Mechanical Reduction of Frictional Resistance of Ninety-Degree PVC Conduit Elbows for Installation of Large Conductors

by

Jay Disberger

B.S., Kansas State University, 2018

A THESIS

submitted in partial fulfillment of the requirements for the degree

MASTER OF SCIENCE

Department of Architectural Engineering and Construction Science
College of Engineering

KANSAS STATE UNIVERSITY
Manhattan, Kansas

2018

Approved by:

Major Professor
Associate Professor Fred Hasler

Copyright

© Jay Disberger 2018.

Abstract

This paper presents the results of an experiment that was purposed with introducing the physical feasibility of a conceptual product that would mechanically reduce frictional resistance of schedule 40 PVC conduit elbows during the installation of large conductors. In the current construction industry, there is a well established and code driven convention for the construction of PVC conduit. For the installation of building service conductors, significant energy is required to pull conductors through the conduit. The service feed is the most expensive and restrictive pull on most projects strictly due the weight of the large conductors which are heavily resistant to deformation. The forces involved necessitate stringent requirements on maximum pull lengths and maximum degrees bent between pull boxes. Cost and risk of costly installation damage are also major characteristics of service feed pulls. The resistance to pulling and highest concentrations of internal forces throughout any conductor pull is located at the elbows or bends. This study is a scaled experimental-based initial establishment of expected evidence to support the feasibility of a product that would essentially reduce the required force to pull large conductors. This product is idealized as a factory PVC elbow that contains mechanical rollers along the inside face of the elbow where the conductors theoretically make the most contact during pulling. This product will ultimately be more expensive, but would be expected to benefit the project by reducing installation time, possibly reduce the number of pull boxes required, and reduce the risk of damaging conductors or conduits. The experiments described in this paper reflect a small-scale set that establishes trends of varying any one significant parameter for single conductor pulls through a single ninety-degree factory PVC elbow. While further research into multi-conductor feeders must be conducted in order to establish full justification for the product development was expected at the onset, the results of this study show that even further additional

research must be conducted to resolve an ambiguity on which a definitive conclusion depends. Due to unforeseen or predicted parameters impacting the reduction of frictional resistance throughout the experimentation, the results both support and counter any benefit of applying mechanical means to reduce frictional resistance. The percentages of reduction range from -37% to +24% across the study's results. The hypothesized sources of the ambiguity that counter expectations can only be verified by future studies. However, the evidence from this study can become definitively directional for the pursuit or lack there of for further investigating the benefits of the idealized product.

Table of Contents

List of Figures

List of Tables

Acknowledgements

Undying thanks is dedicated to Professor Fred Hasler for permitting me to experiment freely under his wise professorship, to Dr. Brian Washburn for the experimental design consulting and analysis advice, to Dr. Don Phillippi for the inspiring brainstorming, to Russell and Mary Disberger for the understanding reminders to get writing, and to Gaby Liuzza for consistently keeping me company while I was writing. Kansas State University's Biological and Agricultural Engineering Department and their research technician Jonathan Zeller are gratefully thanked and recognized for donating their time and resources to machining mechanical components required to run the experiments. Last but not least, an unparalleled special mention and sincere thank you is humbly given up to Travis Whitaker for the outstanding programing that made data acquisition possible. My work has only come to fruition because of all of your care, talent, and support.

Dedication

This paper is dedicated to Amanda Braun for being my rock and source of unconditional encouragement in my every aspiration. This thesis is for you, Amanda.

Chapter 1 - Literature Review of Existing Conditions

1.1 Introduction

It is universally recognized in the construction and architectural engineering industry that the largest and most expensive conductor installation on most jobs is that of the service entrance feed. It is common practice for architectural engineers to make every effort to minimize the distance and total culminated degrees bent in this pull at the design development level. During construction, the larger conductors necessitate significantly more labor and material cost. Existing means to minimize the resistance to pulling a conductor include conductor lubricant or conductors that are designed with outer materials of the most optimal coefficients of friction available (Southwire, 2005). In the available documented history of improvements on conduit technology, there are not easily found records of a conduit product that reduces the frictional resistance through mechanical means. The main purpose of this study to investigate if one such original concept for reducing the frictional resistance of pulling service feed conductors is physically feasible. Such an idealized product that, in short, applies internal rollers to conduit elbows, could potentially have major benefits in reducing labor cost and risks of installation damage. This conceptual product thus has potential in reducing the cost of the most expensive conductor pull on future construction projects thus reducing the overall cost of the projects.

Figure 1-1: Modeled Product Experiment Construction Prior to Securing Roller Elevations

The monetary and risk reducing benefits are attractive but the benefits must be quantifiably understood to pursue developing a product to reduce frictional resistance via mechanical means. While this study is not intended to completely encompass all research and experimentation to validate the development of the idealized product, it frames the groundwork and the results that are essential for rationalizing future studies on this topic. This thesis is constructed to introduce existing industry tools and parameter restrictions in order to create a targeted range for applicable results. The experimental design considered number of scientific concepts and theories that are explained in depth for the sake of reference and completeness in Chapter 2. Chapter 3 describes the experimental design and execution of this study's

experiments in detail. Thereafter, the results are articulated and interpreted with the in-depth narration of Chapter 4. Finally, Chapters 5 and 6 elaborate further on the lessons learned for future researchers and summarize the study.

1.2 Literature Review Over Existing Conditions

In order to establish value and nuance in a well-established construction field, existing solutions resembling the proposed product of a factory conduit elbow containing roller mechanisms must be researched and analyzed. This literature review extends into the background of existing tools that will most likely continue to be utilized in a situation the hypothetical product is applied. It is assumed that the technology currently used today operates at the same performance parameters of their future counterparts.

1.2.1 Other Roller Based Products

One company researched is in the business of cable pulling related products such as sheaves and cable rollers. Among these products are 24” and 36" radius right angle rollers (Current Tools, 2017). These products are primarily used as temporary means for installation of cables that are being supported by a cable tray (Current Tools, 2017). This will largely be applied to data cable installation, but should easily be associated with any power cables that are permitted in cable tray installation. These products are slipped onto empty cable tray right angles of their respective radius and the rollers protrude through the spaces in the cable tray to make contact with cables along the inside and bottom of the bend (Amazon, 2010).

The concept of these products is the same as the product conceptualized for PVC conduit. In pulling the cables through a bend there is a concentration of frictional resistance

relative to pulling along a straight path. This is not only considered as self evident, but is quantified by the experimental data later in this paper. The concept of adding rollers to the main surfaces that cables meet in the bend during the pulling process reduces the required force for pulling. These rollers also reduce the risk of damaging the installation.

The cost of these roller products is extreme as the 24" and 36" radius rollers cost $518 and $585 respectively per a reputable company specializing in the sales and rentals of new and used construction equipment (CESTOOLS.com, 2018). Further online shopping reflects this high cost. A common consumer website in the business of selling anything is selling a similar 24" roller product manufactured for $663.95 (Amazon, 2010). No immediate literature found indicates whether or not this high cost is more reflective of a low demand to high supply or of an extreme cost-to-benefit ratio, but the mere continuing existence of this product indicates that there is a justifiable expense. While this is positive evidence in support of the hypothetical product considered in this paper, there is a major distinction to be made: the conduit rollers that may be developed given enough evidence of their benefit, would remain a permanent part of the installation while the cable tray rollers found here are reusable across countless installations.

The rollers in these cable tray products are segmented in such a way that cables can be installed in sequence without having previously installed cables holding the rollers fixed (Current Tools, 2017). While such division of rolling technology will likely be implemented in the idealized product that prompted the study detailed here within, the testing of such segmentation is beyond the scope of this document. Testing of a more refined prototype after product design and industry feasibility are established will likely be required.

1.2.2. Current Parameters for Installation - Cable Pullers

In addition to products reflecting the concept that is considered as the subject of this study, there are existing cable pulling devices that will likely be used in installations with and without conduit bend rollers. This study is not as concerned about the cost of these tools as much as the available force and speeds associated with operation. These two parameters are of significant interest because they directly define the full-scale parameters that are targets from the mapped small-scale results of the experiments of this study.

Cable pulling catalogs are well-organized references to indicate what cable pullers are capable of, in terms of pulling force and speeds. A common product in such catalogs is the cable feeder. One large example of this product is able to handle up to 200 pounds of force on a single wire with a pulling speed ranging from 4 to 36 feet per second (Greenlee, 2015). This product is helpful in considering a range of results for this study as it is compatible with many cable pulling situations. These ranges should be considered as a fair general target range in future studies.

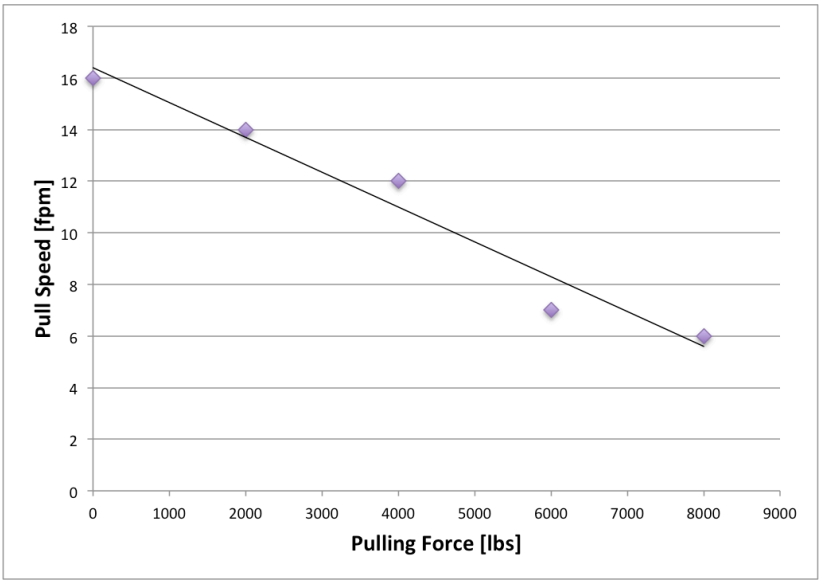

Figure 1-2: Ultra Tugger Tabulated Force vs. Speed (Greenlee, 2015)

While there is a wide range of available cable pullers in such catalogs, only the limits of the largest pullers will be considered due to this study's emphases on the installation of larger conductors. The largest common cable pullers produced are characterized by a maximum pulling force of about 10,000 pounds (Greenlee, 2015). The one considered as reference in this study only lists speeds up to pulls of 8000 pounds (Greenlee, 2015). When graphed, this tabulated data reveals what is potentially a coarsely linear relationship from experimental data. This is highly speculated, as more data points are required to make any definitive conclusion. The range of speeds and applied pulling forces found in this product should also be considered as a background resource when producing a realistic scaled target result from experimental data.

Chapter 2 - Scientific Theories and Experimental Purpose

2.1 Theoretical Basis

The theoretical basis to frictional resistance in this application is far from original. Rollers being applied to flexible entities such as rope may date all the way back to 1500BC Mesopotamia (West, 2017). This marks the initial invention of the pulley as a mechanical tool in hoisting water. The mechanical operation of the conceptual product that is the subject of this paper is simply taking the concept of the pulley and applying it to an in-conduit conductor installation application. The following reviews the physical concepts that theoretically result in mechanically reducing the frictional resistance of conductor installation.

2.1.1. Frictional Concepts

The concept of reducing friction with either pulleys or wheels is fairly intuitive and lightly reviewed here. Consider sliding a block across a smooth floor. While the block slides, across the floor, its kinetic energy is being converted to thermal energy via kinetic frictional interaction between itself and the floor. This energy conversion is continuous until the block's kinetic energy is reduced to zero. Now, consider the same cart with wheels. Relative to the ground, it is a fundamental concept that a rolling wheel is not slipping. The wheel is experiencing static friction relative to the ground. The static friction interaction between the wheel and the ground is not resulting in energy transfer. However, the interface between a static axle and the rotating wheel at the wheel's center is experiencing kinetic friction. This kinetic friction is transferring significantly less energy than the block without wheels, as the energy transferred by friction is significantly less (The University of Tennessee, 2009; Walker, 2013).

The common equation for energy due to work is (Force)x(Distance)=Work. This force in this equation for kinetic friction is determined by the product of the kinetic coefficient of friction experimentally determined to exist between two materials and the normal force at the interface of the two said materials in question. Thus, if the axle and wheel have an interface with a lower associated coefficient of kinetic friction than the interface between the block and the smooth floor, the frictional force present in the case with the wheel will be less than the block alone. This correlates to a slower conversion to thermal energy – lower friction loss. This is why ball bearings and appropriate lubricants can greatly enhance the ability of a wheel to persist in rotation. While the reduction in the frictional force is notable, the other term of the frictional energy equation, distance, is significantly reduced with large wheels (The University of Tennessee, 2009; Walker, 2013).

The distance, in which the block without wheels slides, is finite given a particular coefficient of friction and initial kinetic energy due to the conservation of energy. For the same distance being traveled by the block with wheels, the 'distance' experienced by the frictional force interface is significantly reduced. The constant rate over the span of rotation for a rolling wheel is angular velocity. The actual distance traveled by a particle anywhere on the wheel is directly equal to integrated product of the angular rotation and constant radius from the center of rotation to the particle in question. It is clear that the extreme edge of the wheel will cover a larger summed distance traveled relative to a particle near the inside of the wheel given a finite angle of rotation. Thus, the distance experienced by the interface of the axle and the wheel, near the center of rotation is significantly smaller than the distance traveled by the block which is equivalent to the distance traveled by the outside of the wheel assuming no slipping occurs. This reduction is directly proportional to the radius of the wheel or roller being considered. The

resulting frictional energy loss given the significant reduction in both force and distance terms is often so small that physics textbooks regard the frictional losses in a wheel to be practically negligible (The University of Tennessee, 2009; Walker, 2013).

Considering frictional loss in a roller as negligible is a reasonable assumption when comparing the case of a sliding block and a block with reasonably built or ideal wheels. This translates directly to the concept of pulleys by reconsidering the reference frame of being static with the smooth floor to observe a transient block to tacking with the wheel. This makes the floor look like it is being pulled along a pulley roller like a straight rope. We can now see how a roller reduces the frictional resistance of pulling a conductor through an elbow to practically nothing. Yes, frictional losses still exist. This is especially true if the rollers in the conduit elbow end up locked so that a conductor being pulled is simply sliding across static rollers. This essentially defeats the purpose of the roller product. Design of the future product should take this into account via redundancy and segmentations of rolling elements. For the consideration of the modeling and product concept associated with this experiment, the above is thorough justification for the conception and testing here within described.

2.1.2. Energy and Material Deformation

If the conductors were idealized as perfectly flexible, frictional resistance between the conductor and the conduit would be the only factor that results in higher forces in conduit elbows. This is not a practical consideration for the sake of experimentation. It takes significant force to bend larger conductors. Consider bending a fairly stiff strip of metal back and forth to create deformation that may ultimately lead to separating the strip into two pieces. This action takes energy that is ultimately, like frictional loss, going to end up dissipated as thermal energy.

This can be proven in the action of bending the metal strip as the bending produces heat in the area of bending. A similar and simpler example is how a rubber band heats up when stretched (Walker, 2013).

When the conductors being pulled encounter an elbow, all components of the conductor's construction must deform to accommodate the elbow's bend and then straighten up again in the following conduit run. A wire's construction is not a simple continuous metal. A wire conductor is stranded, annealed metal strands (most commonly copper), heat and moisture resistant PVC insulation, and a very thin outer nylon (Polyamide) or UL-listed equivalent jacket (Southwire, 2017). The composite product and of all three of these materials vary as the wire gauge is increased. For example, the count and size of individual copper strands increases as wire size increases (Wire & Cable Your Way, 2017). Insulation thickness also changes. The interaction during pulling and bending among the strands let alone between the strands and the PVC insulation of the wire during deformation is wildly difficult to analytically model accurately given the number and extreme variation in critical parameters. This is why experimental test data is considered in this study.

At the core of this study, there is a great deal influence from material deformation and internal forces within a given conductor when being pulled through a conduit elbow. The bending must be literally drawn from the energy that is being used to pull the conductor. This is partially why the force to pull a conductor through an elbow is still greater than the force required to pull a conductor through an equivalent distance of straight conduit. The experimental results of this study will isolate the resistance of the material deformation and consider such resistance to be consistent between baseline standard cases and experiments testing rollers. This is a reasonable assumption assuming that the thermal energy dissipated in

pulling the conductor through the standard elbow does not heat the material of the conductor enough to significantly soften the conductor and reduce the energy required to deform the conductor through the bend. Keeping the resistance from deformation in mind, the experimental analysis will focus on the prospects of reducing the frictional resistance with the rollers and compare the reduction to the overall conventional resistance to pulling a conductor through a ninety-degree elbow. In short, the existence and extent of the resistance that is due to friction vs. material deformation is at the heart and core of benefit in reducing frictional resistance.

2.2. Restatement of Experiment Purpose

With existing products and theoretical backing established and reviewed, this section restates the objective of the associated experimental study. This includes the idealized product's experimental design relative to the envisioned full-scale prototype.

2.2.1. Full-sized Product Concept

The objective of the future product in question is to significantly ease the frictional resistance during large conductor installations. This reduction is specifically to be reduced in the portions of conduit with increased concentration of friction – the elbows. The product would locate segmented rollers or rotating entities along the inside face of a standard factory schedule 40 PVC conduit elbow. The rollers will be designed to maintain the sealed environment of a traditional conduit elbow. They will also be segmented throughout to ensure that a stationary obstruction will not hold fixed any portion of any rolling entity that is in contact with a conductor being actively pulled. Such a case would defeat the purpose of the product as well as lead to potential damage of the installation.

Two independently unique constructions of the rolling entities can be classified to accomplish mechanical reduction while maintaining constructability and product integrity. The first of these is a sequence of spherical beads that protrude into the elbow through individual circular openings. Just under half of the spherical rollers would be exposed to the conductor's contact so that they would remain properly fixed and free to rotate. The other end of the spherical roller would be supported by three other rolling entities that are free like beads in a ball bearing. Alterations to the concept of this roller's pocket per more efficient designs are expected during the prototyping of such a product or related. The overall collective mountings of the spherical rollers would be housed by a sealed entity resembling a conduit elbow of a larger size.

The second roller construction is simply of axial construction like a pulley. The rollers themselves are to be lined up along the inside face of the product's bend in order to provide contact with the conductor throughout the entire elbow during installation. The actual rolling portion of the axial roller is to be separated like a stack of washers. This will enable the segmentation mentioned prior in this section. These rollers and the overall elbow may require an overall bulky housing, but such is a detail for prototyping and is beyond the scope of this study.

Both product concepts should be capable of producing results of reduced frictional resistance, but neither can be considered superior to the other without prototyping. For the sake of this experiment, the actual final product construction is considered separate from a proof of concept. The experimental design involving axial rollers is the simplest construction given resources available for the experiment. Thus, the small-scale concept in the experiment is of

axial rollers. The results of this experiment are to be considered validation or lack there of for feasibility of a product implementing either roller construction.

2.2.2. Small Scale Modeling Concepts

Given the financial and space restrictions of this study's experiment, the smallest conduit available was selected for testing. The actual free area within the conduit is considered a negligible parameter in scalability as the modified elbow is the product of interest. Furthermore, conduit is sized per 40% fill on typical power installations per the National Electric Code (NFPA, 2013; Priority Wire & Cable, INC., 2015). Thus, no case is considered in the experiment that exceeds this restriction. The using of a larger conduit, when considering the cable action during installation, can reduce the sharpness of the angle of conductor entry just outside of the elbow and assist in minimizing contact with the inside surface of the elbow. Also, the extra room may also increase the conductor's freedom for random motion that can add to irregularities in resistance of installation. Regardless of the speculated impacts of conductor sizes, the effects are considered negligible in variance for the sake of initial experimental design. Further experimentation with an emphasis on this area would be required to draw any definitive conclusion on the impact of the products total effectiveness or overall frictional resistance.

The physical restrictions of minimizing the conduit size for modeling's sake impose a number of limitations on parameters that are considered, strongly suggested subjects for future areas of research. Such imposed limitations include no tests in varying elbow curvatures. Only one radius elbow was considered in the scaled experiment. All results will only be directly applicable to corresponding elbows after direct scaling factors are applied. Testing on how

rollers impact frictional resistance as a function of the elbow's curvature is thus outside the scope of this experiment and is an area for future research.

Another restriction imposed on the experimental parameters to limit the scope of this study to a manageable result is the number of conductors tested at a time. The simplest case of conductor pulling is the pulling of a single conductor. This case is uncommon in industry, but is the most reduced to avoid variation in experimental error and for accurate data interpretation. It is assumed that by understanding the pulling of a single conductor, further experimentation on multiple conductor pulls will be more intuitive if results build on conclusions of singular conductor experiments. The frictional reactions between conductors and the impact of having conductors over a significantly larger cross-sectional area are factors that may be hard to isolate from results that are solely dependent on conductor size, conductor construction, lubrication, or pull speeds if singular conductors are not tested independently. Thus, interactions among multiple cables are left up to future studies.

Conduit and conductor types are also unvaried factors in this study. The focus of the study is the application to larger installations such as building service feeds. The most typical conduit material for sub-grade service feeds is Polyvinyl chloride (PVC). Thus, this experiment focuses exclusively on PVC conduit. Similarly, the testing of multiple conductor types would result in multiplying the experimental scope by the number of conductors types considered for testing. The variations among cable types include construction, material, and coefficient of friction differences, but the objective of showing feasibility does not require that all conductor types be considered. In academia and industry, copper conductors with THHN insulation and a nylon jacket are incredibly common and will be the exclusive focus of this study (Wire & Cable

Your Way, 2017). Again, the work in varying conductor and conduit types are thus beyond the scope of this study.

The factors that are varied for the sake of scaling and as functionalizing parameters include conductor size, conductor construction, application of lubricant, pull speed, and resulting tension. These factors are isolated and varied independently for the sake of constructing scalable results. The entire construction of the experiment and the experiment's design at its core are both centered on the creation of scalable experimental results that can definitively be used to make remarks about the full-sized case. The details of the actual experiments are outlined in subsequent sections.

2.2.3. Buckingham Pi Theorem

Buckingham Pi Theorem (BPT) is a formal scaling tool that is used in experimental design to conduct dimensional analysis. This tool is very helpful in scaling models that are developed for predicting outcomes of processes that may be too complicated to analytically solve. A good example of a complicated modeled experiment benefited by BPT is using a small wind tunnel to test scaled airfoils for aircrafts. Such experimental work and application of BPT is especially common in the field of fluid mechanics due to the dynamic nature of fluid. While the experimental case considered in this paper is not as dynamically complicated as fluid mechanics, there are enough parameters that experimental results will easily yield more accurate and justifying results (Munson, 2013).

2.2.3.1. Theorem Background

The French mathematician Joseph Bertrand developed BPT in 1878 for the sake of applications to electromagnetics and thermodynamics (Munson, 2013). BPT depends heavily on the dimensional basis of choice for analysis even though using either of the two that are widely accepted will yield identical results. The two dimensional systems that are commonly applied in the fields of physics and engineering are Mass-Length-Time (MLT) and Force-Length-Time (FLT). Temperature may also be applied to either basis and is referenced by the Greek letter theta (Munson, 2013). To understand the difference between the mass based MLT and the force based FLT, consider the English Customary and SI unit systems. In the English system, mass is considered to be of the composite unit 'Slugs' which is equivalent to a pound force times seconds squared divided by feet. This is a force or FLT based systems as force is used to construct the composite unit of mass. This system considers force to be fundamental and is thus using FLT methodology in defining units. Next, consider the SI system's composite unit for force: the Newton. One Newton is equivalent to a kilogram-meter divided by squared seconds. In this case, mass is considered fundamental and is thus based in MLT (Munson, 2013).

The process for executing BPT for dimensional analysis is pretty straightforward given ample practice. A Pi term in the theorem is a dimensionless number of value to the scaling of a model and is constructed by a mixed product of parameters to varying powers that are considered impactful to the dependent variable of interest. Pi terms are systematically constructed by first counting the parameters considered pertinent to scaling as well as the number of dimensions (or consistent combinations of dimensions) present within the set of selected parameters. The dimensions may be listed in MLT or FLT without changing the overall outcome. The difference between the number of parameters considered and the count of their

cumulative repeated dimensions is equivalent to the number of Pi terms that can be constructed. Repeating parameters are then selected to each represent a dimension. Typically the dimension of representation is in its most reduced form in the representative parameter. Each Pi term is then assigned to one of the remaining parameters and all of the repeating parameters taken to a variable power. All of the parameters can then be replaced with their dimensions while still maintaining their variable exponents. The entire equation is set to zero for the sake of a Pi term being defined as dimensionless. A system of equations can then be developed to solve for the exponent variables of the repeating parameters. Isolating each independent dimension and using the corresponding exponents as summed terms that equal zero construct this system of equations results in a system of linear equations. The solution to the linear set of equations yields exponents that can be reapplied to the initial conglomerate of parameters to finally define the Pi term in question. The solving of the system of equations may also be skipped if the solution is self-evident. The writing of a self-evident solution is known as solving by inspection (Munson, 2013).

Once the latter half of this process is repeated to find all of the Pi terms, they can be used to isolate components of a scaled model and solve for expected results of variables that would otherwise be undeterminable. The non-dimensional (unitless) numbers may also be analyzed over multiple iterations of adjusting certain independent parameters to alter the Pi term with dependent parameters. A good example of a typical and valuable non-dimensional number is the Reynolds number. While not having any dimensions, the Reynolds number when plotted against the frictional factor for fluid flow can yield helpful results in determining laminar or turbulent flow of a given fluid within design. This is a common example of a non-dimensional number in fluid mechanics being experimentally useful (Munson, 2013).

2.2.3.2. Experimental Application

The parameter of interest of the experiment is the force that is to be measured during pulling of specified and controlled cases. The large variances that can exist in an industrial case that would alter the amount of force required to pull a conductor include variances in pull speed and wire gauge. Unfortunately, conductors of varying sizes have multiple facets to their construction that change from one size to another (Southwire, 2017; Wire & Cable Your Way, 2017). In order to fully understand the scaled model relative to a full-scale case, the differences in construction must be considered as instrumental and impactful to the results of the small-scale experiments.

By way of BPT, these impacts are to be analyzed through non-dimensional Pi terms. The parameters selected include representation of each significant facet of wire construction and variation in pull speed. The coefficients of friction are excluded from this analysis because they are already dimensionless. Their inclusion, even though they are directly impacting the force required to pull the wire, would be pointless given they have no application throughout the BPT process. This is further explored with the parameter of strand count which is included for academic completeness and emphasis. Furthermore, the modulus of elasticity for both the copper and insulation components of the wires are listed even though their values will remain consistent from a scaled case to the full-sized consideration. Their inclusion is essentially for the consideration of resistance due to material deformation. It is important to be considering the deformational impact from geometry and elastic strengths of the conductors in question. Such resistance is all that is assumed to be significantly impacting the resistance to pulling through an

elbow with applied rollers. The parameters that are theoretically going to impact the force, especially in the context of scaling, are listed in the following table in utilizing FLT dimensions.

Table 2-1: BPT Parameters and Dimensions

Name	Symbol	Units	FLT
Wire Diameter	D	in	L
Strand Count	C_t	#	-
Area of Copper	A_{cu}	in^2	L^2
Area of Insulation	A_{in}	in^2	L^2
Strand Diameter	d	in	L
Copper Modulus of Elasticity	E_{cu}	psi	FL^{-2}
Insulation Modulus of Elasticity	E_p	psi	FL^{-2}
Wire Mass Per Length	λ	lb_f/ft	FT^2L^{-2}
Pull Speed	U	ft/s	LT^{-1}
Pull Force/Tension	T	lbf	F

One of these parameters, strand count, is completely dimensionless and is thus excluded from the BPT analysis. The remaining parameters are applied to BMT by first determining the number of Pi terms to be found. There are clearly three dimensions used among nine usable parameters. Thus, there are a total of six dimensionless numbers that may be constructed for analysis. By selecting wire diameter, pull speed, and tension as the primary repeating parameters representing length, time, and force respectively, all non-dimensional Pi terms may be written by inspection as listed in the following table.

Table 2-2: BPT Pi Terms

Pi Term	Parameters		Dimensions=0
Π_1	=	$D^{-2}A_{cu}$	L^2/L^2
Π_2	=	$D^{-2}A_p$	L^2/L^2
Π_3	=	$D^{-1}d$	L/L
Π_4	=	$T^{-1}D^2E_{cu}$	$L^2(FL^{-2})/F$
Π_5	=	$T^{-1}D^2E_p$	$L^2(FL^{-2})/F$
Π_6	=	$T^{-1}U^2\lambda$	$(L/T)^2*(FT^2L^{-2})/F$

It is also acceptable to multiply or divide Pi terms by each other to create more useful non-dimensional numbers (Munson, 2013). For example, by design, the Pi terms derived do not show strand diameter (d) having a relation to the force of pulling (T). Thus, if this potential relation or dependence is of interest, Pi terms four and five may be multiplied by Pi term three to any power.

Chapter 3 - Experimental Design and Execution

3.1. Experiment Design

The idealized product that is in question of this study is one that may be applied to industry. In being such, there are many facets of operation that will vary widely and can only be properly analyzed by years of field observation and data collection. Statistically, this will be the only way to yield absolutely definitive information. However, this product is not yet developed for field use, and thus must be experimentally isolated in this study with a question of feasibility.

The experimental design of this study has two major hurdles to jump. The first of these is that experimental or lab conditions will not be reflective of field conditions given the isolated parameters and physical restrictions. In order to create useful results, multiple factors that take place in field conditions must be simulated, recreated, or omitted. For example, the service feeders that are focused on by the scope of this study are typically buried underground. The pulling of a conductor through subgrade conduit cannot be replicated without burying the entire system. As is increasingly evident as the experimental design is described, this replication is impractical and inefficient. Thus, the alternative conduit installation designed exclusively for the experiment must be accepted as being close to that of a buried conduit or the effect of the difference must be assumed to be of negligible impact to the results of the study.

The second major hurdle is that a full sized experiment was not fiscally responsible as an initial study of feasibility. Thus, the experimental design must account for being scaled down so that results may be considered valuable to a full sized field condition. For example, the design of the experiment is limited to the speeds available to operate at a small scale. These

speeds may not be found to scale directly to a full sized case. This can be handled by creating a dependency of the speed parameter while experimentally holding all other combinations of parameters constant. Results can then be interpolated or extrapolated to simulate the desired results that were not perfectly replicated on the small scale. This provides a freedom in the scaling of results that would otherwise not exist if the variable were not considered as one to be isolated. The following sections review the facets of the experimental design that was implemented to produce the results discussed thereafter.

3.1.1. Selection of PVC

As stated in the abstract, this study's focus is limited to the effect on larger conductor installations. Such installations are most commonly service feeders that are routed to the building's electrical system through a buried path. It is well understood by engineers and contractors alike that metal conduit is subject to corrosion when exposed to water (NFPA, 2013). Thus, subgrade conduit is most often going to be PVC.

This was not the only consideration in limiting the study to PVC conduit. The product in question is not designed beyond the phase of theoretical conception. The materials and costs for creating this product may necessitate material fabrication that limits the main material to PVC. PVC is likely to be an inexpensive material for prototyping and industry application. Furthermore, the actual product may be restricted to being of a particular material independent of the material of the conduit. In this case, the conduit type used in the experiment should be reflective of the most applicable case for the sake of being valuable to industry. The larger conductor pulls are significantly more challenging and more expensive than smaller conductor pulls. Thus, a product to reduce friction may be most valuable or only valuable in the

installation of large feeders. This reasoning has limited the scope of this study to PVC by way of priority for potential largest benefit and speculated prototype material sequence.

3.1.2. Selection of ½" Conduit

The experiment was restricted heavily from a financial stance. The most cost effective PVC conduit for experimental design was simply the smallest available. Thus, one-half inch schedule 40 PVC was selected for use in the experiments. While testing multiple sizes of conduit would enable this study to comment on the effect that such variation would have on the experimental results, the increasing or decreasing conduit size for installation ease installation is beyond the scope of this experiment. Furthermore, it is assumed that the conductor construction has a much larger impact on the force required for pulling relative to a slight change in conduit size. If the experiment were to have tested multiple conductor pulls, it should be noted that it is speculated that the conduit size would play a larger role in variation of results.

The conduit that was used for the experiment itself was manufactured by Cantex and is labeled as UL compliant. All conduit components that were purchased for the experimental construction were from the same manufacturer and were being sold together at a local home improvement store. The experimental design of the conduit involved two straight legs and one ninety-degree elbow. The legs were constructed in modular pieces that were each approximately 48" in length. These modular sections were combined using typical PVC conduit couplings without any adhesive for the sake of disassembly and reassembly. The leg into which wire is fed measured 113.5" long from end to end. While reasonably similar, the second conduit leg on the pulling side measured 111.25" from end to end. The elbow section was designed to be modularly removable so that the otherwise separate legs could be combined to create a single

longer leg. This longer leg allows testing from the frictional resistance of just pulling the conductors through a straight run. This data was determined for the sake of isolating and separating the frictional resistance of straight elements from the data collected with the elbow installed. The total length of the longer leg was 194.5” as a modular portion of one original leg was omitted from the longer leg. The finer details of the actual PVC conduit run composition are described in more detail under frame construction.

Figure 3-1: Conduit Construction with a Factory Elbow Connecting Two Conduit Legs

3.1.3. Selection of Wire Type and Sizes

As was mentioned in a prior section, the conductor insulation type was selected to be THHN. This selection was made because THHN is a popular selection in industry and because there are numerous variations in wire types. The time required to conduct the experiments in this study would be a direct multiple of insulation types considered. It is also assumed that the differences in results of varying conductor insulations would be minimal compared to the impacts of other parameters being considered. This is largely due to significant similarities among conductor insulation types. This assumption should be verified by future research.

Wire size selection was altered during the process of experimentation. The initial restrictions were well thought out, but a limitation in the measurement equipment cut the testing of larger wires short. The lesson to be considered in future experimentation is to preliminarily compare expected forces involved during pulling to equipment capacities prior to selecting measuring equipment. While this step was conducted in this study, it was not executed to the detail necessary to prevent further limiting the conductors tested.

3.1.3.1. Initial Intent

The 2014 National Electric Code (NEC) is fairly specific about limiting conduit fill, for most power applications, to 40% of the conduit area (NFPA, 2013). For the sake of avoiding considering results that void code compliance, this factor was the primary limitation to conductor selection. As previously discussed, the experimental scope of this study is restricted to testing results of singular conductors for the sake of isolating results that may otherwise be confounded by interactions among multiple conductors. Physically speaking, the singular conduct results are fundamentally an appropriate experimental basis for fully analyzing

experimental results of this and future experiments accurately. Thus, the conductors that would not exceed 40% fill of a ½" PVC conduit per NEC tabulated values include #14, #12, #10, #8, #6, #4, and #2 AWG THHN wires (NFPA, 2013).

The roughly approximated tension required to pull a #14 THHN conductor fell close to being below the range of accuracy for force measuring equipment available. Thus, #14 wires were excluded from the experiment. #2 and #4 wires were also considered to be a bit heavy for the tension gauge purchased to evaluate pulling force. This evaluation was concluded after considering the wires' total weights given the nominal 8'-3" length that all tested conductor samples were to be. The 8'-3" length was selected for the sake of ensuring that the conductor could move completely from one leg of the experimental conduit run to the other without having to exit the conduit. As a result of the preliminary approximations and NEC restrictions, samples were selected and purchased for #12, #10, #8, and #6 wires. These samples were cut to the nominal 8'-3" each and prepared for testing per prescriptions described in subsequent sections.

These conductors, as selected, have one major parameter in common that was initially theorized to be of value in order to fully develop a mapping of results to a full scale. That parameter is the number of copper strands within each wire. These conductors only increase their ampacities by increasing the area per each of their nineteen copper strands. Without a sample set of conductors with a varying number of strands, there can be no measure accounted for in the overall scaling of the results. It should be noted at this juncture that impact may or may not be significant for the scaling of results. Given the findings and relationships developed from maintaining the strand count consistent, further study can easily apply the additional results to those of this study in order to better model any impact that strand count may have on

the overall internal frictional resistance of a conductor when pulled through any conduit bend. This paper still heavily recognizes the strand count parameter in an effort to emphasis the importance of it being held constant when analyzing results, for completeness, and to highlight the recommendation to make the it the subject of a future study.

3.1.3.2. Unforeseen Limitations

There were multiple experimental complications that were worked out before conducting experiments to produce usable data. A substantial adjustment that was made to the wire gauges being considered was that the #8 wire readings were exceeding the maximum force on the dial of the available equipment when tested in the initial baseline case with the fastest of three standard speeds per the experimental design. This is problematic as the #6 wire was clearly going to be too restricted by the force measuring equipment for any valuable results to obtained. The purchasing of a tension gauge to accommodate the restriction would have up to doubled the overall cost of the experiment. This was not a feasible option given the funding available to the study. Thus, the #6 wire was omitted from this study in addition to the data for the #8 wire that was deemed just beyond the equipment limitations. While this restriction is an unfortunate and unpredicted narrowing of the study's initial scope, it was not detrimental to the overall purpose. The trials that were omitted from this restriction are blacked out from the trial summaries provided later in this chapter. Further study using equipment of a higher rated maximum force should be used to study larger single conductors in addition to multi-conductor pulls in future studies. The result of this unforeseen limitation is that the experiments conducted for this study only include data for #12, #10, and #8 THHN conductors.

3.1.4. Speed Variation

In order to generate a model of scaled results that are applicable to industry conditions, the results should be considered over a varying range of speeds in order to fully relate to cable pulling technology limitations and performances. While the idealized case would be to record data from varying speeds over the duration of a continuous pull, the experimental design is best suited to holding a constant speed per finite trial. Thus, it is required by mathematical necessity that at least three different standard experimental speeds for testing must be applied in order to verify a relationship among varying speeds and pulling force. While it is preferable to have more than three speeds, the minimum of three was considered adequate given enough variance and experimental consistency.

3.1.4.1. Method for Pulling

A cable puller acts by winding a braded rope around a spool that is being rotated by a hefty drive motor (Greenlee, 2015). The scaled experiment simulates this scenario in a controlled manner by applying five and a half amp power drill to rotate bolts of varying diameters to pull a fishing line that is fixed to the conductor being pulled. It is assumed that the power drill operates at a consistent angular rotation across all experimental trials as the torque applied to pull the conductors is observed to leave the power drill unstrained. This is per the intended experimental design. While the drill used in the experiment is nominally rated to operate at zero to one thousand six hundred rotations per minute, multiple measures of max rotational speed were experimentally determined. These experiments are described in detail in a following section.

A singular residential receptacle powered the power drill selected in order to avoid any variance in voltages and power loss over the duration of use that would be experienced with a battery source. The power drill was fitted with the appropriate hex head bit to rotate a respective bolt on which the fishing wire was wound. By generating a consistent angular rotation from the power drill, the speed of an experimental pull can easily be changed by selecting bolts of varying diameters. The bolts applied were limited by the hex head bits that were reasonably available for a power drill, but three standard bolts were prepared for use.

Bolts were prepared for use with the assistance of Kansas State University's Biological and Agricultural Engineering department's machine shop. The bolts each had a singular small hole milled perpendicularly through their shafts five-sixteenths inches away from the end of their heads by the machine shop's Research Technician, Jonathan Zeller. These holes are used for anchoring the fishing wire by means of a safety pin that is permanently tied to the end of the fishing wire. The safety pin enables the different conductors that are being tested as well as different bolts to be switched out quickly during the transitions between experiment trials.

The bolts rested in slotted galvanized iron angles that are firmly screwed into the wood frame that acts as the base for the experiment. The bolts are seated through the circular openings in the two parallel iron angles in order to create an acceptable, accessible, and consistent mounting for the bolt being used in any given experiment trial. There were no provisions for creating a perfect fit for all bolts as effects from smoothness of mounting is considered negligible. The bolts were separated from the mounting frictionally by a set of two washers at each interface.

In summary, a mounted bolt with a hole is rotated at a constant angular rotation by a power drill. The bolt in question is modified with a hole that is used for fixing a fishing wire

pulling string to the rotational action via a safety pin. The rotating bolt thus winds the pull string at a constant rate. The pull string is attached to the conductor being tested by the respective trial and is pulled with significant power through the experimental conduit.

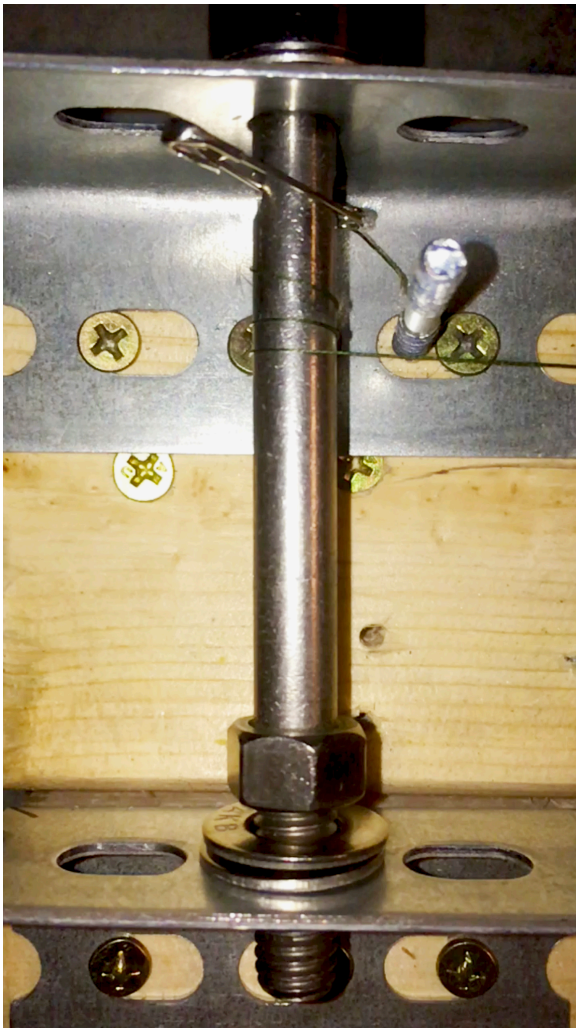

Figure 3-2: Bolt Assembly for Conductor Pulling

3.1.4.2. Bolt Diameters Applied

The bolts applied are nominally four inches long and are of varying diameters. In addition, the hole milled into the bolts is of a different size on each bolt. These holes vary in size strictly for the ease of machining. The bolts are denoted as Bolt 1, Bolt 2, and Bolt 3 and

are 1/4”, 5/16”, and 3/8” in diameter respectively. The holes that are milled into these bolts measure 1/8”, 5/32”, and 3/16” in diameter respectively. Only the last nominal inch of each bolt is threaded for the sake of being fixed to the angle iron frame when in use. The unthreaded majority of the bolt is where the fishing line is wound at a consistent diameter.

3.1.4.3. Method for Defining Angular Speeds

The formula to analytically convert angular velocity to linear velocity is common knowledge among those in the field of physics. A common form and notation for this equation is as follows:

$$V = r * \omega$$

In this equation, *V* represents the linear velocity of a point on a rigid body that is rotating at ω radians per unit time. The point in question is located at radius *r* from the center of rotation of the rigid body (Walker, 2013). Nominally, the rotations per minute of the power drill and the diameters of the bolts used in the experiments are defined. Thus, the nominal linear velocity of the edge of any of our bolts can be found per the above equation. It is important to note that the nominal angular speed of the drill is given as 1600 rotations per minute. This value must be converted to radians per minute in order to be applied to the equation. This is accomplished by the universal definition of one rotation containing 2π radians. The velocity units of interest for this experiment are feet per minute (fpm). Thus, the radius of each bolt is converted from inches to feet in the following calculations:

Bolt 1: $$V_1 = r * \omega = \left(\left(\frac{1}{4}in\right) * \frac{1}{2} * \left(\frac{1\,ft}{12\,in}\right)\right) * \left(\left(1600\frac{rev}{min}\right) * \left(2\pi\frac{rad}{rev}\right)\right) = \mathbf{104.72\ fpm}$$

Bolt 2: $$V_2 = r * \omega = \left(\left(\frac{5}{16}in\right) * \frac{1}{2} * \left(\frac{1\,ft}{12\,in}\right)\right) * \left(\left(1600\frac{rev}{min}\right) * \left(2\pi\frac{rad}{rev}\right)\right) = \mathbf{130.90\ fpm}$$

Bolt 3: $V_3 = r * \omega = \left(\left(\frac{3}{8}in\right) * \frac{1}{2} * \left(\frac{1\,ft}{12\,in}\right)\right) * \left(\left(1600\frac{rev}{min}\right) * \left(2\pi\frac{rad}{rev}\right)\right) = \mathbf{157.08\ fpm}$

These values do not take into account any variance due to the real life parameters that exist in the environment of the experiment. These values may be off if the drill contains production defects or if the experimental environment varies significantly from the test parameters used to rate the power drill. Any experimental value should be smaller than the nominal as the most likely variations potentially impacting rotations per minute of the drill would be applying rotational reduction in power or increase in rotational resistance. Taking these values as absolute would be scientifically irresponsible as there is undoubtedly variation during trials and potential deviations from nominal ratings. Thus, a sub-experiment was designed to establish the linear pull speeds from each bolt independent of nominal or given ratings.

This experiment was conducted by winding a fishing line with knotted and colored demarcations that are spaced out with known spacing. A video of the winding at the drill's full speed was recorded with a slow motion mobile phone camera operating at 240 frames per second. The number of frames between demarcations reaching the edge of a given bolt was recorded in order to calculate time between demarcations during pulling. Demarcations were nominally placed one foot apart from each other. The actual distances were re-measured between all six demarcations and used to ensure accuracy of calculations. The results of the calculated speeds for all five distances in each of the nine trials yielded fifteen results per bolt. The average speeds and statistical uncertainties that were calculated are summarized in the following table.

Table 3-1: Experimental Pulling Speeds Per Bolt

Bolt	Diameter	Average Speed [fpm]	Uncertainty (±) [%]	Approximate fpm	Actual RPM
Bolt 1	1/4	71.7	1.11%	104.72	1096
Bolt 2	5/16	86.5	1.49%	130.90	1057
Bolt 3	3/8	100.7	1.64%	157.08	1027

Figure 3-3: Running Speed Establishment Trial with Bolt #3

The uncertainties were calculated by a common equation for calculating uncertainty from mean quantities of small data sets. The equation is simply taking half of the data set range

divided by the square root of the number of trials in the average. This value is represented as a percentage tolerance by dividing the uncertainty magnitude by the average speed (Taylor, 1997). The measured speeds are consistently smaller than the values found by applying the power drills nominal one thousand six hundred rotations per minute. The actual experimental rotations per minute are calculated for comparison for further comparison by inverting the equation for linear velocity given radius and angular speed.

The experimental averages are stated with +98% certainty and are thus acceptable for application in the study. The values likely vary from the nominal calculations due to systematic and consistent variation in testing conditions relative to the power drill's UL testing. Considering the consistency and certainty of the experimental values, the reason for the variation from the nominal is of no further concern to this study. Future research may make more advanced steps to simultaneously eliminate the majority of this variance in order to alleviate questioning of results.

3.1.5. Gauge Selection and Data Collection

The selection of the force gauge was an incredibly challenging facet of the experimental design. The value of interest that requires measurement in the experiment is the tension on the line pulling the conductor through the conduit. Using a pull spring scale is impractical due to the winding of the fishing line not being able to wind the gauge in with the line. Even in an experiment with an alternate pulling method or extra long string allowing free transit of the gauge over a full duration of pulling, the gauge would still be in motion. If manual, this gauge could not be read consistently. A wired gauge would introduce potential radical variation in

tension from trial to trial due to the connection to the gauge itself interacting with the environment.

The ideal gauge for this experimentation would be integrated into a fixed drive motor. Such a gauge measures torque on the pull while maintaining a constant pulling speed. Digital motor and gauge combinations were found for this experiment, but far exceeded the funding available to the study. It is highly recommended that future research on this topic employ the use of this equipment.

The gauge style that was implemented was a manual dial style device that is commonly applied to measuring the tension on a monofilament being consistently pulled through a machine during its manufacturing. This style of gauge utilizes two fixed rollers and one that is permitted to rotate under an applied force with increasing resistance with progressive displacement. The monofilaments that are typically associated with this style of gauge wind about the rollers in a manner that increases in tension to induce displacement on the movable roller. This gauge applies minimal additional resistance to the system per the application of roller technology discussed earlier in this paper (Check-Line, 2017).

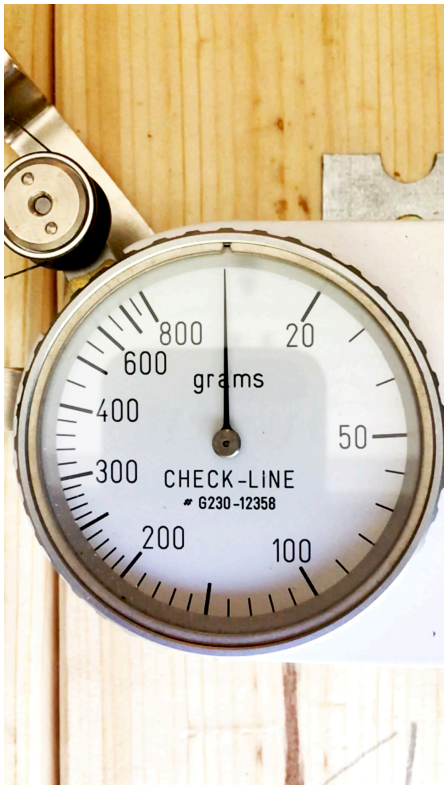

Figure 3-4: Applied Gauge Just Prior to Trial Operation

3.1.5.1. The Applied Gauge

The roller style gauge is available in mechanical and digital models. The digital models result in significantly more accurate data acquisition at a steep monetary expense. While the digital gauge is more desirable, this study utilized the still expensive mechanical gauge to measure the force on the pull string (Check-Line, 2017). The model selected measures tension in grams and has a scale that ranges from twenty to eight hundred grams on a nearly exponential scale. The gauge was received with a certificate of calibration. Two factory provided bolts allowed a means to mount the gauge to the wood frame with a short section of galvanized angle iron (Check-Line, 2017). The gauge is mounted nearly halfway between the end of the conduit and the mounting for the bolts.

3.1.5.2. The Acquisition of Force

As the conductors were pulled during their respective experimental trials, the mechanical tension gauge reads the tension on the pulling string in real time. Given that there is no digital interface for data acquisition, video recording methods were applied as the most appropriate substitute. A smart phone was mounted above the gauge and set to record every trial run at two hundred forty frames per second. The mounting was a separate entity from the experimental wood framing. The phone was firmly fixed to a hardwood board with screws around the phone's edge. The board rested on paint cans and was arranged with the gauge's dial in a consistent location relative to the frame. While this is not the most mechanically consistent setup, it served a flexible and consistent mounting for the phone that isolated it from vibrations from the power drill's interface with the active bolt and mount. The videos were recorded and

meticulously documented for every set of trial treatments as dictated by the experimental design.

3.1.6. Selection of Header and Pull Wire

A method to interface the pulling cable and the conductor was selected per existing industry means, theoretical equivalence, and conductor installation guides. The header is the term used to refer to this interface (MSC Direct, 2018). The header was constructed like that of any header for smaller conductors being installed in the field. The actual scaling of frictional resistance due to header construction is beyond the scope of this study. However, it should be noted that precaution and provisions were made to make the header interface as consistent and reflective to practical application as possible for the sake of successfully modeling a realistic conductor pull. Furthermore, the selection of a pull wire or string from the application of the scaled experiment further reflective industrially practical while conforming to limitations and eliminating complications of the experimental process.

3.1.6.1. Header Composition

The header is often comprised of a pulling grip and electrical tape when larger conductors are installed. These pulling grips include a loop of steel wire and a mesh sleeve that is an extension of the weavings in the loops. As pull rope transfers tension to the pulling grip, the grip holdfast to the conductor using the same concept as Chinese finger traps (MSC Direct, 2018). The mesh of the pulling grip is further fixed to the conductor by a continuous wrapping of electrical tape. This tape also helps protect the inside of the conduit from being damaged by the rough steel mesh. Many variations of this product exist throughout the industry, but they all

function similarly. Smaller conductors can use similar methods, but they may also be pulled with fishing tape that is fixed to the wire by stripped and twisted ends of the conductor itself. This is not reflective of larger conductor pulls that require implementing a braided rope or cable.

In order to best simulate the large conductor header, the pull rope, and comply with requirements of the tension gauge, a fishing wire was selected to stand in for a small-scale pull rope on a string-sized scale. In order to construct a header that performs like a pulling grip, a number of carefully implemented steps were devised. The first step in constructing the experimental pulling header is to use wire cutters to snip the end of the conductor at a bias in order to create a sharply tapered point. This is done to minimize blunt surfaces that may easily catch the joints of the conduit. While this is a realistic happening in field pulls, such interaction between the conduit and conductor is considered noise to the isolated frictional resistance of interest. With the taper established, the very end of the fishing wire is taped to the mid point of the taper as if the fishing wire and conductor shared a mutual end and direction. The fishing wire is then wound tightly around the conductor at a forty-five degree angle until the winding is three inches away from the tapered end of the conductor. While maintaining the same clockwise or counter clockwise direction of winding, the fishing wire is continuously wound at forty-five degrees back over itself back to the tapered end of the conductor. The fishing wire is then anchored next to its origin with the same piece of electrical tape. The result of these steps is a crisscross winding of fishing wire that snugly holds to the first three inches of the conductor to be tested. At the point where the winding switched directions three inches away from the tapered end, a continuous winding of electrical tape is started and continued to the tapered end

of the conductor. At the very end, the tape accentuates the taper to conically reduce the header entity to the singular fishing wire protruding from tapered end.

Figure 3-5: Applied Conductor Header Midway Through Construction

During pulling, the crisscross winding tightens in on itself. The harder the pulling force, the harder the header grips. This reaction is identical to the pulling grip and Chinese finger traps. Furthermore, this header creates an interface that has no noticeable slip and thus achieves its purpose. The fishing wire that continues out of the resulting headers on the tested conductors

was free to run to the bolt mount for winding. The end of the fishing wires used in the experiment were tied to safety pins for ease of attaching and detaching to any winding bolt for the operationalization of the experiments.

3.1.6.2. Pull Wire

The fishing wire described above was not simply selected at random. The process was dictated by necessity of the gauge as well as the model consideration of the full-scale industry standards. Research into the different types of fishing wire was also further necessitated when problems arose due to an initial selection of fishing wire was diagnosed as the source of unacceptable error. The resolved resulting selection of fishing wire proved to be adequately appropriate.

3.1.6.2.1. Initial Intentions

Considering cost and the diameter required by the selected gauge for accuracy strictly dictated the initial selection. The gauge required a filament as close to 0.30mm in diameter in order to read as calibrated (Check-Line, 2017). Any sizable variation would require recalibration of the gauge. The most inexpensive fishing wire is a nylon monofilament. A 0.30mm clear monofilament fishing wire was selected for the initial tests of the experimental trials and ruled inadequate shortly thereafter.

3.1.6.2.2. Stretching Problems

Every trial pulled by the monofilament fishing wire resulted in the gauge reading violently swinging sporadically over the entire reading range. After investigating the experiment

for the source of error and systematic flaw, the monofilament was theorized to have a stretching properties resulting in radical oscillation in tension. Hook's Law can simply and analytically explain this phenomenon. This law simply states that the magnitude of force on a spring like entity is equivalent to the material's spring constant multiplied by the stretch or displacement of the entity. The spring constant is often denoted with a lowercase 'k' and is characterized by larger values representing entities that are harder to stretch (Williams, 2015).

A common and directly relatable physics model that utilizes Hooke's Law is the classic spring mass system where a rigid body of given mass is suspended by a spring of negligible mass. The mass is displaced and proceeds to oscillate up and down in the classic example to a period 'T' that is equal to two pi multiplied by the square root of the ratio of the entity's mass over the springs spring constant. The formula is written as follows (Lumen Learning, 2012, Williams, 2015):

$$T = 2\pi * \sqrt{\frac{m}{k}}$$

This derivation translates to the experiment's case of a conductor being pulled on a spring. While the force of gravity is not acting in the direction of oscillation as it is in the spring mass system, there is a theoretically constant force of kinetic friction acting on the conductor during instances of steady state. By putting our frame of reference in that of the moving wire, the resulting system acts like a gravity spring mass system on its side were the pull string acts as a the nearly massless spring (Lumen Learning, 2012, Williams, 2015).

With this connection established, the above period equation's dependence on the spring constant can be related to the intense oscillation observed when the monofilament was used. During manual pulling, it was duly noted that the monofilament fishing wire was noticeably stretchy. Thus, the value of 'k' must be lower than that of a fishing string characterized by

negligible stretchiness (Lumen Learning, 2012, Williams, 2015). The period is inversely related to the square root of the spring constant. Thus, the smaller spring constant results in a longer period. The period is dimensionally representative of the time it takes an oscillating entity to complete a full cycle of oscillation. Thus, there is more time and variance in the gauge reading in observing pulls from stretchy fishing wire than negligibly stretchy fishing wire.

While this diagnosis was proven true and corrected before conducting official trials, the situation shed light on another drawback of using a mechanical dial gauge. The gauge reads tension by implementing mechanical springs to provide known resistance to the cable under tension. This was not considered as a problem on the onset when the oscillation concerns were unknown, but the presence of any spring in the system ultimately lowers the overall system's effective spring constant. Thus, oscillations are unavoidable and expected in the data results. Any and all adjustments to increase the system's effective spring constant were made after this realization. It is strongly recommended to future researchers to minimize implementing all forms of spring like entities and mechanical gauges for the sake of accuracy and consistency.

3.1.6.2.3. Solution

There are three types of commercially available fishing wires: monofilament, fluorocarbon, and braided. The monofilament type was initially selected as described above. This fishing wire is a single nylon based homogenous entity that is noted by fishing line experts to be stretchy. The fluorocarbon fishing wire is a polyvinylidene fluoride. Fluorocarbon is described as being less absorbent, more ridged, and less stretchy than monofilament. Braided fishing line is identified as having 'no stretch' and intense strength. A braided fishing wire is made of Dacron, Spectra, or Dyneema microfibers that are woven together much like a braided

nylon rope. Thus, the braided fishing wire reflects the full-scale application and virtually eliminates oscillations from stretching. A braded fishing line of identical diameter to the initial monofilament was applied to the experiment. This successfully resolved the unacceptable oscillations previously observed (Sealock, 2014).

The monofilament still served a purpose in the official experimental trials. A header was ultimately applied to both ends. The end tied to the pulling bolt utilized the braided fishing wire while the tail end of the tested conductor consisted of a one and a half inch header for a monofilament connection. The monofilament was drawn in behind the pulled conductor in each trial in order to provide means to pull the conductor backward through the conduit run to the starting test position for another trial. The monofilament was loosely placed at the inlet of the conduit in a manner that permitted free movement and without catching or applying additional frictional resistance during the pull. The monofilament was ideal for this application as it was less expensive than the braided fishing wire and easily managed without tangling. Any effect from this method that was applied to properly operationalize the experiment is assumed to be both negligible and consistent across all trials.

3.1.7. Lubricant

The application of lubricant in the experiment is primarily to reflect the industrial application even though it theoretically has little to no bearing on the interpretive results of this study. The application of lubricant effectively reduces the coefficient of kinetic and static friction between the THHN conductor and the PVC conduit (Dahlke, 2007; General Cable, 2014; Southwire, 2018). This value is then reduced everywhere in the experiment by a linear, constant factor. The effect on the results, however, was speculated to reduce the percentage of

frictional resistance reduction when the idealized product is experimentally compared to the standard baseline. Thus, both a lubricated and un-lubricated set of experiments were conducted.

Because the objectives of applying lubricant to the experimental trial is to compare to the un-lubricated case for variance in percentage reduction and to better simulate industry application, the selection of lubricant was not restricted by any stringent criteria. The lubricant selected was Yellow 77 for being commonly used in industry with THHN conductors (Ideal, 2018). The application directions indicated to lubricate conductors thoroughly with hands or brush while the conductor is being drawn into the conduit. Each time a conductor was loaded for a sequence of five lubricated trials, the conductor was lubricated with a saturated cloth while being drawn into the pre-elbow conduit leg. The five trials were then recorded over an average duration of seven minutes in order to collect data prior to the lubricant drying out.

3.1.8. Frame Construction

The experimental components were all attached to a relatively rigid frame constructed of two by four lumber. The frame was constructed under tight space constraints in multiple locations so the construction is characterized by modular sections that are nominally four feet long for typical, straight runs. Additionally, one angled portion of the frame was used to mount both the baseline and the modeled idealized product for their respective sets of trials. All of these sections of the frame were three and a half inches in width and three inches tall. Lastly, a section of twice the standard width was used for the mounting of the bolt mount, the tension gauge, and a stopper that separated the exiting end of the conduit from the tension gauge. This stopper was implemented to ensure that the conductor would not reach the tension gauge and damage its rollers. The stopper was constructed with two one half inch PVC conduit mounting

straps and electrical tape. One strap was screwed into the lumber frame adjacent to the pulling string's location. The second strap was fixed to the first strap with electrical tape. The pulling string was threaded through one of the second strap's two holes for the sake of stopping the conductor from being pulled to far. The following figures show all components of the experiment in their respective and relative locations.

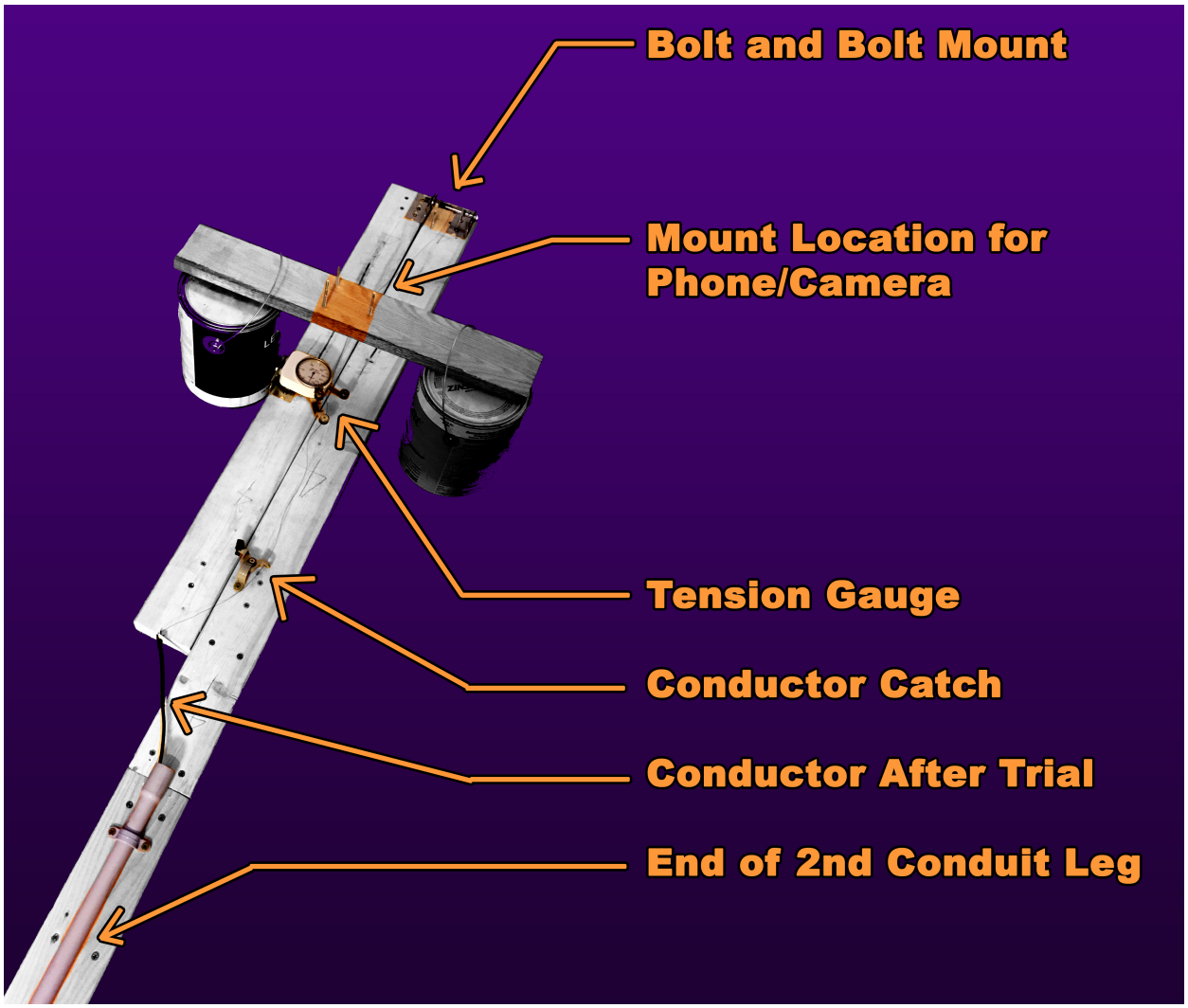

Figure 3-6: Frame Construction and Pulling Component Layout

Figure 3-7: Frame Leg Modular Segmentation

3.1.9. Experiment Category Definitions

There are three main categories of experiments that were conducted for this study. These are classified as the straight baseline, the factory baseline, and the modeled product. All three categories were designed to isolate or characterize data for useful analysis and comparison to achieve the goal of the overall study. The end means of these categories are to establish the magnitude of frictional resistance in the straight portions of the conductor pull, to investigate frictional resistance of the idealized product in questions, and to solidify comparable baseline data for the commonly applied factory elbows currently found in industry.

3.1.9.1. Straight Baseline

The concept behind the straight baseline experiments is straightforward. The tests in this category measure the frictional resistance when a conductor is pulled through a singular straight run of conduit. This straight run, which has already been described in detail, yields data that can be used for isolation of elbow frictional resistance. The other categories of experiments are focused on the elbow, but they each still contain two straight legs of conduit. In the processing data, it is essential to only be considering the resistance from the elbow portion of the pull. Thus the frictional resistance from straight portion of conduit determined by this test category can be subtracted from the net results of the other studies for their respective isolated parameters. The resulting frictional resistance data can then be considered as being strictly associated with the ninety degree elbows' effects. This is usefully essential for comparing the factory case and the idealized product to determine definitive results.

Figure 3-8: Midpoint Connection in Place of Elbow Entity

Figure 3-9: Straight Run Experimental Assembly

3.1.9.2. Factory Baseline

The factory baseline category of testing involves the application of the one half inch schedule 40 PVC factory elbow of four-inch radius. The experimental setup is per the detailed construction established in this chapter for the testing of any applied ninety-degree elbow. The elbow used is a standard bell-end factory elbow that is conforming to UL 651. The purpose of this category is to establish a baseline that is reflective of existing industry. This data is to be used in comparison to the modeled product tests. The interpretation of this comparison is the main inference of most interest to this study.

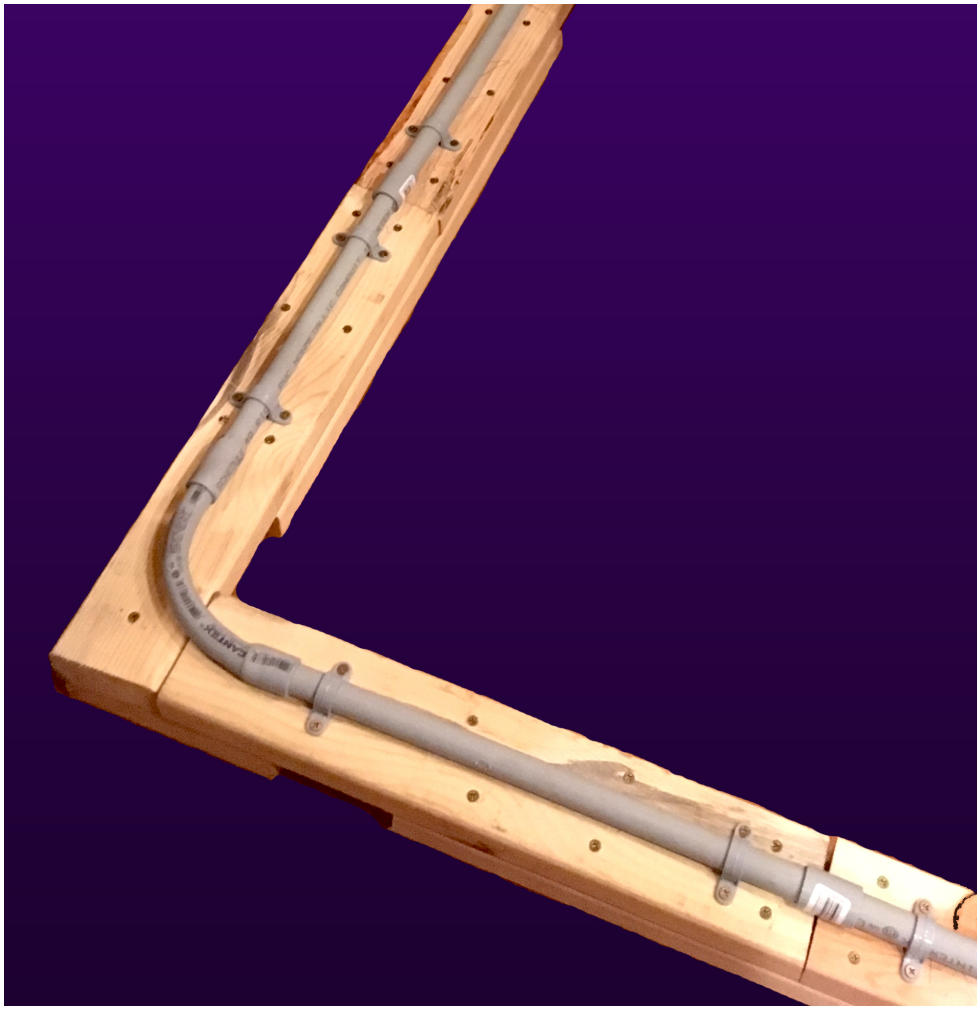

Figure 3-10: Factory Elbow Experiment Construction

3.1.9.3. Modeled Product

The modeled product category is identical to the factory baseline, but with a modified factory elbow designed to simulate a prototype of an elbow containing rollers. The simulated product involved a great deal of construction efforts. The elbow itself was cut open along the inside radius to create a nine-sixteenths inch tall slot for rollers to be inserted. The resulting elbow is best described as a slotted tube bent ninety degrees with a four-inch radius. With the interior of the elbow and immediate connections opened up, the rollers were applied appropriately to ease the resistance on a pulled conductor. The data collected from this

experimental category is considered indicative of a fully prototyped idealized product. The evidence of the benefits of a conduit elbow that implements roller technology is assumed to be reflected by this model.

Each roller was comprised of two modified nylon glass door rollers and a 3/16” diameter headless wood screw with fifty percent machined thread. One flange on each nylon roller was removed so that they could be combined into one roller two-entity roller with flanges on the extreme edges to resemble the curvature of the interior of the unmodified factory elbow. The nylon rollers were purchased with ball-bearing bushings to enable the roller to rotate as freely as possible across all trials. The composite rollers were mounted to the headless screws which were drilled into the timber frame along the inside the modified elbow. Given dimensional constraints, seven rollers were the most that could fit in the modified elbow while still maintaining physical separation among each other. The maximum number of rollers was implemented in order to provide the most nearly continuous bending of the conductor during pulling. Thus, the seven sets of rollers were evenly spaced in this manner with the rollers appropriately protruding into the modified elbow. The first and last rollers in the sequence are also protruding into the connection at the elbow connections to ensure that rollers are supporting the entire pull throughout the elbow. The rollers were held in their respective elevations on the machined portion of the headless screws by appropriate combinations of washers and paired nuts.

Figure 3-11: Modeled Product Experiment Construction Prior to Securing Roller Elevations

3.2. Experiment Execution

The experiment was designed and constructed in multiple locations in and around Salt Lake City, Utah over the course of the summer of 2017. The actual experimental trials were executed in a garaged location in Wamego, Kansas. The order of experimental categories and their respective sequential trials was outlined in detail after the experiment design was proven operable. The operation and ordering of trials were planned out of necessity to minimizing time spent running the experiment. Alternatively, randomization of trials may yield more statistically

sound results, but it is assumed that the systematic and repeatable design by the experiment is sufficient in producing useful results that are independent of randomization.

3.2.1. Location

The experiment was conducted on a level concrete floor of a thermally tempered garage environment. The floor was maintained to be as clean as possible to prevent concentrations of dust and dirt from interfering with the results. The environment provided poorer lighting accommodations than would have been preferred so any task lighting that was available was implemented when possible. The temperature of the space was considered as impactful for the experiment but is not directly quantified into the results analysis. With the understanding that results of significantly colder days would result in higher material resistances as conductors become harder to bend and pull with decreasing temperature. For the sake of analysis, the ambient air temperature of the garage near the centroid of the experiment was recorded prior to each trial. This was achieved with one of the most accurate probe thermometers available. All conductors were thermally acclimated to the ambient environment which thus reflects the thermal state of whole experiment. The temperature data ranged from 66 to 82 degrees Fahrenheit over the course of all experimental trials. It is assumed, for initial analysis, that this variance is not significantly impactful for the general collection of data. The actual temperature values, per trial as indicated by the video ID, are listed in the summary tables below. The ordering of trials in this table is further explained in the following sections as the ordering of the categories is dictated by the order the experiments were conducted.

Table 3-2: Factory Baseline - Dry Trial Temperature and ID

Trial	1		2		3		4		5	
Parameter	**T**	**ID**	**T**	**ID**	**T**	**ID**	**T**	**ID**	**T**	**ID**
Units	°F	#	°F	#	°F	#	°F	#	°F	#
Factory Baseline – Dry										
• #12 Conductor										
Bolt 1	68	1	67	2	67	3	67	4	67	5
Bolt 2	67	6	67	7	67	8	67	9	68	10
Bolt 3	67	11	67	12	66	13	66	14	66	15
• #10 Conductor										
Bolt 1	78	16	78	17	79	18	79	19	79	20
Bolt 2	78	21	79	22	80	23	79	24	79	25
Bolt 3	79	26	79	27	79	28	79	29	78	30
• #8 Conductor										
Bolt 1	79	31	78	32	78	33	78	34	78	35
Bolt 2	78	36	77	37	78	38	78	39	77	40

Table 3-3: Modeled Product - Dry Trial Temperature and ID

Trial	1		2		3		4		5	
Parameter	**T**	**ID**	**T**	**ID**	**T**	**ID**	**T**	**ID**	**T**	**ID**
Units	°F	#	°F	#	°F	#	°F	#	°F	#
Modeled Product - Dry										
• #12 Conductor										
Bolt 1	69	41	69	42	69	43	69	44	69	45
Bolt 2	69	46	69	47	72	48	72	49	72	50
Bolt 3	72	51	73	52	73	53	73	54	73	55
• #10 Conductor										
Bolt 1	75	56	75	57	75	58	75	59	75	60
Bolt 2	75	61	75	62	75	63	75	64	75	65
Bolt 3	75	66	75	67	75	68	75	69	75	70
• #8 Conductor										
Bolt 1	79	71	82	72	81	73	81	74	82	75
Bolt 2	82	76	82	77	82	78	82	79	82	80
Bolt 3	81	81	82	82	82	83	82	84	82	85

Table 3-4: Straight Baseline - Dry Trial Temperature and ID

Trial	1		2		3		4		5	
Parameter	**T**	**ID**	**T**	**ID**	**T**	**ID**	**T**	**ID**	**T**	**ID**
Units	°F	#	°F	#	°F	#	°F	#	°F	#
Straight Baseline - Dry										
• #12 Conductor										
Bolt 1	77	86	78	87	76	88	76	89	76	90
Bolt 2	78	91	77	92	77	93	77	94	77	95
Bolt 3	77	96	77	97	77	98	77	99	77	100
• #10 Conductor										
Bolt 1	77	101	76	102	76	103	77	104	77	105
Bolt 2	77	106	77	107	77	108	77	109	77	110
Bolt 3	77	111	77	112	77	113	77	114	77	115
• #8 Conductor										
Bolt 1	77	116		117		118		119		120
Bolt 2	77	121		122		123		124		125
Bolt 3	77	126	77	127	77	128	77	129	77	130

Table 3-5: Straight Baseline - Lubricated Trial Temperature and ID

Trial	1		2		3		4		5	
Parameter	**T**	**ID**	**T**	**ID**	**T**	**ID**	**T**	**ID**	**T**	**ID**
Units	°F	#	°F	#	°F	#	°F	#	°F	#
Straight Baseline - Lubricated										
• #12 Conductor										
Bolt 1	70	176		177		178		179		180
Bolt 2	70	181		182		183		184		185
Bolt 3	70	186	70	187	70	188	70	189	70	190
• #10 Conductor										
Bolt 1	71	191		192		193		194		195
Bolt 2	71	196		197		198		199		200
Bolt 3	71	201	71	202	71	203	71	204	71	205
• #8 Conductor										
Bolt 1	71	206		207		208		209		210
Bolt 2	69	211		212		213		214		215
Bolt 3	69	216	69	217	69	218	69	219	69	220

Table 3-6: Modeled Product - Lubricated Trial Temperature and ID

Trial	1		2		3		4		5	
Parameter	**T**	**ID**	**T**	**ID**	**T**	**ID**	**T**	**ID**	**T**	**ID**
Units	°F	#	°F	#	°F	#	°F	#	°F	#
Modeled Product - Lubricated										
• #12 Conductor										
Bolt 1	76	221	76	222	76	223	76	224	76	225
Bolt 2	76	226	76	227	76	228	76	229	76	230
Bolt 3	76	231	76	232	76	233	76	234	76	235
• #10 Conductor										
Bolt 1	74	236	74	237	74	238	75	239	74	240
Bolt 2	75	241	75	242	75	243	75	244	75	245
Bolt 3	75	246	75	247	75	248	75	249	75	250
• #8 Conductor										
Bolt 1	75	251	75	252	75	253	75	254	75	255
Bolt 2	75	256	75	257	76	258	76	259	76	260
Bolt 3	75	261	75	262	75	263	76	264	76	265

Table 3-7: Factory Baseline - Lubricated Trial Temperature and ID

Trial	1		2		3		4		5	
Parameter	**T**	**ID**	**T**	**ID**	**T**	**ID**	**T**	**ID**	**T**	**ID**
Units	°F	#	°F	#	°F	#	°F	#	°F	#
Factory Baseline – Lubricated										
• #12 Conductor										
Bolt 1	75	266	75	267	75	268	75	269	75	270
Bolt 2	75	271	75	272	75	273	75	274	75	275
Bolt 3	75	276	75	277	75	278	75	279	75	280
• #10 Conductor										
Bolt 1	75	281	75	282	75	283	75	284	75	285
Bolt 2	75	286	75	287	75	288	75	289	75	290
Bolt 3	75	291	75	292	75	293	75	294	75	295
• #8 Conductor										
Bolt 1	79	296	79	297	79	298	79	299	79	300
Bolt 2	79	301	79	302	79	303	79	304	79	305
Bolt 3	79	306	79	307	79	308	79	309	79	310

Table 3-8: Speed Establishment Trial Temperature and ID

Trial	1		2		3		4		5	
Parameter	**T**	**ID**	**T**	**ID**	**T**	**ID**	**T**	**ID**	**T**	**ID**
Units	°F	#	°F	#	°F	#	°F	#	°F	#
Speed Establishment										
Bolt 1	77	141		132		133		134		135
Bolt 2	77	146		137		138		139		140
Bolt 3	77	131		142		143		144		145

3.2.2. Sequence of Operations

The operational sequence of each set of trials, in general, is conducted systematically per the following. The leading end of the conductor to be tested is pulled into the leg that precedes the elbow from the conduit inlet. Once the conductor is just completely in the first leg of conduit, the associated pull string is loosely drawn through the catch, by the tension gauge, and to the bolt mount. The monofilament fishing wire on the tail end of the conductor is arranged behind the inlet to the conduit to ensure that it will not catch during pulling. Bolt 1 is inserted into the bolt mount. The pull string is attached to Bolt 1 via the hole in the bolt and a safety pin. The pull string is then wound about the drive bolt in order to provide minimum tension on the pull string. The pull string is properly placed about the rollers of the tension gauge. The temperature and time is recorded prior to engaging the trial. A mobile phone placed in testing in the jig above the gauge is set ready to record. The power drill is mated with the drive bolt for pulling. The tension on the pull string is adjusted so the needle on the tension gauge barely just reads zero grams of force. At this point, the camera recording begins, the trial or video ID is stated out loud, and the power drill is quickly engaged to full power. The conductor is pulled until its end just barely protrudes from the outlet of the second conduit leg. At this point, the drill is disengaged, the video is stopped, and the trial ends.

The experiment is reset for five subsequent identical trials. To reset, the pull string is unloaded from the tension gauge rollers. The monofilament line is then used to pull the conductor back to the starting position. At this point, setup can proceed as usual after another temperature and time is recorded. After a total of five identical runs are complete, Bolt 1 is switched out for Bolt 2 for another set of five trials. This repeats for Bolt 3 and then subsequent conductor samples. The sequence is applied to all categories of experimentation until all trials are complete.

3.2.3. Sequencing of Experimental Categories

The sequence of experimental categories was dictated by a need for efficiency over randomization. The first divide that was necessitated was between trial with and without lubrication. The experimental system would be difficult to clean after a lubricated trial in order to conduct a proper dry trial. Thus, all dry trials were conducted prior to all lubricated trials. The initial construction of the experiment had the factory elbow installed, so those dry trials ran first. Additionally, for consistency, the trials under the modeled product category required a consistent construction and thus no disassembly/reassembly after between dry and lubricated trials. The elbow section of the frame could be removed from the experiment without discontinuity caused by reassembly. Thus, the straight baseline category, dry and lubricated, was processed in between dry and lubricated modeled product trials. The following resulting categorical sequence of trial categories was used to satisfy these experimental constraints and considerations:

1. Factory Baseline – Dry
2. Modeled Product - Dry
3. Straight Baseline - Dry
4. Straight Baseline - Lubricated
5. Modeled Product - Lubricated
6. Factory Baseline – Lubricated

As trials were conducted, the date and time were recorded alongside the temperature and each unique trial ID. The records of the sequencing, dates, times, and trials are provided in the appendices.

3.2.4. Crashes

There was one glaring complication that arose during the execution of the experiment. While there was a catch implemented between the conduit outlet and the tension gauge in order to prevent damaging, damage was not preventable in three cases that necessitated repairs and the introduction of a potential systematic error. In three failed runs the power drill was not fully disengaged prior to the conductor reaching the catch. At the point the conductor gets stopped and the power continues to apply increasing tension to the pull string, the gauge suffers a crash. The movable roller on the gauge is maxed out and bent out of position by the pull string in the event of a crash. In addition, all three crashes from this experiment resulted in the pull string snapping at the header of the conductor.

The repairs included bending the roller on the gauge back into its original position and replacing the pull string and damaged header. While the material deformation experience did

not cause observable damage to the tension gauge's inner workings (likely by design), it is possible that the roller experienced damage. The result would be a minor calibration shift in the readings of the gauge in trials following the crash. After each crash, a previously successful trial was re-conducted and the resulting videos were compared for noticeable deviation. The results of this analysis are that there was no permanent or detrimental damages resulting in a variance of data that exceeds the experiments tolerance in precision. In short, the events of crashing did indeed happen and are important to note, but the crashed did not observably alter the integrity of the experiment. Similar experiments to continue this study should have appropriate measures taken to accommodate for detrimental crash prevention and correction.

3.2.5. Data Acquisition Comments

The data acquisition has already received comment, but further details demand additional discussion. In order to record the data from the mechanical tension gauge, the mobile phone camera set to 240 frames per second was consistently applied. The recordings were compiled for digitization. Taking readings manually from the video over a consistent interval of frames was considered but deemed impractical. After months of work, the videos were processed into quantifiable numerical readings with proper time dependency via the gauge reader program that was custom tailored for this experiment. The gauge reader program is able to take a video and appropriate parameters and convert the readings into time dependent tabulated values. The robust results, outputs, and complications introduced by the programming are covered thoroughly in Chapter 4.

For the experimental process, it was essential for the successful application of the program that the videos be recorded and doctored as consistently as possible. This process still

dictated complicated and exhaustive efforts to produce reasonable, reliable results. Relatively speaking, a digital tension gauge would have been much more practical and is recommended all the more for the sake of future researchers being able to avoid the video image processing convolutions. The source code developed for this study is provided in the appendices for development of any future application.

Chapter 4 - Experimental Results

4.1. Experimental Results

This chapter goes into detail in the processing of the data acquired from the study's experiments. After the processes that were applied to digitize the collected data are sufficiently detailed, the specifics on the statistical processing of tabulated data sets per category are presented. This detail is important to note for the understanding of the cumulative results summary where all the data is summarized for interpretation. While the findings reveal a notable degree of ambiguity and lack of accuracy, the potential causes for the result deviations from expected values are explored in the end of the chapter.

4.1.1. Manual Data Processing Preparation

The videos that were recorded for each trial required manual video processing to be properly prepared for digitization via the gauge reader program. The processing steps were systematically applied to all trial videos to produce constancy among all data samples. The first step taken to prepare the videos was to reduce shaking using a shake reduction in a standard movie-editing program. Some of the videos were subject to vibrations during the trial run, and this processing minimized the noise and error introduced by the vibration. This editing program was also used to automatically enhance the color and contrast of the videos for further processing. Finally, the beginning and end of each video was checked for any camera movement or long durations of inactivity. All videos were trimmed appropriately.

Once this first series of processing was complete, the videos were all processed through an image editing software to be cropped and rotated to a consistent size and orientation. The

center of the gauge was also relocated to the very center of every video for the sake of minimizing error from the gauge reader program which mathematically defines the center of the frame to be the origin of its applied coordinate system. This same image-processing tool was then used to boost the brightness and contrast of each video in order to eliminate noise from shadows and lighting inconsistencies. Lastly, the gauge numbers and tick marks that are on the gauge were masked with white. The gauge reader program locates dark pixels and locates the maximum in a transformation of the video. In the transform, the black markings on the gauge read as noise that clutters the actual needle reading. The masking eliminated a vast majority of the noise in the videos. This improved the reliability and accuracy of the collected data. These collective steps of manual video processing cleanly and completely prepared all videos for digitization via the gauge reader program.

Figure 4-1: Example Frame from a Manually Processed Trial Video

4.1.2. Data Digitization

The gauge reader program is capable of producing three useful outputs in order to represent data for debugging and analysis. These outputs are classified by the gauge reader program as ‘cropdebug’, ‘transdebug’, and ‘maketable’. The ‘cropdebug’ output of the program is the binary video processed from the manually doctored videos. This outputted video is circularly cropped to just show the face of the gauge without including the frame or unmasked shadows. Binary conversion of the video also eliminated all bright pixels leaving the dark needle and the occasional residual noise. The needle is displayed as white against a completely black background in the video output. The binary format is most easily manipulated for further processing by the gauge reader program. This output is helpful for showing if excessive noise is being misread as actual data as well as that the final program output is reading the intended area of the doctored video. This debugging of the cropped binary video was used primarily in successfully identifying videos that required further boosting of brightness to eliminate noise due to shadows. The binary video also showed how a few videos were processed with an un-filterable shadow that was cast by the needle. By all measures taken to verify data, this needle shadow was not proven to skew the data results, but its presence necessitates documentation.

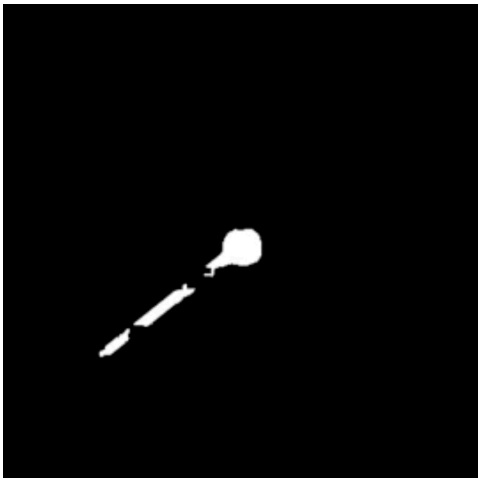

Figure 4-2: Example Frame From 'cropdebug' Processing

The ‘transdebug’ output is that of a mathematically transformed coordinate space. This step simply transforms the polar coordinate system of the physical gauge to a sinusoidal space that is more convenient for finding the actual gauge reading via coding. This space simplifies the functions required to integrate over the binary pixels of the needle and isolate the angle on which the most pixels are aligned. This maximum is indicated on the transformed video file as a bright spot that moves back and forth along the center of the output. The only ambiguity introduced by this approach is that the coordinate transform involves inverse trigonometry limitations where the actual angle may be pi away from the range of the transform zero to pi. Logic in the gauge reader program resolves the issue by adding pi to the angle identified if the concentration of the pixels present in the respective frame dominates the left half of the original video. The remaining ambiguity of the transform is then that the gauge reader is not able to completely distinguish the needle’s reading when the needle points straight up or down. Thus, occasionally when the needle crosses over the bottom or the top of the gauge, the tabular angle identified in the transform is a shifted pi away from being continuous. In the transformed space, this is identified when two bright spots are visible on the extreme edges of the video output.

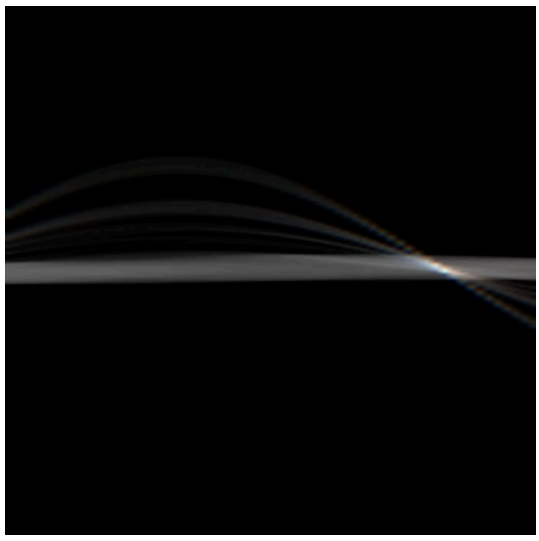

Figure 4-3: Example Frame From 'transdebug' Processing

This ambiguity carries over to the ‘maketable’ output of the program. The bottom of the gauge most nearly reads 121grams and the top would most nearly read the 1100 grams when the exponential scale of the gauge readings is extrapolated out beyond the max reading of 800 grams. The tabular output of the ‘maketable’ is a CSV file that lists the angle found from the transform with respect to the time that is relative to the video frame rate per frame for all frames. The gauge readings are also included in the CSV as they are solved for as a mapped function of the angle. The readings in and around 121 grams are often rattled with 1100 gram spikes. These spikes exist all throughout the 500,000+ data points produced by the gauge reader program. The tabulated data was smoothed via linear interpolation formulas applied to the spikes that were identified via a conditional formatting of colors within ranges to easily recognize discontinuity in the overall pool of data.

4.1.3. Construction of Data Analysis

The resulting cleaned pool was also trimmed on the ends to eliminate extensive inactivity that was not eliminated from video editing detailed previously in this chapter. The tabulated data was then broken up into sets representative of each of their respective isolated parameters. These isolated groupings were sorted per their experimental categories. Each trial was graphed with consistent formatting and analyzed for statistical areas of clear noise or inconsistency. These areas were removed per the next section’s detailed description of each data set category. The graphs included the full duration of the videos’ readings even though only the region of data of interest is limited to the data collected while the conductor in the respective trial is being steadily pulled through the ninety-degree entity. Graphs of this isolated area of interest were produced in addition to the culminated cleaned results from each trial. For

ensuring the consistency among trial sets of five, all five trials per set were graphed over each other. The average of each data set was also graphed in the interest of observing behavior that persists across samples in addition to tamed generalities. While the trials within each data set were not synchronized in their time dependency, the results of the superposition and average graphs are still considered observationally informative. All of the produced graphs are included in the appendix while the following sections include a collection of the most relevant and exemplary graphs for elaboration.

While the graphs and independent section analysis is informative of the behavior of the individual experiments, the main interest is the culminated categorical data. This was accomplished by statistically collecting the mean value of all data points of interest collected in each respective set of five trials. This average value for the tension is taken to be the expected value of the frictional resistance for each set of isolated parameters. This analysis does not forgo error analysis. The standard uncertainty of the tension averages is calculated by taking the standard deviation of the respective sets and dividing said value by the square root of the number of data points there within applied. This standard uncertainty is multiplied by 1.96 to yield a standard uncertainty of 95% confidence. Due to the vast quantity of data points collected from the experiment, the resulting tolerance on a data set to data set basis is indicated as being very reliable and precise in all cases. However, outside factors that impact the accuracy of the intensions of the experiment are not included in this uncertainty. Outside factors are hypothesized later given constituted deviations from expected results (Taylor, 1997).

4.1.4. Result Details Per Category

The following sections break down the observations for all trials per their respective categories. The observations made are relative to the graphical representation of individual trial data. In general, the common and complete data from any given trial involving an elbow can be described in three graphical regions that are directly correlated to the instantaneous physical state of experiment given time dependency. These regions exist physically in each experiment even though some are not graphically translated in the data due to ambiguity or data trimming. The first of these regions relative to increasing time is simply denoted a Region 1. Leading up to this region is the initial transition of the gauge reading while the power drill is initially engaging the pull bolt and string. Either a sharp spike or a seaming exponential increase in tension often initially characterizes this transition. The difference between these two starts of the data directly correlated to the speed in which the power drill was engaged. Trials involving large values of tension were often more slowly engaged to reduce the risk of damaging the gauge. The transition leads into Region 1 with the behavior of an under-damped spring mass system due to the influence and reaction of the mechanical gauge. Region 1 is representative of the physical state where the conductor being tested is entirely within the first conduit leg but not the elbow in question. This region shows higher frictional resistance relative to trials of straight pulls due to the resistance of the pull string itself being pulled through the elbow. As soon as tested conductor header enters the elbow, the transition in frictional resistance often induces a sharp jump or spike in the gauge reading. This is followed by a transition that is again mostly characteristic of an underdamped spring-mass oscillation.

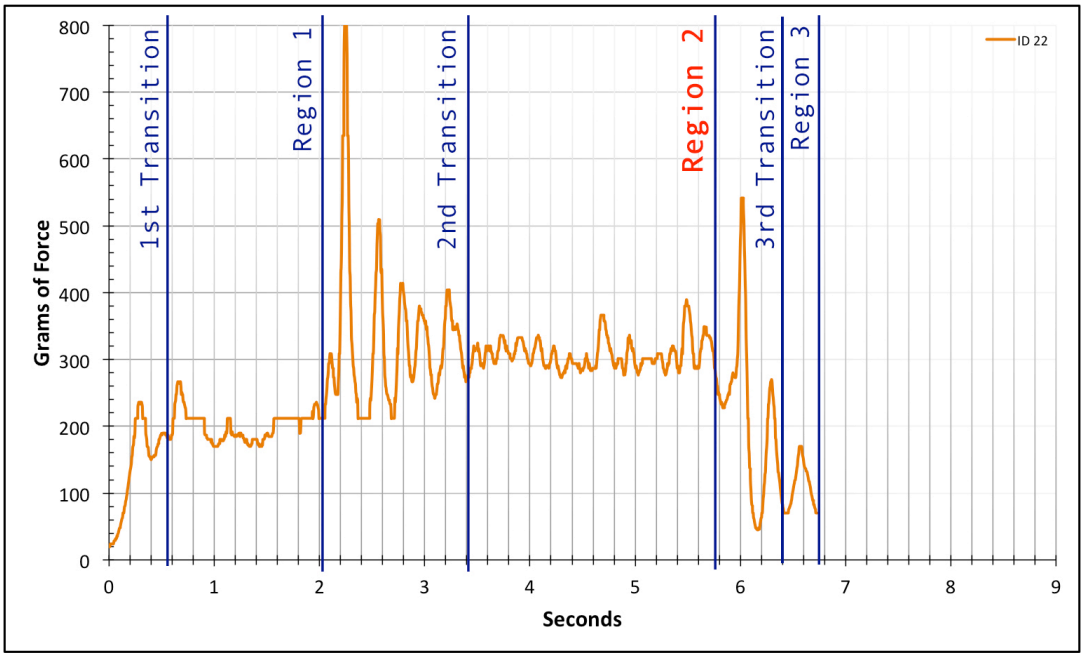

Figure 4-4: Typical Transition and Region Identification

Once the transition region dissipates into a stabilized state, the data has successfully entered Region 2. This region is representative of the conductor being steadily pulled through the elbow in question. Most often, Region 2 averages gauge readings that are higher than Region 1, but this is not always the case. The inferred reason for this is covered in the analysis of the individual cases. Region 2 is the region of most interest to this study. For this reason, the figures labeled as being statistical are representative of the respective trial's Region 2 alone. It is this data that is applied to the statistical means and standard errors that are tabulated at the end of this chapter.

The final region is preceded by another transition that is indicative of the conductor table transitioning out of the elbow. This transition is characterized by a change in the average gauge reading given another under-damped settling of the oscillations. The following Region 3 is physically representative of the tested conductor being entirely contained within the second straight conduit leg after having completely exited the elbow entity. This region is often very

short and ends with the occasionally recorded gauge reading drop indicating the applied pulling tension has been terminated along with the end of the trial.

The straight baseline categories do not have the division of regions in their data sets due to the lack of an elbow entity that results in the variance in physical states of operation. These trials are mostly represented by graphs that beautifully reflect the behavior of an under-damped spring mass system with a stable, constant value post initial transition. Thus, these trials are also mathematically defined as the most precise of this study. The statistical trimming in these categories was strictly limited to removing areas of transition on both ends of the stable data.

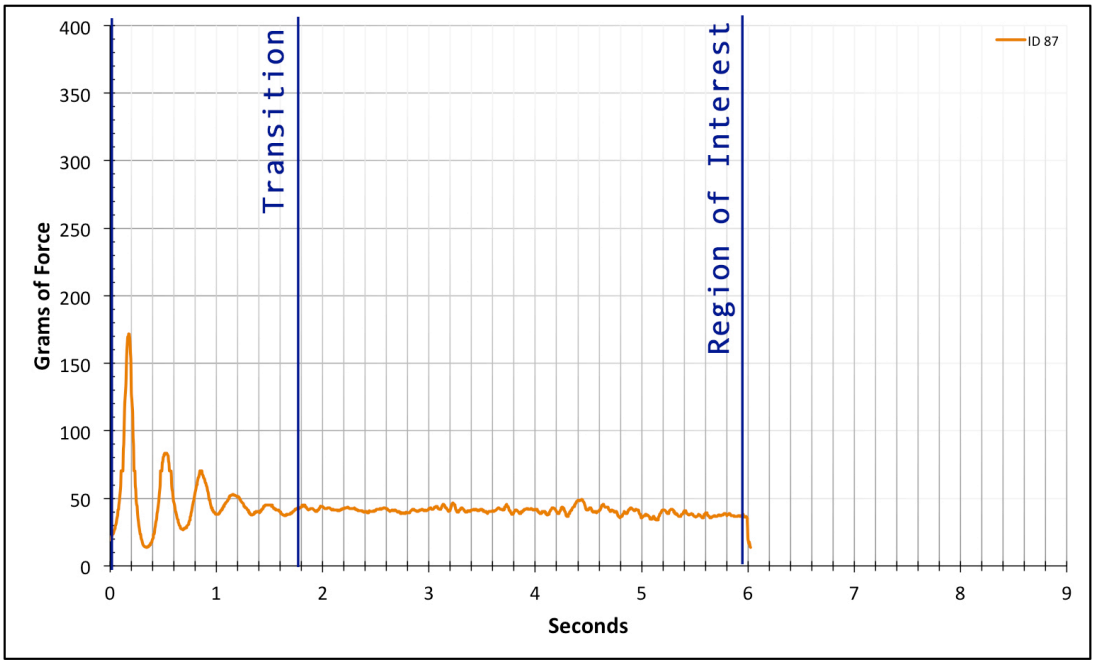

Figure 4-5: Straight Baseline Transition and Region of Interest Identification

It should be noted the values that are marked on the gauge range from 20 grams to 800 grams of tension force. The function used in the program to map the angle to a gram reading does not actually ever read 0 grams due to mechanical construction and calibration of the physical gauge. Thus, most trials indicate the start of the graphical data when the gauge reading enters the range indicated on the gauge. Past the 800 gram mark, some data was collected given

an extrapolation of the formula. These values are understood to be outside the certified accuracy of the gauge, but are included for interpretation and complete data estimation.

Throughout the entire time data was being processed, it was understood that the collected data must, at the very least, satisfy the Nyquist Theorem. The Nyquist Theorem states that the sampling rate (in Hz) of any analog signal should be at least twice the frequency of the highest frequency component of the signal in question. In other words, the frequency of the sampling rate should be at least twice that of the highest frequency in the signal. This theorem exists to ensure that the full effect of the signal is being captured without overlooking the effect of the aliasing of the signal. The data collected may have been sampled at any rate between double a max-observed frequency of needle oscillation and the frame rate of the video samples. If this range were determined to not exist, the data collected would be invalid. The sampling rate applied in this study's sampling was the frame rate of the videos and the resolution of full oscillations in the data clearly show that the Nyquist Theorem is here within satisfied (Rouse, 2005).

In the processing, it is also noted that applying a Fourier transform to isolate and omit the sinusoidal response from the mechanical gauge would be an additional processing step that was not conducted here. This is largely because the points of interest are the centers of the oscillations. This center is preserved even with the mechanical response. Thus, the Fourier transform would only be helpful in improving the precision of the data per the standard uncertainty calculations. Future researchers may choose to apply this level of processing if a deeper level of processing dictates finer precision in regions of relatively few data points. For example, A Fourier transform would be incredibly valuable if the trials were to be synchronized and their time dependence would require instantaneous uncertainty to be displayed along the

curves of force for instantaneous analysis. This level of analysis is beyond the scope of this study (Washburn).

4.1.4.1. Factory Baseline – Dry

The category includes videos 1 through 40 to cover the factory baseline category without the application of lubricant. The data set for the #12 conductor and Bolt 1 (ID 1 – ID 5) is plagued by a consistent bubble of increased amplitude within Region 2. This is likely due to a systematic error from a defect in the conductor's header repeatedly catching in a break or inconsistency in the conduit. This increased amplitude has an effect of increasing the standard error for this data set. A general experimental note is that the difference among the three regions within this set is measurable but small. The graph of the overall average indicates a bowing of Region 2 due to the constructive/destructive superposition of the systematic error. The result from this data set's Region 2 is an expected frictional resistance of 133.1±1.1 grams.

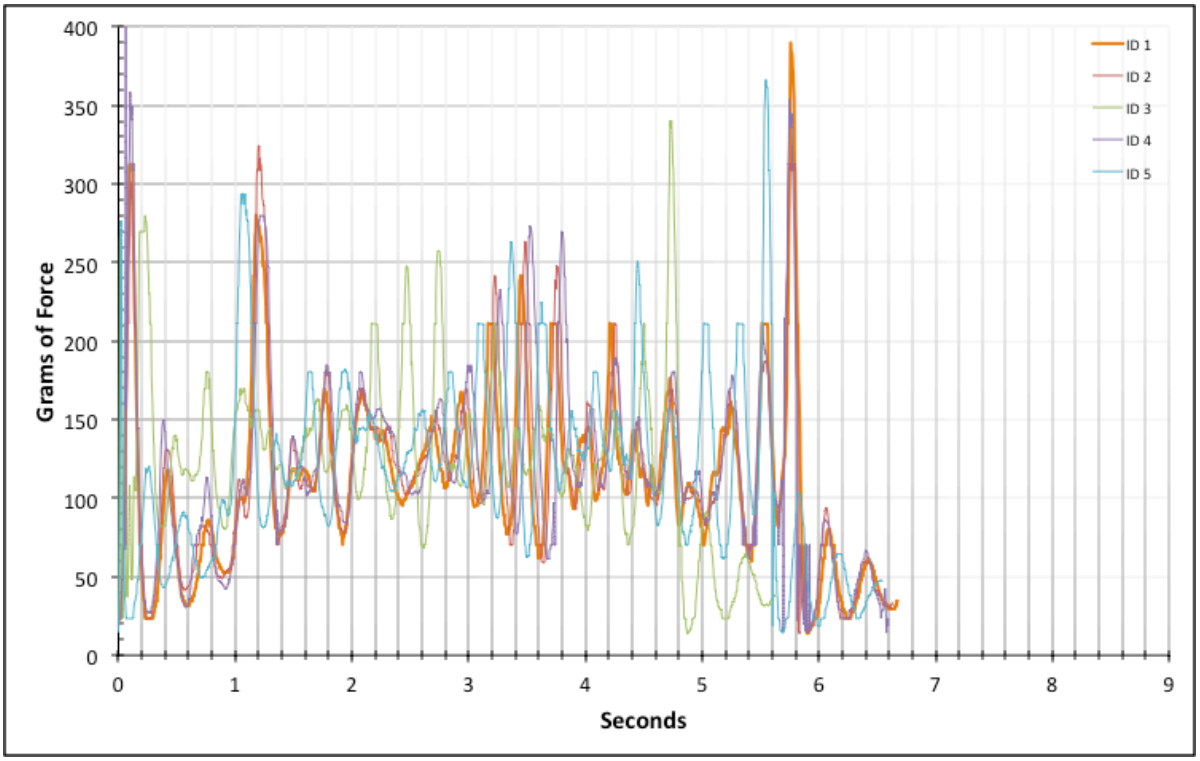

Figure 4-6: Full Composite Data for ID 1-5

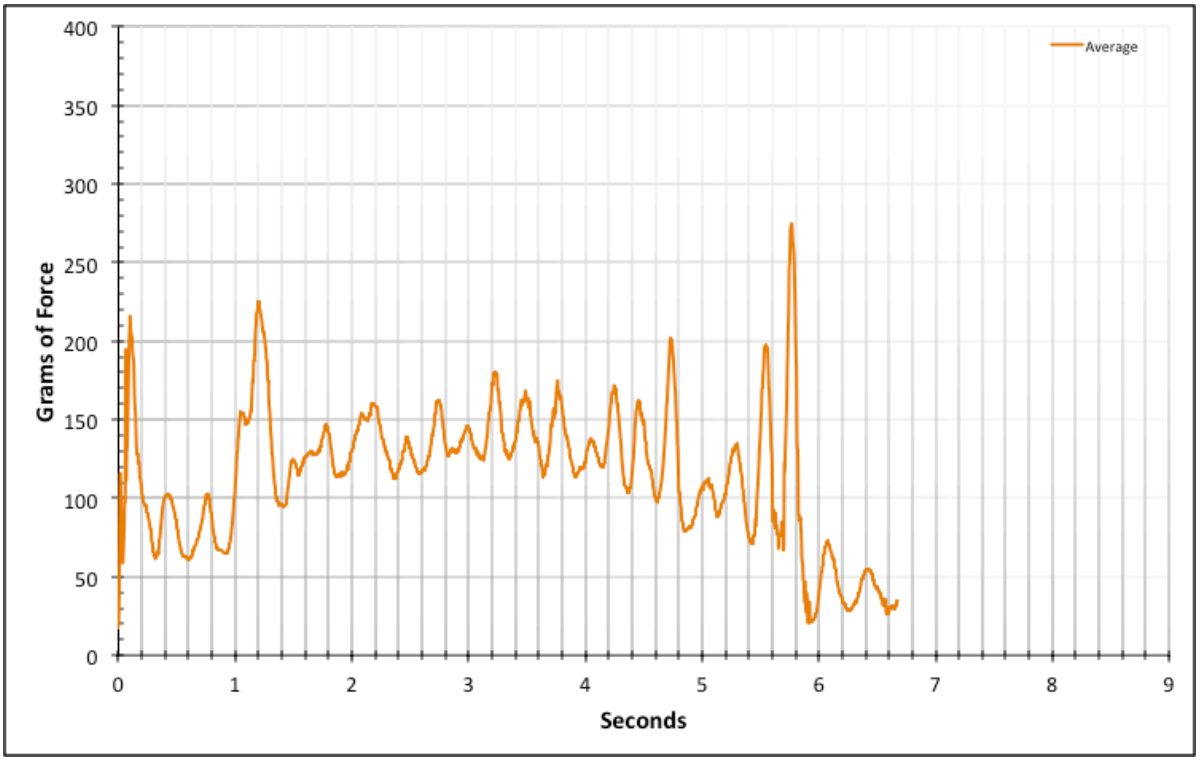

Figure 4-7: Full Average Data for ID 1-5

The very same systematic error repeats in the data set for #12 conductors and Bolt 2 (ID 6 – ID 10). This further supports that the systematic error is due to a defect in the conductor's header construction. The average graph in this data set clearly indicates the constructive evidence of systematic error. The result from this data set's Region 2 is an expected frictional resistance of 138.7±1.0 grams.

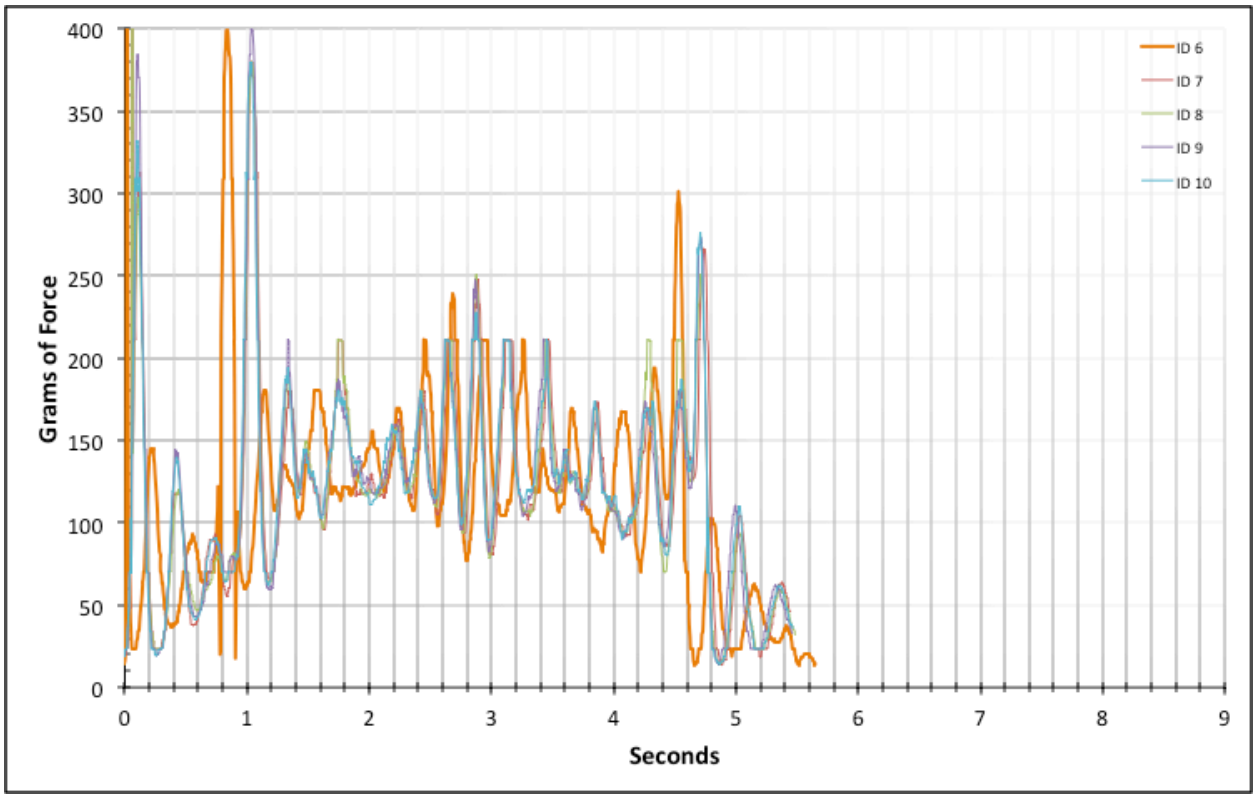

Figure 4-8: Full Composite Data for ID 6-10

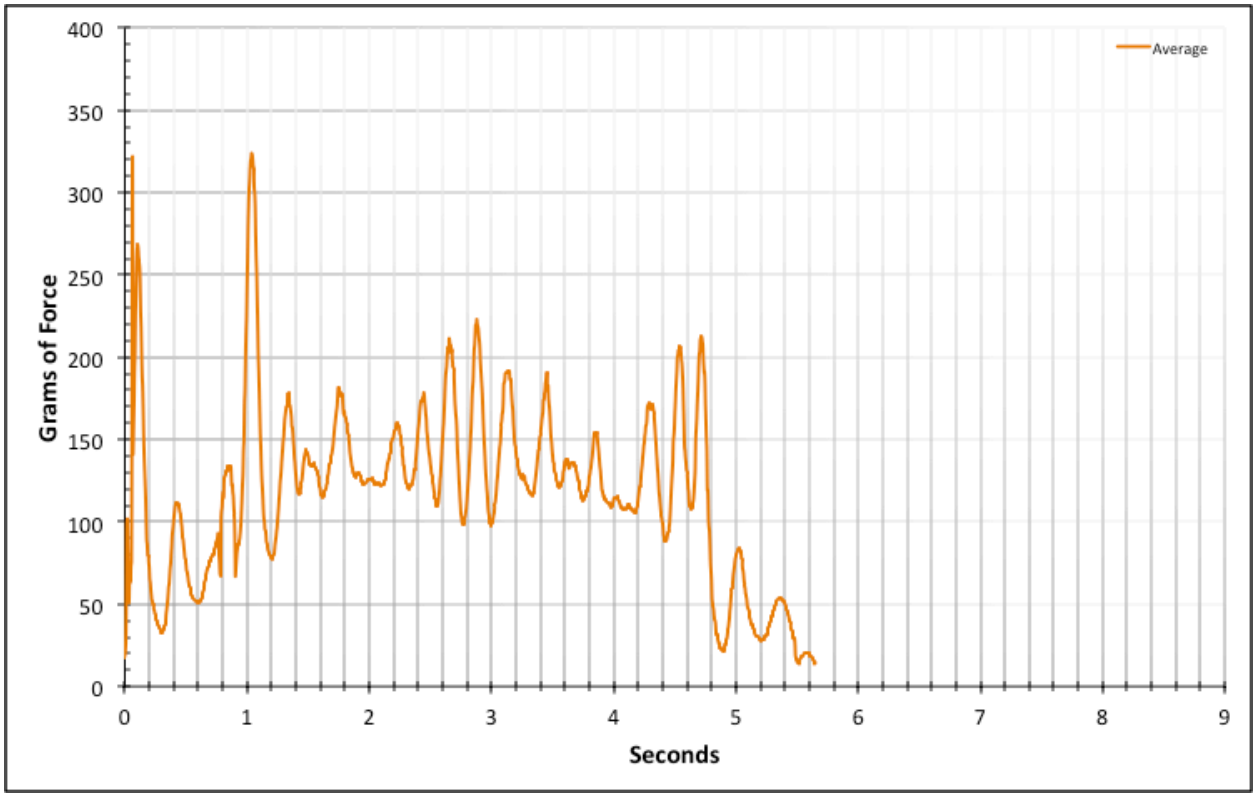

Figure 4-9: Full Average Data for ID 6-10

The data set representing the #12 conductor and Bolt 3 (ID 11 – ID 15) continues the systematic disturbance but to a lesser extent. The results are also characterized by major under damped oscillations. Both of these observations are likely due to the increased speed of Bolt 3. An abnormality from these trials is found in video ID 12. This trial consistently shows tension values higher than all others in the data set. For this reason, the trial is considered a systematic anomaly and is completely omitted from the statistically analyzed data. The result from this data set's Region 2 is an expected frictional resistance of 141.7±1.3 grams.

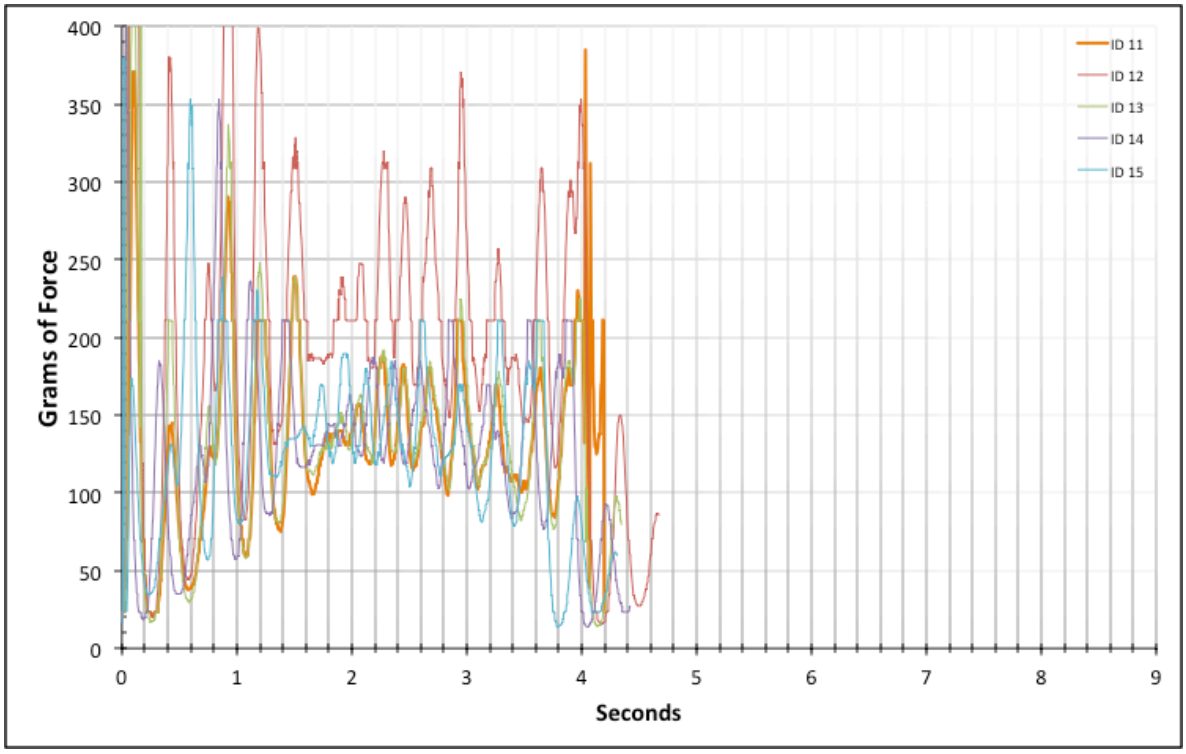

Figure 4-10: Full Composite Data for ID 11-15

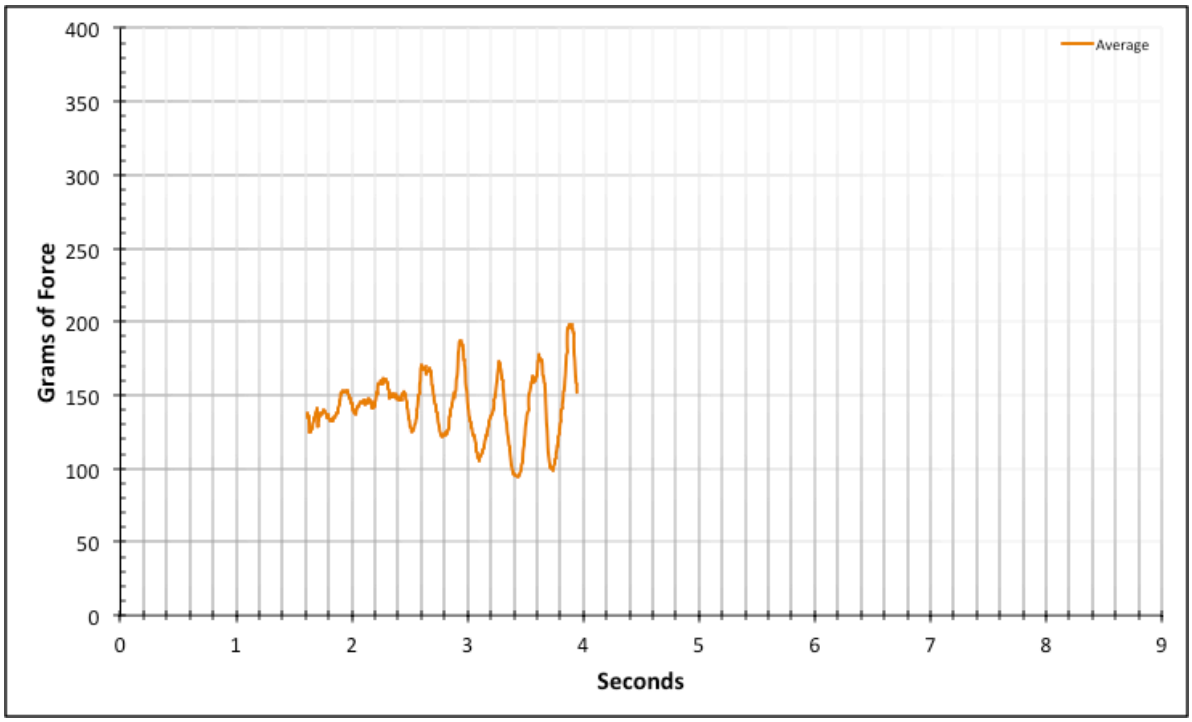

Figure 4-11: Region 2 Average Data for ID 11-15

The data set representing the #10 conductor and Bolt 1 (ID 16 – ID 20) is a clean example with a large Region 2 that is relatively ideal. The result from this data set's Region 2 is an expected frictional resistance of 309.2±1.1 grams.

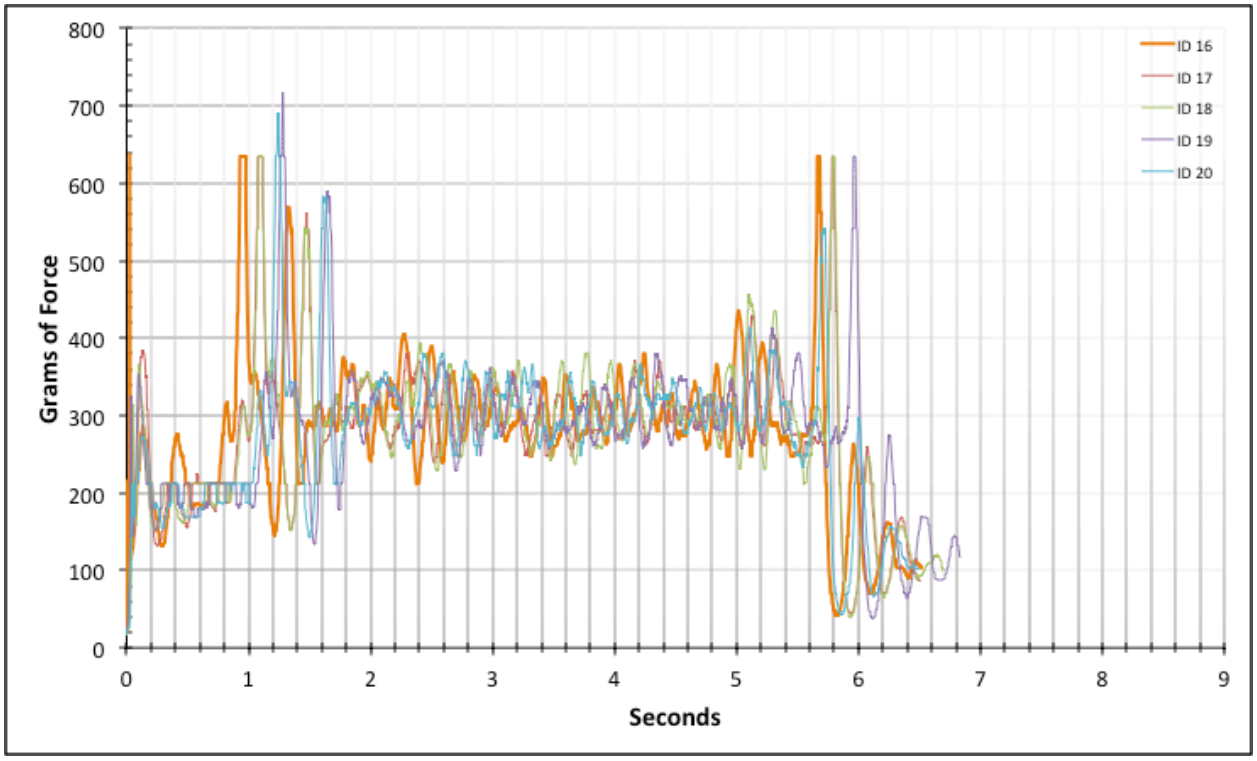

Figure 4-12: Full Composite Data for ID 16-20

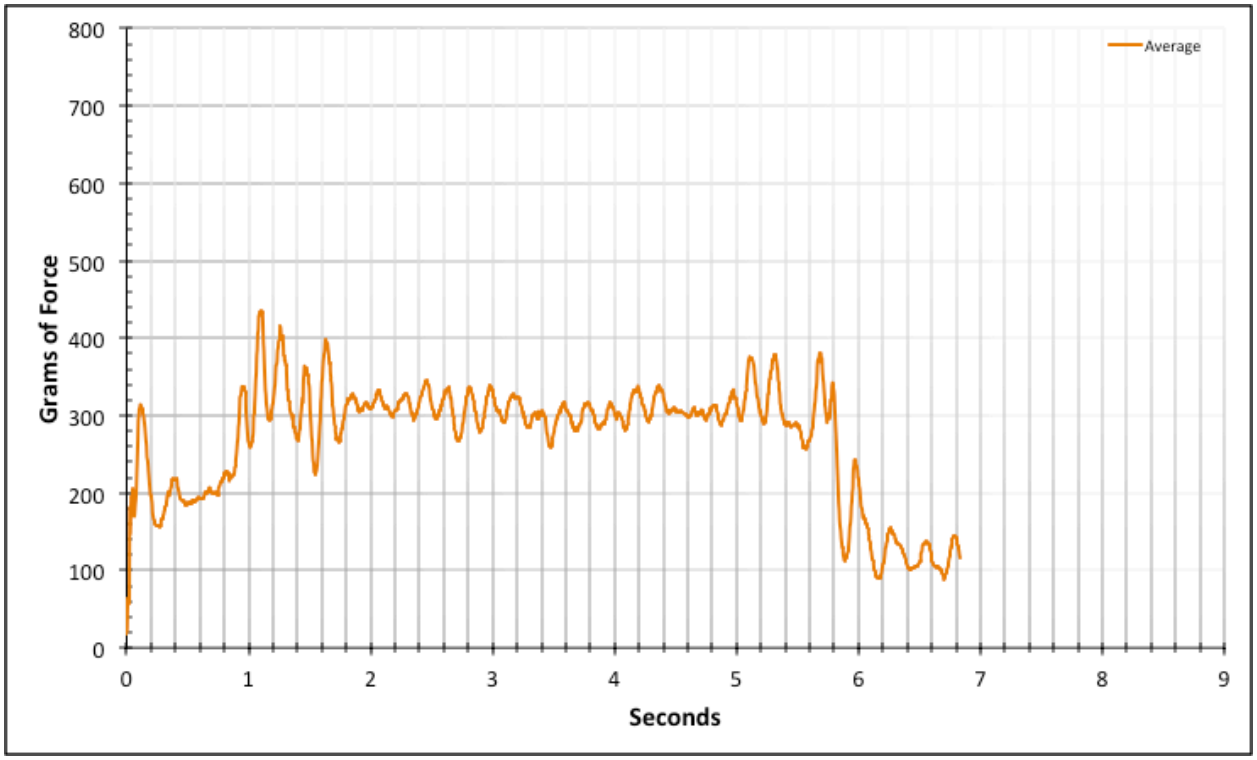

Figure 4-13: Full Average Data for ID 16-20

The data set representing the #10 conductor and Bolt 2 (ID 21 – ID 25) is a clean example with a large Region 2 that is relatively ideal. The result from this data set's Region 2 is an expected frictional resistance of 307.2±0.9 grams.

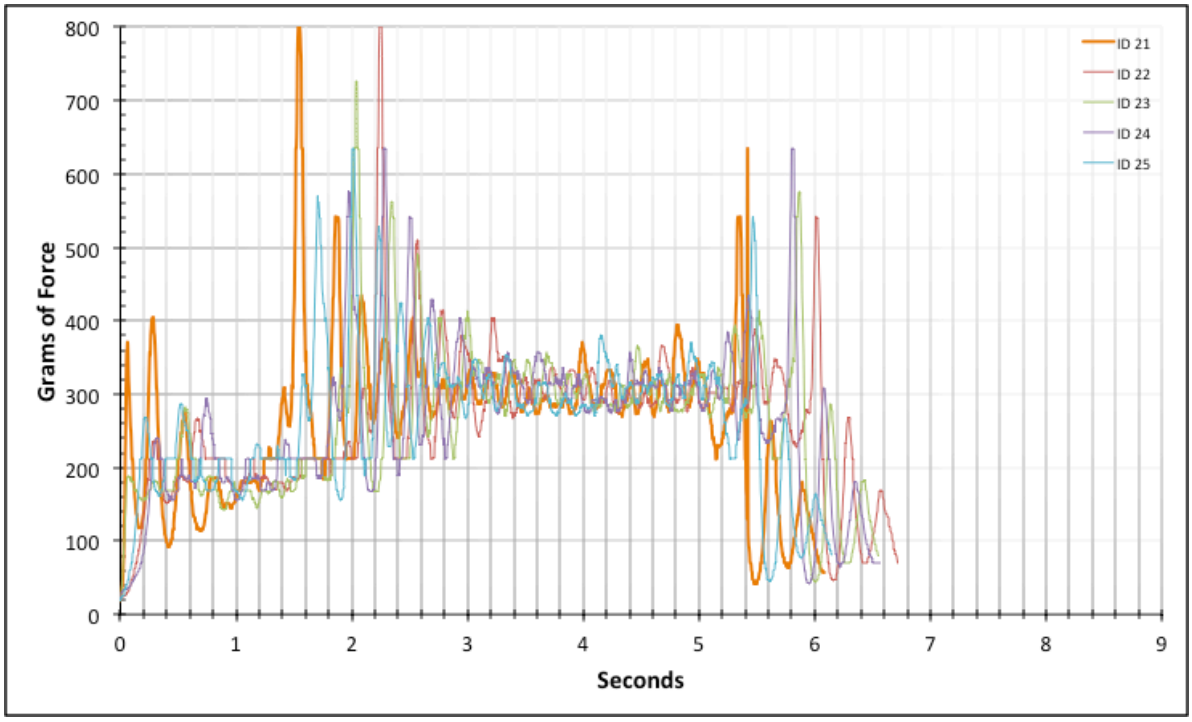

Figure 4-14: Full Composite Data for ID 21-25

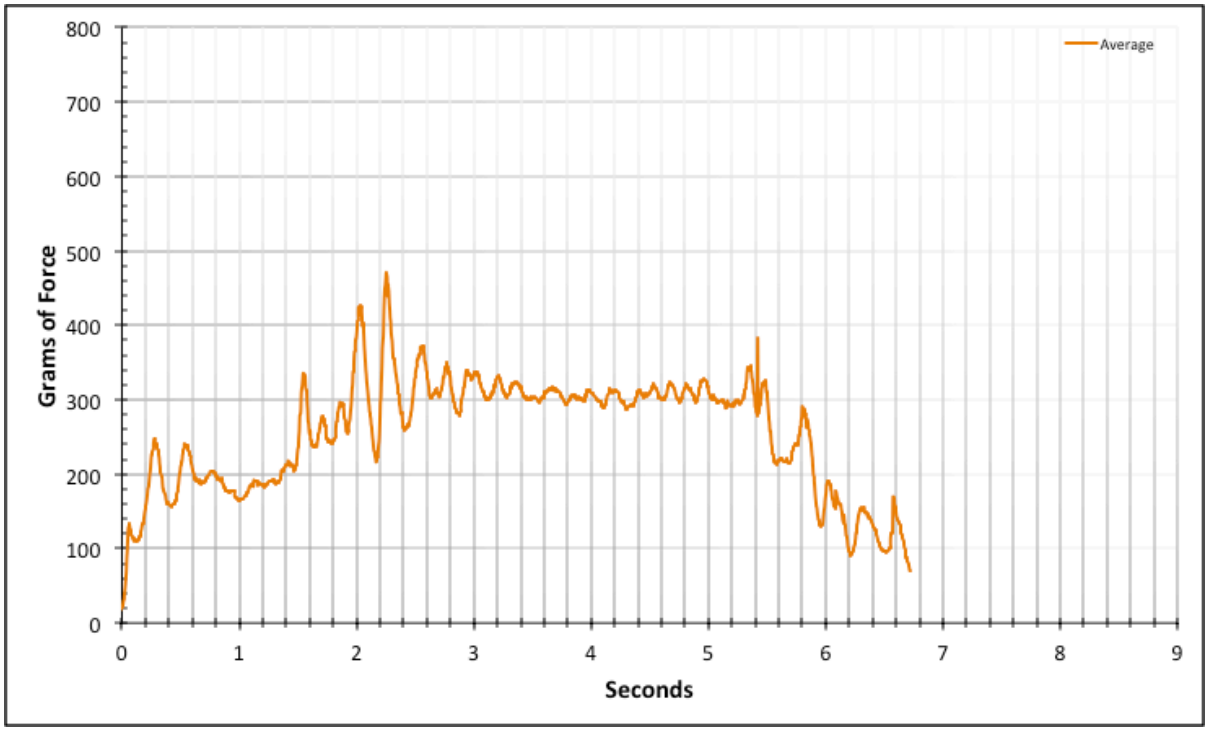

Figure 4-15: Full Average Data for ID 21-25

The data set representing the #10 conductor and Bolt 3 (ID 26 – ID 30) is a clean example with a good Region 2 that is relatively ideal. The transition from Region 1 to Region 2 is a bit longer than others likely due to the higher speed of Bolt 3. The result from this data set's Region 2 is an expected frictional resistance of 328.1±0.9 grams.

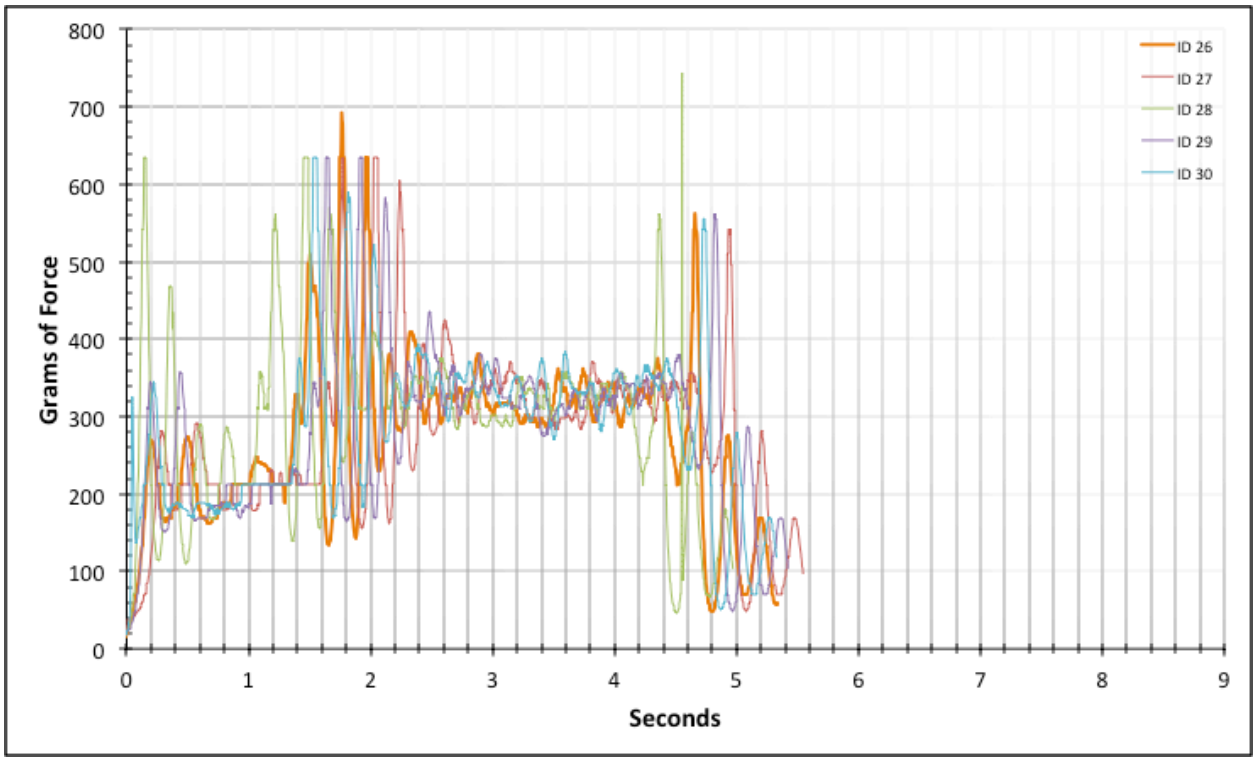

Figure 4-16: Full Composite Data for ID 26-30

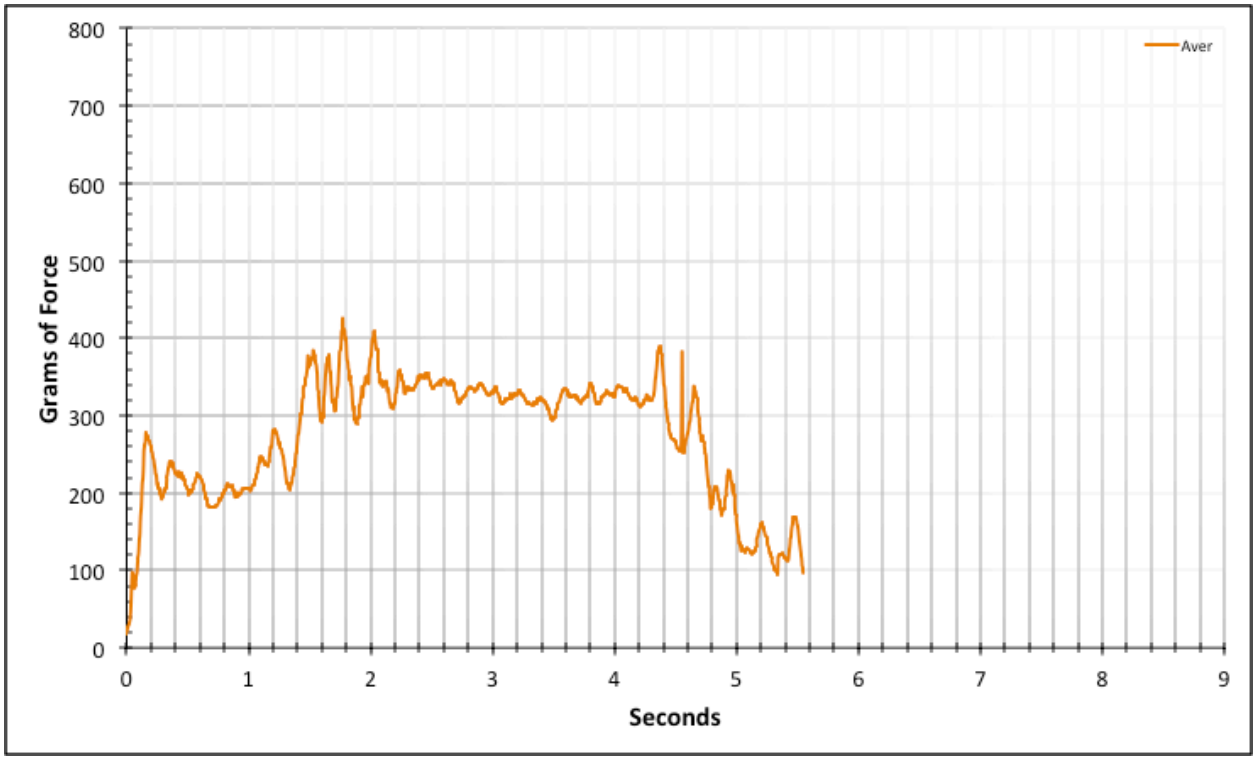

Figure 4-17: Full Average Data for ID 26-30

The data set representing the #8 conductor and Bolt 1 (ID 31 – ID 35) is a good set with a fair Region 2 that is a bit noise ridden in the first half. This is also the first data set with notable flat spots around 635 grams. These flat spots repeat in later data sets as well. It is most likely an error introduced by the gauge reader program not being able to effectively read the precise value while the needle was near this reading. Observations of the raw video footage do confirm near steady readings that repeat near 635 grams. The systematic error of flat spots has no applied or known correction and is accepted as systematic error. The statistical results were only conducted on the second half of Region 2 in order to include as little flat spot error as possible. The latter half also includes the fewest spikes outside of the gauge's certified range. The result from this data set's Region 2 is an expected frictional resistance of 760.6±1.5 grams.

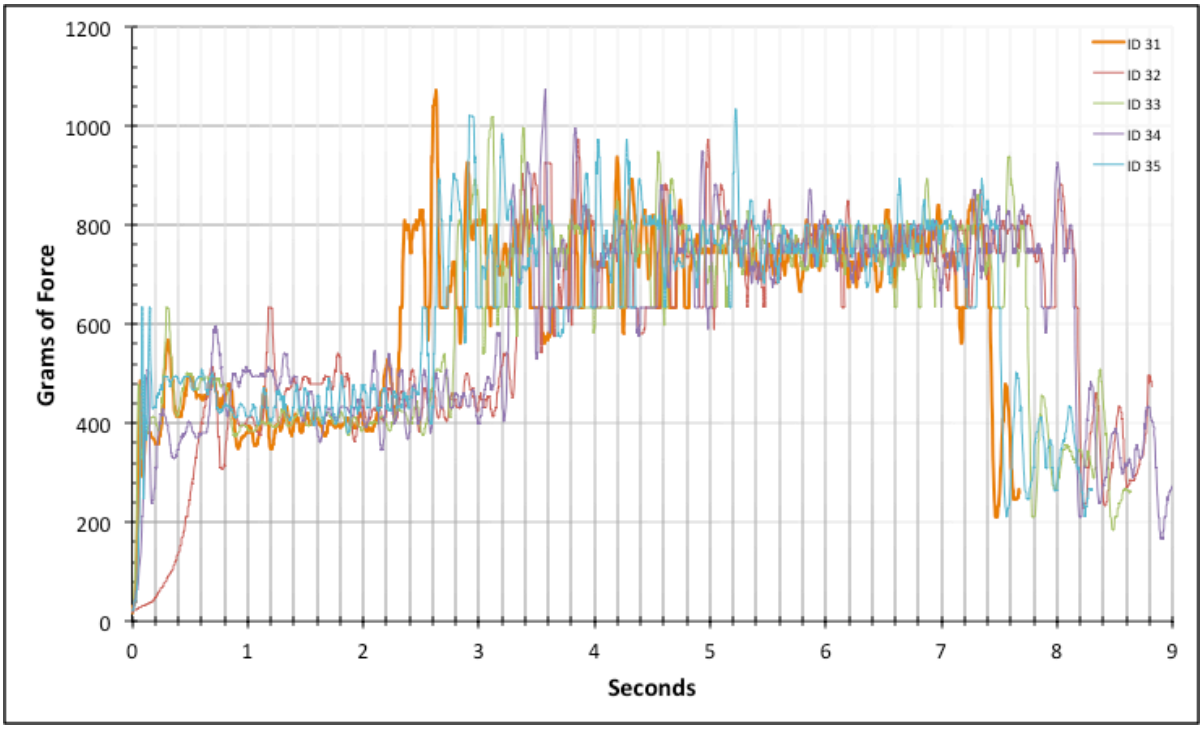

Figure 4-18: Full Composite Data for ID 31-35

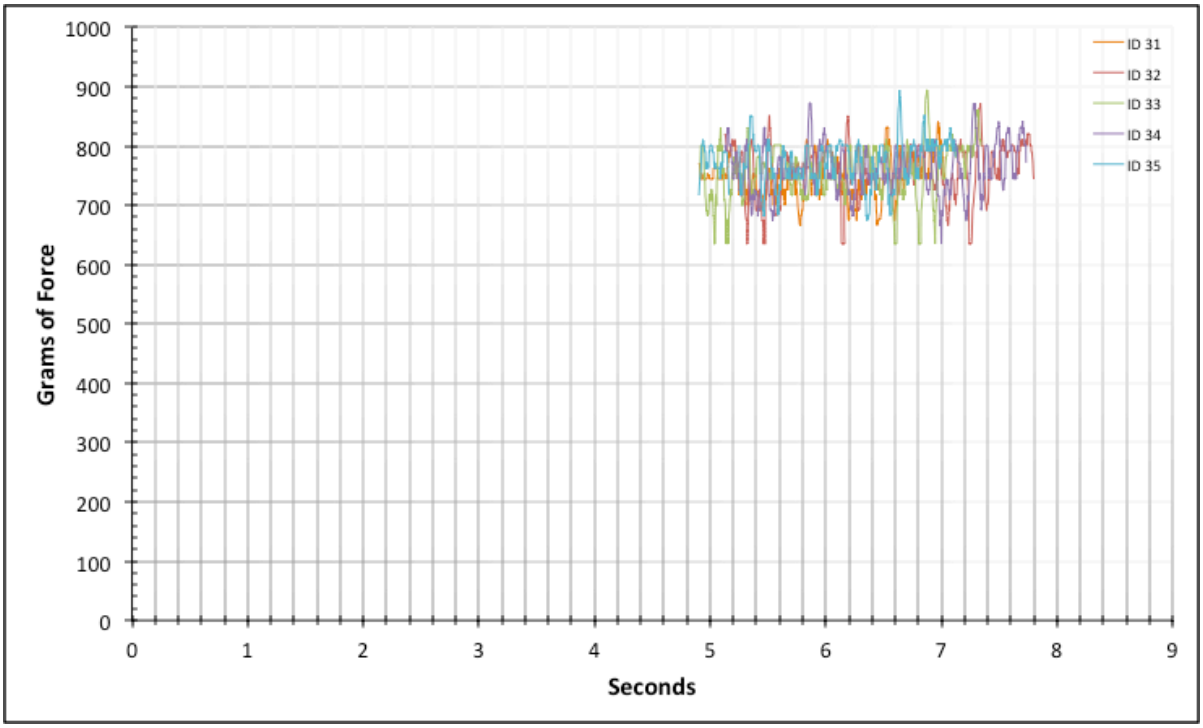

Figure 4-19: Region 2 Composite Data for ID 31-35

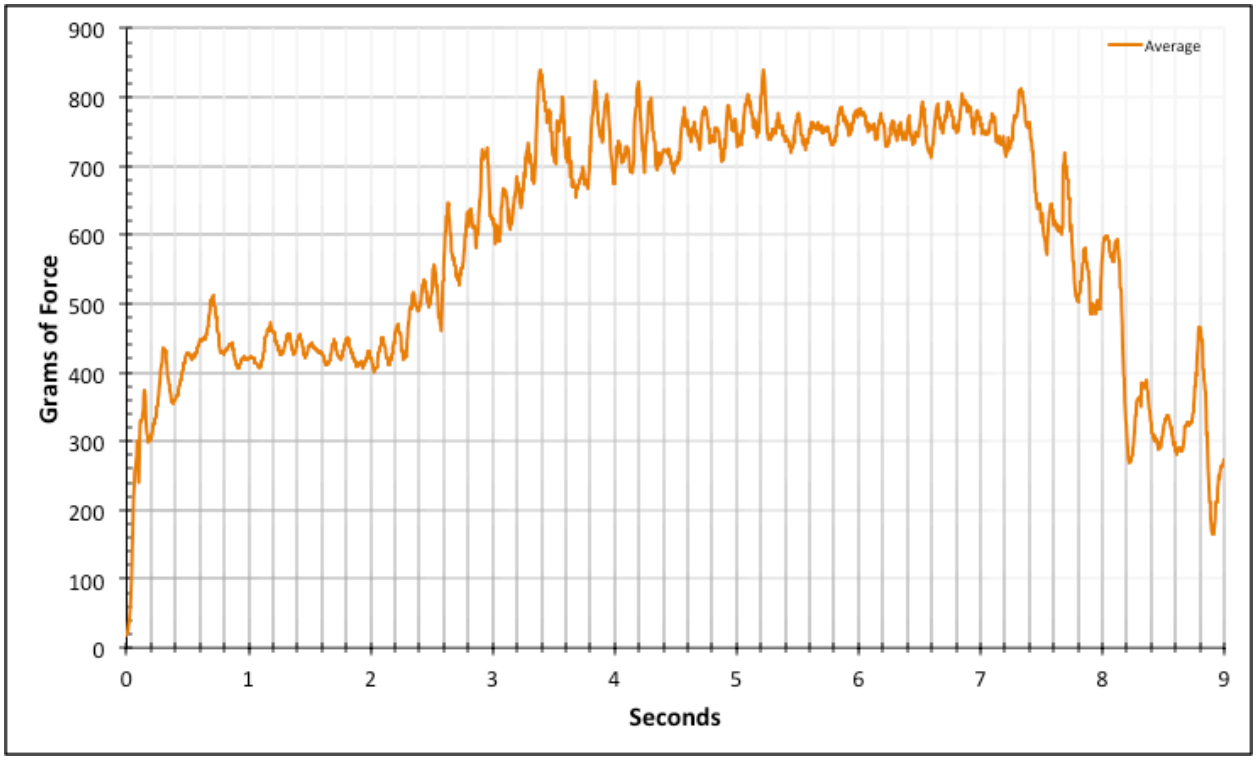

Figure 4-20: Full Average Data for ID 31-35

The data set representing the #8 conductor and Bolt 2 (ID 36 – ID 40) beautifully represents expected behavior and a consistent Region 2. The notable concern with this data set is that the result's mean value is very close to the gauge's max reading of 800 grams. This does yield the potential of skewed results due to readings that fluctuate above 800 grams throughout the trial. Due to the closeness to 800 grams observed during the experimental execution, the trials that should have been recorded for the #8 conductor and Bolt 3 were omitted from the study in an effort to avoid damaging the gauge. The result from this data set's Region 2 is an expected frictional resistance of 782.4±1.6 grams.

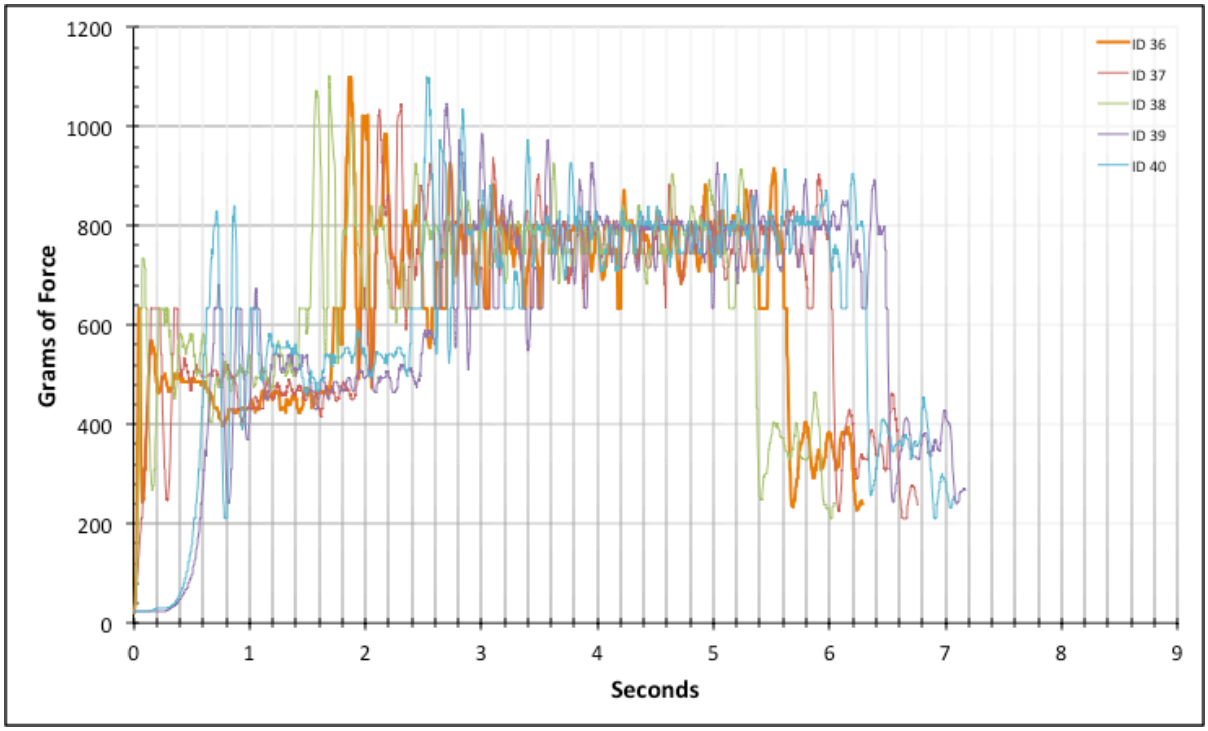

Figure 4-21: Full Composite Data for ID 36-40

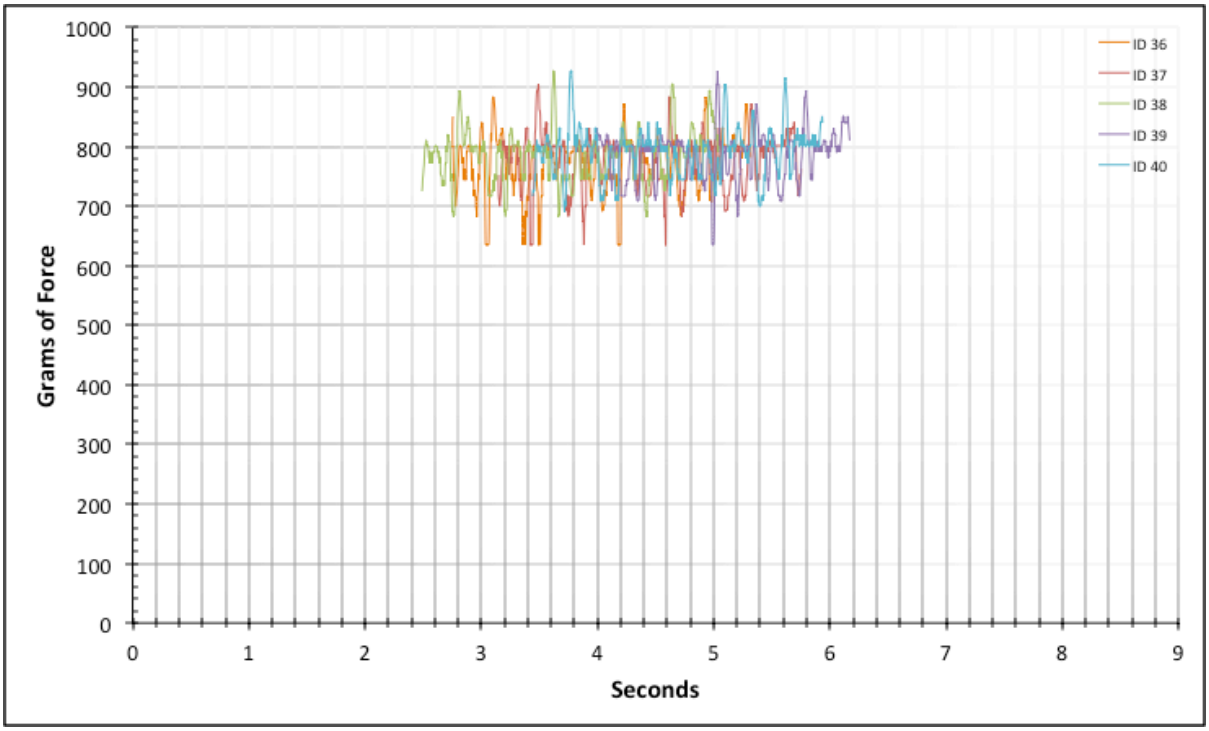

Figure 4-22: Region 2 Composite Data for ID 36-40

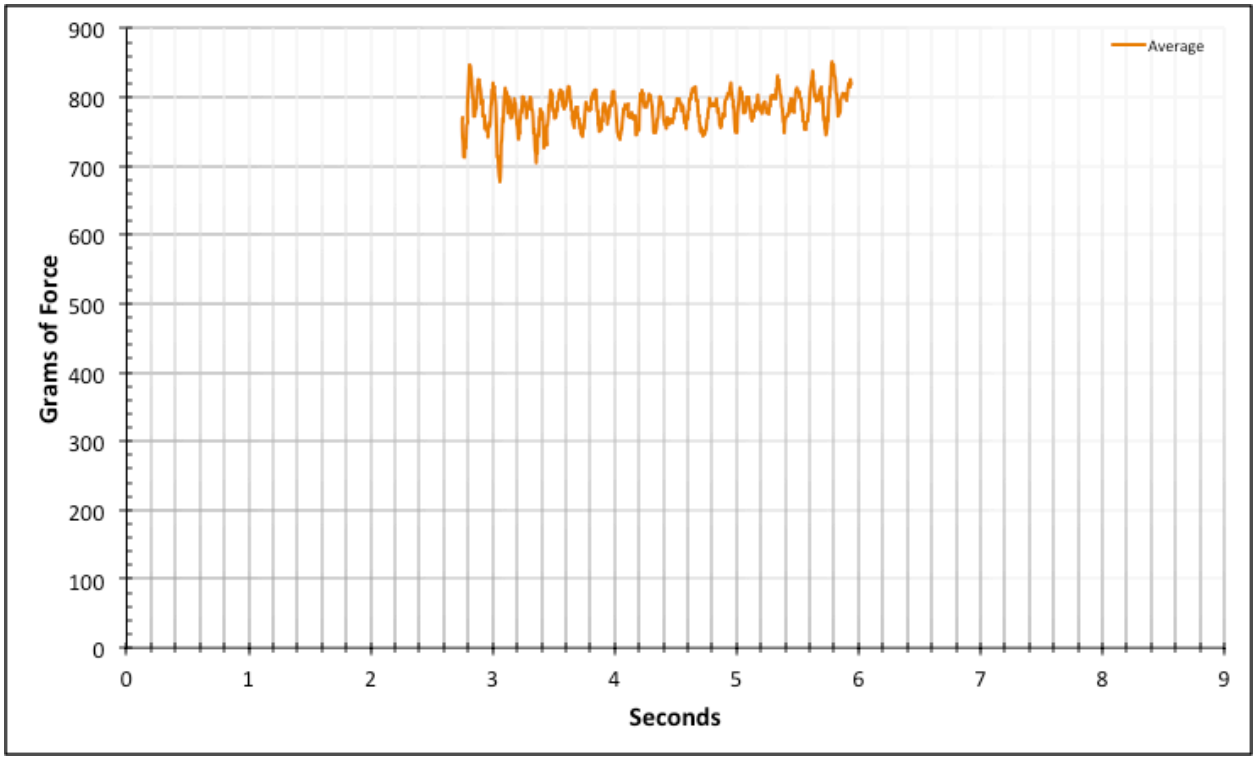

Figure 4-23: Region 2 Average Data for ID 36-40

4.1.4.2. Modeled Product - Dry

The category includes videos 41 through 85 to cover the modeled product category without the application of lubricant. The data set for the #12 conductor and Bolt 1 (ID 41 – ID 45) is plagued by a consistent bubble of increased amplitude within Region 2 similar to the factory baseline case. The bubble is less distinguished in amplitude and spans over more time. This is likely due to a systematic error from a defect in the conductor's header repeatedly catching in a break or inconsistency in the conduit along with a reduced damping from reduced friction in the elbow. This systematic error has an effect of increasing the standard error for this data set. The graph of the overall average indicates above average noise in Region 2 likely due to the constructive/destructive superposition of the systematic error. The result from this data set's Region 2 is an expected frictional resistance of 143.9±1.0 grams.

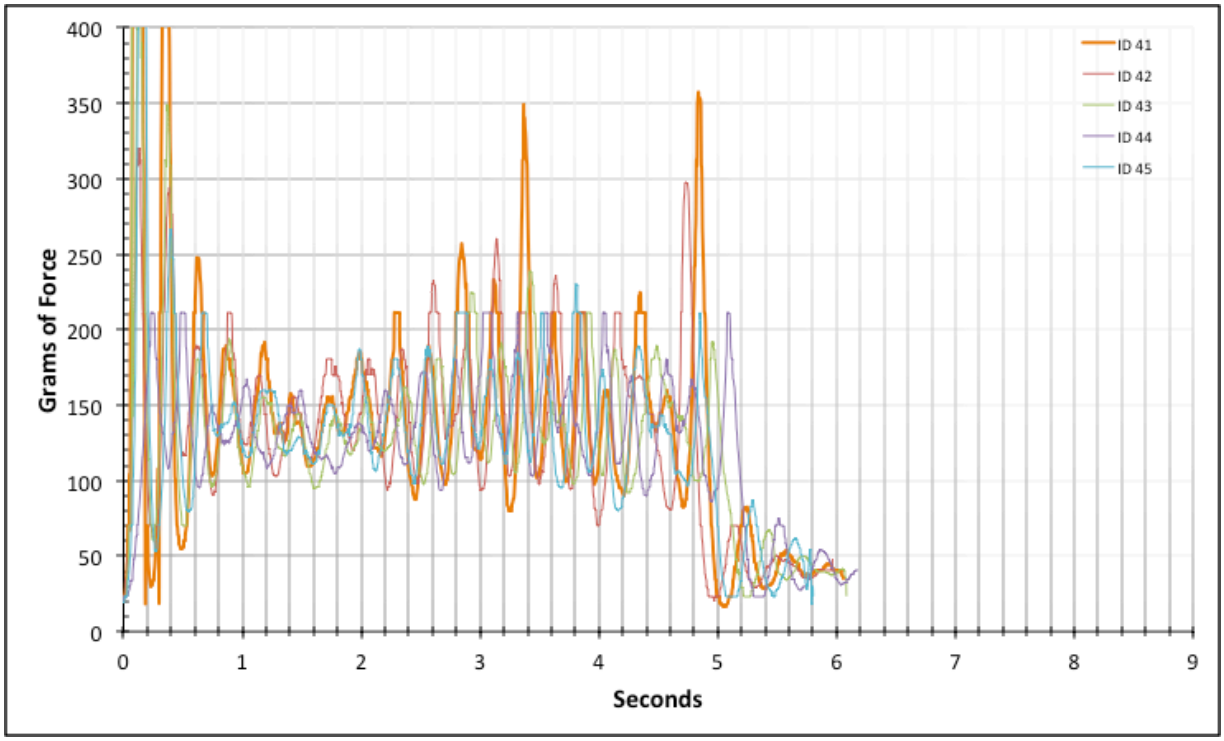

Figure 4-24: Full Composite Data for ID 41-45

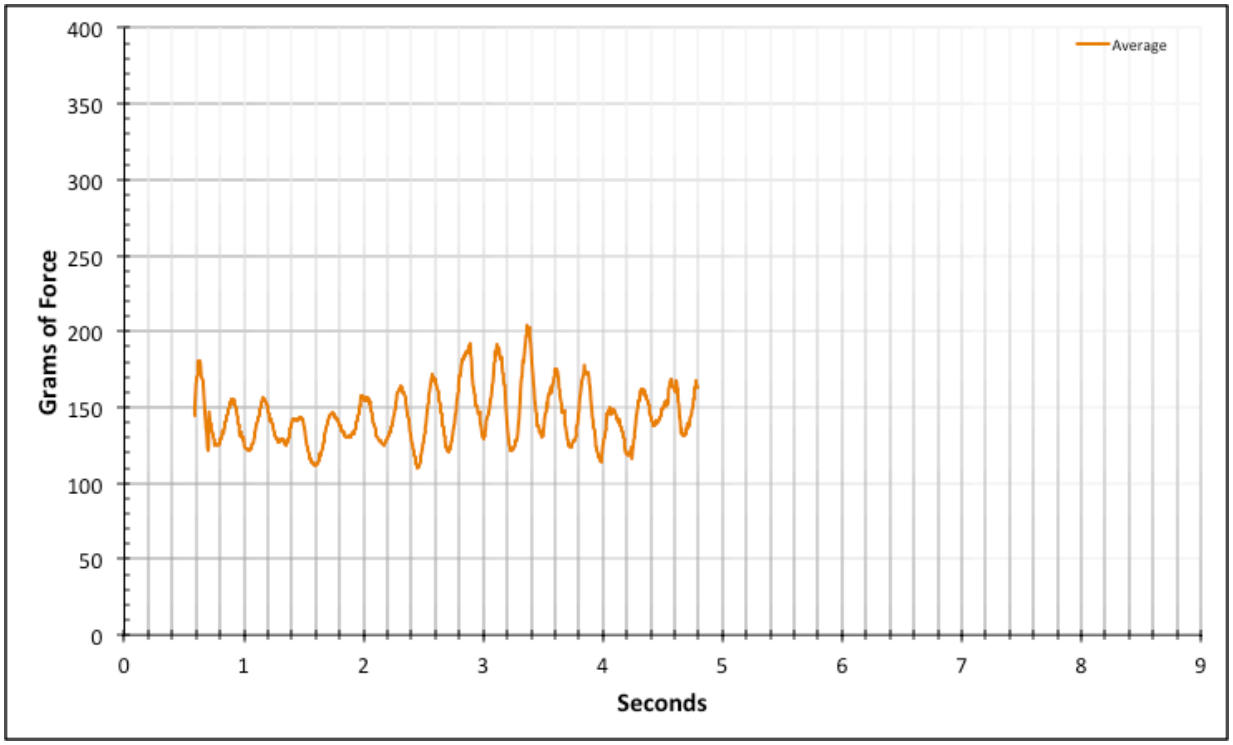

Figure 4-25: Region 2 Average Data for ID 41-45

The data set for the #12 conductor and Bolt 2 (ID 46 – ID 50) is not indicative of visually definitive systematic error. The trials are out of sync due to data cropping. The resulting graphs thus appear noisier than the data truly is. The result from this data set's Region 2 is an expected frictional resistance of 151.2±0.9 grams.

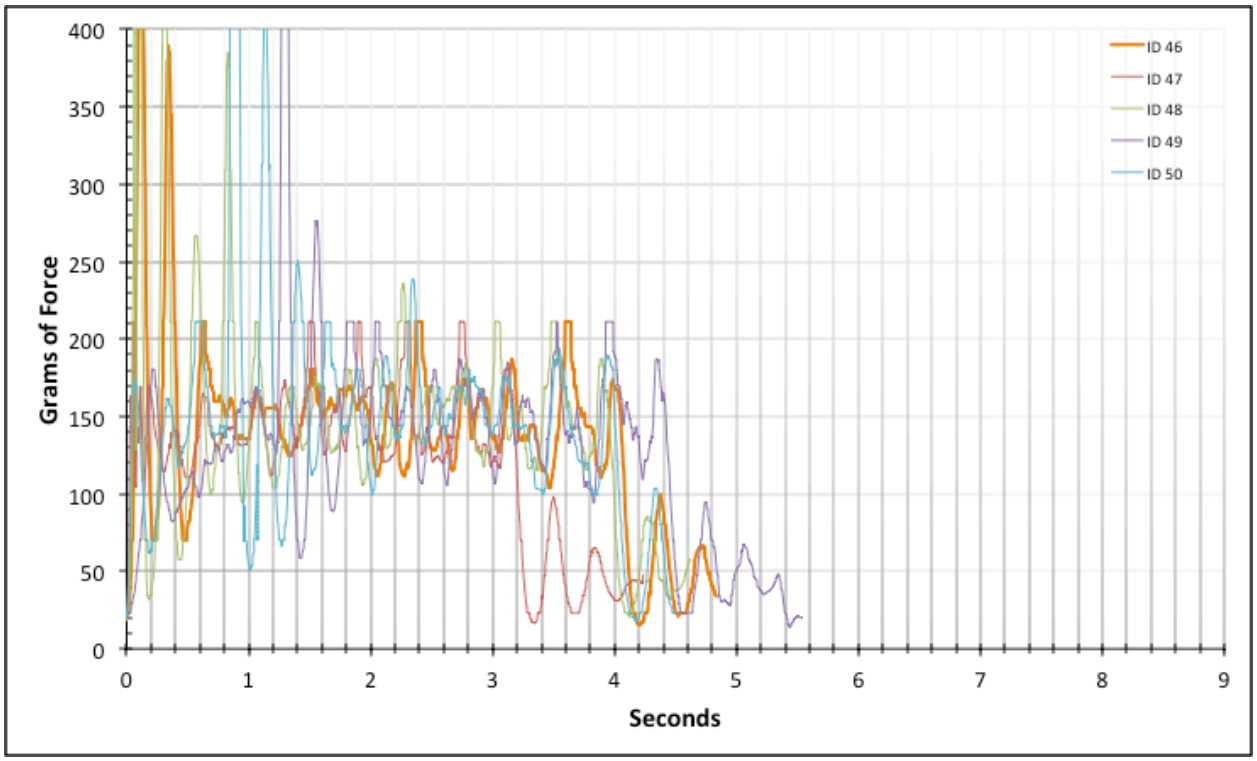

Figure 4-26: Full Composite Data for ID 46-50

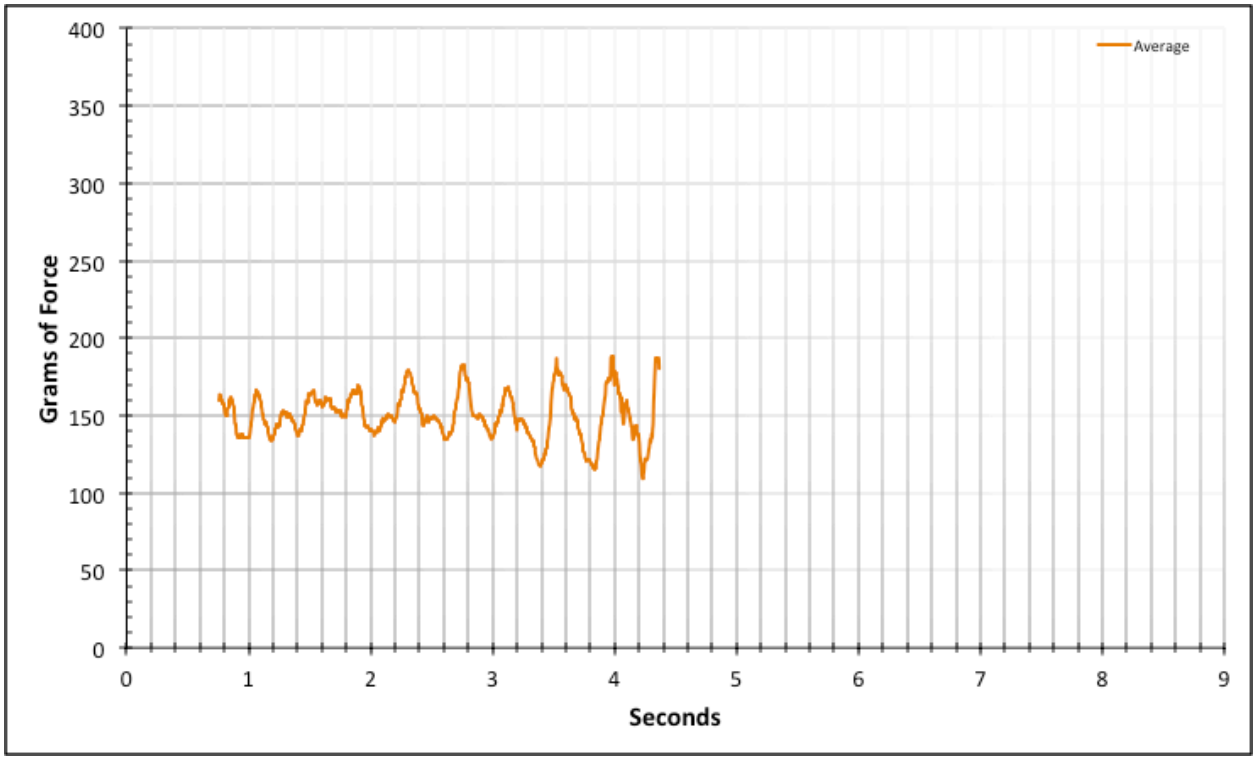

Figure 4-27: Region 2 Average Data for ID 46-50

The data set for the #12 conductor and Bolt 3 (ID 51 – ID 55) is not indicative of visually definitive systematic error. The trials are out of sync due to data cropping. The resulting graphs thus appear noisier than the data truly is. The result from this data set's Region 2 is an expected frictional resistance of 160.9±0.9 grams.

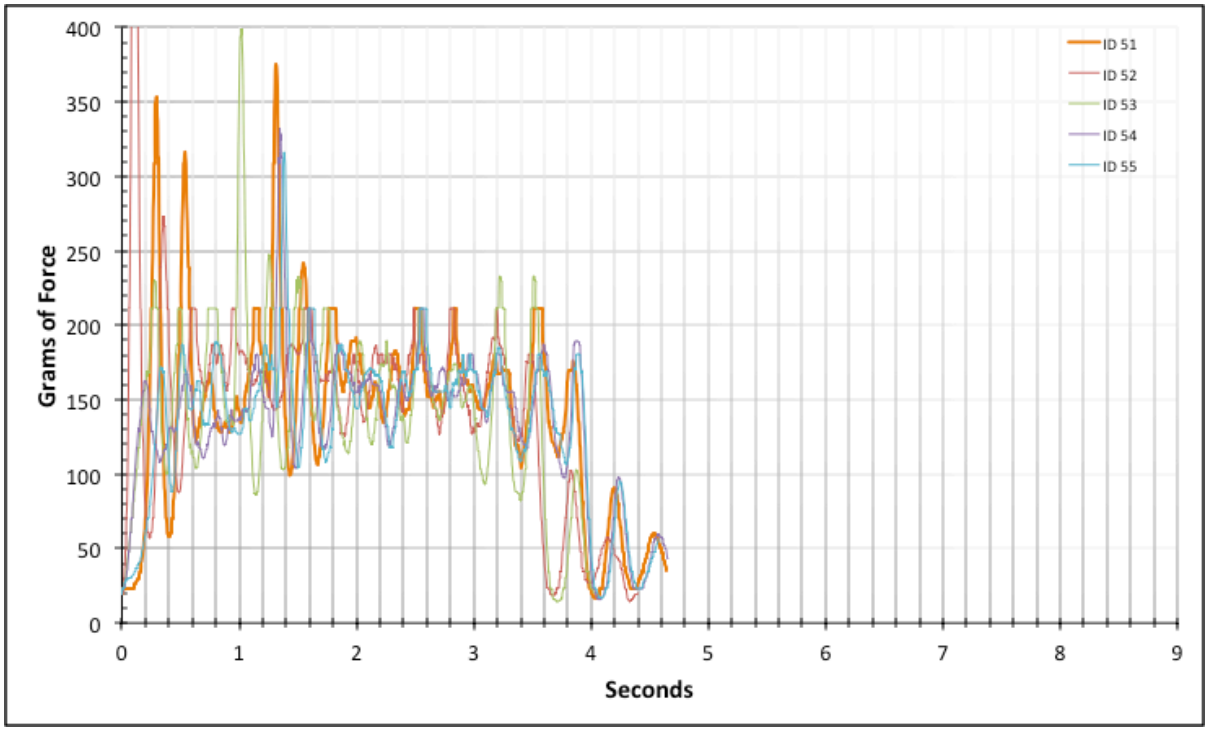

Figure 4-28: Full Composite Data for ID 51-55

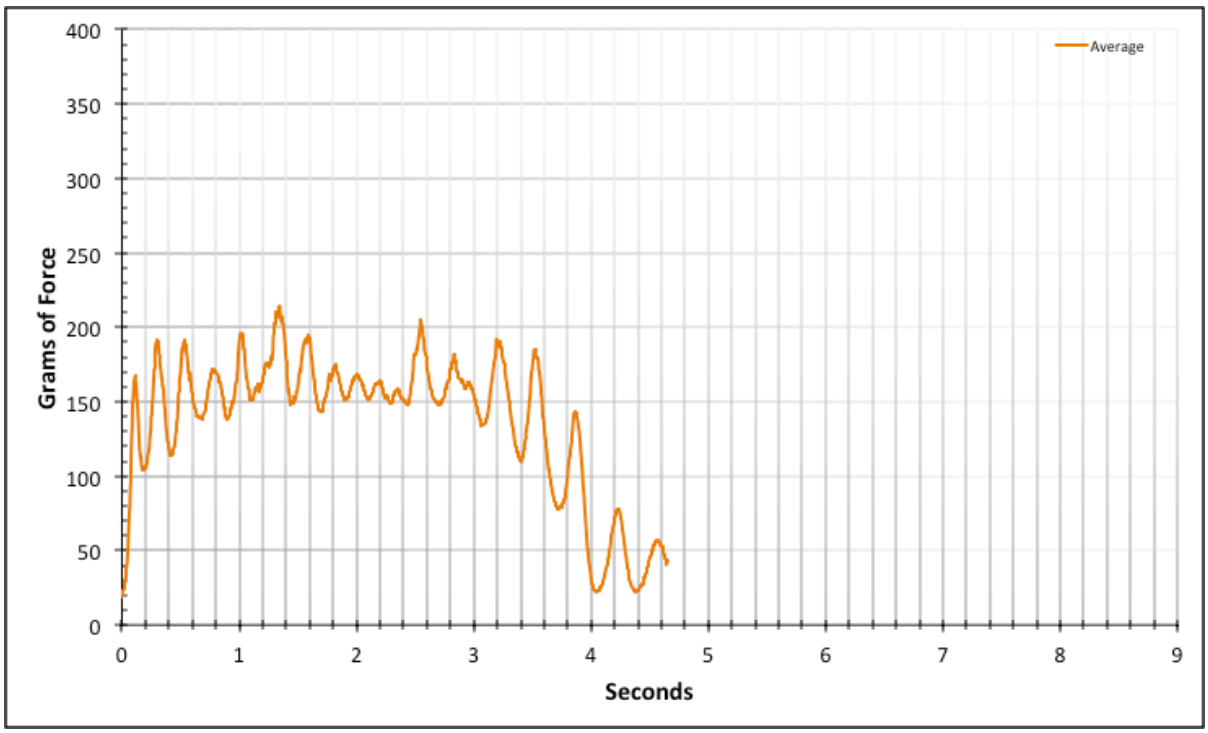

Figure 4-29: Full Average Data for ID 51-55

The data set for the #10 conductor and Bolt 1 (ID 56 – ID 60) is noisier than the average data set. There are a couple of large spikes in the 2nd Transition that were omitted from the statistically relevant data set. The result from this data set's Region 2 is an expected frictional resistance of 279.8±1.4 grams.

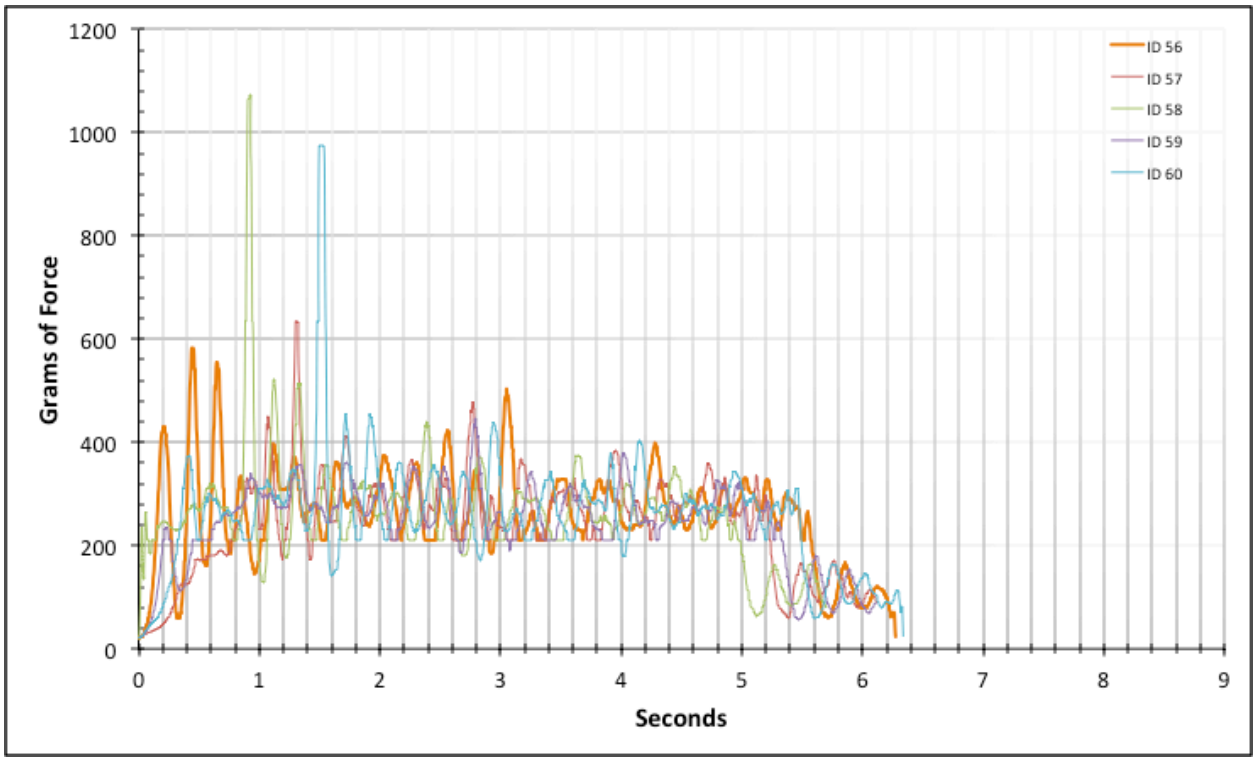

Figure 4-30: Full Composite Data for ID 56-60

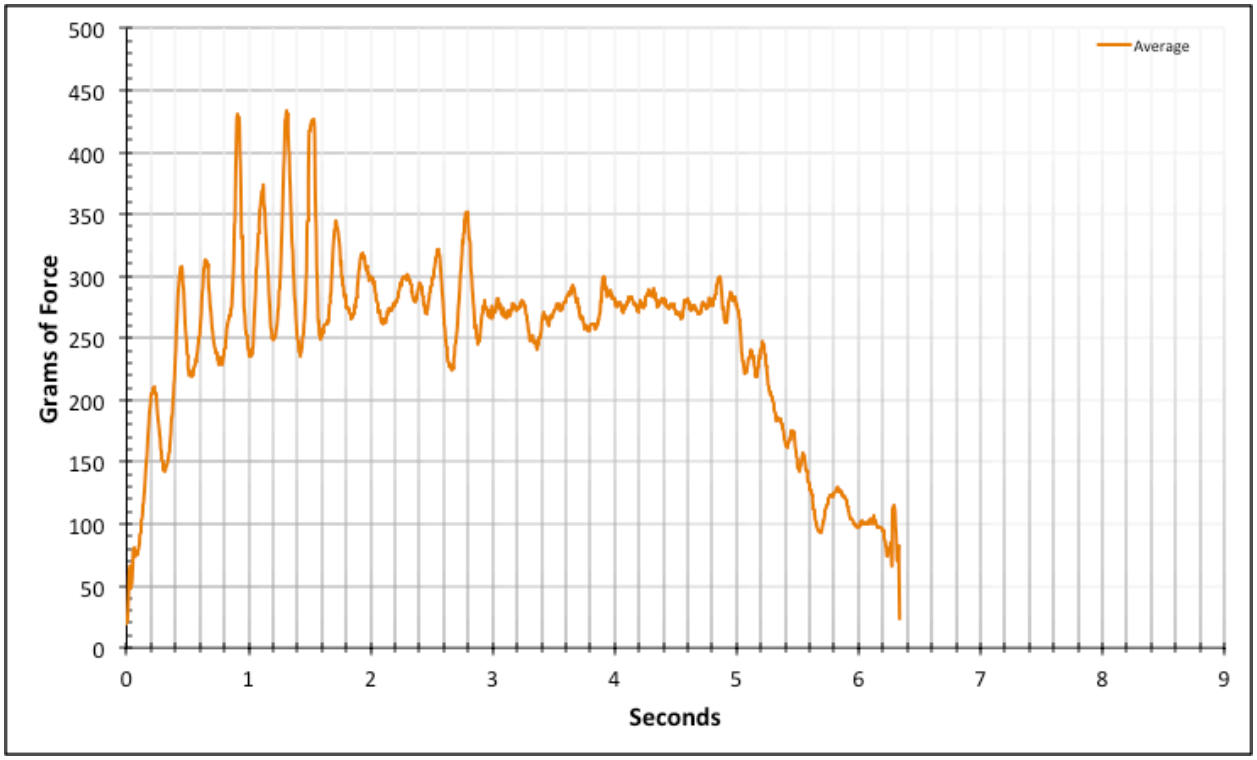

Figure 4-31: Full Average Data for ID 56-60

The data set for the #10 conductor and Bolt 2 (ID 61 – ID 65) is characterized by a bubble of systematic error that consumes a majority of Region 2. The most likely cause is a repeated catching defect of the header. The standard error from this data set is thus relatively high. The result from this data set's Region 2 is an expected frictional resistance of 299.8±1.9 grams.

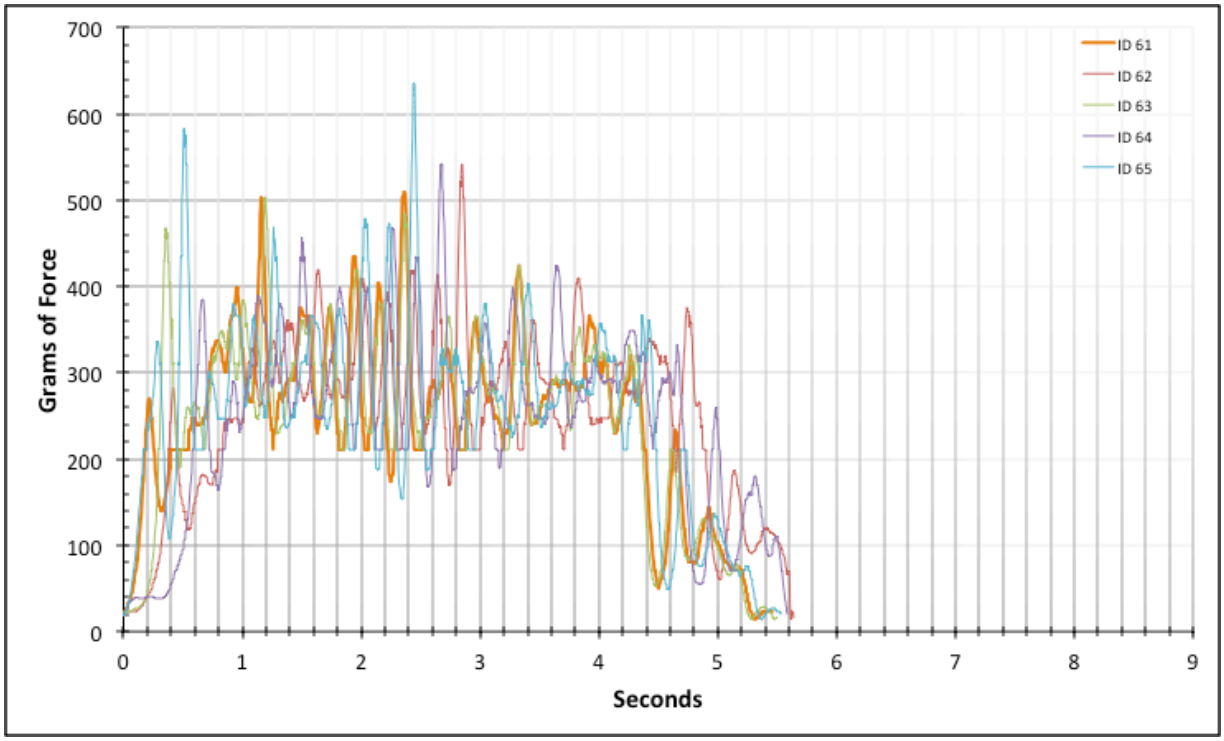

Figure 4-32: Full Composite Data for ID 61-65

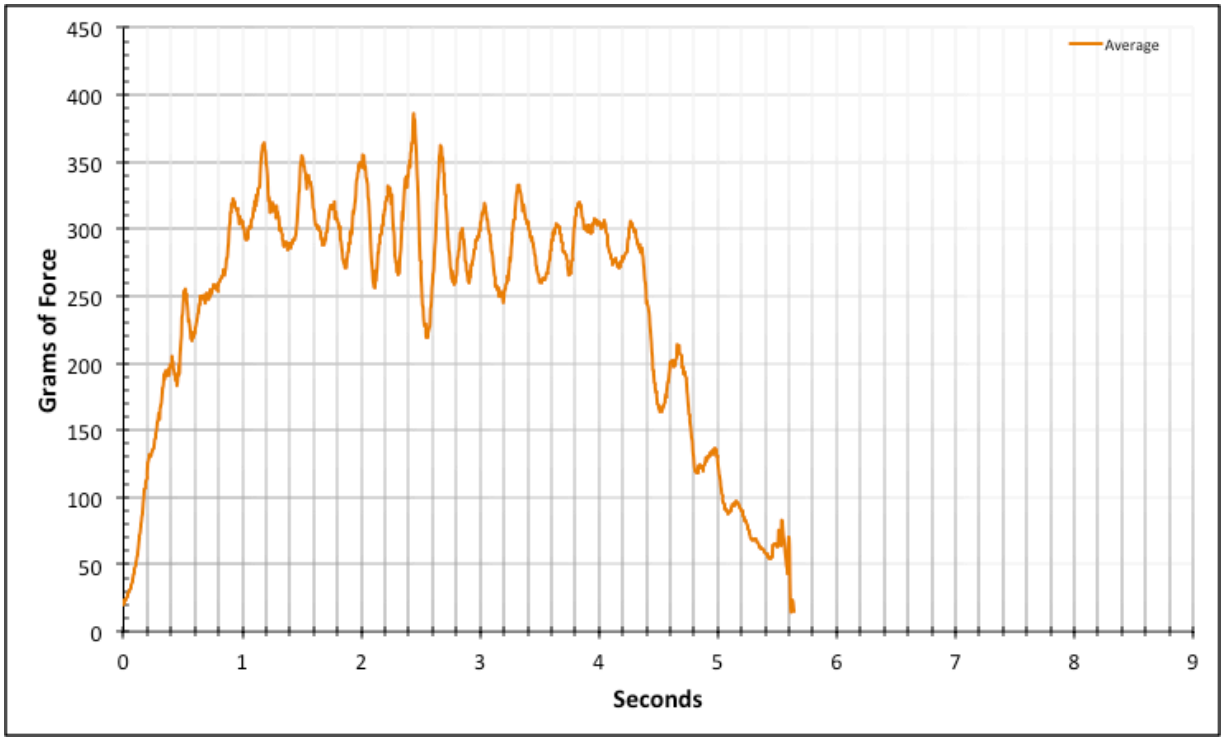

Figure 4-33: Full Average Data for ID 61-65

The data set for the #10 conductor and Bolt 3 (ID 66 – ID 70) is more noisy than the previous data set. The one abnormality that must be noted here is that video 68 was corrupted. The raw footage blacks out at the onset of the 2nd Transition. This video is thus completely omitted from the statistical data. The result from this data set's Region 2 is an expected frictional resistance of 308.9±2.3 grams.

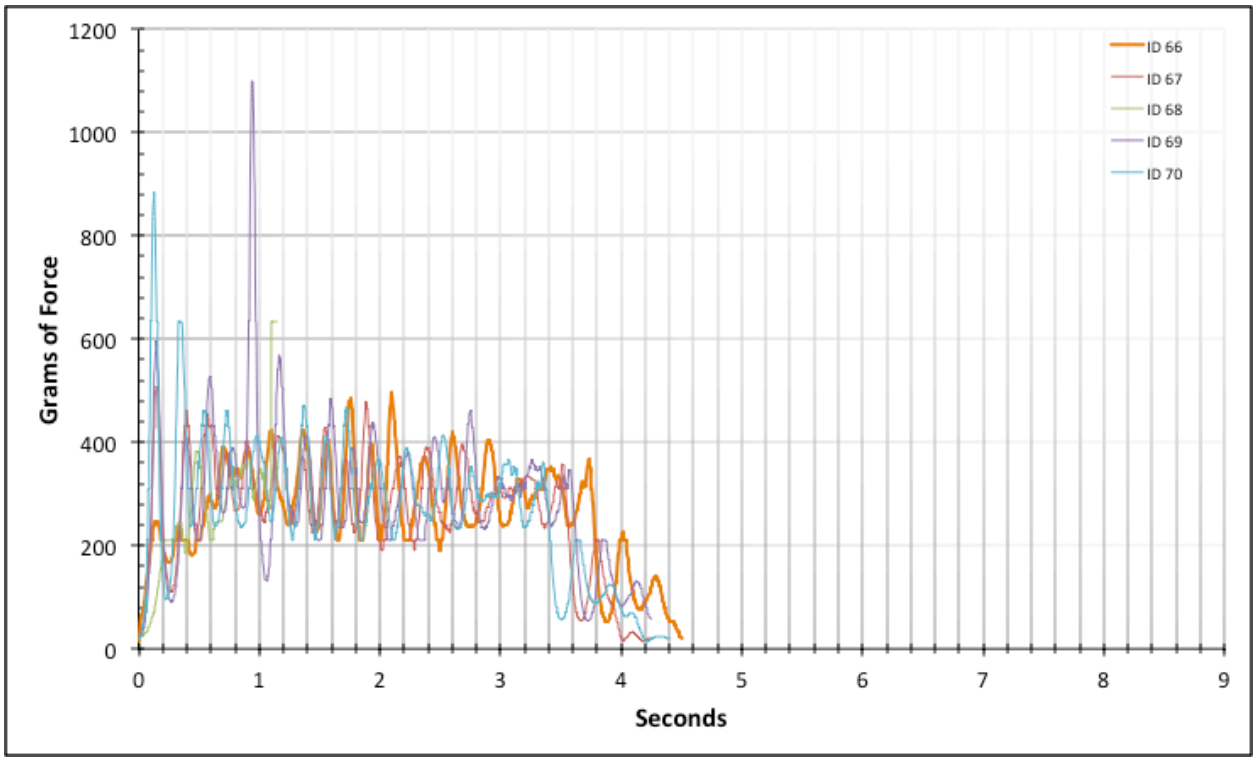

Figure 4-34: Full Composite Data for ID 66-70

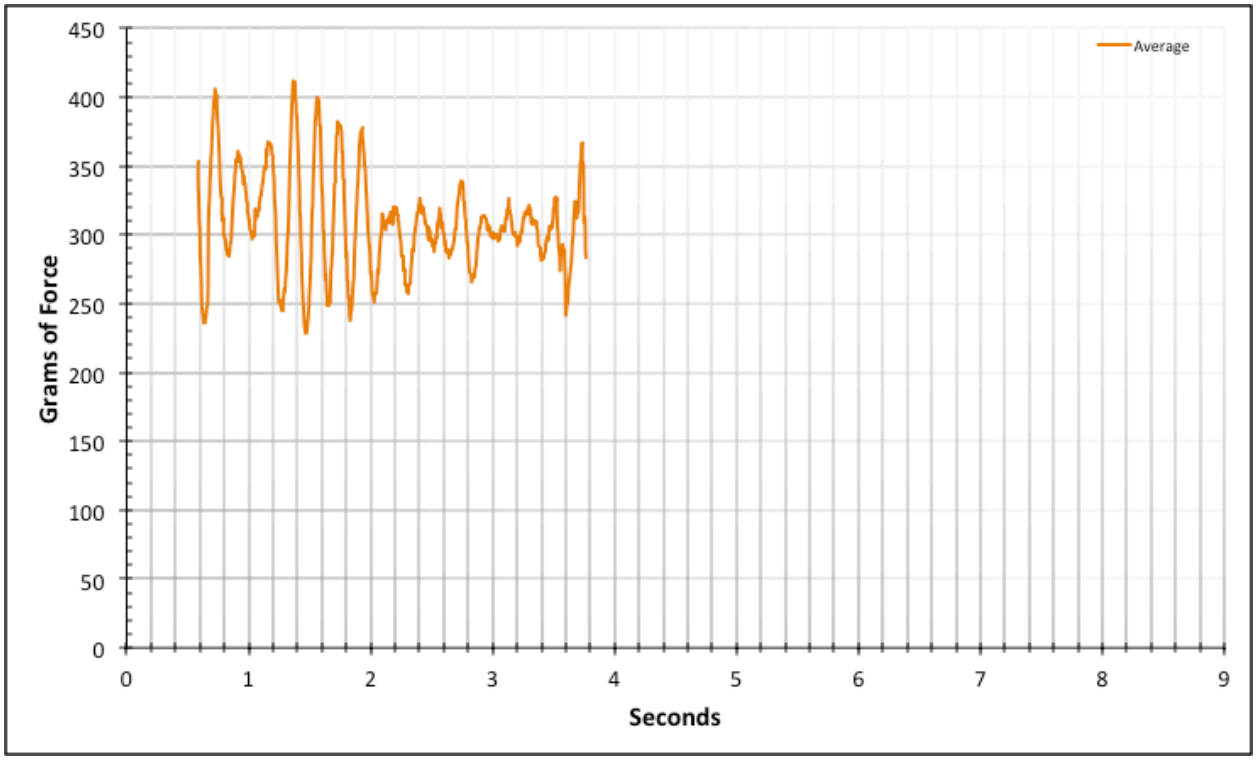

Figure 4-35: Region 2 Average Data for ID 66-70

The data set for the #8 conductor and Bolt 1 (ID 71 – ID 75) is largely consistent yet subject to ample flat spots. Also, video 74 was corrupted during processing. The corruption in this instance was due to an inconsistency in frame rate from a file conversion. The results were all there, but compressed into about 50% of the typical time duration of a trial. Thus, to avoid potential skewing, ID 74 is completely omitted from the statistical data. The result from this data set's Region 2 is an expected frictional resistance of 672.7±1.6 grams.

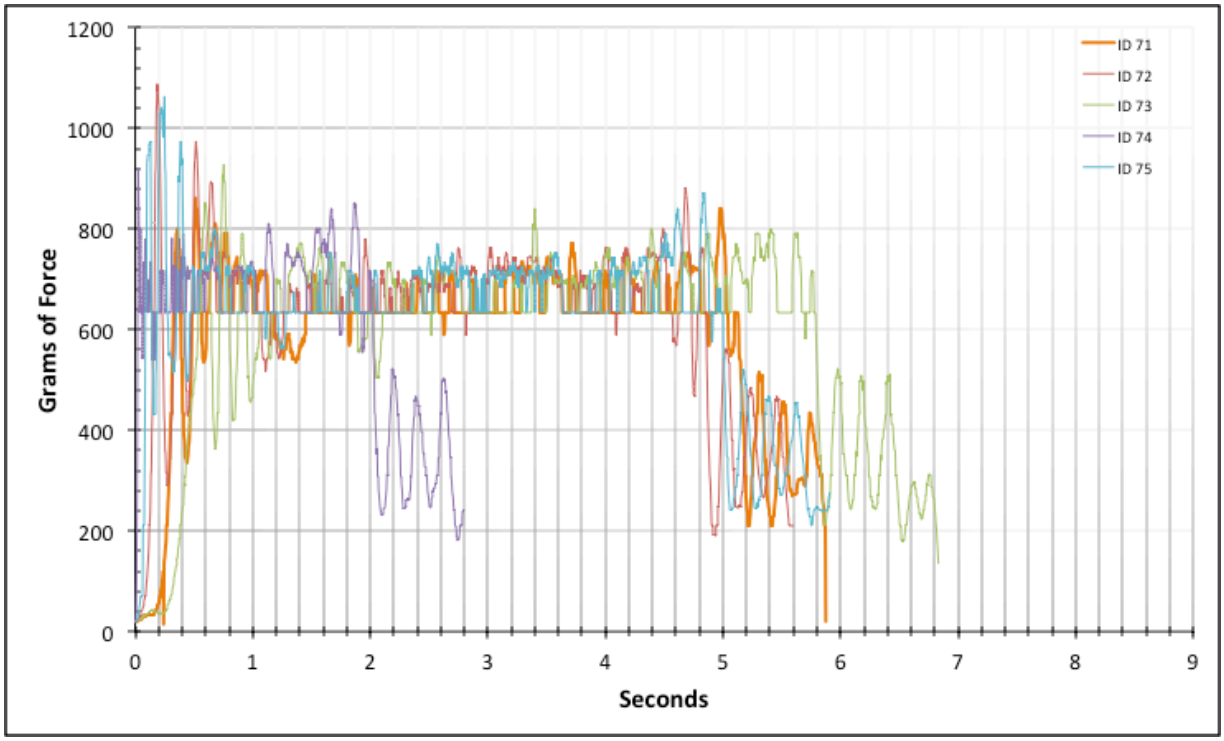

Figure 4-36: Full Composite Data for ID 71-75

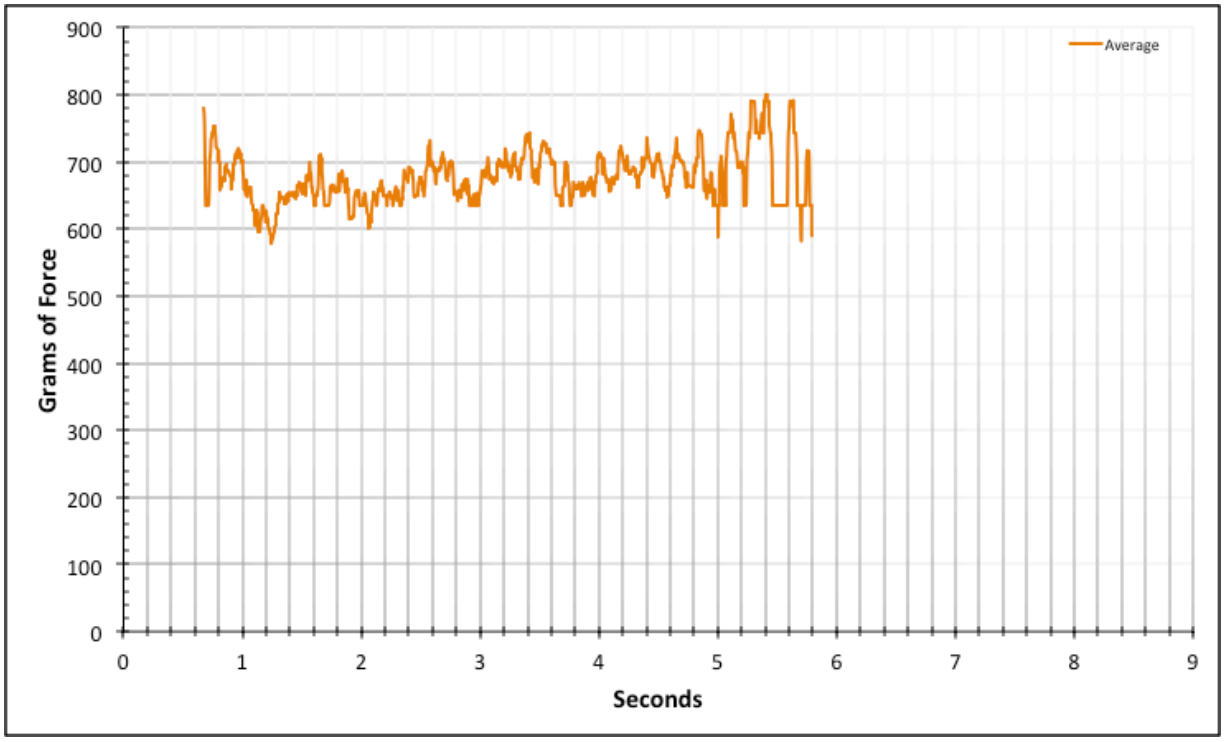

Figure 4-37: Region 2 Average Data for ID 71-75

The data set for the #8 conductor and Bolt 2 (ID 76 – ID 80) yields fairly consistent data. The individual trials are still subject to some flat spot error. The result from this data set's Region 2 is an expected frictional resistance of 715.6±1.7 grams.

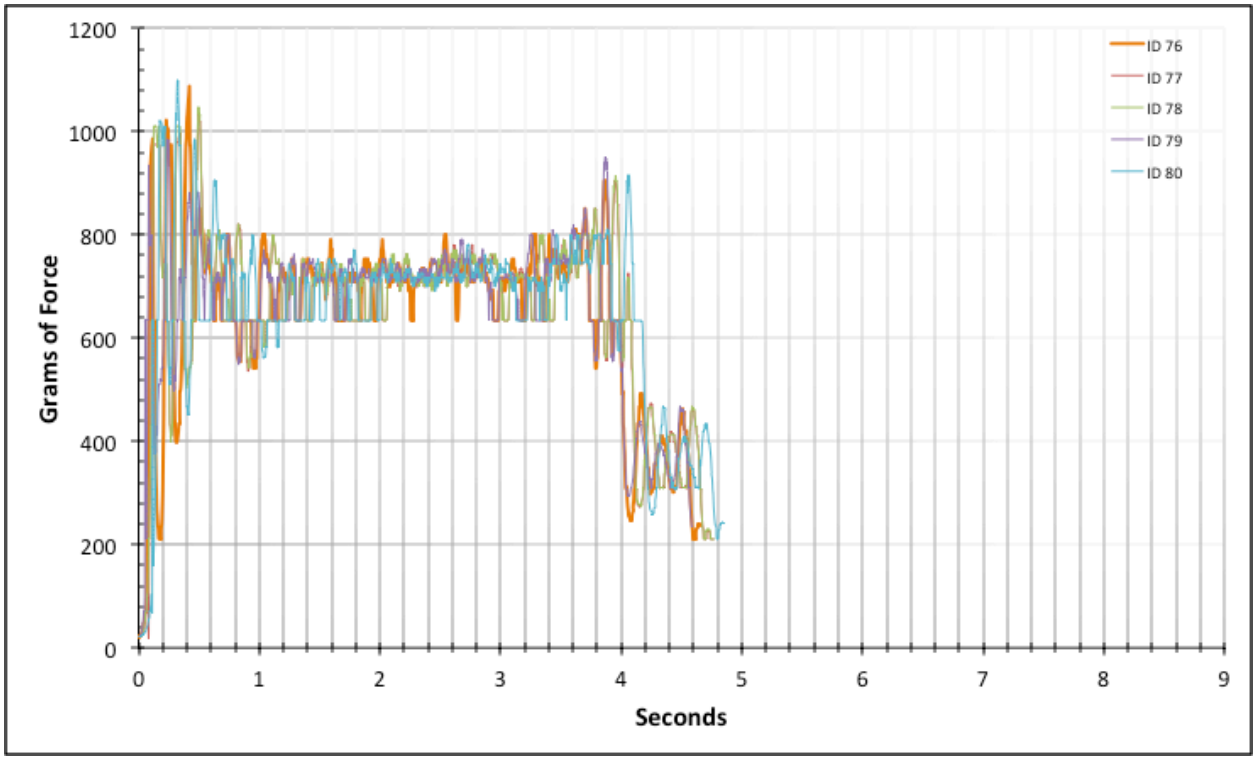

Figure 4-38: Full Composite Data for ID 76-80

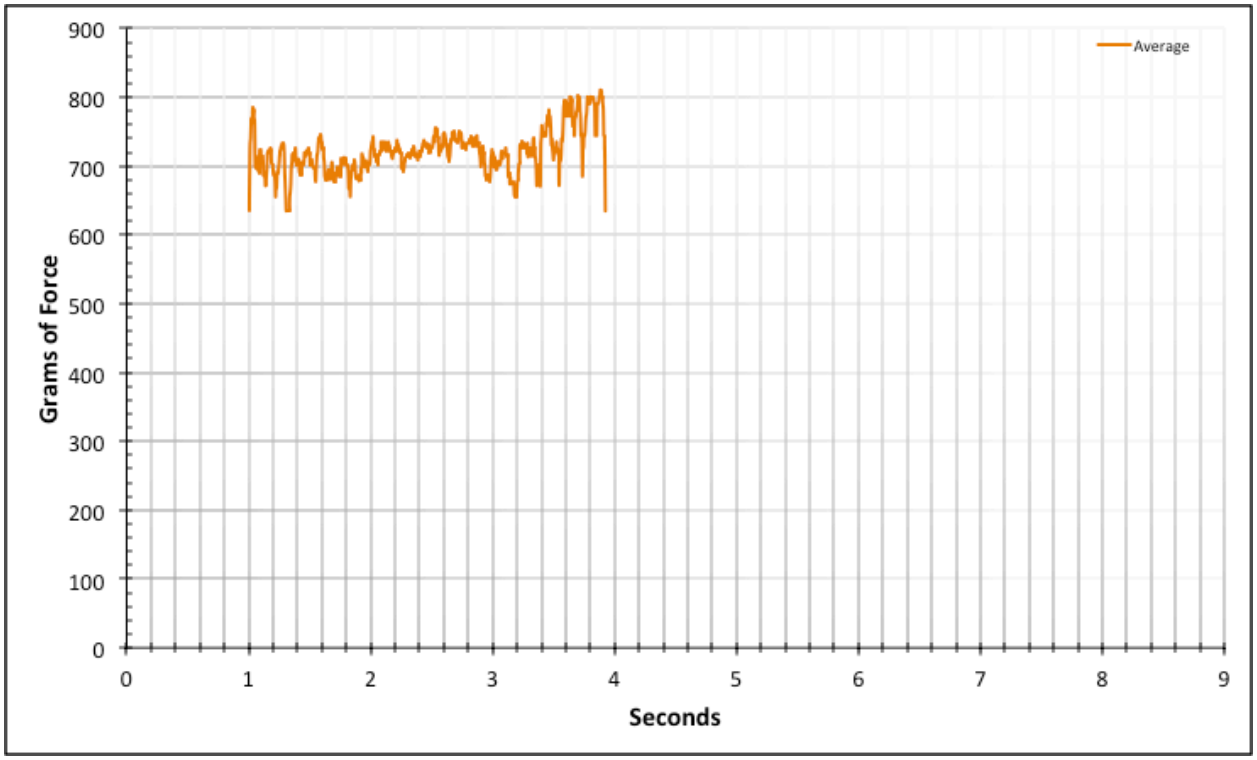

Figure 4-39: Region 2 Average Data for ID 76-80

The data set for the #8 conductor and Bolt 3 (ID 81 – ID 85) is also plagued by some flat spot error. The end results are still graphically acceptable. The result from this data set's Region 2 is an expected frictional resistance of 730.6±1.8 grams.

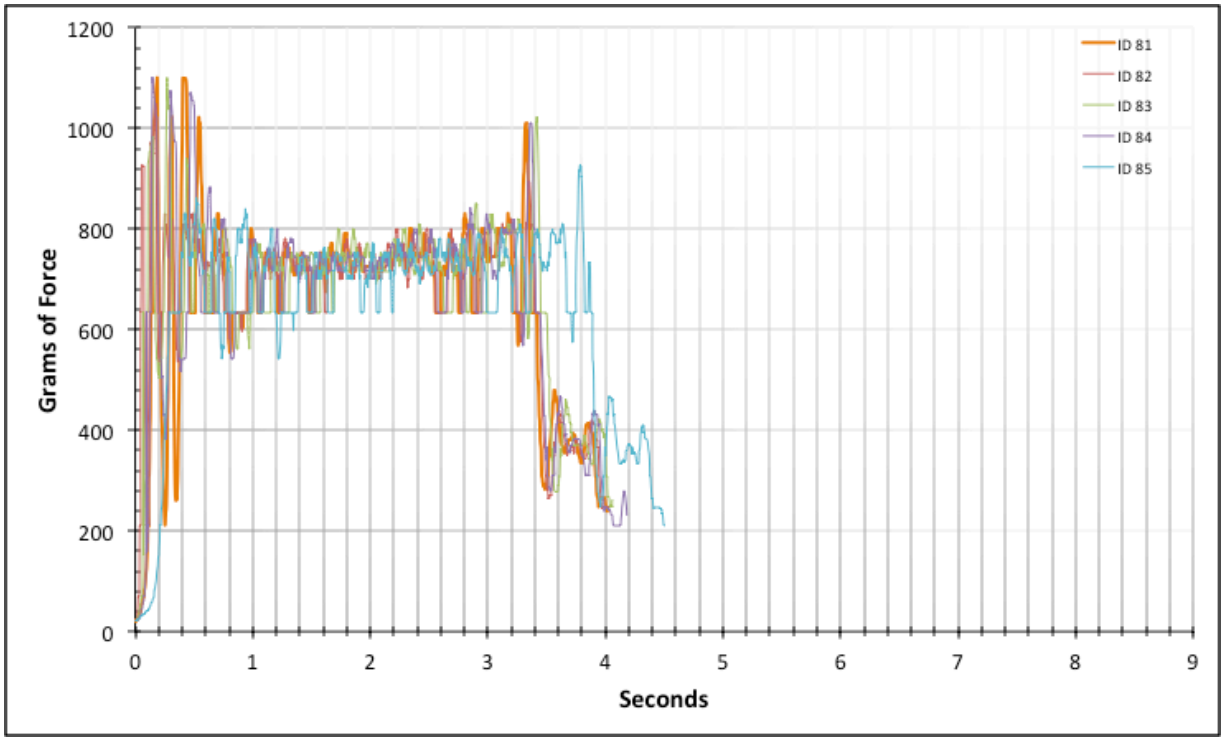

Figure 4-40: Full Composite Data for ID 81-85

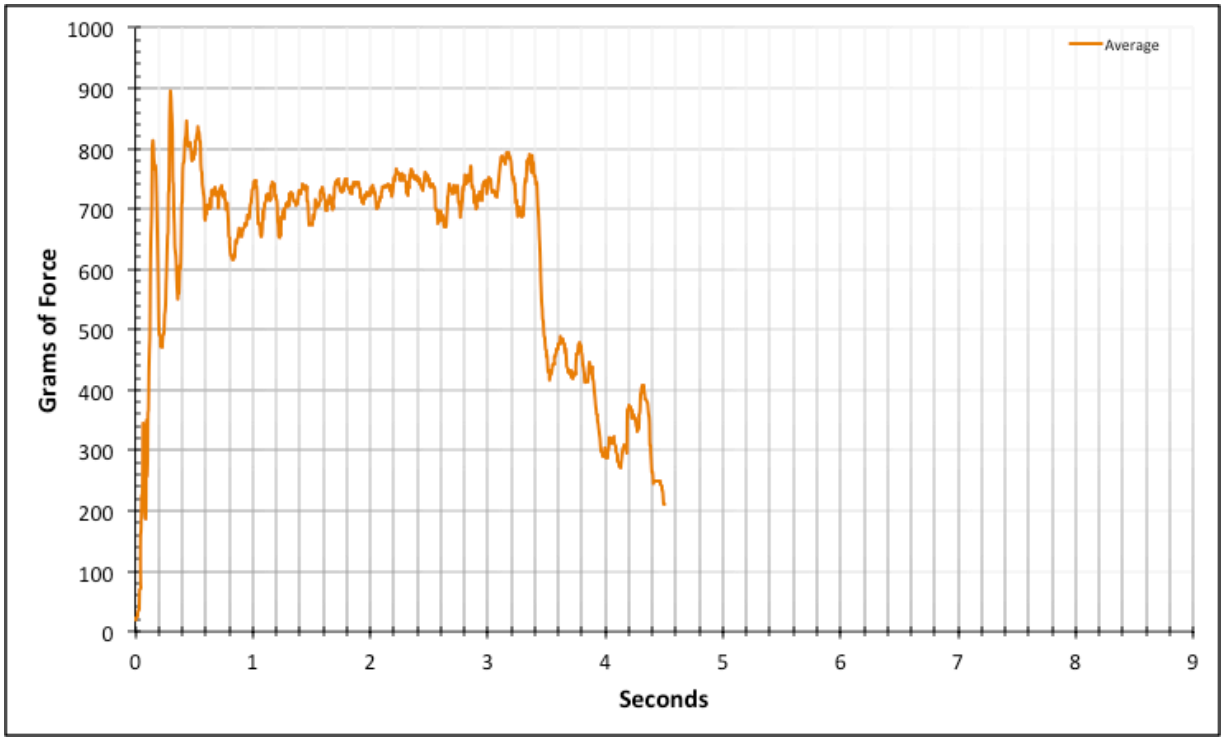

Figure 4-41: Full Average Data for ID 81-85

4.1.4.3. Straight Baseline - Dry

The category includes videos 86 through 130 to cover the straight baseline category without the application of lubricant. The data set for the #12 conductor and Bolt 1 (ID 86 – ID 90) is very consistent and a beautiful example of what idealized results for the straight run categories should be. In fact, the results are so consistent with the data sets describing the #12 conductor with Bolts 2 and 3 (ID 91 – ID 100) that the pure friction force measured is observed to be independent of velocity. This is scientifically proclaimed in the definition of friction in the field of physics. (Walker, 2013) Thus the following are graphs representative of all #12 conductor trials in this category. It should be noted that video 98 is completely omitted due to a file corruption upon recording. The original video file did not survive. The result from these data sets' region of interest is an expected frictional resistance of 42.2±0.1 grams.

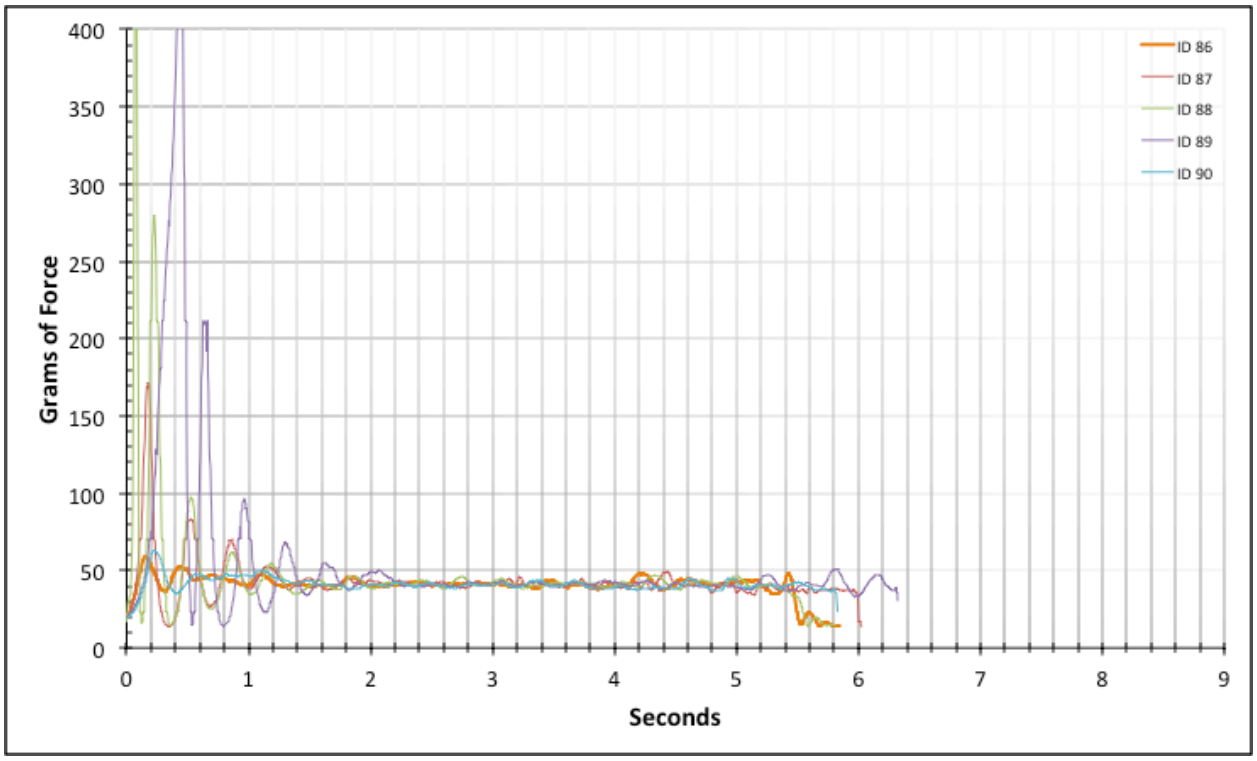

Figure 4-42: Full Composite Data for ID 86-90

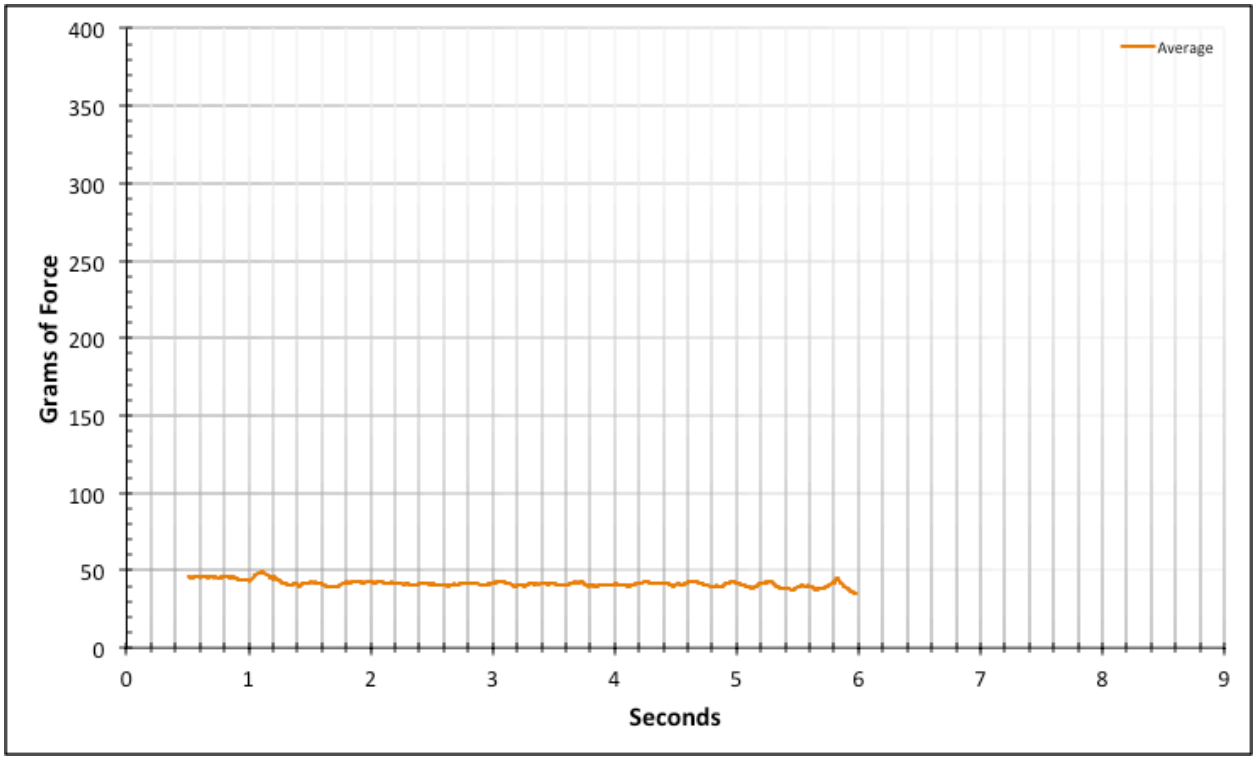

Figure 4-43: Regional Average Data for ID 86-90

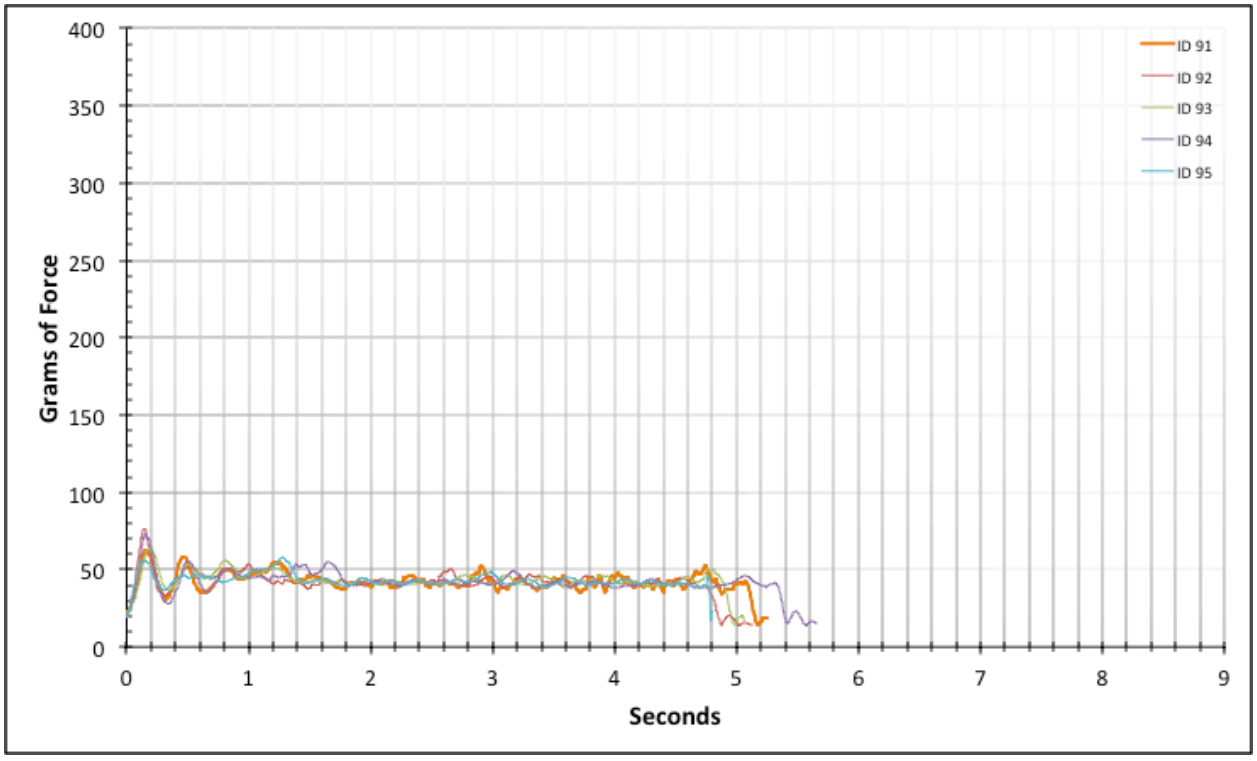

Figure 4-44: Full Composite Data for ID 91-95

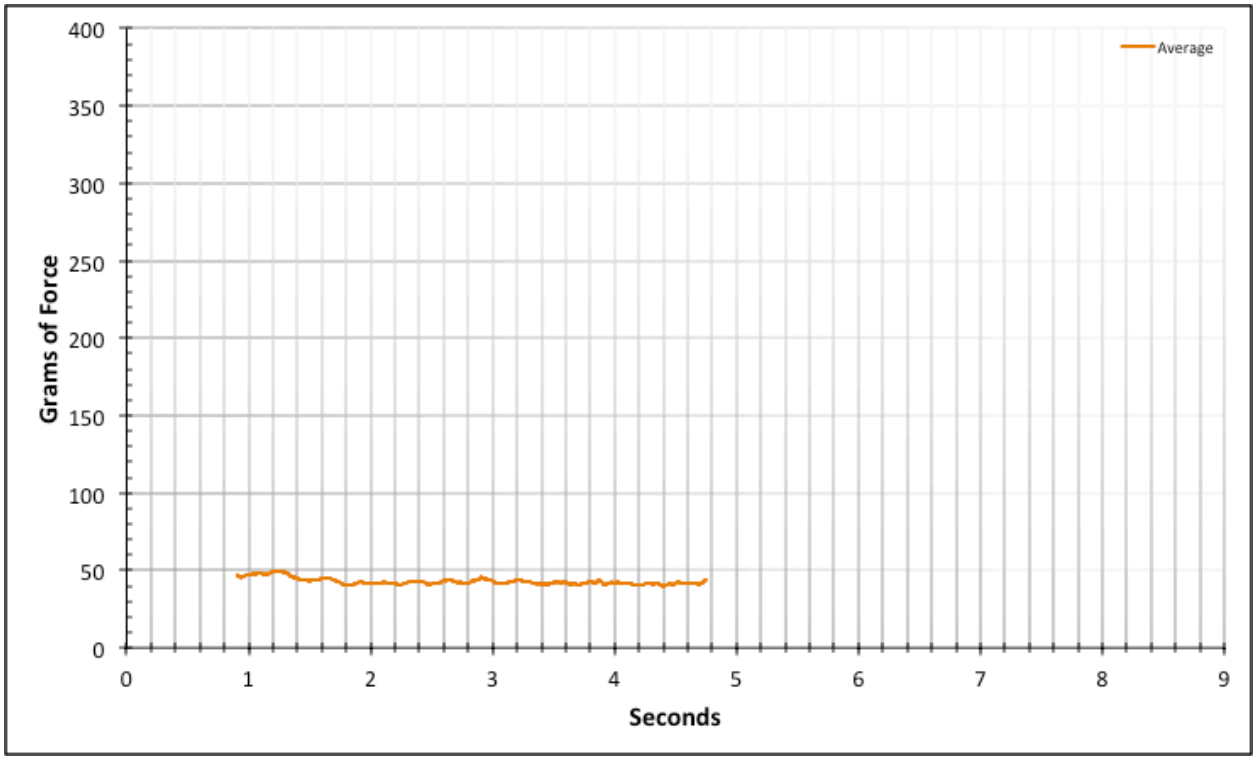

Figure 4-45: Regional Average Data for ID 91-95

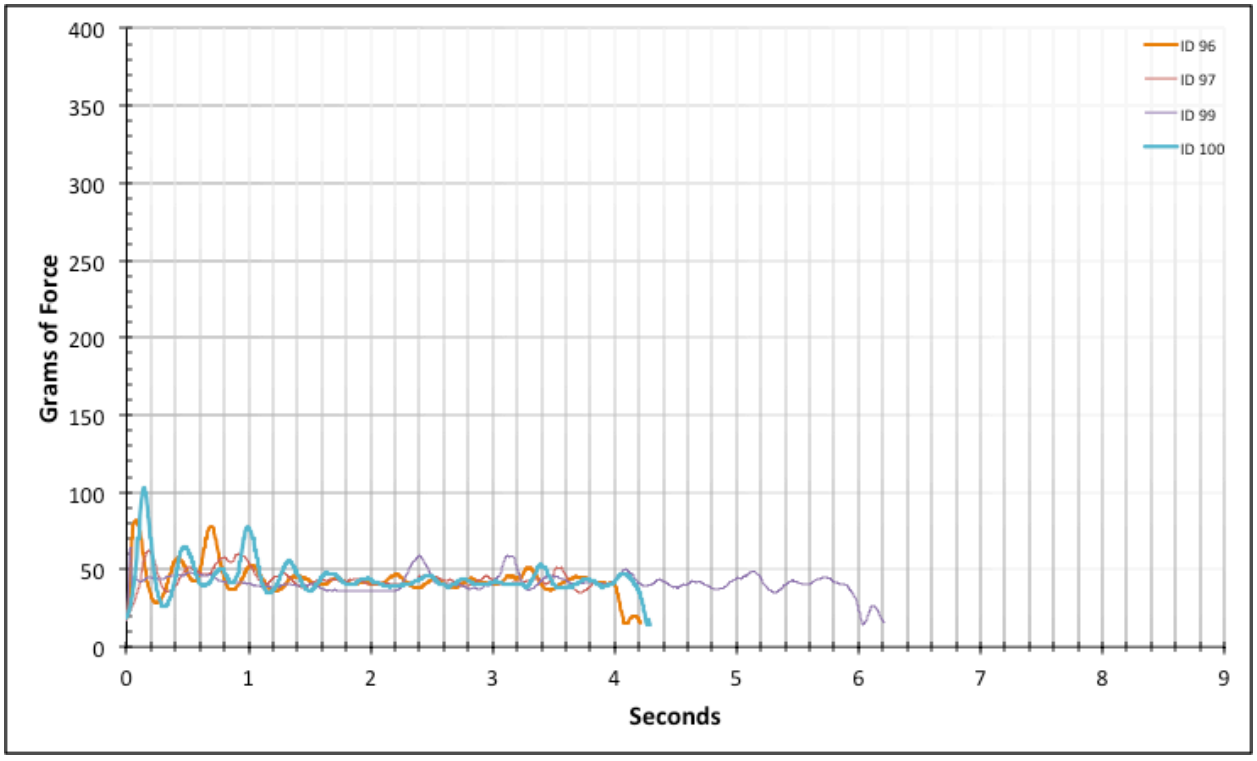

Figure 4-46: Full Composite Data for ID 96-100

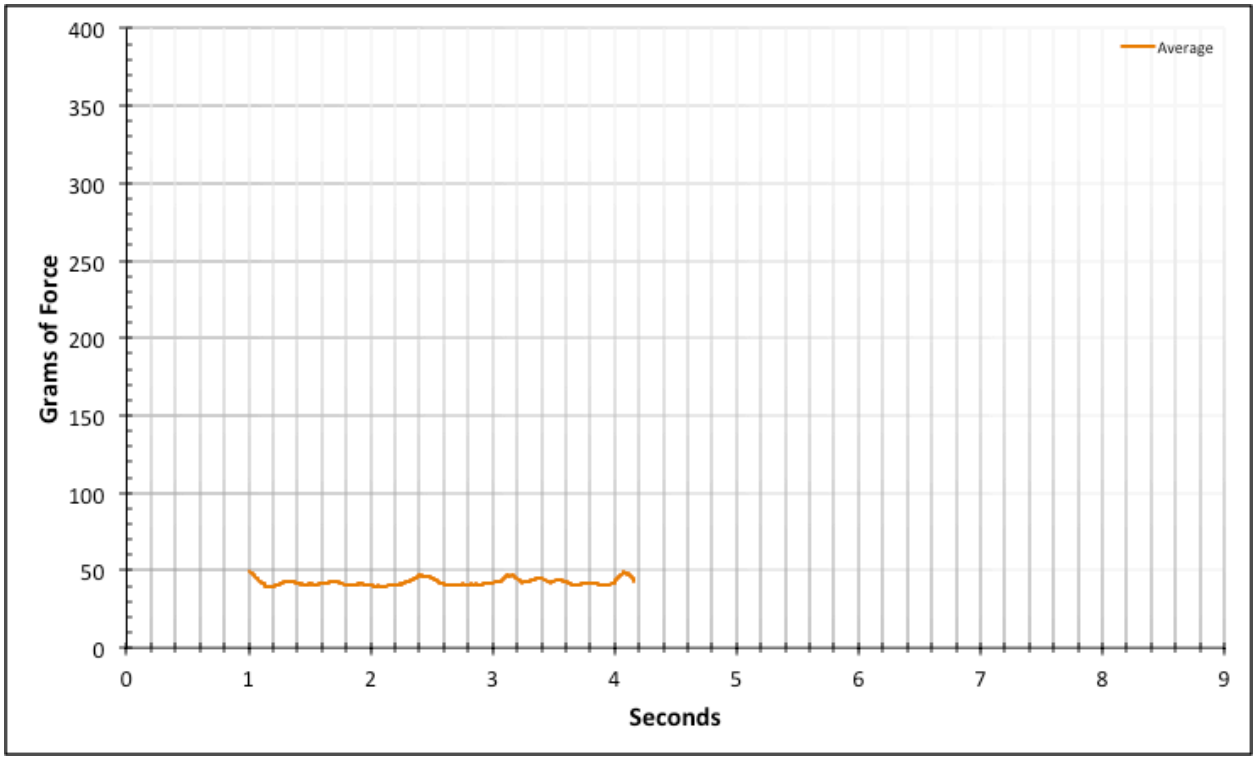

Figure 4-47: Regional Average Data for ID 96-100

The data sets for the #10 conductor and Bolts 1, 2, and 3 (ID 101 – ID 115) are consistent and free of systematic inconsistencies with expectations. Video 107 was subject to an unusual spiking of amplitude that was removed from the statistical data. The result from these data sets' region of interest is an expected frictional resistance of 95.5±0.3 grams.

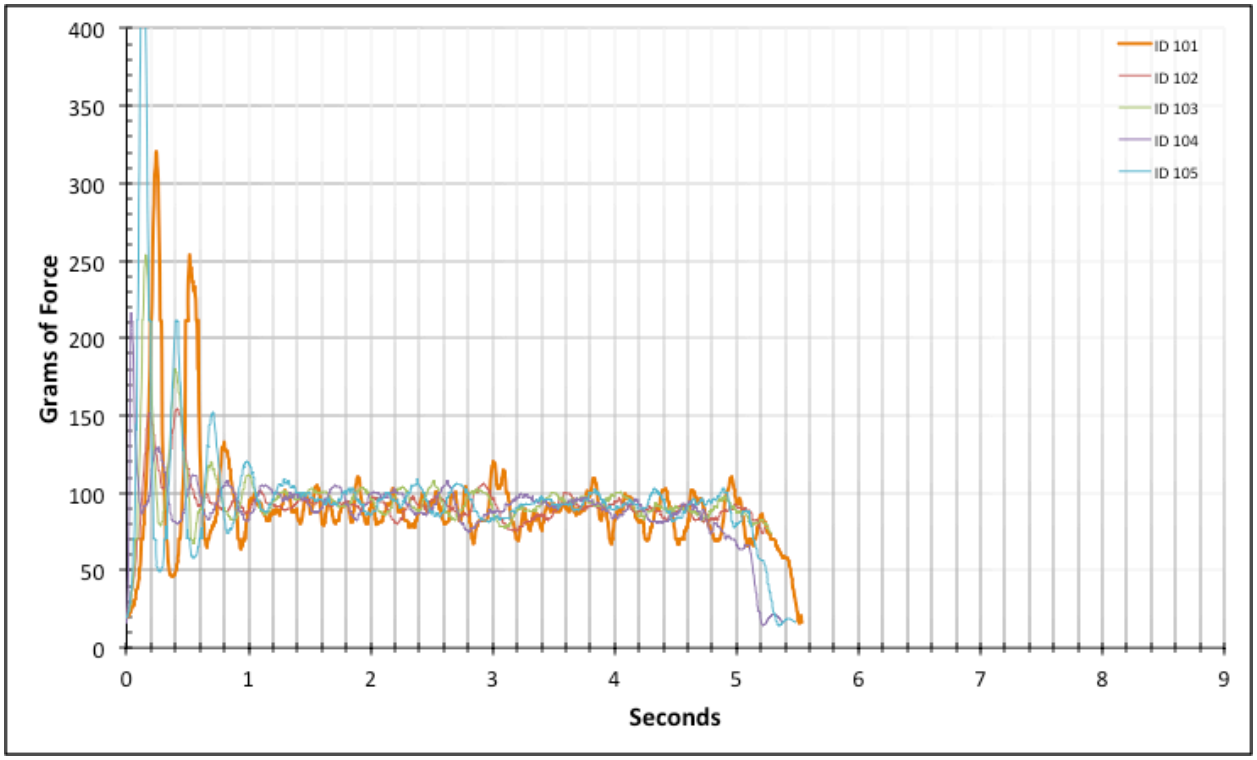

Figure 4-48: Full Composite Data for ID 101-105

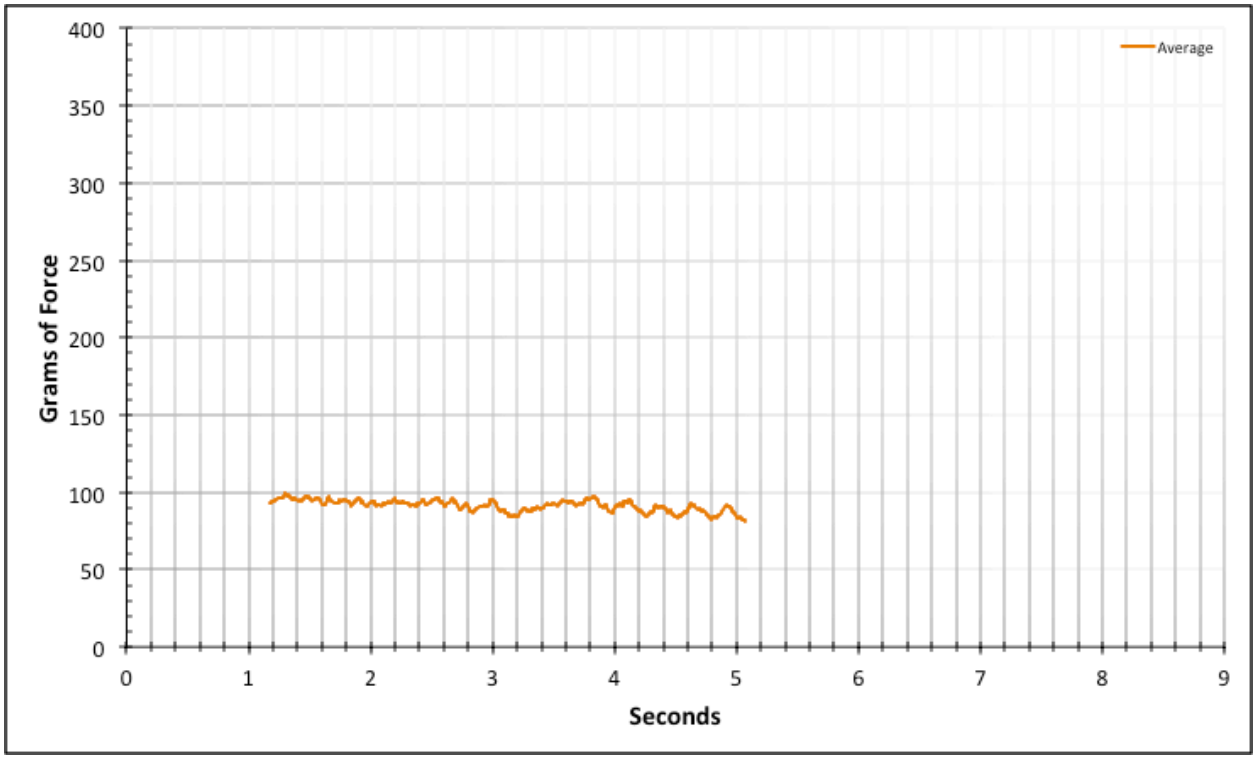

Figure 4-49: Regional Average Data for ID 101-105

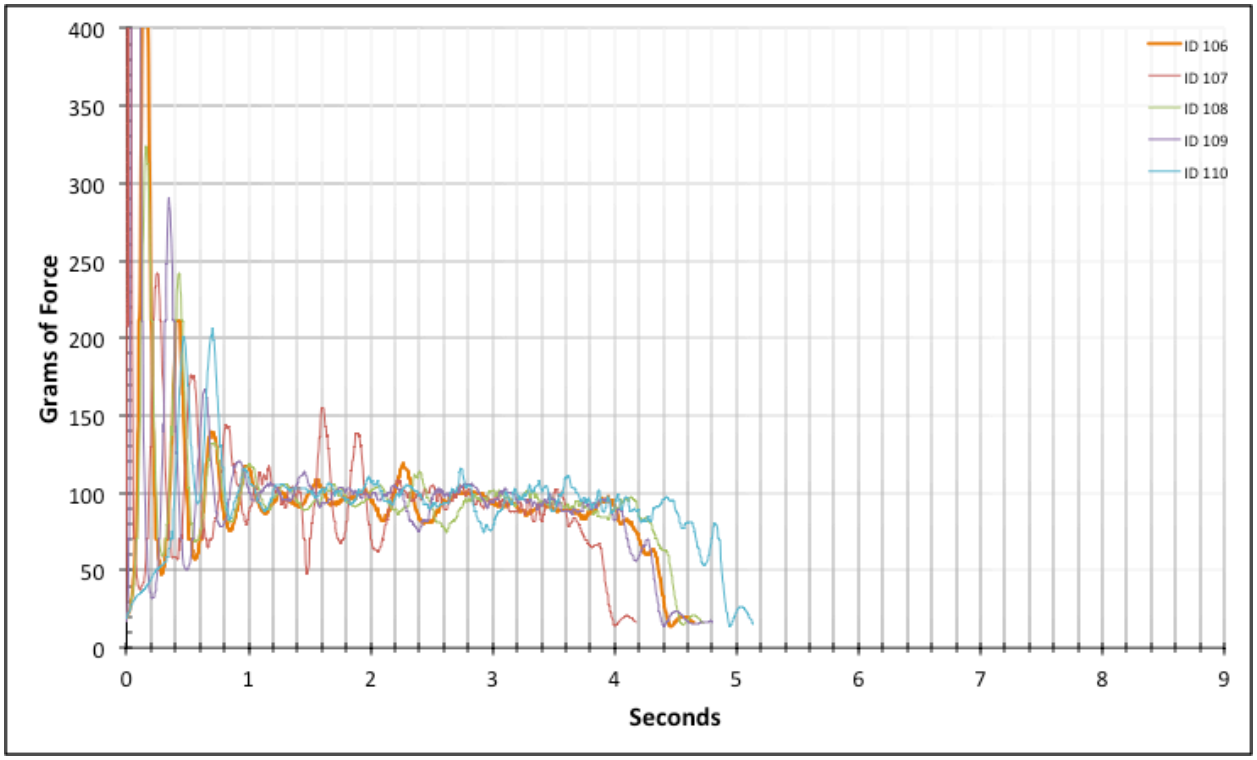

Figure 4-50: Full Composite Data for ID 106-110

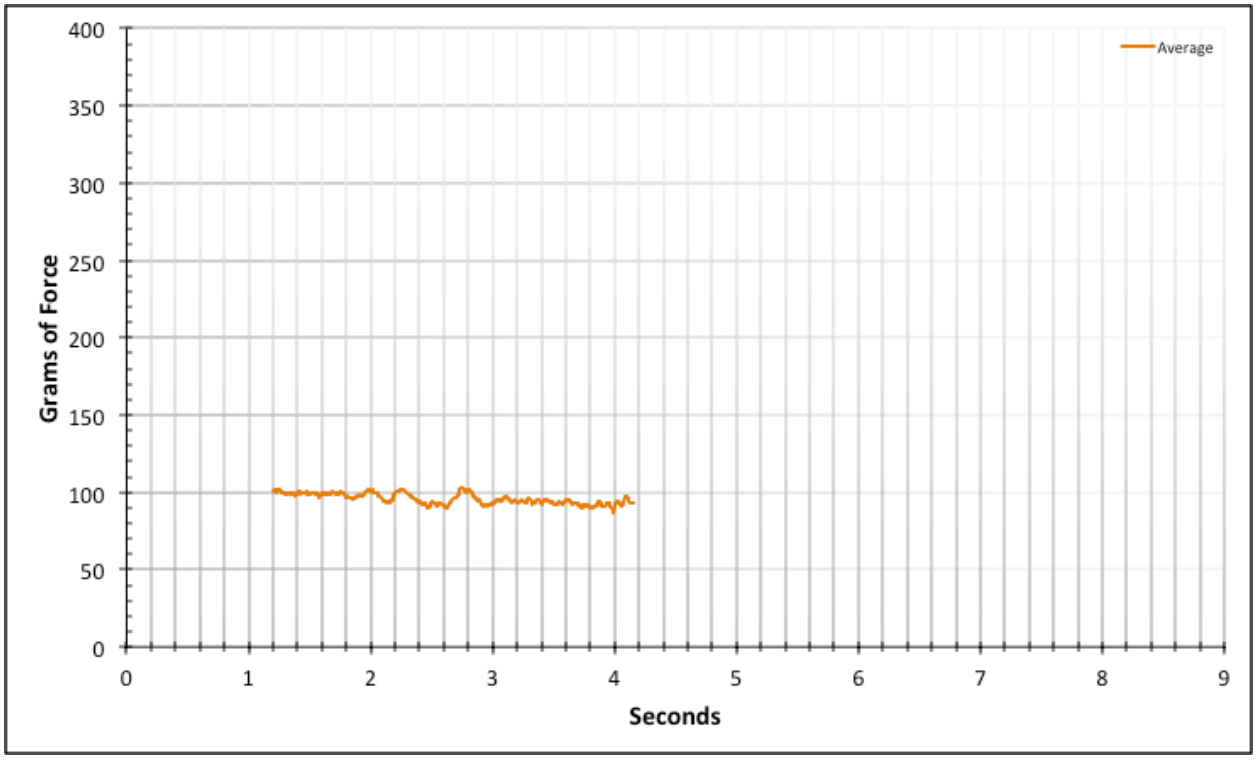

Figure 4-51: Regional Average Data for ID 106-110

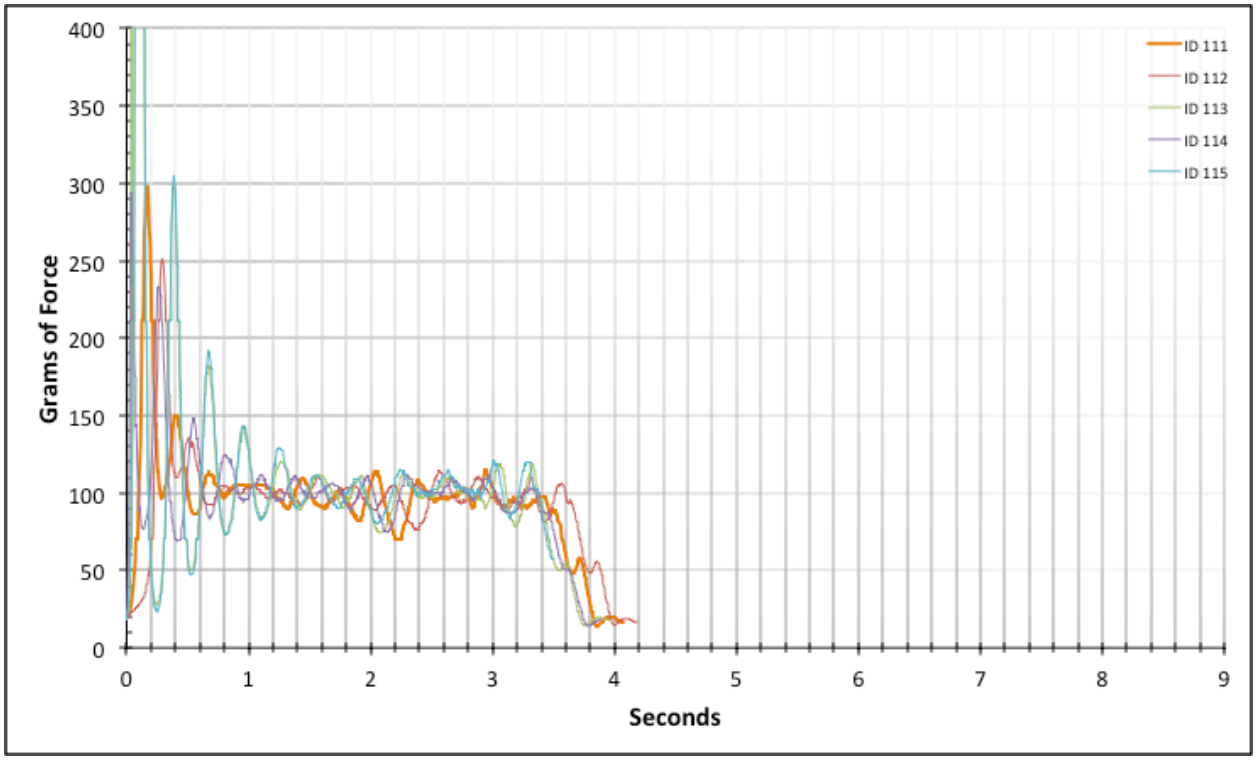

Figure 4-52: Full Composite Data for 111-115

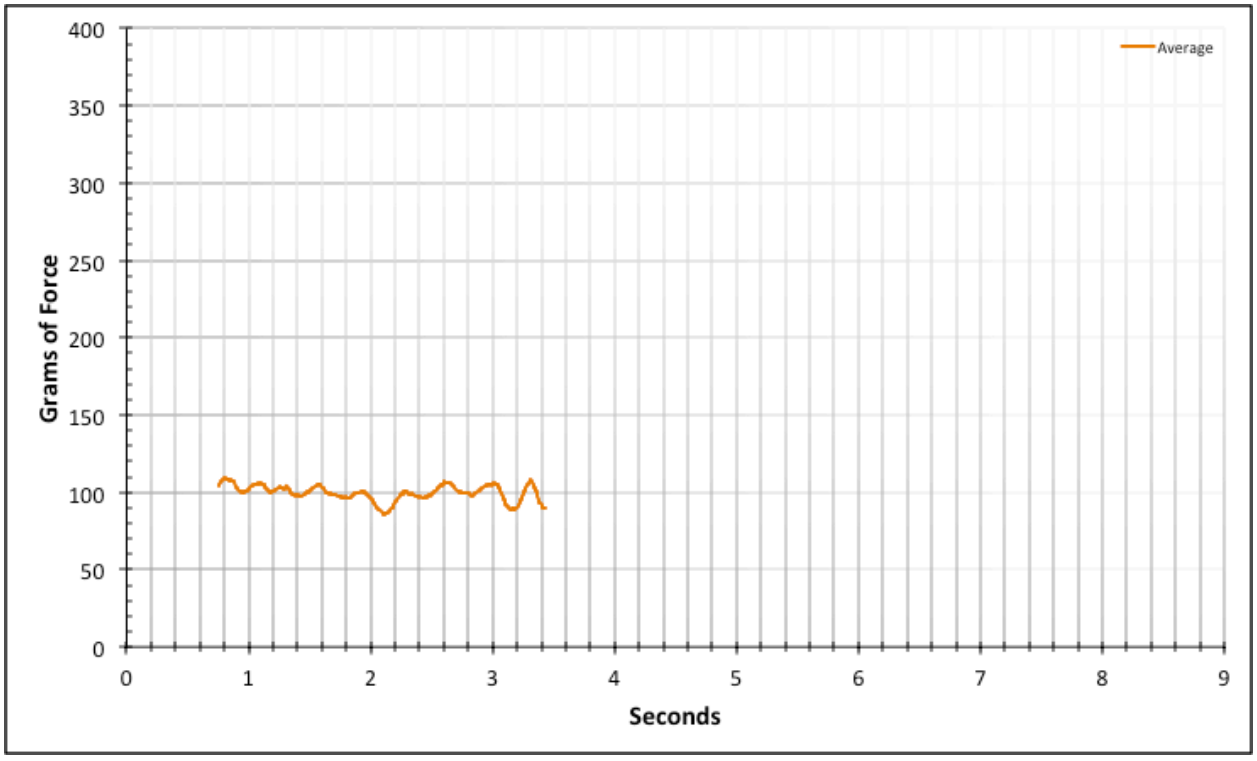

Figure 4-53: Regional Average Data for 111-115

The data set for the #8 conductor and Bolts 1, 2, and 3 (ID 116, ID 121, ID 126 – ID 130) is subject to a singular violent spike in amplitude that is likely a systematic catching of the conductor or conductor header on a break in the conduit. This systematic error is present in all trials in this data set. The error is omitted from the statistically processed data. This single set also varies from the previous conductors' data in this category because, during the experiment, it was realized that the pure friction force in this category is not depended on speed. Thus, one trial was run with each of Bolts 1 and 2 and a full five trials were conducted with Bolt #3. While it would have been more appropriate to run the five trials with Bolt 1 given that doing so would likely result in more data points and a lower standard deviation given the trend of the #12 and #10 conductor data sets, this fact was not known at the time Bolt 3 was selected. The results are still more than adequately precise for the necessity of this study. The pattern of running singular trials for Bolts 1 and 2 while running a full five trials with Bolt three is continued with all three conductors in lubricated straight baseline category. The singular trials are conducted for graphical verification of the theory that the resistance measured in the absence of the elbow is not dependent on speed. The following two graphs were composed using the data from this resulting seven-trial data set. The result from this data set's region of interest is an expected frictional resistance of 389.3±0.7 grams.

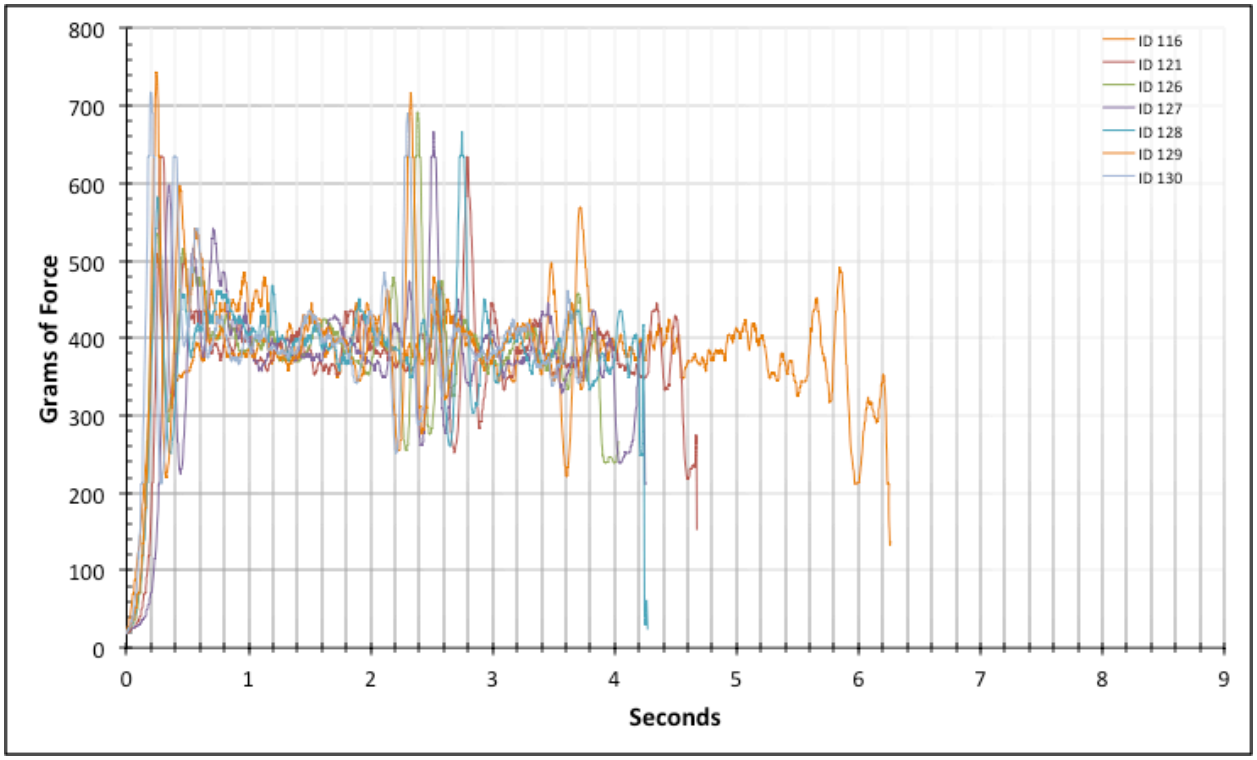

Figure 4-54: Full Composite Data for 116-130

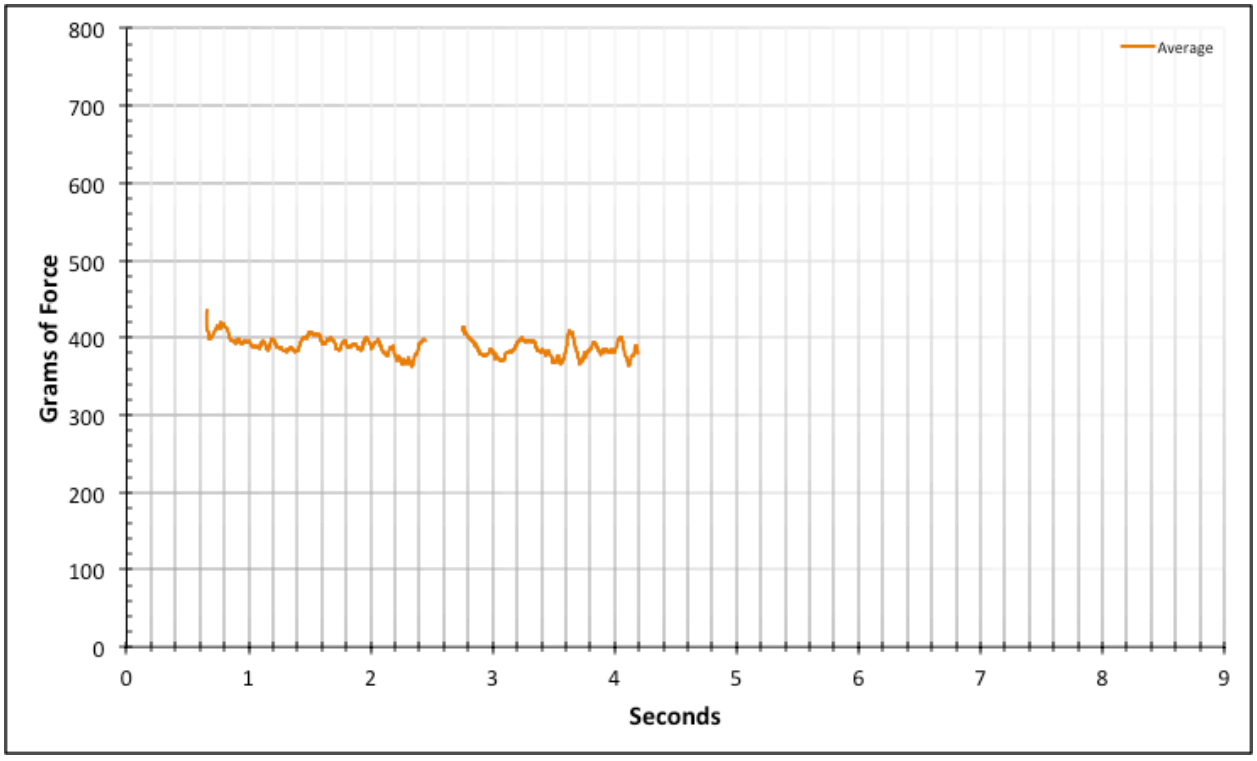

Figure 4-55: Regional Average Data for ID 116-130

4.1.4.4. Straight Baseline - Lubricated

The category includes videos 176 through 220 to cover the straight baseline category with the application of lubricant. The data set for the #12 conductor (ID 176 – ID 190) is consistent but not quite as much as its un-lubricated counterpart. This is a theme generally continued throughout the remaining data sets. It appears as though the introduction of lubricant creates and inherent inconsistency as the behavior and predictability of the lubricant is significantly more variable than cases defined by its absence. The result from this data set's region of interest is an expected frictional resistance of 49.9±0.1 grams.

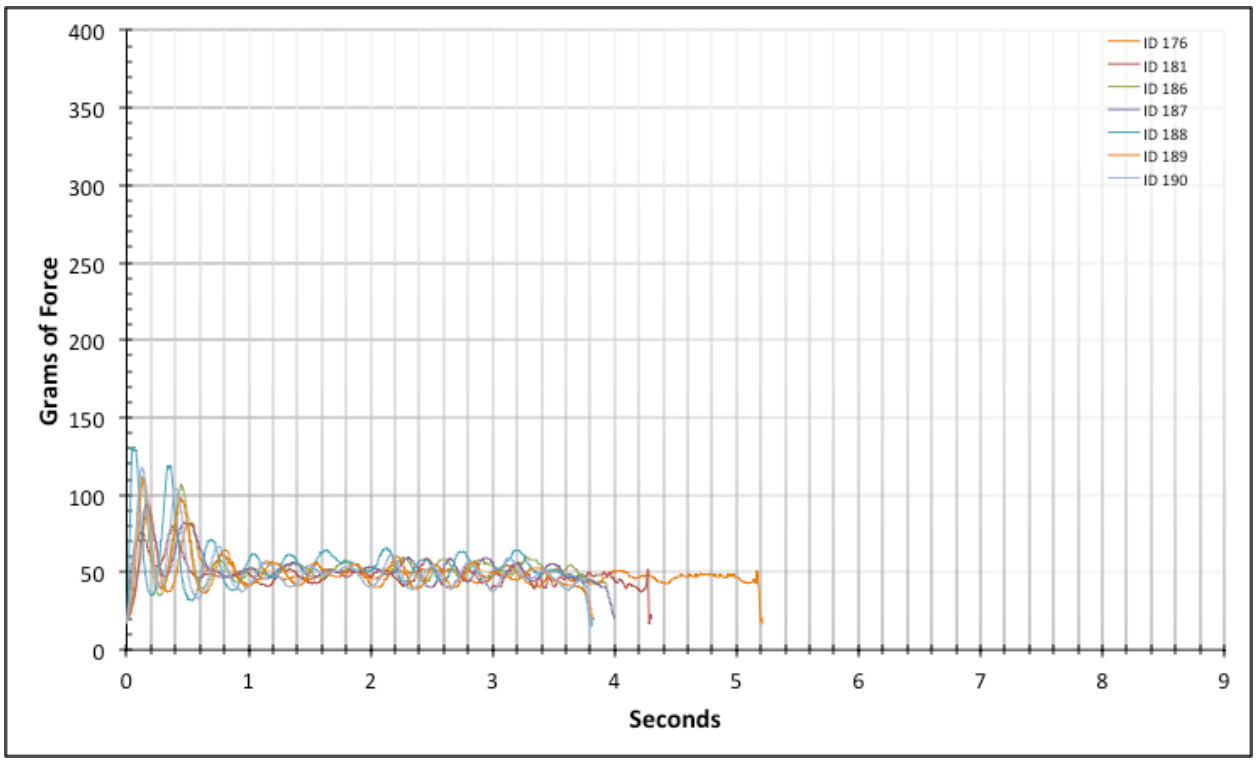

Figure 4-56: Full Composite Data for ID 176-190

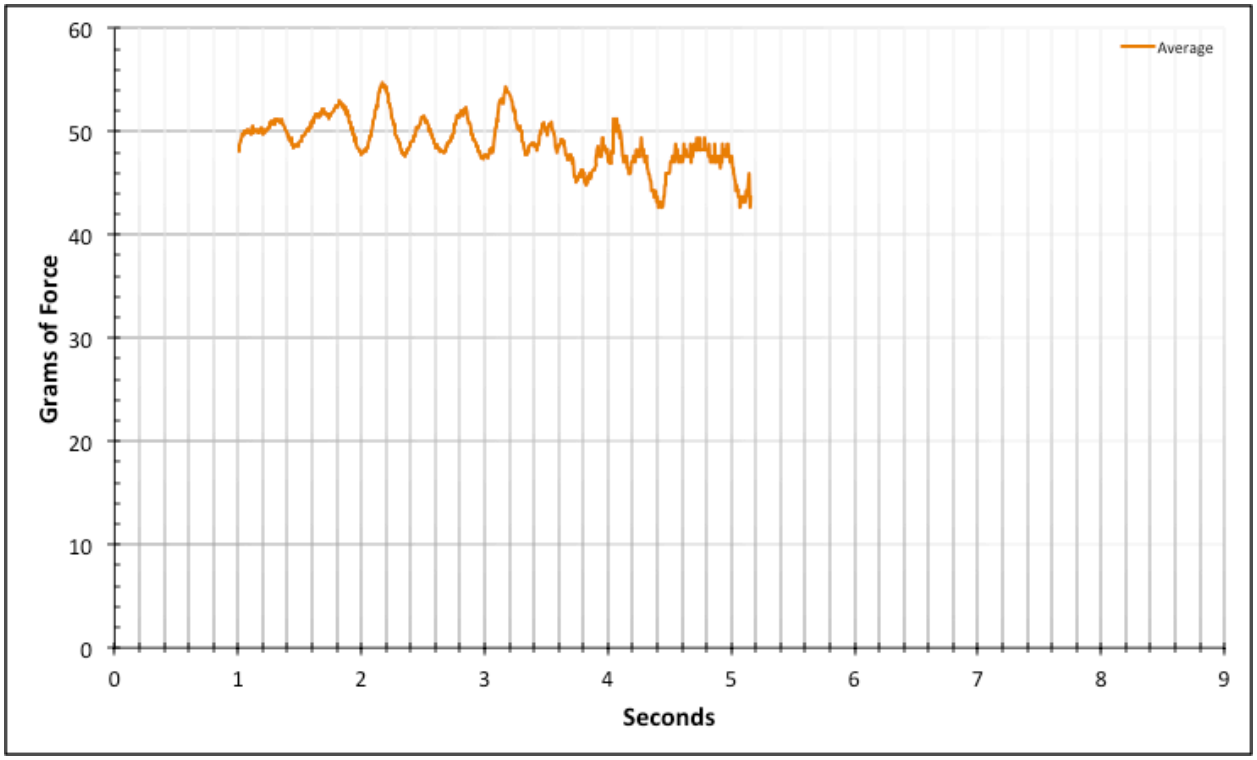

Figure 4-57: Regional Average Data for ID 176-190

The data set for the #10 conductor (ID 191 – ID 205) is consistent but resulting in a negative notable slope unlike the nearly flat data sets before it. This data set is still treated the same way for the sake of analysis, but the slope indicates that the conductor slides more easily with the passage of time, as the lubricant must be redistributing in a manner that results in lower resistance with the progression of time. This evidence is not enough to establish a definitive trend as the parameters that would impact the slope of the data and the behavior of the lubricant are not isolated, recorded, or of significant interest to this study. The result from this data set's region of interest is an expected frictional resistance of 71.9±0.3 grams.

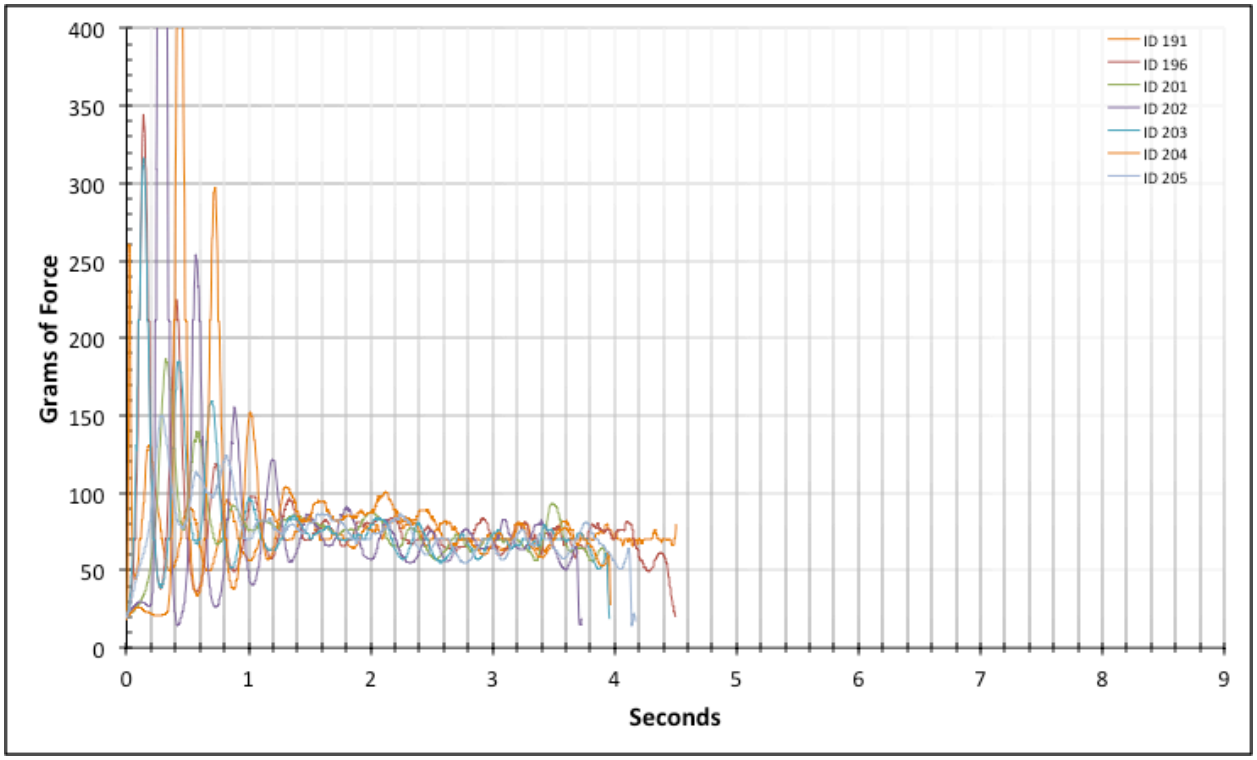

Figure 4-58: Full Composite Data for ID 191-205

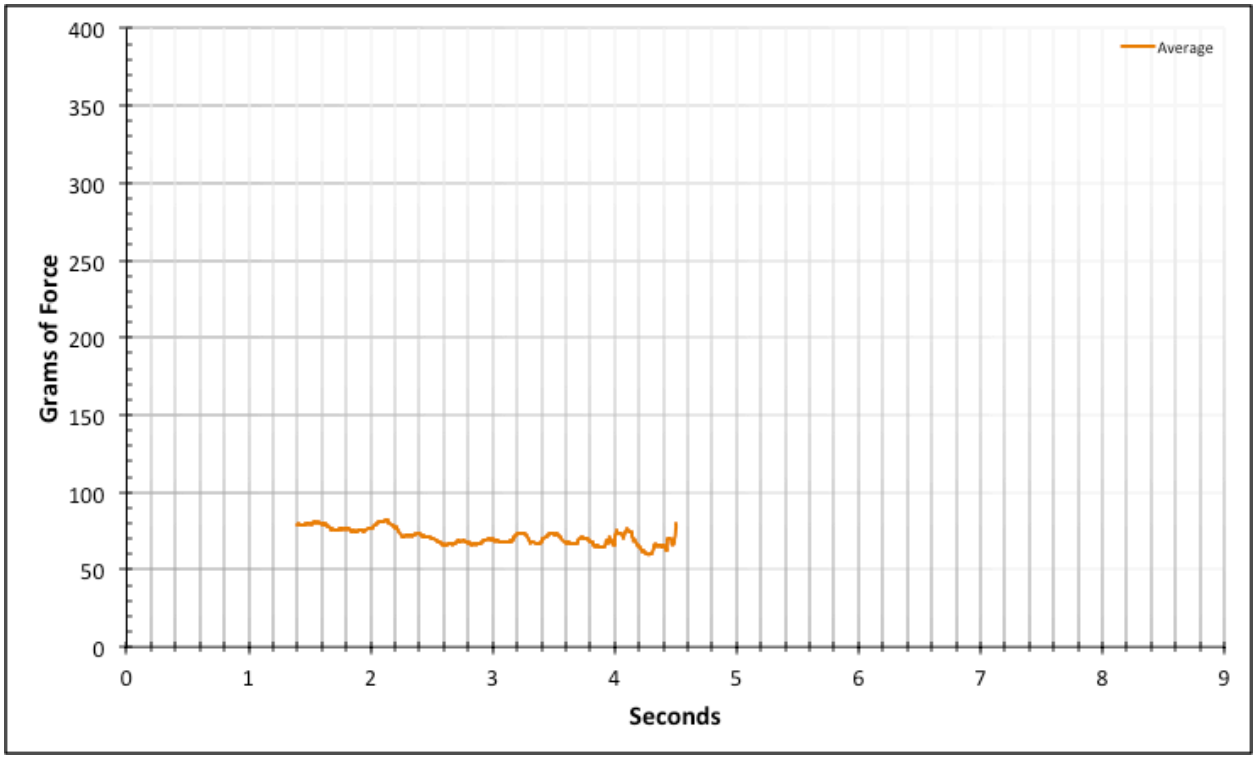

Figure 4-59: Regional Average Data for ID 191-205

The data set for the #8 conductor (ID 206 – ID 215) is mostly consistent but suffers from the same systematic spike in amplitude that its un-lubricated counterpart experienced. This indicates that there is indeed a systematic catch between the #8 conductor or conductor header tested in both trials and the conduit. The systematic error is omitted from the statistically analyzed data. This data also results in a slight positive slope implying the possibility of the lubricant redistributing in a manner that increases frictional resistance with increasing time with the heavier conductor. This further highlights the inconsistency introduced by the complicated parameters on which lubricant depends. Regardless, the treatment of the data is the same as the slope is considered negligible and reflective of the behavior that this test statistic should capture. The result from this data set's region of interest is an expected frictional resistance of 327.0±0.7 grams.

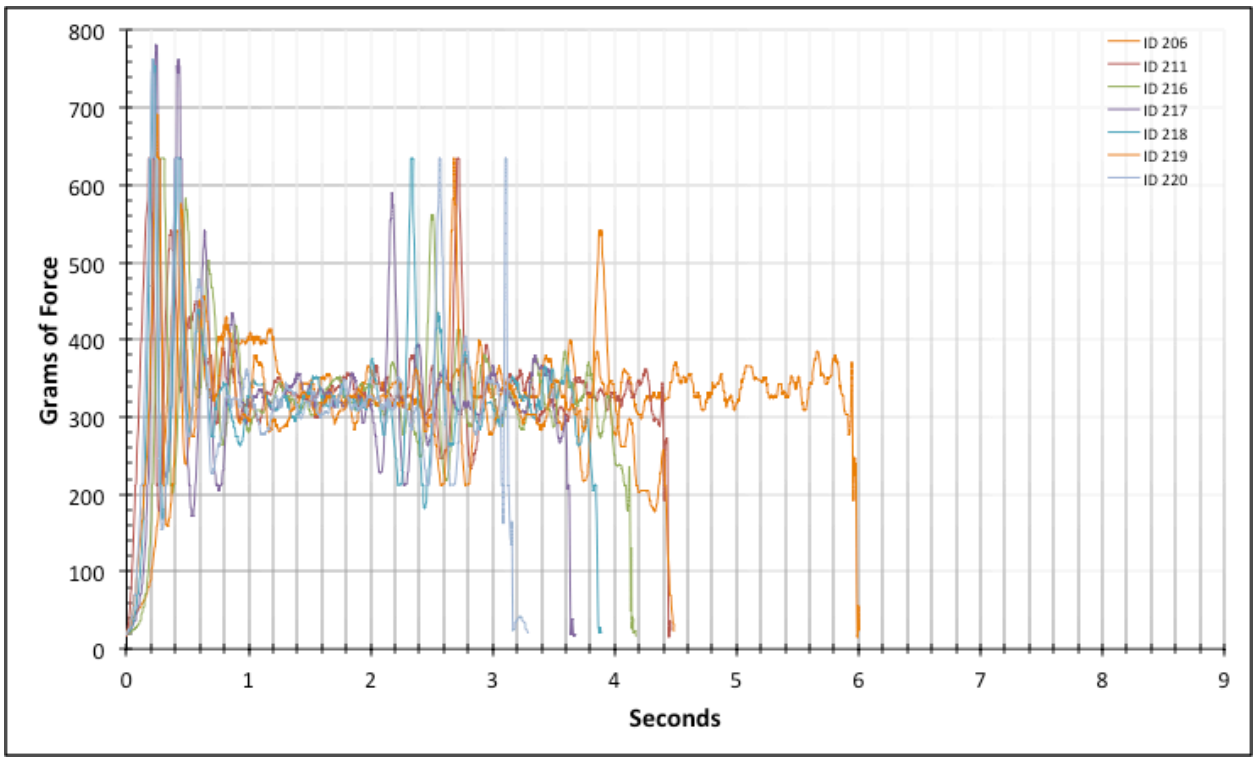

Figure 4-60: Full Composite Data for ID 206-220

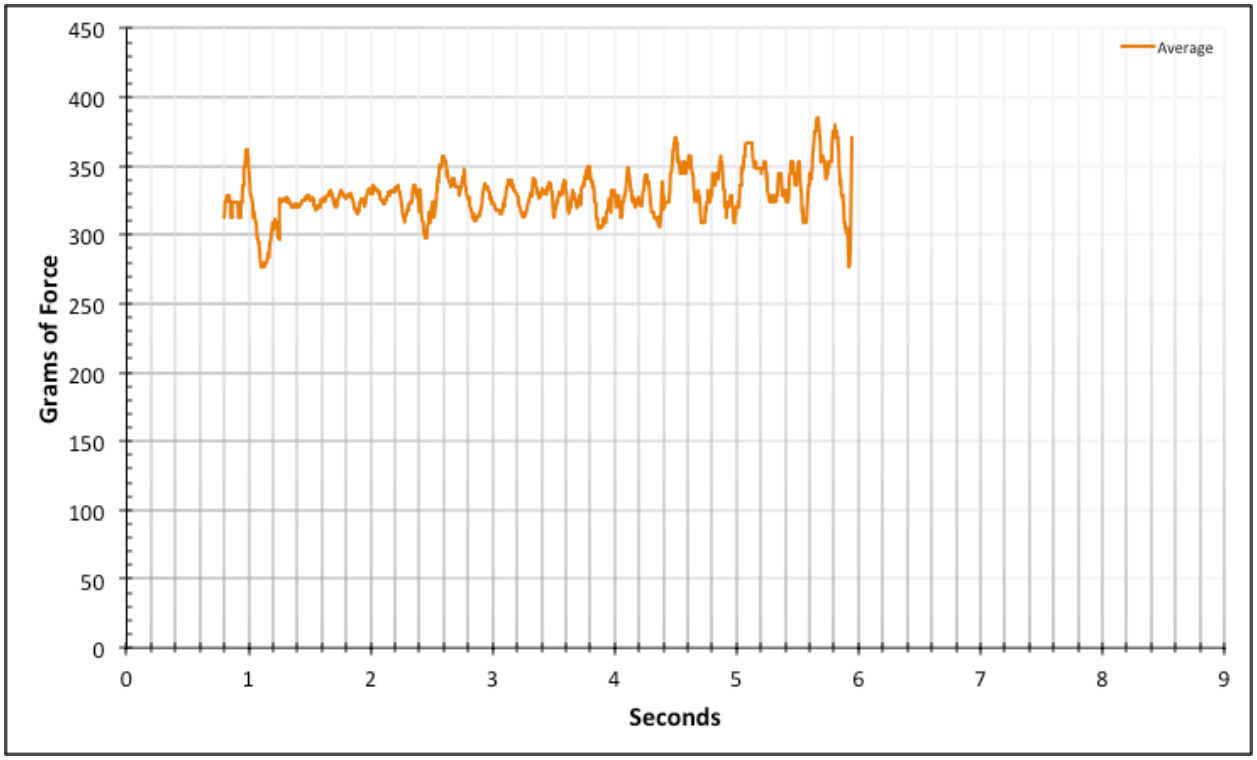

Figure 4-61: Regional Average Data for ID 206-220

4.1.4.5. Modeled Product - Lubricated

The category includes videos 221 through 265 to cover the modeled product category with the application of lubricant. The data set for the #12 conductor and Bolt 1 (ID 221 – ID 225) is relatively consistent in amplitude throughout Region 2. The smoother results indicate a reduction in oscillation driving defects and/or an increase in damping. Upon further comparison to relatable trials, the cleaner results here are most likely due to a reduction of interaction from physical defects in the system. The result from this data set's Region 2 is an expected frictional resistance of 85.5±0.4 grams.

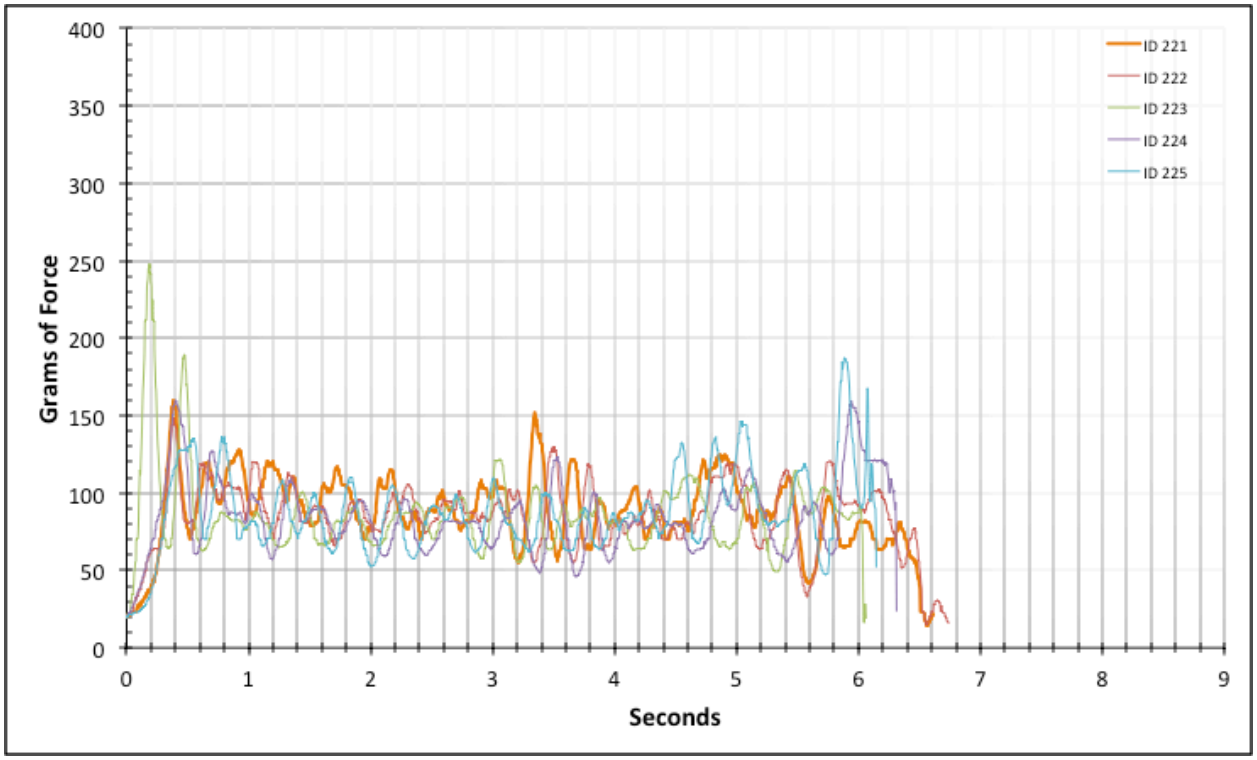

Figure 4-62: Full Composite Data for ID 221-225

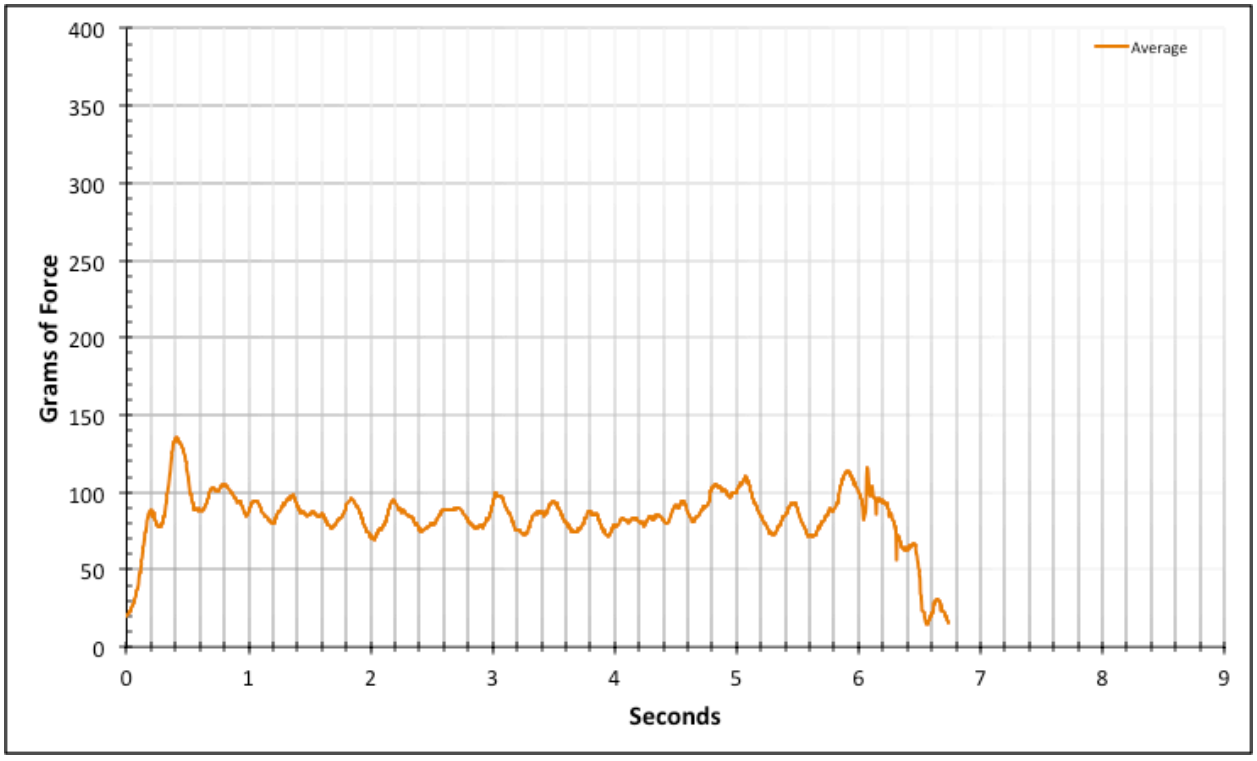

Figure 4-63: Full Average Data for 221-225

The data set for the #12 conductor and Bolt 2 (ID 226 – ID 230) is relatively consistent in amplitude throughout Region 2. There is a singular spike from video 226 that is identified as an experimental anomaly. This anomaly is excluded from the statistical data. The result from this data set's Region 2 is an expected frictional resistance of 83.3±0.5 grams.

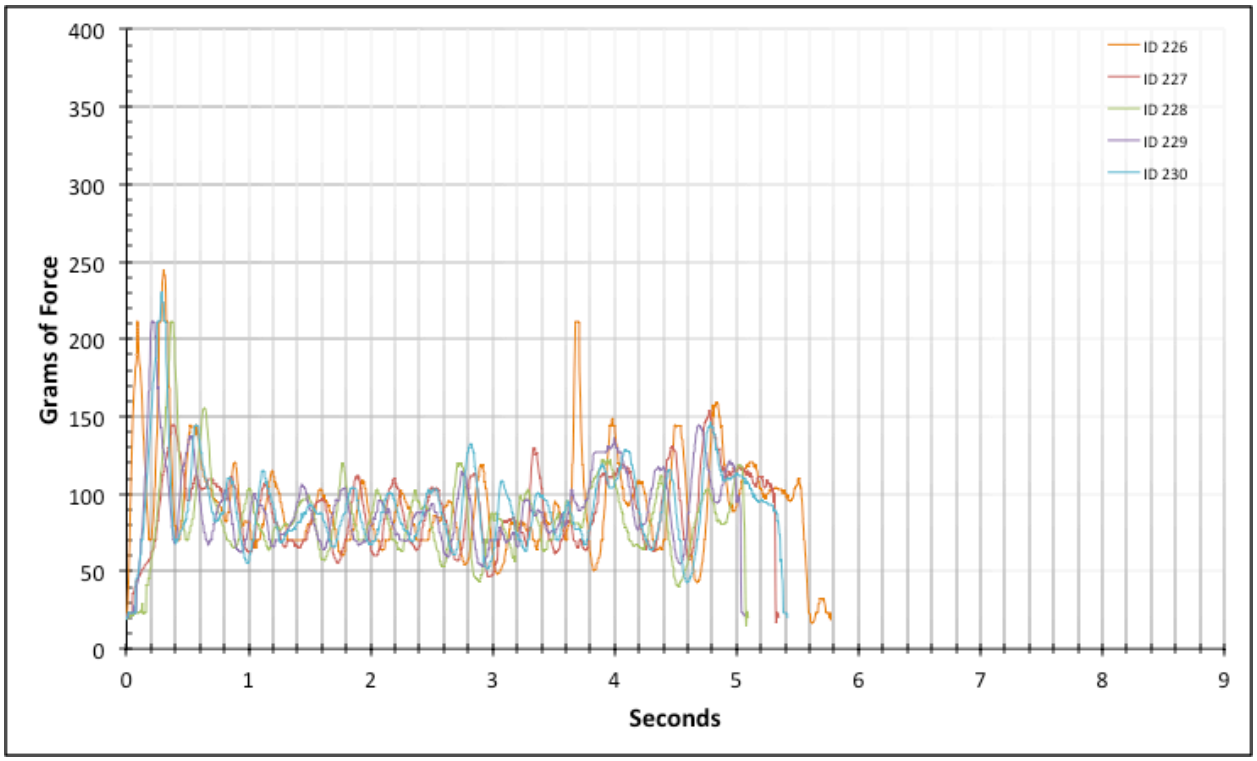

Figure 4-64: Full Composite Data for ID 226-230

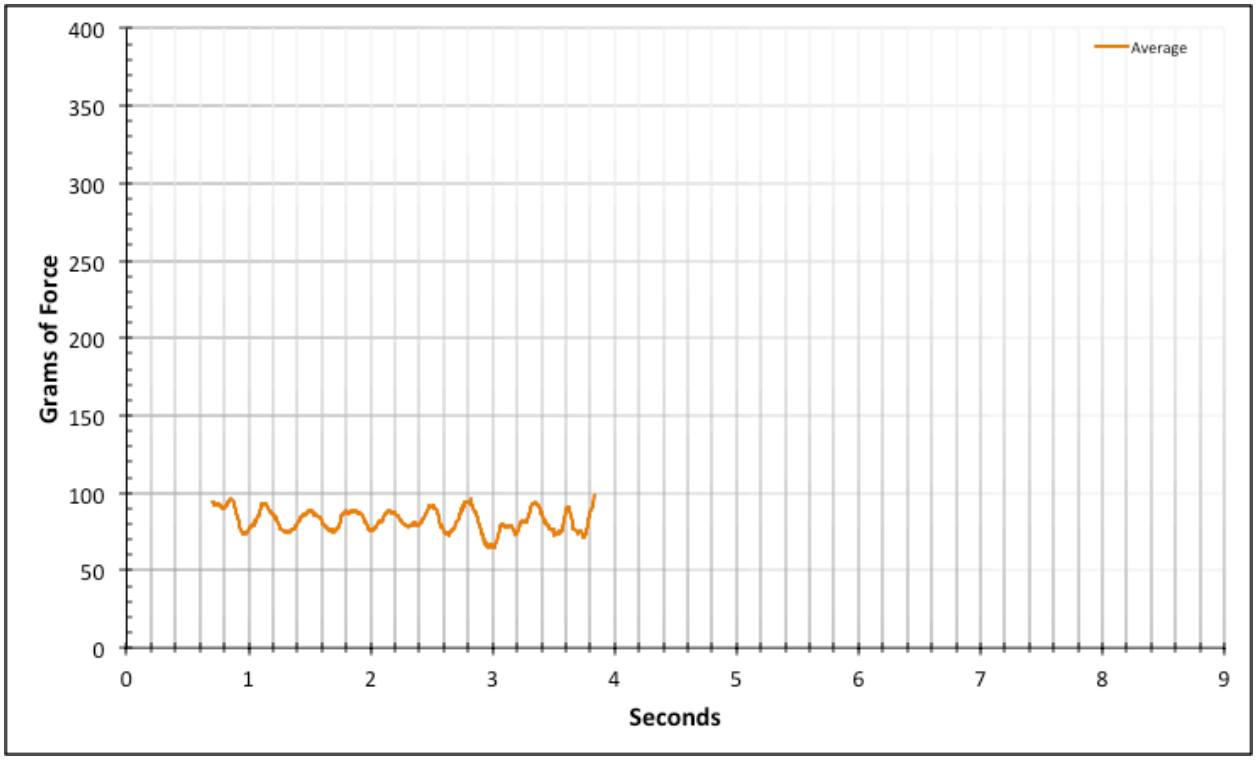

Figure 4-65: Region 2 Average Data for 226-230

The data set for the #12 conductor and Bolt 3 (ID 231 – ID 235) is relatively consistent in amplitude throughout Region 2. Video 231 is of higher amplitude throughout all of Region 2 than the rest of the videos in this data set. The result from this data set's Region 2 is an expected frictional resistance of 78.7.3±0.6 grams.

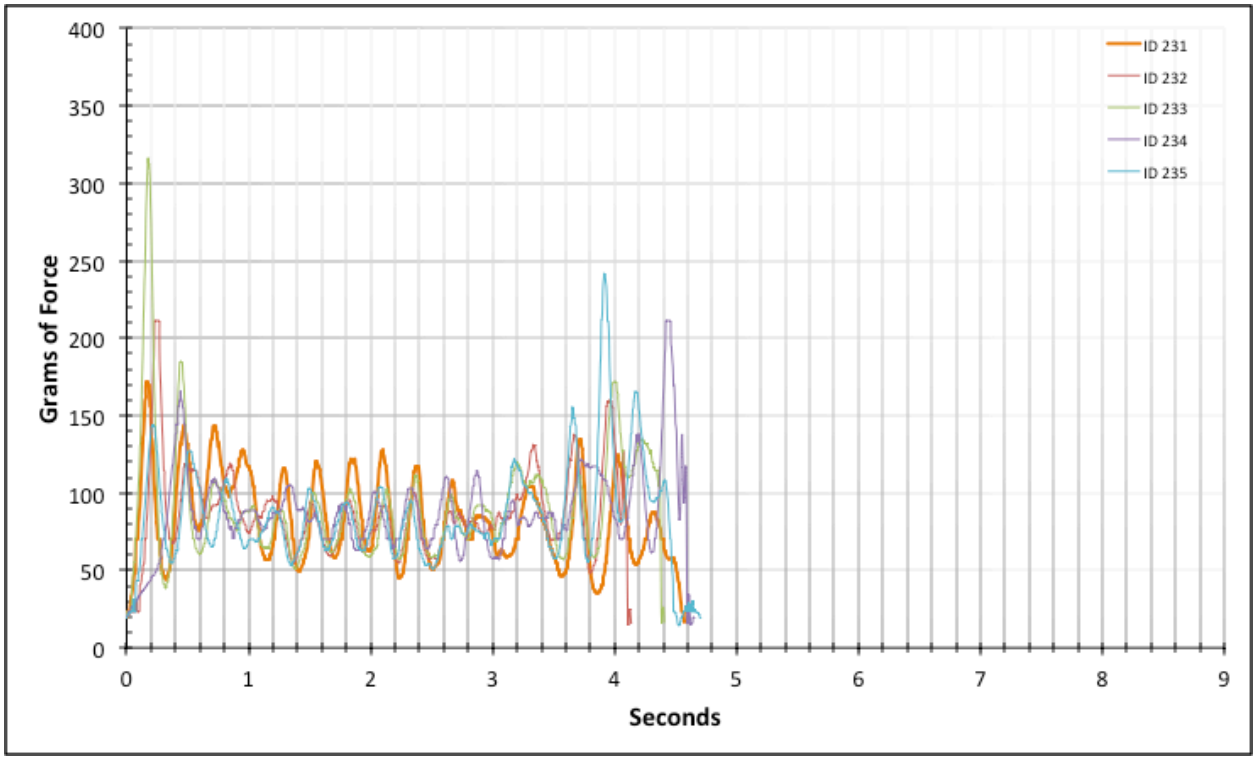

Figure 4-66: Full Composite Data for ID 231-235

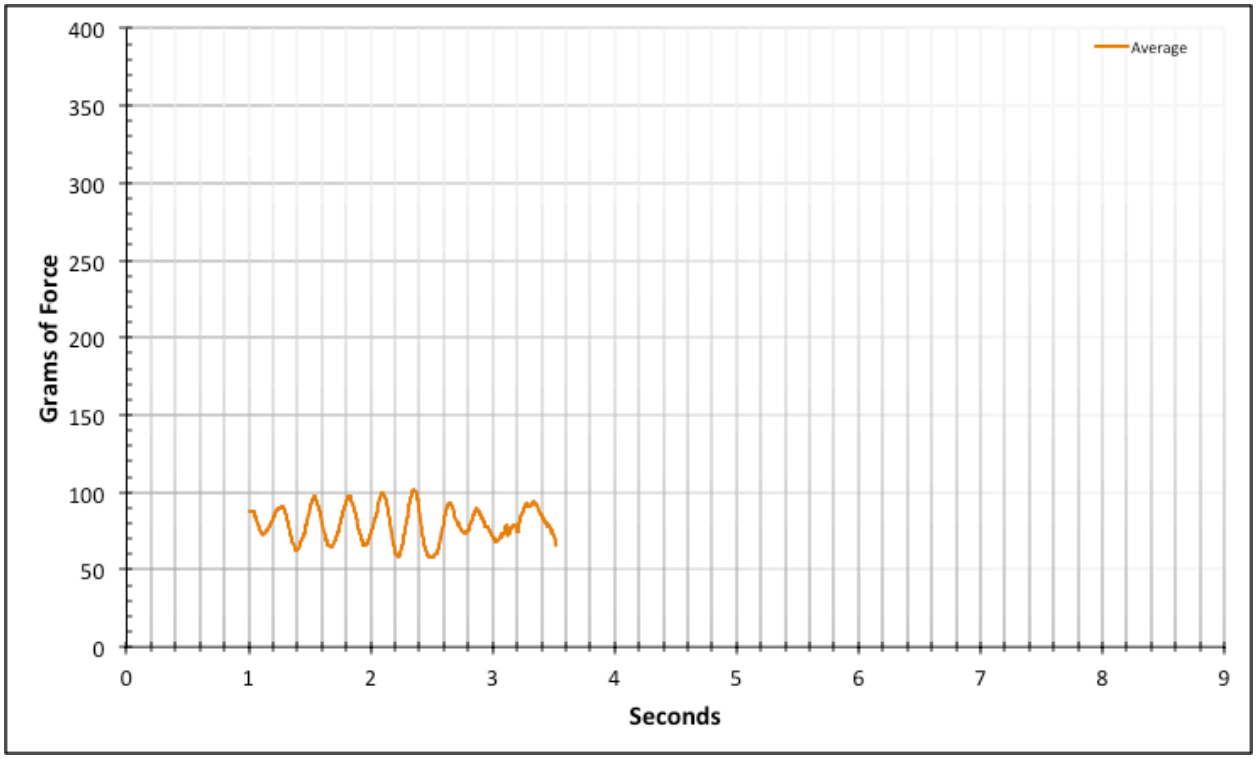

Figure 4-67: Region 2 Average Data for ID 231-235

The data set for the #10 conductor and Bolt 1 (ID 236 – ID 240) is relatively consistent in amplitude throughout Region 2. However, this data set is subject to the flat spot error as can be seen near the center of Region 2. The result from this data set's Region 2 is an expected frictional resistance of 203.4±1.0 grams.

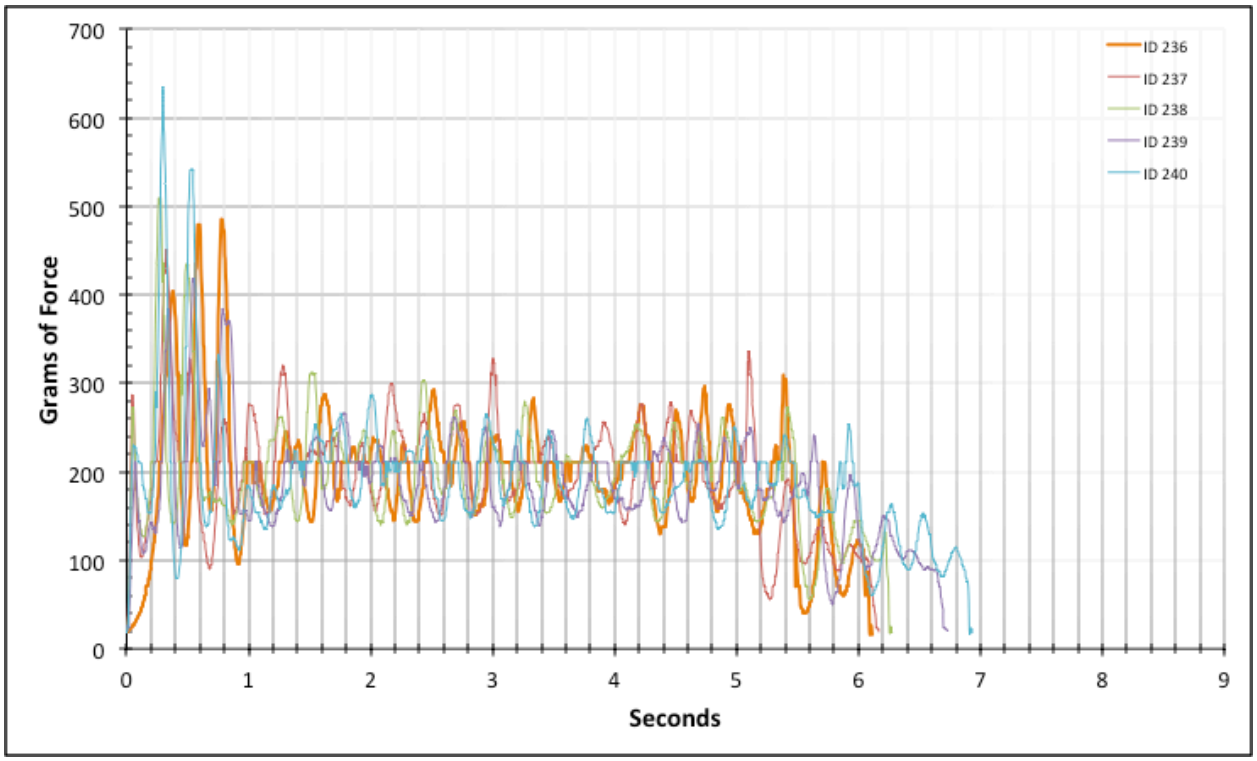

Figure 4-68: Full Composite Data for ID 236-240

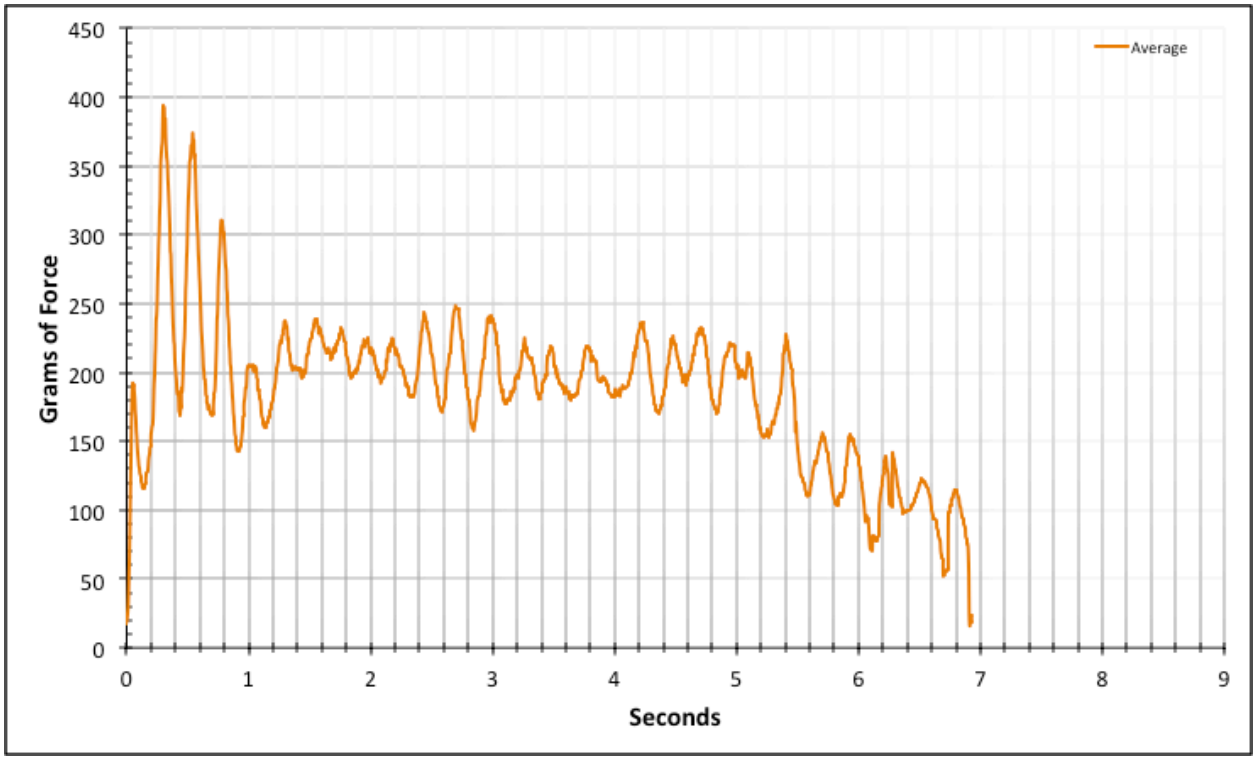

Figure 4-69: Full Average Data for ID 236-240

The data set for the #10 conductor and Bolt 2 (ID 241 – ID 245) is notably noisy yet consistent throughout Region 2. This data set is also subject to the flat spot error as can be seen near the center of Region 2. The result from this data set's Region 2 is an expected frictional resistance of 196.1±1.0 grams.

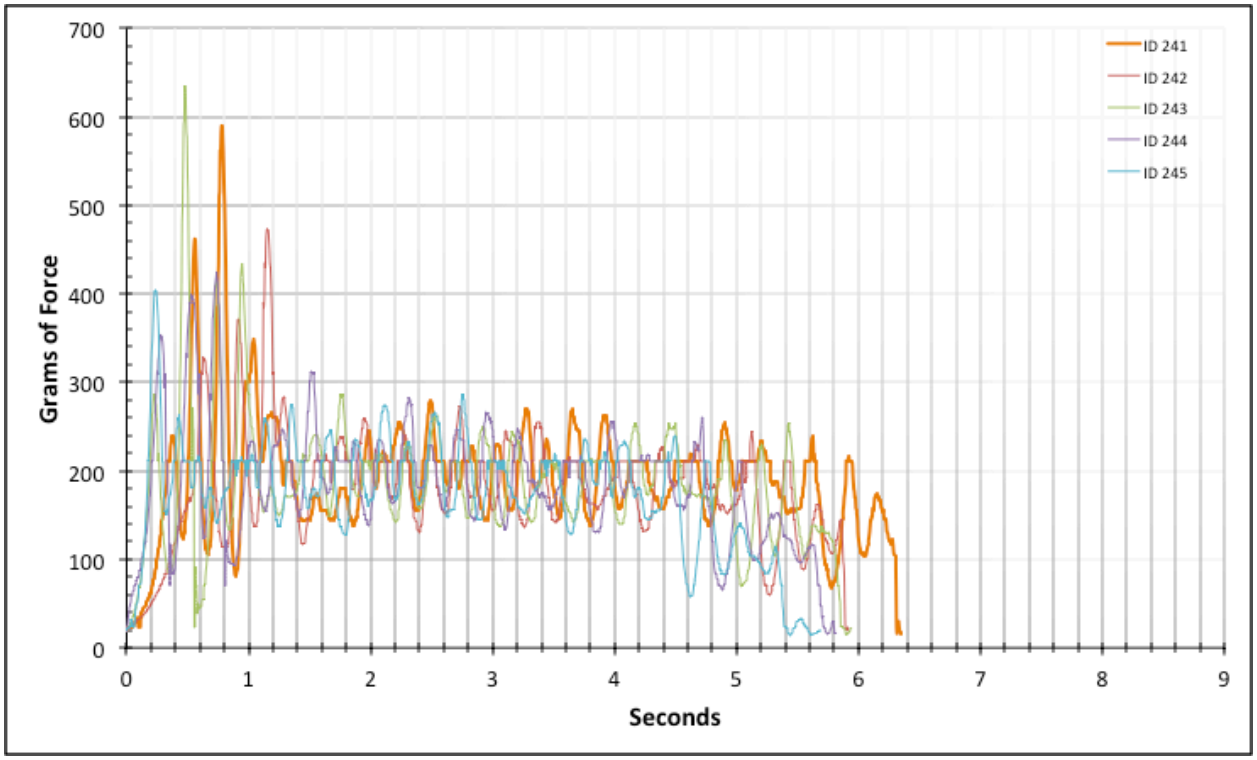

Figure 4-70: Full Composite Data for ID 241-245

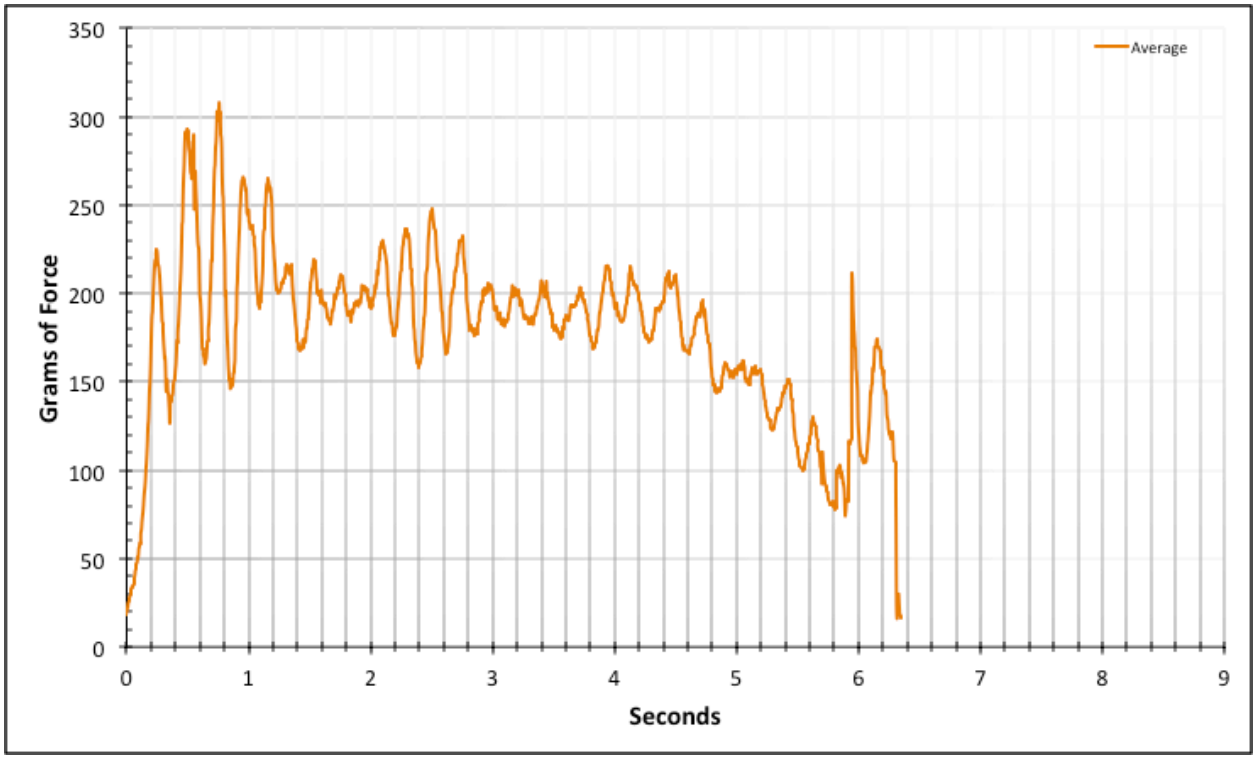

Figure 4-71: Full Average Data for ID 241-245

The data set for the #10 conductor and Bolt 3 (ID 246 – ID 250) is slightly noisier than the previous data set. The cause is possibly due to the increase in speed from Bolt 2 to Bolt 3. This data set is also subject to the flat spot error as can be seen near the center of Region 2. The result from this data set's Region 2 is an expected frictional resistance of 196.0±1.1 grams.

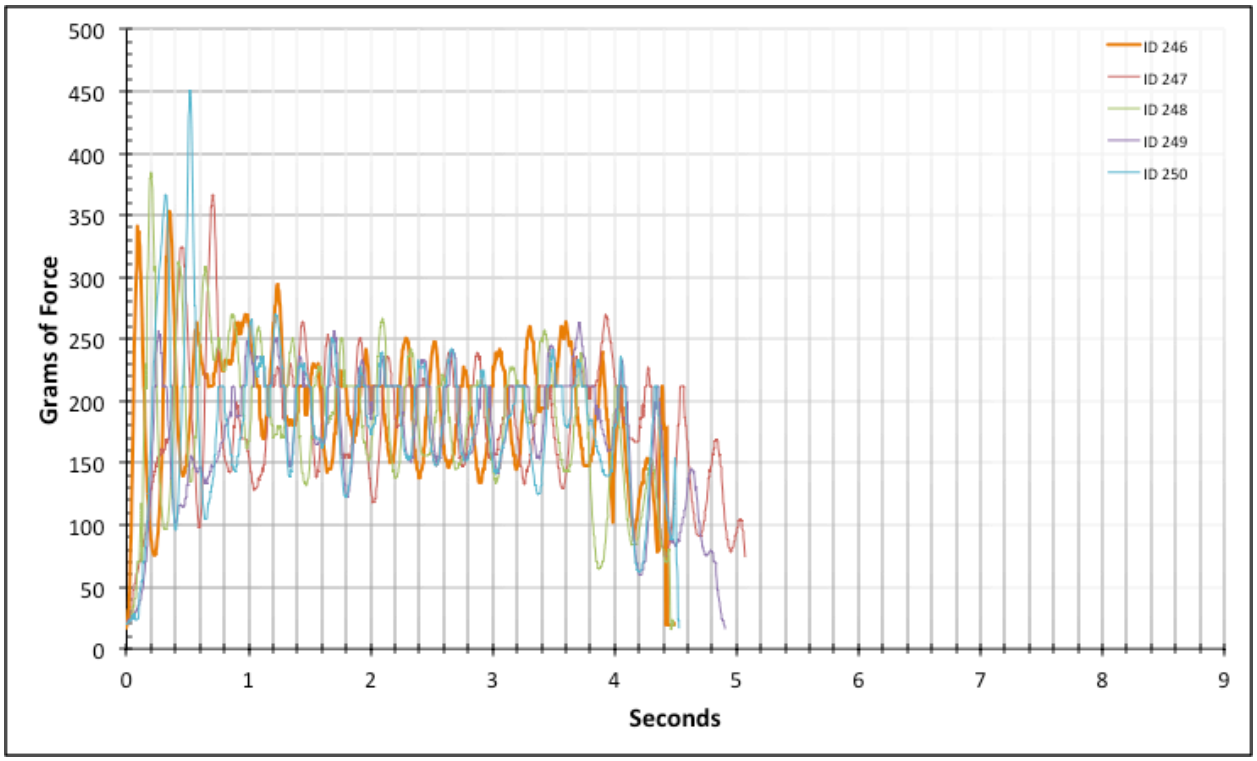

Figure 4-72: Full Composite Data for ID 246-250

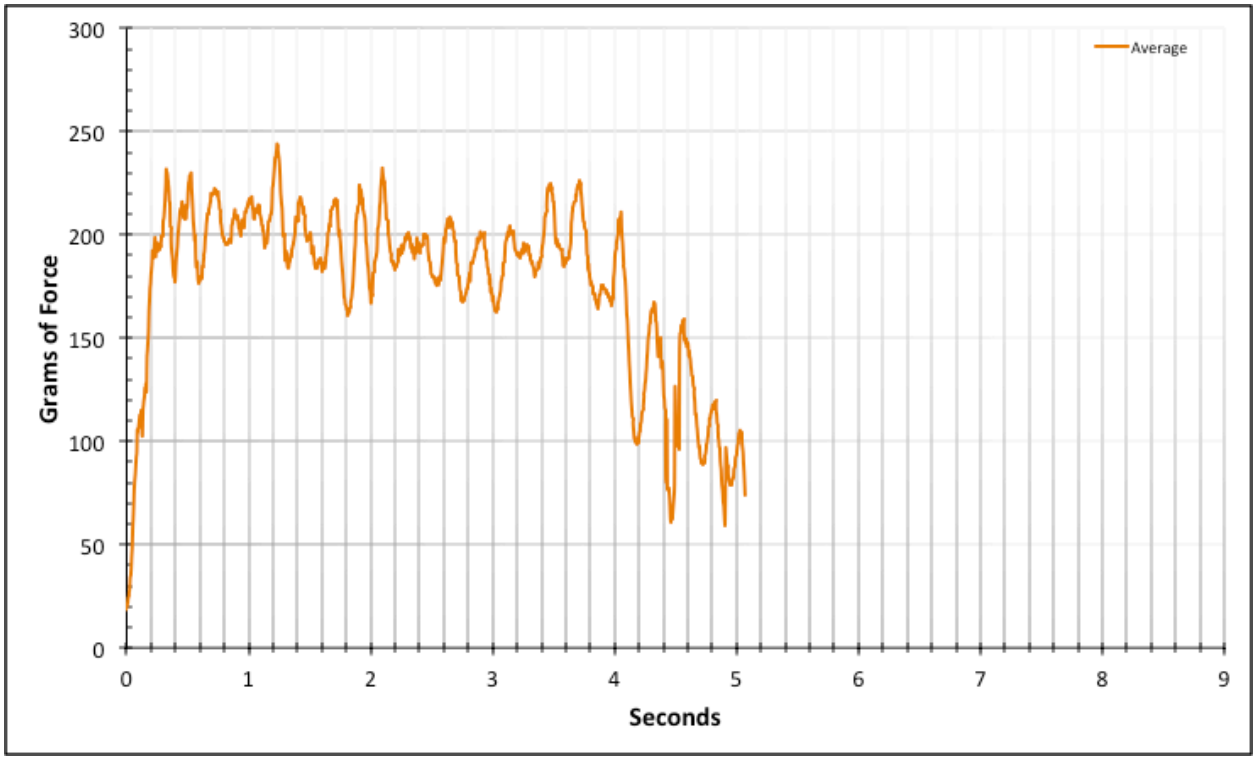

Figure 4-73: Full Average Data for ID 246-250

The data set for the #8 conductor and Bolt 1 (ID 251 – ID 255) is victim to ample noise and flat spot error. This error is appears to be giving the data an inflated value. The result from this data set's Region 2 is an expected frictional resistance of 524.8±1.6 grams

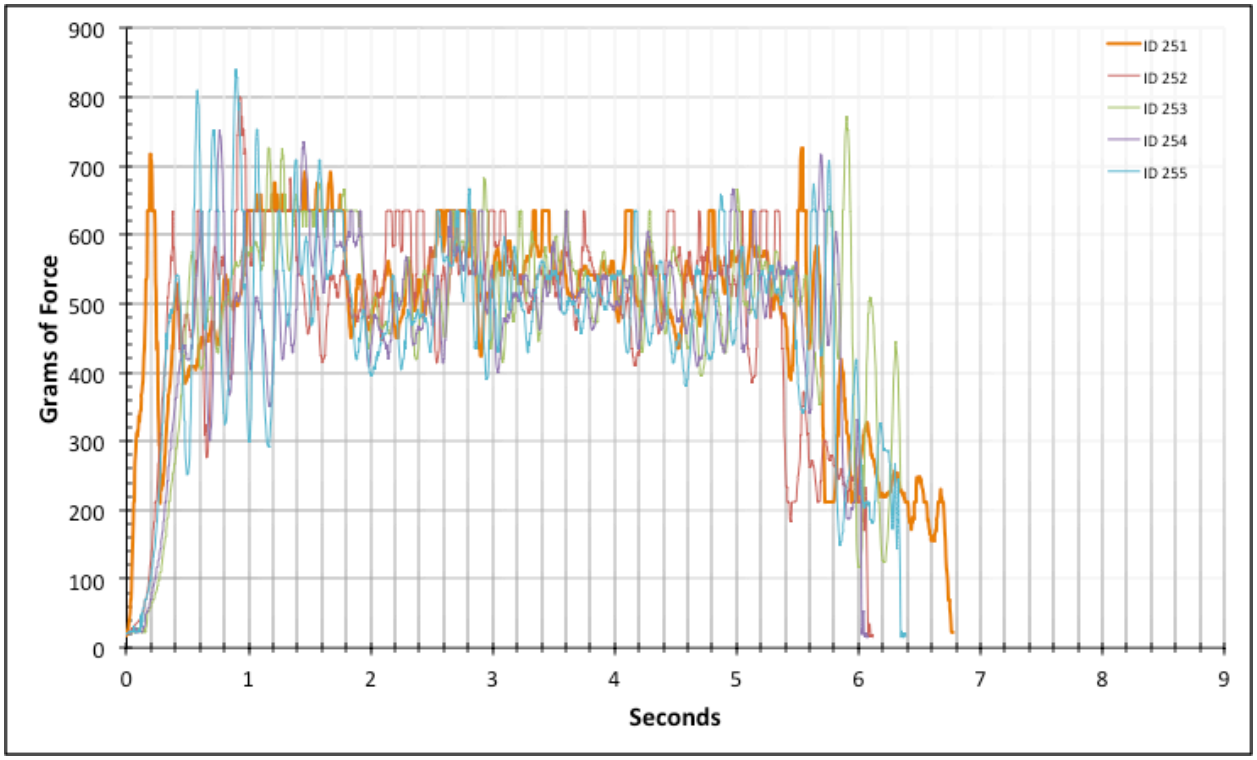

Figure 4-74: Full Composite Data for ID 251-255

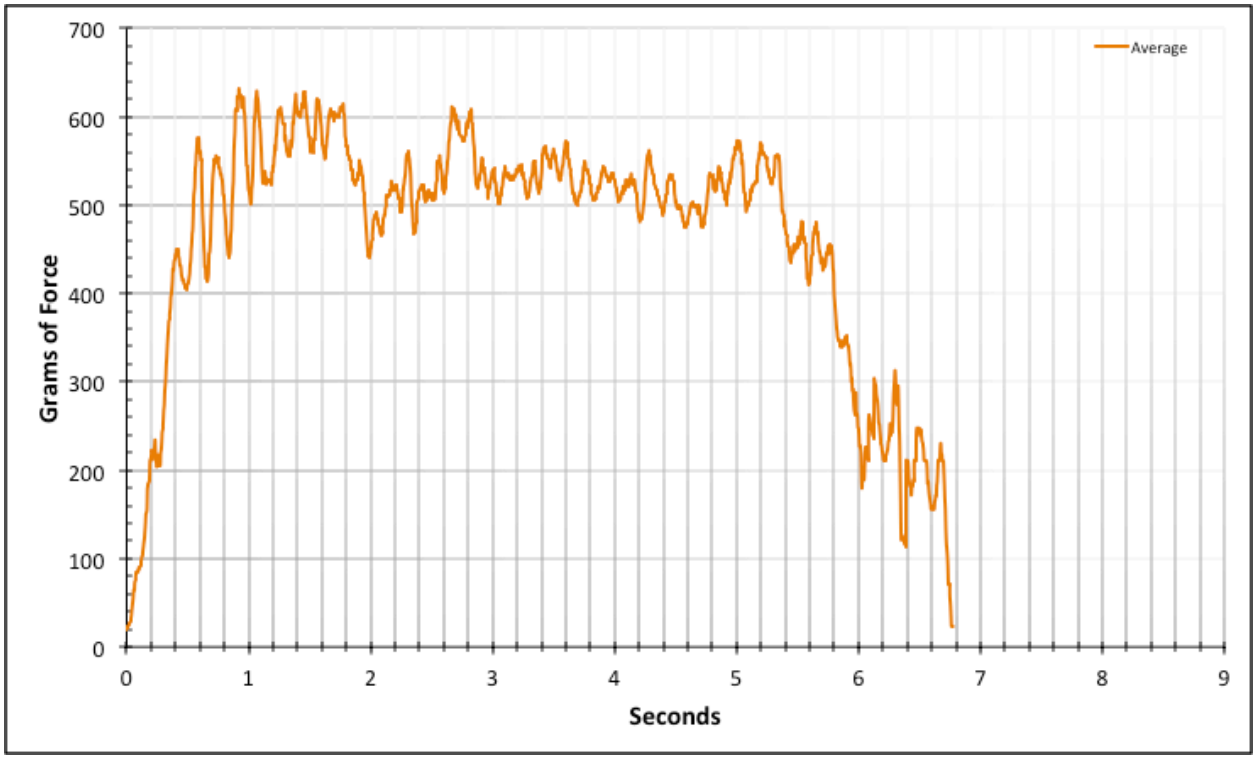

Figure 4-75: Full Average Data for ID 251-255

The data set for the #8 conductor and Bolt 2 (ID 256 – ID 260) is more stable than the last data set. The transition region does appear to be inflated. This inflation may be due to lubricant potentially not being immediately effective because of inconsistency in the application. This data set is also characterized by the common flat spot error. This error is appears to be giving the data an inflated value. The result from this data set's Region 2 is an expected frictional resistance of 499.9±1.8 grams

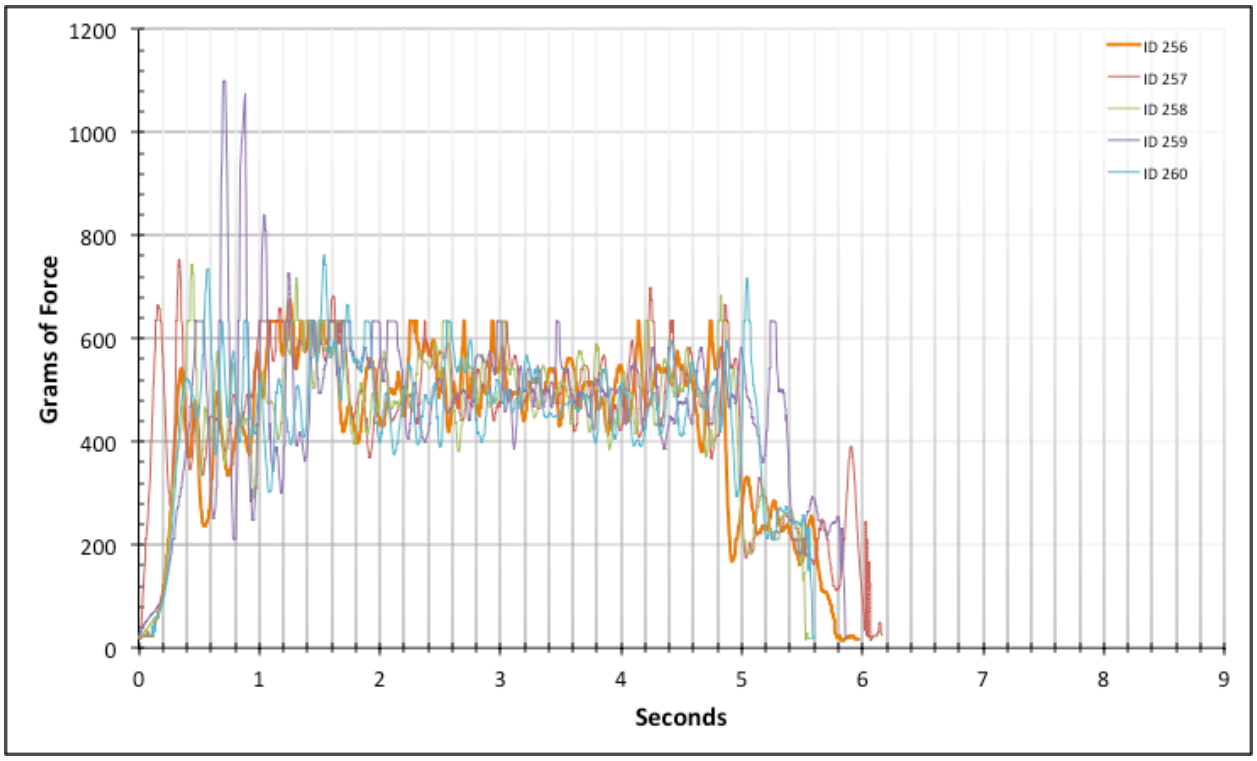

Figure 4-76: Full Composite Data for ID 256-260

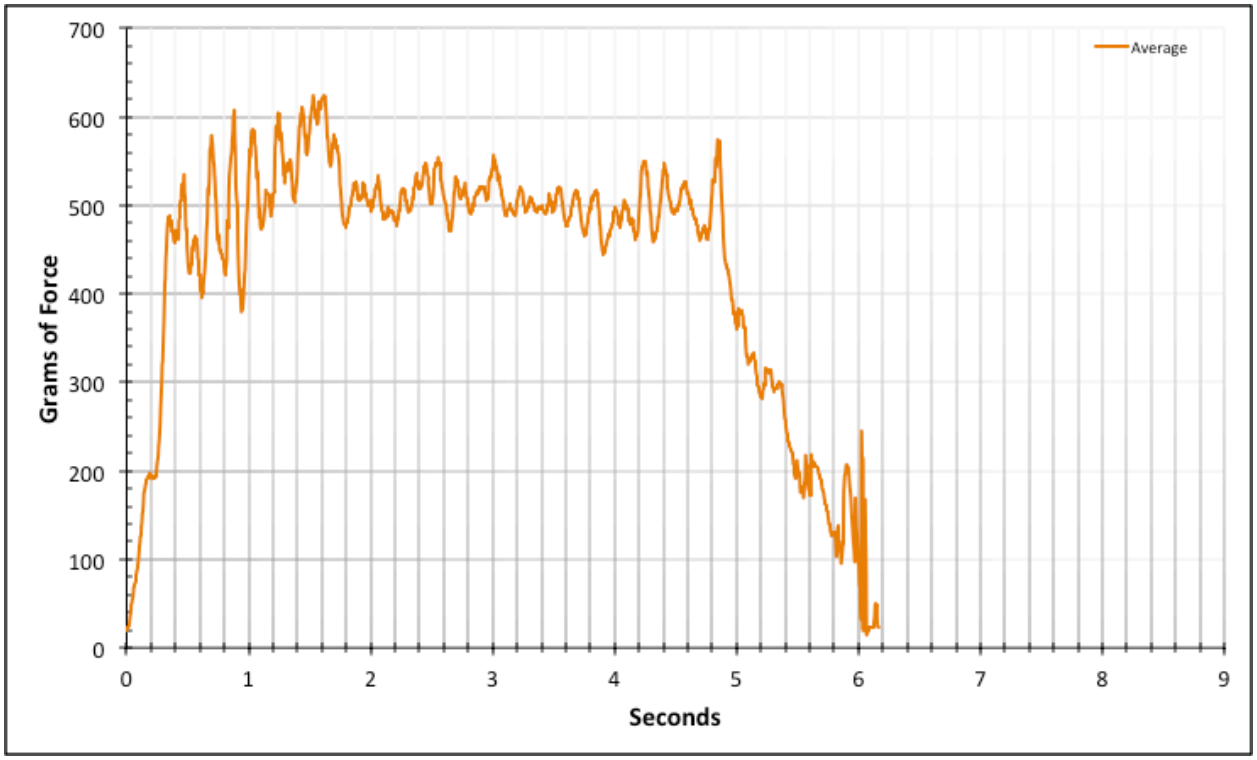

Figure 4-77: Full Average Data for ID 256-260

The data set for the #8 conductor and Bolt 3 (ID 261 – ID 265) is the most consistent set for the #8 conductor in this category and is subject to the least flat spot error. This may be the reason for this data set being the lowest of the three if the other values were inflated from the flat spot error. The result from this data set's Region 2 is an expected frictional resistance of 491.7±2.0 grams

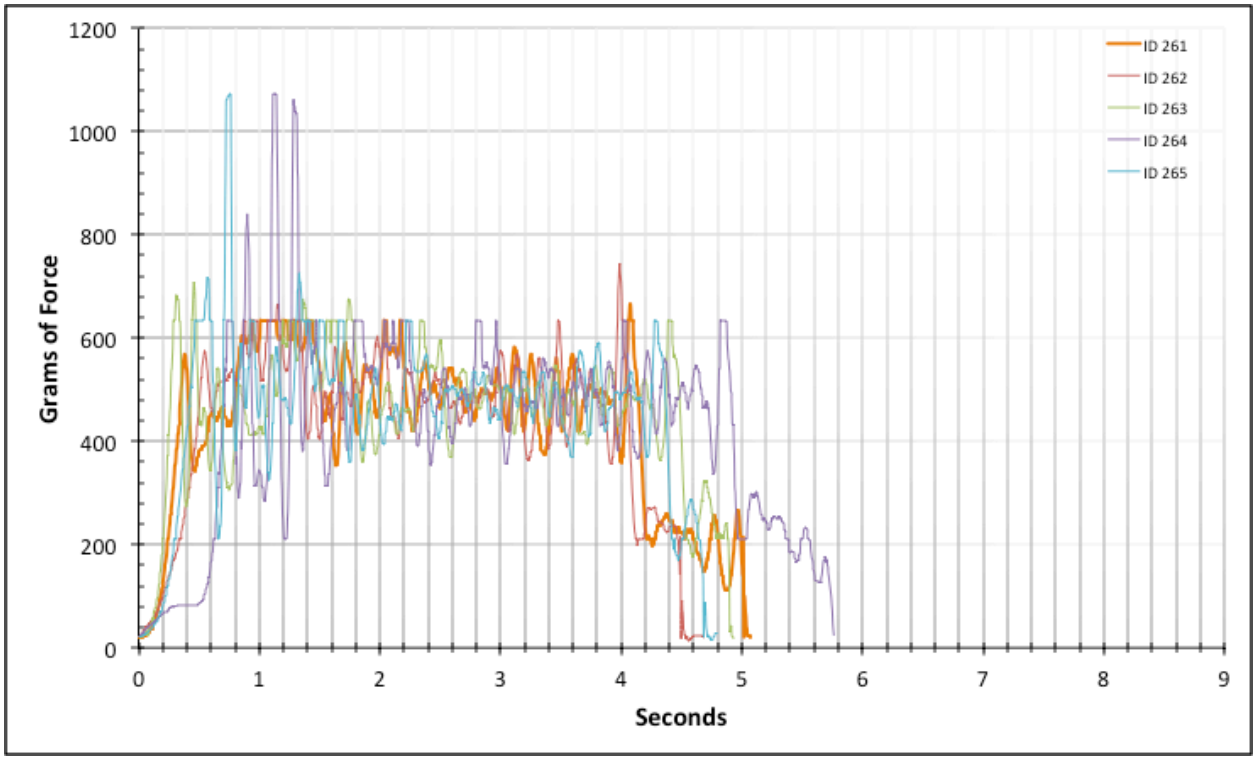

Figure 4-78: Full Composite Data for ID 261-265

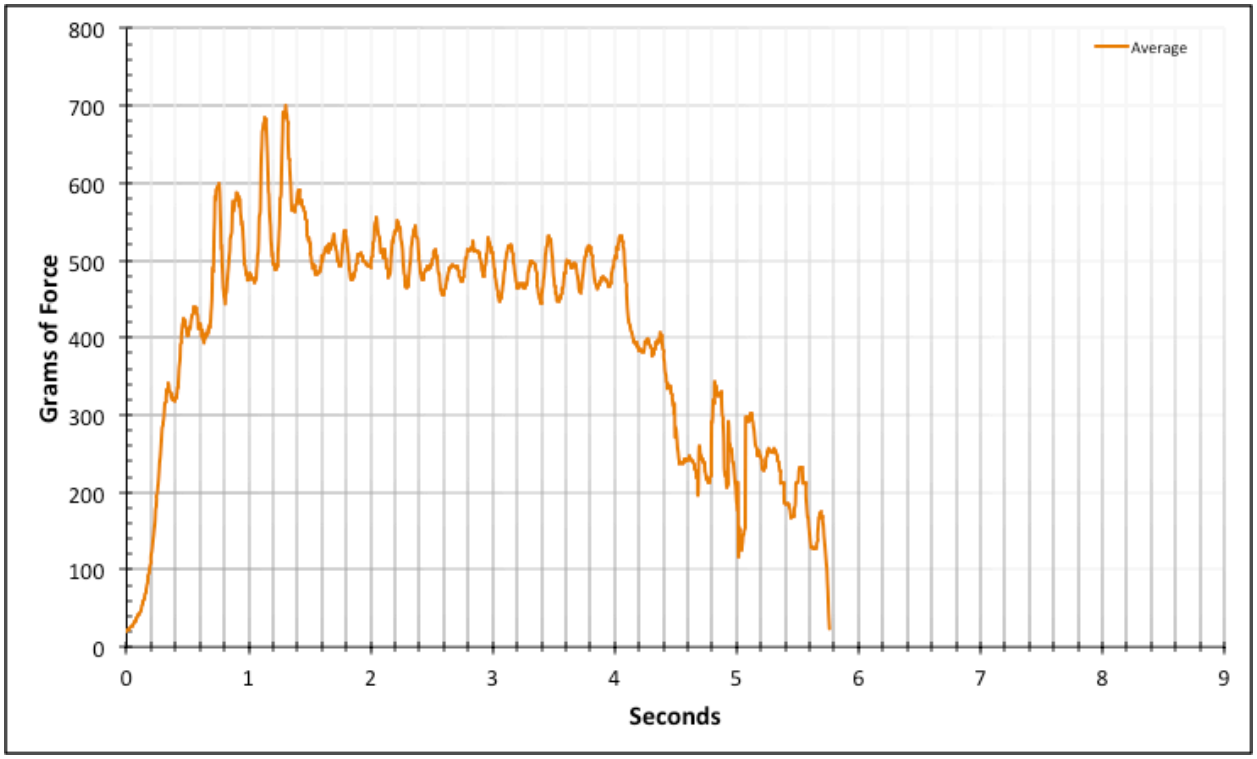

Figure 4-79: Full Average Data for ID 261-265

4.1.4.6. Factory Baseline – Lubricated

The category includes videos 266 through 310 to cover the factory baseline category with the application of lubricant. The data set for the #12 conductor and Bolt 1 (ID 266 – ID 270) is inconsistent near the 2nd Transition, but fairly stable there after. This is likely due to the unpredictability of the lubricant. The result from this data set's Region 2 is an expected frictional resistance of 89.0±0.4 grams.

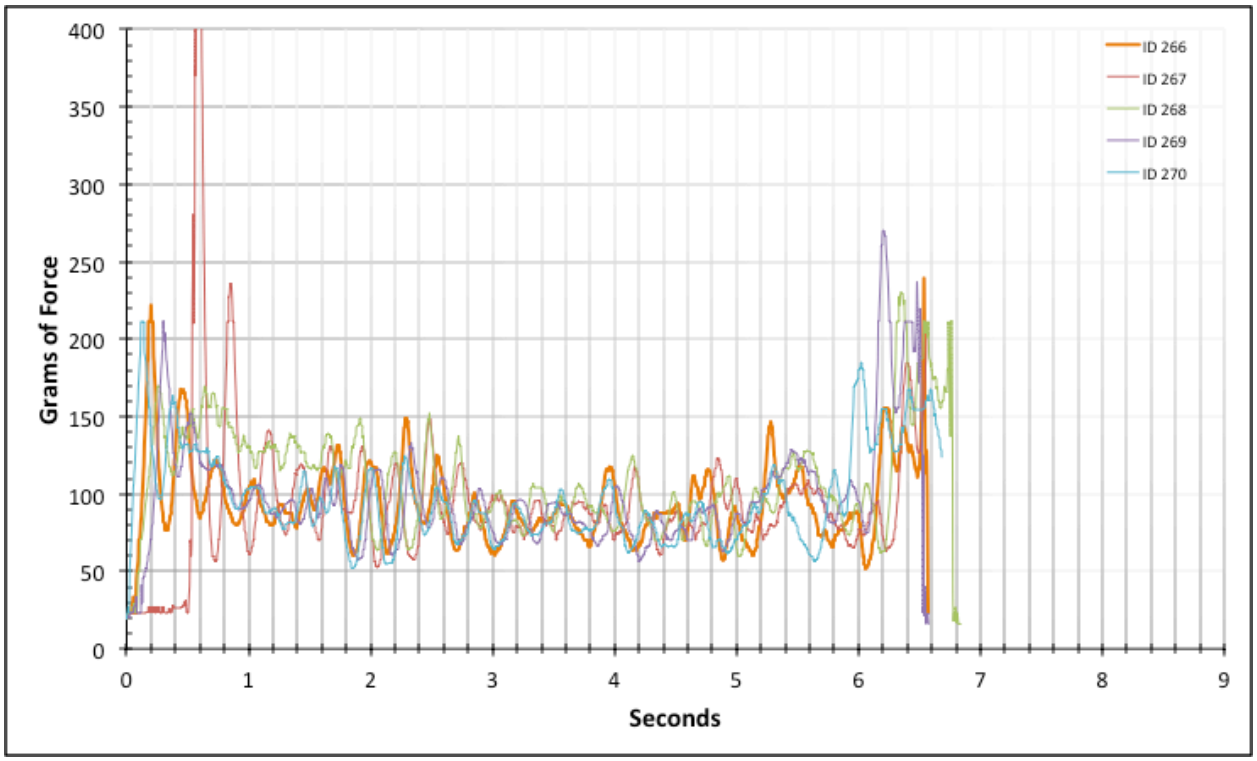

Figure 4-80: Full Composite Data for ID 266-270

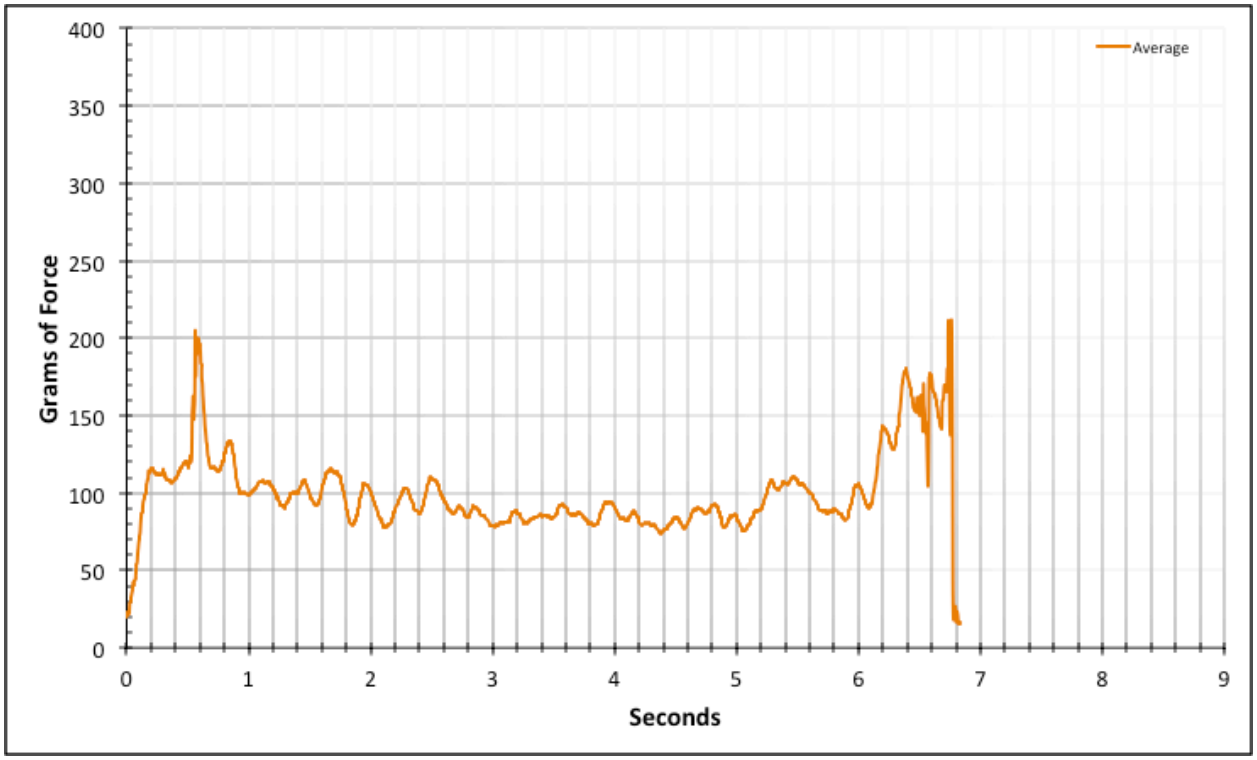

Figure 4-81: Full Average Data for ID 266-270

The data set for the #12 conductor and Bolt 2 (ID 271 – ID 275) is inconsistent near the 2nd Transition, but fairly stable there after. It is clear that this inconsistency is linearly decreasing of tension to the point of stability. This is likely due to the lubricant stabilizing from an initially less effective state. The result from this data set's Region 2 is an expected frictional resistance of 83.6±0.5 grams.

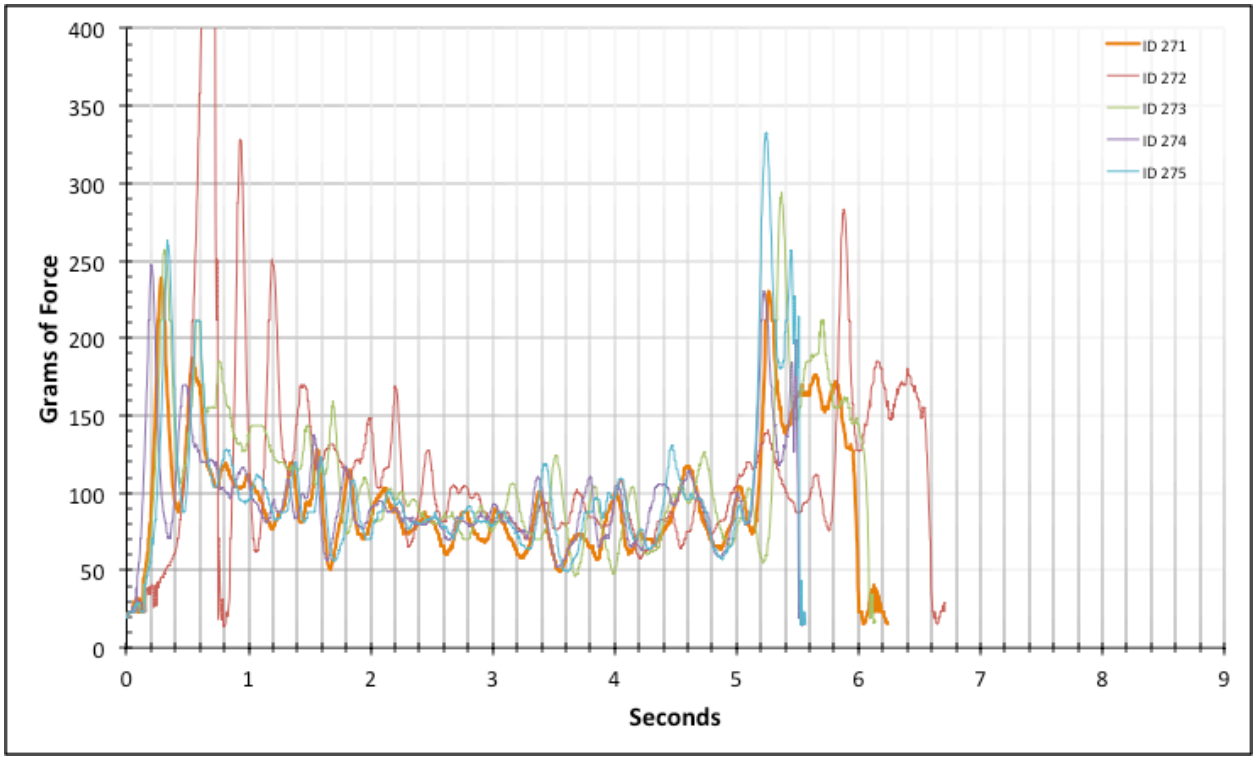

Figure 4-82: Full Composite Data for ID 271-275

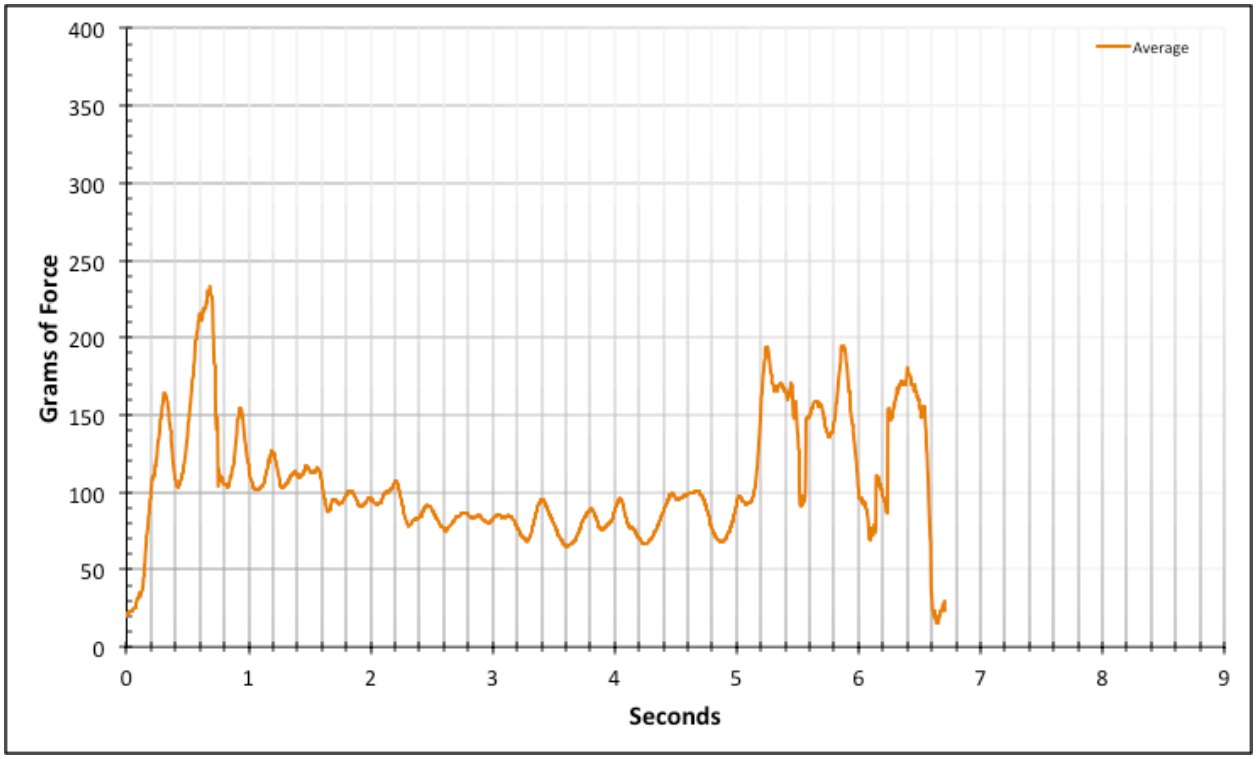

Figure 4-83: Full Average Data for ID 271-275

The data set for the #12 conductor and Bolt 3 (ID 276 – ID 280) is mostly stable and reasonably consistent. There are not abnormalities here to challenge the norm. The result from this data set's Region 2 is an expected frictional resistance of 79.9±0.5 grams.

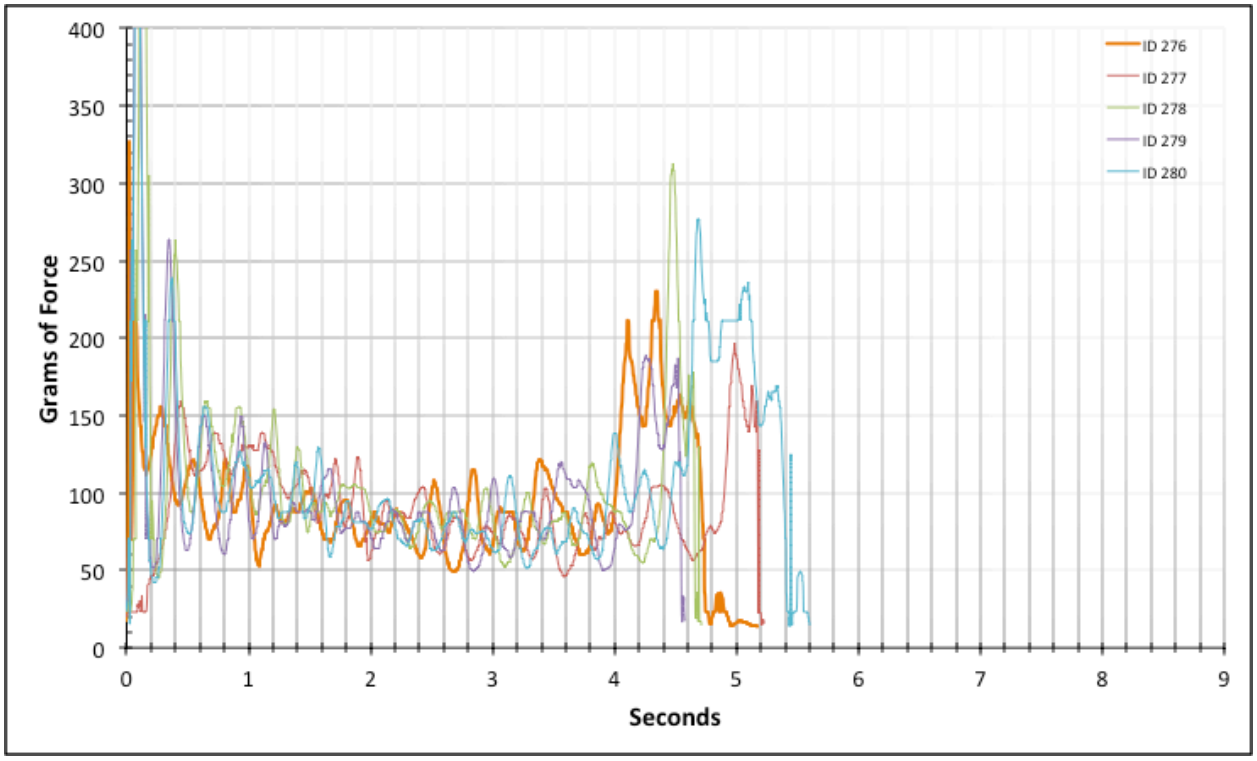

Figure 4-84: Full Composite Data for ID 276-280

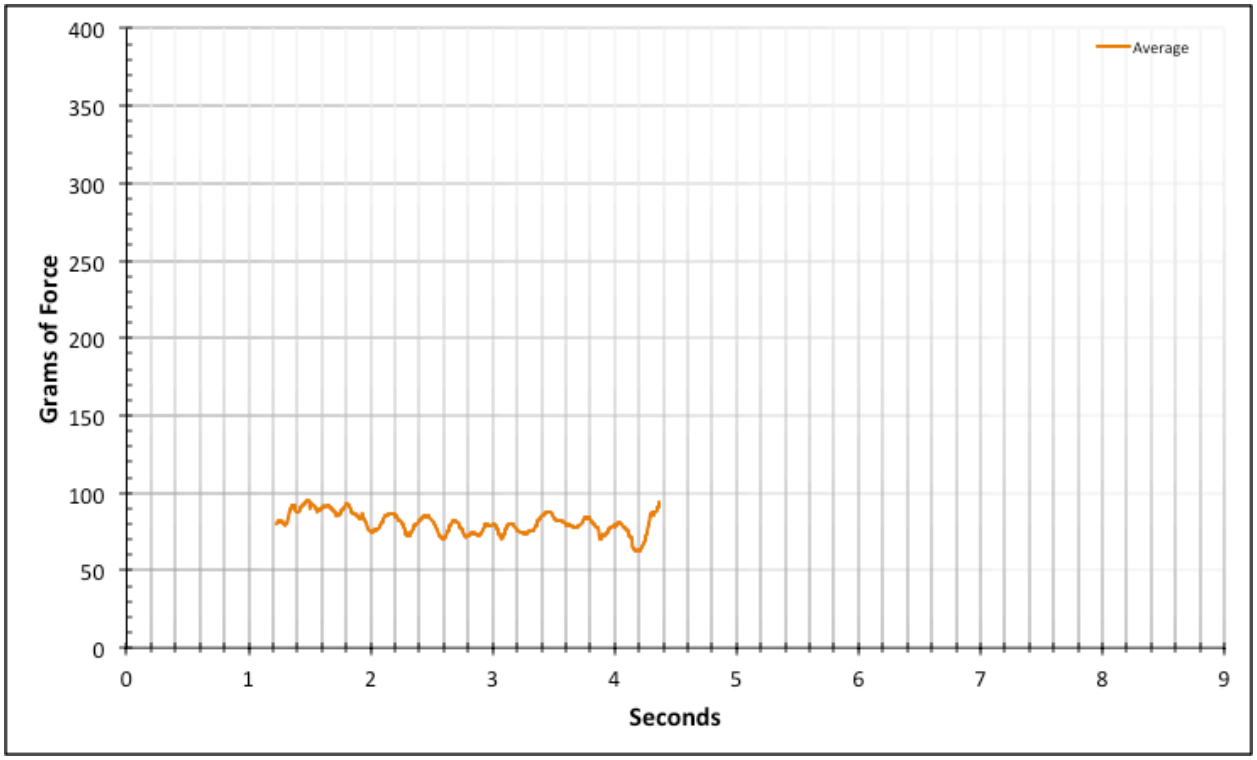

Figure 4-85: Region 2 Average Data for ID 276-280

The data set for the #10 conductor and Bolt 1 (ID 281 – ID 285) is noisy and impacted by the flat spot error. A slight positive slope from lubricant effects once again characterizes this data. The result from this data set's Region 2 is an expected frictional resistance of 190.6±0.8 grams.

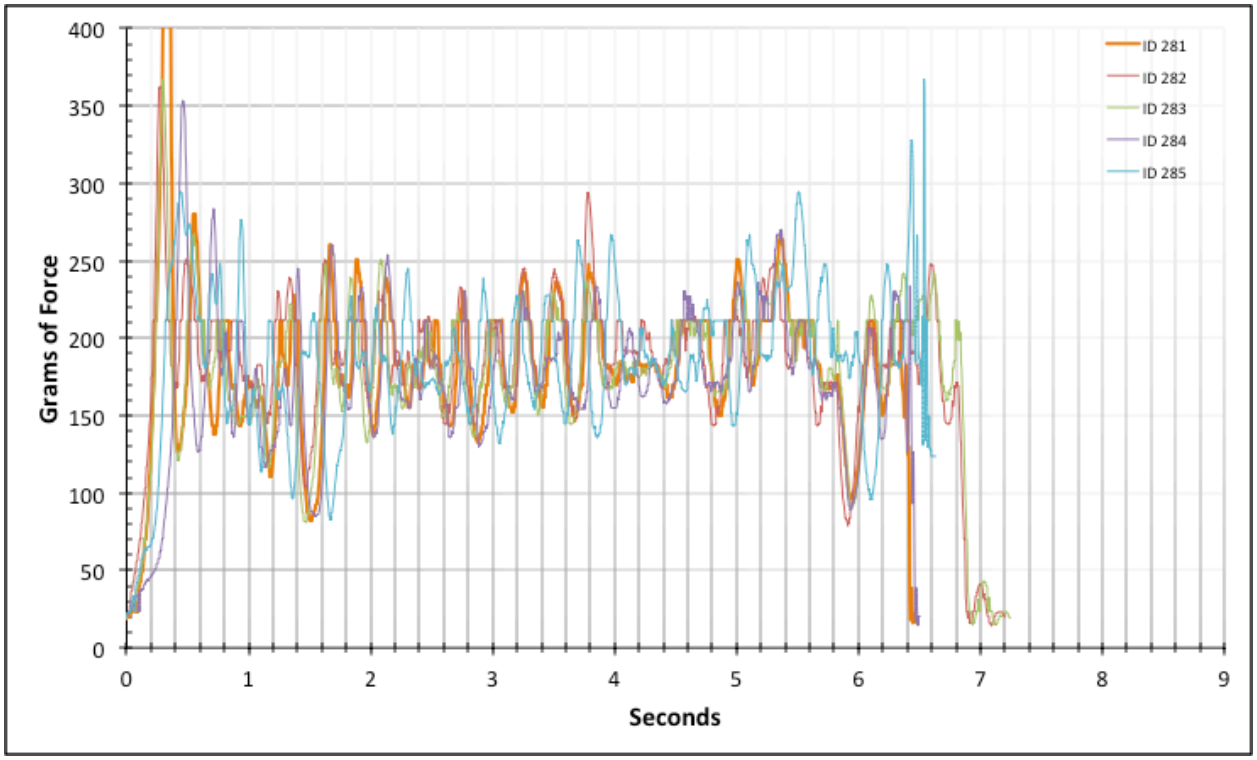

Figure 4-86: Full Composite Data for ID 281-285

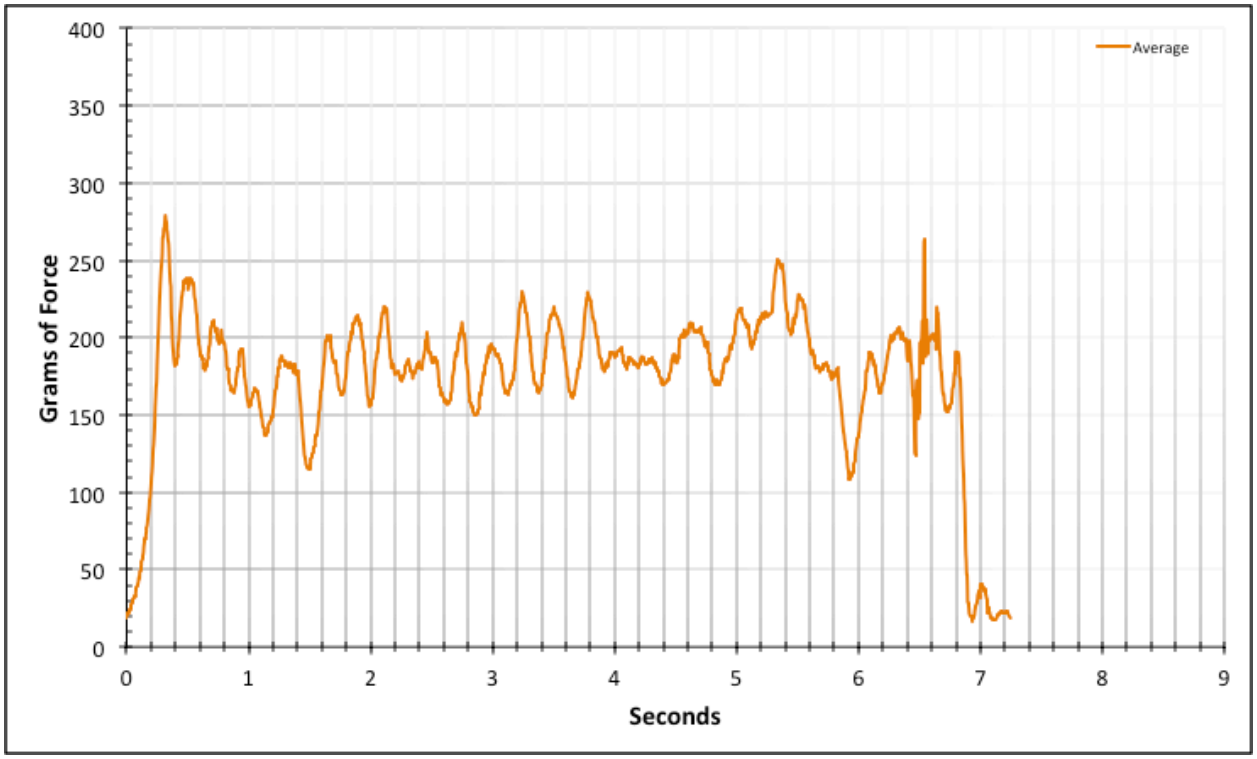

Figure 4-87: Full Average Data for ID 281-285

The data set for the #10 conductor and Bolt 2 (ID 286 – ID 290) is noisier than the last set and also impacted by the flat spot error. A slight positive slope from lubricant effects once again characterizes this data to a more visually apparent degree. The result from this data set's Region 2 is an expected frictional resistance of 206.9±1.2 grams.

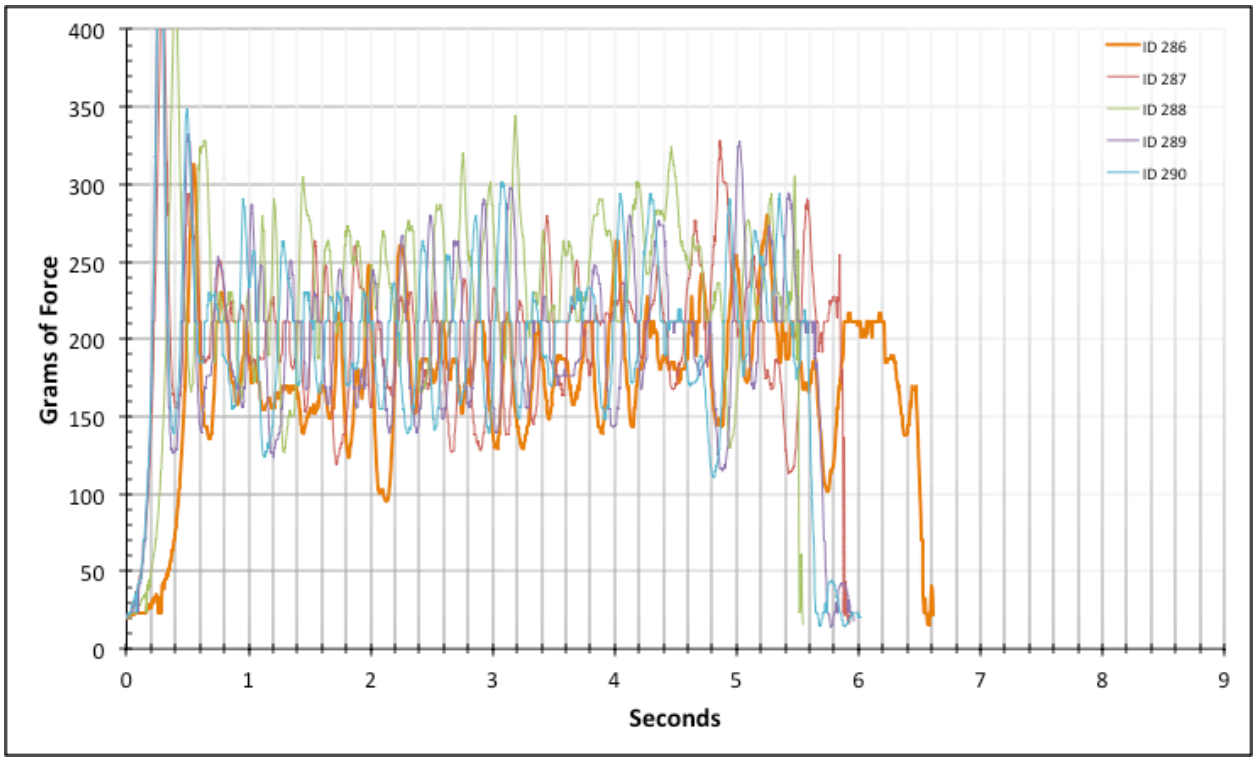

Figure 4-88: Full Composite Data for ID 286-290

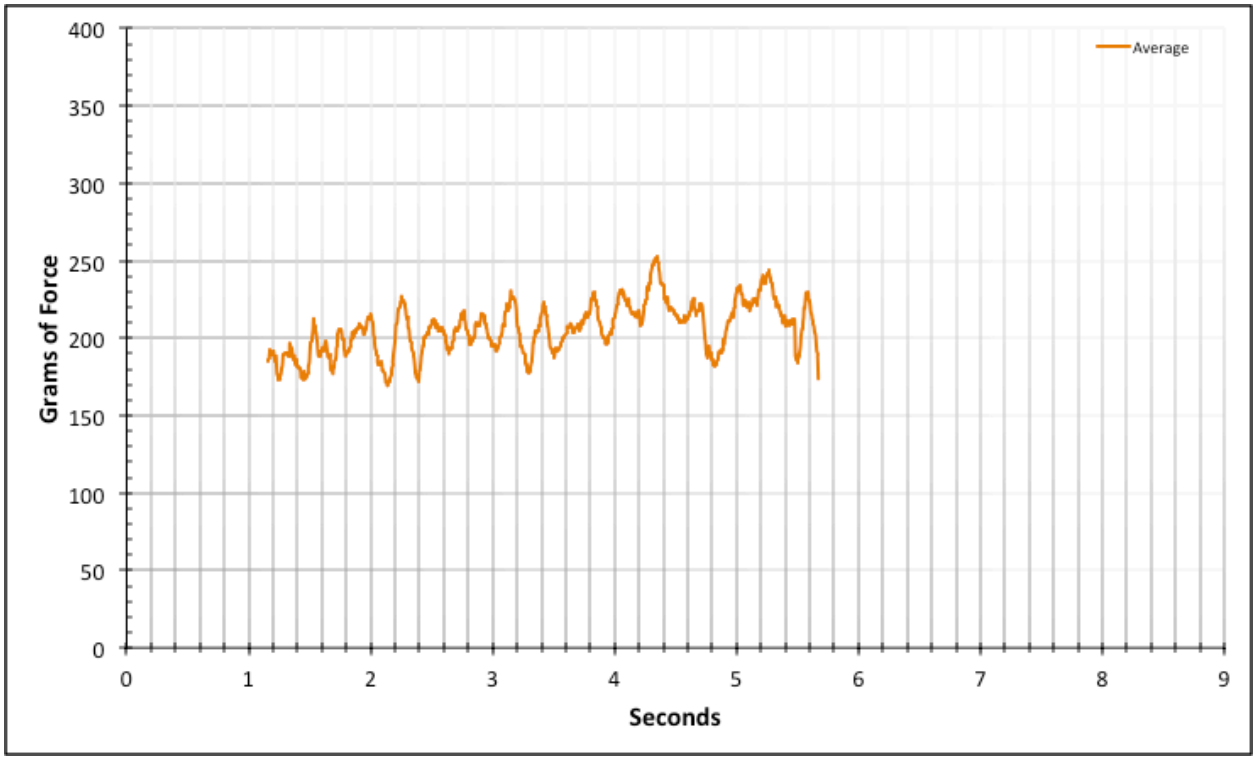

Figure 4-89: Region 2 Average Data for ID 286-290

The data set for the #10 conductor and Bolt 3 (ID 291 – ID 295) is just as noisy as the last set and also impacted by the flat spot error. Unlike the last two data sets for the #10 conductor, here is no apparent slope from lubricant effects. The result from this data set's Region 2 is an expected frictional resistance of 198.2±1.1 grams.

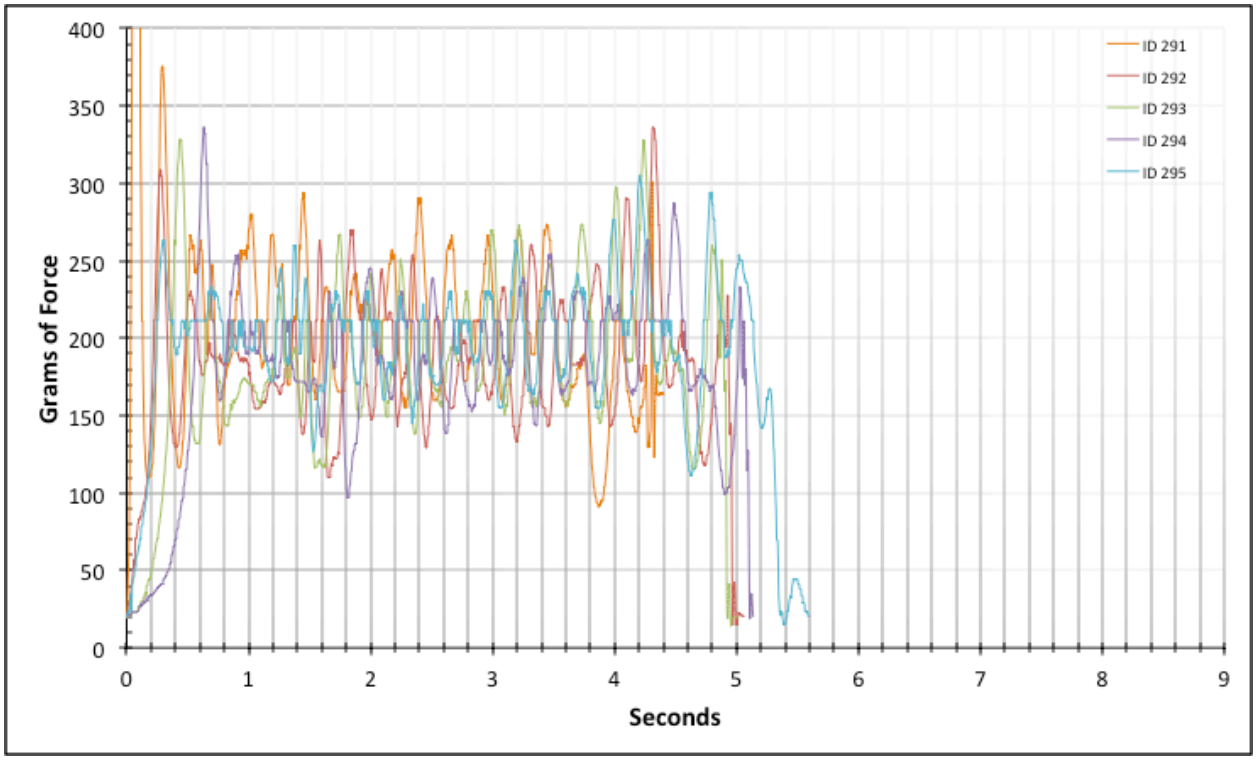

Figure 4-90: Full Composite Data for ID 291-295

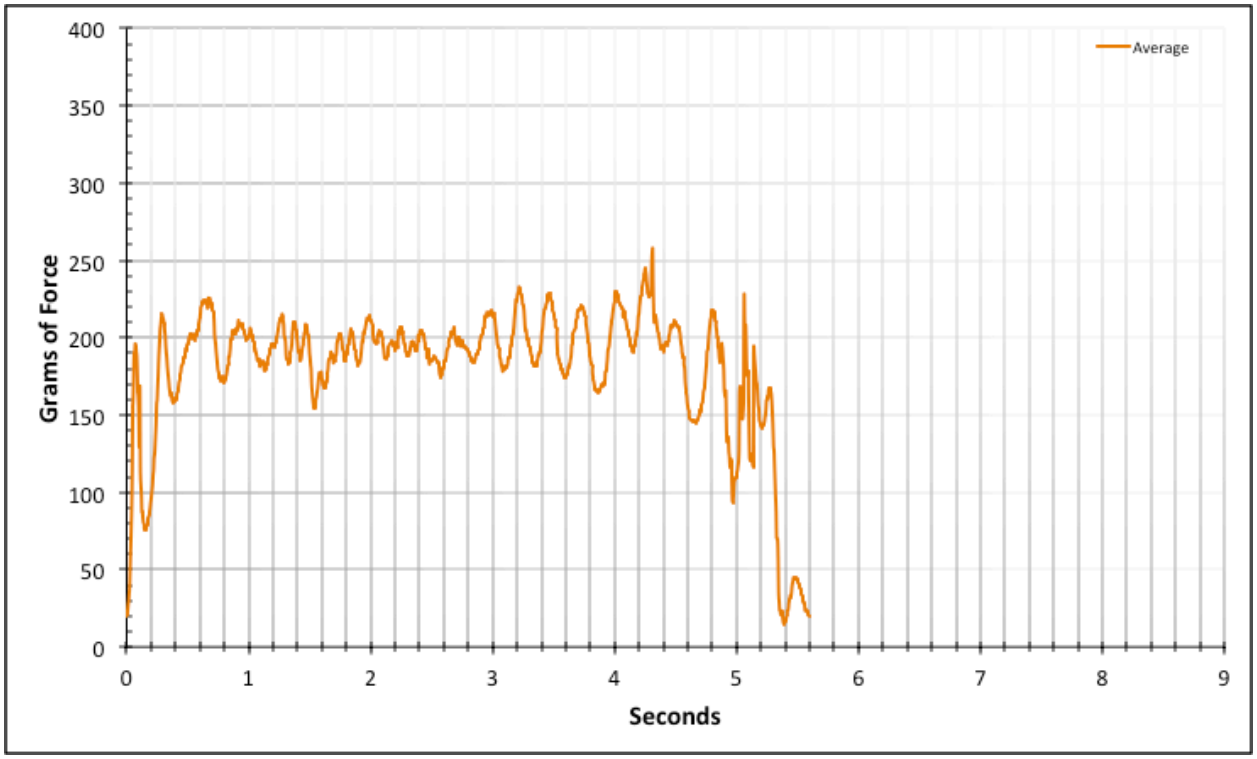

Figure 4-91: Full Average Data for ID 291-295

The data set for the #8 conductor and Bolt 1 (ID 296 – ID 300) is noisy throughout the first half of Region 2. The second half of Region 2 is relatively consistent and most nearly avoids the flat spot error. The result from this data set's Region 2 is an expected frictional resistance of 479.2±1.9 grams.

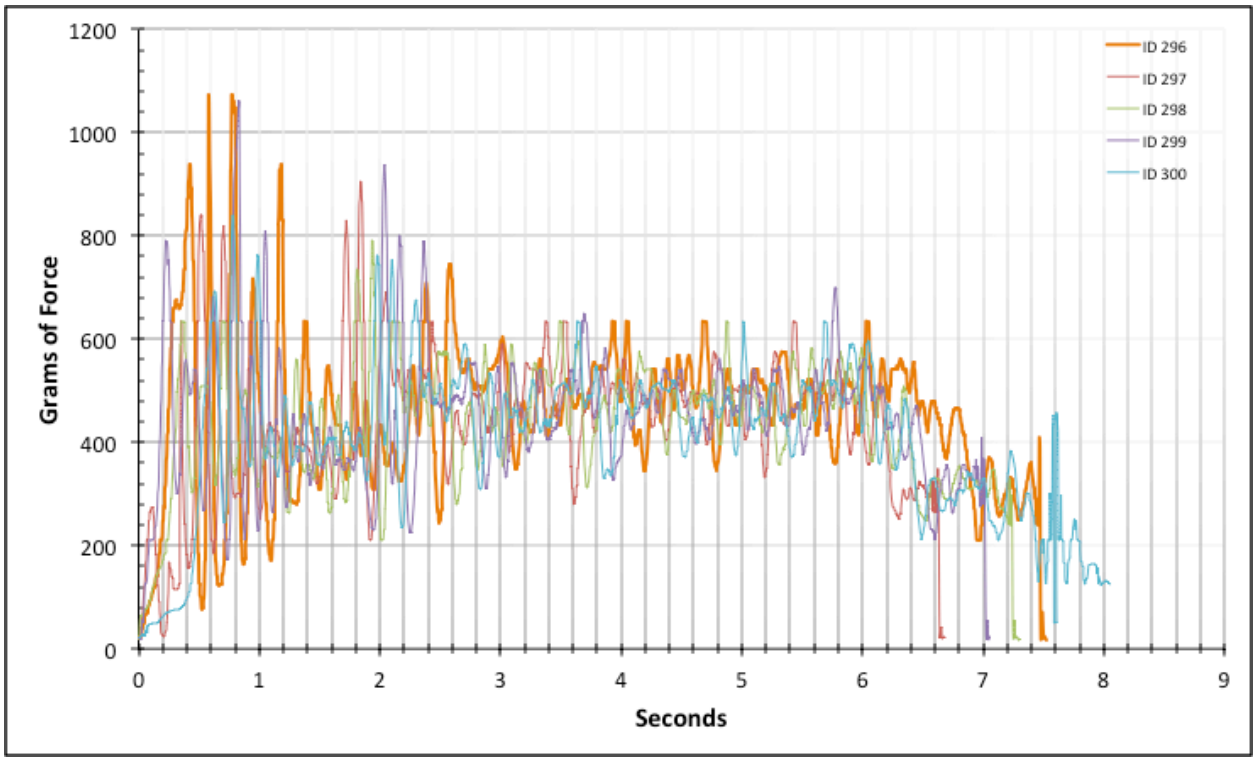

Figure 4-92: Full Composite Data for ID 296-300

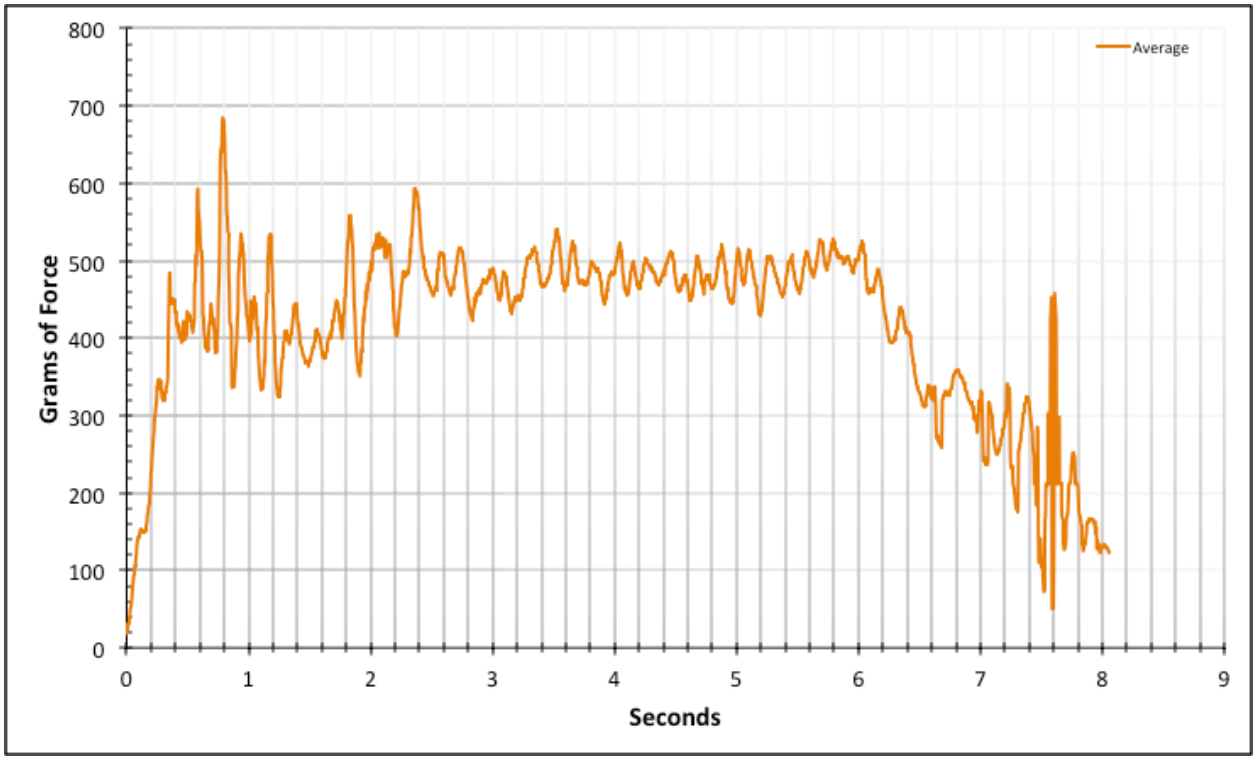

Figure 4-93: Full Average Data for ID 296-300

The data set for the #8 conductor and Bolt 2 (ID 301 – ID 305) is noisy mostly noisy throughout the Region 2. Video 303 is particularly extreme in amplitude for an extensive duration but is still included in the statistical data. A slight positive slope is present in this data set. The result from this data set's Region 2 is an expected frictional resistance of 460.1±1.9 grams.

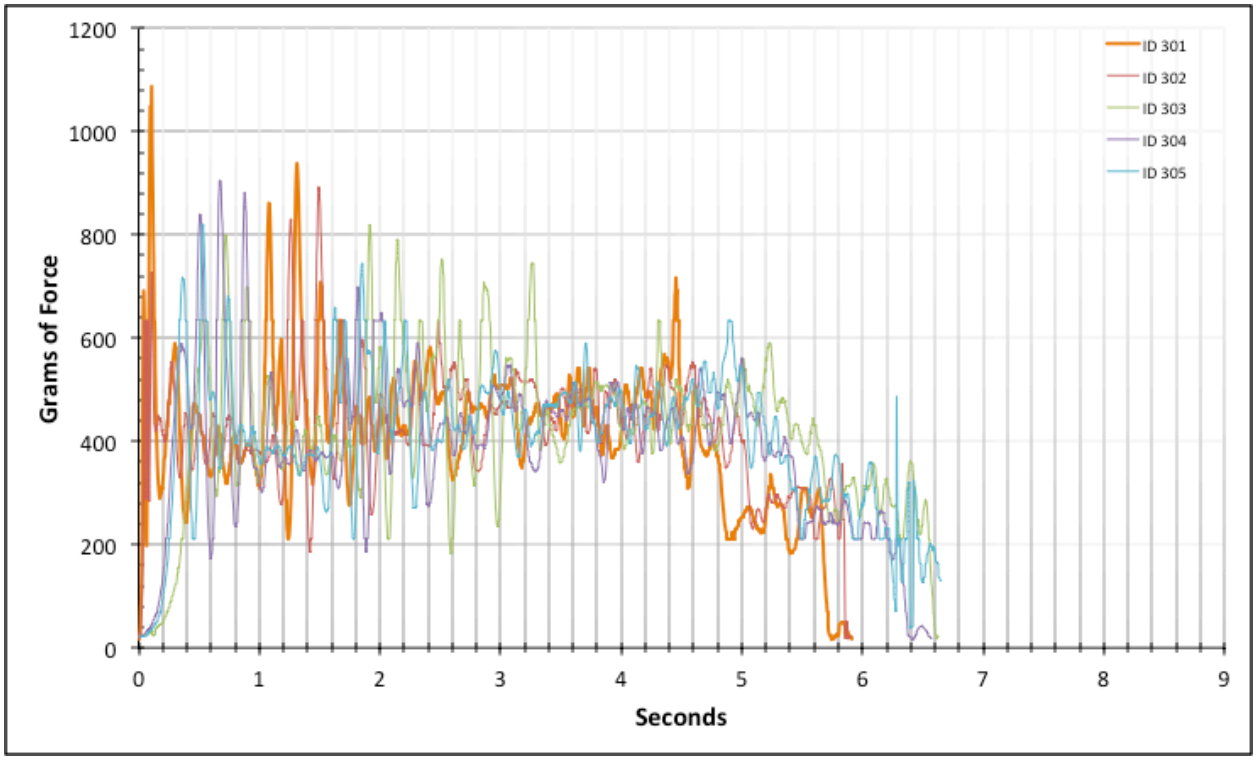

Figure 4-94: Full Composite Data for ID 301-305

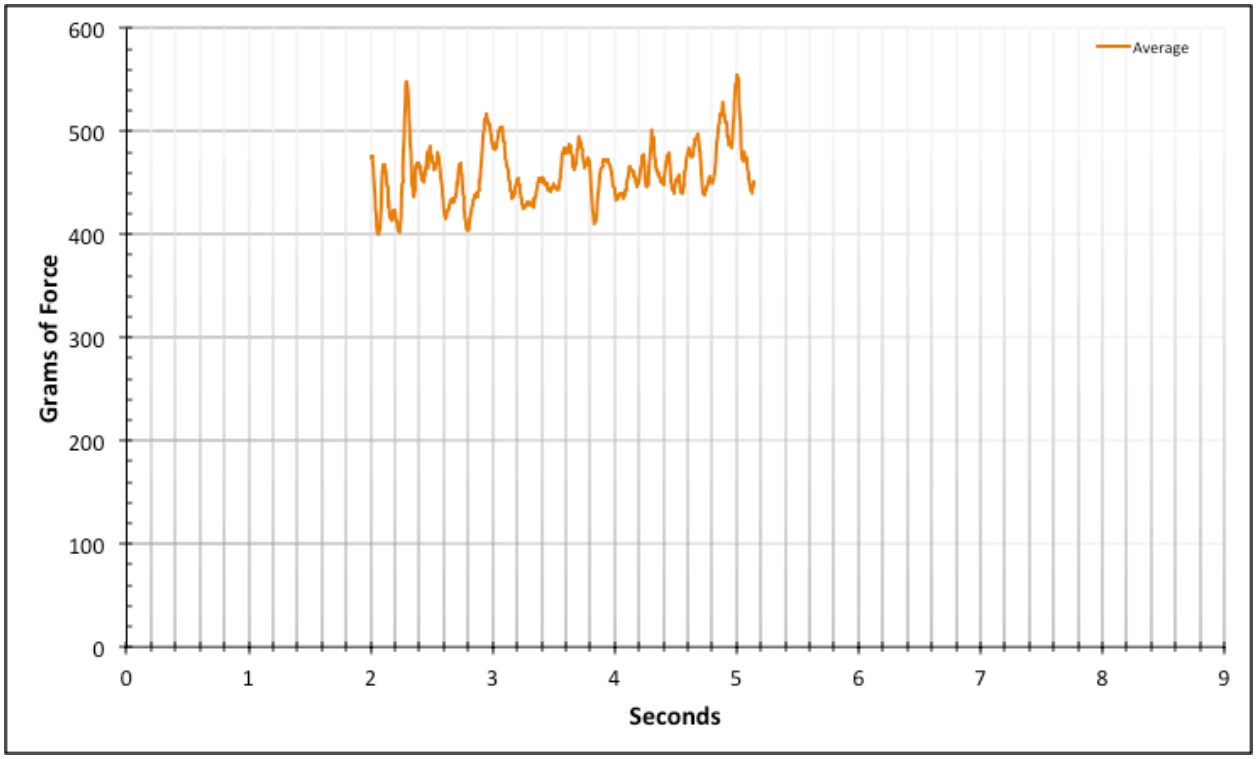

Figure 4-95: Region 2 Average Data for ID 301-305

The data set for the #8 conductor and Bolt 3 (ID 306 – ID 310) is subject to a systematic bubble of higher amplitude after a brief instance of stability in Region 2. This area is omitted from the statistical data. A relatively moderate positive slope is present in this data set. The result from this data set's Region 2 is an expected frictional resistance of 447.1±1.8 grams.

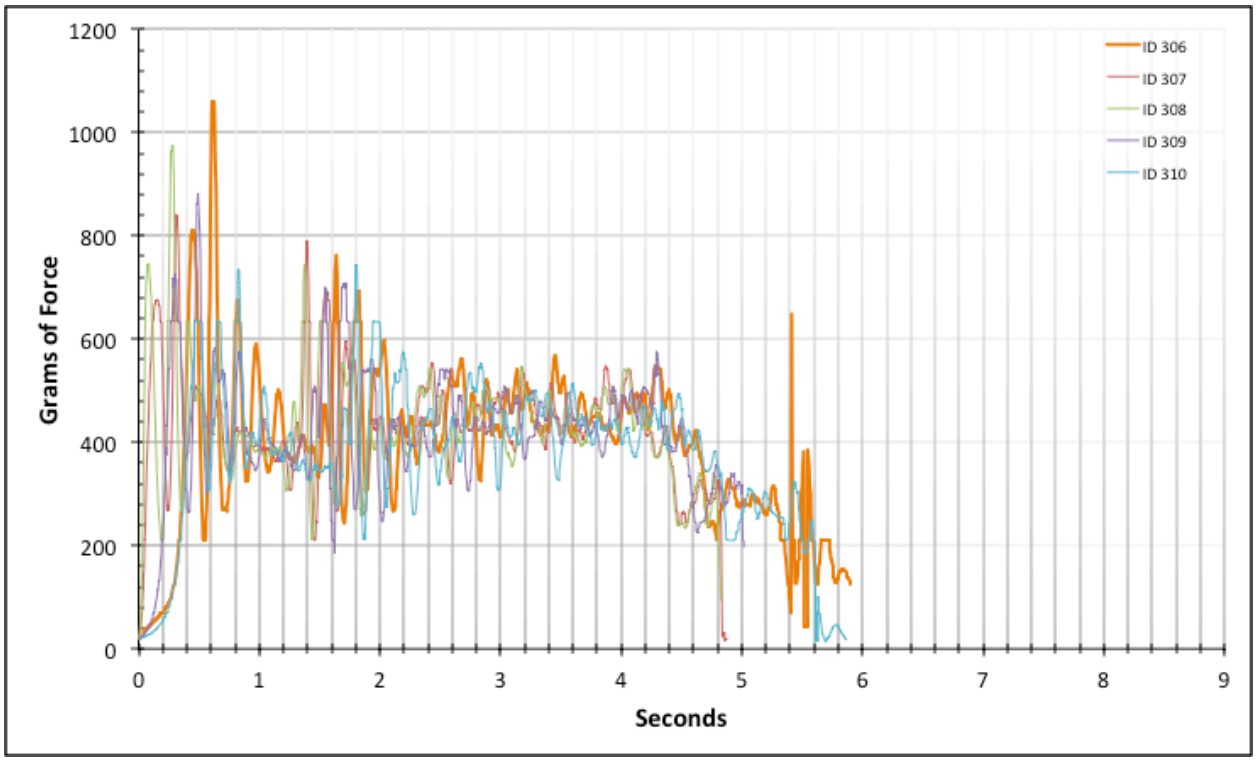

Figure 4-96: Full Composite Data for ID 306-310

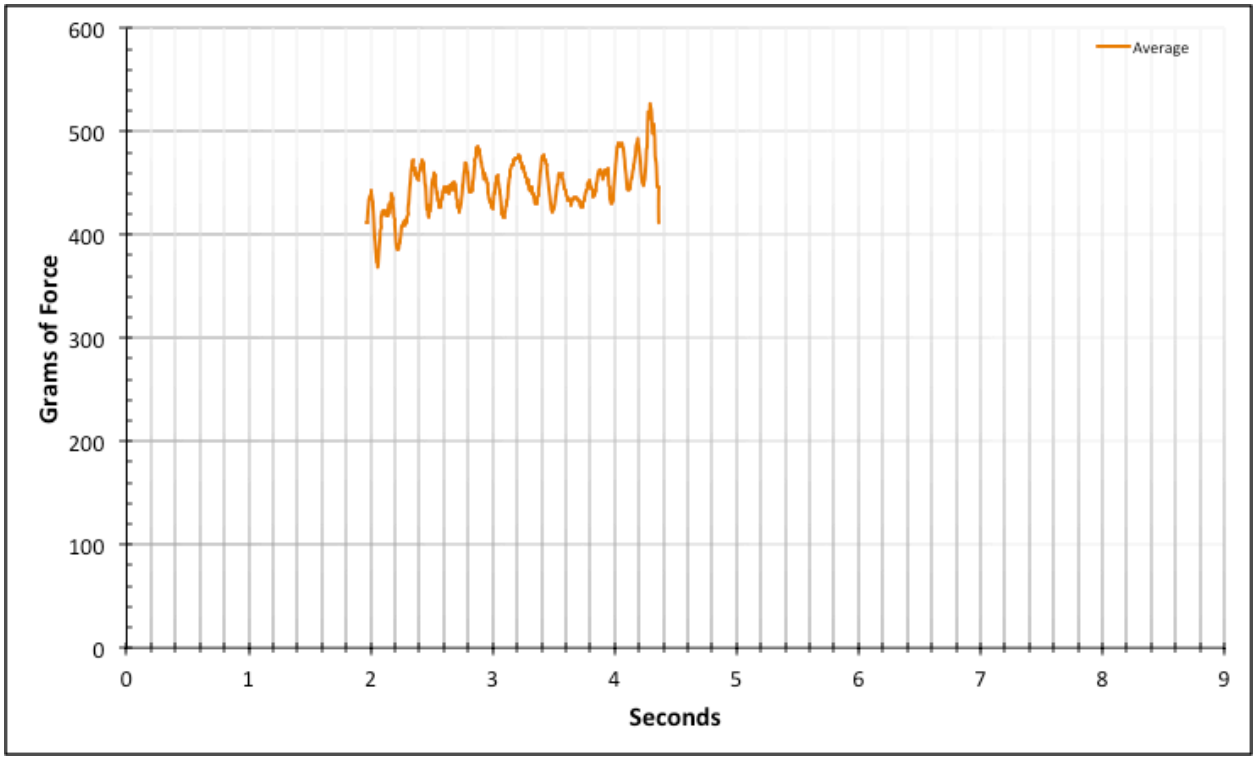

Figure 4-97: Region 2 Average Data for ID 306-310

4.1.5. Culminated Results Summary

In order to clearly present experimental conclusions, this section summarizes all of the results from the last section and executes the essential comparisons of interest. **Table 4-1** is simply the expected mean frictional resistances from each data set. The 95% standard uncertainty is included on this and all following tables. The Factory Baseline categories are treated in this study as the control values. They are intended to represent the existing frictional resistances in today's conductor pulls given the tabulated fixed parameters. The Modeled Product categories are representative of the experiments subject that is hypothesized to ultimately reduce the overall frictional resistance measured in a pull with otherwise identical parameters. Finally, the Straight Baseline categories represent the isolated frictional resistance of the conductor being pulled through the straight legs of conduit in the experiment.

Considering the focus of this experiment is to isolate the resistance of the elbow entities alone, all data sets involving the factory elbow and the modeled product require that their resulting mean values be reduced by subtracting the straight baseline value that correlates with the respective set's conductor size and elbow type. For example, the first data set in **Table 4-1** is for the #12 conductor and Bolt 1 being pulled through the un-lubricated factory elbow. The mean frictional value from this data set is 133.1±1.1 grams. The straight baseline value for an un-lubricated #12 conductor is 42.2±0.1 grams. Note that the straight baseline value is theoretically treated to be independent of speed and thus bolt size. The isolated frictional resistance from the factory elbow for an un-lubricated #12 conductor being pulled by Bolt 1 is thus taken to be ((133.1±1.1) - (42.2±0.1)) grams = *(90.9±1.2) grams*. Note that standard uncertainties are always added in addition and subtraction functions. **Table 4-2** is the summarized execution of this calculation being processed for every data set of this study. Experimental notes about any observed abnormalities

Table 4-1: Expected Mean Frictional Resistance Per Data Set

Category		Conductor and Bolt	Mean (Grams)		95% Confidence Uncertainty
Dry	Factory Baseline – Dry	#12 - Bolt 1	133.1	±	1.1
		#12 - Bolt 2	138.7	±	1.0
		#12 - Bolt 3	141.7	±	1.3
		#10 - Bolt 1	309.2	±	1.1
		#10 - Bolt 2	307.2	±	0.9
		#10 - Bolt 3	328.1	±	0.9
		#8 - Bolt 1	760.6	±	1.5
		#8 - Bolt 2	782.4	±	1.6
		#8 - Bolt 3	-		-
	Modeled Product - Dry	#12 - Bolt 1	143.9	±	1.0
		#12 - Bolt 2	151.2	±	0.9
		#12 - Bolt 3	160.9	±	0.9
		#10 - Bolt 1	279.8	±	1.4
		#10 - Bolt 2	299.8	±	1.9
		#10 - Bolt 3	308.9	±	2.3
		#8 - Bolt 1	672.7	±	1.6
		#8 - Bolt 2	715.6	±	1.7
		#8 - Bolt 3	730.6	±	1.8
	Straight Baseline - Dry	#12 - Bolt 1	41.35	±	0.1
		#12 - Bolt 2	42.9	±	0.1
		#12 - Bolt 3	42.4	±	0.1
		#12 - Bolt 1-3	42.2	±	0.1
		#10 - Bolt 1	91.4	±	0.2
		#10 - Bolt 2	95.7	±	0.2
		#10 - Bolt 3	99.3	±	0.3
		#10 - Bolt 1-3	95.5	±	0.3
		#8 - Bolt 1-3	389.3	±	0.7
Lubricated	Straight Baseline - Lubricated	#12 - Bolt 1	49.9	±	0.1
		#10 - Bolt 3	71.9	±	0.3
		#8 - Bolt 1	327.0	±	0.7
	Modeled Product - Lubricated	#12 - Bolt 1	85.5	±	0.4
		#12 - Bolt 2	83.3	±	0.5
		#12 - Bolt 3	78.7	±	0.6
		#10 - Bolt 1	203.4	±	1.0
		#10 - Bolt 2	196.1	±	1.0
		#10 - Bolt 3	196.0	±	1.1
		#8 - Bolt 1	524.8	±	1.6
		#8 - Bolt 2	499.9	±	1.8
		#8 - Bolt 3	491.7	±	2.0
	Factory Baseline – Lubricated	#12 - Bolt 1	89.0	±	0.4
		#12 - Bolt 2	83.6	±	0.5
		#12 - Bolt 3	79.9	±	0.5
		#10 - Bolt 1	190.6	±	0.8
		#10 - Bolt 2	206.9	±	1.2
		#10 - Bolt 3	198.2	±	1.1
		#8 - Bolt 1	479.2	±	1.9
		#8 - Bolt 2	460.1	±	1.9
		#8 - Bolt 3	447.1	±	1.8

in the data are made for the sake of simplifying the cross referencing results to the original analysis. These notes are heavily referenced in Section 4.1.6.

Table 4-2: Isolated Elbow Frictional Resistances and Comments

Category	Conductor and Bolt	Isolated Elbow Friction (Grams)			Experimental Comments
Factory Baseline – Dry	#12 - Bolt 1	90.9	±	1.2	Systematic Increase in Amplitude Included
	#12 - Bolt 2	96.5	±	1.1	Systematic Increase in Amplitude Included
	#12 - Bolt 3	99.5	±	1.4	Omitted ID 12
	#10 - Bolt 1	213.8	±	1.3	Clean Results
	#10 - Bolt 2	211.8	±	1.1	Clean Results
	#10 - Bolt 3	232.6	±	1.2	Clean Results
	#8 - Bolt 1	371.3	±	2.1	Minor +800g Spikes
	#8 - Bolt 2	393.1	±	2.2	+800g Spikes
	#8 - Bolt 3	-	-	-	Unconducted
Modeled Product - Dry	#12 - Bolt 1	101.7	±	1.1	Systematic Increase in Amplitude Included
	#12 - Bolt 2	109.0	±	1.0	Very Minor High Flat Spots
	#12 - Bolt 3	118.7	±	1.0	Very Minor High Flat Spots
	#10 - Bolt 1	184.3	±	1.7	Omitted Spikes, Minor Low Flat Spots
	#10 - Bolt 2	204.3	±	2.2	Major Systematic Increase in Amplitude Included
	#10 - Bolt 3	213.4	±	2.6	Omitted ID 68
	#8 - Bolt 1	283.4	±	2.3	Omitted ID 74, Ample Low Flat Spots
	#8 - Bolt 2	326.3	±	2.3	Low Flat Spots
	#8 - Bolt 3	341.3	±	2.4	Low Flat Spots
Modeled Product - Lubricated	#12 - Bolt 1	35.6	±	0.6	Clean Results
	#12 - Bolt 2	33.4	±	0.7	Omitted Spike
	#12 - Bolt 3	28.8	±	0.7	Mostely Clean Results
	#10 - Bolt 1	131.6	±	1.2	Mid Flat Spots
	#10 - Bolt 2	124.2	±	1.2	Mid/High Flat Spots
	#10 - Bolt 3	124.1	±	1.3	Mid/High Flat Spots, High Amplitude
	#8 - Bolt 1	197.8	±	2.3	High Flat Spots
	#8 - Bolt 2	172.9	±	2.4	High Flat Spots
	#8 - Bolt 3	164.7	±	2.7	High Flat Spots
Factory Baseline – Lubricated	#12 - Bolt 1	39.1	±	0.6	Clean Results
	#12 - Bolt 2	33.7	±	0.6	First Half Negative Slope (Inflating)
	#12 - Bolt 3	30.0	±	0.6	Minor First Half Negative Slope (Inflating)
	#10 - Bolt 1	118.8	±	1.1	High Flat Spots
	#10 - Bolt 2	135.1	±	1.4	Wide Spread Trials, Mid/High Flat Spots
	#10 - Bolt 3	126.4	±	1.4	Mid/High Flat Spots
	#8 - Bolt 1	152.1	±	2.5	Mostly Clean Results
	#8 - Bolt 2	133.0	±	2.5	High Amplitute In ID 303, Full Positive Slope
	#8 - Bolt 3	120.1	±	2.4	Full Positive Slope

With the isolated elbow entity resistance values for each data set in the four categories of interested computed, simple tabulations of respective differences need only be presented. **Table 4-3** shows these differences in addition to percentages in frictional resistance due to the modeled product with respect to the factory elbow baseline control.

Table 4-3: Isolated Frictional Resistance Modeled Product Reduction Results

Category	Conductor and Bolt	Factory (Grams)			Modeled Product (Grams)			Force Reduction (Grams)			Percentage Reduced		
Dry	#12 - Bolt 1	90.9	±	1.2	101.7	±	1.1	-10.8	±	2.3	-12%	±	2.5%
	#12 - Bolt 2	96.5	±	1.1	109.0	±	1.0	-12.5	±	2.1	-13%	±	2.2%
	#12 - Bolt 3	99.5	±	1.4	118.7	±	1.0	-19.2	±	2.4	-19%	±	2.4%
	#10 - Bolt 1	213.8	±	1.3	184.3	±	1.7	29.4	±	3.0	14%	±	1.4%
	#10 - Bolt 2	211.8	±	1.1	204.3	±	2.2	7.5	±	3.3	4%	±	1.6%
	#10 - Bolt 3	232.6	±	1.2	213.4	±	2.6	19.2	±	3.8	8%	±	1.6%
	#8 - Bolt 1	371.3	±	2.1	283.4	±	2.3	87.9	±	4.4	24%	±	1.2%
	#8 - Bolt 2	393.1	±	2.2	326.3	±	2.3	66.9	±	4.6	17%	±	1.2%
	#8 - Bolt 3	-	±	-	341.3	±	2.4	-	±	-	-	±	-
Lubricated	#12 - Bolt 1	39.1	±	0.6	35.6	±	0.6	3.5	±	1.2	9%	±	3.0%
	#12 - Bolt 2	33.7	±	0.6	33.4	±	0.7	0.3	±	1.3	1%	±	3.8%
	#12 - Bolt 3	30.0	±	0.6	28.8	±	0.7	1.2	±	1.4	4%	±	4.6%
	#10 - Bolt 1	118.8	±	1.1	131.6	±	1.2	-12.8	±	2.3	-11%	±	1.9%
	#10 - Bolt 2	135.1	±	1.4	124.2	±	1.2	10.8	±	2.6	8%	±	2.0%
	#10 - Bolt 3	126.4	±	1.4	124.1	±	1.3	2.3	±	2.7	2%	±	2.2%
	#8 - Bolt 1	152.1	±	2.5	197.8	±	2.3	-45.7	±	4.8	-30%	±	3.2%
	#8 - Bolt 2	133.0	±	2.5	172.9	±	2.4	-39.8	±	5.0	-30%	±	3.7%
	#8 - Bolt 3	120.1	±	2.4	164.7	±	2.7	-44.6	±	5.1	-37%	±	4.3%

These force reduction findings are a mix of supportive and unsupportive evidence to the expected values given the implication of a frictional reducing invention. The lubricated #8 conductor's results are starkly counterintuitive as they show that the modeled product likely increases frictional resistance by more than 30%. Given that the data shows the modeled product is not a consistent improvement, no positive information can be gained by scaling the model up to predict the behavior of larger conductors being pulled through an elbow with rollers. However, some trends can be observed and discussed given these small-scale results.

It would appear that faster conductor pulls correlate with a less effective reduction in frictional resistance through any elbow. This can be what would be expected if a conductor were to act more ridged under more intense impulses. These results could mean that a conductor does indeed deform less easily with faster pulling. This trend appears in the dry and lubricated trials even though dry trials are characterized by increasing force with speed while lubricated trials experience less resistance with increased speed. Thus, it may be noted that the trend of reduction effectiveness may not be dependent on material resistance and that lubricant may have an effect on the ease of deforming a material that is more effective with speed.

Conductors may also experience an increase in random jostling during faster pulls. This more frequent or intense random motion could result in more resistance during pulling. This hypothesis is supported by the fact that pulls of higher speeds were characterized by higher amplitudes of stable and randomly induced oscillations. However, the parameters to make a definitive claim for this trend were not controlled or observed throughout this study.

Further elaboration on observed patterns are continued in the next section. Before continuing the narration on the results of interest, **Table 4-4** needs to be introduced and discussed. This table is similar to **Table 4-3**, but the values being subtracted focus on the reduction of friction introduced by applying lubrication.

Table 4-4: Isolated Frictional Resistance Lubricant Reduction Results

Category	Conductor and Bolt	Dry			Lubricated			Force Reduction in Grams			Percentage Reduced		
Factory Baseline	#12 - Bolt 1	90.9	±	1.2	39.1	±	0.6	51.8	±	1.8	57%	±	2%
	#12 - Bolt 2	96.5	±	1.1	33.7	±	0.6	62.8	±	1.8	65%	±	2%
	#12 - Bolt 3	99.5	±	1.4	30.0	±	0.6	69.5	±	2.0	70%	±	2%
	#10 - Bolt 1	213.8	±	1.3	118.8	±	1.1	95.0	±	2.4	44%	±	1%
	#10 - Bolt 2	211.8	±	1.1	135.1	±	1.4	76.7	±	2.5	36%	±	1%
	#10 - Bolt 3	232.6	±	1.2	126.4	±	1.4	106.2	±	2.6	46%	±	1%
	#8 - Bolt 1	371.3	±	2.1	152.1	±	2.5	219.2	±	4.7	59%	±	1%
	#8 - Bolt 2	393.1	±	2.2	133.0	±	2.5	260.1	±	4.7	66%	±	1%
	#8 - Bolt 3	-	±	-	120.1	±	2.4	-	±	-	-	±	-
Modeled Product	#12 - Bolt 1	101.7	±	1.1	35.6	±	0.6	66.1	±	1.7	65%	±	2%
	#12 - Bolt 2	109.0	±	1.0	33.4	±	0.7	75.6	±	1.6	69%	±	2%
	#12 - Bolt 3	118.7	±	1.0	28.8	±	0.7	89.9	±	1.7	76%	±	1%
	#10 - Bolt 1	184.3	±	1.7	131.6	±	1.2	52.7	±	2.9	29%	±	2%
	#10 - Bolt 2	204.3	±	2.2	124.2	±	1.2	80.1	±	3.4	39%	±	2%
	#10 - Bolt 3	213.4	±	2.6	124.1	±	1.3	89.3	±	3.9	42%	±	2%
	#8 - Bolt 1	283.4	±	2.3	197.8	±	2.3	85.6	±	4.5	30%	±	2%
	#8 - Bolt 2	326.3	±	2.3	172.9	±	2.4	153.4	±	4.8	47%	±	1%
	#8 - Bolt 3	341.3	±	2.4	164.7	±	2.7	176.7	±	5.1	52%	±	2%

The immediate and obvious observation from this table is that lubrication not only consistently reduces friction but it does so with significant effect. The secondary trend is that lubricant seems to reduce friction most effectively on faster pulls, but this inference may be convoluted with the ordering of the trials. More often than not, conductors were tested with Bolts 1, 2, and 3 in respective order. Thus a buildup or unintended concentration of lubrication may be responsible for this trend. Regardless, the most definitive claim that can be asserted by comparing the reductions due to the modeled product verses lubricant shows that lubricant is by far in a way more effective and consistent than the applied mechanical effort to reduce frictional resistance. Even with the ambiguity and inferences to be gained for the sake of this area of study, it can be claimed, given that the modeled product is taken to be an acceptably functioning representation of the idealized product, that lubricant is more effective than mechanical efforts to reduce the friction in ninety-degree elbows characterized by rollers arranged to ease pulling.

In other words, the product in question is not likely a beneficial avenue for improving large conductor installation.

4.1.6. Possible Causes for Inconsistencies

This section first considers the unexpected inconsistency between the expected results and the negative frictional resistance reduction for the dry #12 conductor data sets. This conductor, being of the smallest diameter, is most likely to experience pinching from the duel roller entity. The #12 conductor trials may have had at least one roller pair that lifted or separated enough to allow the conductor to be pinched in between them. If this is true, the rollers may have been experiencing unintended restrictions to rotation thus acting as a counterproductive entity that added resistance to pulling. This is the only hypothesized cause for inconsistency that explicitly applies to this case. The remaining trials covered in the un-lubricated or dry trials followed expectations.

The inconstancy is that of the lubricated #10 conductor trials associated with Bolt 1. This one instance has flat spot error, but considerations of the theoretical effect of the flat spot error work against the causes for this inconstancy as the assumed impacts of the error should have resulted in an inflated positive effect. Given no other recorded potential cause for inconsistency, the result is assumed to be the result of the later explained generalized sources of error.

The inflated negative values of frictional resistance reduction for the lubricated #8 conductor may be due to the flat spot error. This inflation is present in the modeled case but not the factory case. High flat spot error is assumed to result in higher calculated mean frictional resistances if the flat spot is taking the place of an oscillation that may have found itself on the

other side of the actual mean value. In comparison, the data of the factory elbow case is not notably subject to any type of flat spot error. This error is most likely due to a systematic video processing error associated with the input to the gauge reader program or within the gauge reader program itself. Thus, the inflation of the modeled product values may at least be a partial cause for the negative effect on frictional resistance.

There are five general, overarching potential sources that may have impacted the data the most. First, the crashes experienced may have effected the gauge in a manner that through off it's calibration. The simple extensive use of the gauge may have also worked it out of calibration, but the crashes should be more concerning. This scenario is considered fairly unlike given the consistency within each data set.

Second, the recording and processing of the videos involved a great deal of effort to ensure the greatest degree of consistency. However, it is noted that any degree of variance in the video editing or recording, if systematically additive in a detrimental direction, could be responsible for the otherwise unexplainable. The pinnacle for this concern is that the gauge reader program integrated an exponential function to very nearly map the needle angle to the gauge reading. The program is not able to calibrate itself or eliminate any systematic error existing prior. This source of error is observed to be unlikely given the consistency of the location of multiple datum points on the videos correlating with the time dependent data output and the fact that all results are relative to each other. Regardless, the lesson learned here for future researchers is to utilize a digital gauge and circumvent these and previously mentioned mechanical sources of error.

The third potential source of notable error is that the ordering of the experiments was systematic and not random. This introduces the impact of any fatigue or systematic

improvement impacting data in a finite and skewing progression. It is strongly advised that future researchers develop a way to randomize the order of trials even though the resulting study would necessitate significantly more time. This randomization should include randomizing all trial parameters including the sample conductor selected.

Fourth, the modeled product in this study was well conceptualized but under prioritized due to lack of funding. A majority of available funds were allocated to a quality tension gauge over the construction of the modeled product. The result may have been a construction that most poorly or inconsistently represented the theoretical benefit. Evidence of this scenario lies in the logical interpretation of the increased frictional resistance of the dry #12 conduction trials being the result of the conductor being pinched in the duel roller assembly.

Last but not least, this experiment considered relatively short lengths of conductors which may have introduced end effects that threw the data due to physical interactions beyond analytical modeling. This can be resolved by increasing the conduit leg and sample conductor lengths. The concept for testing a finite length conductor is only valid if the conductor tested behaves continuously at the elbow for a duration of time that permits a steady state behavior to be clearly observed. This was achieved in this study, but the impact of the length of the conductor was indeed assumed to be non-impactful to the results given consistency among all trials. This is a topic that all future researchers in this area should consider.

Chapter 5 - Alternative Future Testing and Future Research

5.1. Speculation in Alternate Experimentation and Recommendations

Given the ambiguity of the results, their deviation from expectations, and the mention of future recommendations due to complications, this chapter is purposed with restating the recommendations for future research and experimentation. This conglomeration of recommendations should not be considered a scientifically absolute as the recommendations are primarily derived from the experienced and educated opinions resulting from singularly conducting the entirety of the study. There are many lessons to be learned and many developments from this study that should be applied in future studies on conductor pulling improvement.

5.1.1. Modeled Product Construction

The modeled product in this study was constructed as individual roller assemblies fixed to the experiment's frame. The roller assemblies themselves were also simply constructed without extensive sub-experimental verification of their effectiveness. Due to this situation, any variation in the conduit orientation during or in-between experimental trials could easily alter the relationship among the rollers and the conduit and the conductor. These hypothesized variations may theoretically be conductor or speed dependent. Thus, the very nature of construction may be a soul source of dominant ambiguity in the results.

Thus, the recommendation for future experimental construction is to rigidly fix the rolling entities to the modified elbow. This assembly would likely be more complicated than the modeled product considered in this study, but it would remove the potential of this hypothesized

error. Additionally, the alternative modeled product construction should be tested for effectiveness and constancy prior to conducting official trials. This sub-experimental verification is not designed here within, but it is recommended that the sub-experiment be conducted in a quantifiable manner that shows a comparison to the individual roller performance and the respective performance within the modeled product construction.

5.1.2. Speed Control

The speed control, though not quantifiably applied, in the study suffered from a variation of the manufacturer's nominal revolutions per minute and the experimentally determined rotations per minute. Furthermore, the application of the drill as the driving power pulling the conductor operated under the assumption that the torque from the drill was much higher than the torque applied by the pulling cable during a trial. This assumption was left unverified. However, the results of the experiment are relative to each other and thus only depend on a high rate of consistency in application and trial comparison. This exists in this study and the frictional resistance reduction results should be independent of this parameter. However, if a future study does indeed successfully scale up results such as those expected by this study, then speed verification and measurable certainty is highly desirable. Thus, it is recommended that future experiments be conducted with the application of a constant speed, variable torque servo. If this servo motor is applied and is capable of running at multiple fixed speeds, the need for variation in the pulling axle (or the bolts as they were in this study) is eliminated.

5.1.3. Conductor Isolation and End Effects

The results in this experiment showed some time dependency on data stability outside of the transition regions. This was mostly highlighted in trials that included the treatment of lubricant. While the causes of this dependency mostly embodied in the slopping of Region 2 are thoroughly discussed, some trials exemplified a lack of slope completely as well as a point of stability. This implies that some trials may have been subject to a secondary transient state to stability. The trials in this study that sloped without a final point of stability may simply have been too short for the phenomenon to be fully observed and treated accordingly. Thus, the inclusion of slopped data in this study may have inflated or deflated mean frictional resistance values to the point of ambiguity. The sloped data included in this study, without sufficient evidence for invalidation, is taken to be reflective the actual physical states of interest.

In addition, the ends of Region 2 were often subject to secondary steps in stability up or down prior to entering the identified transition region. The lines between this effect and the effect of sloping data is somewhat blurred. The potential cause for the hypothesized step in stability is that the conductor behaves differently once the end of the conductor is no longer much farther away from the elbow relative to the arc length spanned by the elbow. In short, the behavior of the conductor may change in a way that is not reflective of a continuous pull due to end effects.

While both of these hypothesized problems are different, the solution to resolve and distinguish their separate existences clearly may be the same. This recommended solution is to lengthen the legs on both ends of the elbow as well as increased the length of the conductors being tested. The duration of time in which Region 2 exists in this study is as little as one to two seconds in some trials. If either situation described above impacted the results as discussed, the

extended length applied to future experiments would yield a proportionally longer Region 2 given similar applied speed treatments. Alternatively, the speeds applied to testing can be lowered, but this approach risks the potential for insufficient scalable results. If speeds are not varied enough, extrapolation of relationships of data too closely associated to each other may be inaccurately representative. It is recommended that future studies investigate lubricated trials with varying lengths of conductors in order to document any observation that could support the existence of either. If a conductor and conduit leg length can be selected to provide a minimum length of Region 2 that can capture a clear difference among end effects, transient states, and stability, then that length can be applied to the official trials. This application could then lead to only statistically considering the stable data within Region 2 to yield more refined and informative data.

5.1.4. Scale

This was most nearly the smallest scale experiment possible for testing the mechanical reduction of frictional resistance in pulling conductors. The small scale does mean that the differences among varying regions, transitions, and trials, are more likely to be of greater relative uncertainty and to be potentially indistinguishable. This was an unfortunate restriction of this study due to lack of funding. It would be desirable to consider larger conductors and conduit combinations per the outlined process in this study. This would enable the production of potentially more defined results and the investigation parameters considered to be beyond the scope of this study. For example, the number of strands contained within a conductor was excluded from consideration here as the conductor sizes tested all contained nineteen copper strands each. Ultimately, studies of slightly to moderately larger scale would likely yield more

informative and diverse results. If evidence is found that mechanical means do indeed ease the installation of large conductors, a full sized experiment would be the most definitive and advantageous source of the product effectiveness.

5.1.5. Gauge Application

The application of a mechanical gauge in this study clearly led to multiple potential sources of errors and data processing complications. The most restrictive impact to the study was the extensive time that had to be dedicated to video processing. The only notable functional benefit that a mechanical gauge may have over a digital alternative is the long response time that acts as a dampening agent to inconsistencies in a pull such as a conductor or conductor header catching the inside of the conduit. This reduces the risk of damage to the system, as the impulse from a catch or inconsistency is longer and thus of lower maximum force.

Regardless, if a digital gauge is robust enough to handle the spikes in tension of future testing, it would result in directly digitized data that circumvents all sources of error associated with video data digitization. Avoiding the extensive process to obtain data from a mechanical gauge is an intense motivation for this recommendation. It should also be noted that the gauge selected for testing should cover a readable range well over the maximum expected force given the largest conductor intended for testing. This is to ensure that the omission of intended trials does not become a necessity as it was in this study with the un-lubricated #8 conductor being pulled by Bolt 3. Additionally, it is recommended that the gauge selected be easily fixed to the experiment frame. That was a very positive feature of the mechanical gauge used in this study.

5.1.6. Crash Protection

The potentially damaging crashes experienced during this study had the potential to render further experimentation with the given equipment impossible. Crash protection should be a major concern for future studies for the sake of protecting the investment of the experimental equipment. The method applied with the catch in this study was clearly unsuccessful due to being too rigid. There are three ideas for crash protection that developed after this study's experiments were conducted. The first is that a catch be suspended through the path of the pulling wire with elastic bands that reach their maximum extension just prior to the conductor reaching the tension gauge. This mechanism would be more effective by implementing the much more flexible elastic. This should also give much more obvious and prolonged warning to disengage the conductor pulling before a crash occurs.

The second concept for crash protection would be to provide a breakaway connection shortly after the header on the pull string. The pulling side of the breakaway connection would have to be narrow enough to be pulled through the gauge rollers without sustaining damage to the gauge. This concept would have to be applied with a catch that is fixed enough to permit the breakaway connection to function prior to the gauge sustaining damage. This concept is conceptually effective, but actual constructions should be tested in the absence of the gauge to ensure proper function. It should also be tested to ensure that it does not breakaway at force levels that are reached during normal spikes that occur during a pull. A breakaway connection that is too weak will leave the conductor being tested disconnected midway through a trial and necessitate chronic retesting.

5.1.7. Conductor Selection

In selecting conductors for future experimentation, it is recommended that the selected conductors share and vary in properties that can be applied to non-dimensional numbers for the sake of scaling. In this study, parameters such as strand count were taken as beyond the experiment's scope due to other limiting factors. For more overarching and conclusive results, future studies should consider what parameters are to be considered within and beyond their scope. Conductors and the overall experimental design should respectively include and accommodate the included parameters intended.

5.1.8. Header Preparation

Header preparation skills appeared to improve as this study progressed. Impact from defects in header construction was more prominent in earlier trials. One of the most important facets of header construction is the bias cut on the end of the conductor used to produce an appropriately pointed end. This pointing of the conductor reduces the odds of catching on the inside of conduit joints during pulling. It is recommended that future experimenters practice their header construction of choice multiple times prior to official tests to ensure constant and quality constructions. While the header construction applied to this study was appropriate, it is a facet of the experiment that may be improved for the sake of minimizing error.

5.1.9. Bolt and Mount Design

The bolts used to wind the pull string in this study were mounted into a universally compatible mounting. While this was beneficial for the ease of the experiment execution and trial transition, the smaller bolts were subject to minor movement as the mount holes were

larger than need be for them. To reduce noise and variation, it is recommended that future experiments be designed to ensure appropriate mounting for each respective bolt if the varying diameters to vary speed is recycled from this study's experimental design.

5.1.10.Randomization Factors

This study executed experimental trials systematically due to necessity and time restrictions. As mentioned in the last chapter, this systematic approach introduces the potential to systematically fatigue facets of the system that skew the results of later trials relative to the earlier trials. This is not the healthiest approach for future experimentation given the level of ambiguity in this study's results. An example of this fatigue is the built up of lubrication from one trial to the next. Additional lubricant was applied throughout the conducting of trials in order to attain consistency, but the buildup of lubricant over time may have had an effect. This is especially true since the lubricant does dry and all lubricated trials were not conducted on the same day. A second example of systematic fatigue that could be impactful is that a conductor sample may not maintain the same level of resistance to bending over time. Thus, the samples that were used could have easily been deflating the results of later trials. This impact is would be completely masked without the application of randomization.

To randomize future experiments, it is recommended that every trial's set of treatments or parameters be represented finitely in pools of objects that are selected randomly to define the next trial to be conducted. For example, consider taking a bucket of marbles that are of colors that correlate to conductor sizes, another bucket with marbles that correlate to applied speeds, a bucket with marbles that correlate to trial categories, and a bucket that contains two marble colors that correlate to lubricated and un-lubricated experiments. Each type of marble will only

exist as many times as it's representative parameter is supposed to occur in the study's cumulative trials. These buckets may need to be broken up into further subsets so that a sequence of drawing marbles will identify the next trial to be conducted without unintended repetition until all intended trials are conducted. As long as quantities are sufficiently mixed and partitioned to satisfy the experimental design, this approach adequately randomizes the sequence of trials. Alternatively, a statistical computer program can be used to randomize the sequence of all intended trials. The randomization will necessitate more time in setting up and transitioning between trials, but the result of executing a proper randomization would ensure that fatigue effects do not systematically skew future results.

5.1.11. Lubricant Treatment

The application of lubricant resulted in some subtle inconsistencies that were not present in the un-lubricated trails. The lubricant application is also time and air sensitive since it dries out. There are many parameters that need considered and some may be beyond reasonable control. This may be acceptable as long as the experimental design considers appropriate relationship to field installation conditions. The main concerns expressed about the impact of lubricant are resolved in other sections of this chapter. However, there are two recommendations that apply exclusively to lubrication. The application of the lubricant must be systematically consistent as was the case in this study. There may be more precise ways to ensure consistency of the application, and it is recommended that future researchers do not gloss over this area, as it is rather impactful to the quality of the results. The second recommendation is that future researchers should have provisions to systematically clean the lubricant from the system trials to avoid the impact of lubricant build up. This approach may require testing to

determine how often the system needs to be cleaned out to ensure consistent results with the least labor. Furthermore, the cleaning to be applied must not impact the coefficient of friction of the conduit or leave a residue that would not be present in the field or consistent in-between trials.

5.1.12. Conduit and Segmentation

The conduit construction in this study was modularized along with the frame for the sake of transportation. The negative aspect to the modular approach is the increased frequency of connections throughout straight conduit legs. This increases the chances of the conductor header catching during a trial. This is undesirable even though such is reflective of field conditions. It is recommended that segmentation be minimalized as much as possible in future experimentation.

The conduit type and size were held constant in this study. The same is true about the elbow size in all respects. It is recommended that future studies vary these parameters if more promise for mechanical reduction of frictional resistance is discovered. This would diversify the results in a manner than may very well find an optimal case for the application of the idealized product.

5.1.13. Data Analysis

In processing the data in this study, there were many complications and tedious cleanings due to the processing from video data. While selecting a digital gauge would eliminate the majority of these processing challenges, there are data specific recommendations that should continue to be applicable regardless of gauge selection.

It is recommended that the raw data be processed in chunks per category, as the data collected for this study was too much to process in one collection with standard spreadsheet processing. Systematic templates and linked files ease the processing of data and reduce crashing substantially. While handling these large sums of data, it is most helpful to consider graphical representations that are synced for comparison. The time dependency in this study was not required to gain the data of interest, but the data sets that were most nearly synced produced more informative charts. It is recommended that time dependent data be presented in a manner that syncs results as much as is reasonable. Lastly, the mount of data as processed in this study is desirable for minimizing standard uncertainty, but the larger data set is cumbersome to process. Regardless of how data is collected, it is recommended that the frequency in which data is collected be lengthened relative to this study while still maintaining satisfaction of the Nyquist Theorem. This is ultimately a light recommendation that should be considered as a polite suggestion to ease the speed of processing without compromising the certainty of the results.

Chapter 6 - Conclusion

6.1. Conclusion from the Experiment

The experiment conducted by this study was, according to the research conducted for the literature review, the first of its kind. The experimental design successfully isolated a narrowed scope that was still substantial enough to claim definitive progress. Additionally, the theories and scientific backing for investigating this avenue experientially are well documented for ample justification. Existing conditions and limitations of field conditions were used to select parameters for individualized isolation and variation for varying data sets. The experimental design for scaled testing is well intended and outlined in extensive detail per Buckingham Pi Theorem. The experiment's physical parameters for design were carefully crafted with some level of trial and error into what is ultimately detailed heavily in Chapter 3. While not problem or error free, the execution of the experiments themselves was still successfully conducted in a repeatable and consistent manner thought the early fall of 2017. Videos collected from the experiment were processed with magnificent resolution and detail by the gauge reader program even though extensive cleaning and handling was required before and after the execution of the program. In the end, reflection on the quantized data led to the hypothesis of physical elements of the experiment design that resulted in a clouding level of unexpected ambiguity. The most notable of these hypothesized sources of error was the disjointing of the roller and modified elbow assemblies. This and other potential physical flaws were evaluated in detail for the sake of making thorough recommendations for future researchers.

6.2. Conclusion from the Data

The data from the experiment was originally intended to be applied for scaling up for the prediction of frictional resistance reduction of large conductors given the application of the idealized product. Unfortunately this intention was stunted by the ambiguity of unexpected results. The mix of reduction and increased frictional resistance of the isolated elbow values show that some uncontrolled elements of the experiment were impacting the results on a basis that was nearly entirely dependent on the category considered. There were still informative trends that can be used to extrapolate beneficial and productive results. The first of these is that faster conductor pulls are less affected by the modeled product while lubricant seems to be increasingly effective with increased speed. The data also highlighted an increase in oscillation amplitude on faster pulls. This implies that faster pulls are potentially subject to more end effects that may be resolved in future studies by increasing the lengths of tested conductors. Lastly, the experiment does show a consistent and significant friction reduction as a result of the application of lubricant. Even in the face of ambiguity, there is a significant difference between the level of effectiveness of the modeled product and the lubricant. Thus the conclusion that can be made given the assumption that the modeled product of this study is representative of the idealized application of rollers is that lubricant is effective enough to render the application of mechanical means to reduce frictional resistance none beneficial.

6.3. Conclusion of the Study

While the overall interpretation of the data indicates that this mechanical reduction of frictional resistance is not effective, there are more qualitative factors to consider. The main contradiction to this statement and what prevents it from being definitive is that fact the

evidence exists to hypothesis that the separation of the rolling assemblies and the conduit elbow resulted in a categorically dependent reduction in effectiveness. This hypothesis resolves the contradictions in the data and further supports the theory on which the product is based. As shown in Chapter 2, rollers are applied to pulling cables through bends in data trays. Furthermore, the fundamental fact that properly applied rollers should reduce frictional resistance is sound. It should also be remembered that this experiment was purposed with the narrowed scope of a singular conductor. A singular conductor pull is rare in the field, and the stunted modeling of this study further prevents a statement to be made to build toward establishing how much the idealized product would or would not reduce frictional resistance. Thus the effectiveness of the idealized product can neither be confirmed nor denied. What can be said is that future research conducted to resolve the ambiguity from the hypothesized sources of error can resolve conflict between the following two options for a definitive conclusion: 1) If a future experiment that is developed from this study proves the ineffectiveness or relatively small effectiveness of the idealized product, it can be concluded that the further development toward establishing value of applying mechanical means to reduce the frictional resistance of pulling large conductors is an empty endeavor as the frictional reduction from lubricant will be physically and economically dominate thus rendering the idealized product irrelevant. 2) If a future experiment that is developed from this study can resolve the ambiguity of the results to yield a sizable and expected net reduction in frictional resistance, further future studies should be pursued to investigate the full scale modeling of the idealized product to completely and economically quantify the benefits of applying mechanical means to reduce the frictional resistance of pulling large conductors.

References

Munson, B. R. (2013). *Fundamentals of fluid mechanics*(7th ed.). Hoboken, NJ: Wiley.

Amazon. (2010, October). Greenlee 20249R Right Angle Rollers, 24-Inch, Radius 90-Degree. Retrieved October, 2017, from https://www.amazon.com/Greenlee-20249R-Rollers-24-Inch-90-Degree/dp/B00125IVDU

CESTOOLS.com. (2018). Current Tools 95036RA 90° Right Angle Rollers With 36" Radius. Retrieved October, 2017, from http://www.cestools.com/current-tools-95036ra-90-right-angle-rollers-with-36-radius/

Check-Line. (2017). ODT Stationary Tension Meter. Retrieved June, 2017, from https://www.checkline.com/stationary_tension_meters/odt

Current Tools. (2017). 24" Radius Right Angle Roller. Retrieved October, 2017, from http://www.currenttools.com/products/sheaves-and-cable-rollers/385-24-radius-right-angle-roller.html

Dahlke, S. (2007, January 01). Tension reduction, lubrication on high-performance data cable. Retrieved January, 2018, from http://www.cablinginstall.com/articles/print/volume-15/issue-1/features/cable-sharing/tension-reduction-lubrication-on-high-performance-data-cable.html

General Cable. (2011, September). Cable Installation Manual for Power and Control Cable. Retrieved November, 2017, from http://cdn.generalcable.com/assets/documents/information-center/downloads/brochures/01$GC_Cable-Install_Manual_PowerControl_Cables-7_14.pdf?ext=.pdf

General Cable. (2014). Dynamic Friction: Slick Solutions for Sticky Situations. Retrieved February, 2018, from https://cdn.generalcable.com/assets/documents/North America Documents/Information-Center/Brochures-Sell Sheets/Industrial/GC-Coefficient-of-Dynamic-Friction.PDF

Greenlee. (2015). CABLE PULLING. Retrieved December, 2017, from https://greenlee-cdn.ebizcdn.com/media/2015 Cable Pulling.pdf

Ideal. (2018). Yellow 77® Wire Pulling Lubricant. Retrieved February, 2018, from https://www.idealind.com/ideal-electrical/us/en/products/electrical-supplies/25-wire-pulling-lubricant/1-yellow-77-wire-pulling-lubricant.aspx

Lumen Learning. (2012). Periodic Motion. Retrieved February, 2018, from https://courses.lumenlearning.com/boundless-physics/chapter/periodic-motion/

MSC Direct. (2018). Double Eye, Closed Mesh, Bronze Wire Pulling Grip. Retrieved February, 2018, from https://www.mscdirect.com/product/details/70498258

NFPA. (2013). NFPA 70: National Electrical Code (2014 Edition ed.). Quincy, MA: National Fire Protection Association.

Priority Wire & Cable, INC. (2015). NEC CONDUIT FILL. Retrieved February, 2018, from http://www.prioritywire.com/techdocs/conduitfill.pdf

Professional Data Analysis Recommendations From Dr. Brian Washburn [Personal interview]. (2018, March 2).

Rouse, M. (2005, September). What is Nyquist Theorem? - Definition from WhatIs.com. Retrieved March, 2018, from http://whatis.techtarget.com/definition/Nyquist-Theorem

Sealock, J. (2014, February 26). How to Choose Bass Fishing Line. Retrieved February, 2018, from https://scout.com/outdoors/bass-fishing/Article/How-to-Choose-Bass-Fishing-Line-106128234

Southwire. (2005). Power Cable Installation Guide. Retrieved November, 2017, from https://www.anixter.com/content/dam/Suppliers/Southwire/Literature/envirotectPowerCableInstallManual.pdf

Southwire. (2007). Installation and Application Guide for 600V Conductors. Retrieved November, 2017, from http://www.simpullsolutions.com/documents/simpullthhninstallationandapplicationguide8-15-07.pdf

Southwire. (2017). THHN/THWN/TWN75/T90. Retrieved January, 2018, from http://www.southwire.com/ProductCatalog/XTEInterfaceServlet?contentKey=prodcatsheetOEM5

Southwire. (2018). Pulling Cables? Keep Them Slippery! Retrieved February, 2018, from http://www.southwire.com/support/PullingCablesKeepthemSlippery.htm

Taylor, J. R. (1997). *An introduction to error analysis: The study of uncertainties in physical measurements*(2nd ed.). Sausalito (Calif.): University Science Books.

The University of Tennessee. (2009, August). Wheels. Retrieved March 16, 2018, from http://electron6.phys.utk.edu/101/CH2/wheels.htm

Walker, J. (2013). *Fundamentals of Physics Extended (10th Edition)*(10th ed.). Wiley.

West, S. (2017, November 13). Origin of the pulley system and how a block and tackle work. Retrieved February, 2018, from https://www.ronstanindustrial.com/how-pulley-system-changed-the-world/

Williams, M. (2015, February 16). What is Hooke's Law? Retrieved February, 2018, from https://phys.org/news/2015-02-law.html

Wire & Cable Your Way. (2017). THHN/THWN-2 Wire • Cut by the Foot from $0.09/ft | Wire & Cable Your Way. Retrieved July, 2017, from https://www.wireandcableyourway.com/THHN-THWN/

Appendix A - Experimental Data

A.1. Factory Baseline – Dry

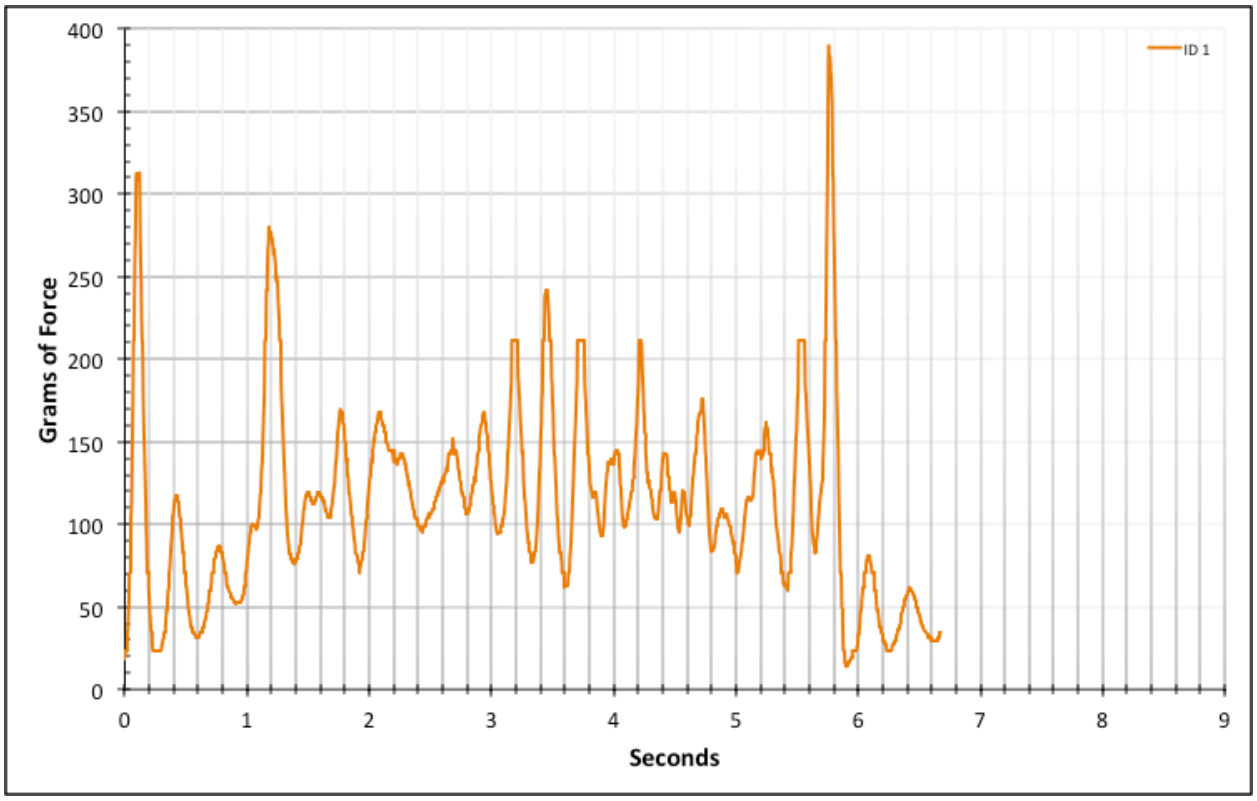

Figure A-6-1: Full Factory Baseline - Dry - ID 1 - #12, Bolt 1

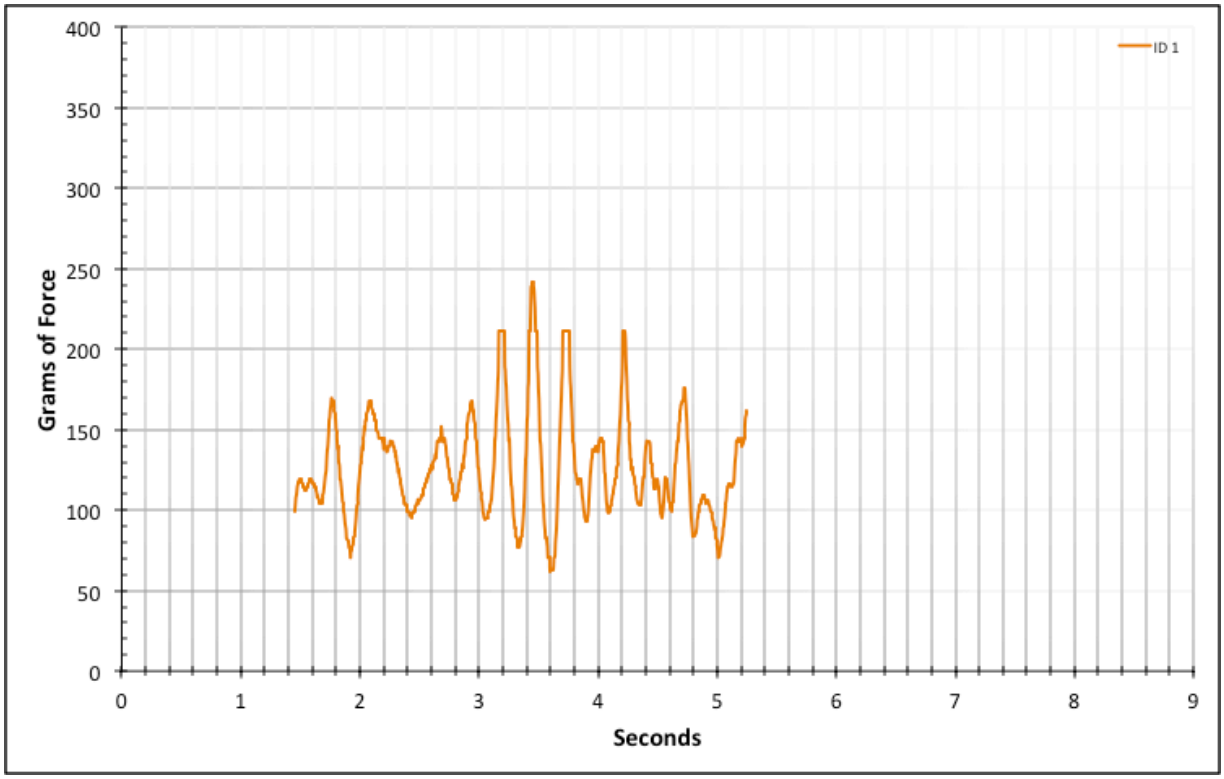

Figure A-6-2: Statistical Region Factory Baseline - Dry - ID 1 - #12, Bolt 1

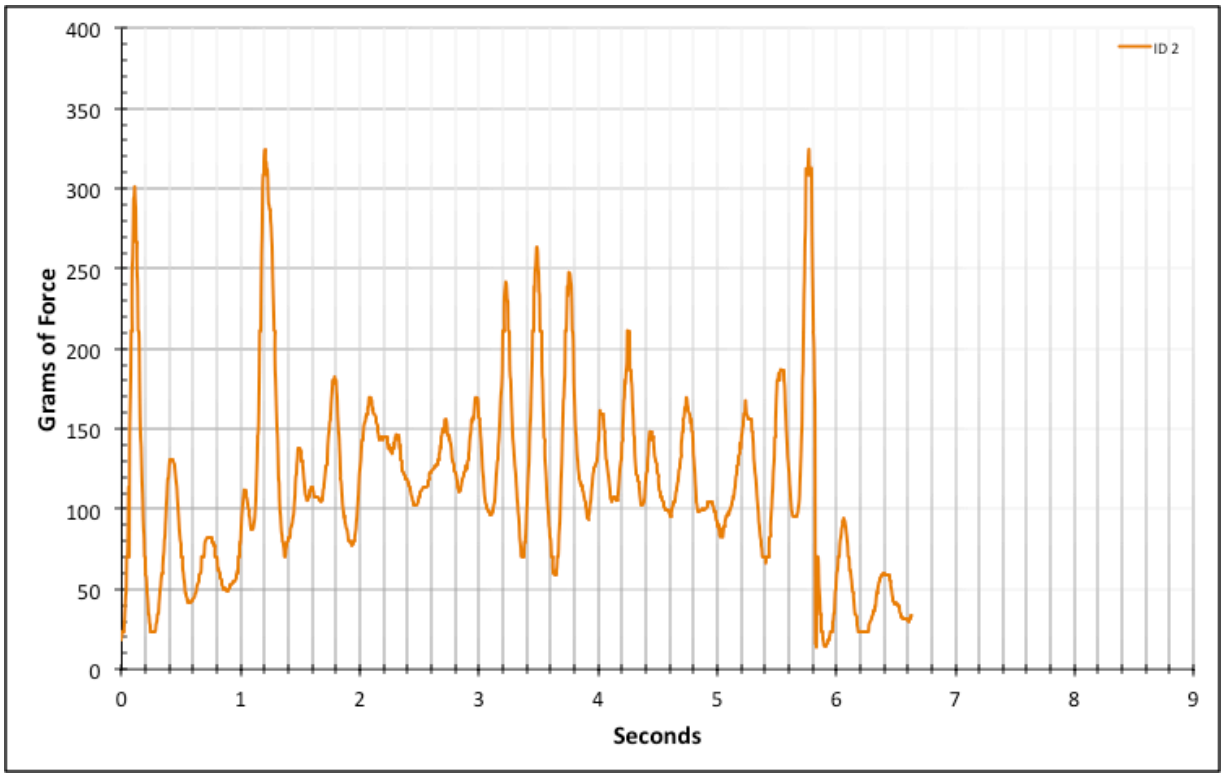

Figure A-6-3: Full Factory Baseline - Dry - ID 2 - #12, Bolt 1

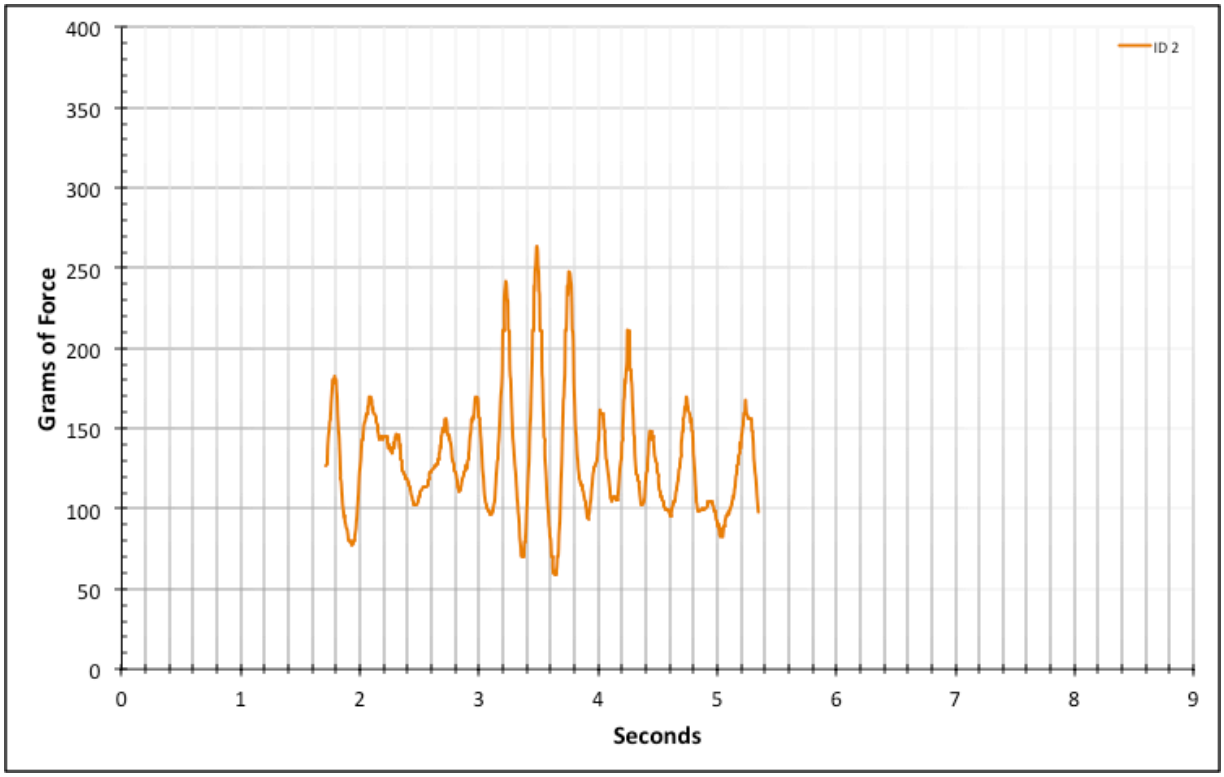

Figure A-6-4: Statistical Region Factory Baseline - Dry - ID 2 - #12, Bolt 1

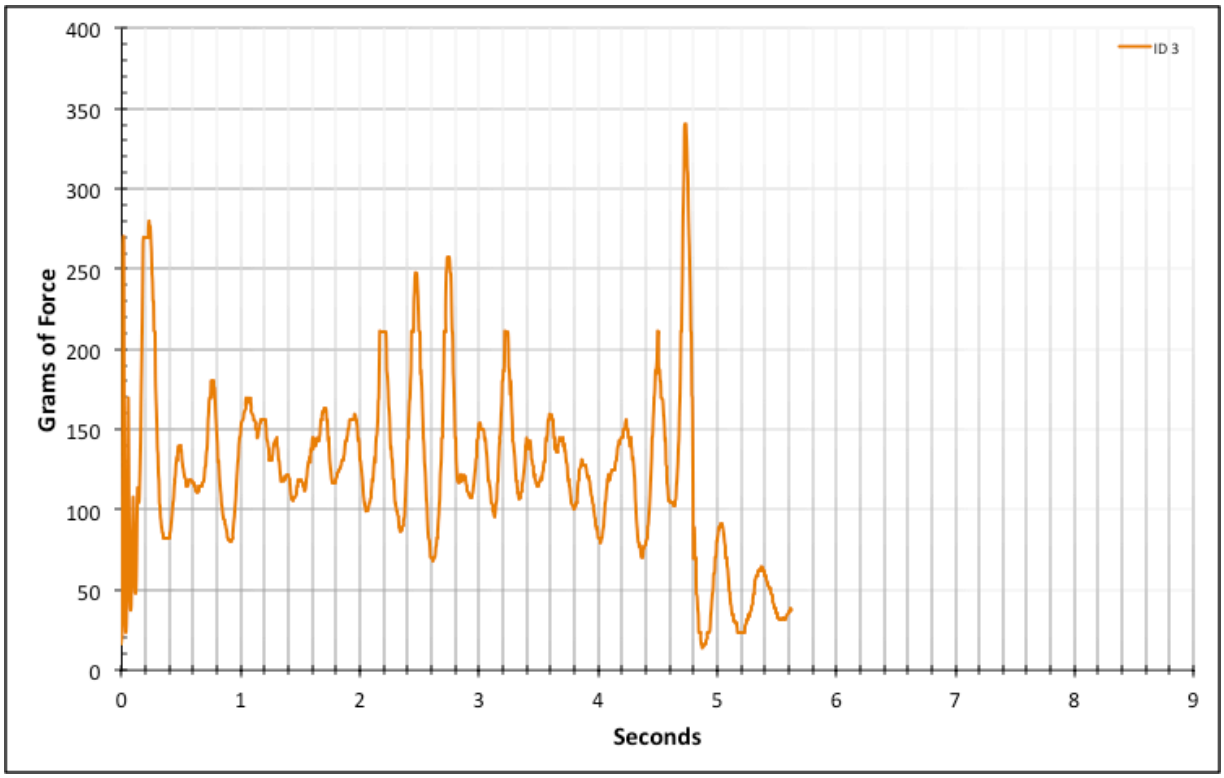

Figure A-6-5: Full Factory Baseline - Dry - ID 3 - #12, Bolt 1

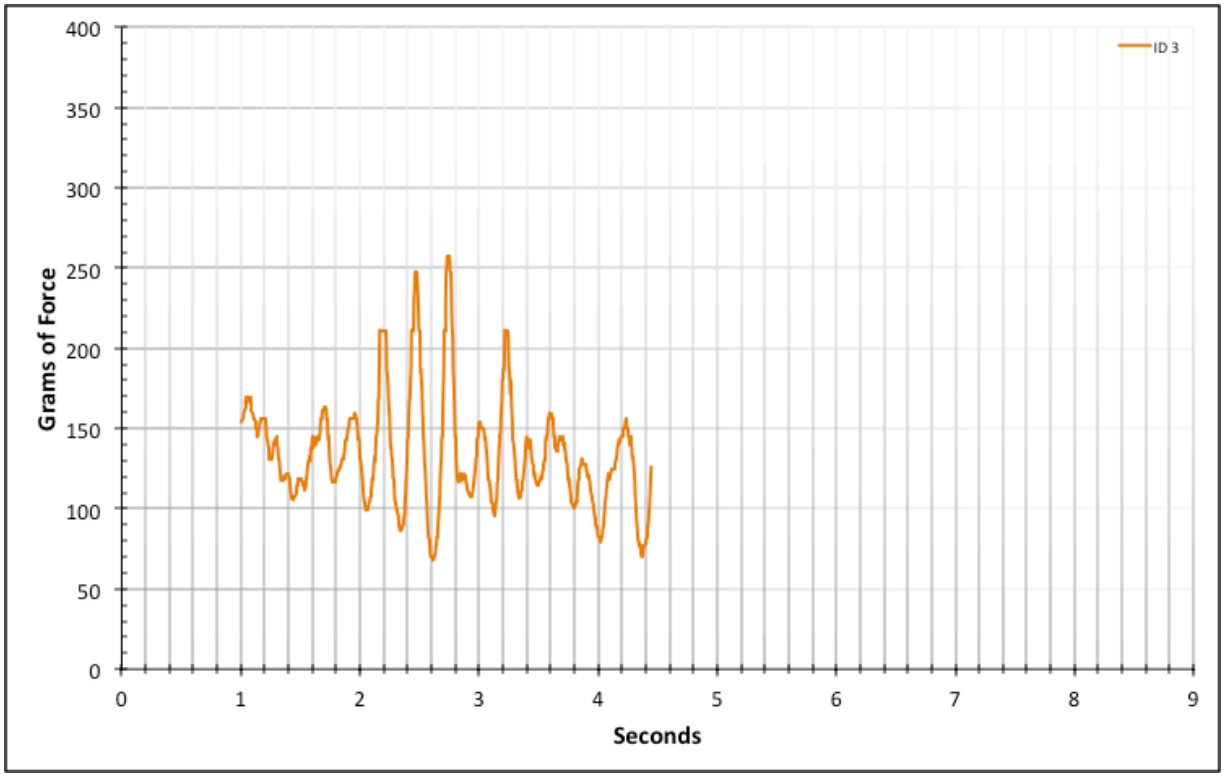

Figure A-6-6: Statistical Region Factory Baseline - Dry - ID 3 - #12, Bolt 1

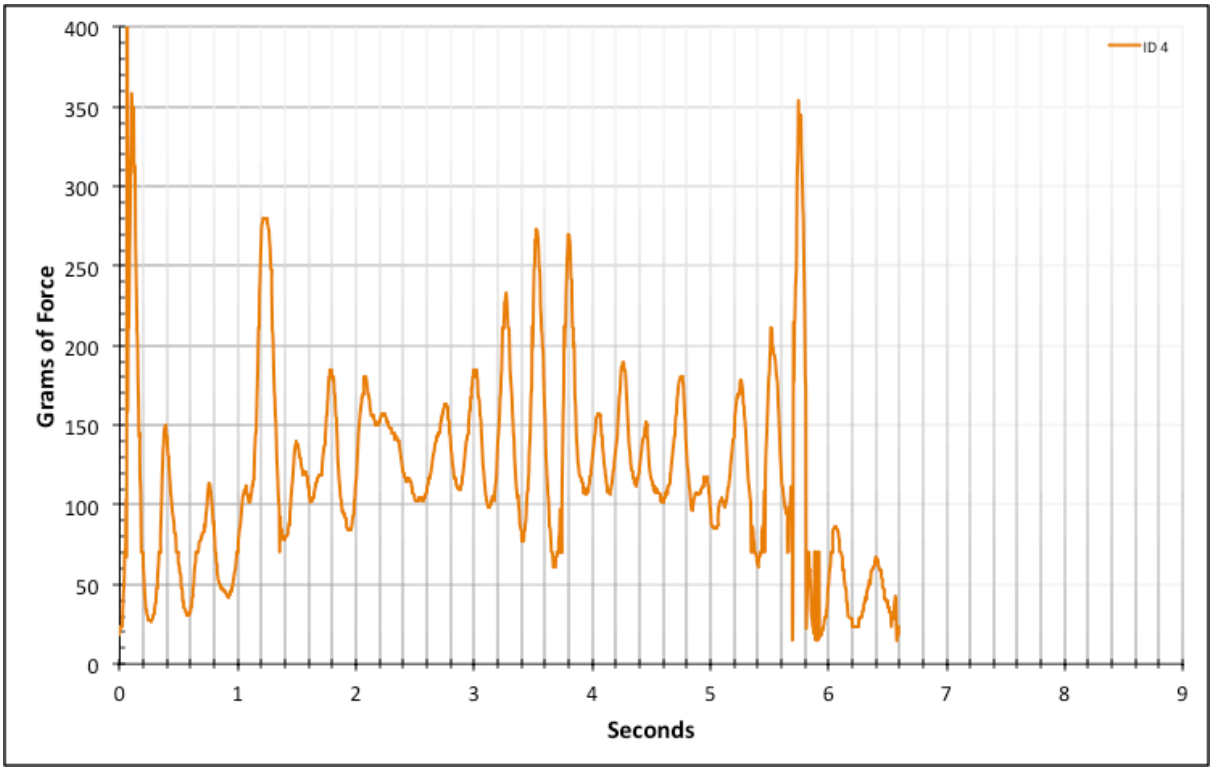

Figure A-6-7: Full Factory Baseline - Dry - ID 4 - #12, Bolt 1

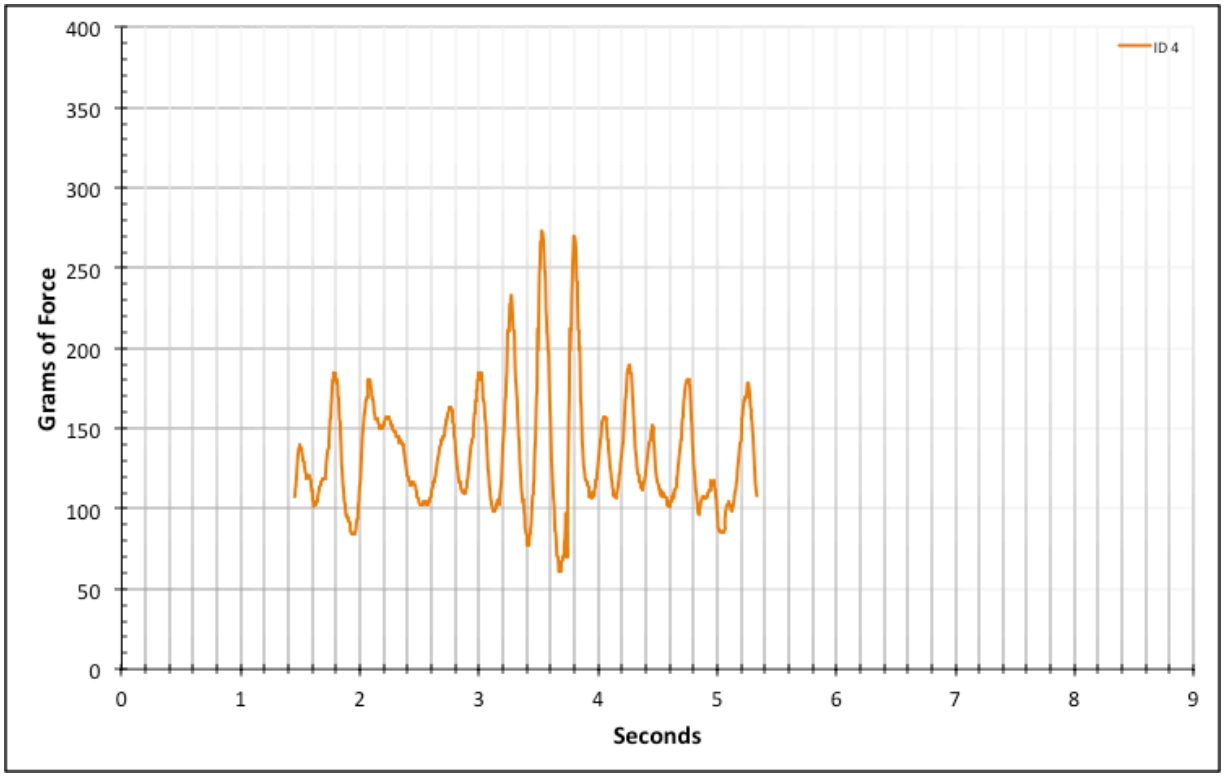

Figure A-6-8: Statistical Region Factory Baseline - Dry - ID 4 - #12, Bolt 1

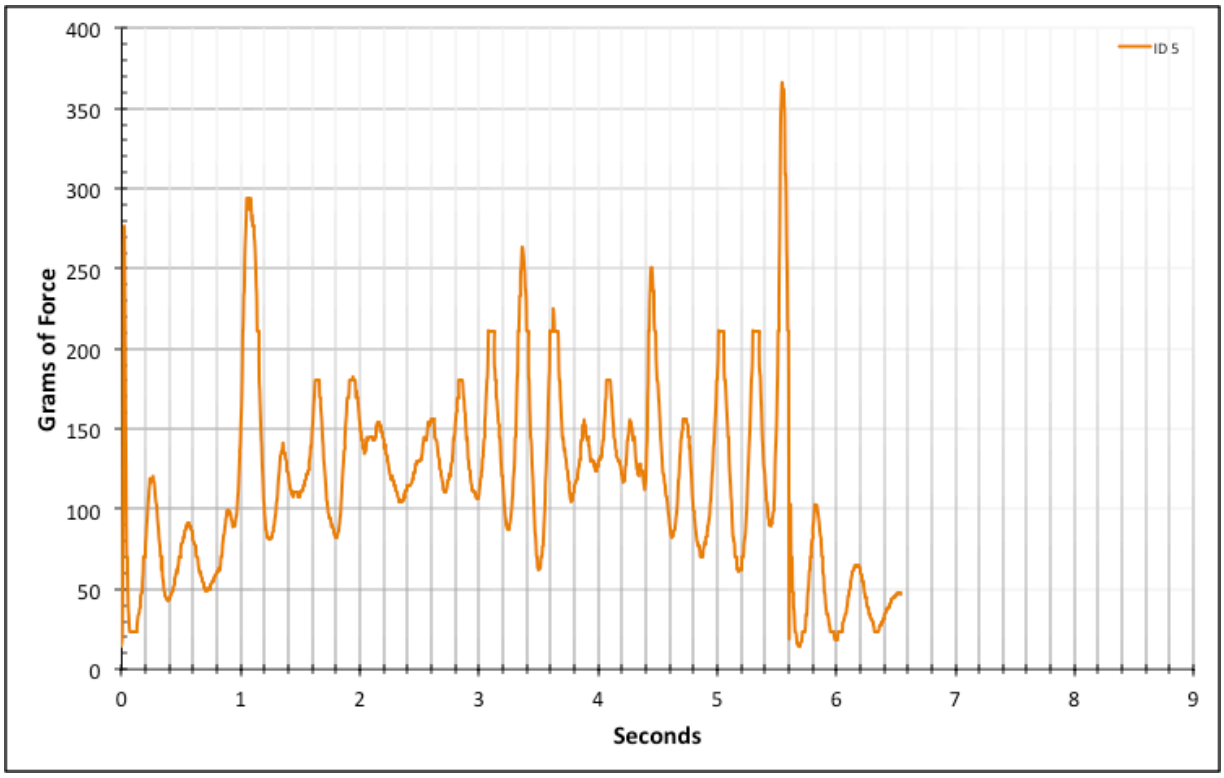

Figure A-6-9: Full Factory Baseline - Dry - ID 5 - #12, Bolt 1

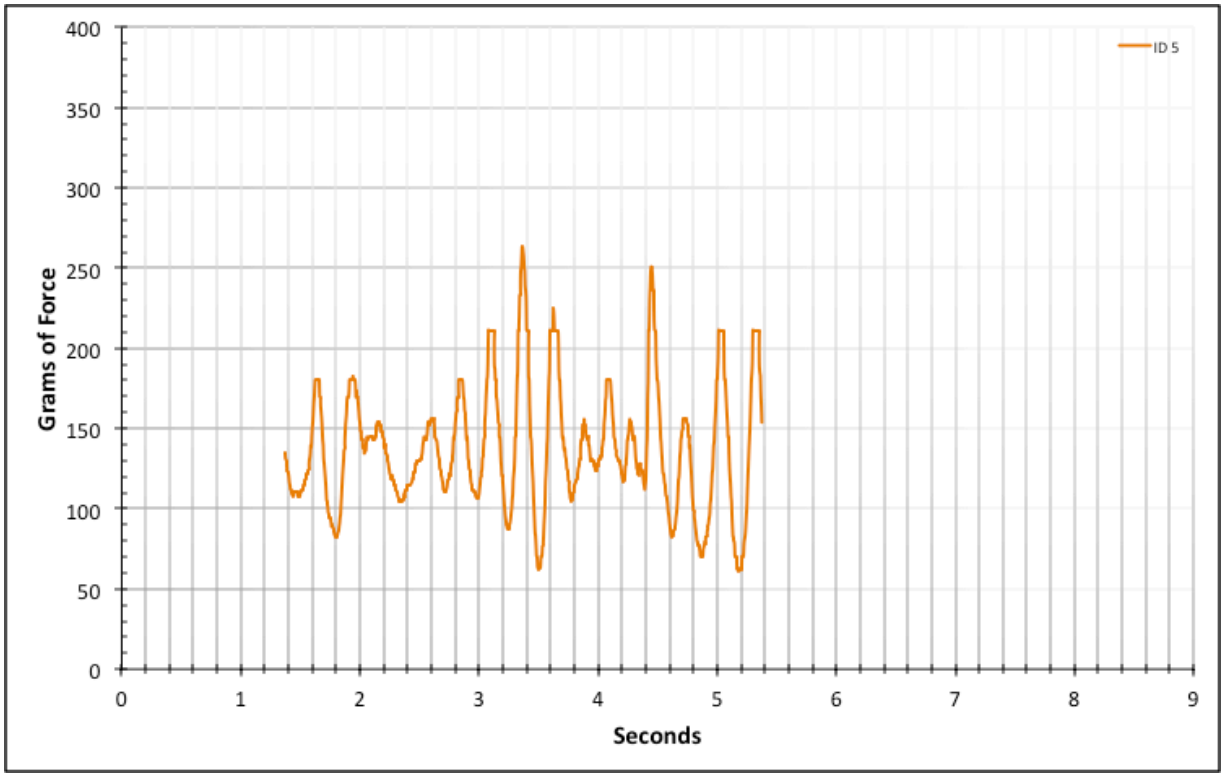

Figure A-6-10: Statistical Region Factory Baseline - Dry - ID 5 - #12, Bolt 1

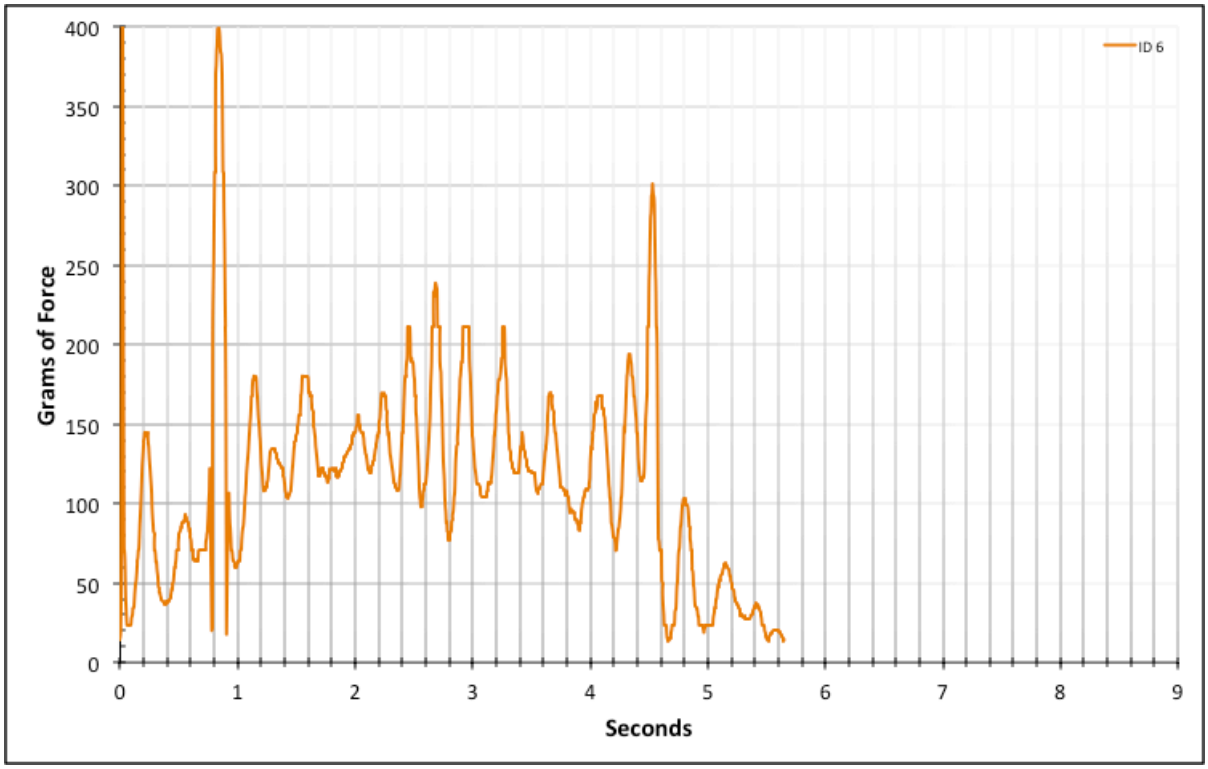

Figure A-6-11: Full Factory Baseline - Dry - ID 6 - #12, Bolt 2

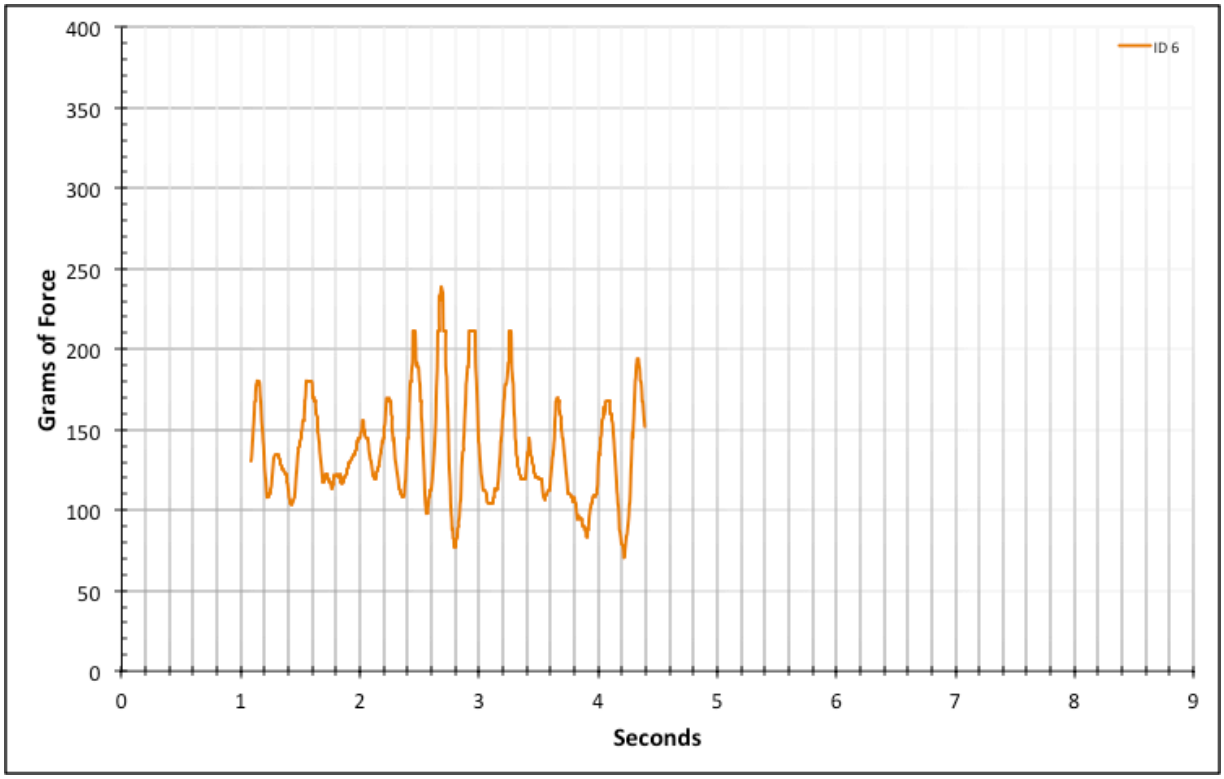

Figure A-6-12: Statistical Region Factory Baseline - Dry - ID 6 - #12, Bolt 2

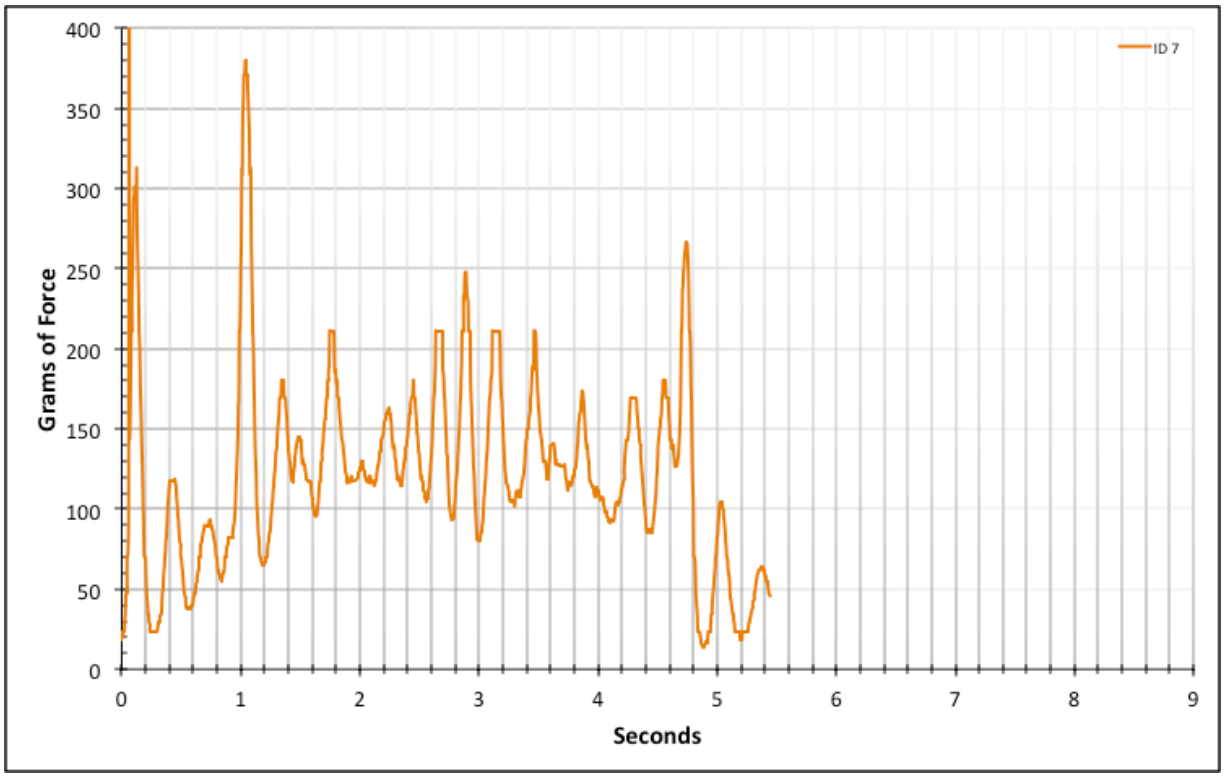

Figure A-6-13: Full Factory Baseline - Dry - ID 7 - #12, Bolt 2

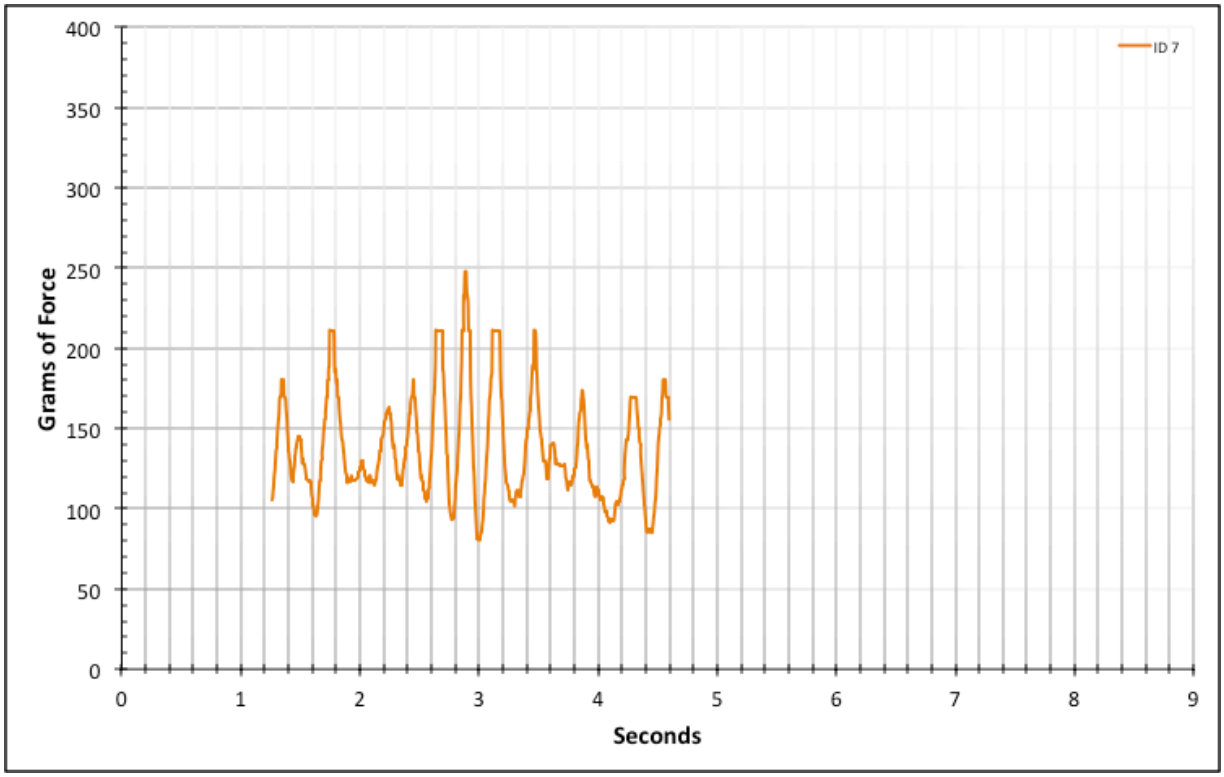

Figure A-6-14: Statistical Region Factory Baseline - Dry - ID 7 - #12, Bolt 2

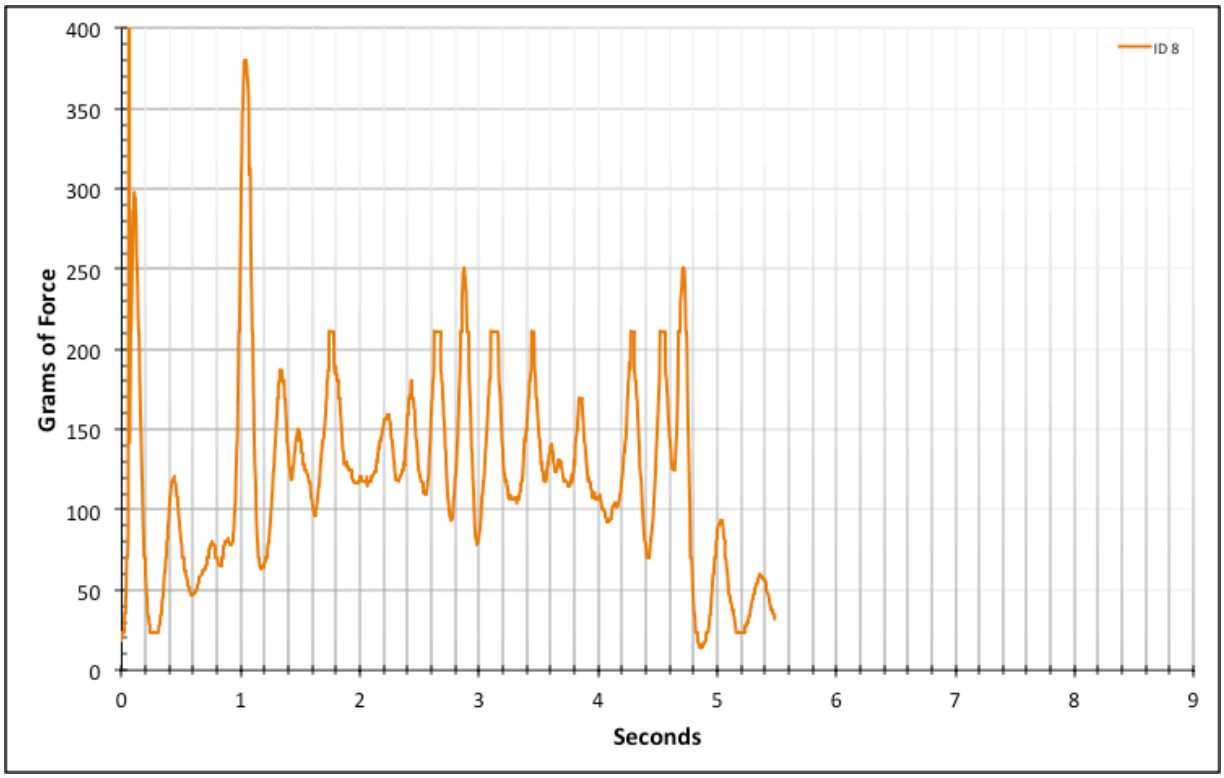

Figure A-6-15: Full Factory Baseline - Dry - ID 8 - #12, Bolt 2

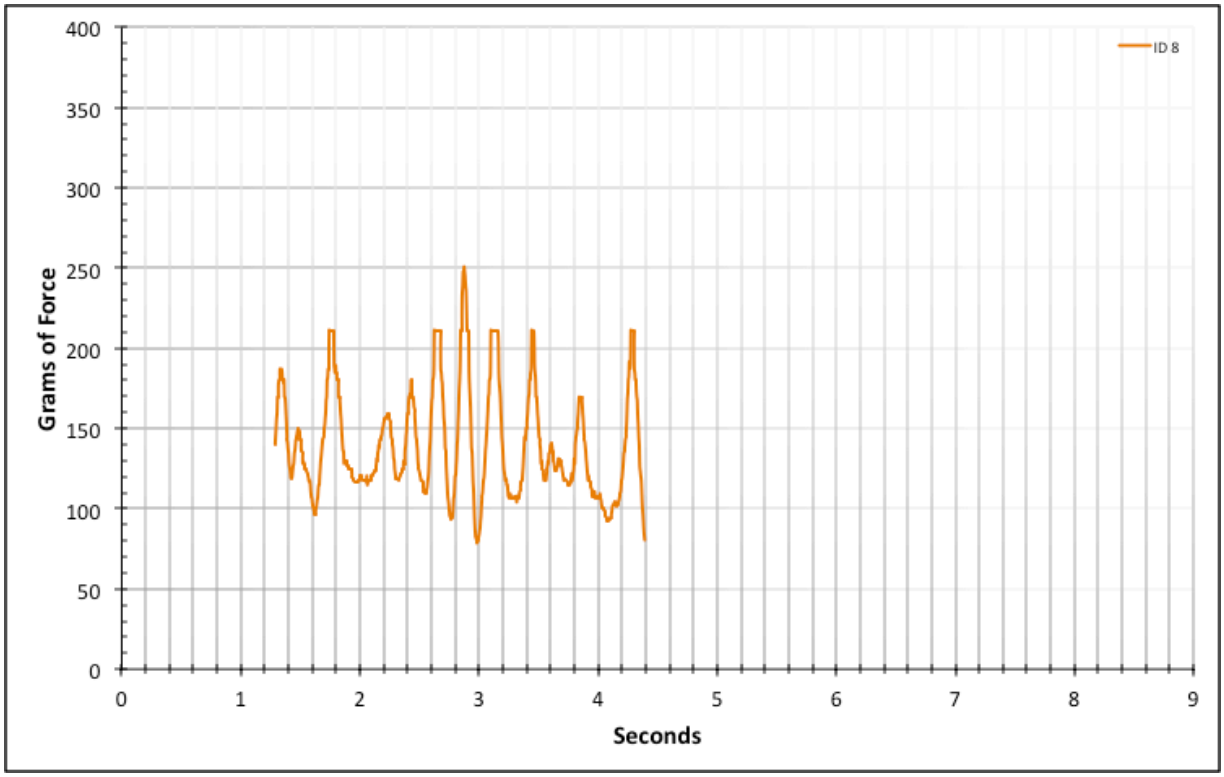

Figure A-6-16: Statistical Region Factory Baseline - Dry - ID 8 - #12, Bolt 2

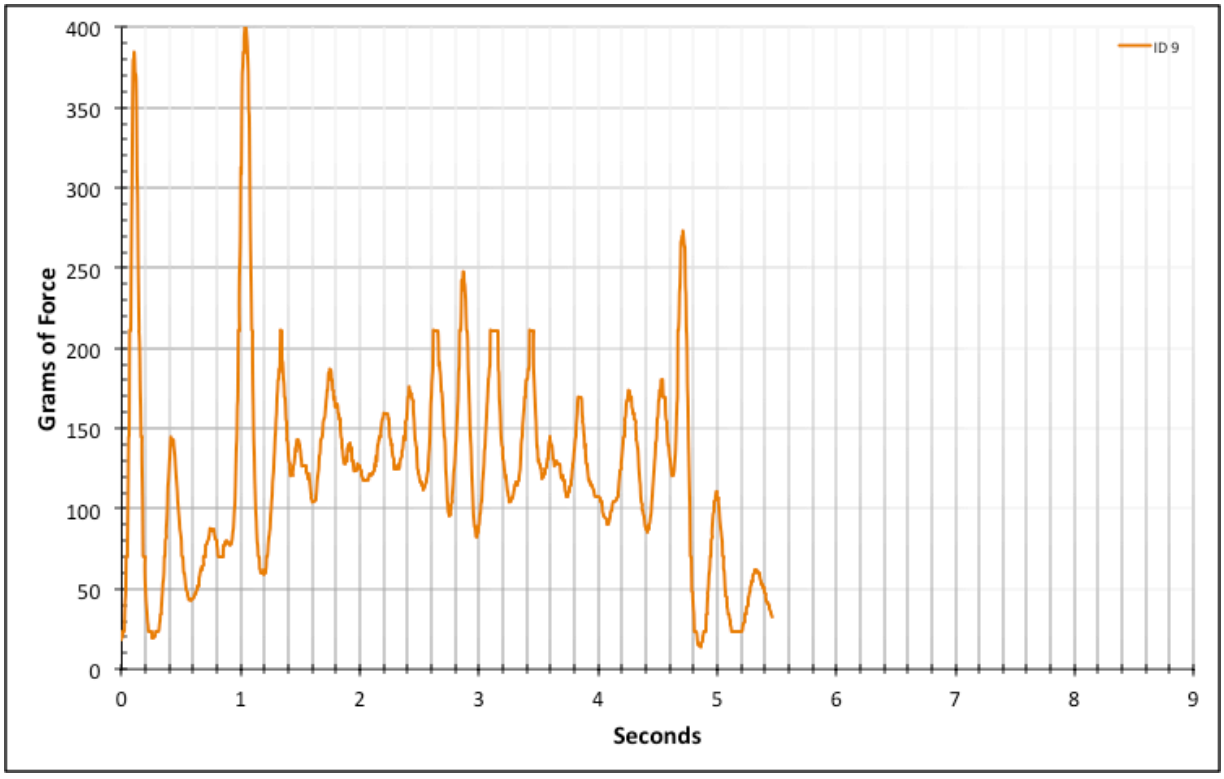

Figure A-6-17: Full Factory Baseline - Dry - ID 9 - #12, Bolt 2

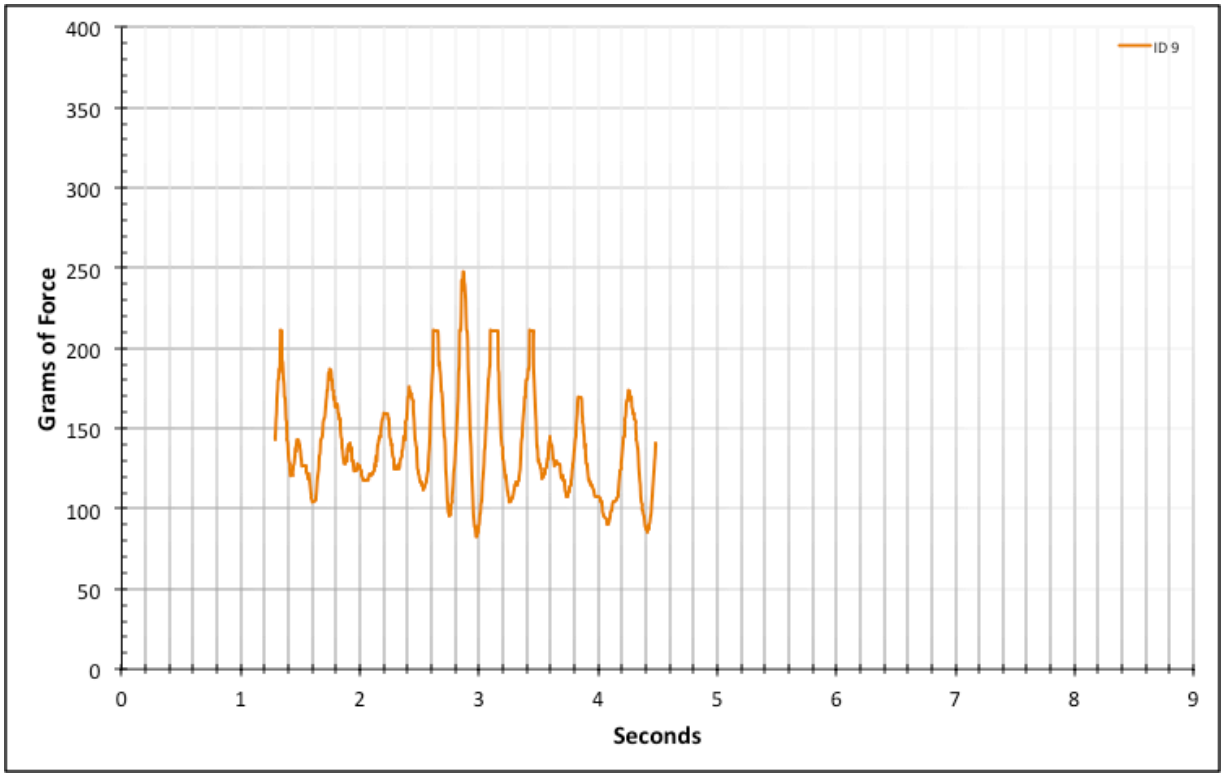

Figure A-6-18: Statistical Region Factory Baseline - Dry - ID 9 - #12, Bolt 2

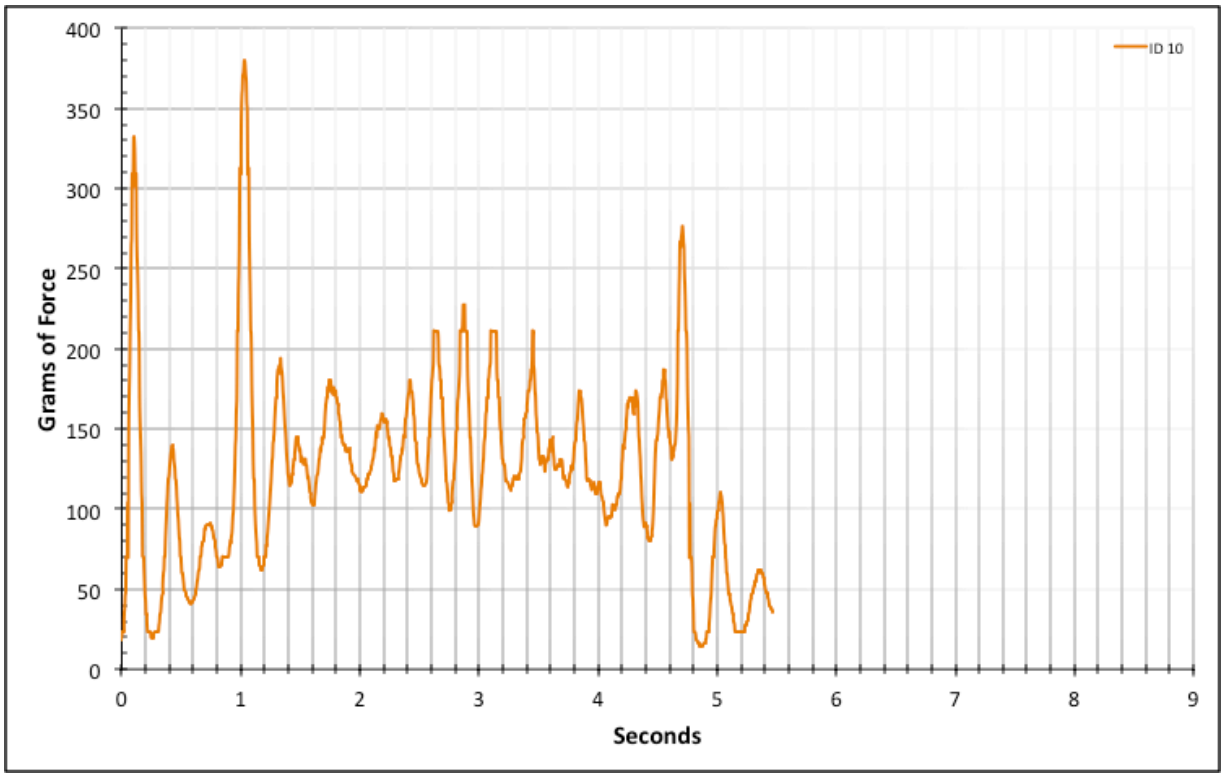

Figure A-6-19: Full Factory Baseline - Dry - ID 10 - #12, Bolt 2

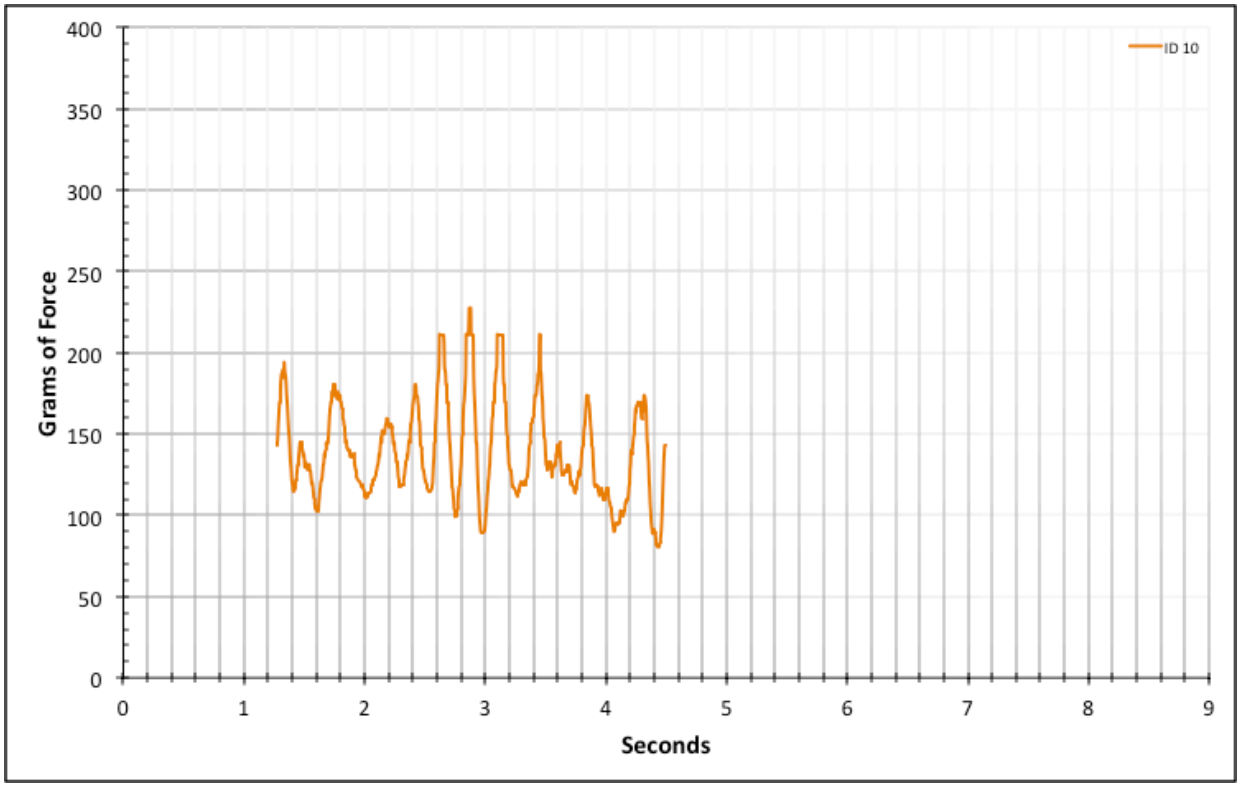

Figure A-6-20: Statistical Region Factory Baseline - Dry - ID 10 - #12, Bolt 2

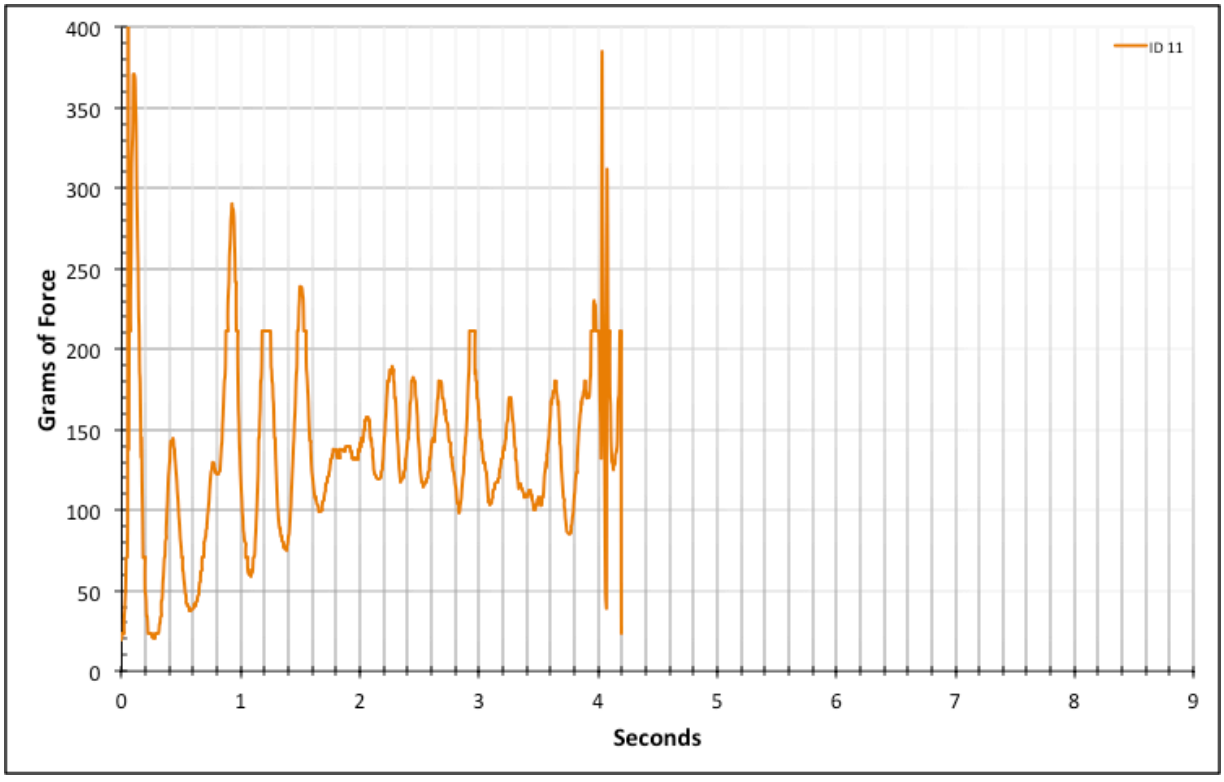

Figure A-6-21: Full Factory Baseline - Dry - ID 11 - #12, Bolt 3

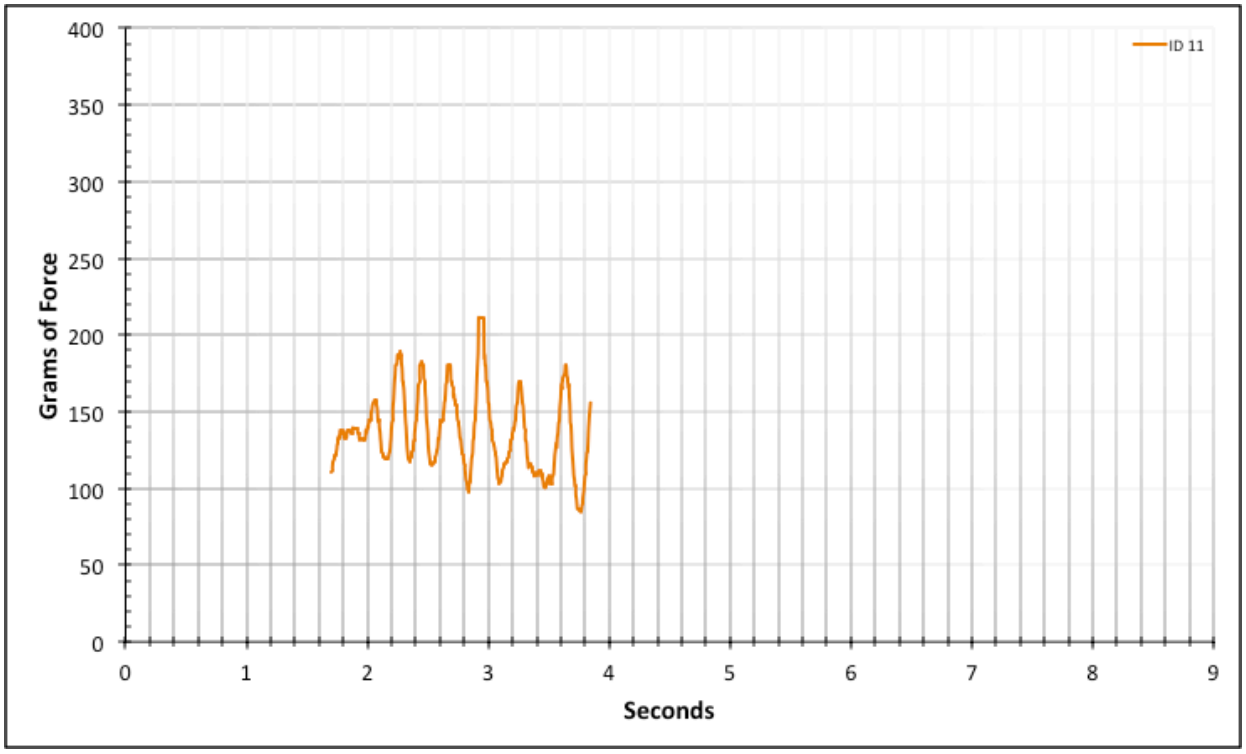

Figure A-6-22: Statistical Region Factory Baseline - Dry - ID 11 - #12, Bolt 3

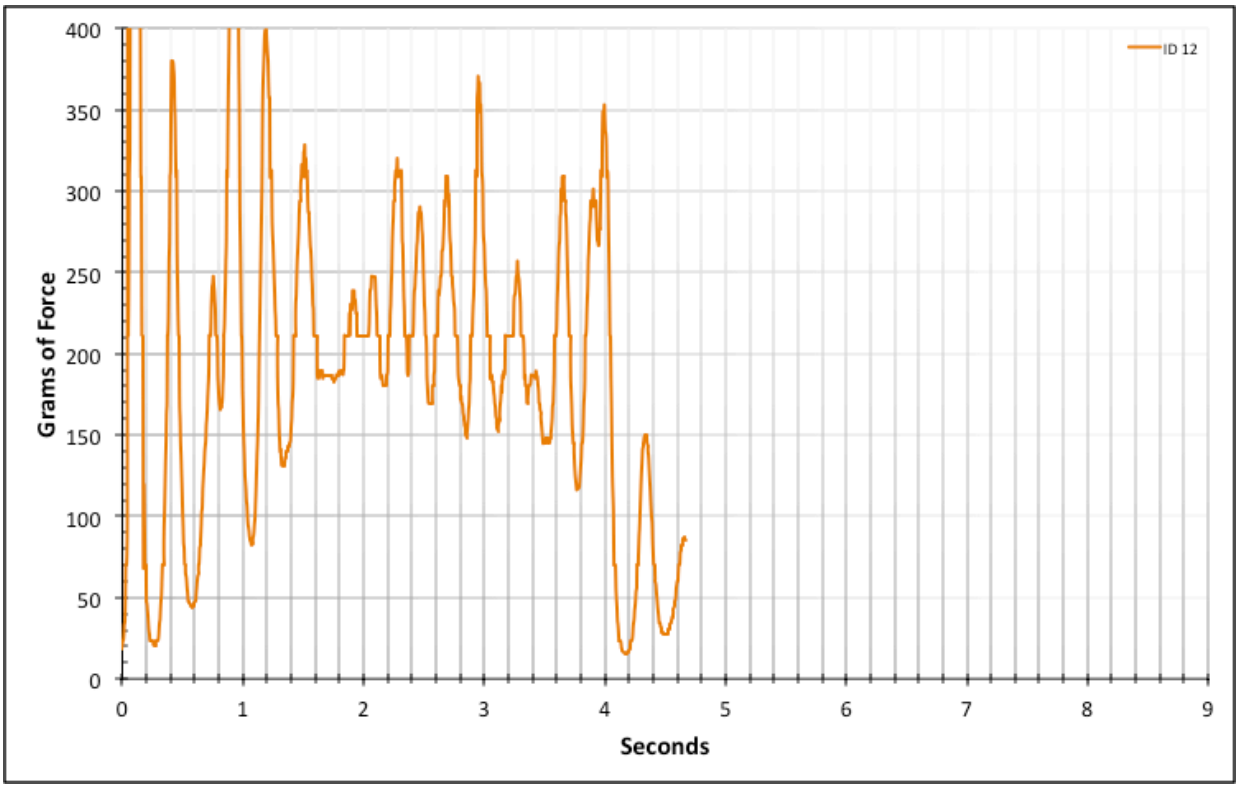

Figure A-6-23: Full Factory Baseline - Dry - ID 12 - #12, Bolt 3

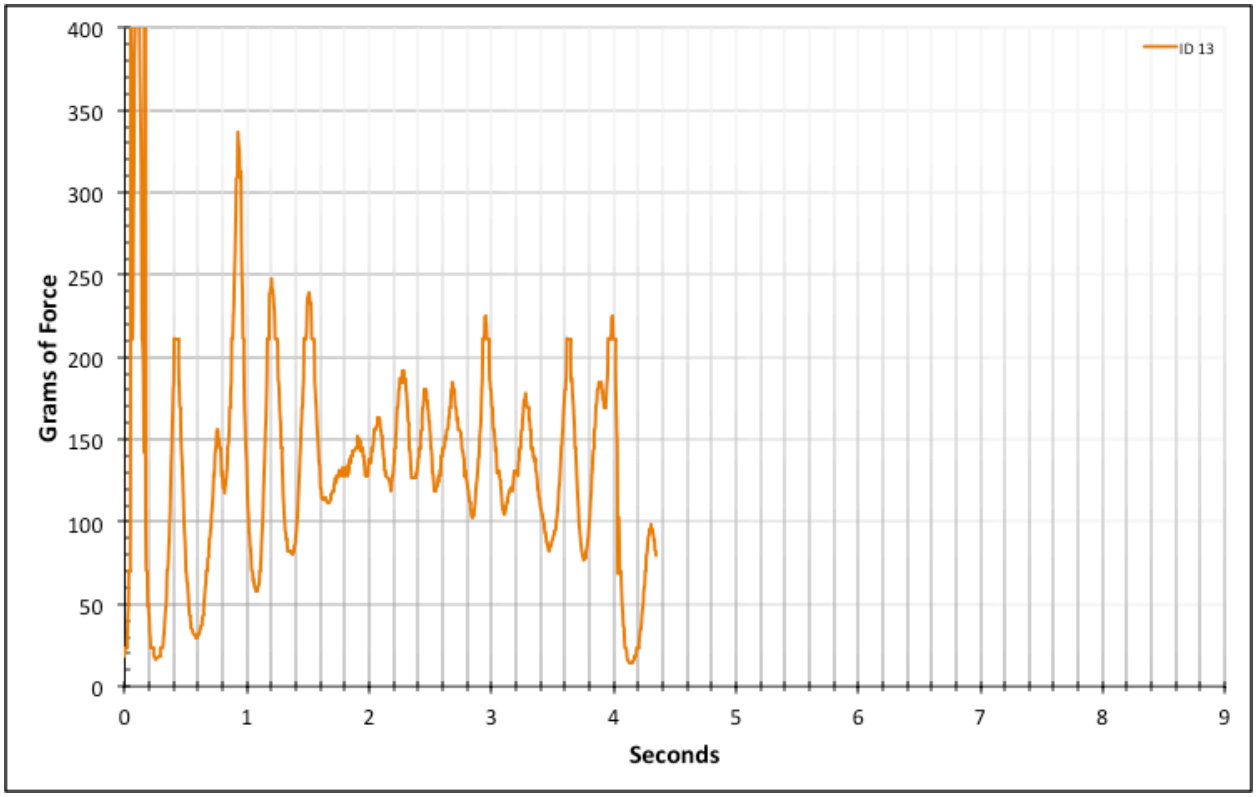

Figure A-6-24: Full Factory Baseline - Dry - ID 13 - #12, Bolt 3

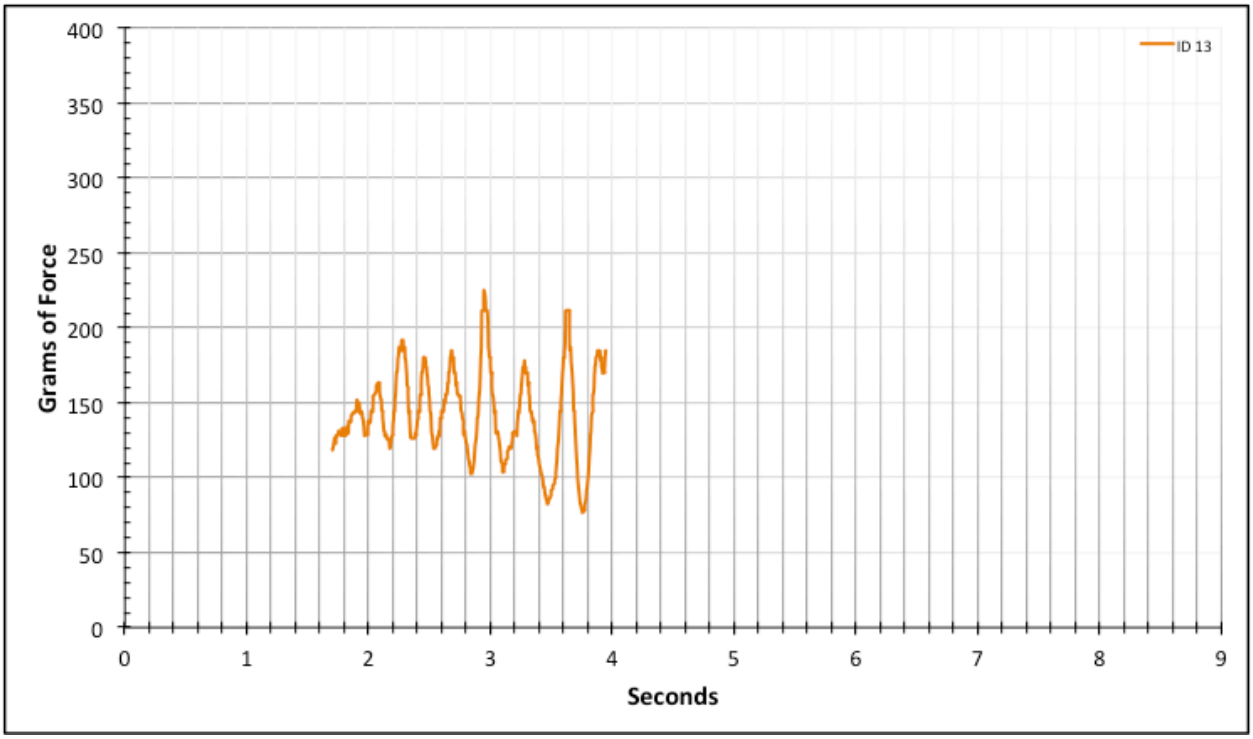

Figure A-6-25: Statistical Region Factory Baseline - Dry - ID 13 - #12, Bolt 3

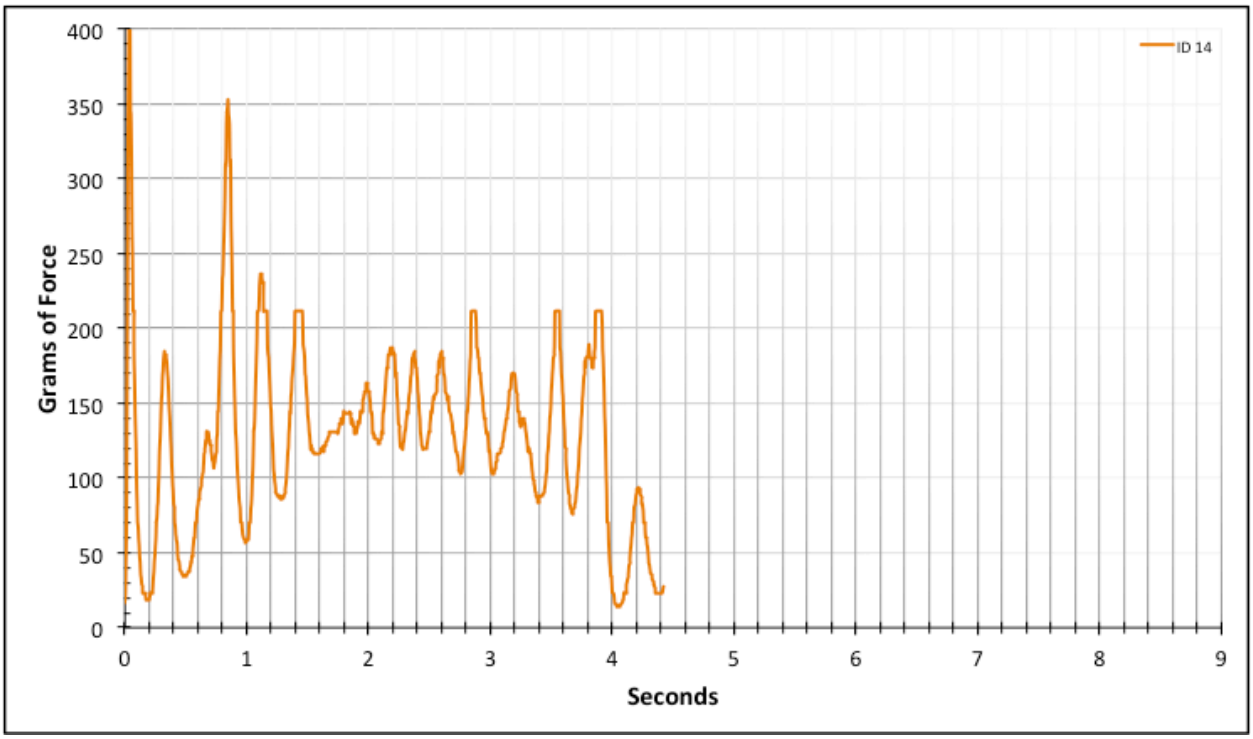

Figure A-6-26: Full Factory Baseline - Dry - ID 14 - #12, Bolt 3

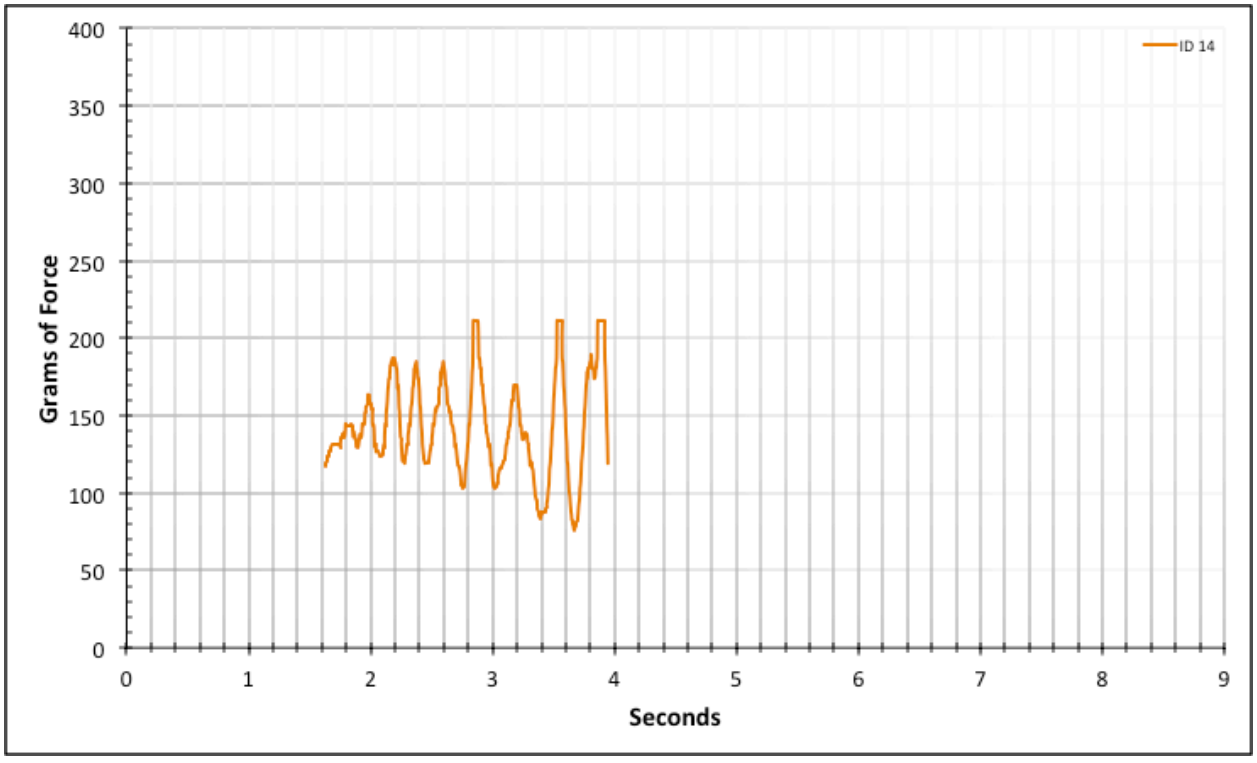

Figure A-6-27: Statistical Region Factory Baseline - Dry - ID 14 - #12, Bolt 3

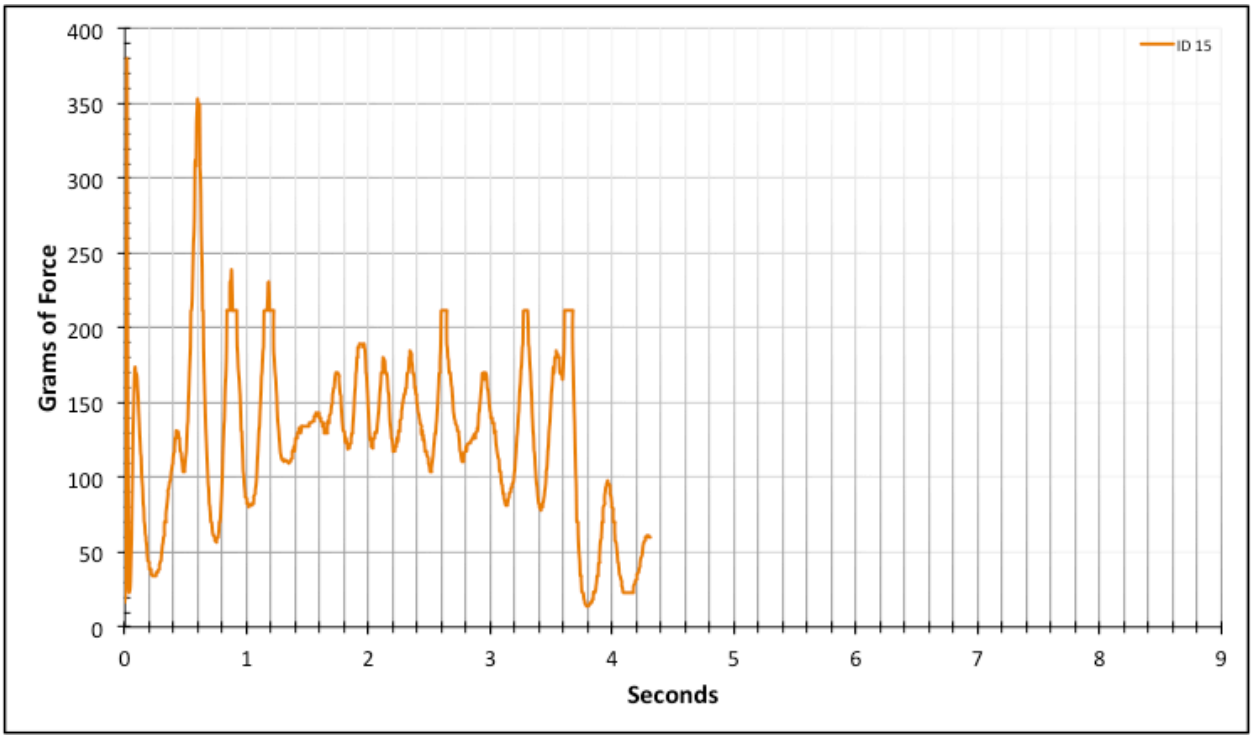

Figure A-6-28: Full Factory Baseline - Dry - ID 15 - #12, Bolt 3

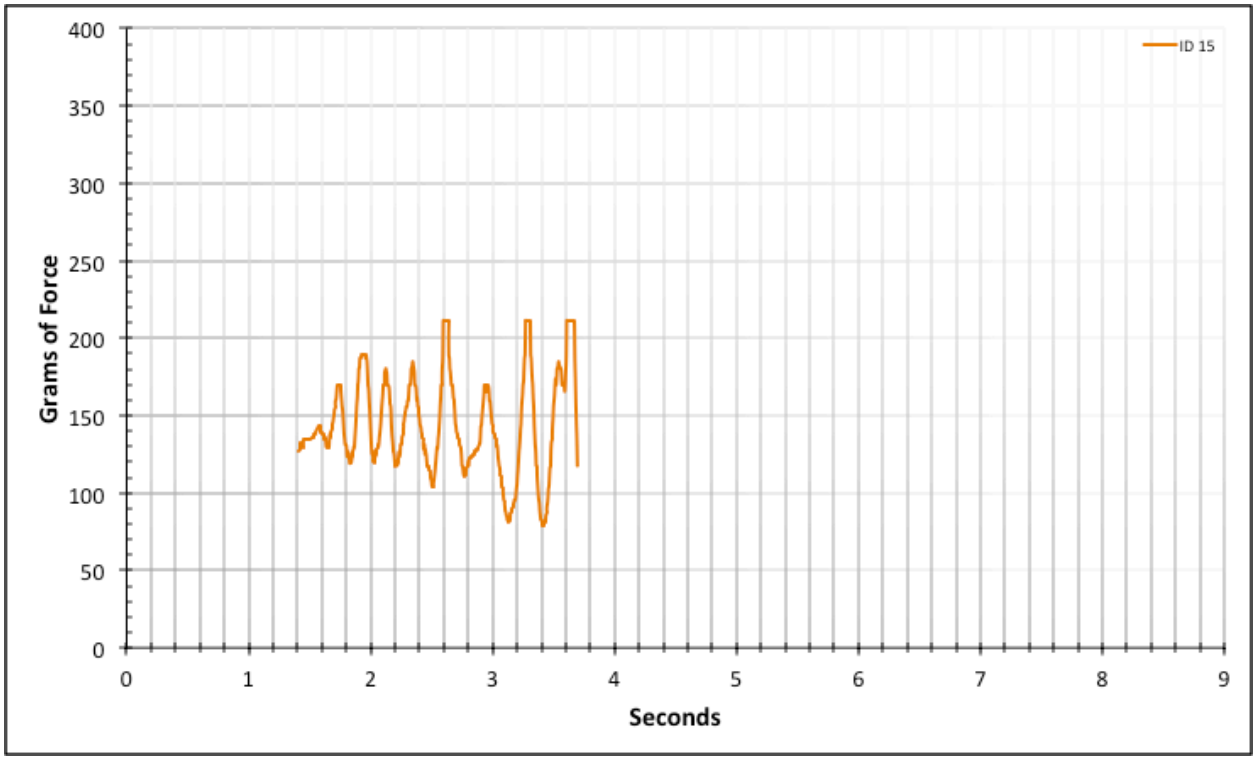

Figure A-6-29: Statistical Region Factory Baseline - Dry - ID 15 - #12, Bolt 3

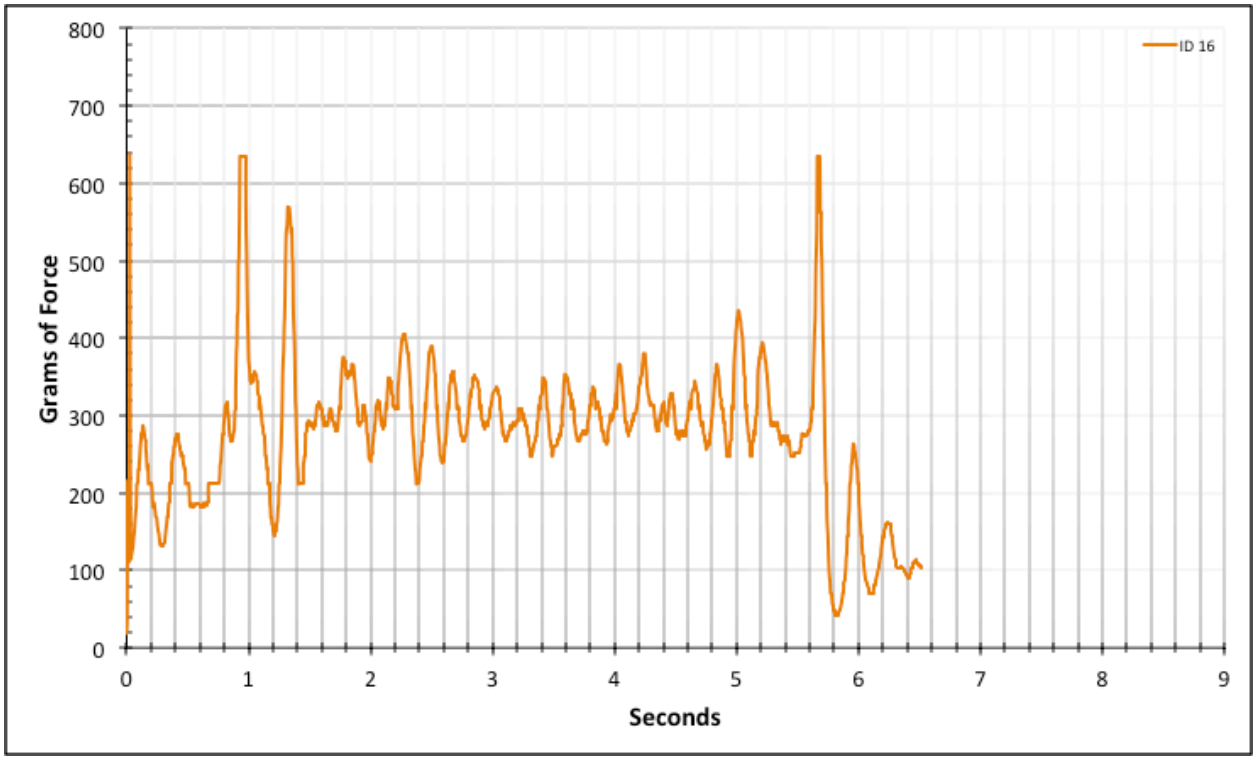

Figure A-6-30: Full Factory Baseline - Dry - ID 16 - #10, Bolt 1

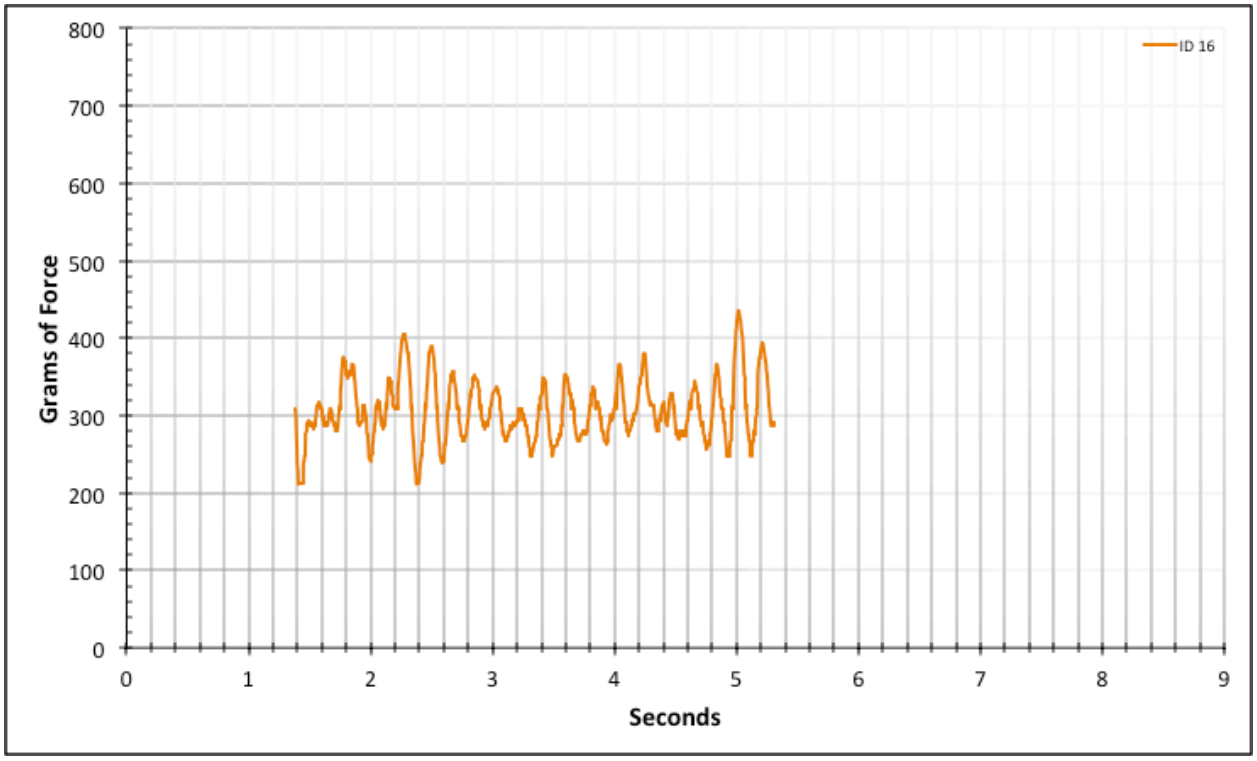

Figure A-6-31: Statistical Region Factory Baseline - Dry - ID 16 - #10, Bolt 1

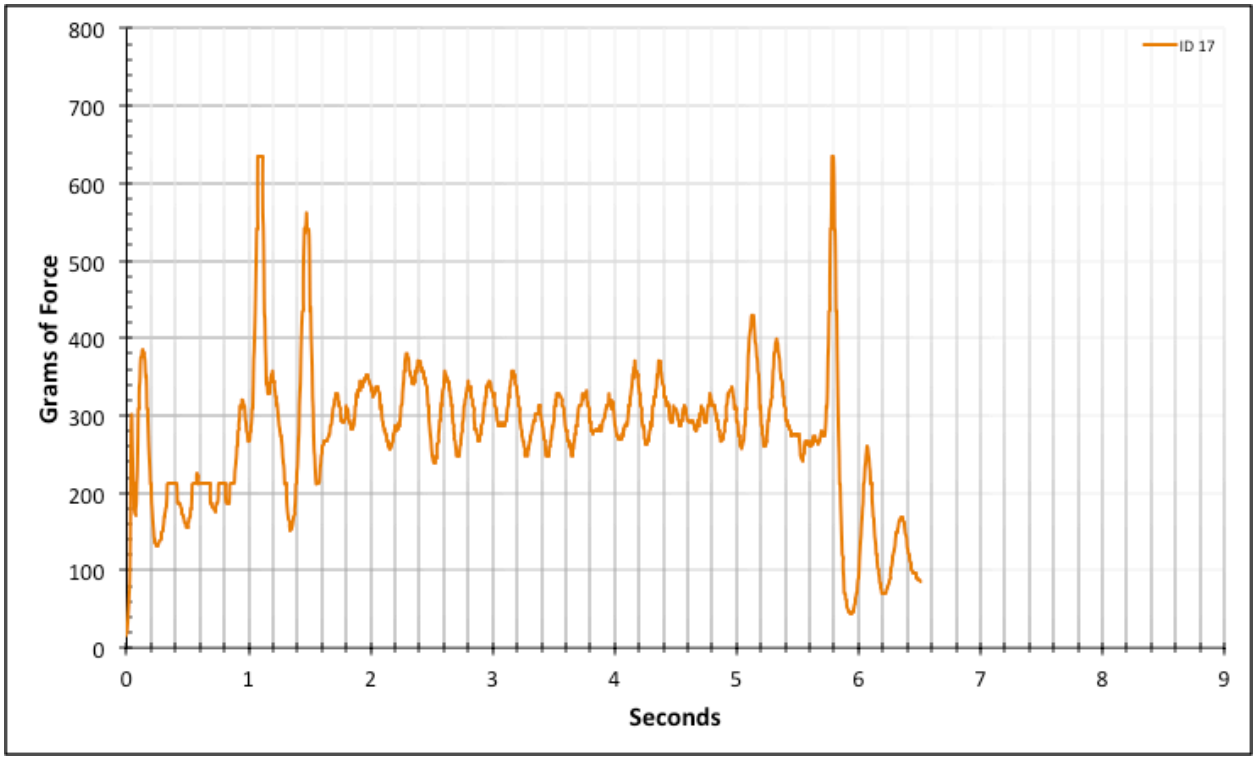

Figure A-6-32: Full Factory Baseline - Dry - ID 17 - #10, Bolt 1

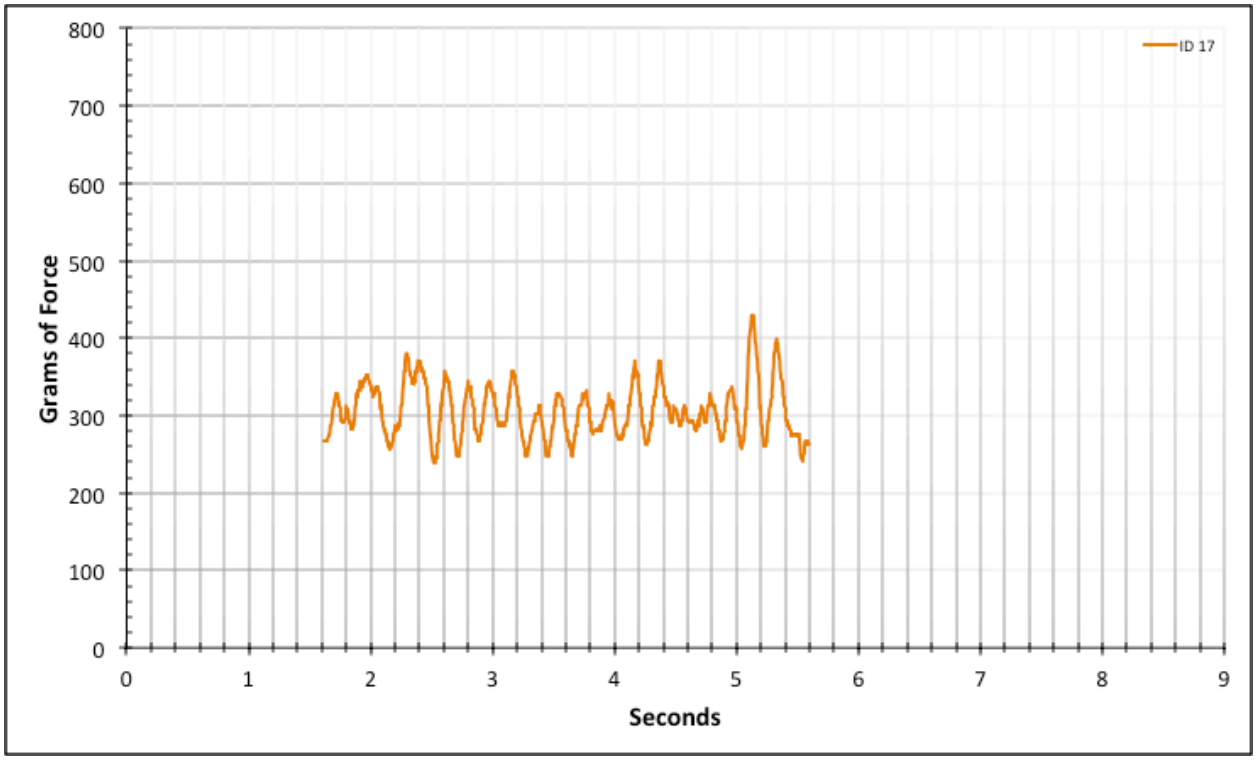

Figure A-6-33: Statistical Region Factory Baseline - Dry - ID 17 - #10, Bolt 1

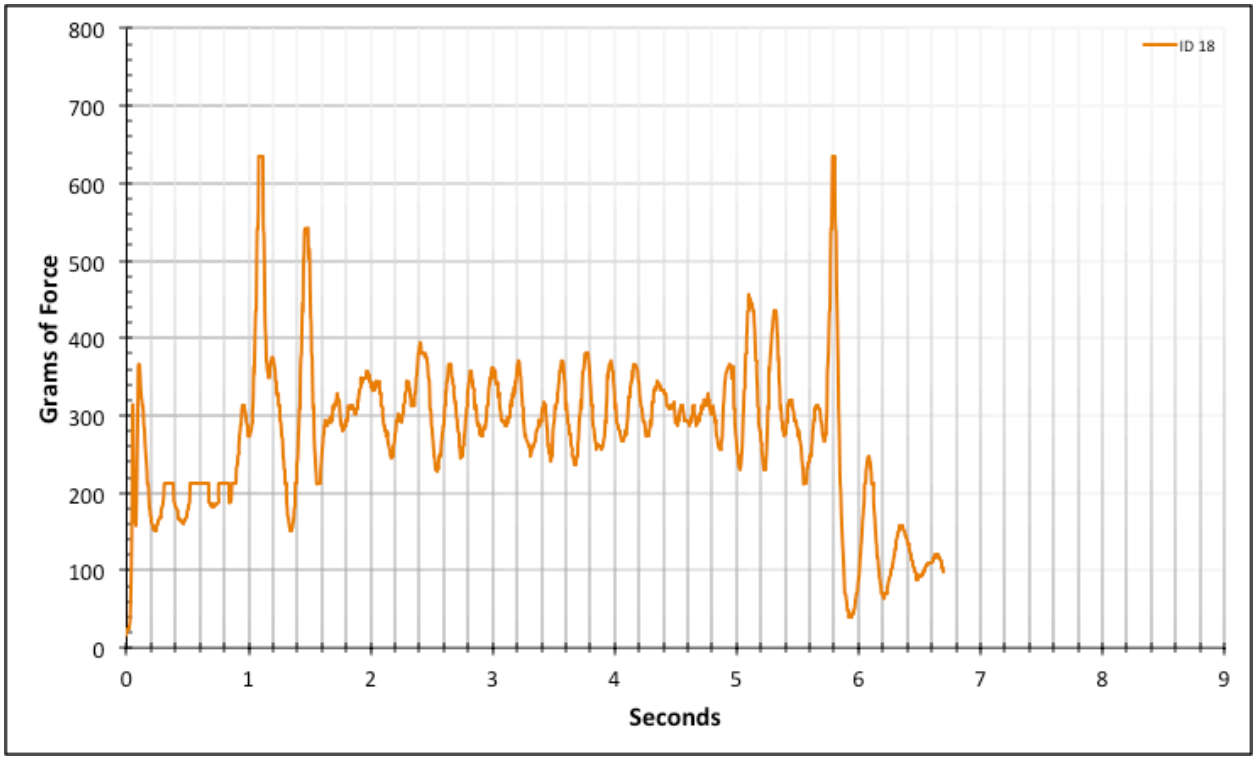

Figure A-6-34: Full Factory Baseline - Dry - ID 18 - #10, Bolt 1

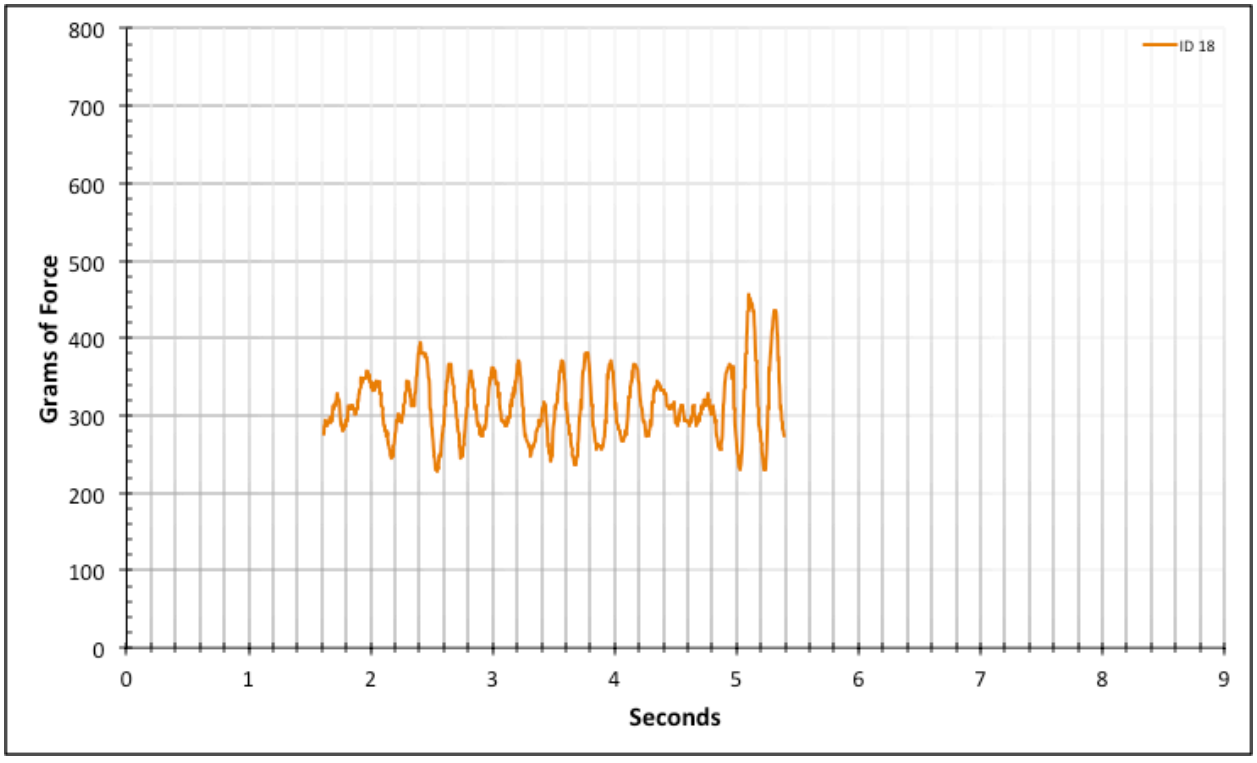

Figure A-6-35: Statistical Region Factory Baseline - Dry - ID 18 - #10, Bolt 1

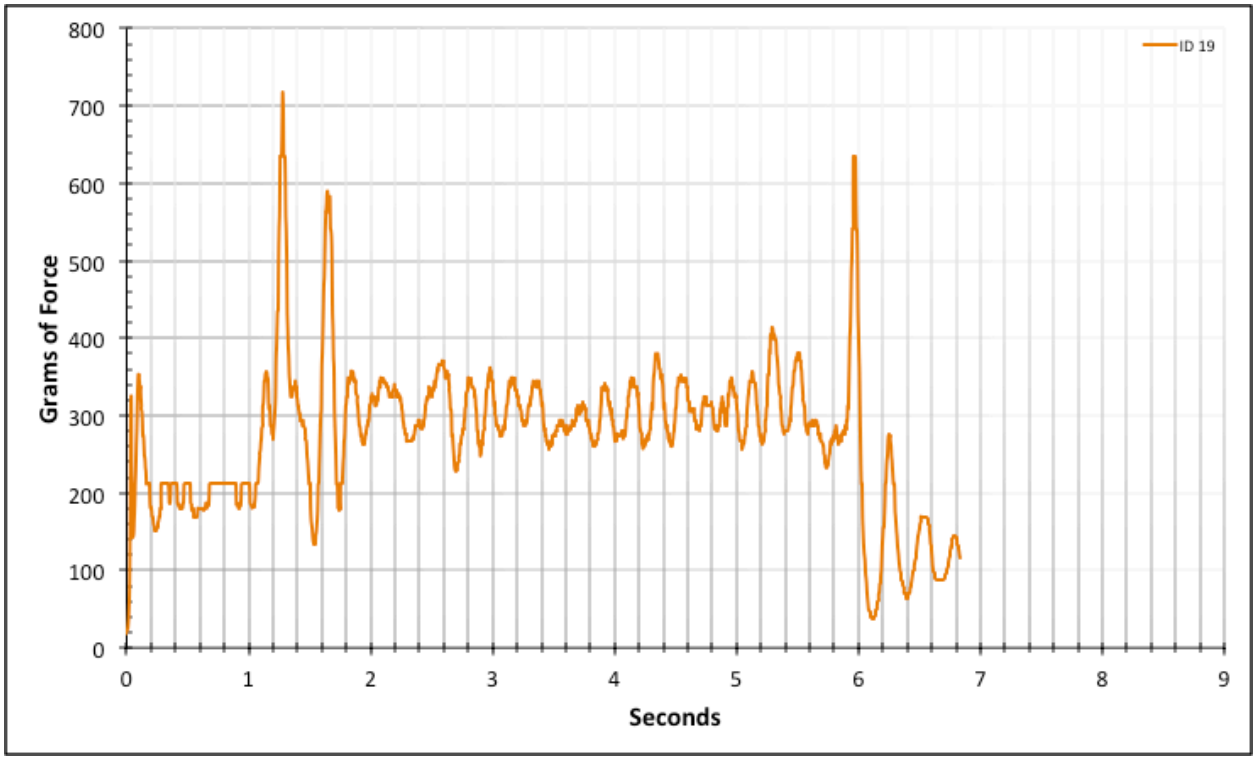

Figure A-6-36: Full Factory Baseline - Dry - ID 19 - #10, Bolt 1

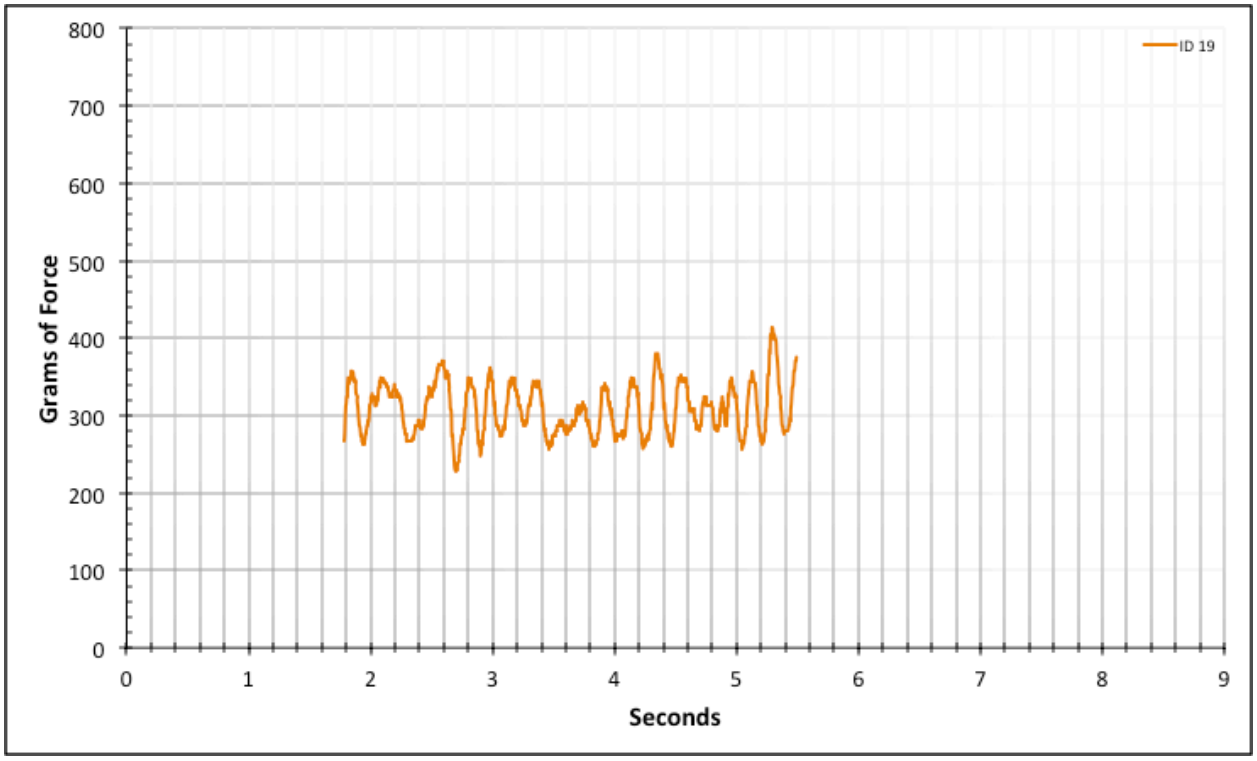

Figure A-6-37: Statistical Region Factory Baseline - Dry - ID 19 - #10, Bolt 1

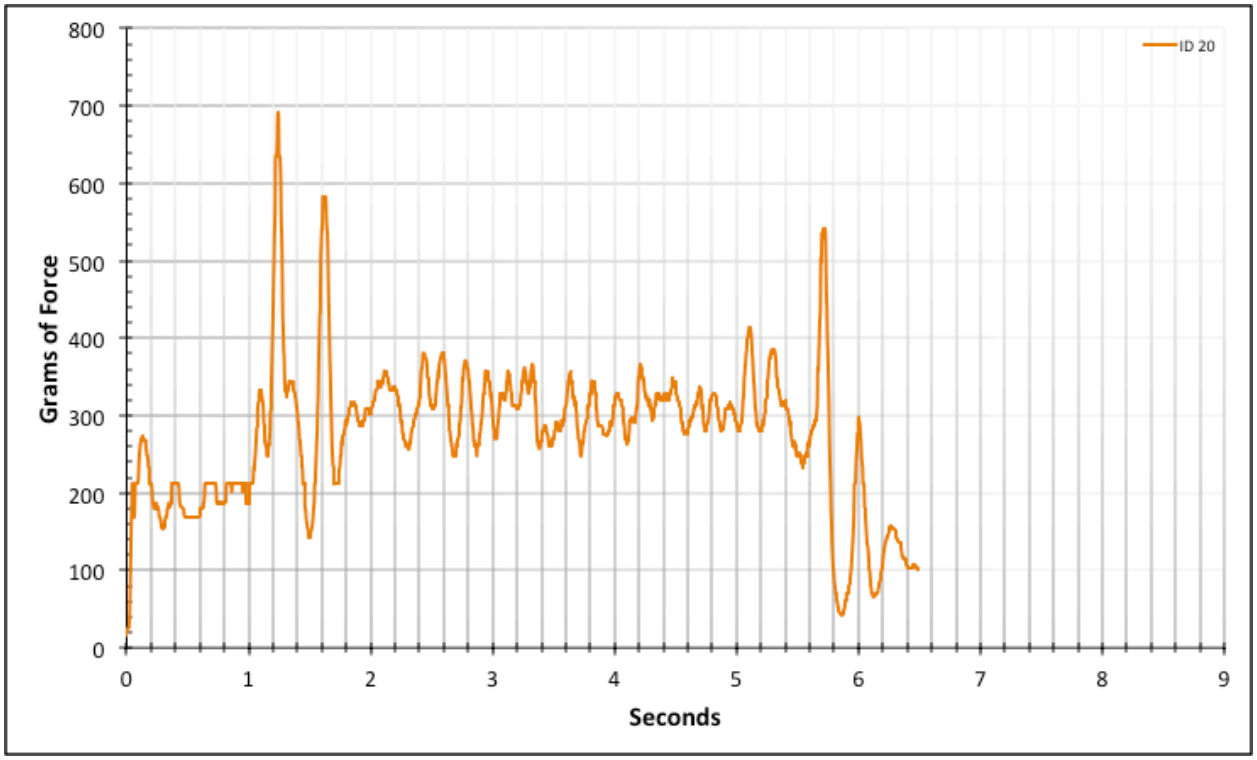

Figure A-6-38: Full Factory Baseline - Dry - ID 20 - #10, Bolt 1

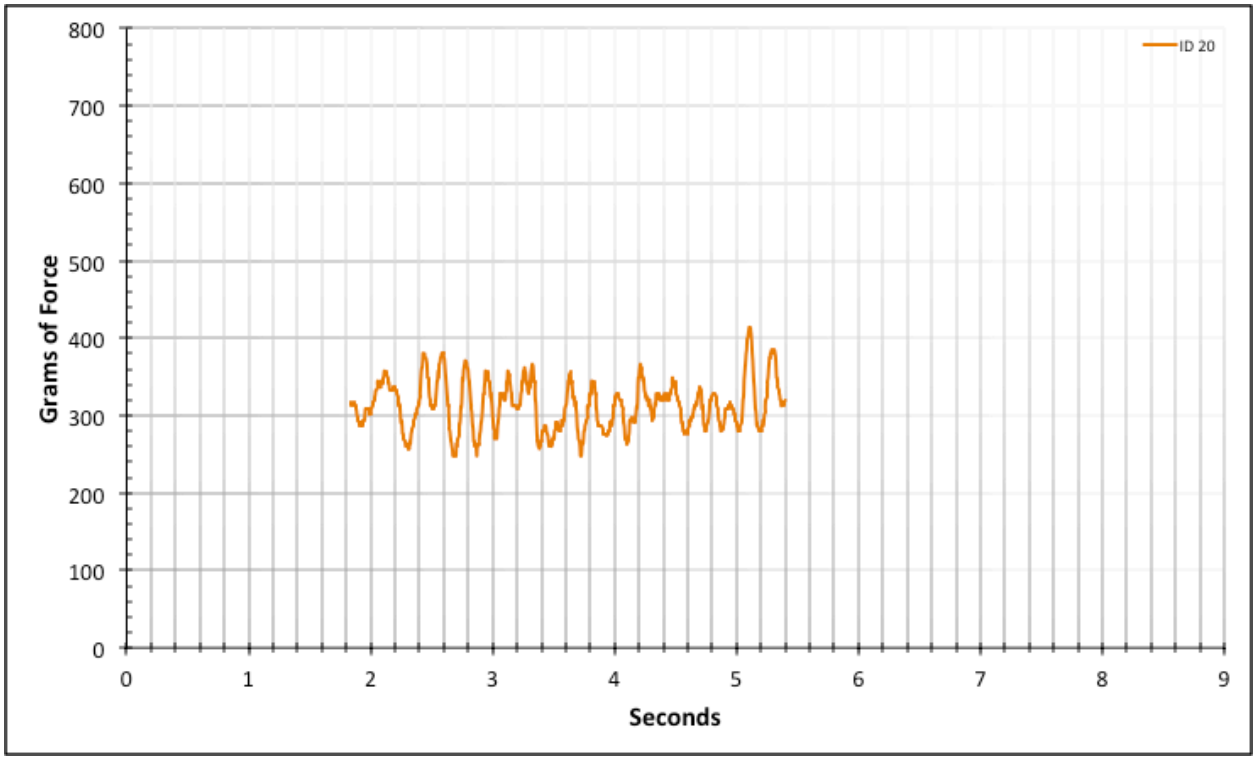

Figure A-6-39: Statistical Region Factory Baseline - Dry - ID 20 - #10, Bolt 1

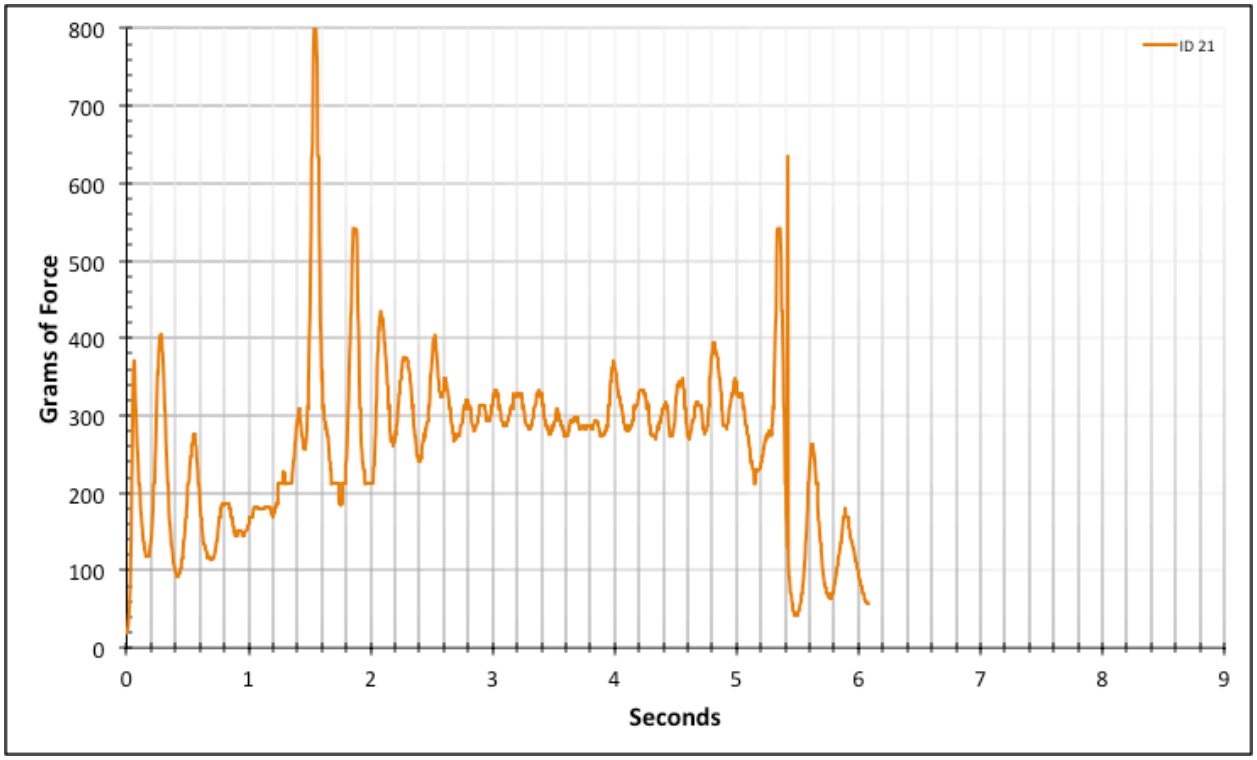

Figure A-6-40: Full Factory Baseline - Dry - ID 21 - #10, Bolt 2

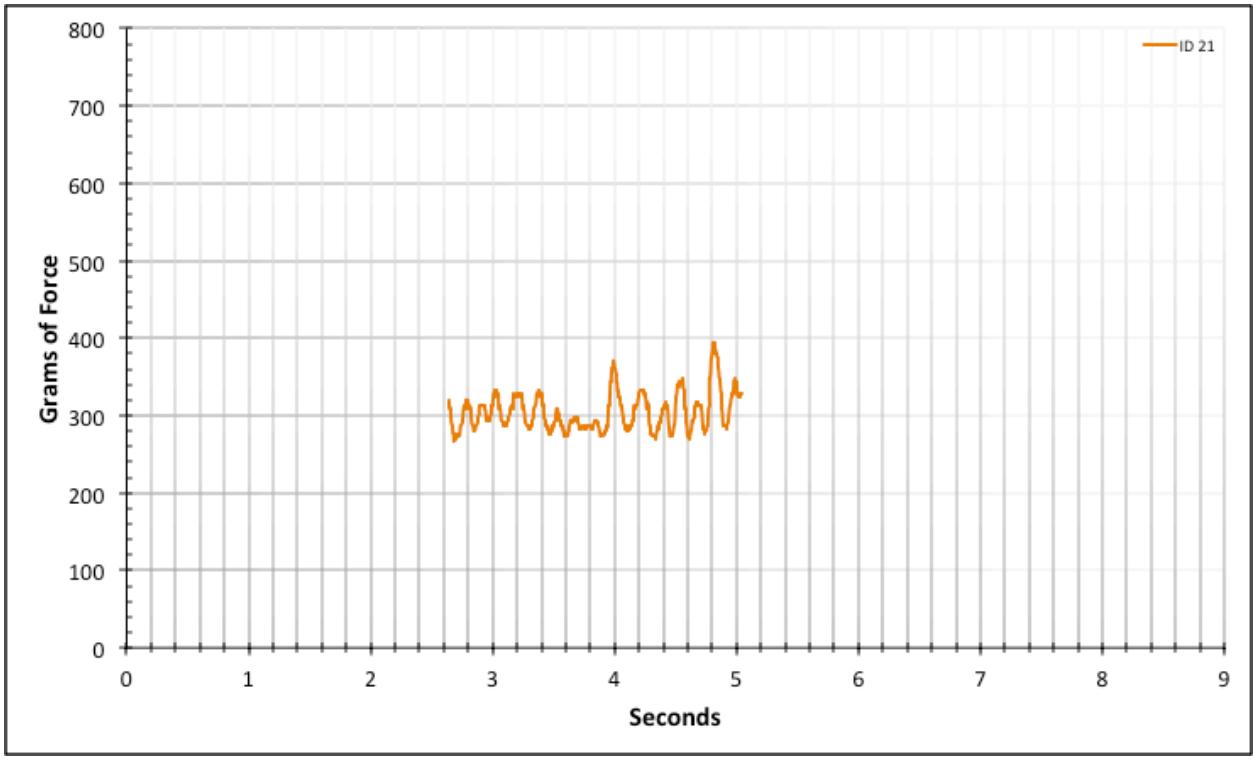

Figure A-6-41: Statistical Region Factory Baseline - Dry - ID 21 - #10, Bolt 2

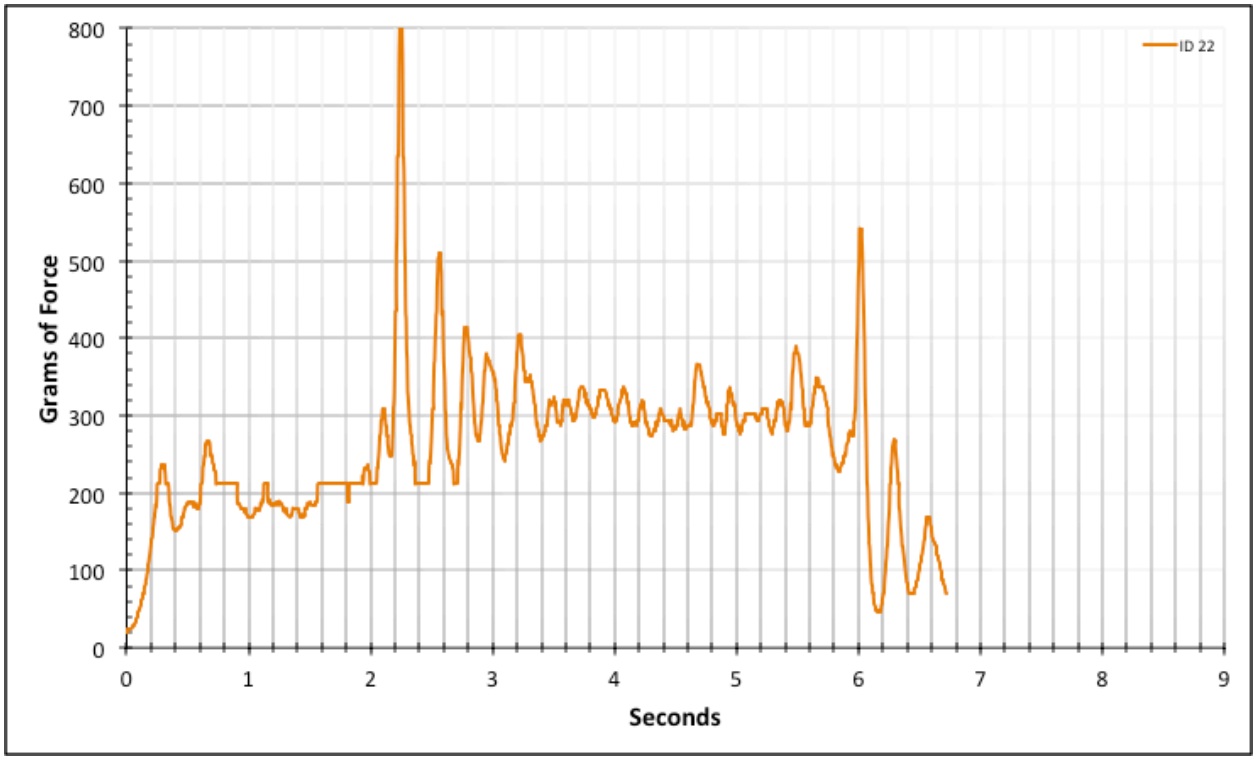

Figure A-6-42: Full Factory Baseline - Dry - ID 22 - #10, Bolt 2

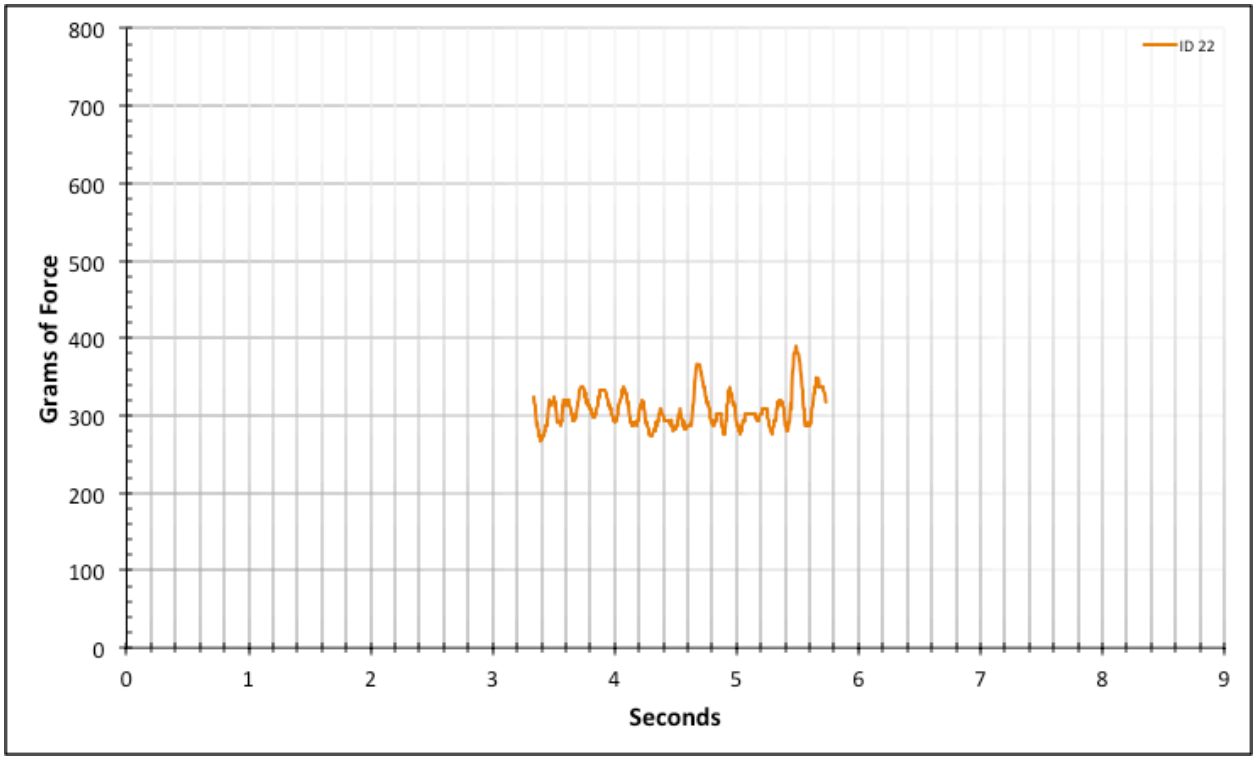

Figure A-6-43: Statistical Region Factory Baseline - Dry - ID 22 - #10, Bolt 2

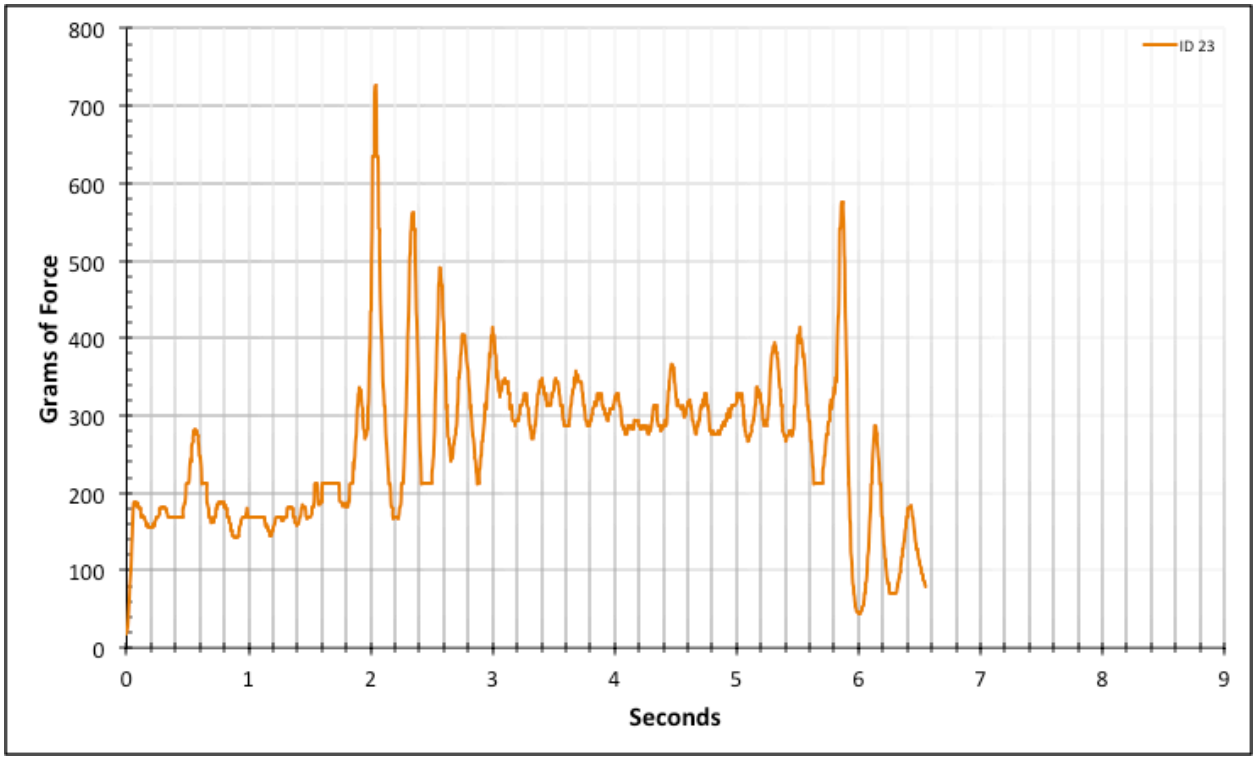

Figure A-6-44: Full Factory Baseline - Dry - ID 23 - #10, Bolt 2

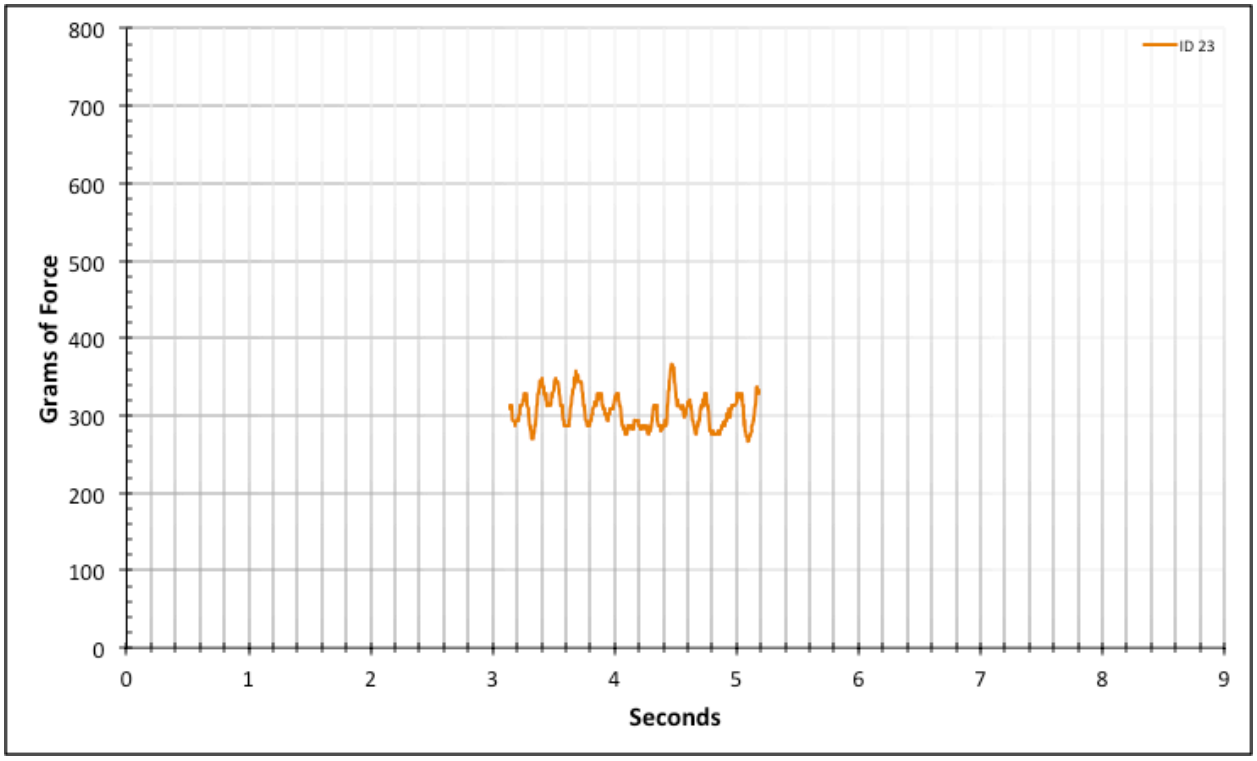

Figure A-6-45: Statistical Region Factory Baseline - Dry - ID 23 - #10, Bolt 2

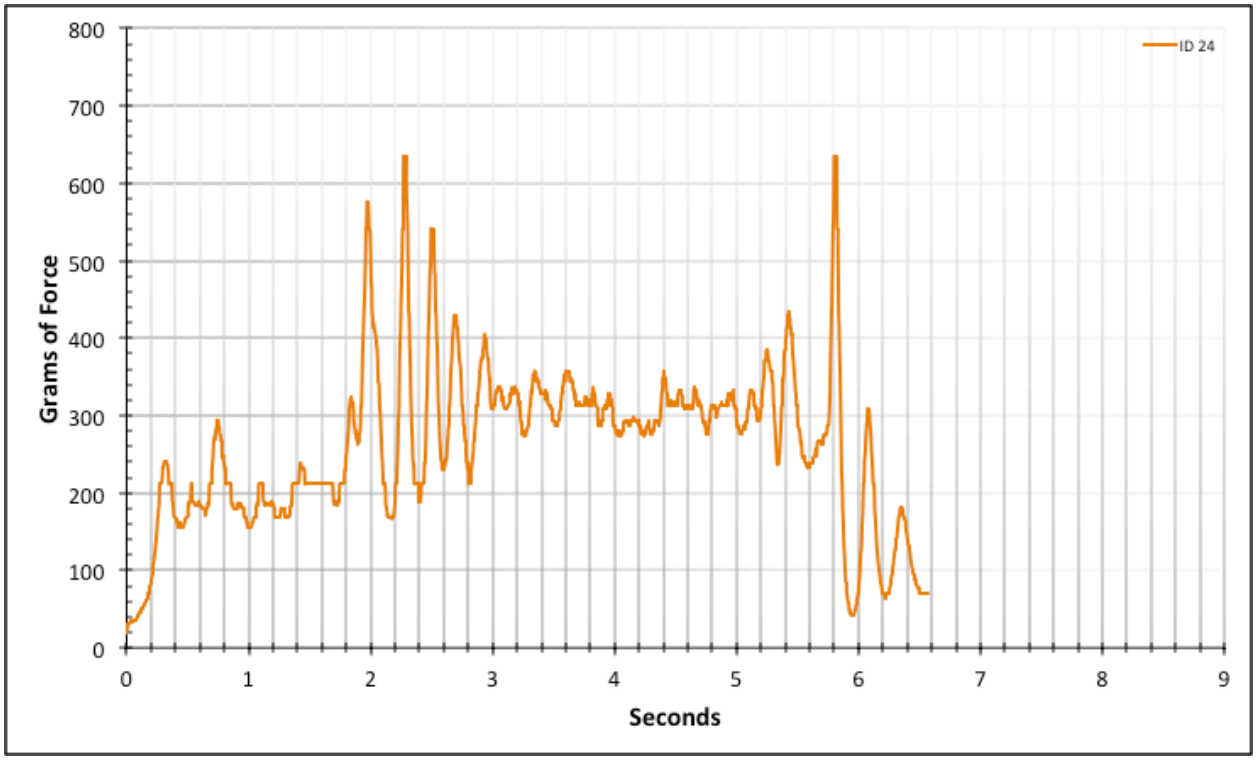

Figure A-6-46: Full Factory Baseline - Dry - ID 24 - #10, Bolt 2

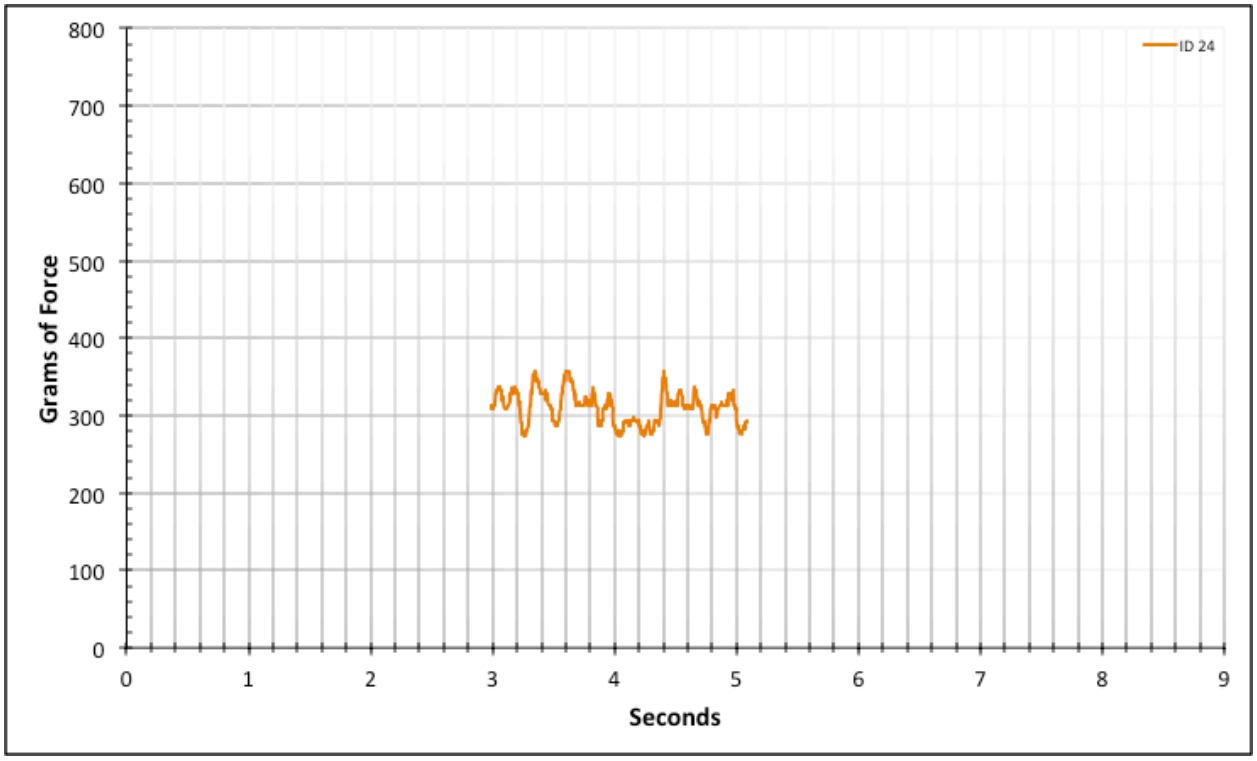

Figure A-6-47: Statistical Region Factory Baseline - Dry - ID 24 - #10, Bolt 2

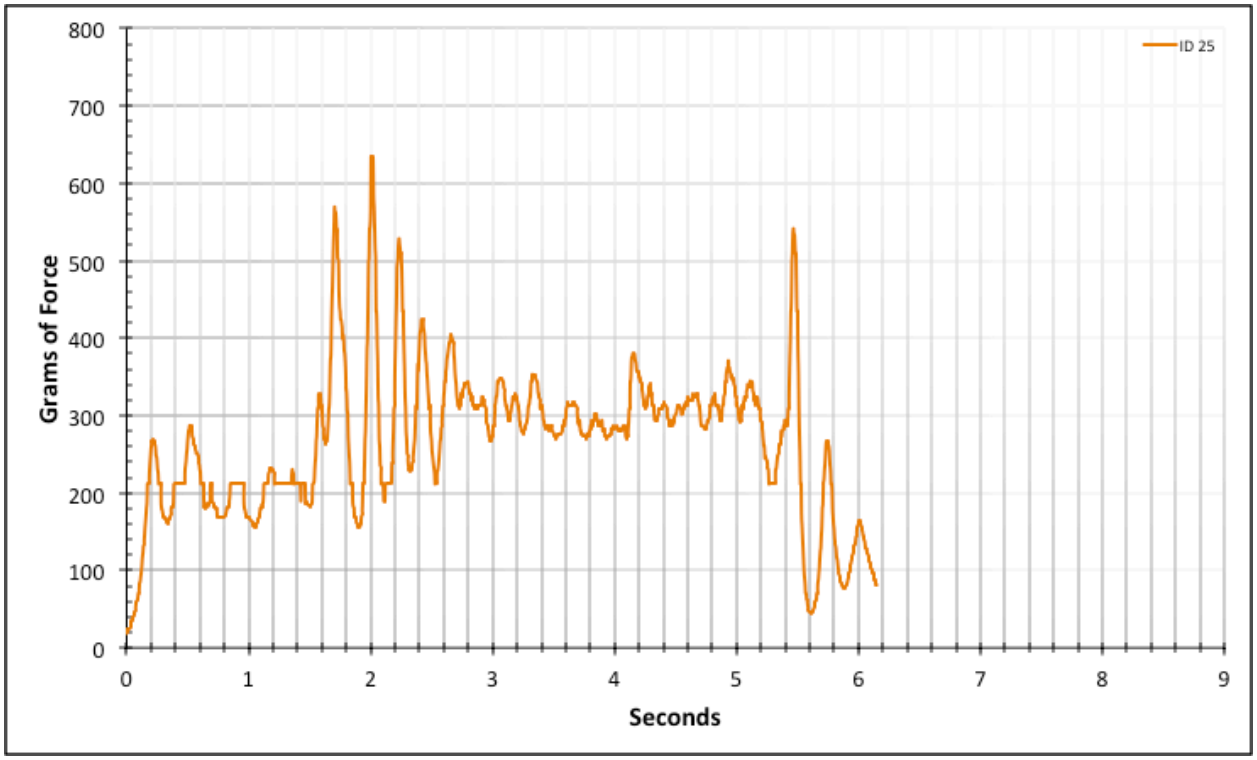

Figure A-6-48: Full Factory Baseline - Dry - ID 25 - #10, Bolt 2

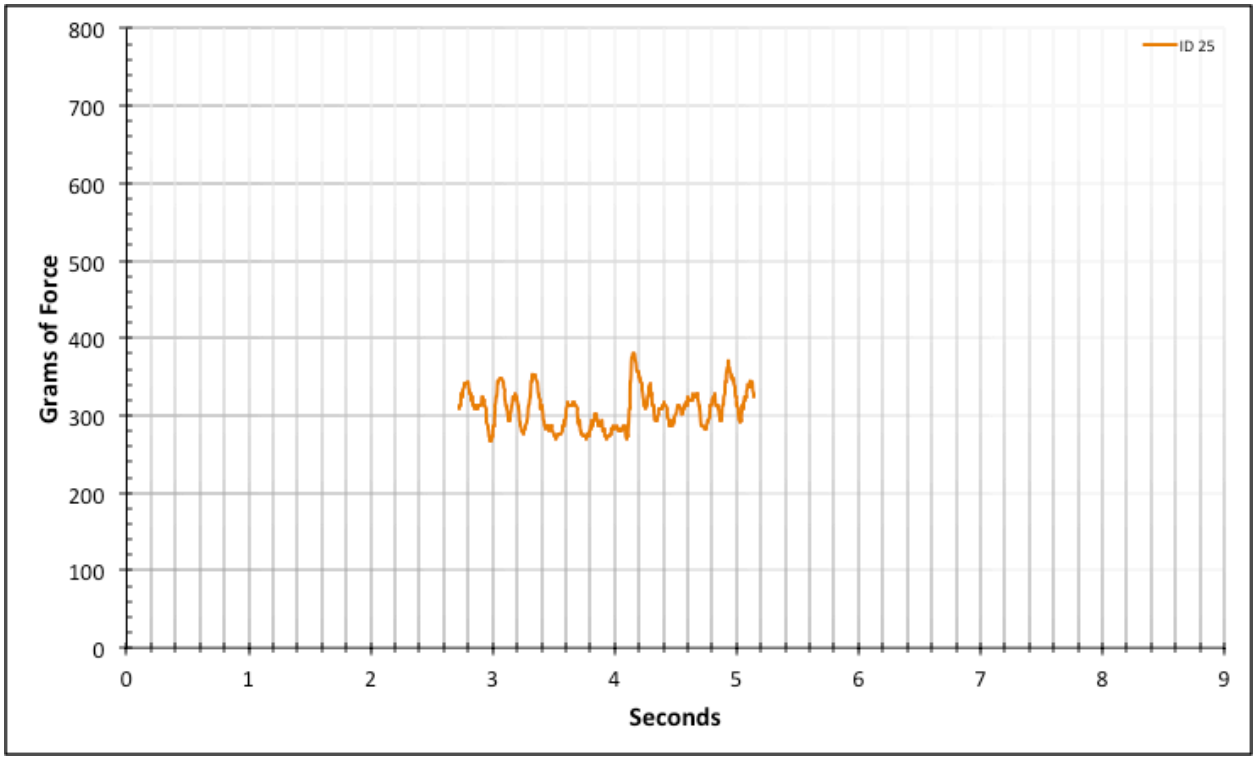

Figure A-6-49: Statistical Region Factory Baseline - Dry - ID 25 - #10, Bolt 2

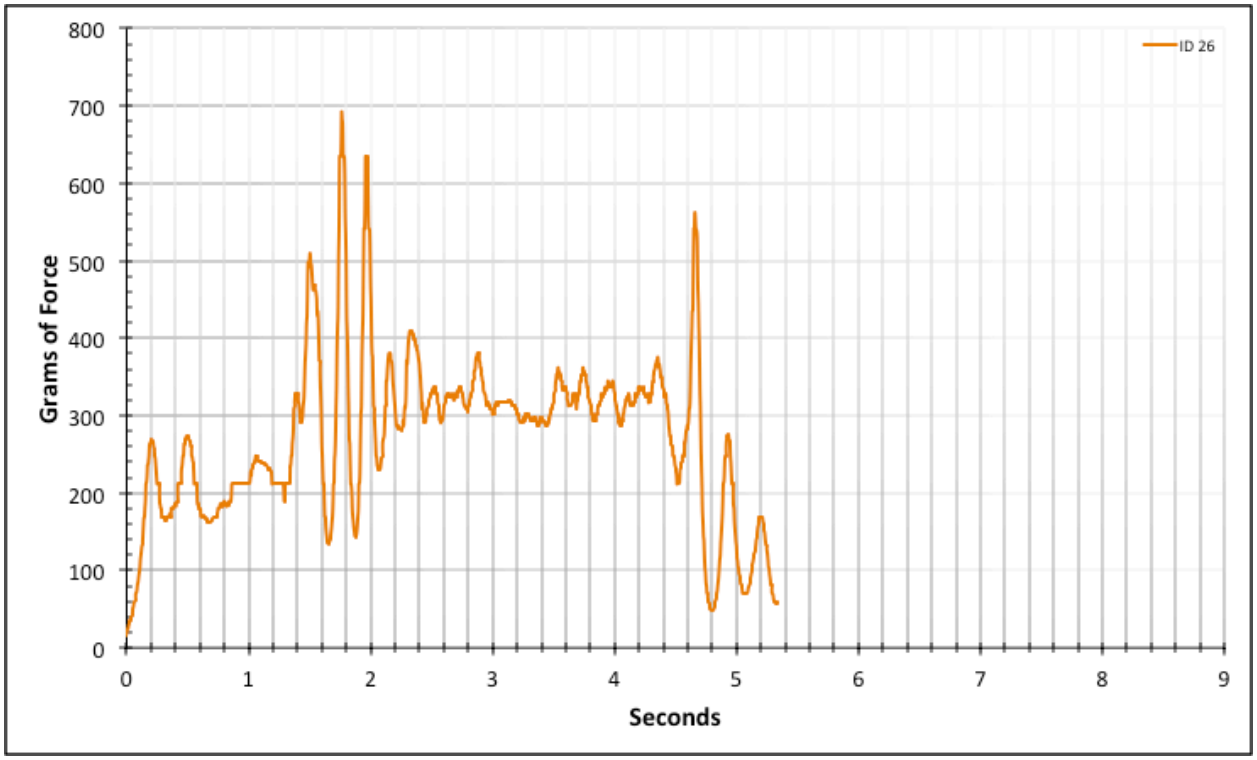

Figure A-6-50: Full Factory Baseline - Dry - ID 26 - #10, Bolt 3

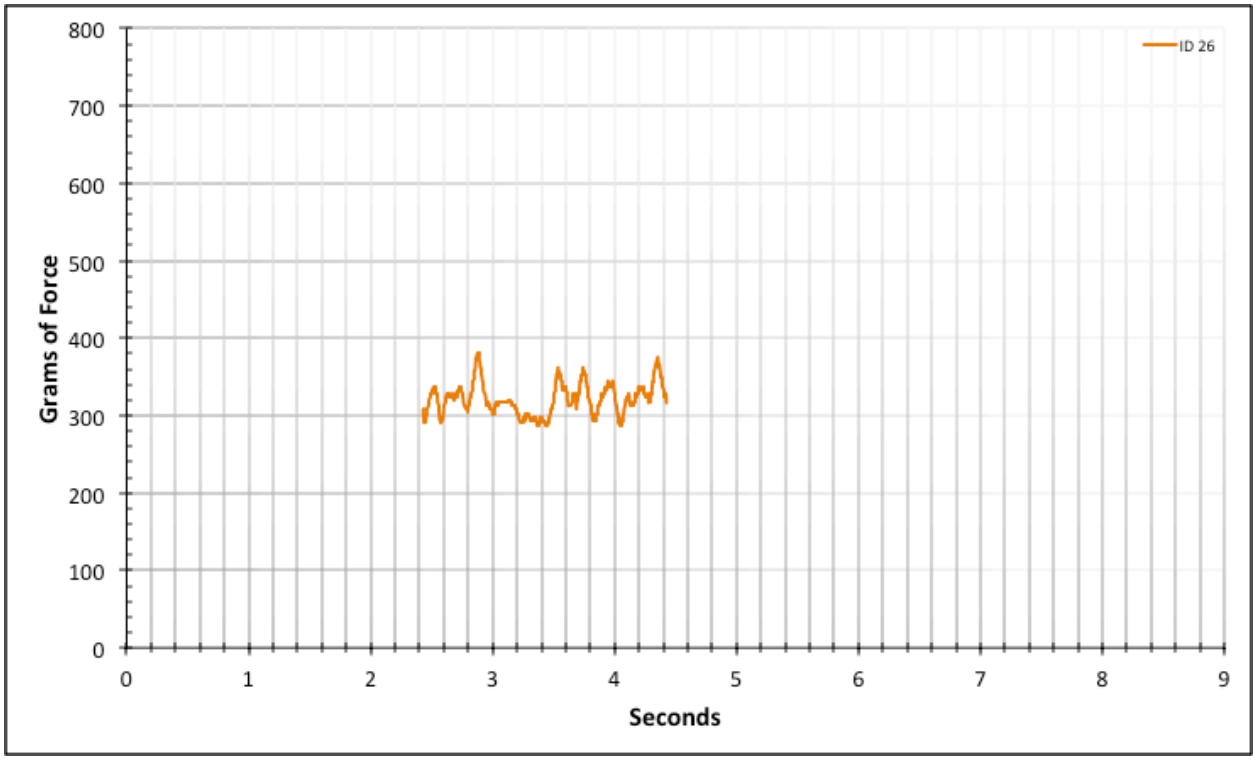

Figure A-6-51: Statistical Region Factory Baseline - Dry - ID 26 - #10, Bolt 3

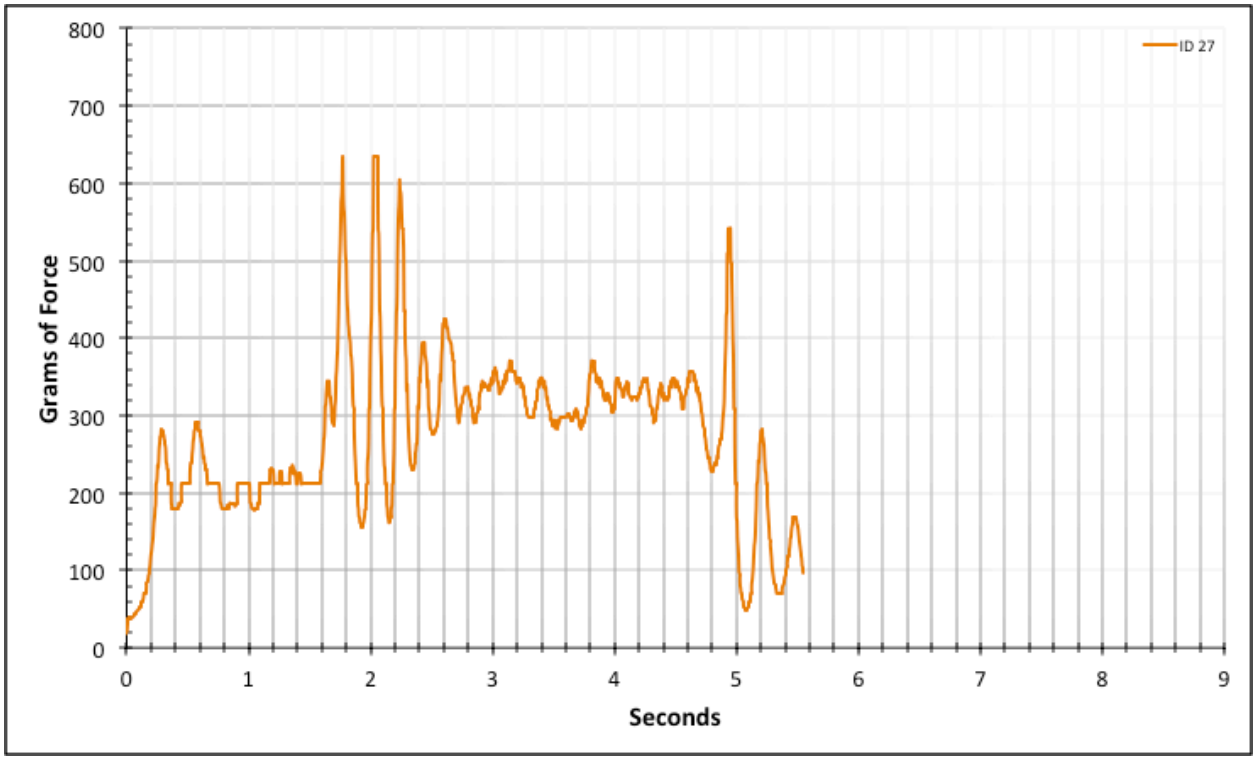

Figure A-6-52: Full Factory Baseline - Dry - ID 27 - #10, Bolt 3

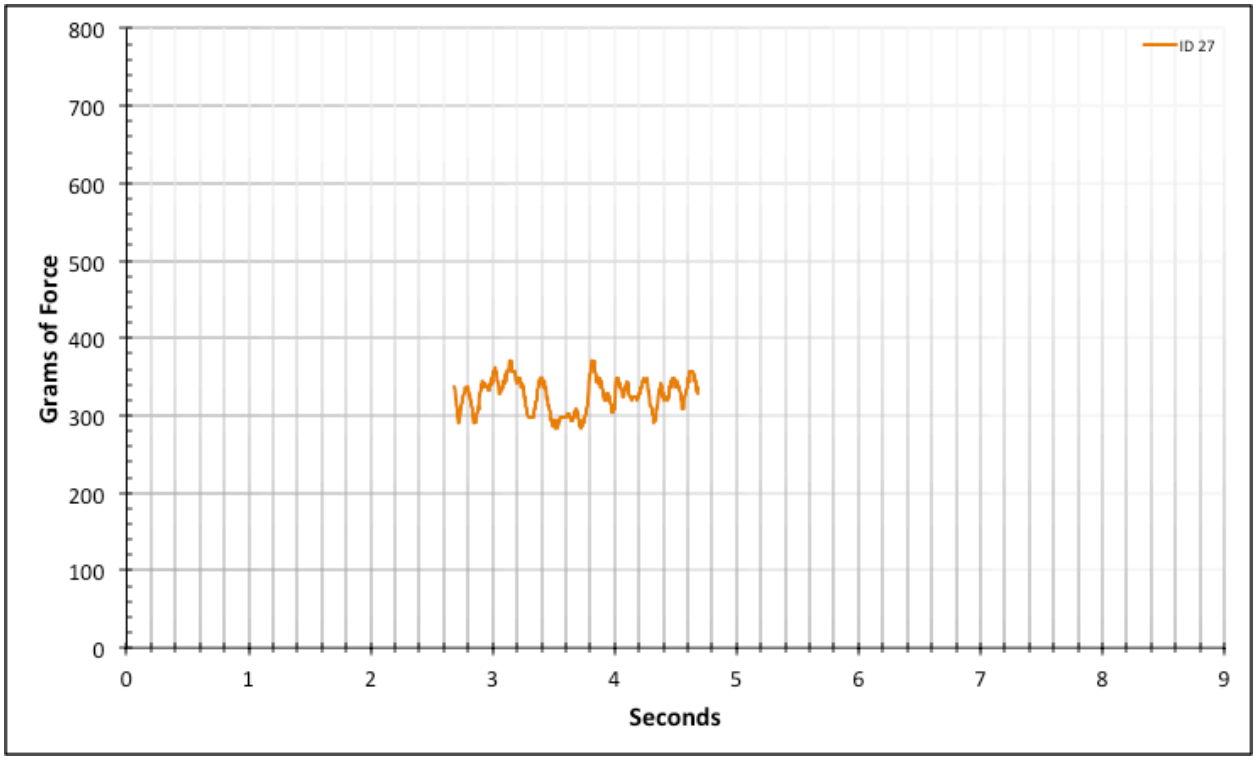

Figure A-6-53: Statistical Region Factory Baseline - Dry - ID 27 - #10, Bolt 3

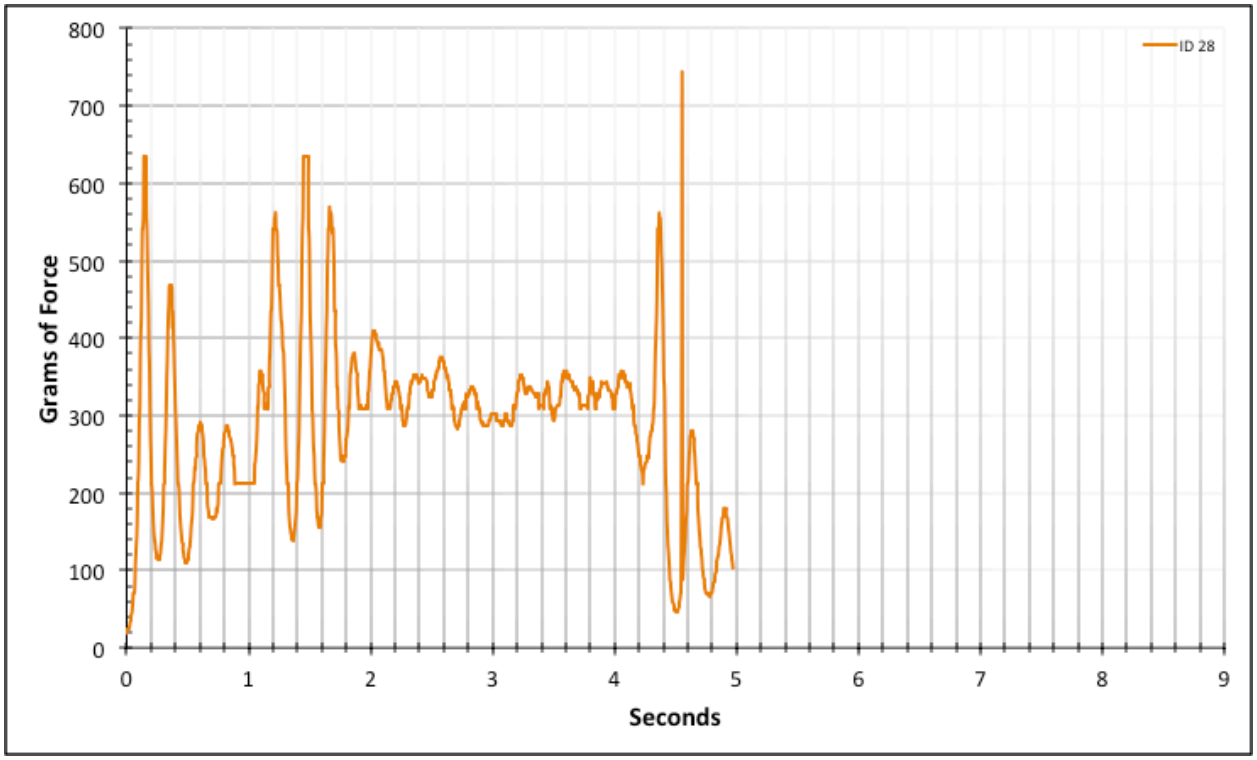

Figure A-6-54: Full Factory Baseline - Dry - ID 28 - #10, Bolt 3

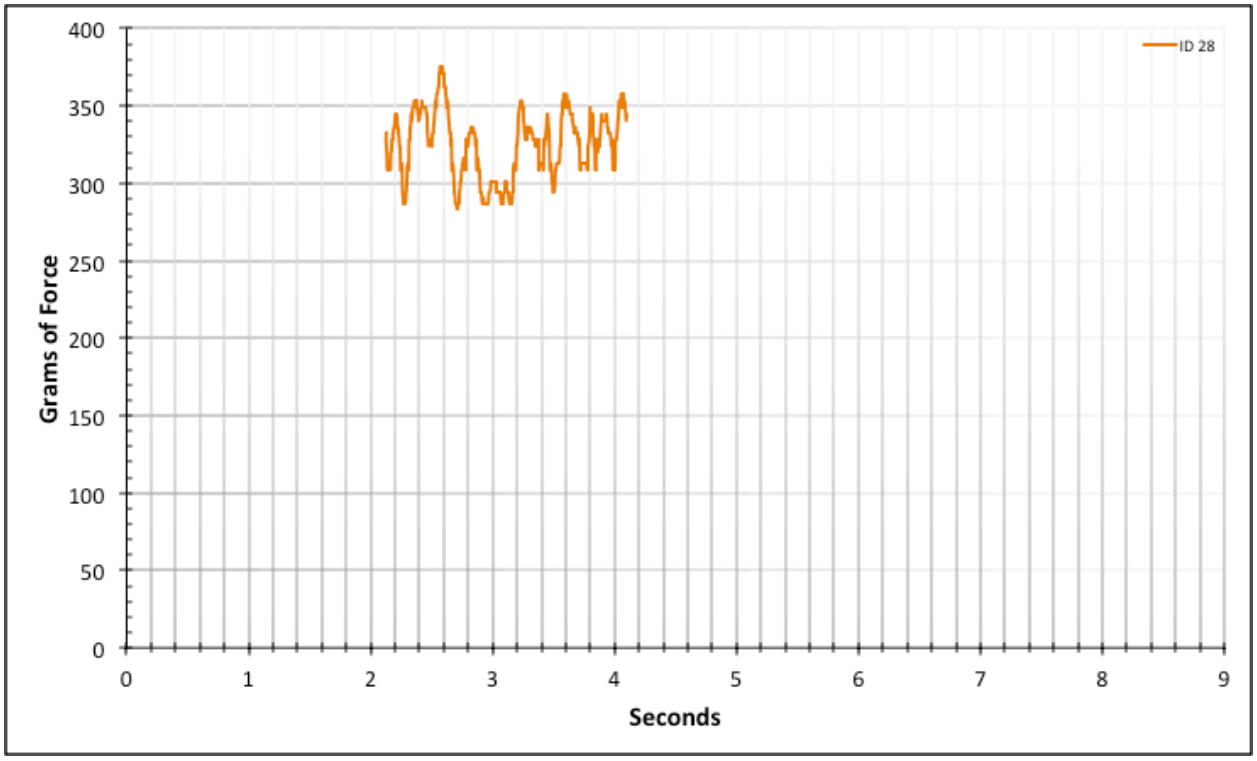

Figure A-6-55: Statistical Region Factory Baseline - Dry - ID 28 - #10, Bolt 3

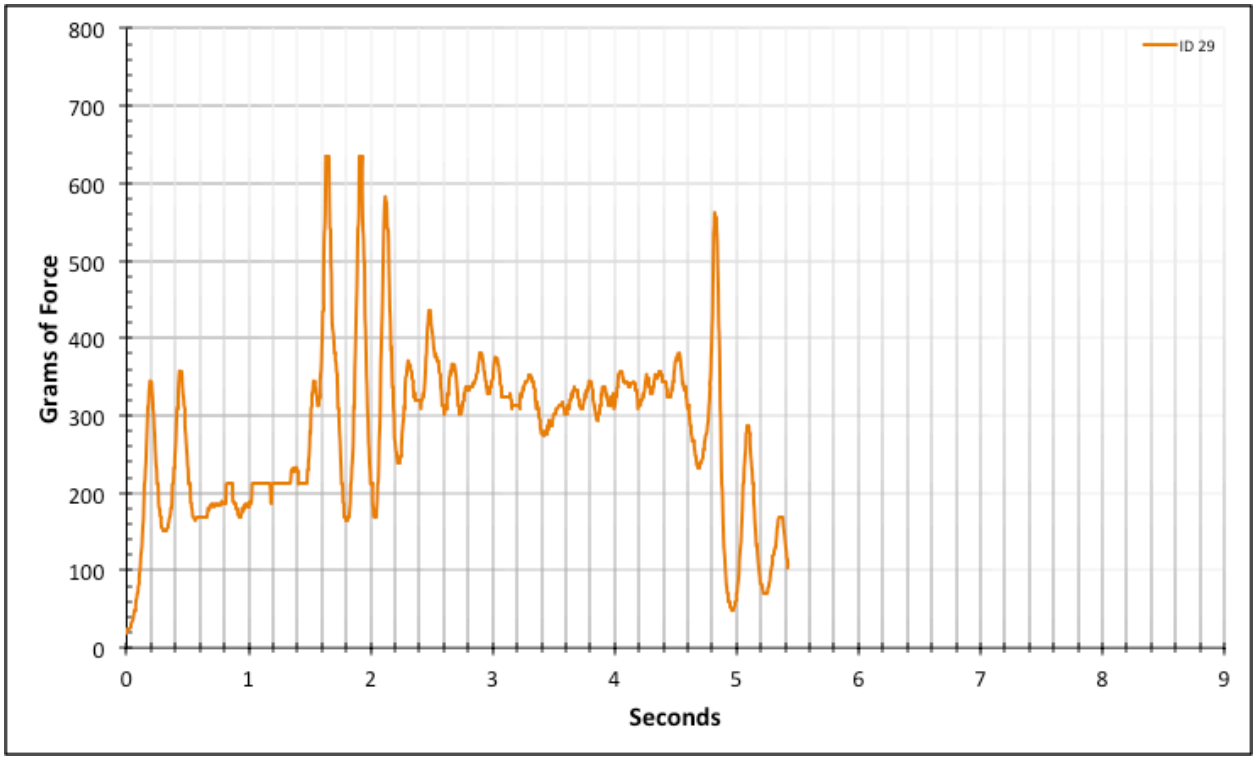

Figure A-6-56: Full Factory Baseline - Dry - ID 29 - #10, Bolt 3

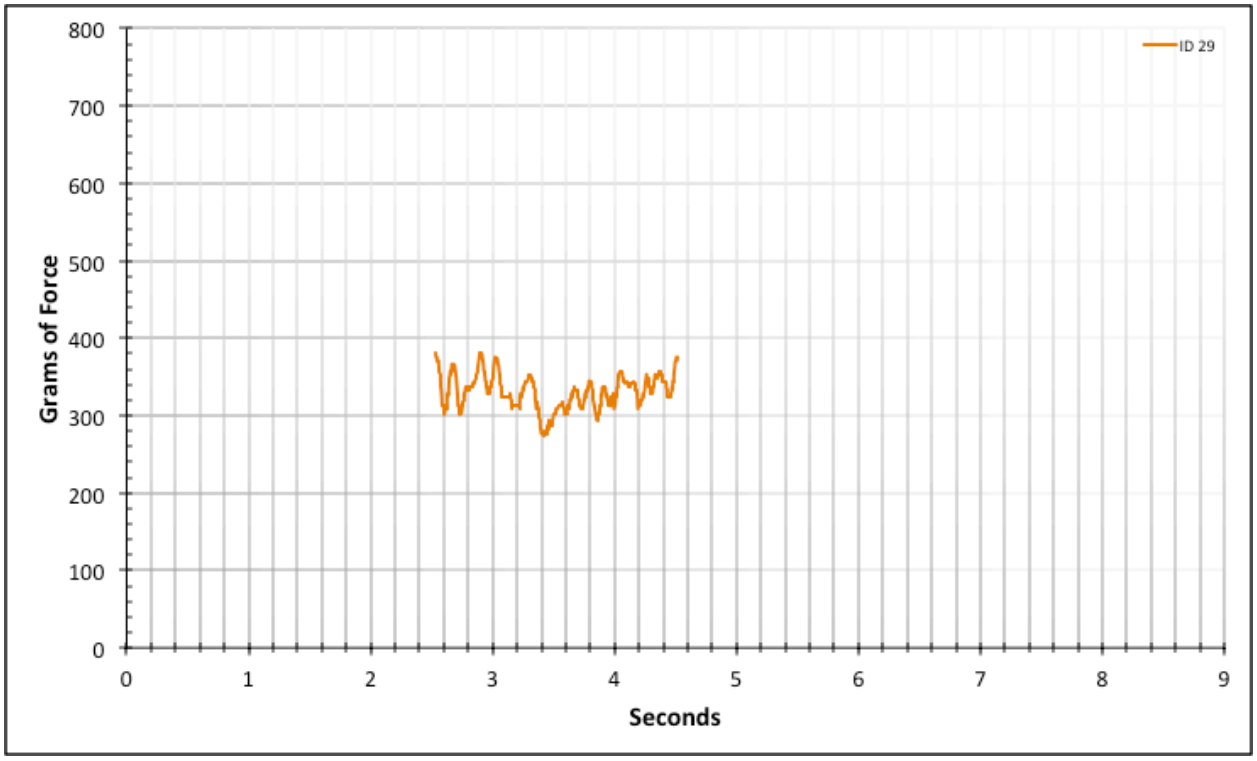

Figure A-6-57: Statistical Region Factory Baseline - Dry - ID 29 - #10, Bolt 3

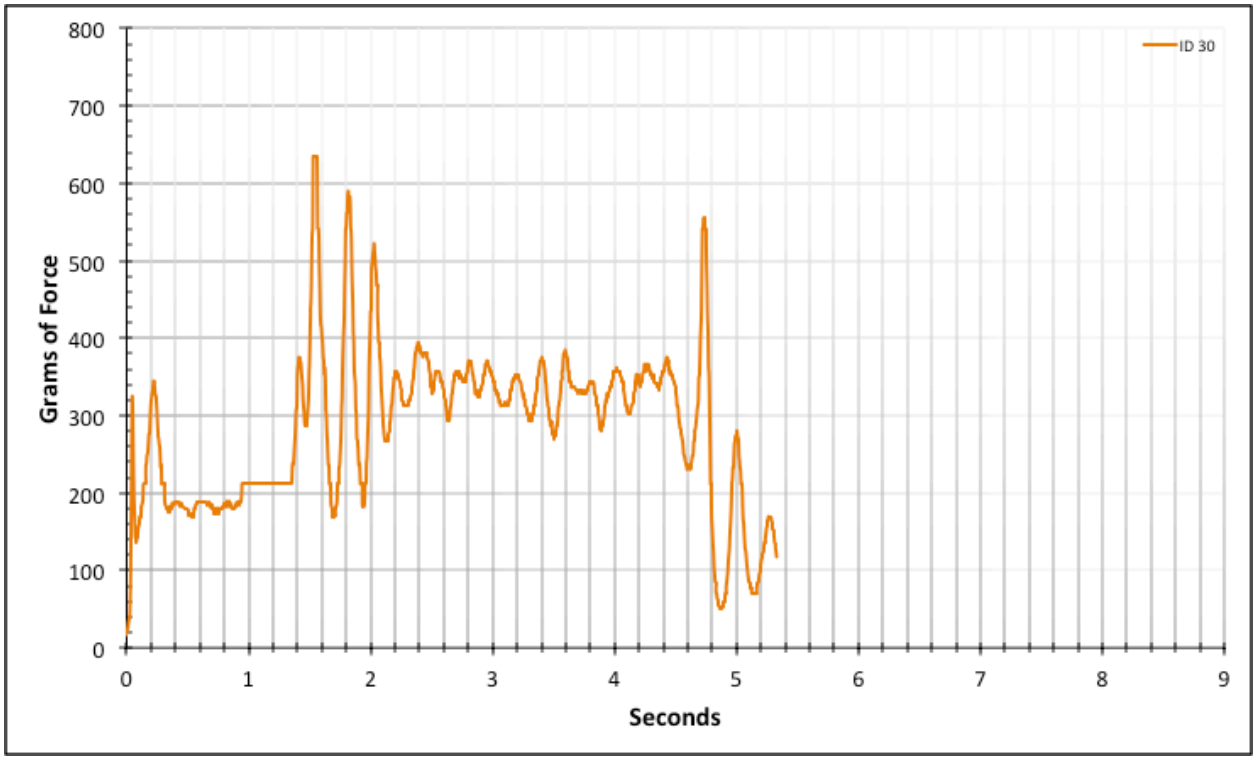

Figure A-6-58: Full Factory Baseline - Dry - ID 30 - #10, Bolt 3

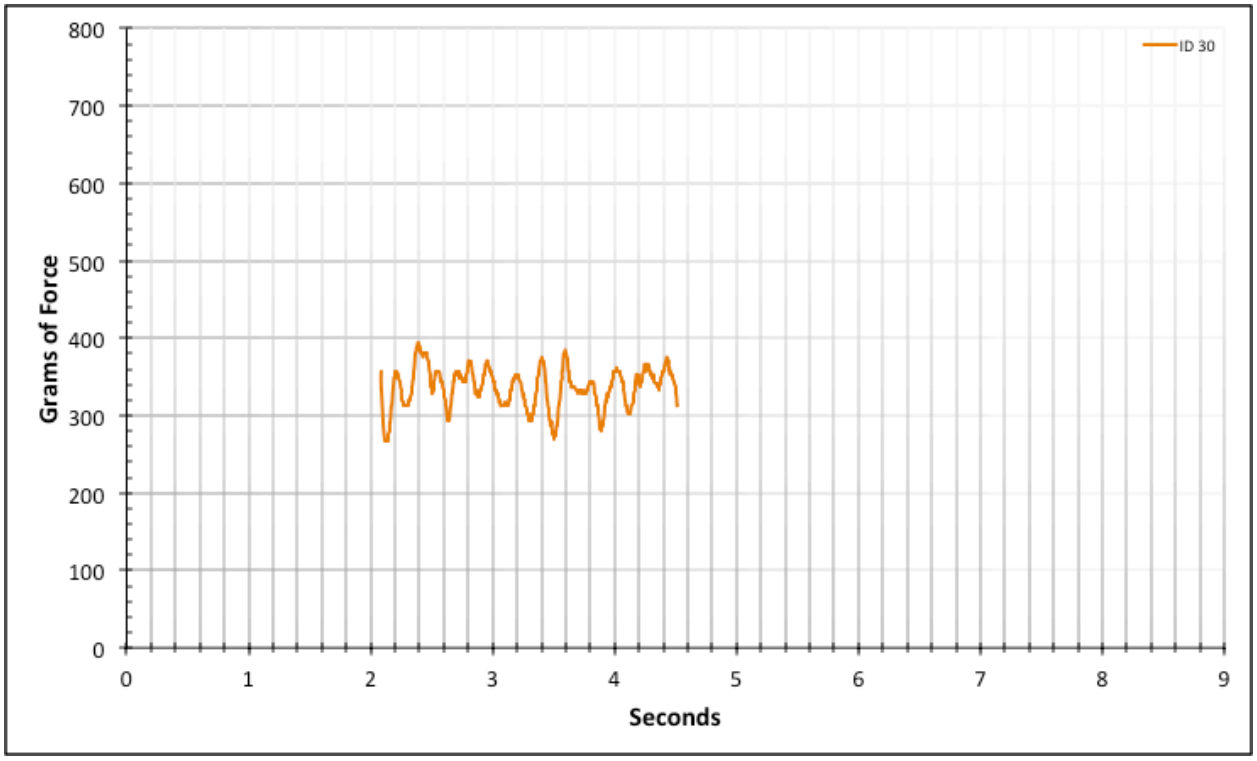

Figure A-6-59: Statistical Region Factory Baseline - Dry - ID 30 - #10, Bolt 3

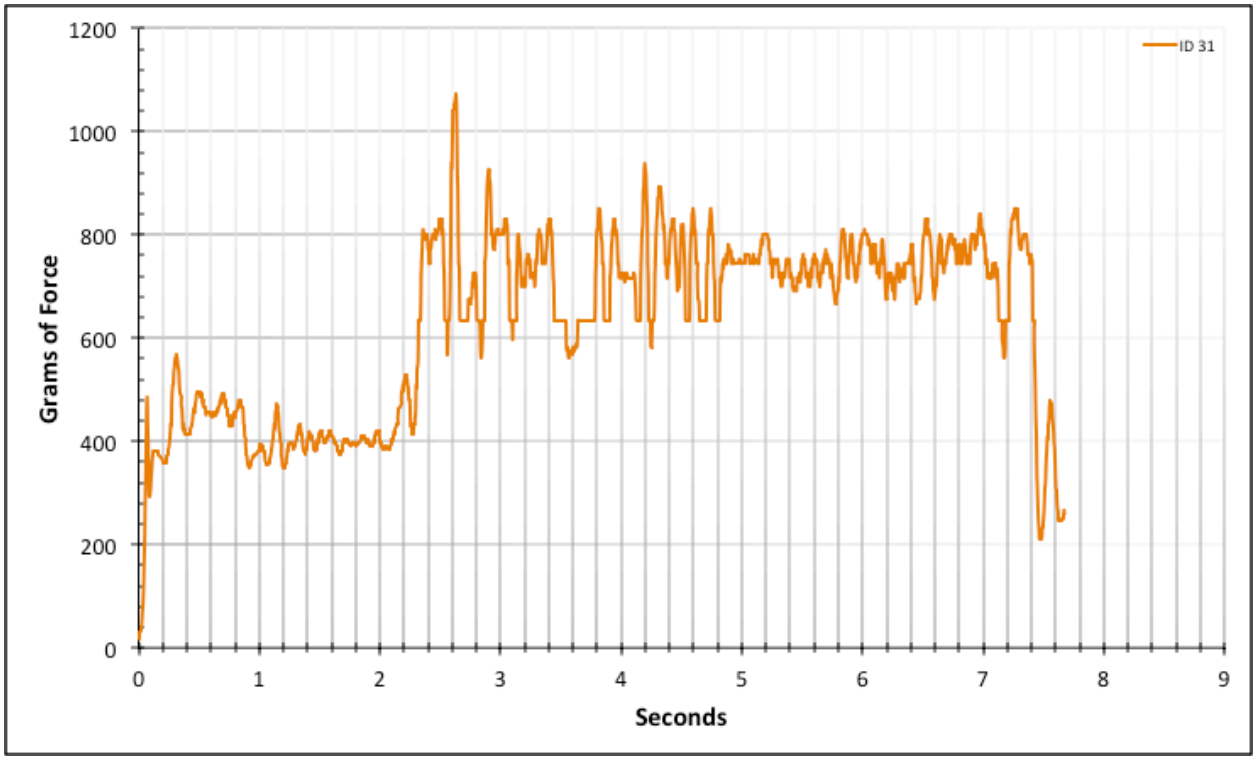

Figure A-6-60: Full Factory Baseline - Dry - ID 31 - #8, Bolt 1

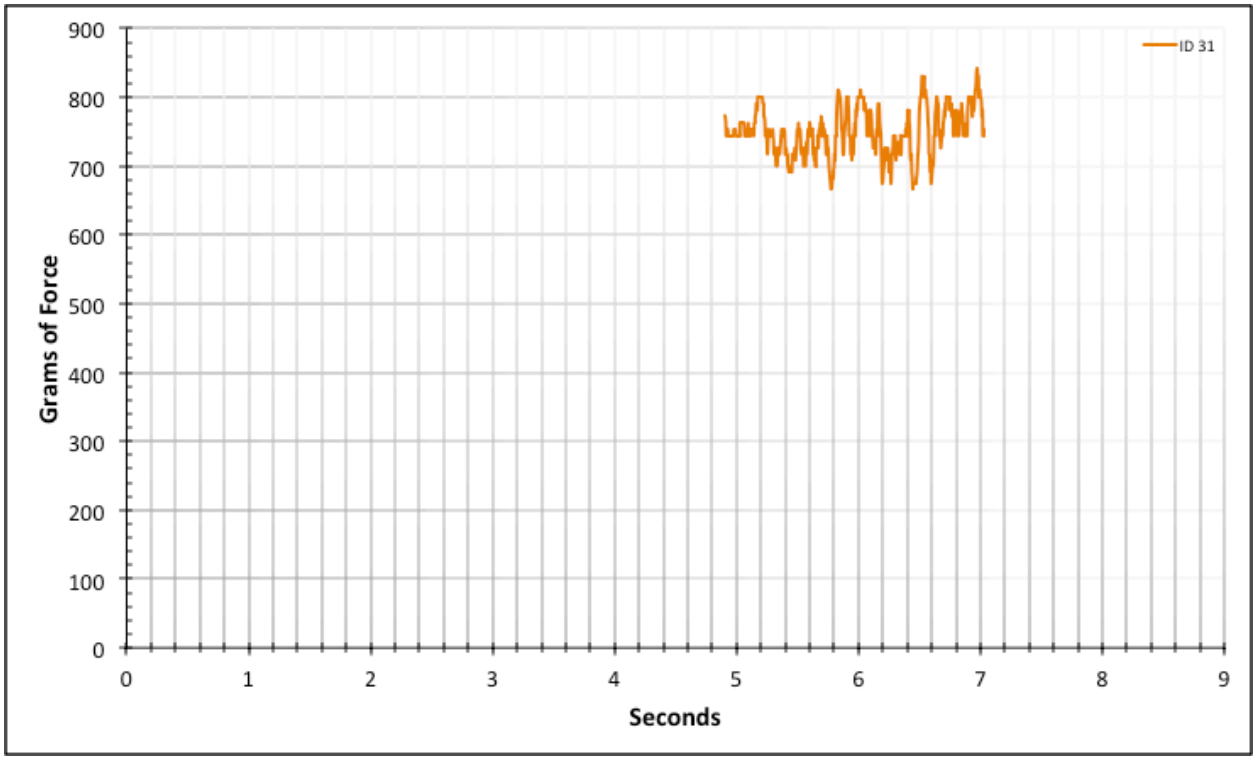

Figure A-6-61: Statistical Region Factory Baseline - Dry - ID 31 - #8, Bolt 1

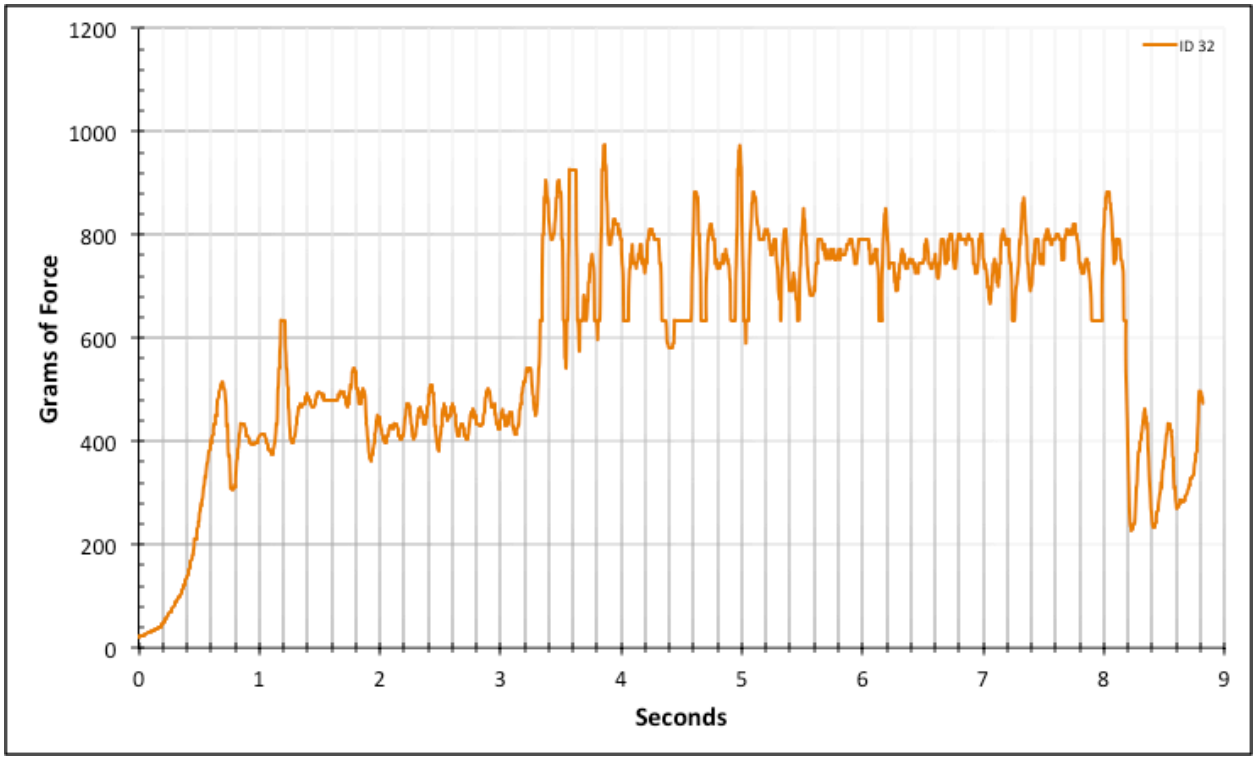

Figure A-6-62: Full Factory Baseline - Dry - ID 32 - #8, Bolt 1

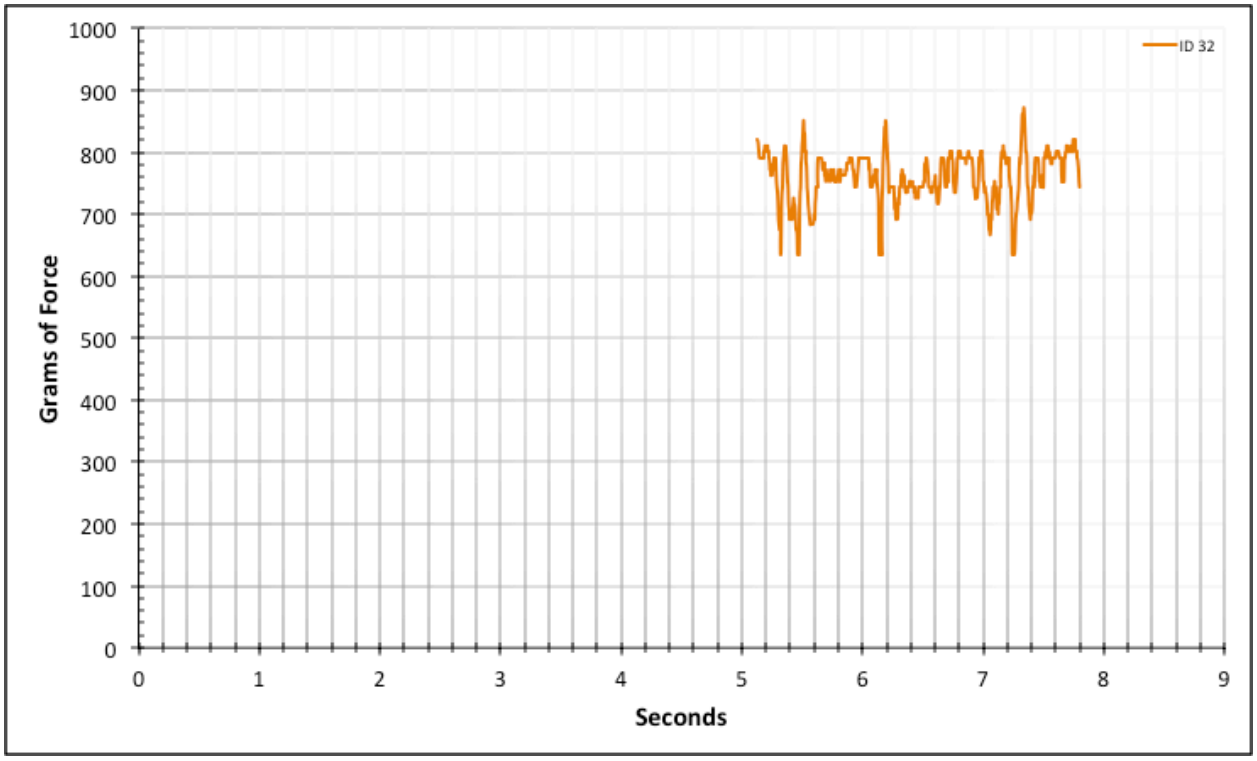

Figure A-6-63: Statistical Region Factory Baseline - Dry - ID 32 - #8, Bolt 1

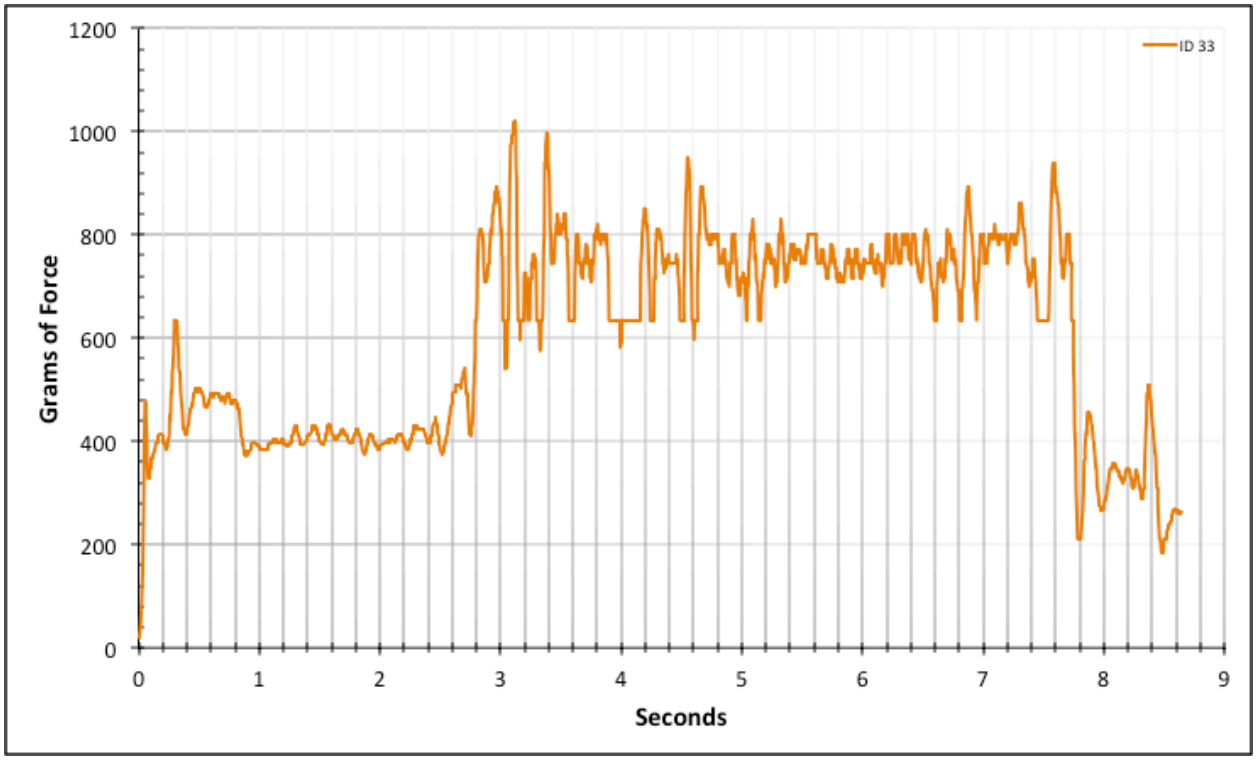

Figure A-6-64: Full Factory Baseline - Dry - ID 33 - #8, Bolt 1

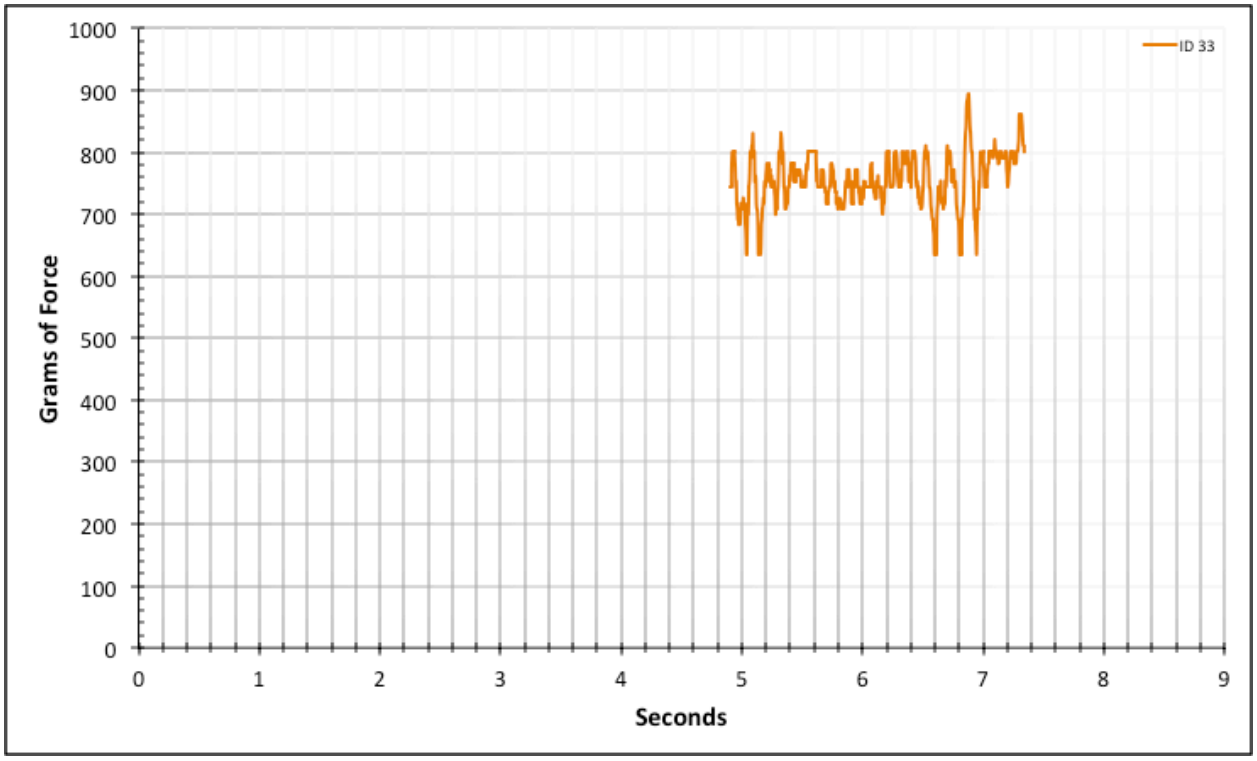

Figure A-6-65: Statistical Region Factory Baseline - Dry - ID 33 - #8, Bolt 1

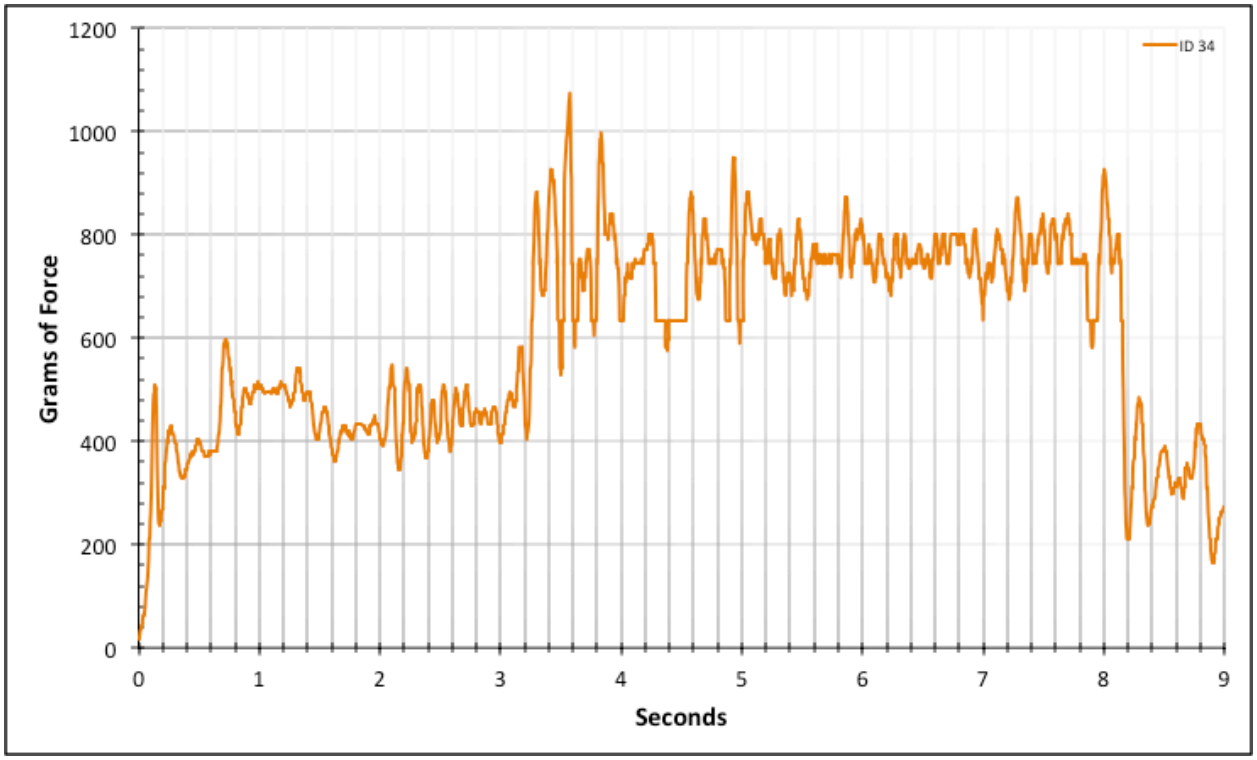

Figure A-6-66: Full Factory Baseline - Dry - ID 34 - #8, Bolt 1

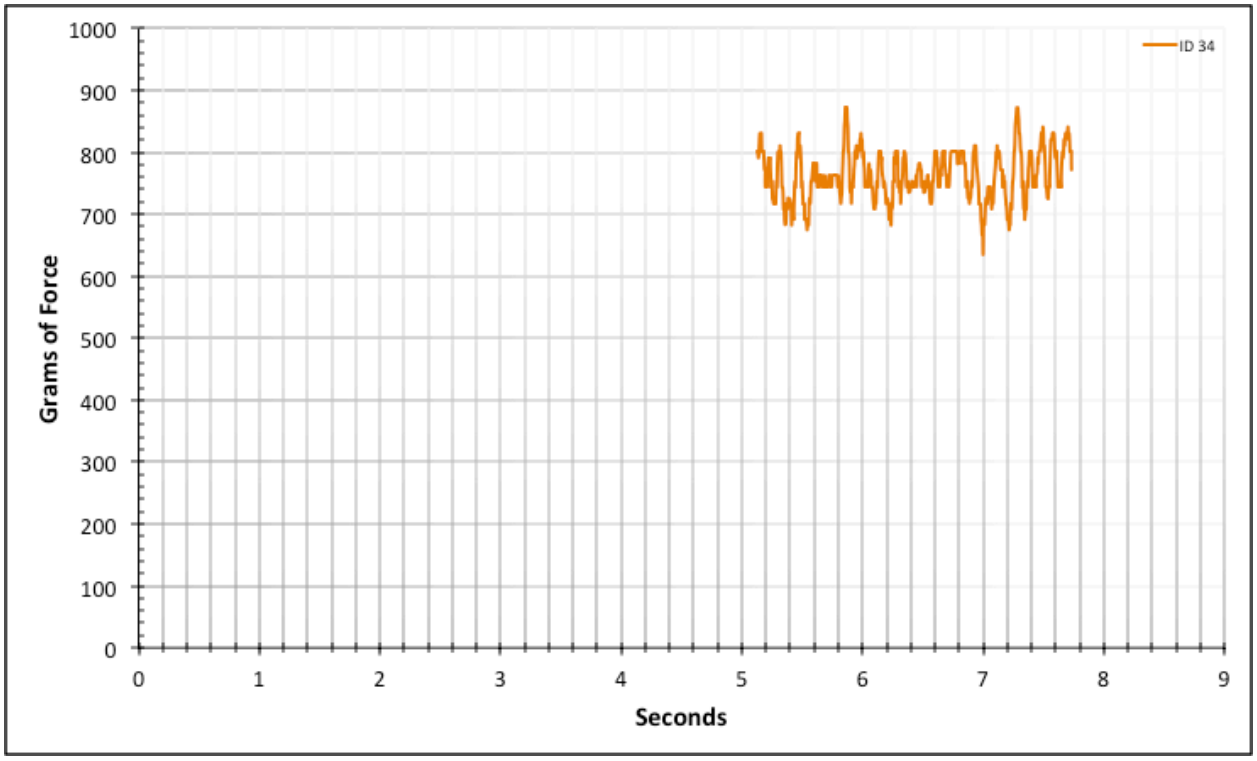

Figure A-6-67: Statistical Region Factory Baseline - Dry - ID 34 - #8, Bolt 1

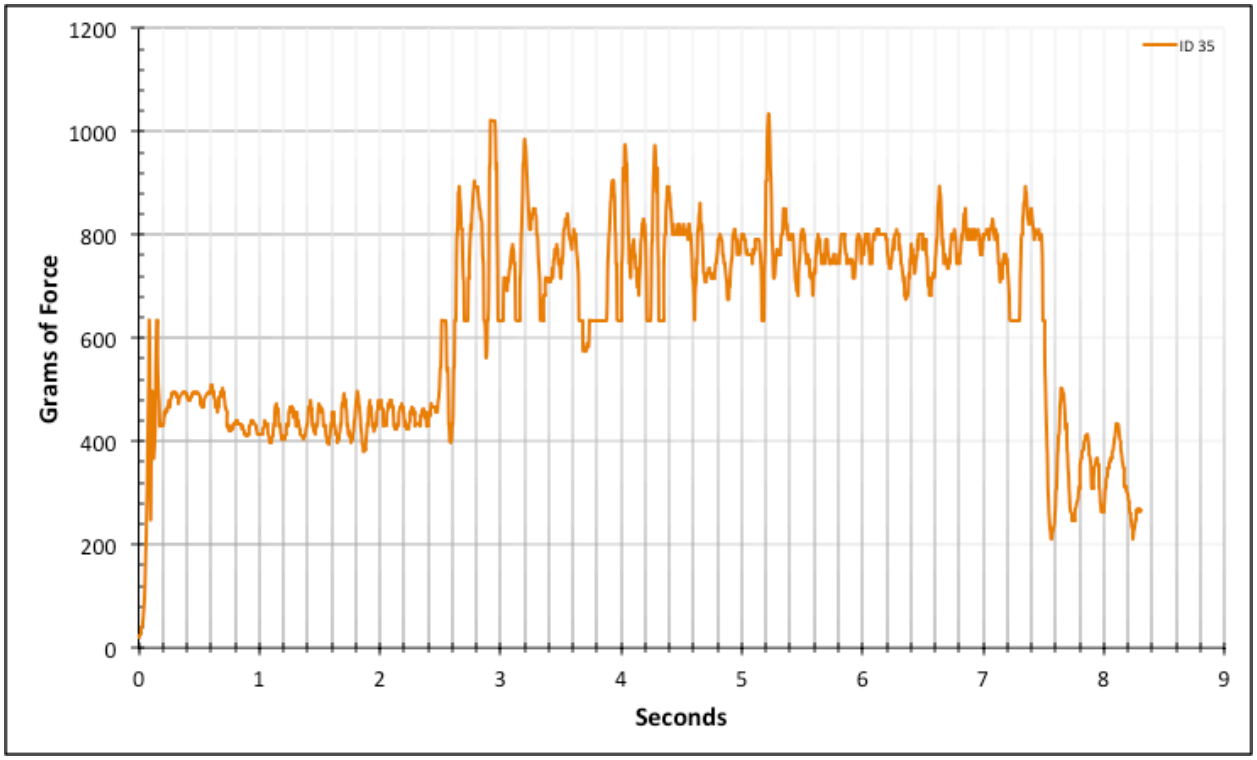

Figure A-6-68: Full Factory Baseline - Dry - ID 35 - #8, Bolt 1

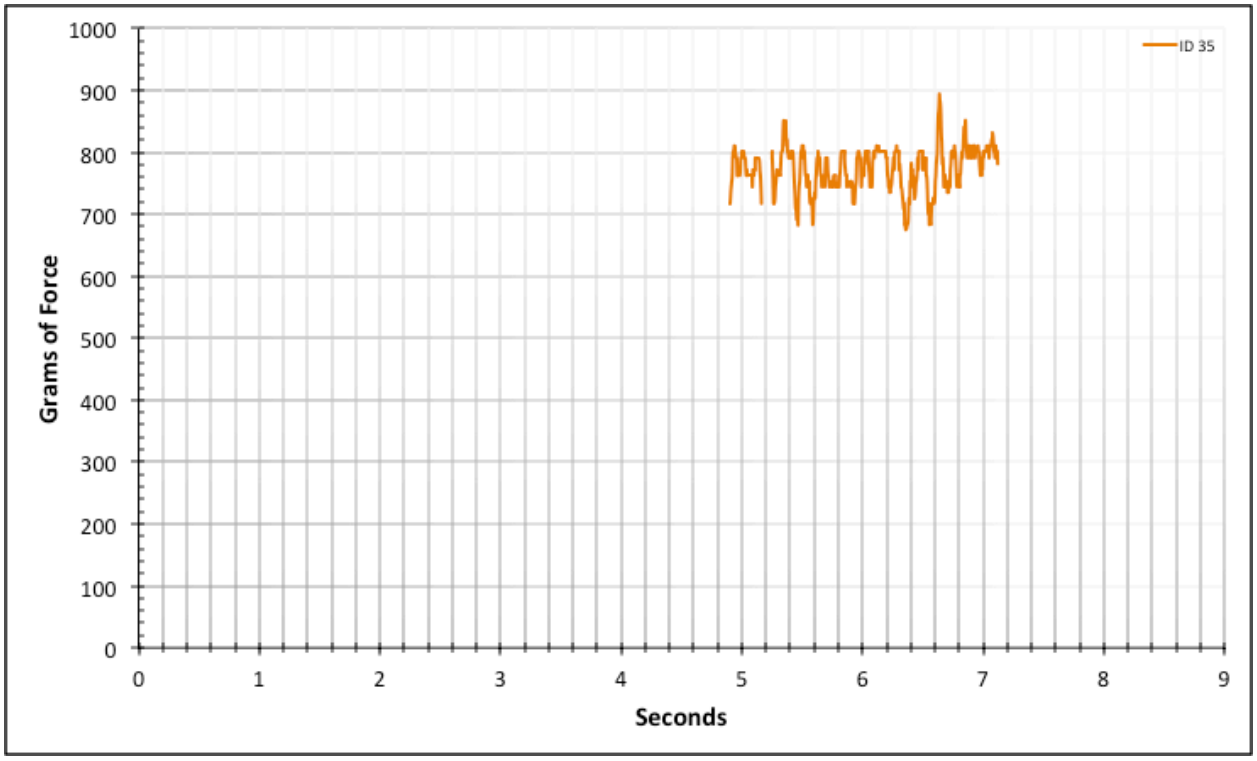

Figure A-6-69: Statistical Region Factory Baseline - Dry - ID 35 - #8, Bolt 1

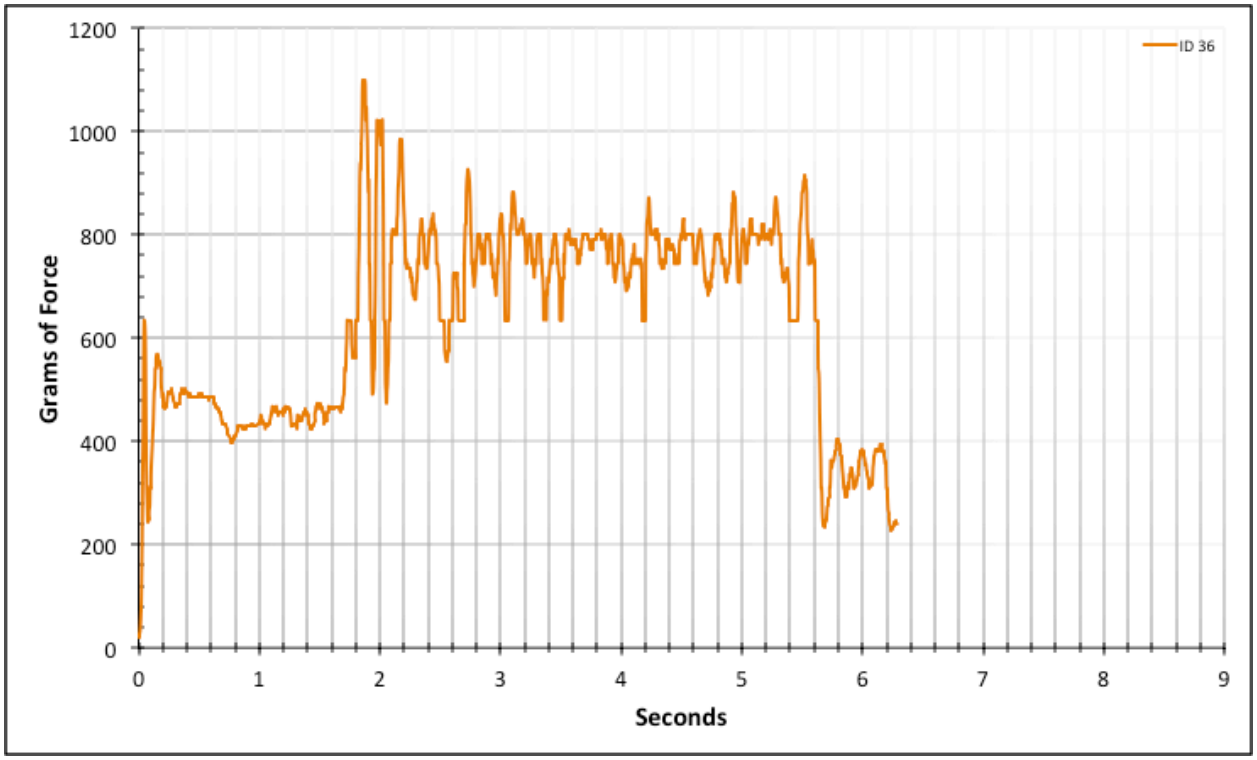

Figure A-6-70: Full Factory Baseline - Dry - ID 36 - #8, Bolt 2

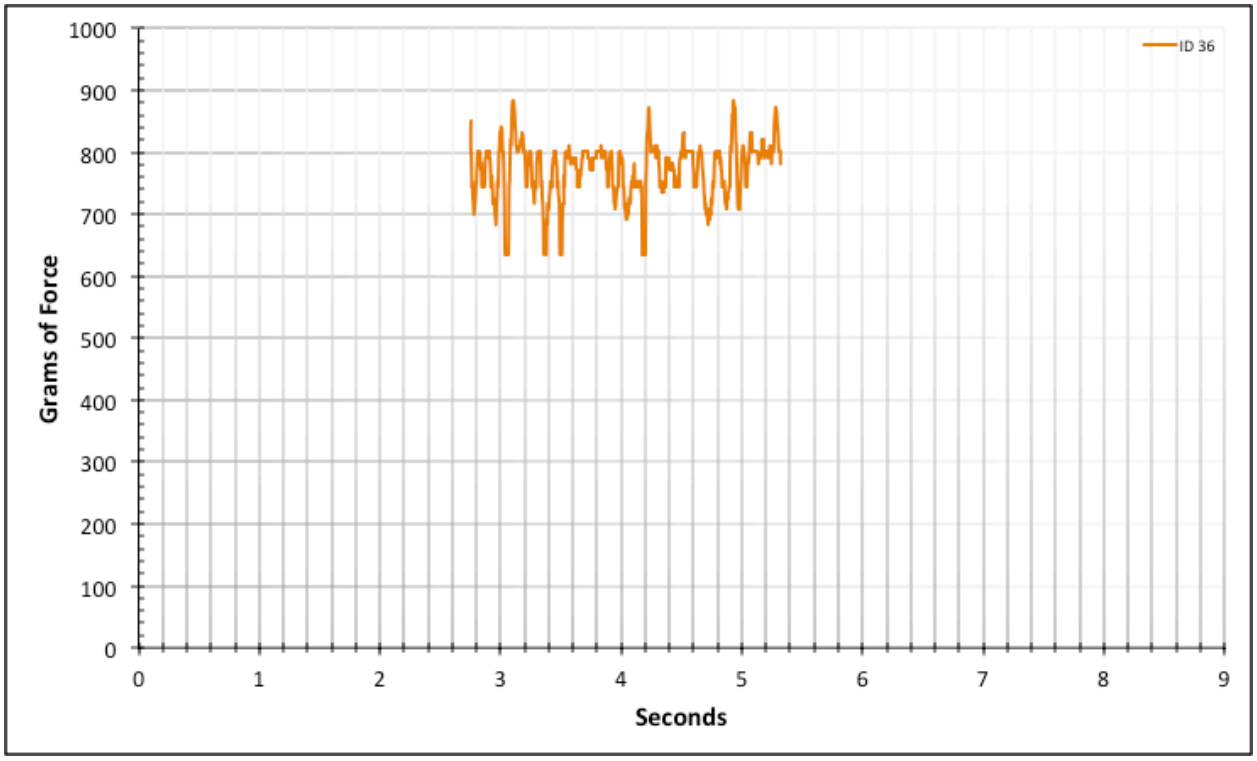

Figure A-6-71: Statistical Region Factory Baseline - Dry - ID 36 - #8, Bolt 2

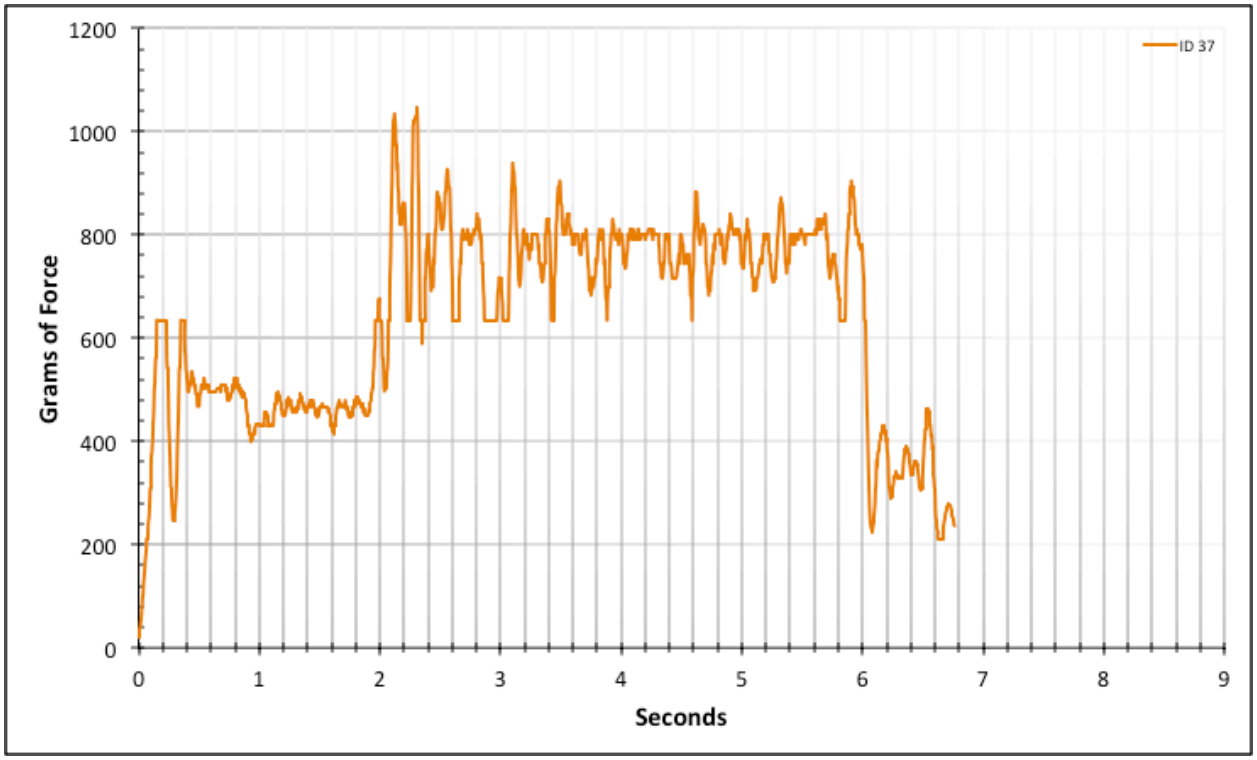

Figure A-6-72: Full Factory Baseline - Dry - ID 37 - #8, Bolt 2

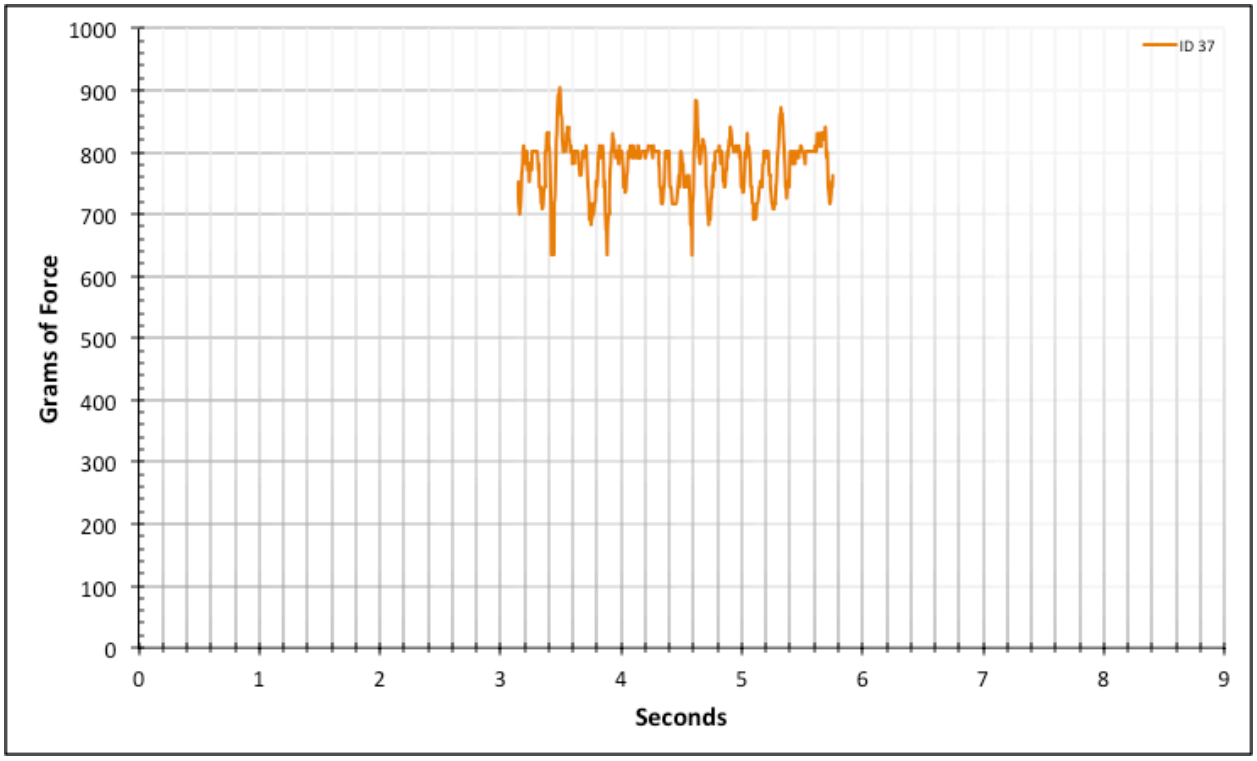

Figure A-6-73: Statistical Region Factory Baseline - Dry - ID 37 - #8, Bolt 2

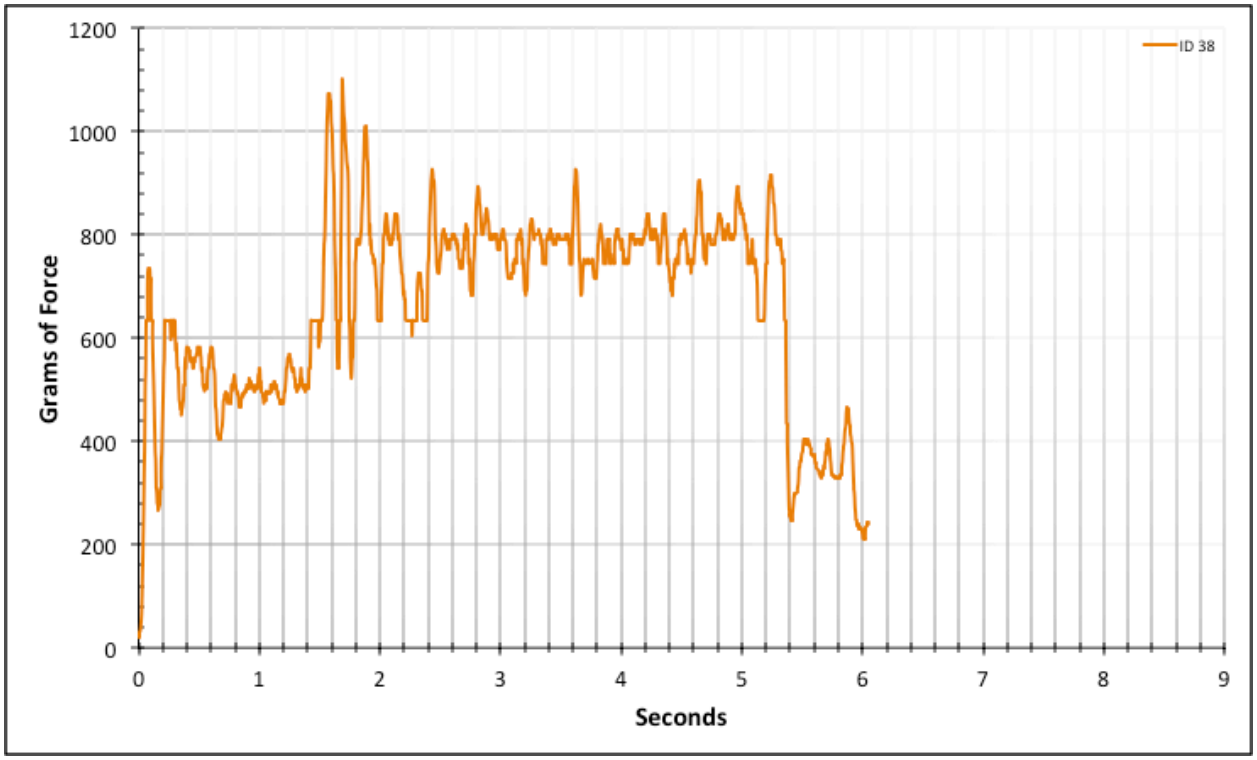

Figure A-6-74: Full Factory Baseline - Dry - ID 38 - #8, Bolt 2

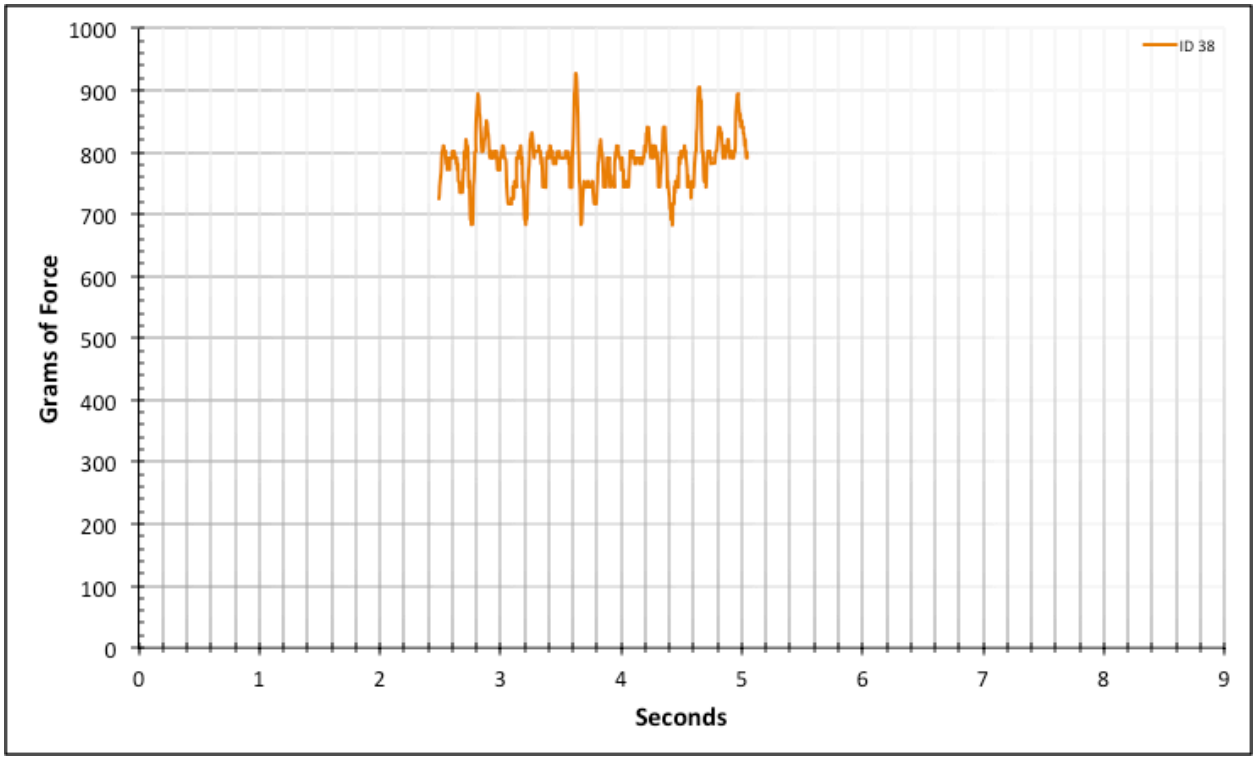

Figure A-6-75: Statistical Region Factory Baseline - Dry - ID 38 - #8, Bolt 2

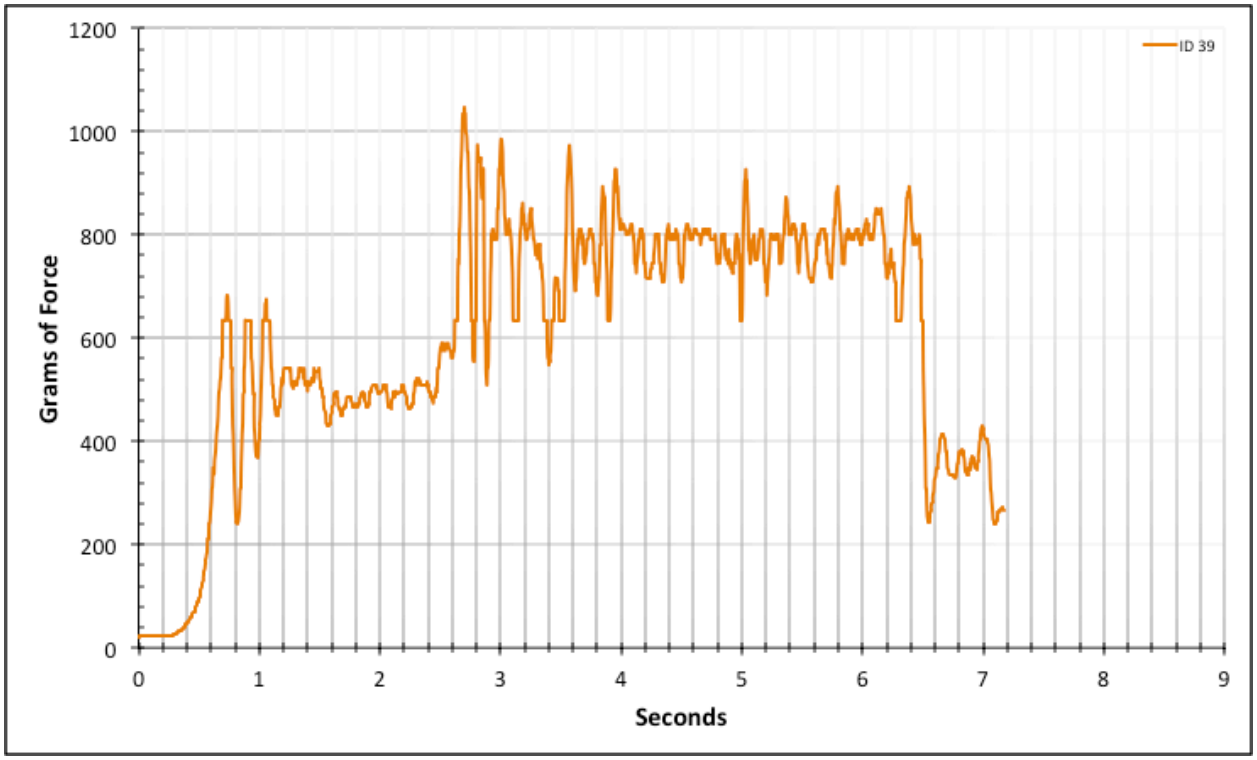

Figure A-6-76: Full Factory Baseline - Dry - ID 39 - #8, Bolt 2

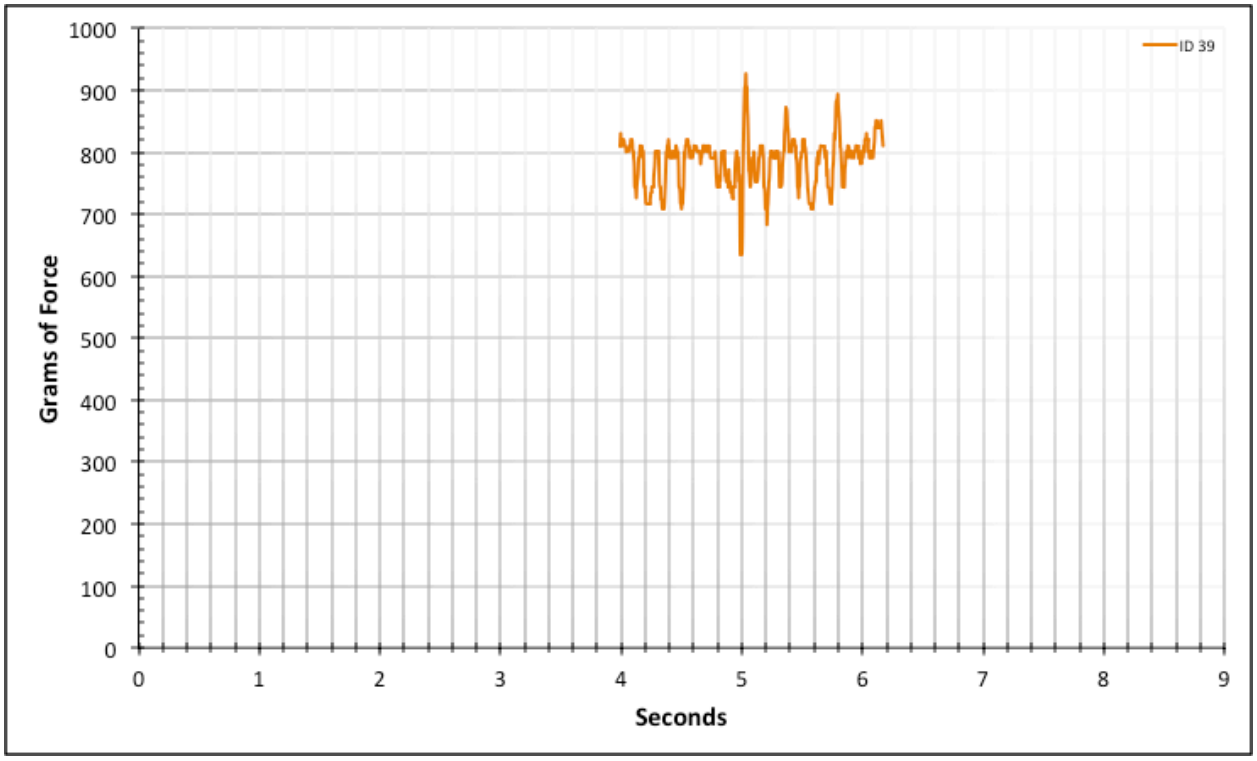

Figure A-6-77: Statistical Region Factory Baseline - Dry - ID 39 - #8, Bolt 2

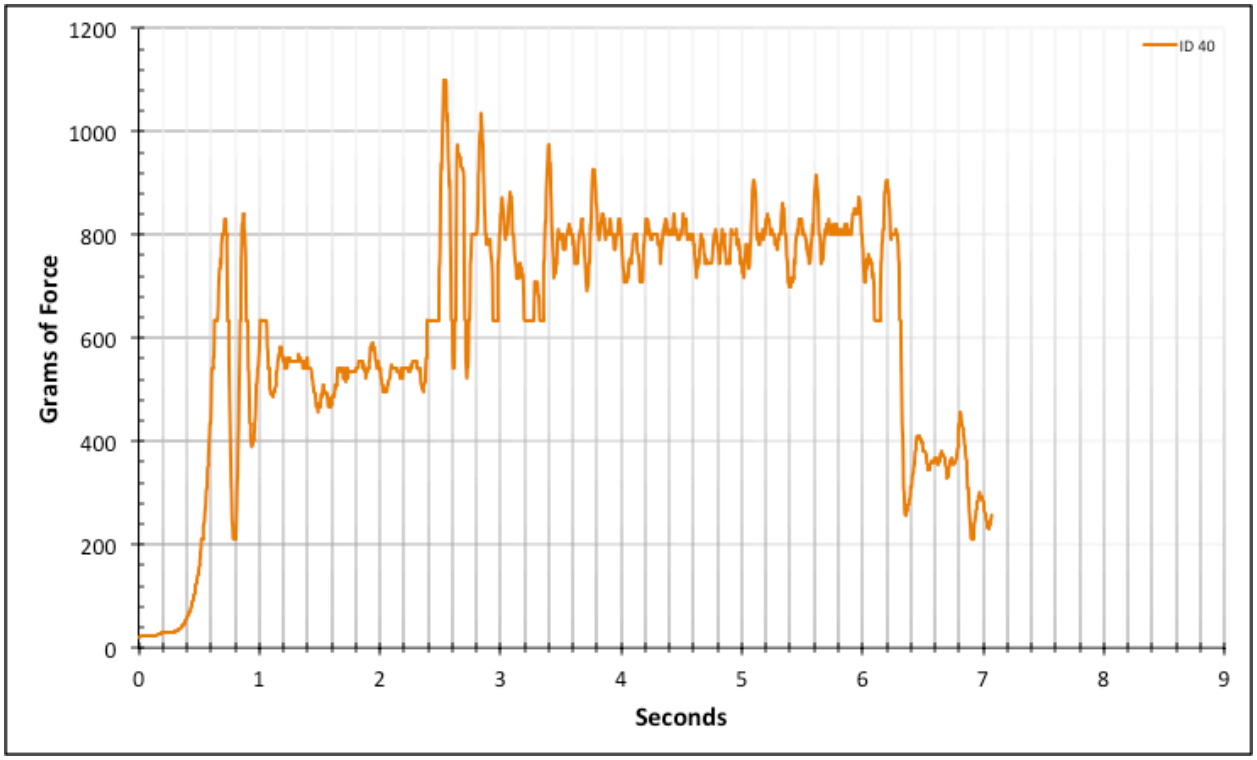

Figure A-6-78: Full Factory Baseline - Dry - ID 40 - #8, Bolt 2

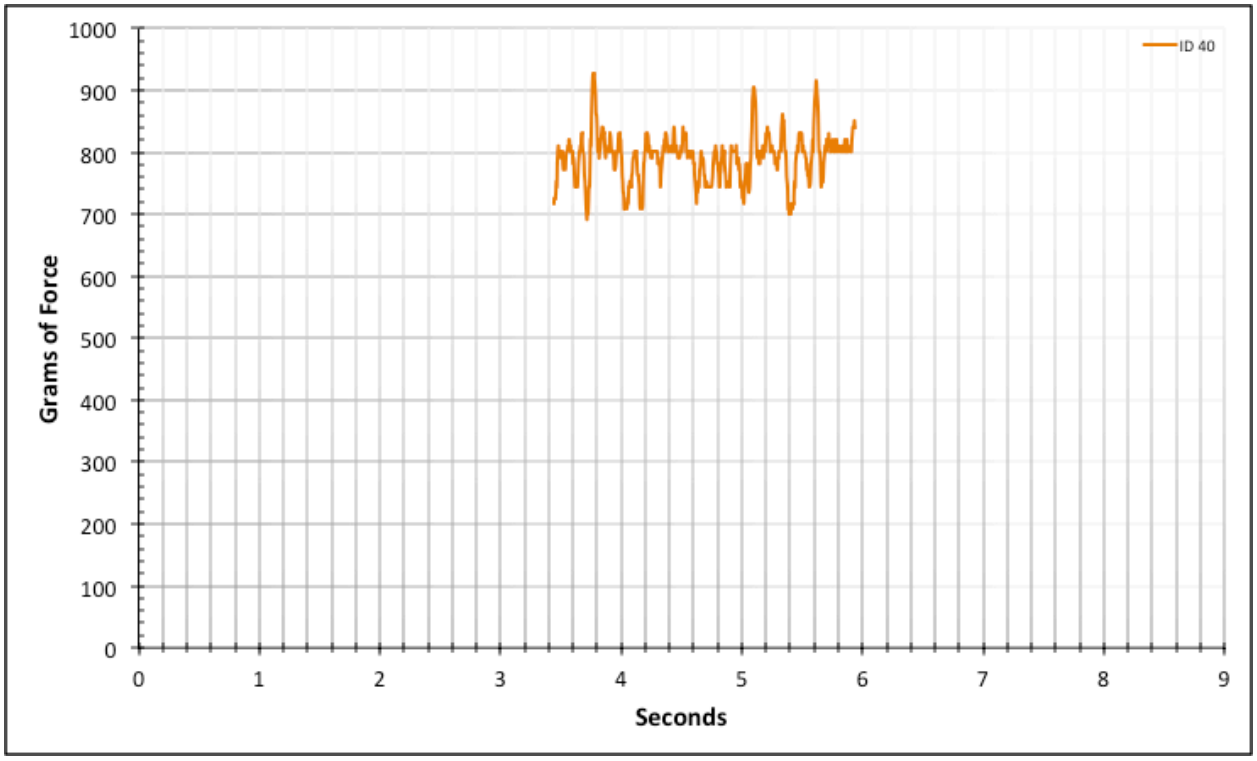

Figure A-6-79: Statistical Region Factory Baseline - Dry - ID 40 - #8, Bolt 2

A.2. Modeled Product – Dry

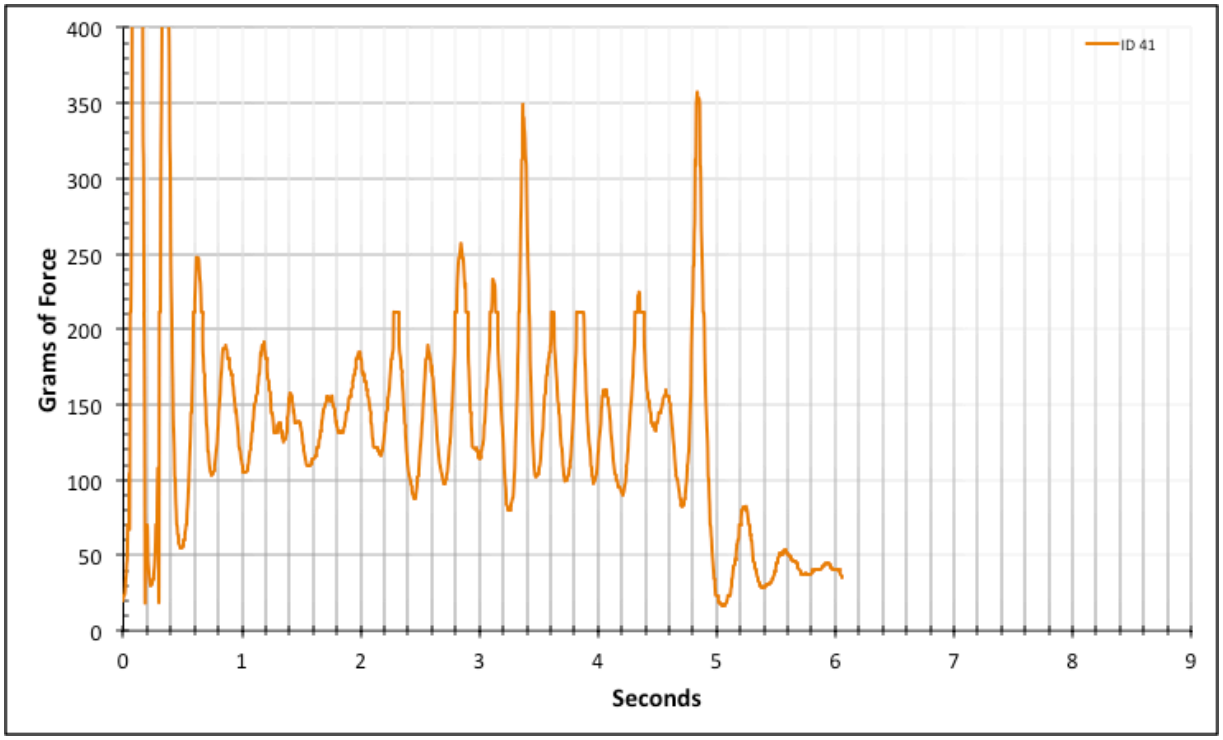

Figure A-6-80: Full Modeled Product - Dry - ID 41 - #12, Bolt 1

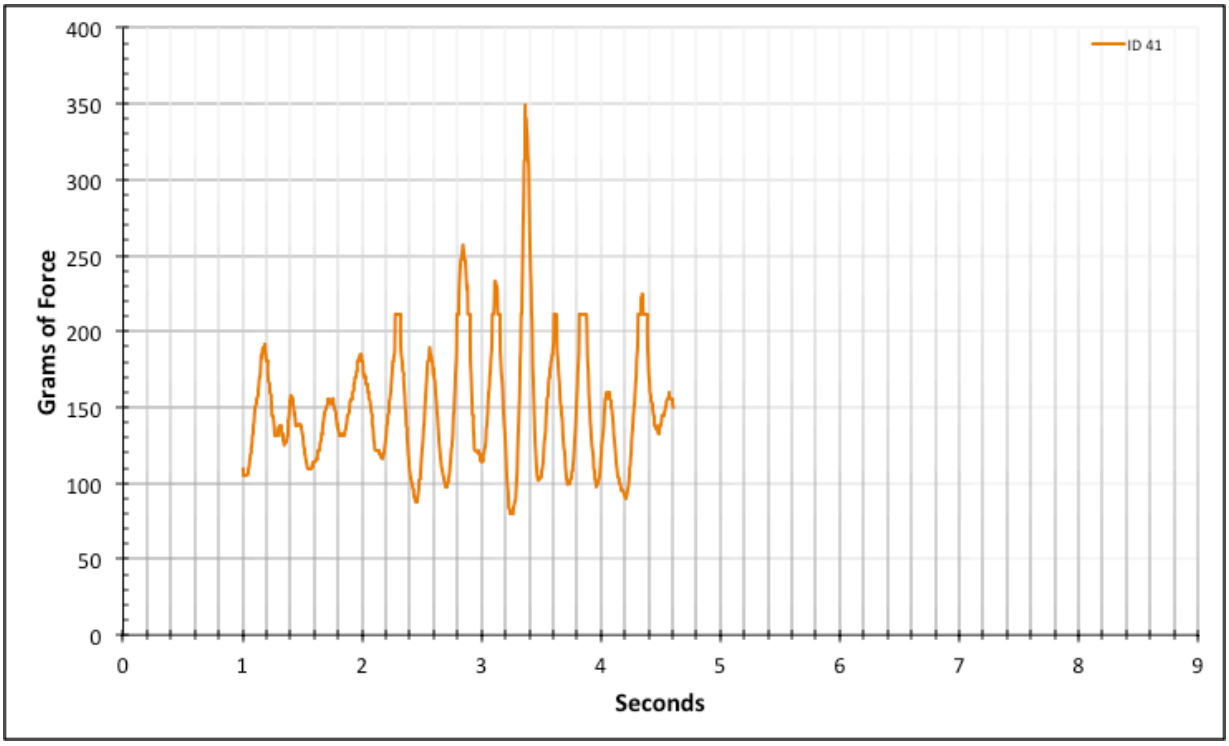

Figure A-6-81: Statistical Region Modeled Product - Dry - ID 41 - #12, Bolt 1

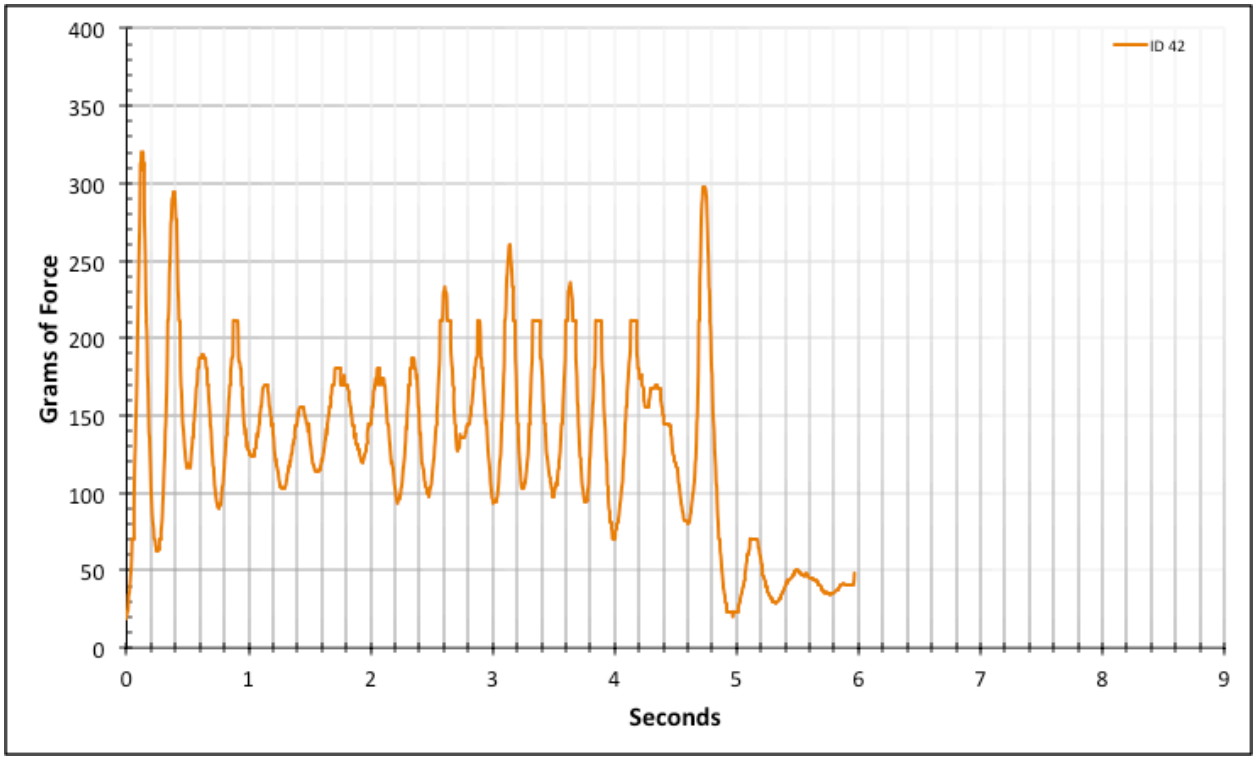

Figure A-6-82: Full Modeled Product - Dry - ID 42 - #12, Bolt 1

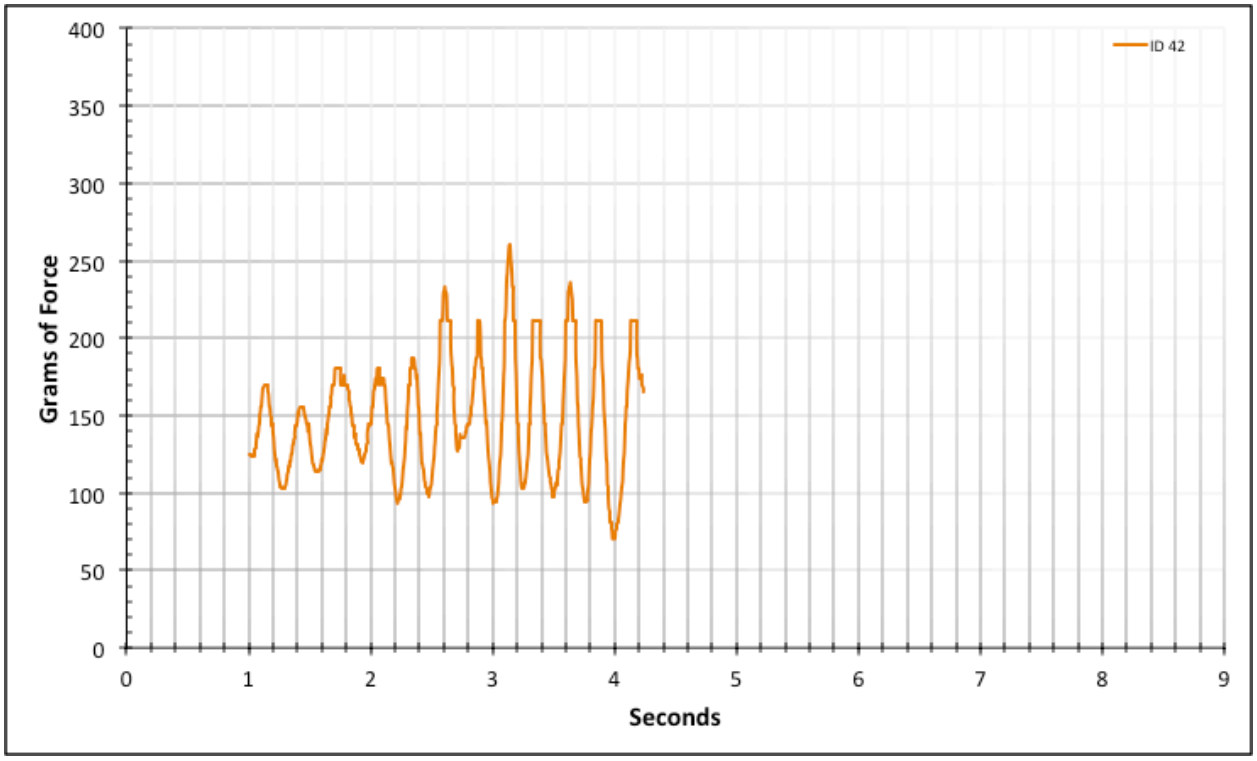

Figure A-6-83: Statistical Region Modeled Product - Dry - ID 42 - #12, Bolt 1

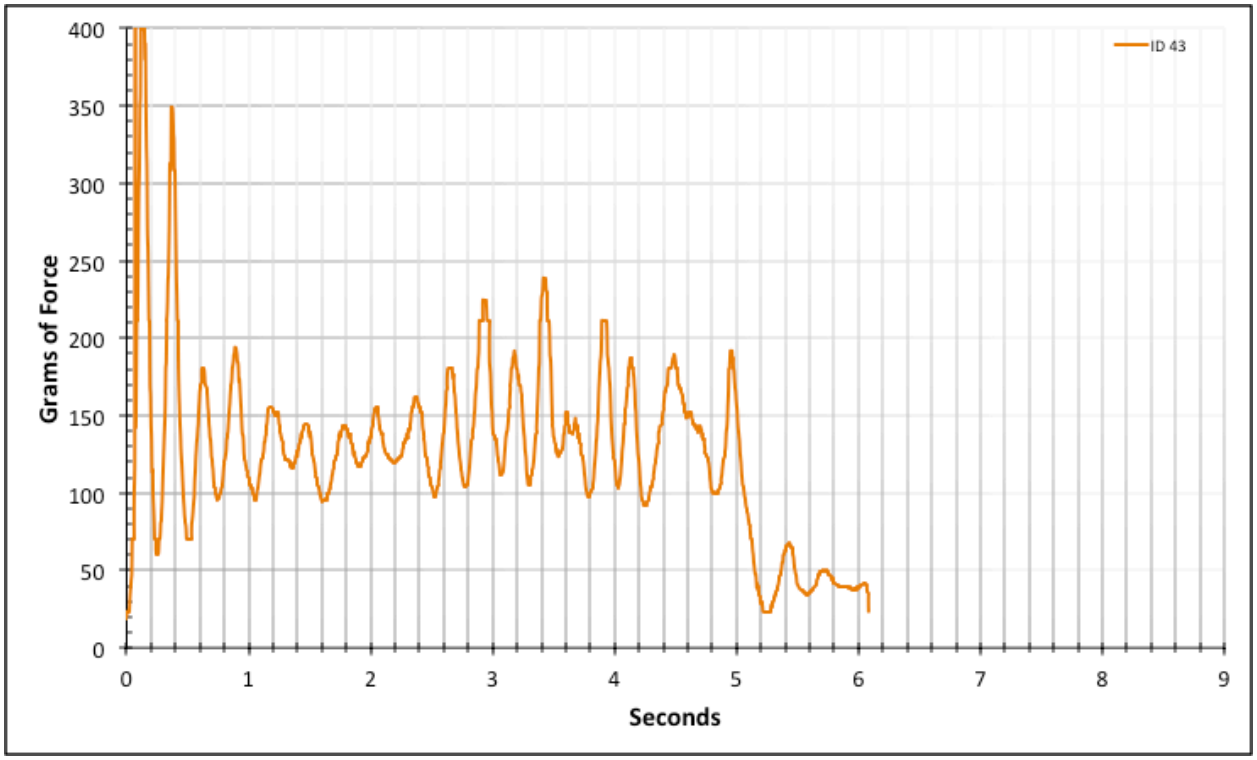

Figure A-6-84: Full Modeled Product - Dry - ID 43 - #12, Bolt 1

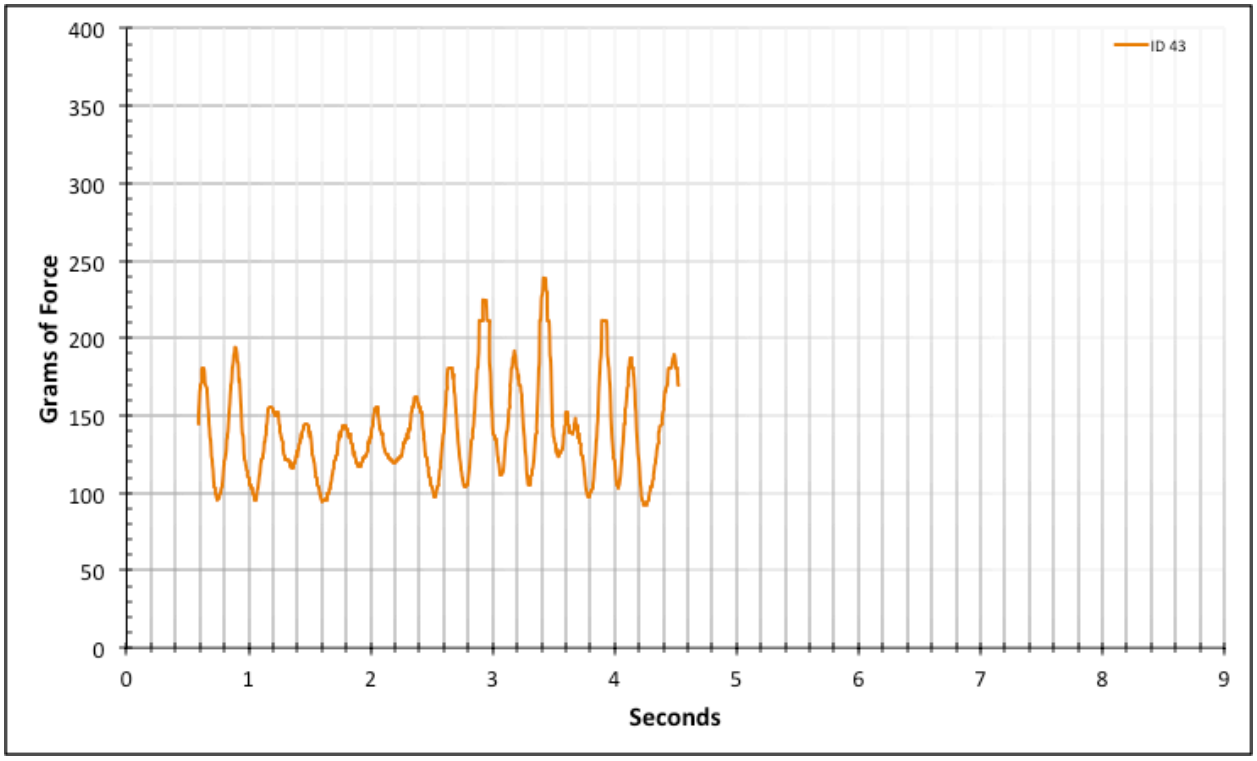

Figure A-6-85: Statistical Region Modeled Product - Dry - ID 43 - #12, Bolt 1

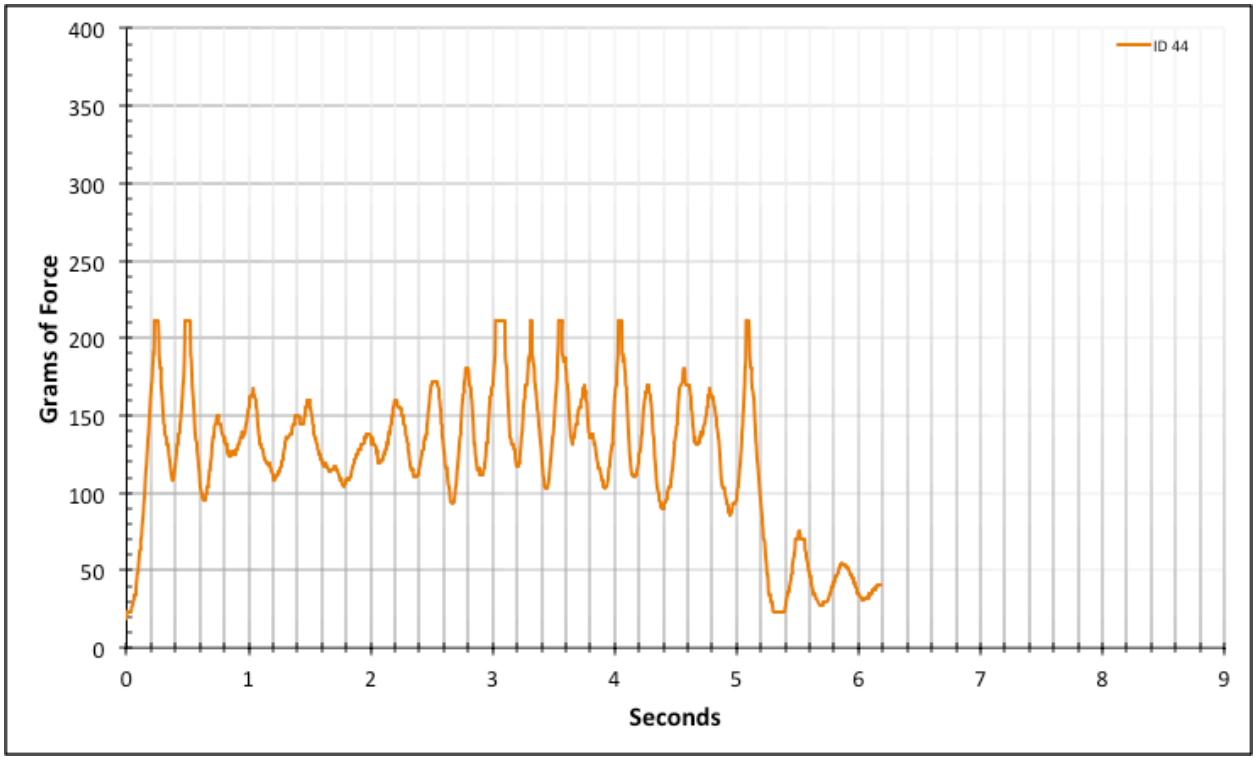

Figure A-6-86: Full Modeled Product - Dry - ID 44 - #12, Bolt 1

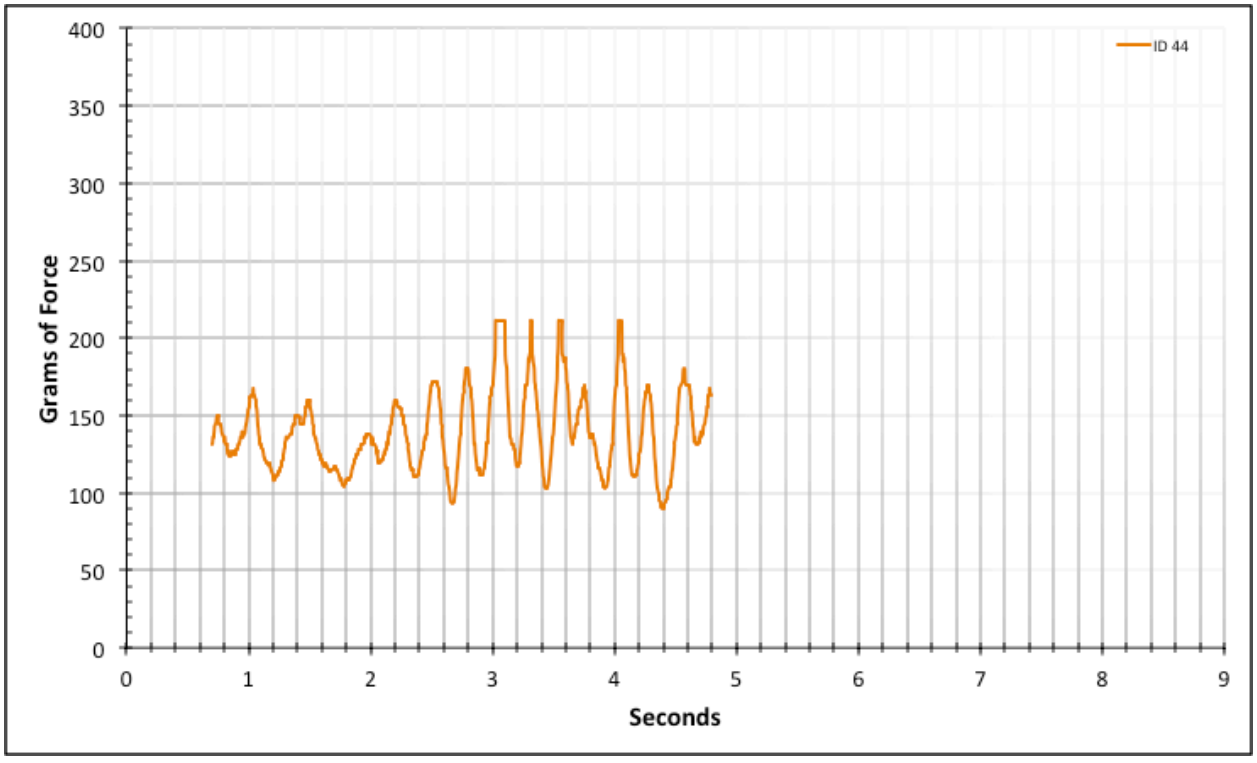

Figure A-6-87: Statistical Region Modeled Product - Dry - ID 44 - #12, Bolt 1

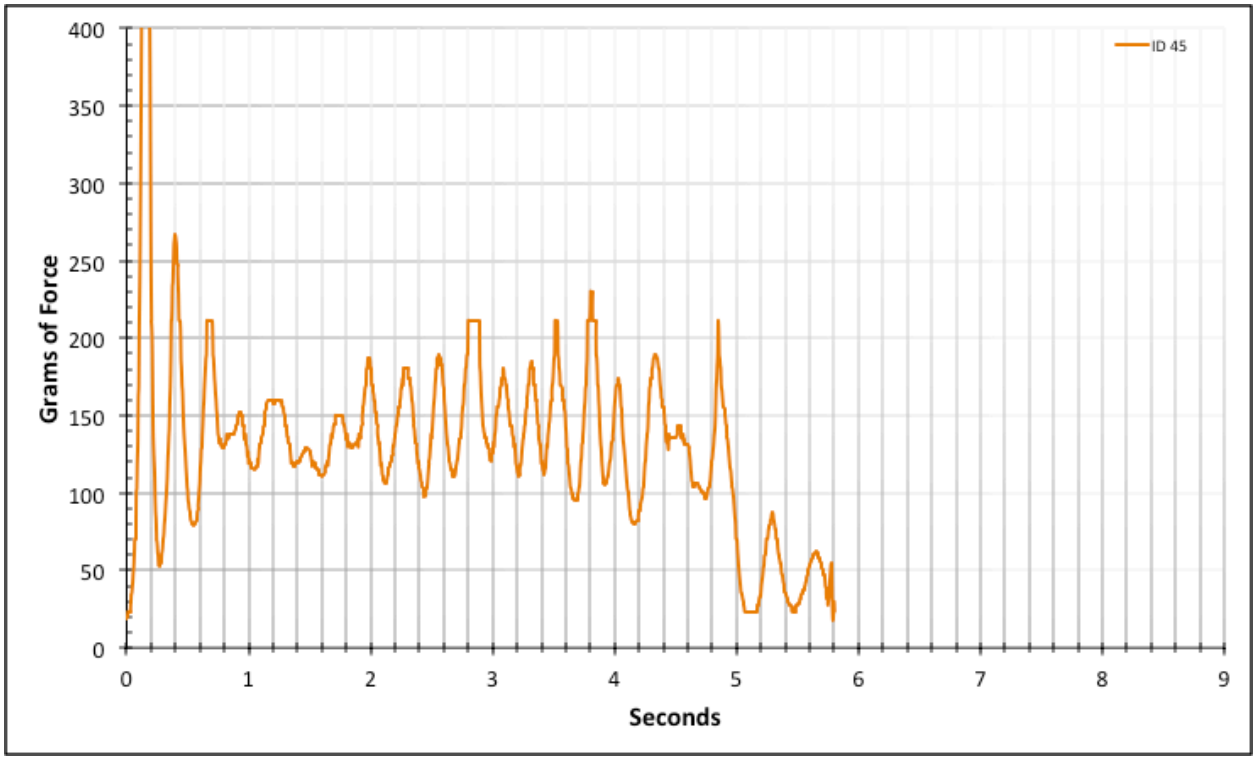

Figure A-6-88: Full Modeled Product - Dry - ID 45 - #12, Bolt 1

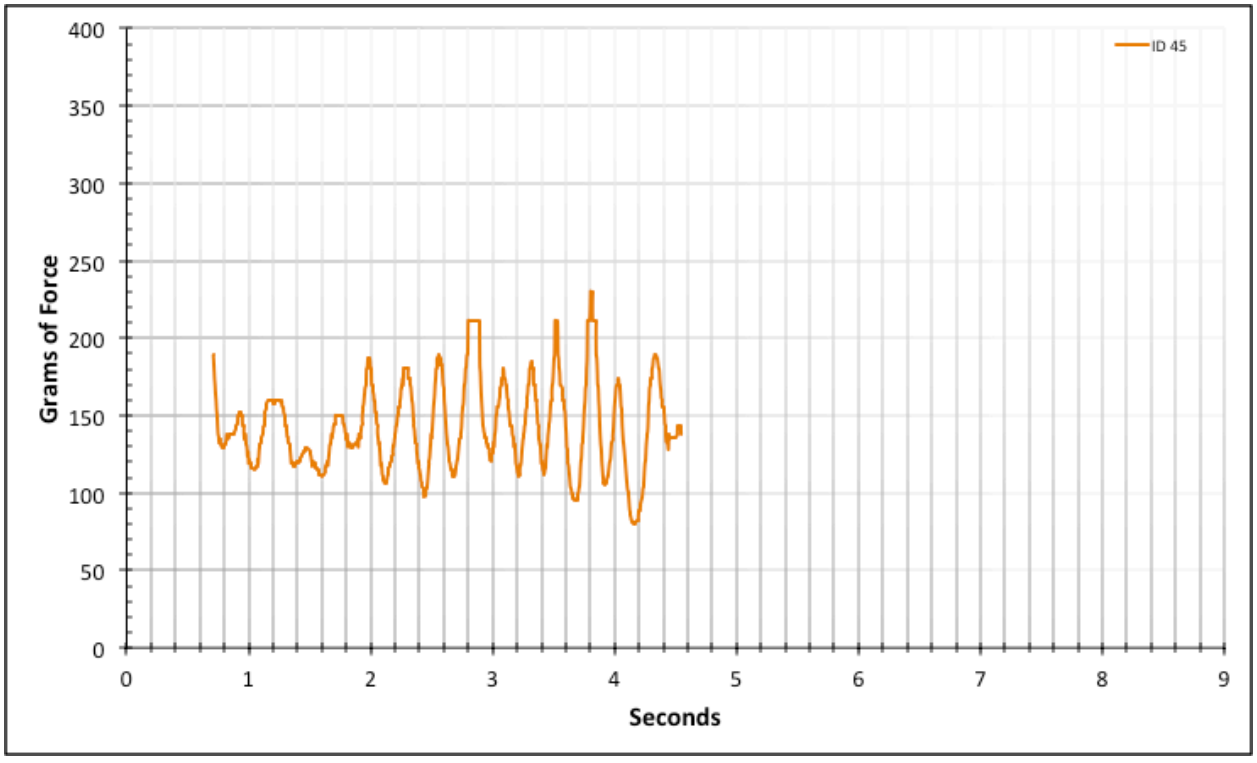

Figure A-6-89: Statistical Region Modeled Product - Dry - ID 45 - #12, Bolt 1

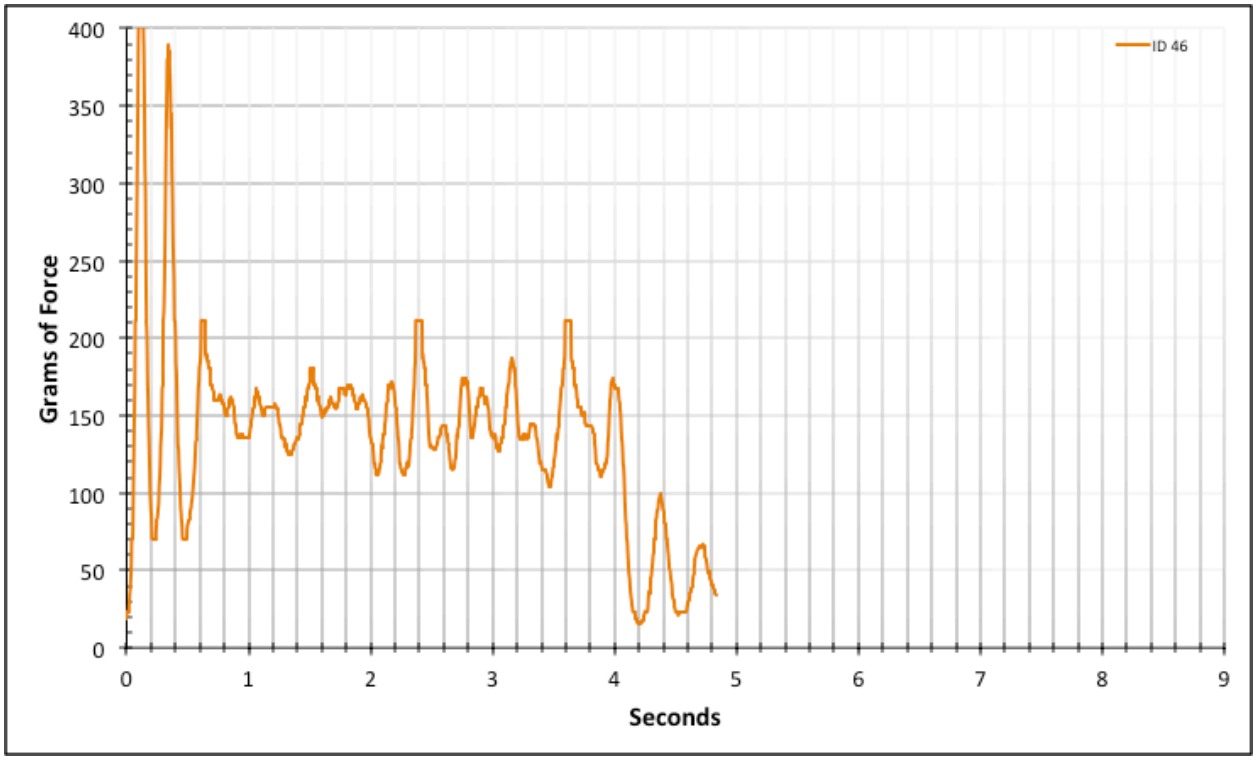

Figure A-6-90: Full Modeled Product - Dry - ID 46 - #12, Bolt 2

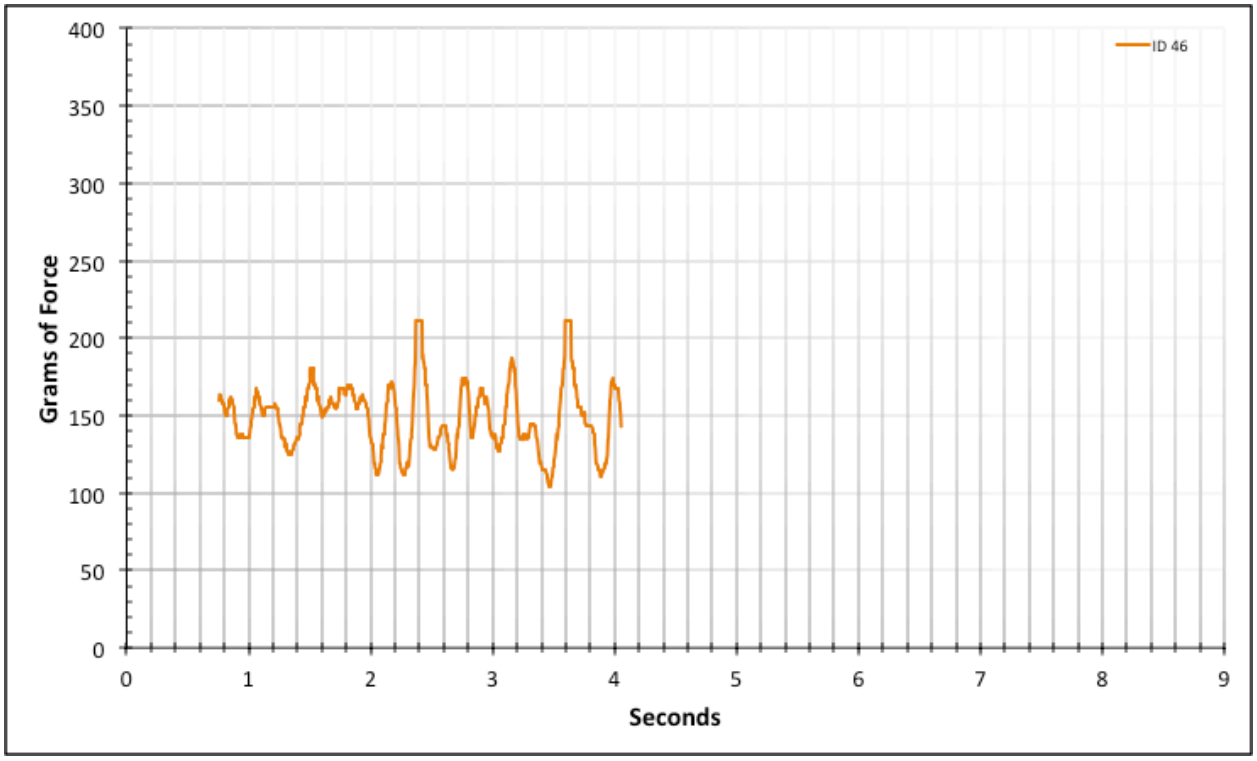

Figure A-6-91: Statistical Region Modeled Product - Dry - ID 46 - #12, Bolt 2

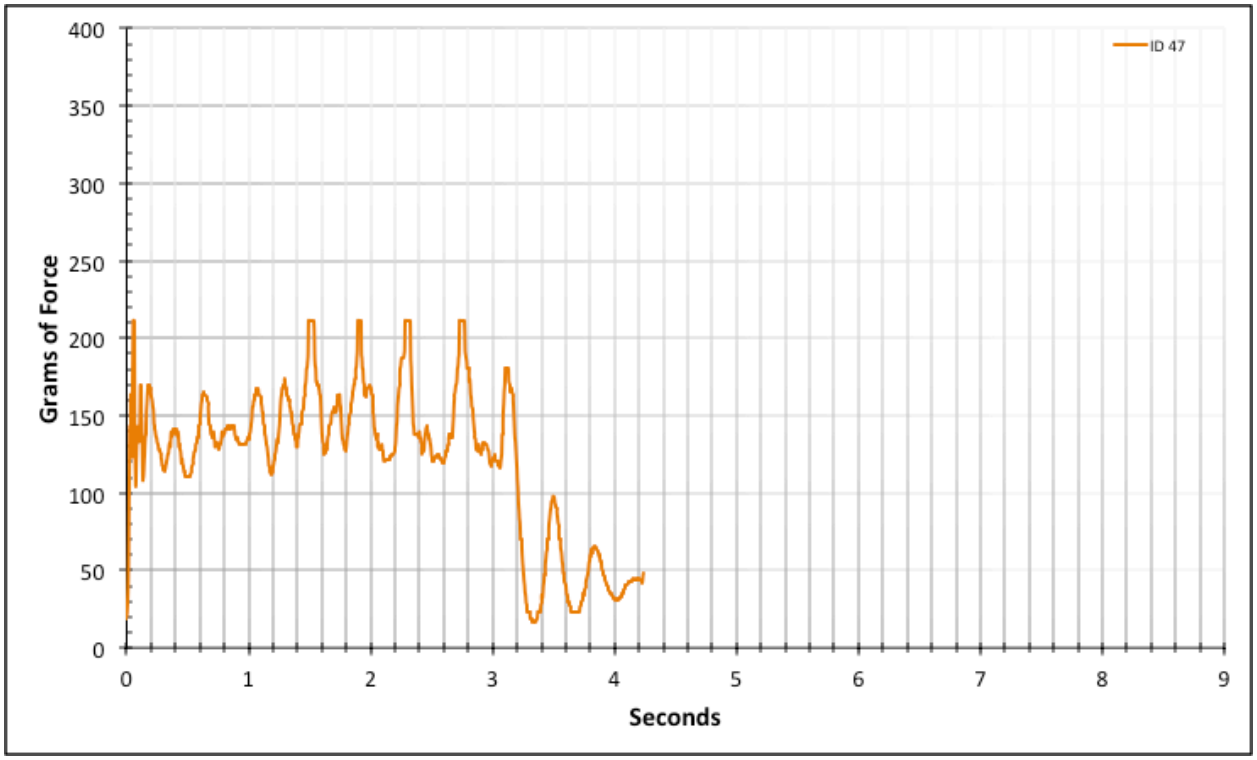

Figure A-6-92: Full Modeled Product - Dry - ID 47 - #12, Bolt 2

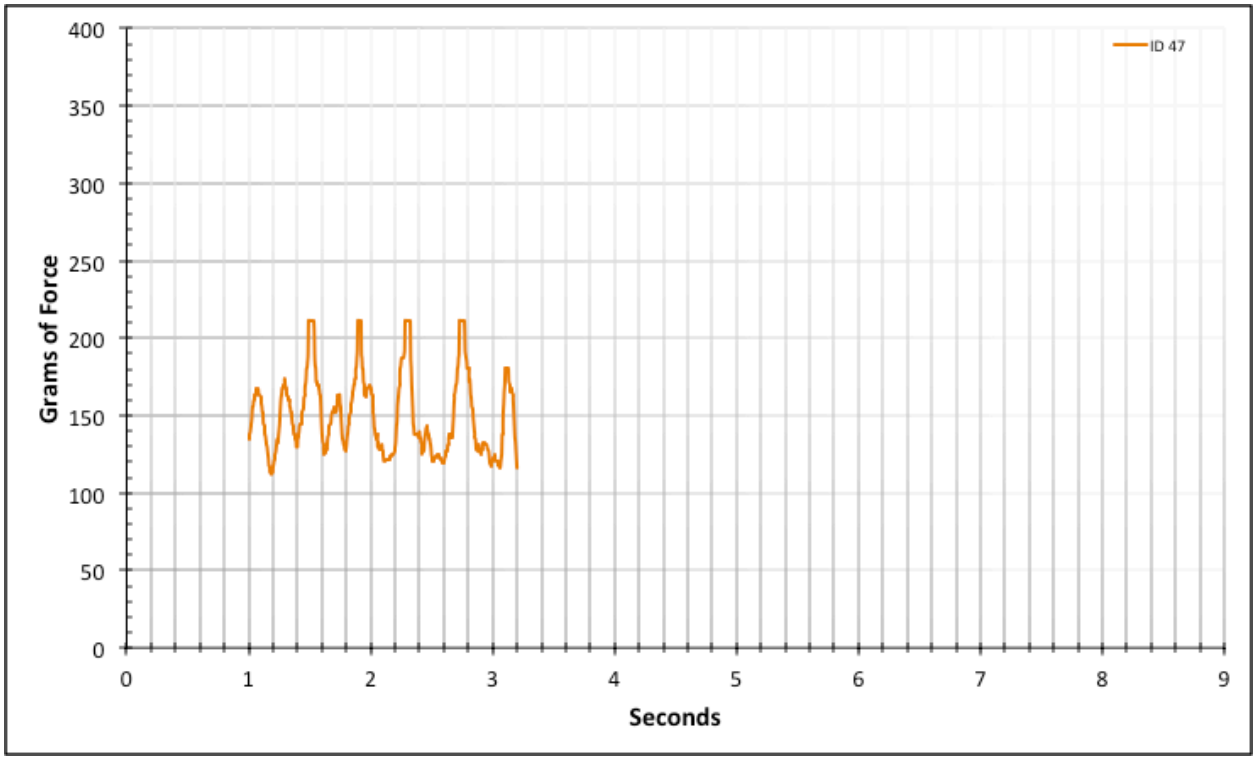

Figure A-6-93: Statistical Region Modeled Product - Dry - ID 47 - #12, Bolt 2

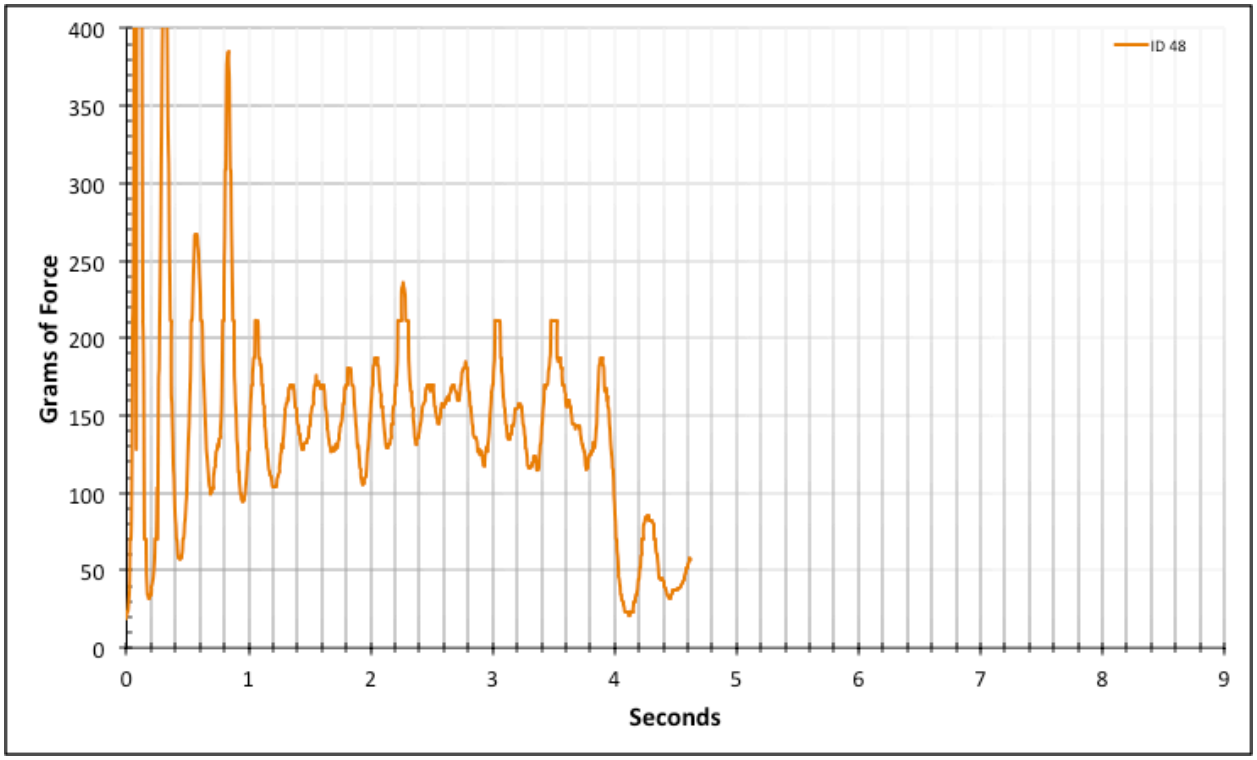

Figure A-6-94: Full Modeled Product - Dry - ID 48 - #12, Bolt 2

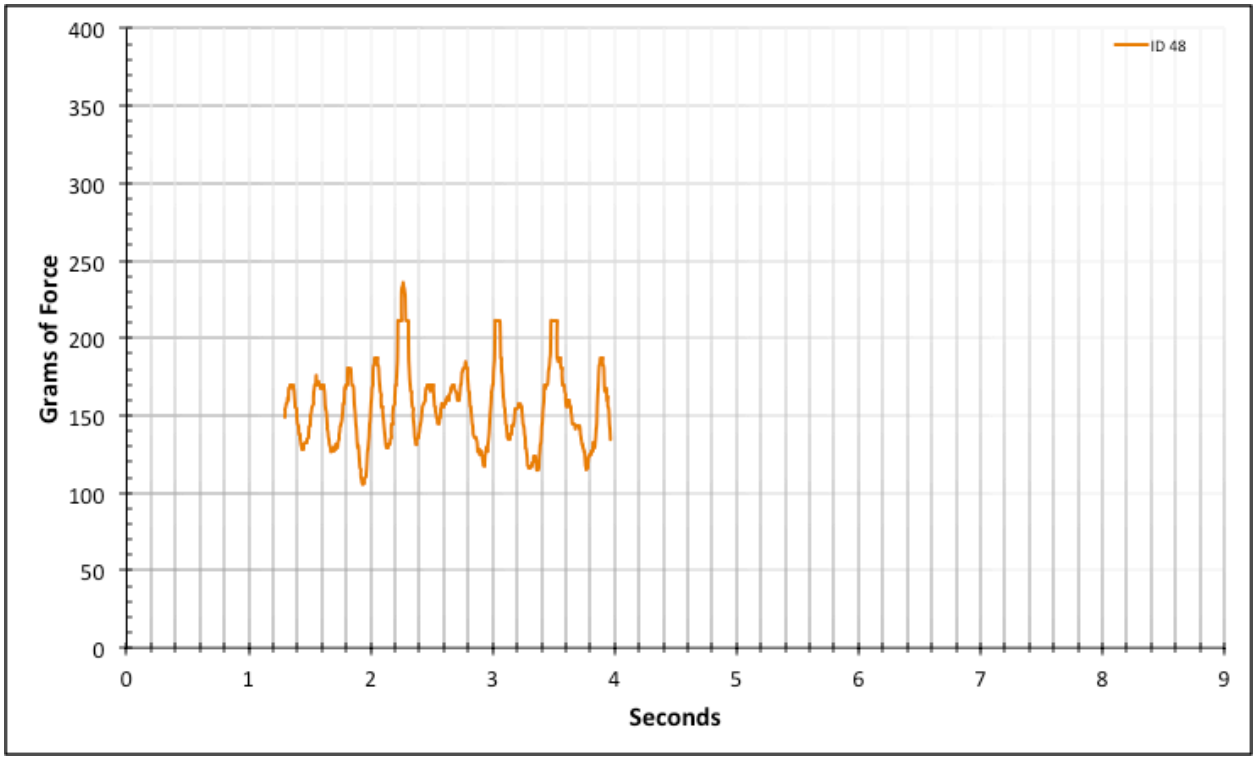

Figure A-6-95: Statistical Region Modeled Product - Dry - ID 48 - #12, Bolt 2

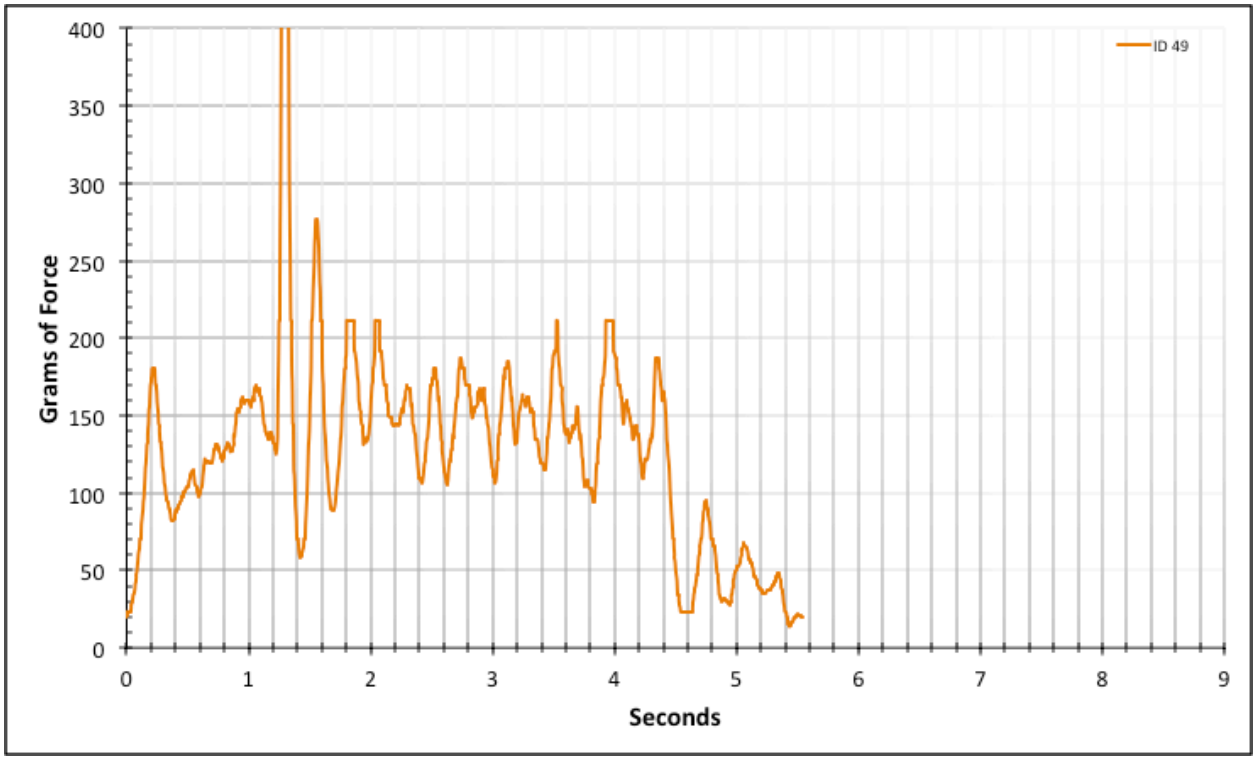

Figure A-6-96: Full Modeled Product - Dry - ID 49 - #12, Bolt 2

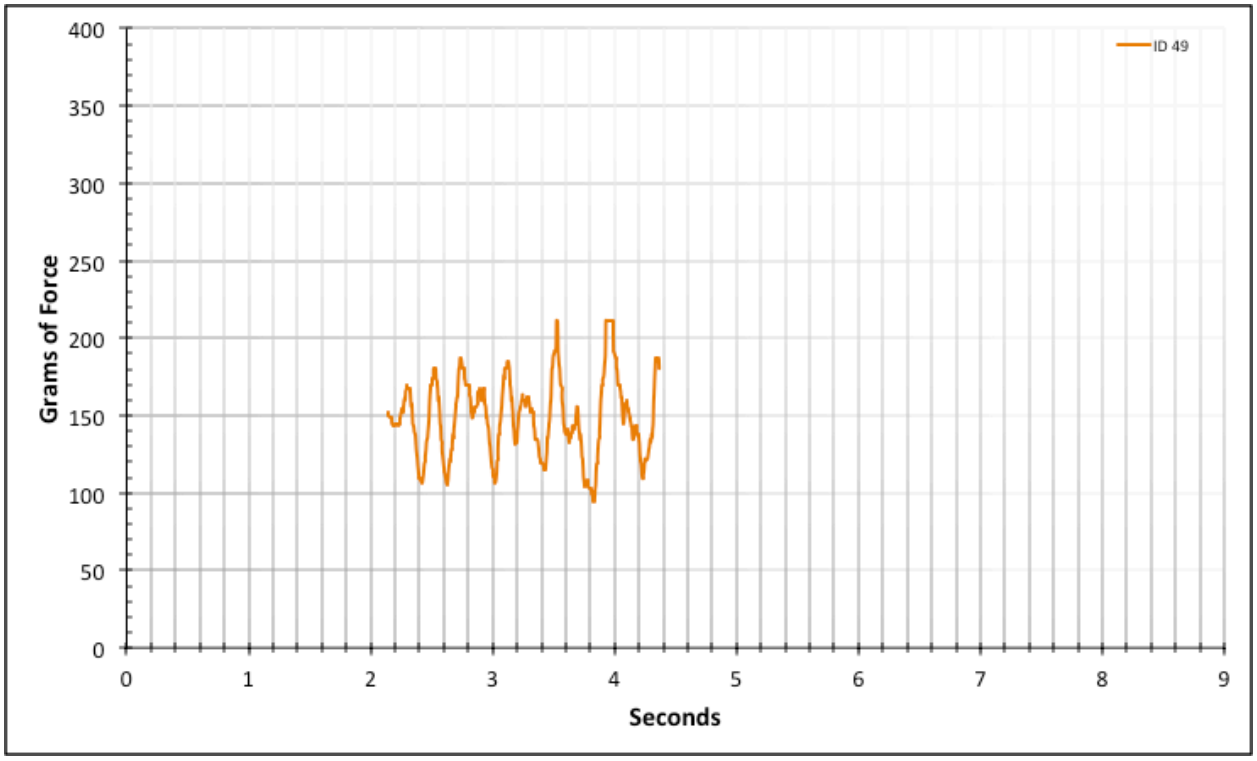

Figure A-6-97: Statistical Region Modeled Product - Dry - ID 49 - #12, Bolt 2

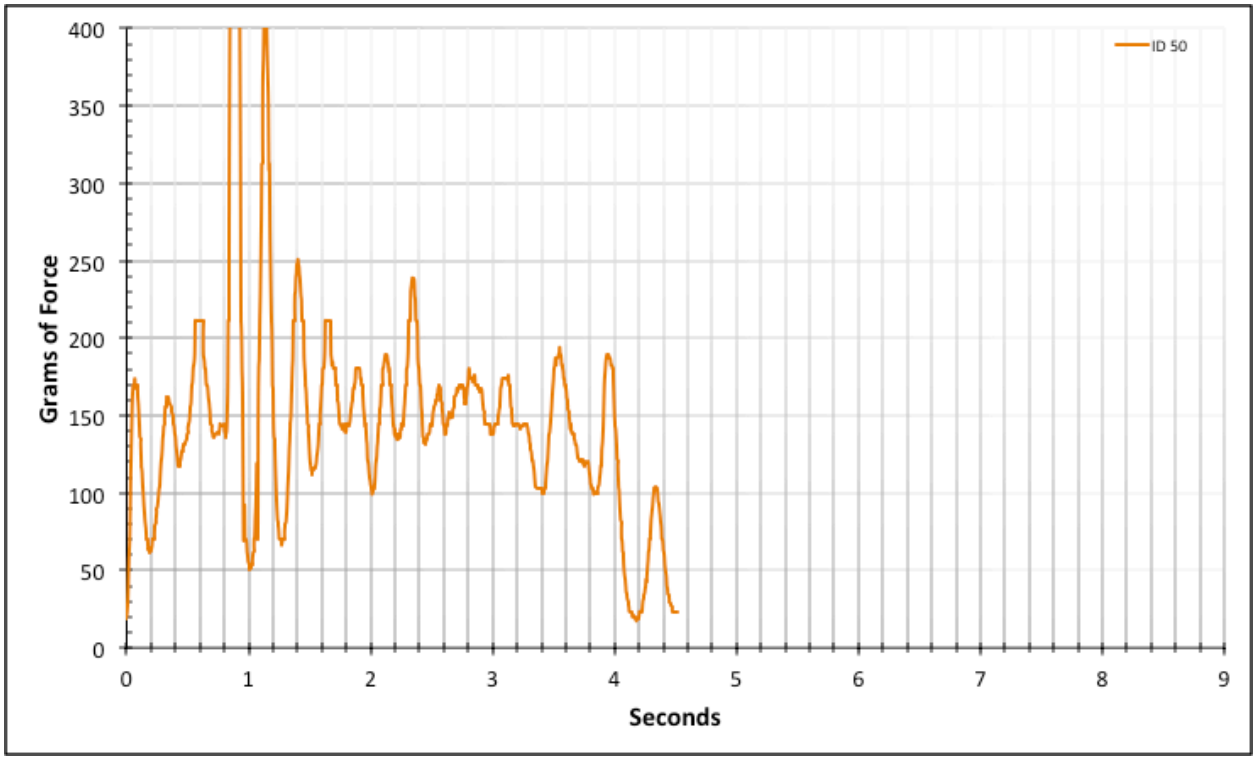

Figure A-6-98: Full Modeled Product - Dry - ID 50 - #12, Bolt 2

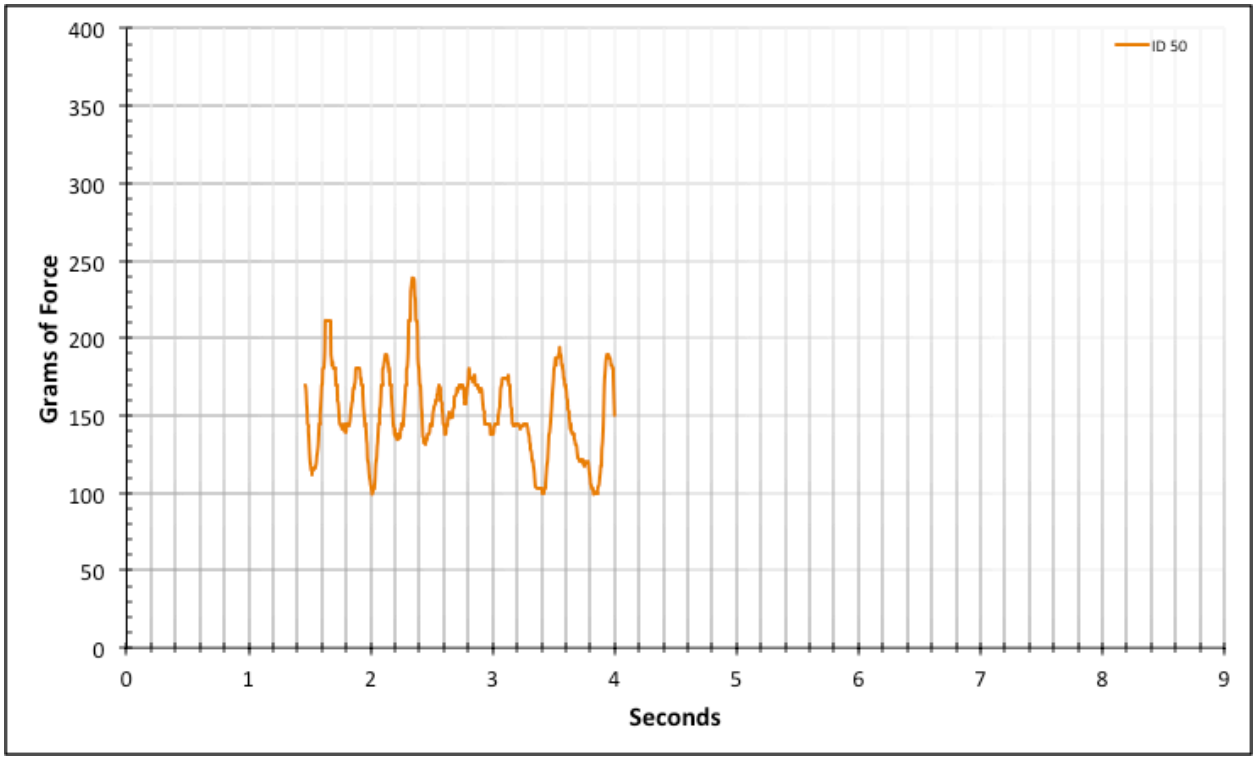

Figure A-6-99: Statistical Region Modeled Product - Dry - ID 50 - #12, Bolt 2

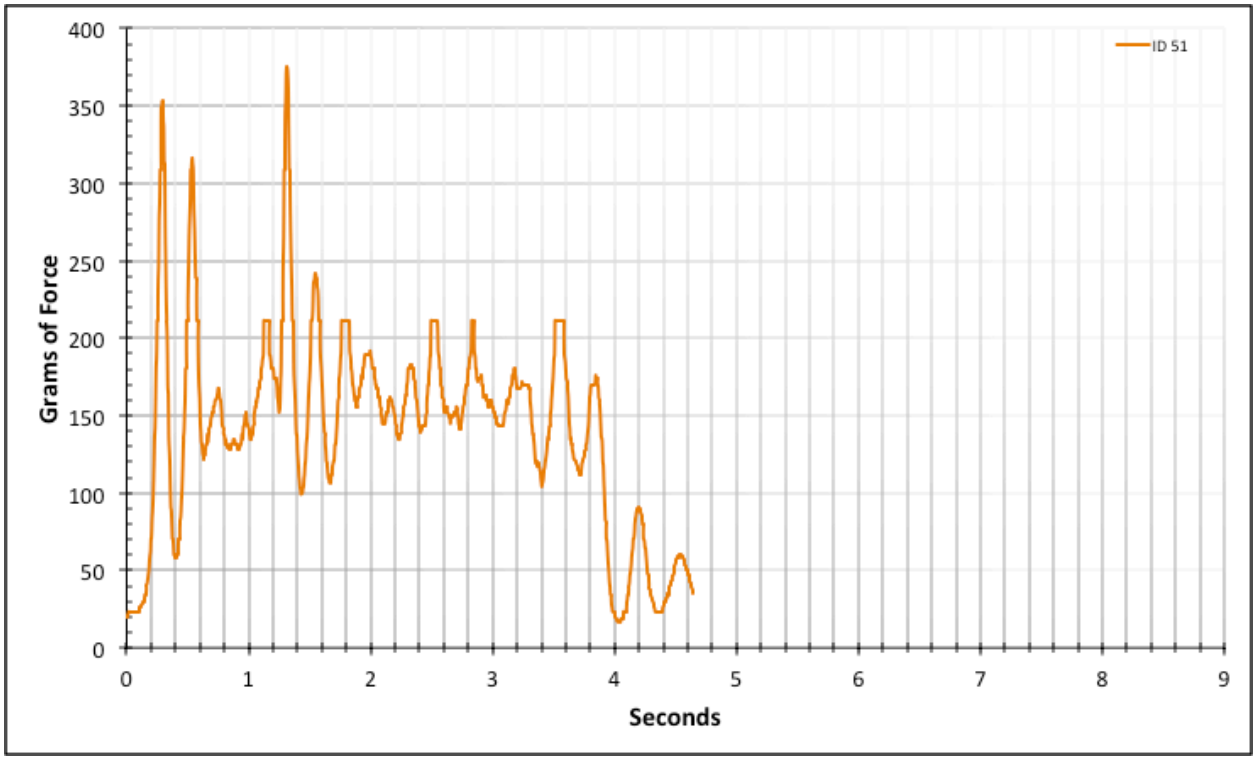

Figure A-6-100: Full Modeled Product - Dry - ID 51 - #12, Bolt 3

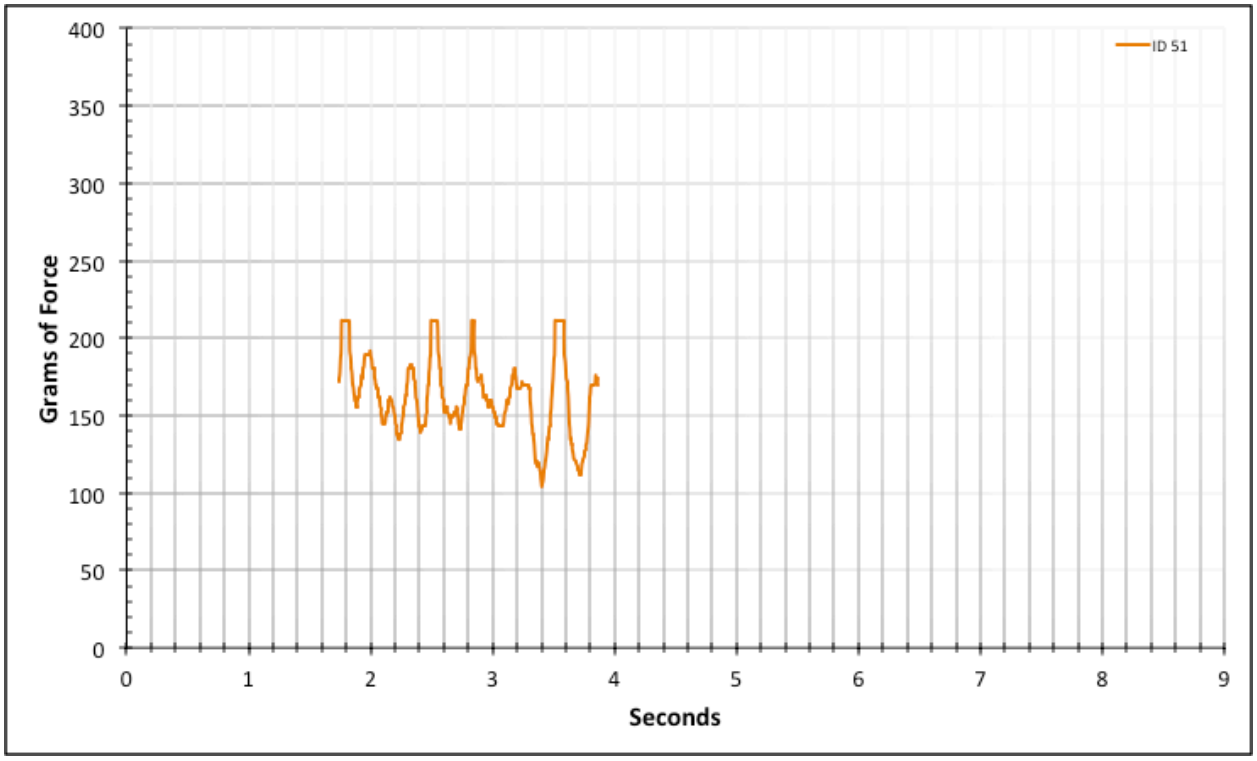

Figure A-6-101: Statistical Region Modeled Product - Dry - ID 51 - #12, Bolt 3

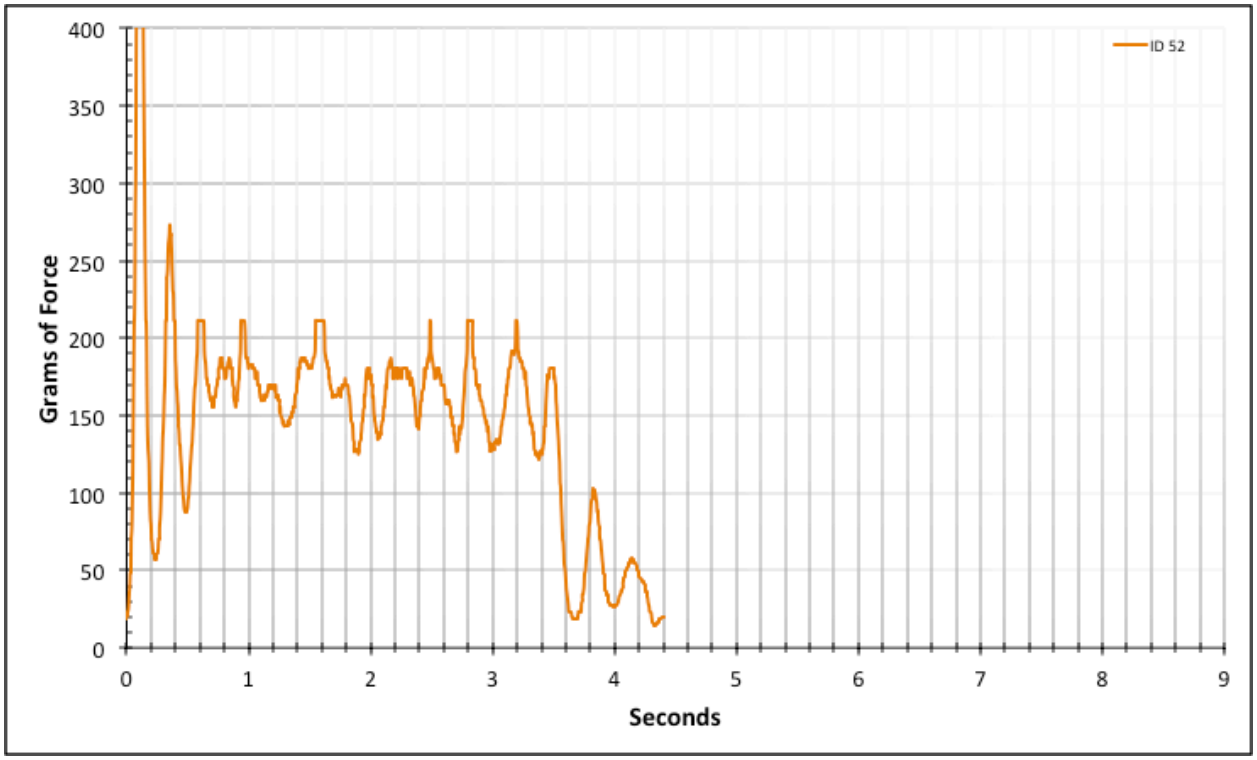

Figure A-6-102: Full Modeled Product - Dry - ID 52 - #12, Bolt 3

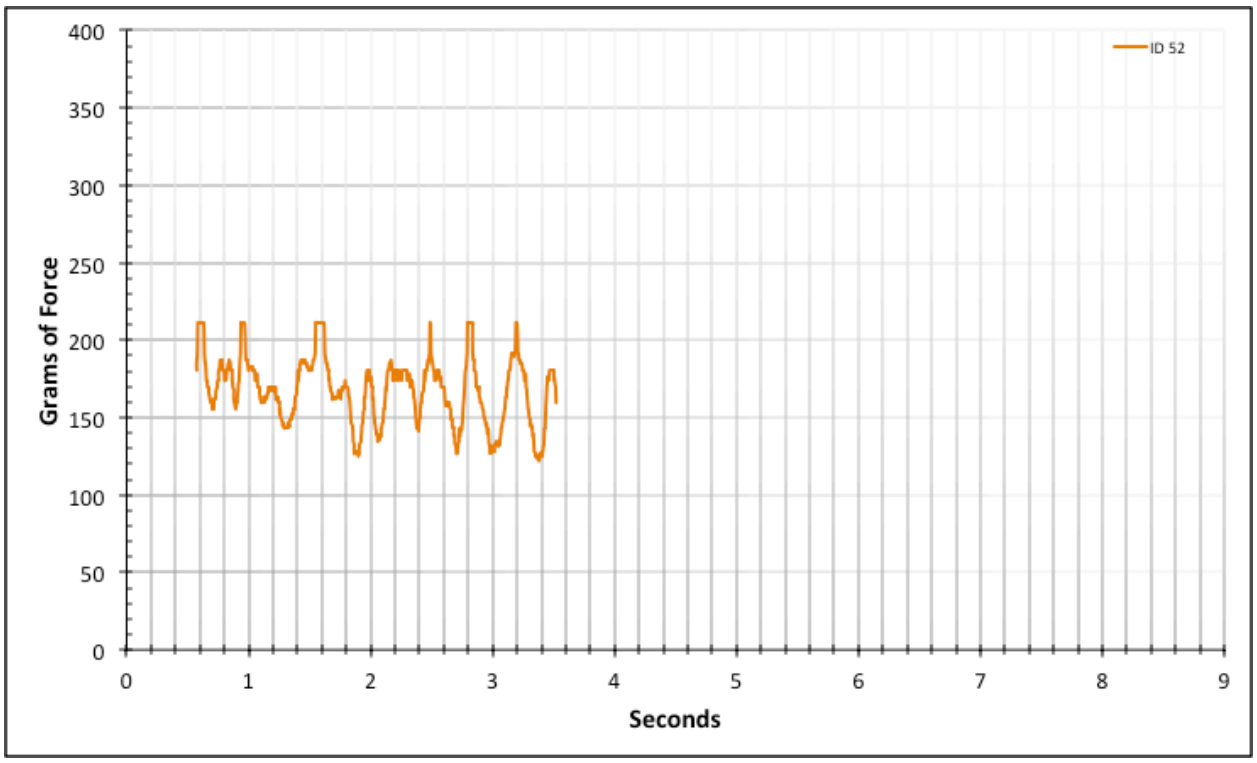

Figure A-6-103: Statistical Region Modeled Product - Dry - ID 52 - #12, Bolt 3

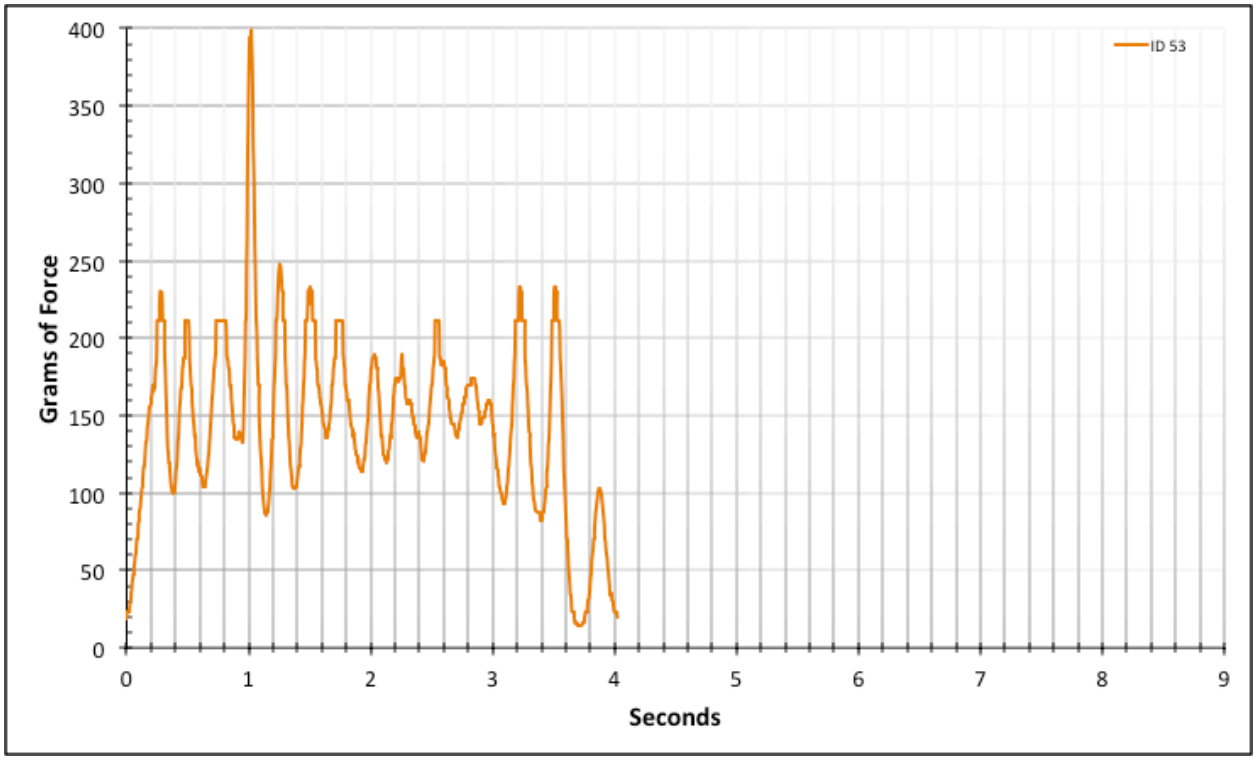

Figure A-6-104: Full Modeled Product - Dry - ID 53 - #12, Bolt 3

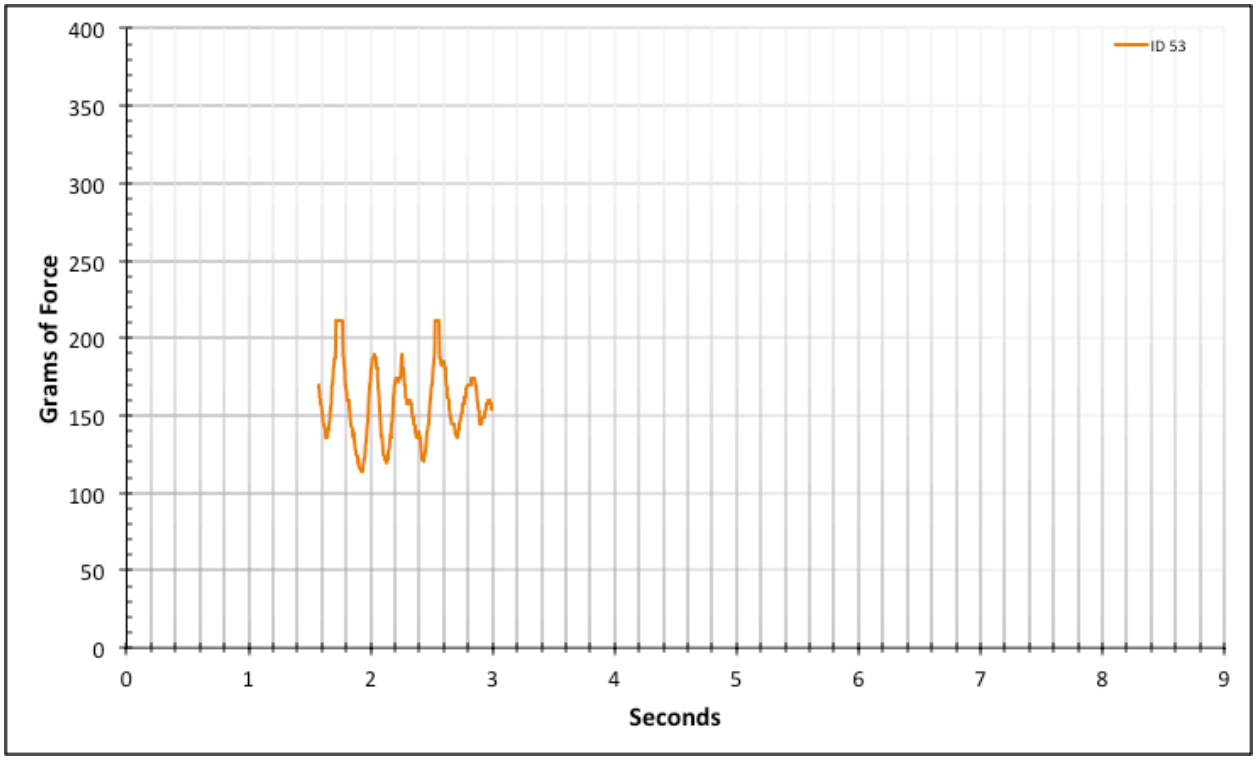

Figure A-6-105: Statistical Region Modeled Product - Dry - ID 53 - #12, Bolt 3

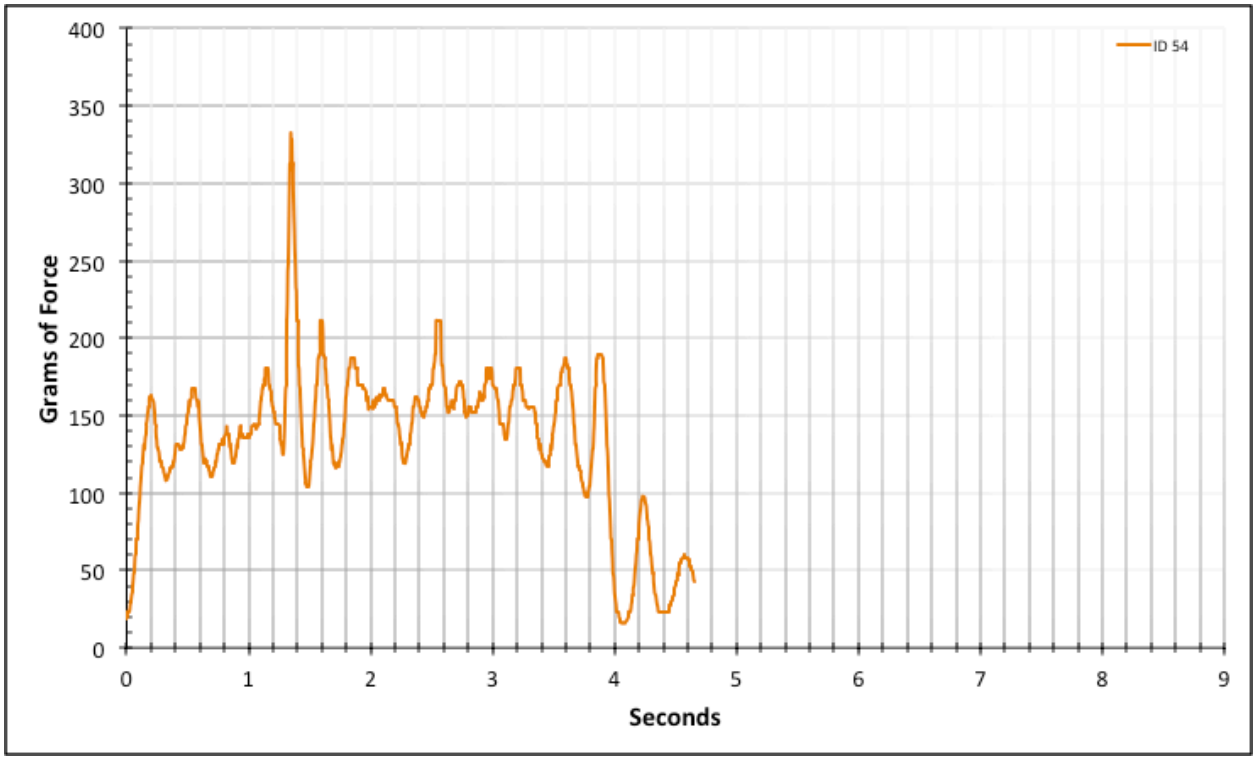

Figure A-6-106: Full Modeled Product - Dry - ID 54 - #12, Bolt 3

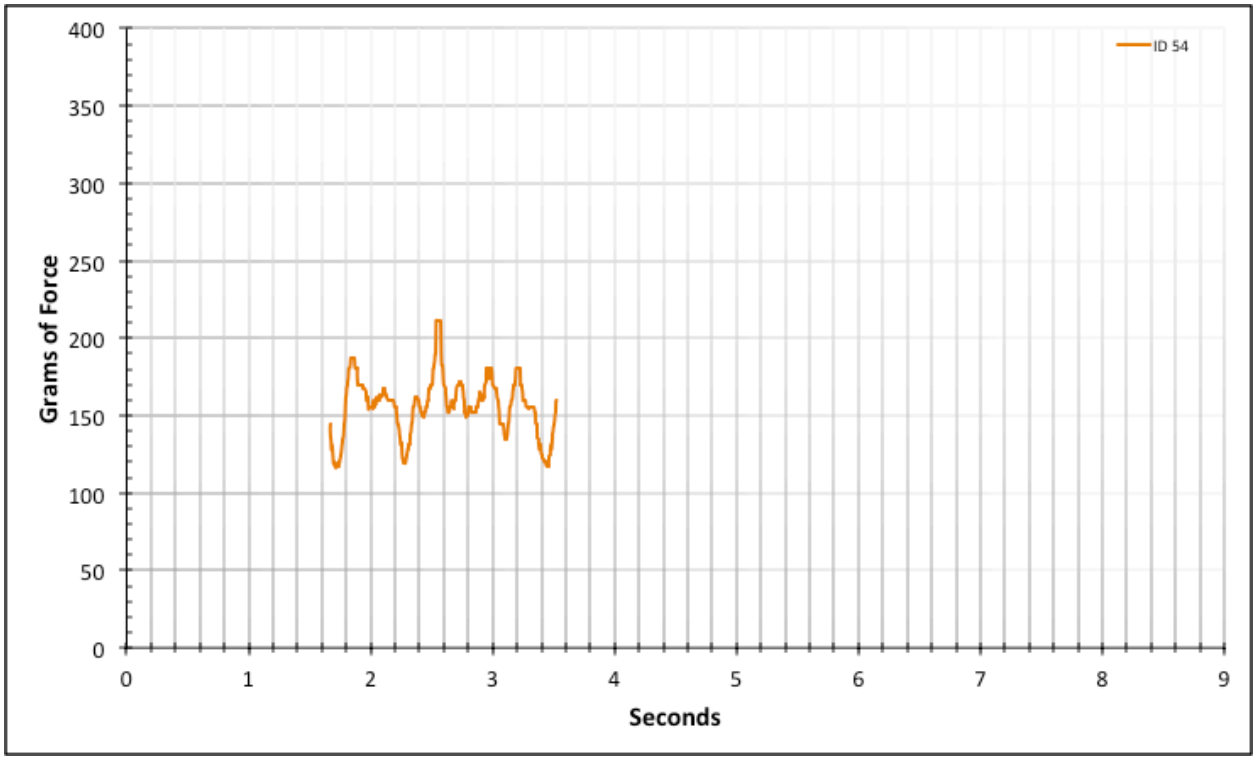

Figure A-6-107: Statistical Region Modeled Product - Dry - ID 54 - #12, Bolt 3

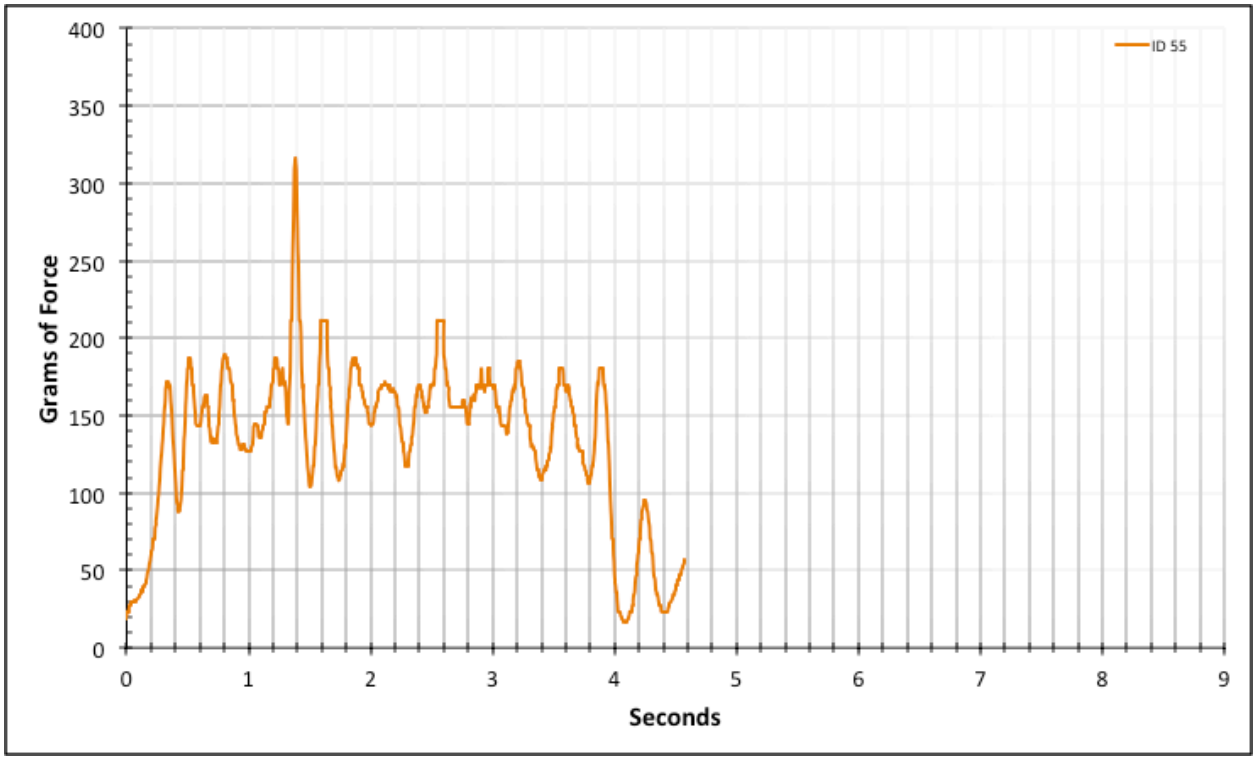

Figure A-6-108: Full Modeled Product - Dry - ID 55 - #12, Bolt 3

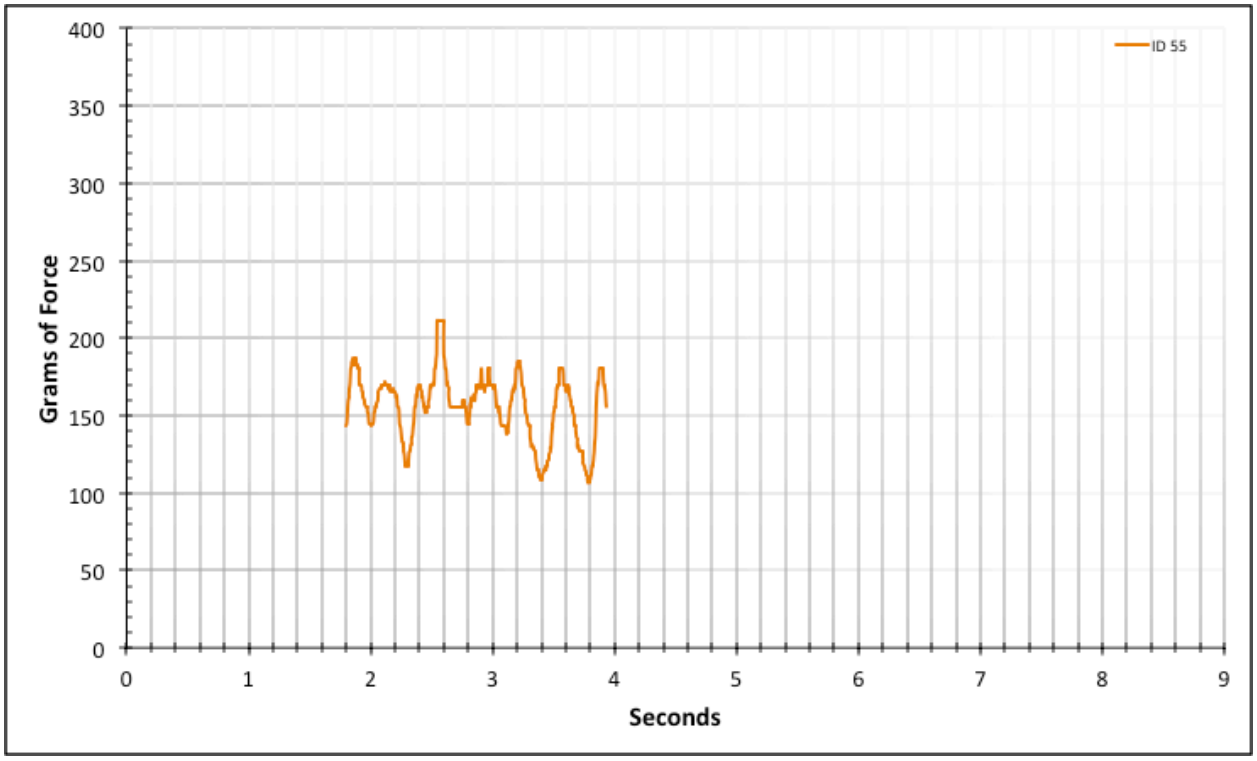

Figure A-6-109: Statistical Region Modeled Product - Dry - ID 55 - #12, Bolt 3

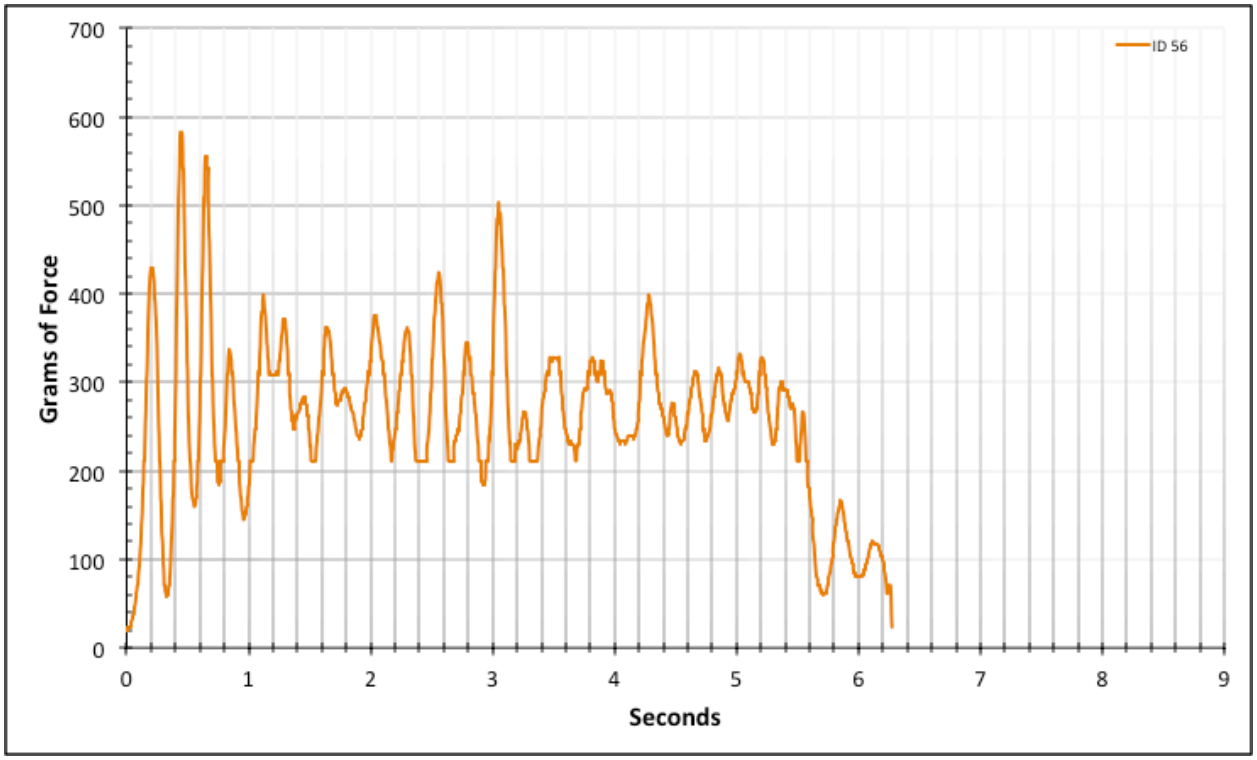

Figure A-6-110: Full Modeled Product - Dry - ID 56 - #10, Bolt 1

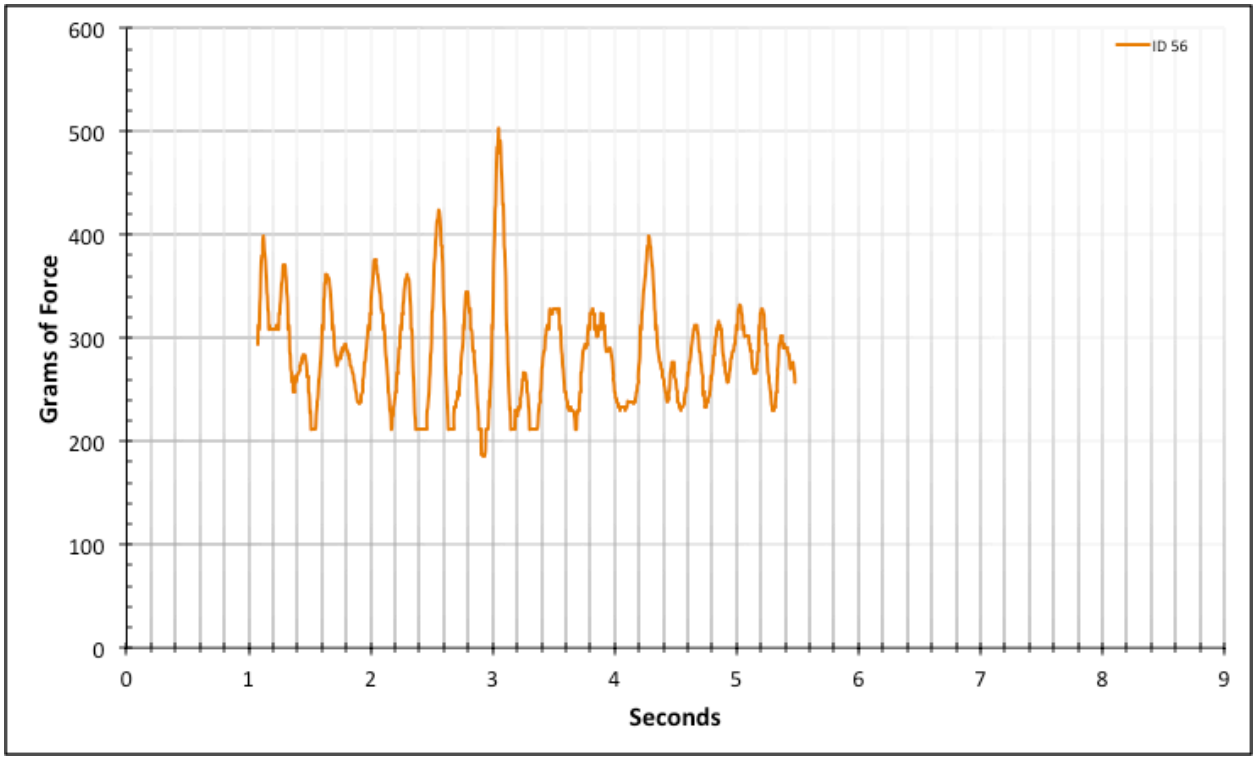

Figure A-6-111: Statistical Region Modeled Product - Dry - ID 56 - #10, Bolt 1

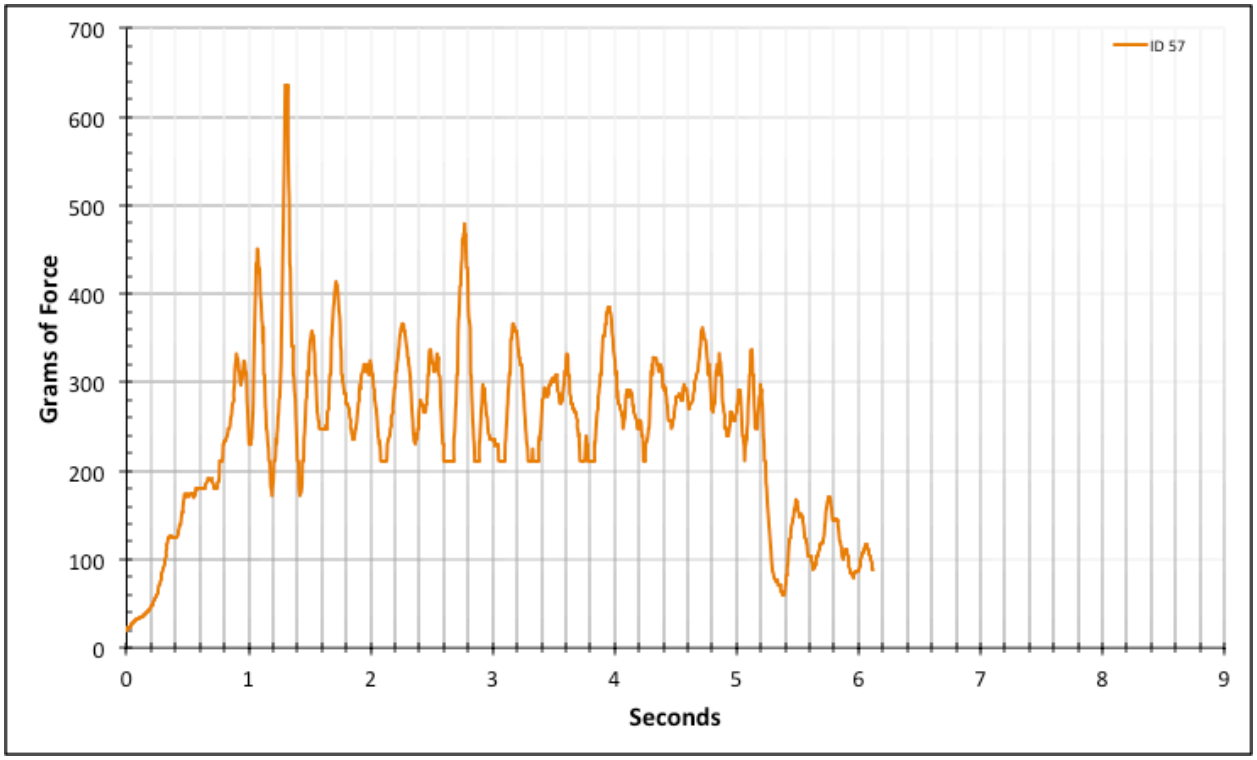

Figure A-6-112: Full Modeled Product - Dry - ID 57 - #10, Bolt 1

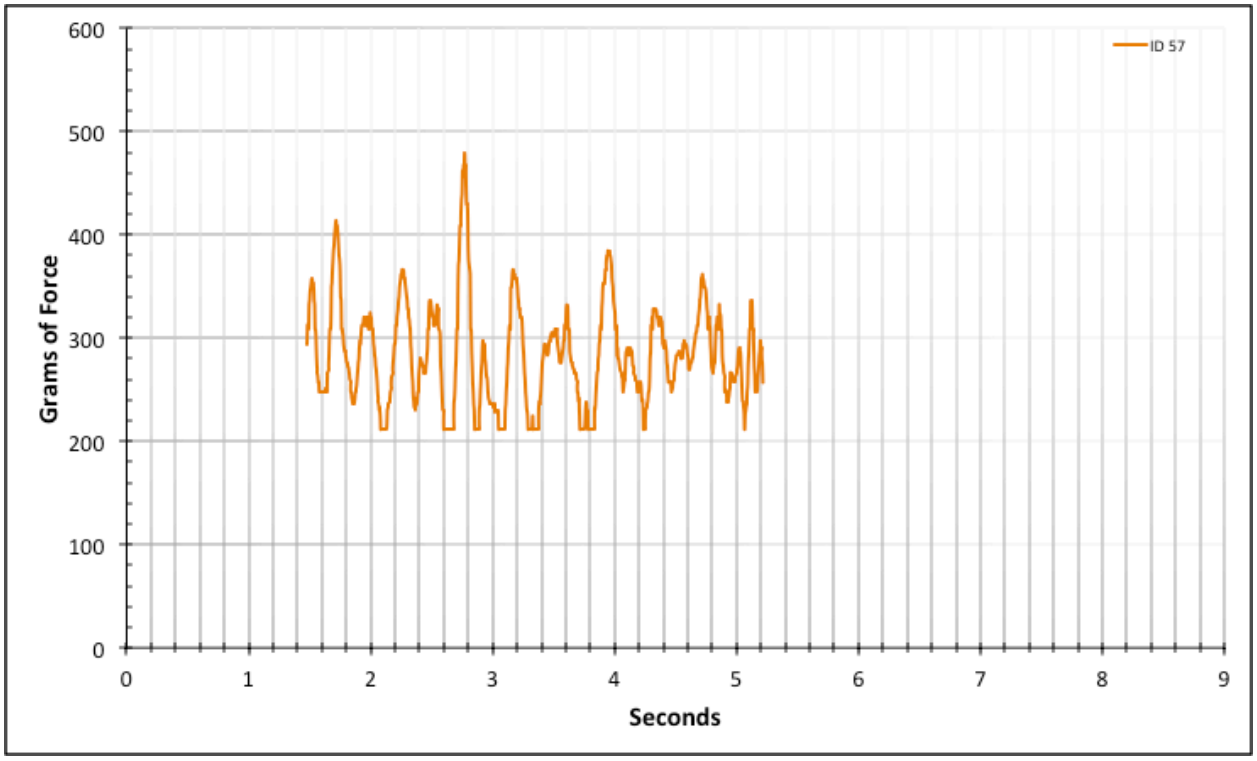

Figure A-6-113: Statistical Region Modeled Product - Dry - ID 57 - #10, Bolt 1

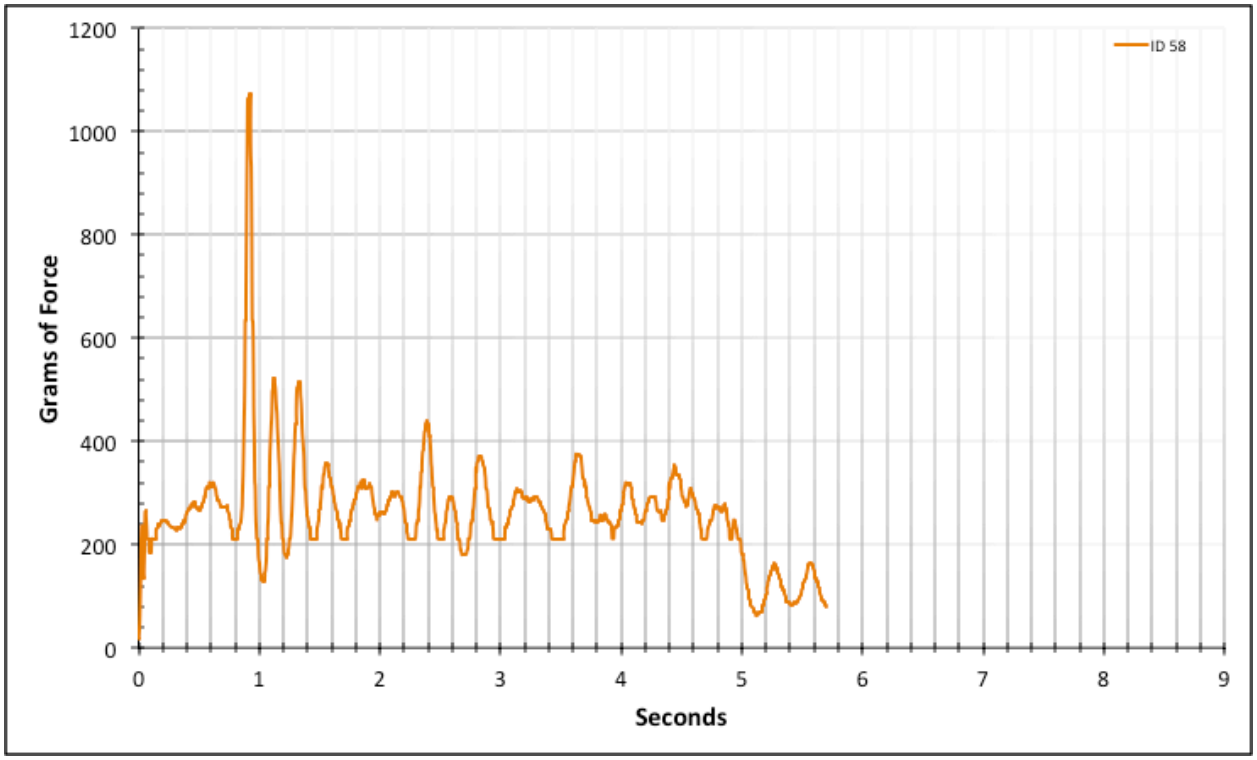

Figure A-6-114: Full Modeled Product - Dry - ID 58 - #10, Bolt 1

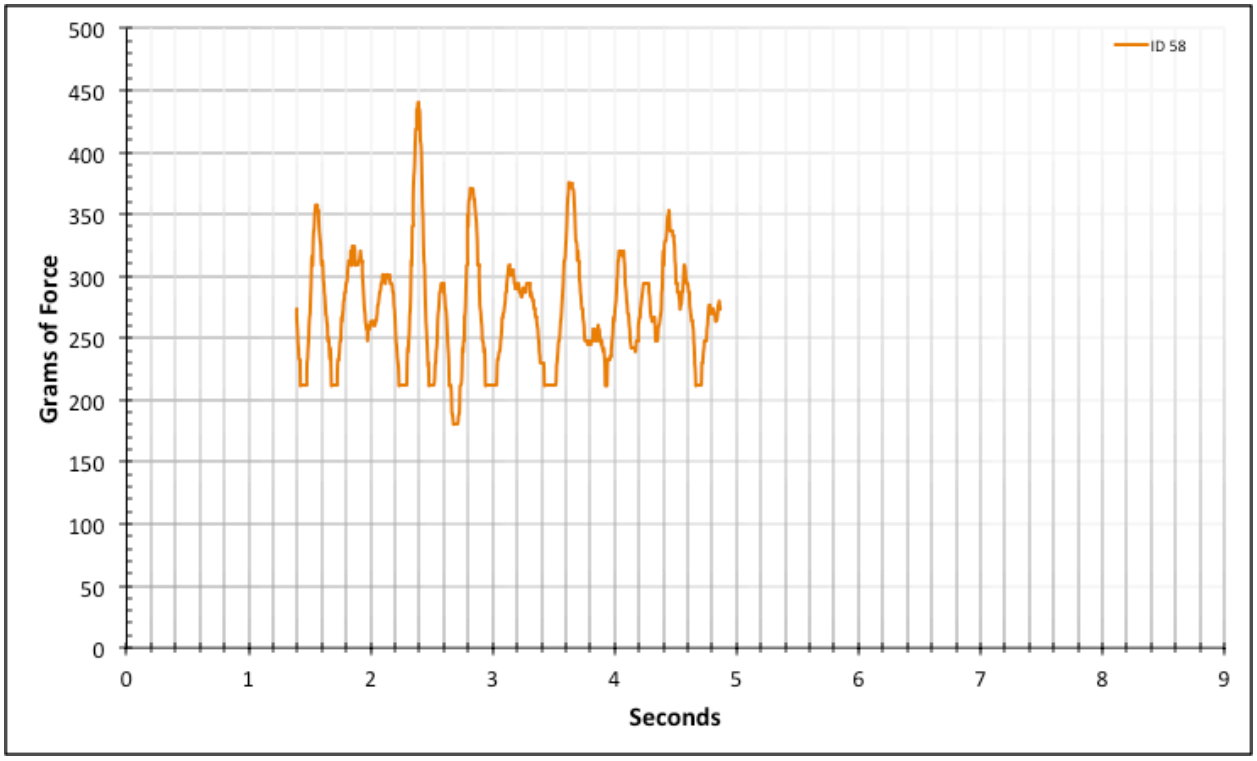

Figure A-6-115: Statistical Region Modeled Product - Dry - ID 58 - #10, Bolt 1

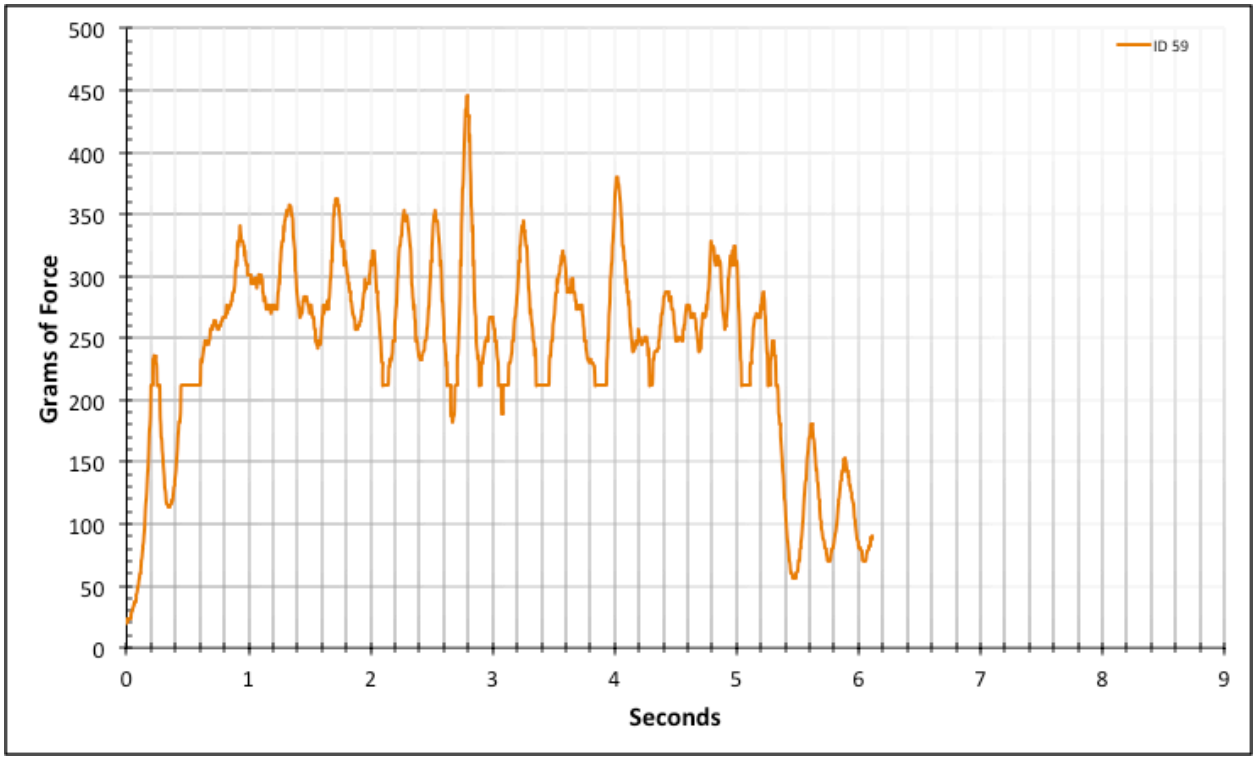

Figure A-6-116: Full Modeled Product - Dry - ID 59 - #10, Bolt 1

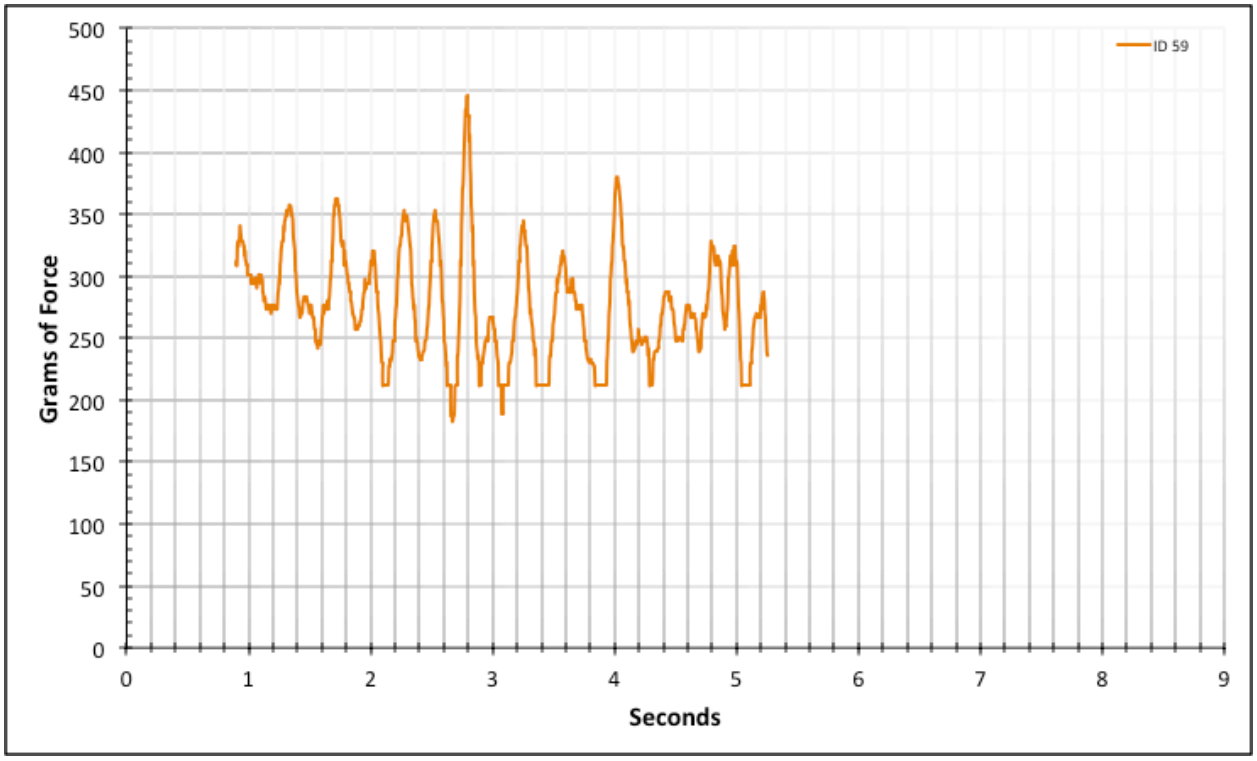

Figure A-6-117: Statistical Region Modeled Product - Dry - ID 59 - #10, Bolt 1

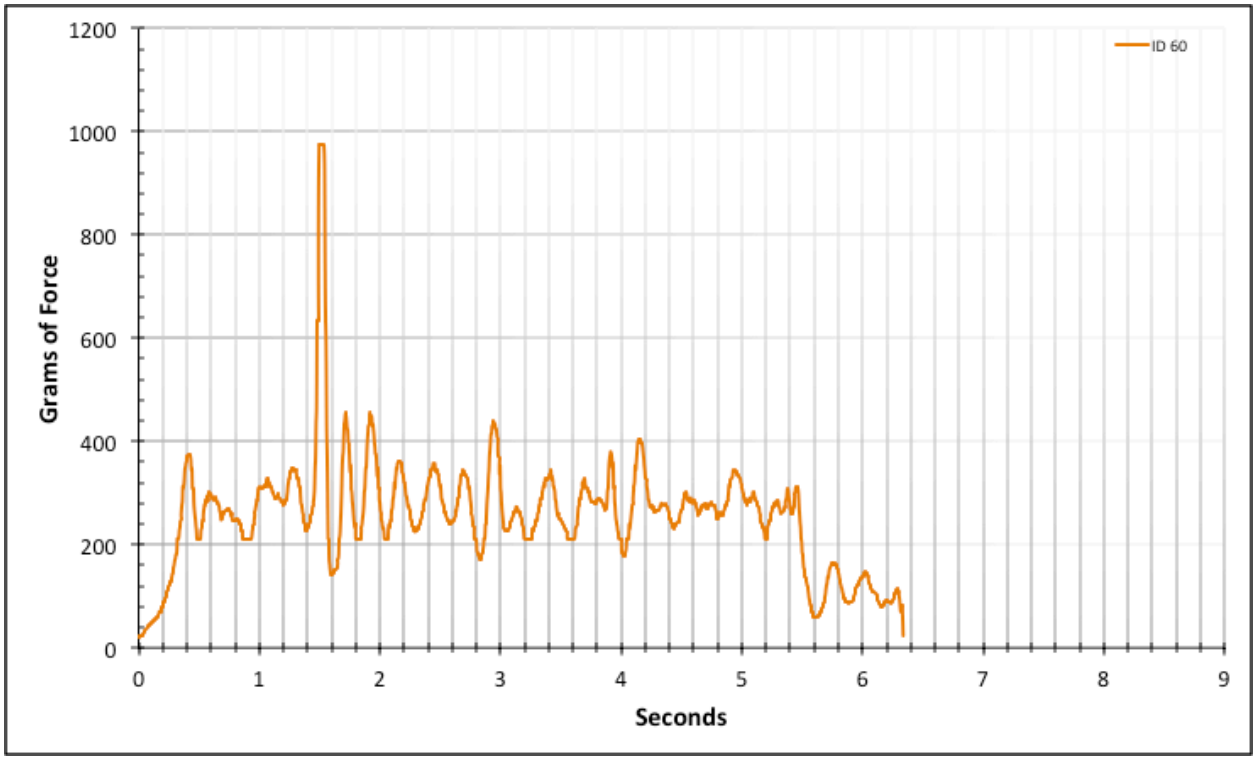

Figure A-6-118: Full Modeled Product - Dry - ID 60 - #10, Bolt 1

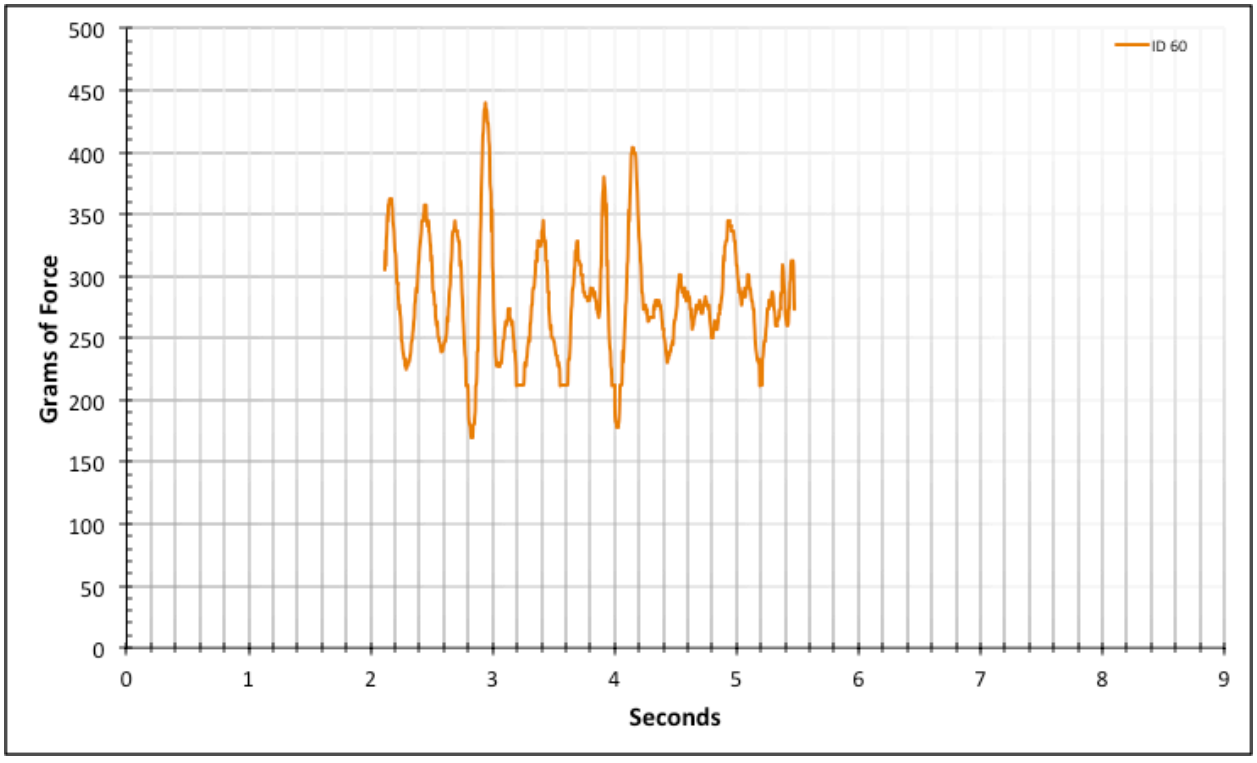

Figure A-6-119: Statistical Region Modeled Product - Dry - ID 60 - #10, Bolt 1

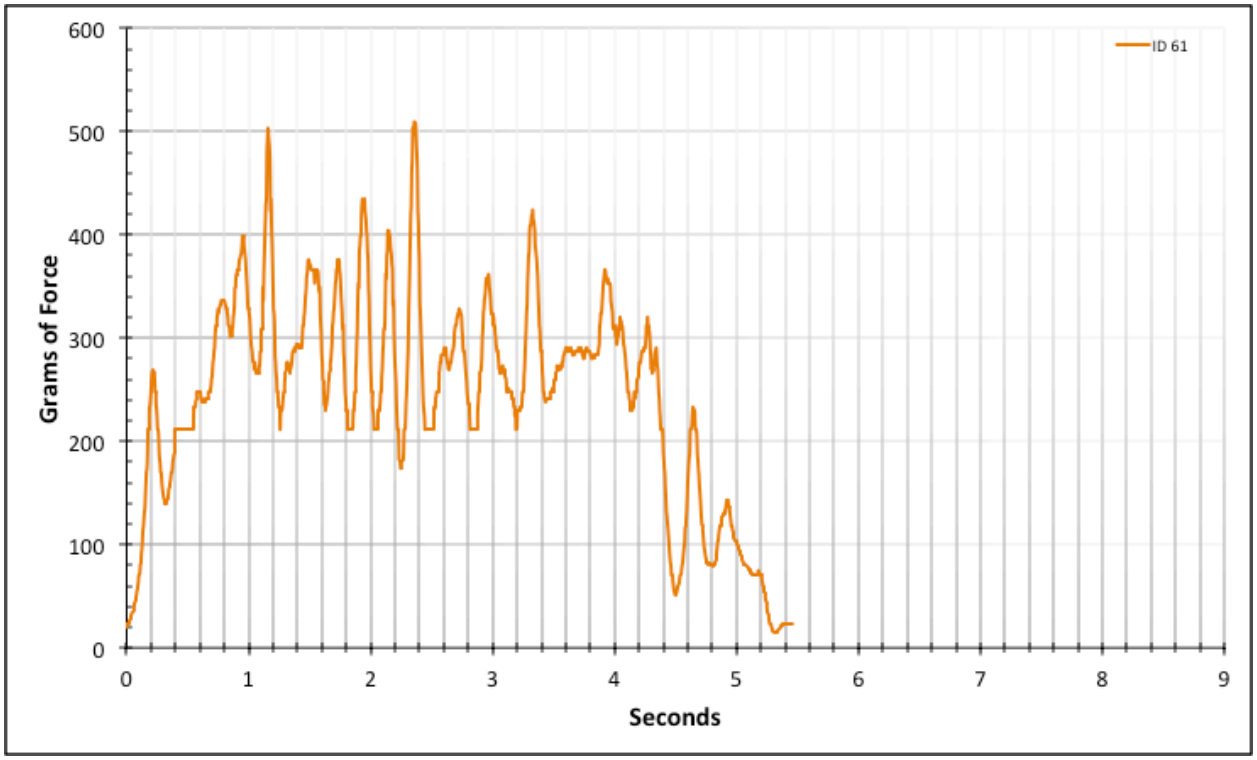

Figure A-6-120: Full Modeled Product - Dry - ID 61 - #10, Bolt 2

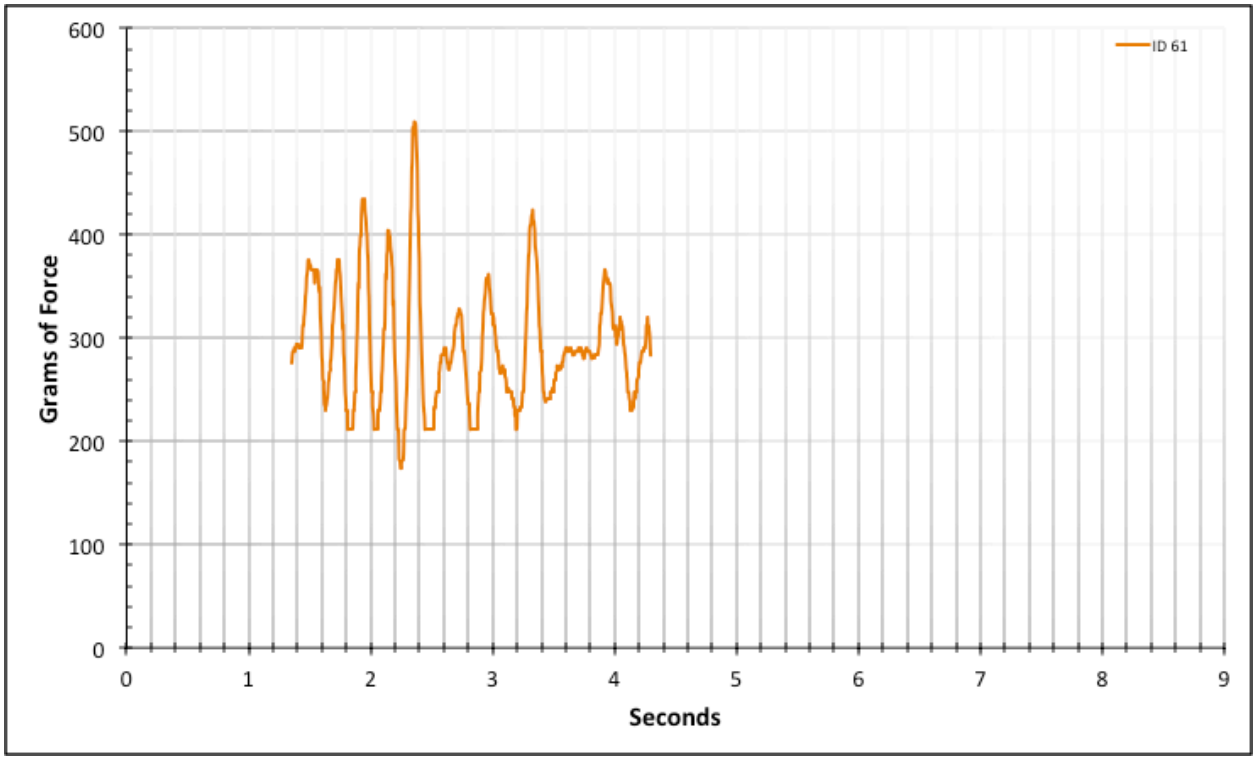

Figure A-6-121: Statistical Region Modeled Product - Dry - ID 61 - #10, Bolt 2

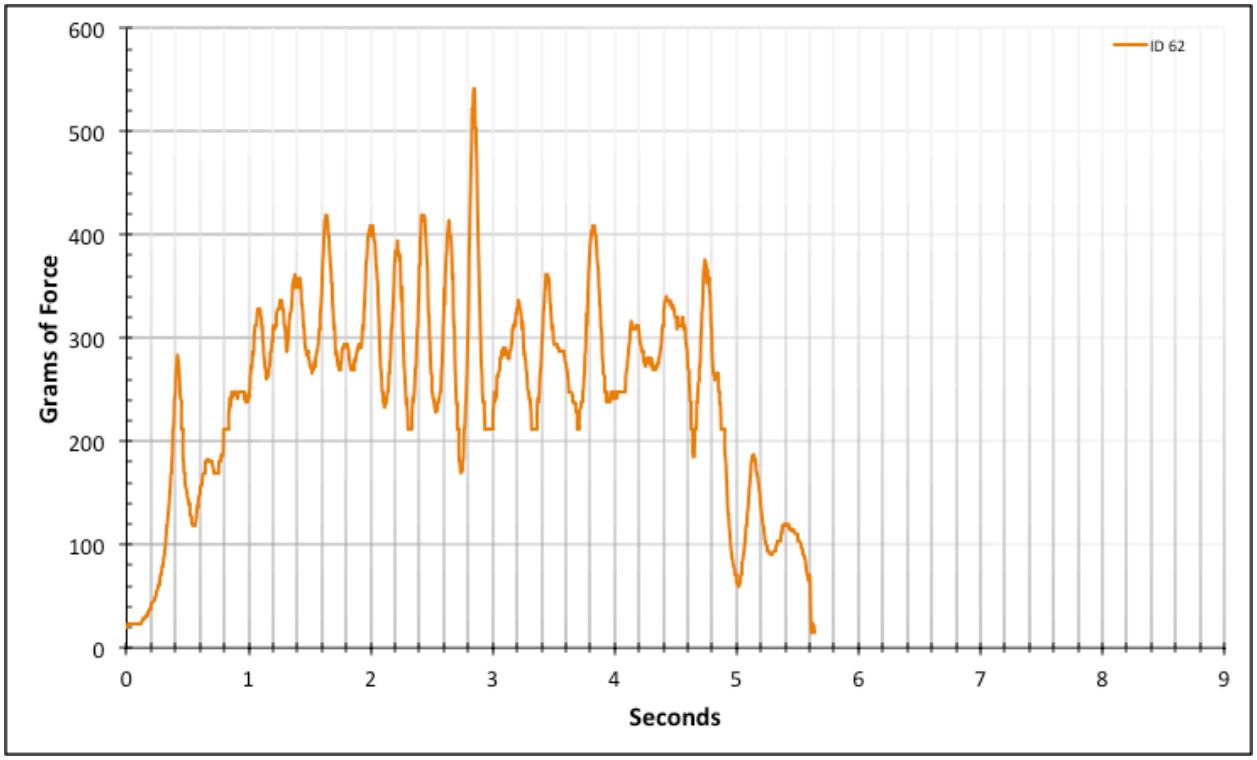

Figure A-6-122: Full Modeled Product - Dry - ID 62 - #10, Bolt 2

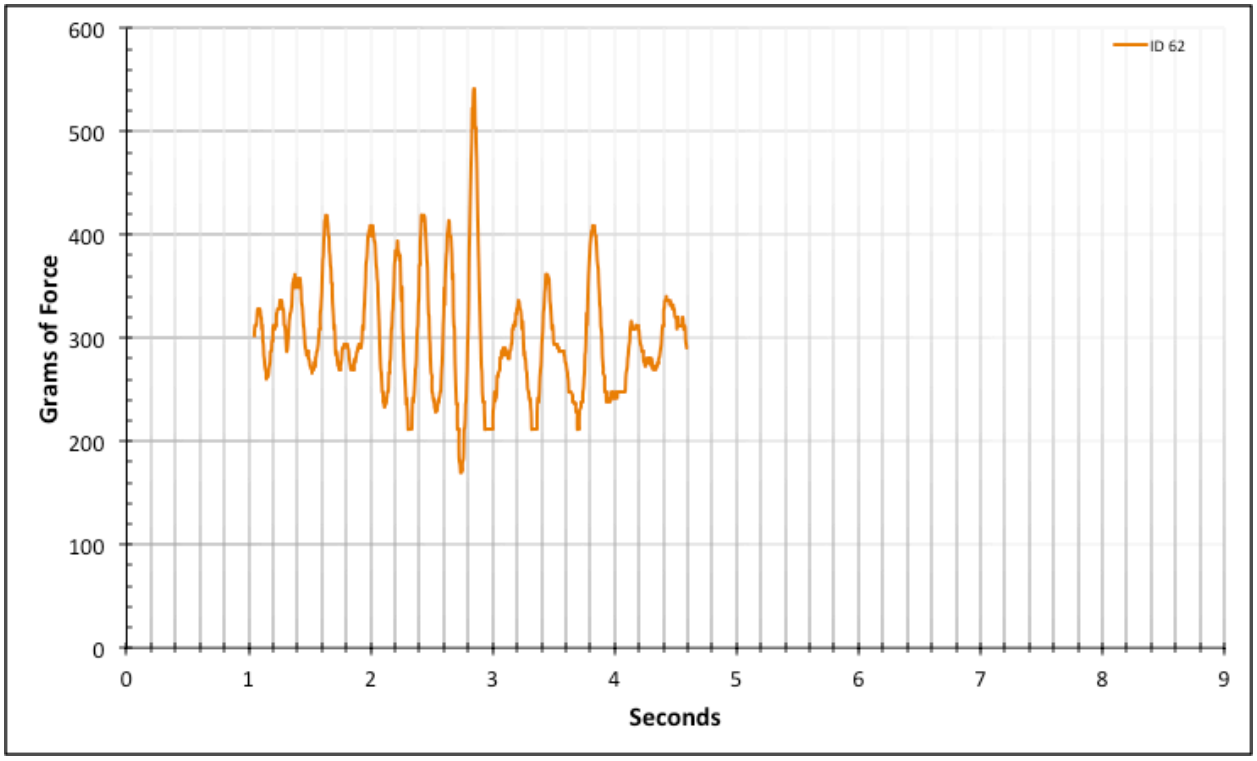

Figure A-6-123: Statistical Region Modeled Product - Dry - ID 62 - #10, Bolt 2

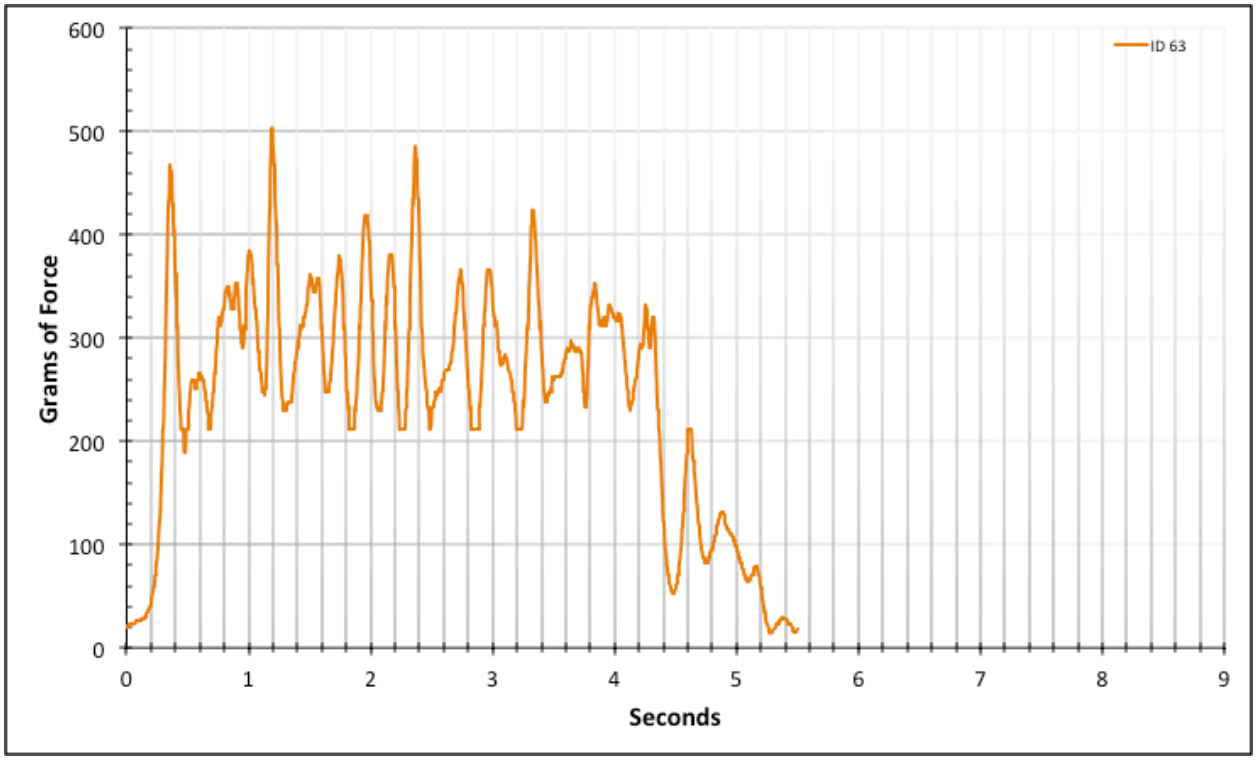

Figure A-6-124: Full Modeled Product - Dry - ID 63 - #10, Bolt 2

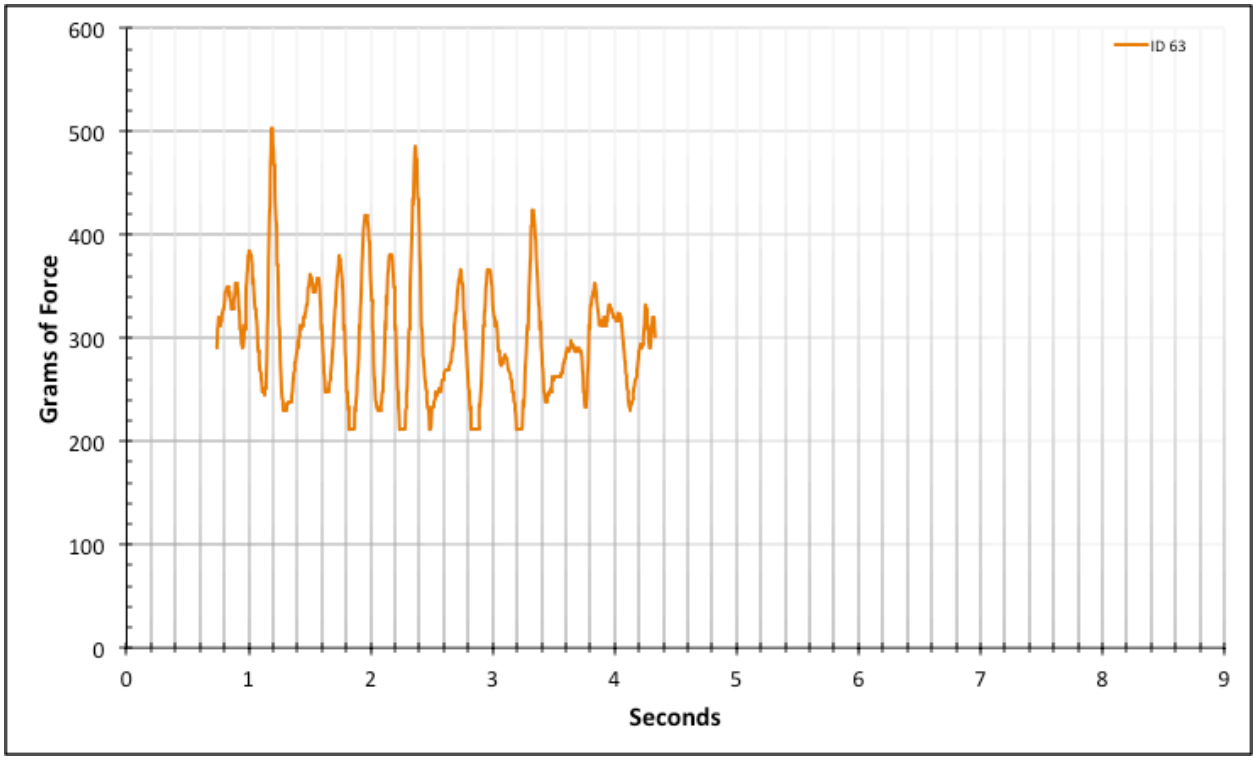

Figure A-6-125: Statistical Region Modeled Product - Dry - ID 63 - #10, Bolt 2

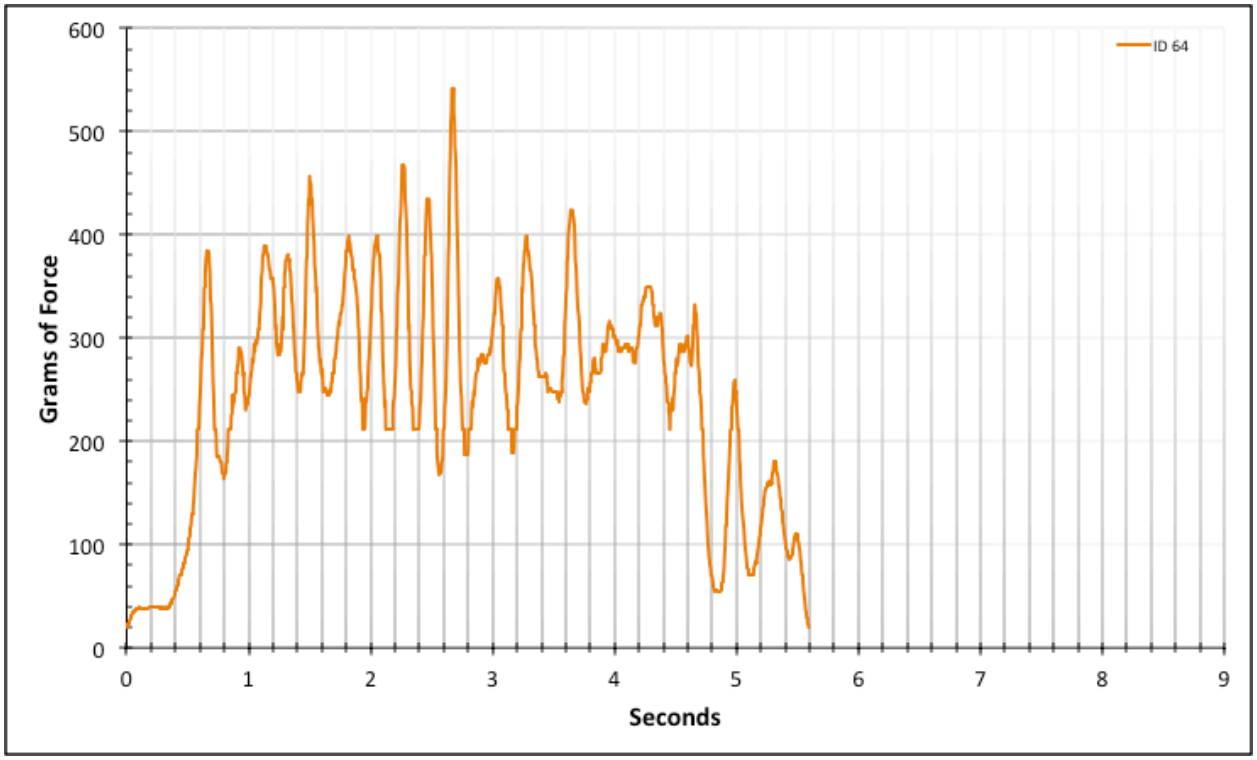

Figure A-6-126: Full Modeled Product - Dry - ID 64 - #10, Bolt 2

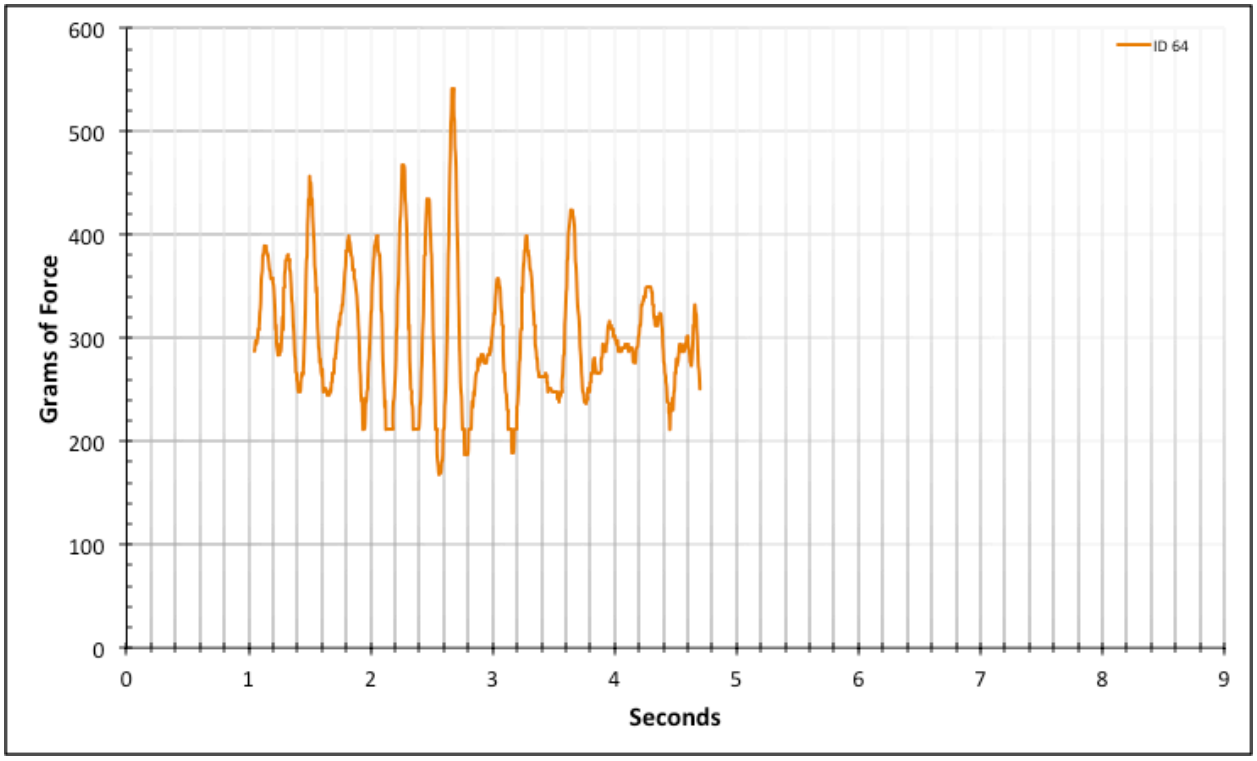

Figure A-6-127: Statistical Region Modeled Product - Dry - ID 64 - #10, Bolt 2

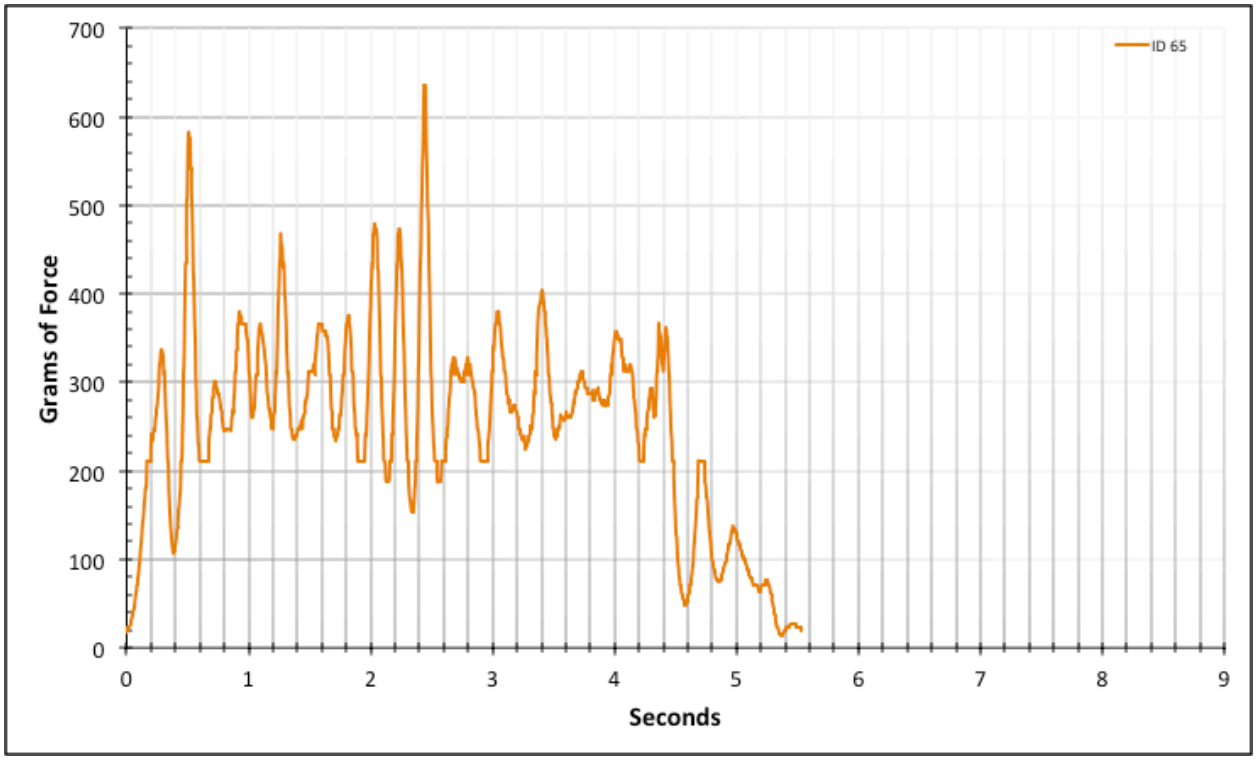

Figure A-6-128: Full Modeled Product - Dry - ID 65 - #10, Bolt 2

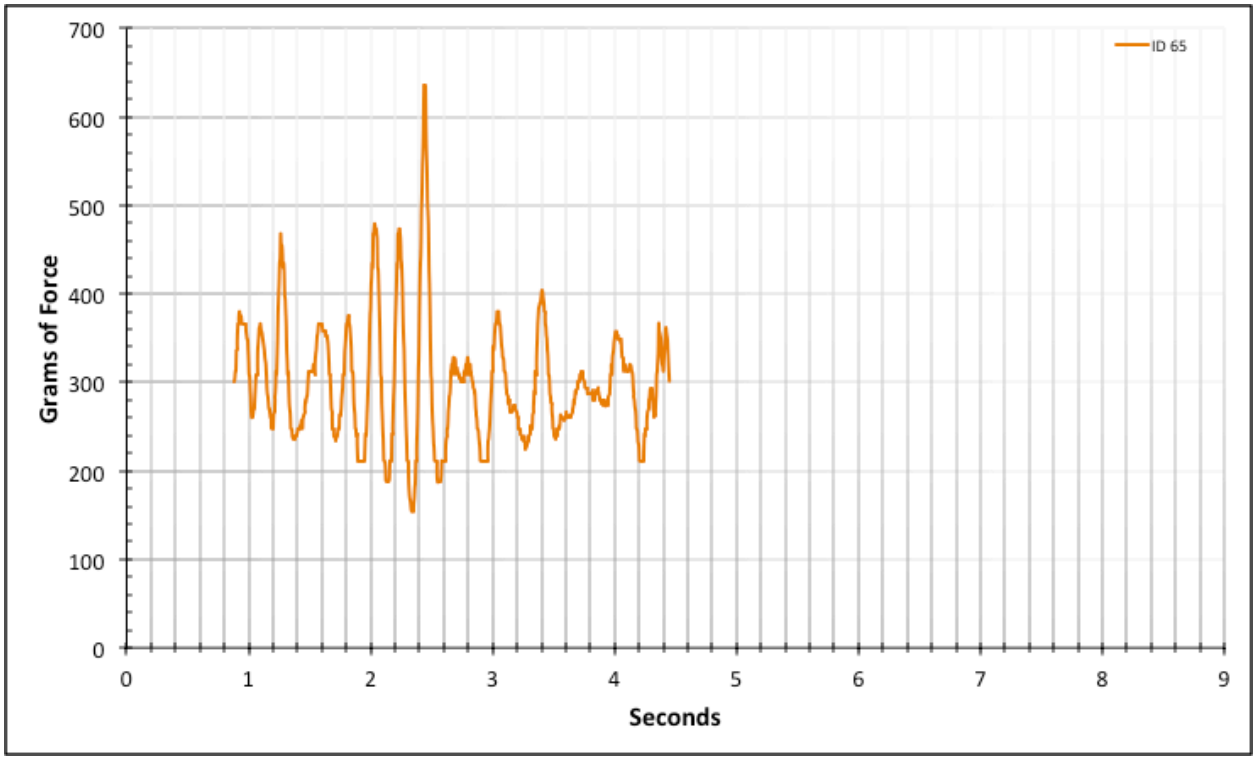

Figure A-6-129: Statistical Region Modeled Product - Dry - ID 65 - #10, Bolt 2

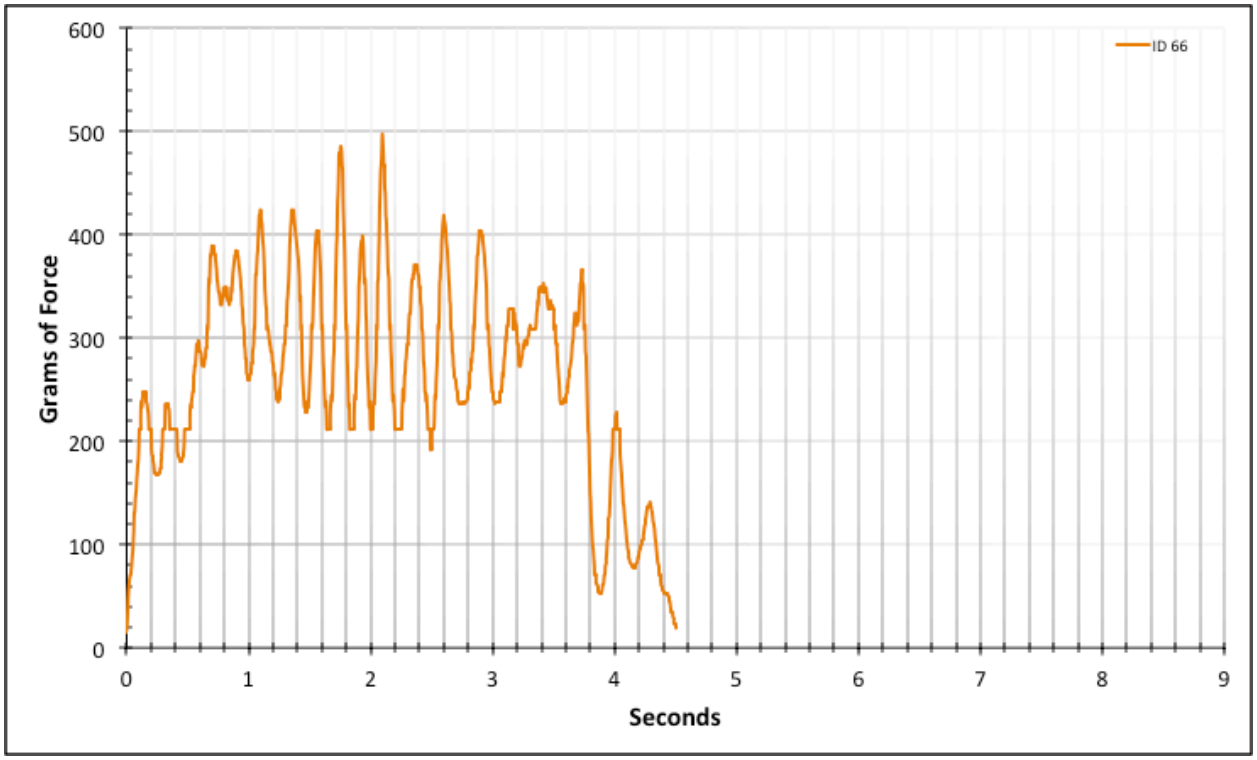

Figure A-6-130: Full Modeled Product - Dry - ID 66 - #10, Bolt 3

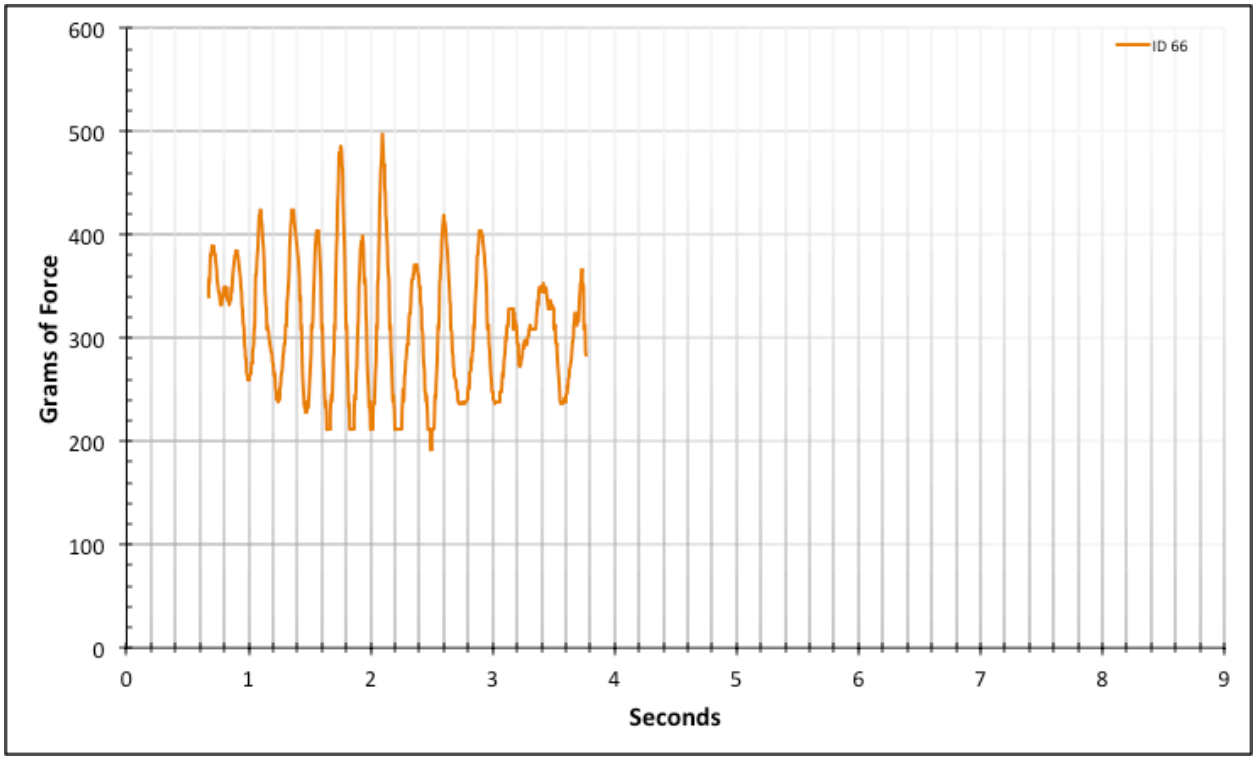

Figure A-6-131: Statistical Region Modeled Product - Dry - ID 66 - #10, Bolt 3

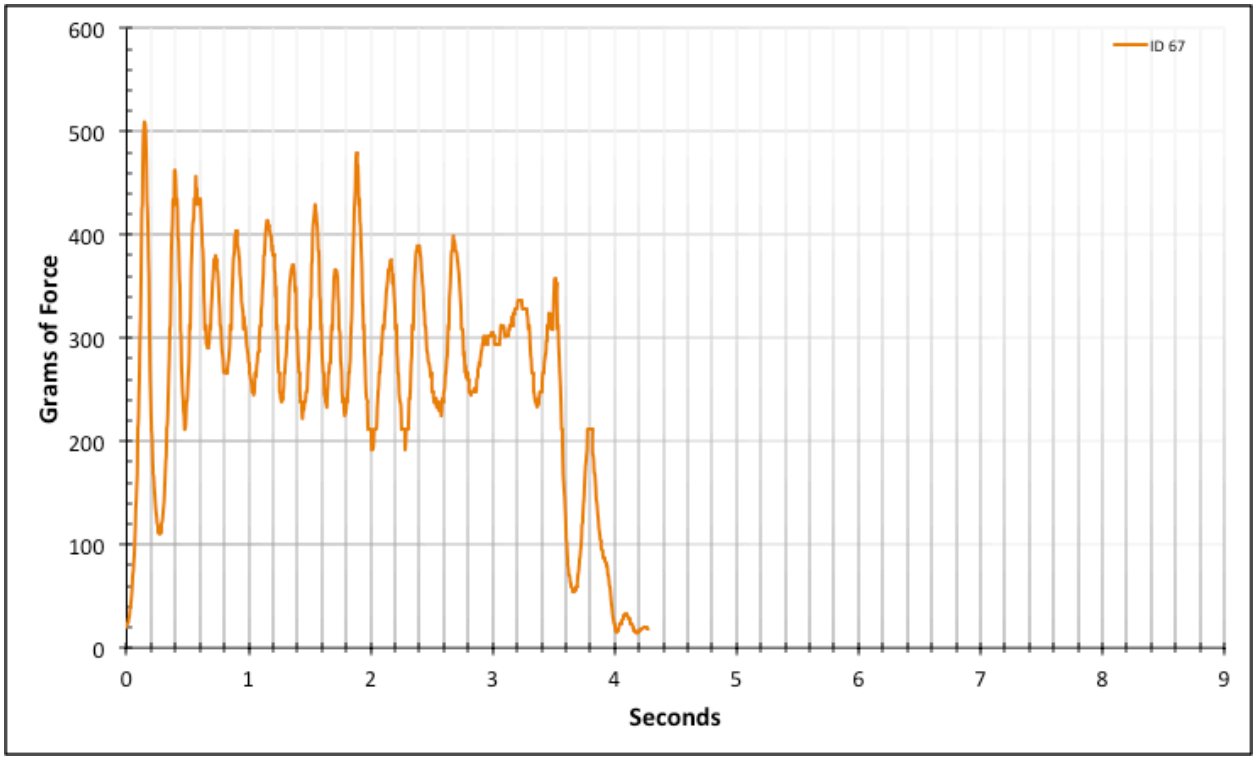

Figure A-6-132: Full Modeled Product - Dry - ID 67 - #10, Bolt 3

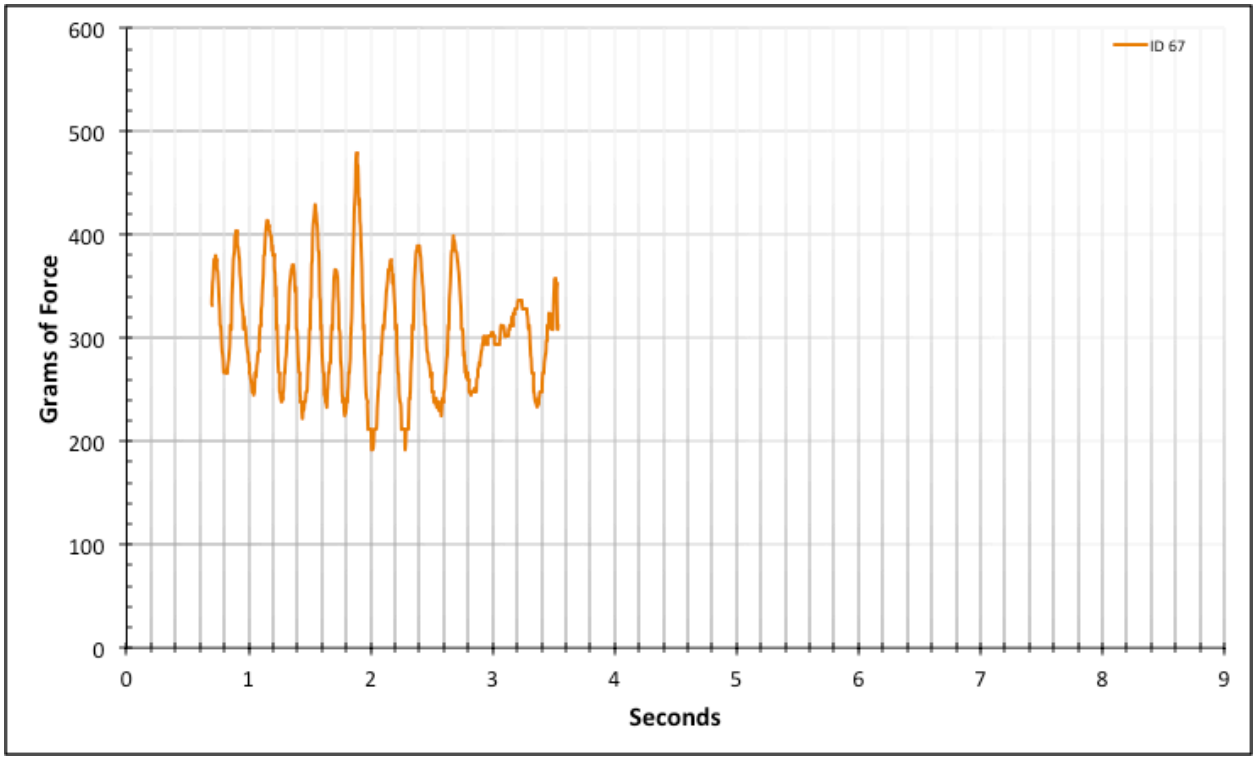

Figure A-6-133: Statistical Region Modeled Product - Dry - ID 67 - #10, Bolt 3

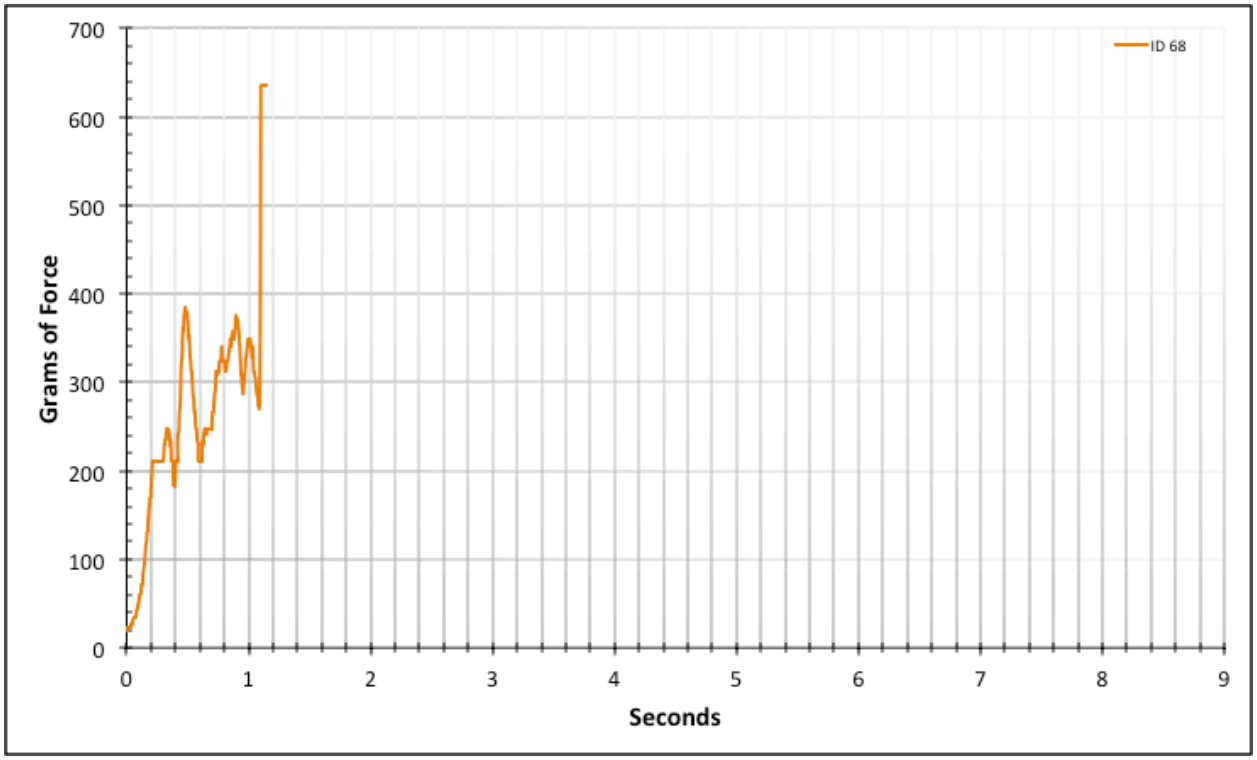

Figure A-6-134: Full Modeled Product - Dry - ID 68 - #10, Bolt 3

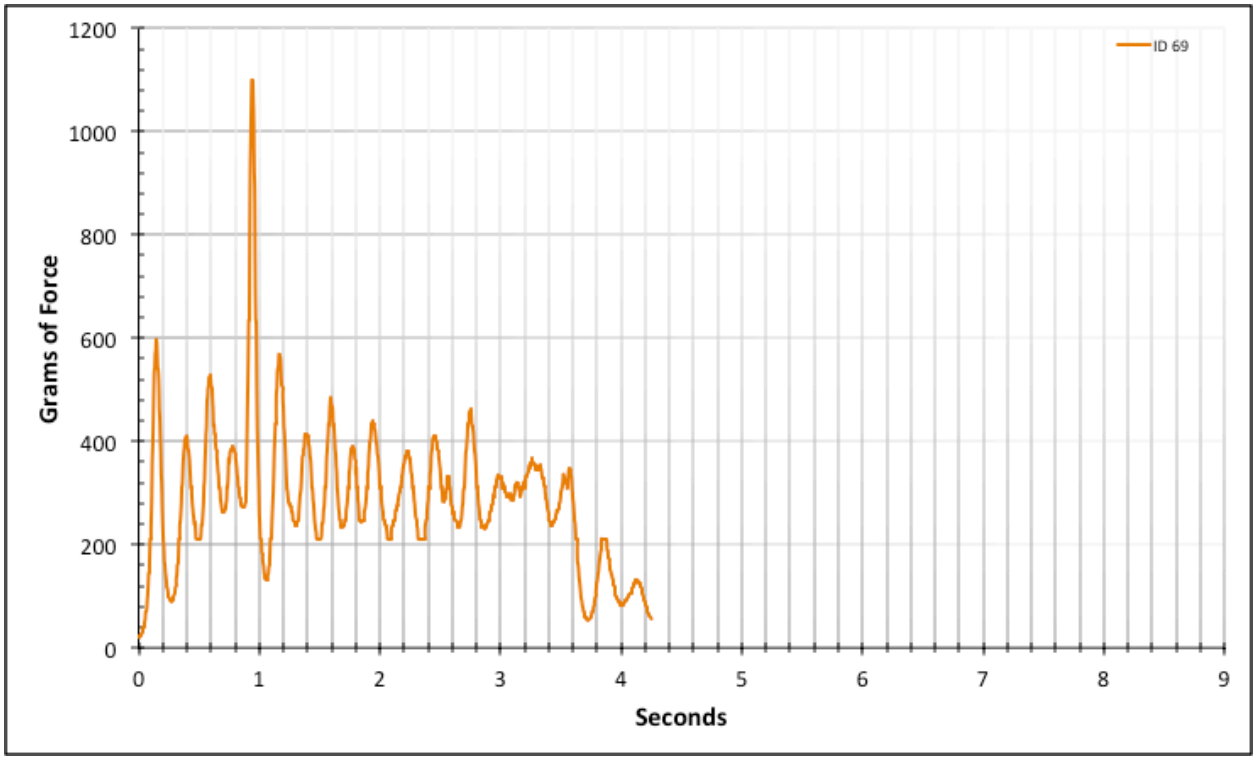

Figure A-6-135: Full Modeled Product - Dry - ID 69 - #10, Bolt 3

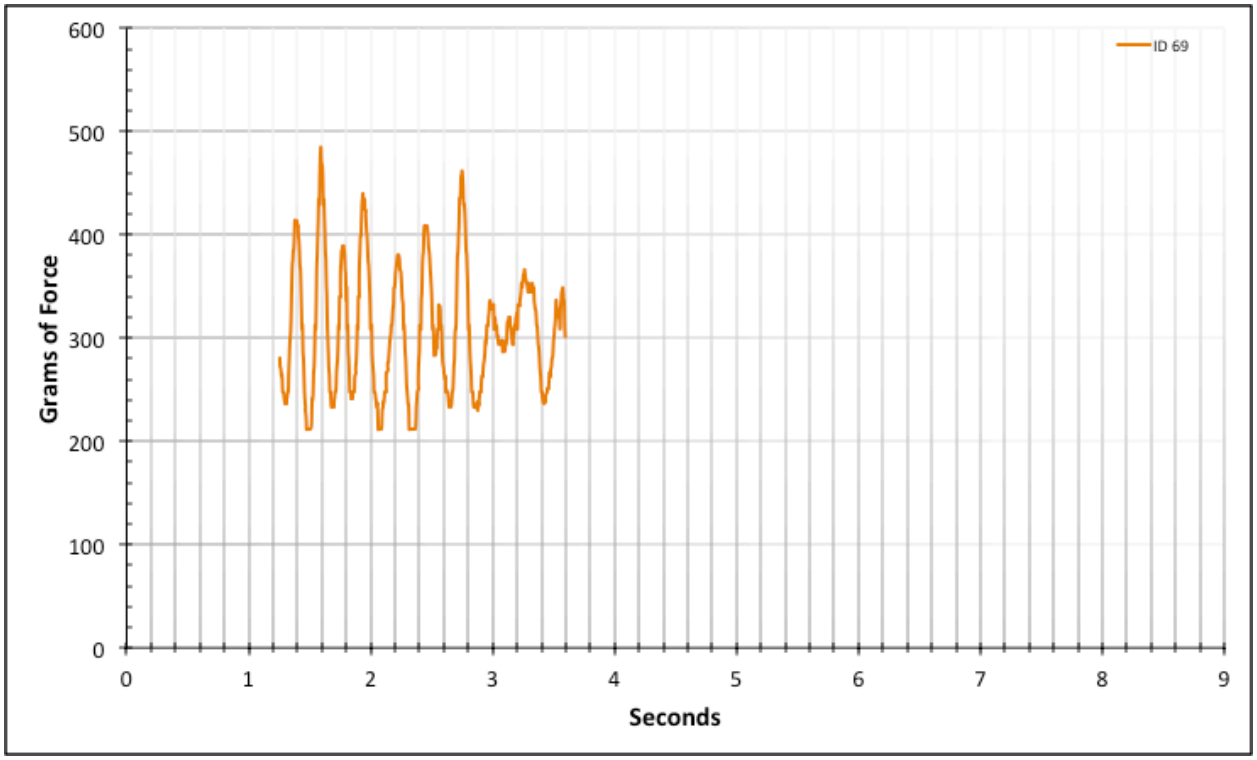

Figure A-6-136: Statistical Region Modeled Product - Dry - ID 69 - #10, Bolt 3

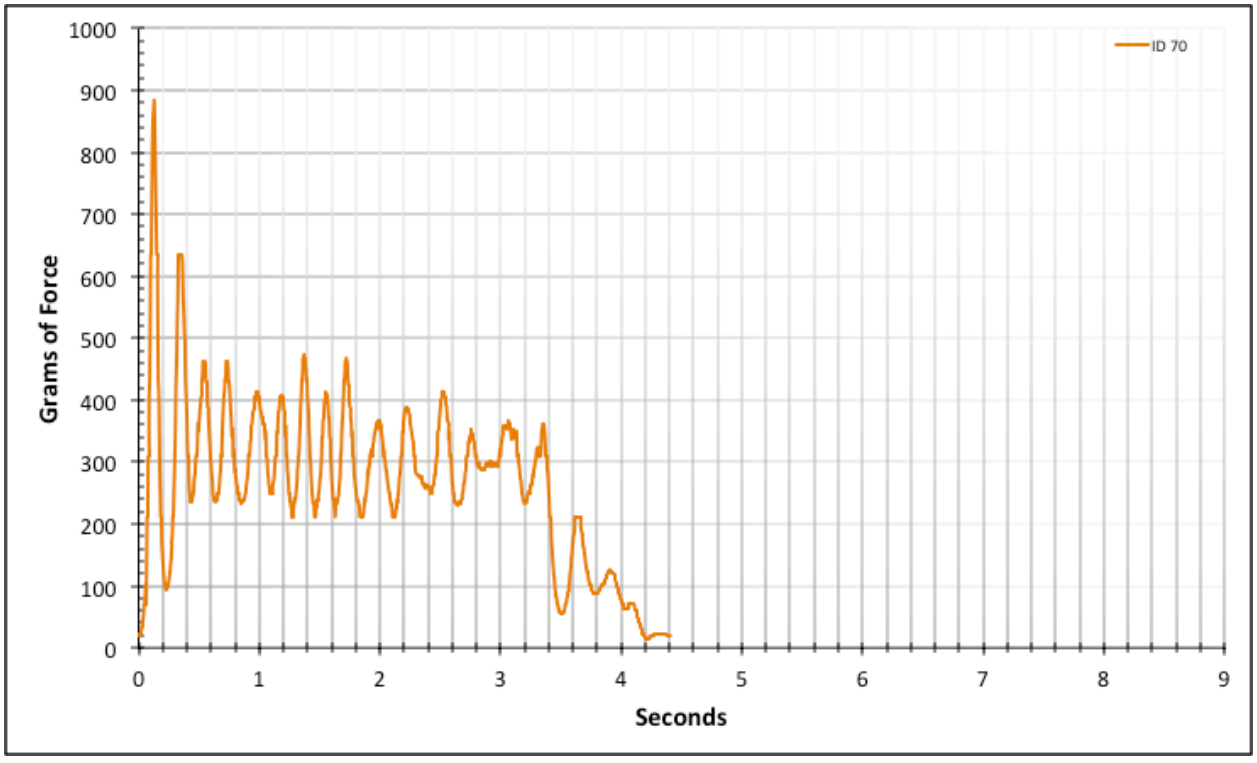

Figure A-6-137: Full Modeled Product - Dry - ID 70 - #10, Bolt 3

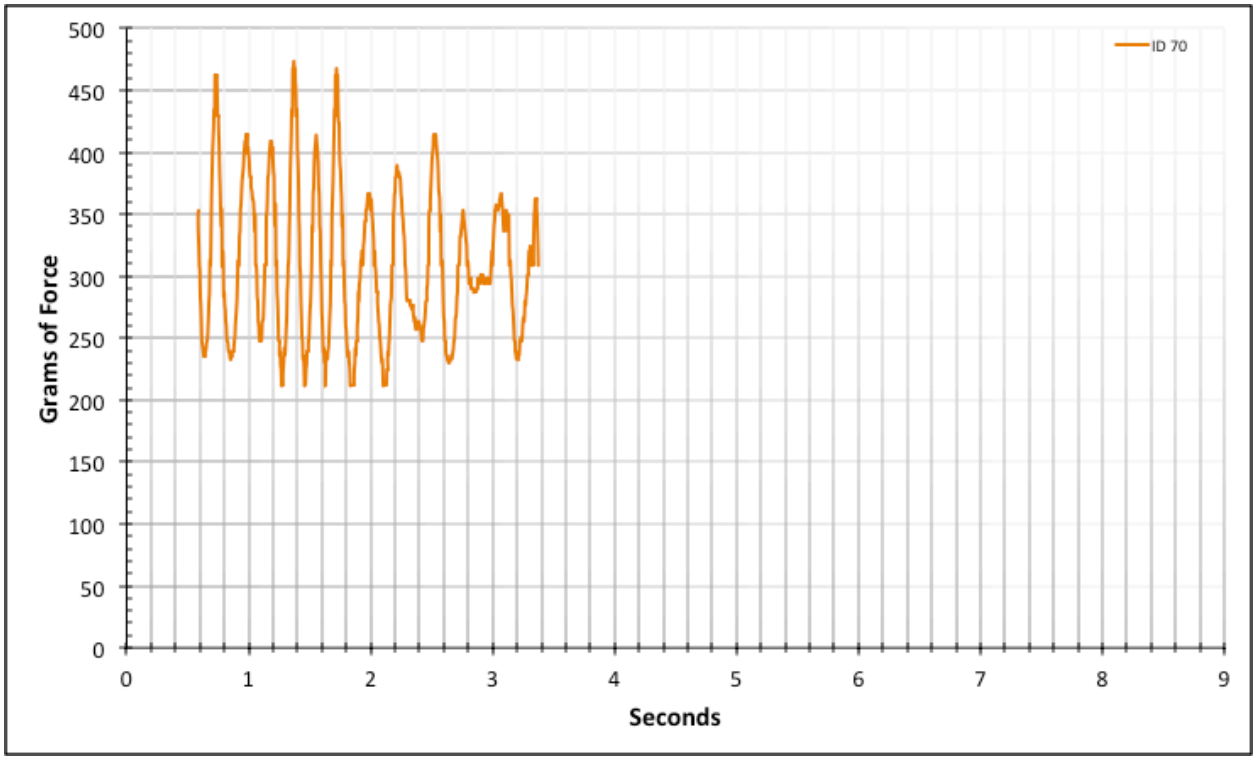

Figure A-6-138: Statistical Region Modeled Product - Dry - ID 70 - #10, Bolt 3

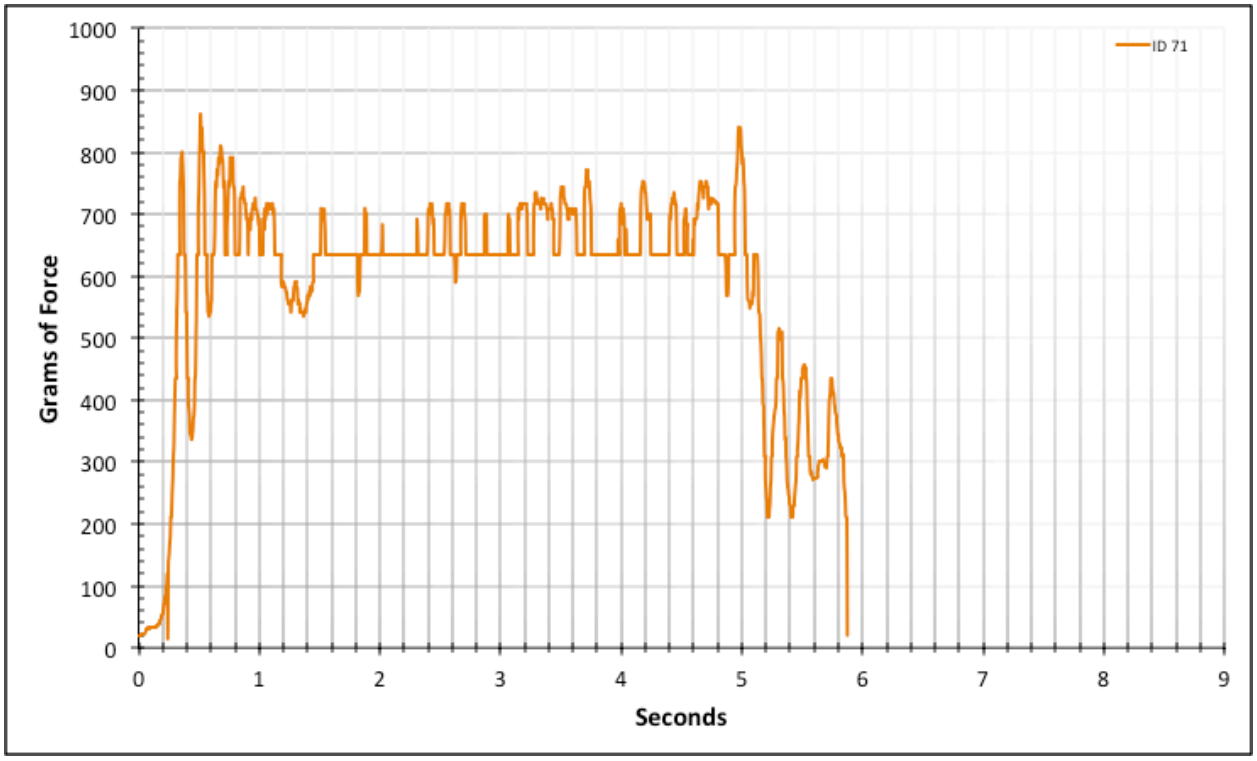

Figure A-6-139: Full Modeled Product - Dry - ID 71 - #8, Bolt 1

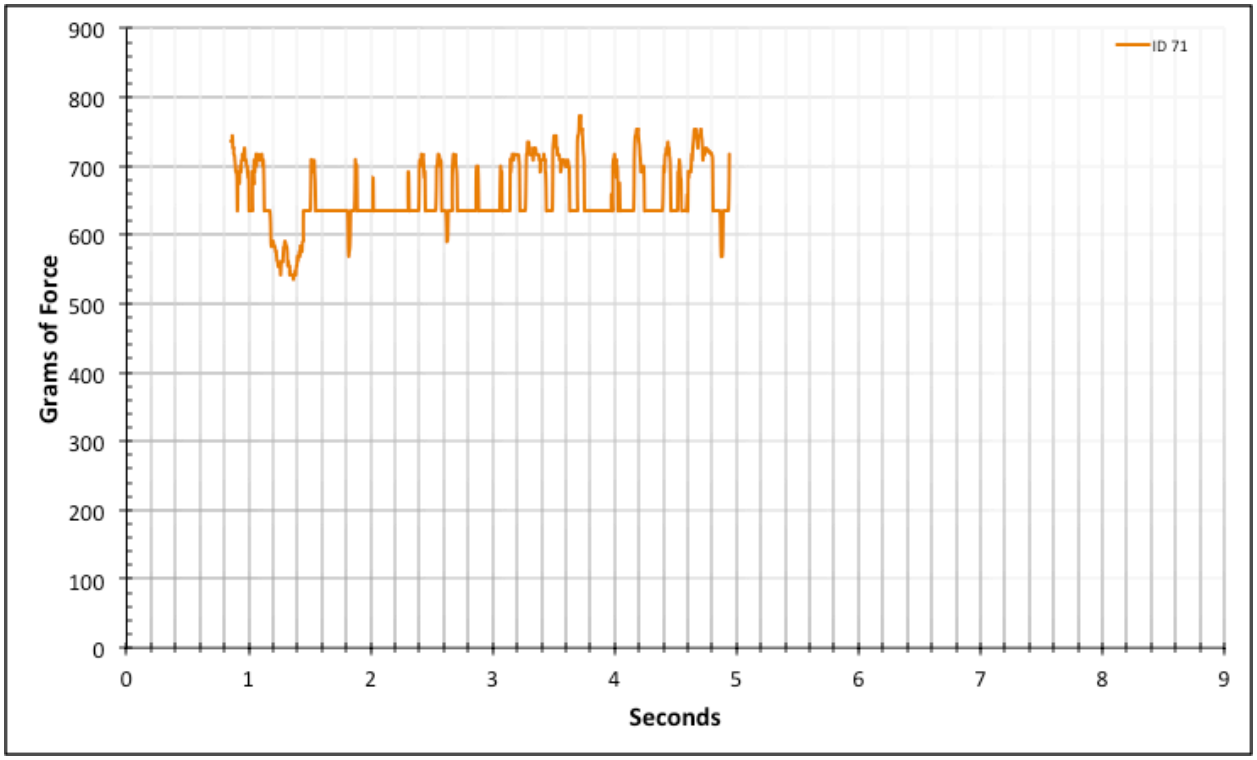

Figure A-6-140: Statistical Region Modeled Product - Dry - ID 71 - #8, Bolt 1

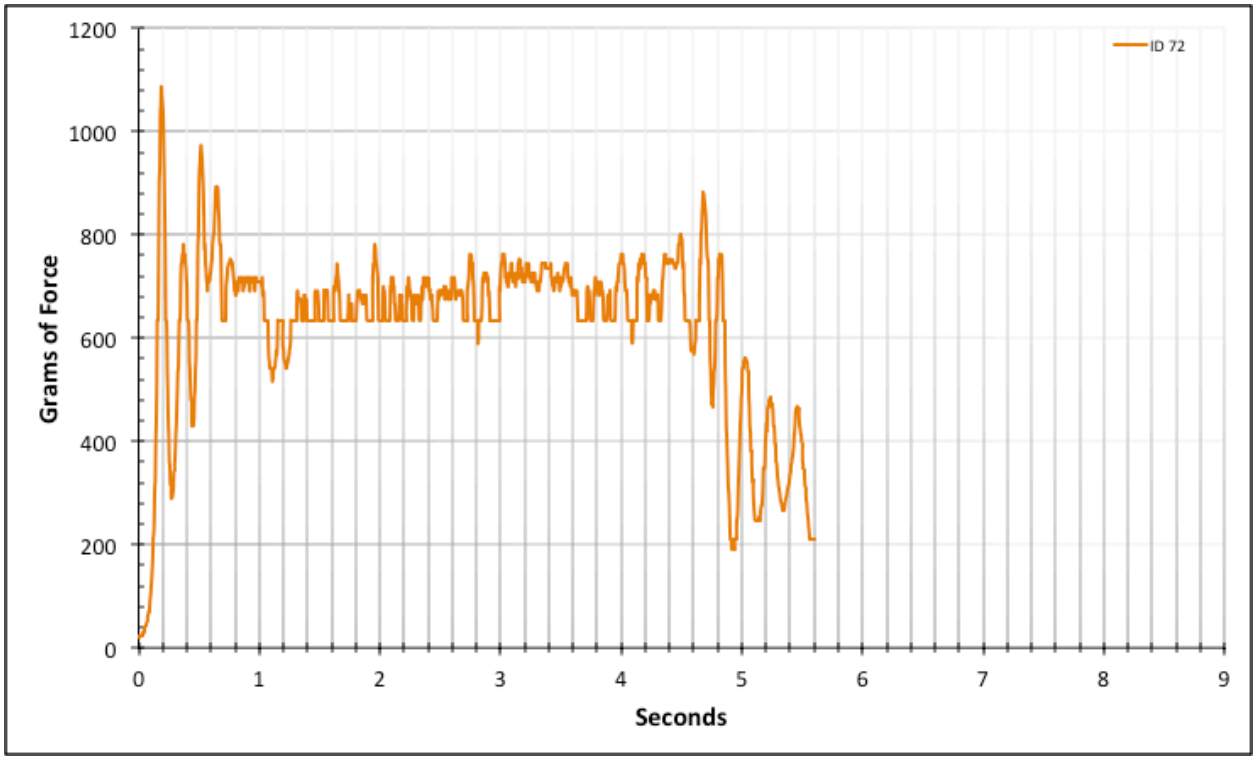

Figure A-6-141: Full Modeled Product - Dry - ID 72 - #8, Bolt 1

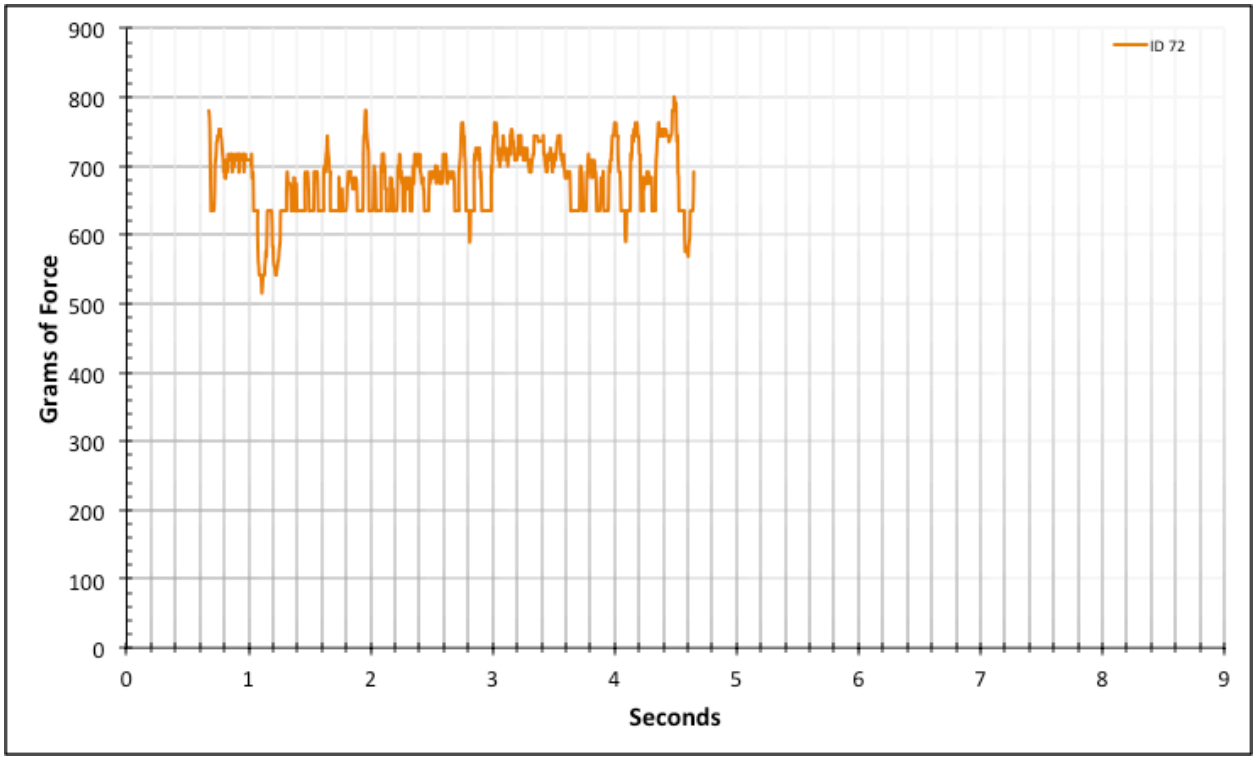

Figure A-6-142: Statistical Region Modeled Product - Dry - ID 72 - #8, Bolt 1

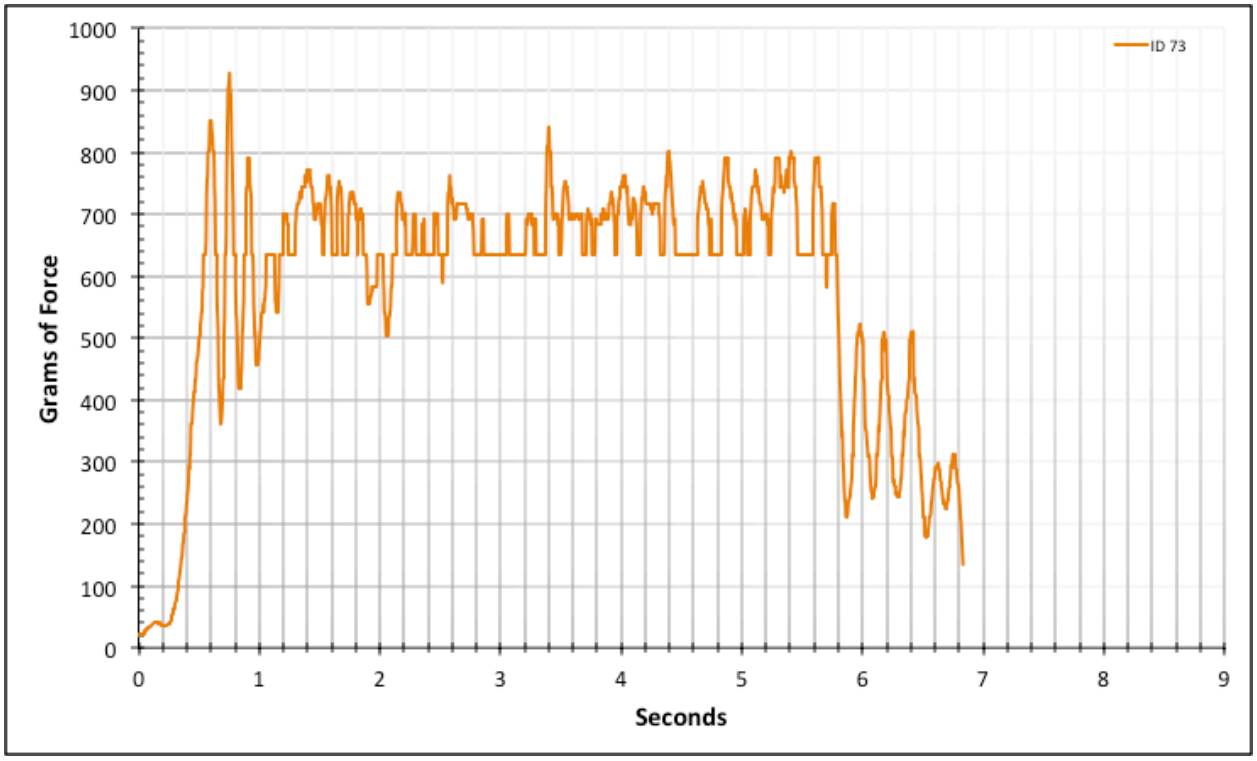

Figure A-6-143: Full Modeled Product - Dry - ID 73 - #8, Bolt 1

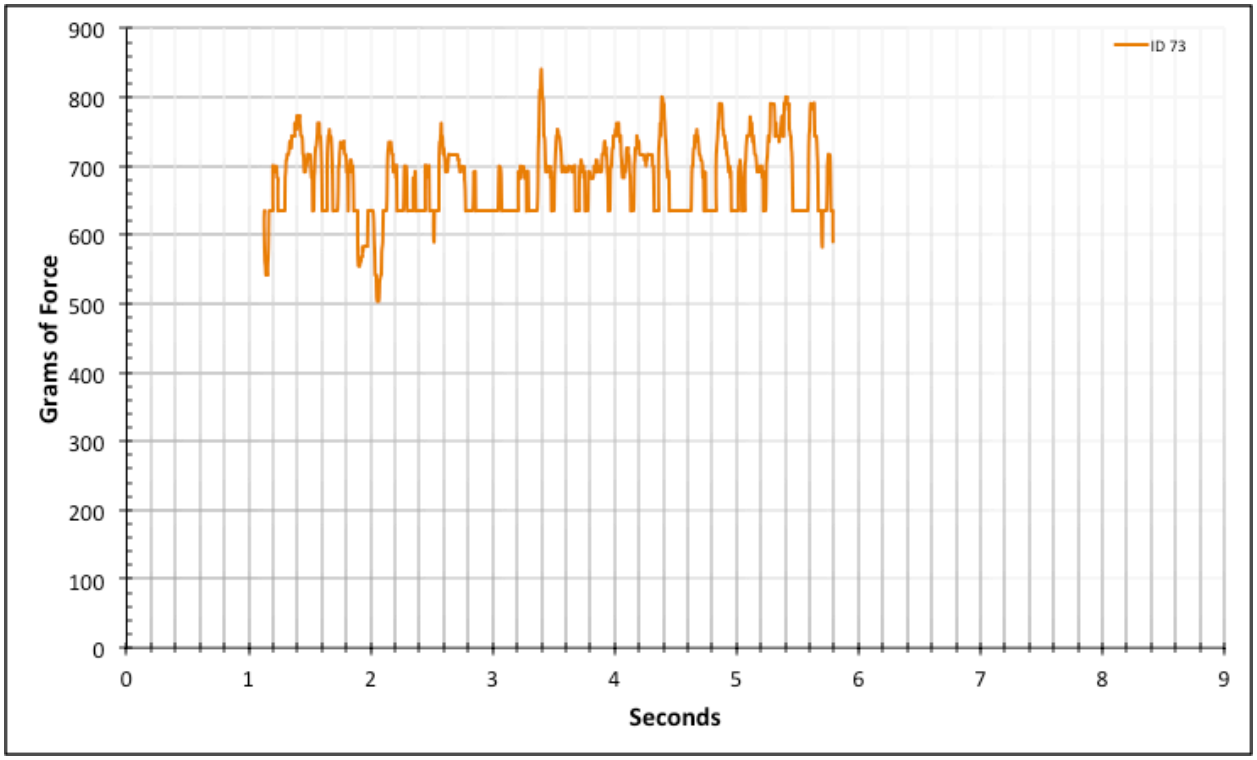

Figure A-6-144: Statistical Region Modeled Product - Dry - ID 73 - #8, Bolt 1

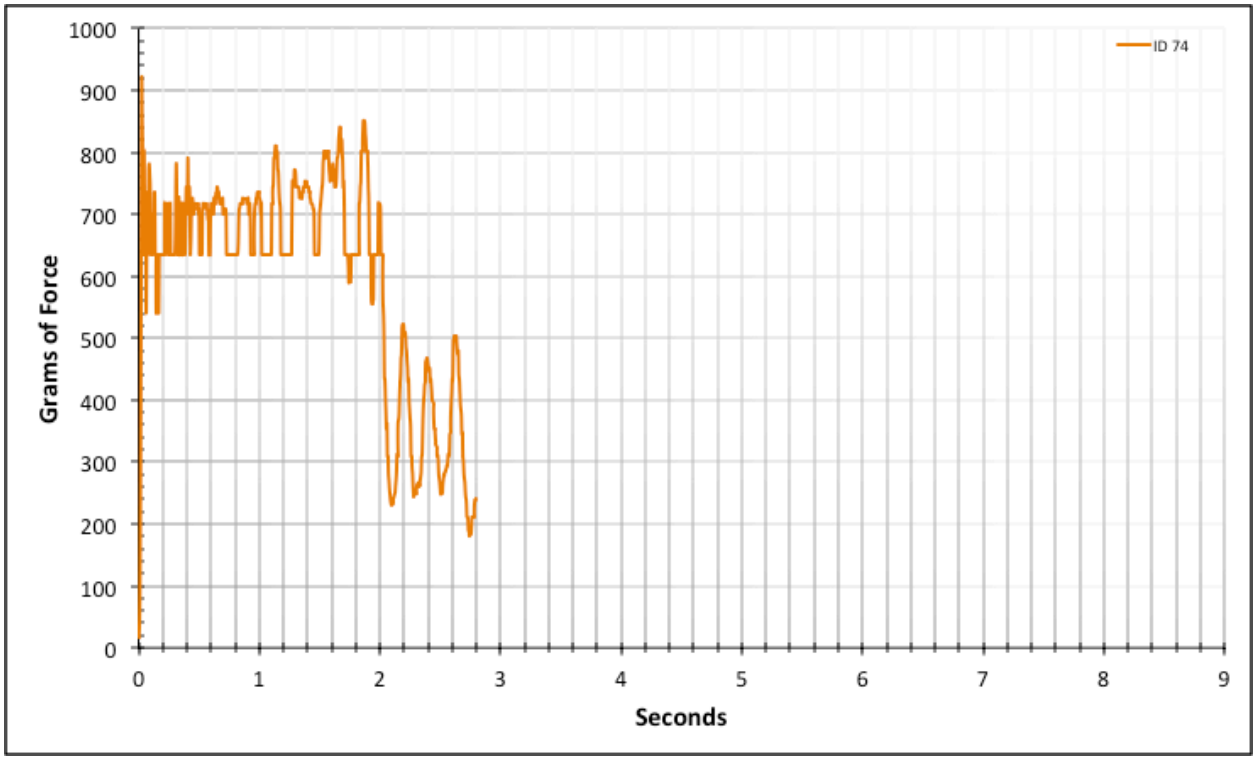

Figure A-6-145: Full Modeled Product - Dry - ID 74 - #8, Bolt 1

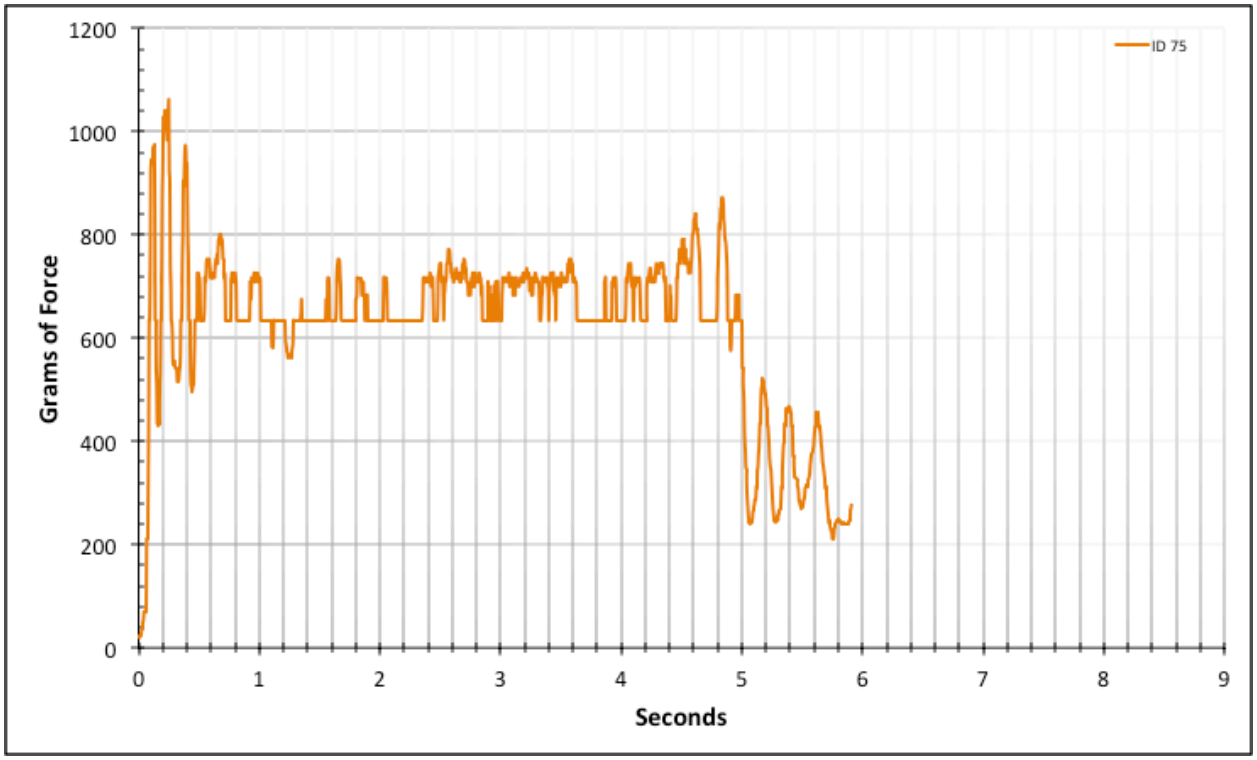

Figure A-6-146: Full Modeled Product - Dry - ID 75 - #8, Bolt 1

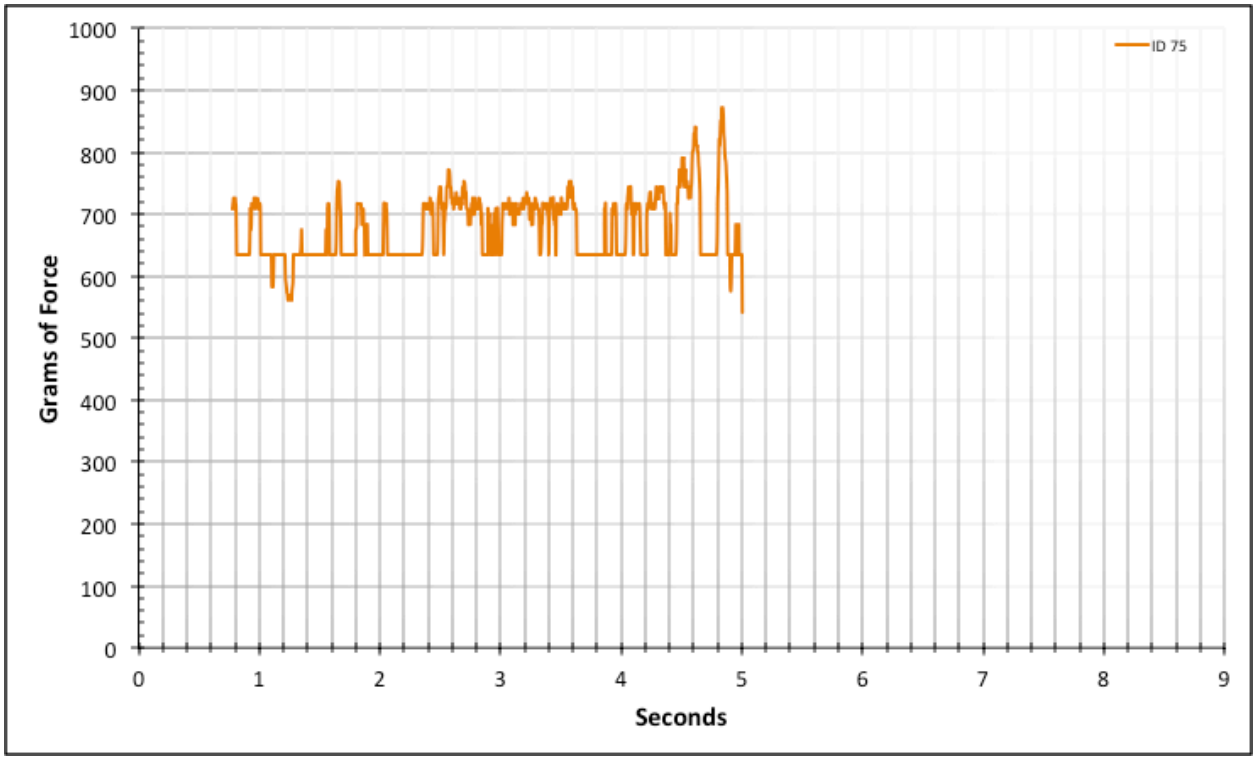

Figure A-6-147: Statistical Region Modeled Product - Dry - ID 75 - #8, Bolt 1

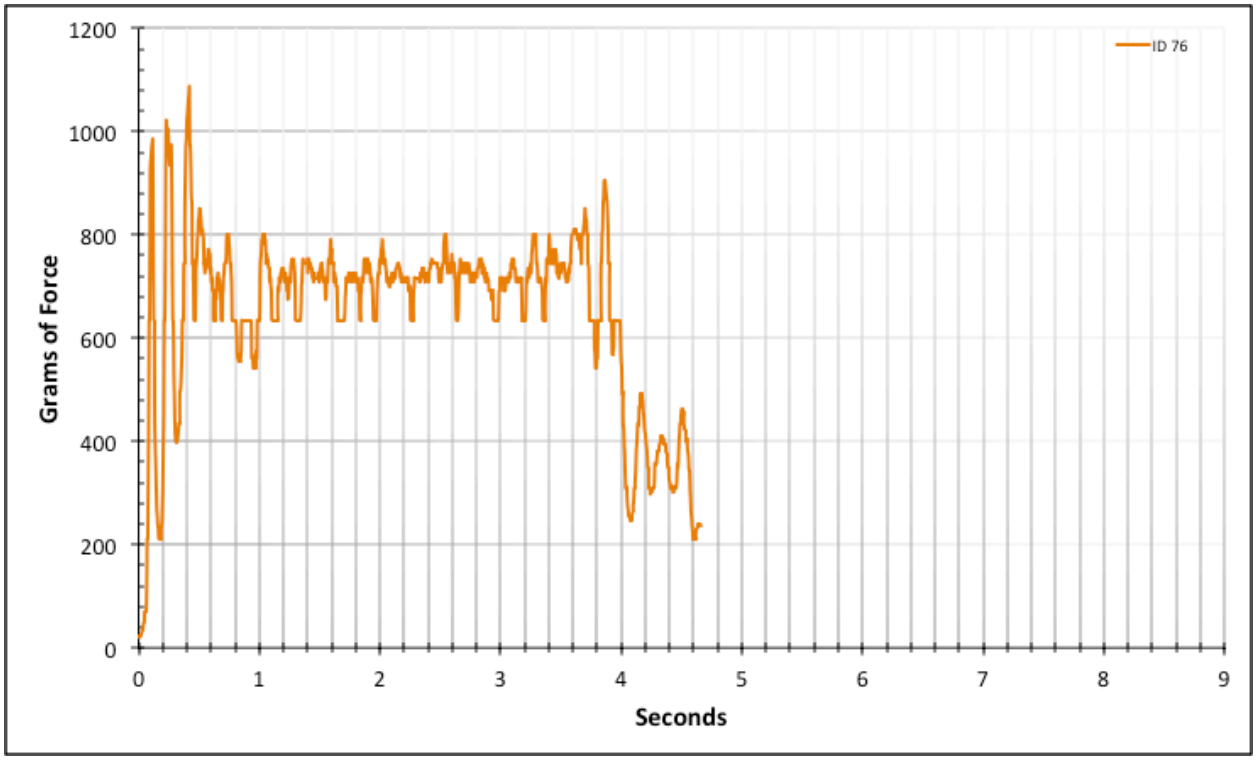

Figure A-6-148: Full Modeled Product - Dry - ID 76 - #8, Bolt 2

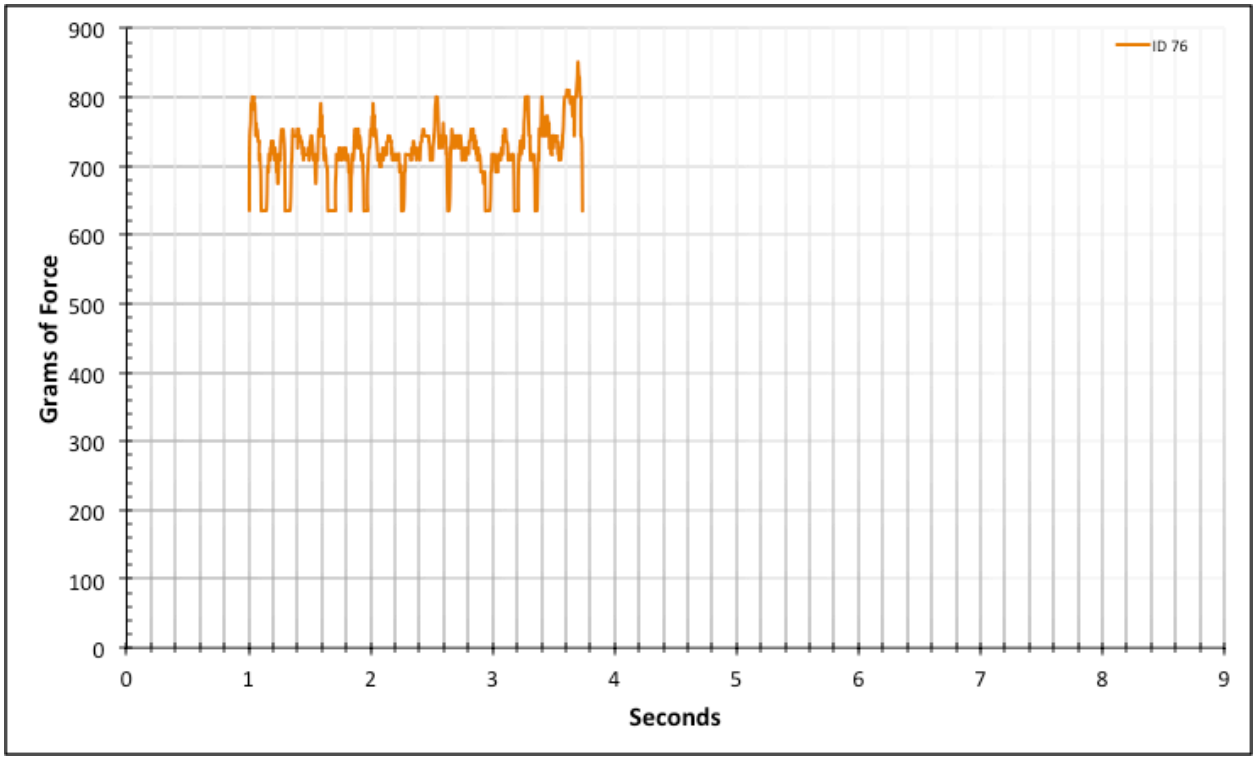

Figure A-6-149: Statistical Region Modeled Product - Dry - ID 76 - #8, Bolt 2

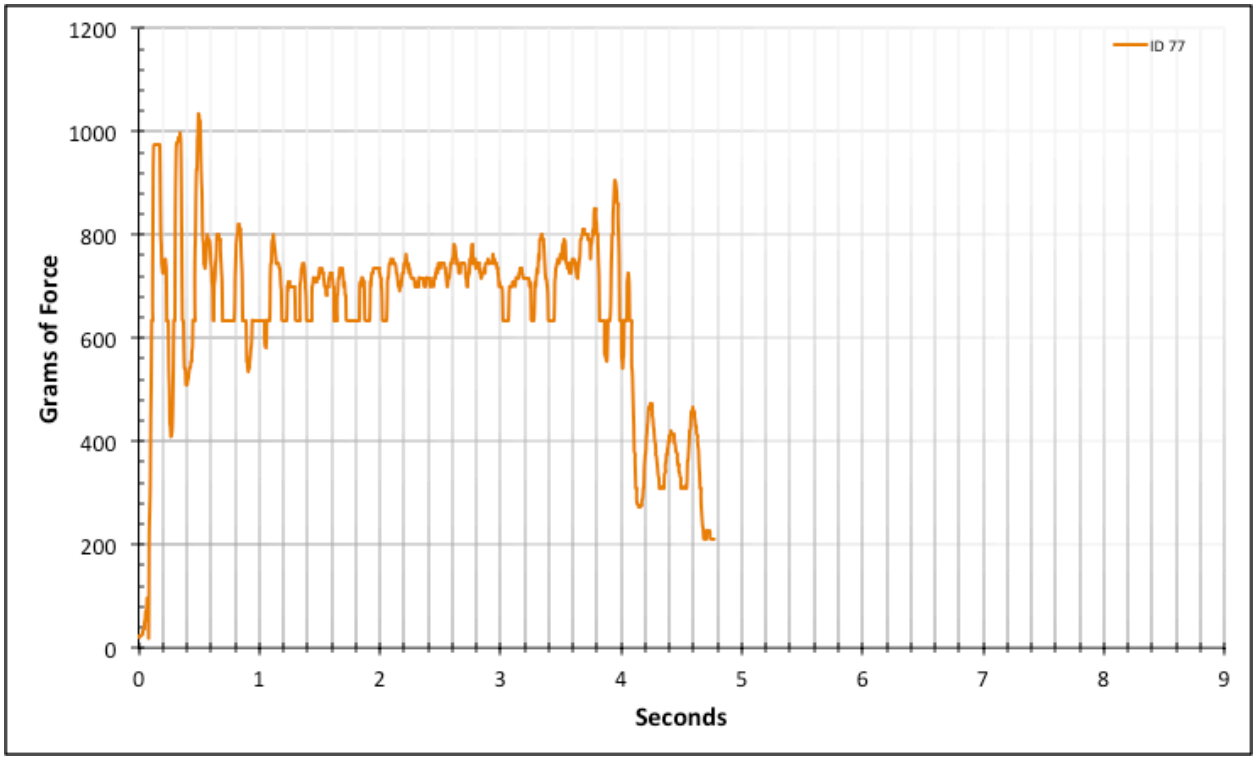

Figure A-6-150: Full Modeled Product - Dry - ID 77 - #8, Bolt 2

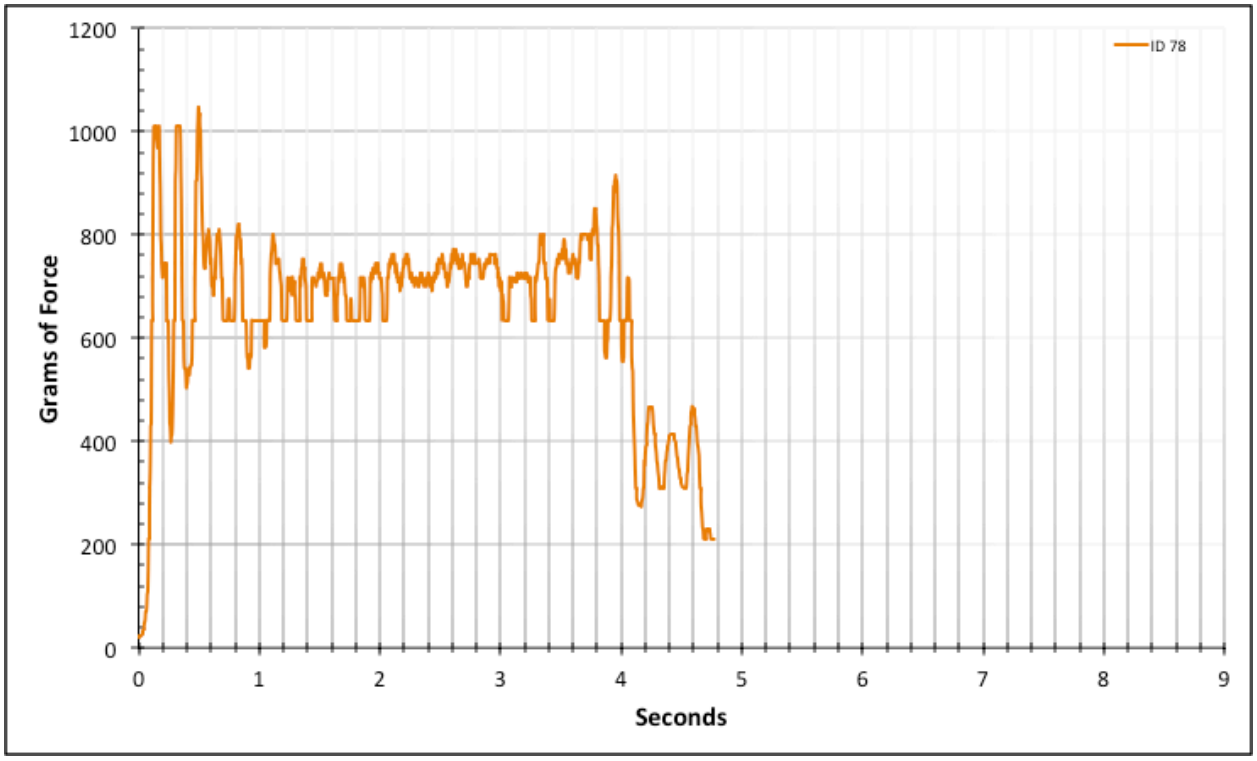

Figure A-6-151: Full Modeled Product - Dry - ID 78 - #8, Bolt 2

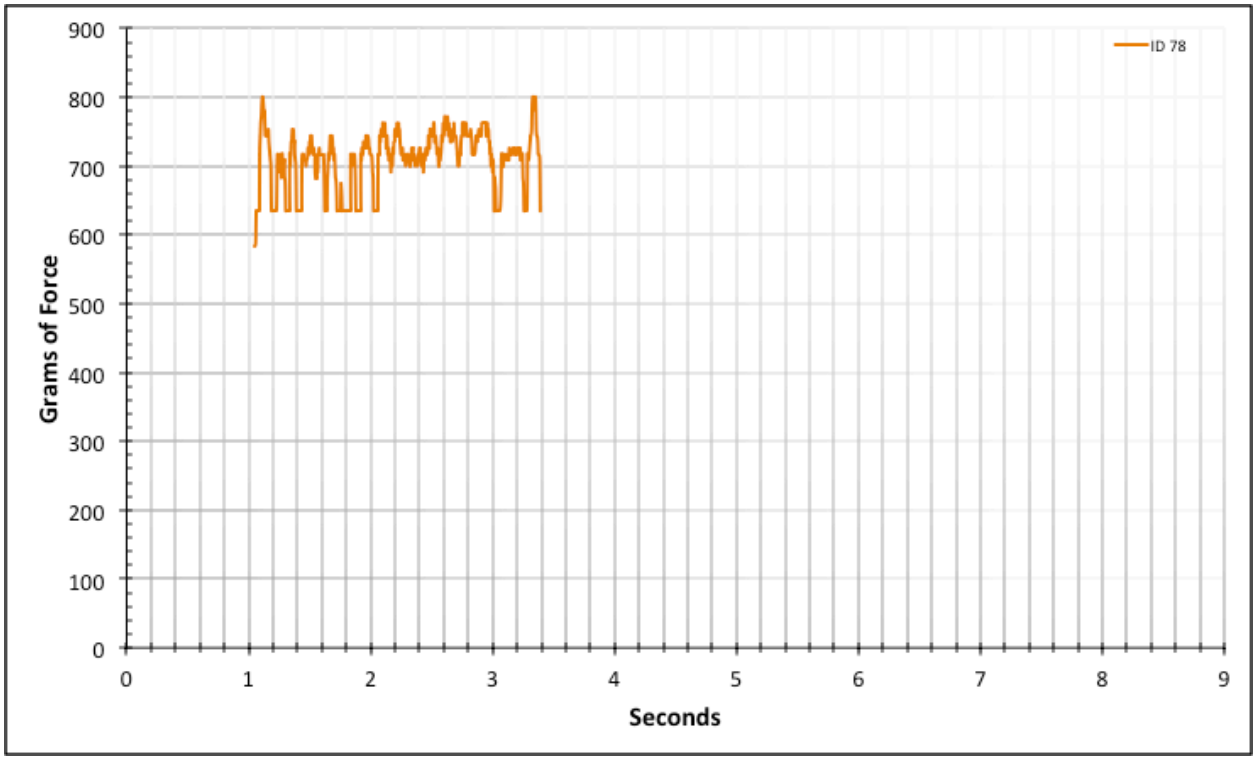

Figure A-6-152: Statistical Region Modeled Product - Dry - ID 78 - #8, Bolt 2

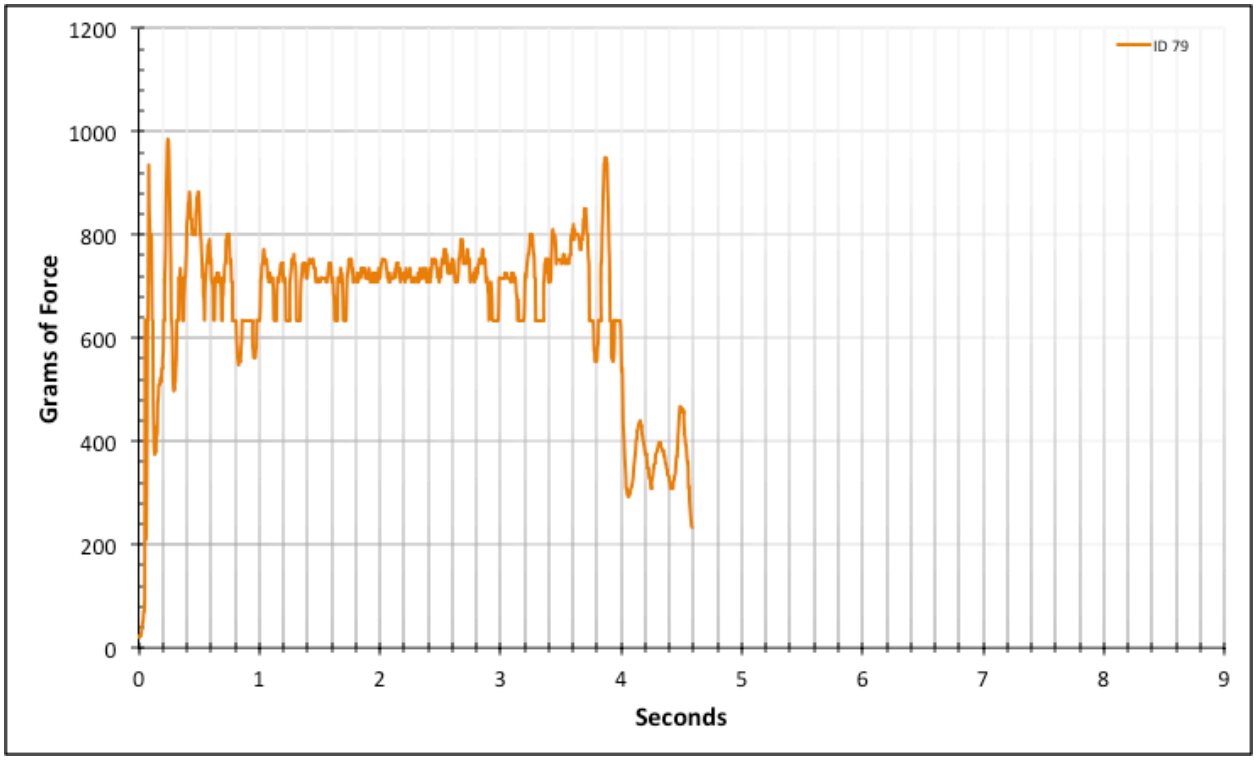

Figure A-6-153: Full Modeled Product - Dry - ID 79 - #8, Bolt 2

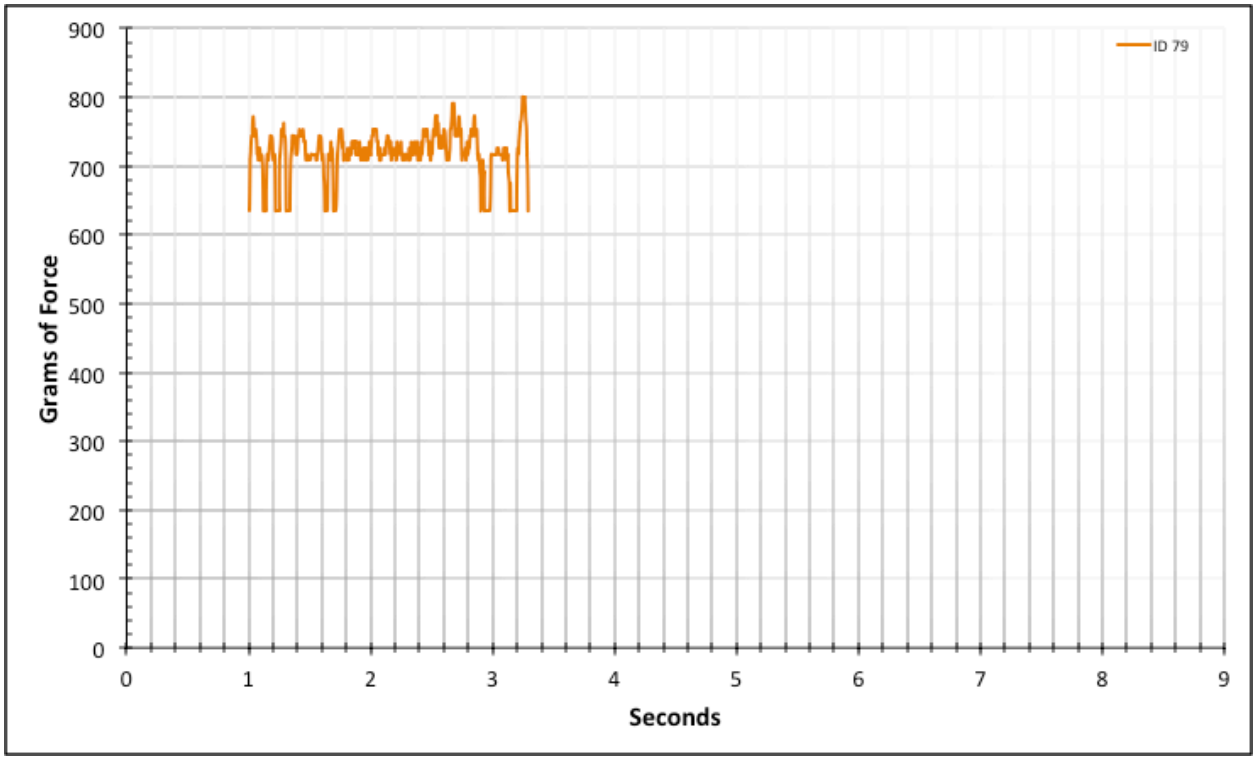

Figure A-6-154: Statistical Region Modeled Product - Dry - ID 79 - #8, Bolt 2

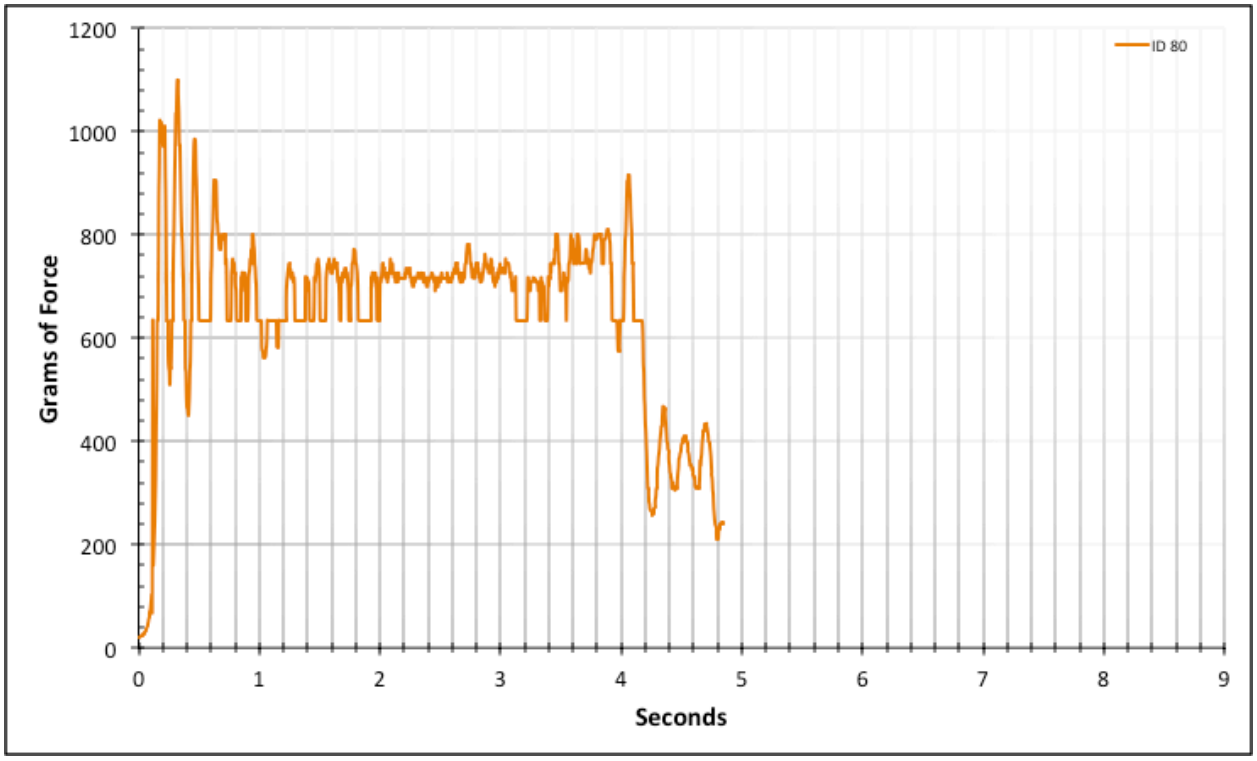

Figure A-6-155: Full Modeled Product - Dry - ID 80 - #8, Bolt 2

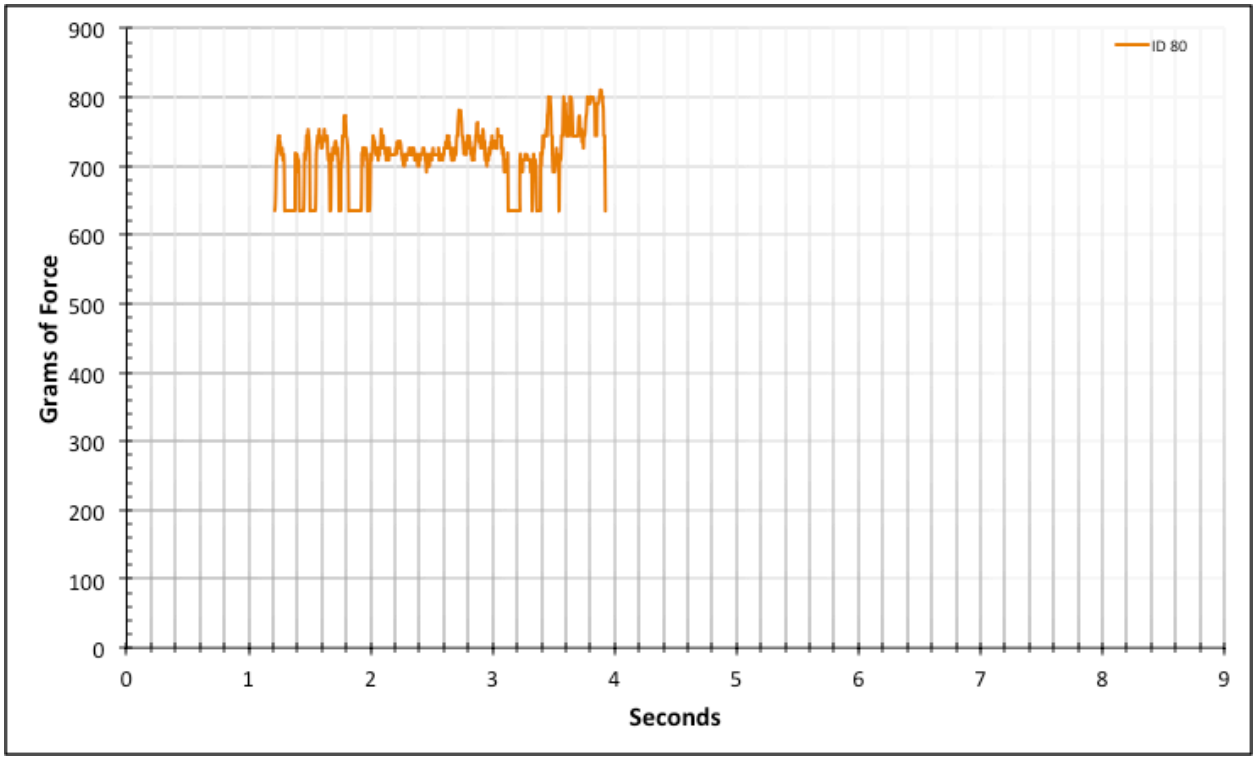

Figure A-6-156: Statistical Region Modeled Product - Dry - ID 80 - #8, Bolt 2

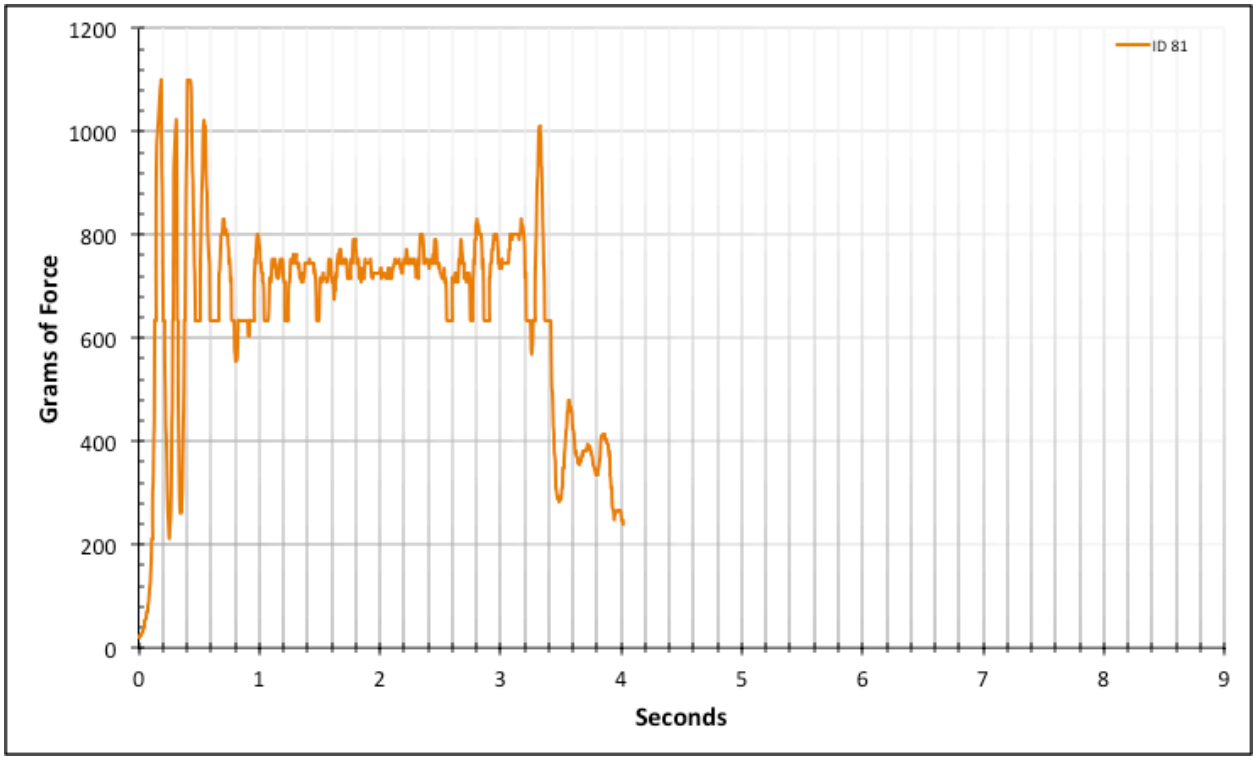

Figure A-6-157: Full Modeled Product - Dry - ID 81 - #8, Bolt 3

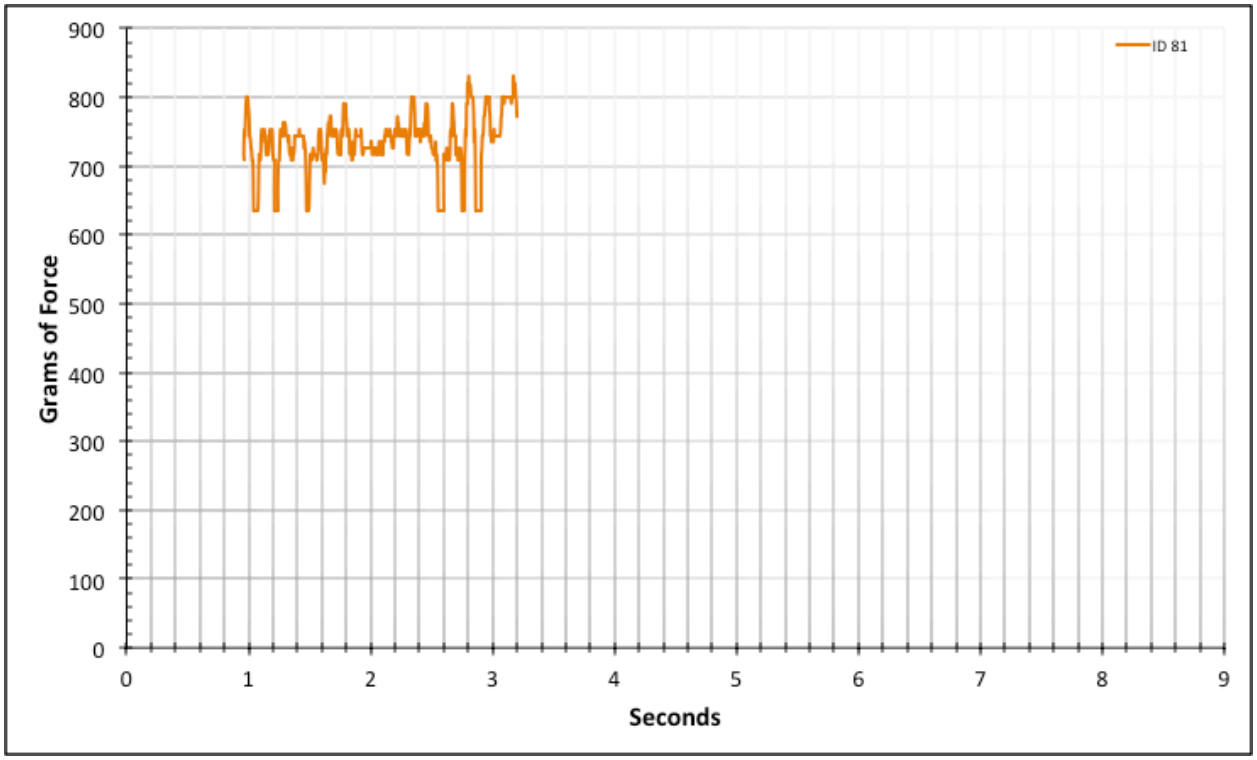

Figure A-6-158: Statistical Region Modeled Product - Dry - ID 81 - #8, Bolt 3

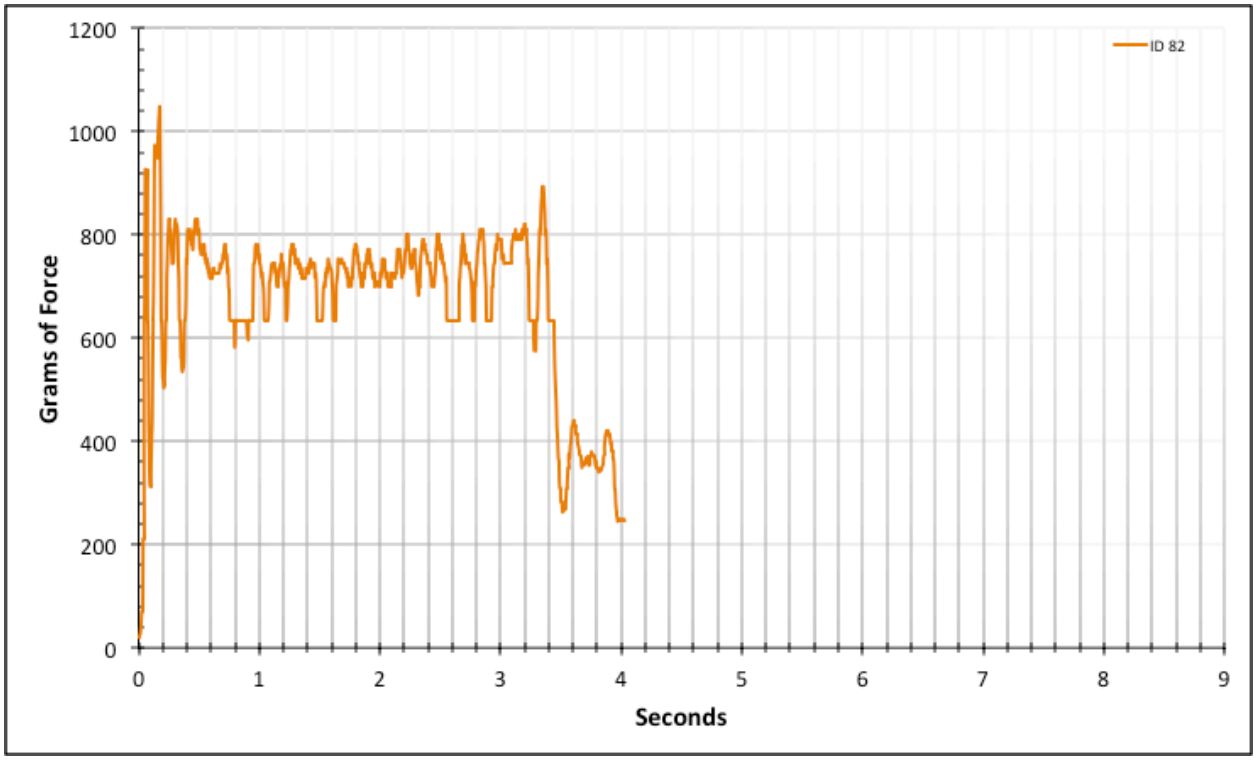

Figure A-6-159: Full Modeled Product - Dry - ID 82 - #8, Bolt 3

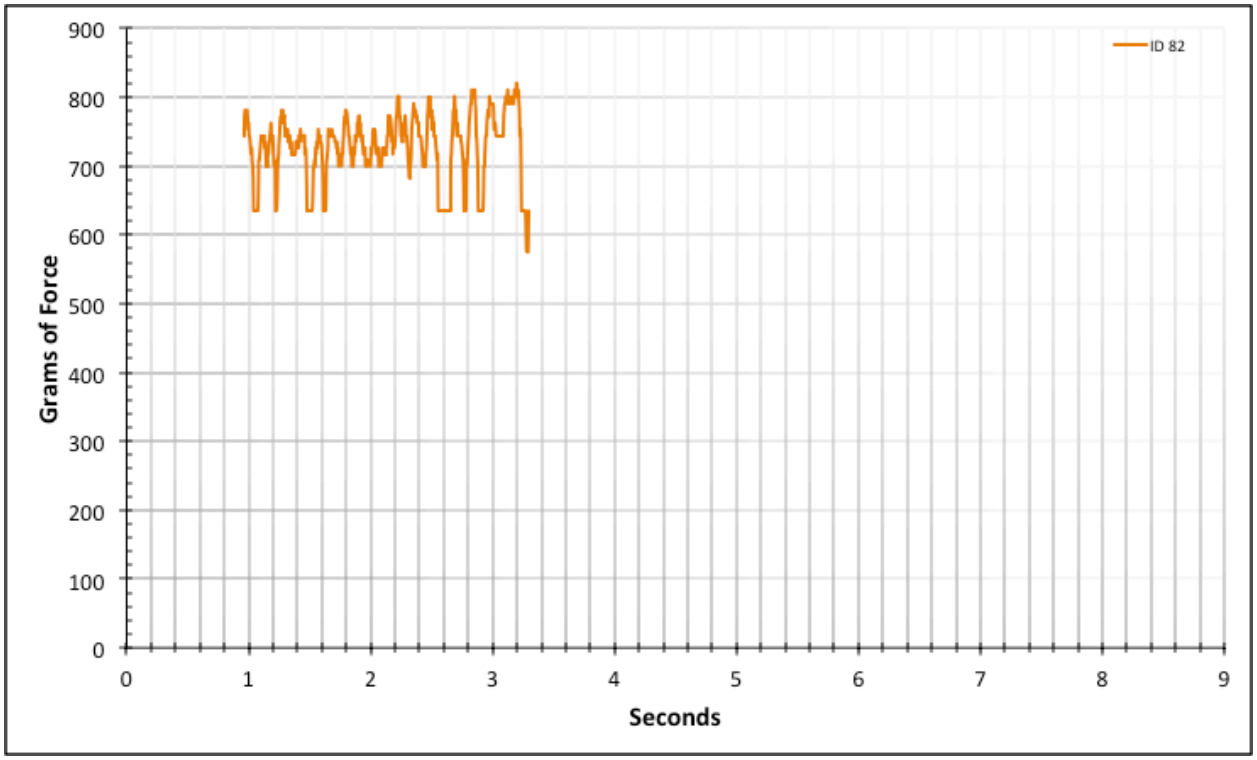

Figure A-6-160: Statistical Region Modeled Product - Dry - ID 82 - #8, Bolt 3

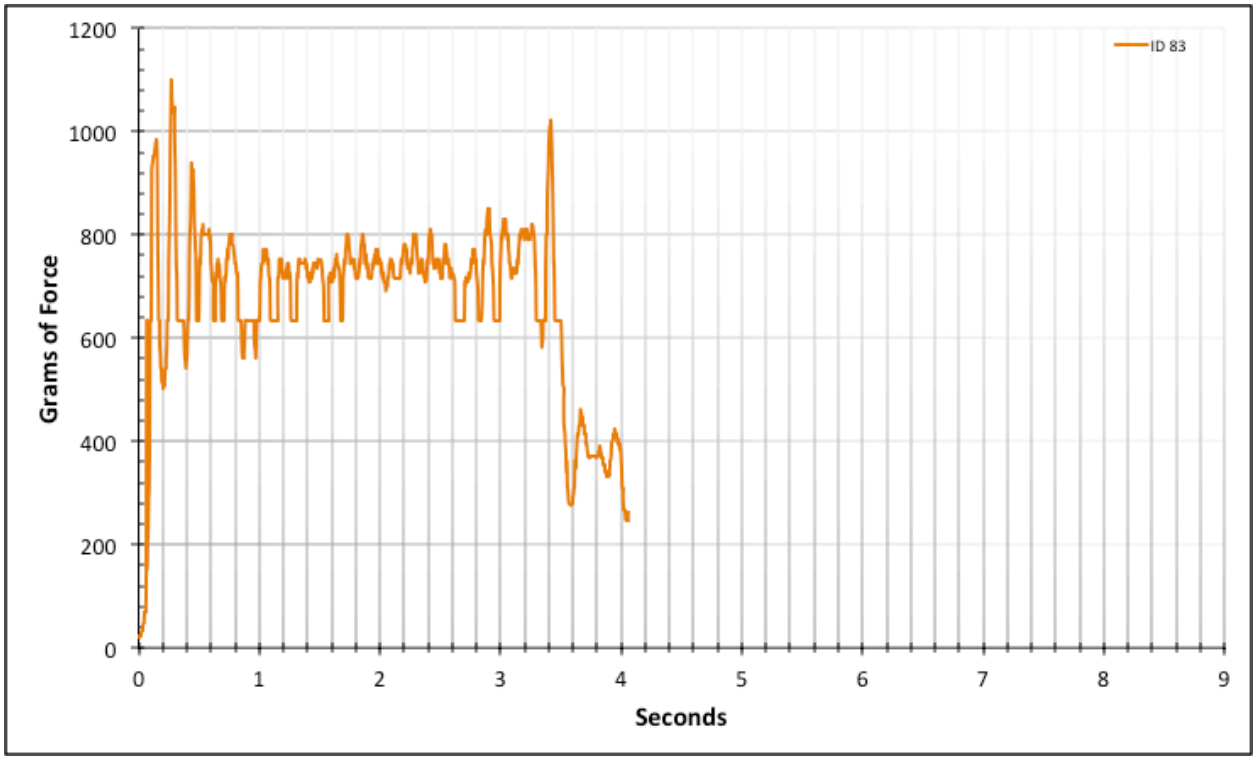

Figure A-6-161: Full Modeled Product - Dry - ID 83 - #8, Bolt 3

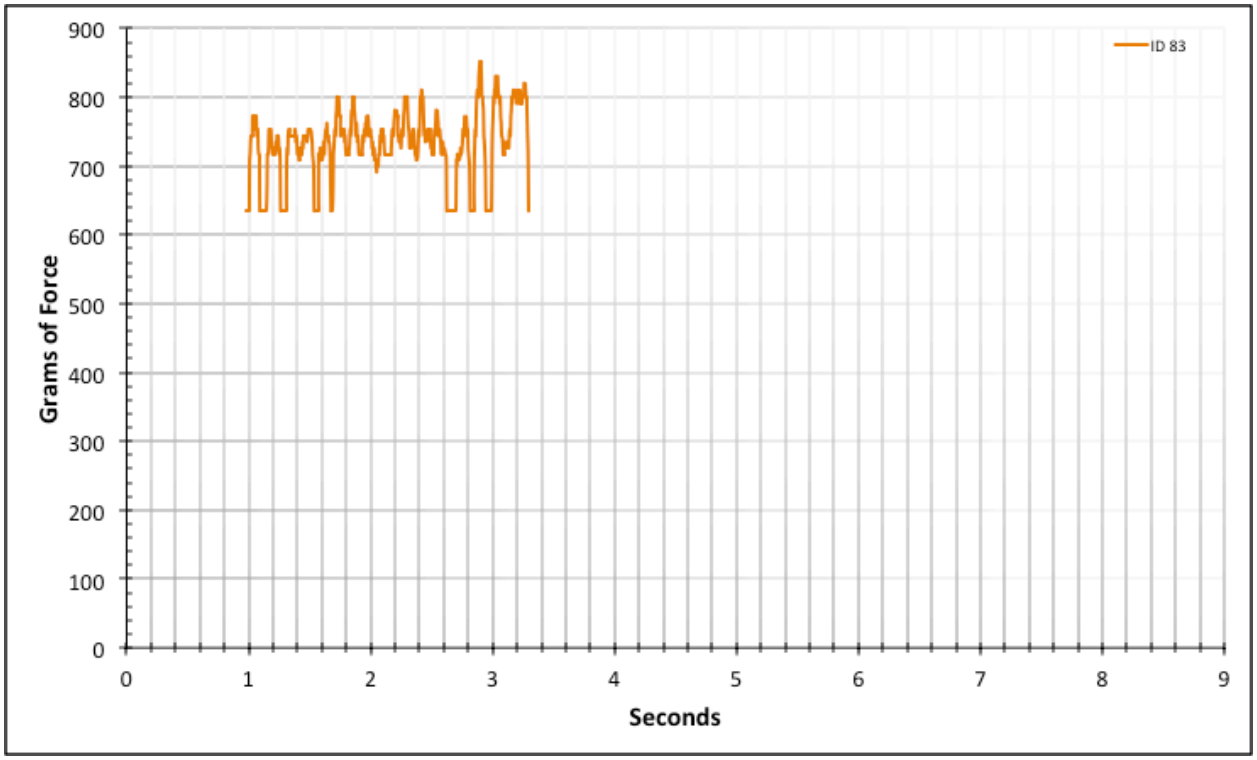

Figure A-6-162: Statistical Region Modeled Product - Dry - ID 83 - #8, Bolt 3

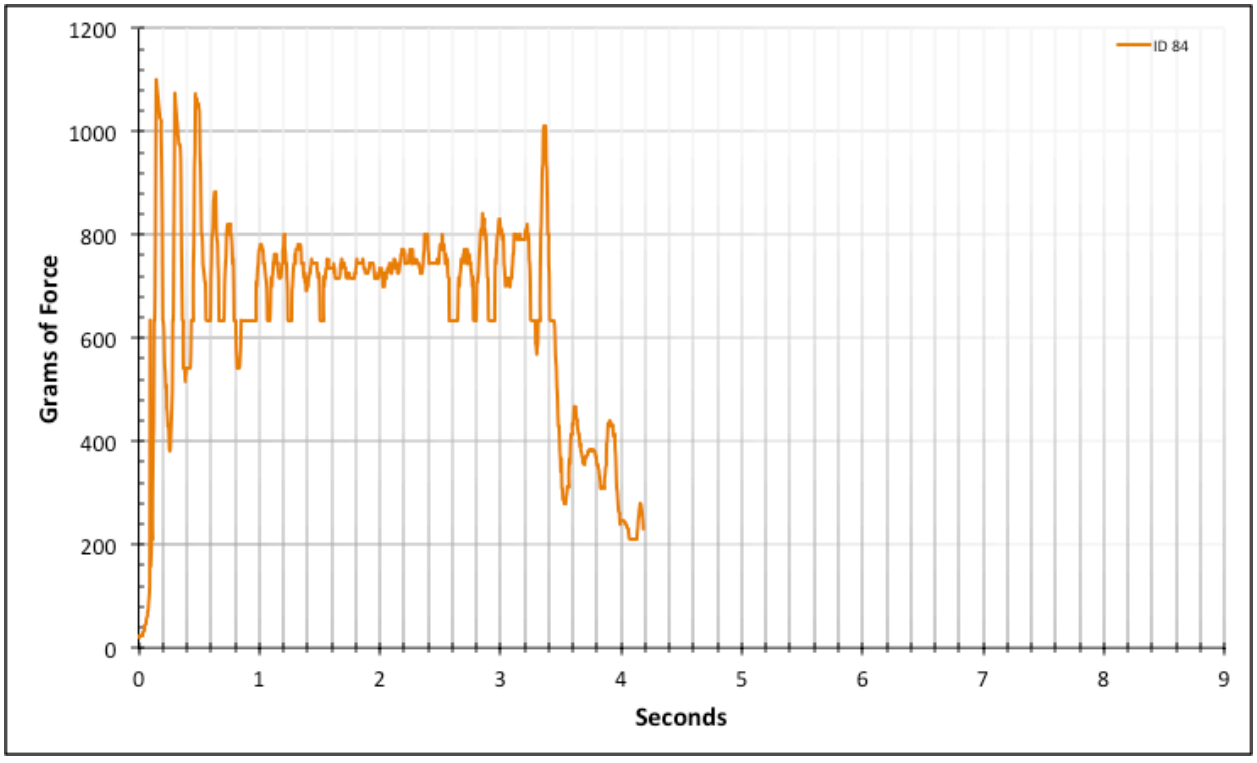

Figure A-6-163: Full Modeled Product - Dry - ID 84 - #8, Bolt 3

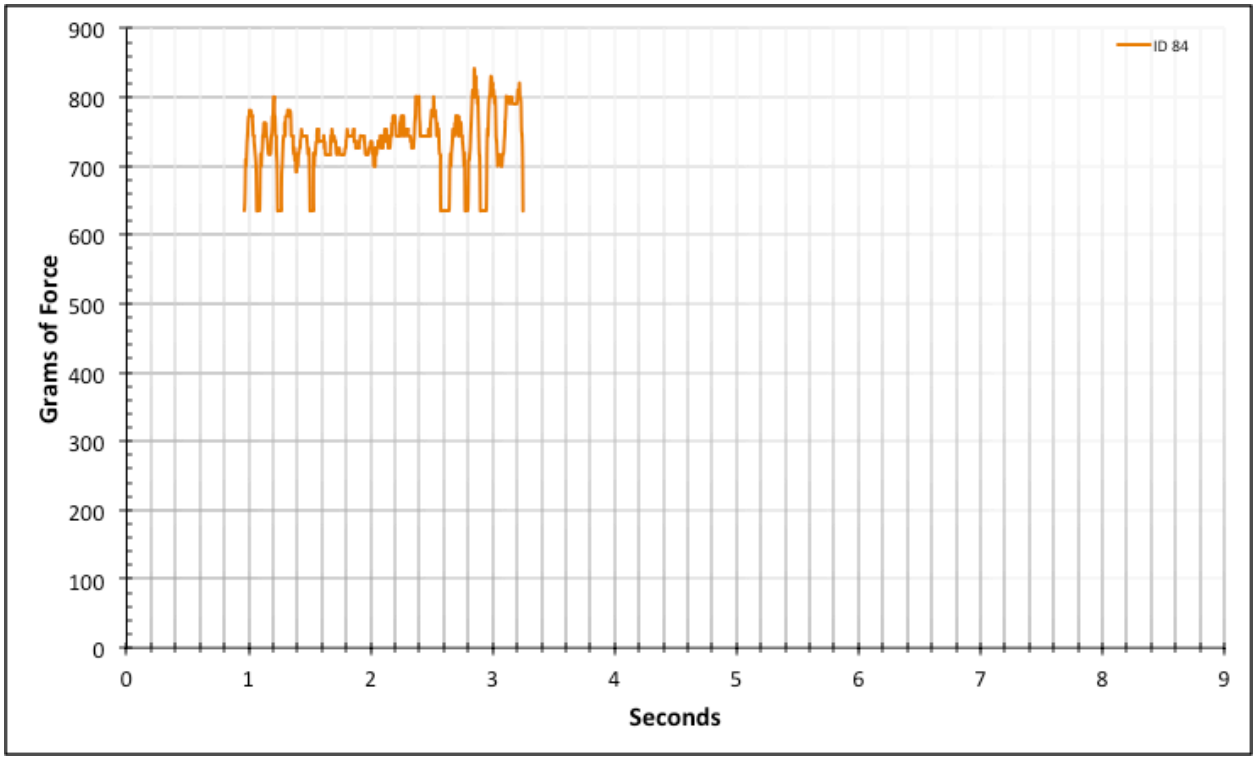

Figure A-6-164: Statistical Region Modeled Product - Dry - ID 84 - #8, Bolt 3

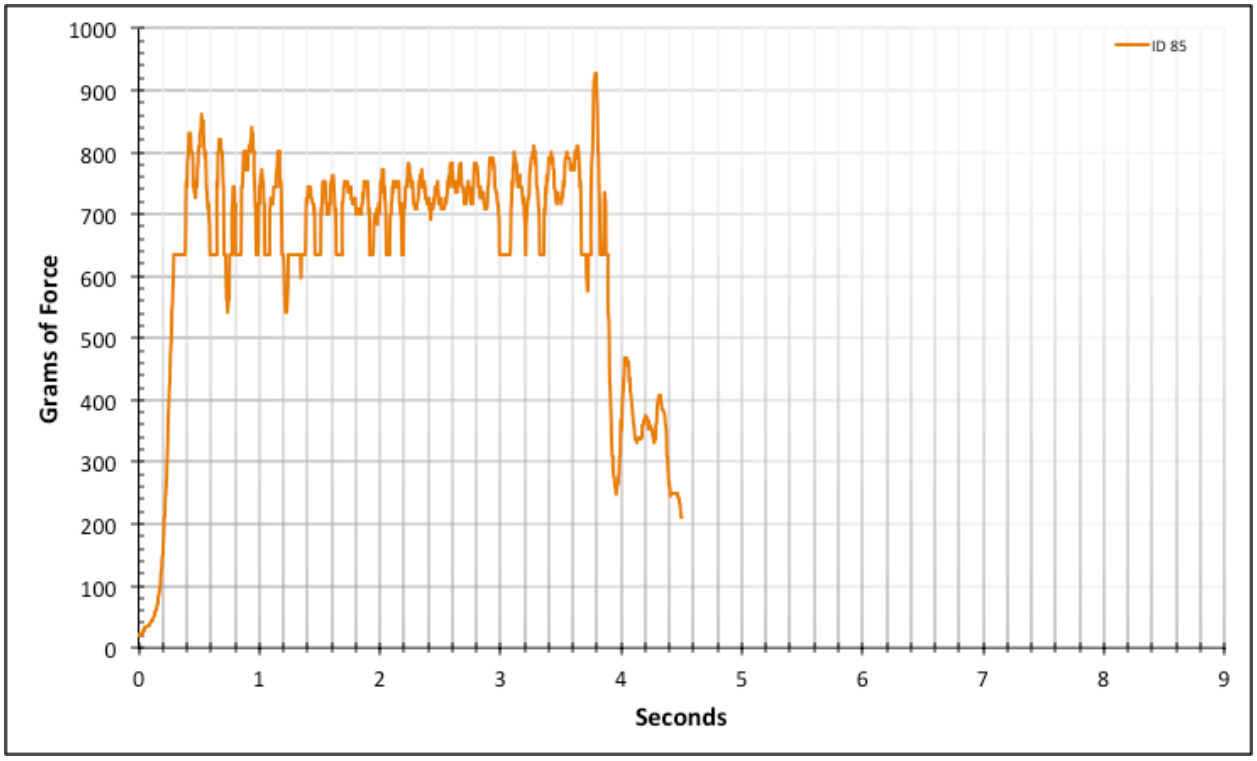

Figure A-6-165: Full Modeled Product - Dry - ID 85 - #8, Bolt 3

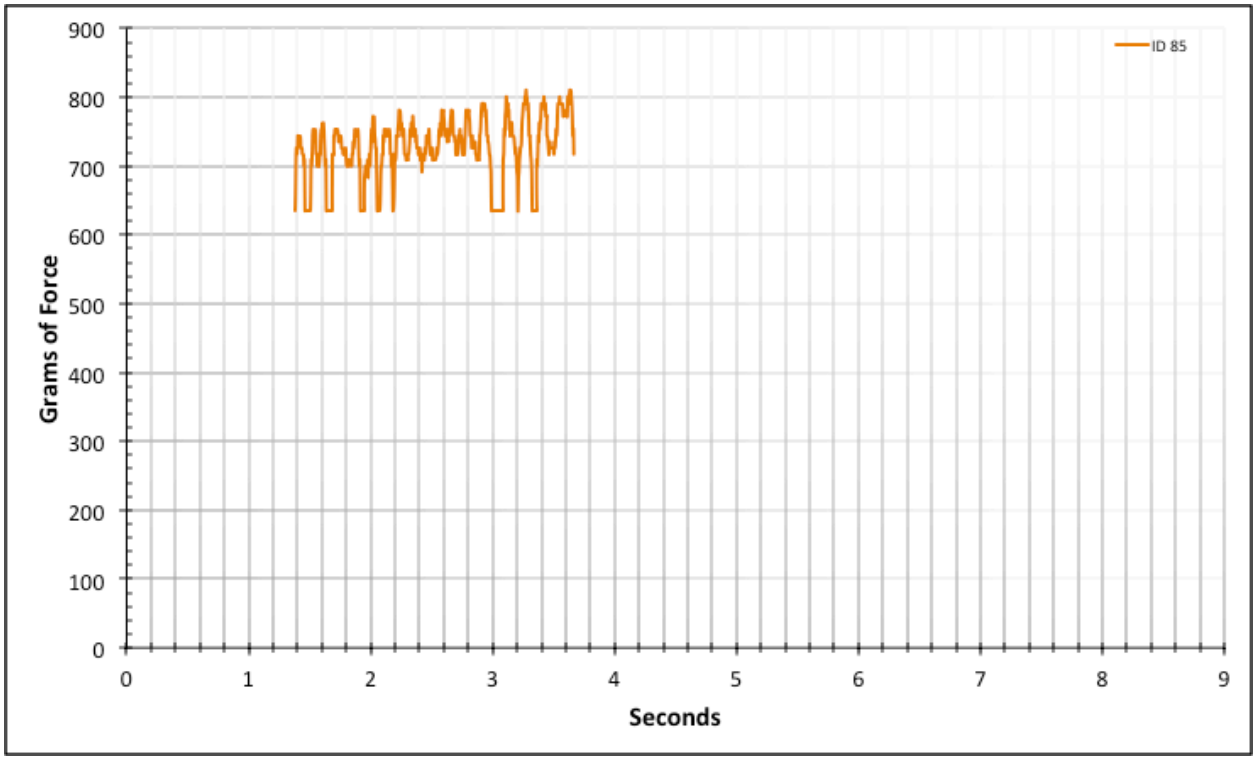

Figure A-6-166: Statistical Region Modeled Product - Dry - ID 85 - #8, Bolt 3

A.3. Straight Baseline – Dry

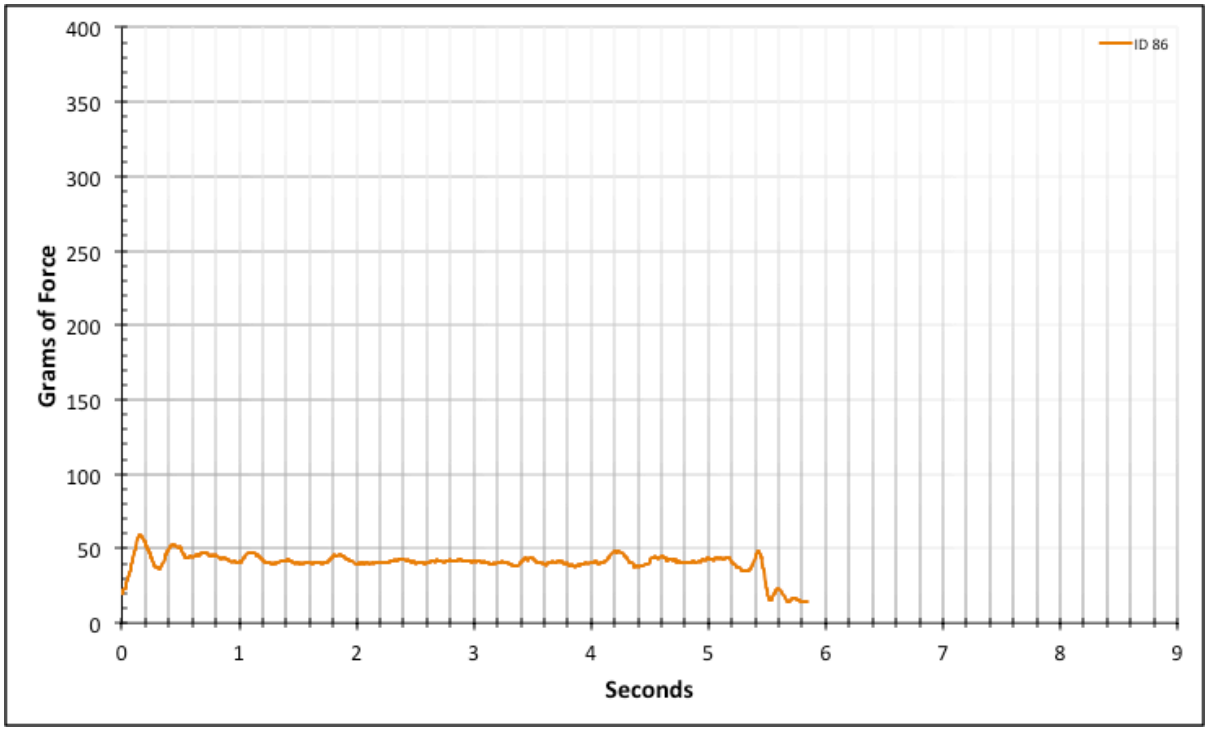

Figure A-6-167: Full Straight Baseline - Dry - ID 86 - #12, Bolt 1

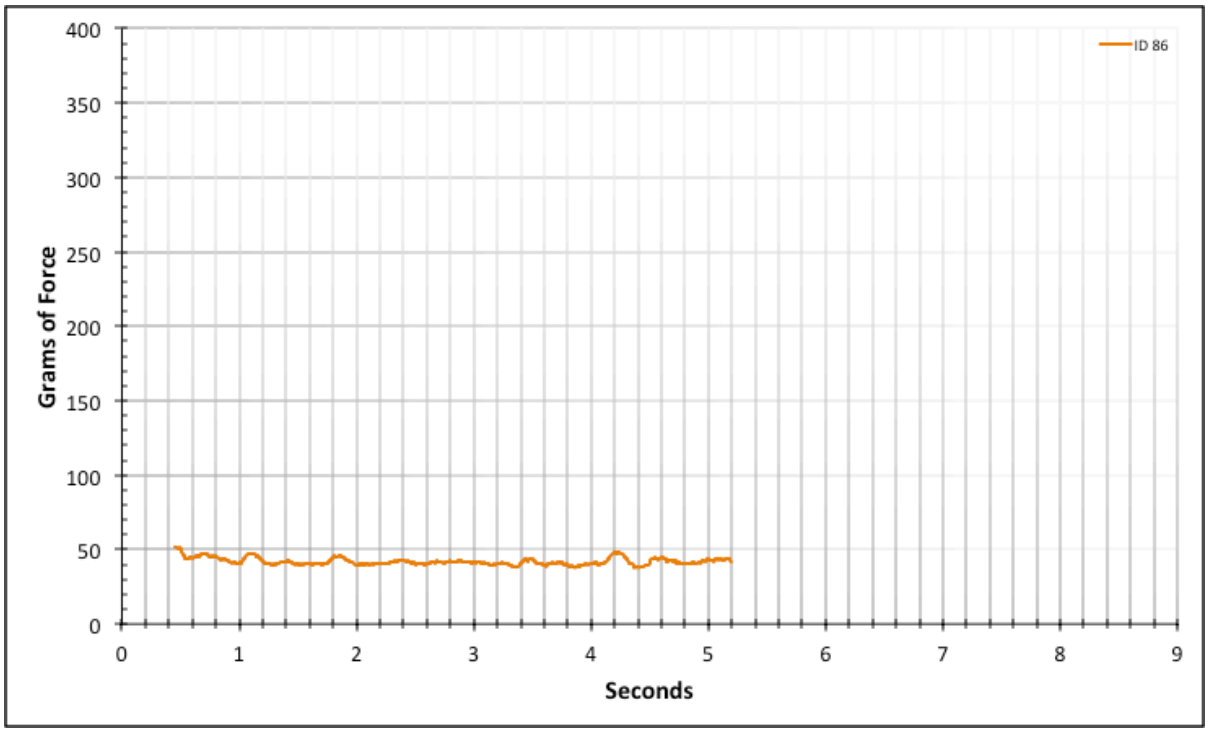

Figure A-6-168: Statistical Region Straight Baseline - Dry - ID 86 - #12, Bolt 1

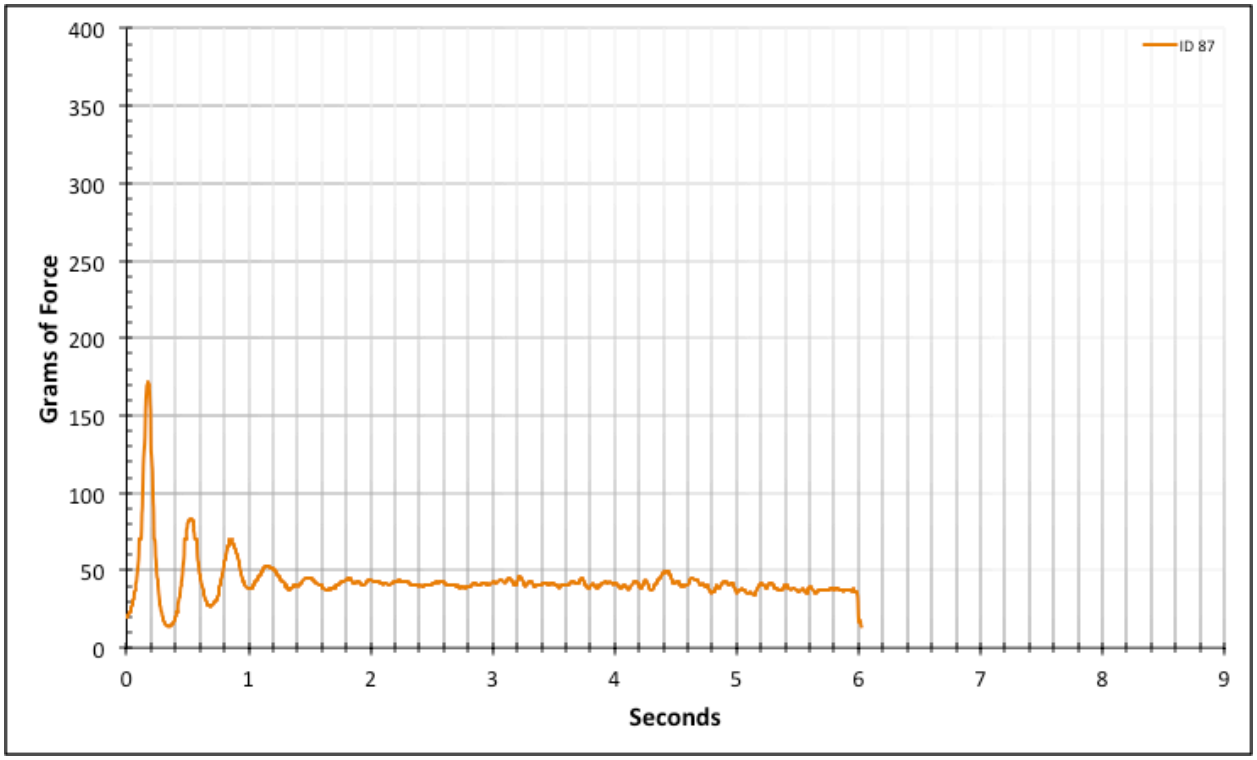

Figure A-6-169: Full Straight Baseline - Dry - ID 87 - #12, Bolt 1

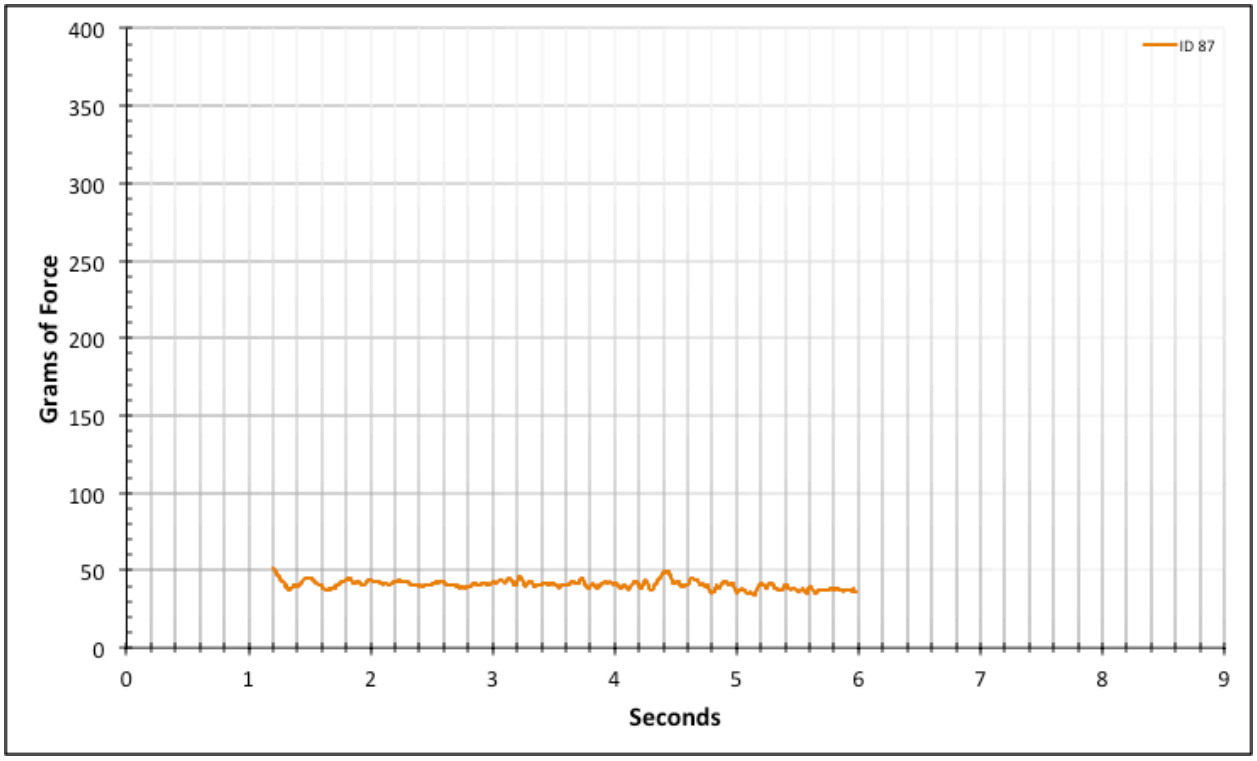

Figure A-6-170: Statistical Region Straight Baseline - Dry - ID 87 - #12, Bolt 1

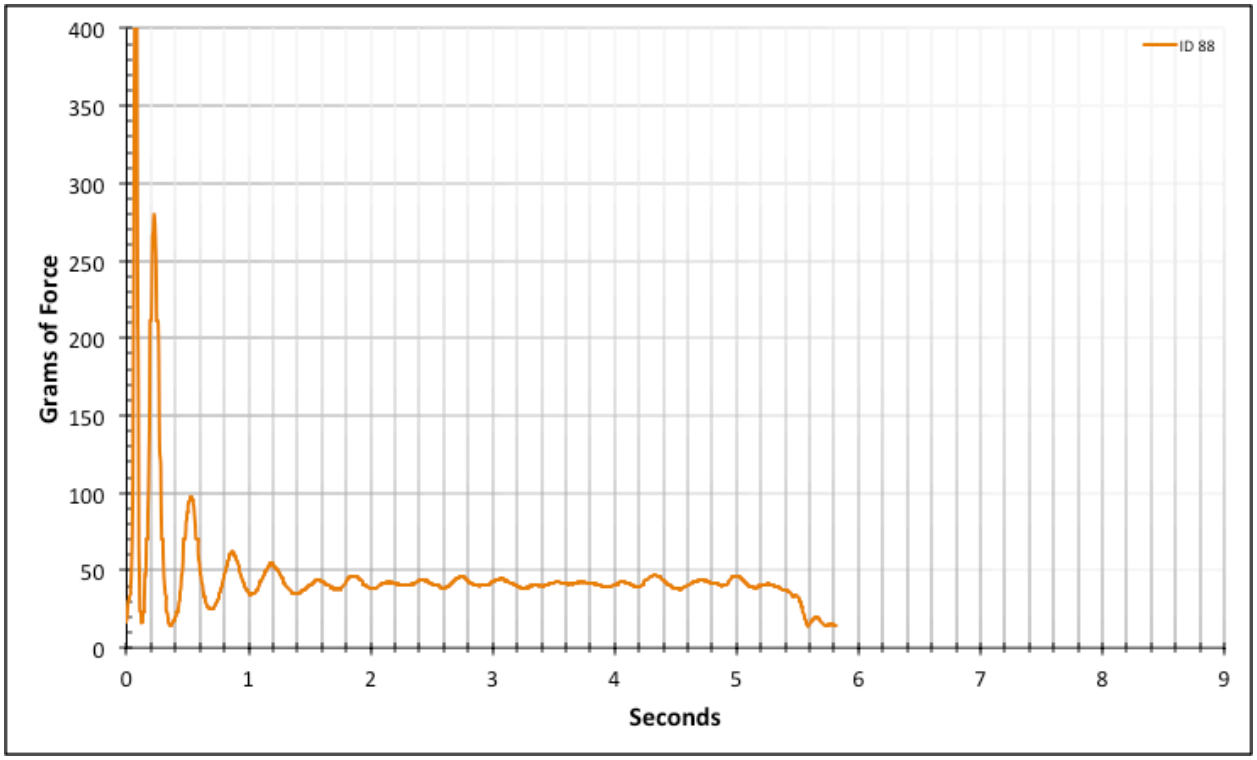

Figure A-6-171: Full Straight Baseline - Dry - ID 88 - #12, Bolt 1

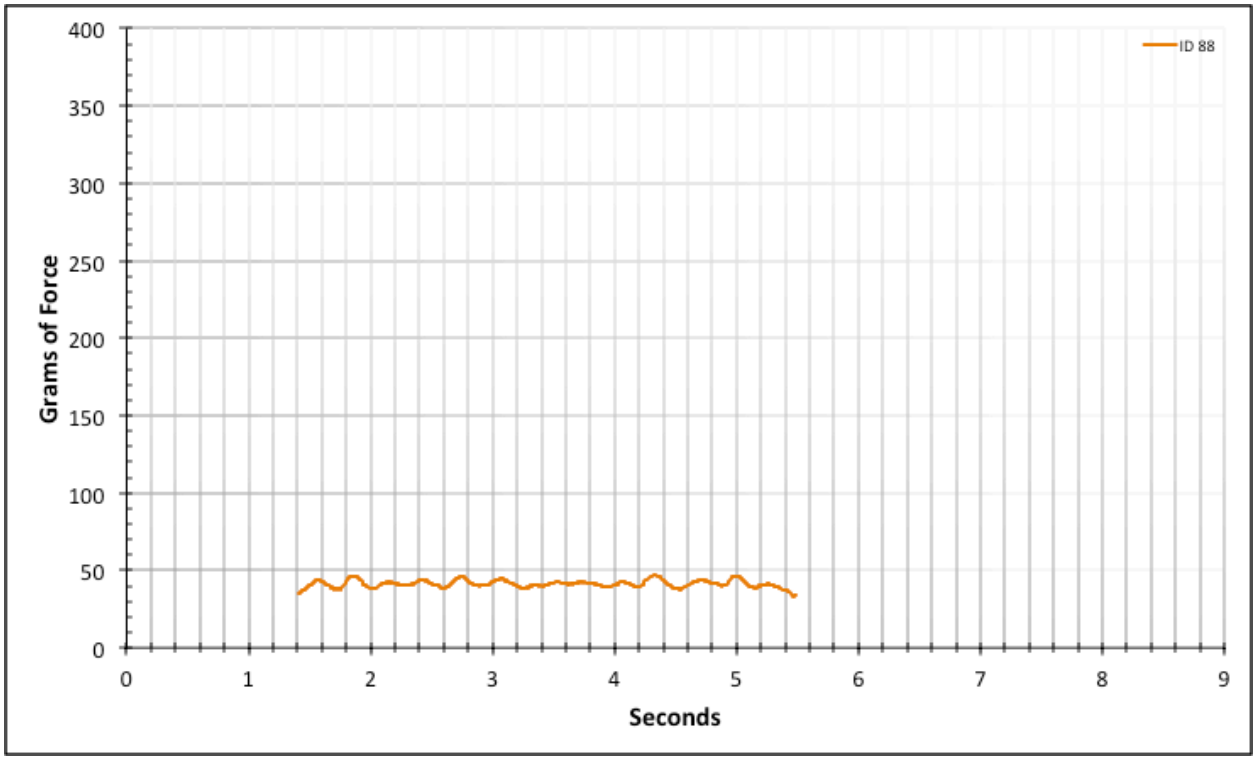

Figure A-6-172: Statistical Region Straight Baseline - Dry - ID 88 - #12, Bolt 1

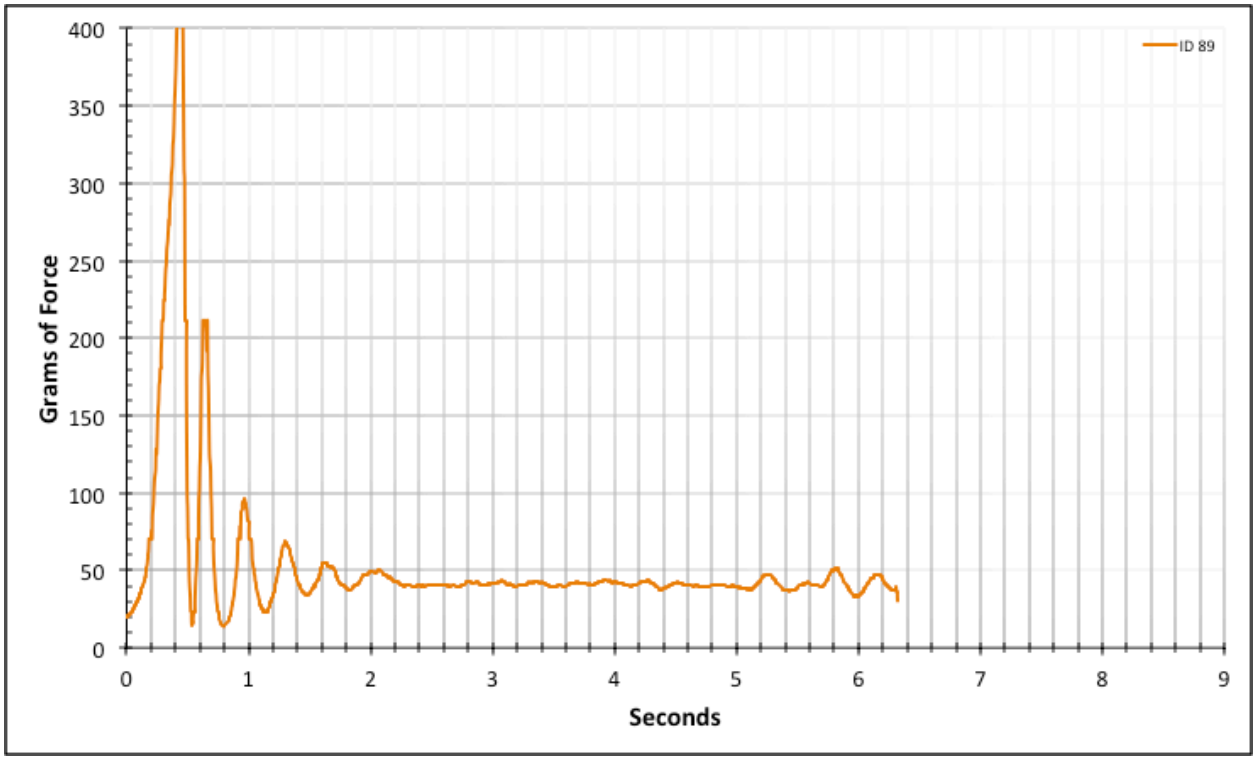

Figure A-6-173: Full Straight Baseline - Dry - ID 89 - #12, Bolt 1

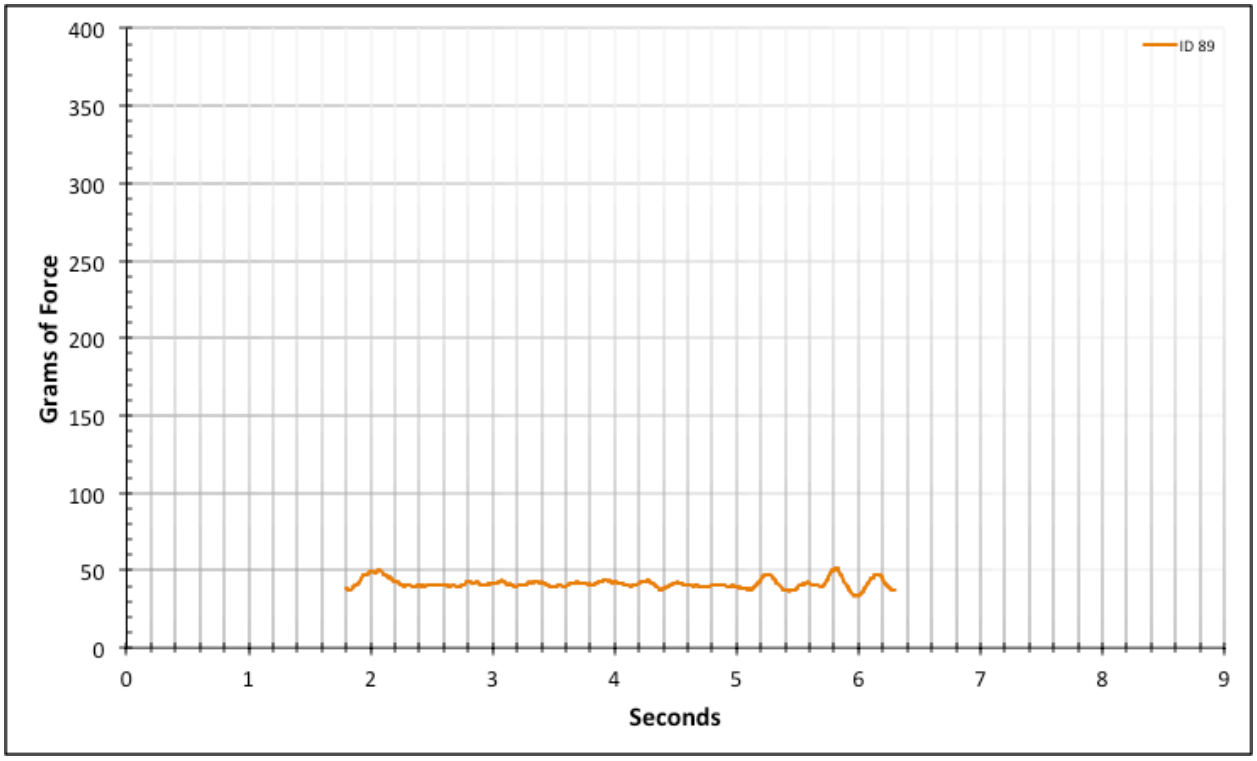

Figure A-6-174: Statistical Region Straight Baseline - Dry - ID 89 - #12, Bolt 1

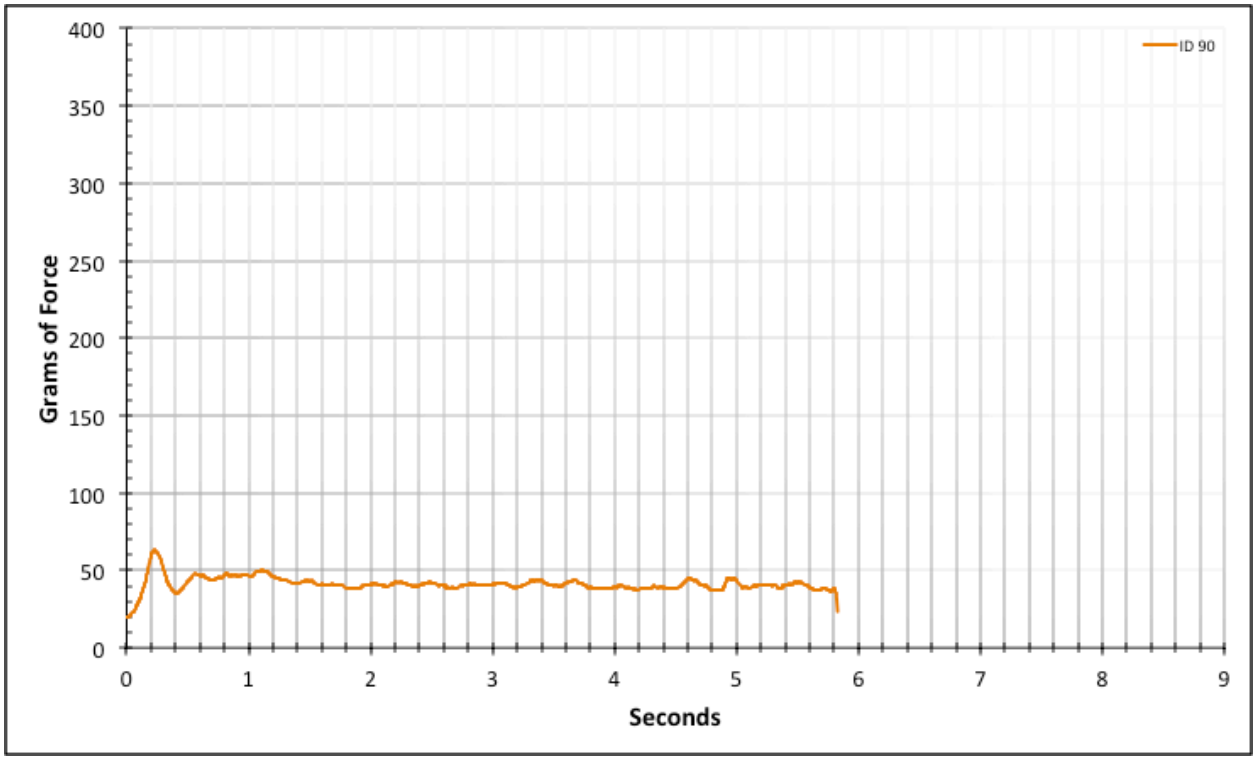

Figure A-6-175: Full Straight Baseline - Dry - ID 90 - #12, Bolt 1

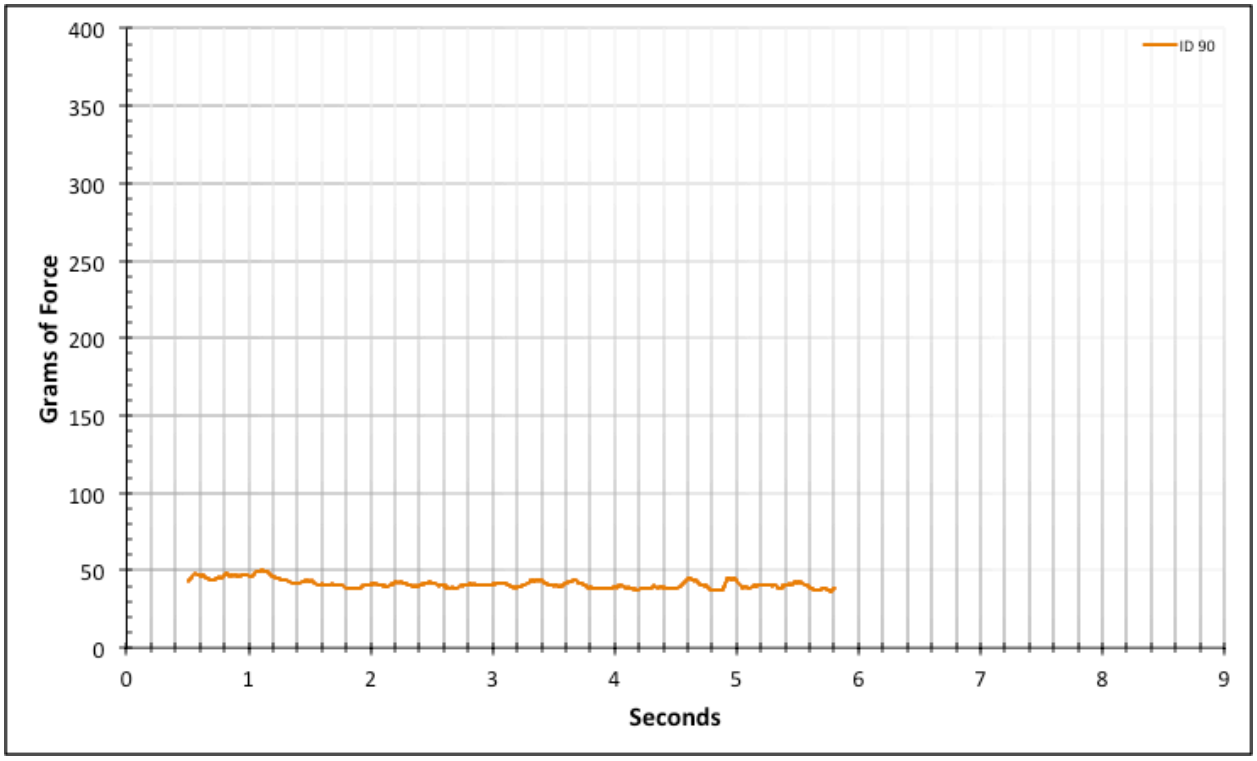

Figure A-6-176: Statistical Region Straight Baseline - Dry - ID 90 - #12, Bolt 1

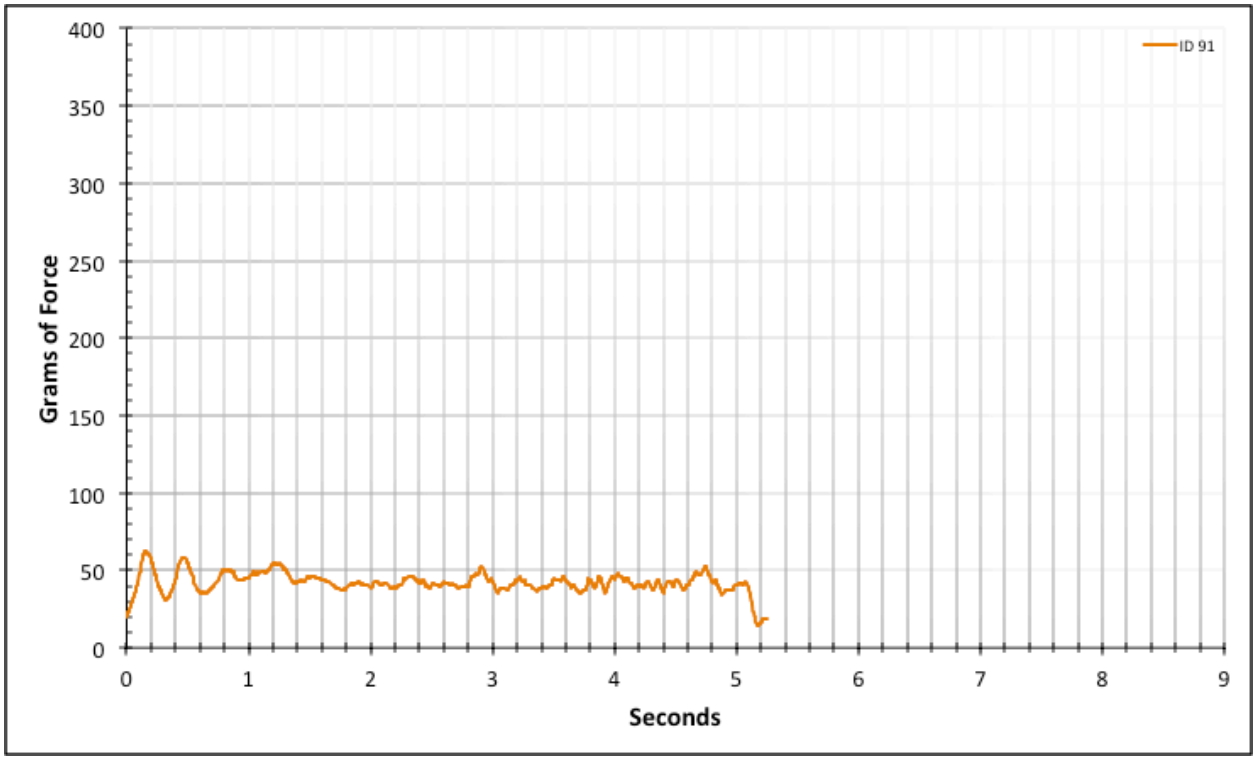

Figure A-6-177: Full Straight Baseline - Dry - ID 91 - #12, Bolt 2

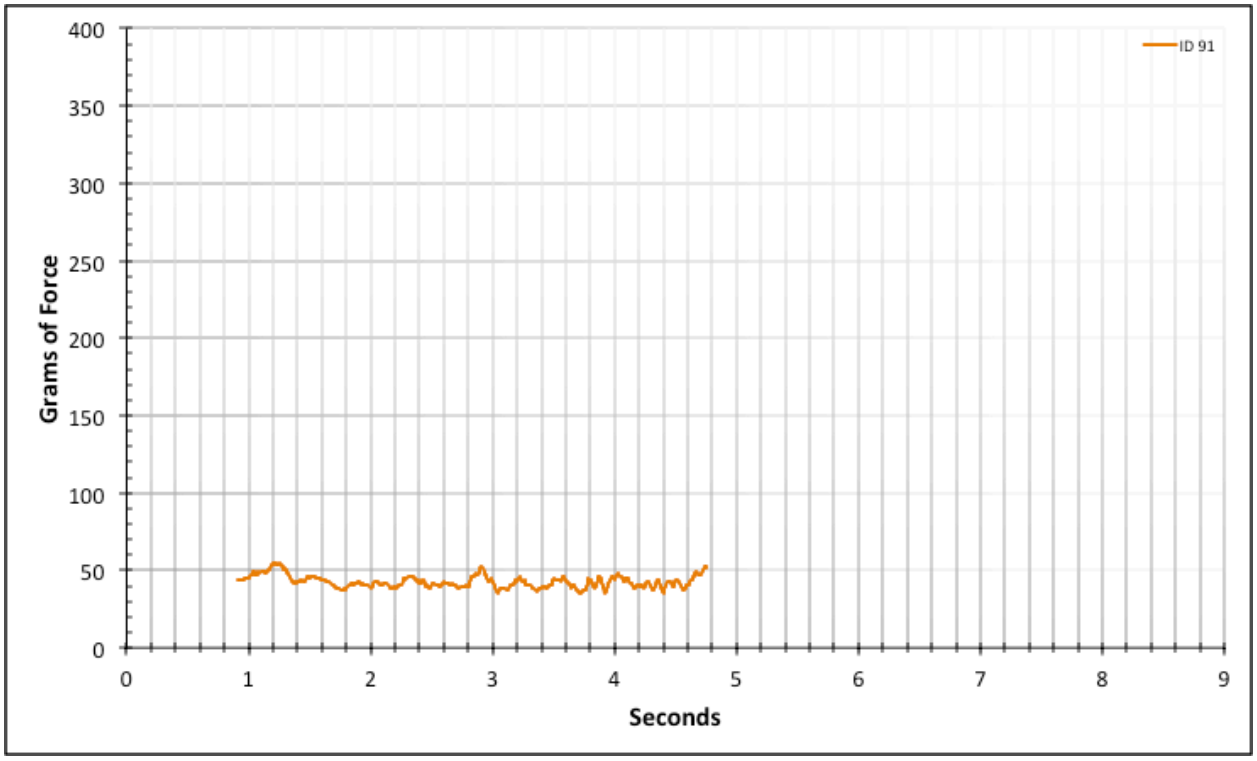

Figure A-6-178: Statistical Region Straight Baseline - Dry - ID 91 - #12, Bolt 2

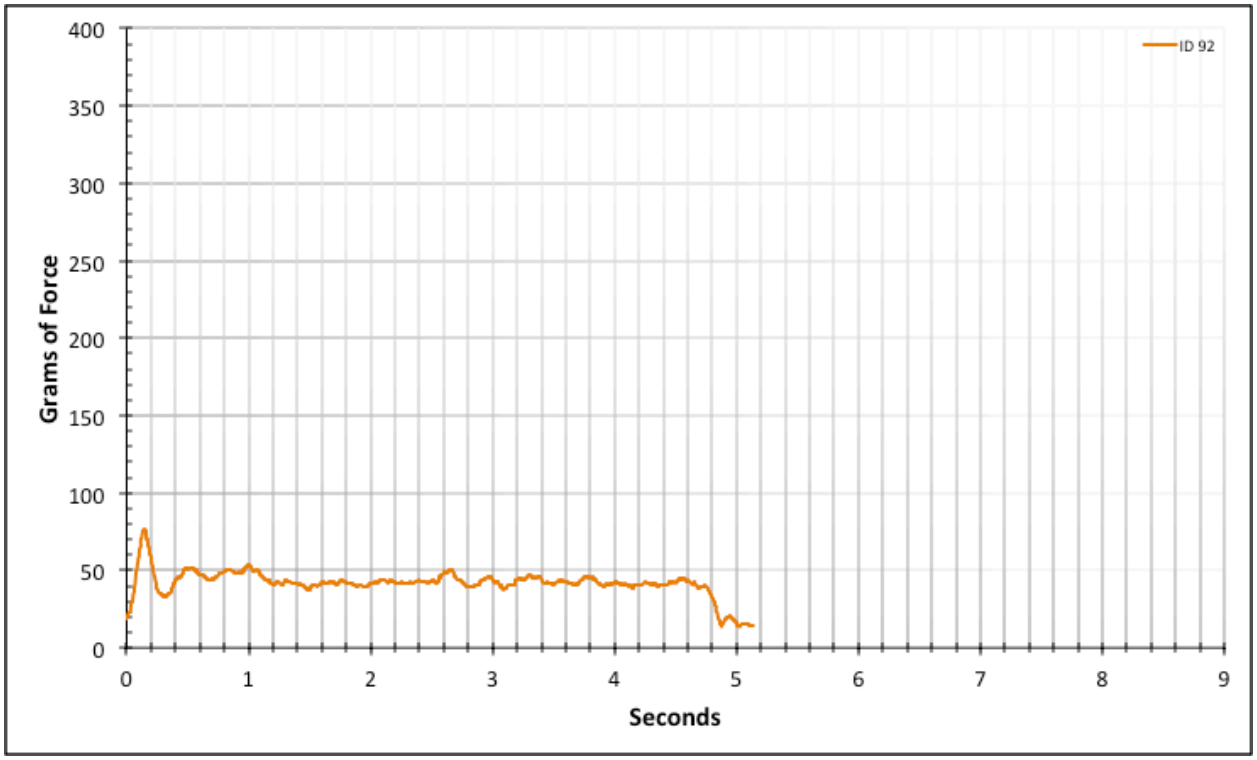

Figure A-6-179: Full Straight Baseline - Dry - ID 92 - #12, Bolt 2

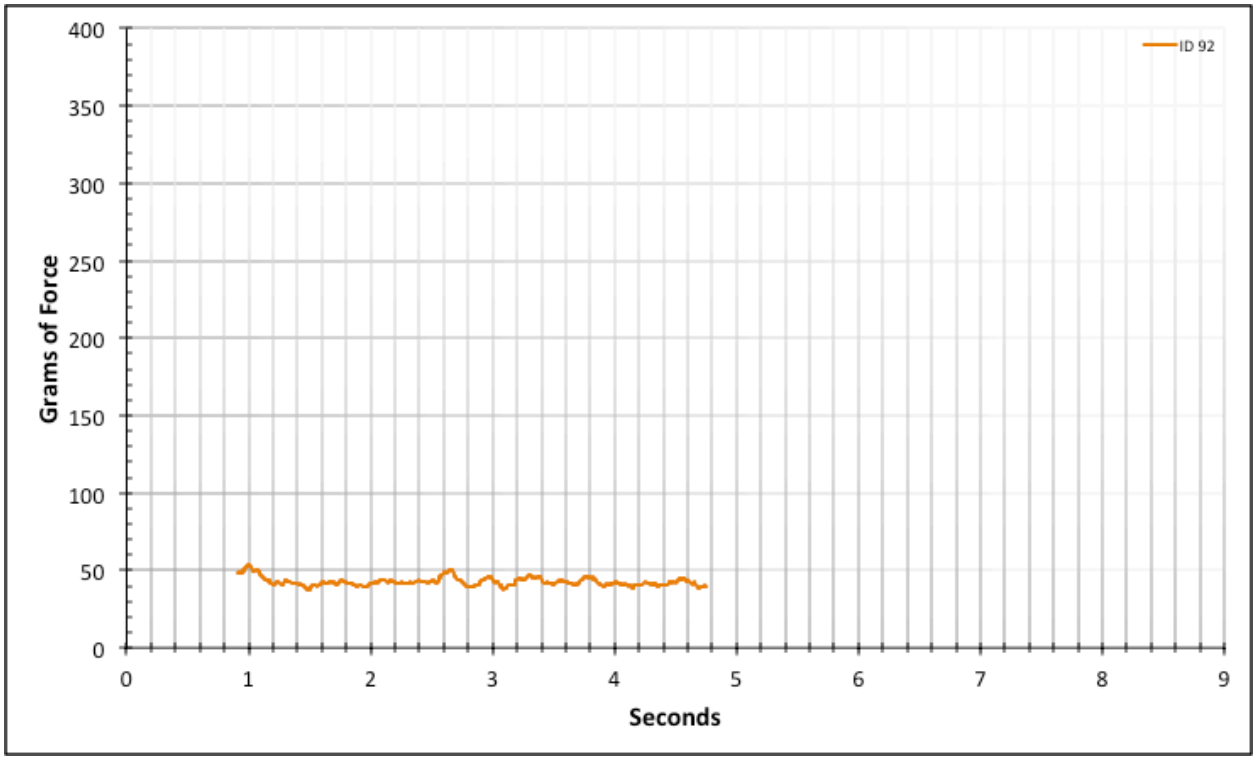

Figure A-6-180: Statistical Region Straight Baseline - Dry - ID 92 - #12, Bolt 2

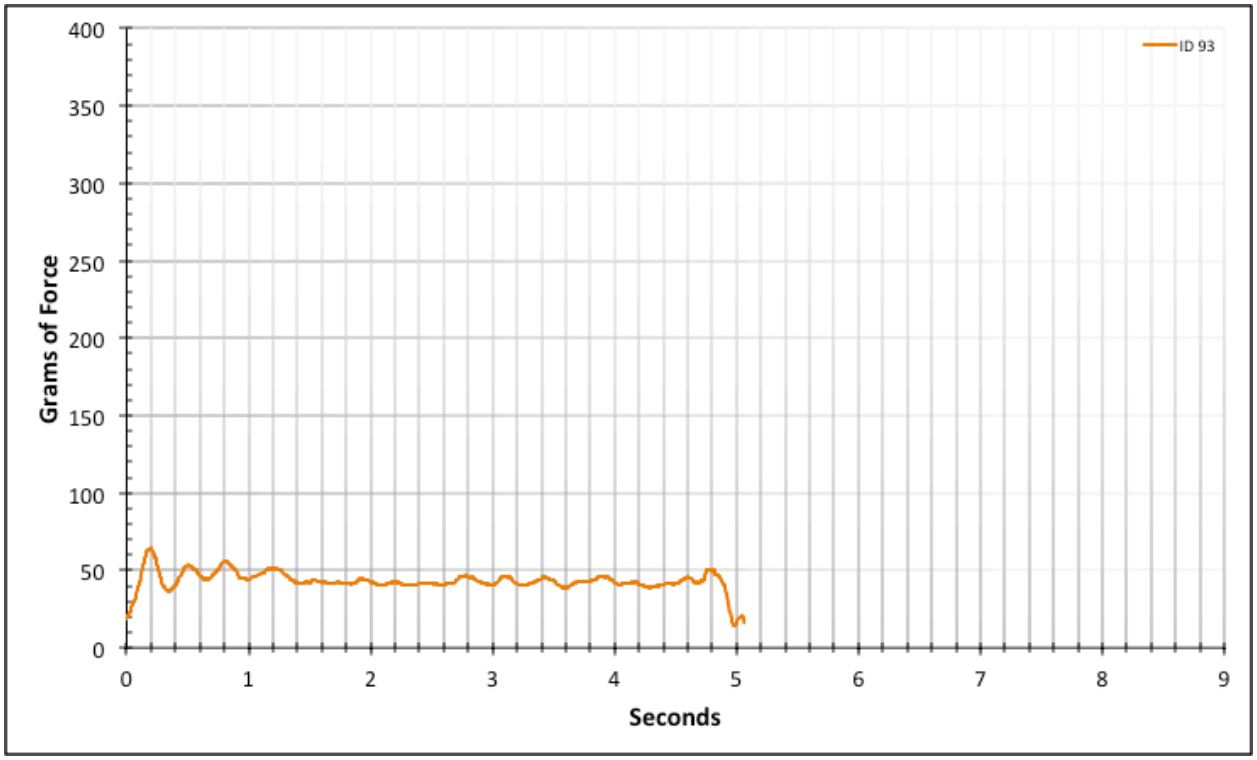

Figure A-6-181: Full Straight Baseline - Dry - ID 93 - #12, Bolt 2

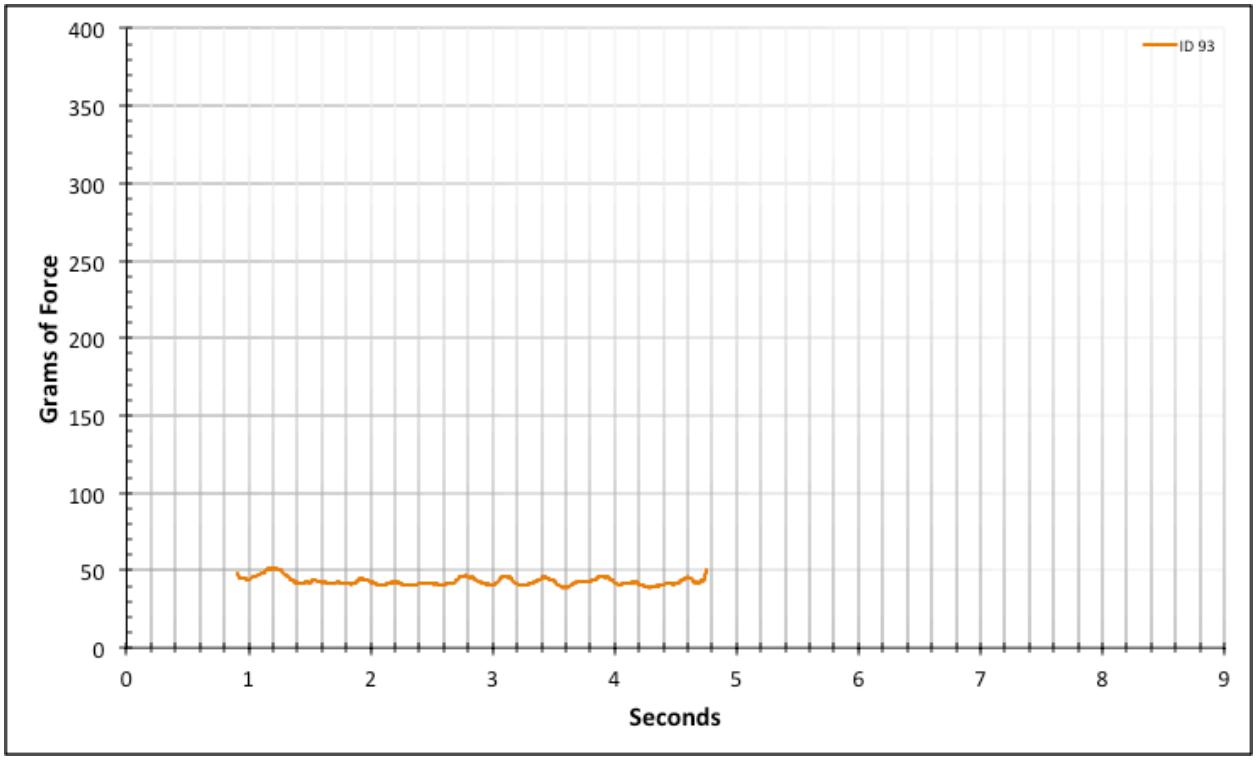

Figure A-6-182: Statistical Region Straight Baseline - Dry - ID 93 - #12, Bolt 2

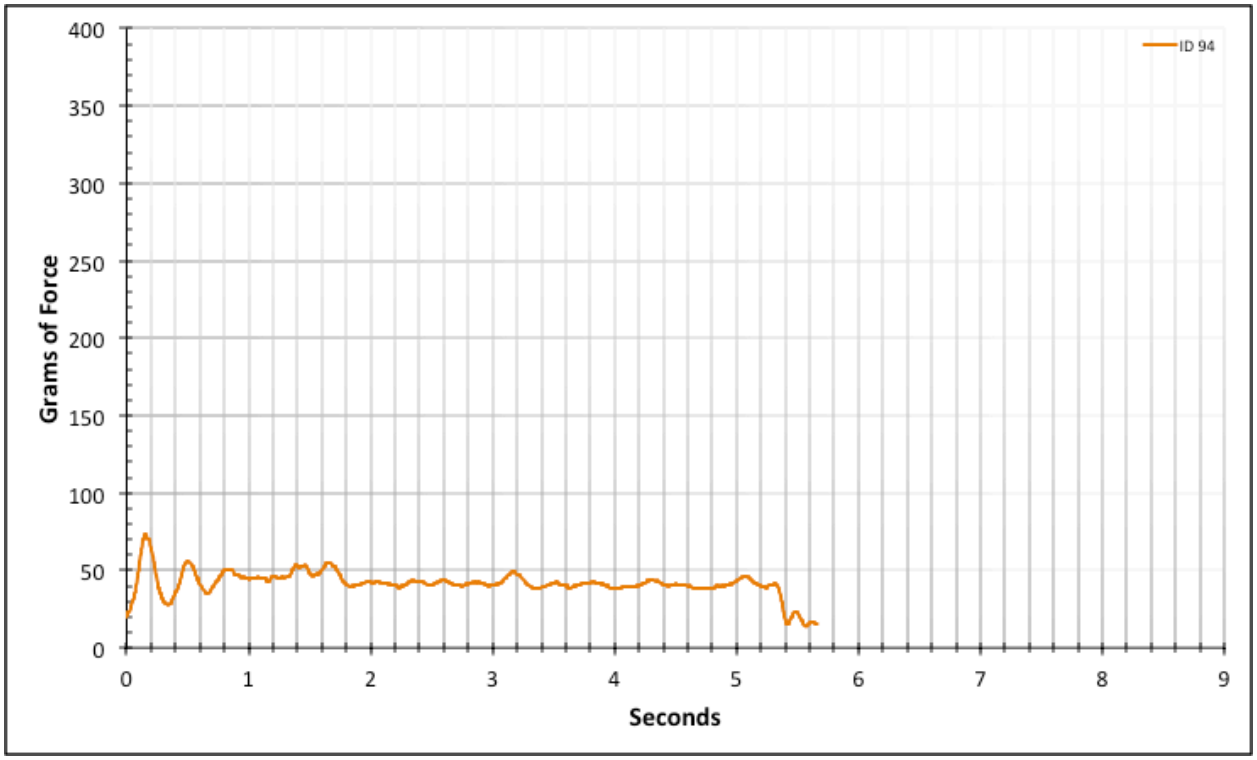

Figure A-6-183: Full Straight Baseline - Dry - ID 94 - #12, Bolt 2

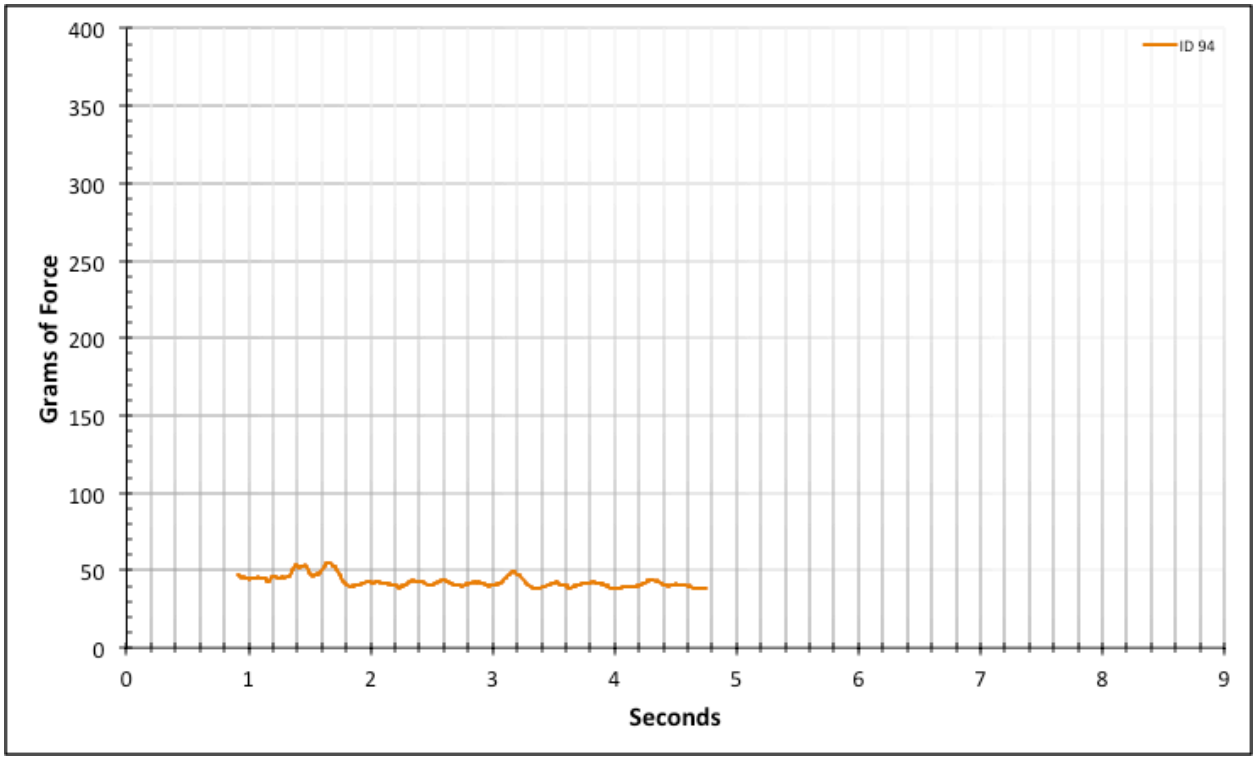

Figure A-6-184: Statistical Region Straight Baseline - Dry - ID 94 - #12, Bolt 2

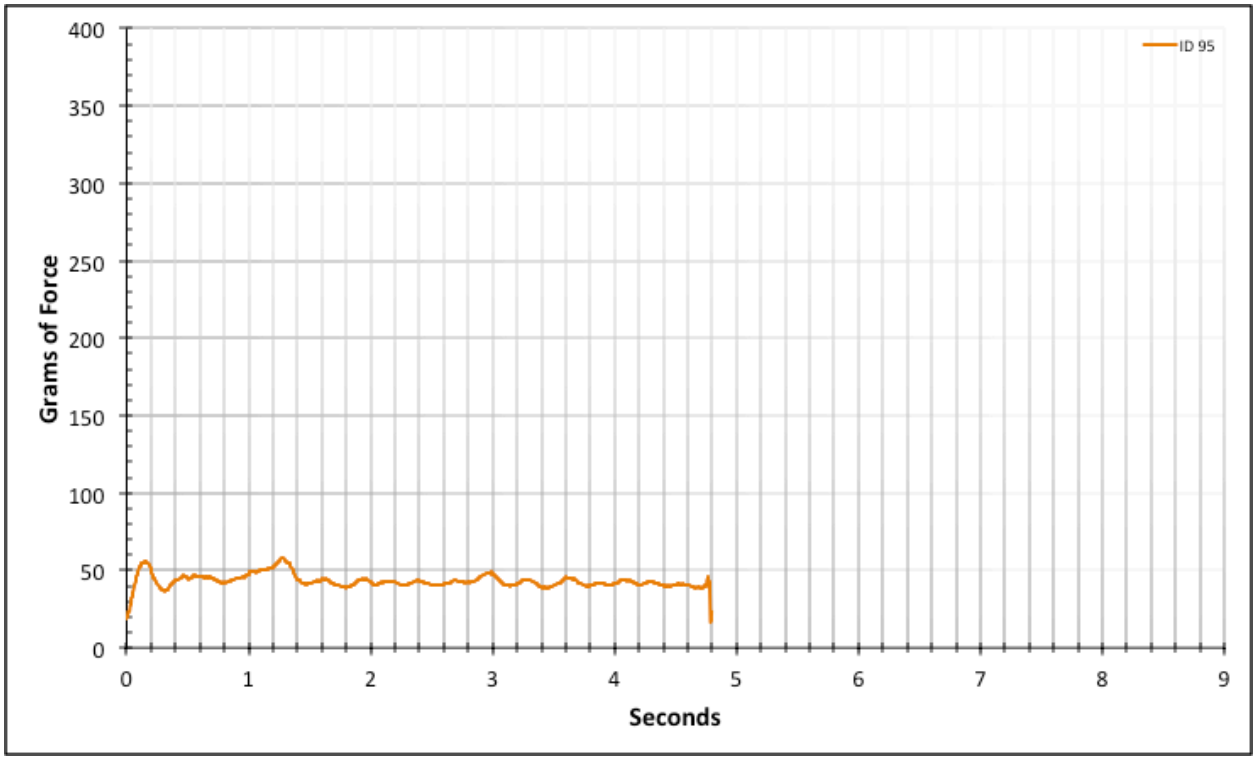

Figure A-6-185: Full Straight Baseline - Dry - ID 95 - #12, Bolt 2

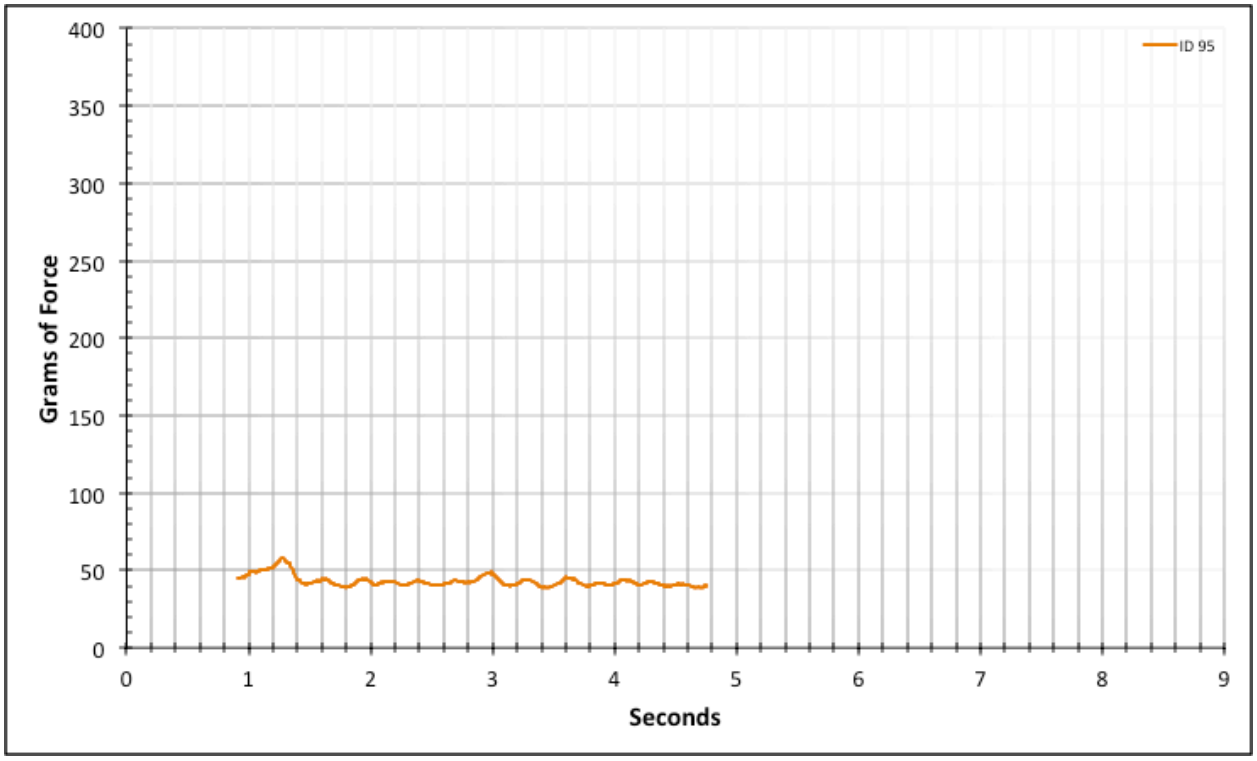

Figure A-6-186: Statistical Region Straight Baseline - Dry - ID 95 - #12, Bolt 2

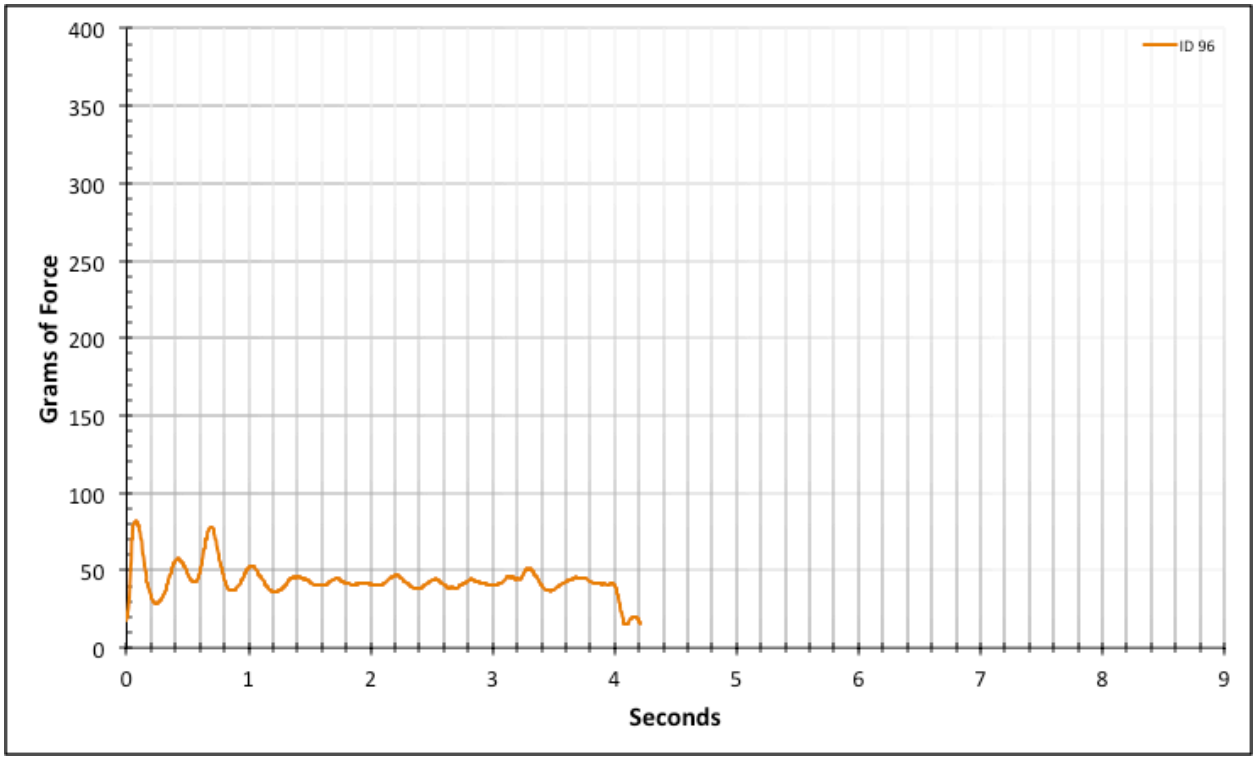

Figure A-6-187: Full Straight Baseline - Dry - ID 96 - #12, Bolt 3

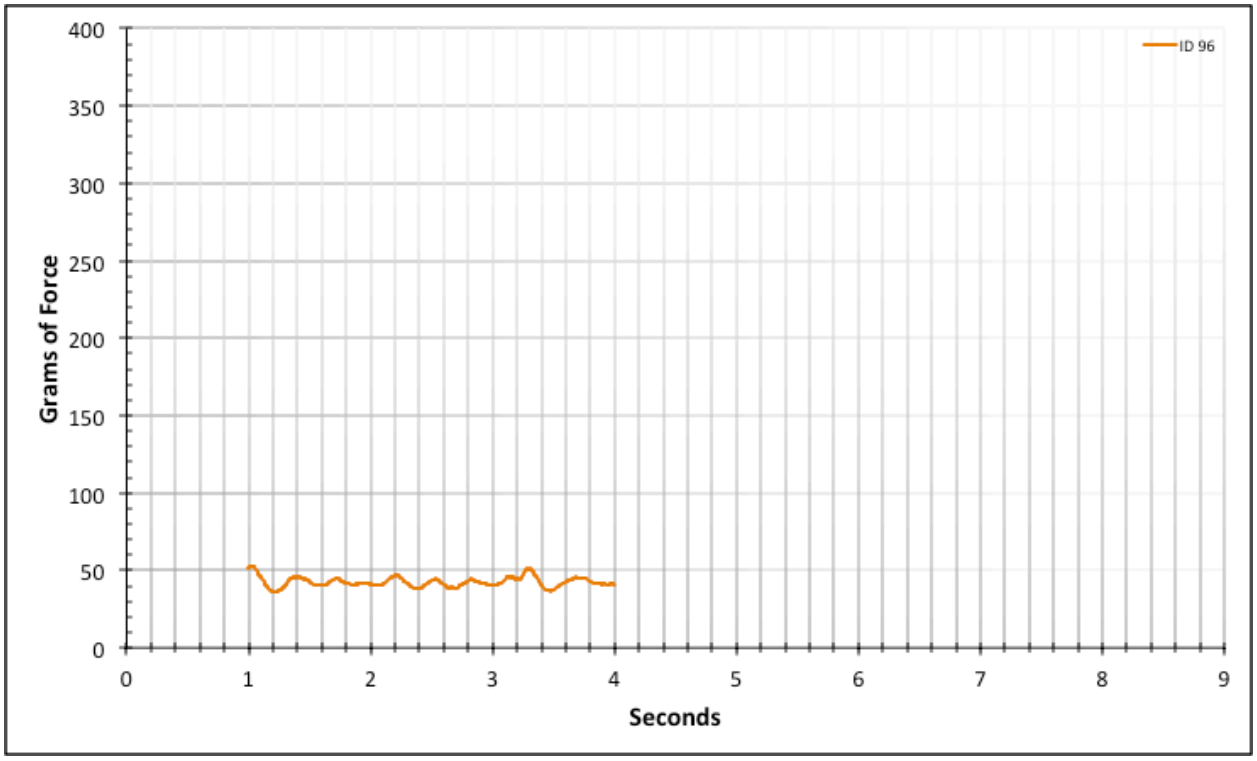

Figure A-6-188: Statistical Region Straight Baseline - Dry - ID 96 - #12, Bolt 3

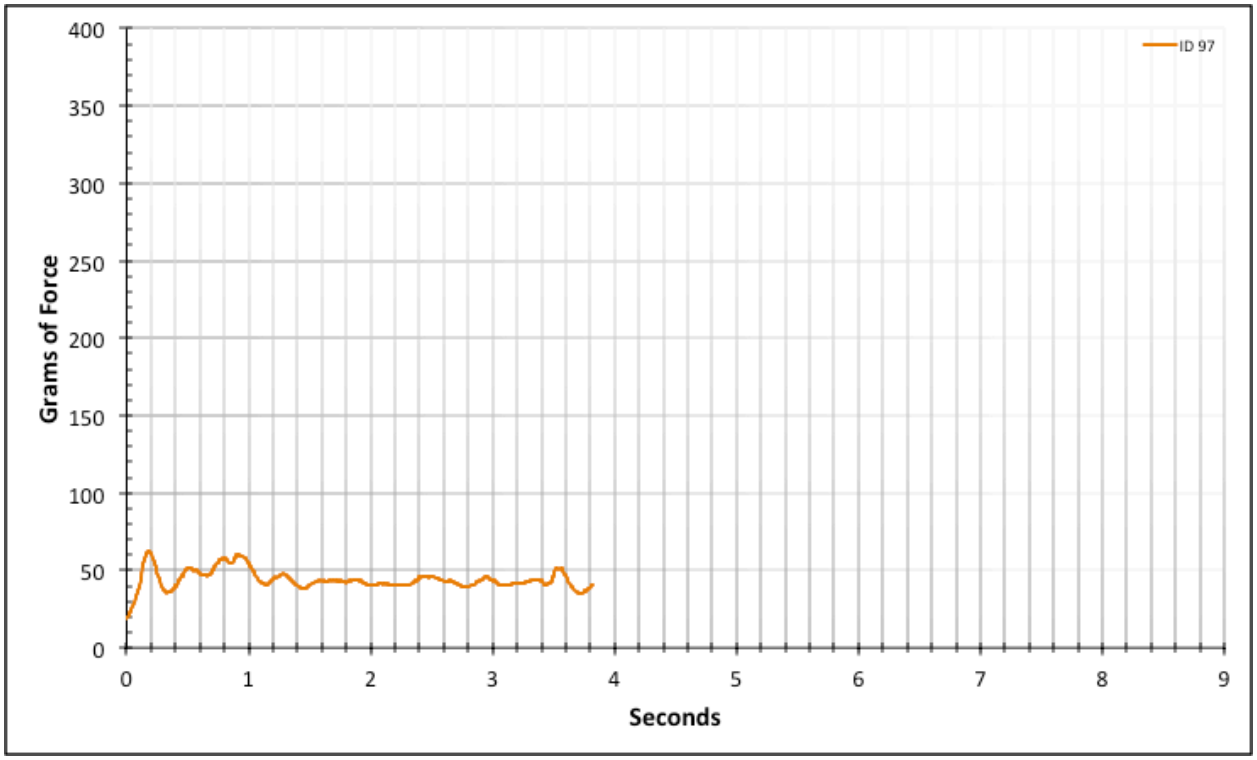

Figure A-6-189: Full Straight Baseline - Dry - ID 97 - #12, Bolt 3

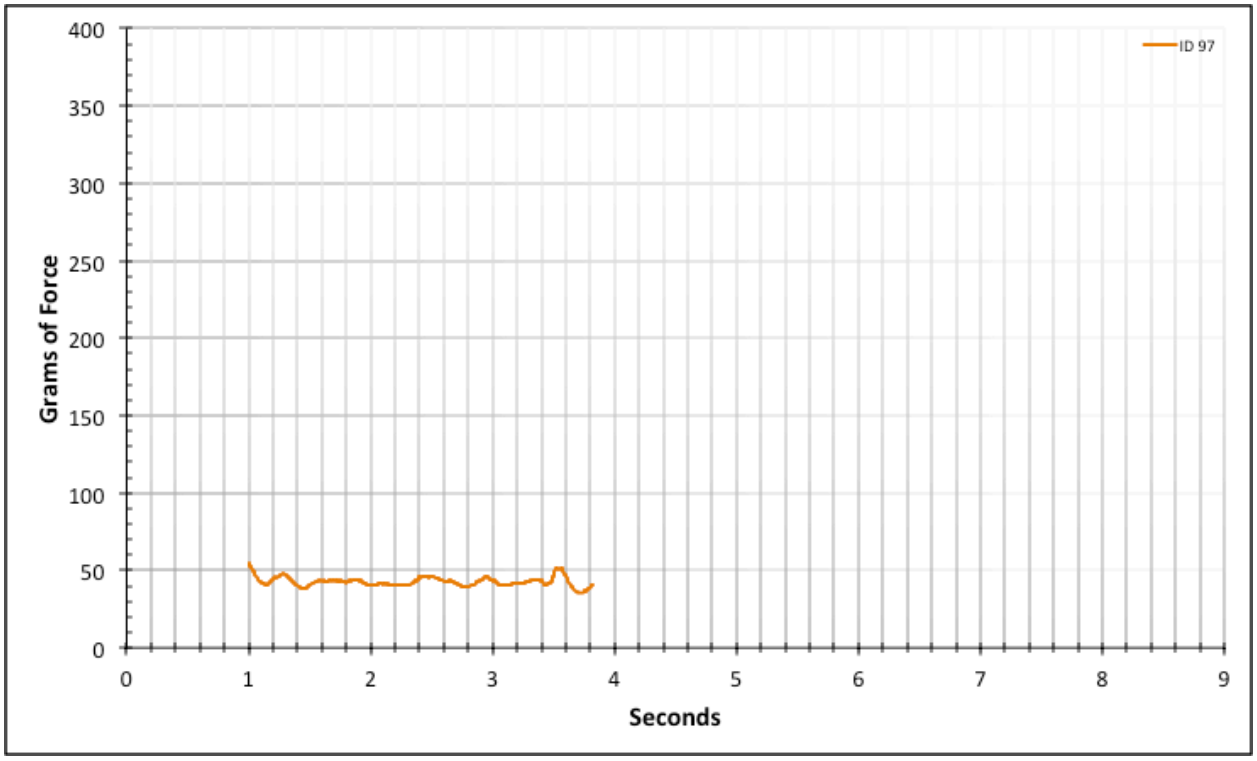

Figure A-6-190: Statistical Region Straight Baseline - Dry - ID 97 - #12, Bolt 3

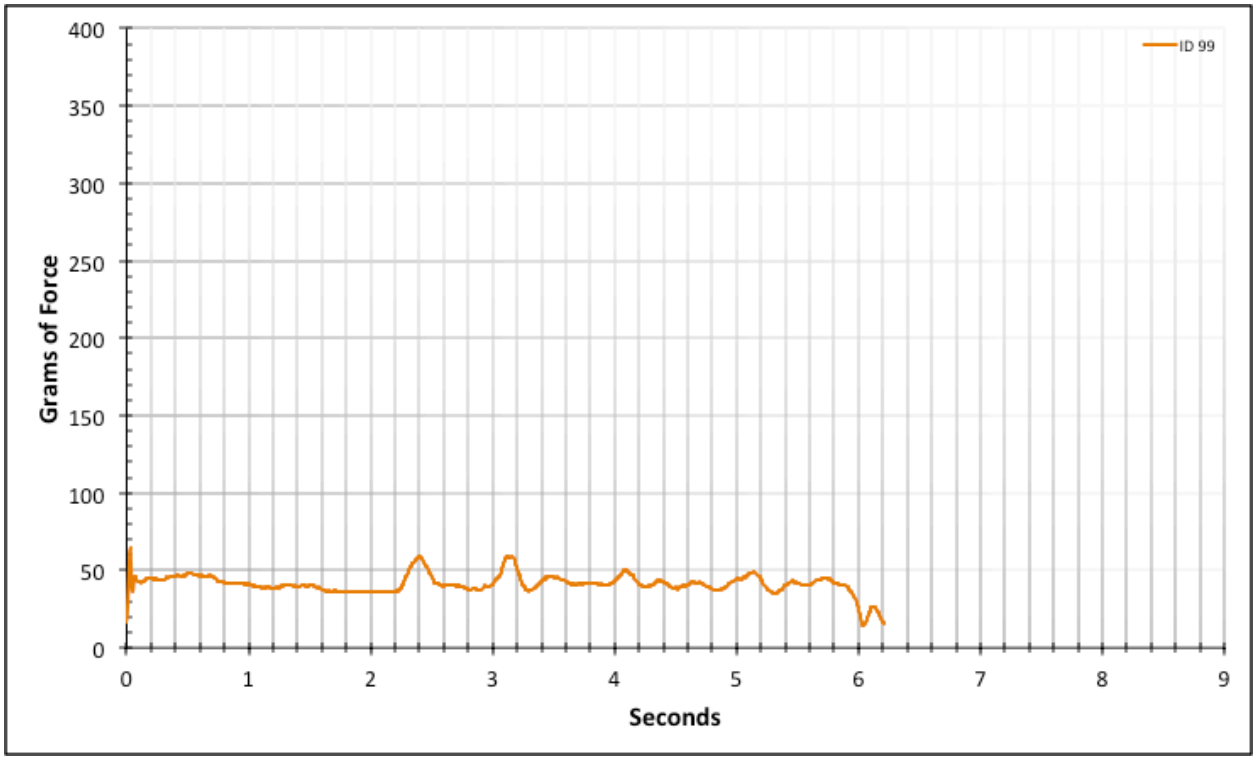

Figure A-6-191: Full Straight Baseline - Dry - ID 99 - #12, Bolt 3

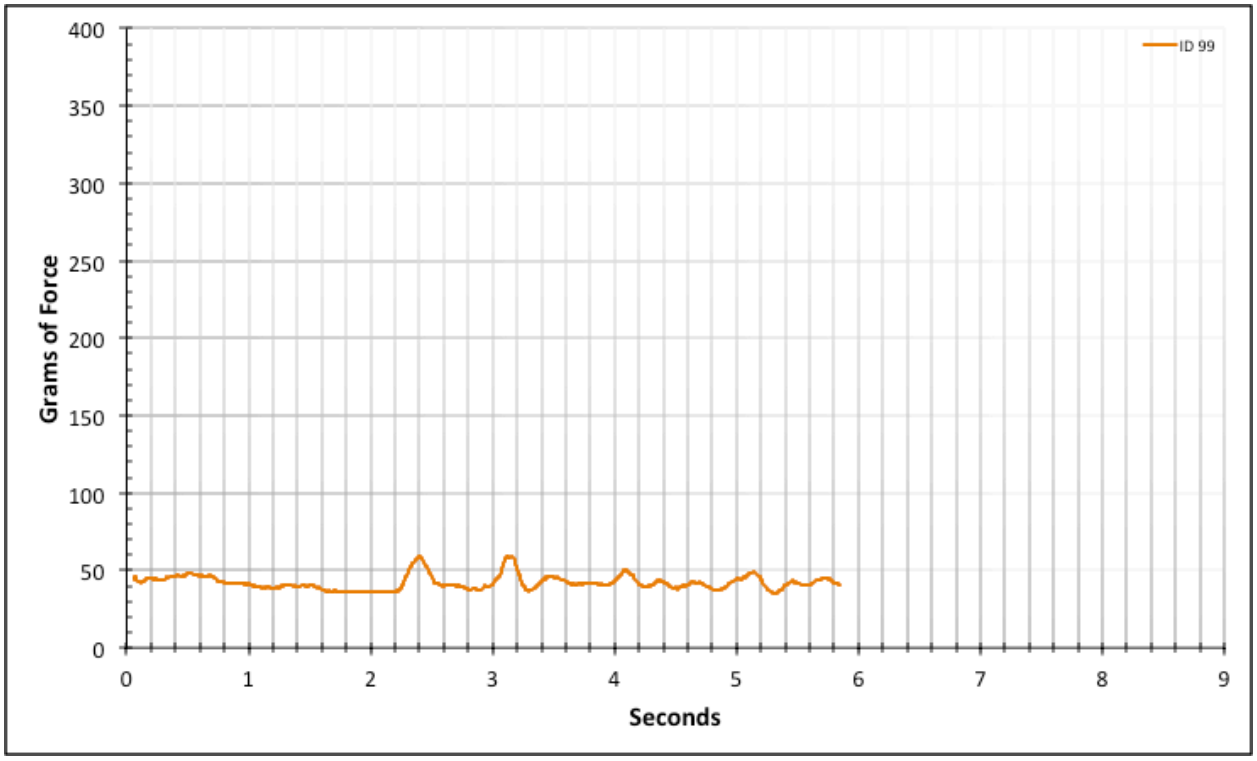

Figure A-6-192: Statistical Region Straight Baseline - Dry - ID 99 - #12, Bolt 3

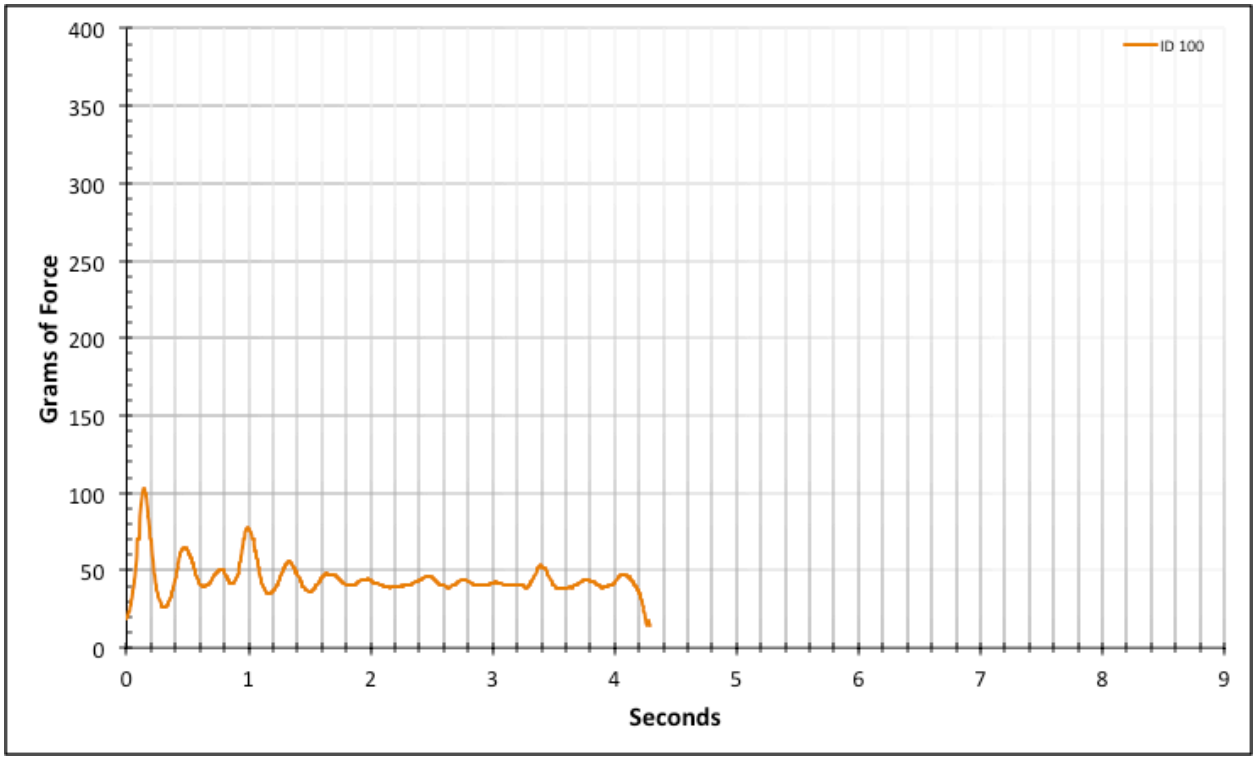

Figure A-6-193: Full Straight Baseline - Dry - ID 100 - #12, Bolt 3

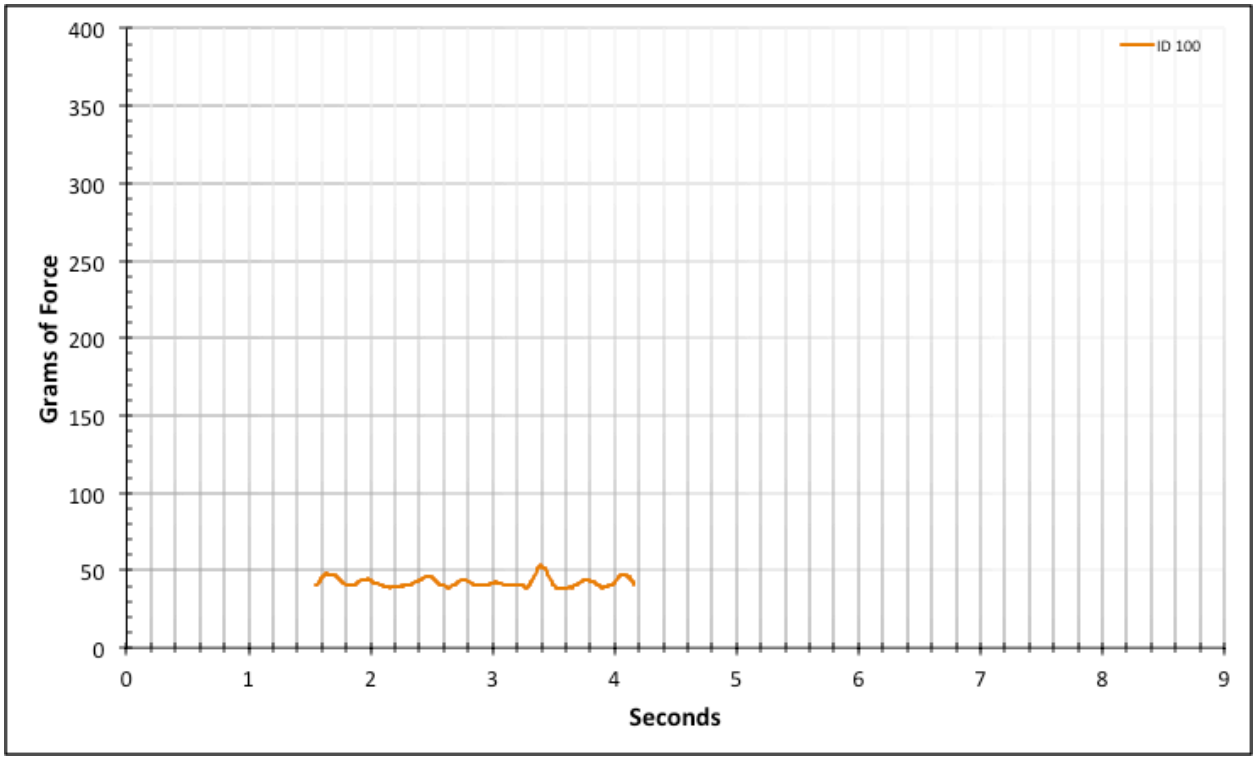

Figure A-6-194: Statistical Region Straight Baseline - Dry - ID 100 - #12, Bolt 3

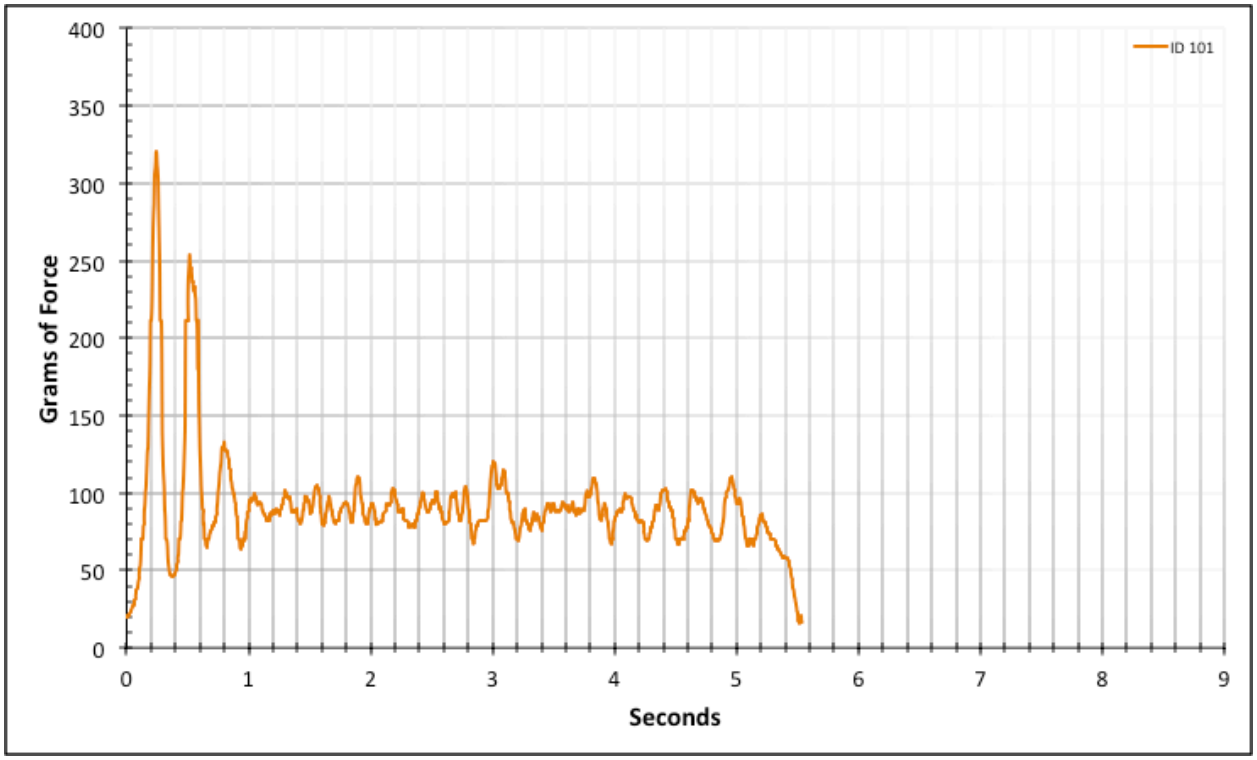

Figure A-6-195: Full Straight Baseline - Dry - ID 101 - #10, Bolt 1

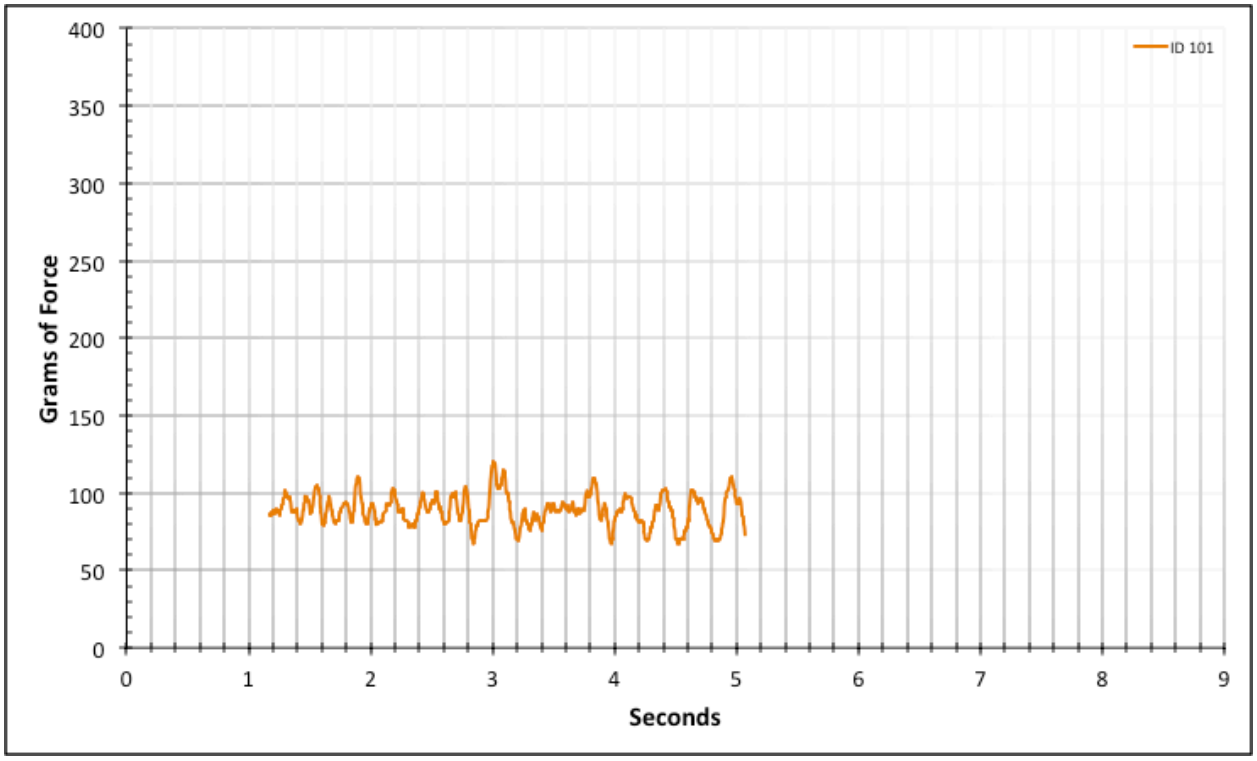

Figure A-6-196: Statistical Region Straight Baseline - Dry - ID 101 - #10, Bolt 1

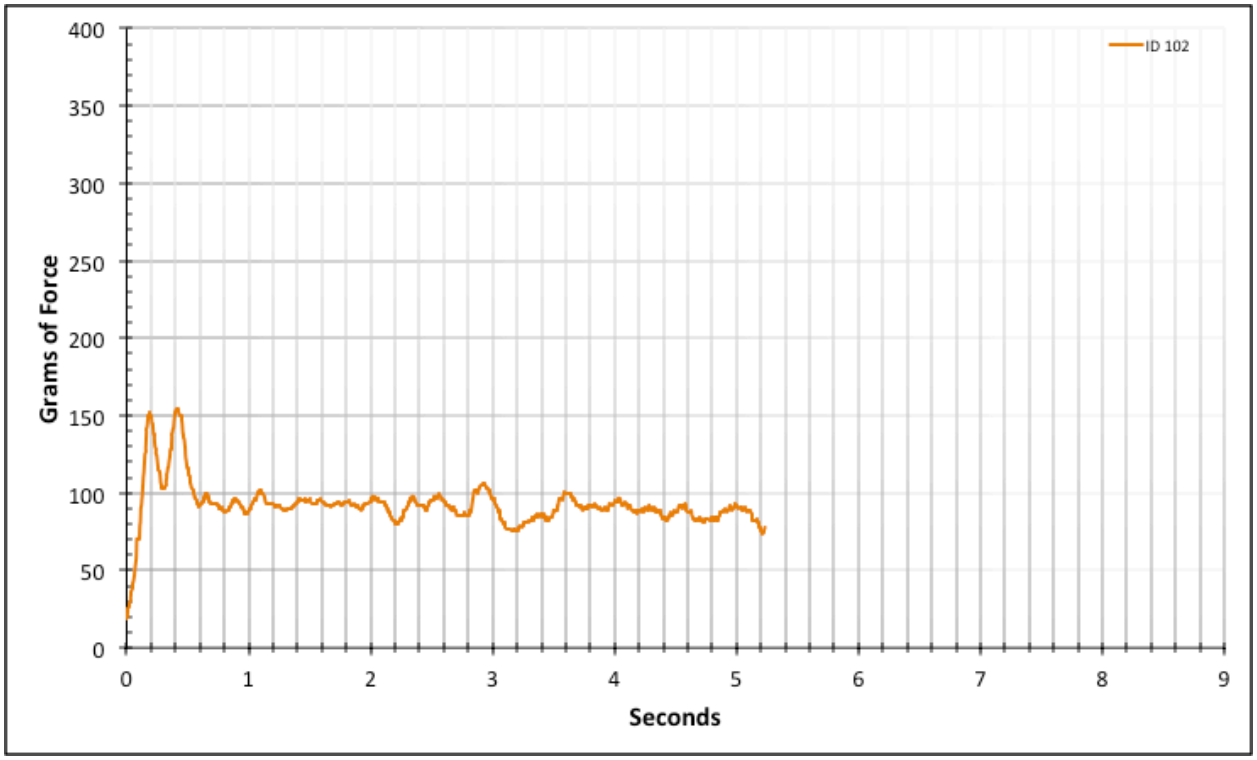

Figure A-6-197: Full Straight Baseline - Dry - ID 102 - #10, Bolt 1

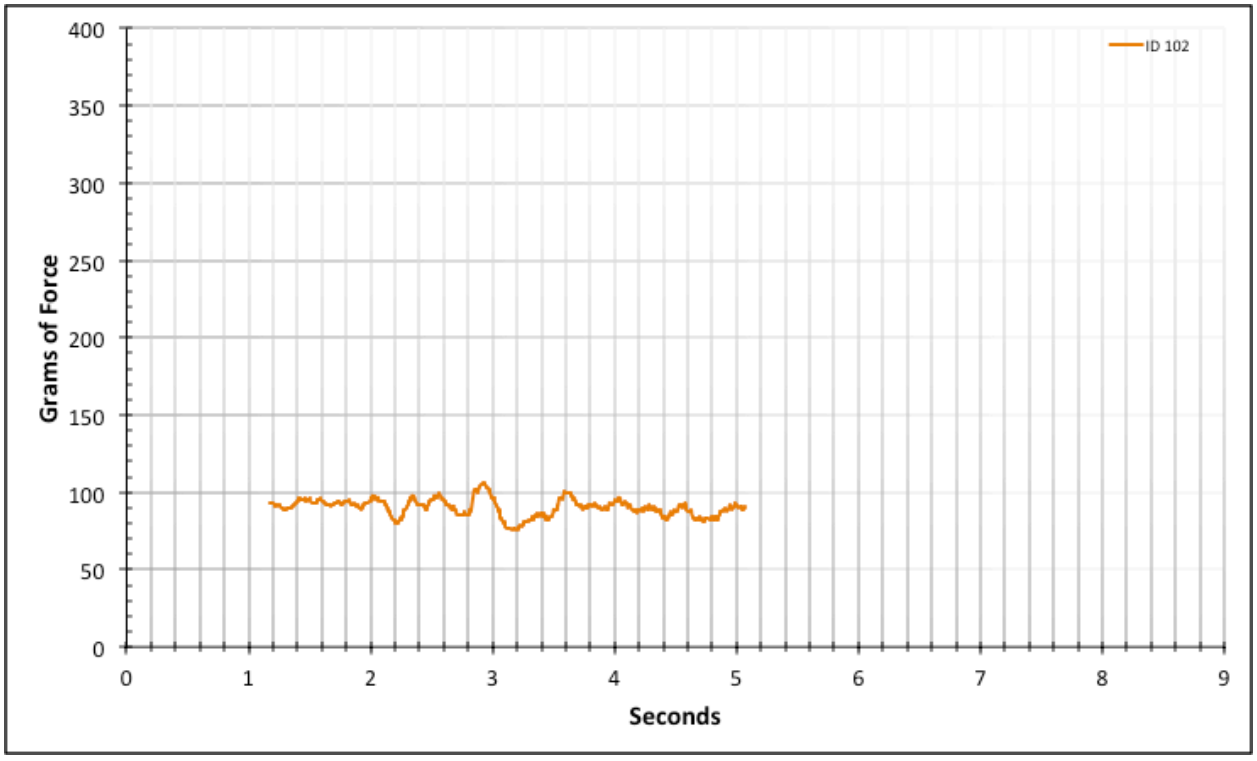

Figure A-6-198: Statistical Region Straight Baseline - Dry - ID 102 - #10, Bolt 1

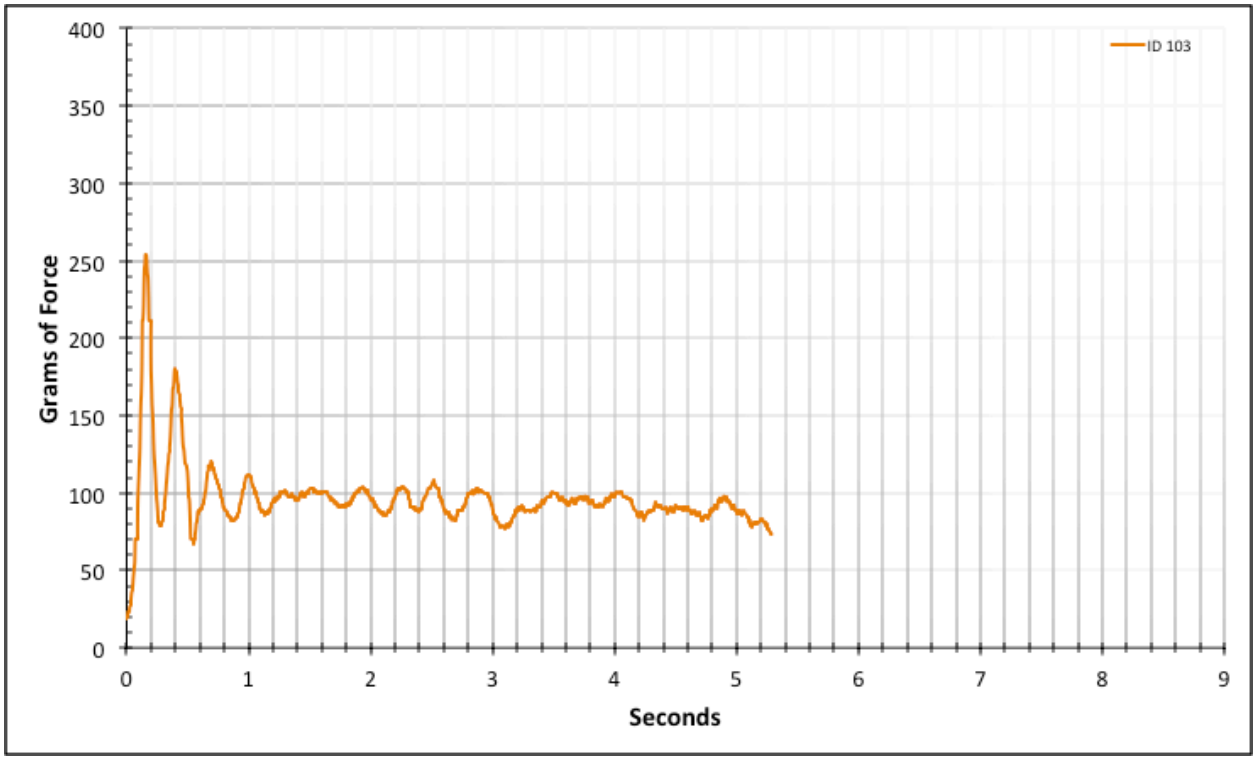

Figure A-6-199: Full Straight Baseline - Dry - ID 103 - #10, Bolt 1

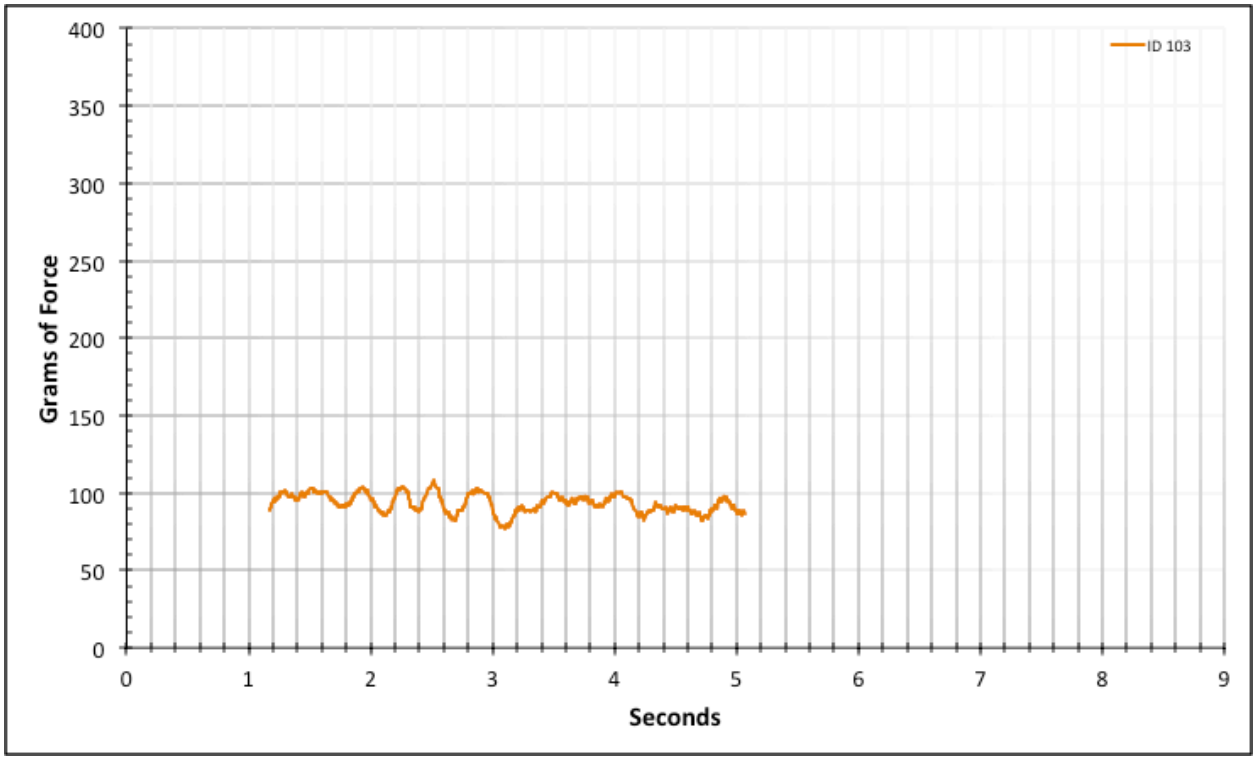

Figure A-6-200: Statistical Region Straight Baseline - Dry - ID 103 - #10, Bolt 1

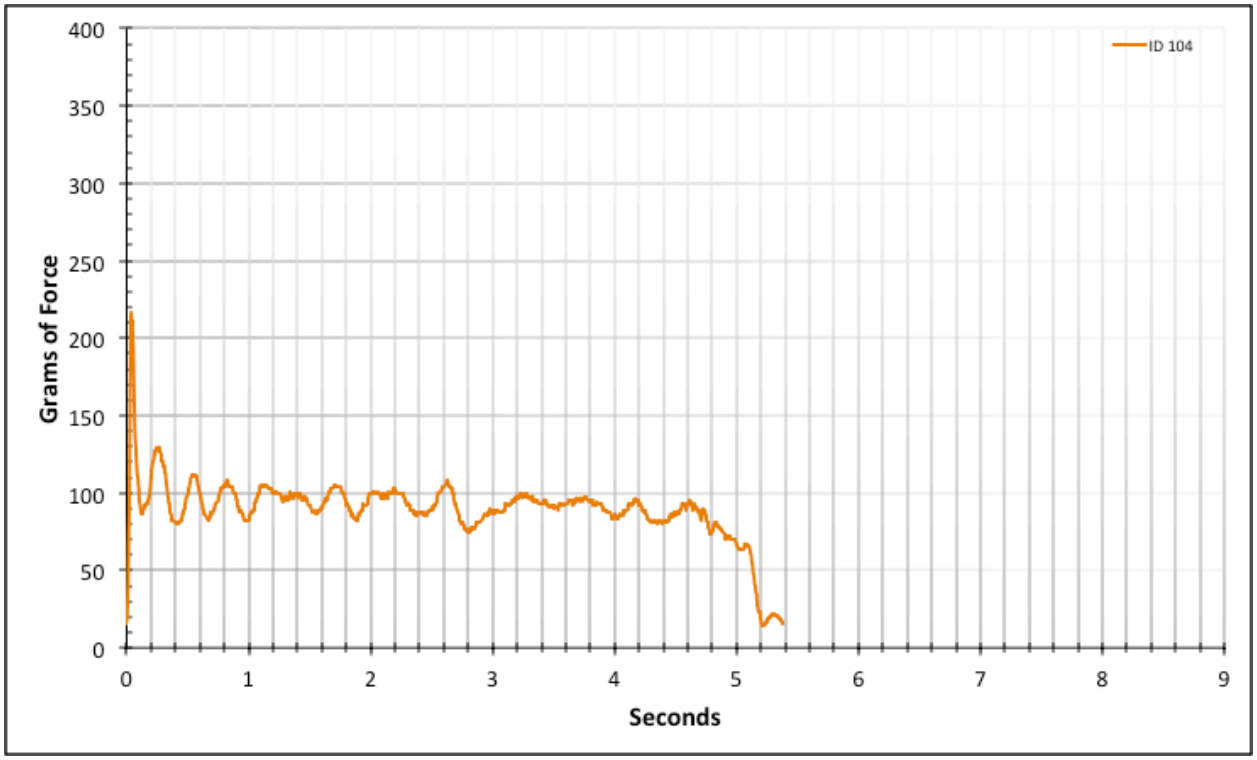

Figure A-6-201: Full Straight Baseline - Dry - ID 104 - #10, Bolt 1

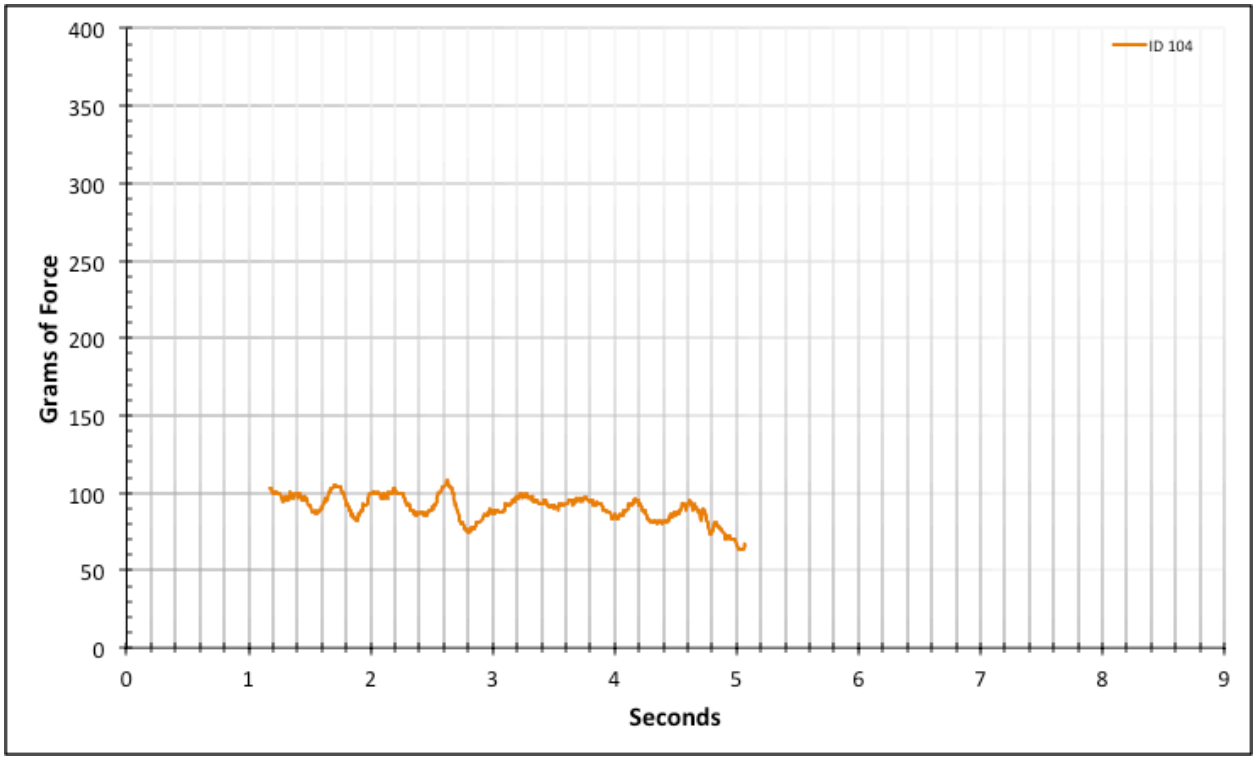

Figure A-6-202: Statistical Region Straight Baseline - Dry - ID 104 - #10, Bolt 1

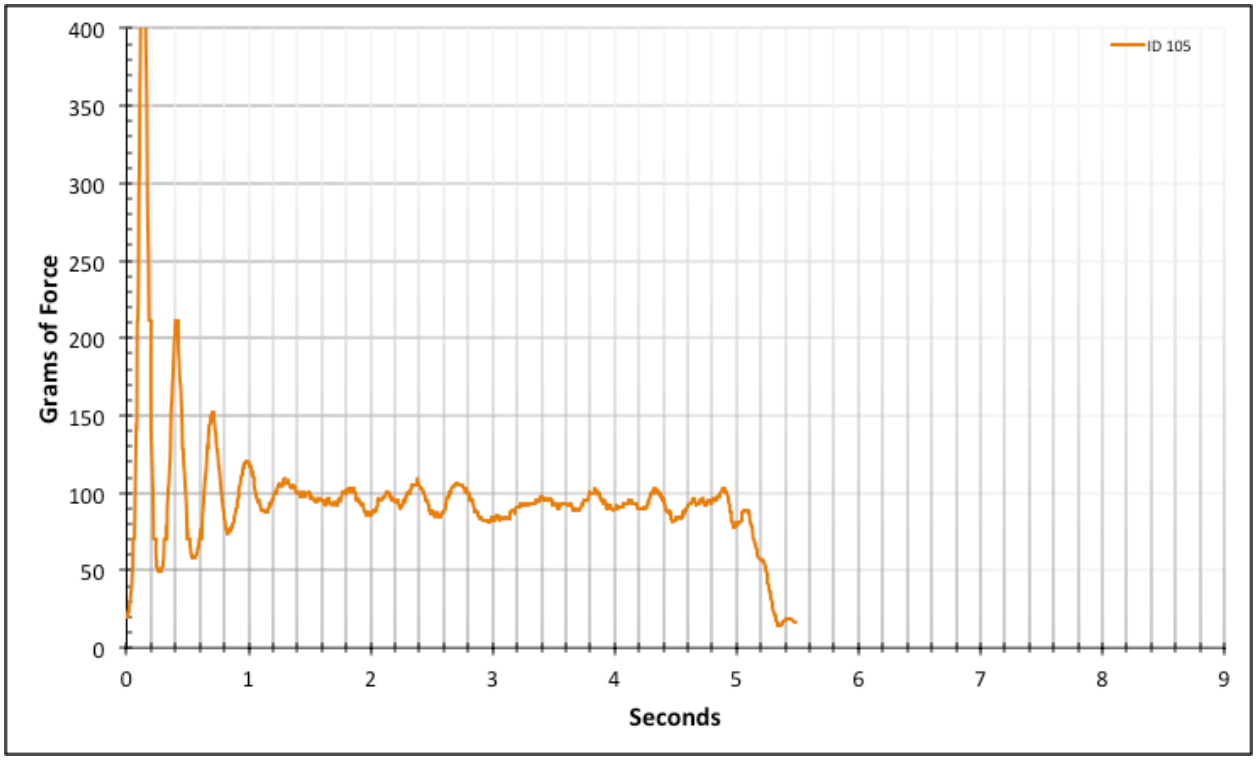

Figure A-6-203: Full Straight Baseline - Dry - ID 105 - #10, Bolt 1

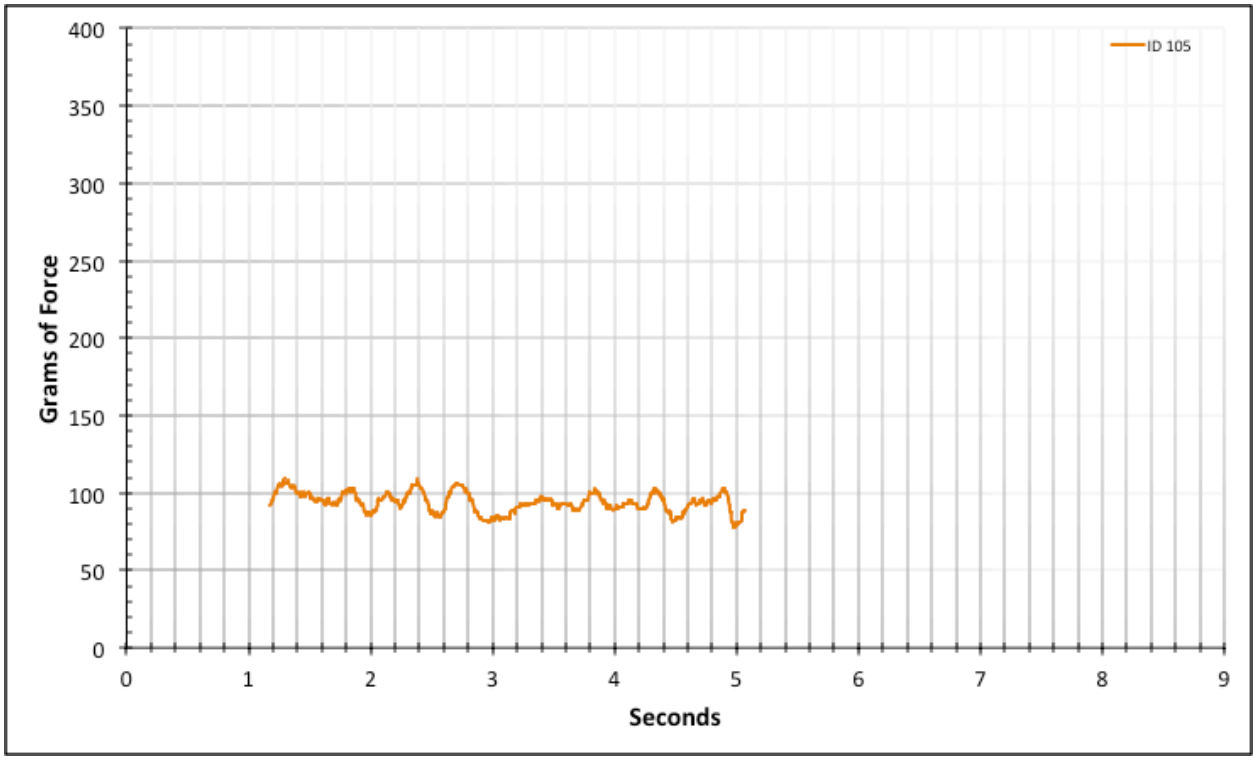

Figure A-6-204: Statistical Region Straight Baseline - Dry - ID 105 - #10, Bolt 1

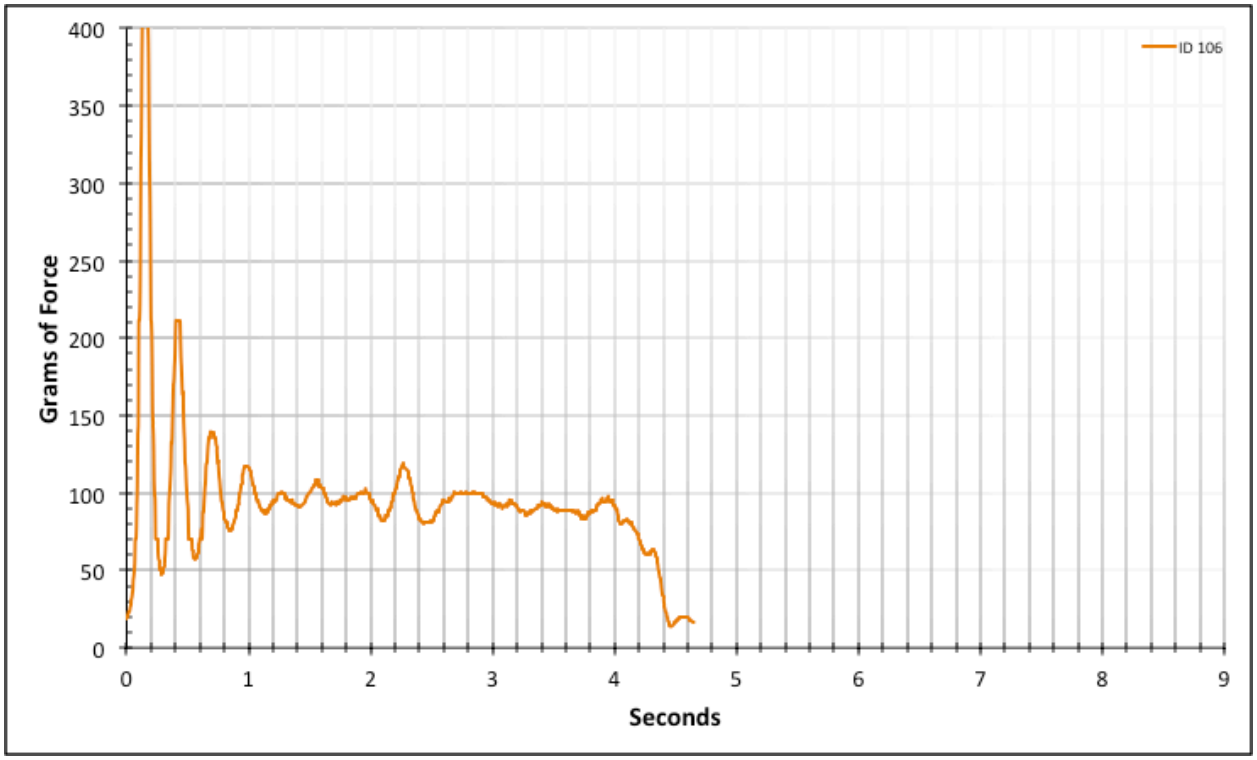

Figure A-6-205: Full Straight Baseline - Dry - ID 106 - #10, Bolt 2

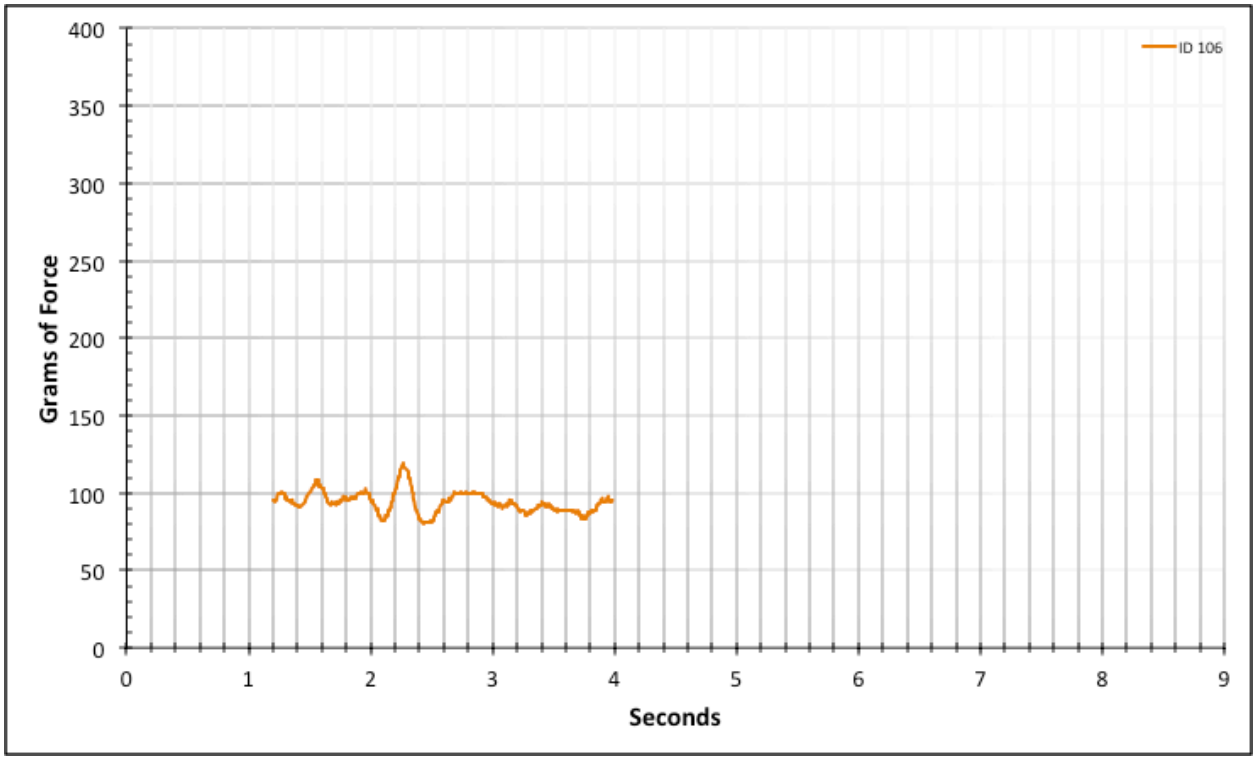

Figure A-6-206: Statistical Region Straight Baseline - Dry - ID 106 - #10, Bolt 2

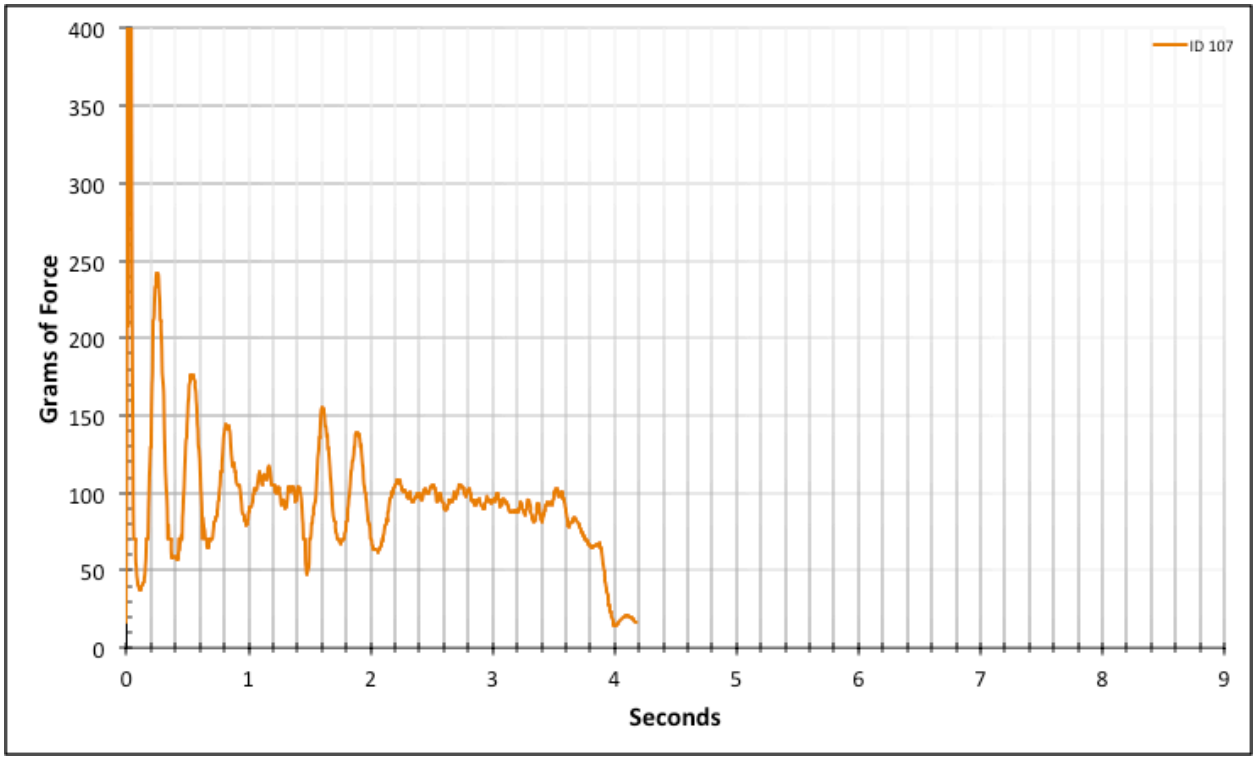

Figure A-6-207: Full Straight Baseline - Dry - ID 107 - #10, Bolt 2

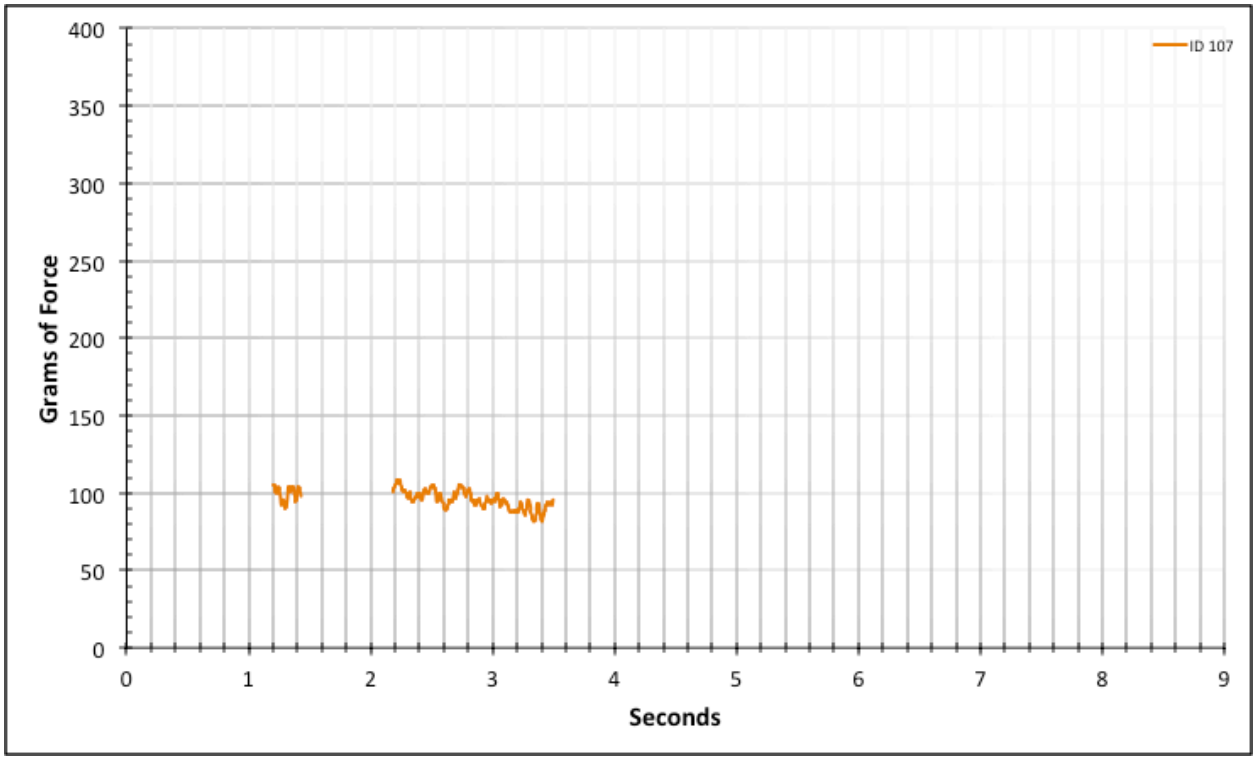

Figure A-6-208: Statistical Region Straight Baseline - Dry - ID 107 - #10, Bolt 2

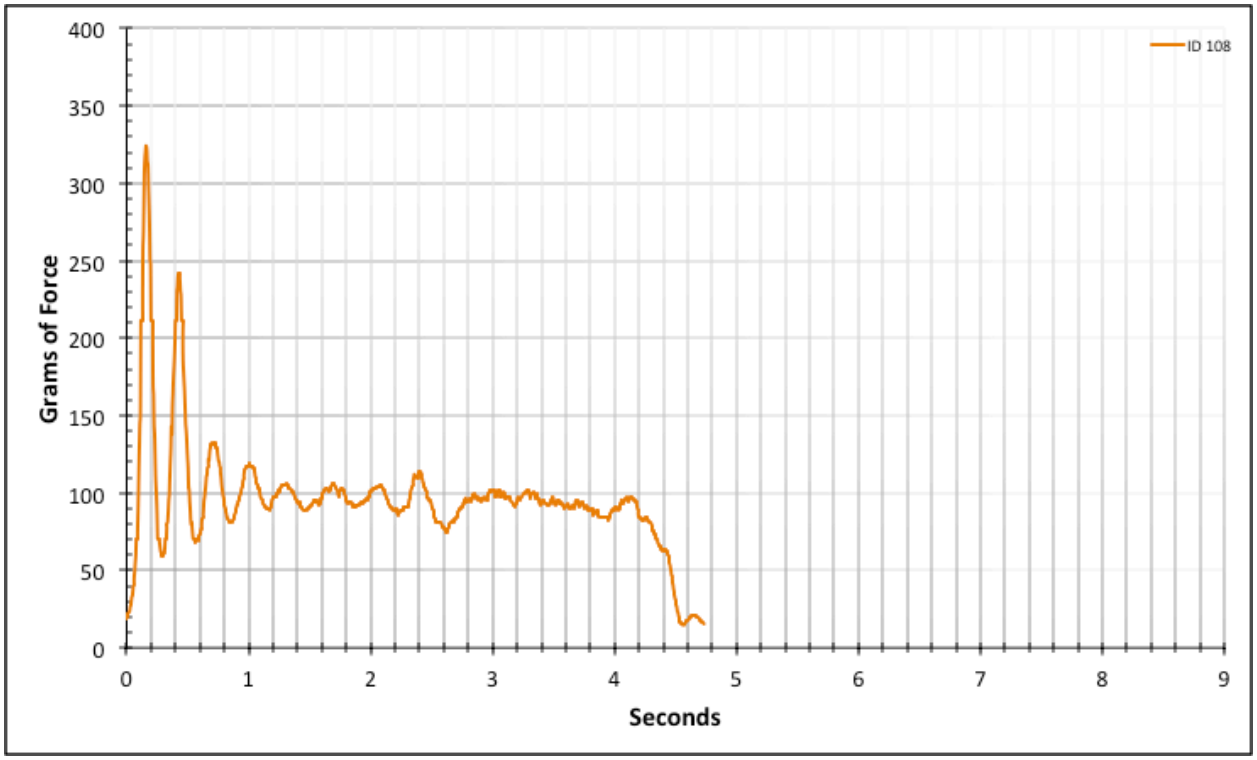

Figure A-6-209: Statistical Region Straight Baseline - Dry - ID 108 - #10, Bolt 2

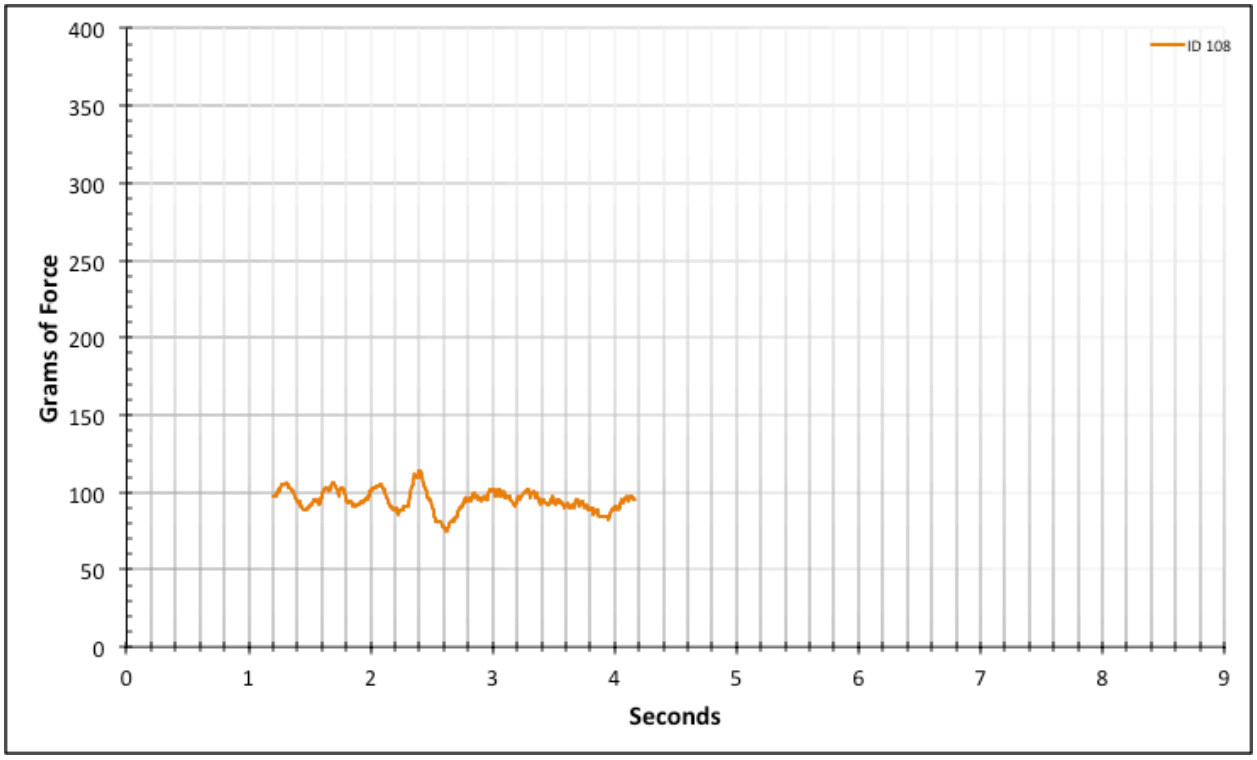

Figure A-6-210: Full Straight Baseline - Dry - ID 108 - #10, Bolt 2

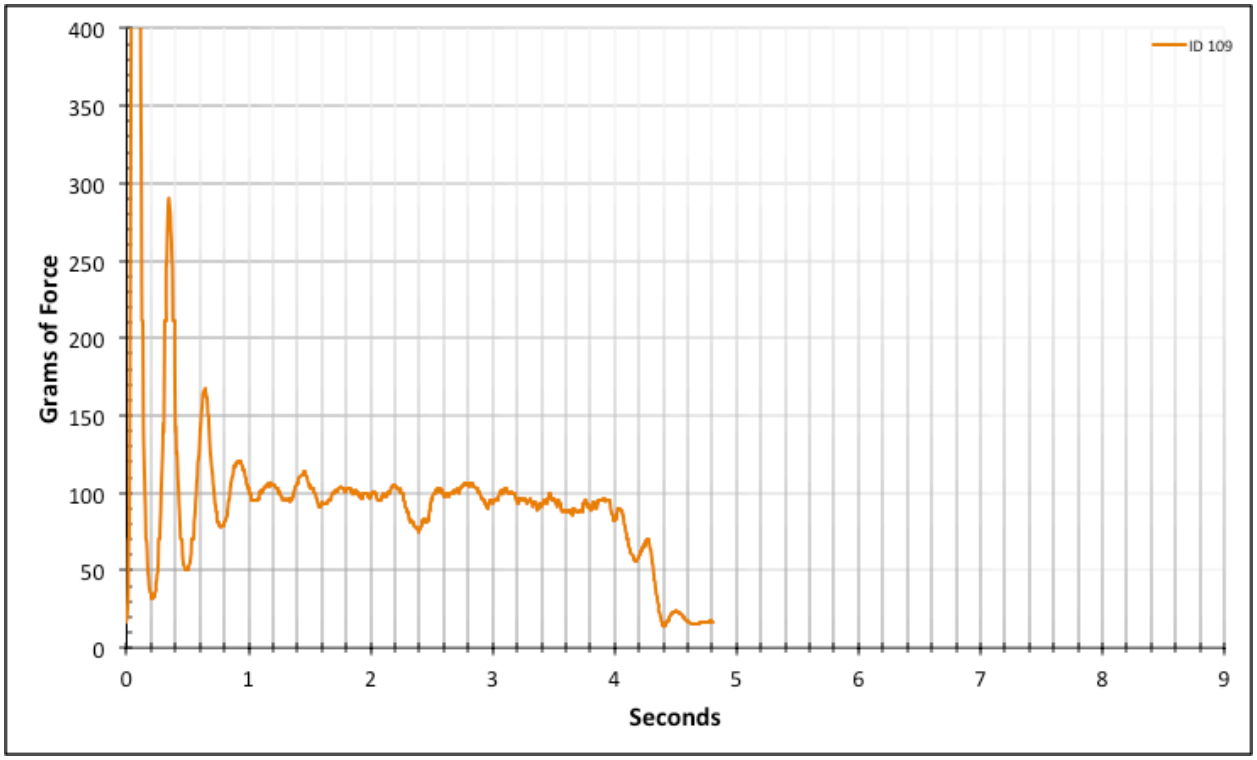

Figure A-6-211: Full Straight Baseline - Dry - ID 109 - #10, Bolt 2

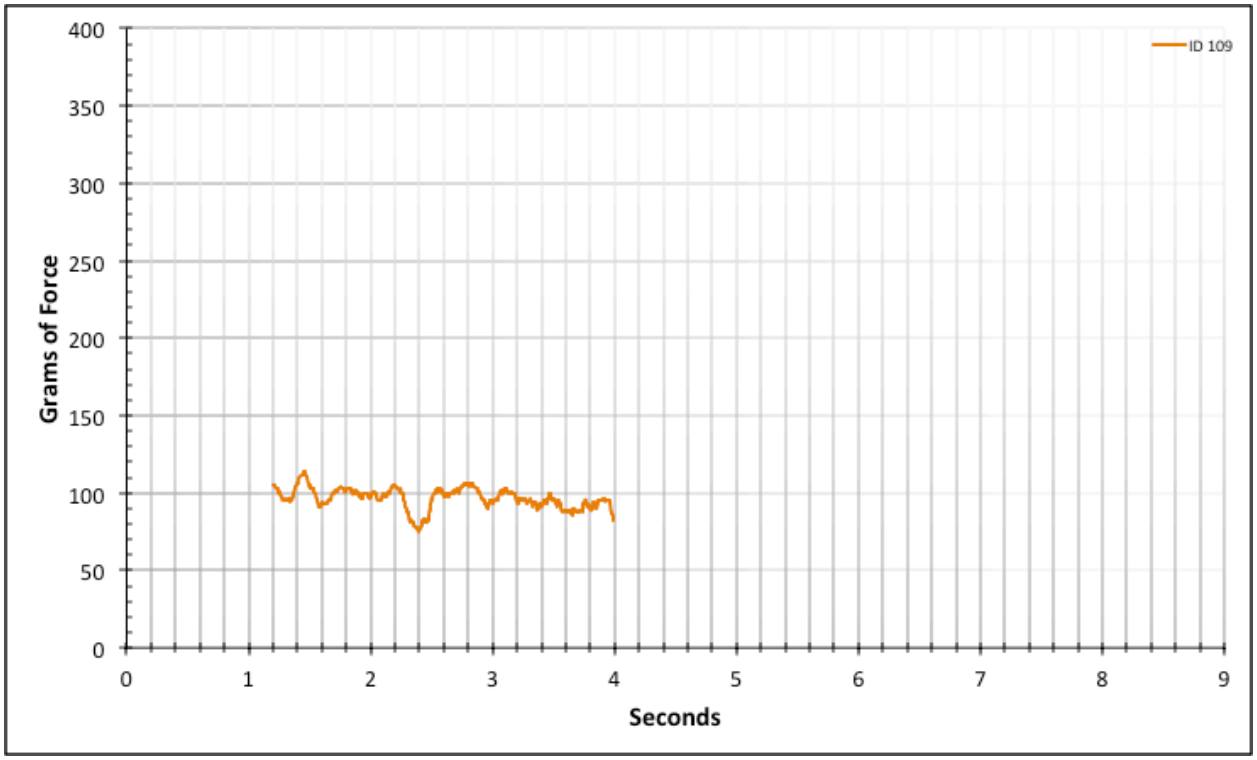

Figure A-6-212: Statistical Region Straight Baseline - Dry - ID 109 - #10, Bolt 2

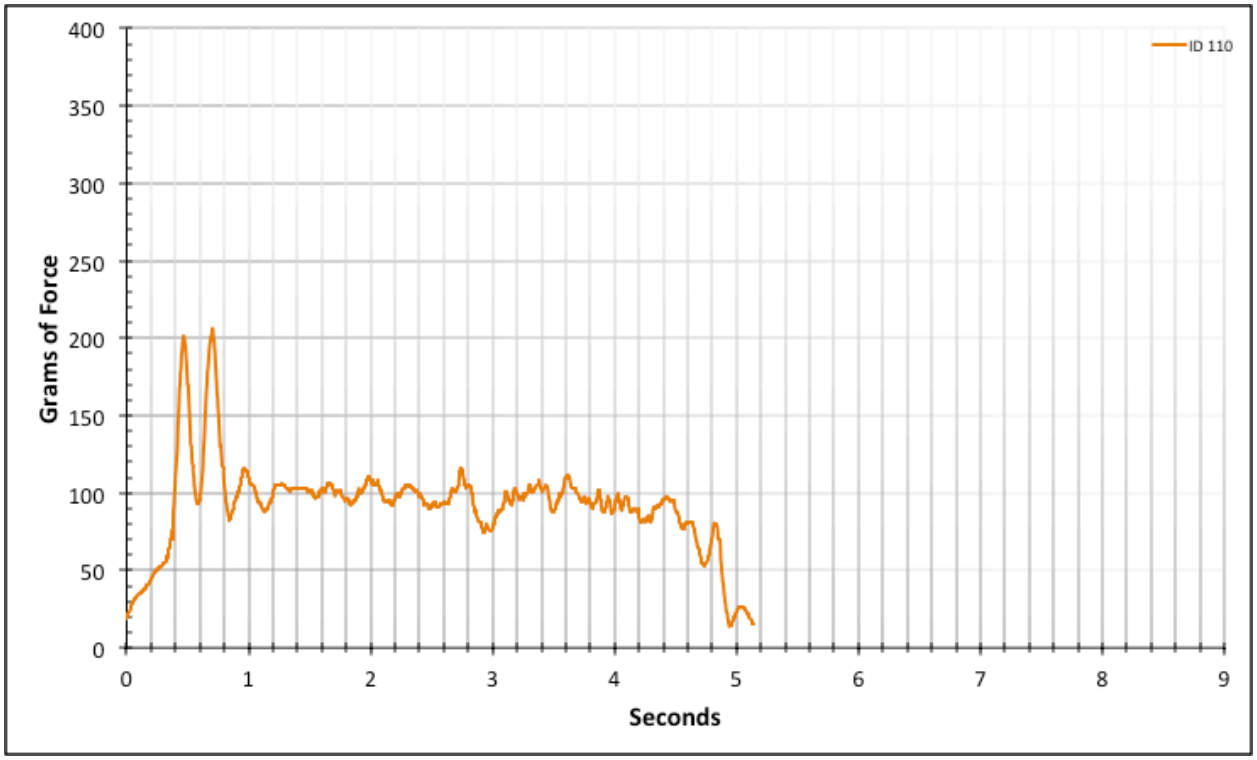

Figure A-6-213: Full Straight Baseline - Dry - ID 110 - #10, Bolt 2

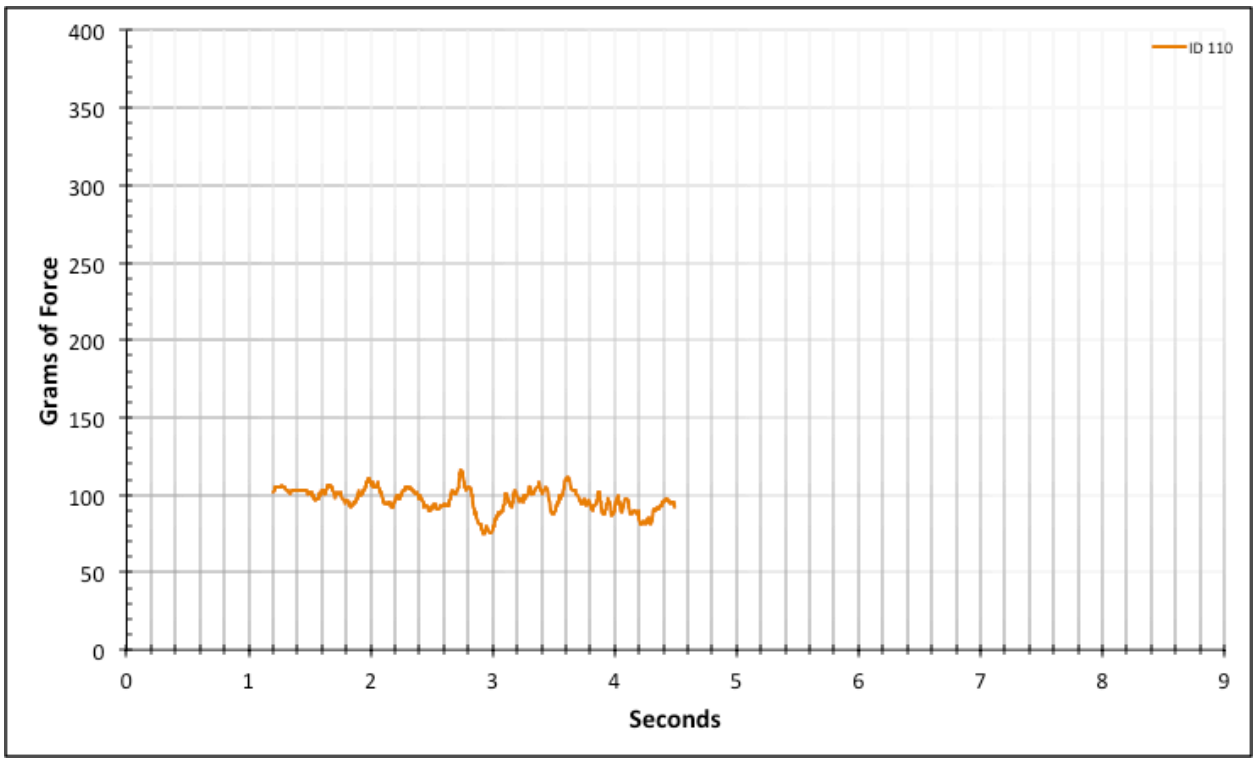

Figure A-6-214: Statistical Region Straight Baseline - Dry - ID 110 - #10, Bolt 2

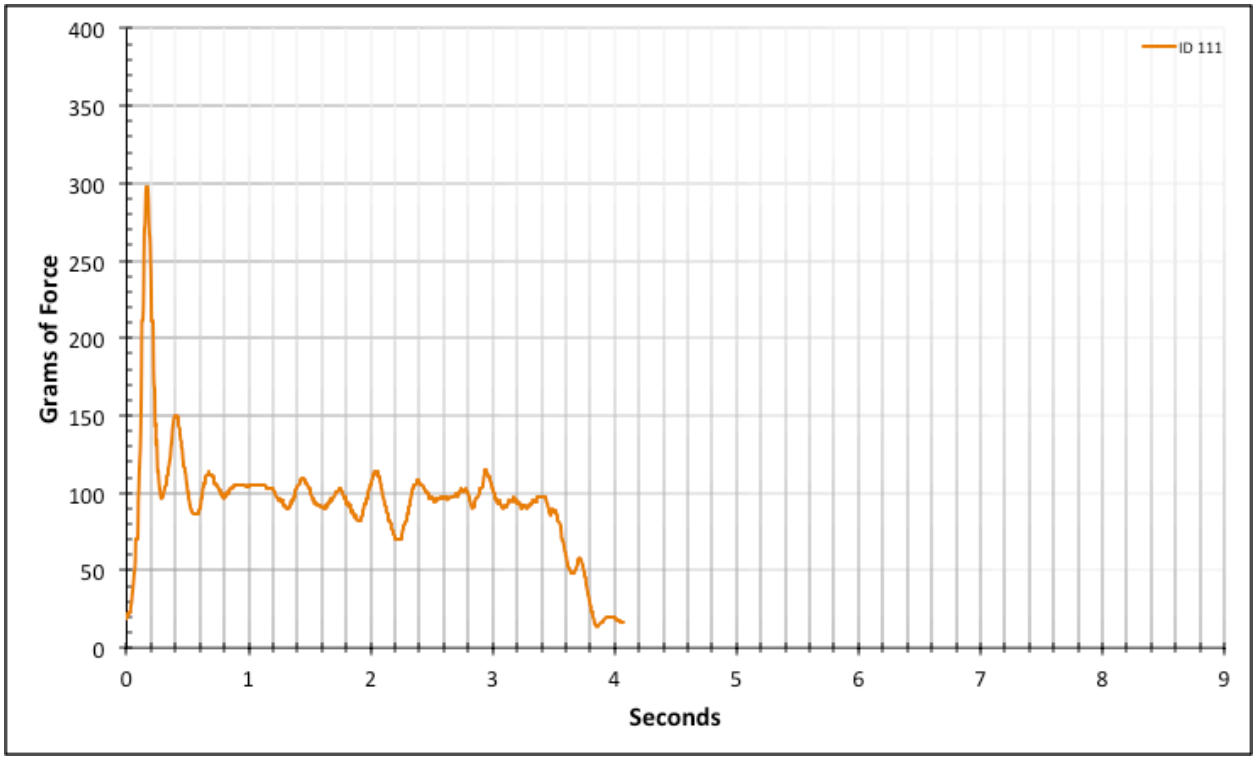

Figure A-6-215: Full Straight Baseline - Dry - ID 111 - #10, Bolt 3

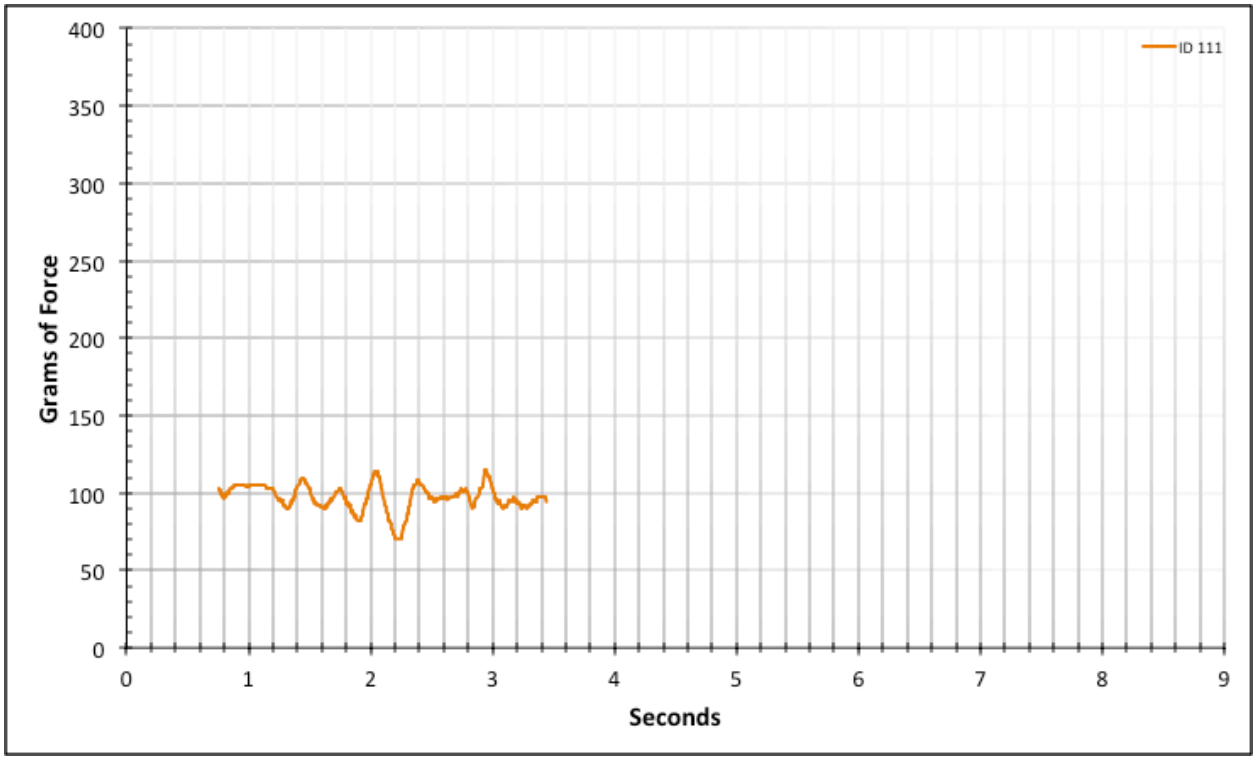

Figure A-6-216: Statistical Region Straight Baseline - Dry - ID 111 - #10, Bolt 3

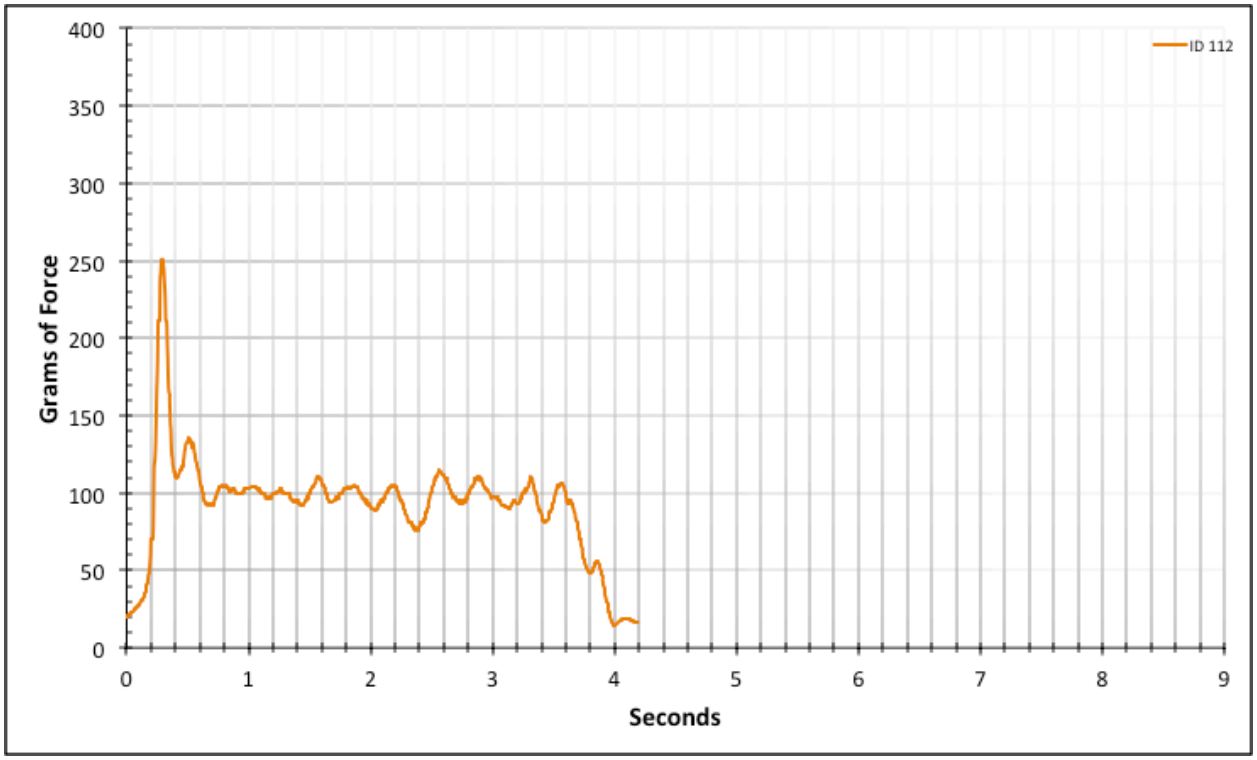

Figure A-6-217: Full Straight Baseline - Dry - ID 112 - #10, Bolt 3

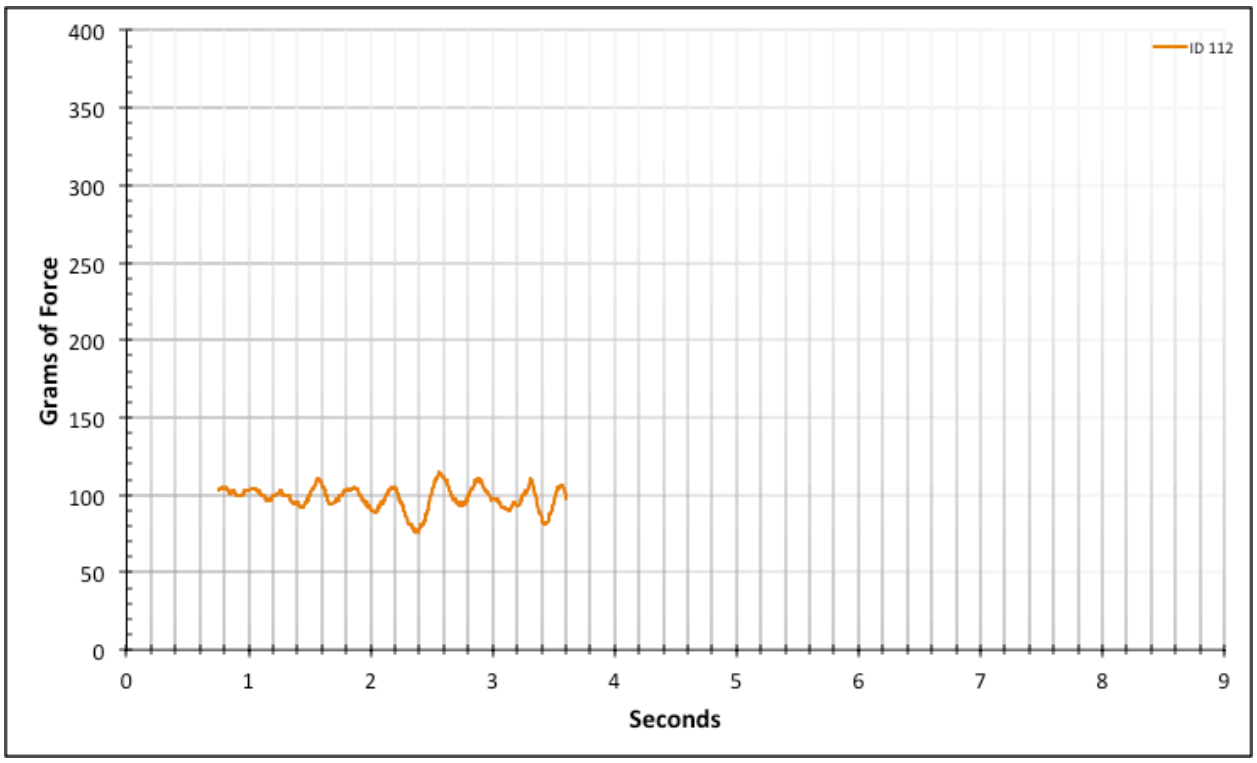

Figure A-6-218: Statistical Region Straight Baseline - Dry - ID 112 - #10, Bolt 3

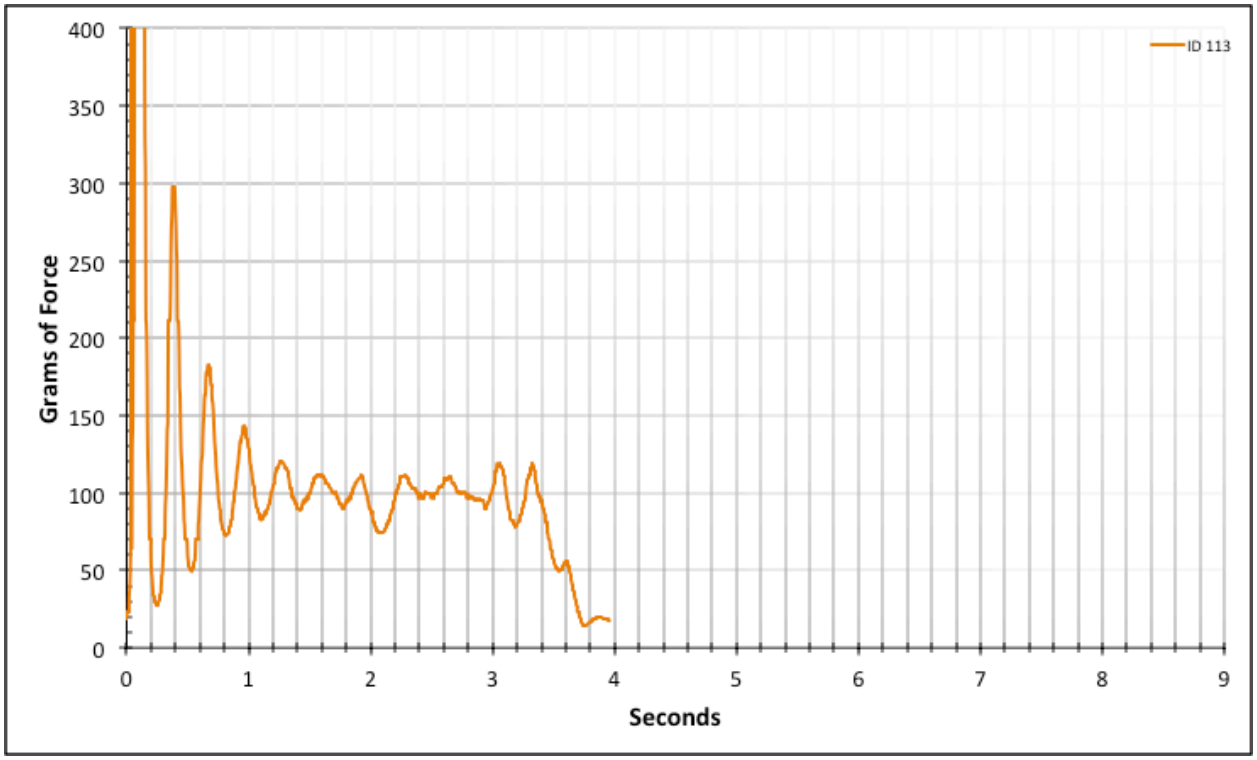

Figure A-6-219: Full Straight Baseline - Dry - ID 113 - #10, Bolt 3

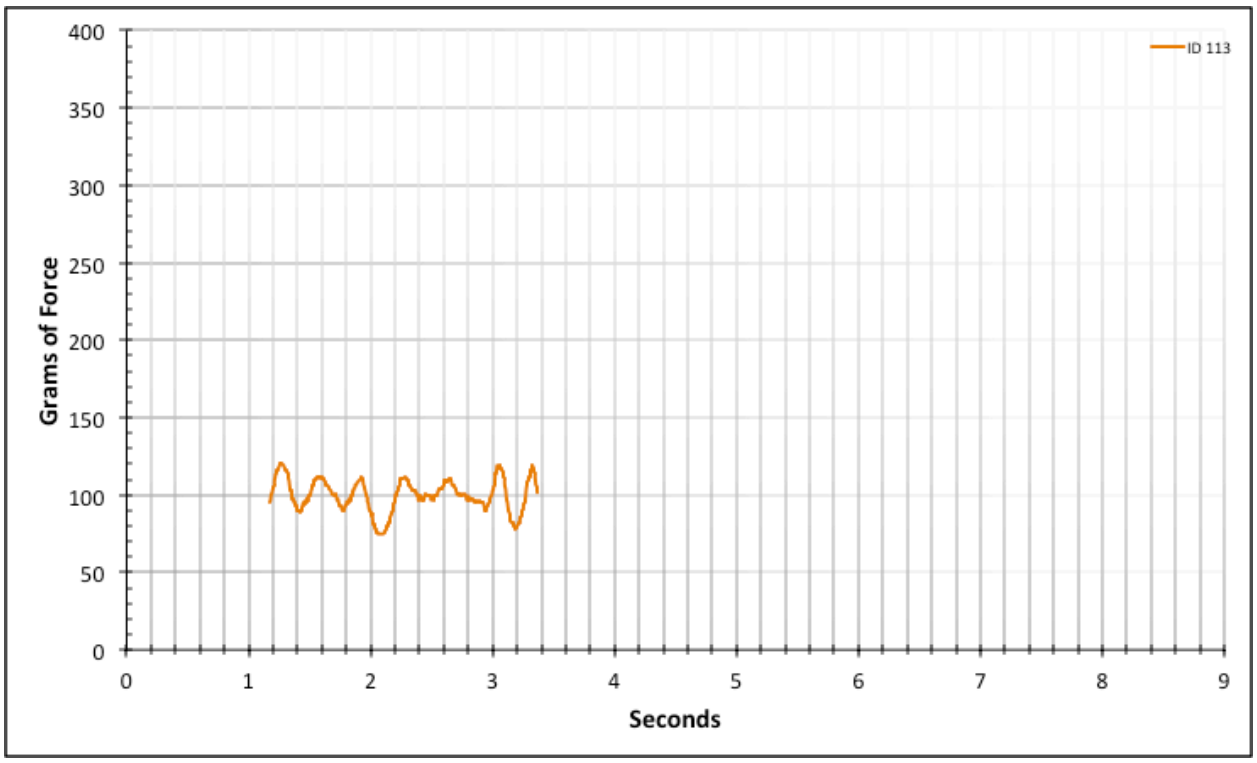

Figure A-6-220: Statistical Region Straight Baseline - Dry - ID 113 - #10, Bolt 3

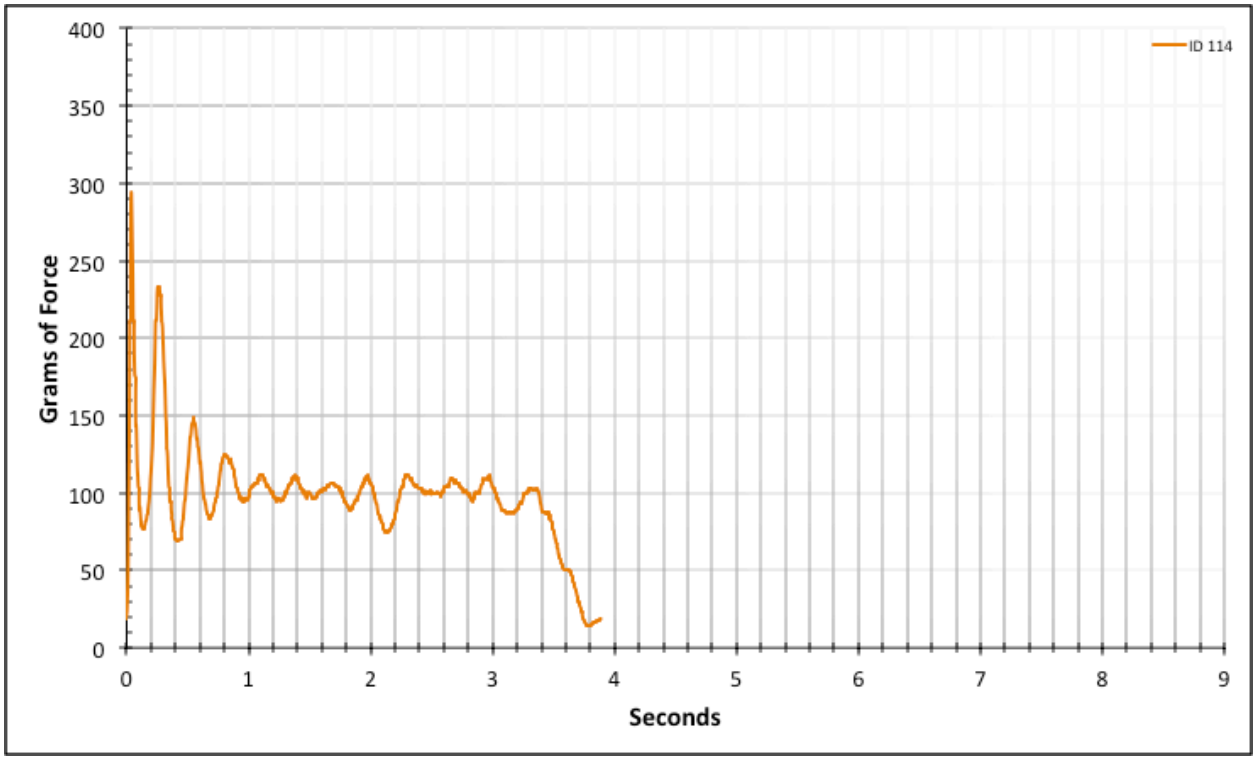

Figure A-6-221: Full Straight Baseline - Dry - ID 114 - #10, Bolt 3

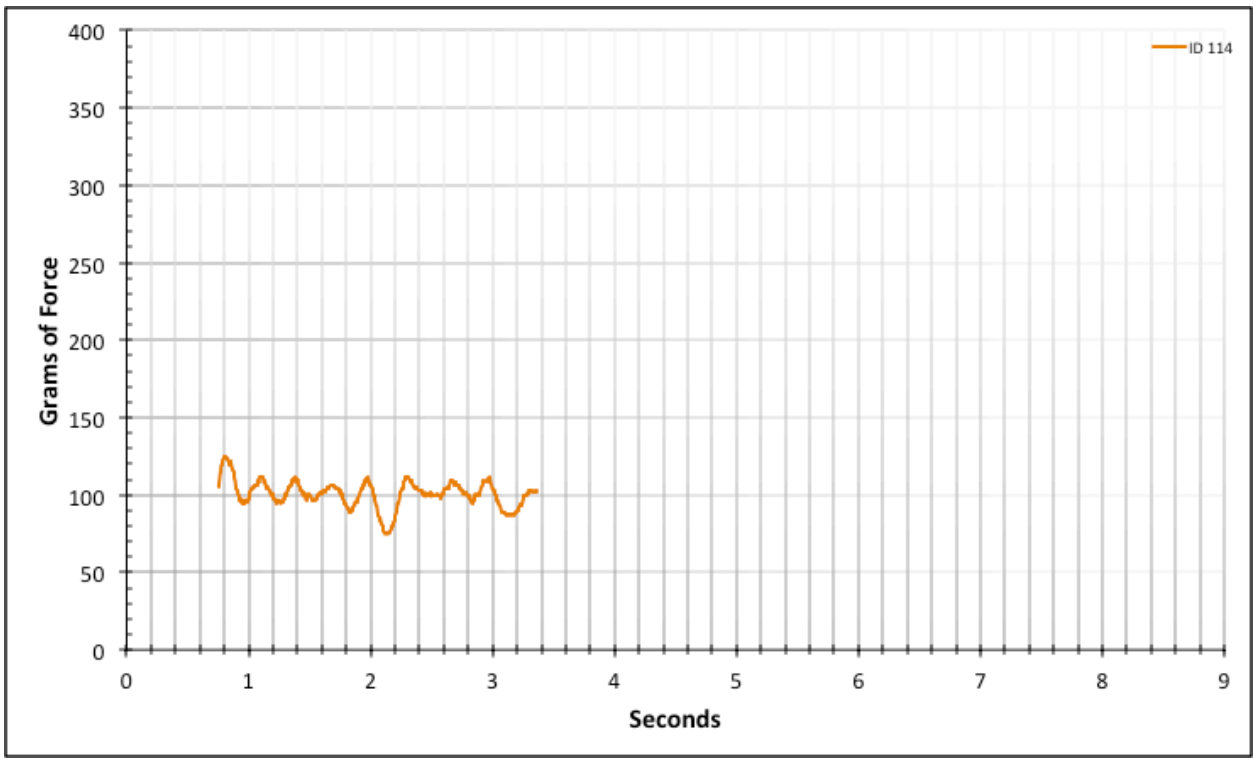

Figure A-6-222: Statistical Region Straight Baseline - Dry - ID 114 - #10, Bolt 3

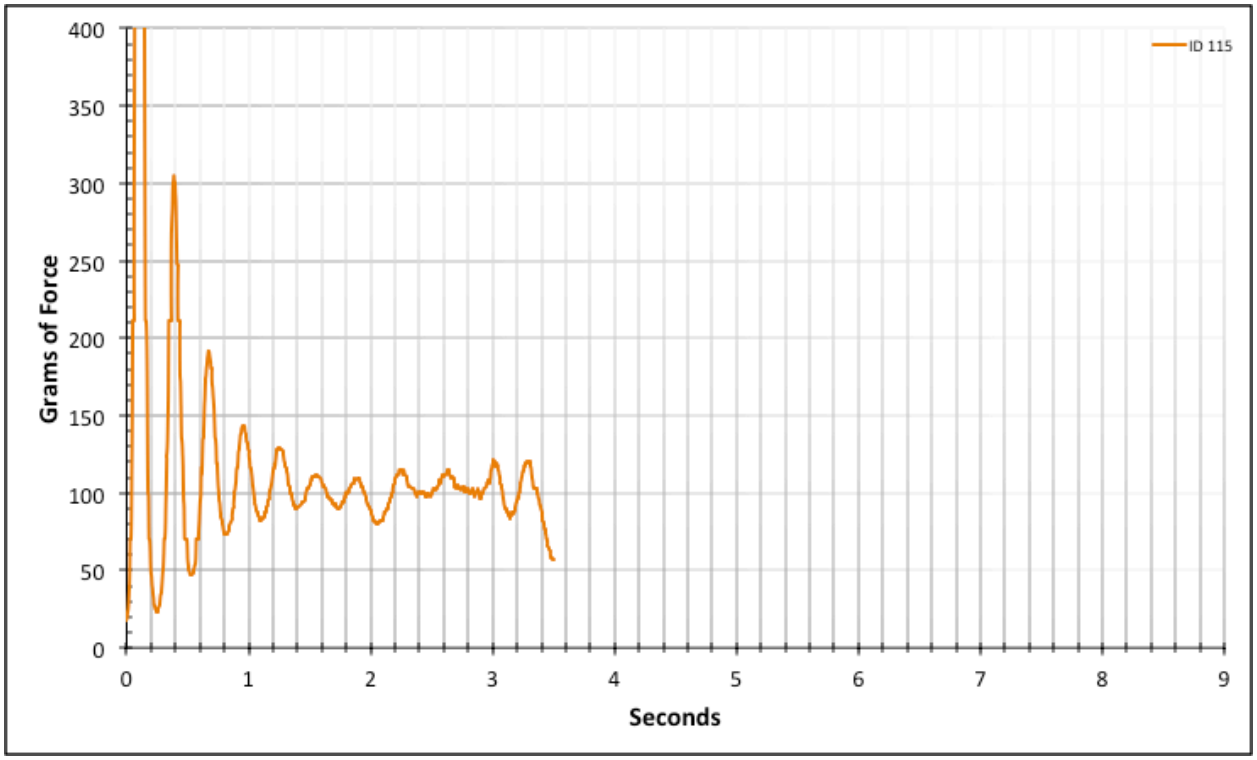

Figure A-6-223: Full Straight Baseline - Dry - ID 115 - #10, Bolt 3

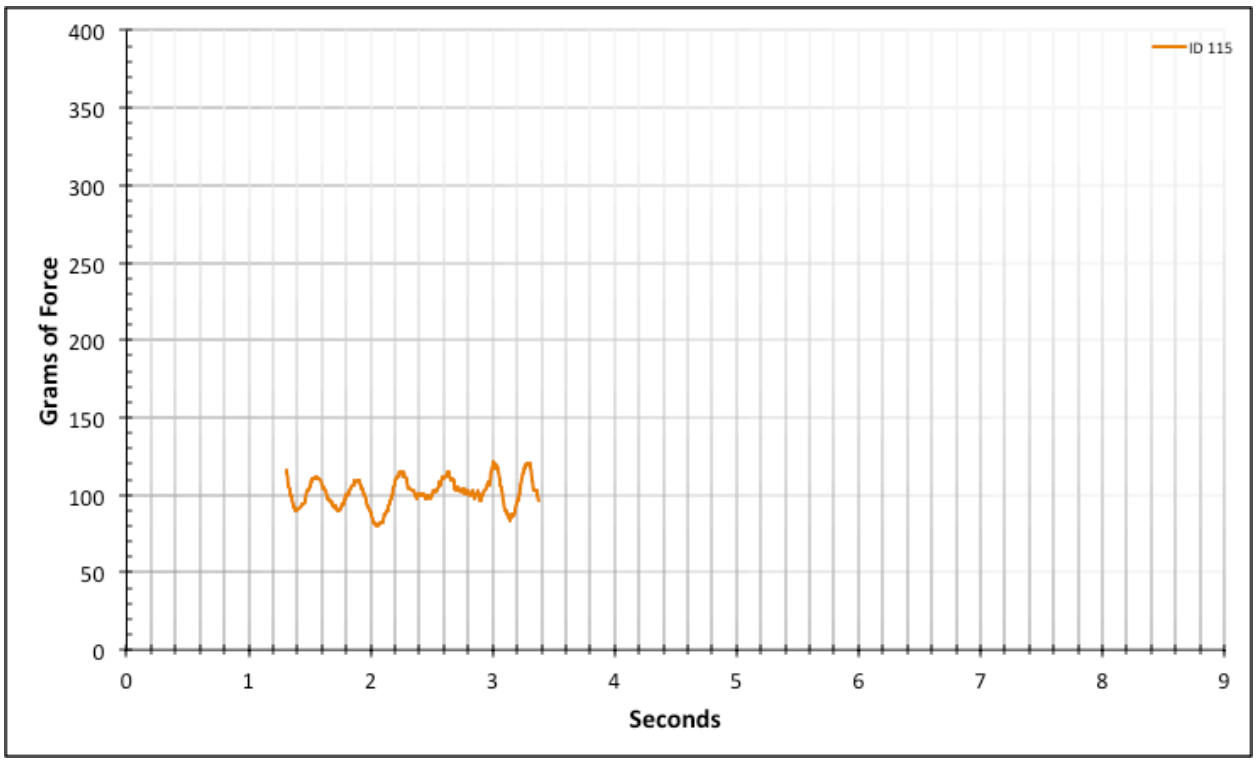

Figure A-6-224: Statistical Region Straight Baseline - Dry - ID 115 - #10, Bolt 3

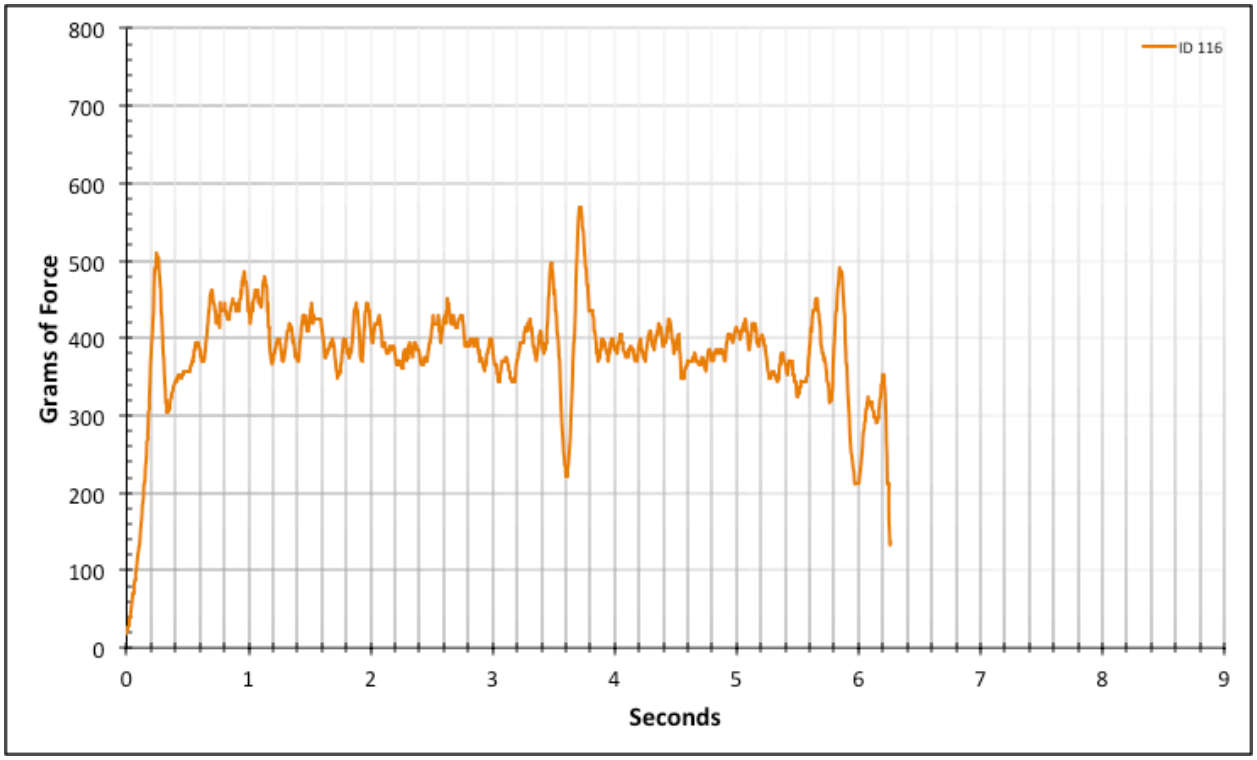

Figure A-6-225: Full Straight Baseline - Dry - ID 116 - #8, Bolt 1

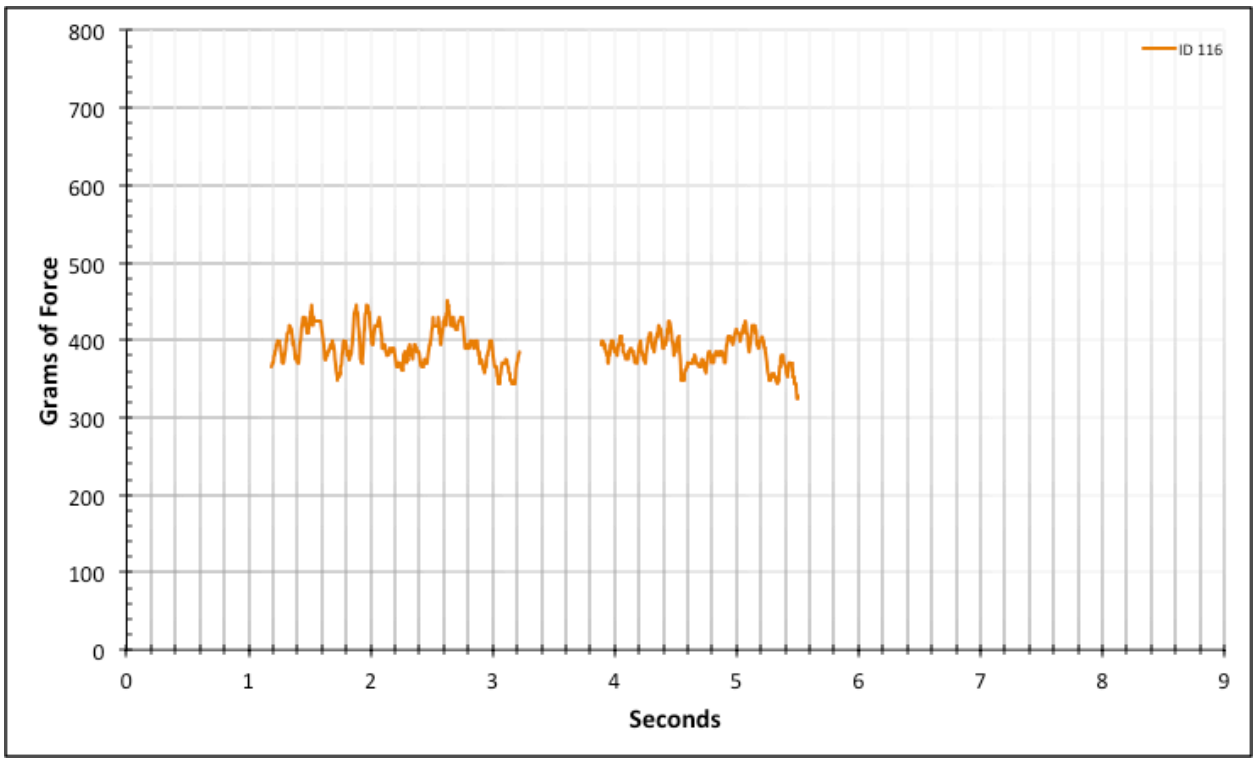

Figure A-6-226: Statistical Region Straight Baseline - Dry - ID 116 - #8, Bolt 1

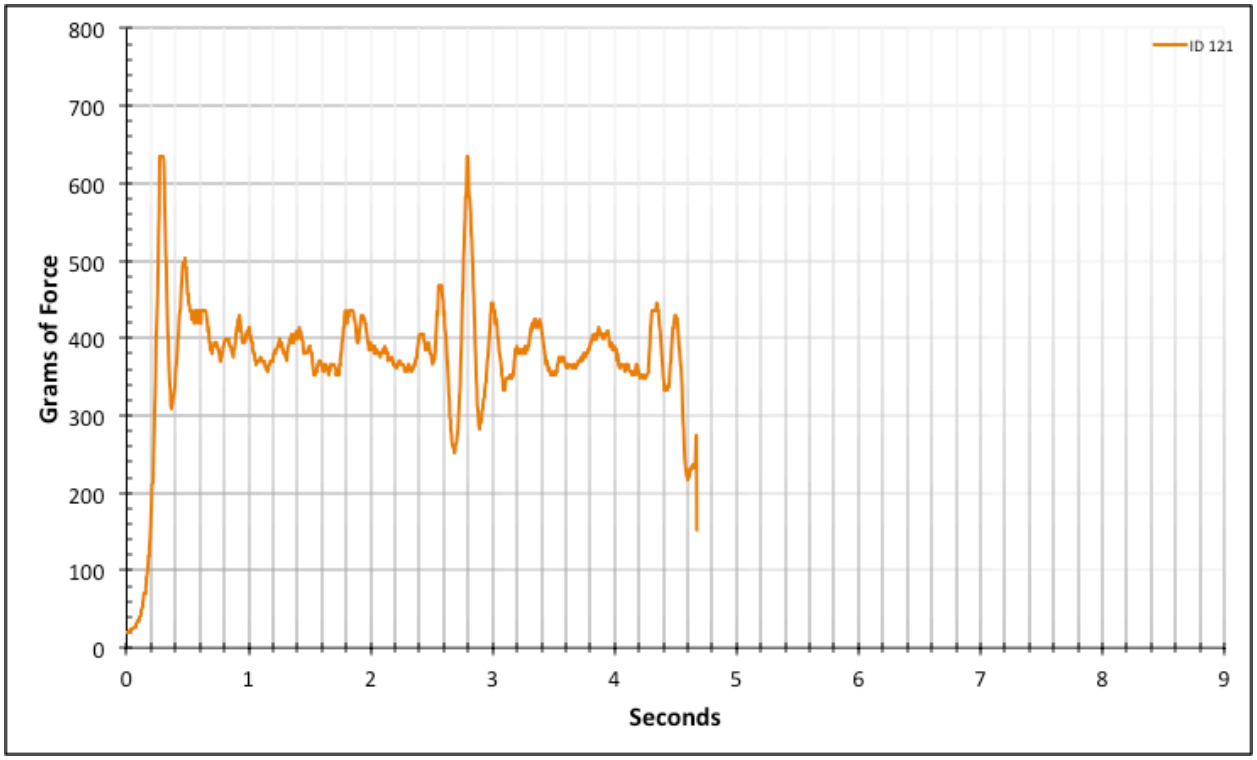

Figure A-6-227: Full Straight Baseline - Dry - ID 121 - #8, Bolt 2

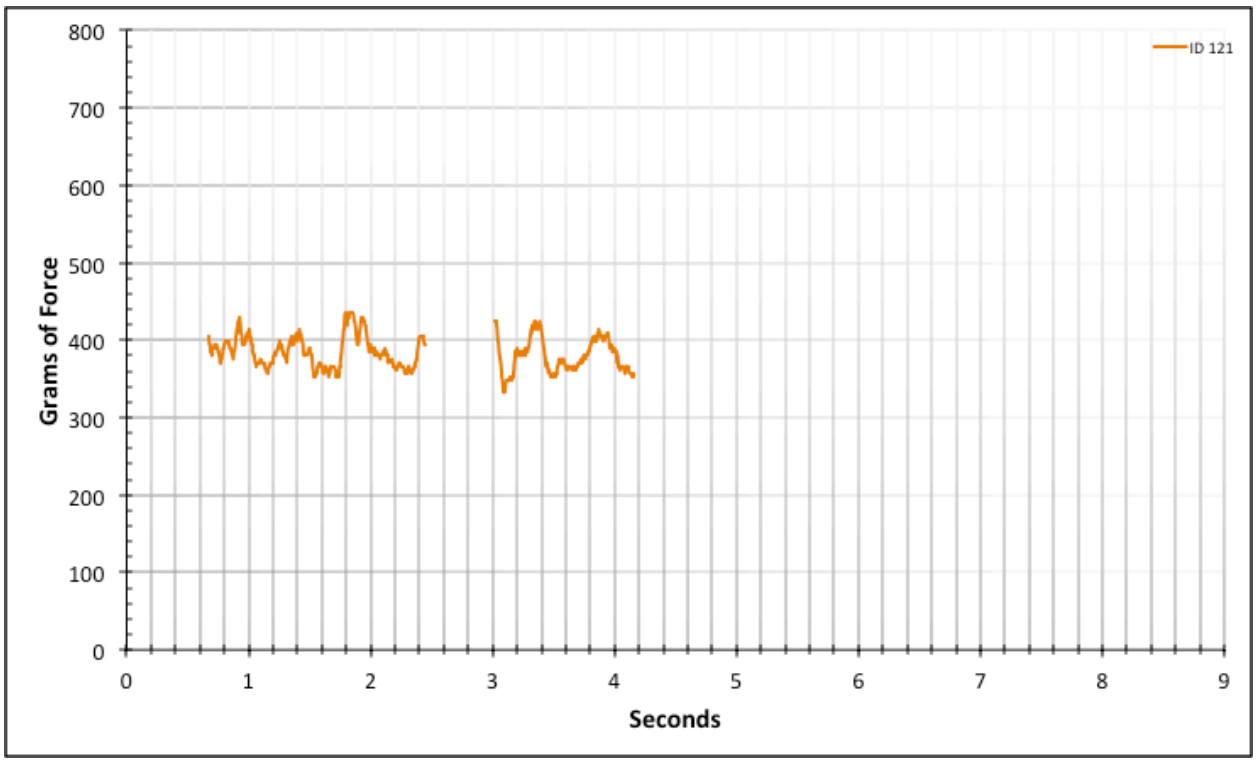

Figure A-6-228: Statistical Region Straight Baseline - Dry - ID 121 - #8, Bolt 2

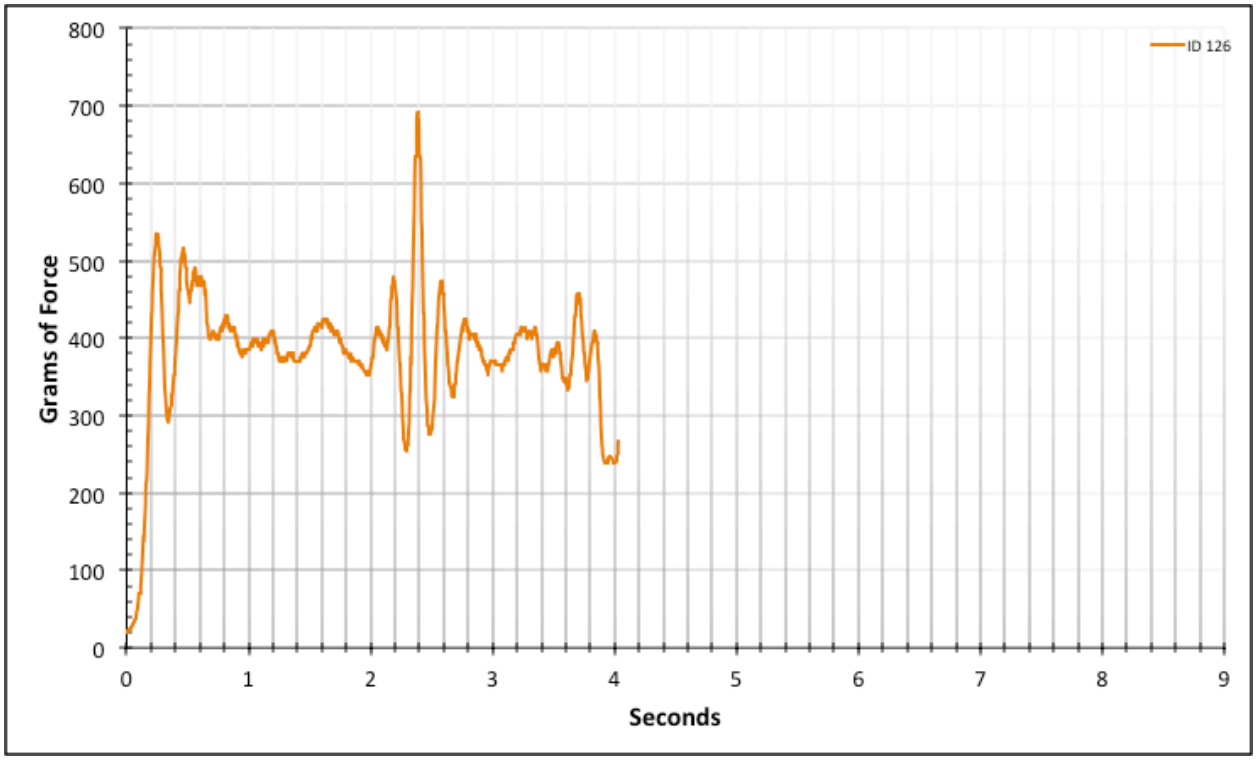

Figure A-6-229: Full Straight Baseline - Dry - ID 126 - #8, Bolt 3

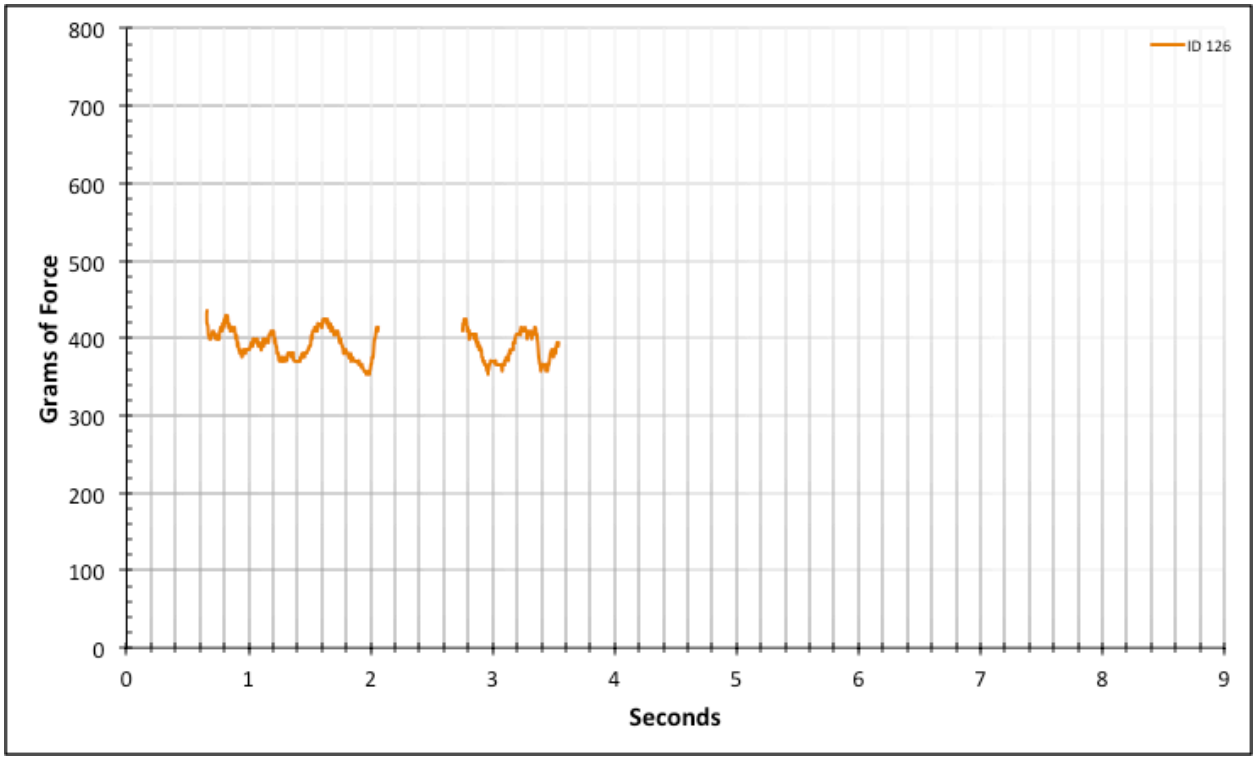

Figure A-6-230: Statistical Region Straight Baseline - Dry - ID 126 - #8, Bolt 3

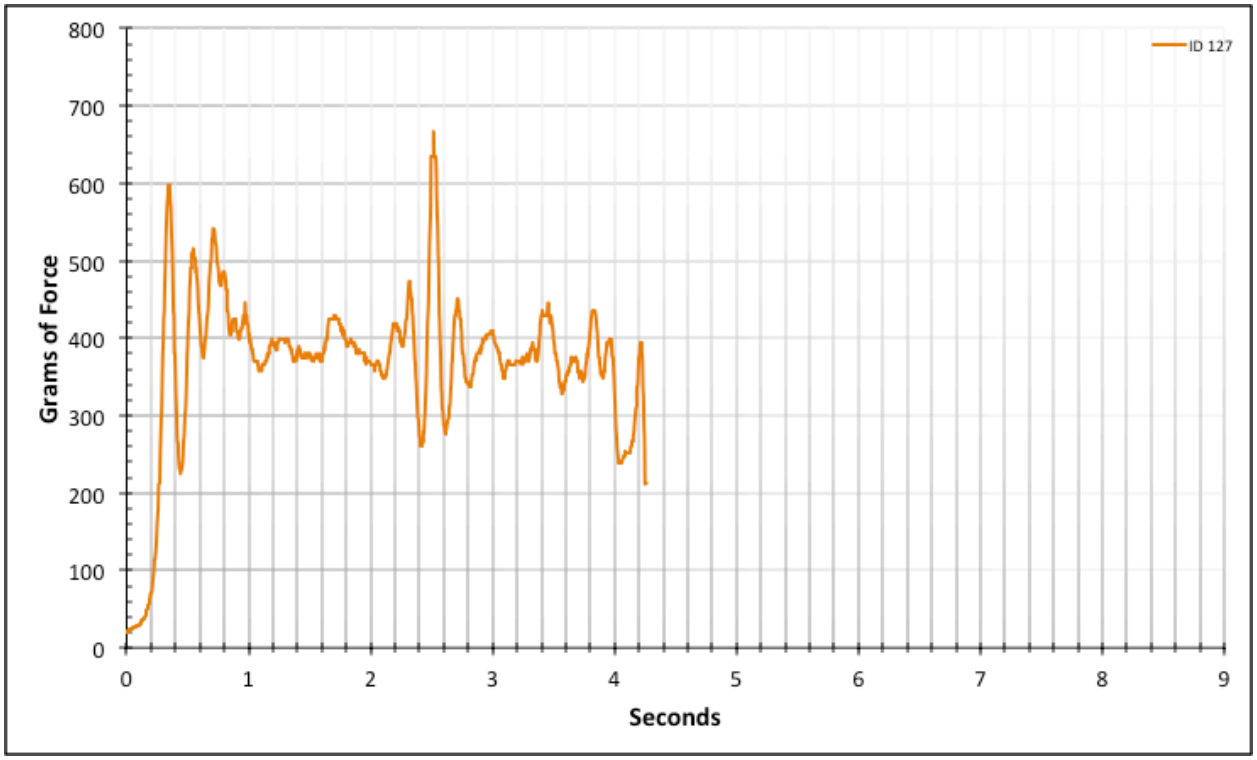

Figure A-6-231: Full Straight Baseline - Dry - ID 127 - #8, Bolt 3

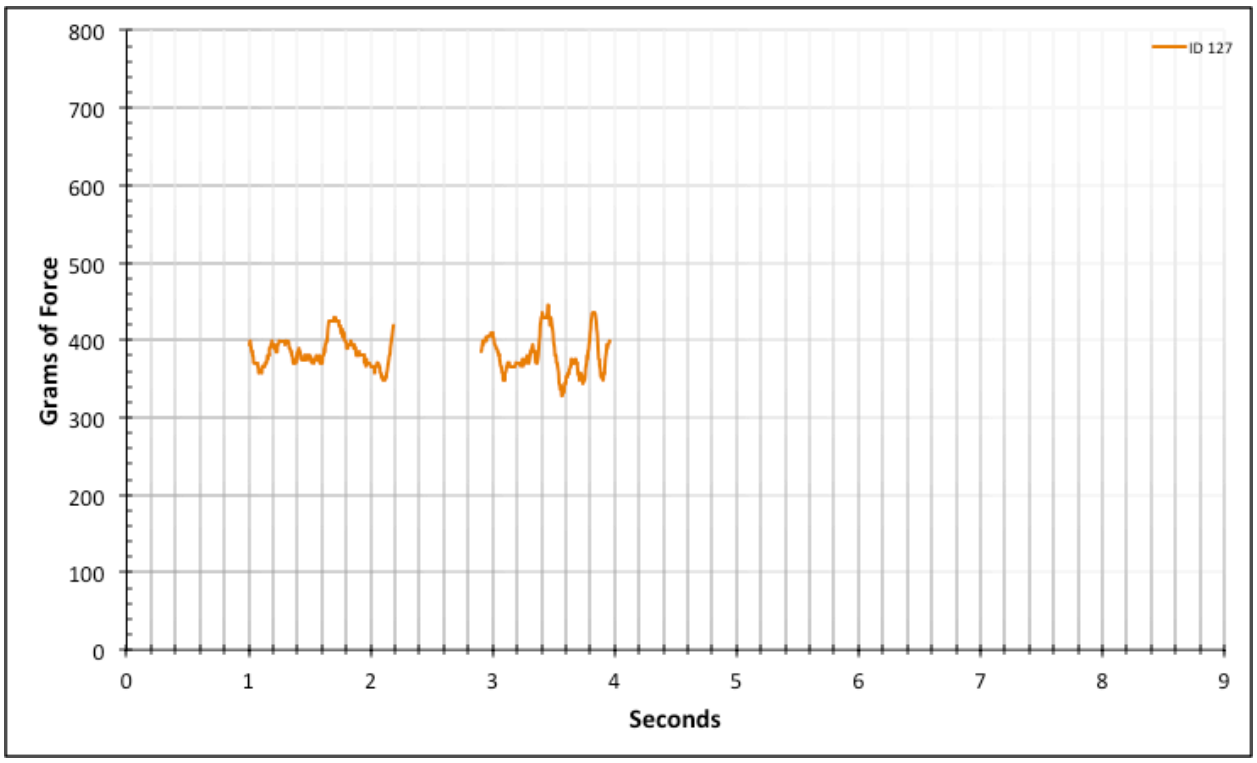

Figure A-6-232: Statistical Region Straight Baseline - Dry - ID 127 - #8, Bolt 3

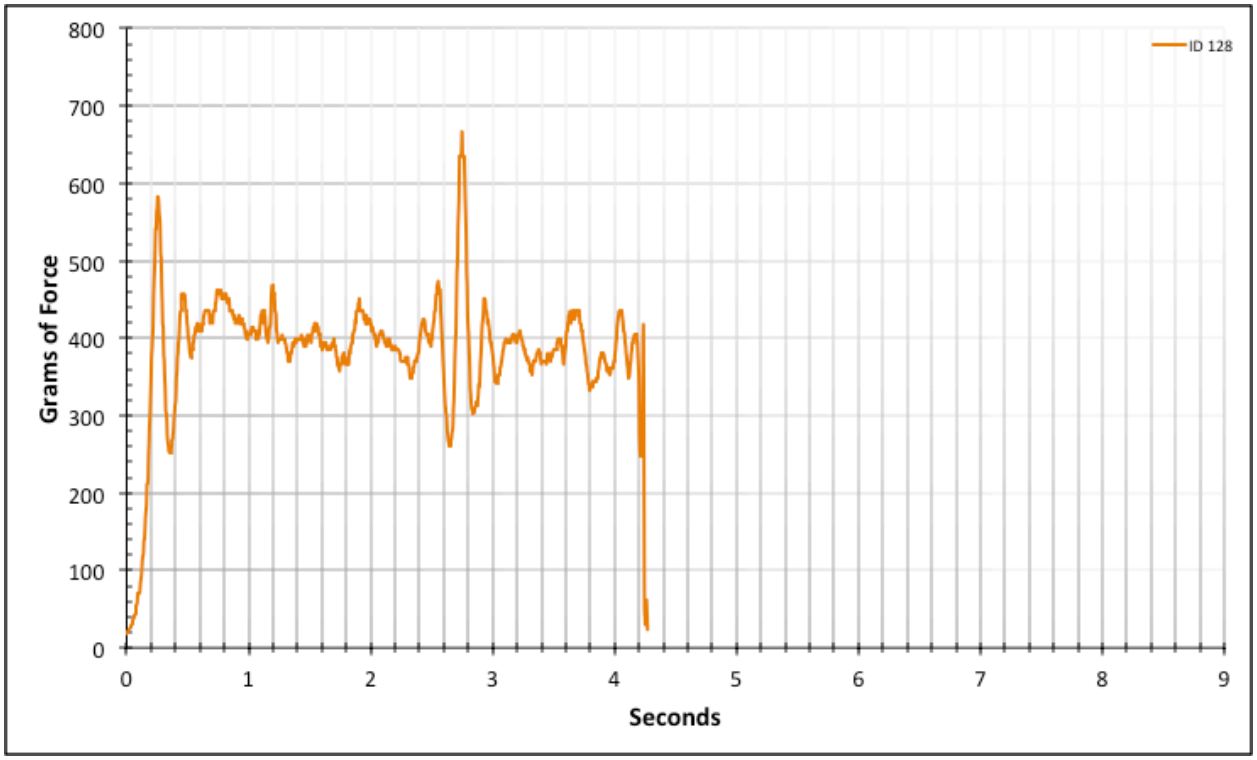

Figure A-6-233: Full Straight Baseline - Dry - ID 128 - #8, Bolt 3

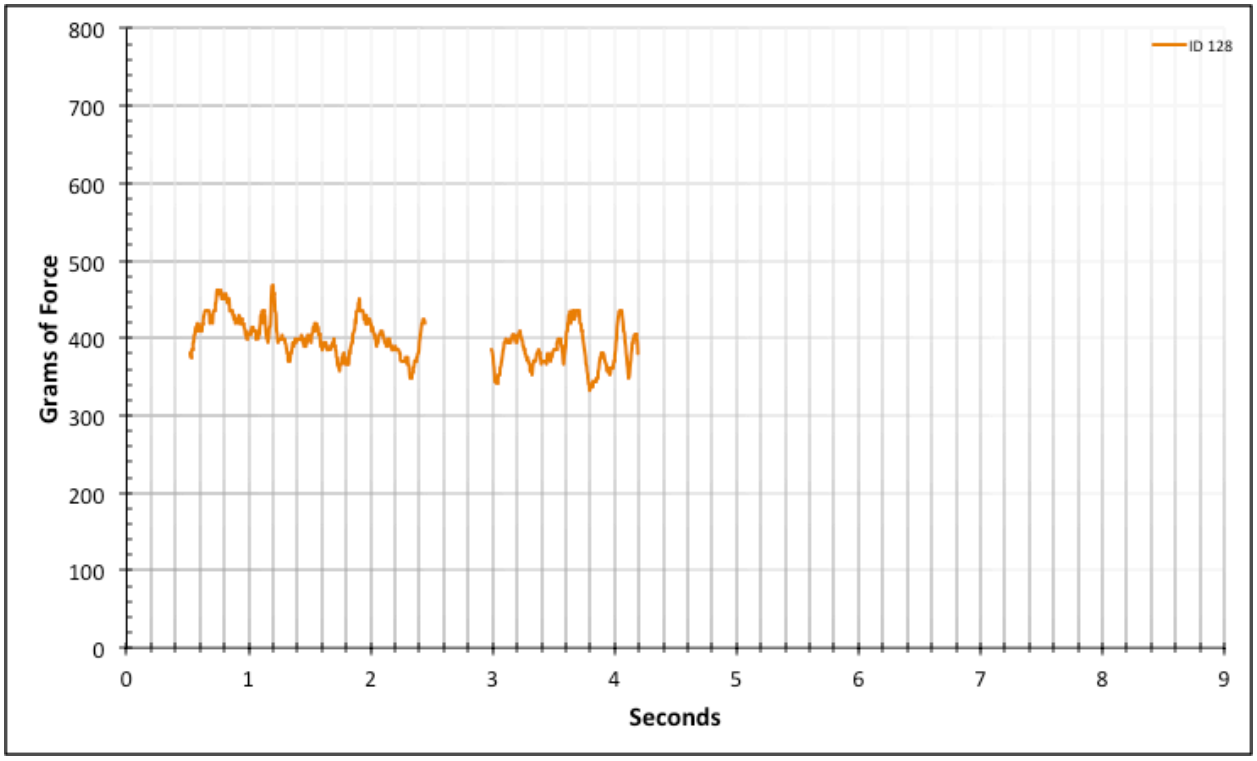

Figure A-6-234: Statistical Region Straight Baseline - Dry - ID 128 - #8, Bolt 3

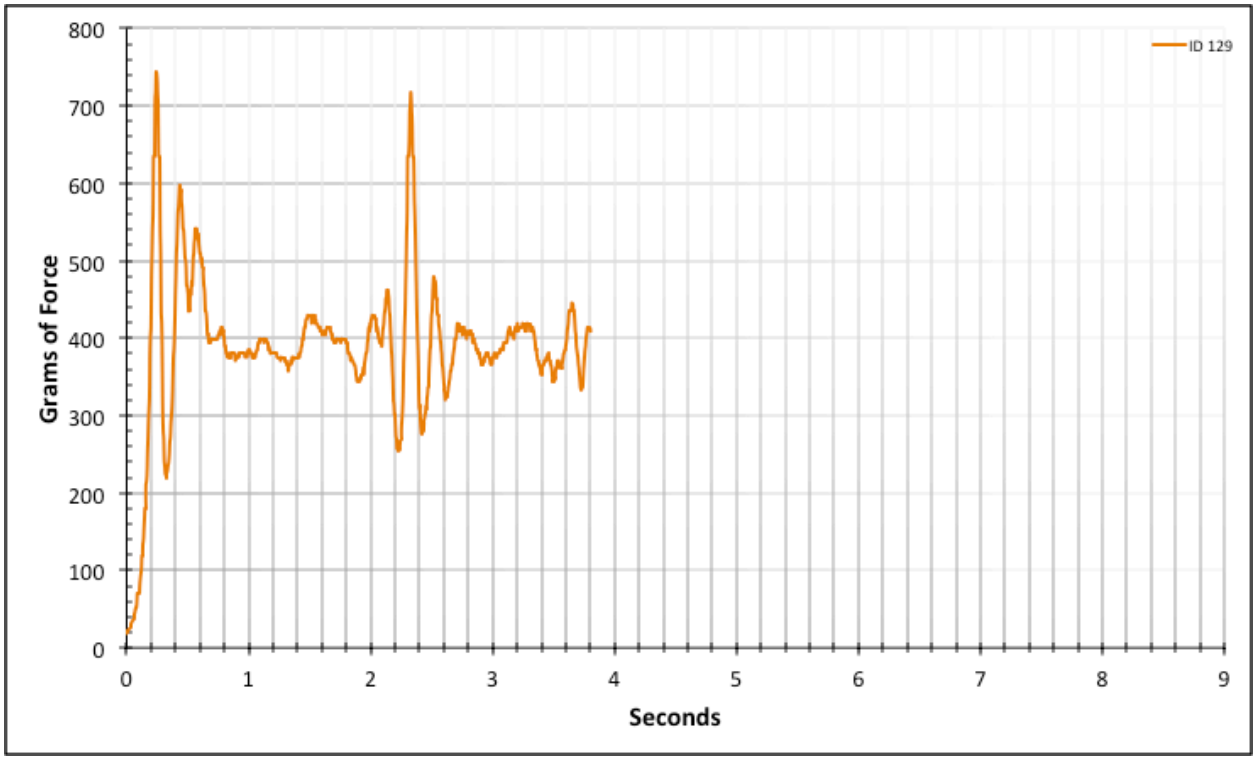

Figure A-6-235: Full Straight Baseline - Dry - ID 129 - #8, Bolt 3

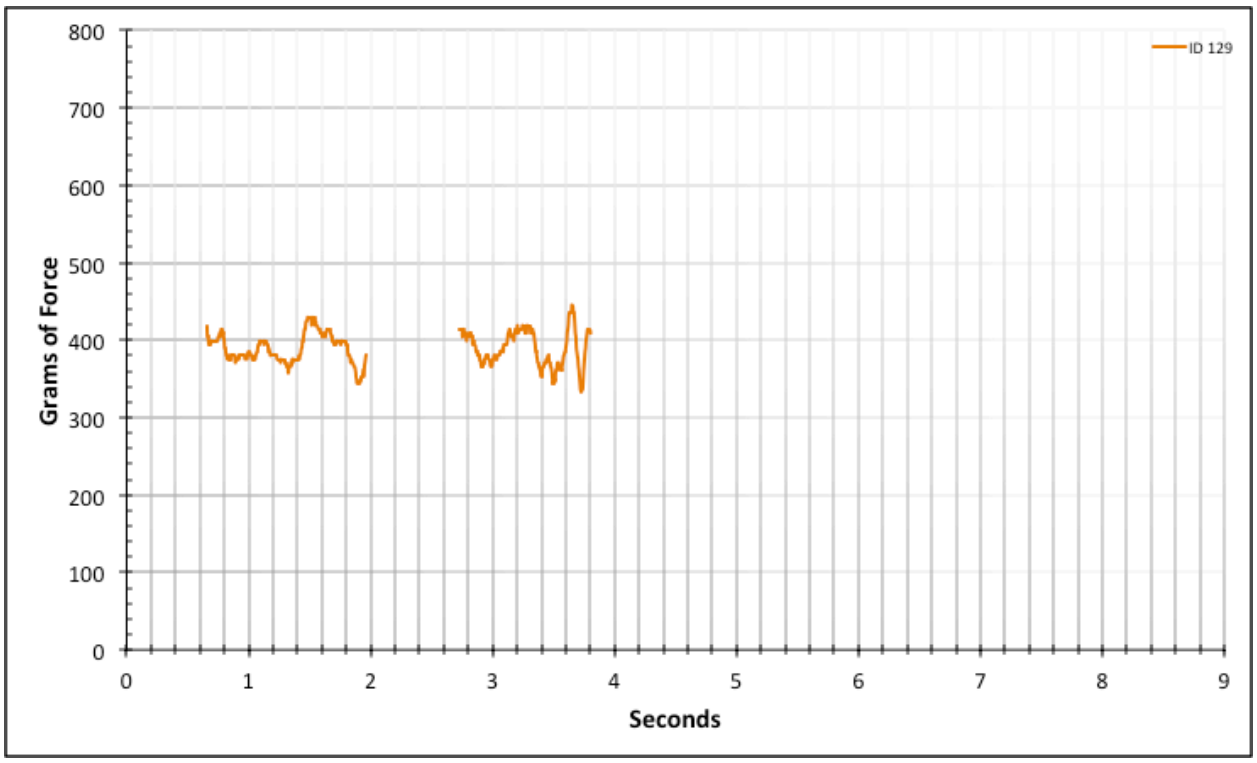

Figure A-6-236: Statistical Region Straight Baseline - Dry - ID 129 - #8, Bolt 3

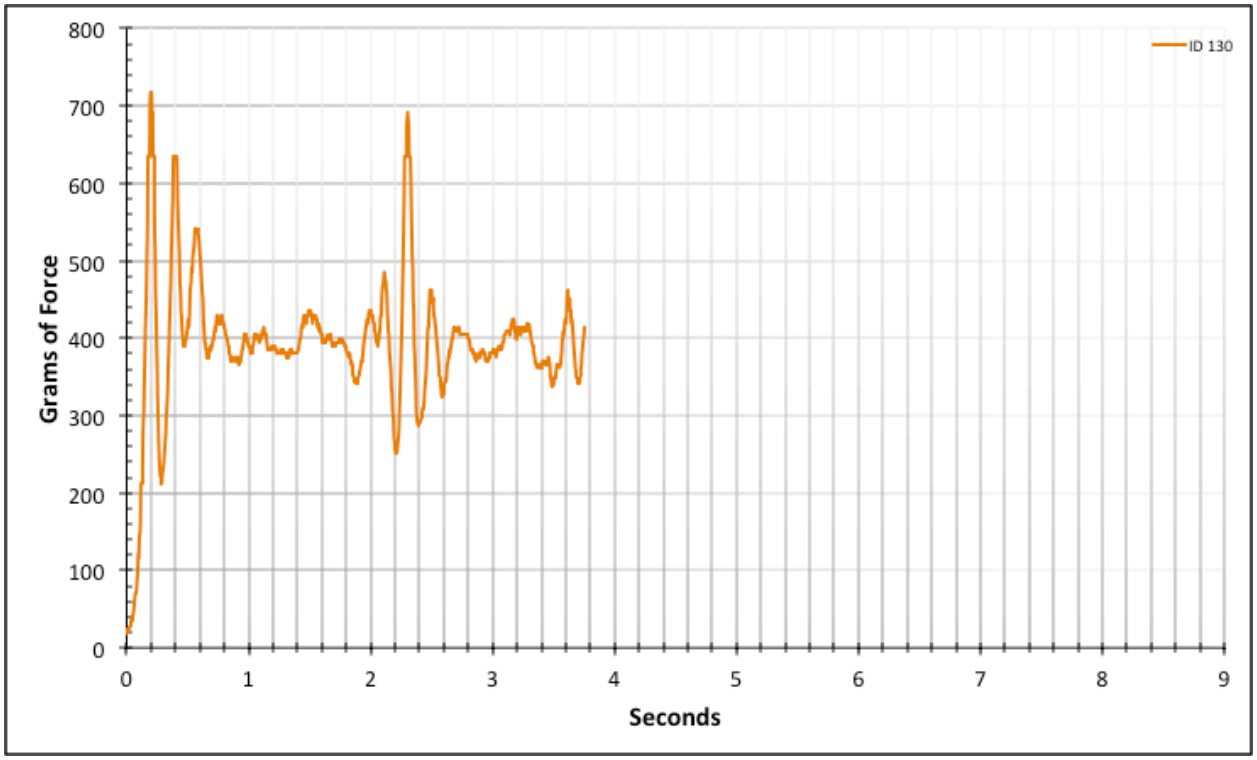

Figure A-6-237: Full Straight Baseline - Dry - ID 130 - #8, Bolt 3

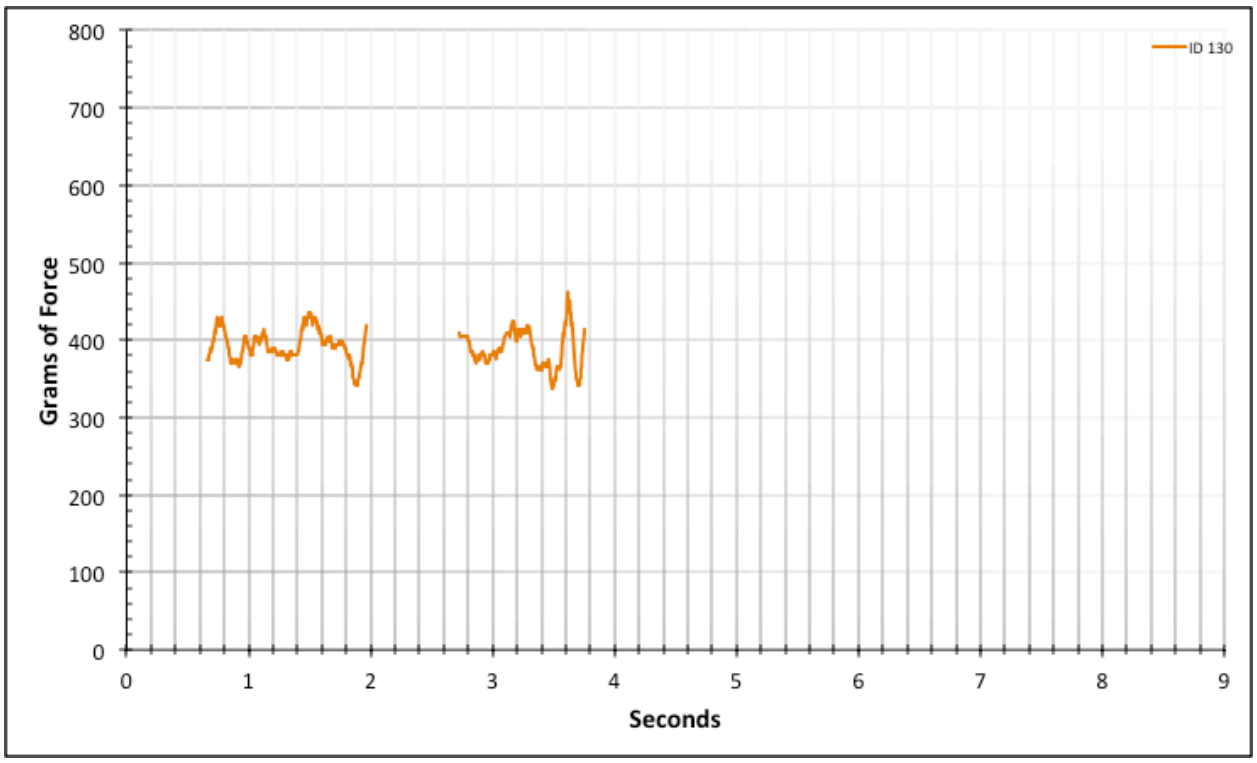

Figure A-6-238: Statistical Region Straight Baseline - Dry - ID 130 - #8, Bolt 3

A.4. Straight Baseline – Lubricated

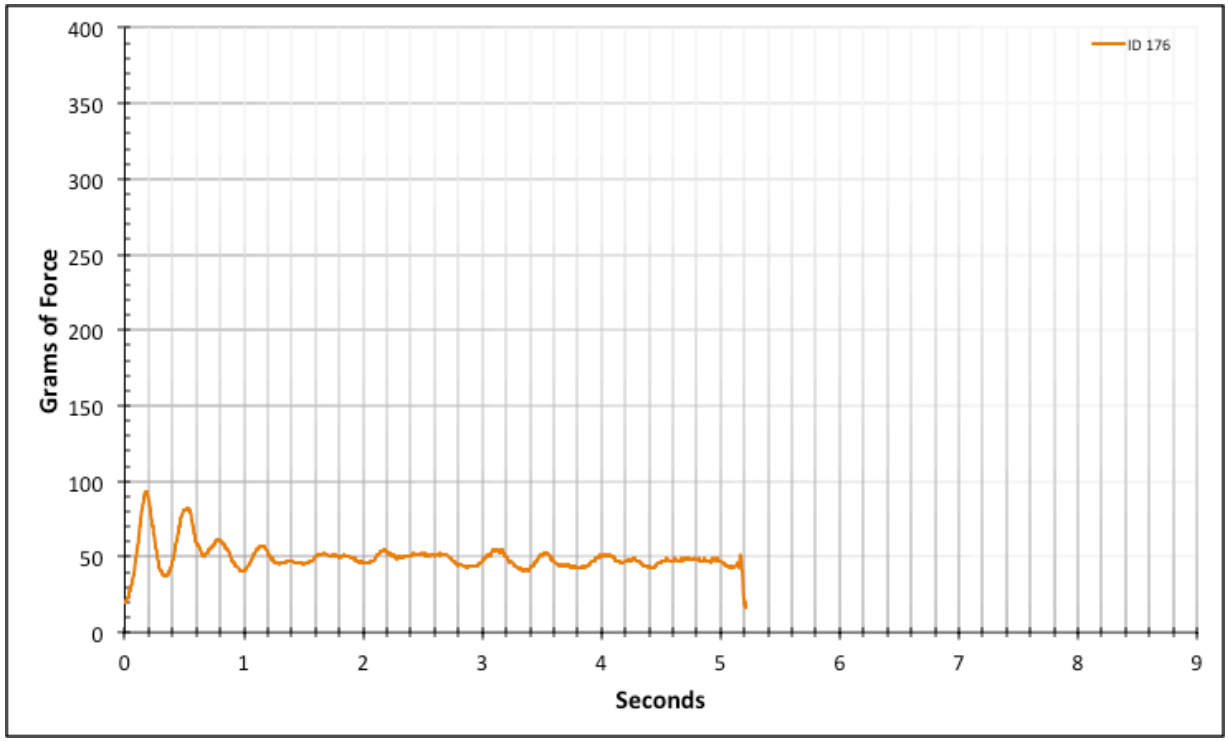

Figure A-6-239: Full Straight Baseline - Lubricated - ID 176 - #12, Bolt 1

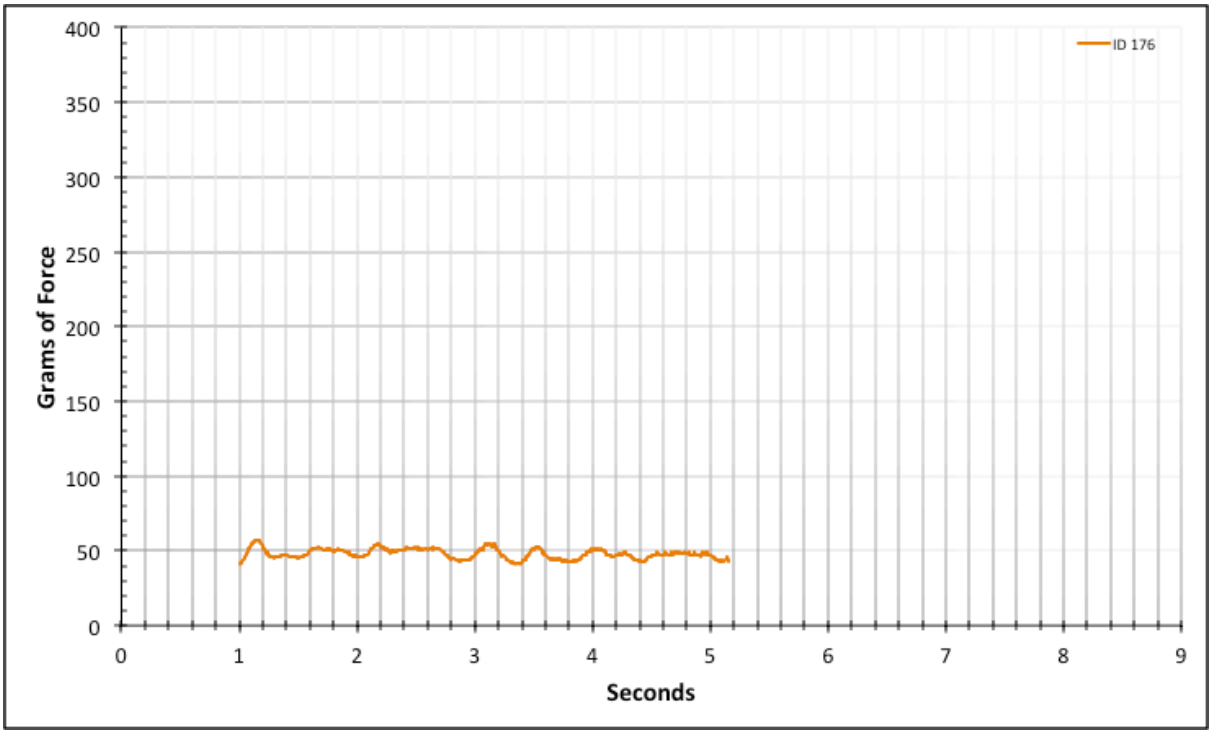

Figure A-6-240: Statistical Region Straight Baseline - Lubricated - ID 176 - #12, Bolt 1

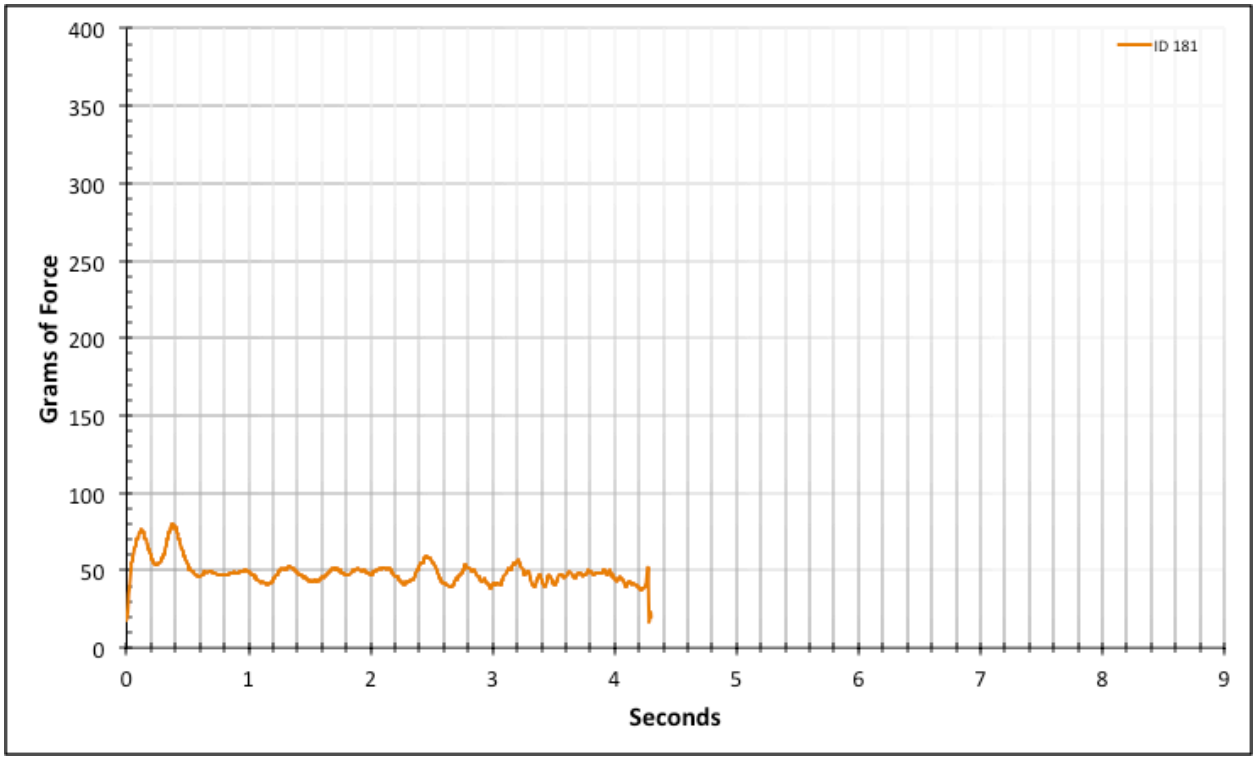

Figure A-6-241: Full Straight Baseline - Lubricated - ID 181 - #12, Bolt 2

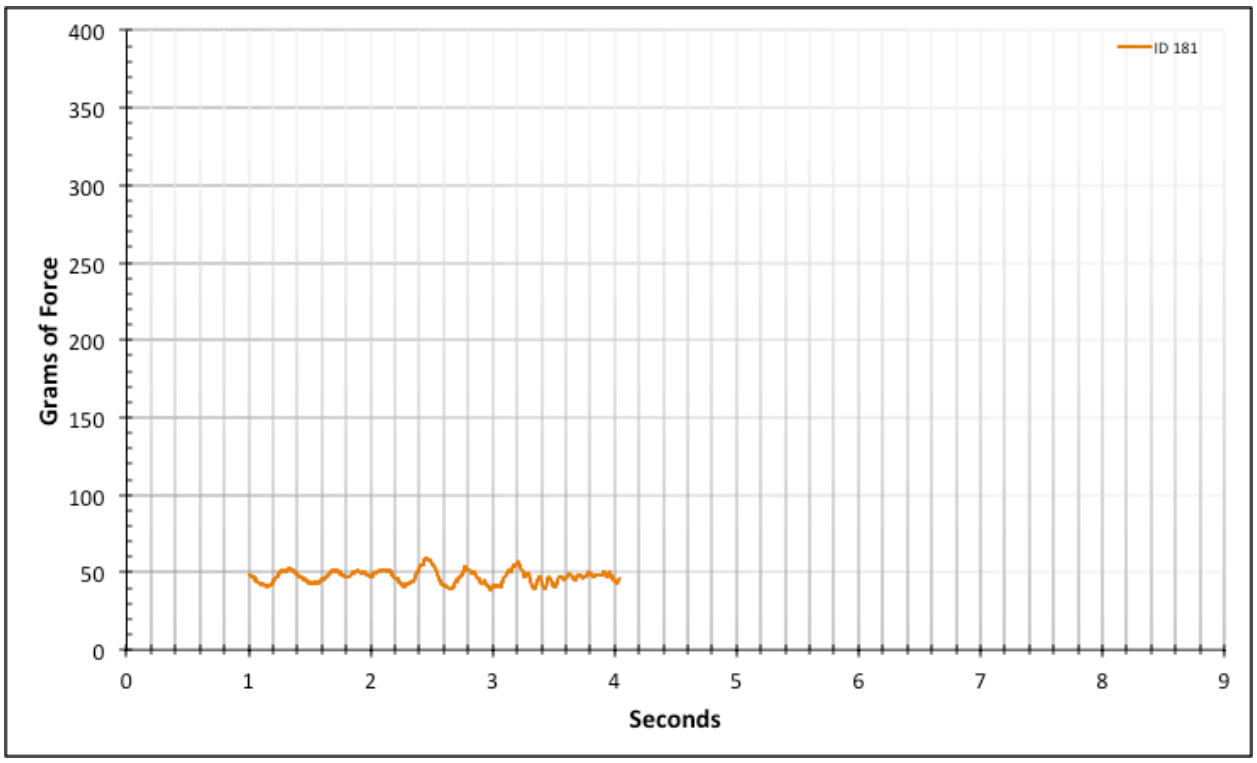

Figure A-6-242: Statistical Region Straight Baseline - Lubricated - ID 181 - #12, Bolt 2

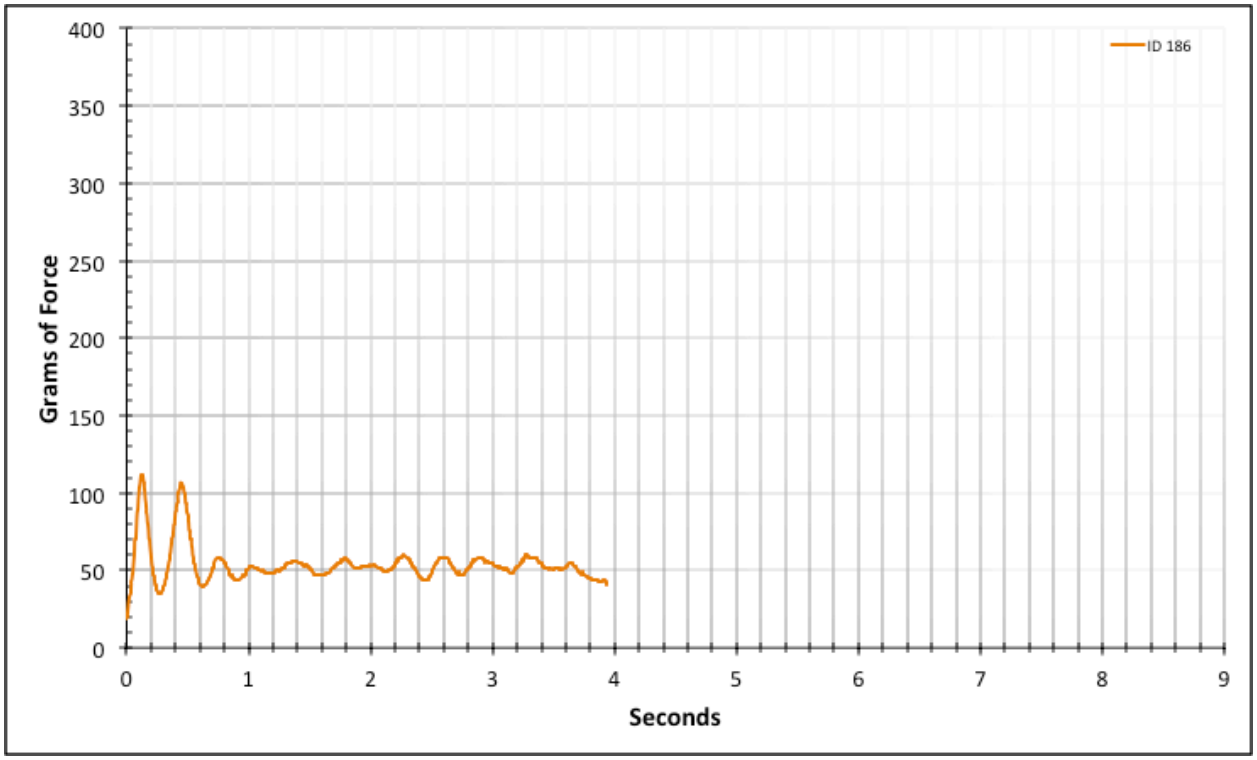

Figure A-6-243: Full Straight Baseline - Lubricated - ID 186 - #12, Bolt 3

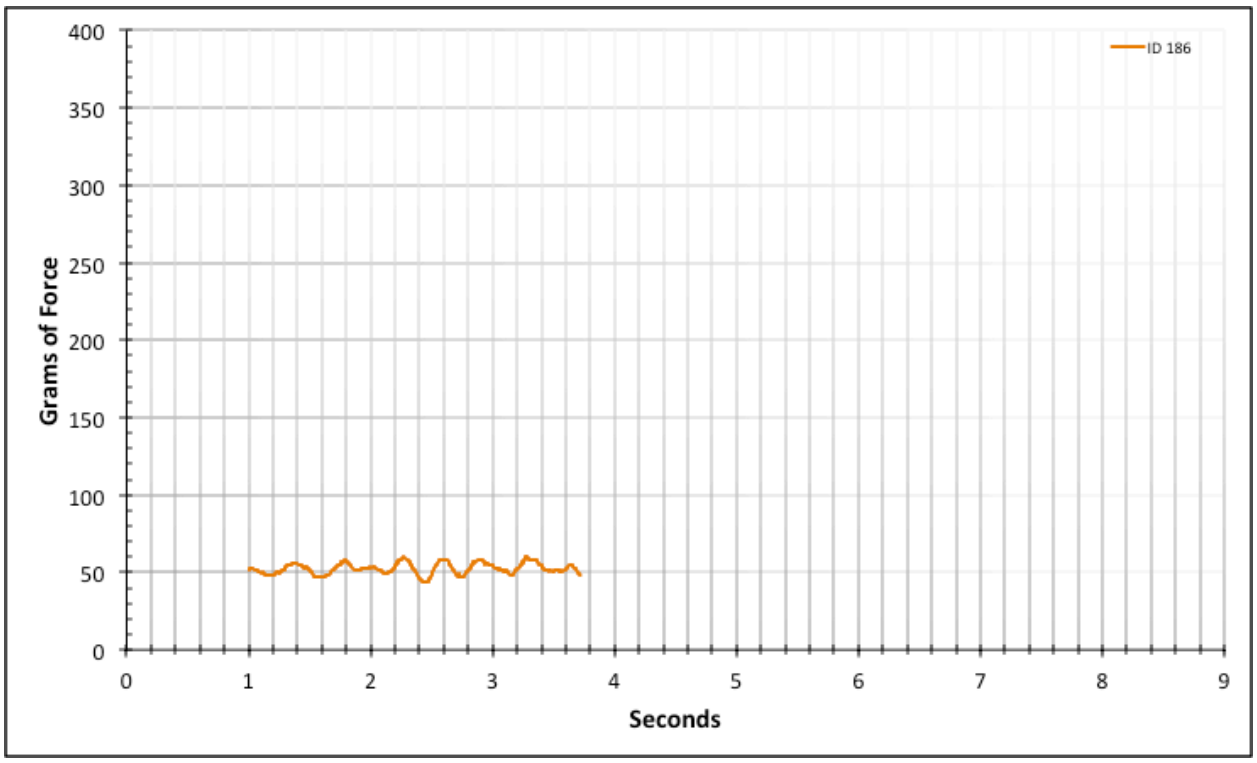

Figure A-6-244: Statistical Region Straight Baseline - Lubricated - ID 186 - #12, Bolt 3

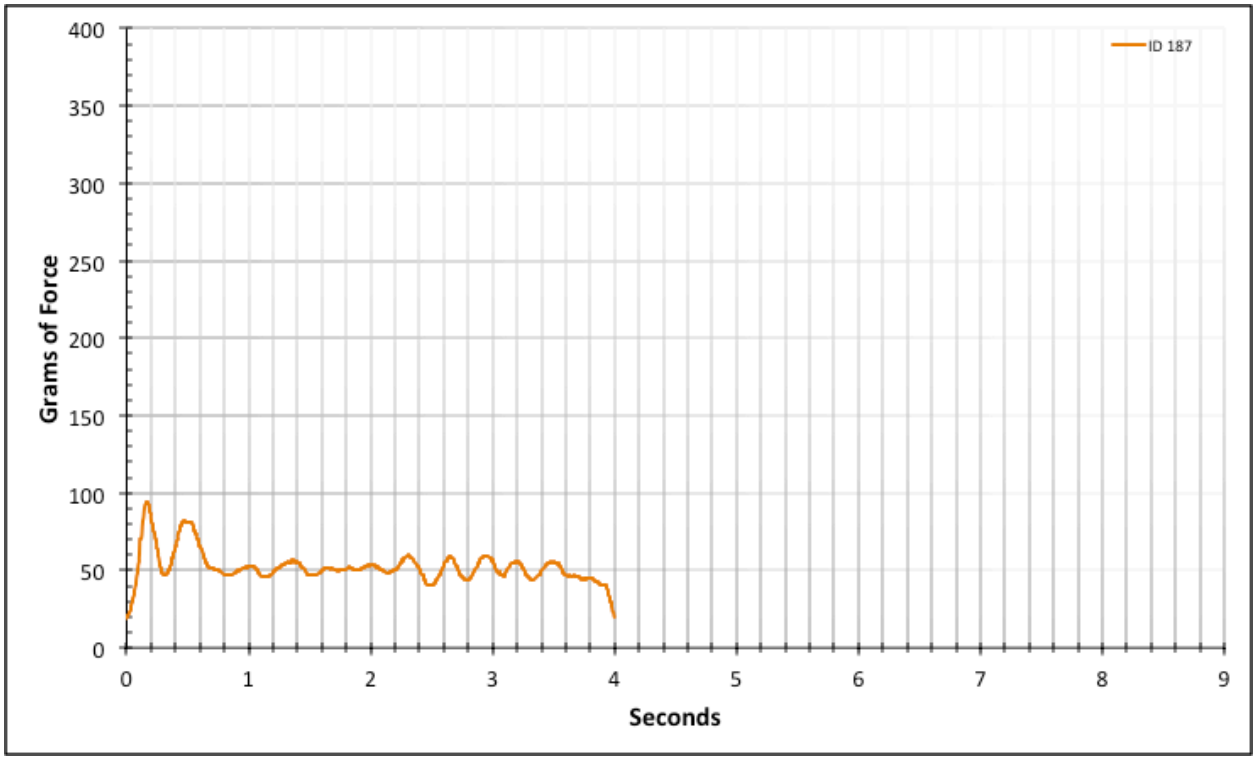

Figure A-6-245: Full Straight Baseline - Lubricated - ID 187 - #12, Bolt 3

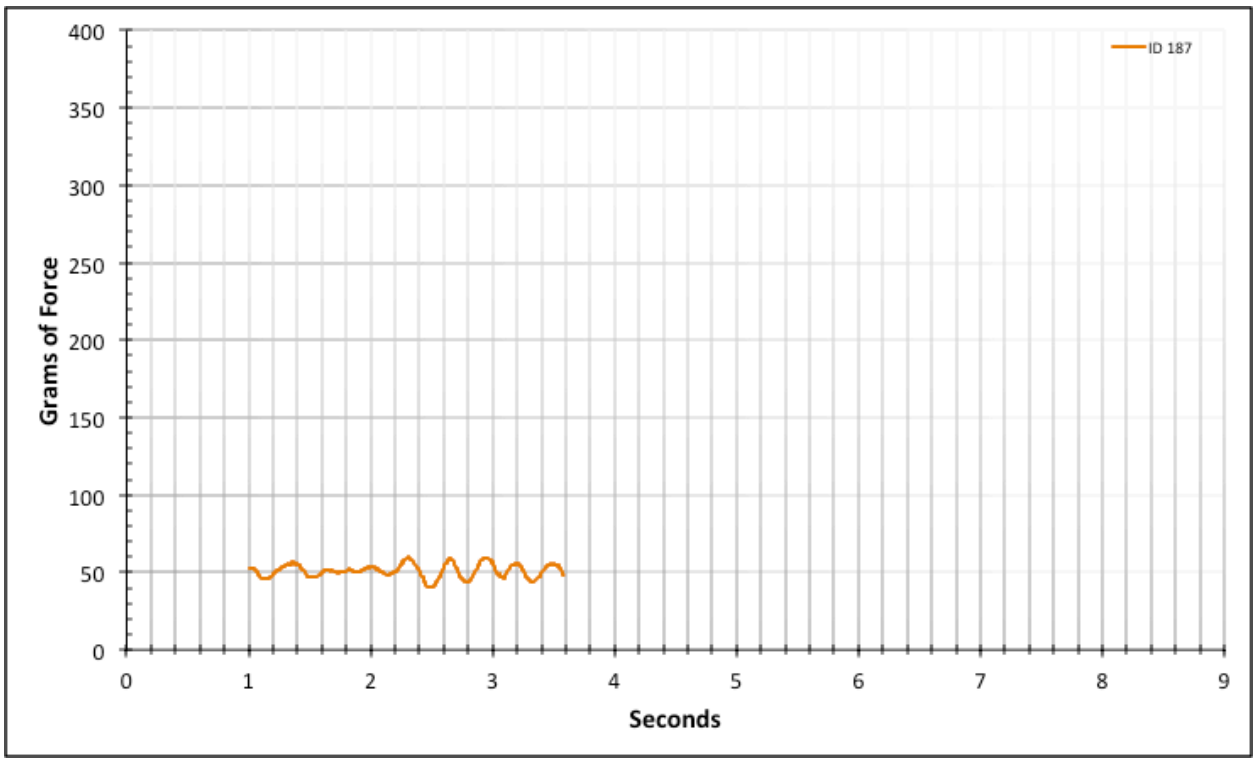

Figure A-6-246: Statistical Region Straight Baseline - Lubricated - ID 187 - #12, Bolt 3

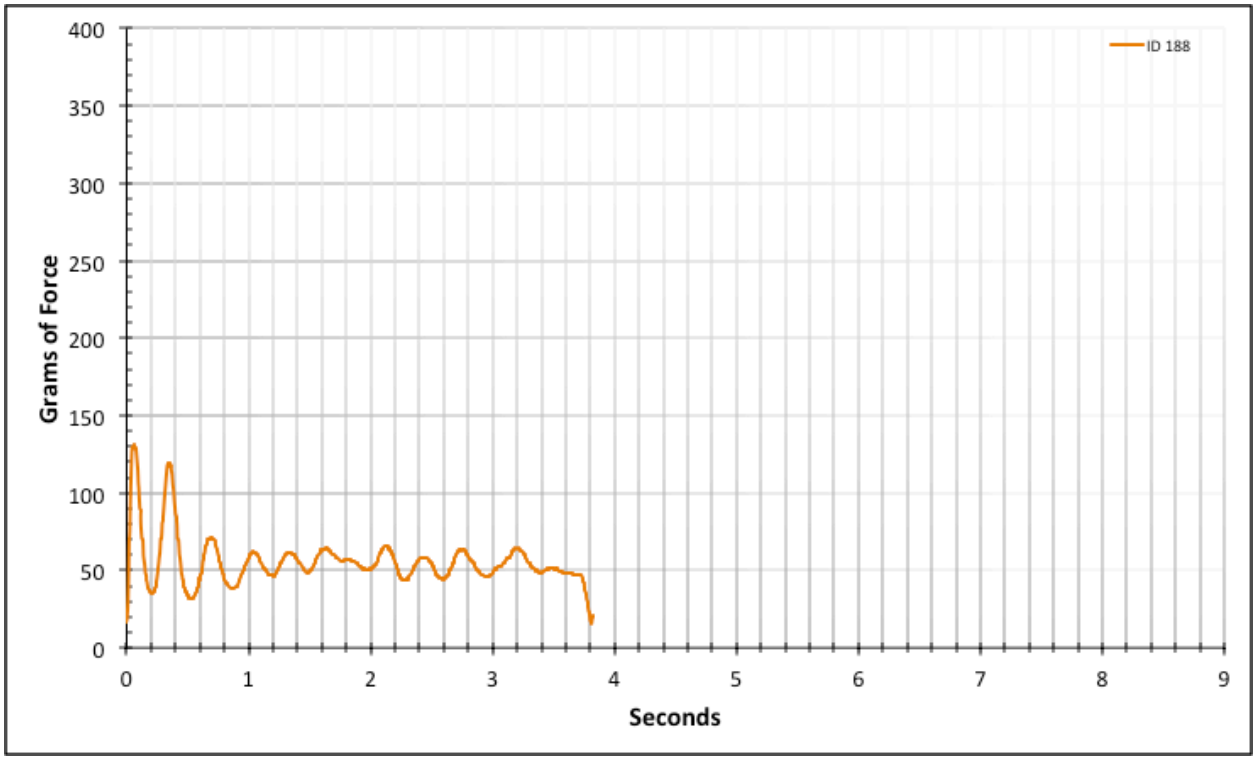

Figure A-6-247: Full Straight Baseline - Lubricated - ID 188 - #12, Bolt 3

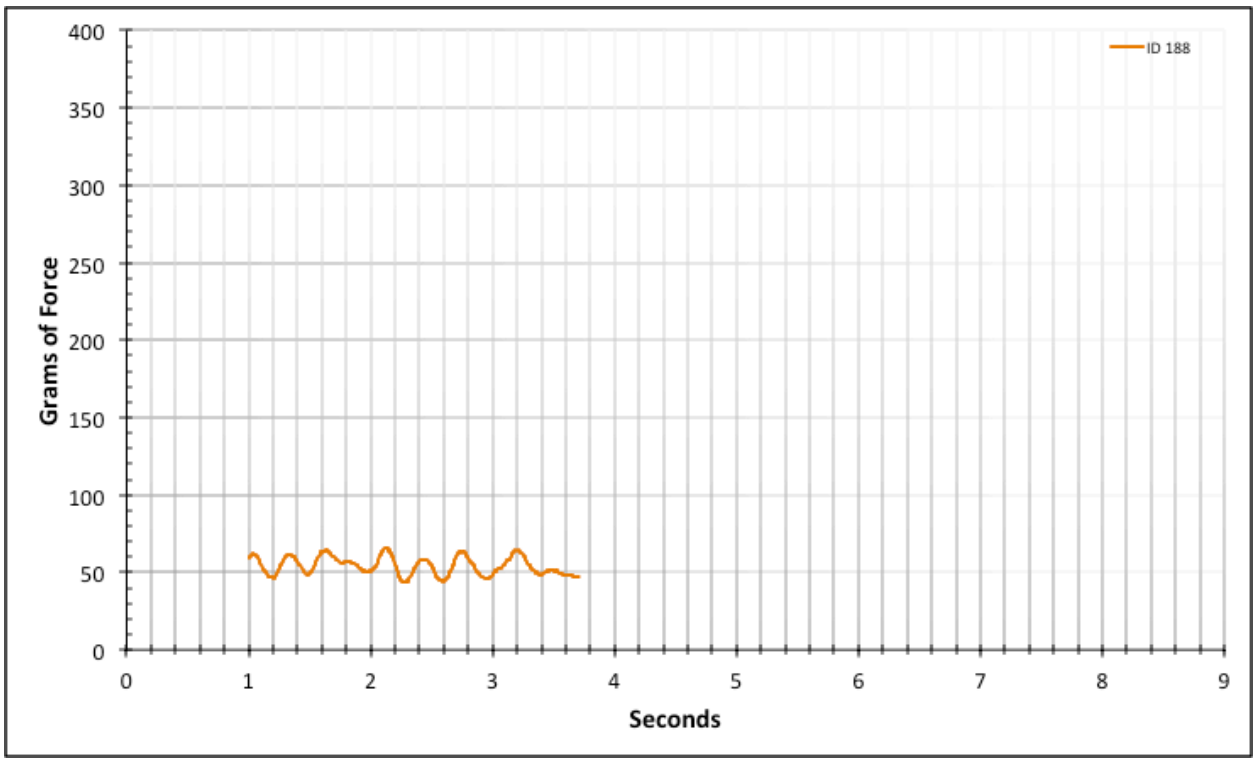

Figure A-6-248: Statistical Region Straight Baseline - Lubricated - ID 188 - #12, Bolt 3

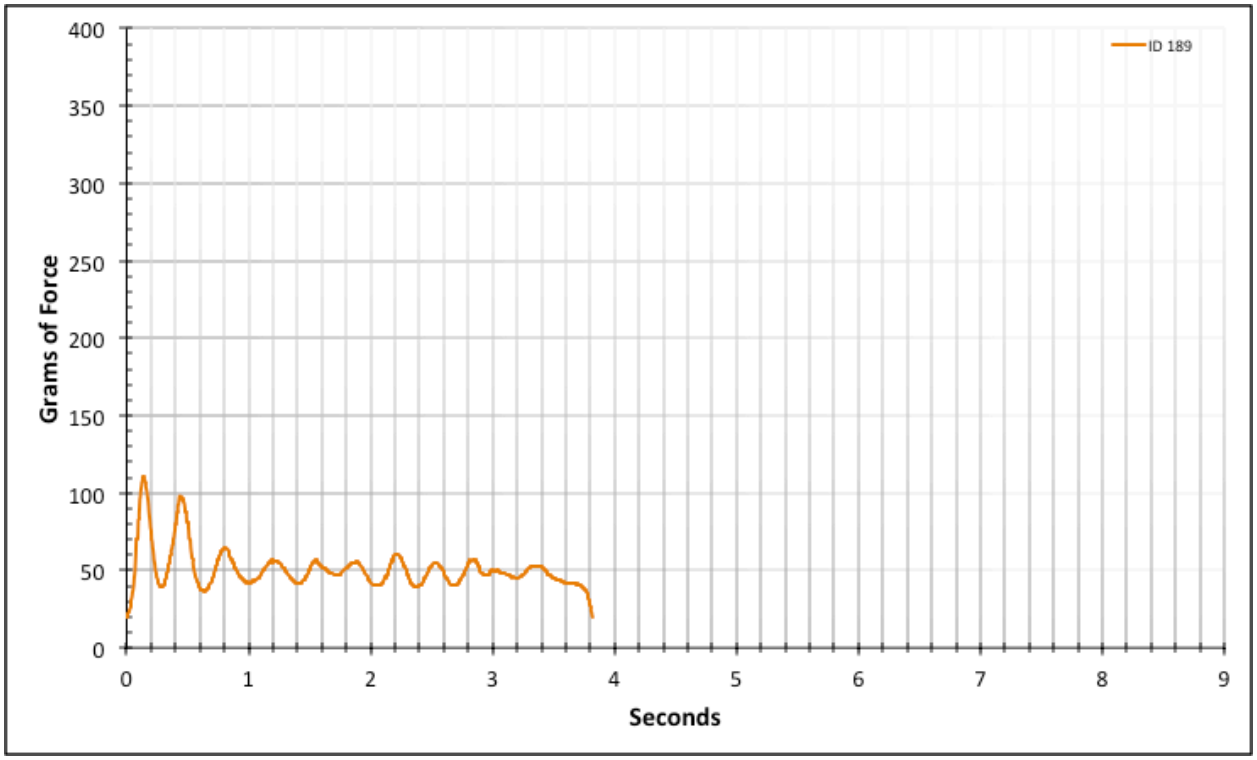

Figure A-6-249: Full Straight Baseline - Lubricated - ID 189 - #12, Bolt 3

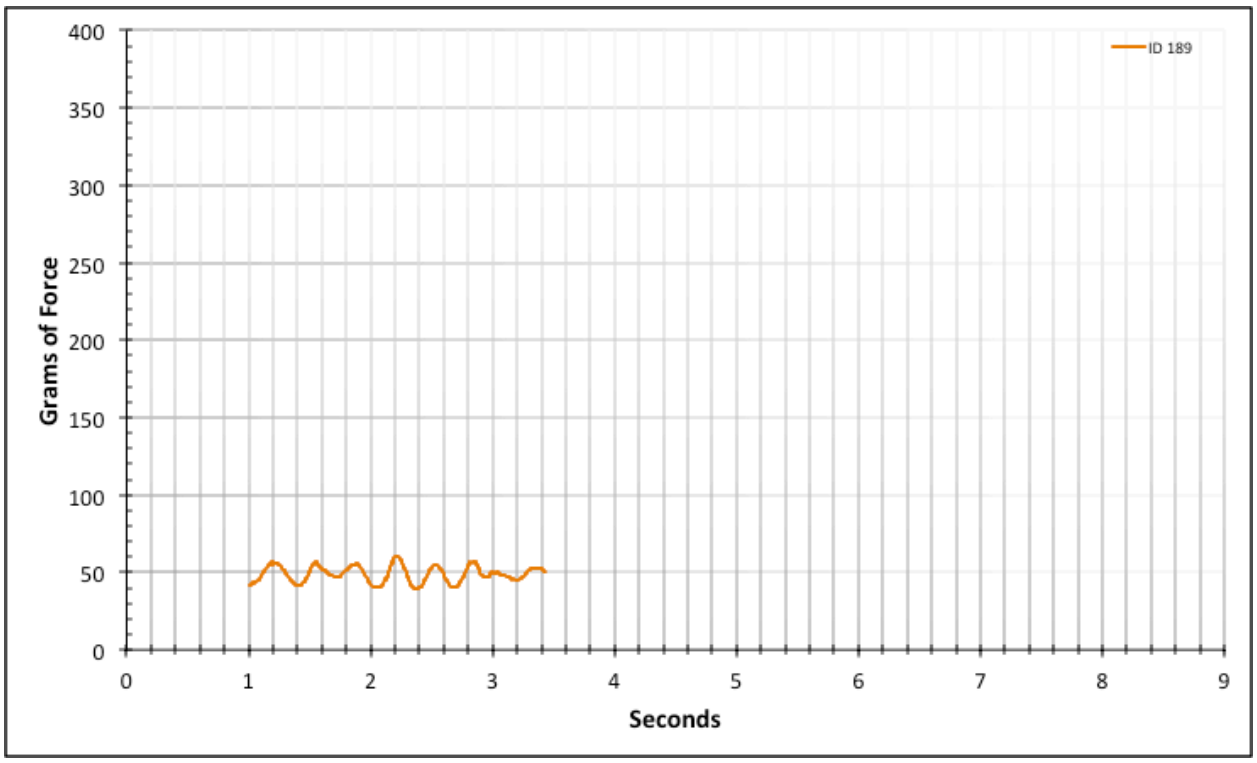

Figure A-6-250: Statistical Region Straight Baseline - Lubricated - ID 189 - #12, Bolt 3

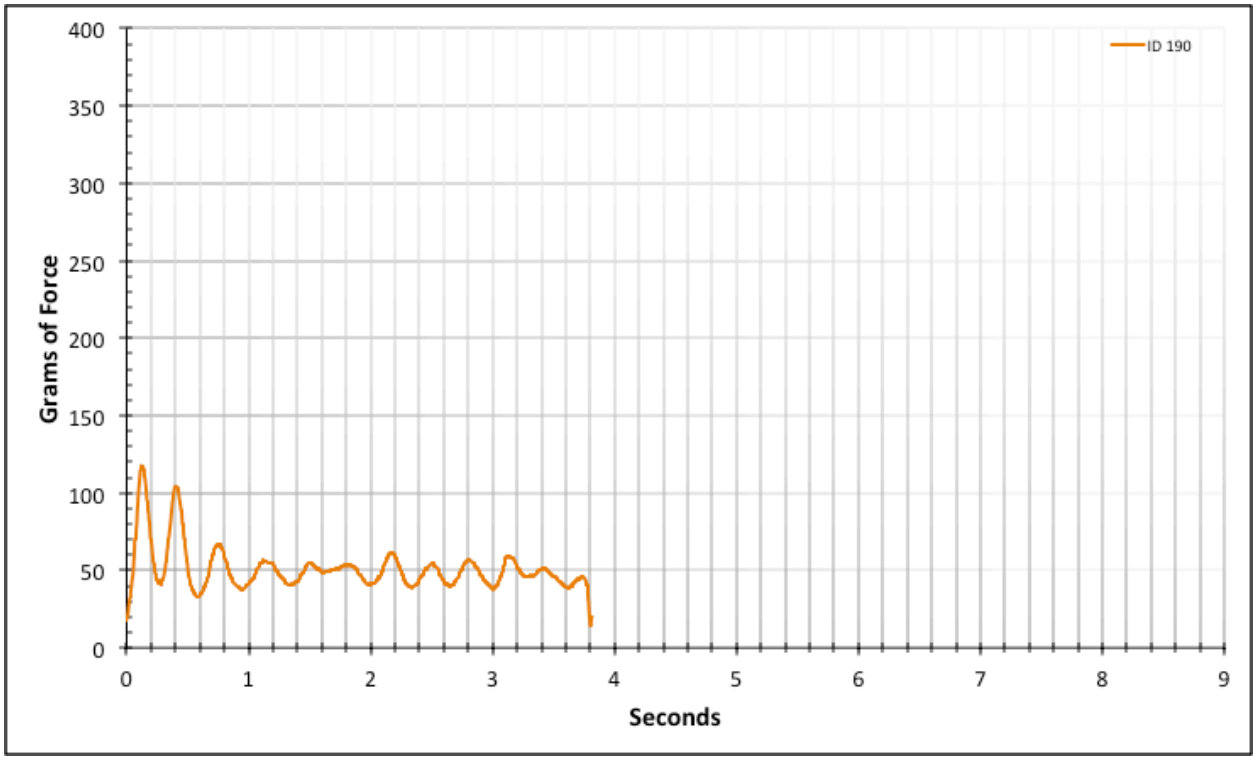

Figure A-6-251: Full Straight Baseline - Lubricated - ID 190 - #12, Bolt 3

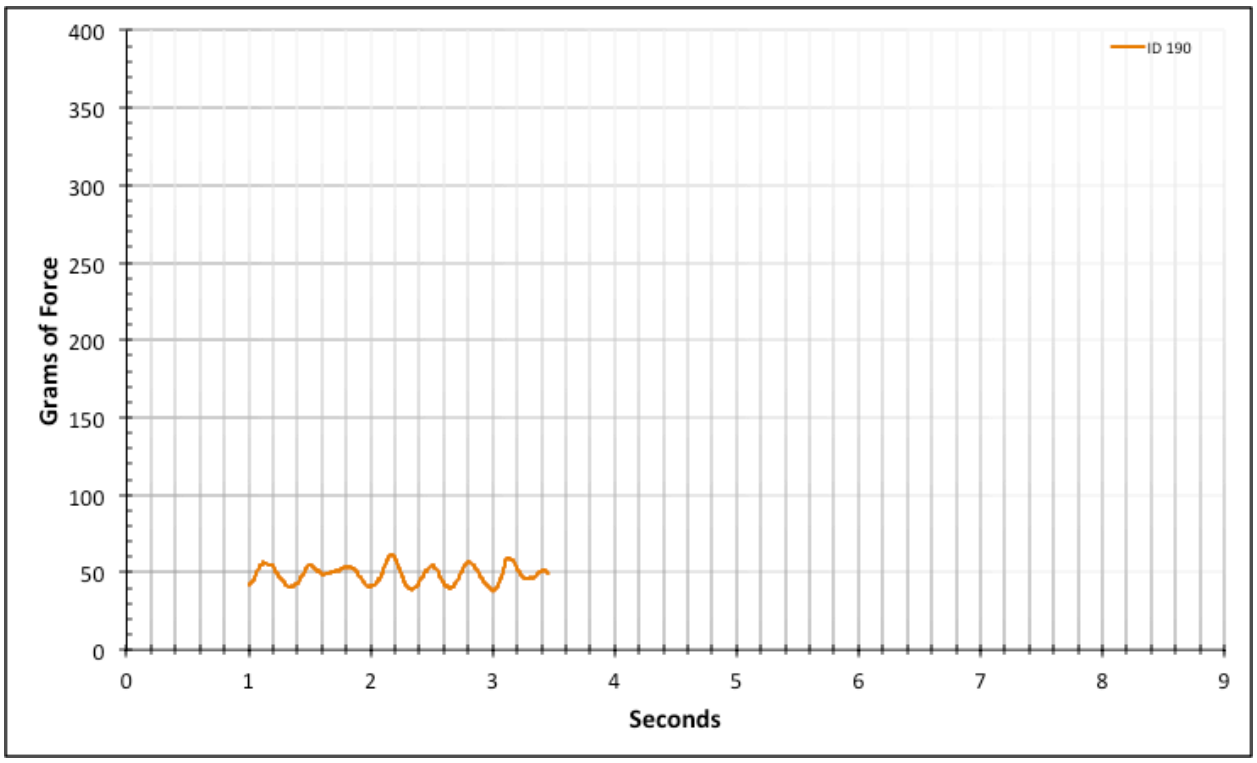

Figure A-6-252: Statistical Region Straight Baseline - Lubricated - ID 190 - #12, Bolt 3

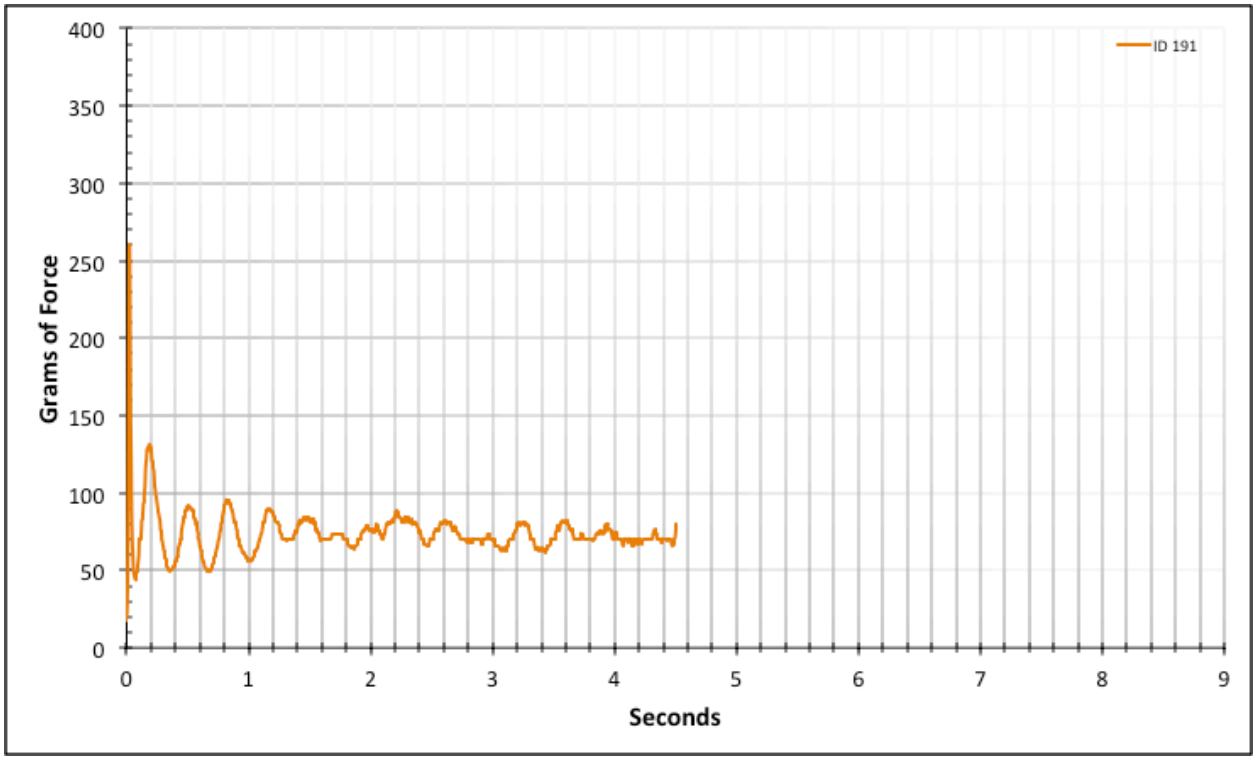

Figure A-6-253: Full Straight Baseline - Lubricated - ID 191 - #10, Bolt 1

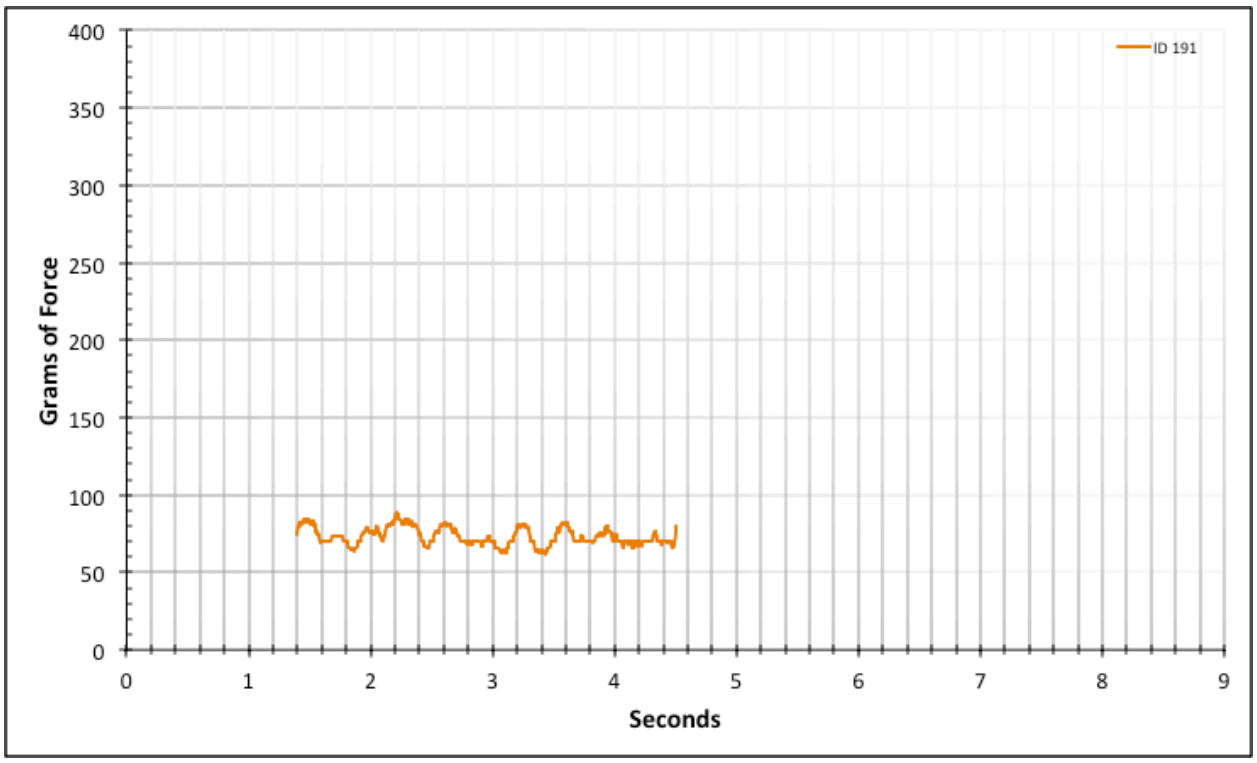

Figure A-6-254: Statistical Region Straight Baseline - Lubricated - ID 191 - #10, Bolt 1

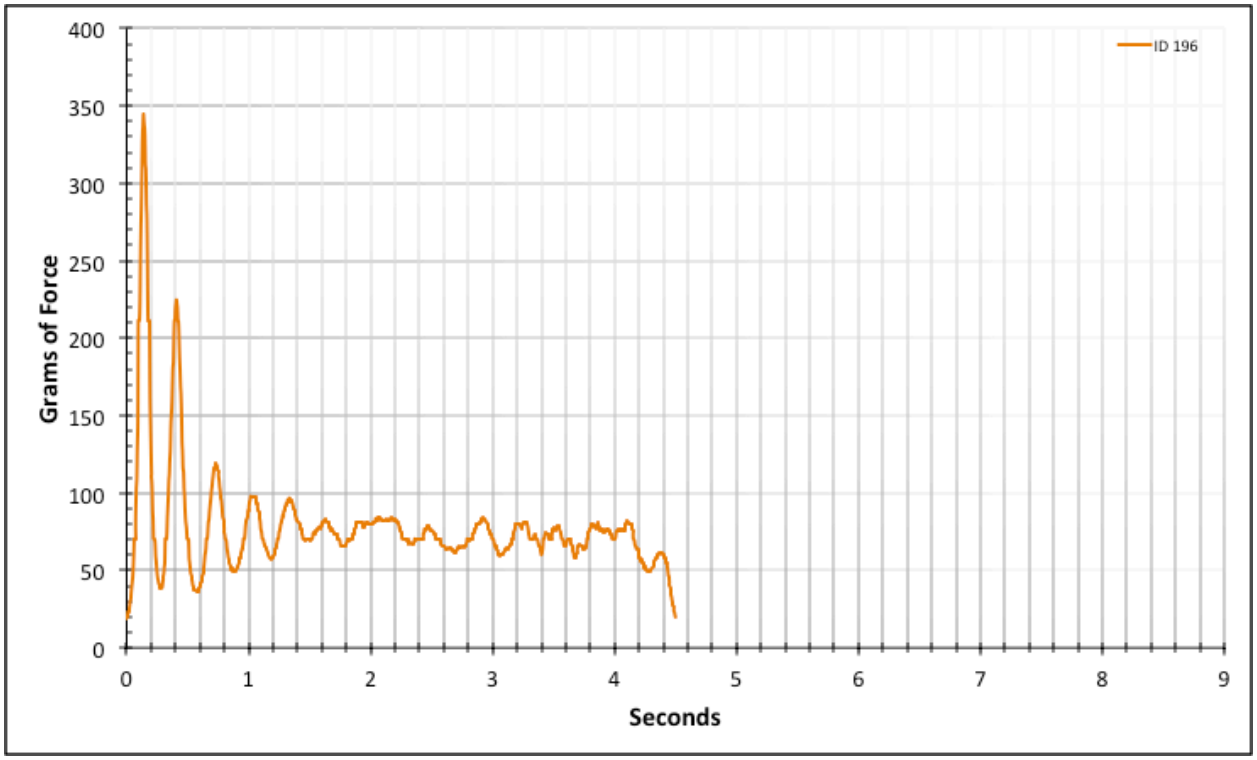

Figure A-6-255: Full Straight Baseline - Lubricated - ID 196 - #10, Bolt 2

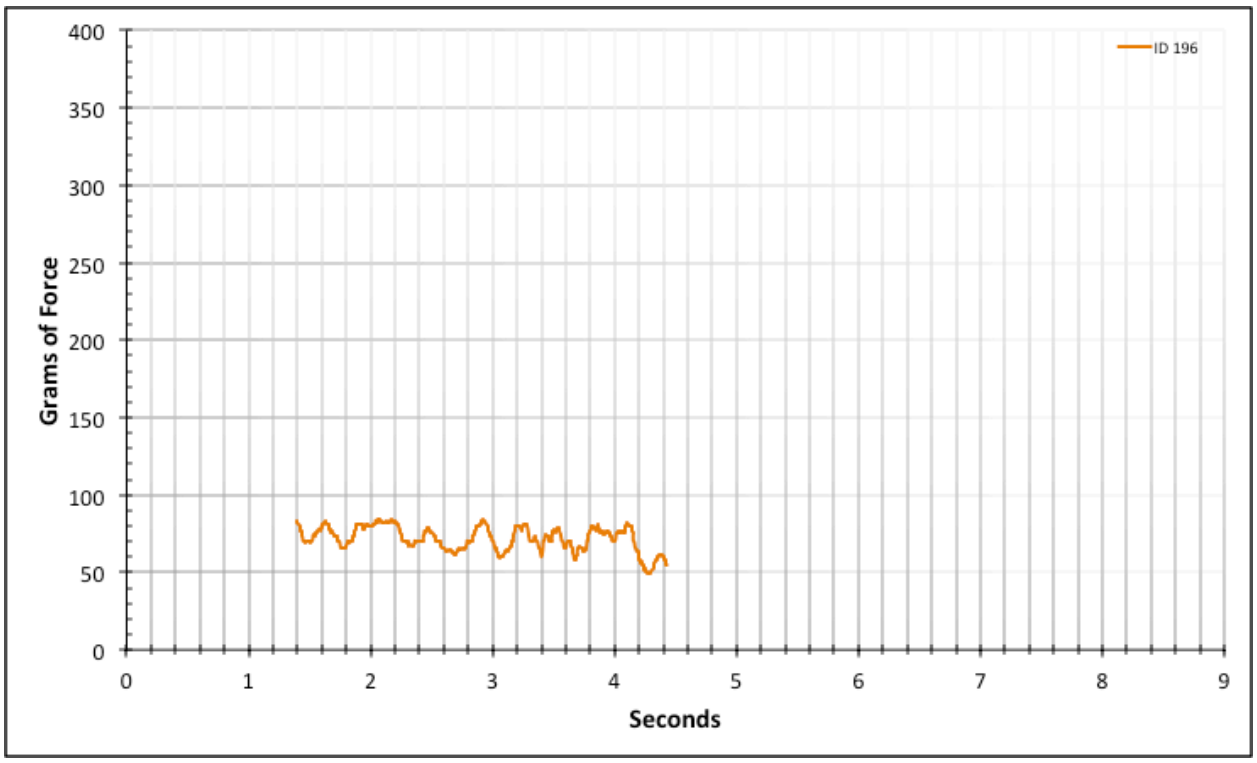

Figure A-6-256: Statistical Region Straight Baseline - Lubricated - ID 196 - #10, Bolt 2

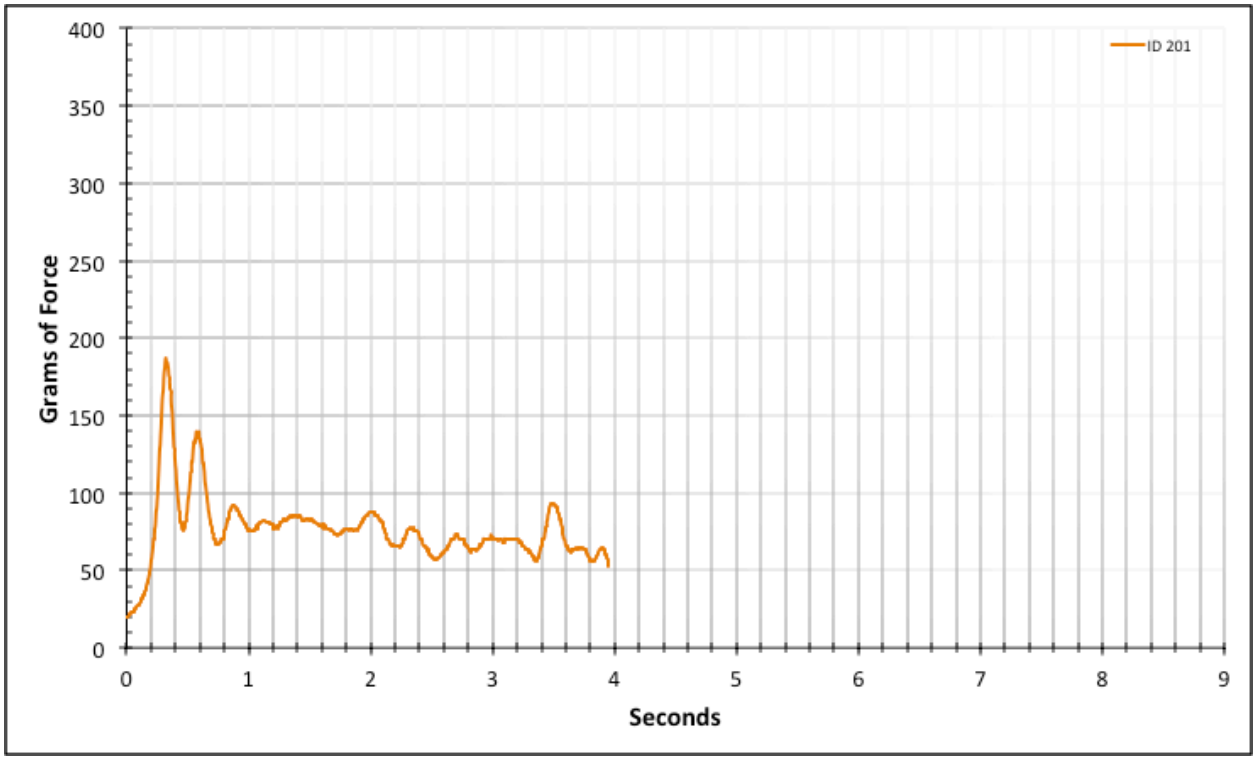

Figure A-6-257: Full Straight Baseline - Lubricated - ID 201 - #10, Bolt 3

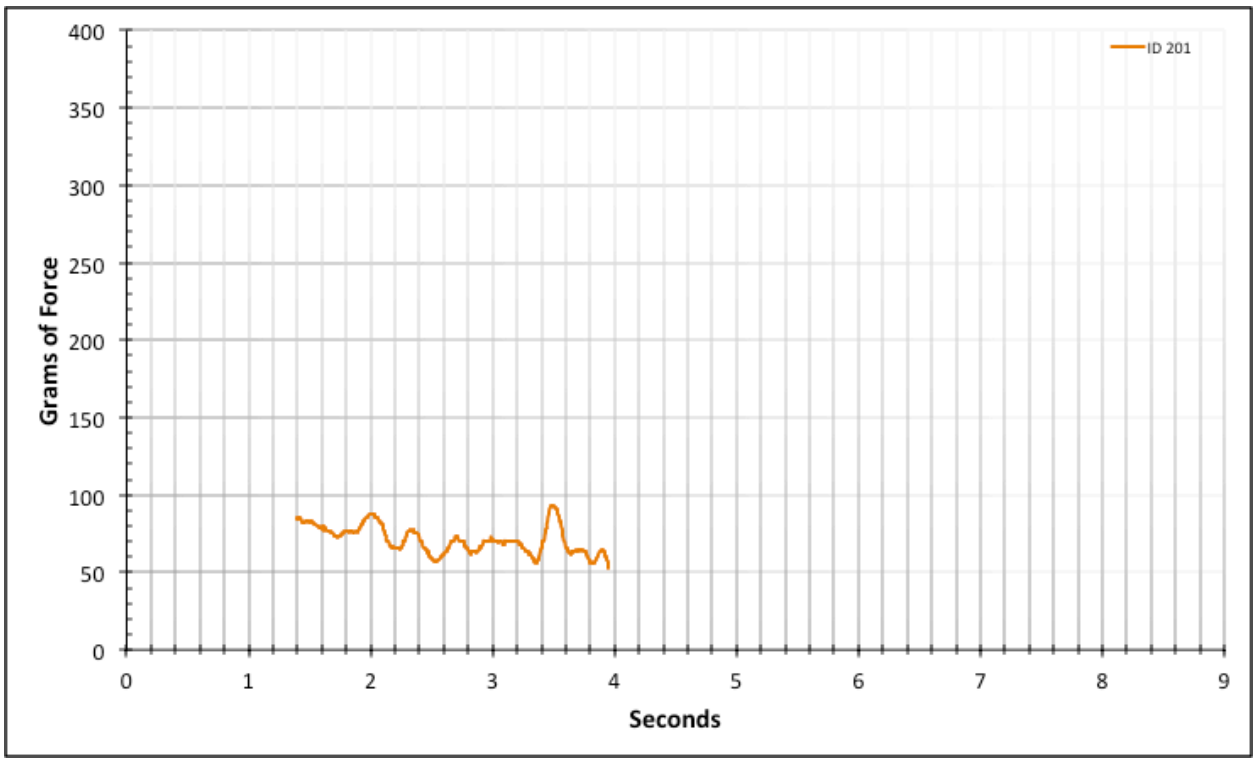

Figure A-6-258: Statistical Region Straight Baseline - Lubricated - ID 201 - #10, Bolt 3

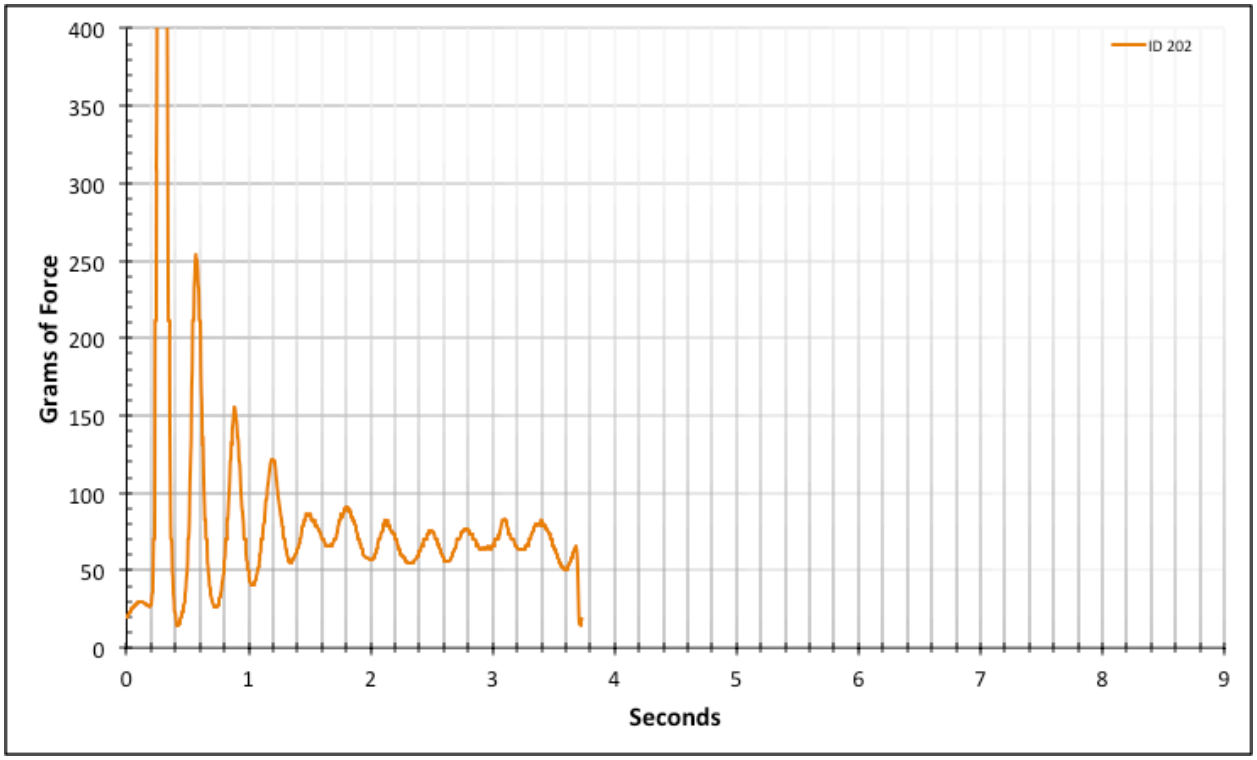

Figure A-6-259: Full Straight Baseline - Lubricated - ID 202 - #10, Bolt 3

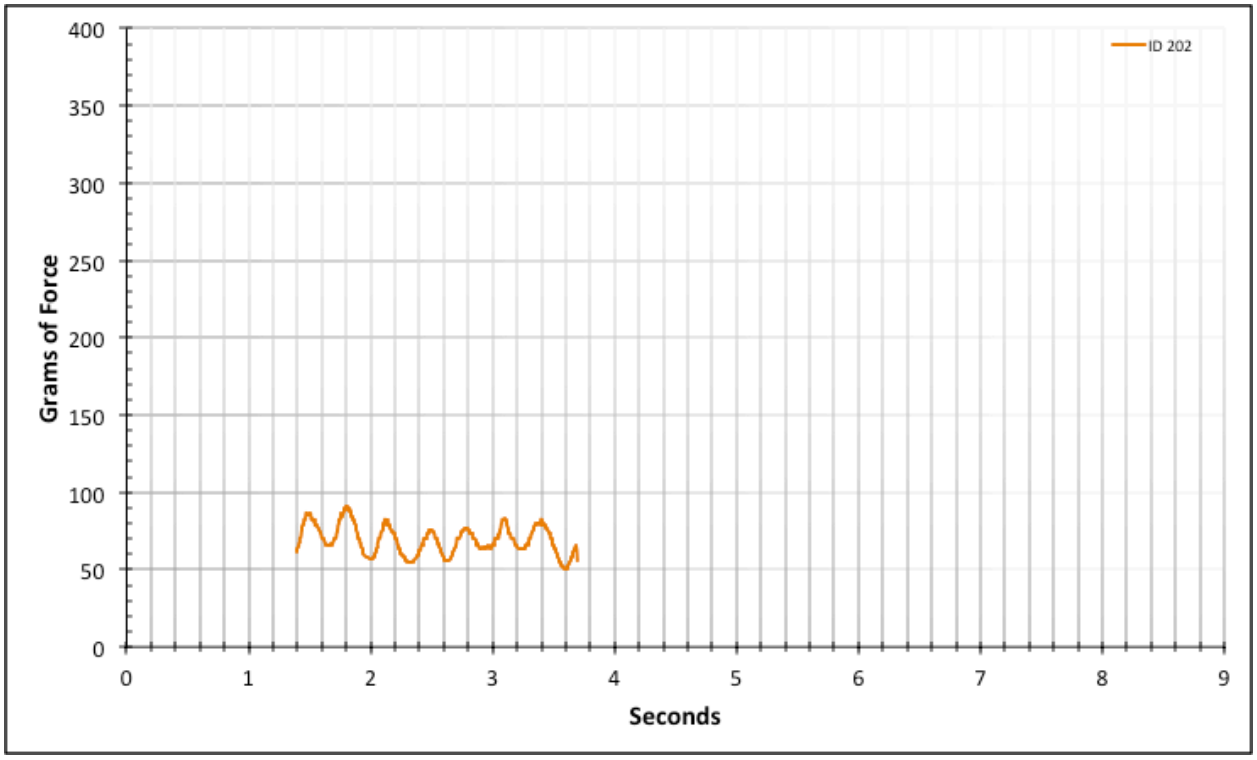

Figure A-6-260: Statistical Region Straight Baseline - Lubricated - ID 202 - #10, Bolt 3

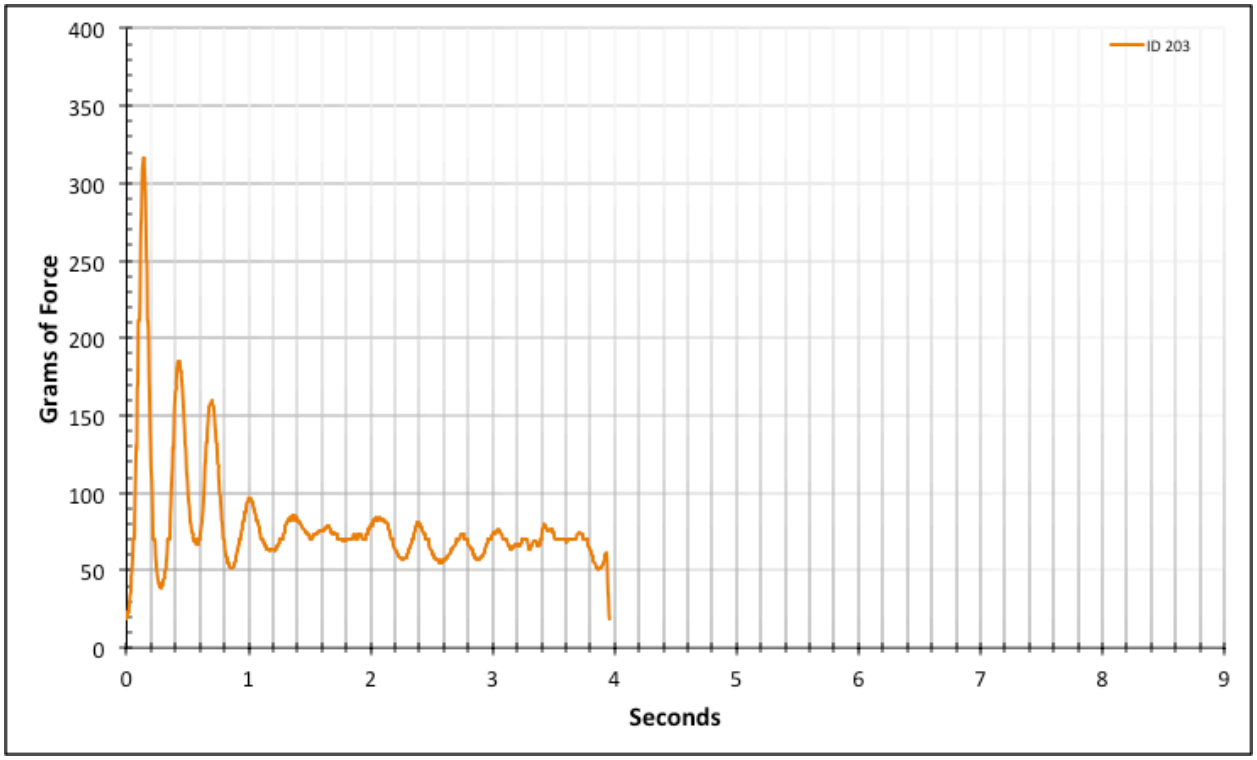

Figure A-6-261: Full Straight Baseline - Lubricated - ID 203 - #10, Bolt 3

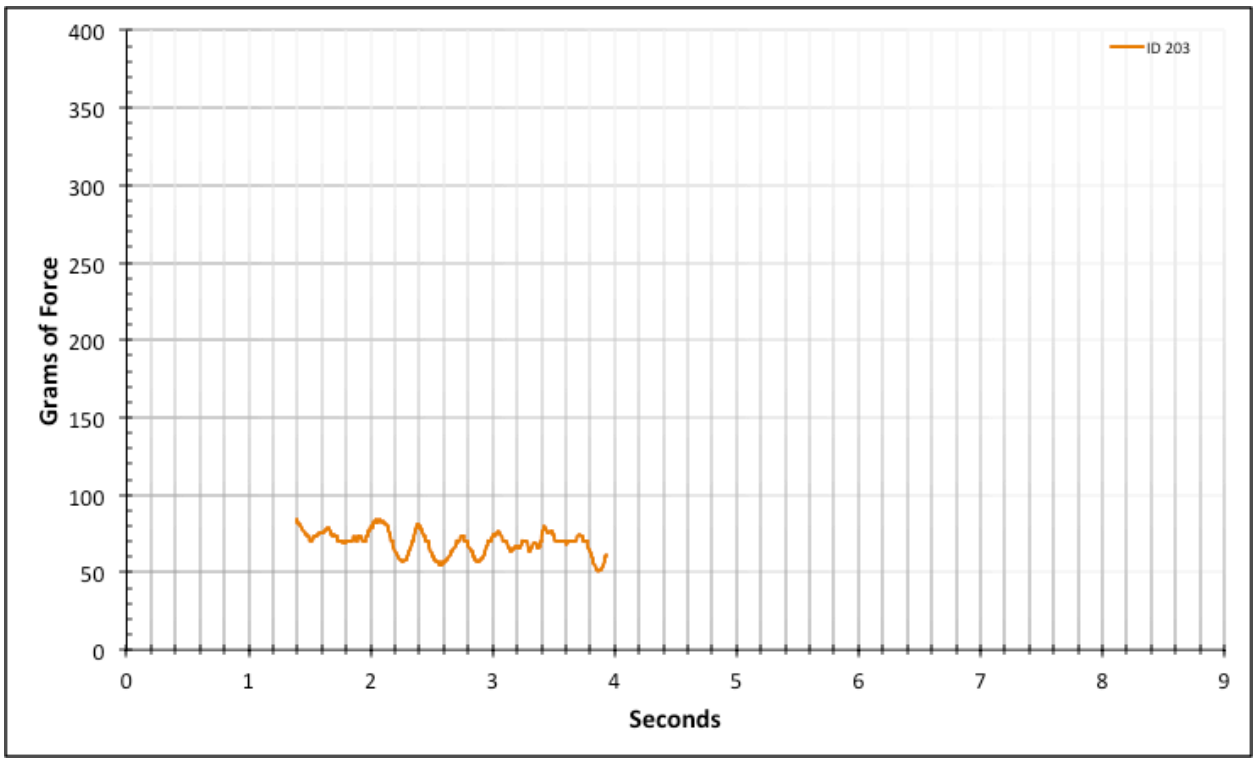

Figure A-6-262: Statistical Region Straight Baseline - Lubricated - ID 203 - #10, Bolt 3

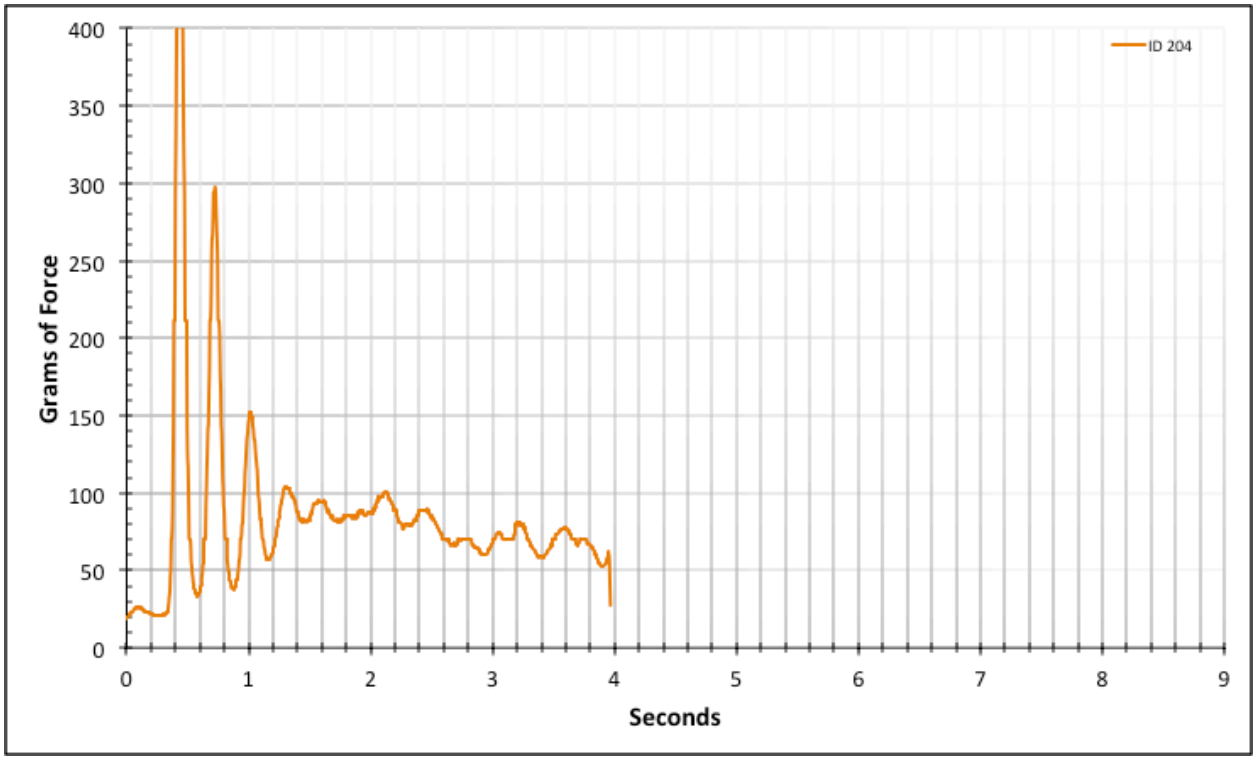

Figure A-6-263: Full Straight Baseline - Lubricated - ID 204 - #10, Bolt 3

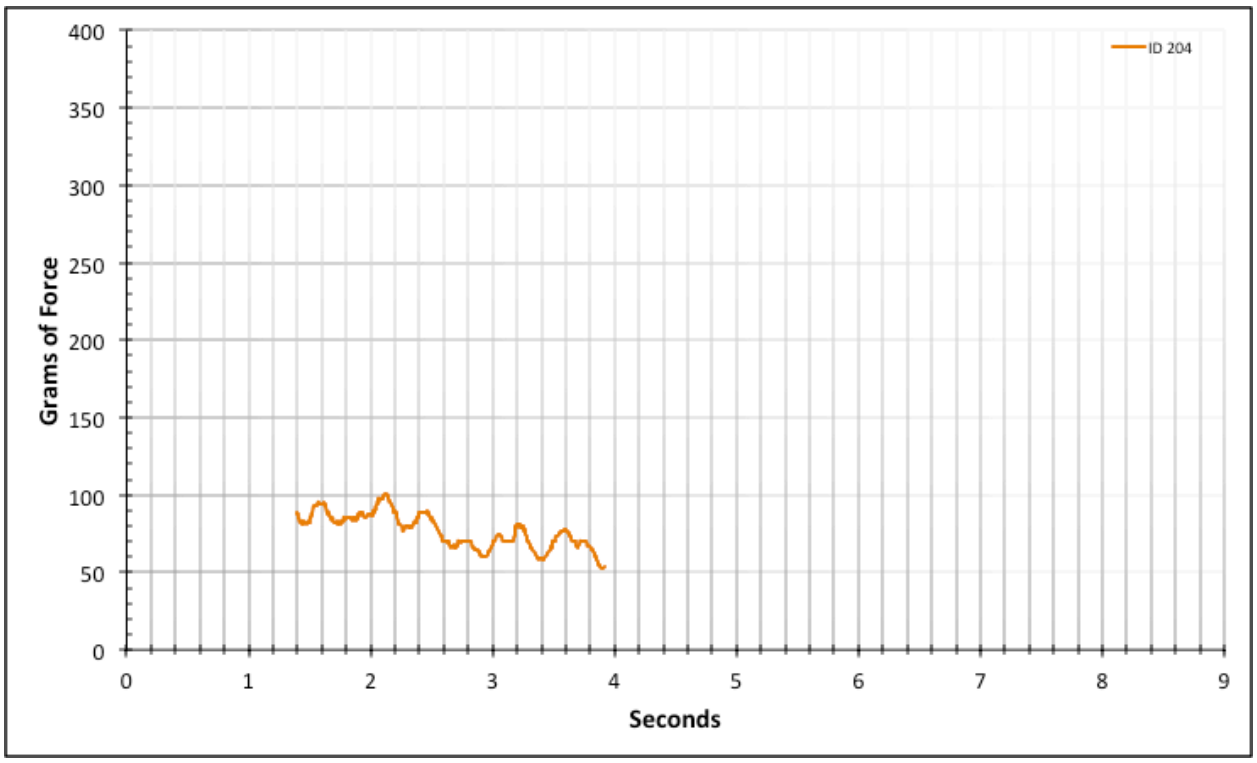

Figure A-6-264: Statistical Region Straight Baseline - Lubricated - ID 204 - #10, Bolt 3

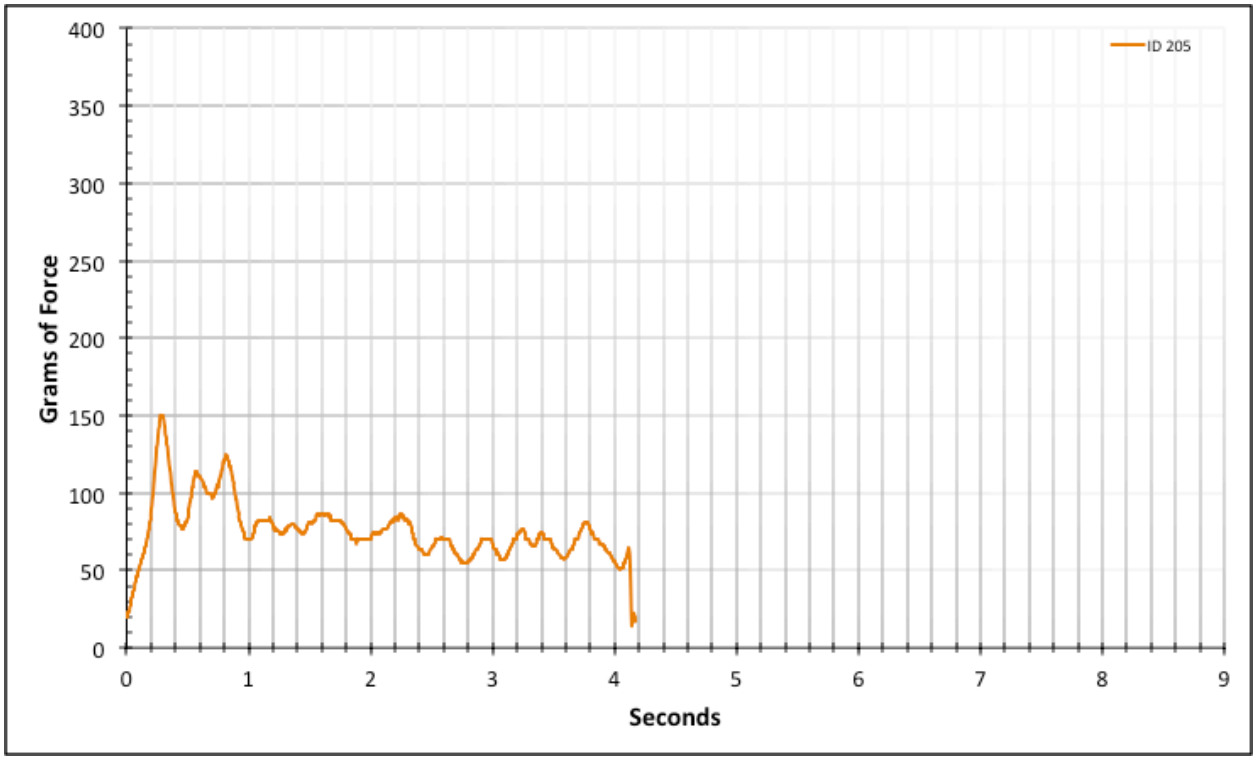

Figure A-6-265: Full Straight Baseline - Lubricated - ID 205 - #10, Bolt 3

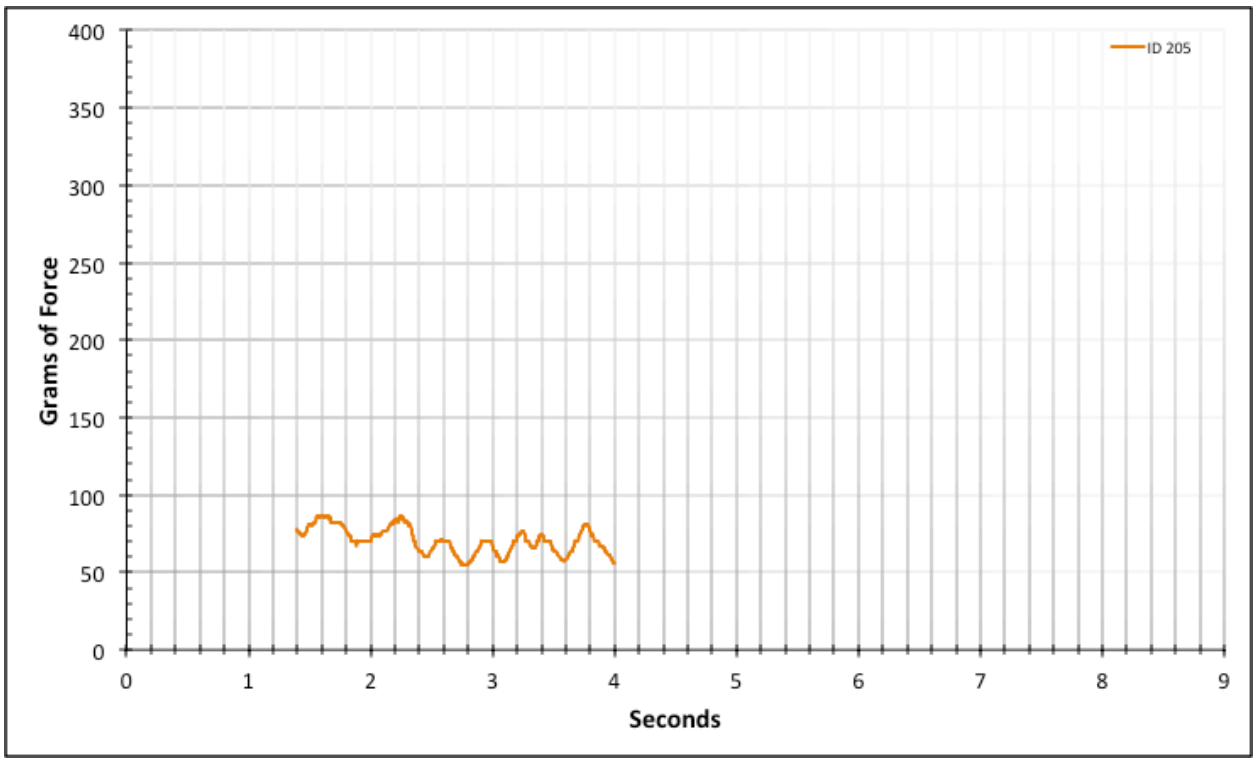

Figure A-6-266: Statistical Region Straight Baseline - Lubricated - ID 205 - #10, Bolt 3

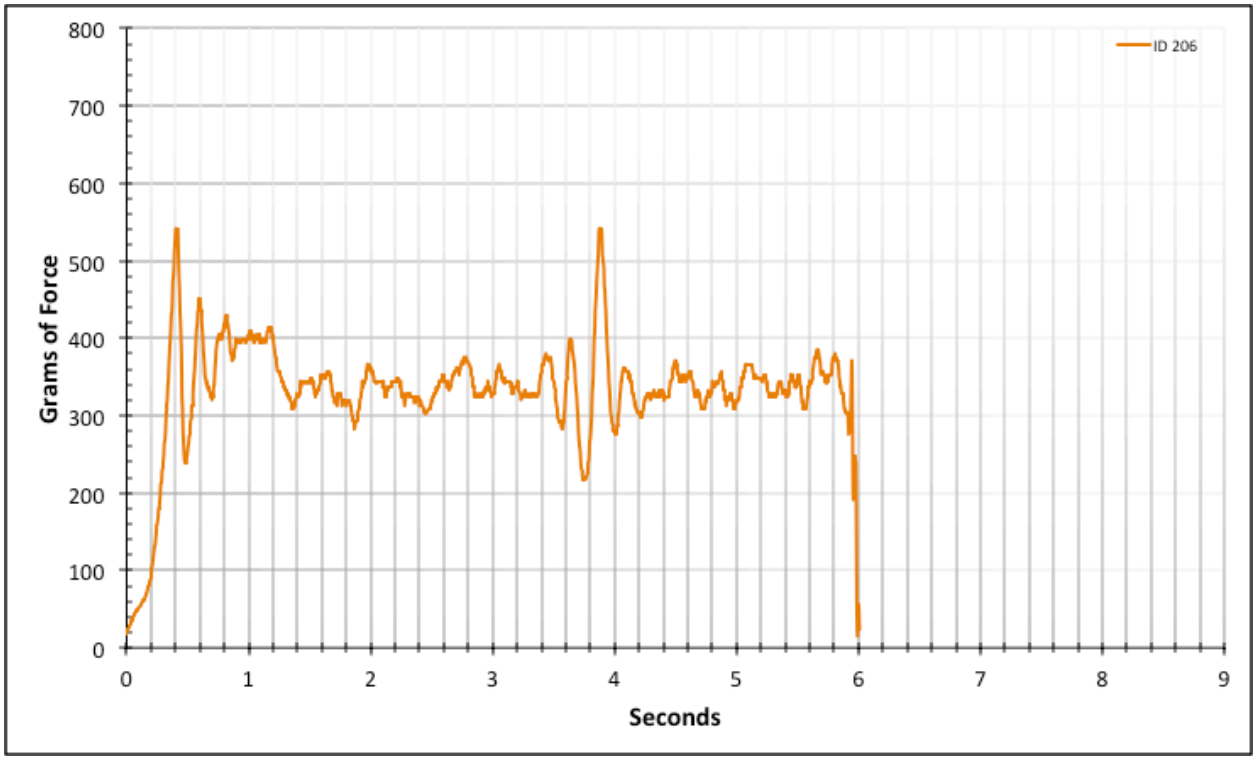

Figure A-6-267: Full Straight Baseline - Lubricated - ID 206 - #8, Bolt 1

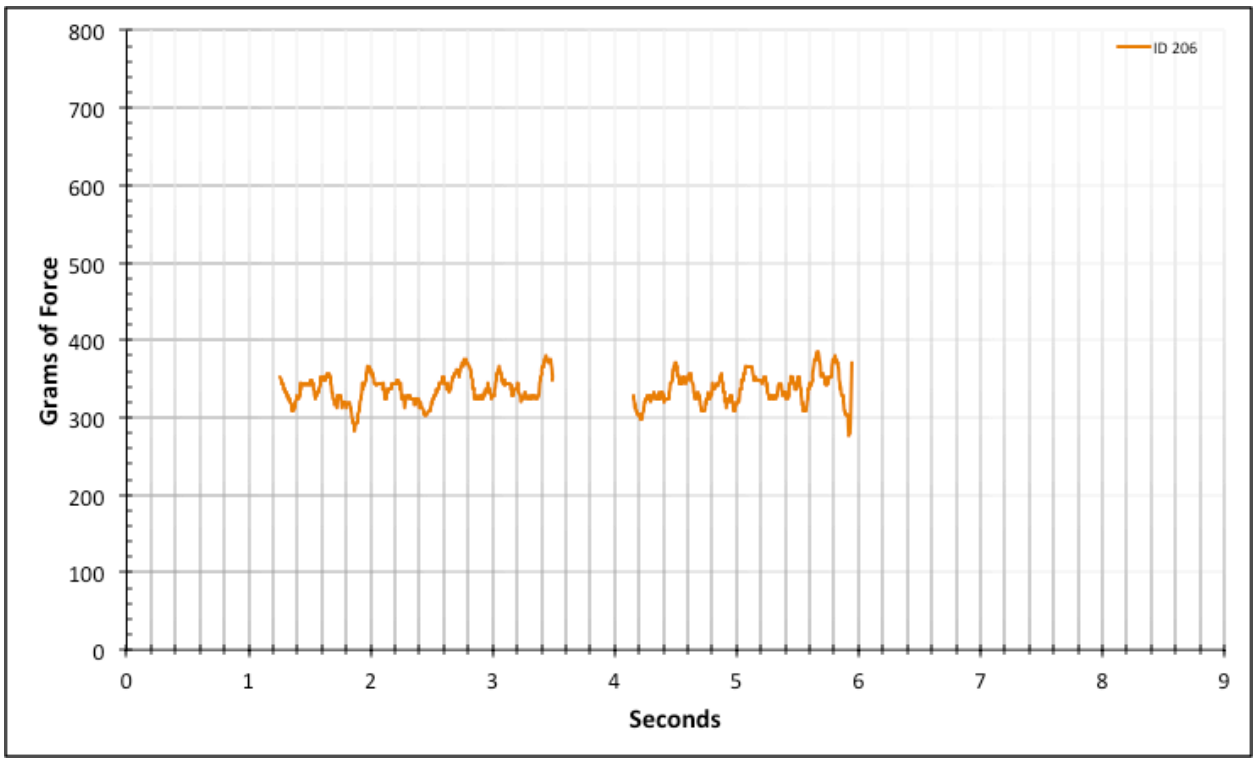

Figure A-6-268: Statistical Region Straight Baseline - Lubricated - ID 206 - #8, Bolt 1

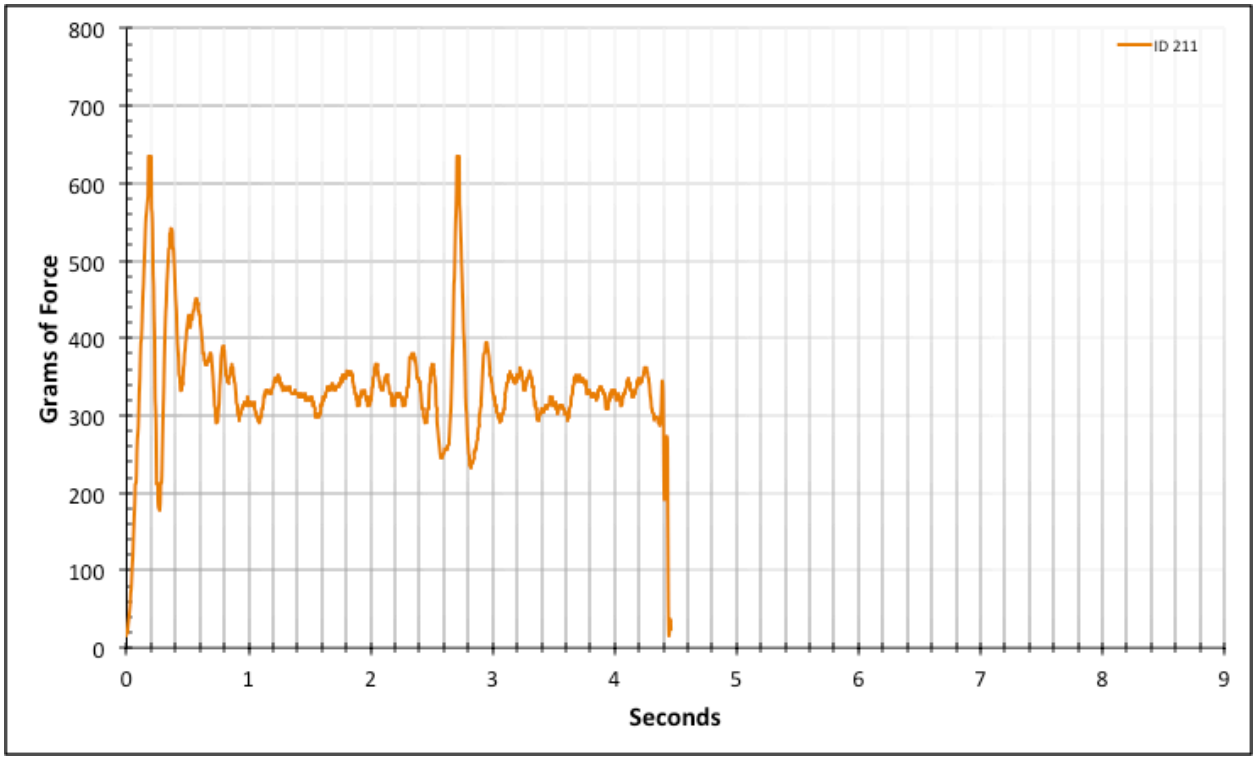

Figure A-6-269: Full Straight Baseline - Lubricated - ID 211 - #8, Bolt 2

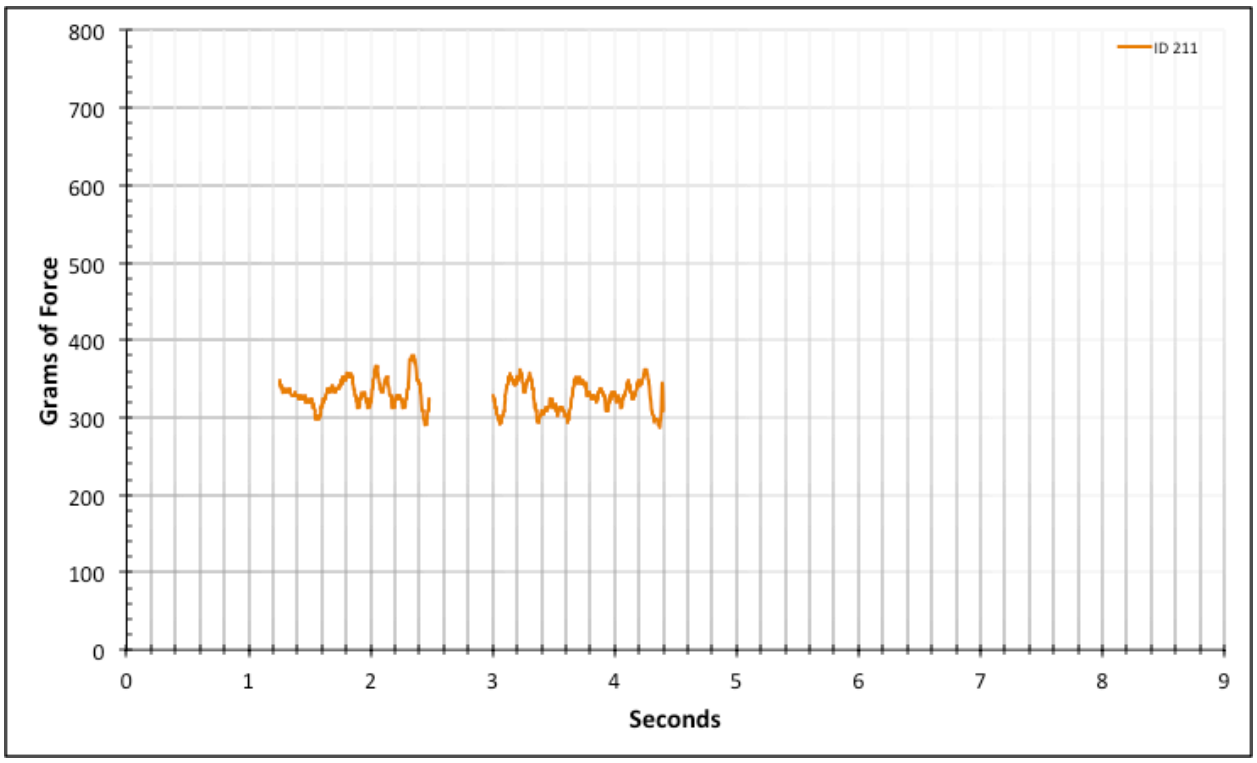

Figure A-6-270: Statistical Region Straight Baseline - Lubricated - ID 211 - #8, Bolt 2

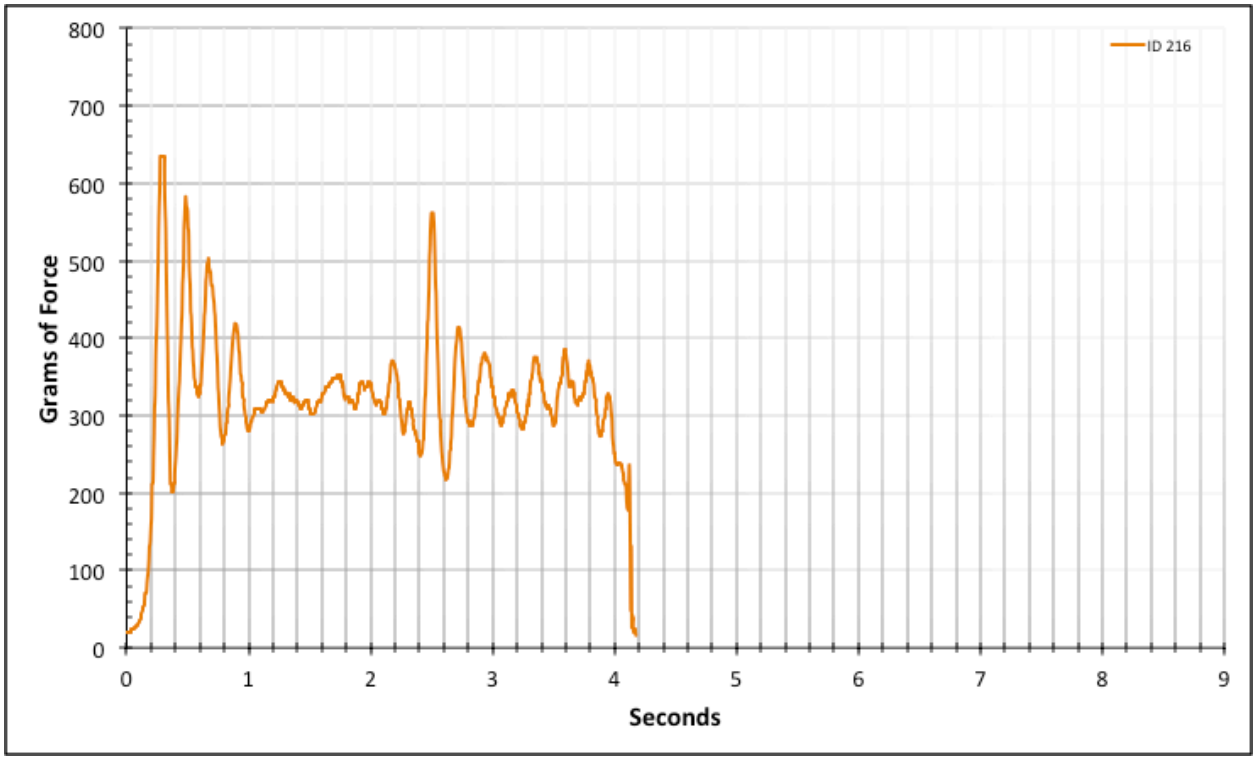

Figure A-6-271: Full Straight Baseline - Lubricated - ID 216 - #8, Bolt 3

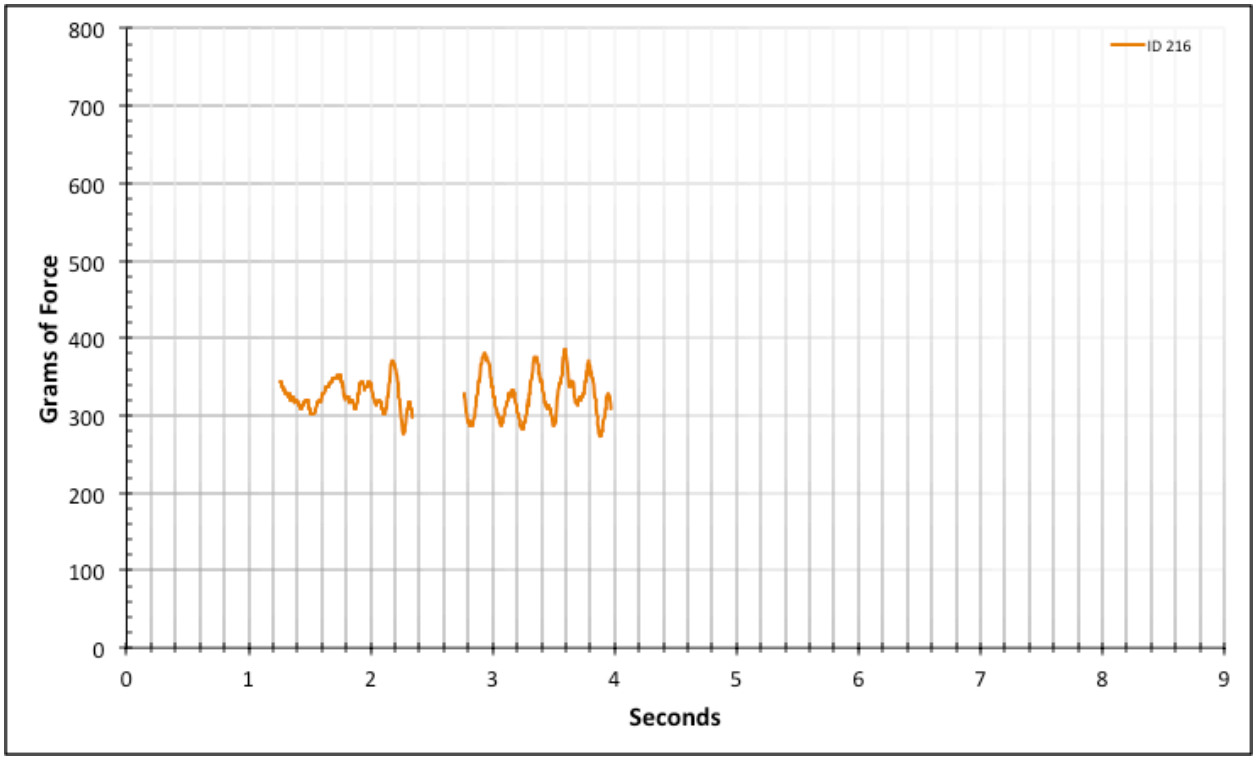

Figure A-6-272: Statistical Region Straight Baseline - Lubricated - ID 216 - #8, Bolt 3

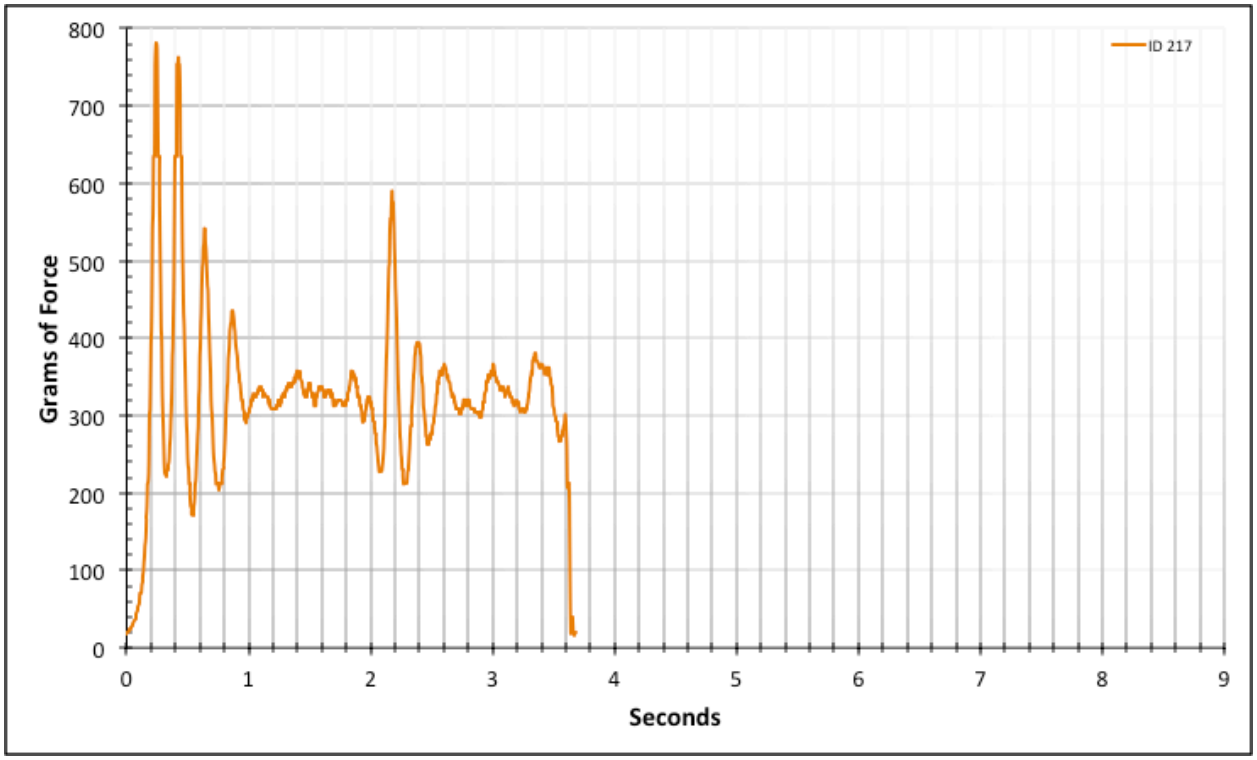

Figure A-6-273: Full Straight Baseline - Lubricated - ID 217 - #8, Bolt 3

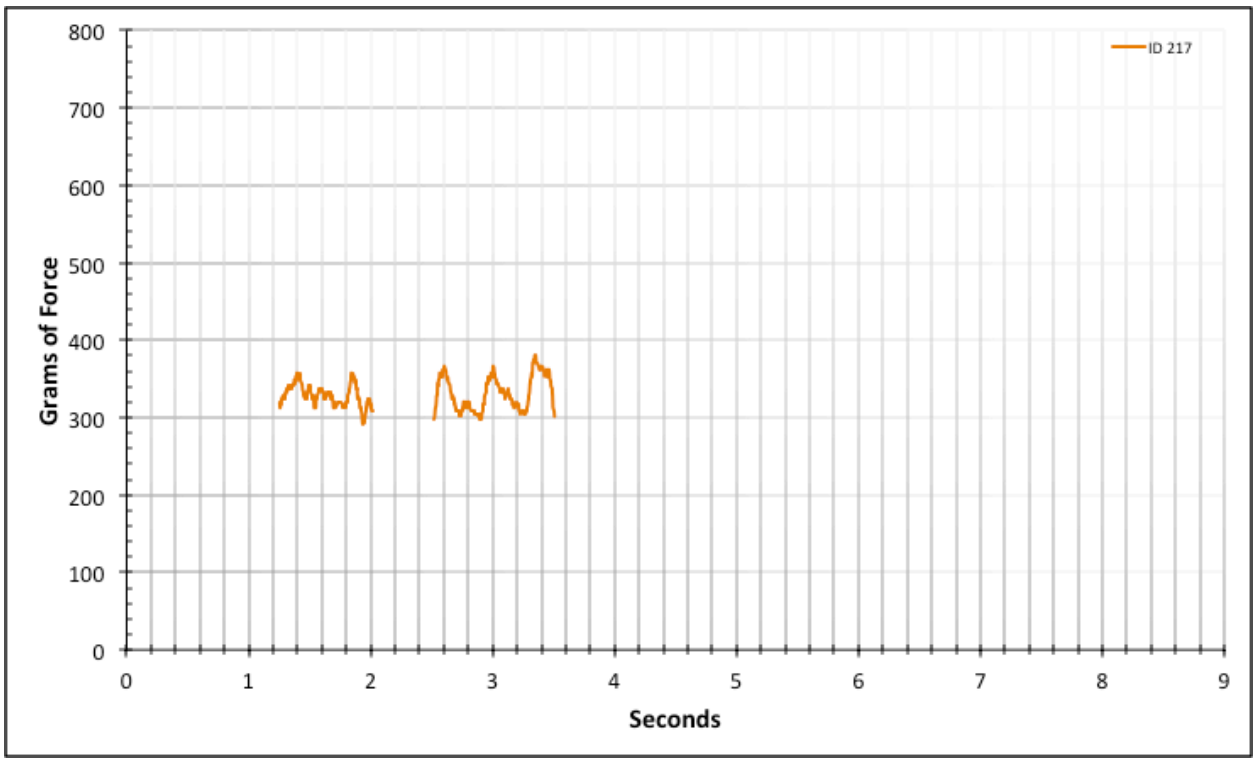

Figure A-6-274: Statistical Region Straight Baseline - Lubricated - ID 217 - #8, Bolt 3

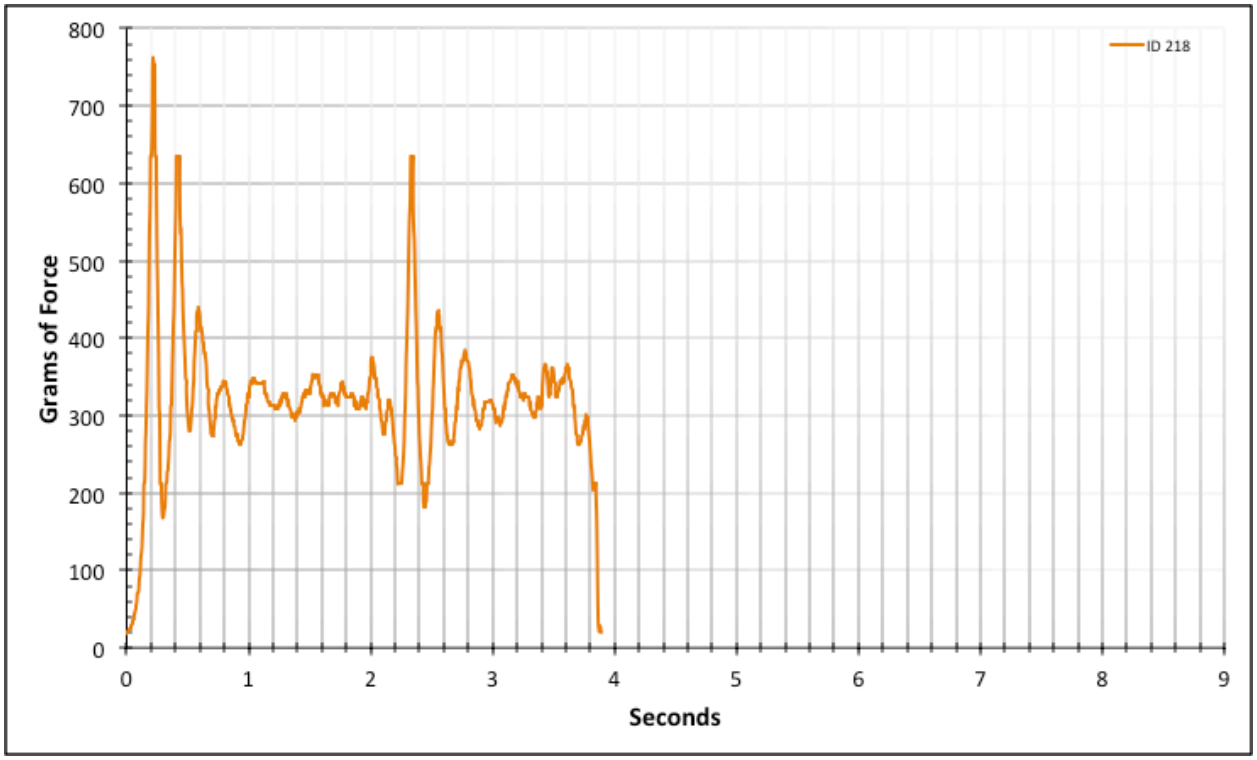

Figure A-6-275: Full Straight Baseline - Lubricated - ID 218 - #8, Bolt 3

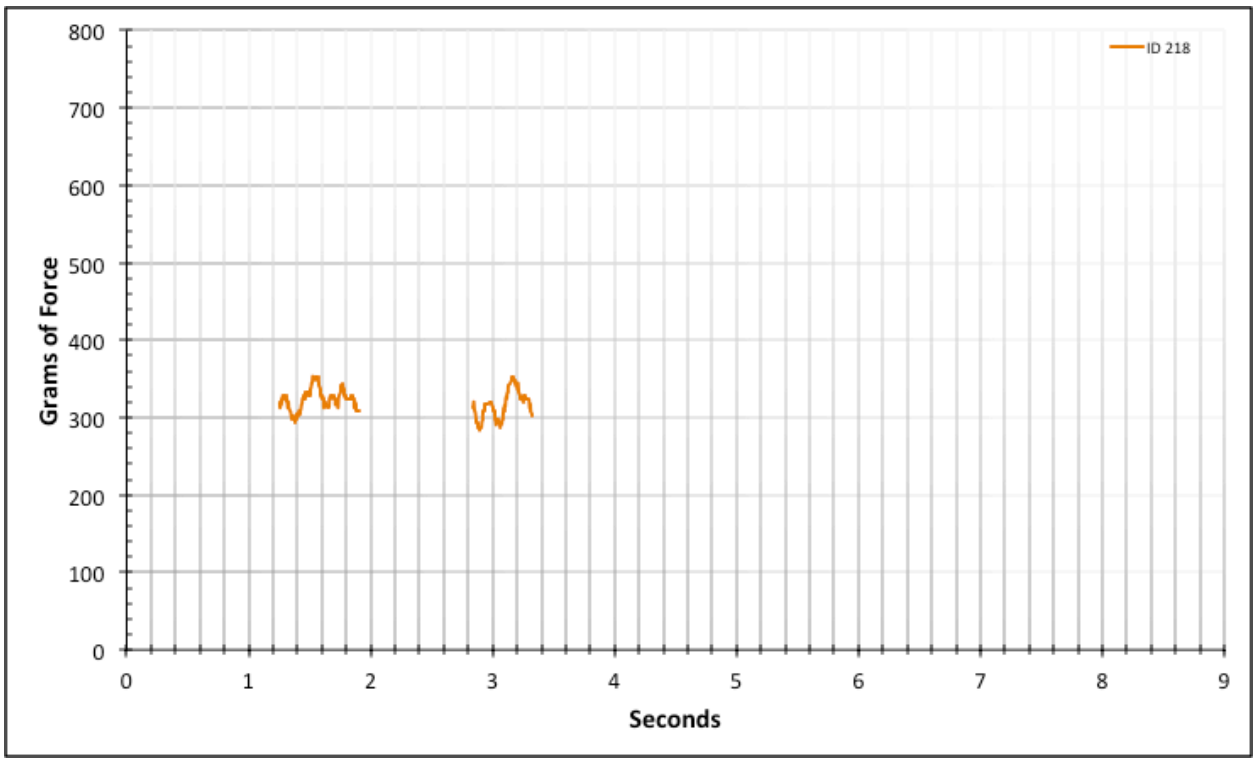

Figure A-6-276: Statistical Region Straight Baseline - Lubricated - ID 218 - #8, Bolt 3

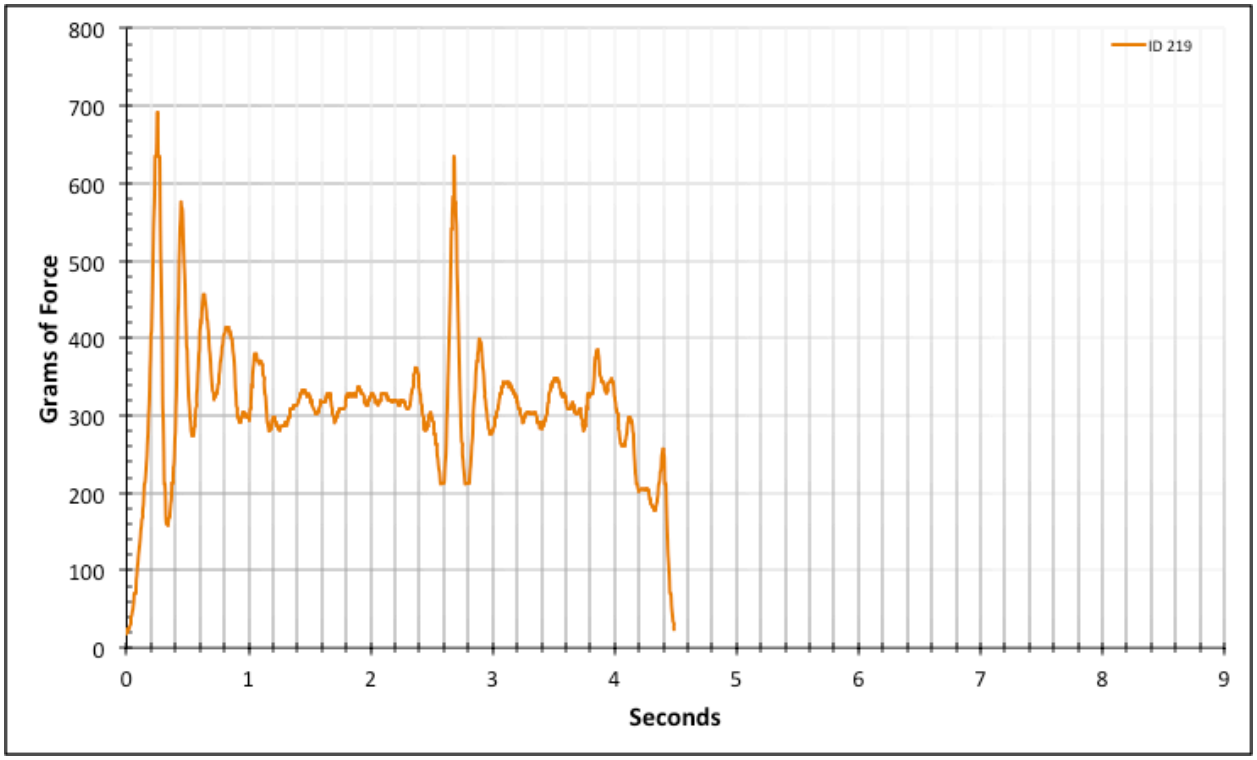

Figure A-6-277: Full Straight Baseline - Lubricated - ID 219 - #8, Bolt 3

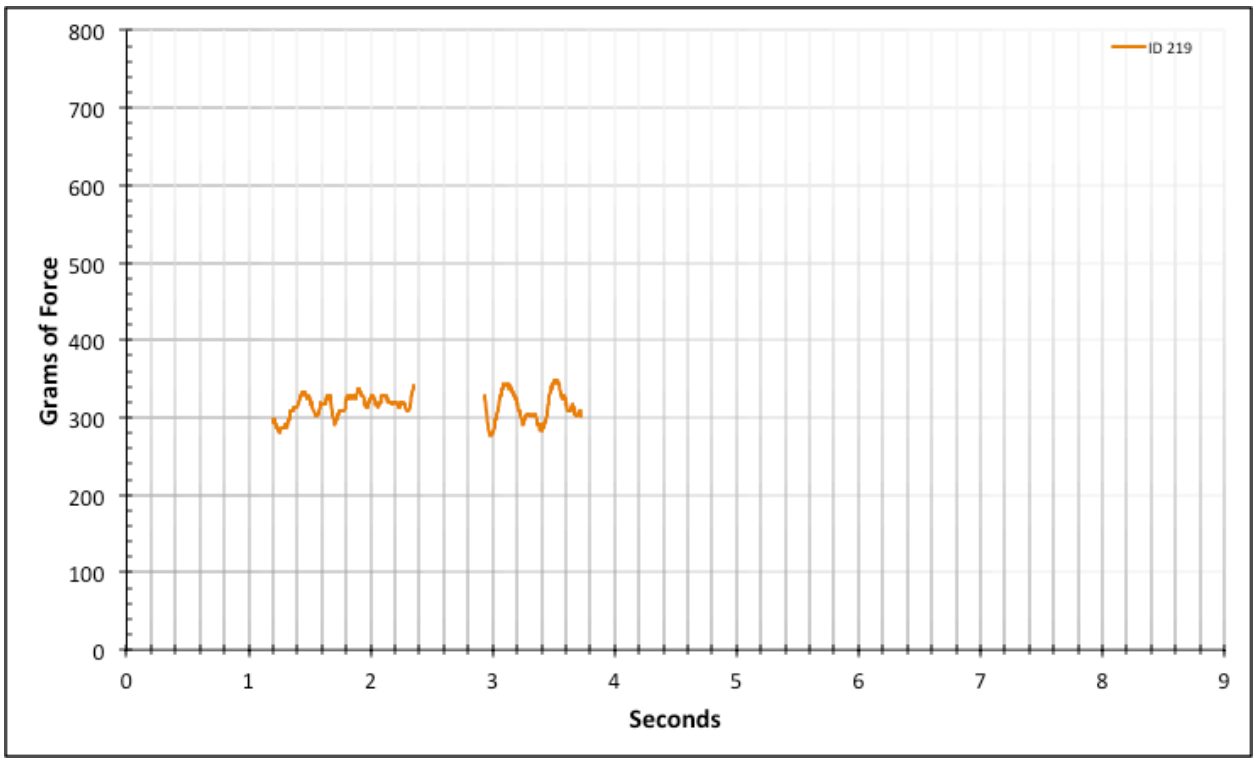

Figure A-6-278: Statistical Region Straight Baseline - Lubricated - ID 219 - #8, Bolt 3

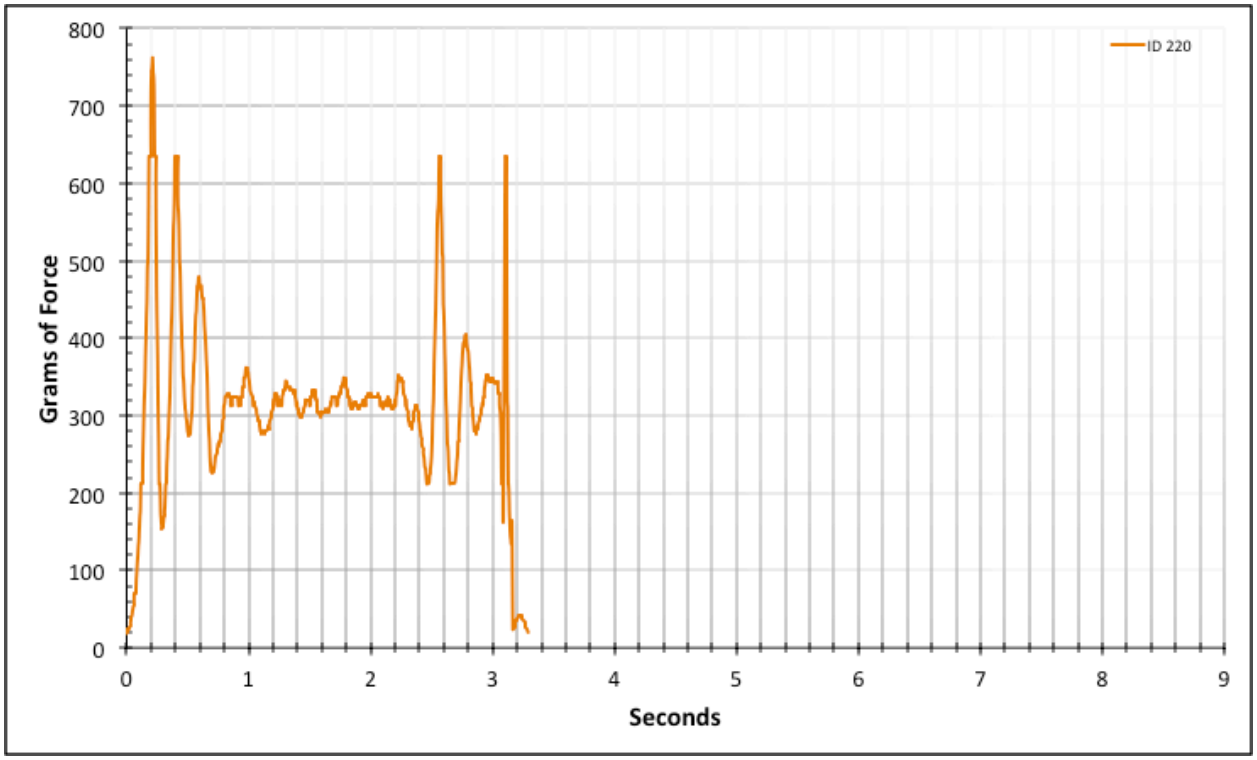

Figure A-6-279: Full Straight Baseline - Lubricated - ID 220 - #8, Bolt 3

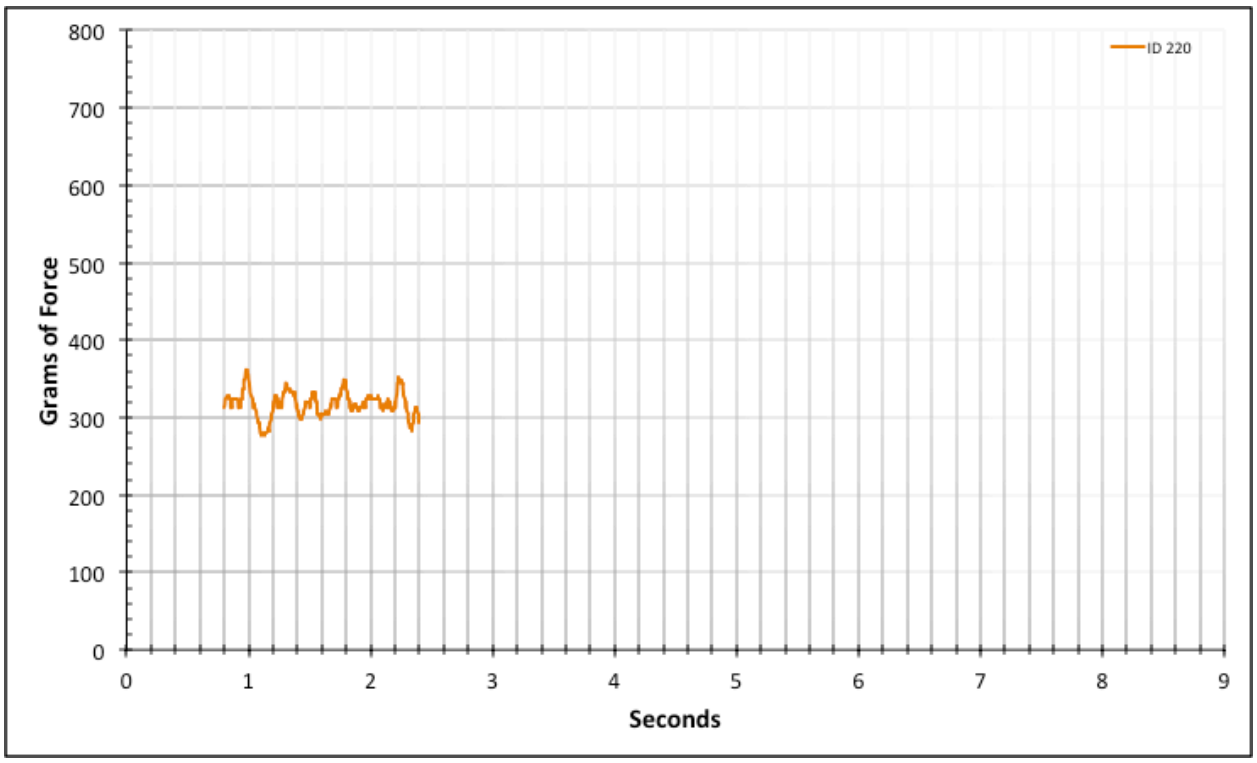

Figure A-6-280: Statistical Region Straight Baseline - Lubricated - ID 220 - #8, Bolt 3

A.5. Modeled Product – Lubricated

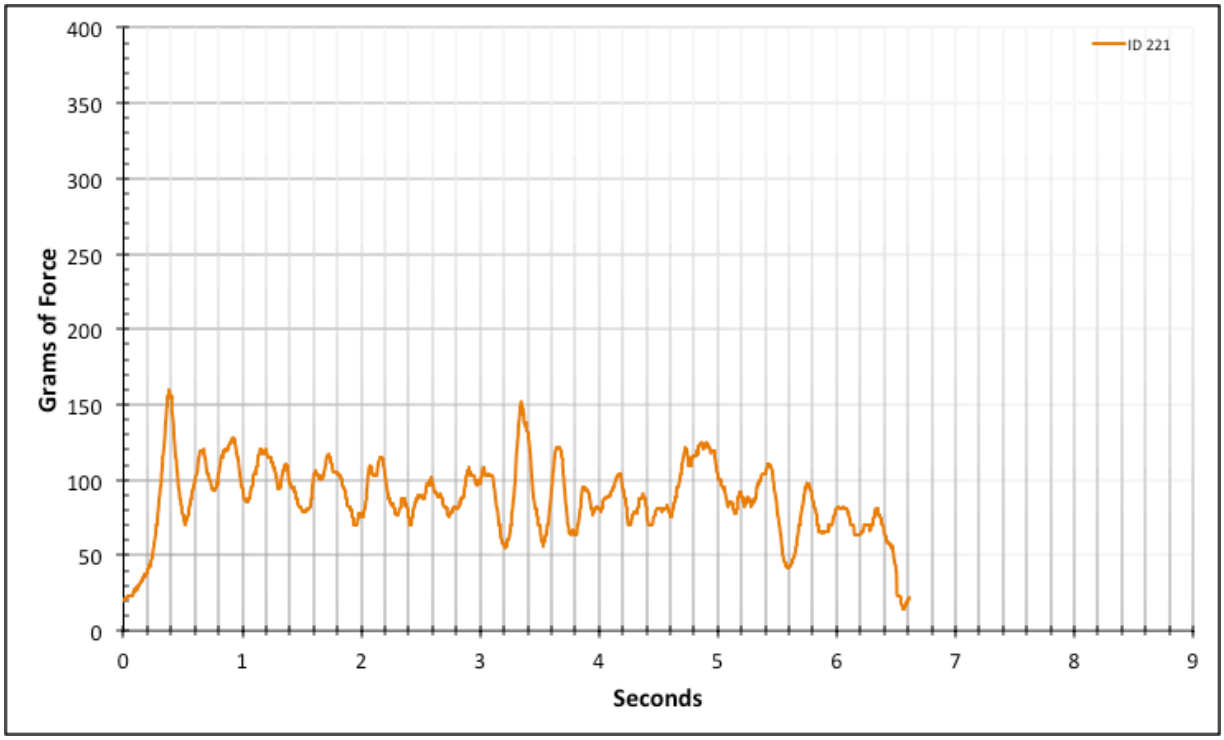

Figure A-6-281: Full Modeled Product - Lubricated - ID 221 - #12, Bolt 1

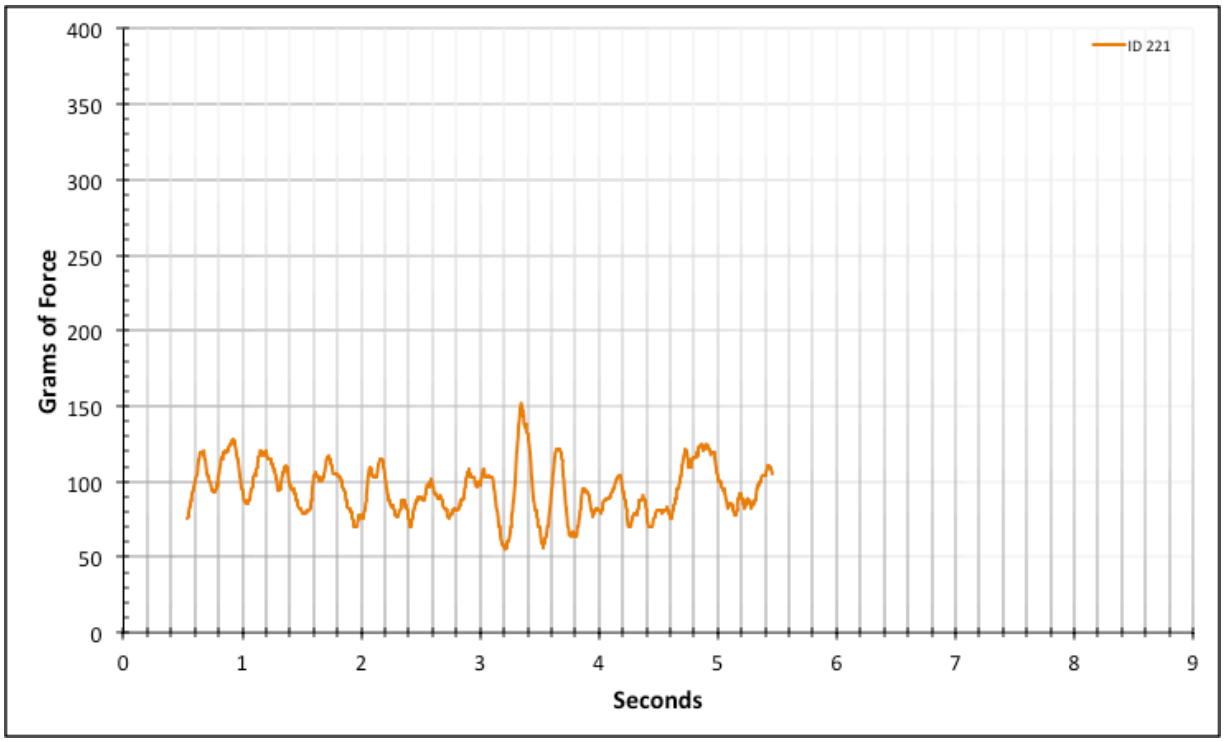

Figure A-6-282: Statistical Region Modeled Product - Lubricated - ID 221 - #12, Bolt 1

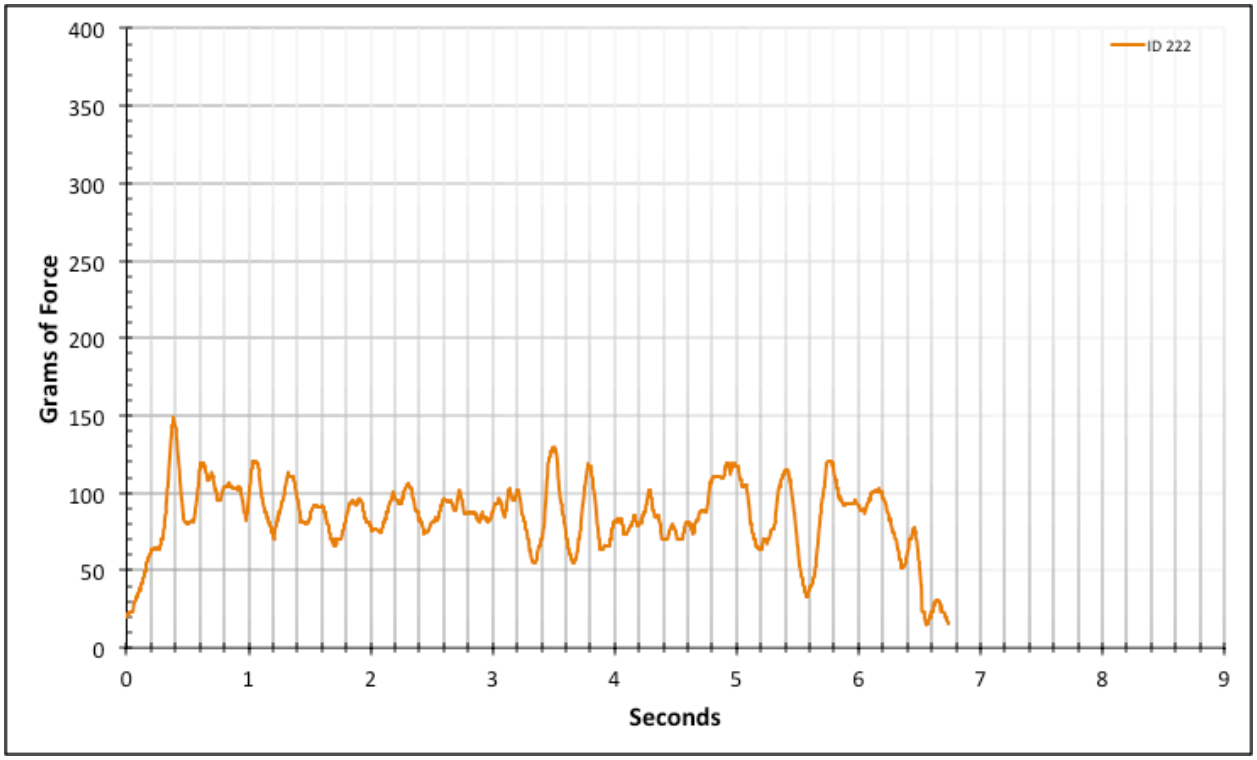

Figure A-6-283: Full Modeled Product - Lubricated - ID 222 - #12, Bolt 1

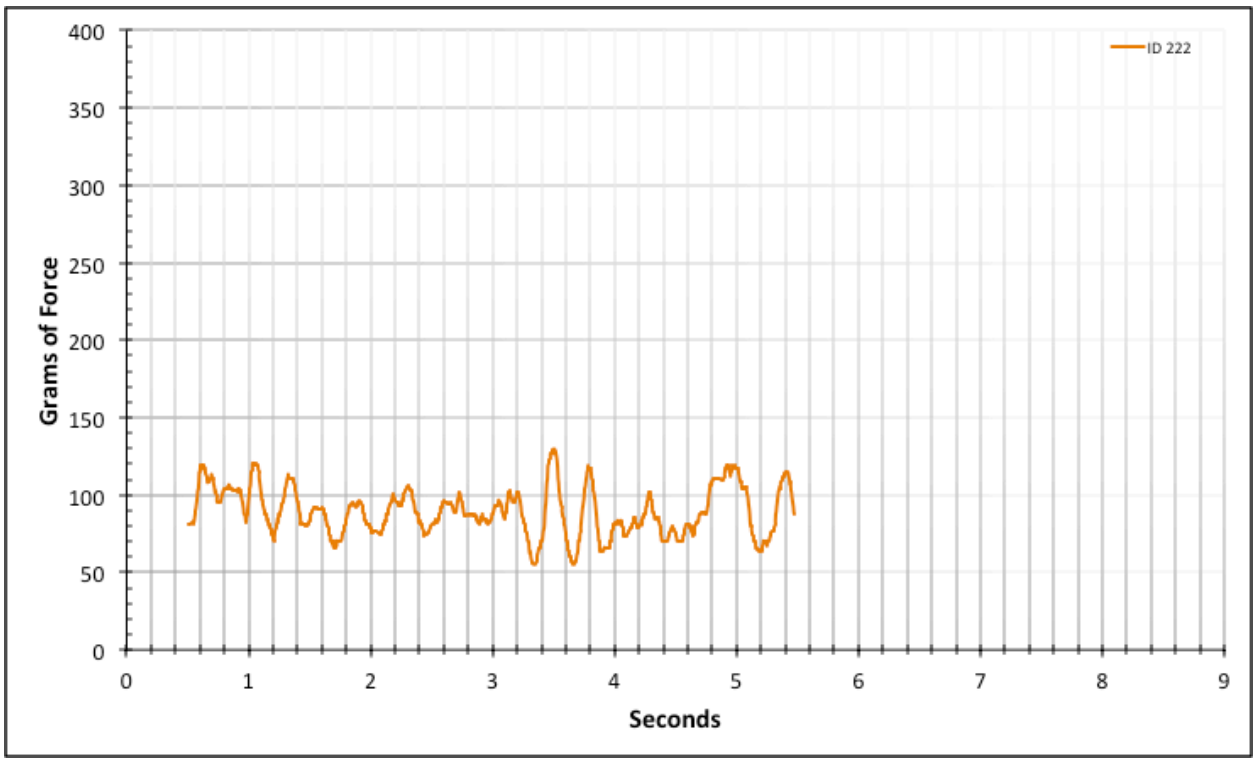

Figure A-6-284: Statistical Region Modeled Product - Lubricated - ID 222 - #12, Bolt 1

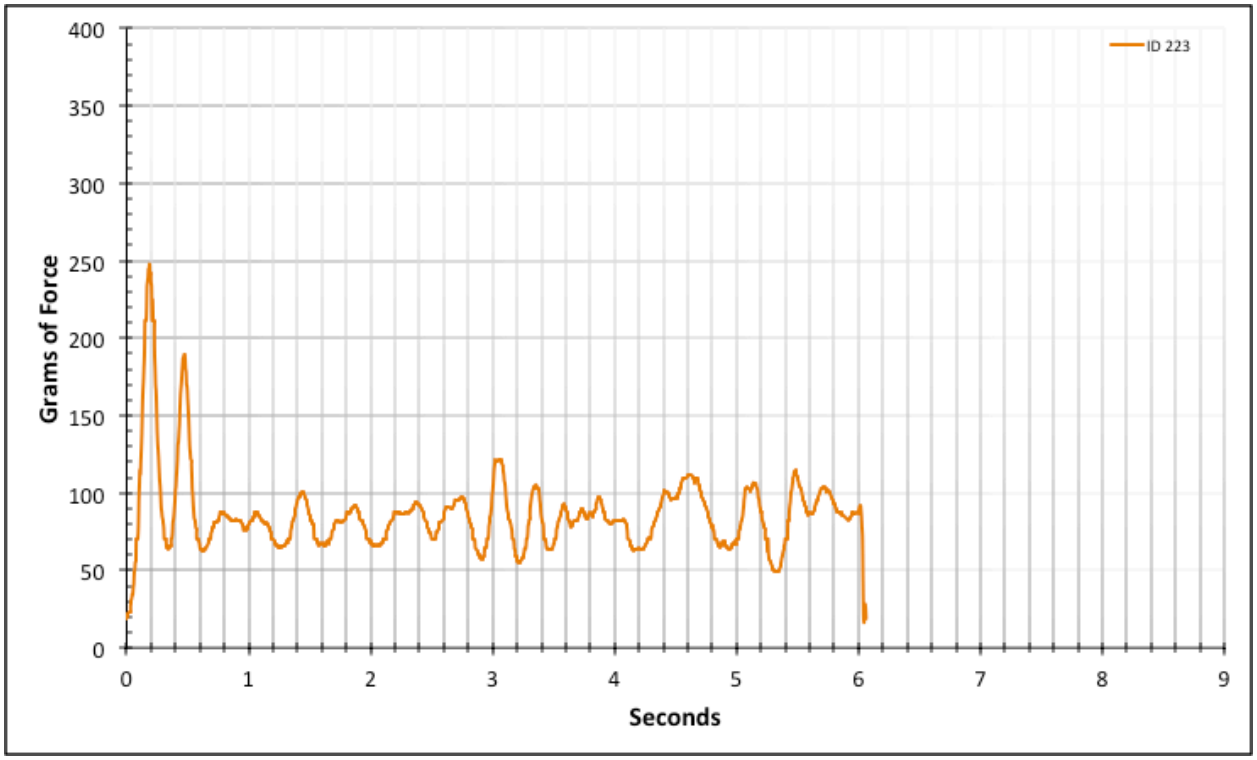

Figure A-6-285: Full Modeled Product - Lubricated - ID 223 - #12, Bolt 1

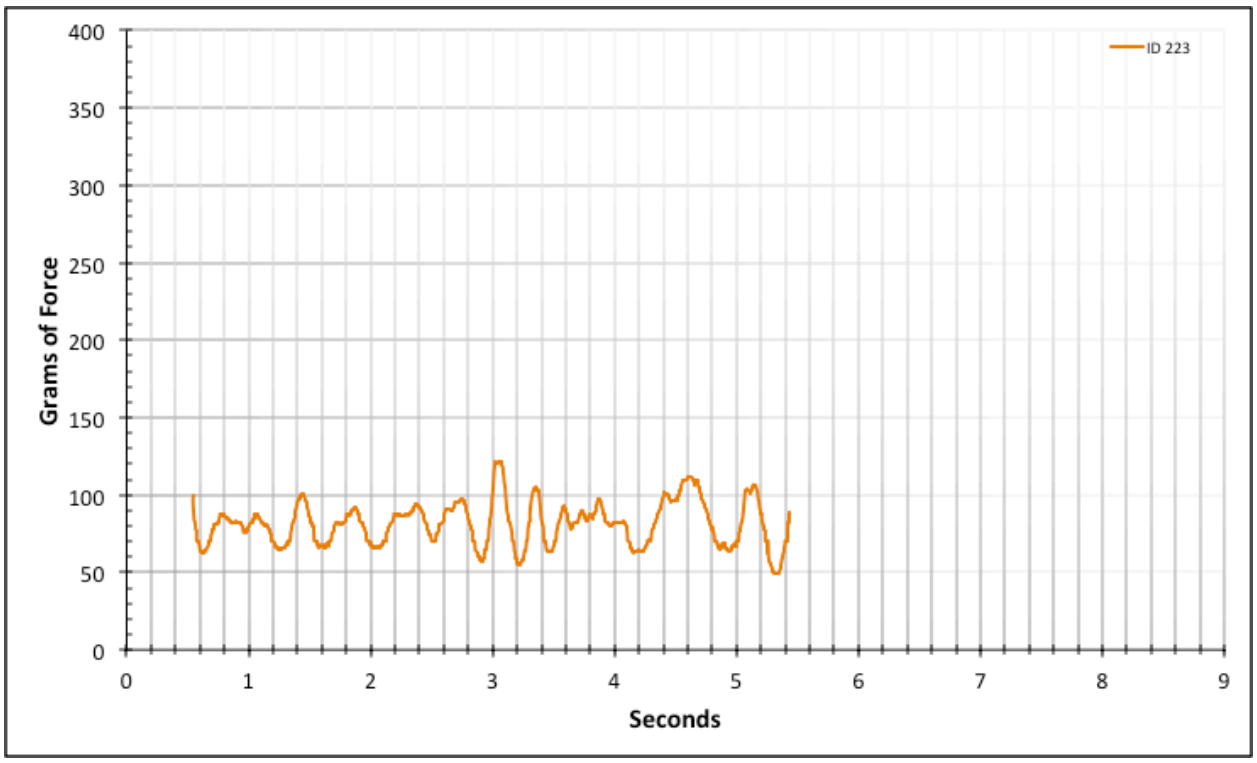

Figure A-6-286: Statistical Region Modeled Product - Lubricated - ID 223 - #12, Bolt 1

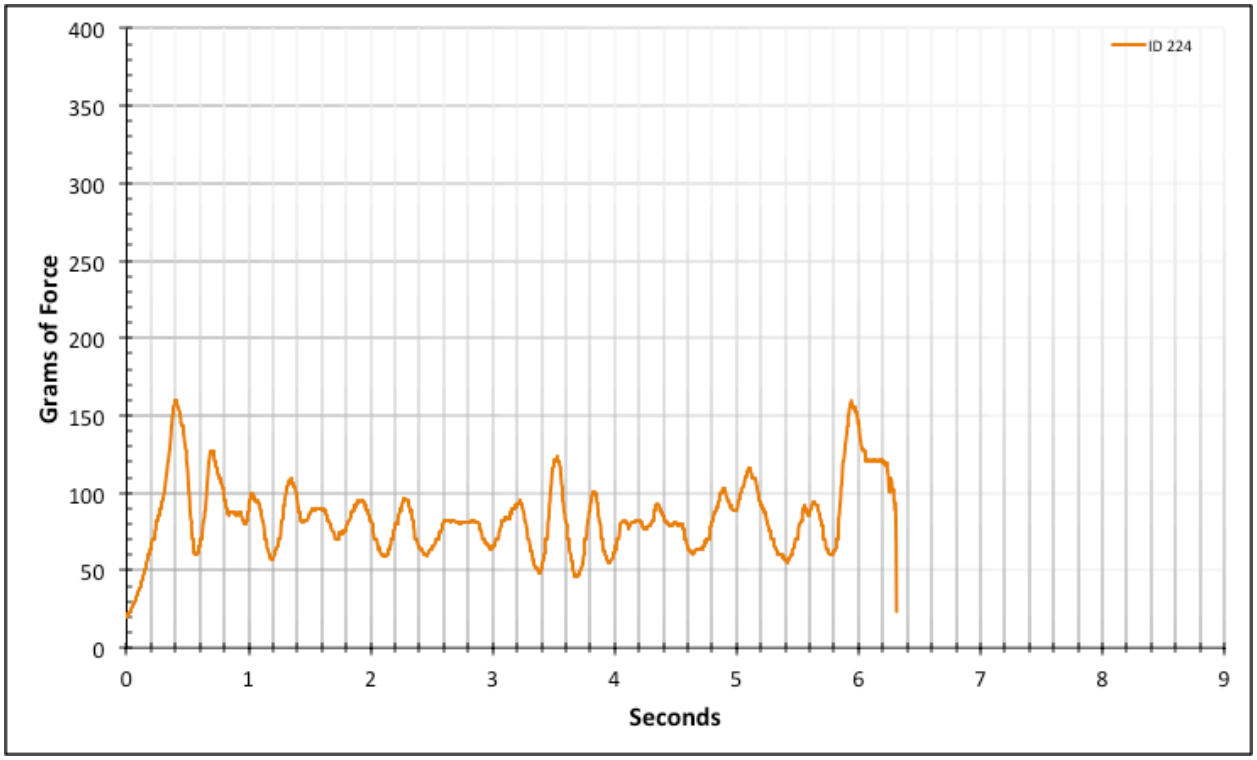

Figure A-6-287: Full Modeled Product - Lubricated - ID 224 - #12, Bolt 1

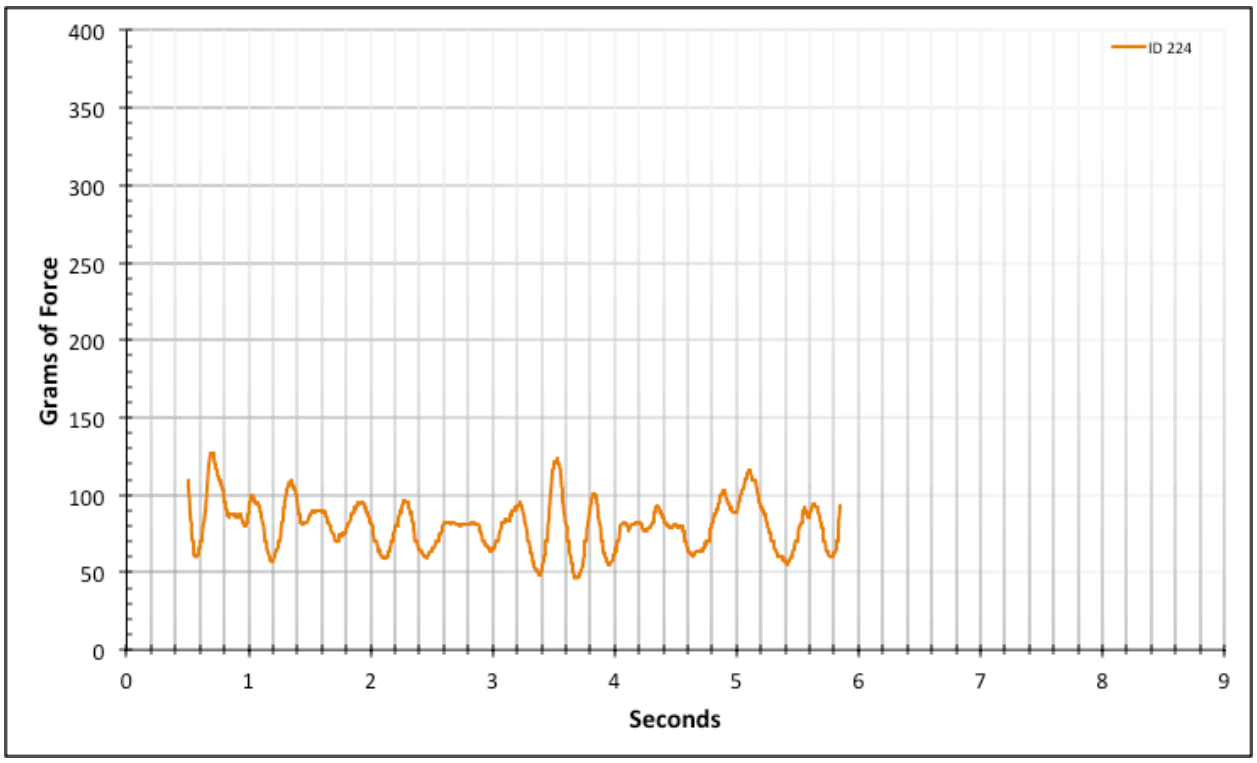

Figure A-6-288: Statistical Region Modeled Product - Lubricated - ID 224 - #12, Bolt 1

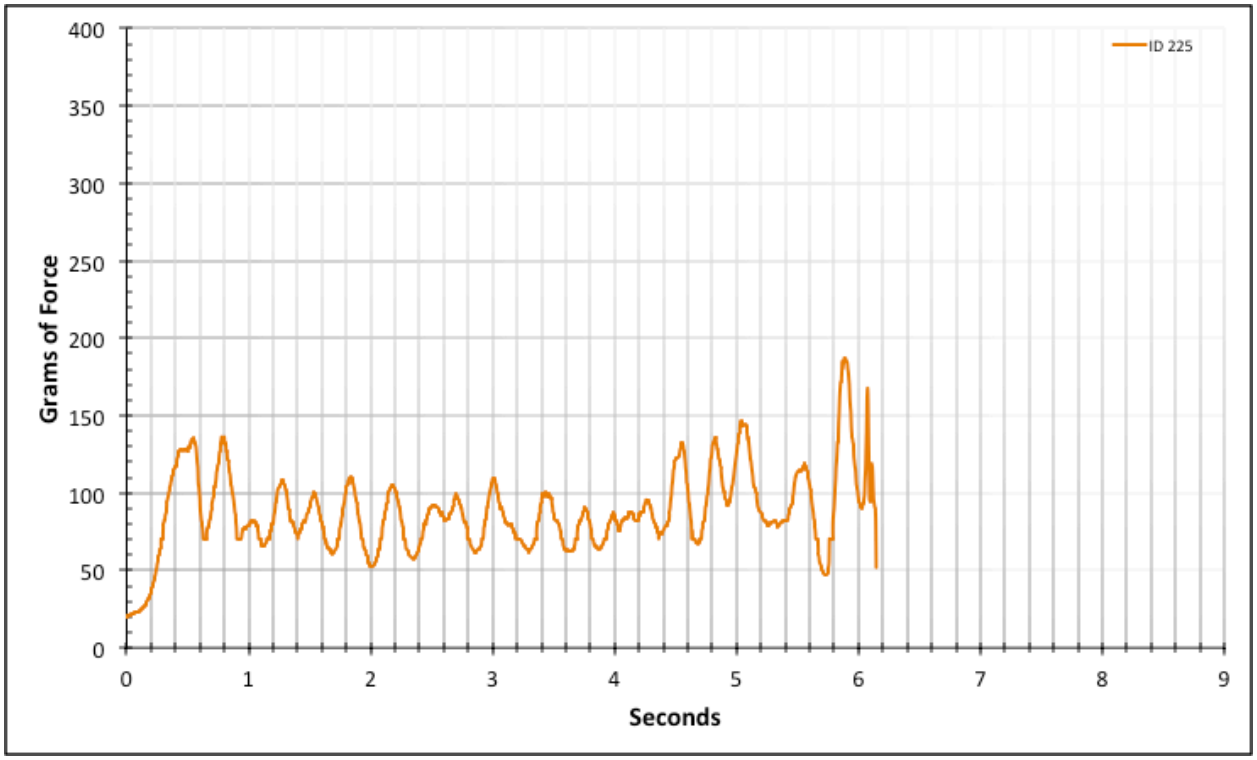

Figure A-6-289: Full Modeled Product - Lubricated - ID 225 - #12, Bolt 1

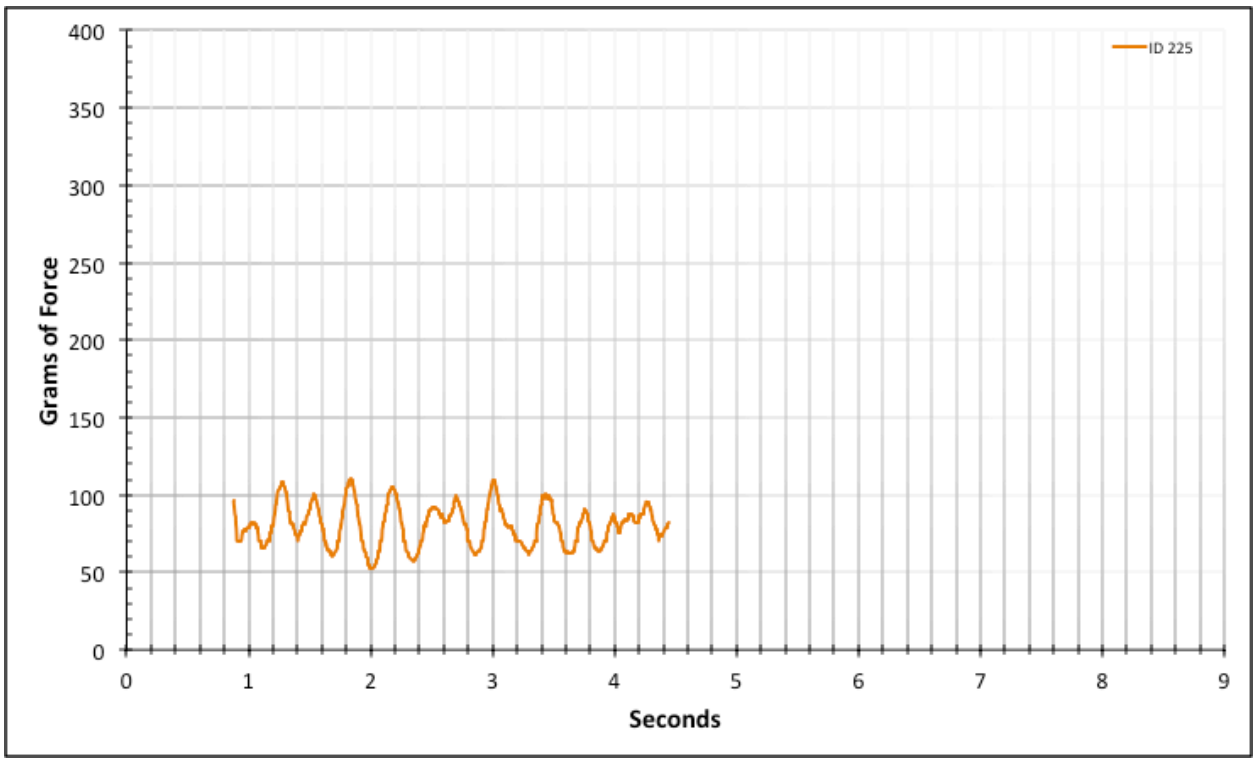

Figure A-6-290: Statistical Region Modeled Product - Lubricated - ID 225 - #12, Bolt 1

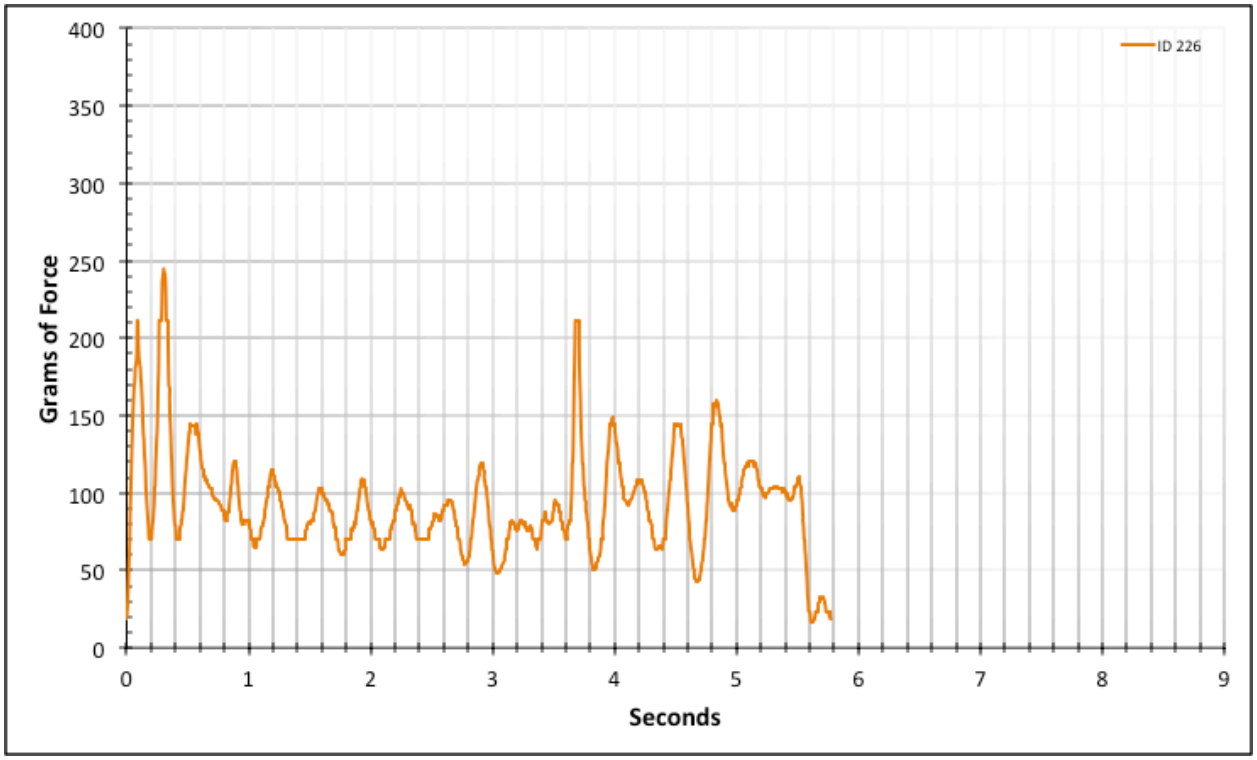

Figure A-6-291: Full Modeled Product - Lubricated - ID 226 - #12, Bolt 2

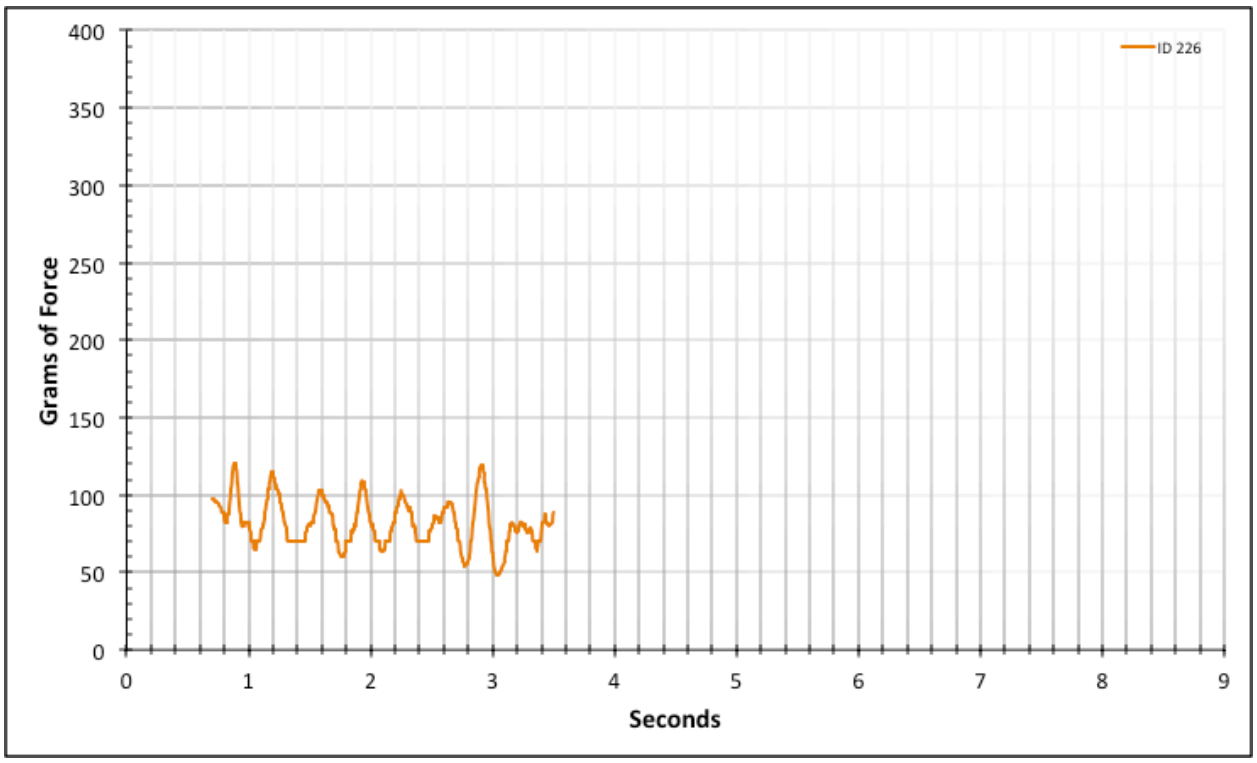

Figure A-6-292: Statistical Region Modeled Product - Lubricated - ID 226 - #12, Bolt 2

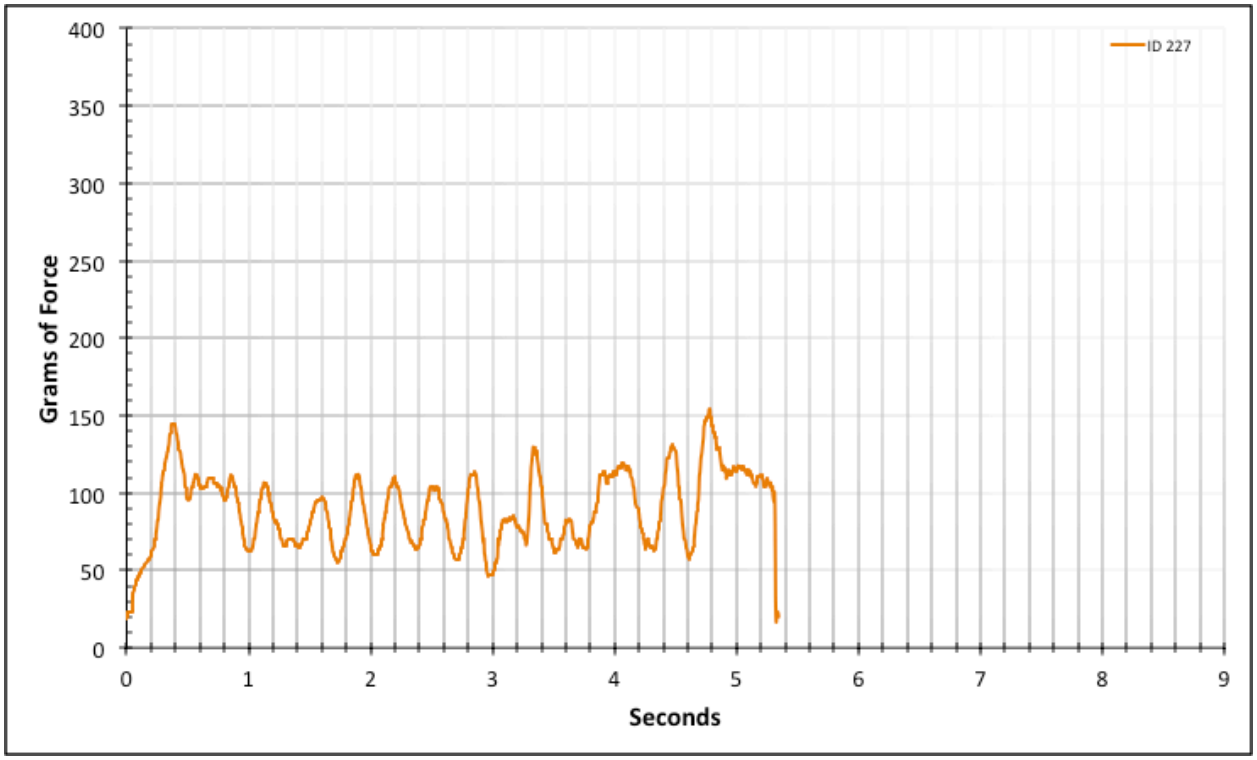

Figure A-6-293: Full Modeled Product - Lubricated - ID 227 - #12, Bolt 2

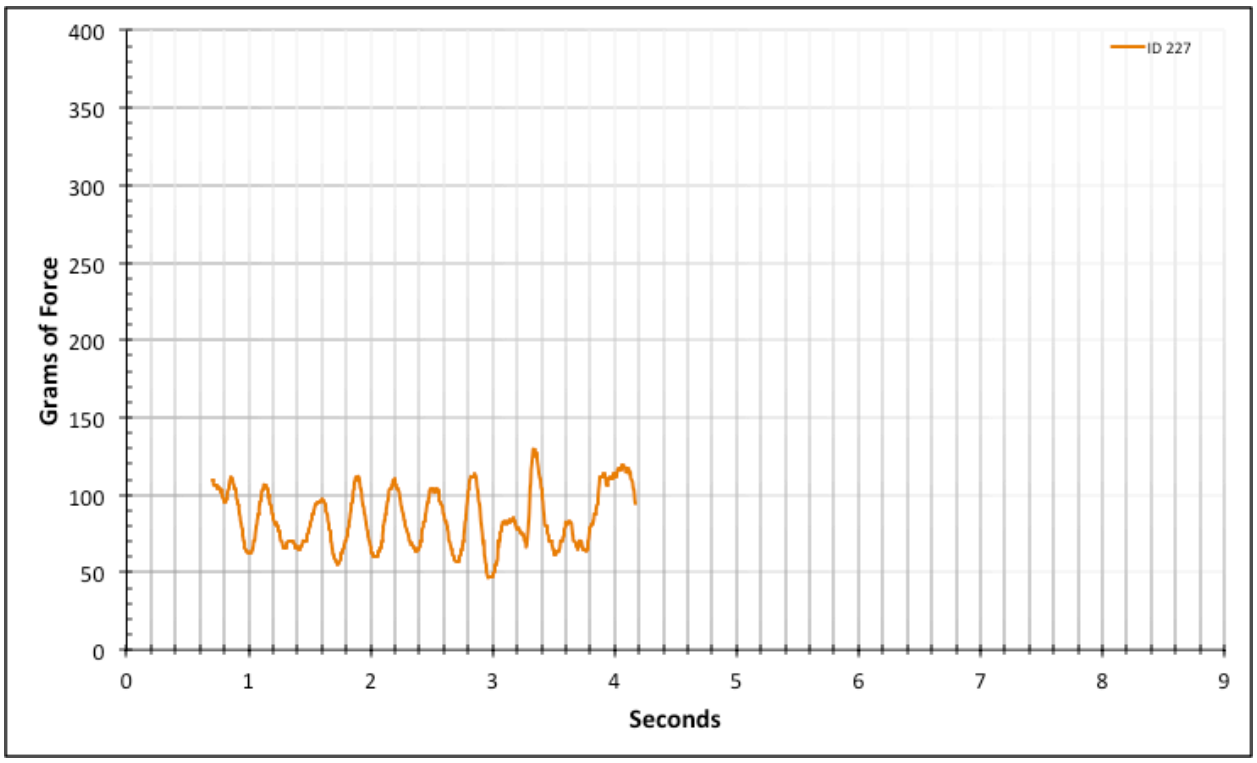

Figure A-6-294: Statistical Region Modeled Product - Lubricated - ID 227 - #12, Bolt 2

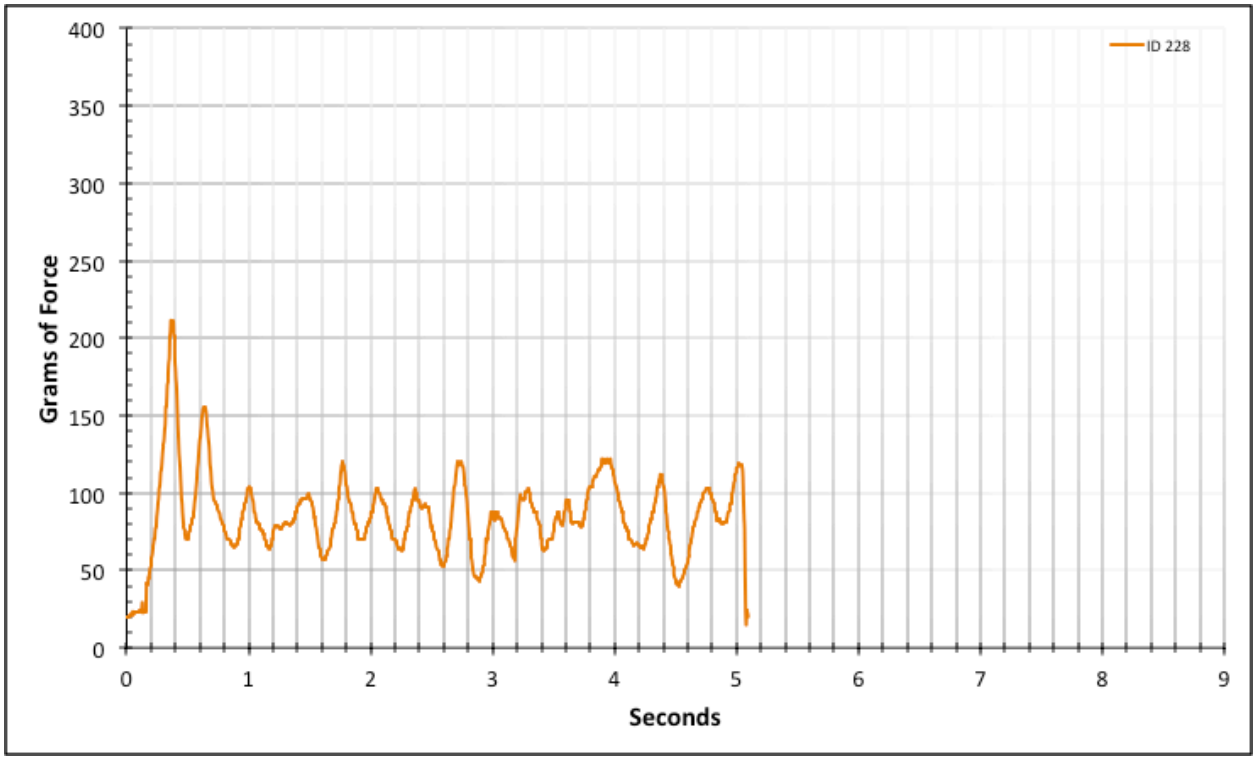

Figure A-6-295: Full Modeled Product - Lubricated - ID 228 - #12, Bolt 2

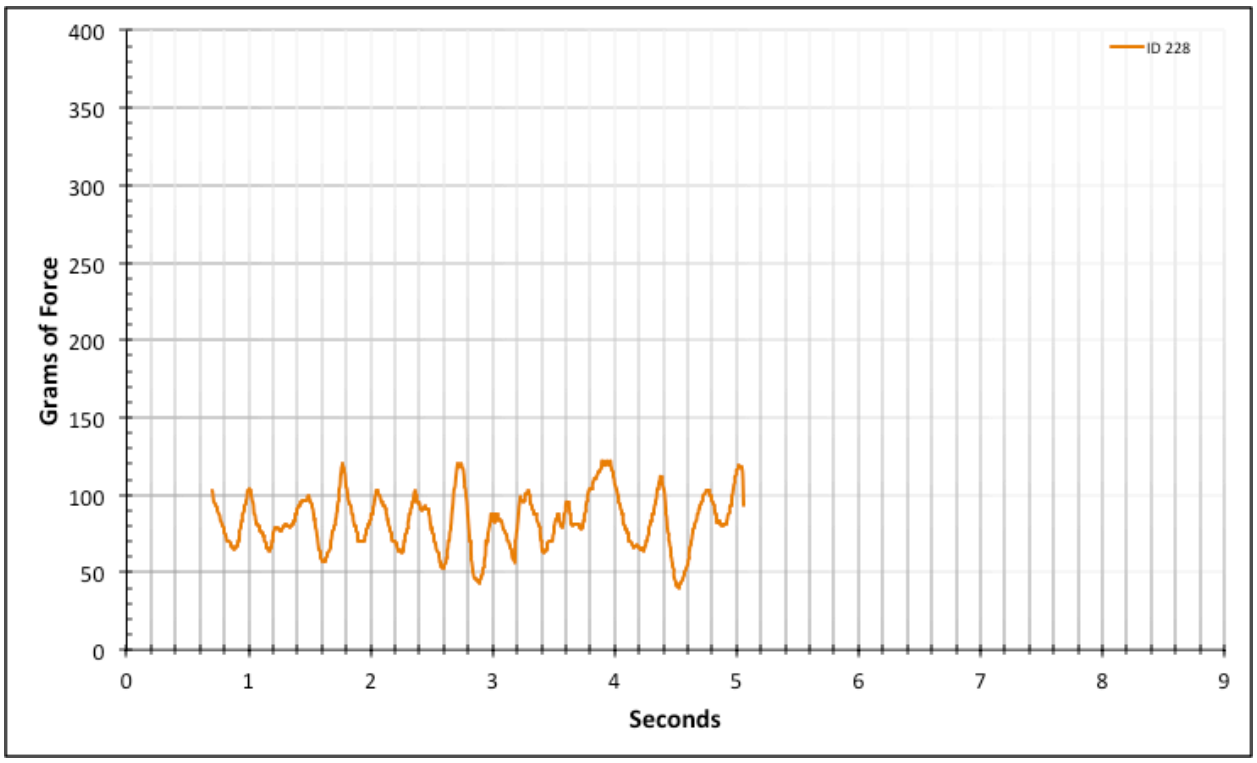

Figure A-6-296: Statistical Region Modeled Product - Lubricated - ID 228 - #12, Bolt 2

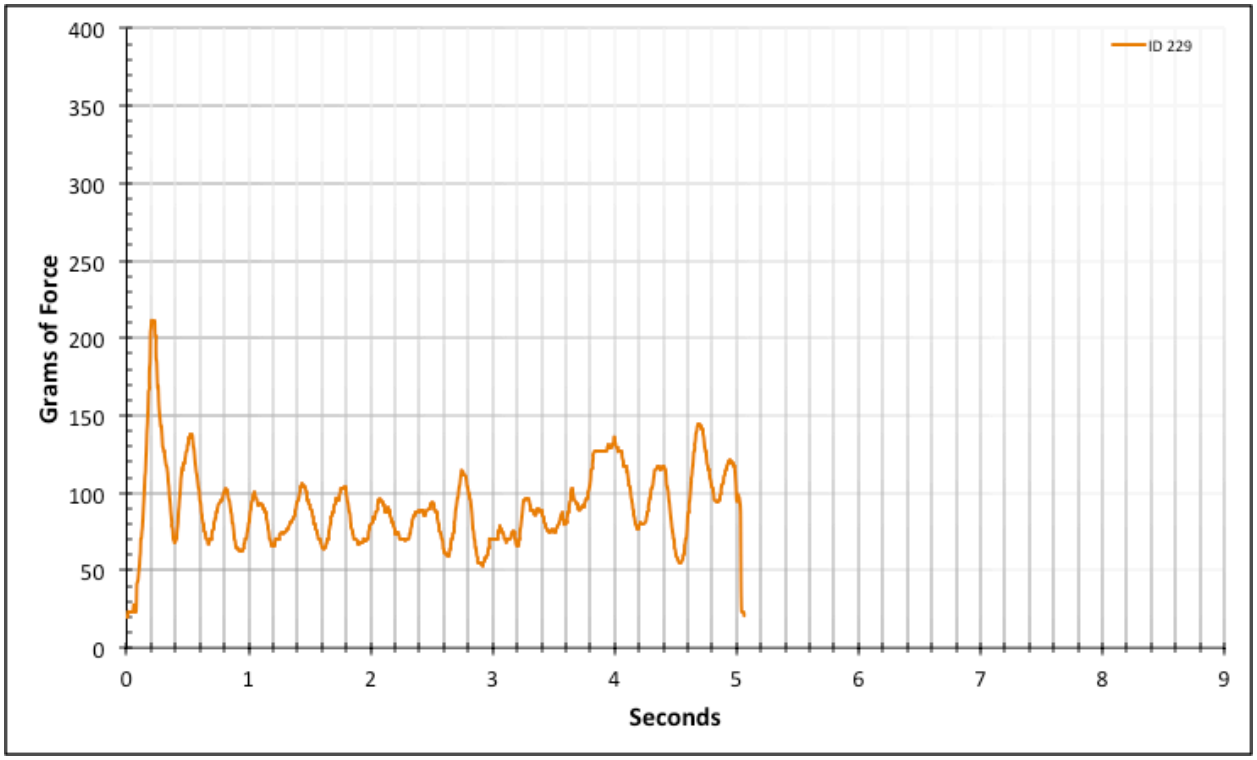

Figure A-6-297: Full Modeled Product - Lubricated - ID 229 - #12, Bolt 2

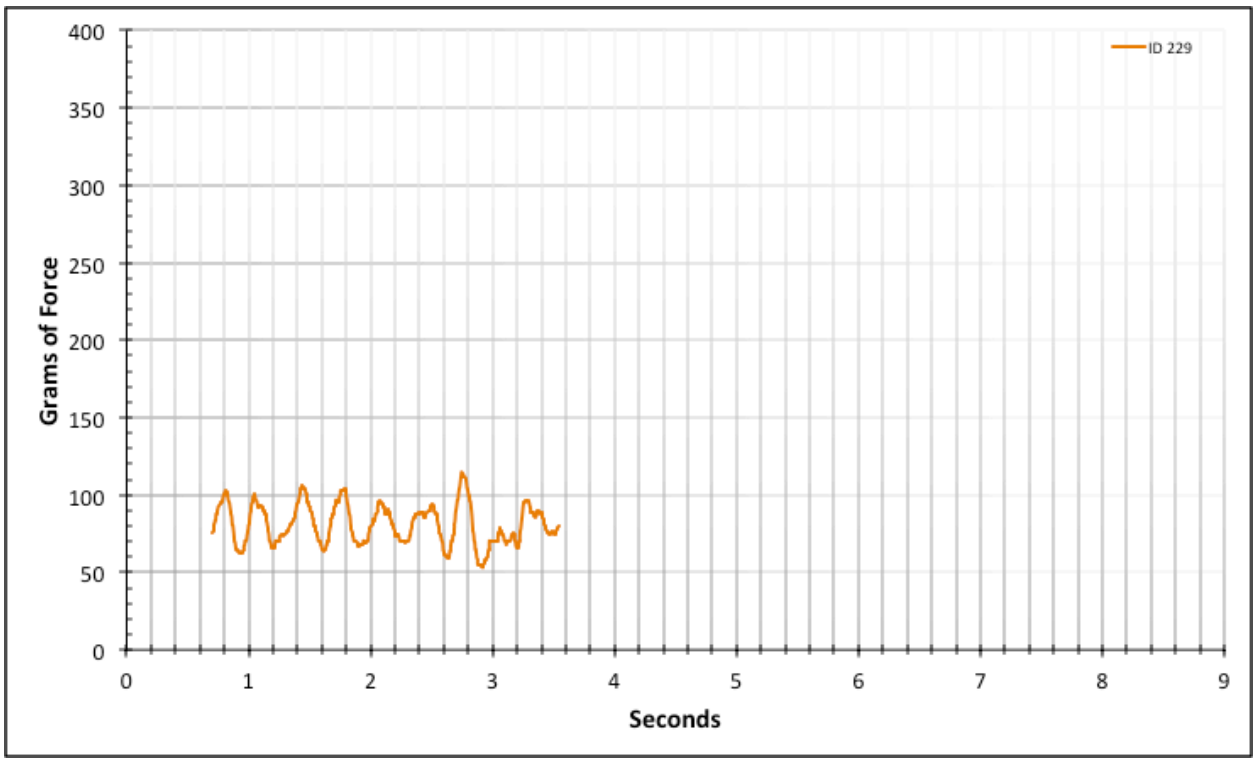

Figure A-6-298: Statistical Region Modeled Product - Lubricated - ID 229 - #12, Bolt 2

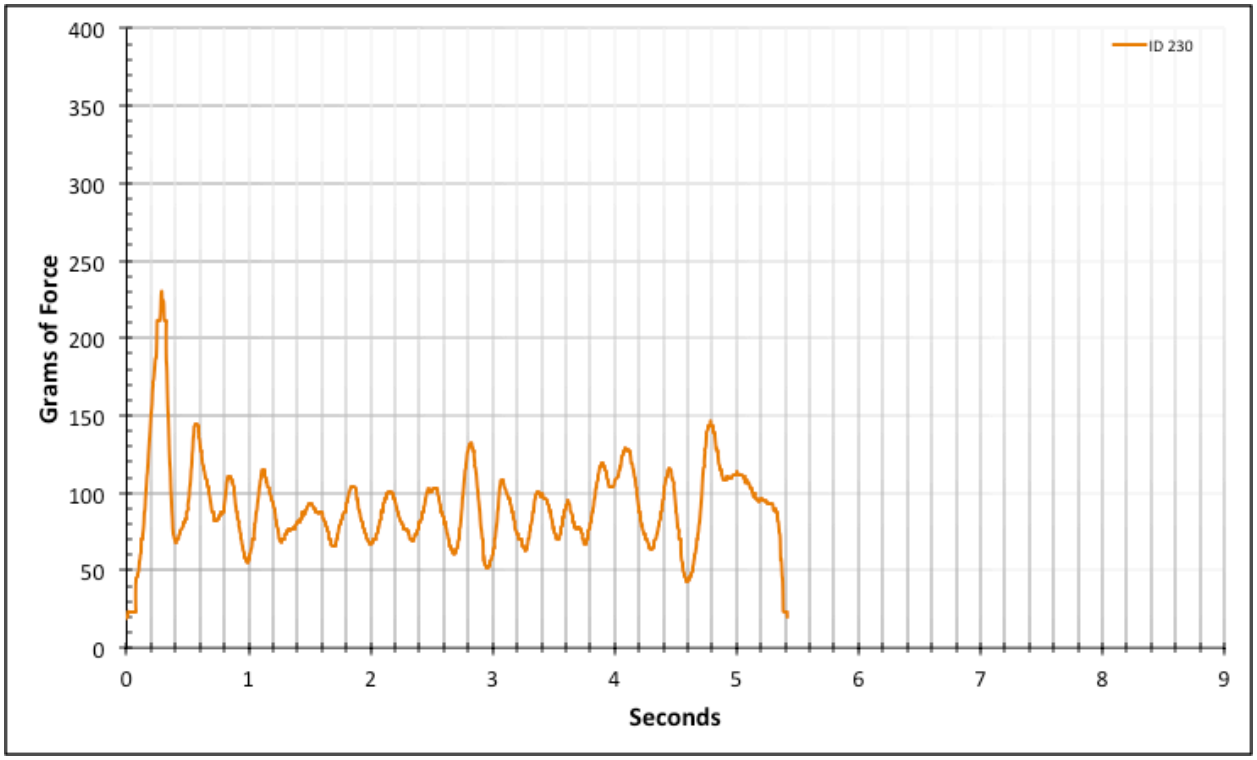

Figure A-6-299: Full Modeled Product - Lubricated - ID 230 - #12, Bolt 2

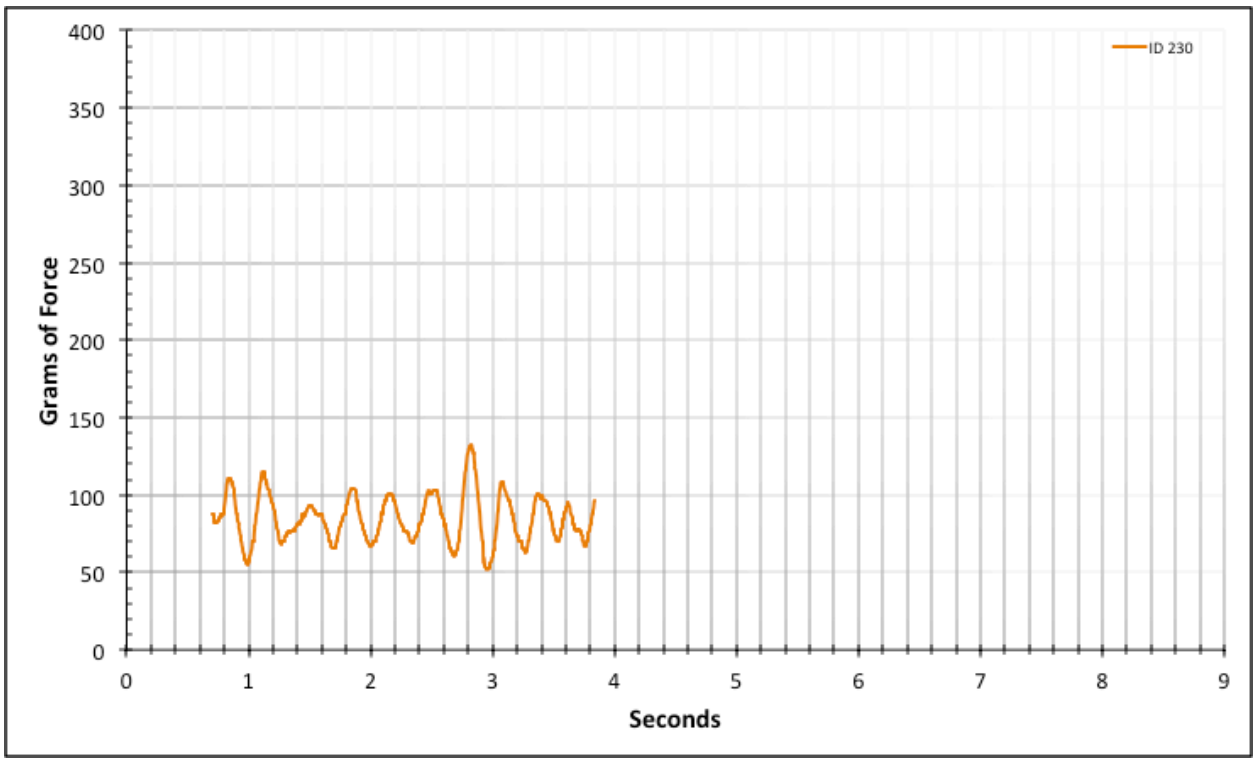

Figure A-6-300: Statistical Region Modeled Product - Lubricated - ID 230 - #12, Bolt 2

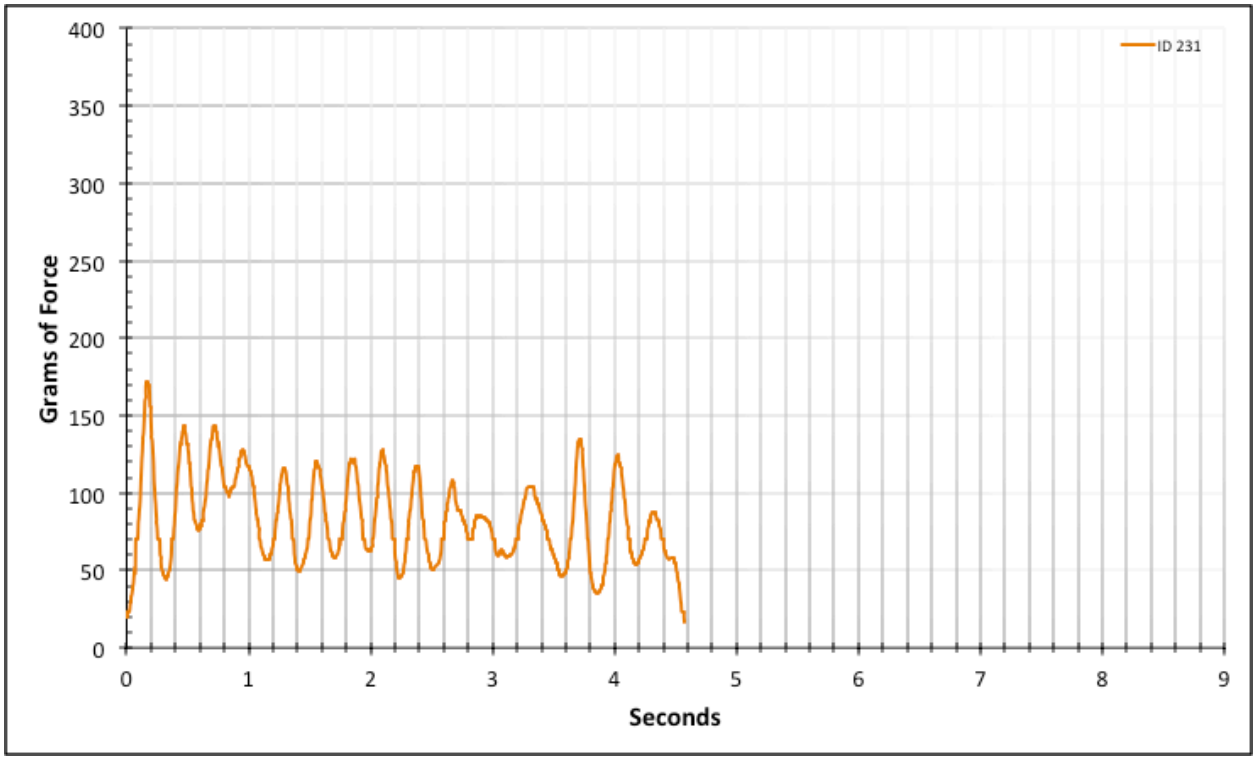

Figure A-6-301: Full Modeled Product - Lubricated - ID 231 - #12, Bolt 3

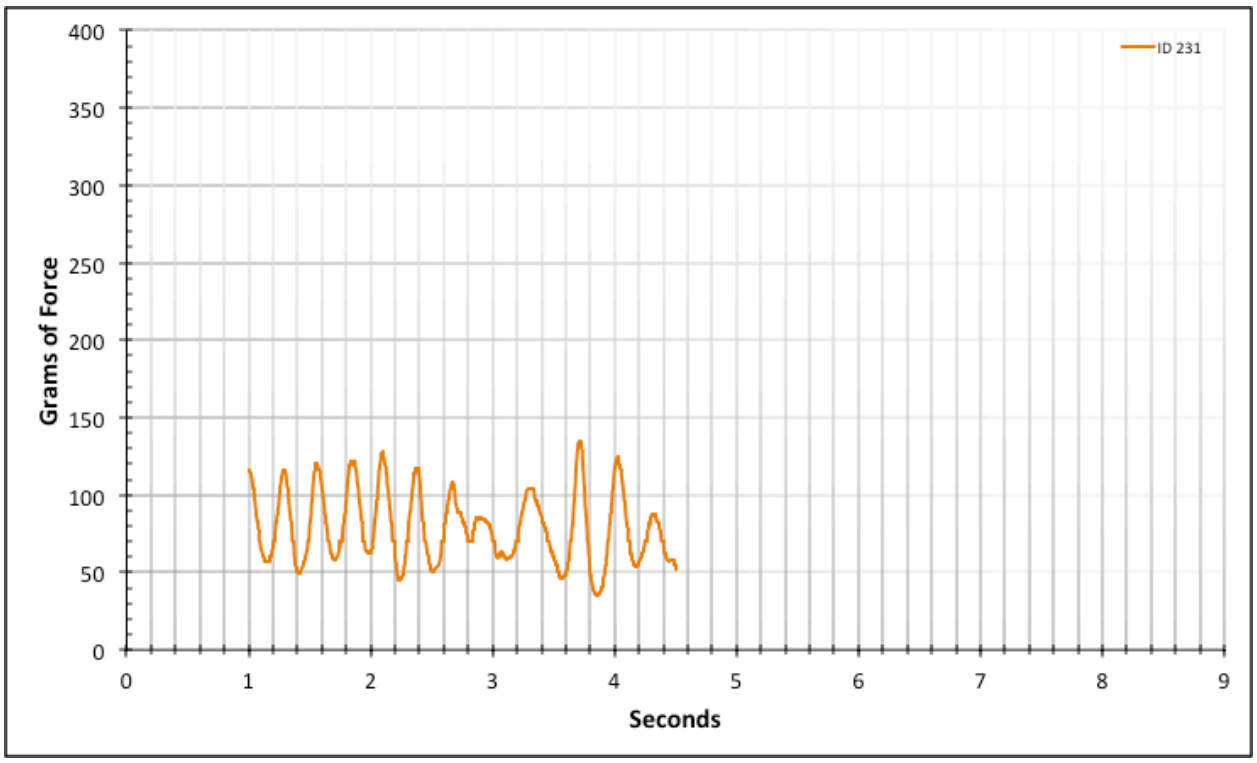

Figure A-6-302: Statistical Region Modeled Product - Lubricated - ID 231 - #12, Bolt 3

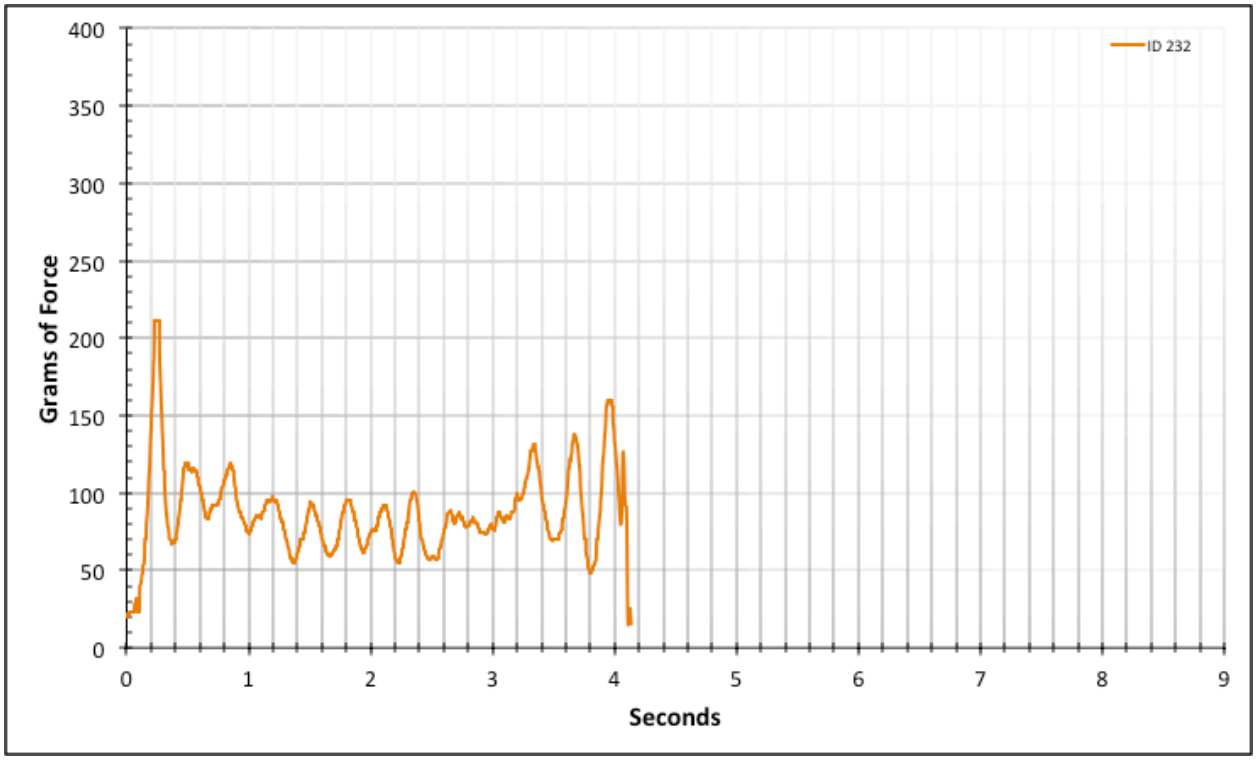

Figure A-6-303: Full Modeled Product - Lubricated - ID 232 - #12, Bolt 3

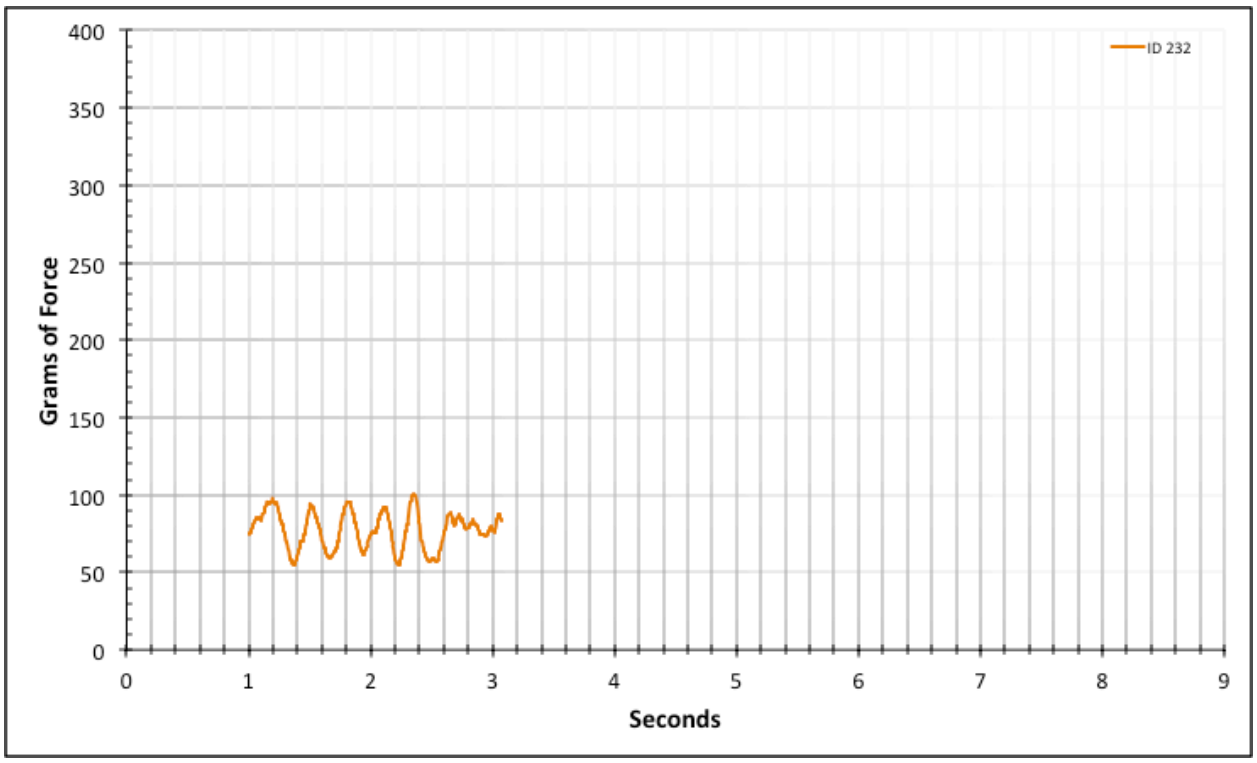

Figure A-6-304: Statistical Region Modeled Product - Lubricated - ID 232 - #12, Bolt 3

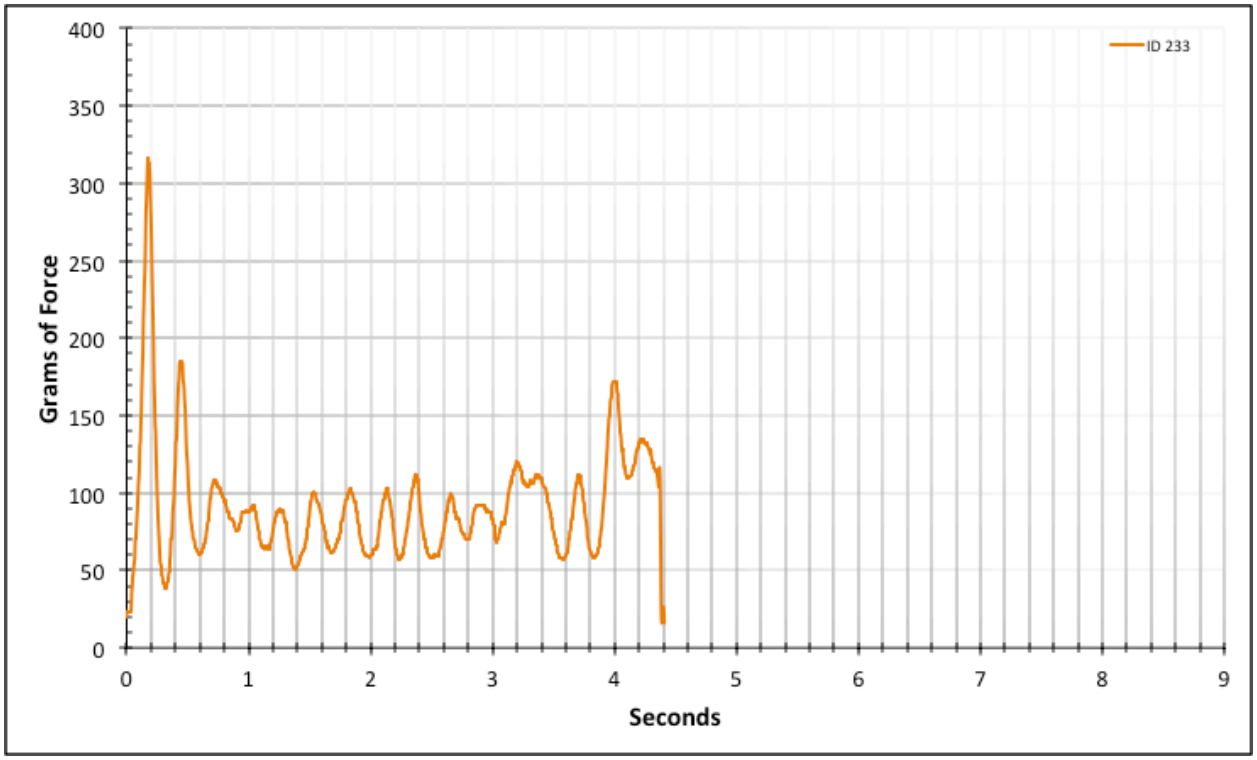

Figure A-6-305: Full Modeled Product - Lubricated - ID 233 - #12, Bolt 3

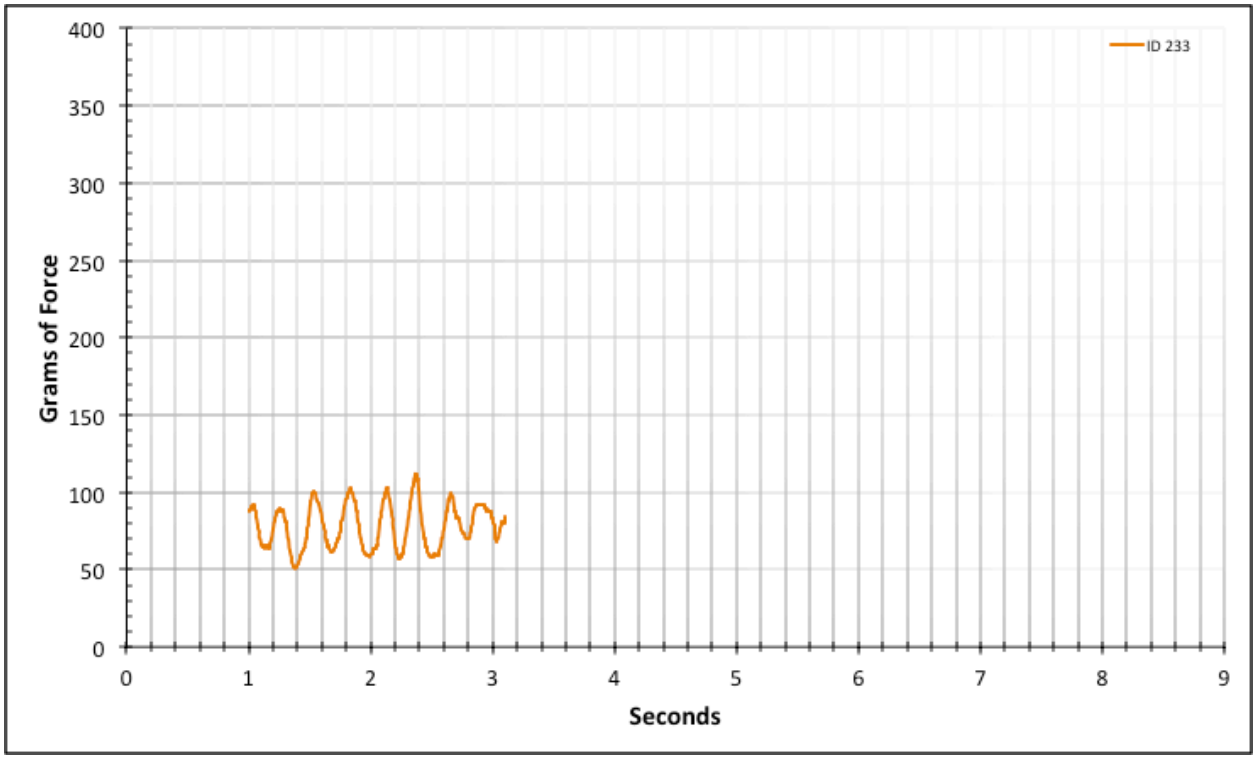

Figure A-6-306: Statistical Region Modeled Product - Lubricated - ID 233 - #12, Bolt 3

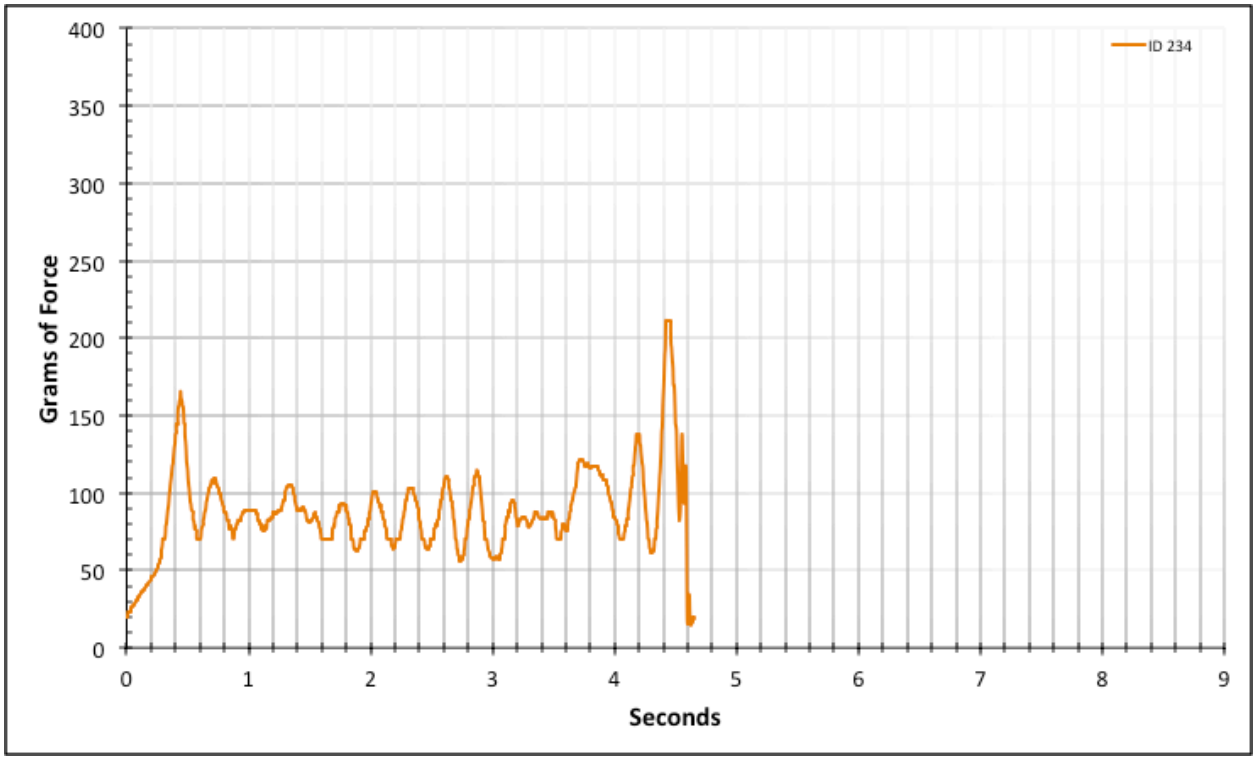

Figure A-6-307: Full Modeled Product - Lubricated - ID 234 - #12, Bolt 3

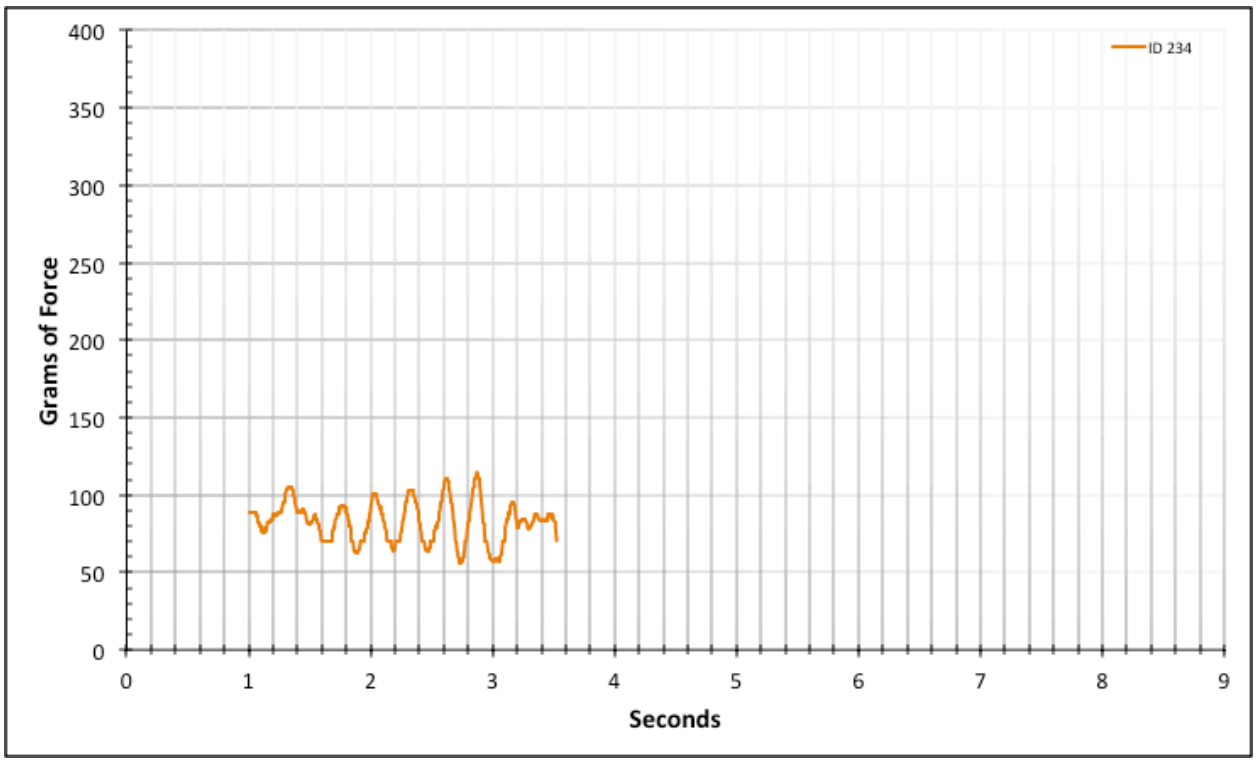

Figure A-6-308: Statistical Region Modeled Product - Lubricated - ID 234 - #12, Bolt 3

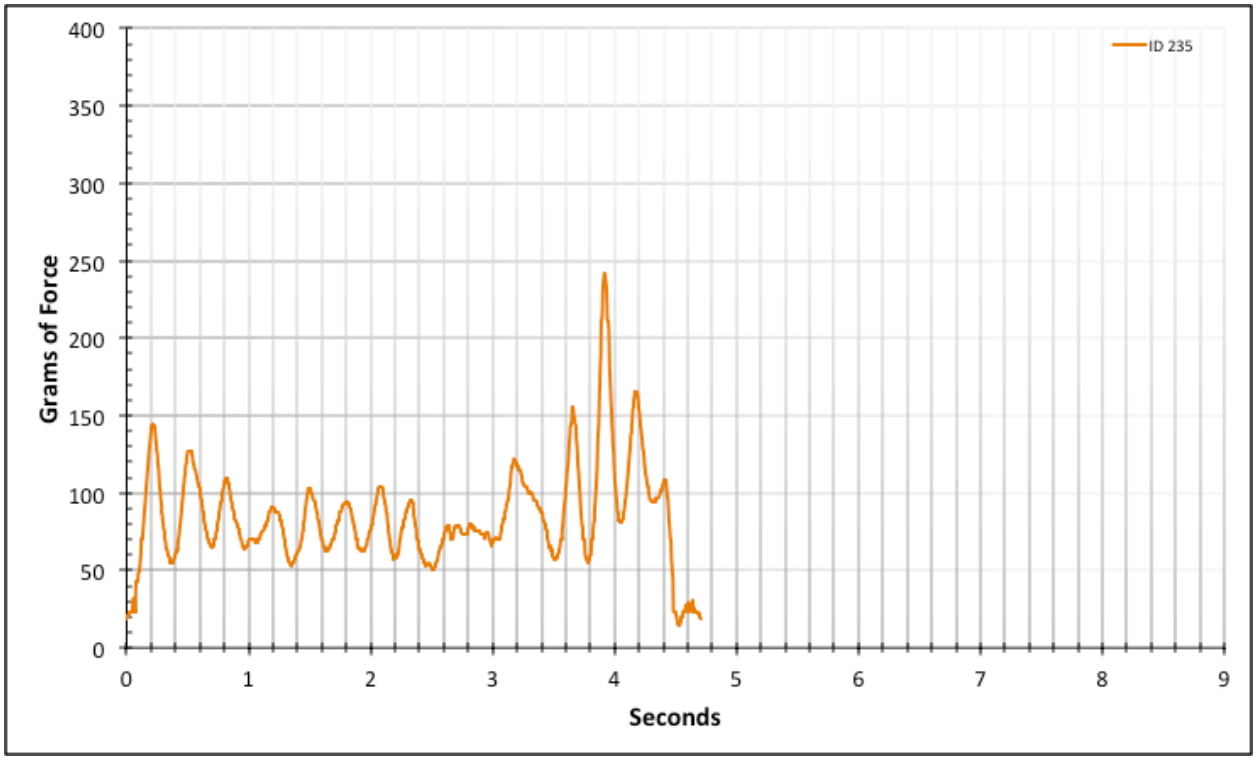

Figure A-6-309: Full Modeled Product - Lubricated - ID 235 - #12, Bolt 3

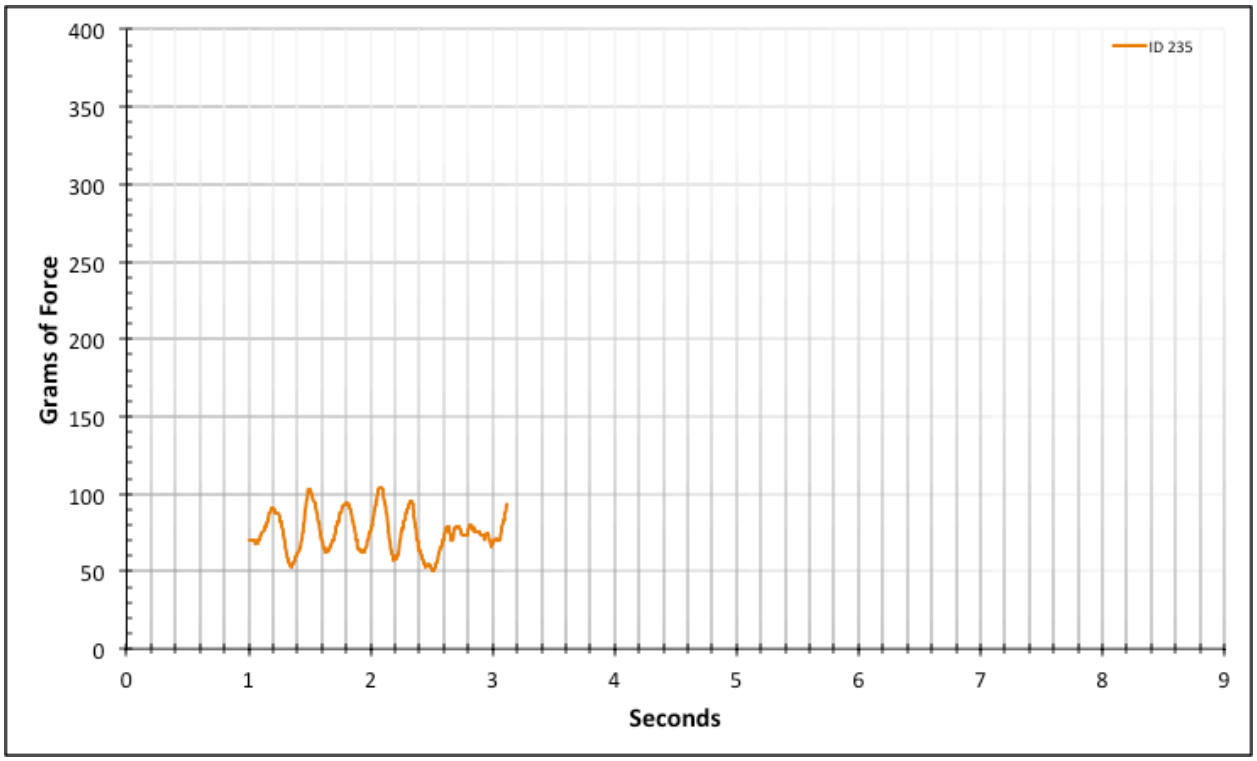

Figure A-6-310: Statistical Region Modeled Product - Lubricated - ID 235 - #12, Bolt 3

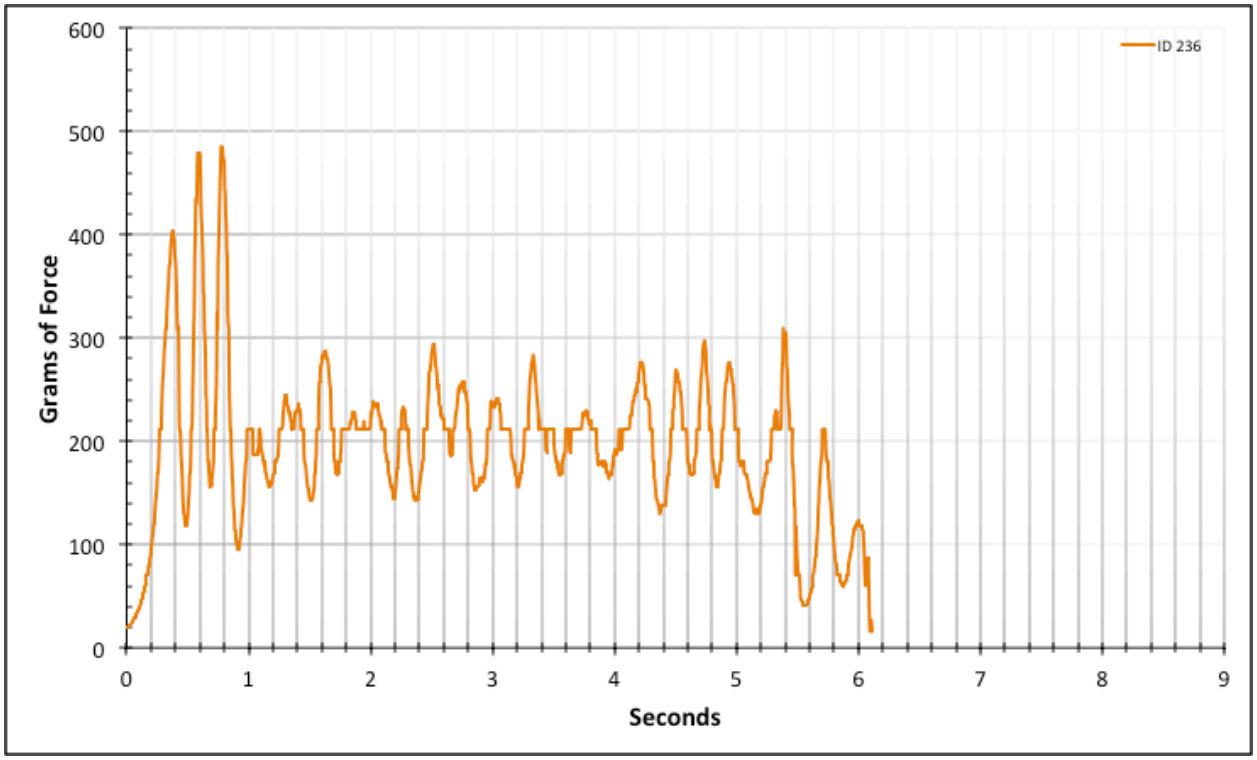

Figure A-6-311: Full Modeled Product - Lubricated - ID 236 - #10, Bolt 1

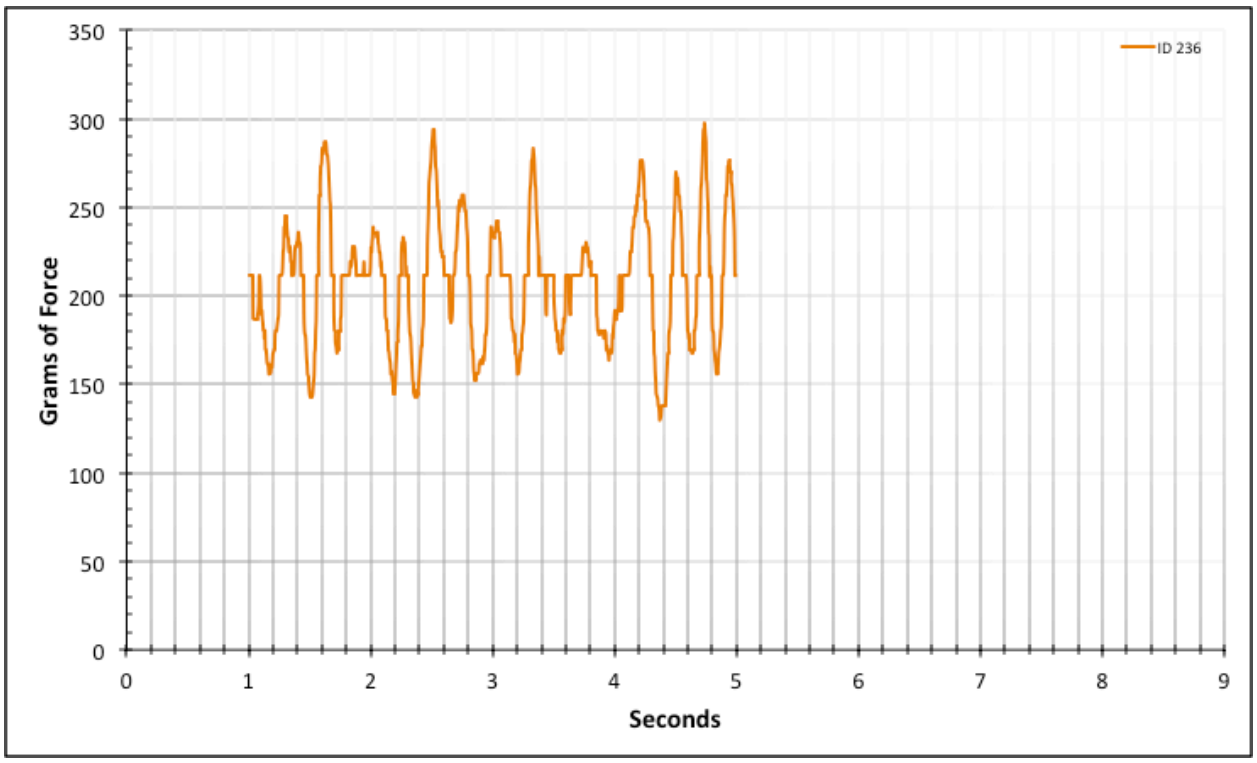

Figure A-6-312: Statistical Region Modeled Product - Lubricated - ID 236 - #10, Bolt 1

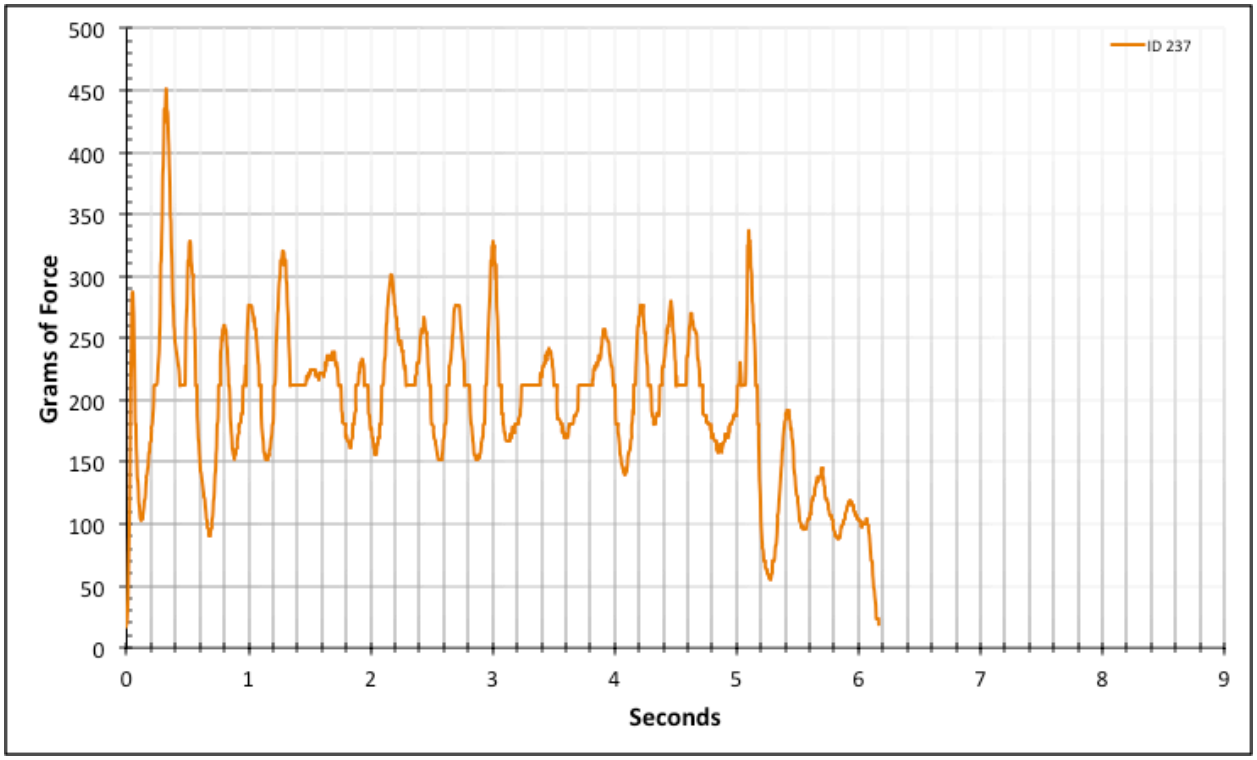

Figure A-6-313: Full Modeled Product - Lubricated - ID 237 - #10, Bolt 1

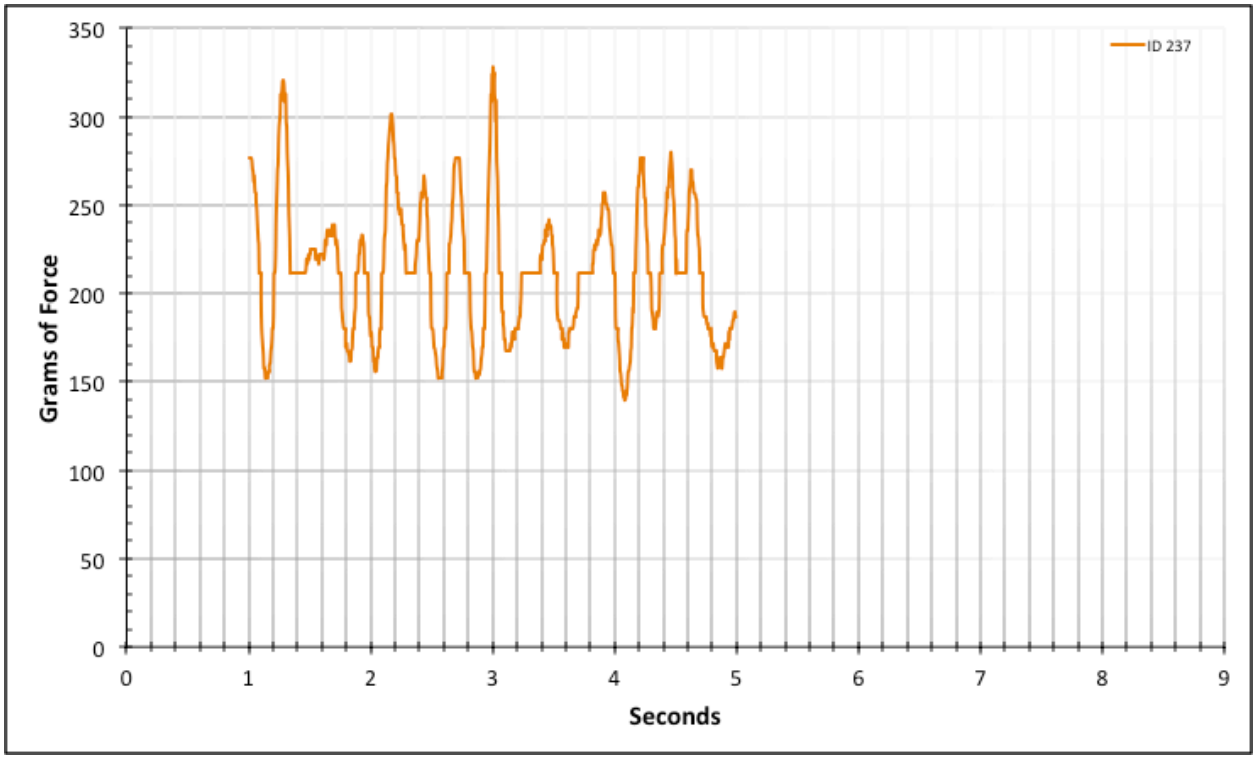

Figure A-6-314: Statistical Region Modeled Product - Lubricated - ID 237 - #10, Bolt 1

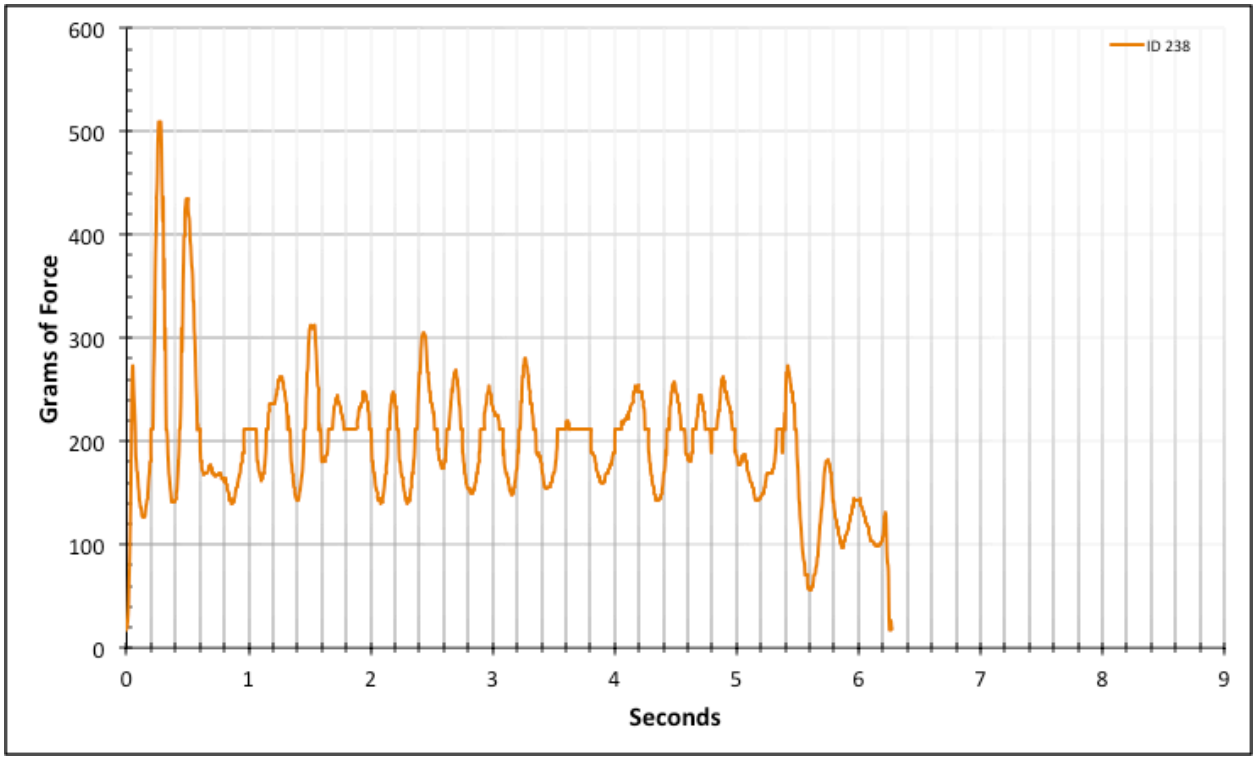

Figure A-6-315: Full Modeled Product - Lubricated - ID 238 - #10, Bolt 1

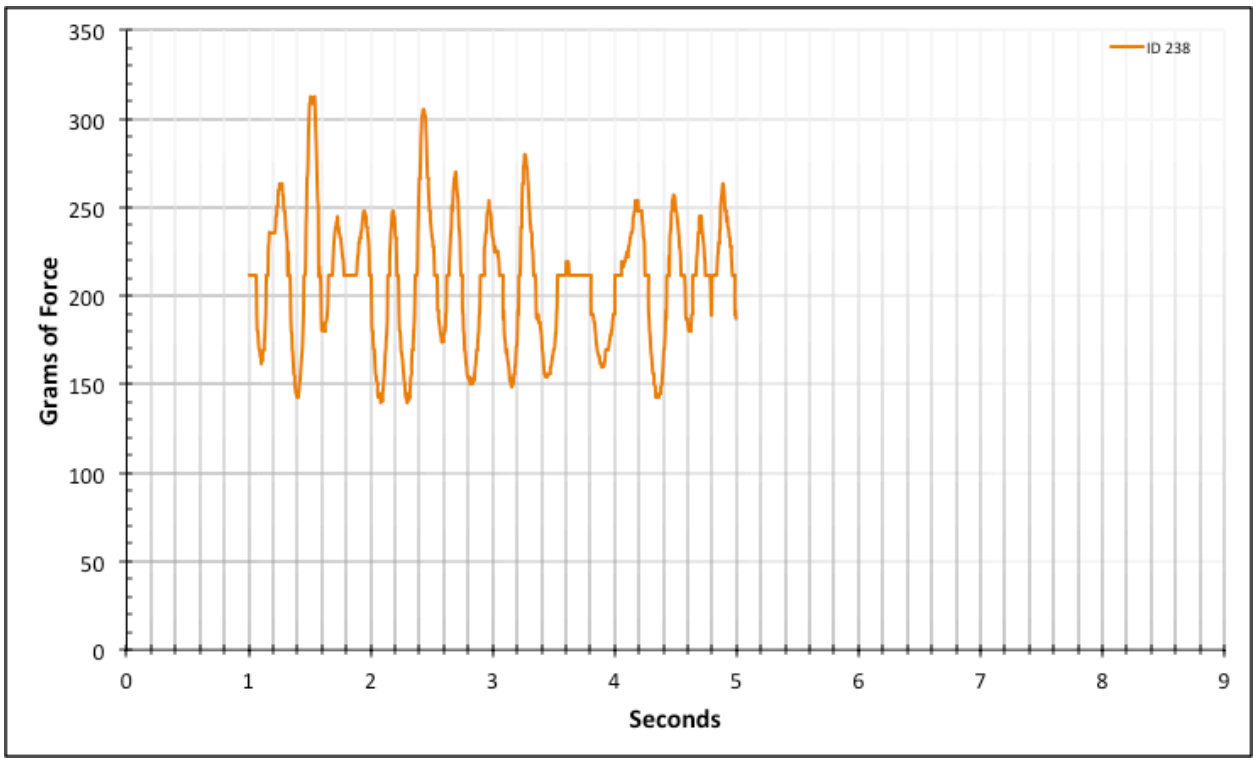

Figure A-6-316: Statistical Region Modeled Product - Lubricated - ID 238 - #10, Bolt 1

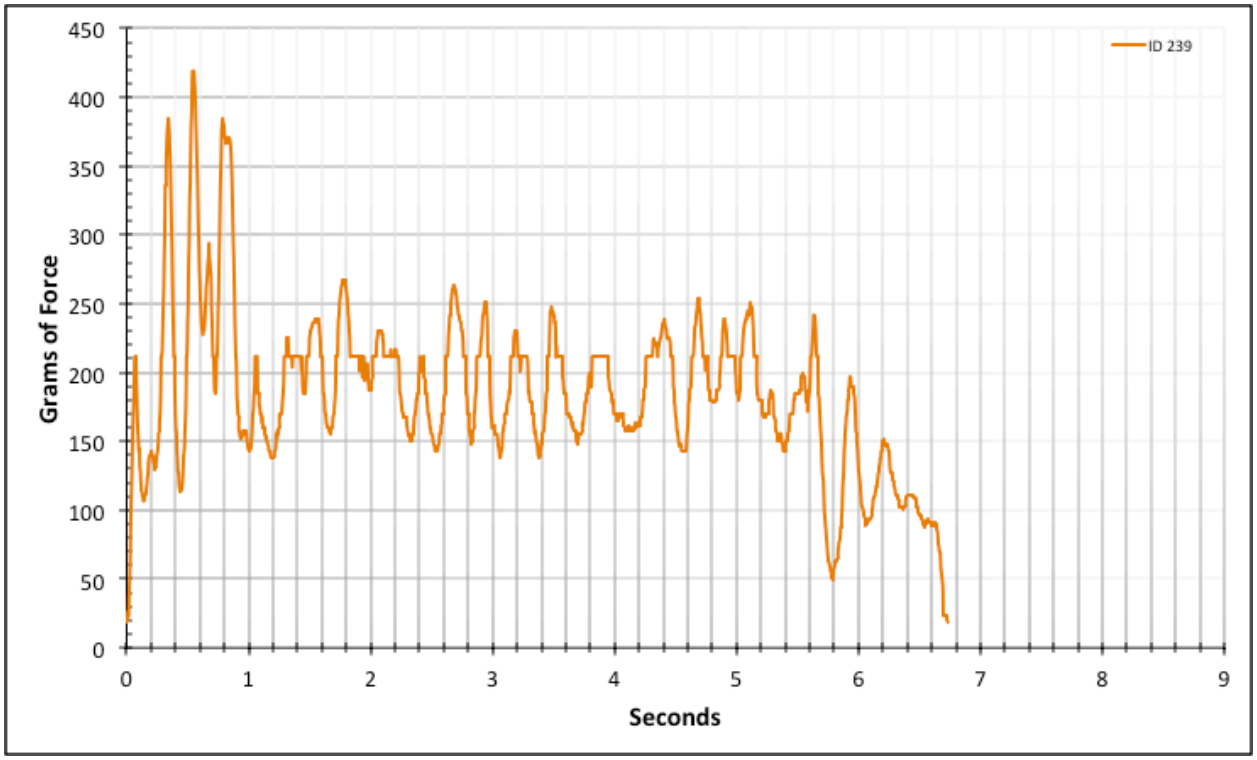

Figure A-6-317: Full Modeled Product - Lubricated - ID 239 - #10, Bolt 1

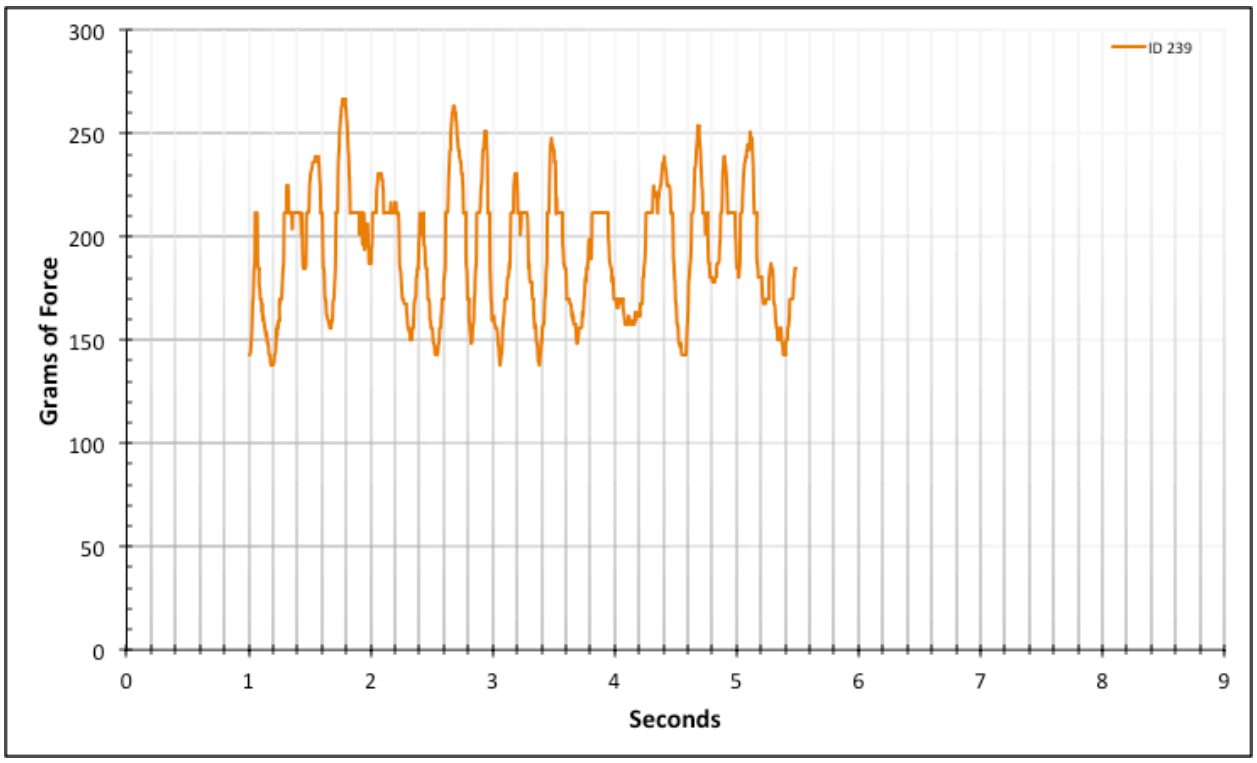

Figure A-6-318: Statistical Region Modeled Product - Lubricated - ID 239 - #10, Bolt 1

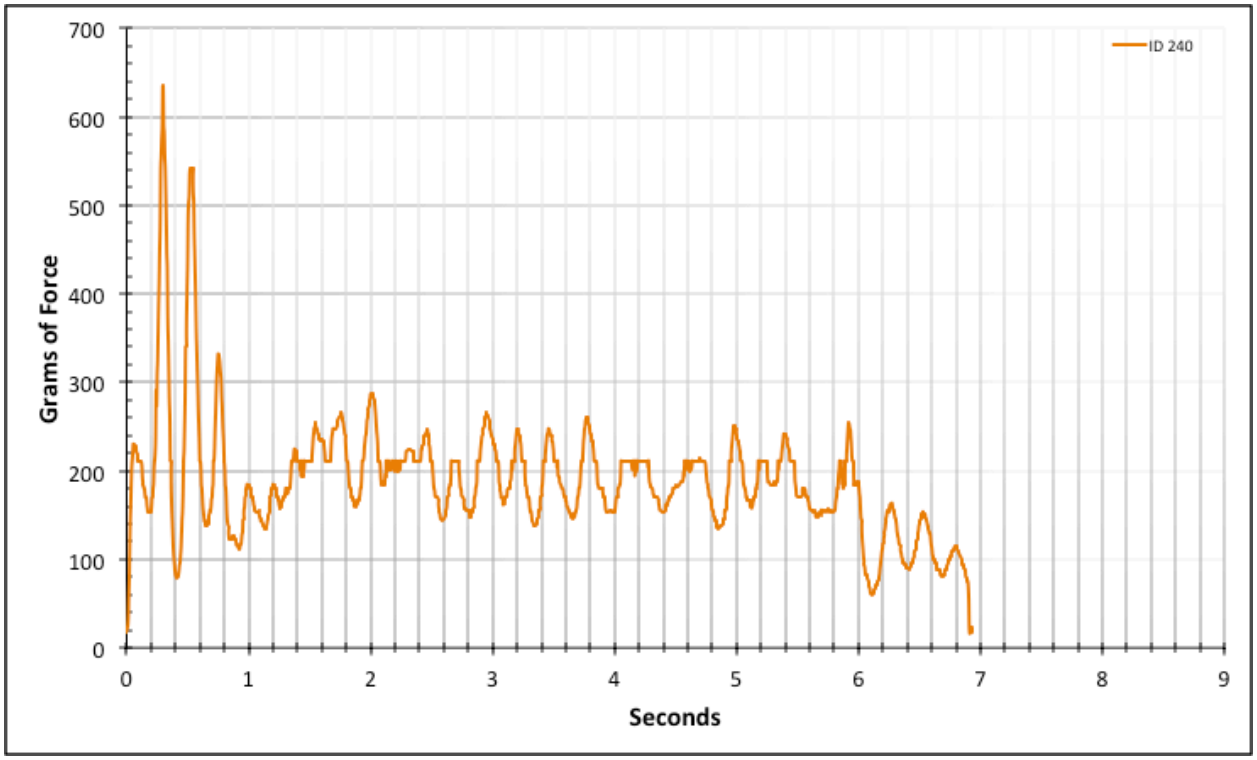

Figure A-6-319: Full Modeled Product - Lubricated - ID 240 - #10, Bolt 1

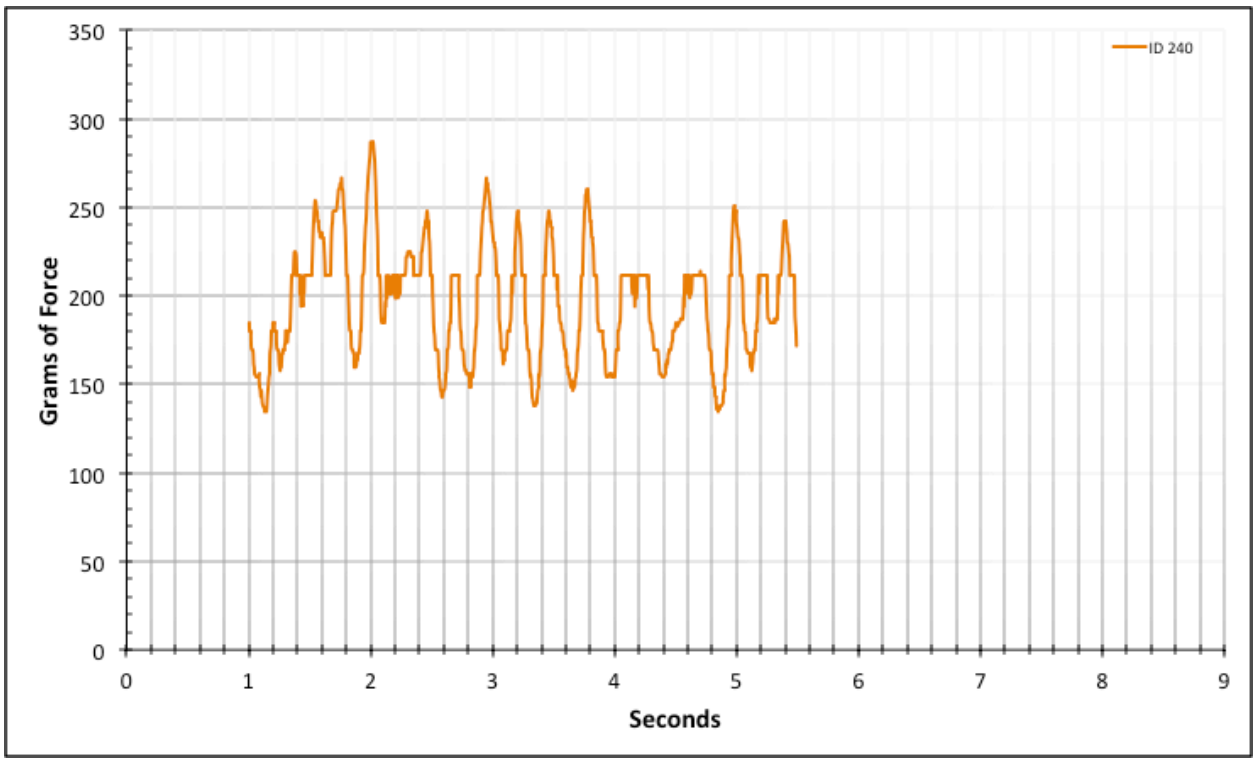

Figure A-6-320: Statistical Region Modeled Product - Lubricated - ID 240 - #10, Bolt 1

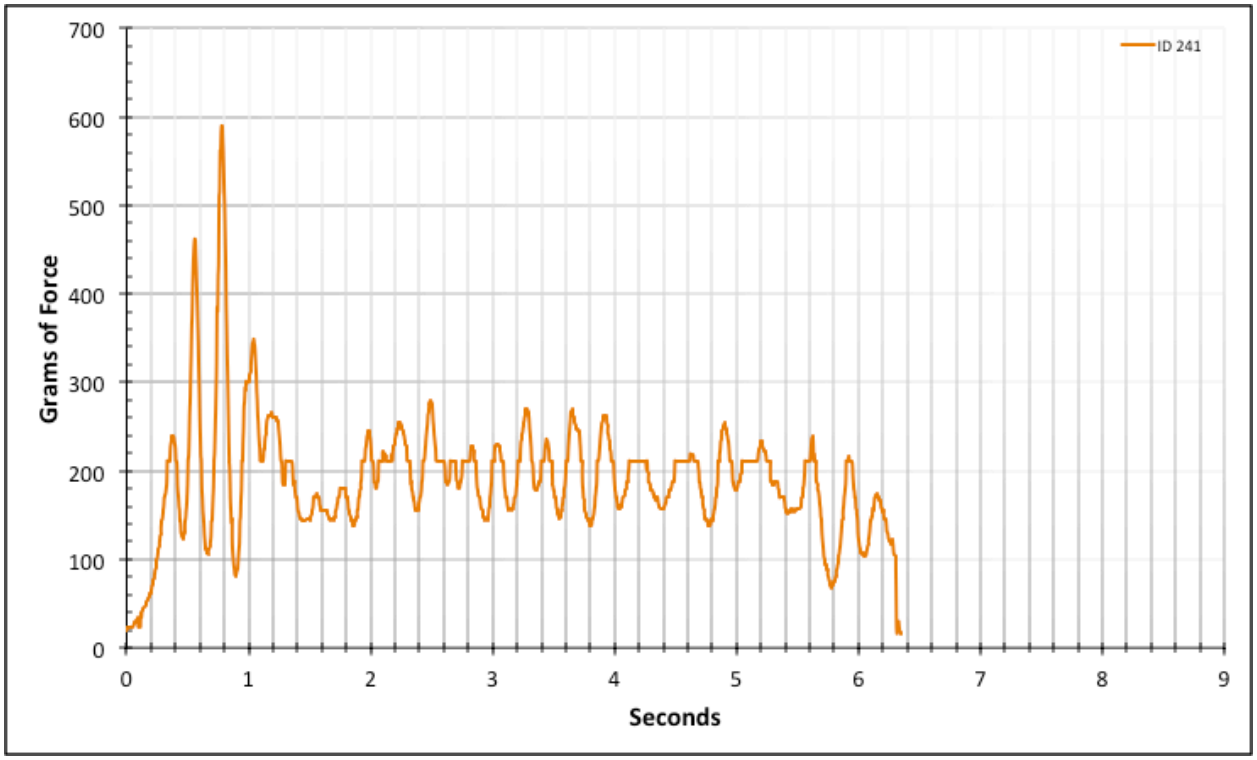

Figure A-6-321: Full Modeled Product - Lubricated - ID 241 - #10, Bolt 2

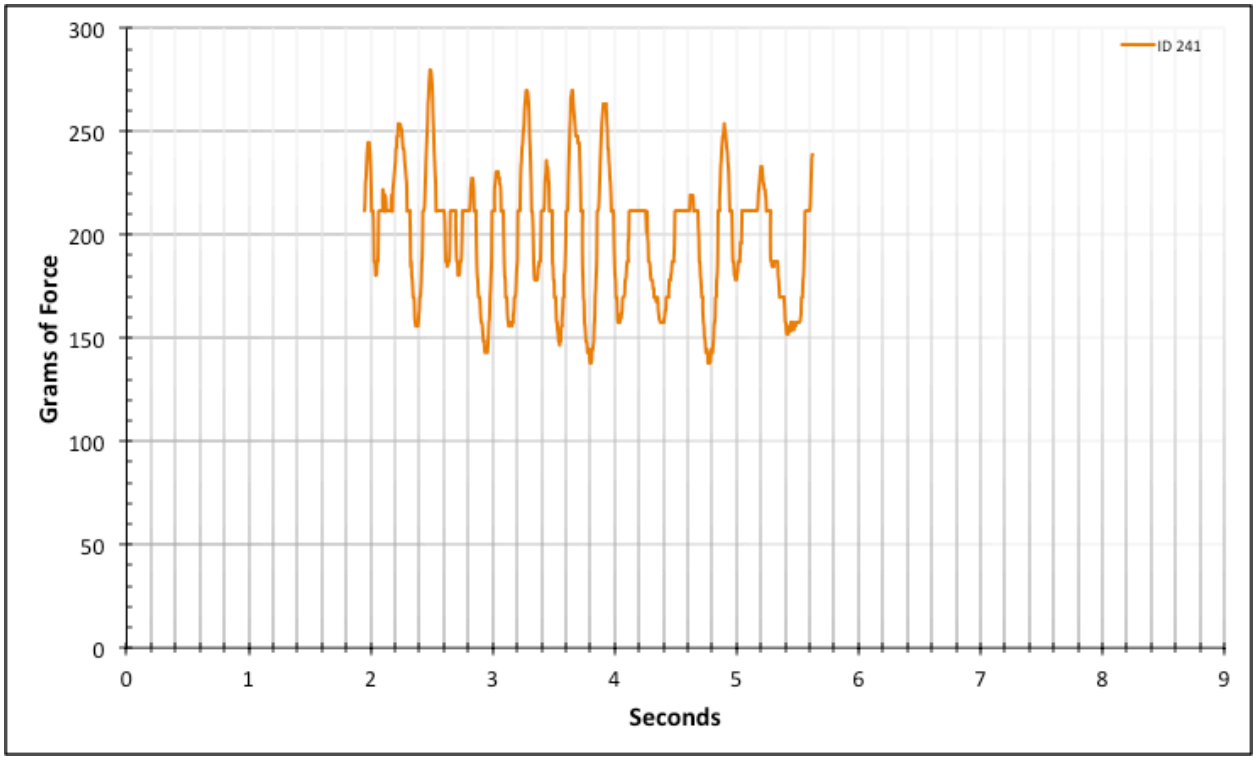

Figure A-6-322: Statistical Region Modeled Product - Lubricated - ID 241 - #10, Bolt 2

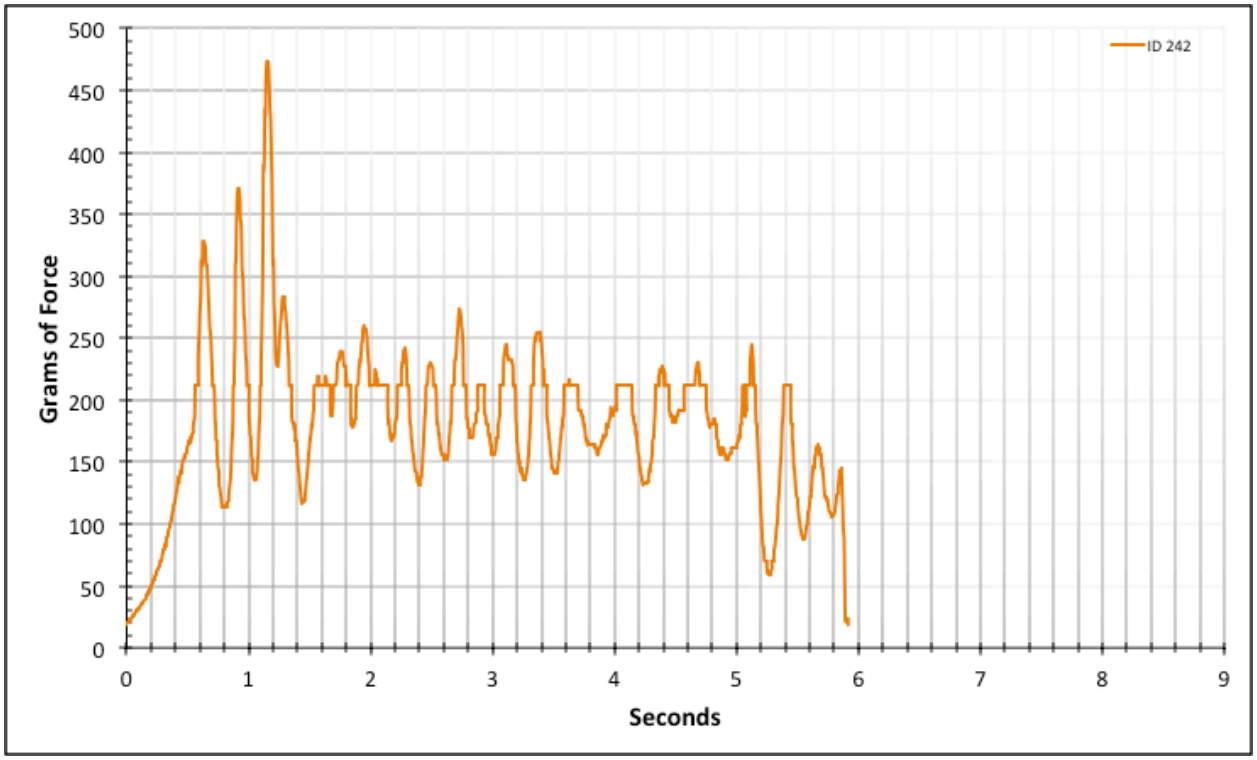

Figure A-6-323: Full Modeled Product - Lubricated - ID 242 - #10, Bolt 2

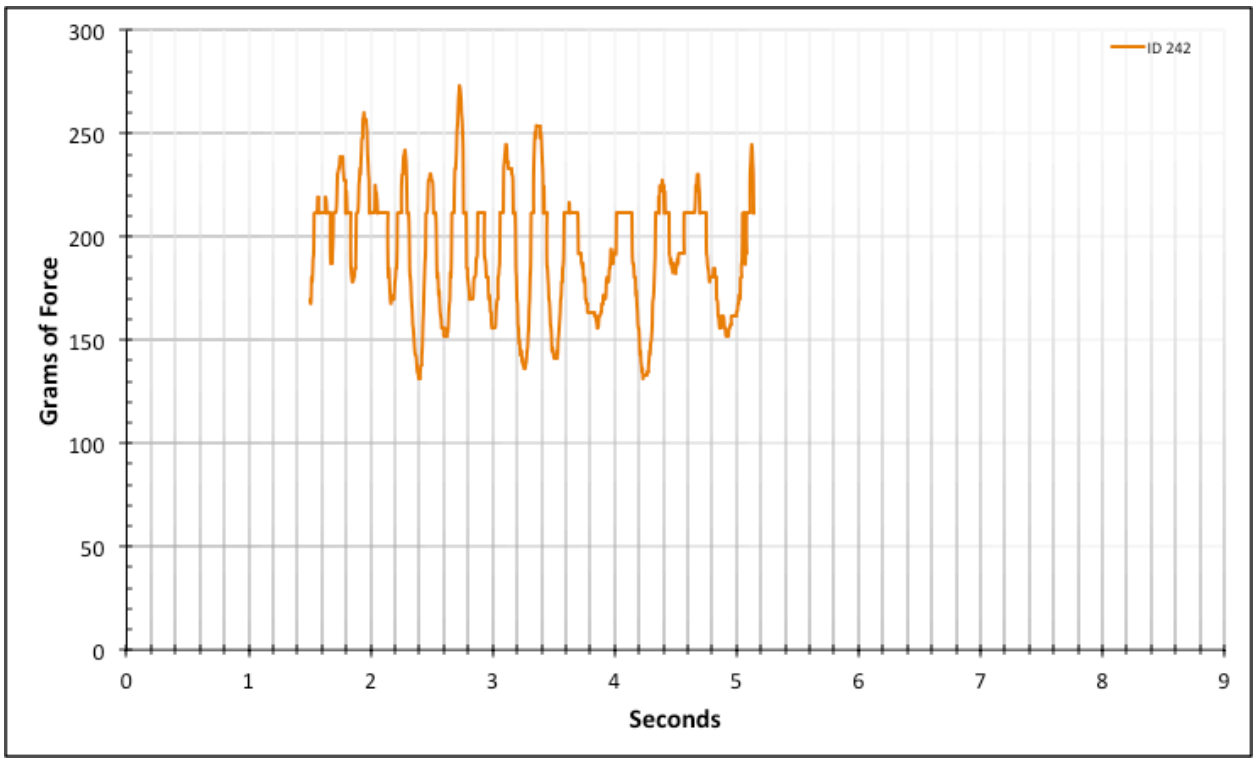

Figure A-6-324: Statistical Region Modeled Product - Lubricated - ID 242 - #10, Bolt 2

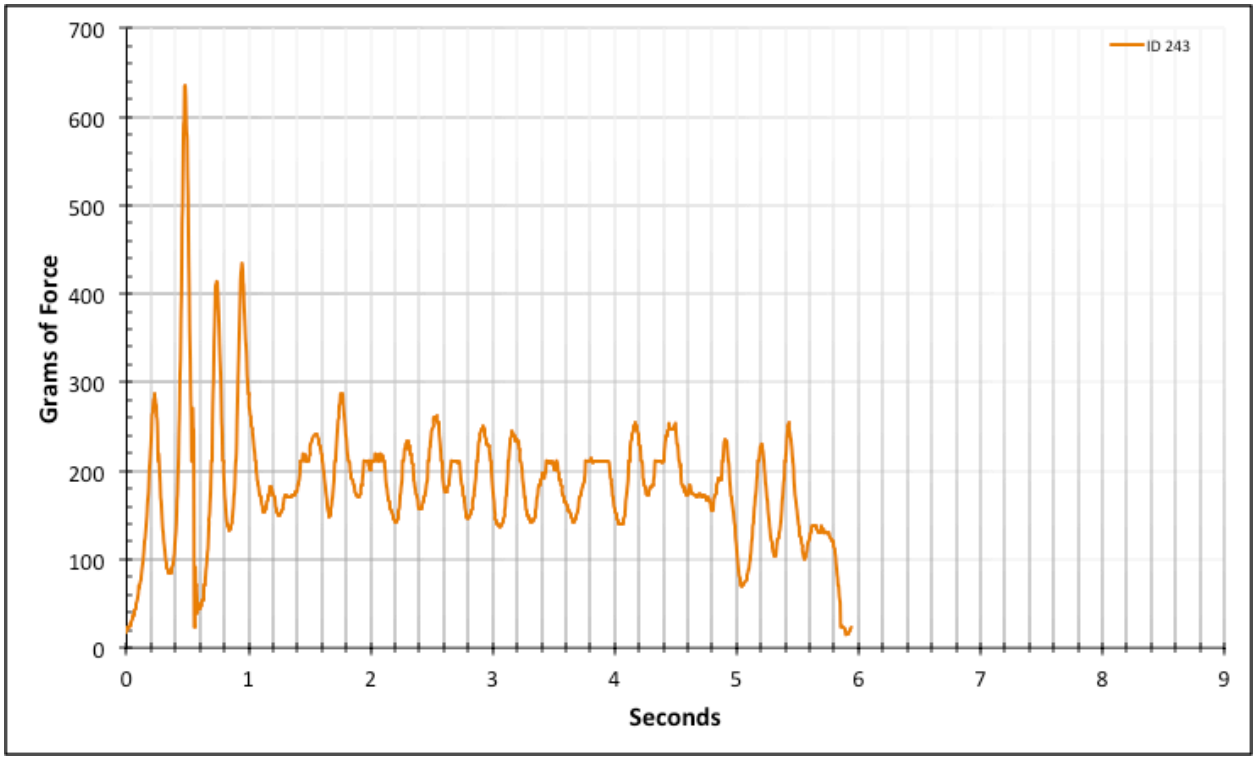

Figure A-6-325: Full Modeled Product - Lubricated - ID 243 - #10, Bolt 2

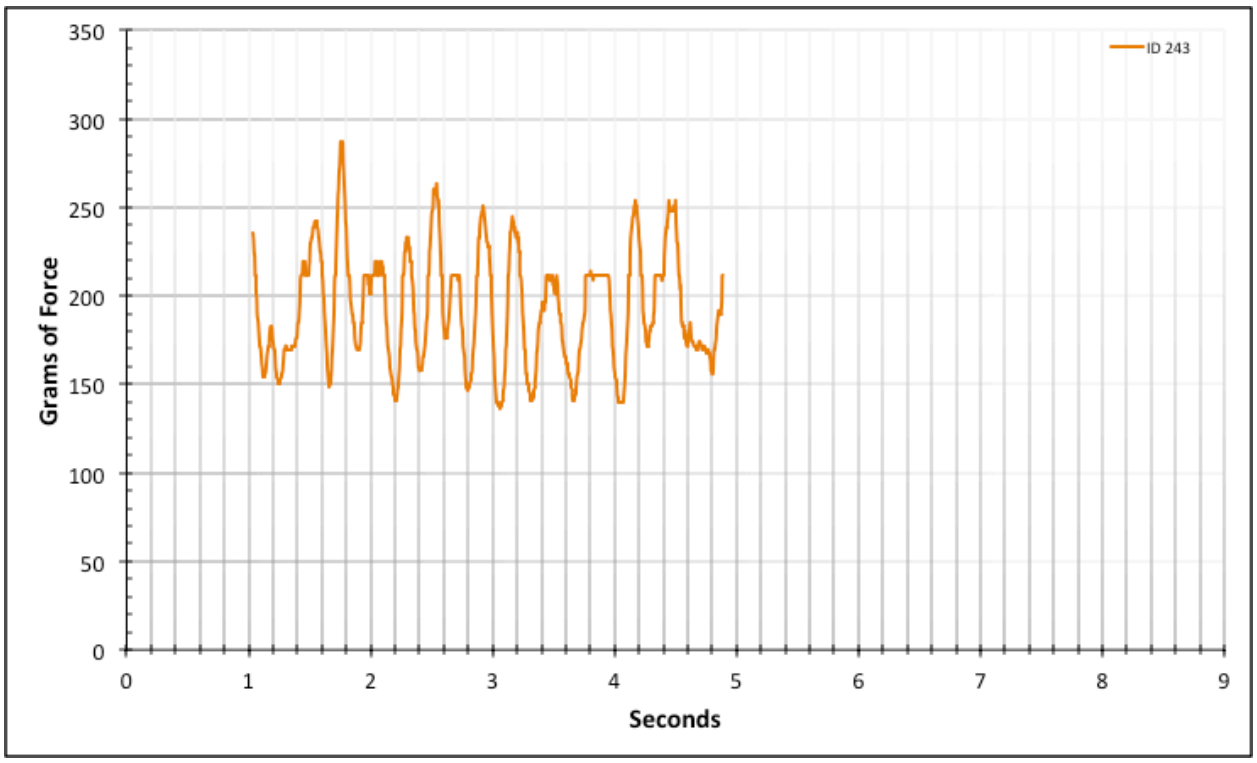

Figure A-6-326: Statistical Region Modeled Product - Lubricated - ID 243 - #10, Bolt 2

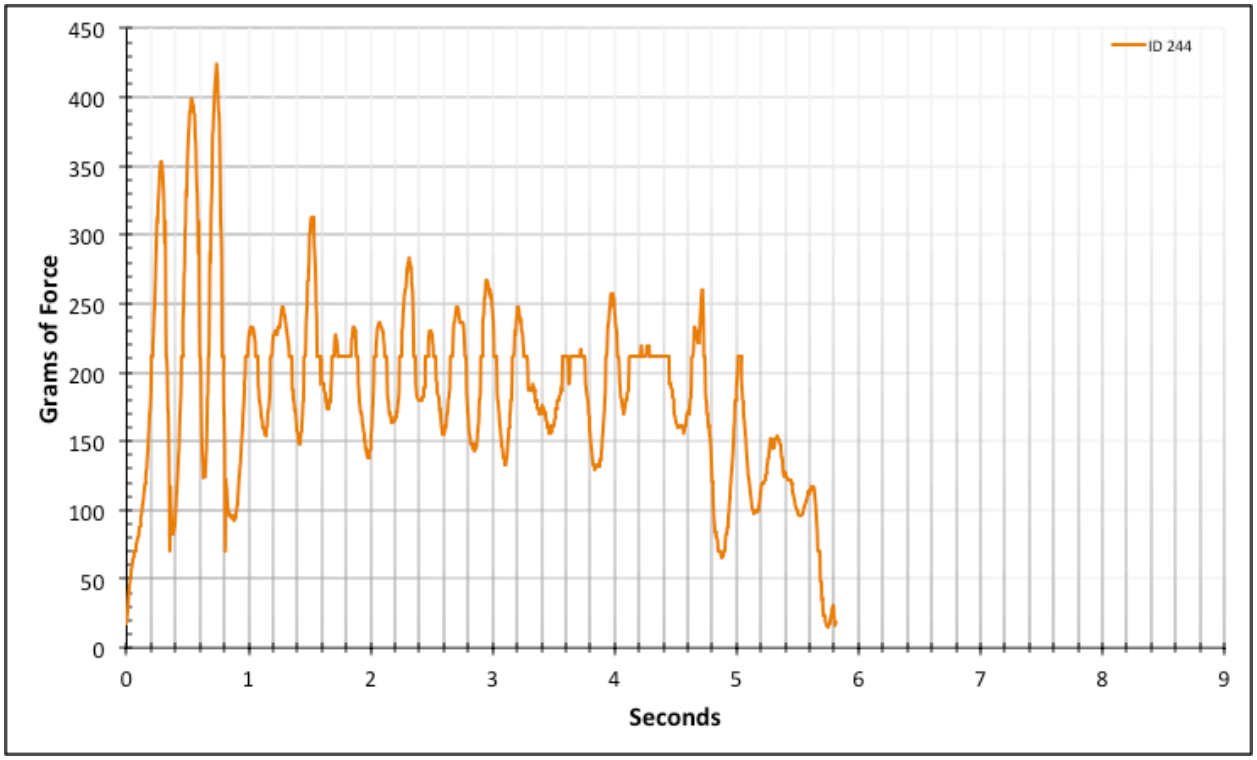

Figure A-6-327: Full Modeled Product - Lubricated - ID 244 - #10, Bolt 2

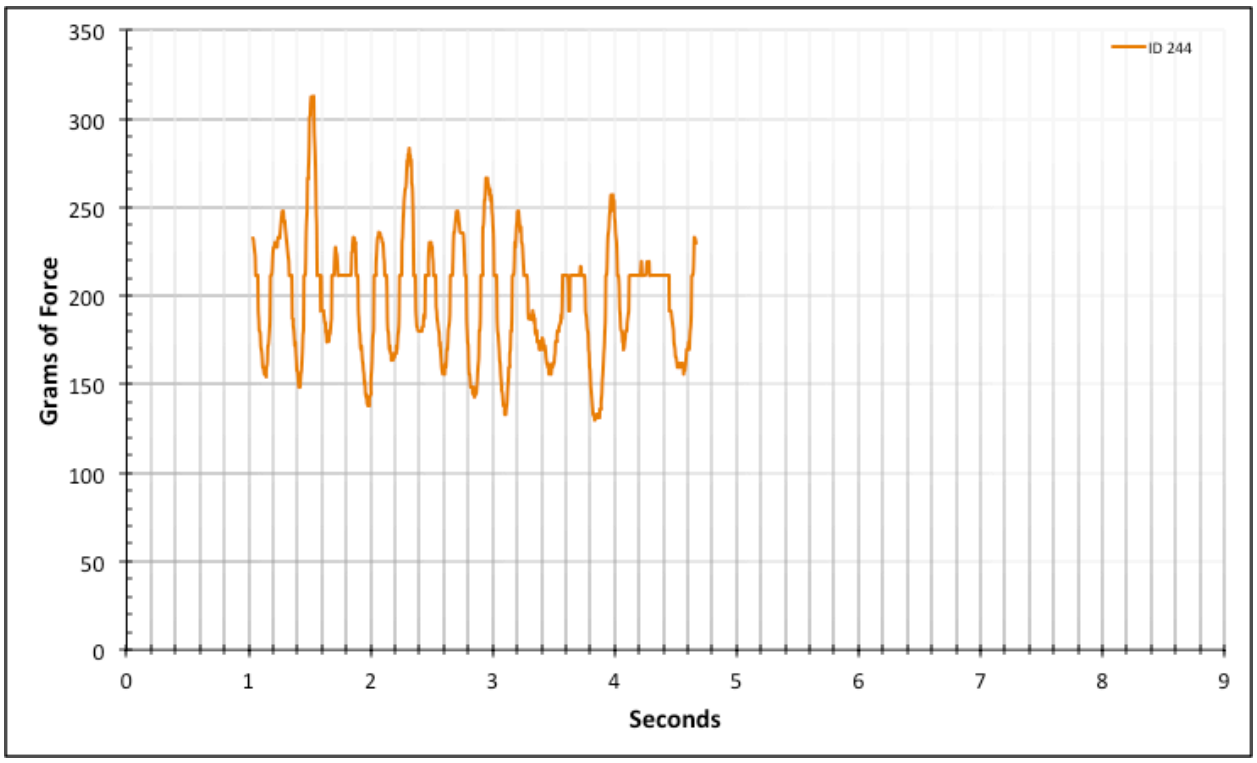

Figure A-6-328: Statistical Region Modeled Product - Lubricated - ID 244 - #10, Bolt 2

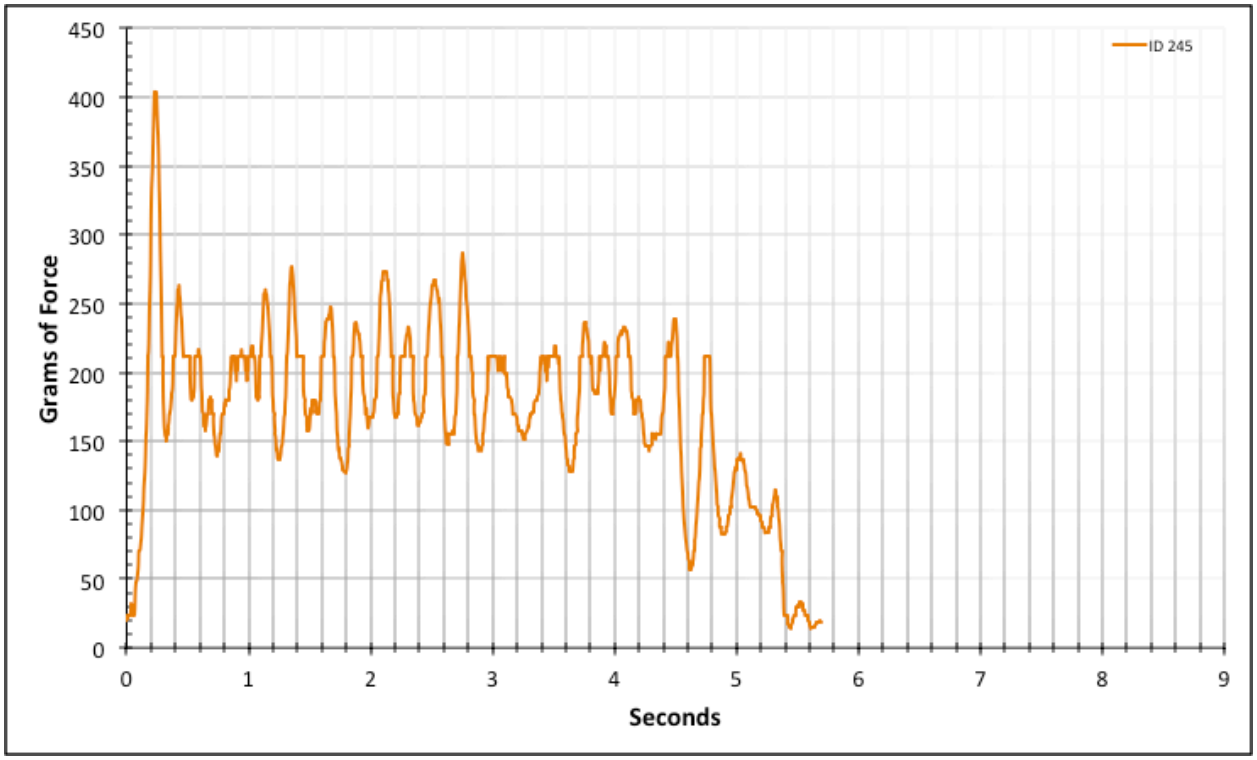

Figure A-6-329: Full Modeled Product - Lubricated - ID 245 - #10, Bolt 2

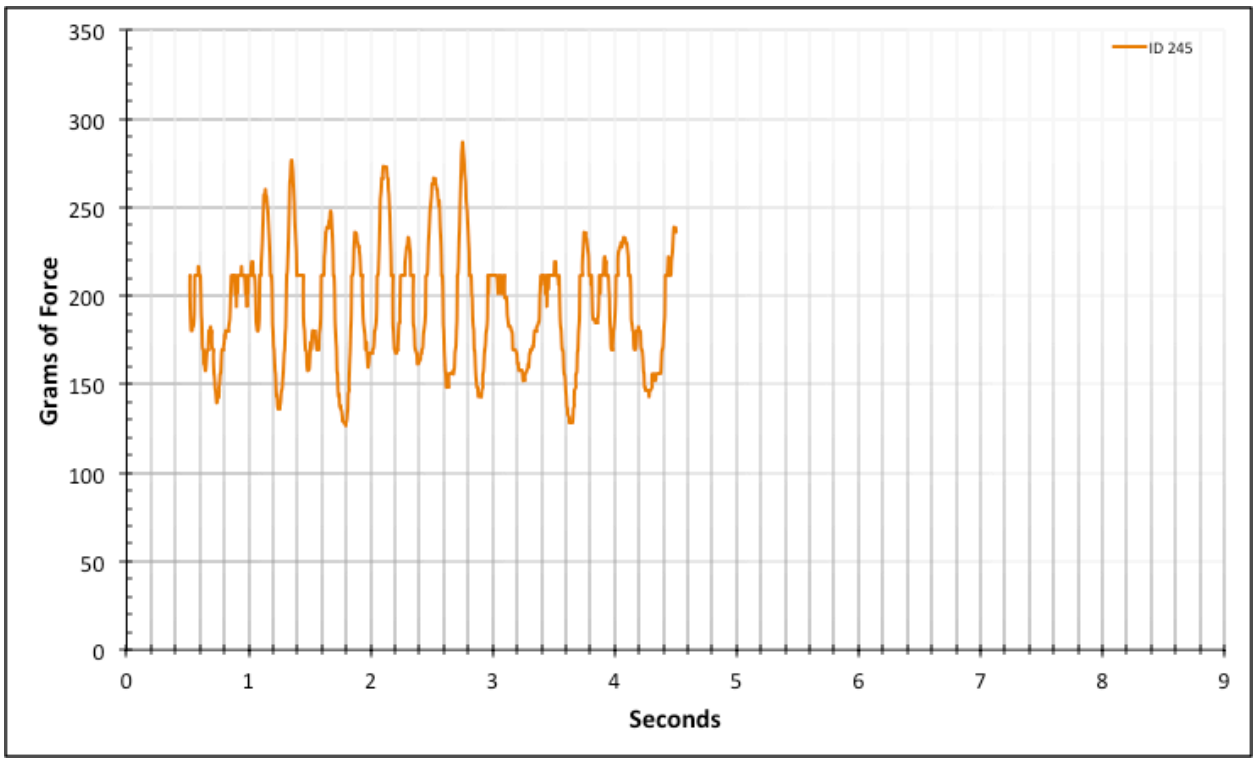

Figure A-6-330: Statistical Region Modeled Product - Lubricated - ID 245 - #10, Bolt 2

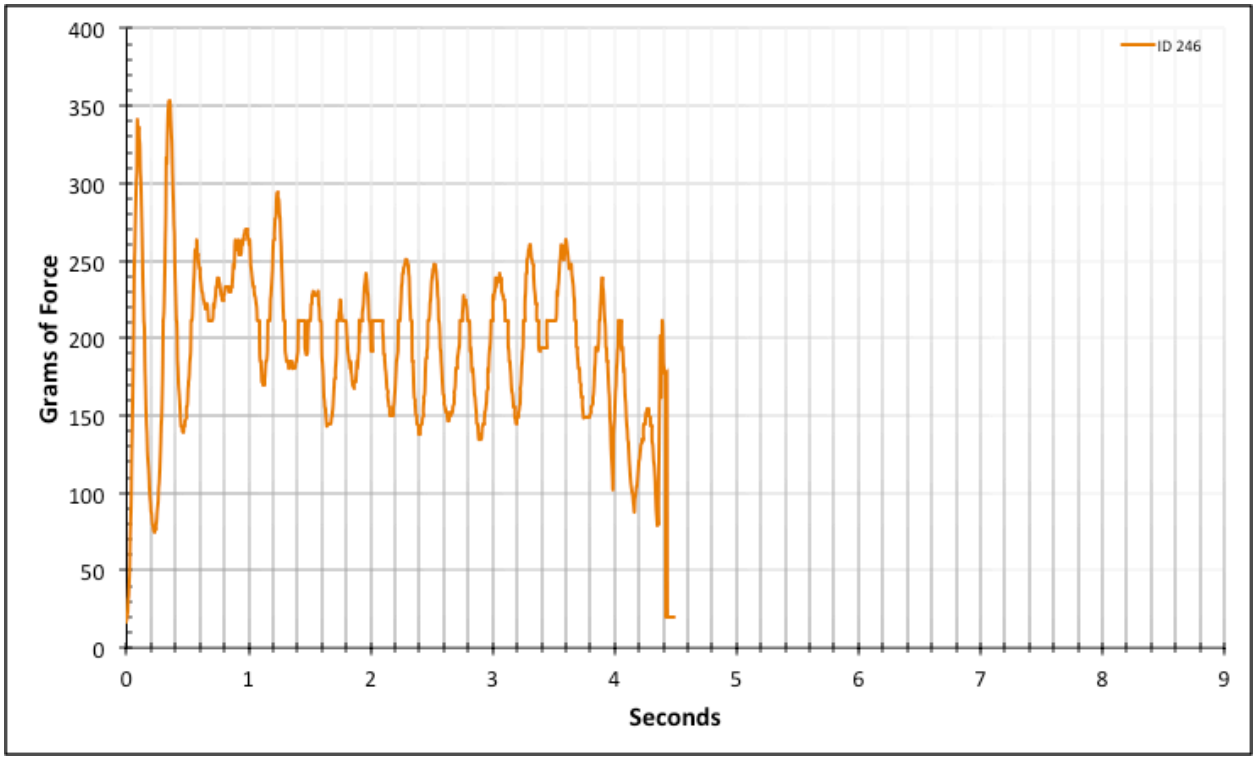

Figure A-6-331: Full Modeled Product - Lubricated - ID 246 - #10, Bolt 3

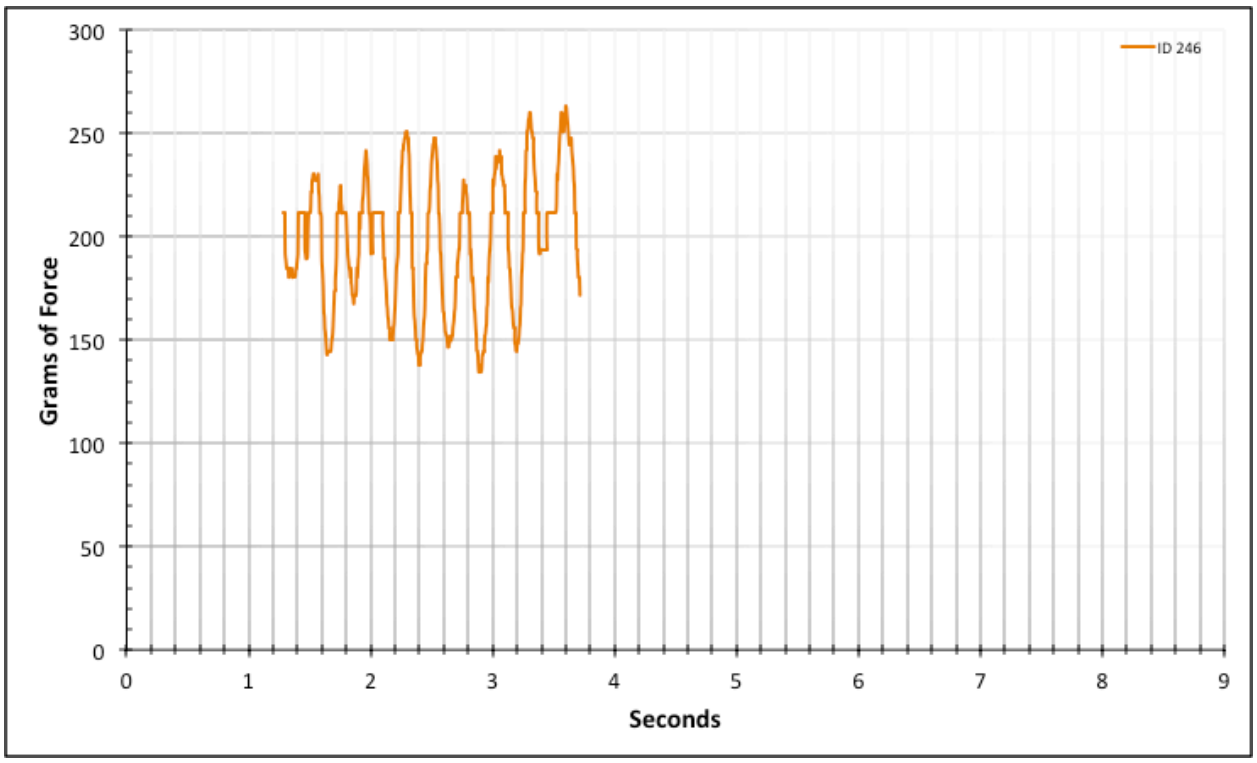

Figure A-6-332: Statistical Region Modeled Product - Lubricated - ID 246 - #10, Bolt 3

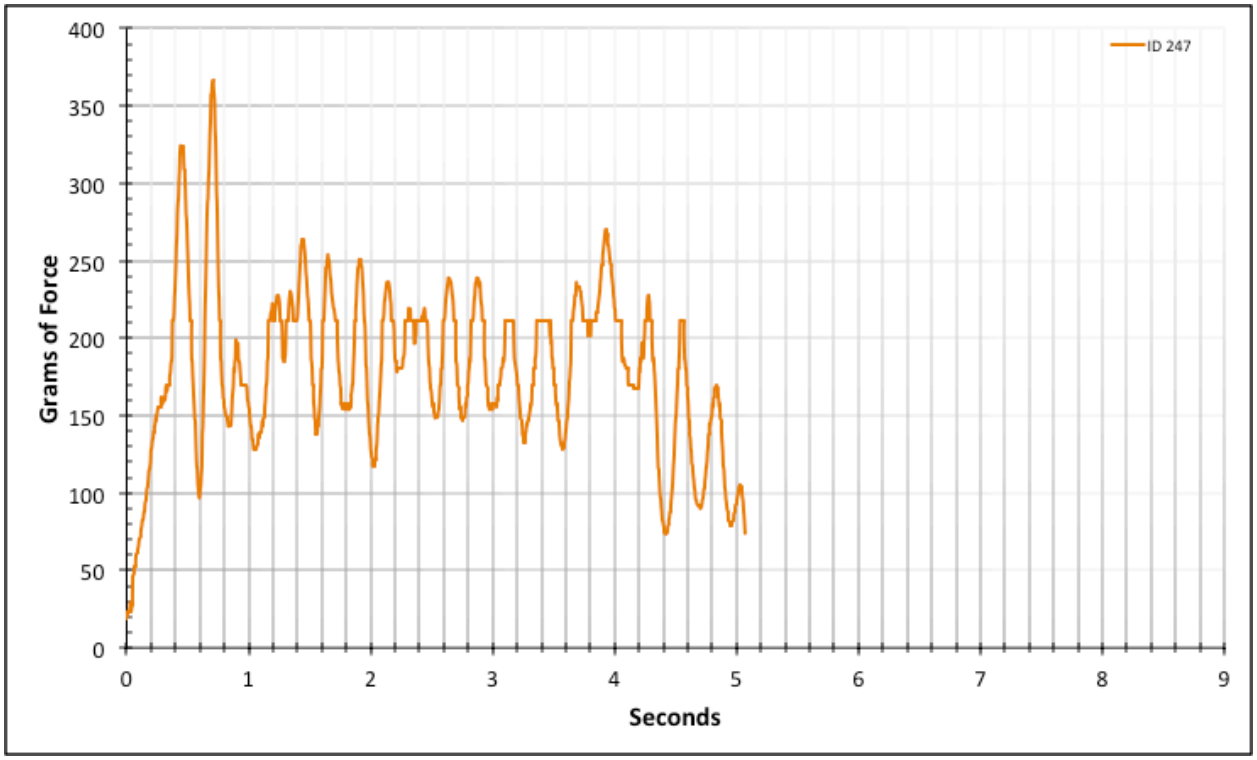

Figure A-6-333: Full Modeled Product - Lubricated - ID 247 - #10, Bolt 3

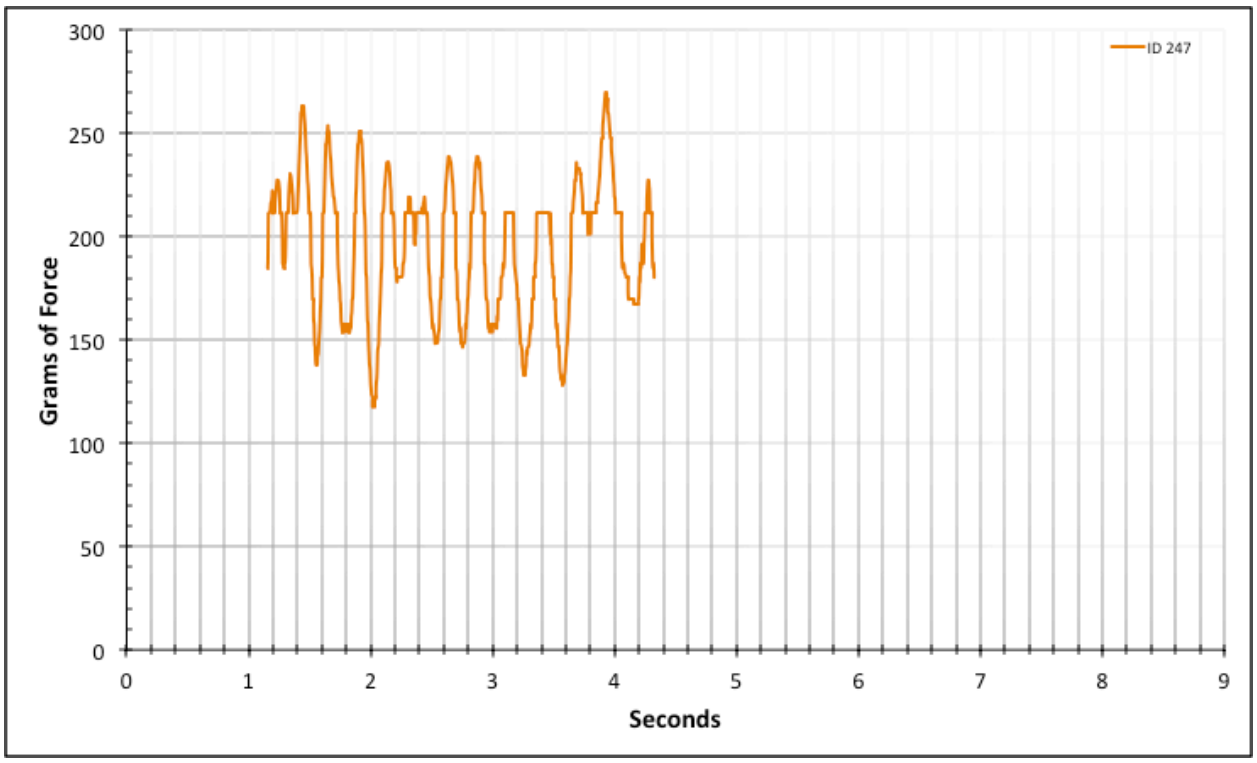

Figure A-6-334: Statistical Region Modeled Product - Lubricated - ID 247 - #10, Bolt 3

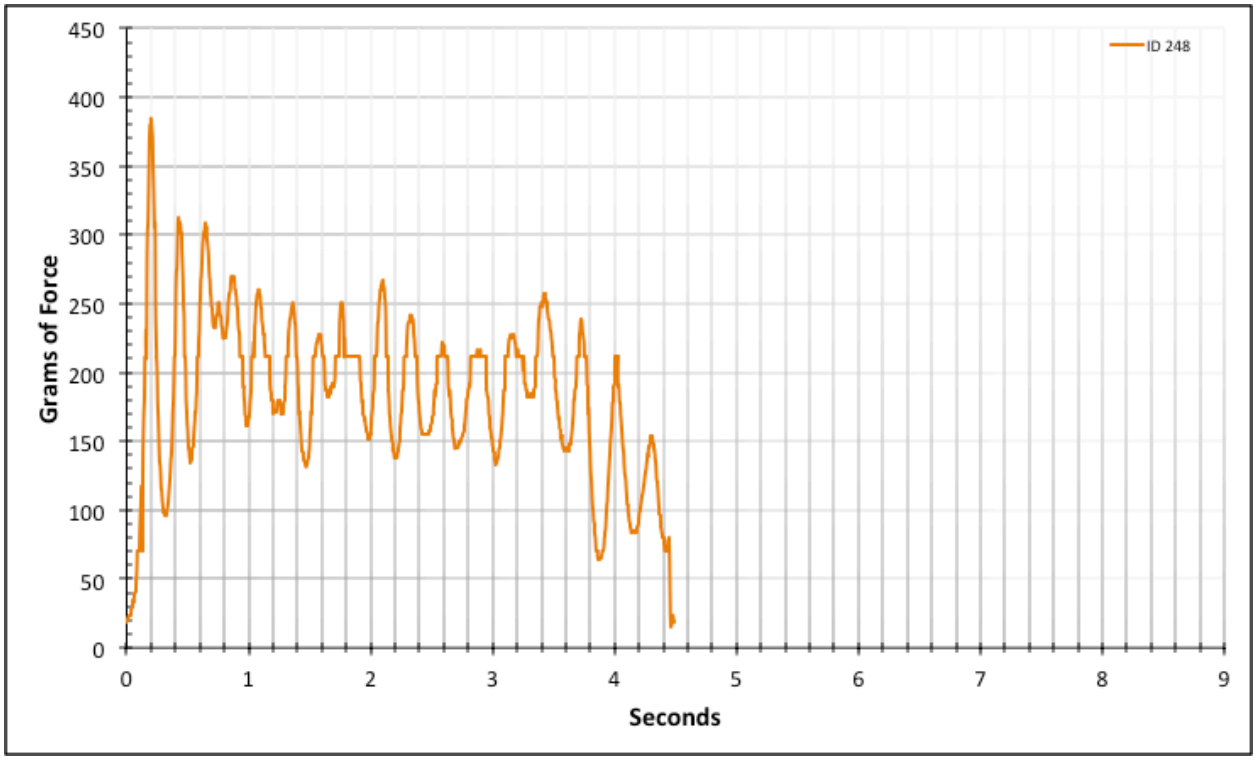

Figure A-6-335: Full Modeled Product - Lubricated - ID 248 - #10, Bolt 3

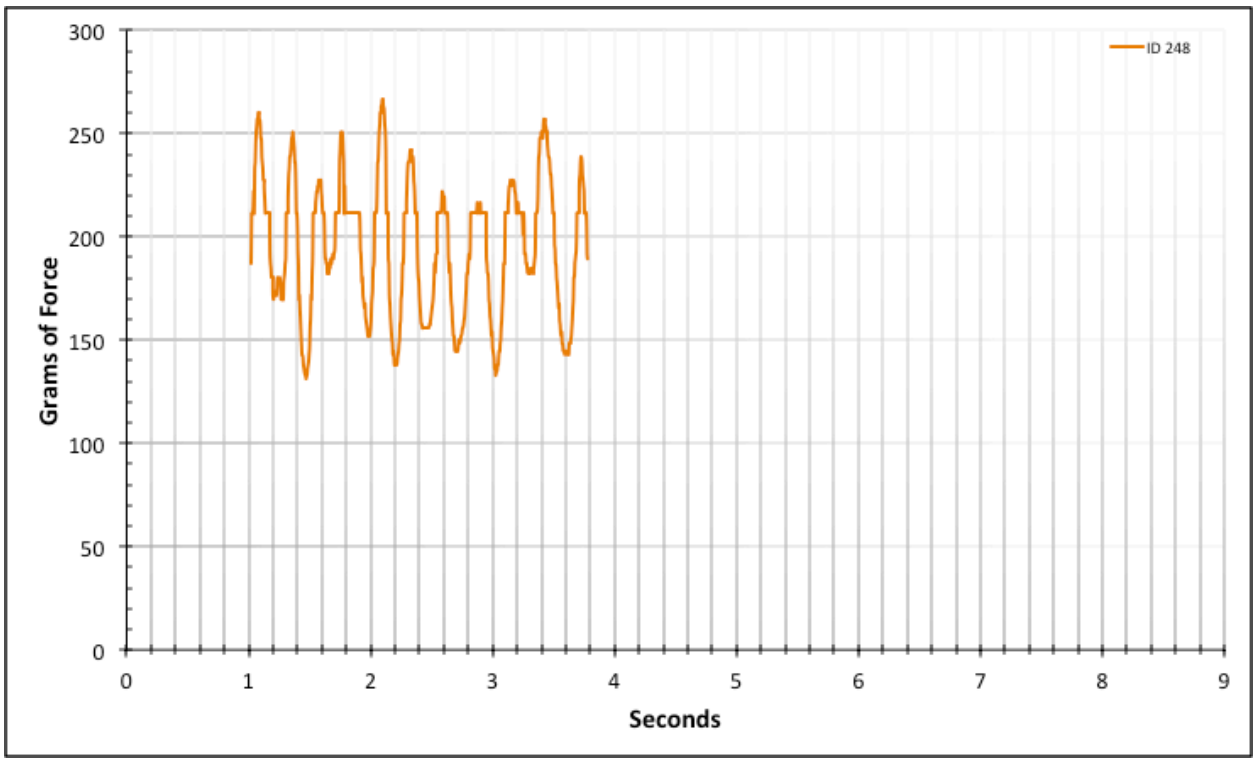

Figure A-6-336: Statistical Region Modeled Product - Lubricated - ID 248 - #10, Bolt 3

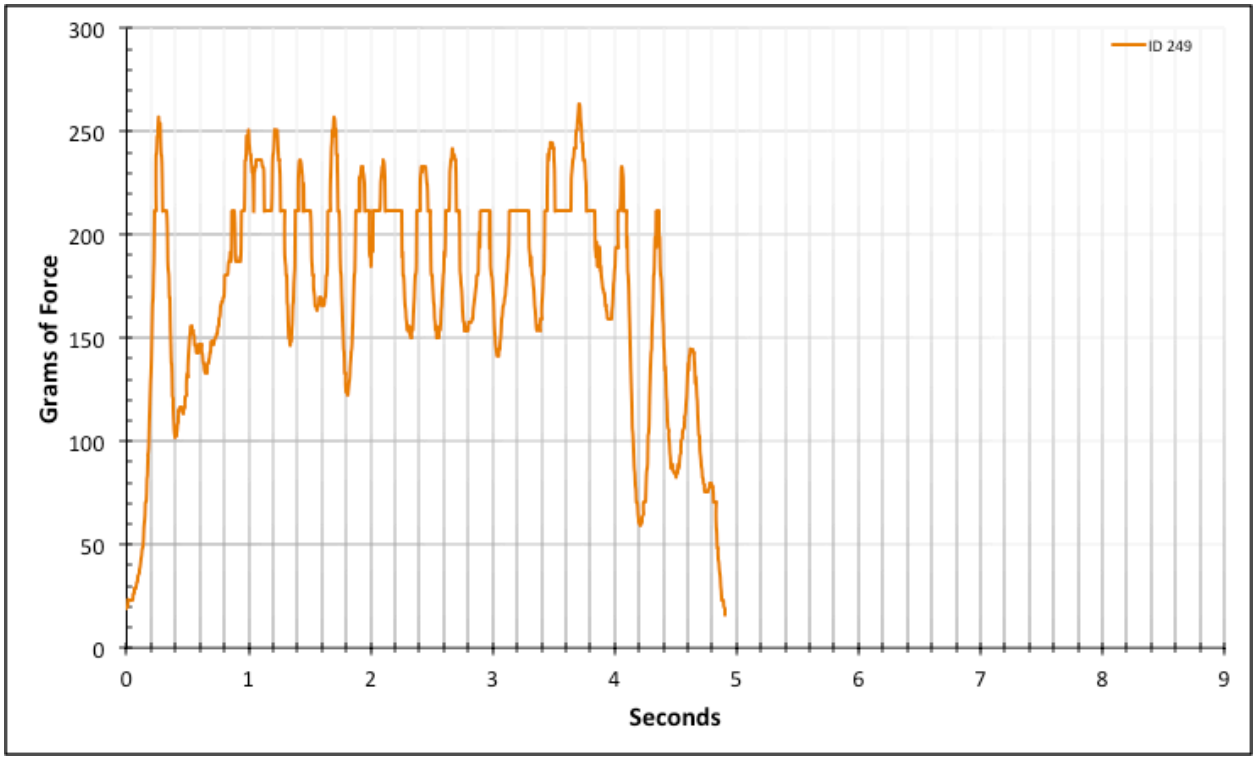

Figure A-6-337: Full Modeled Product - Lubricated - ID 249 - #10, Bolt 3

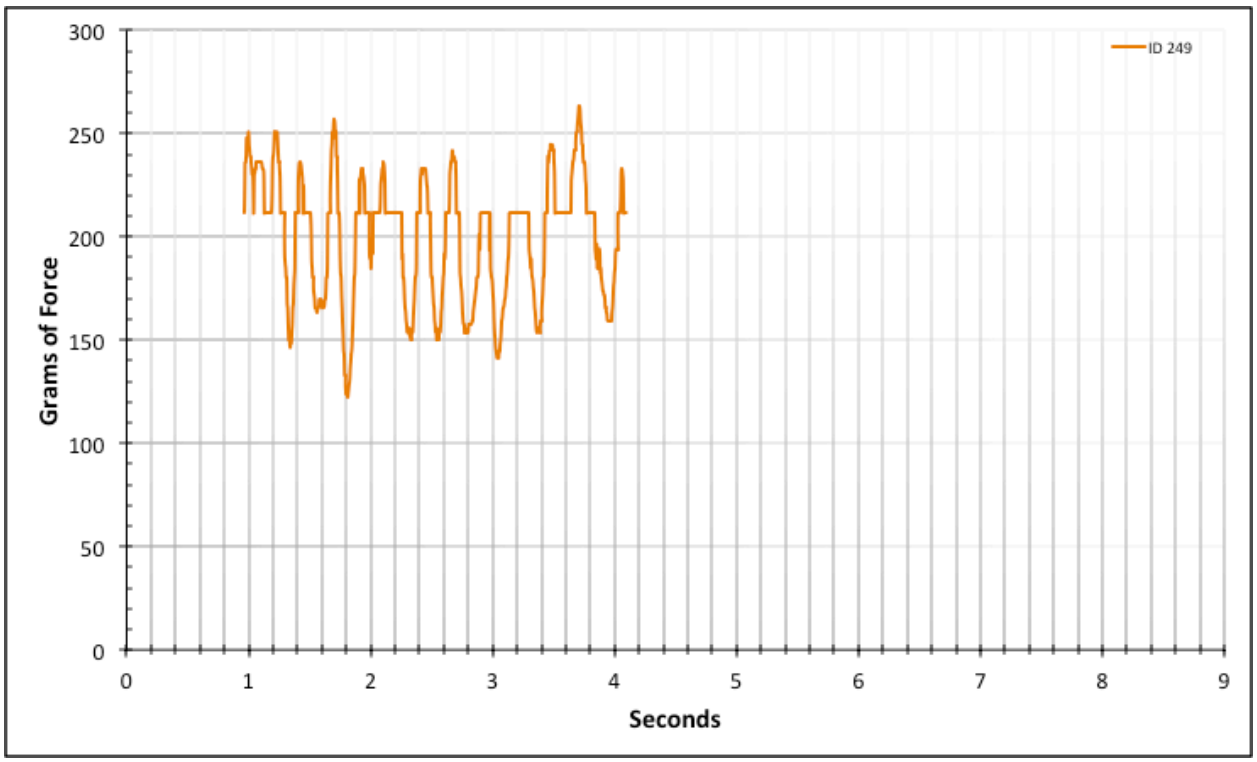

Figure A-6-338: Statistical Region Modeled Product - Lubricated - ID 249 - #10, Bolt 3

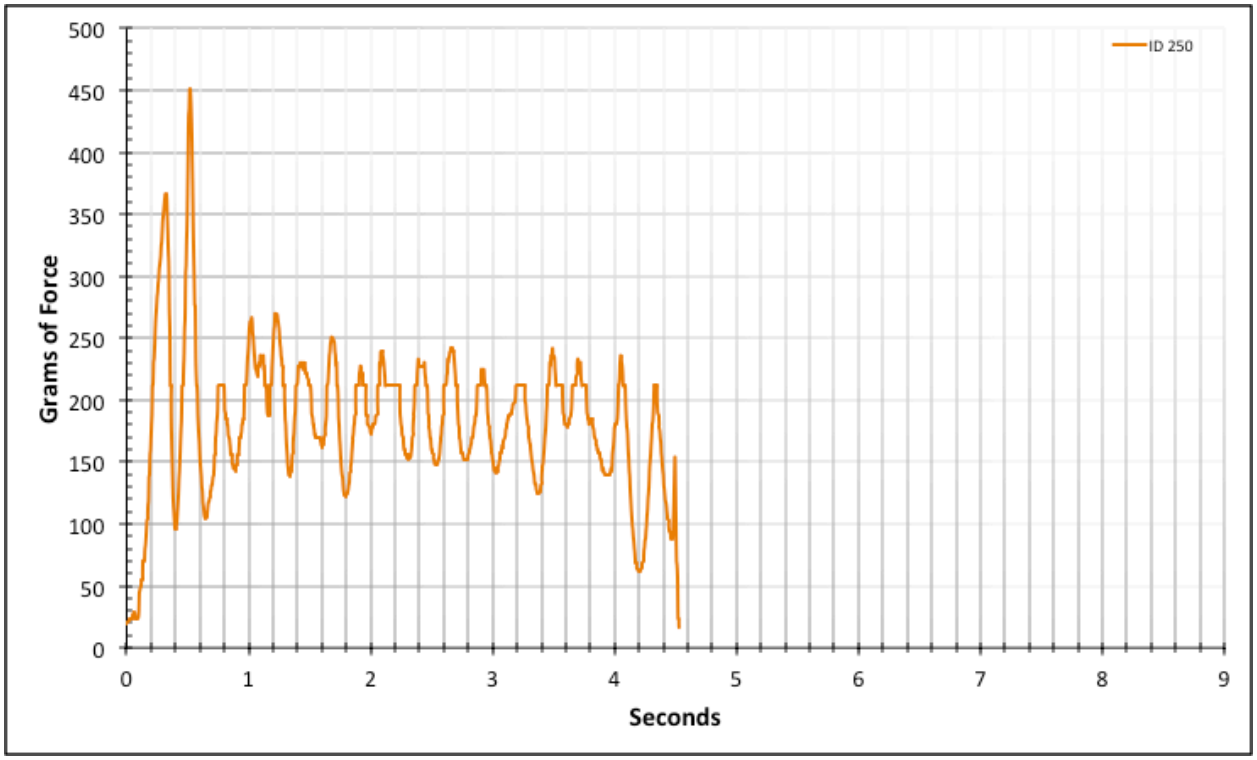

Figure A-6-339: Full Modeled Product - Lubricated - ID 250 - #10, Bolt 3

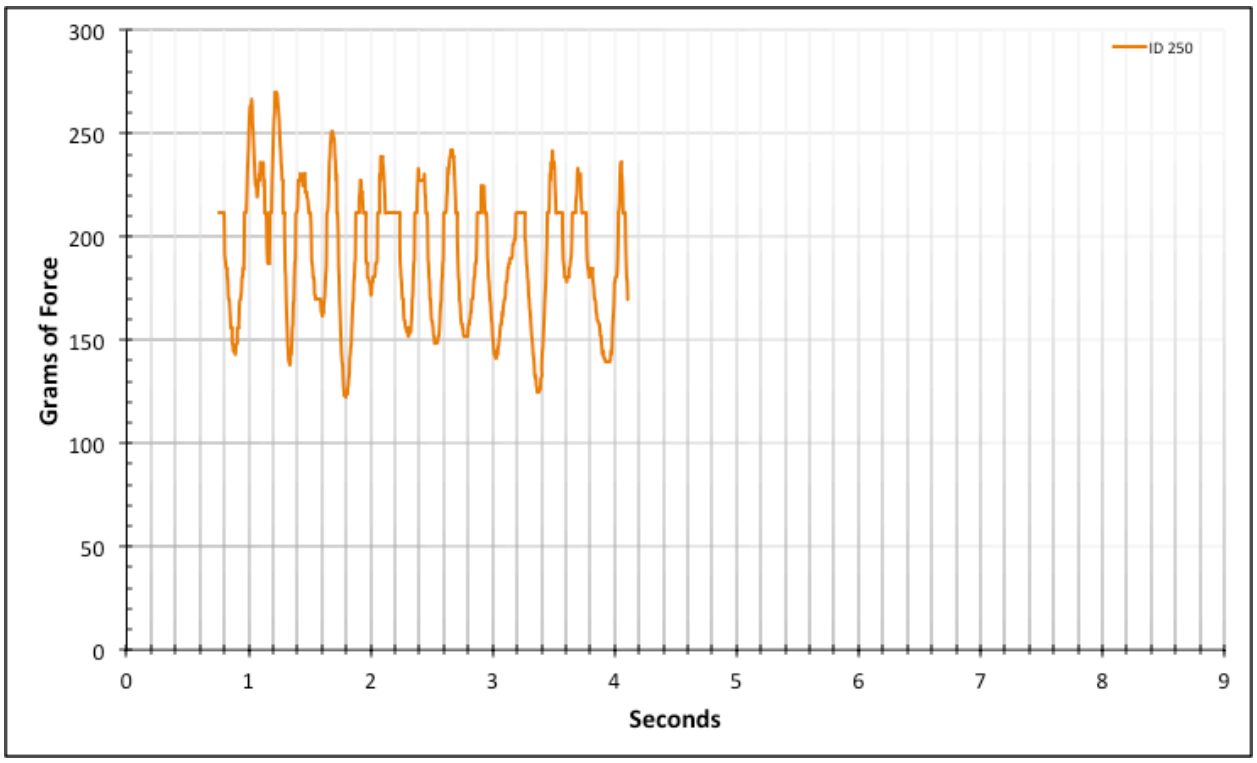

Figure A-6-340: Statistical Region Modeled Product - Lubricated - ID 250 - #10, Bolt 3

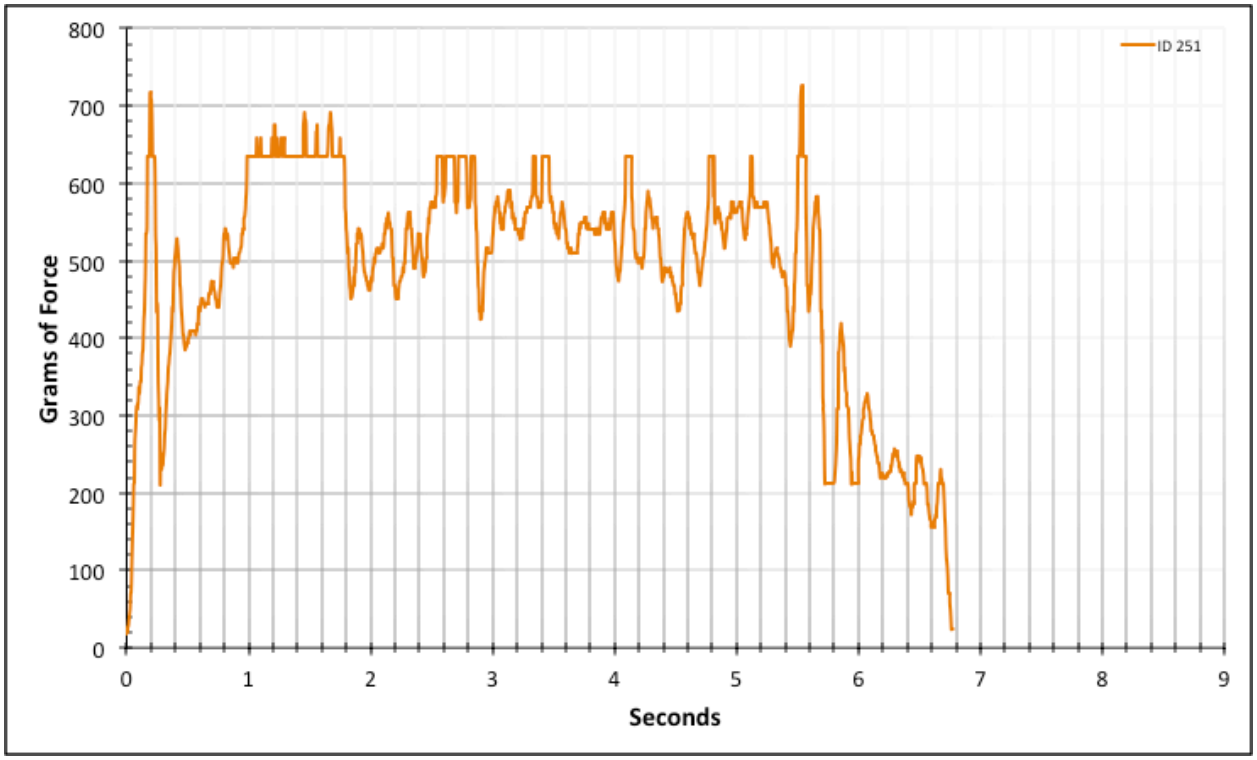

Figure A-6-341: Full Modeled Product - Lubricated - ID 251 - #8, Bolt 1

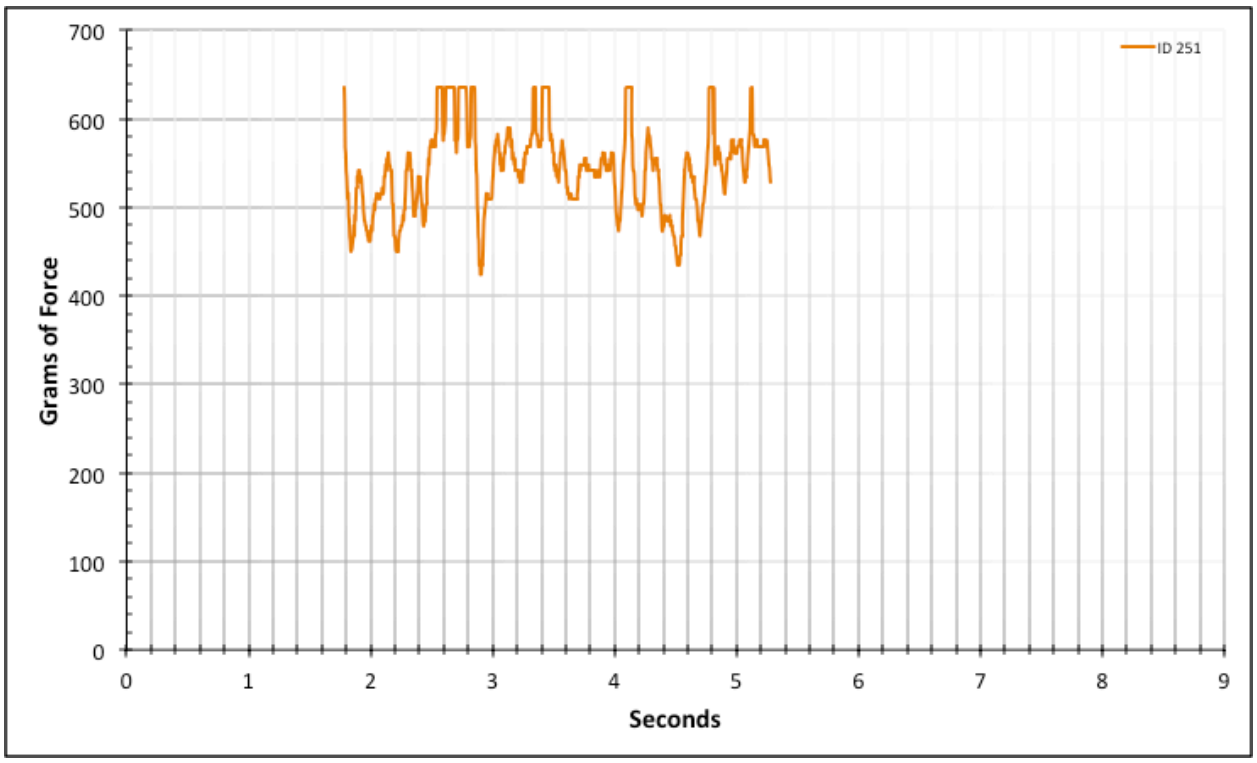

Figure A-6-342: Statistical Region Modeled Product - Lubricated - ID 251 - #8, Bolt 1

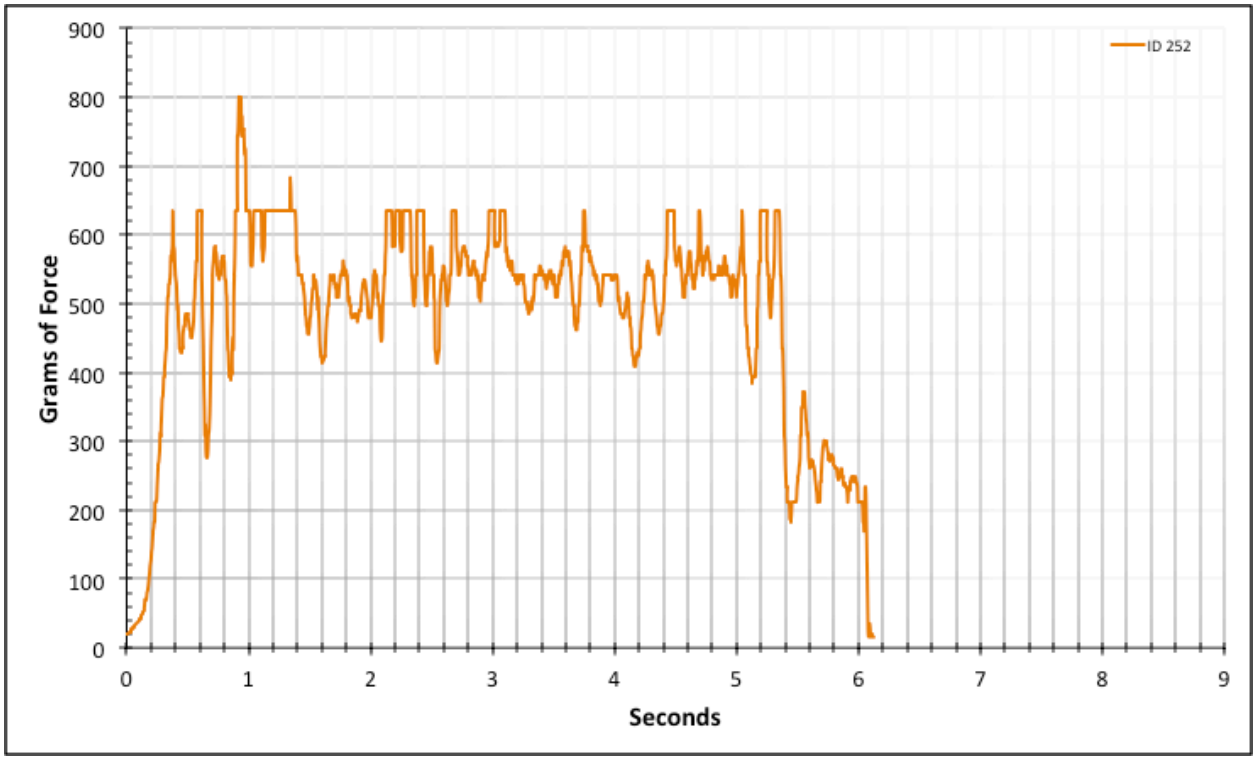

Figure A-6-343: Full Modeled Product - Lubricated - ID 252 - #8, Bolt 1

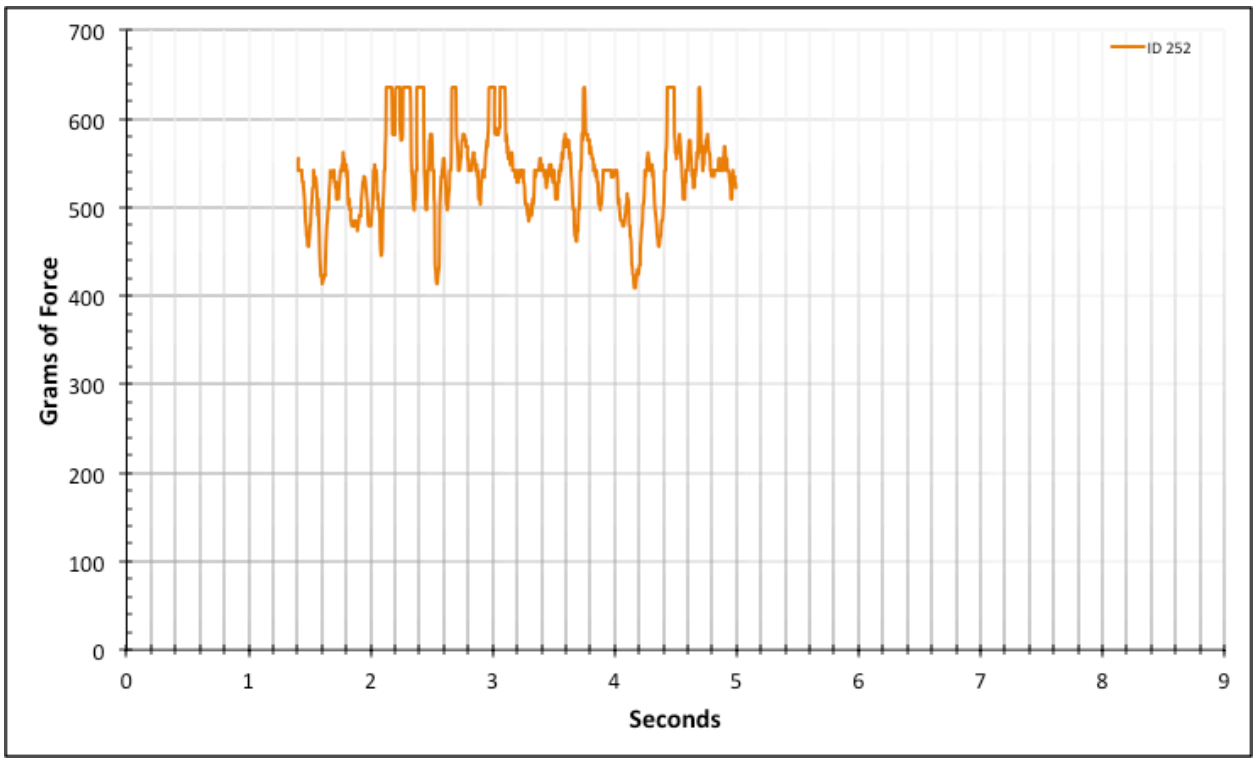

Figure A-6-344: Statistical Region Modeled Product - Lubricated - ID 252 - #8, Bolt 1

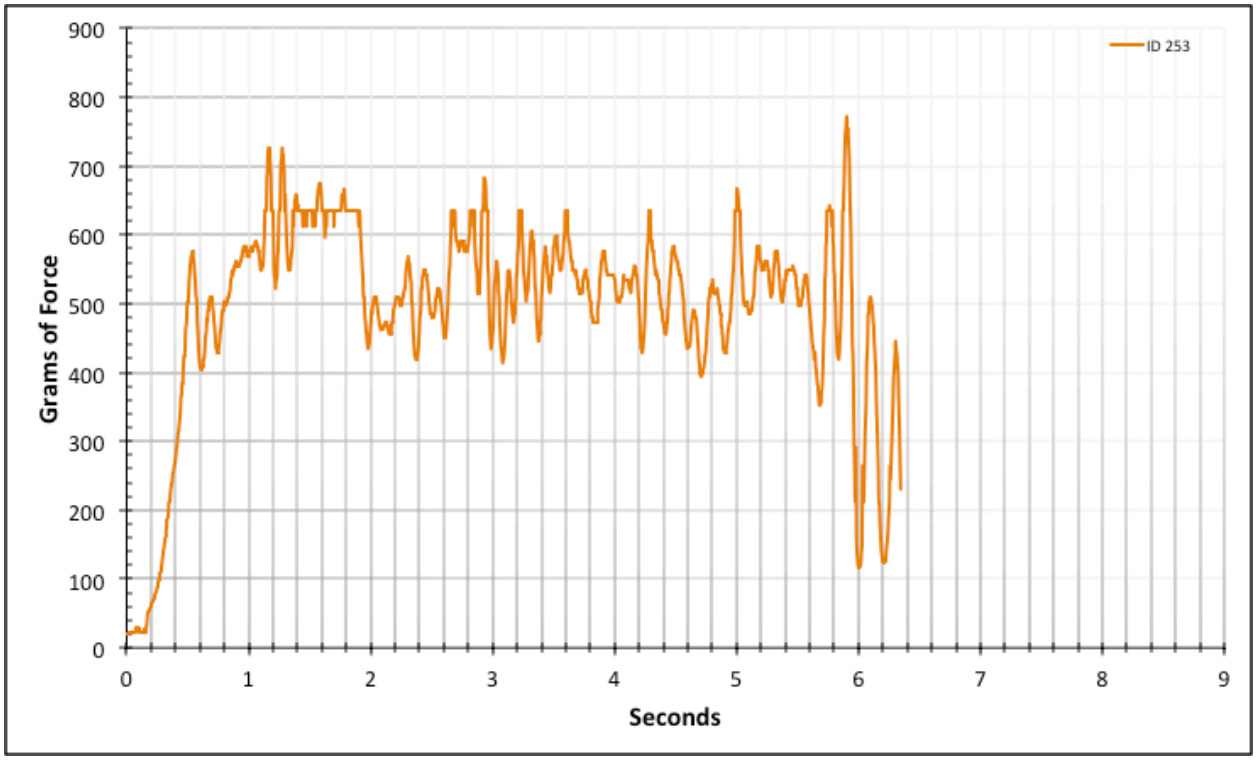

Figure A-6-345: Full Modeled Product - Lubricated - ID 253 - #8, Bolt 1

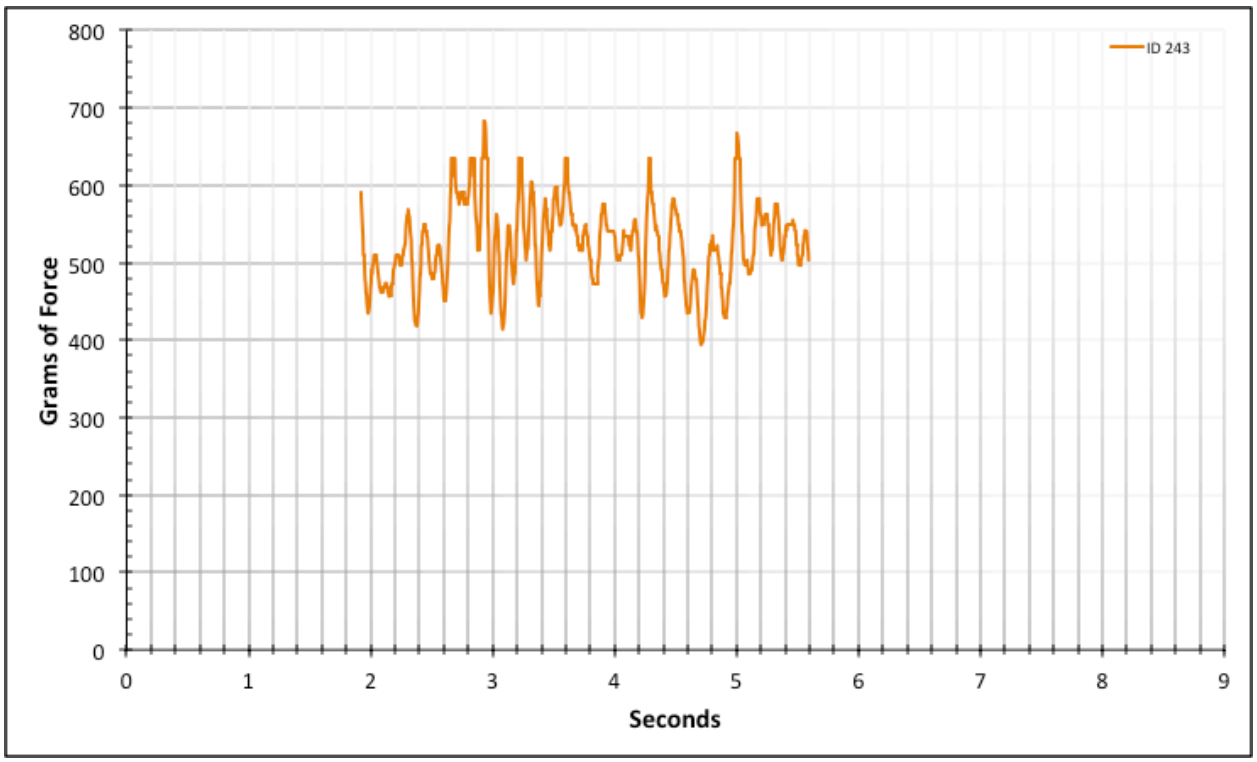

Figure A-6-346: Statistical Region Modeled Product - Lubricated - ID 253 - #8, Bolt 1

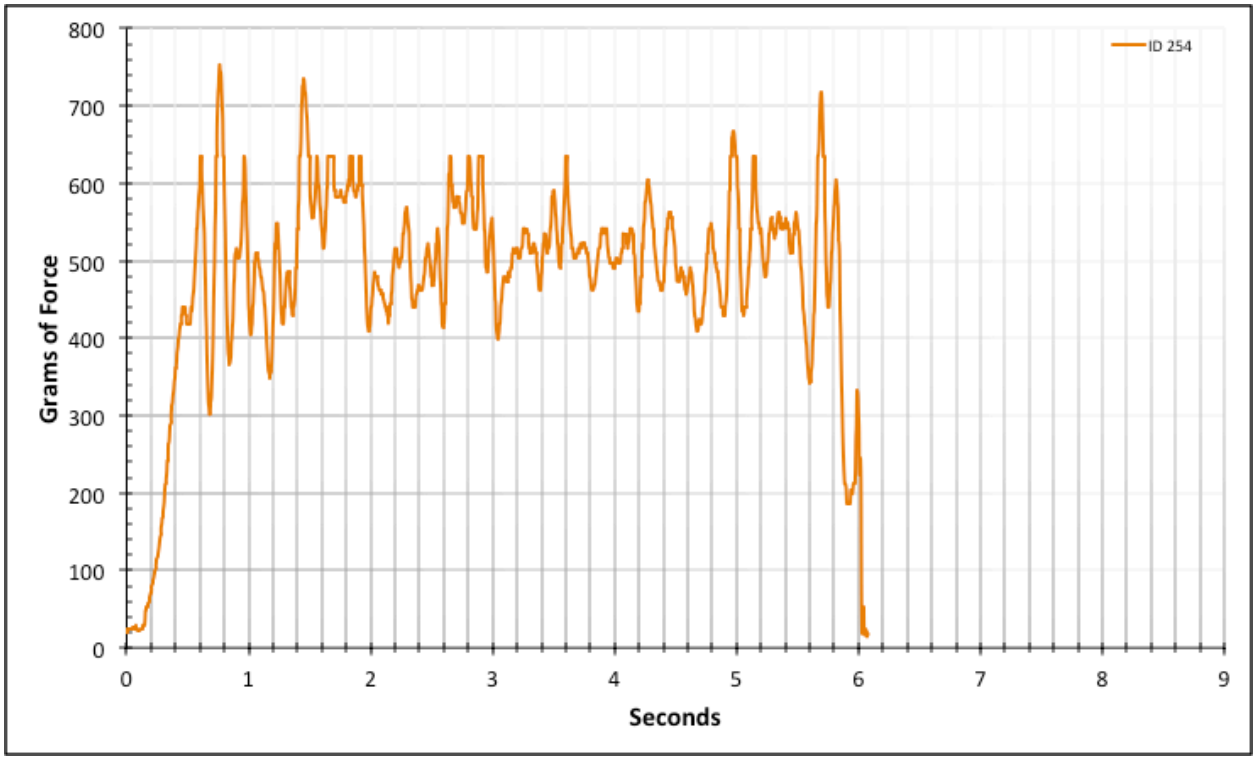

Figure A-6-347: Full Modeled Product - Lubricated - ID 254 - #8, Bolt 1

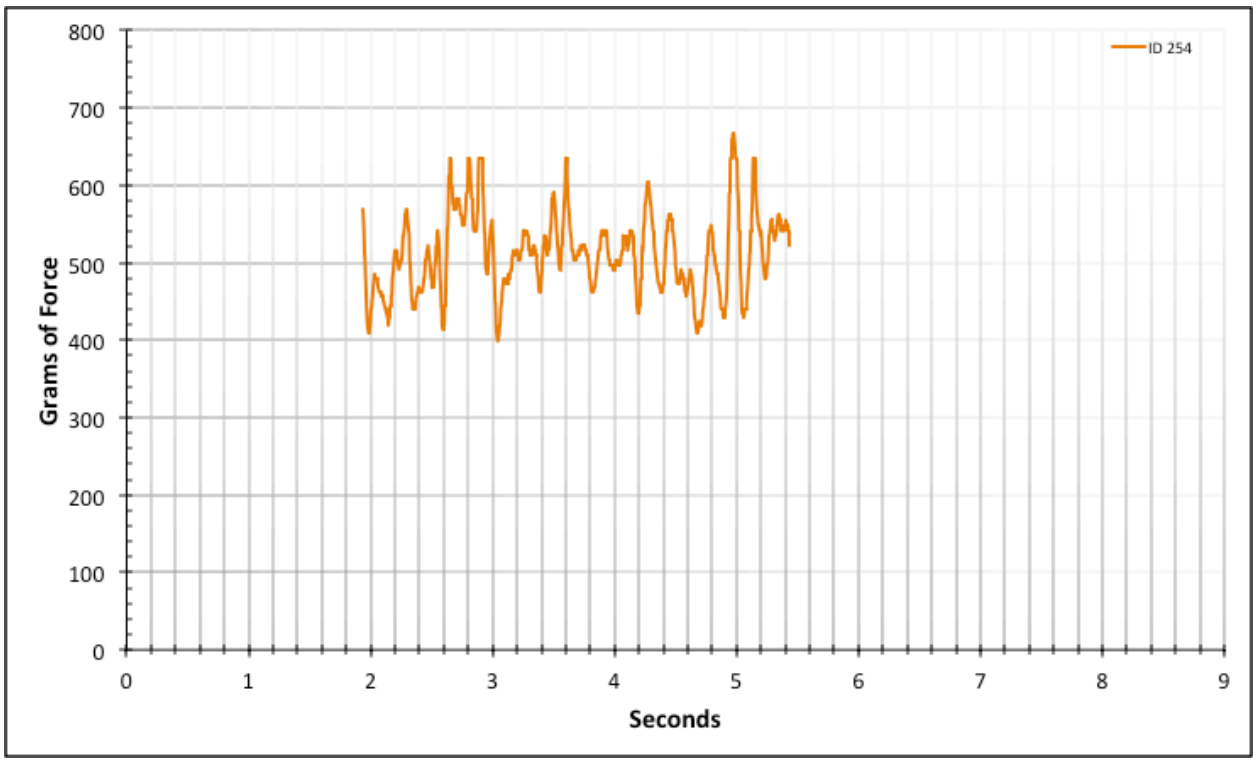

Figure A-6-348: Statistical Region Modeled Product - Lubricated - ID 254 - #8, Bolt 1

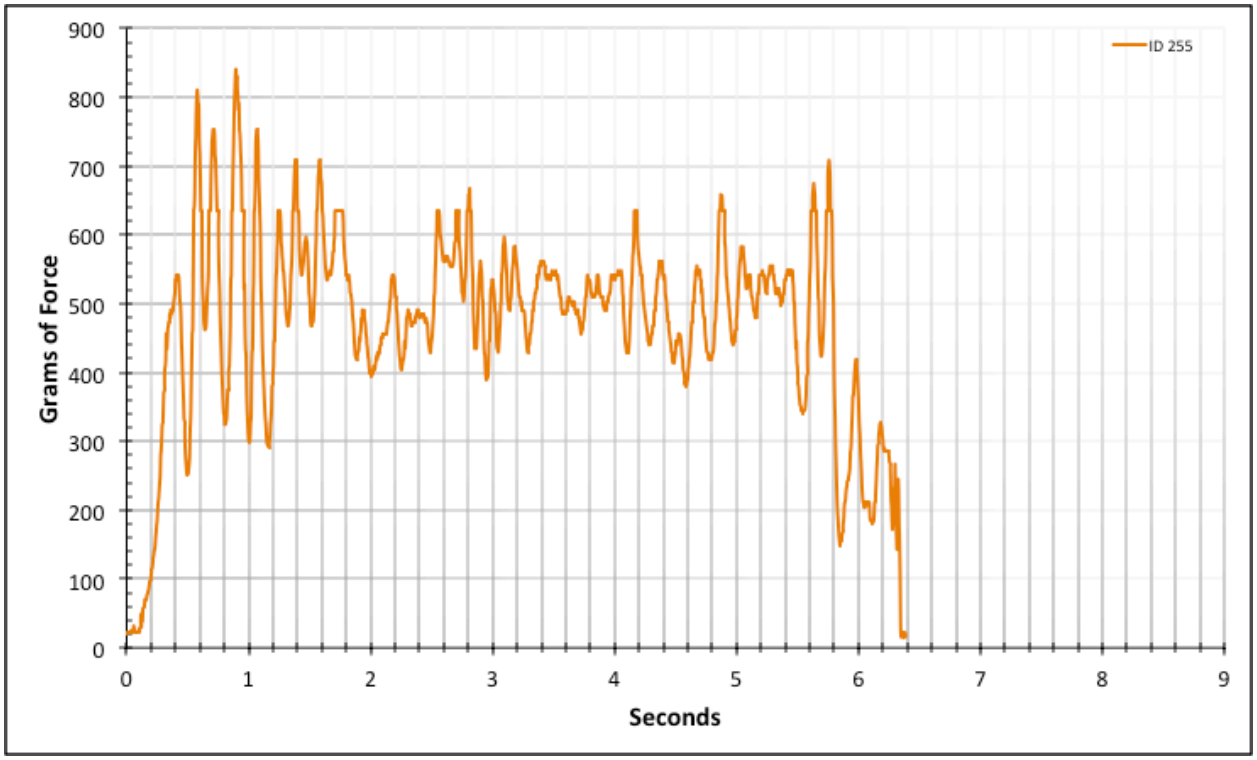

Figure A-6-349: Full Modeled Product - Lubricated - ID 255 - #8, Bolt 1

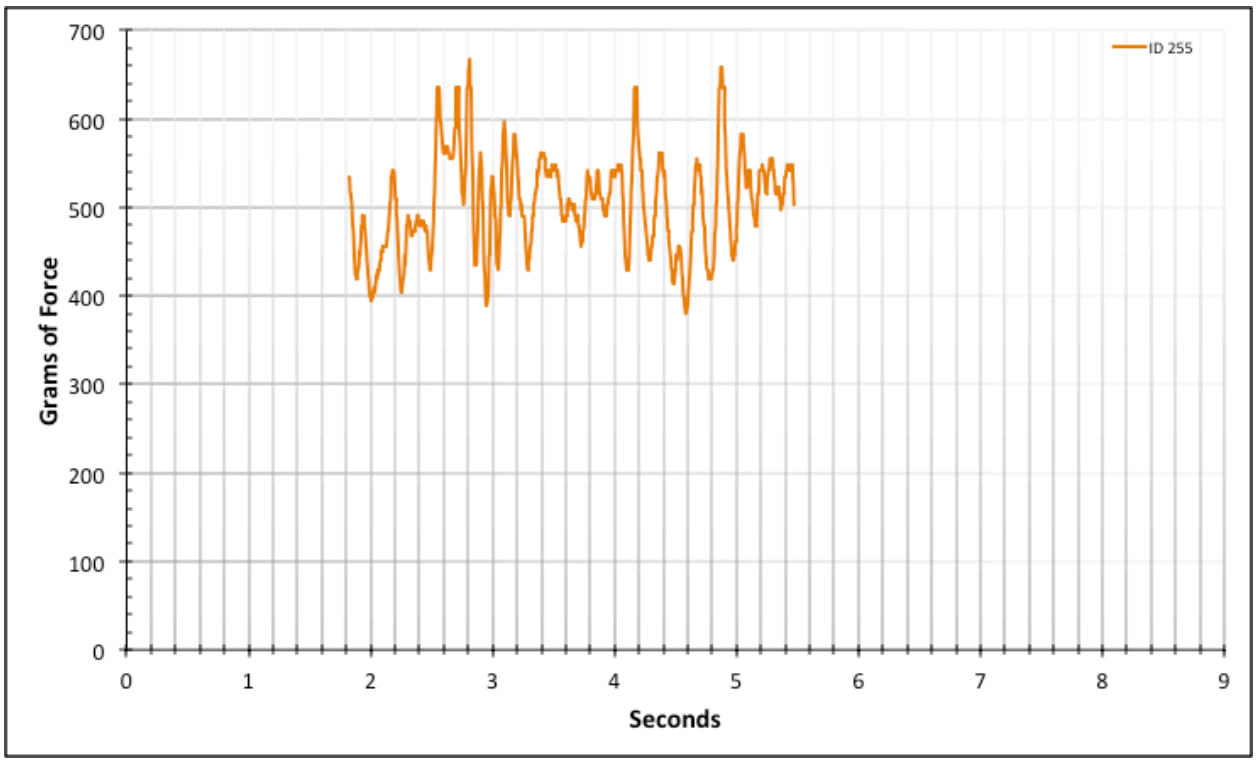

Figure A-6-350: Statistical Region Modeled Product - Lubricated - ID 255 - #8, Bolt 1

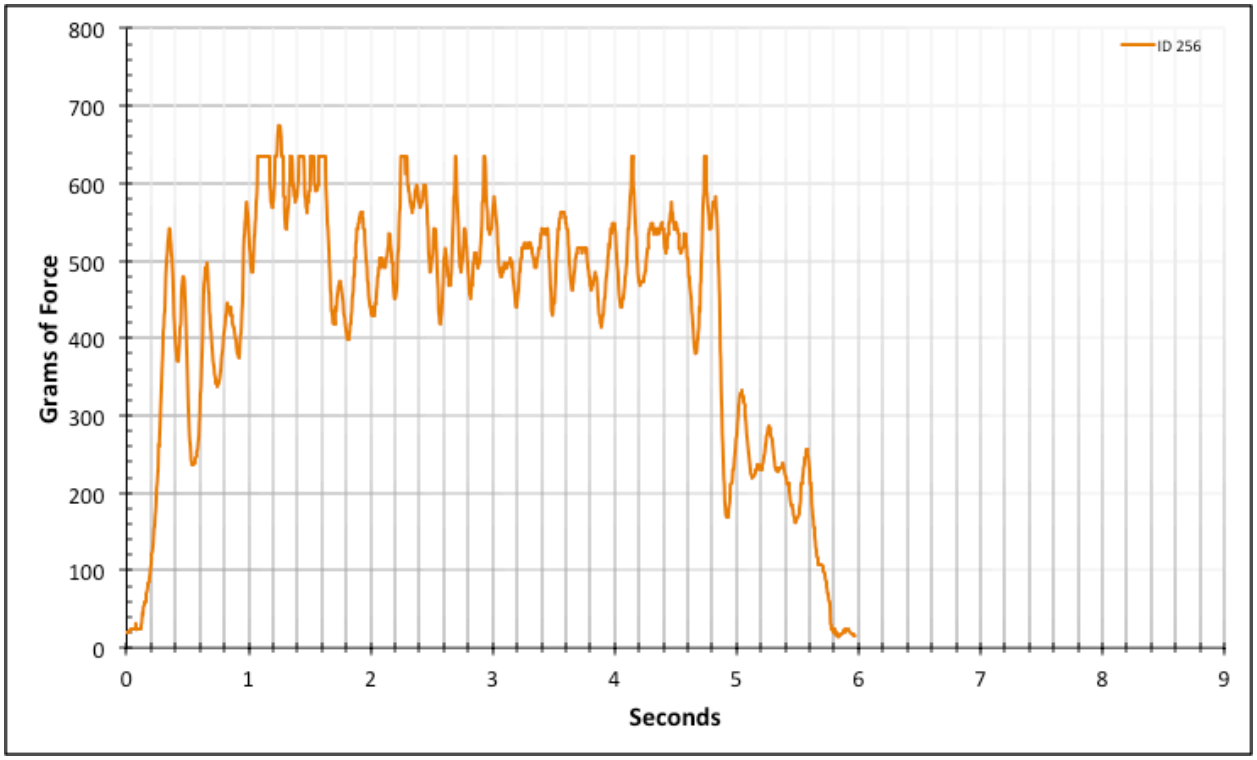

Figure A-6-351: Full Modeled Product - Lubricated - ID 256 - #8, Bolt 2

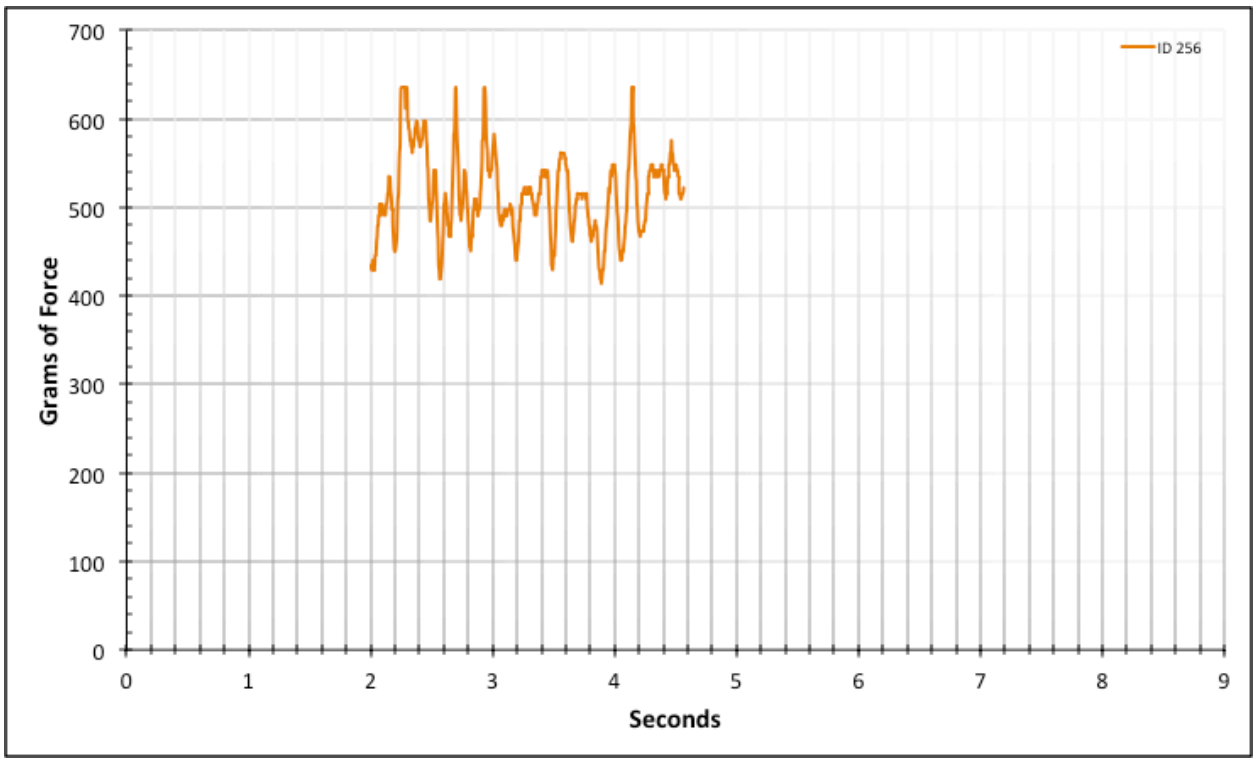

Figure A-6-352: Statistical Region Modeled Product - Lubricated - ID 256 - #8, Bolt 2

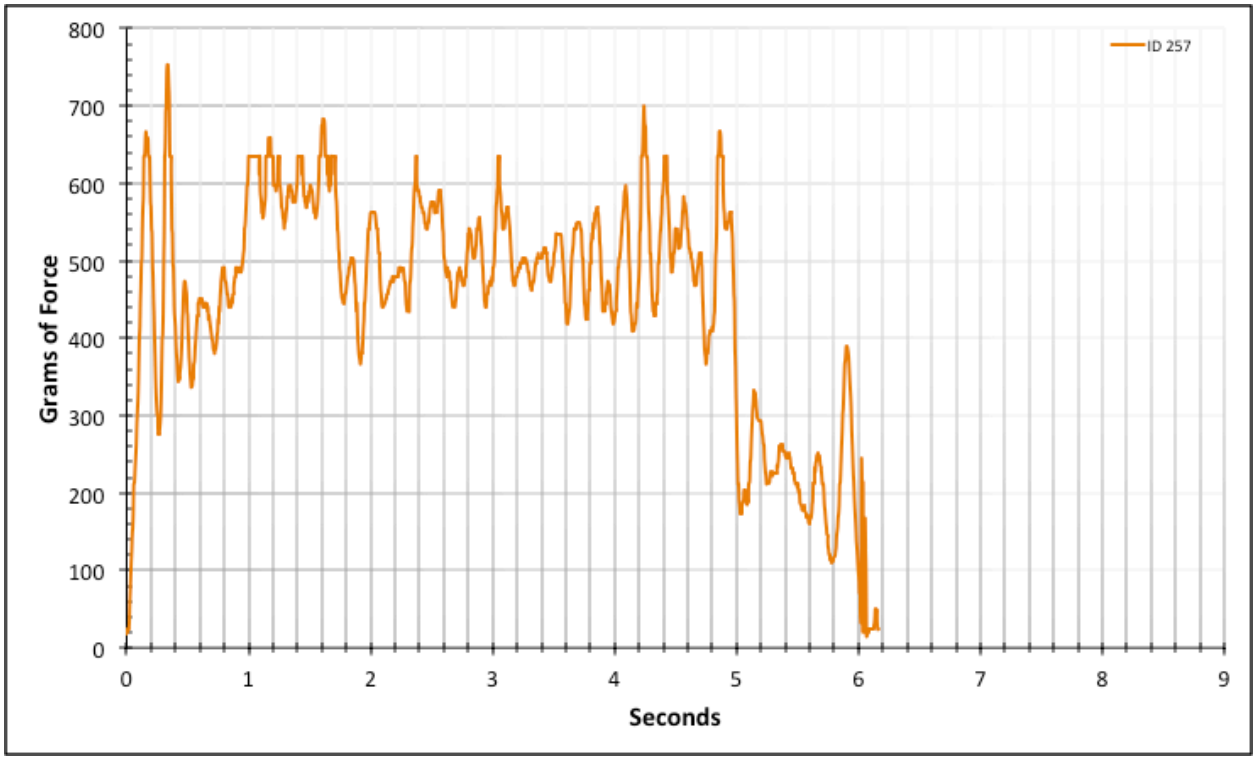

Figure A-6-353: Full Modeled Product - Lubricated - ID 257 - #8, Bolt 2

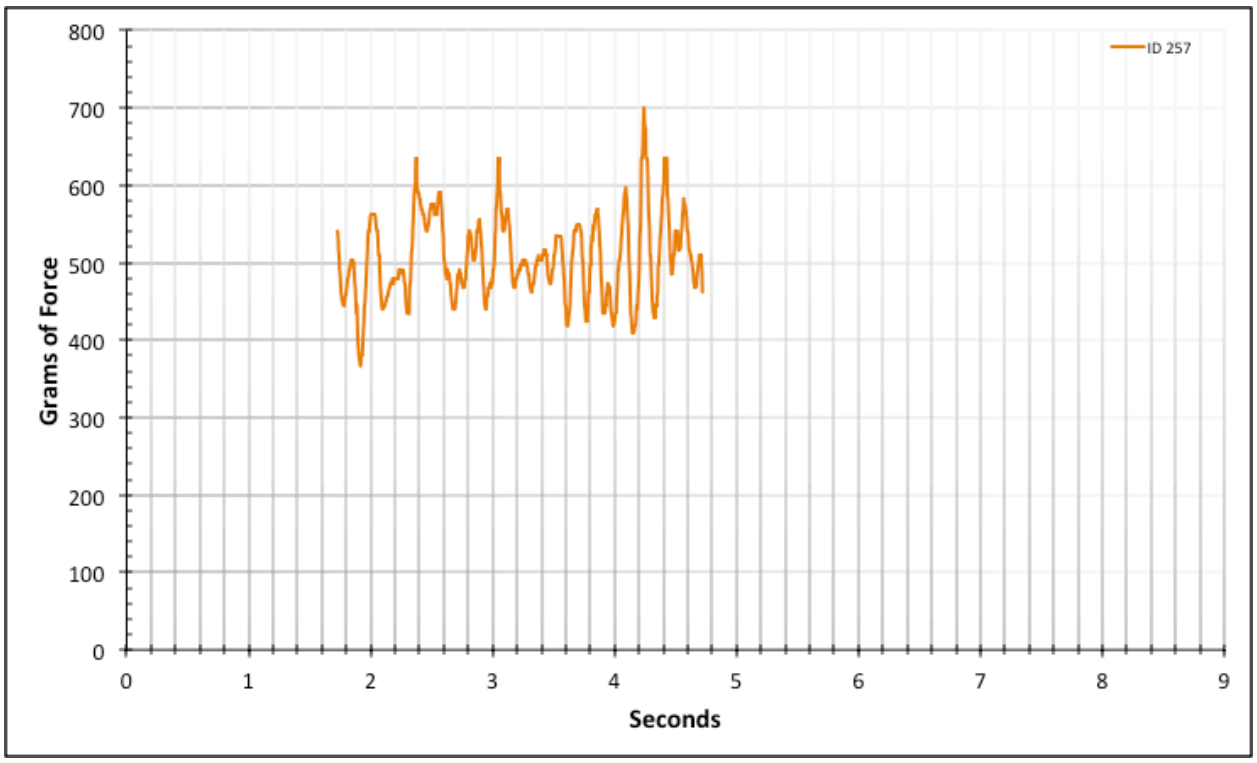

Figure A-6-354: Statistical Region Modeled Product - Lubricated - ID 257 - #8, Bolt 2

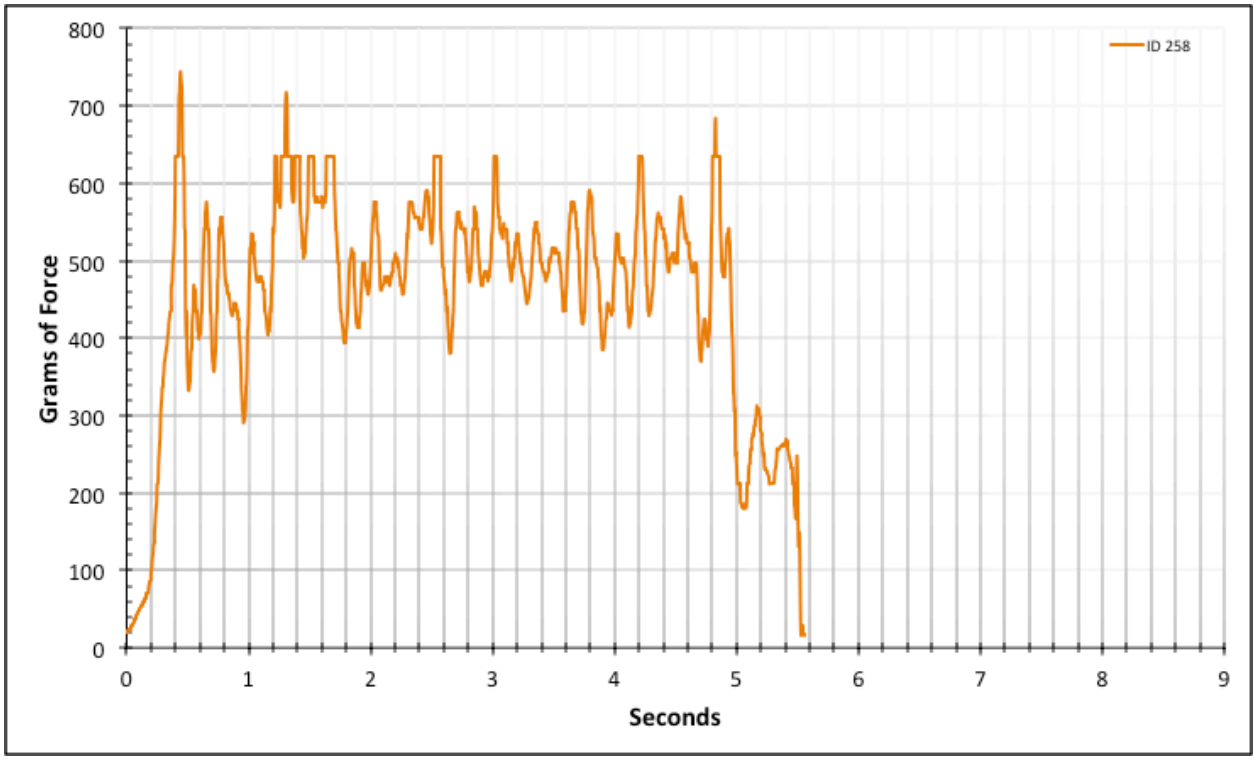

Figure A-6-355: Full Modeled Product - Lubricated - ID 258 - #8, Bolt 2

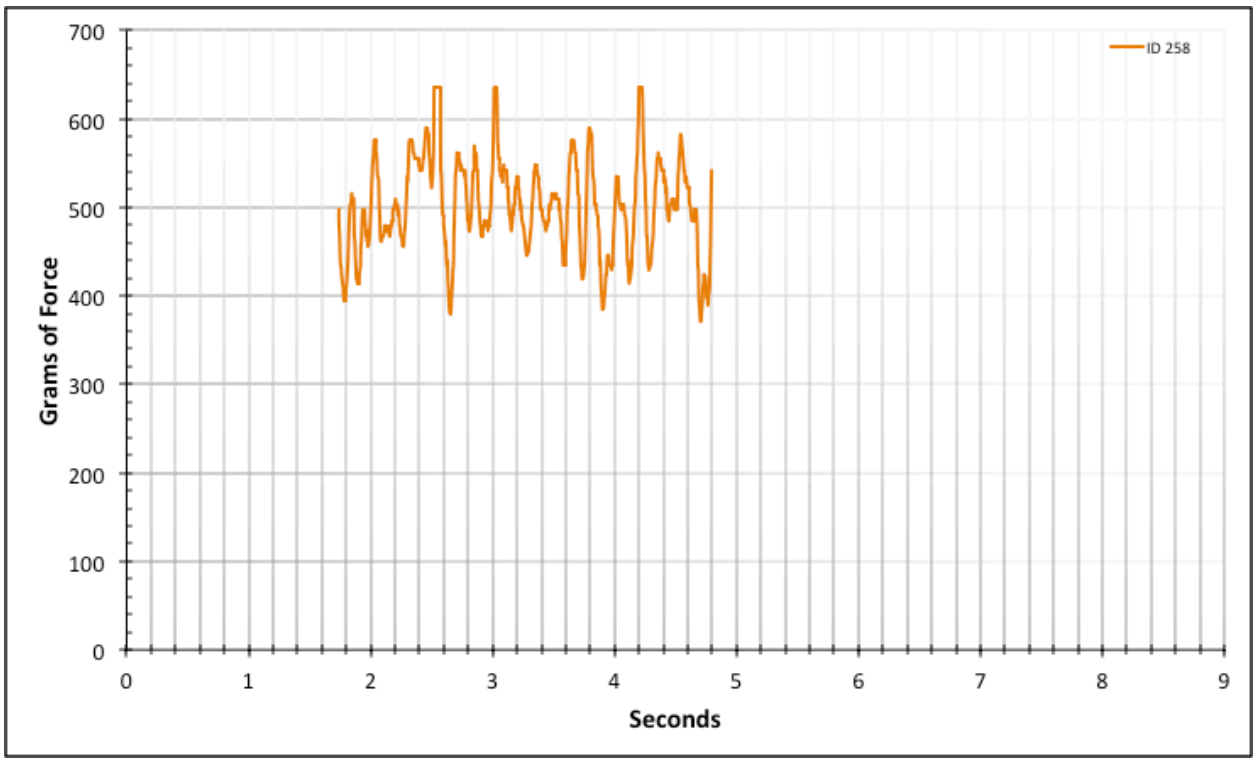

Figure A-6-356: Statistical Region Modeled Product - Lubricated - ID 258 - #8, Bolt 2

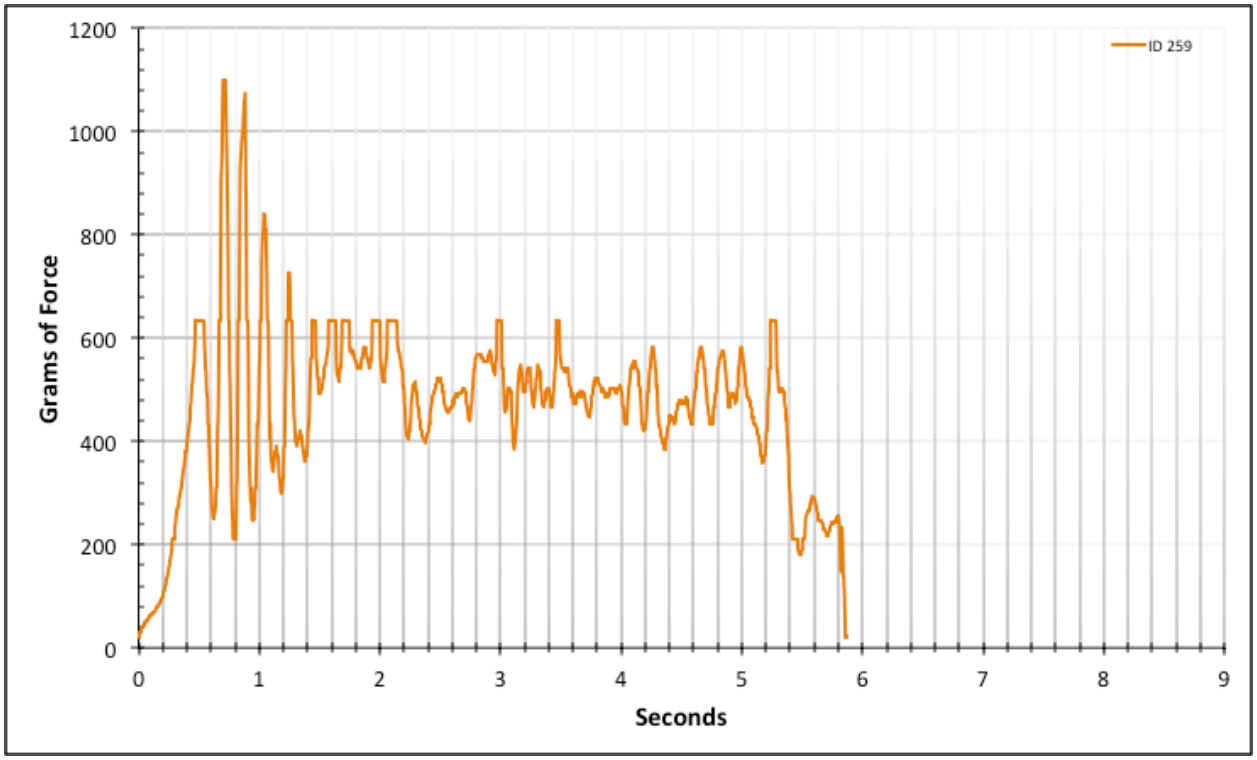

Figure A-6-357: Full Modeled Product - Lubricated - ID 259 - #8, Bolt 2

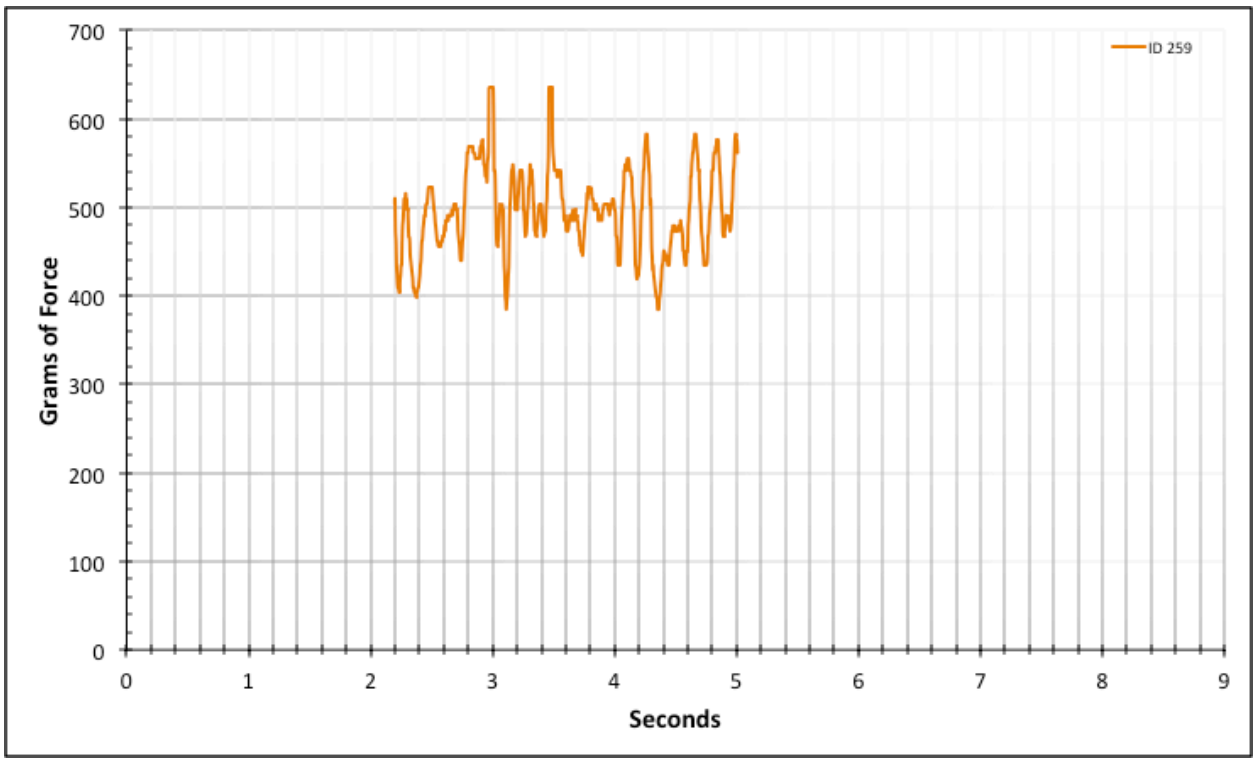

Figure A-6-358: Statistical Region Modeled Product - Lubricated - ID 259 - #8, Bolt 2

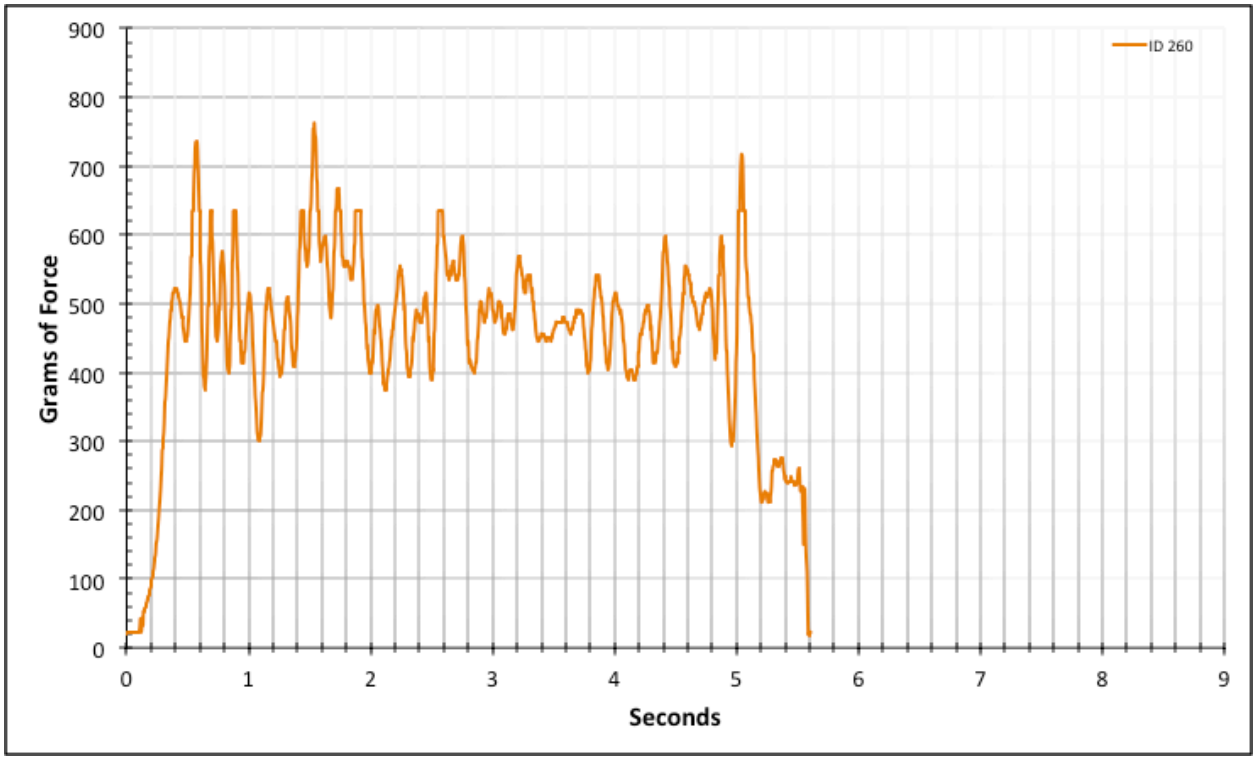

Figure A-6-359: Full Modeled Product - Lubricated - ID 260 - #8, Bolt 2

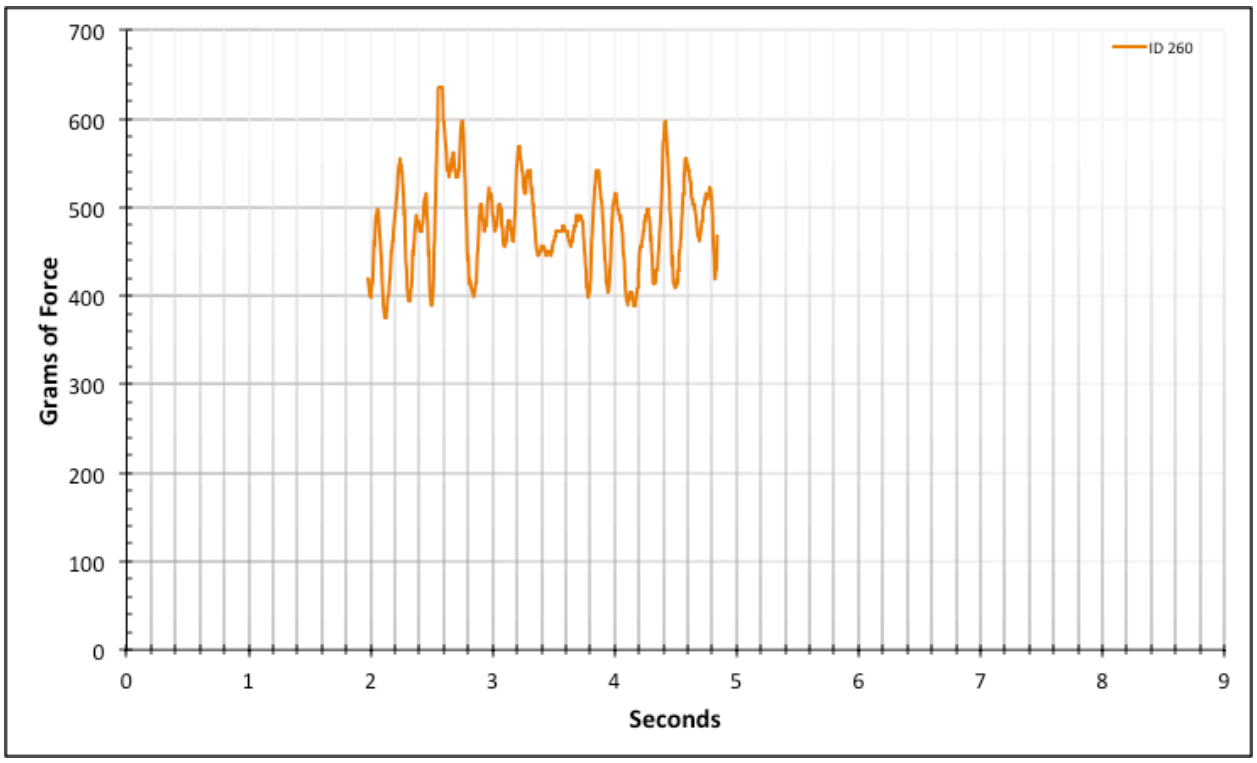

Figure A-6-360: Statistical Region Modeled Product - Lubricated - ID 260 - #8, Bolt 2

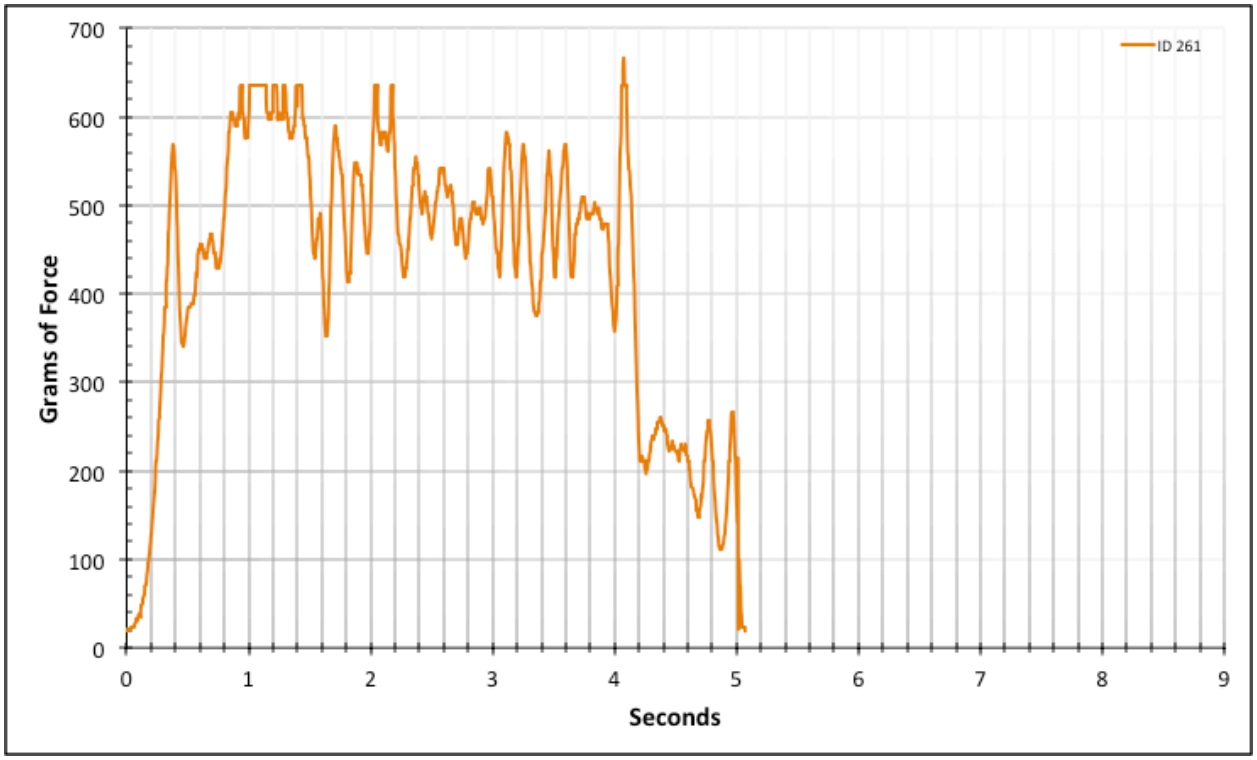

Figure A-6-361: Full Modeled Product - Lubricated - ID 261 - #8, Bolt 3

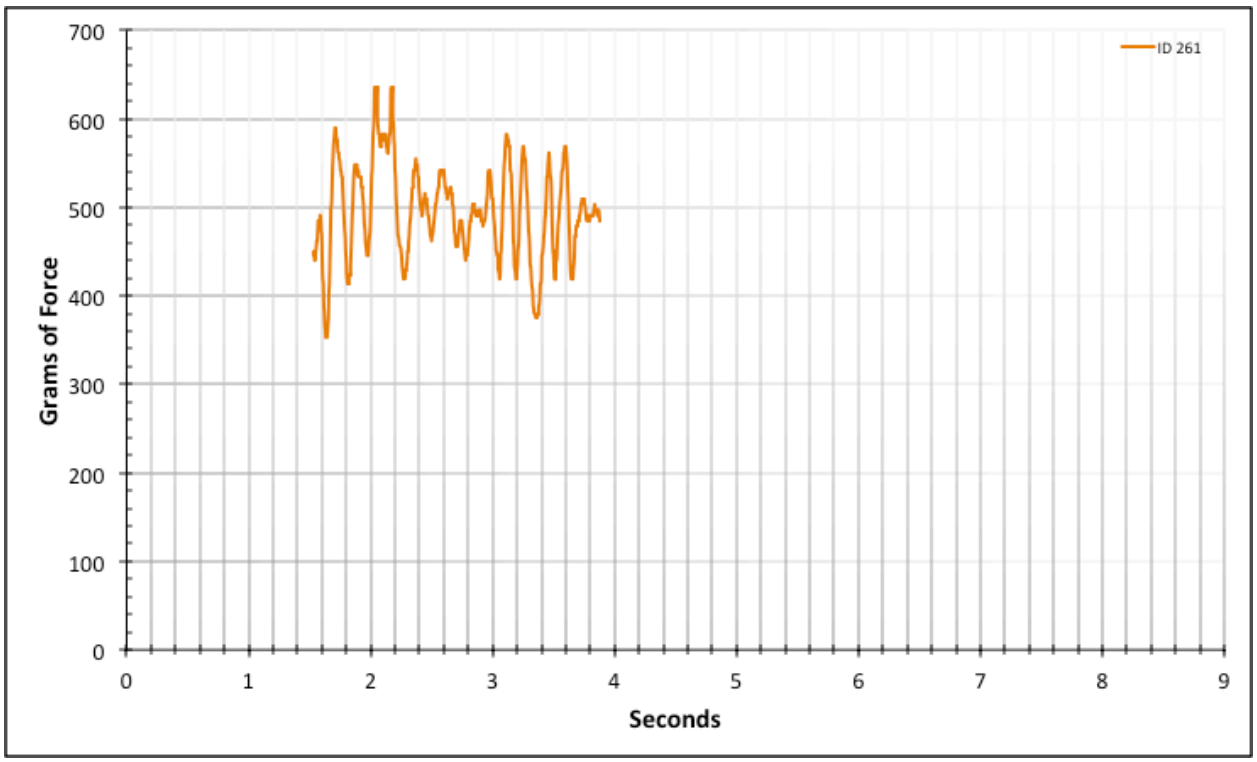

Figure A-6-362: Statistical Region Modeled Product - Lubricated - ID 261 - #8, Bolt 3

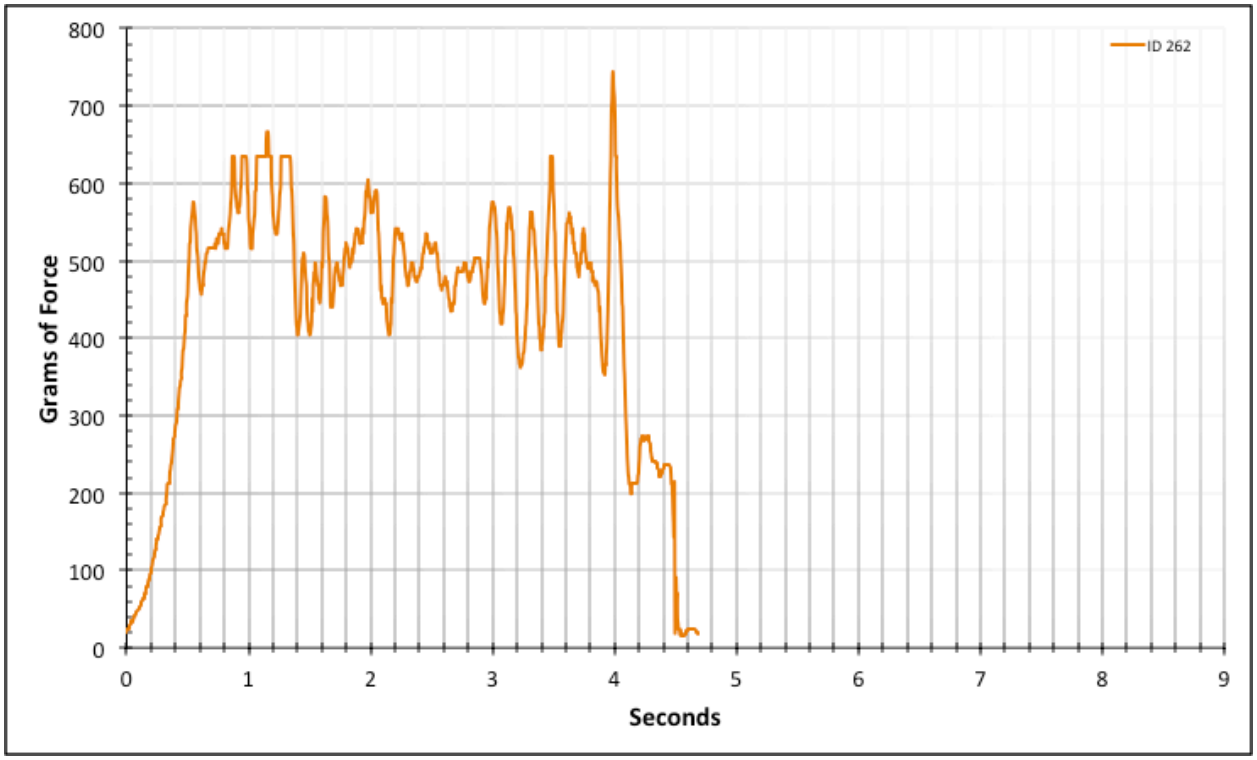

Figure A-6-363: Full Modeled Product - Lubricated - ID 262 - #8, Bolt 3

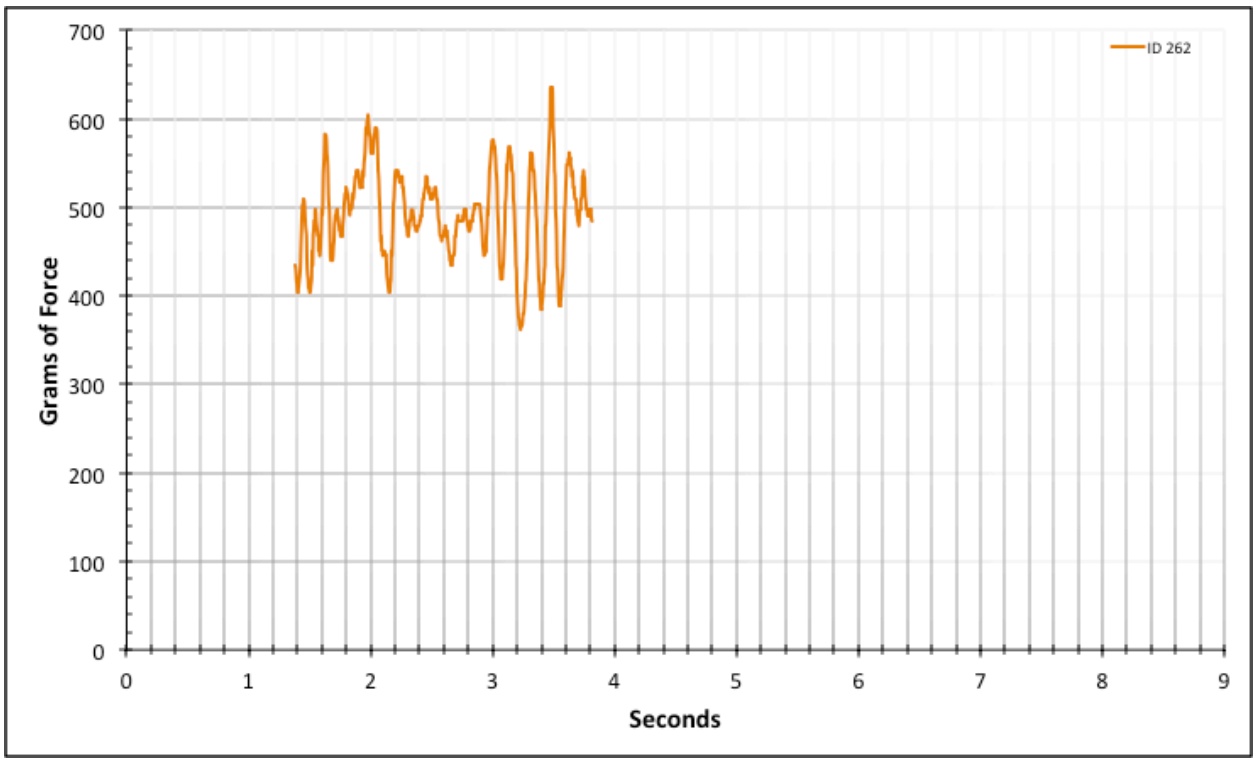

Figure A-6-364: Statistical Region Modeled Product - Lubricated - ID 262 - #8, Bolt 3

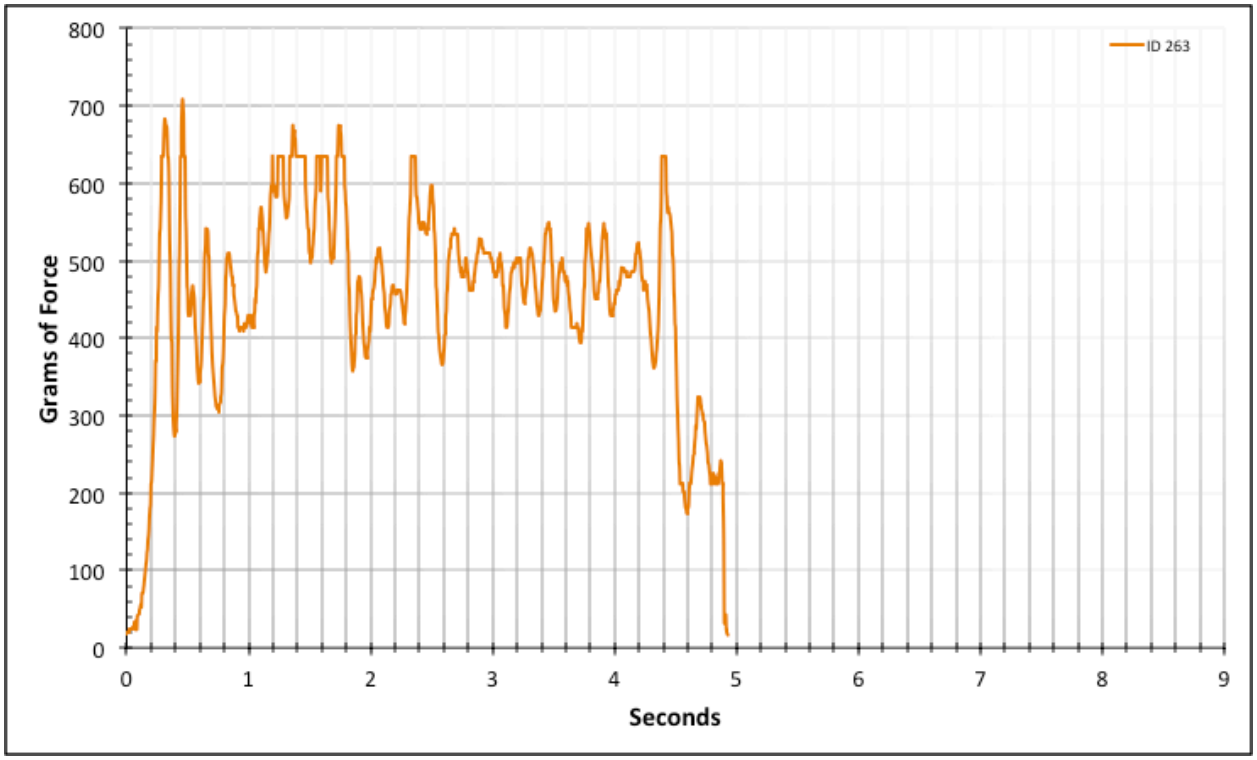

Figure A-6-365: Full Modeled Product - Lubricated - ID 263 - #8, Bolt 3

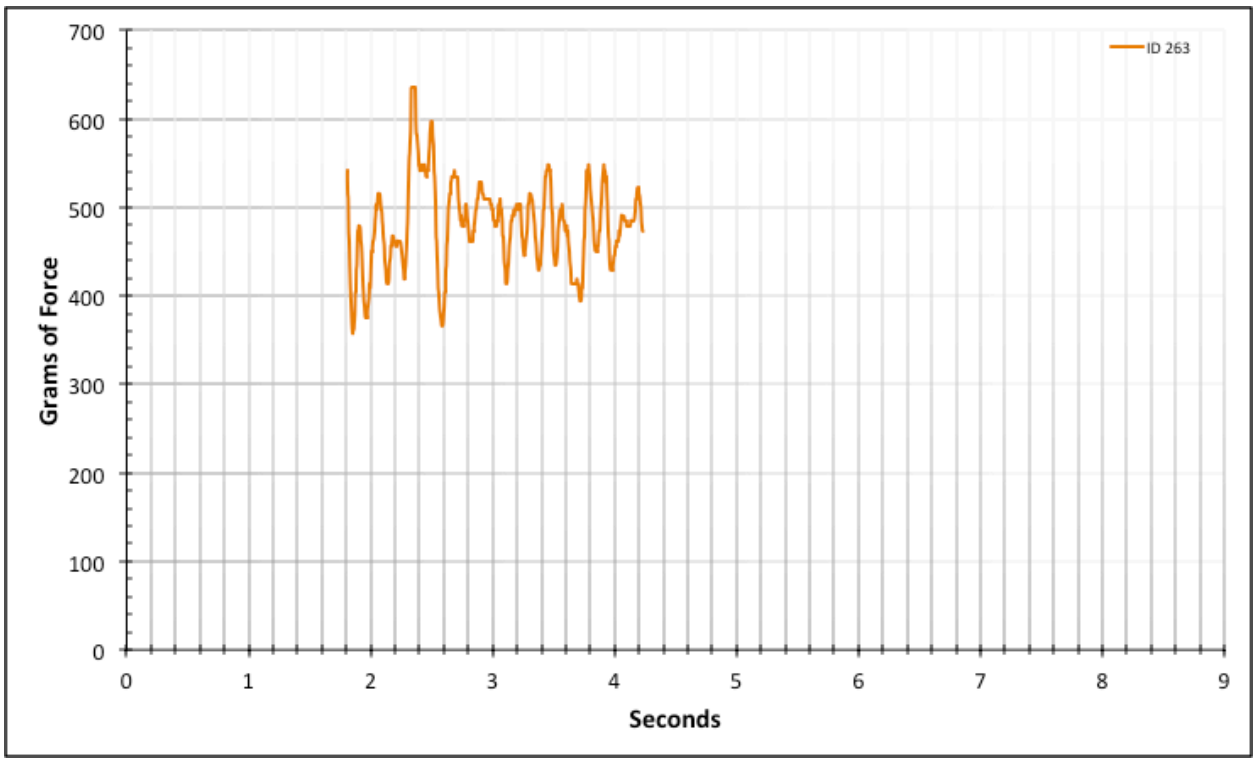

Figure A-6-366: Statistical Region Modeled Product - Lubricated - ID 263 - #8, Bolt 3

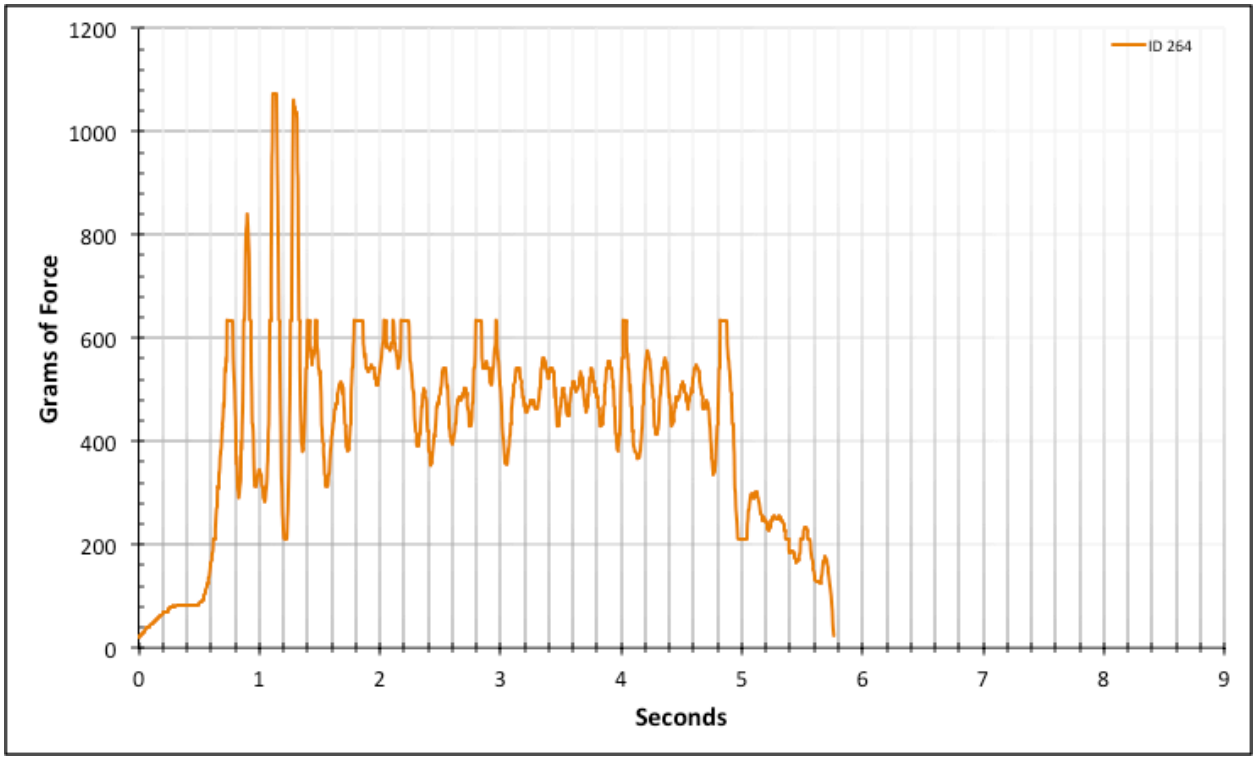

Figure A-6-367: Full Modeled Product - Lubricated - ID 264 - #8, Bolt 3

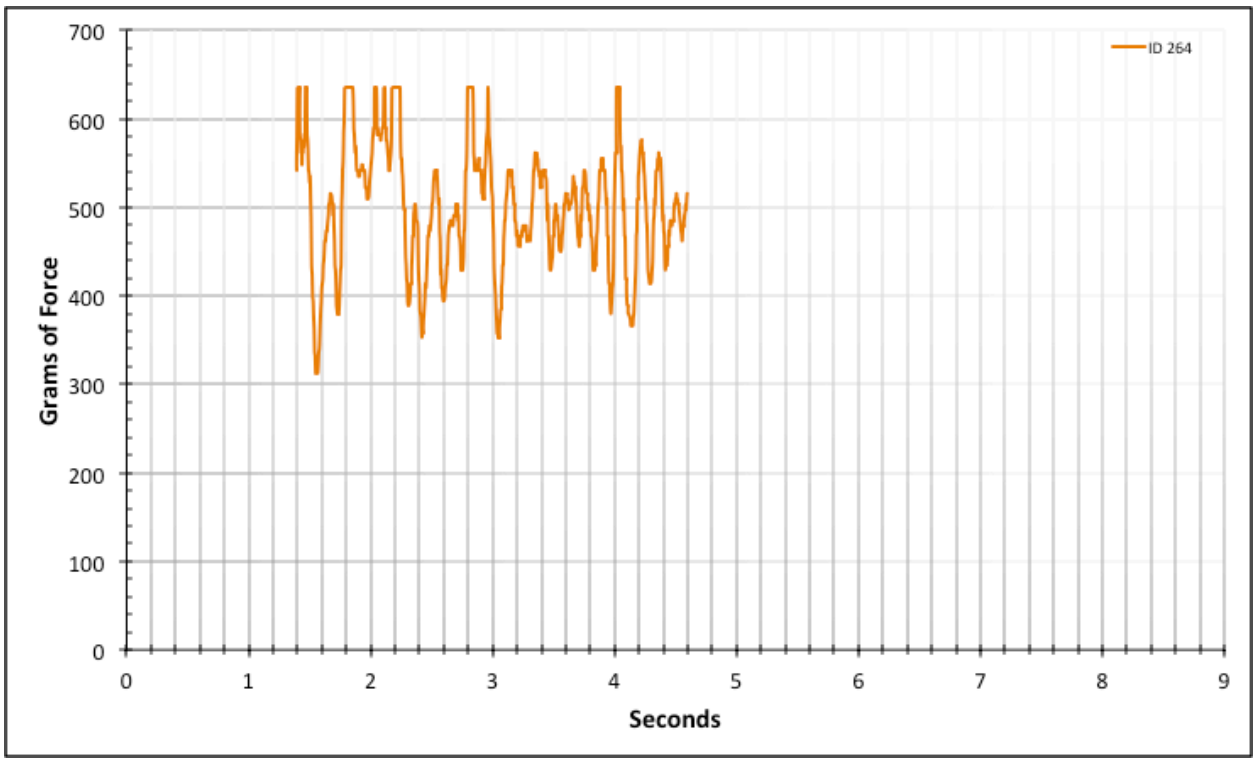

Figure A-6-368: Statistical Region Modeled Product - Lubricated - ID 264 - #8, Bolt 3

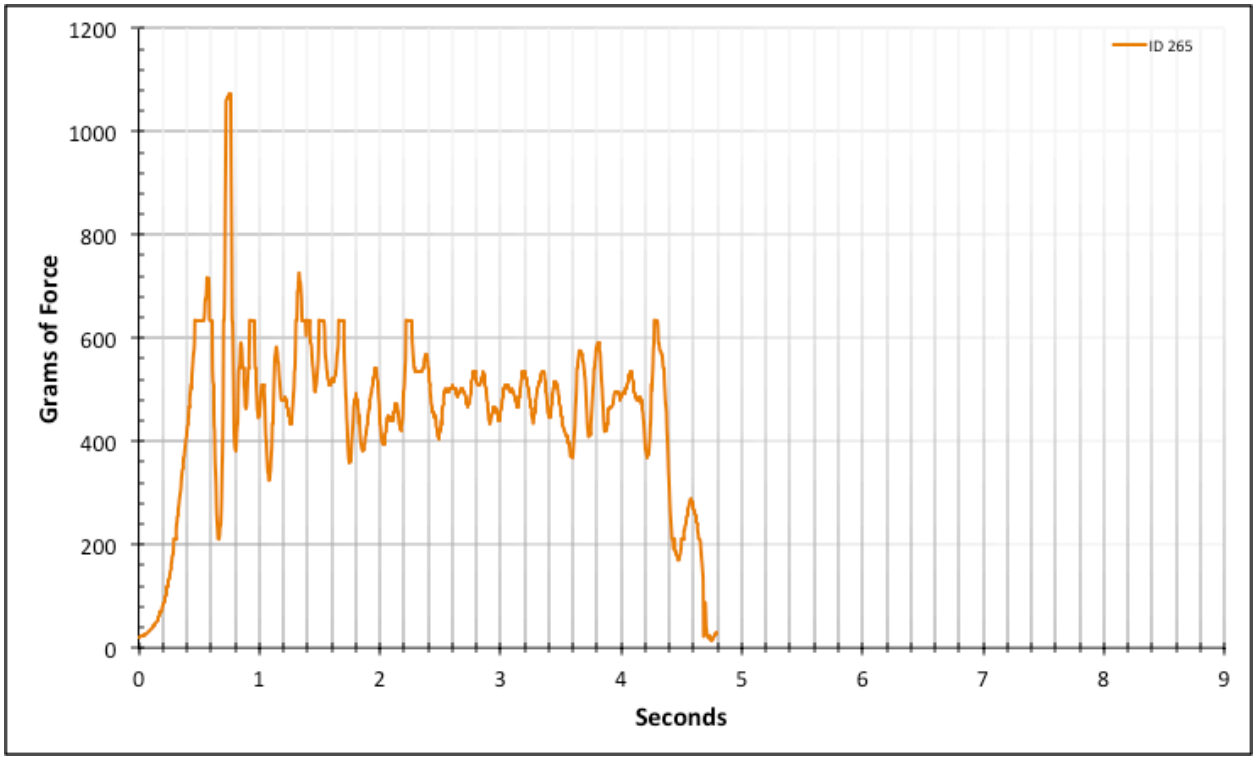

Figure A-6-369: Full Modeled Product - Lubricated - ID 265 - #8, Bolt 3

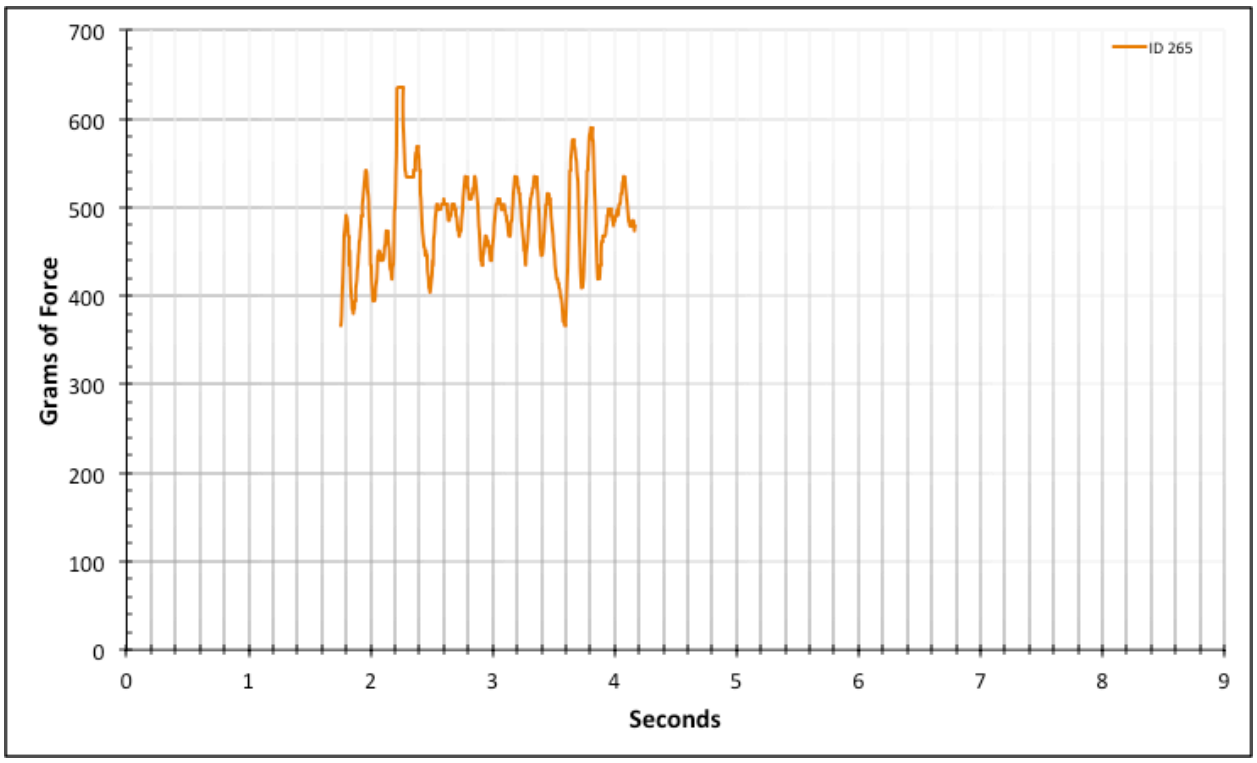

Figure A-6-370: Statistical Region Modeled Product - Lubricated - ID 265 - #8, Bolt 3

A.6. Factory Baseline – Lubricated

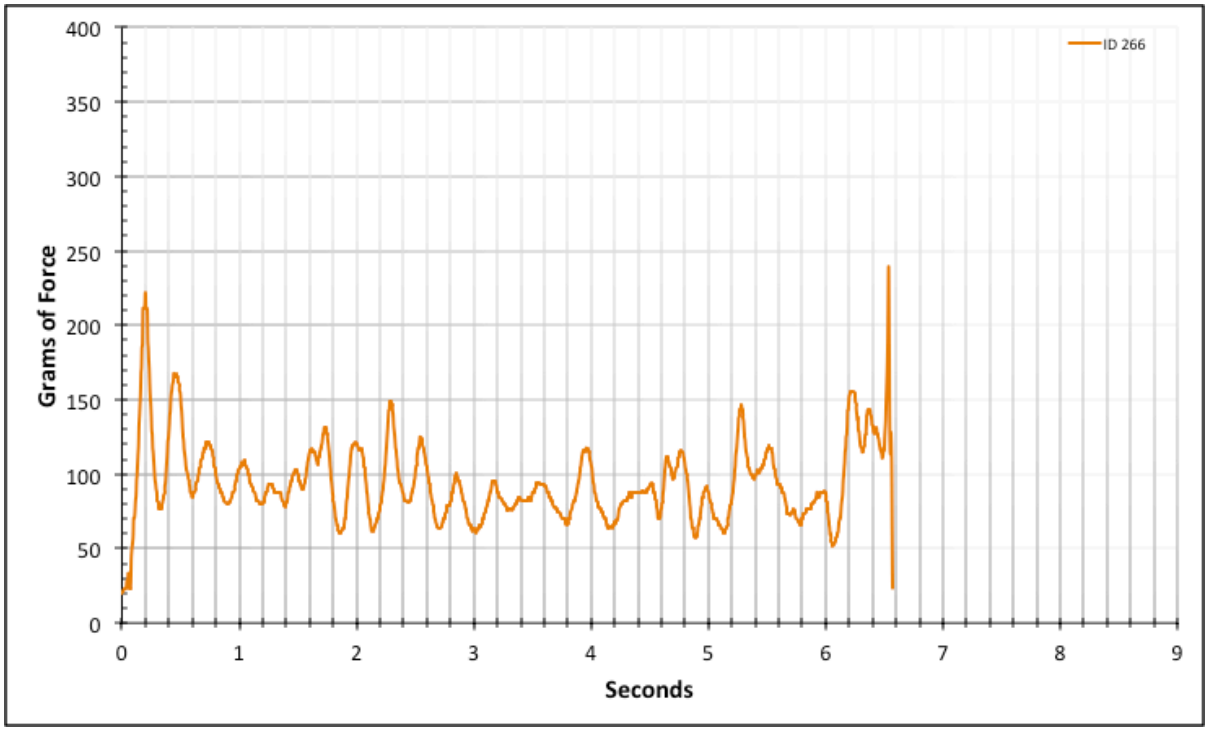

Figure A-6-371: Full Factory Baseline - Lubricated - ID 266 - #12, Bolt 1

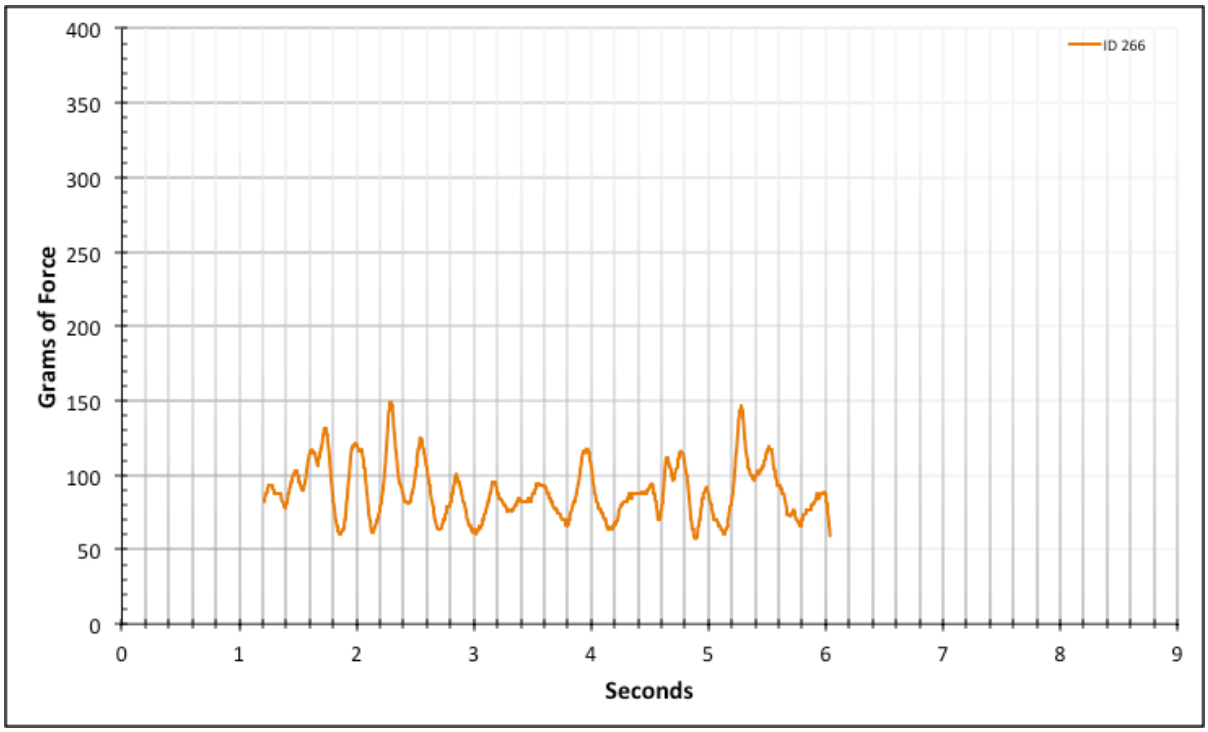

Figure A-6-372: Statistical Region Factory Baseline - Lubricated - ID 266 - #12, Bolt 1

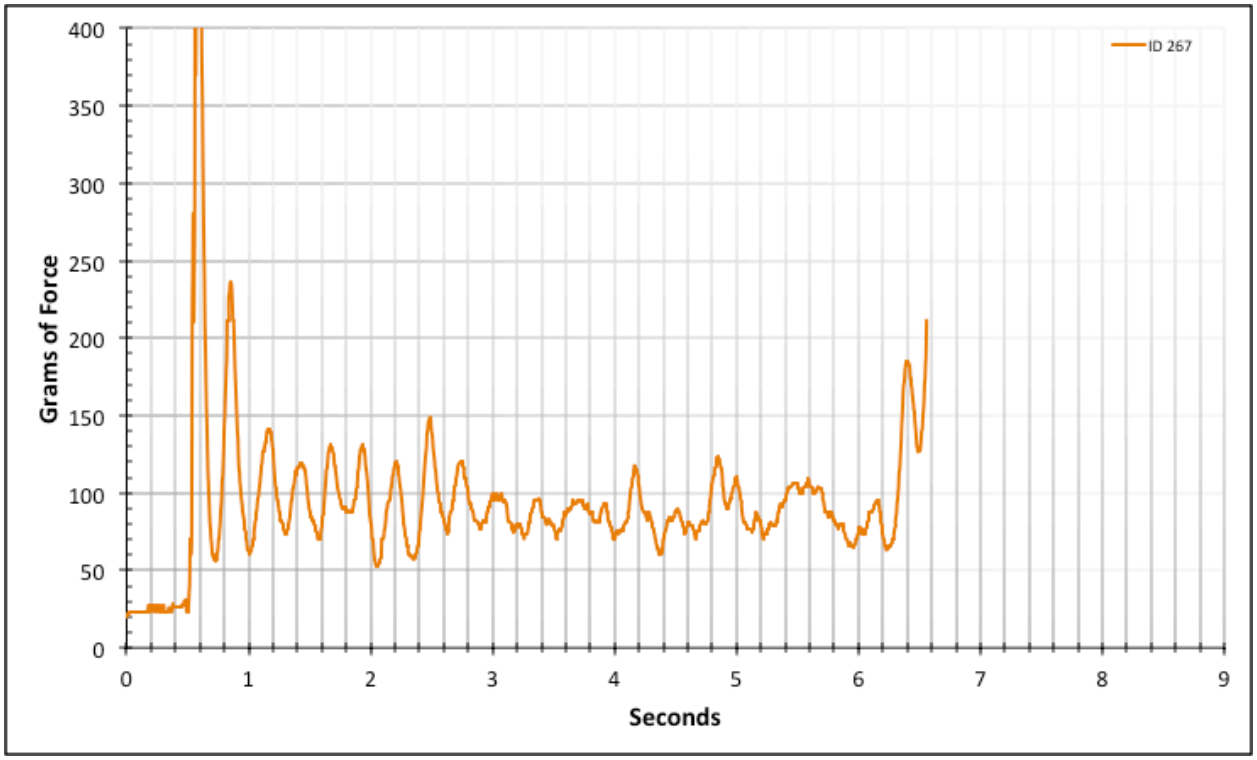

Figure A-6-373: Full Factory Baseline - Lubricated - ID 267 - #12, Bolt 1

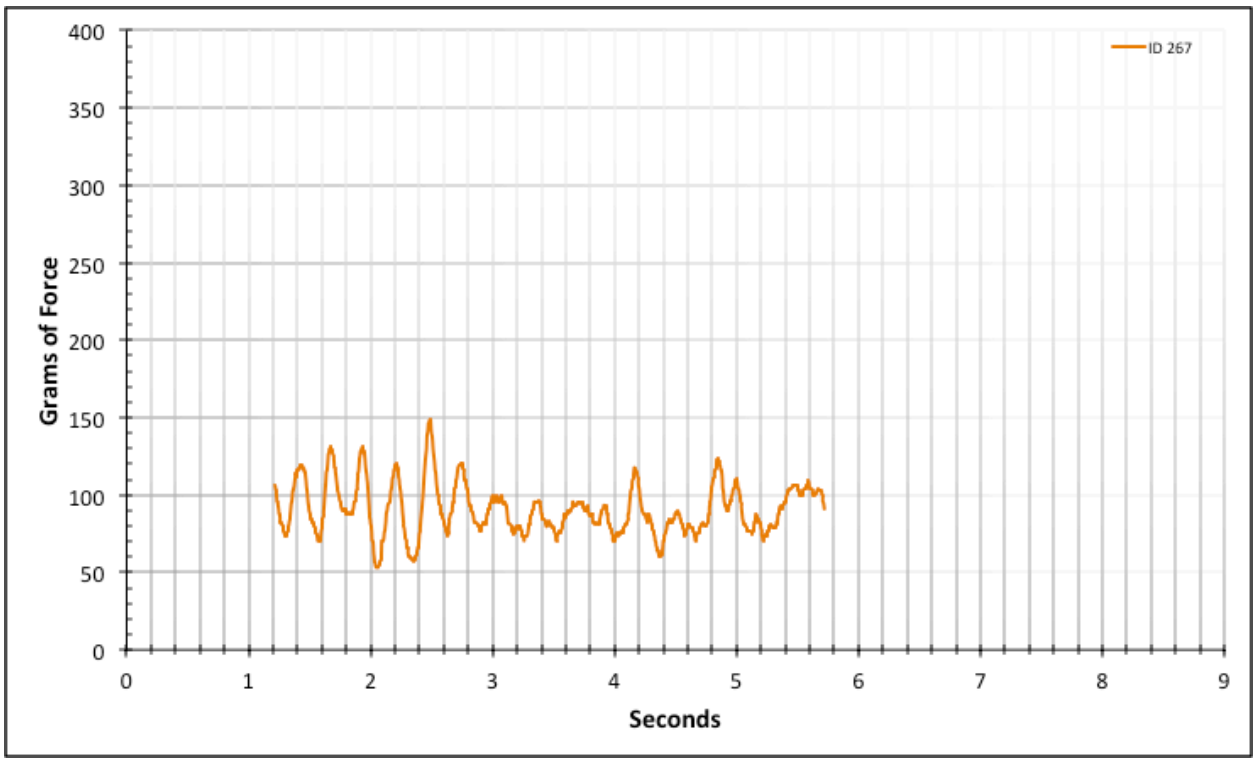

Figure A-6-374: Statistical Region Factory Baseline - Lubricated - ID 267 - #12, Bolt 1

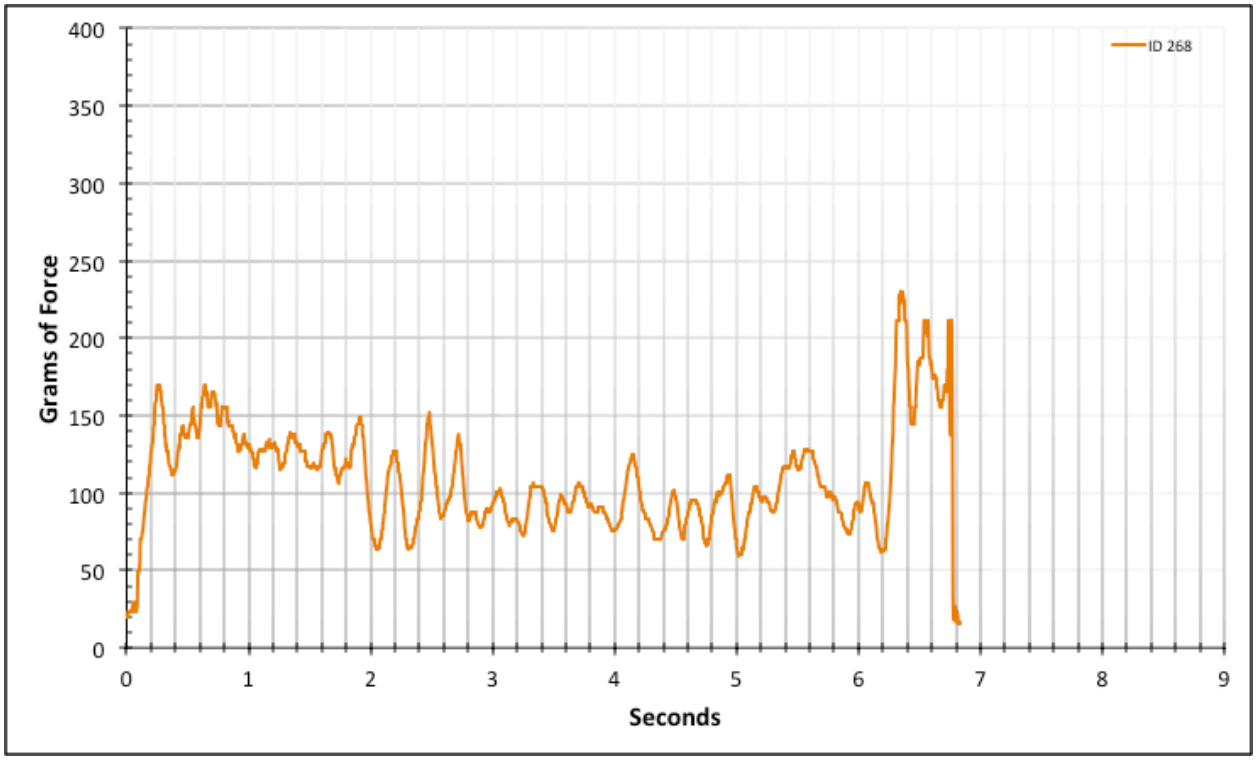

Figure A-6-375: Full Factory Baseline - Lubricated - ID 268 - #12, Bolt 1

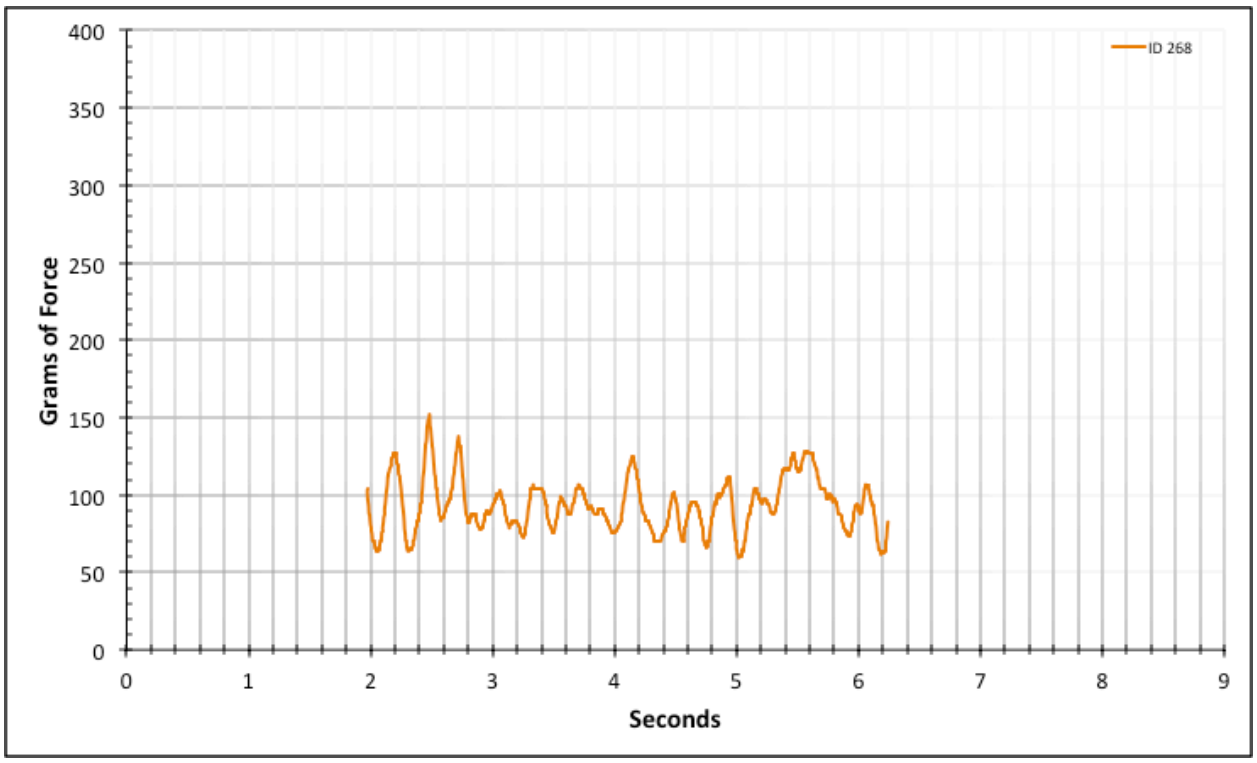

Figure A-6-376: Statistical Region Factory Baseline - Lubricated - ID 268 - #12, Bolt 1

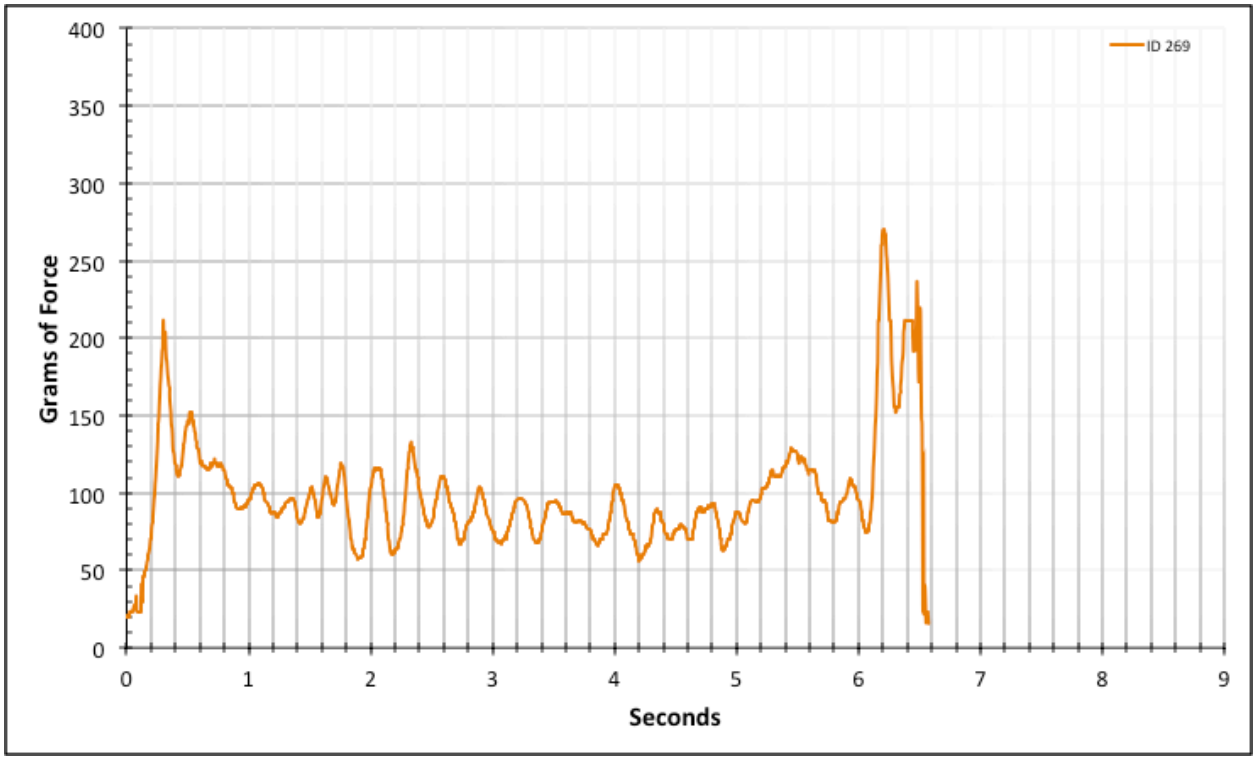

Figure A-6-377: Full Factory Baseline - Lubricated - ID 269 - #12, Bolt 1

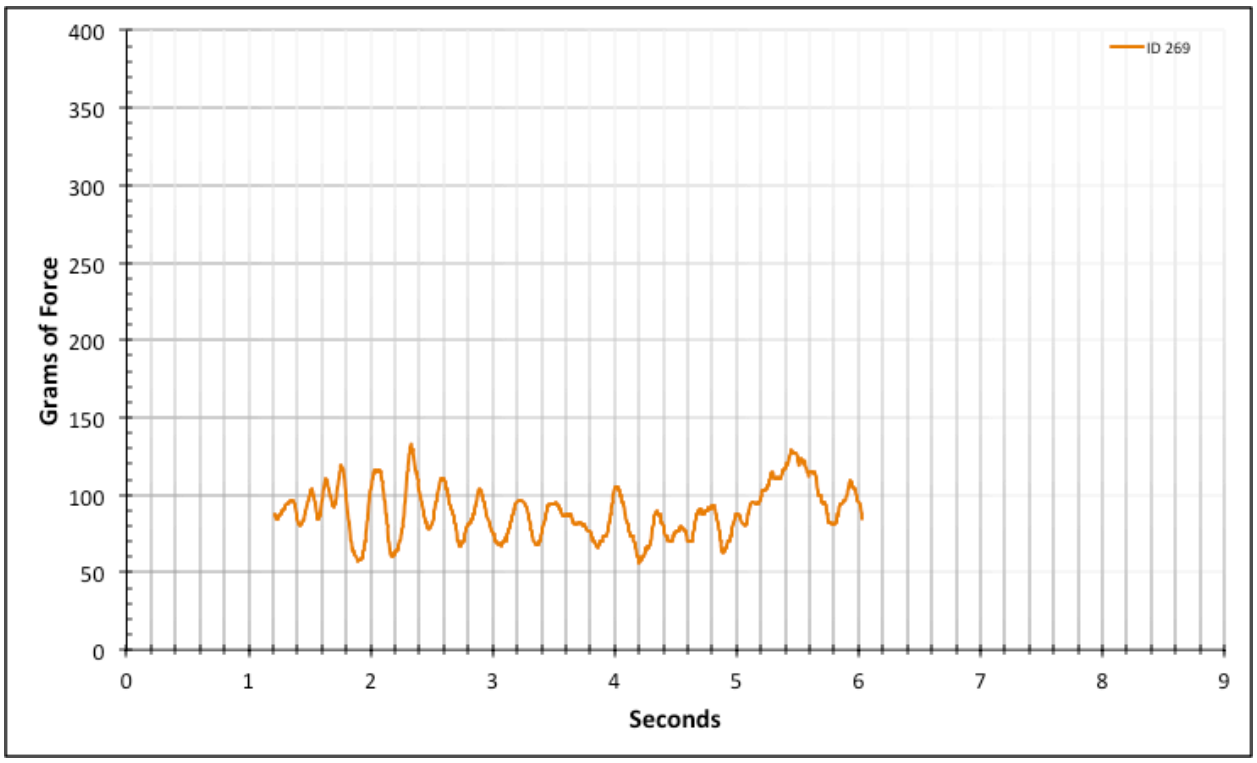

Figure A-6-378: Statistical Region Factory Baseline - Lubricated - ID 269 - #12, Bolt 1

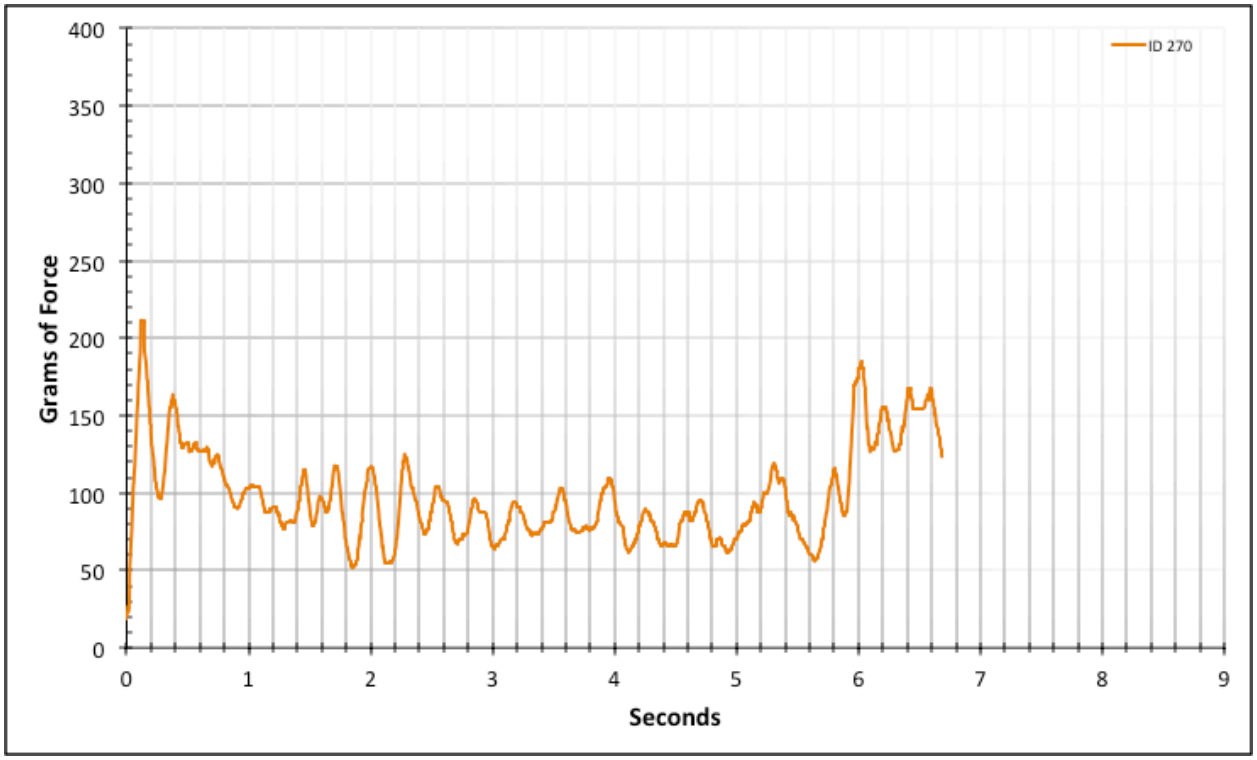

Figure A-6-379: Full Factory Baseline - Lubricated - ID 270 - #12, Bolt 1

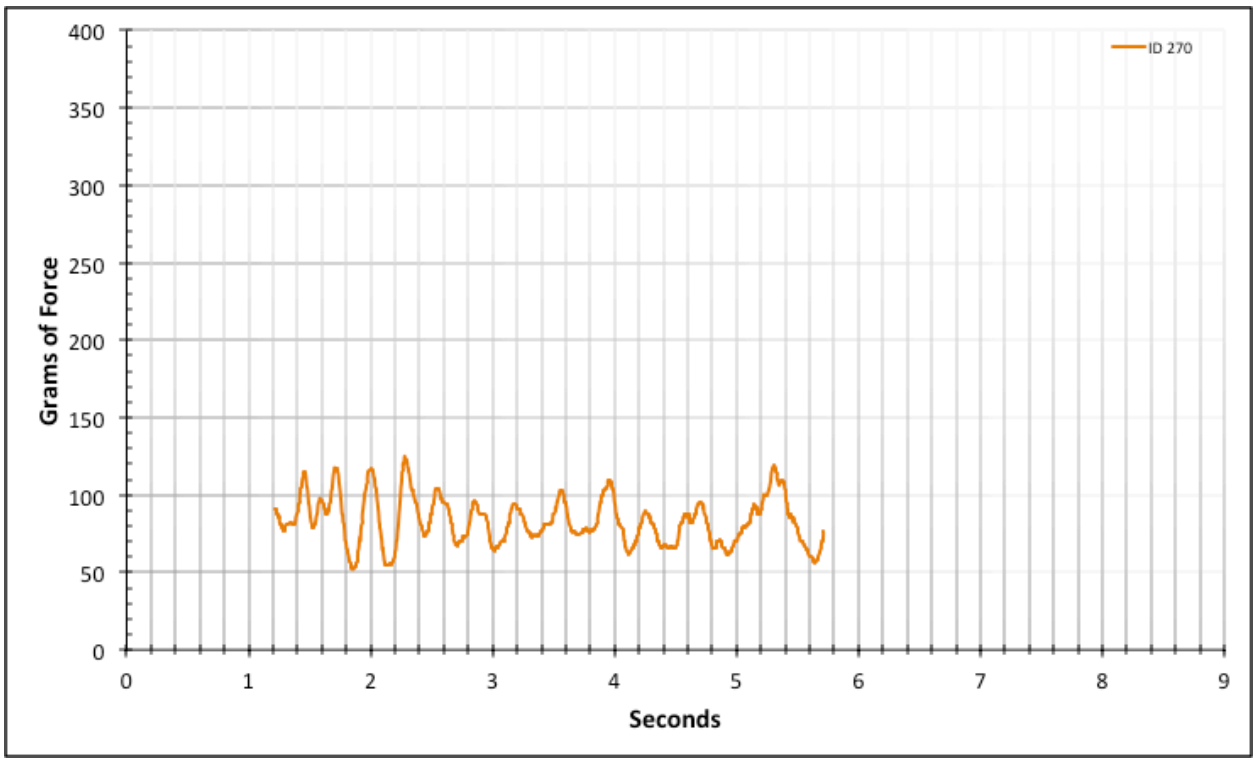

Figure A-6-380: Statistical Region Factory Baseline - Lubricated - ID 270 - #12, Bolt 1

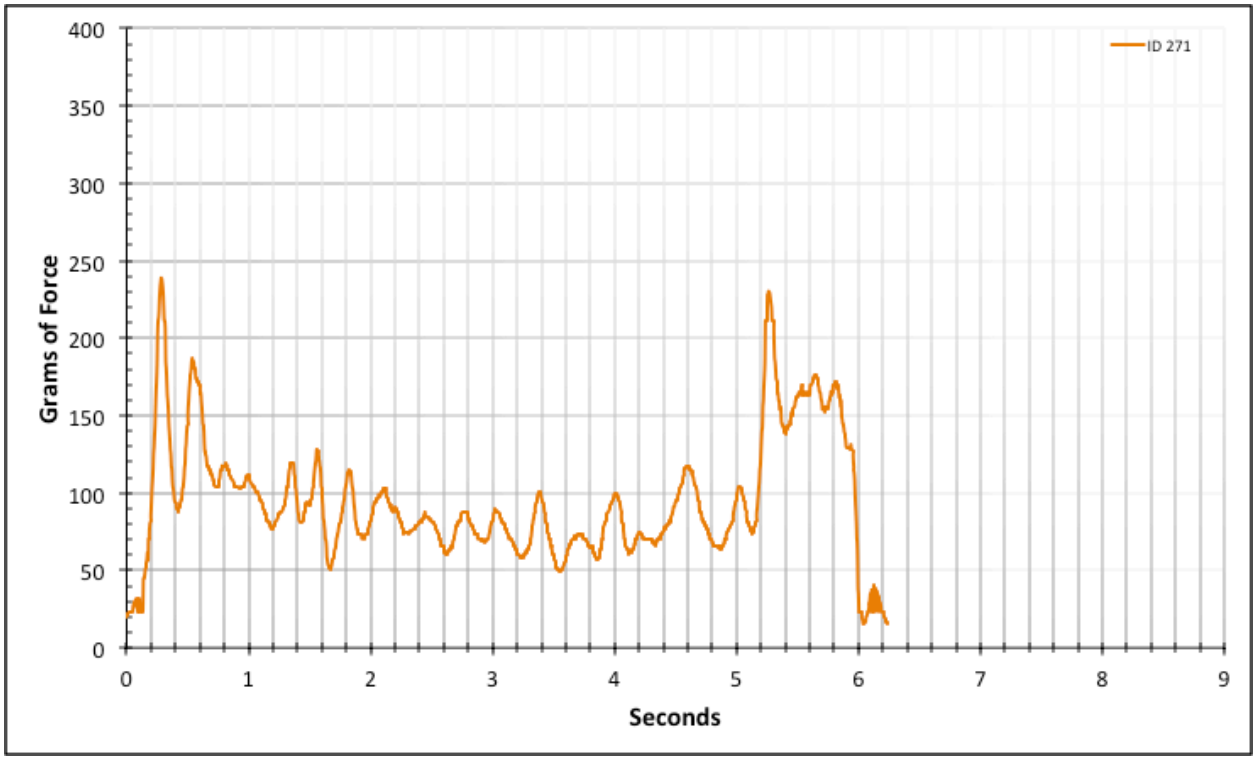

Figure A-6-381: Full Factory Baseline - Lubricated - ID 271 - #12, Bolt 2

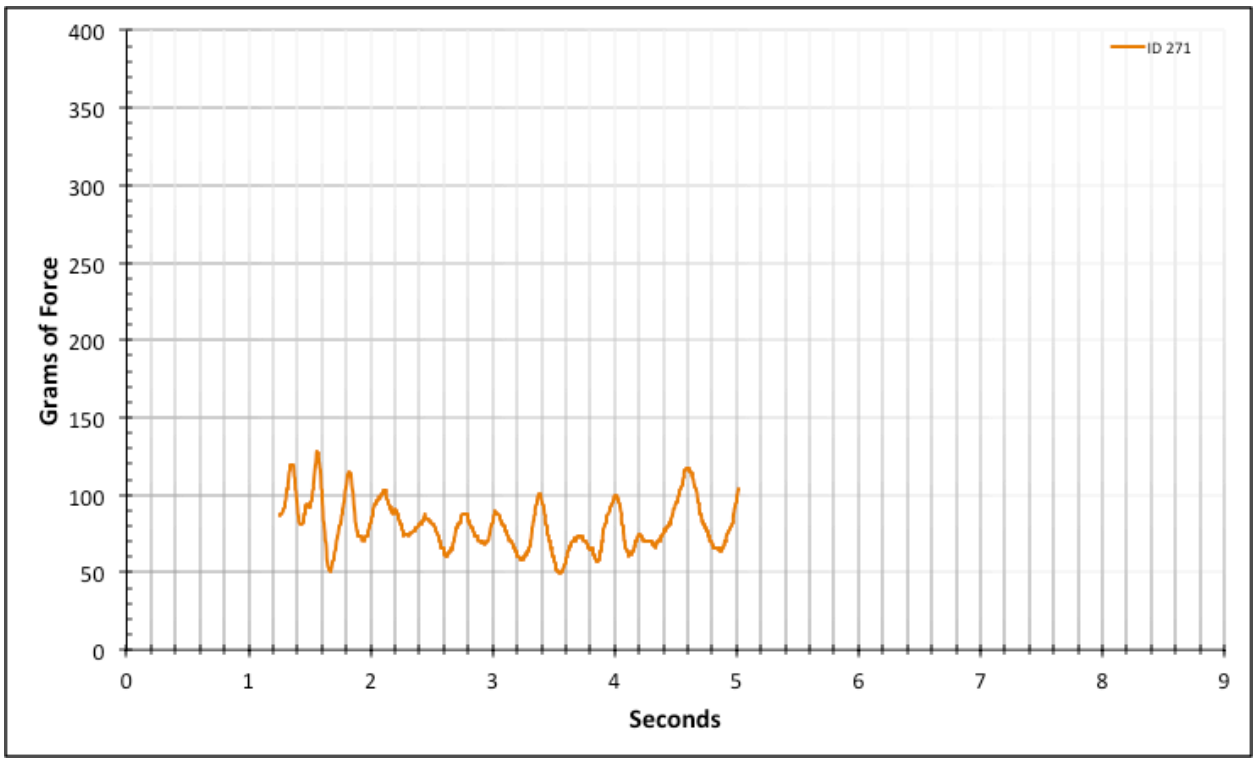

Figure A-6-382: Statistical Region Factory Baseline - Lubricated - ID 271 - #12, Bolt 2

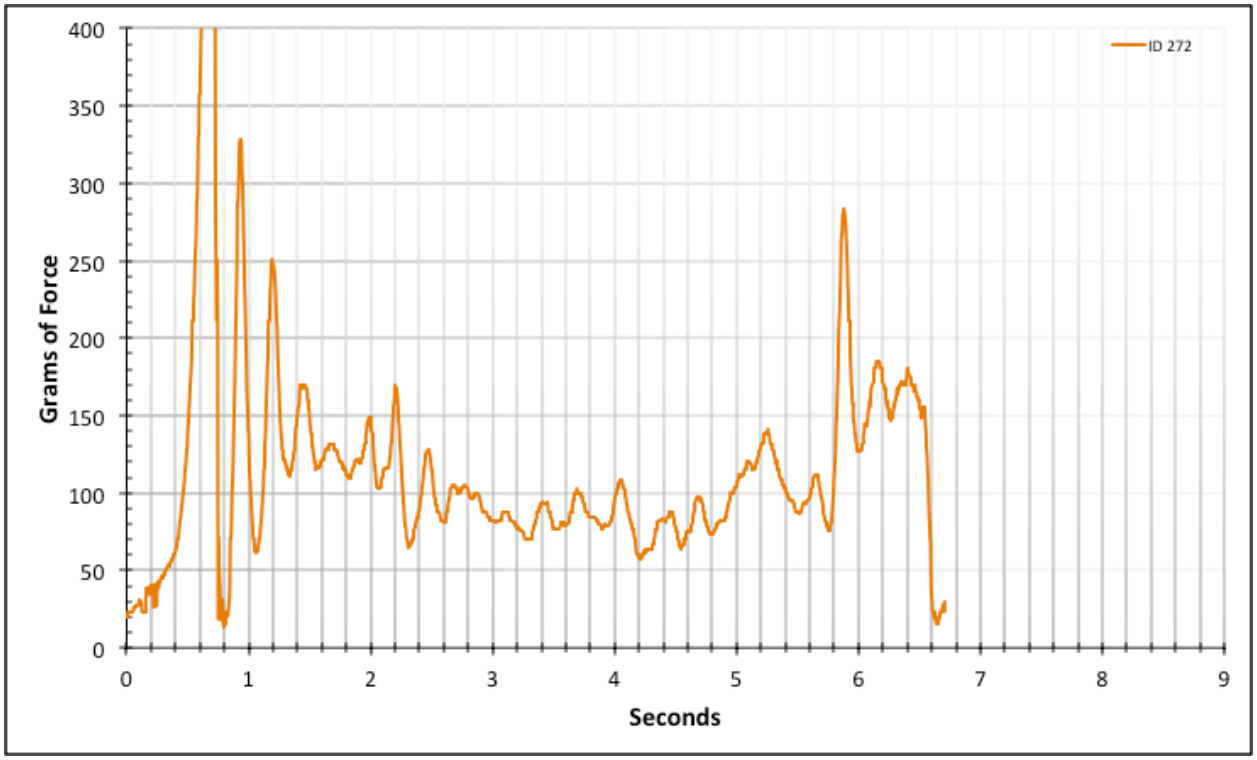

Figure A-6-383: Full Factory Baseline - Lubricated - ID 272 - #12, Bolt 2

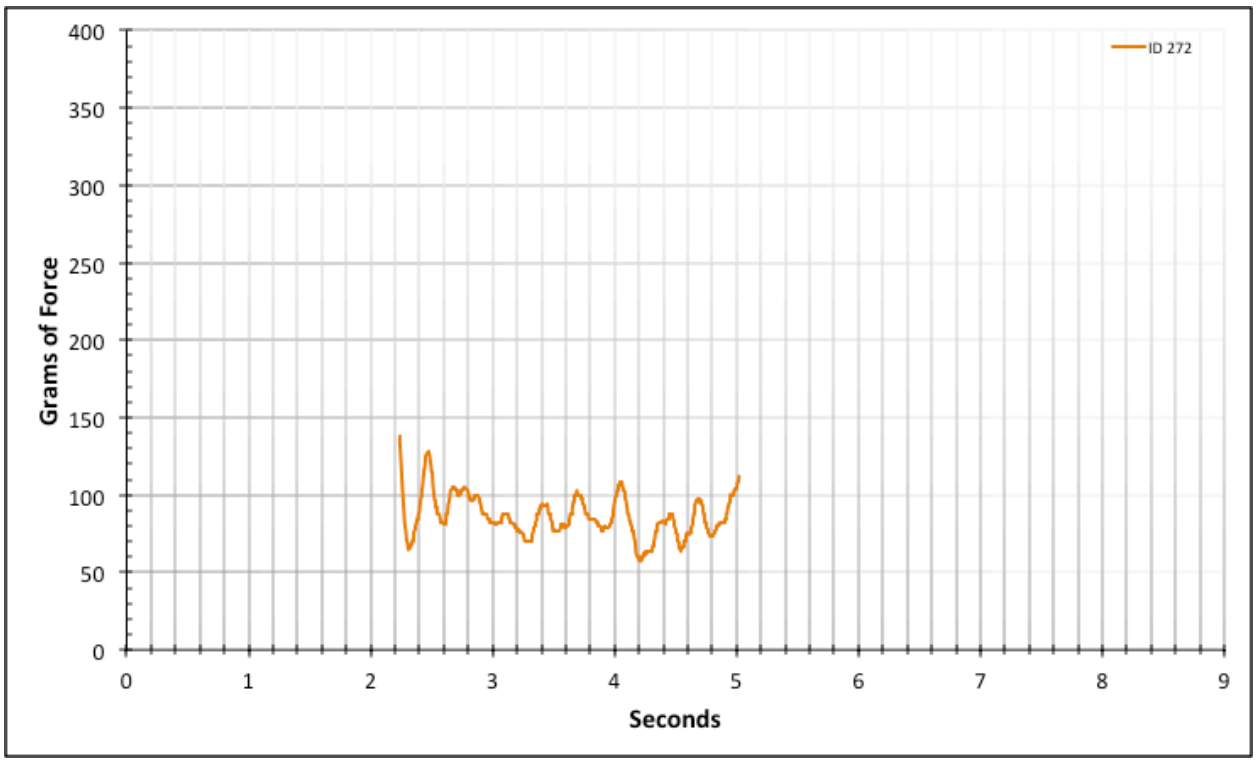

Figure A-6-384: Statistical Region Factory Baseline - Lubricated - ID 272 - #12, Bolt 2

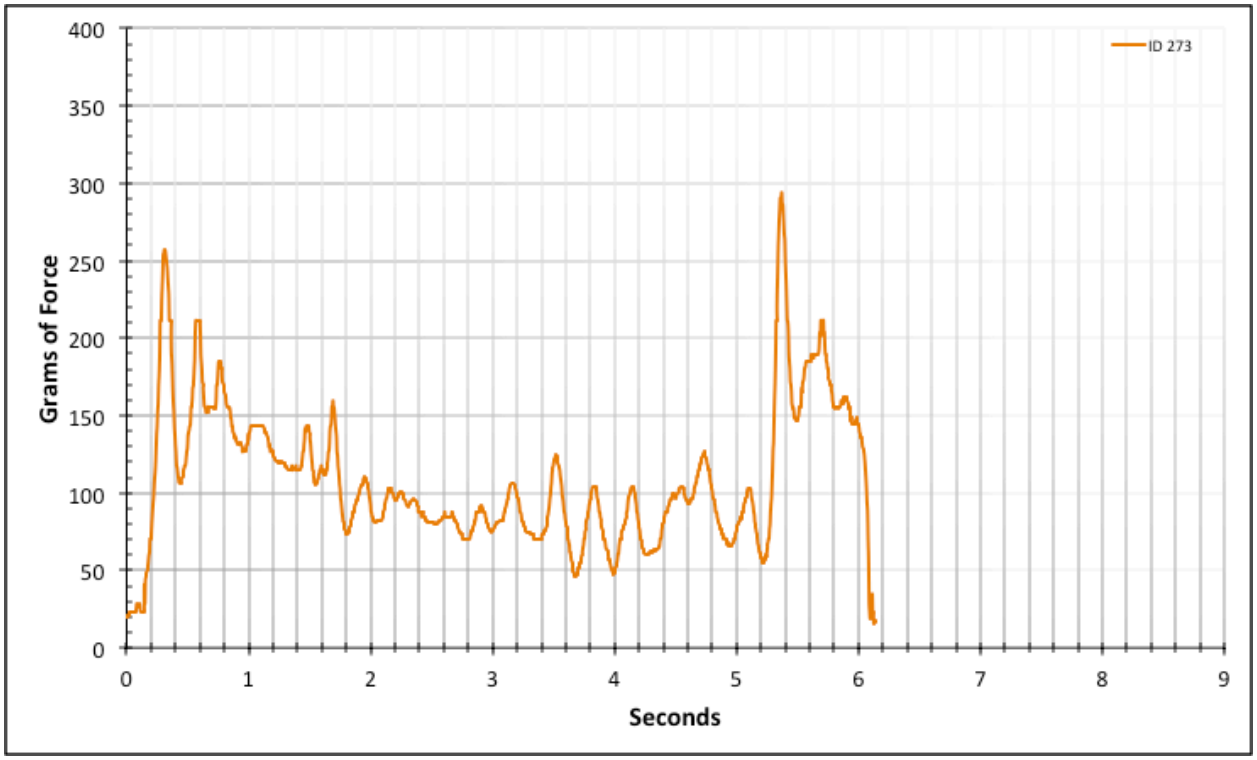

Figure A-6-385: Full Factory Baseline - Lubricated - ID 273 - #12, Bolt 2

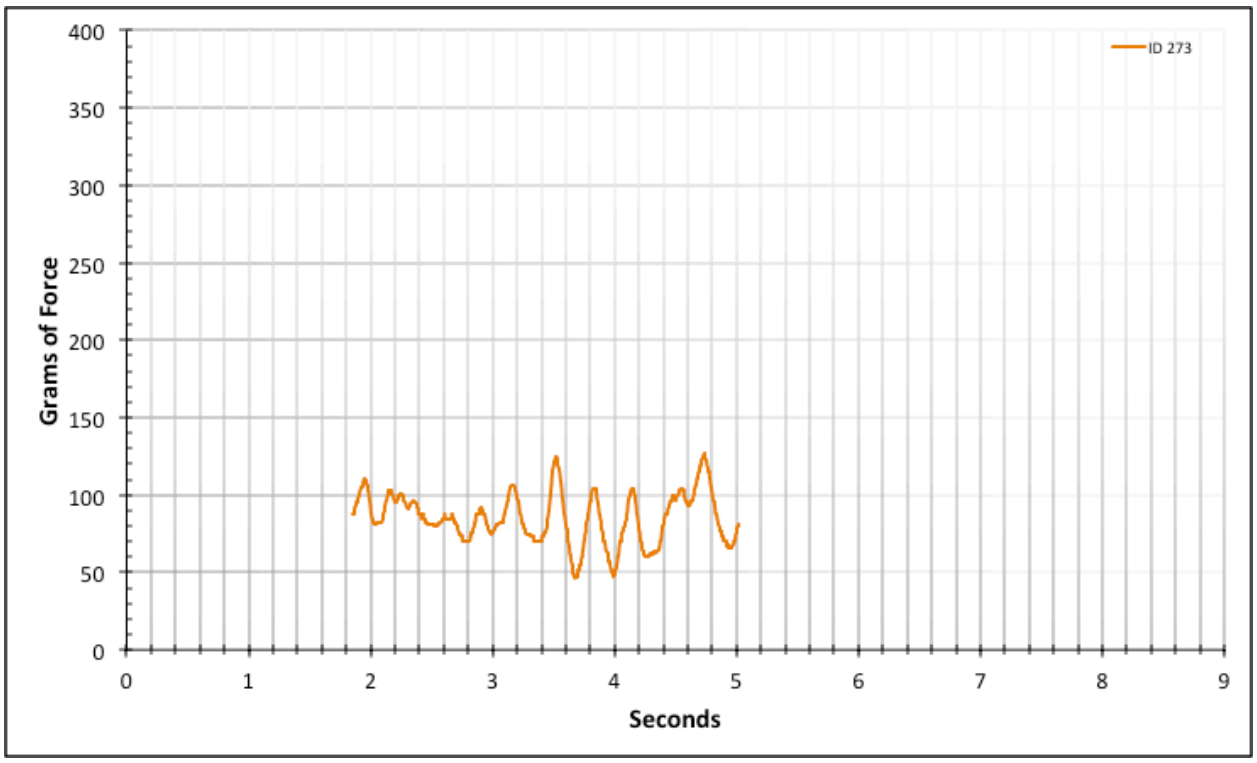

Figure A-6-386: Statistical Region Factory Baseline - Lubricated - ID 273 - #12, Bolt 2

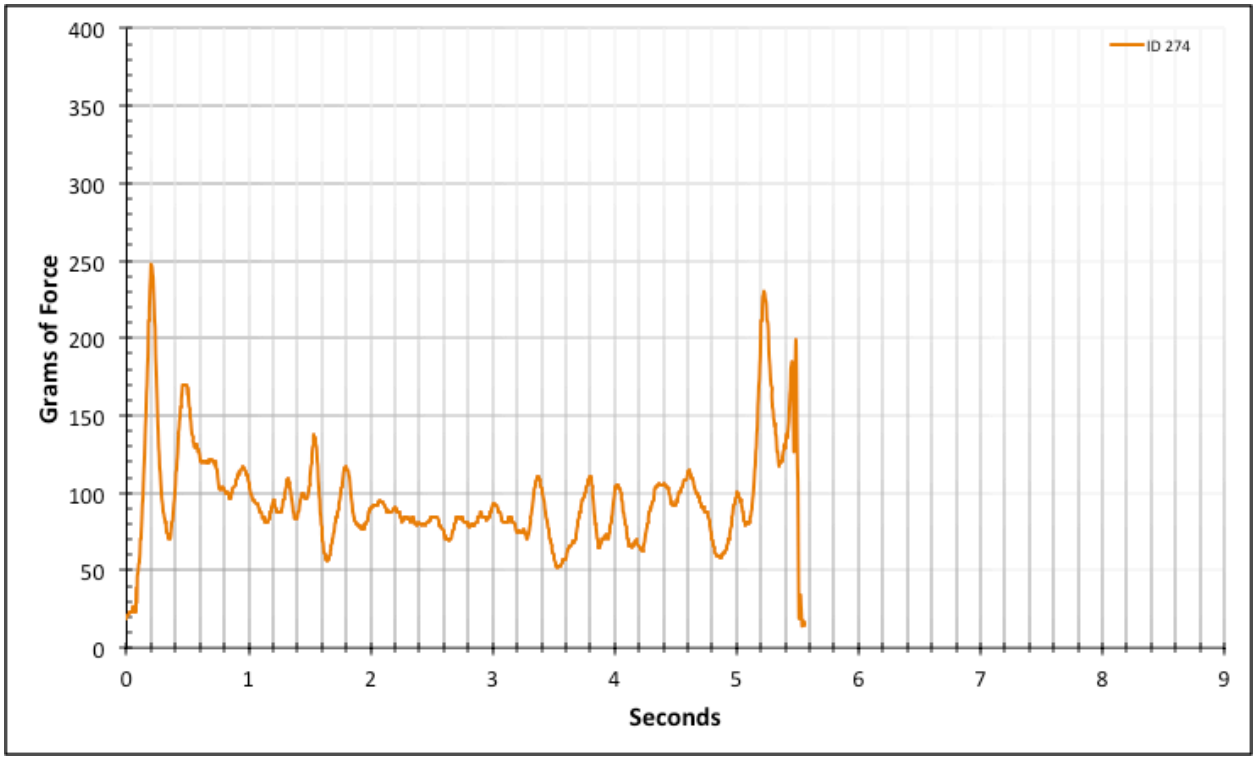

Figure A-6-387: Full Factory Baseline - Lubricated - ID 274 - #12, Bolt 2

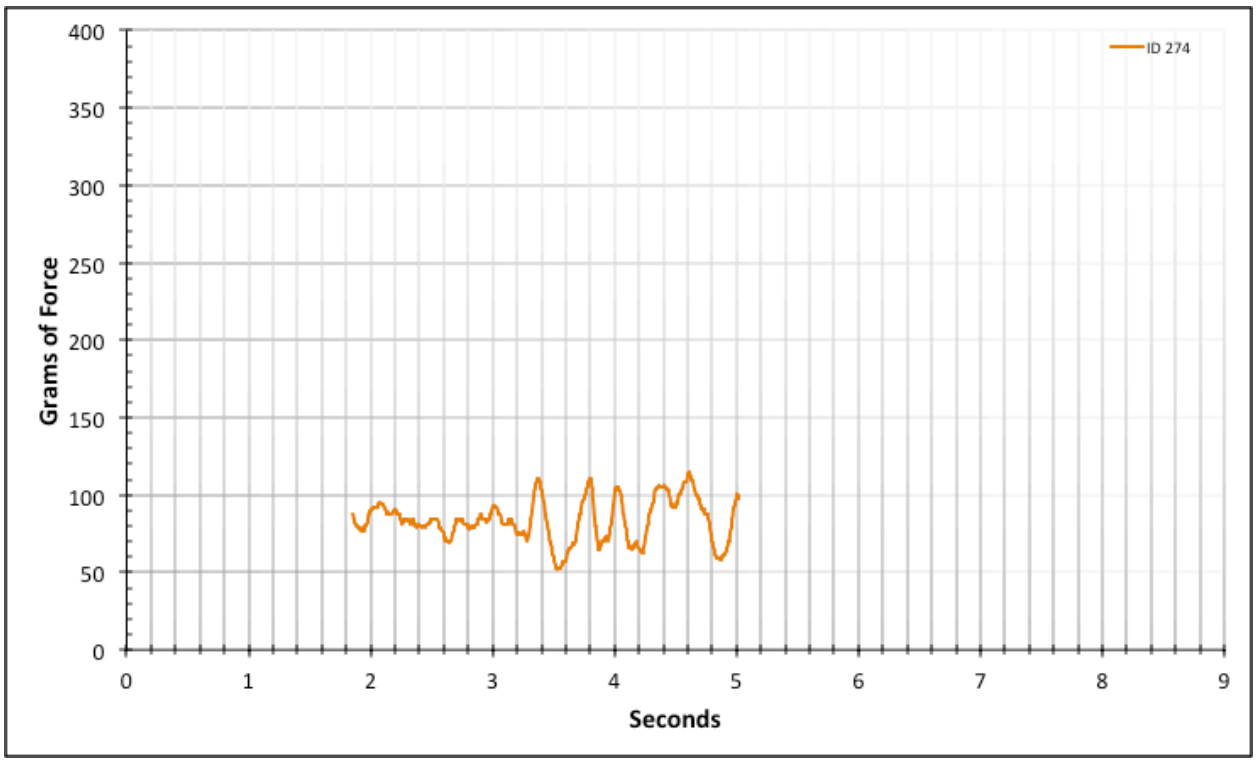

Figure A-6-388: Statistical Region Factory Baseline - Lubricated - ID 274 - #12, Bolt 2

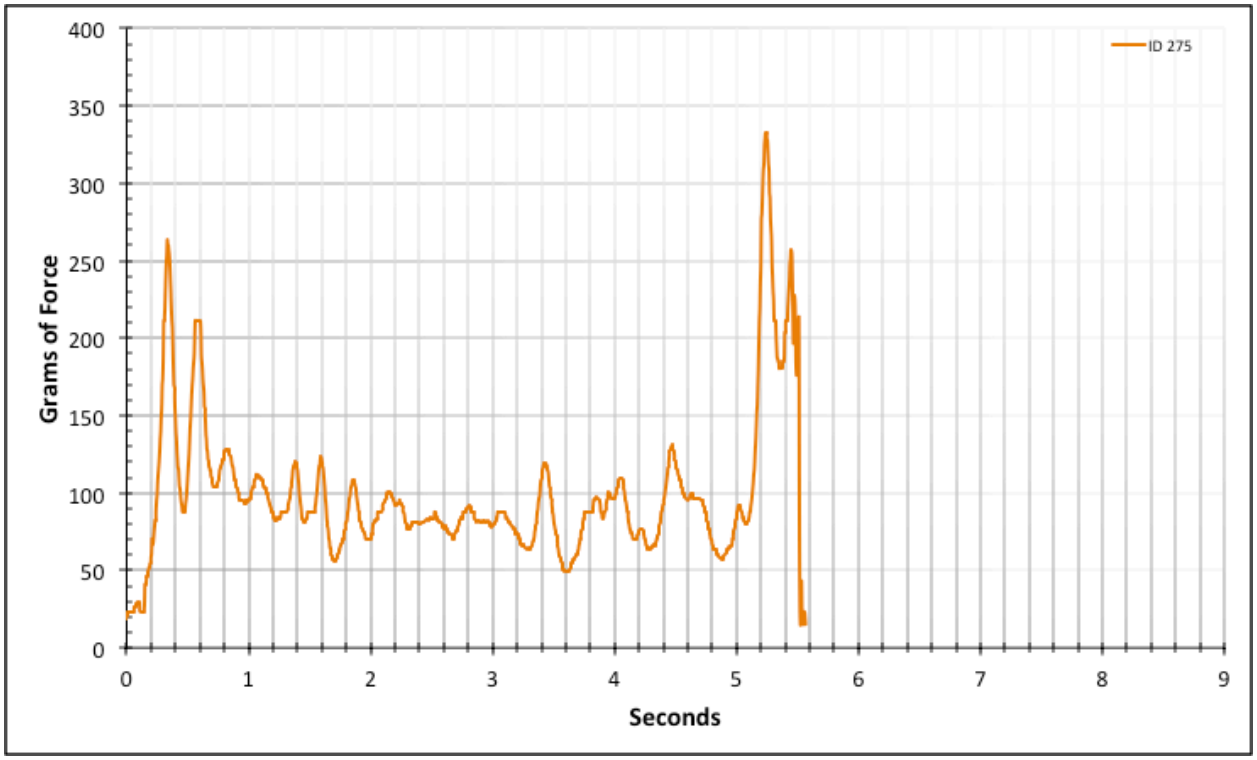

Figure A-6-389: Full Factory Baseline - Lubricated - ID 275 - #12, Bolt 2

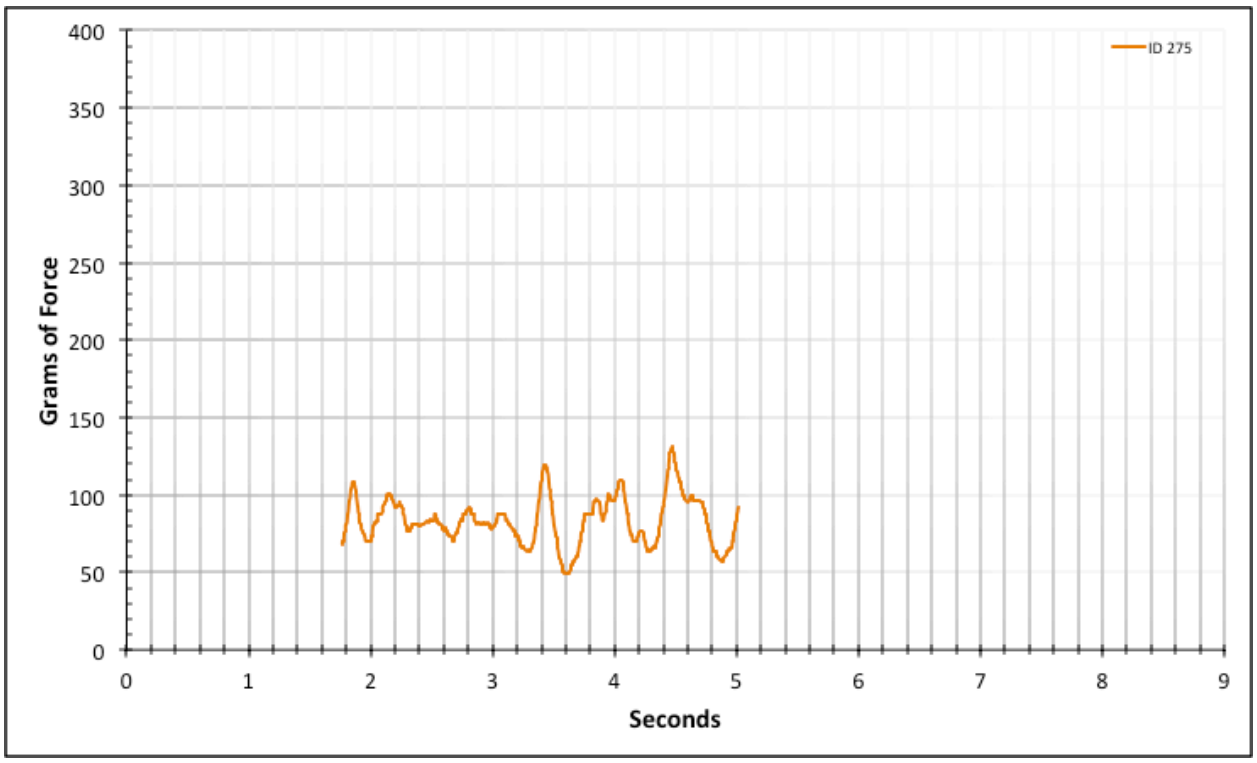

Figure A-6-390: Statistical Region Factory Baseline - Lubricated - ID 275 - #12, Bolt 2

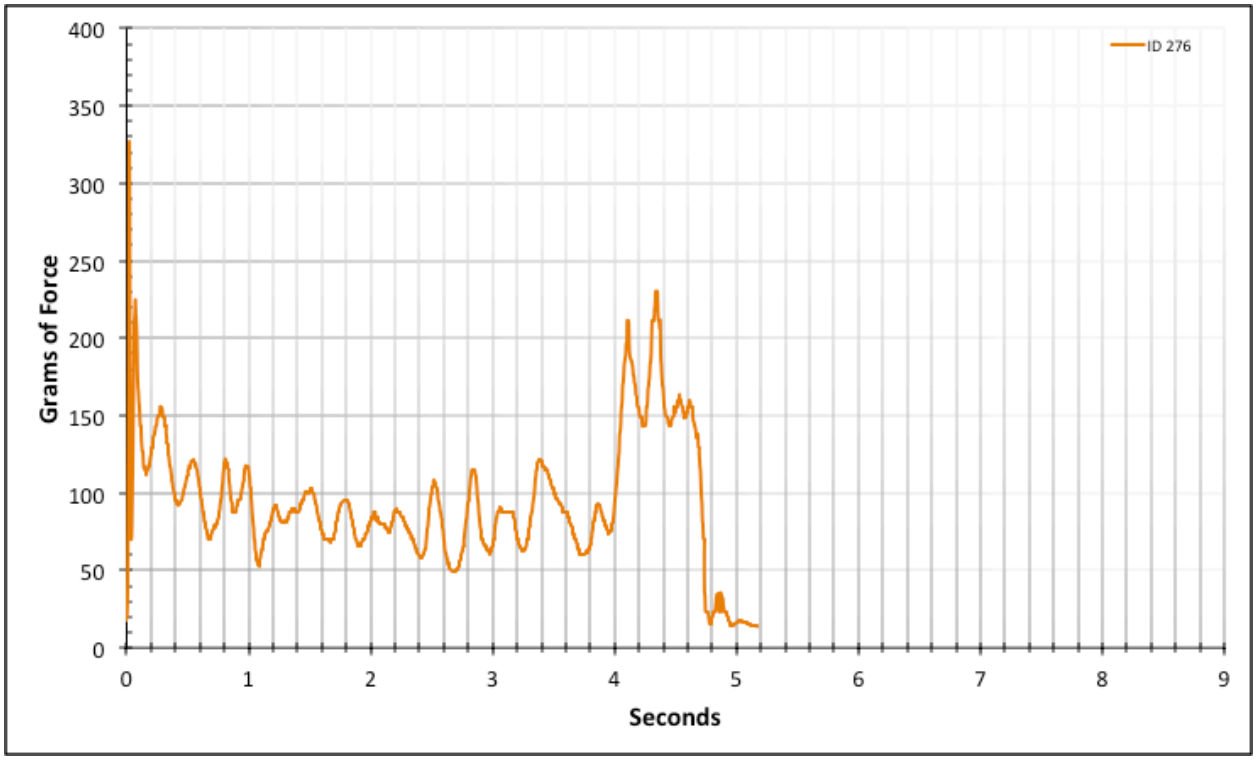

Figure A-6-391: Full Factory Baseline - Lubricated - ID 276 - #12, Bolt 3

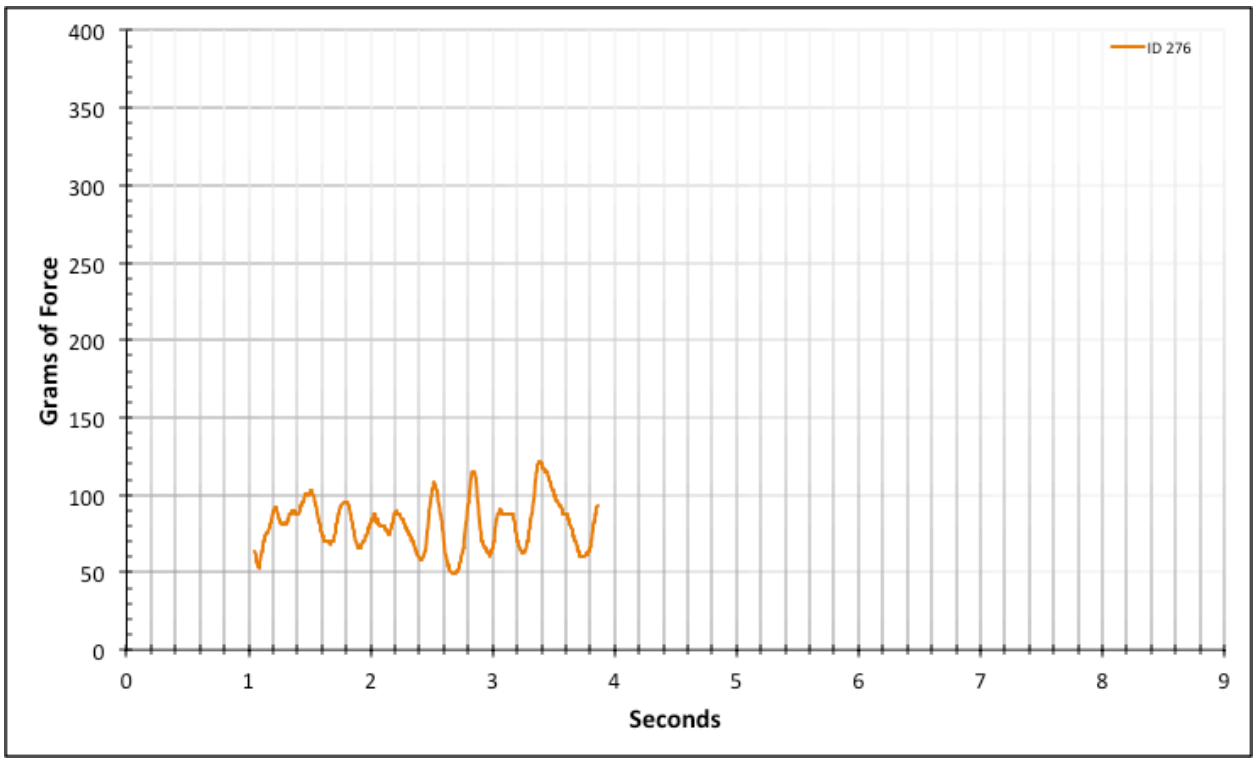

Figure A-6-392: Statistical Region Factory Baseline - Lubricated - ID 276 - #12, Bolt 3

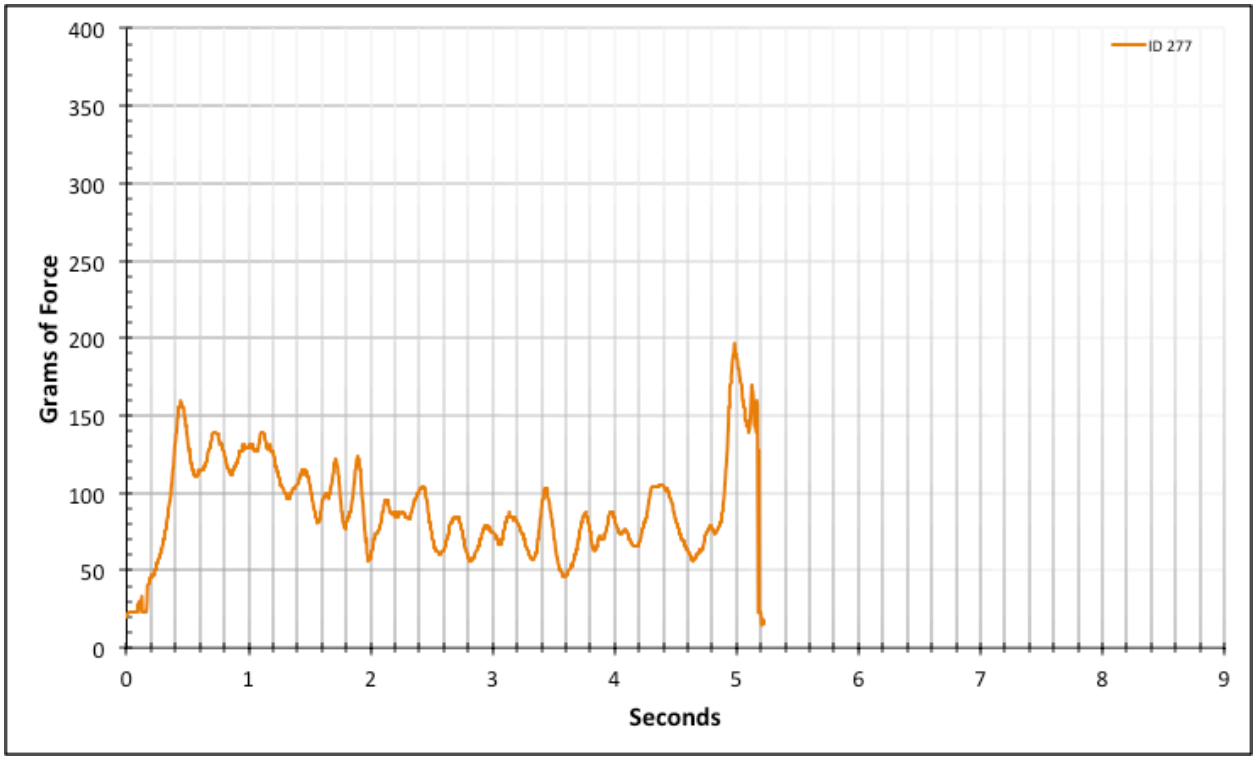

Figure A-6-393: Full Factory Baseline - Lubricated - ID 277 - #12, Bolt 3

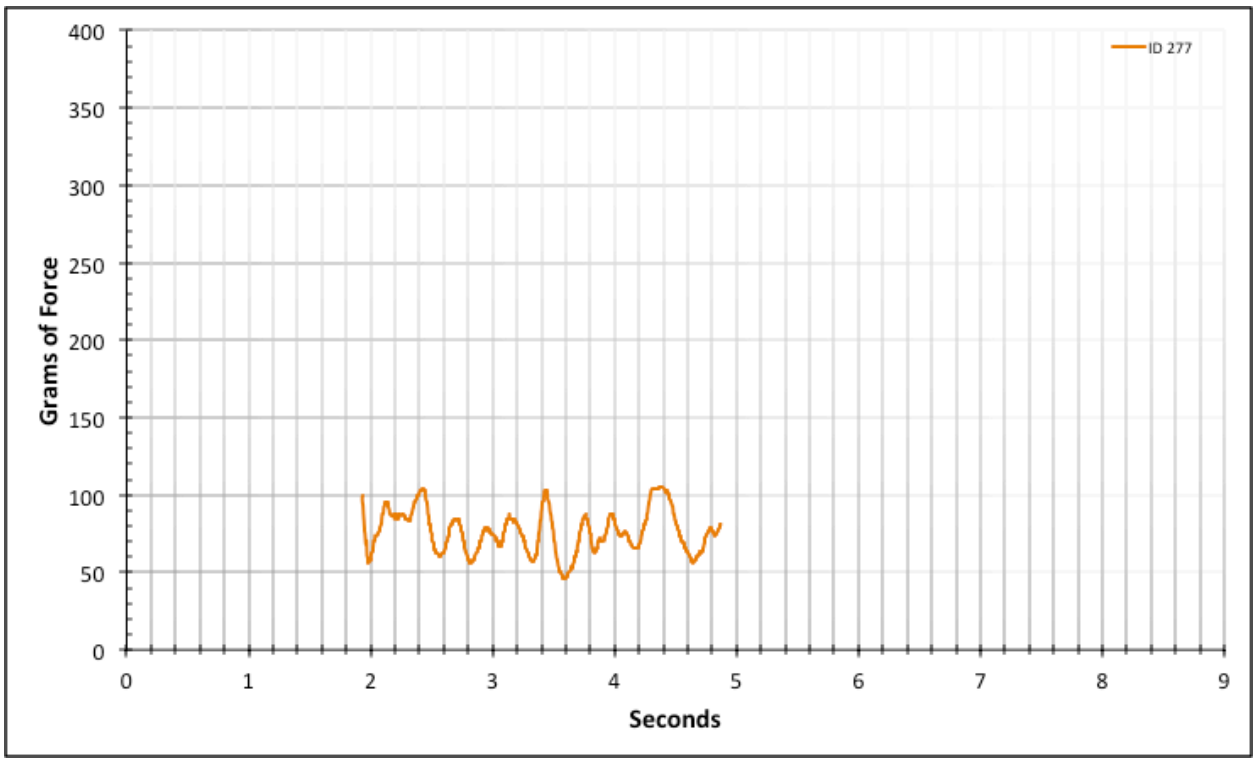

Figure A-6-394: Statistical Region Factory Baseline - Lubricated - ID 277 - #12, Bolt 3

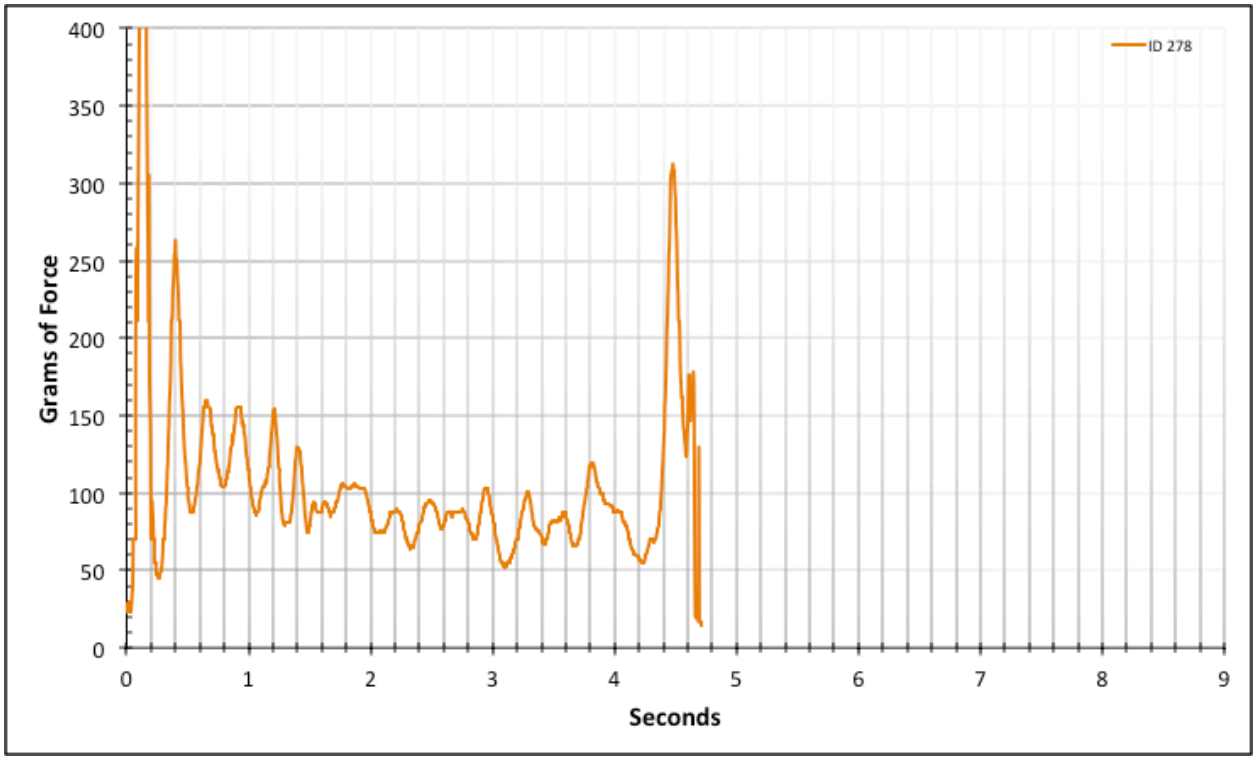

Figure A-6-395: Full Factory Baseline - Lubricated - ID 278 - #12, Bolt 3

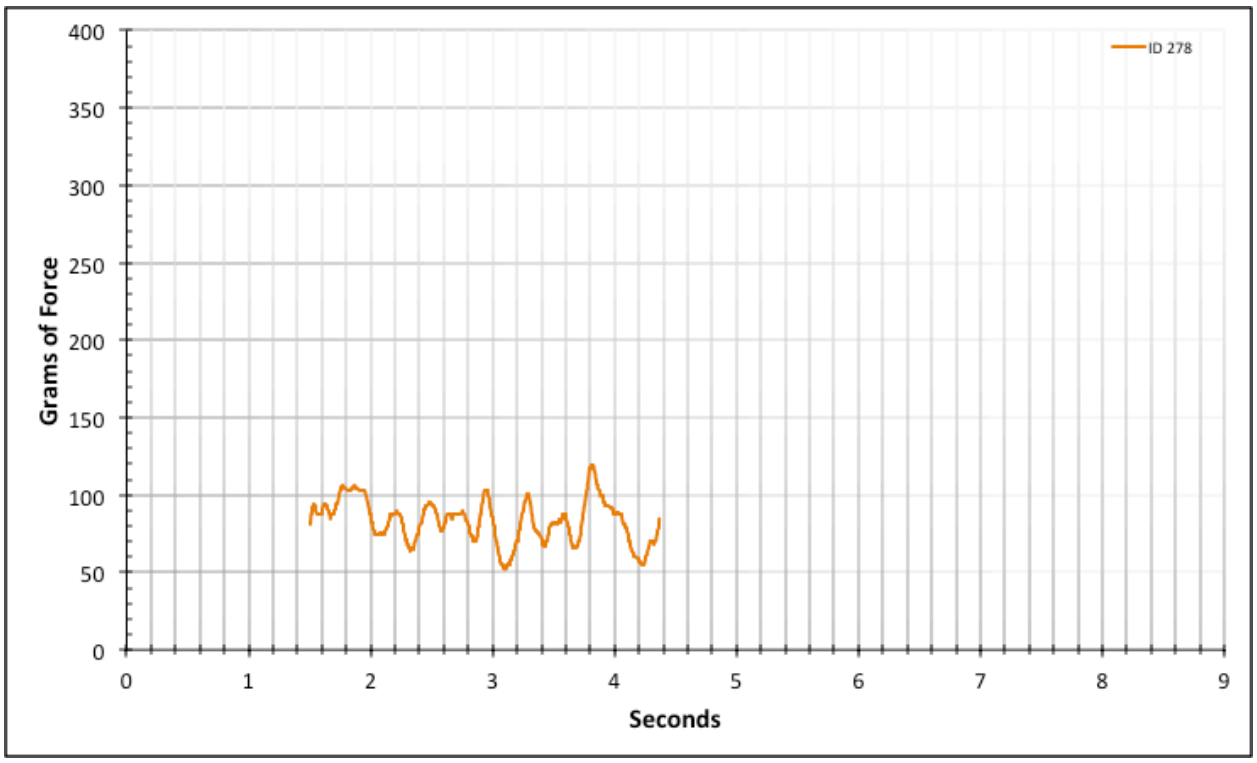

Figure A-6-396: Statistical Region Factory Baseline - Lubricated - ID 278 - #12, Bolt 3

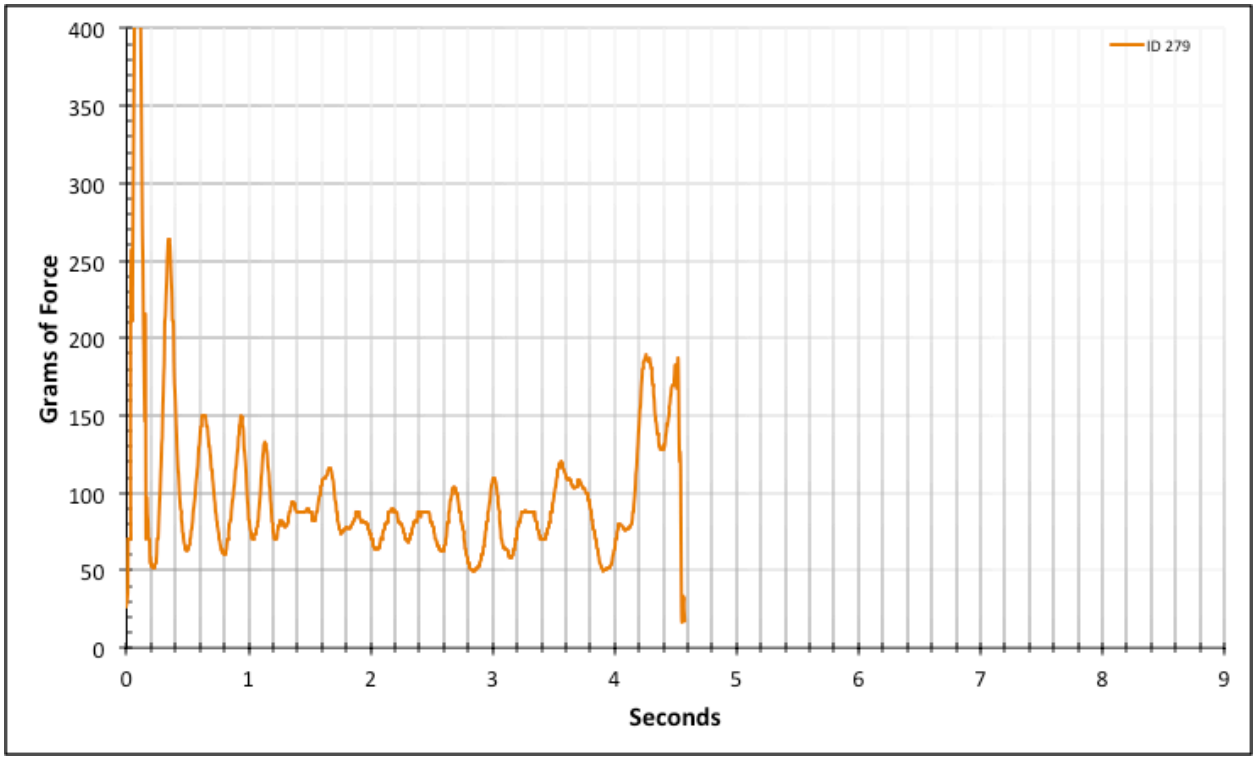

Figure A-6-397: Full Factory Baseline - Lubricated - ID 279 - #12, Bolt 3

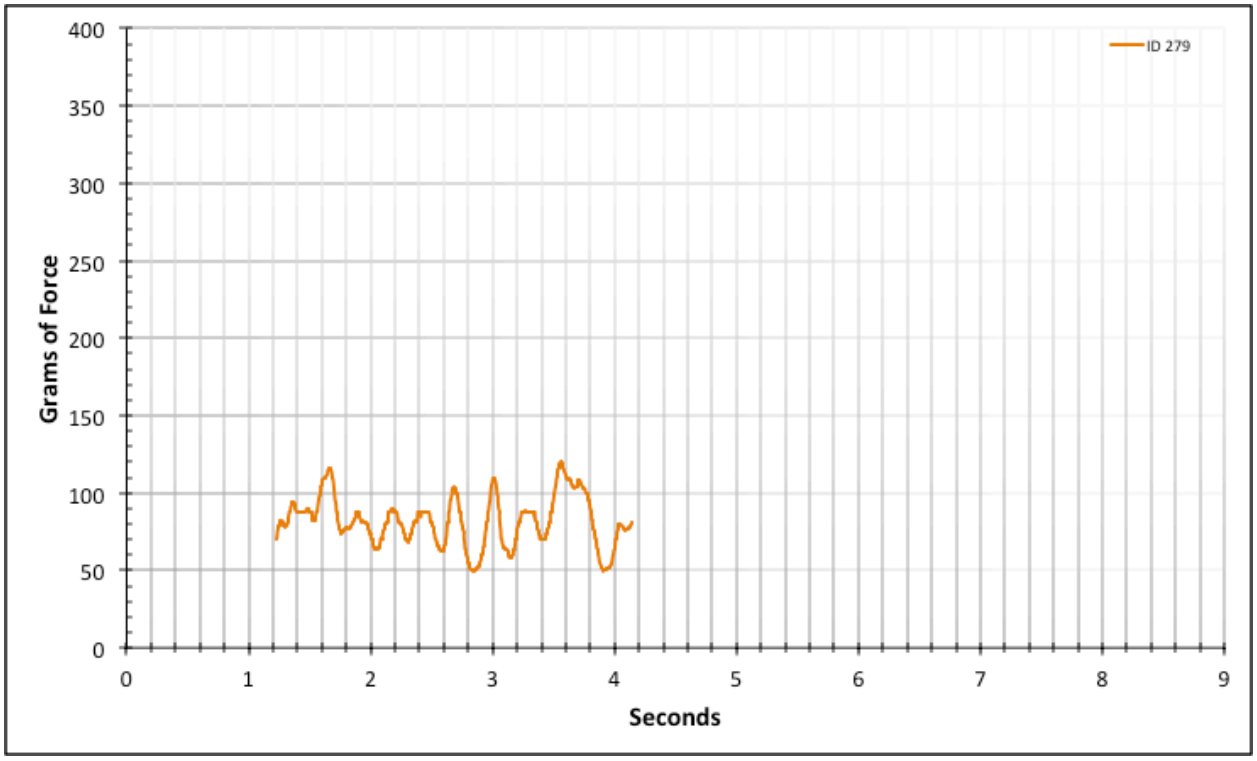

Figure A-6-398: Statistical Region Factory Baseline - Lubricated - ID 279 - #12, Bolt 3

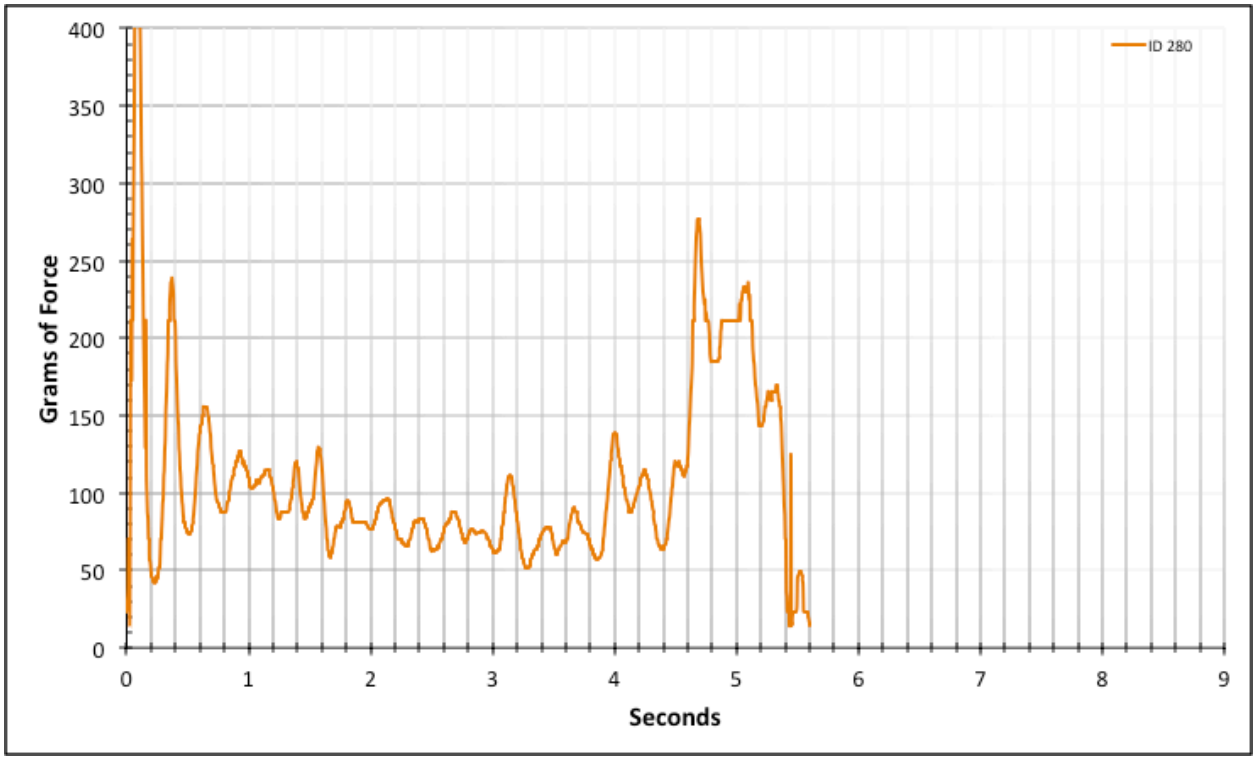

Figure A-6-399: Full Factory Baseline - Lubricated - ID 280 - #12, Bolt 3

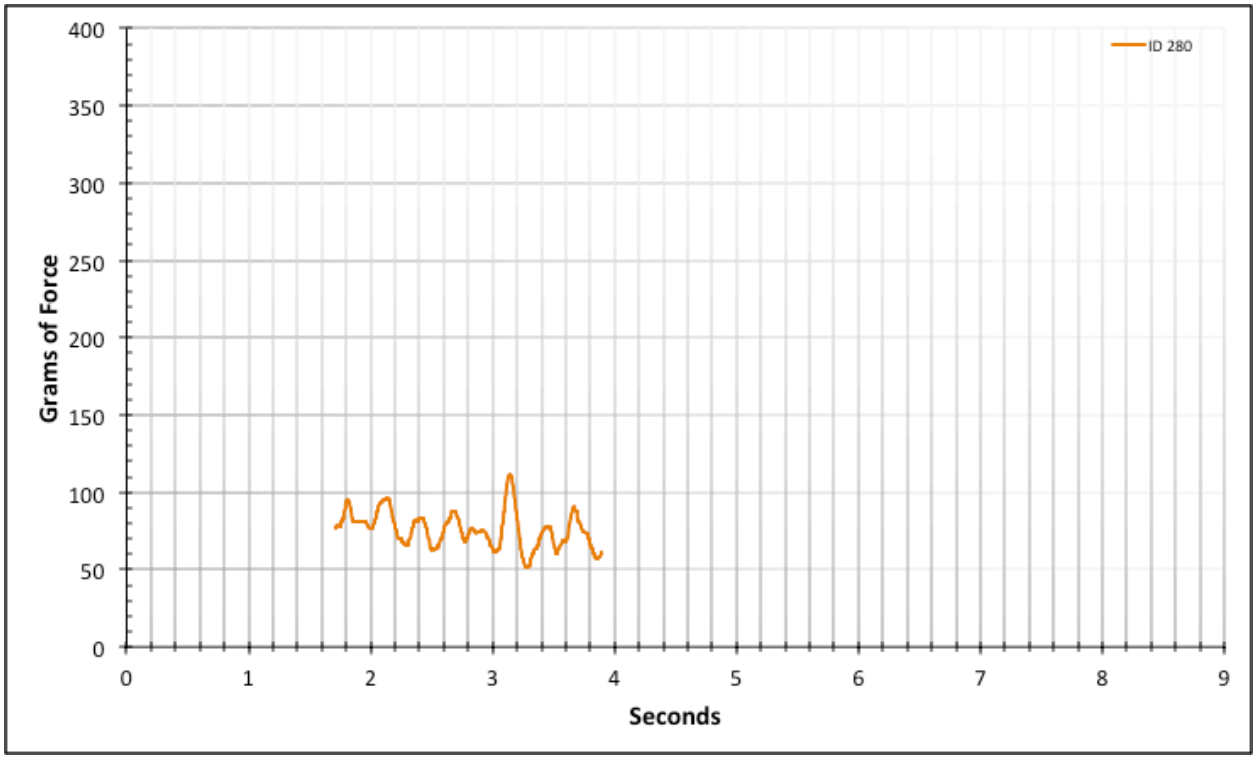

Figure A-6-400: Statistical Region Factory Baseline - Lubricated - ID 280 - #12, Bolt 3

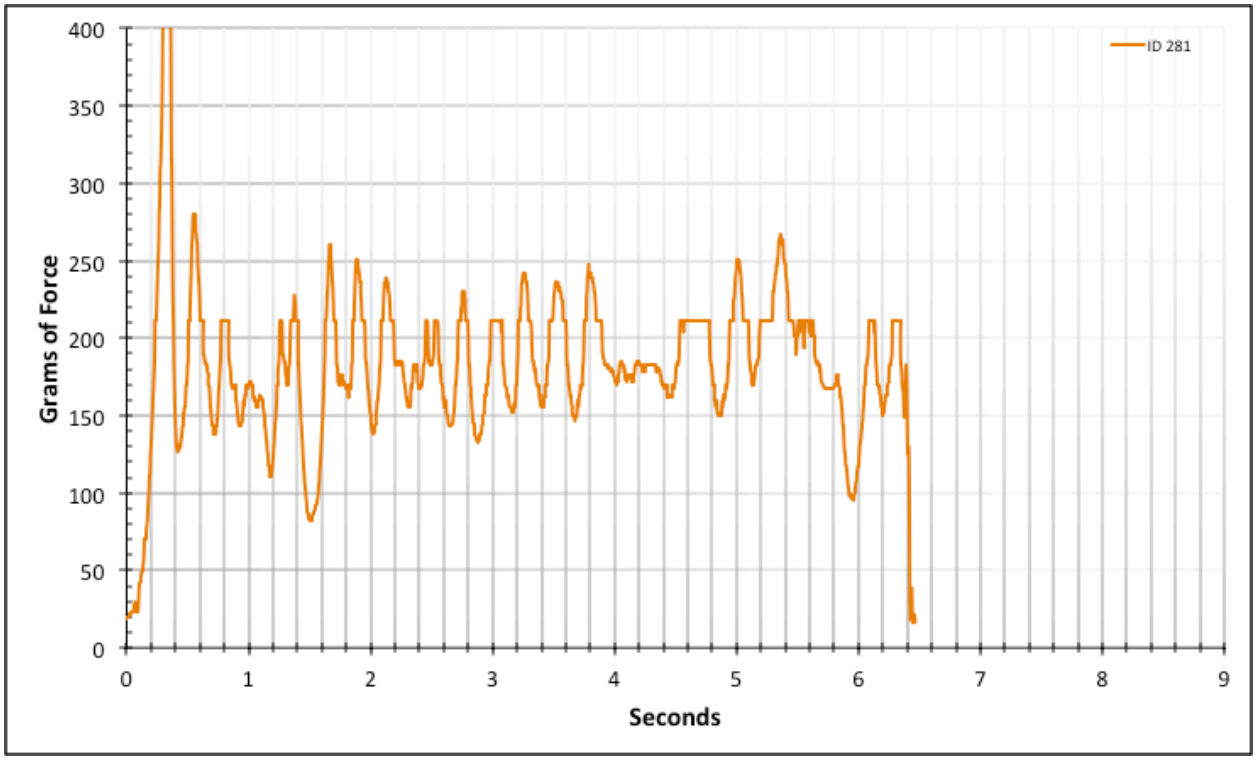

Figure A-6-401: Full Factory Baseline - Lubricated - ID 281 - #10, Bolt 1

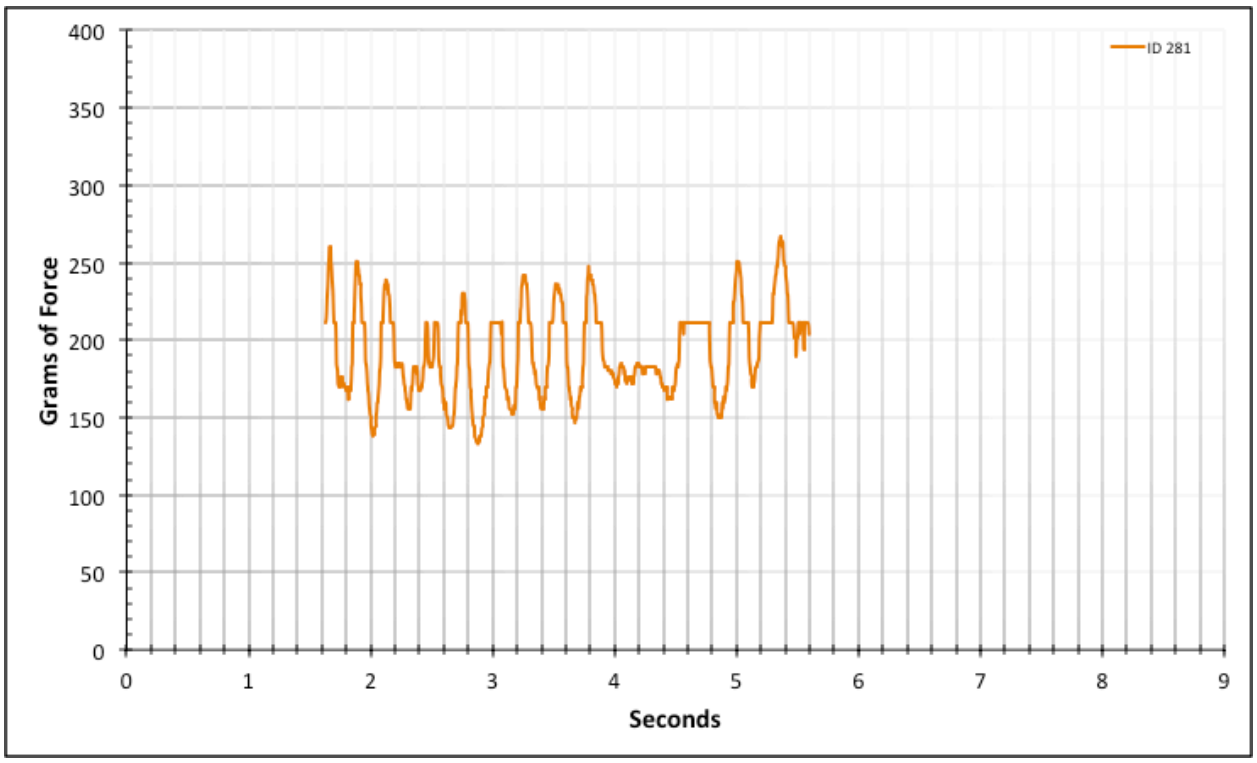

Figure A-6-402: Statistical Region Factory Baseline - Lubricated - ID 281 - #10, Bolt 1

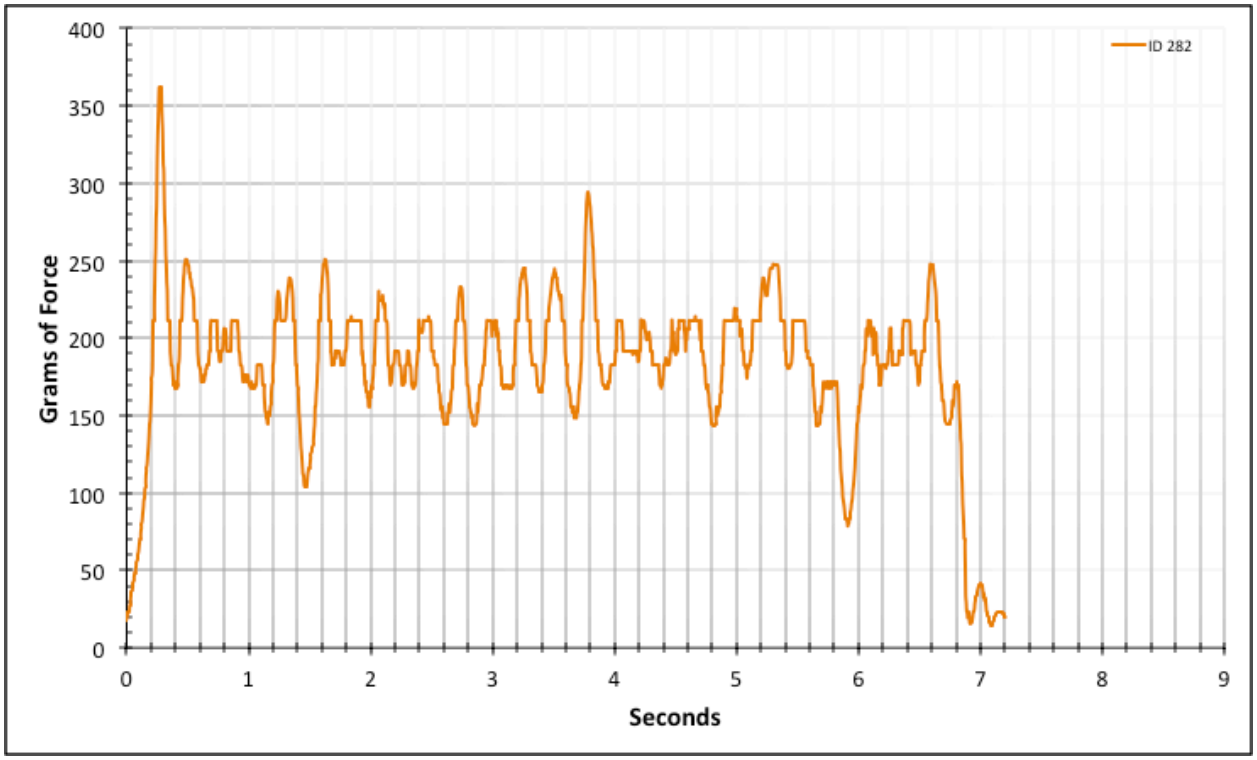

Figure A-6-403: Full Factory Baseline - Lubricated - ID 282 - #10, Bolt 1

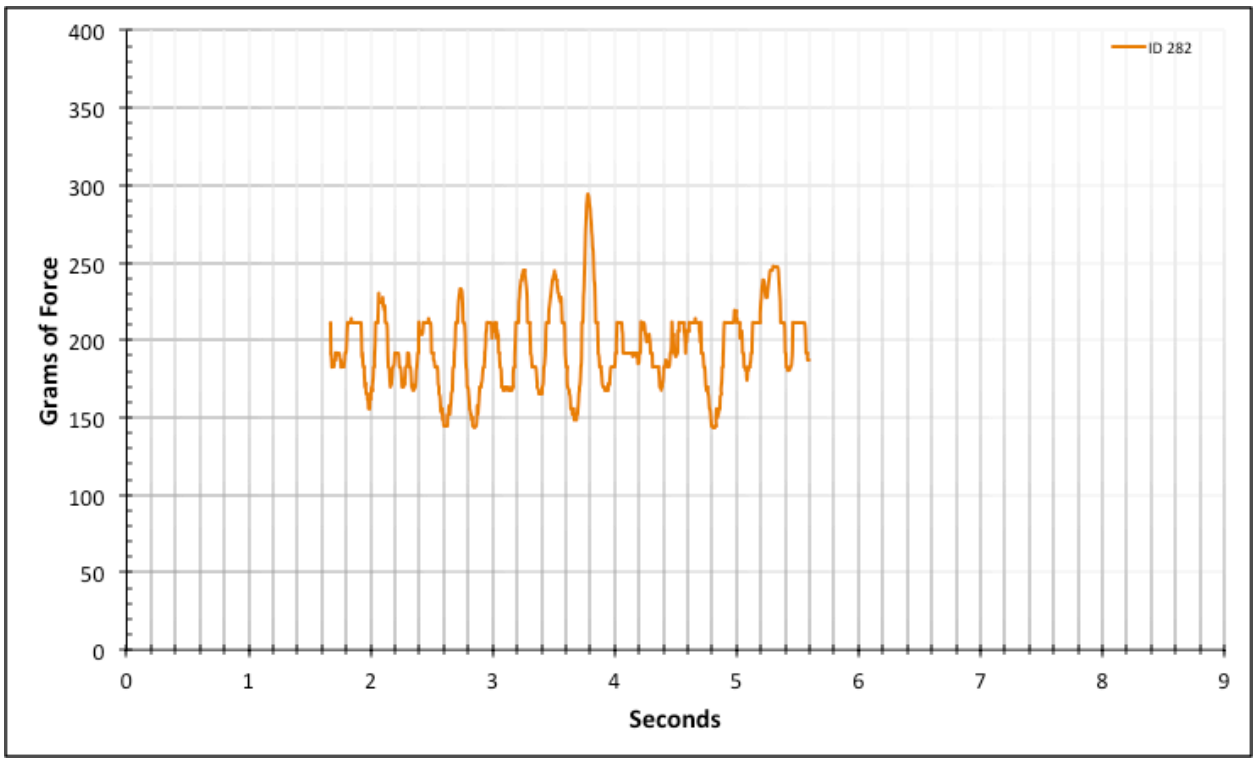

Figure A-6-404: Statistical Region Factory Baseline - Lubricated - ID 282 - #10, Bolt 1

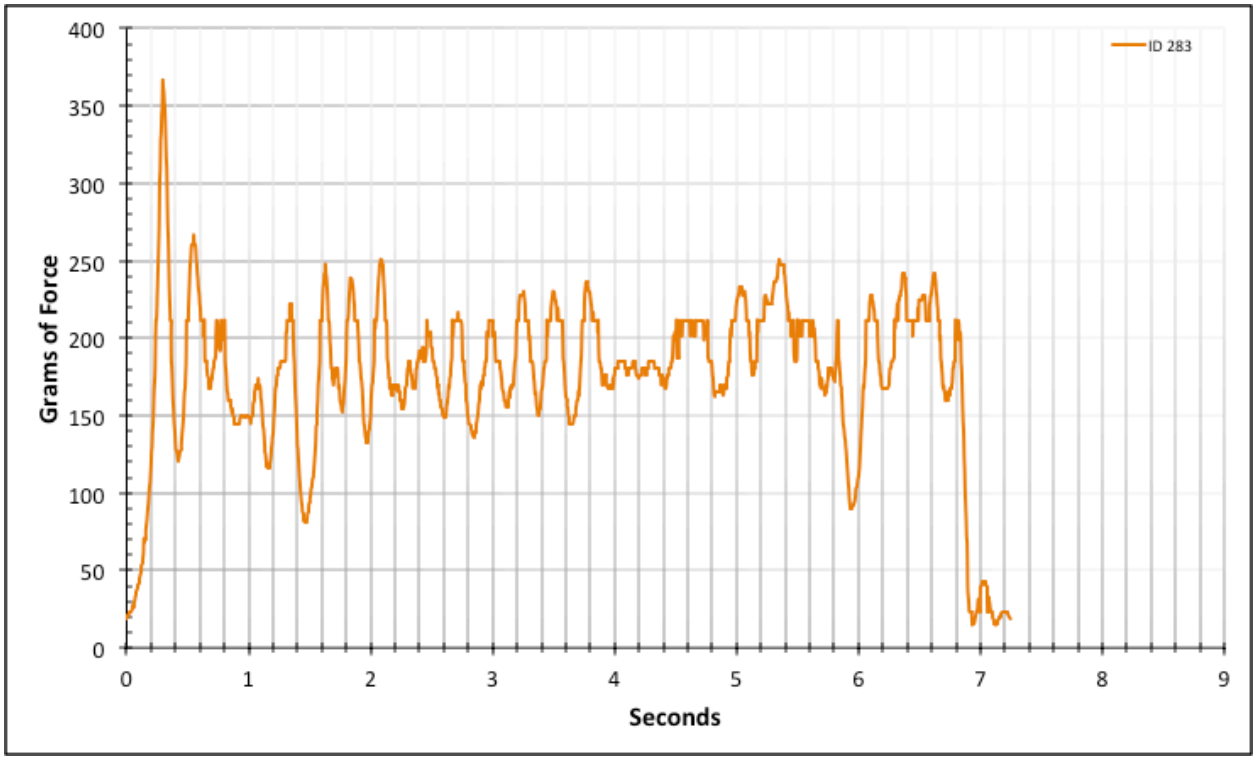

Figure A-6-405: Full Factory Baseline - Lubricated - ID 283 - #10, Bolt 1

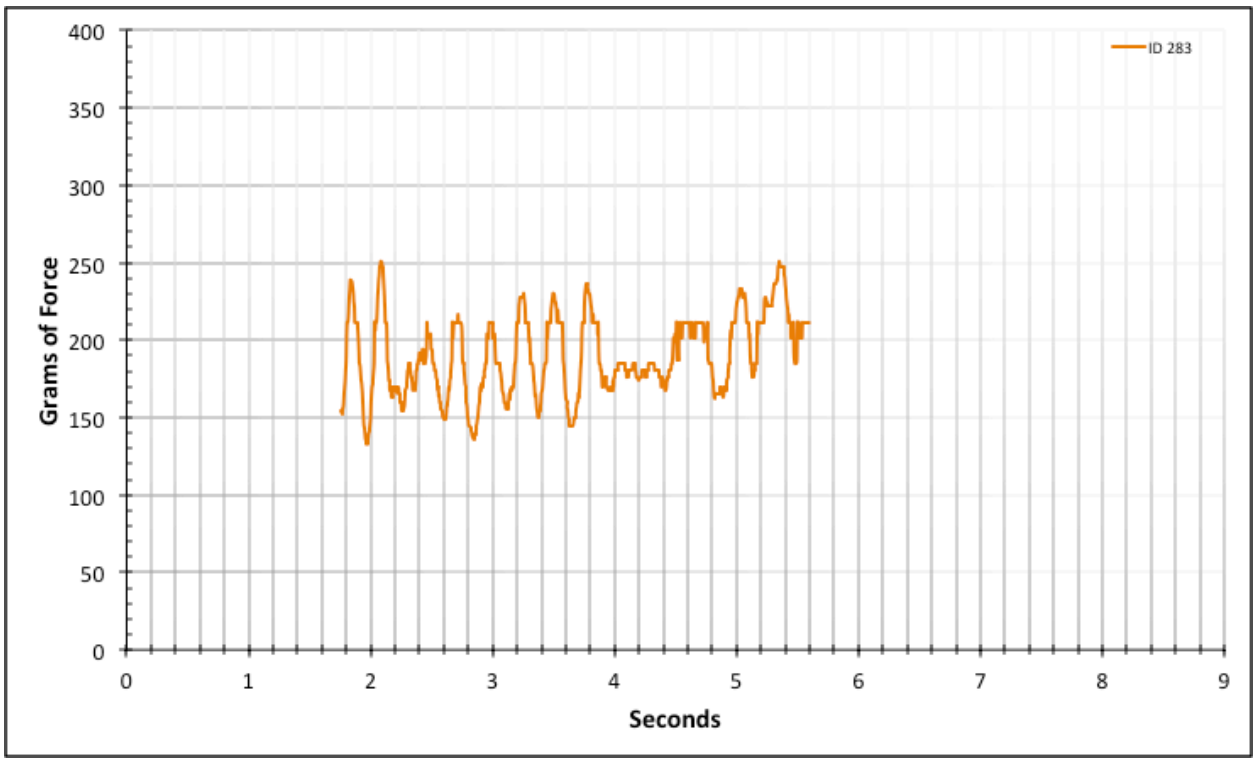

Figure A-6-406: Statistical Region Factory Baseline - Lubricated - ID 283 - #10, Bolt 1

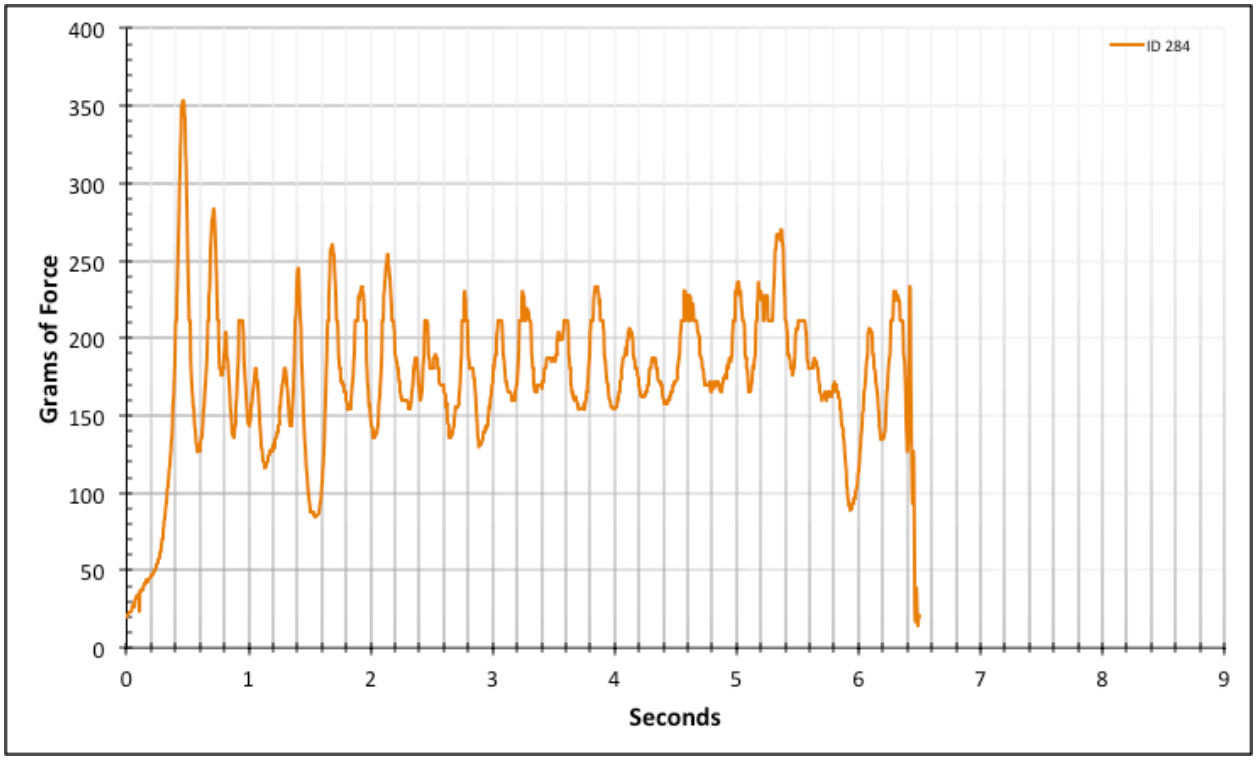

Figure A-6-407: Full Factory Baseline - Lubricated - ID 284 - #10, Bolt 1

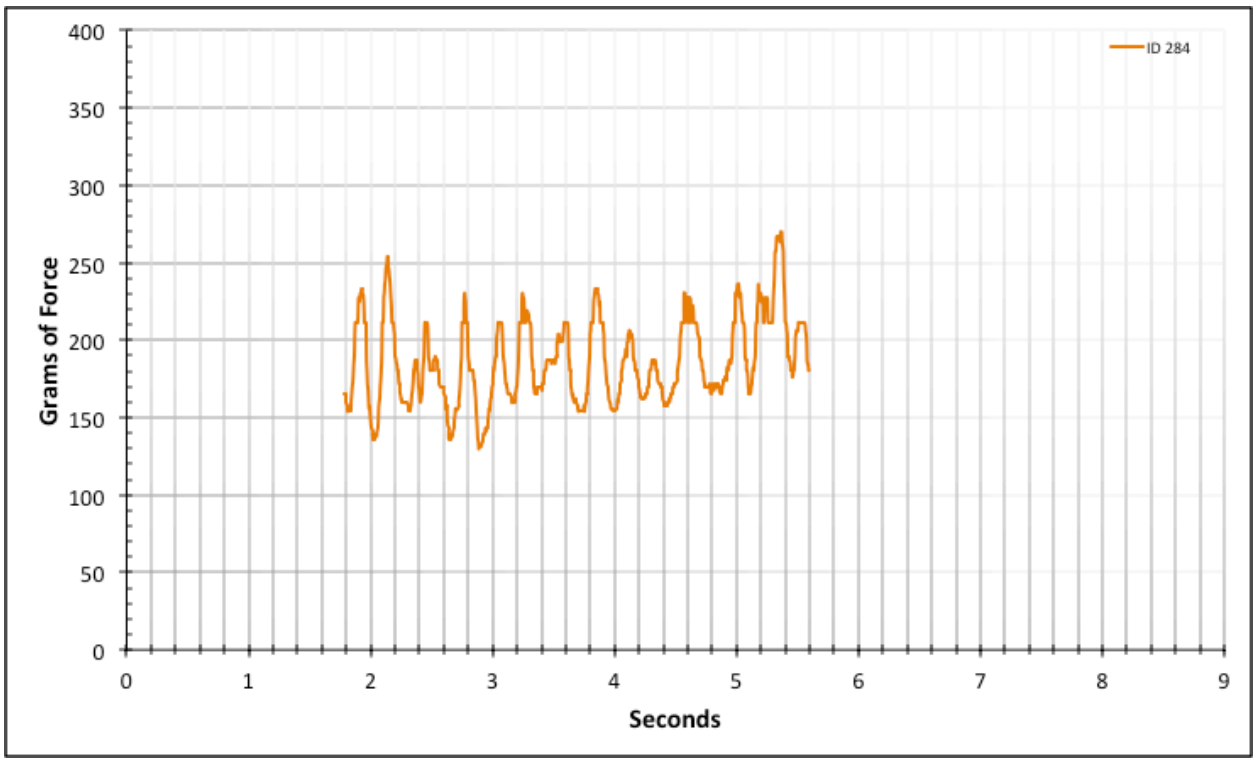

Figure A-6-408: Statistical Region Factory Baseline - Lubricated - ID 284 - #10, Bolt 1

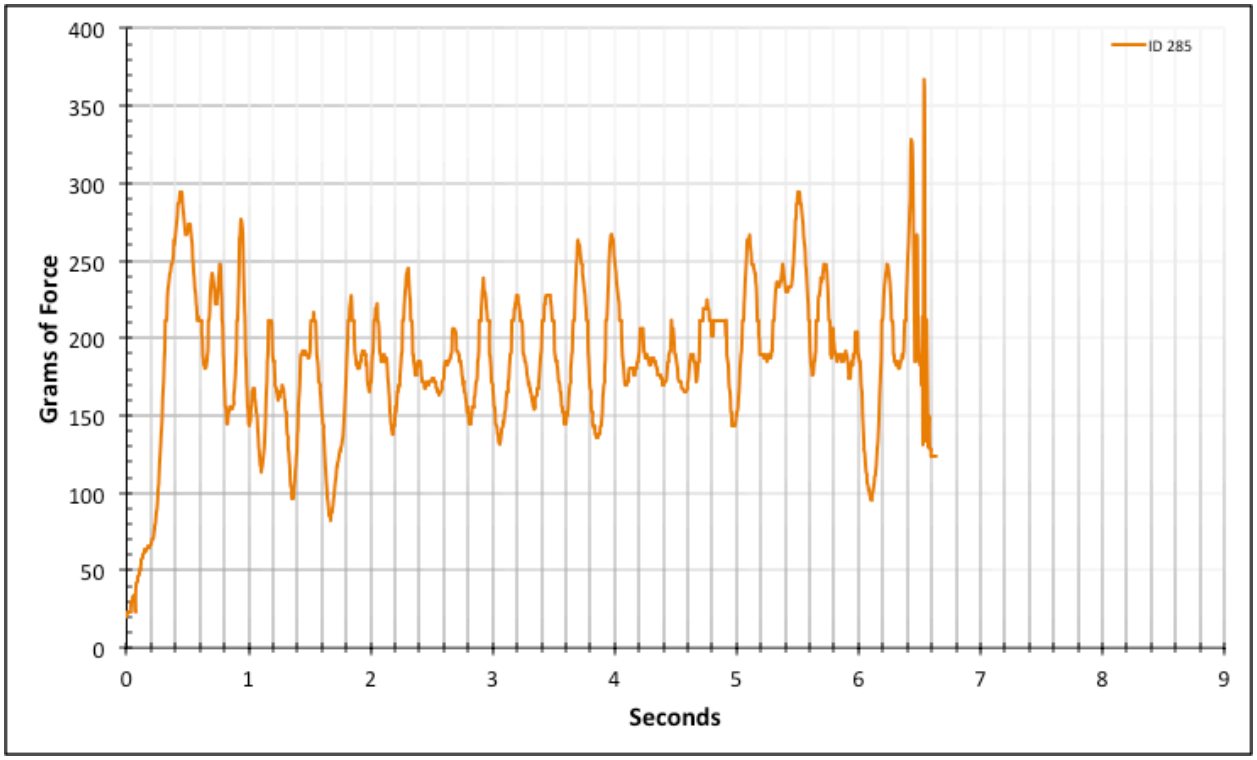

Figure A-6-409: Full Factory Baseline - Lubricated - ID 285 - #10, Bolt 1

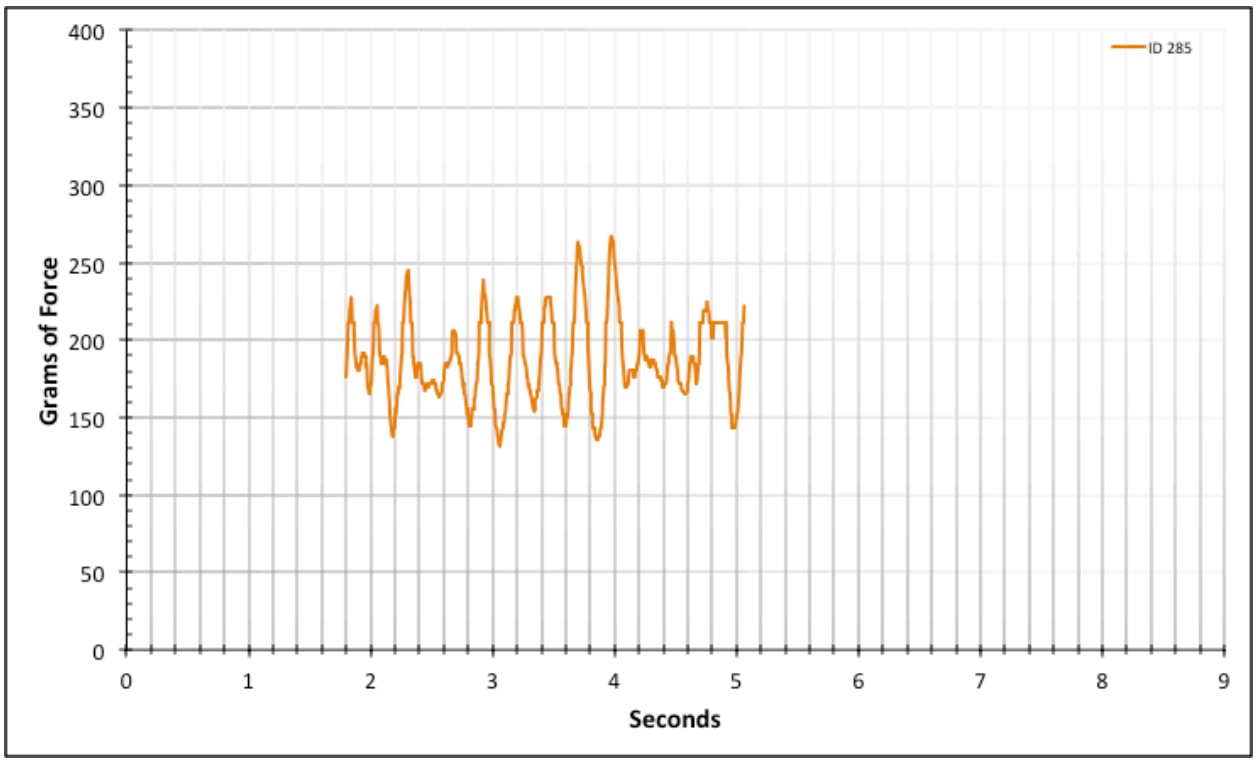

Figure A-6-410: Statistical Region Factory Baseline - Lubricated - ID 285 - #10, Bolt 1

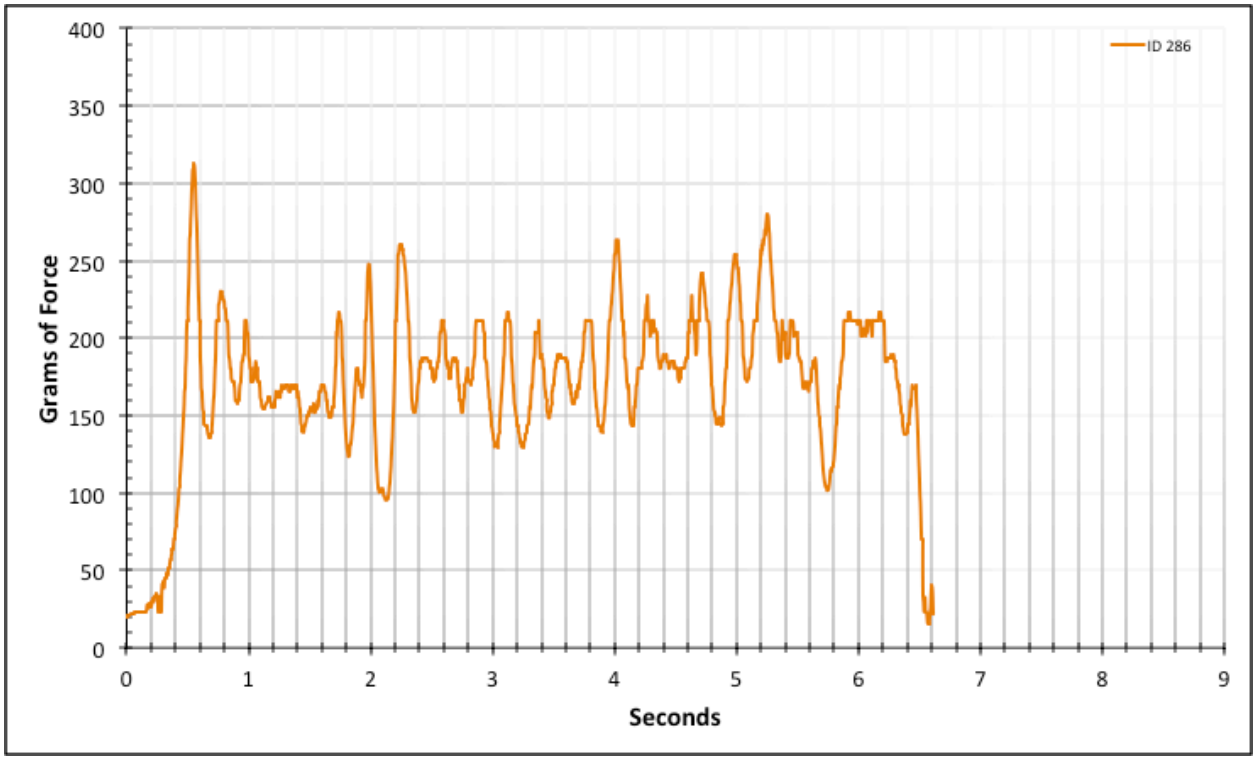

Figure A-6-411: Full Factory Baseline - Lubricated - ID 286 - #10, Bolt 2

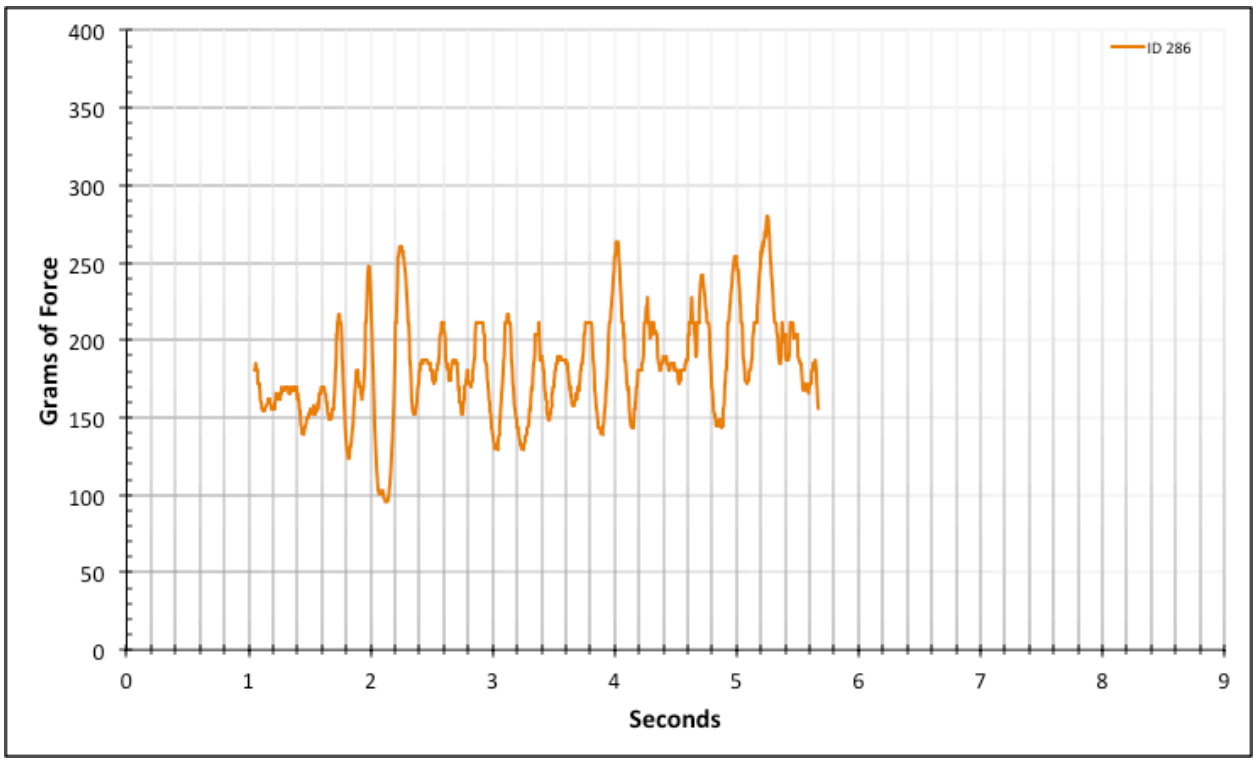

Figure A-6-412: Statistical Region Factory Baseline - Lubricated - ID 286 - #10, Bolt 2

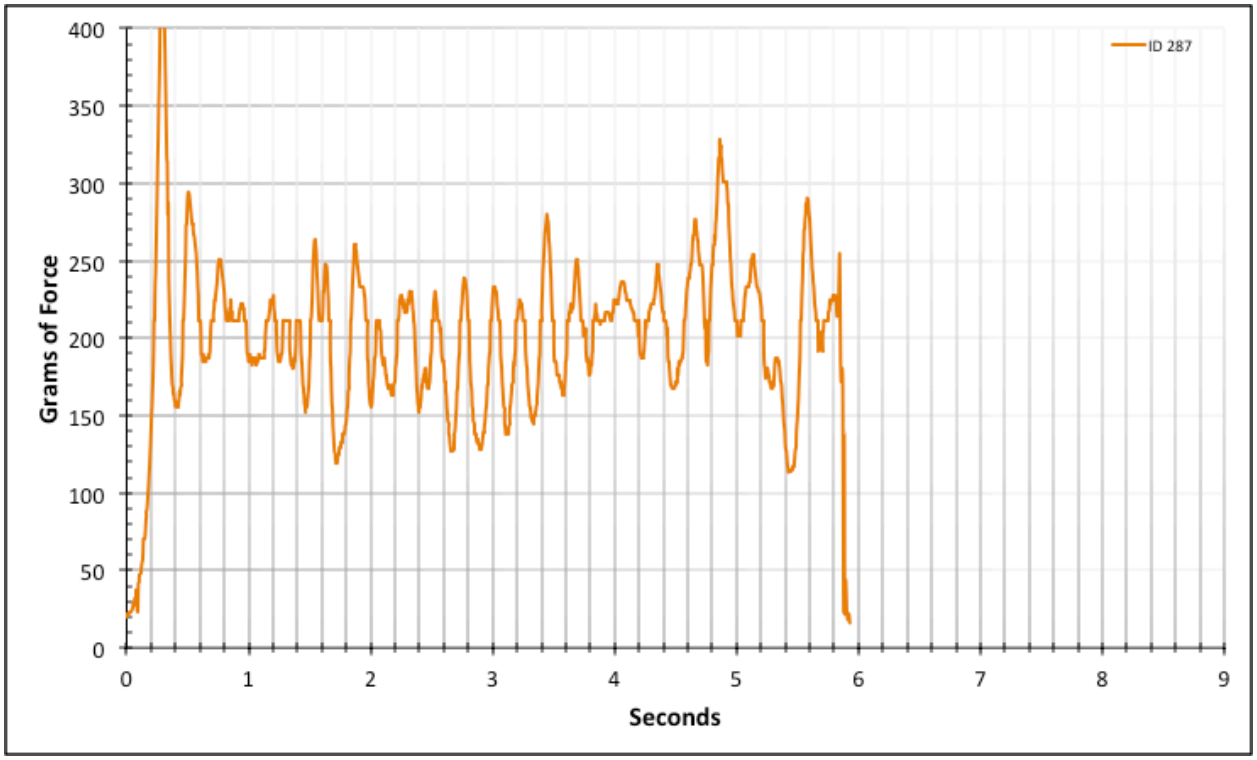

Figure A-6-413: Full Factory Baseline - Lubricated - ID 287 - #10, Bolt 2

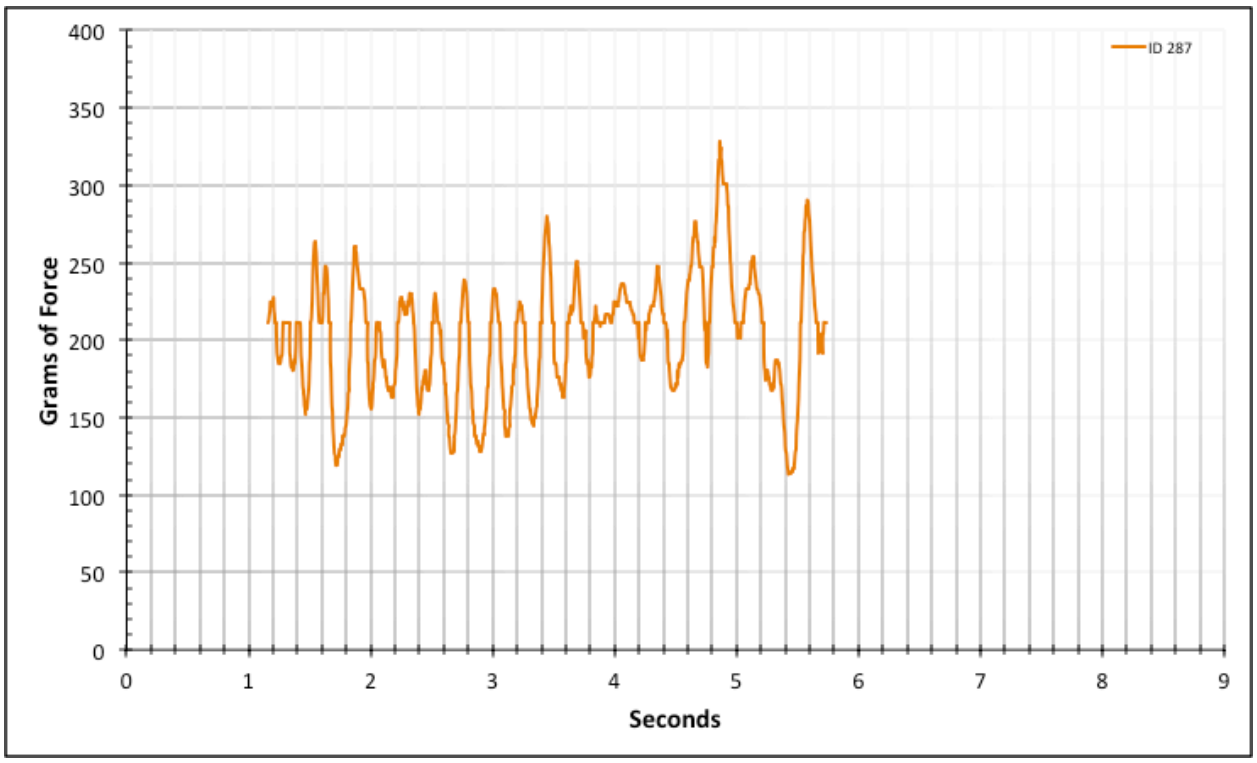

Figure A-6-414: Statistical Region Factory Baseline - Lubricated - ID 287 - #10, Bolt 2

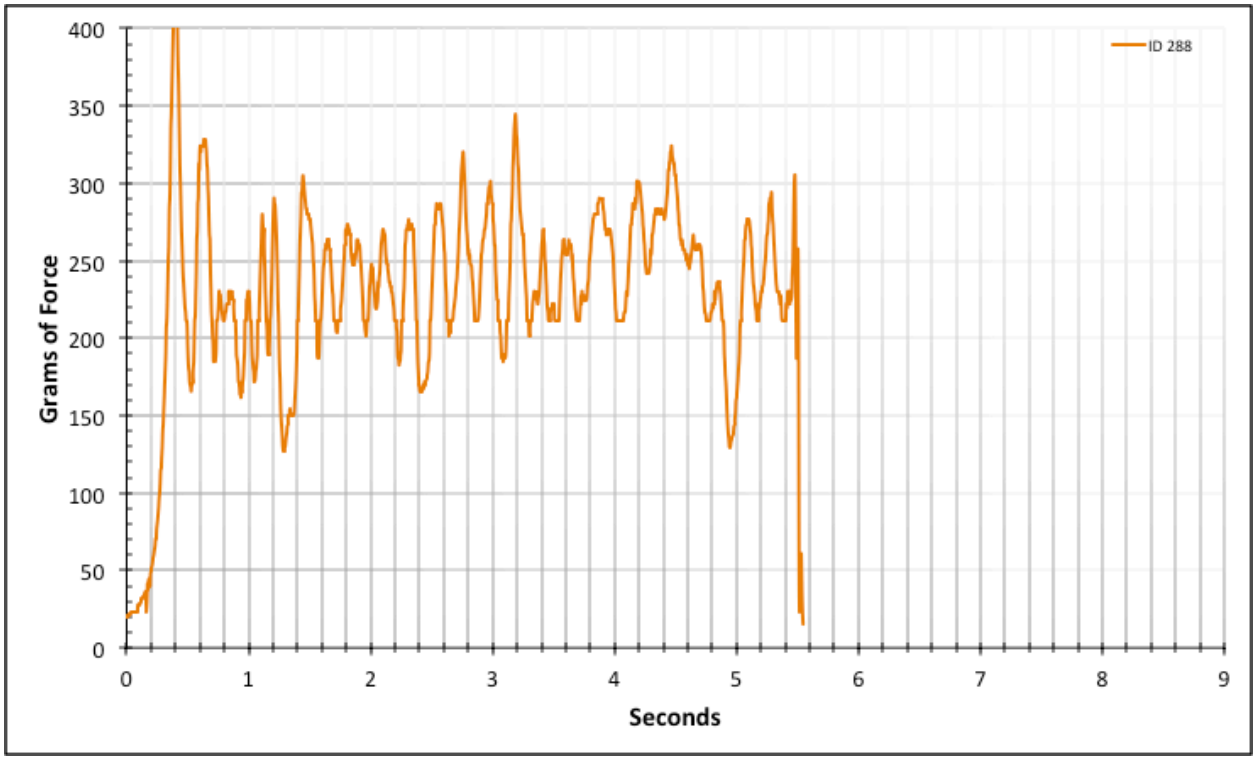

Figure A-6-415: Full Factory Baseline - Lubricated - ID 288 - #10, Bolt 2

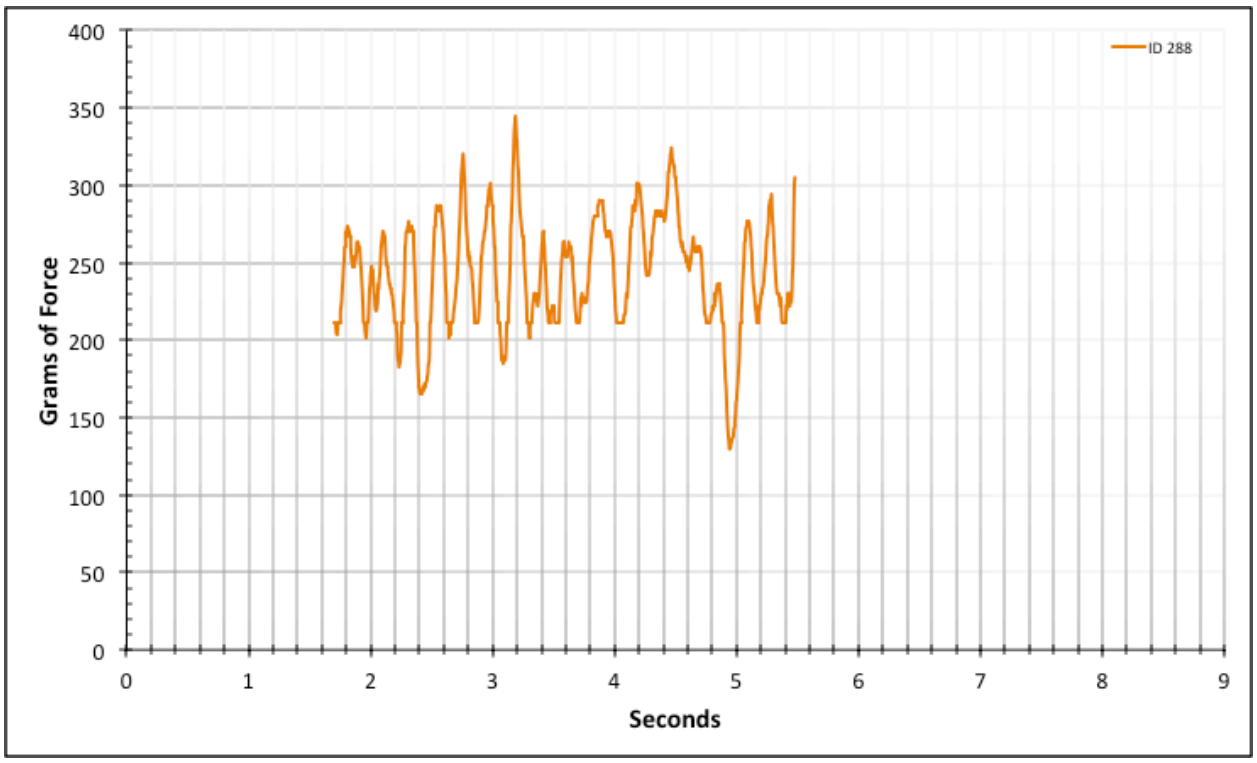

Figure A-6-416: Statistical Region Factory Baseline - Lubricated - ID 288 - #10, Bolt 2

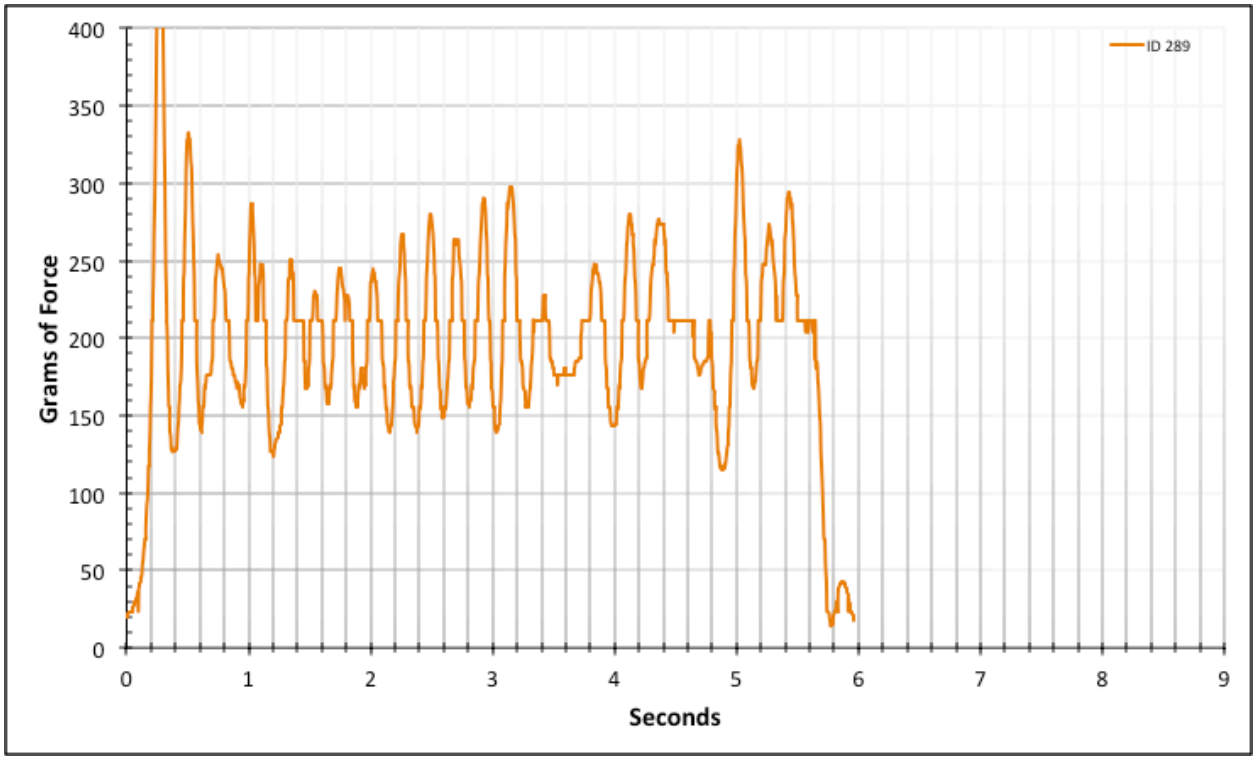

Figure A-6-417: Full Factory Baseline - Lubricated - ID 289 - #10, Bolt 2

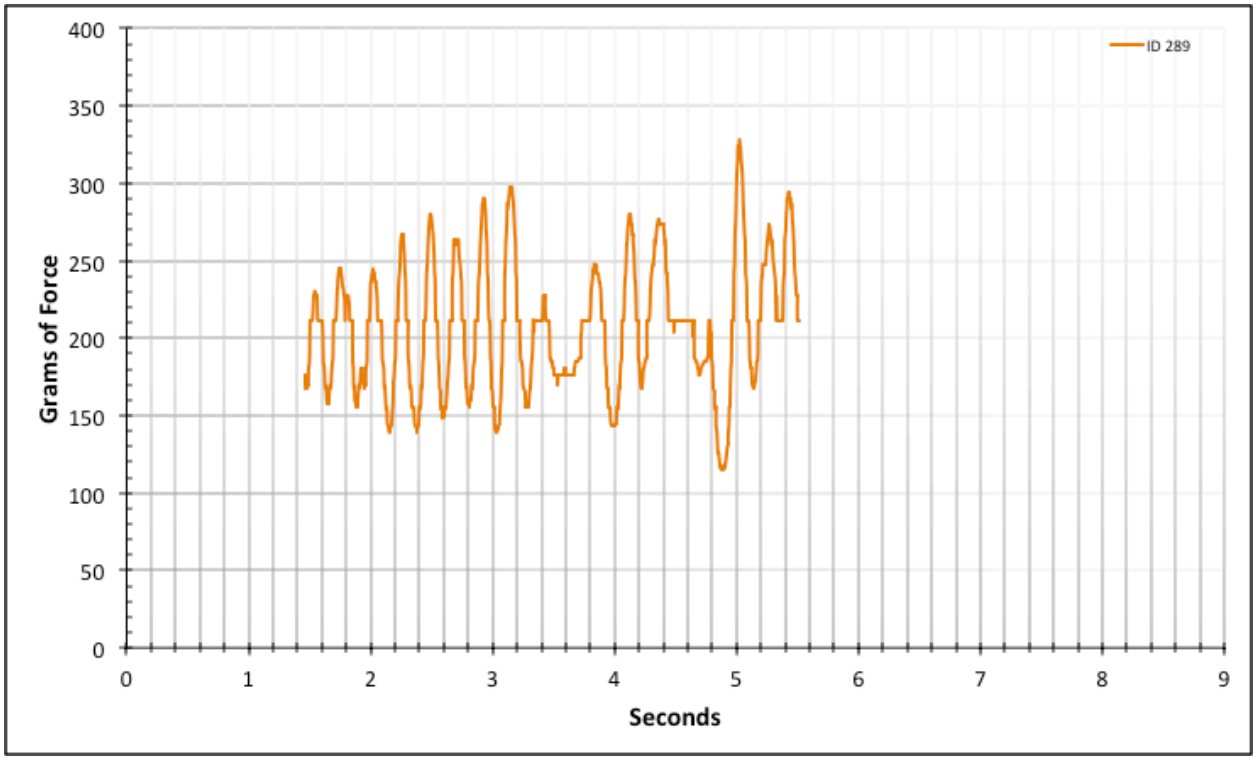

Figure A-6-418: Statistical Region Factory Baseline - Lubricated - ID 289 - #10, Bolt 2

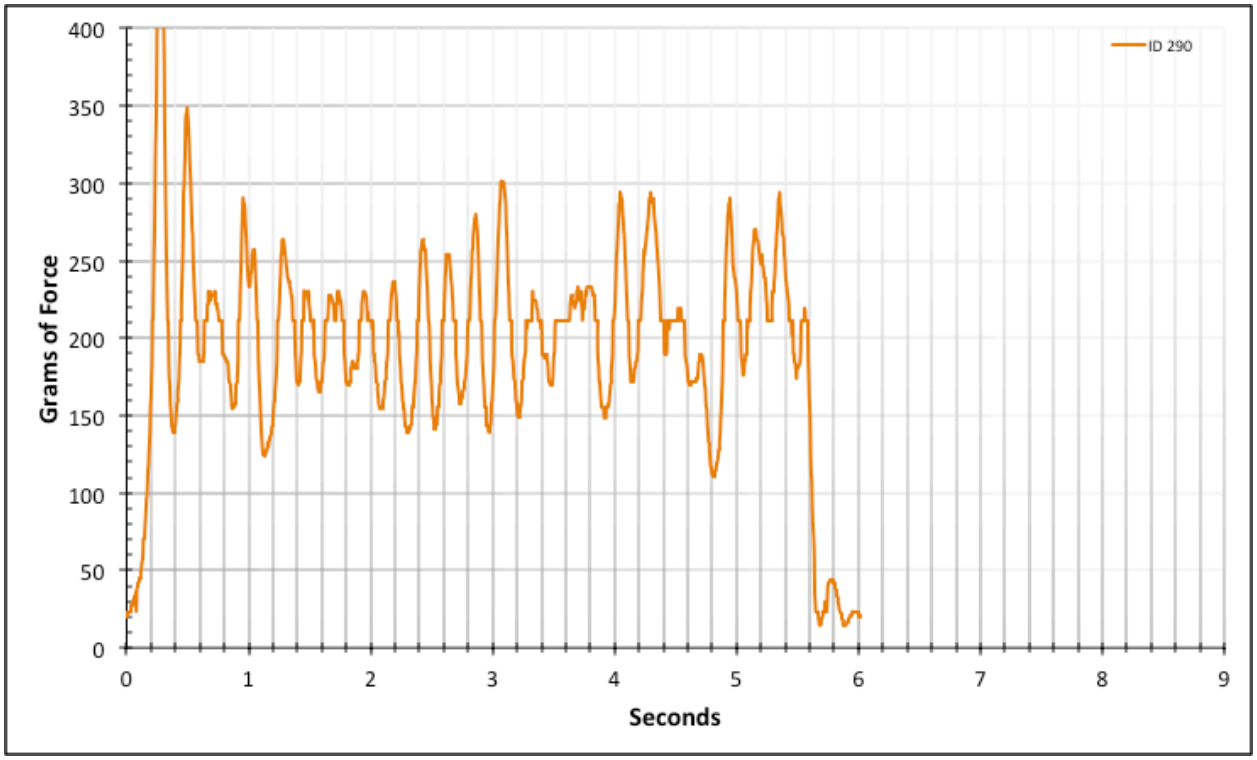

Figure A-6-419: Full Factory Baseline - Lubricated - ID 290 - #10, Bolt 2

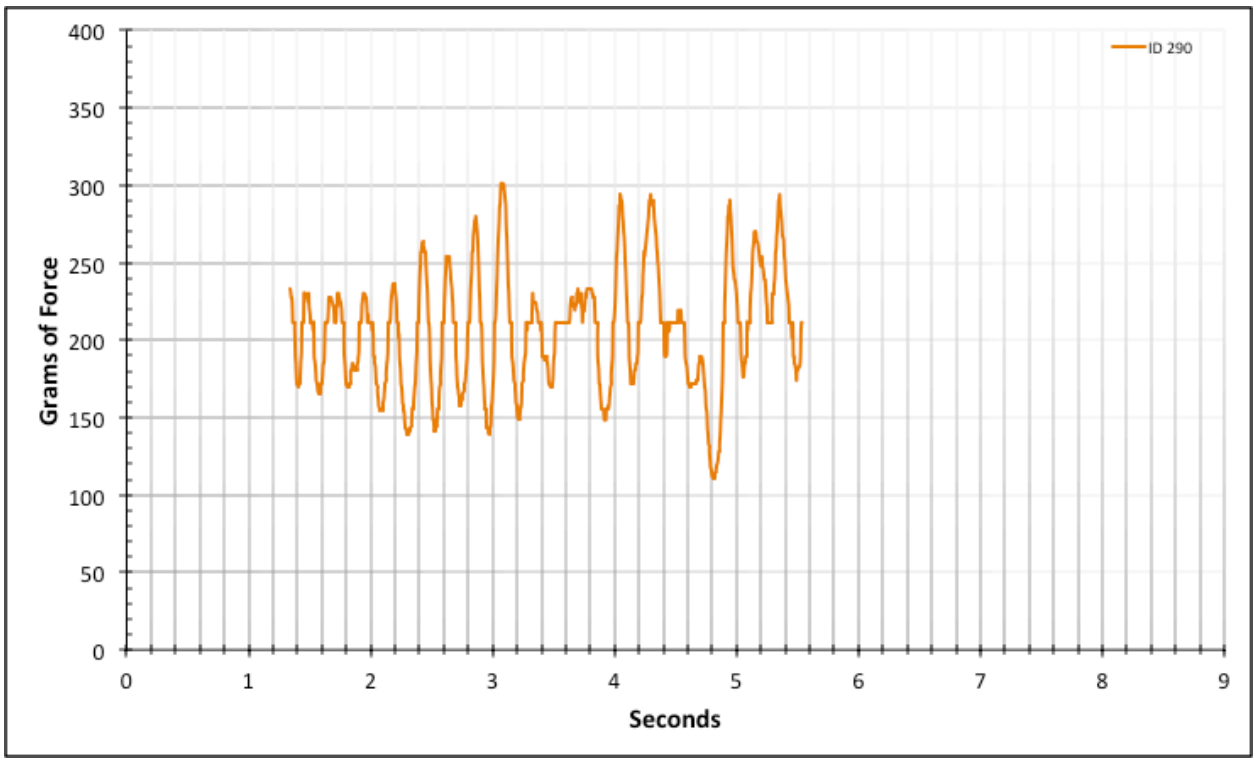

Figure A-6-420: Statistical Region Factory Baseline - Lubricated - ID 290 - #10, Bolt 2

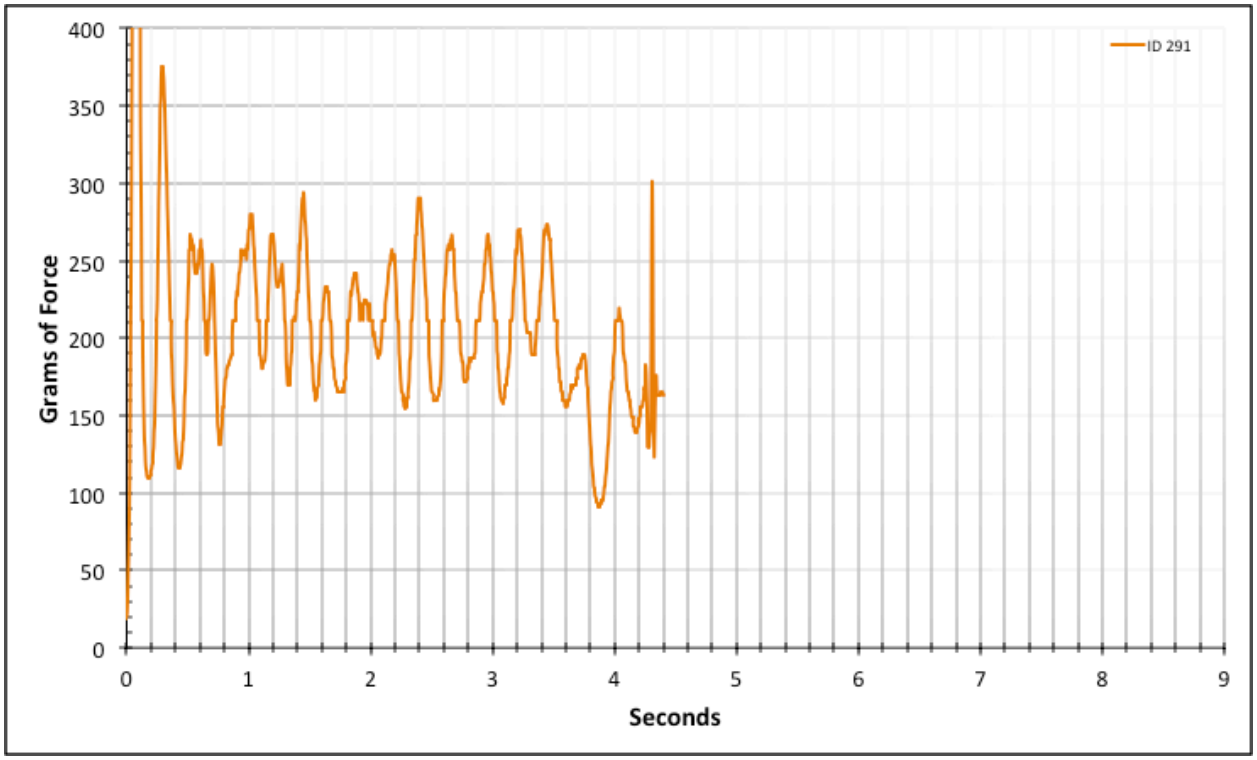

Figure A-6-421: Full Factory Baseline - Lubricated - ID 291 - #10, Bolt 3

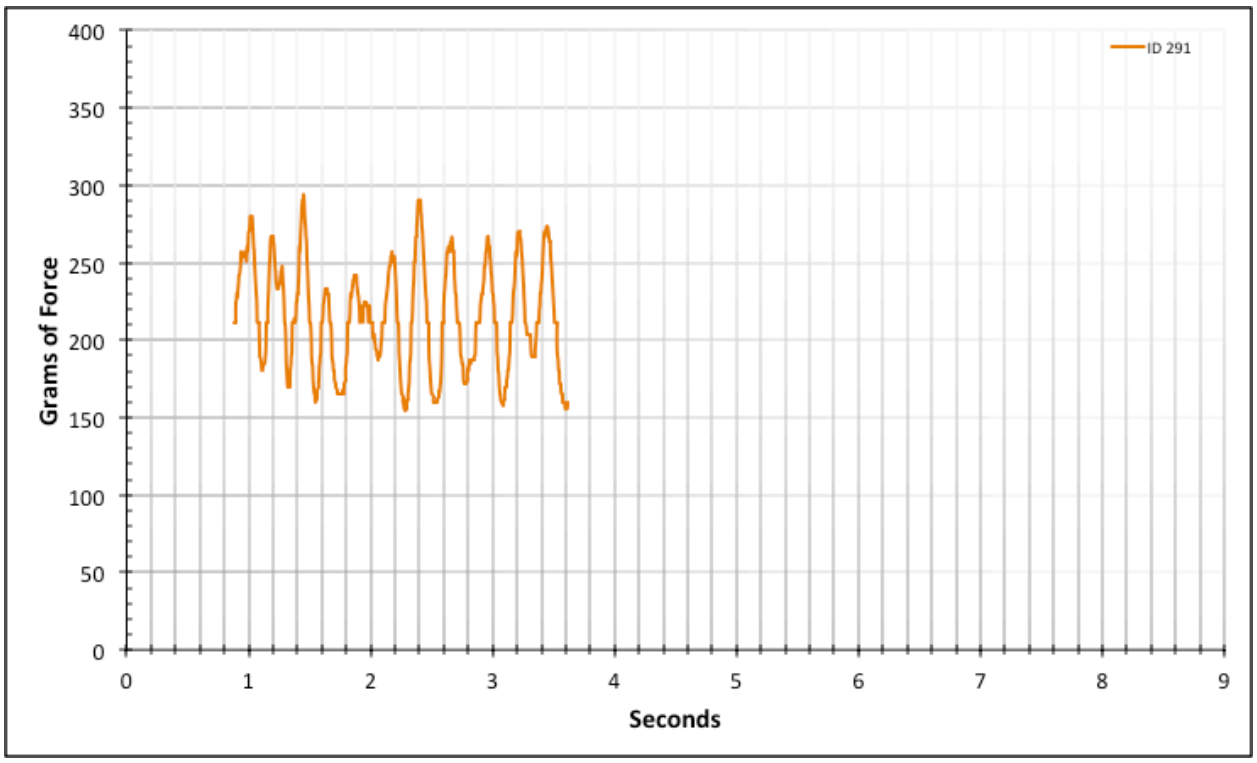

Figure A-6-422: Statistical Region Factory Baseline - Lubricated - ID 291 - #10, Bolt 3

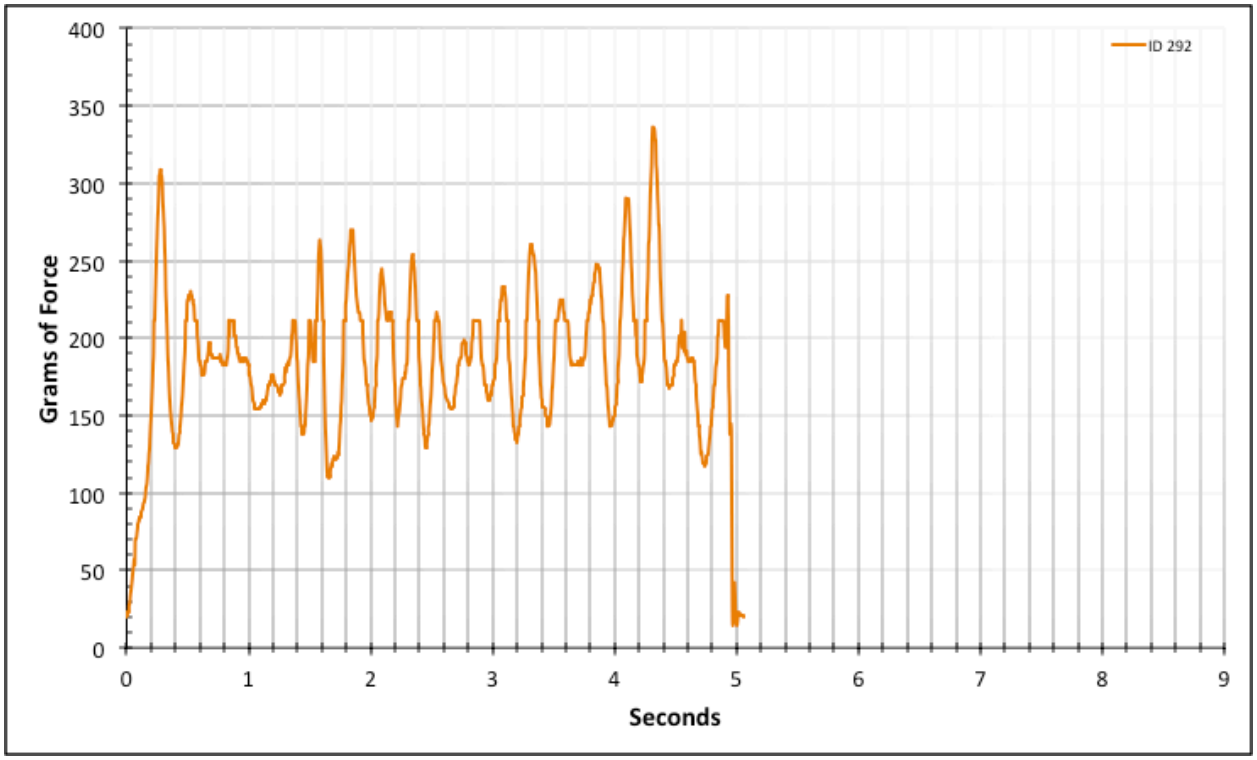

Figure A-6-423: Full Factory Baseline - Lubricated - ID 292 - #10, Bolt 3

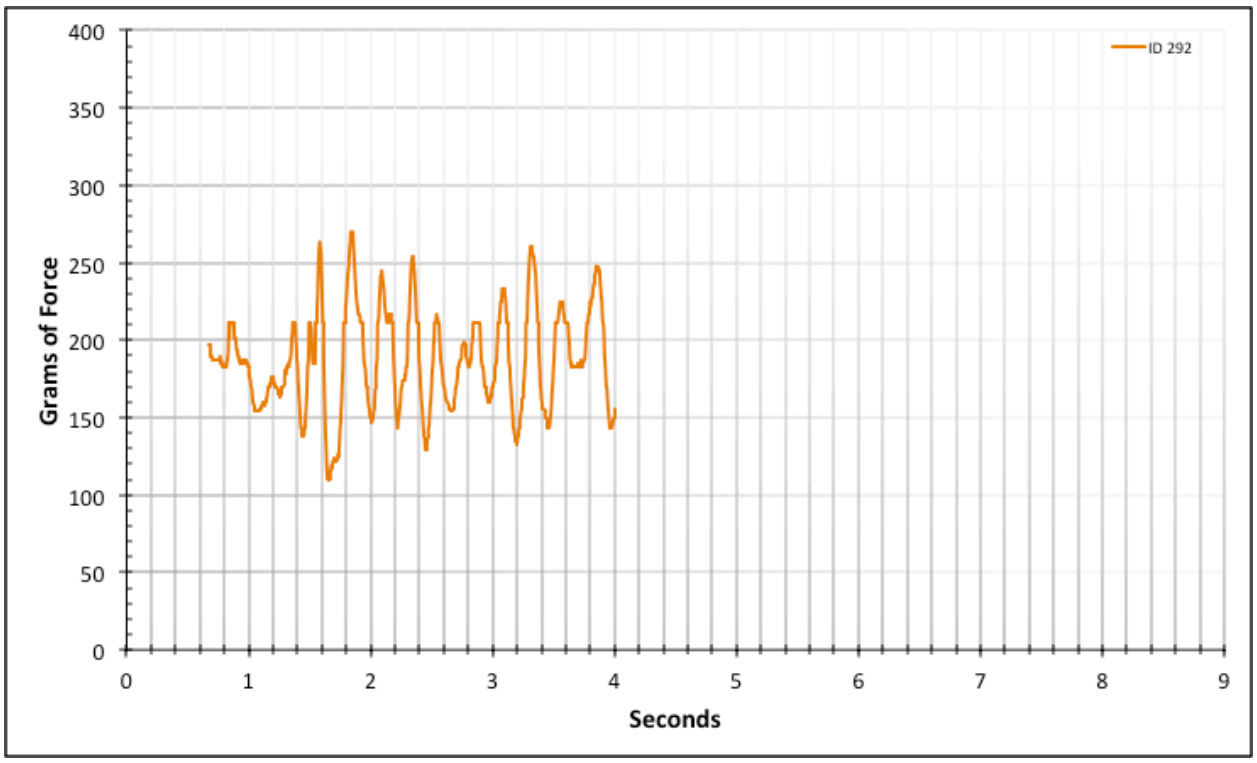

Figure A-6-424: Statistical Region Factory Baseline - Lubricated - ID 292 - #10, Bolt 3

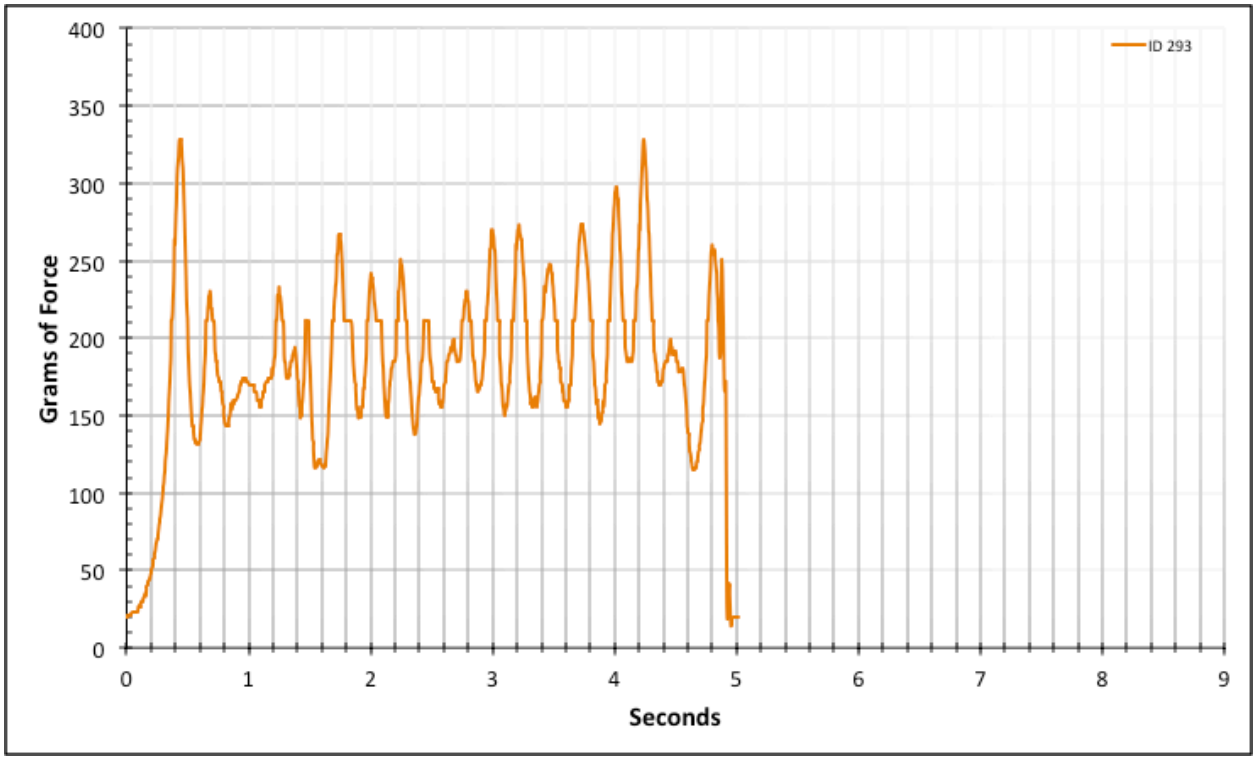

Figure A-6-425: Full Factory Baseline - Lubricated - ID 293 - #10, Bolt 3

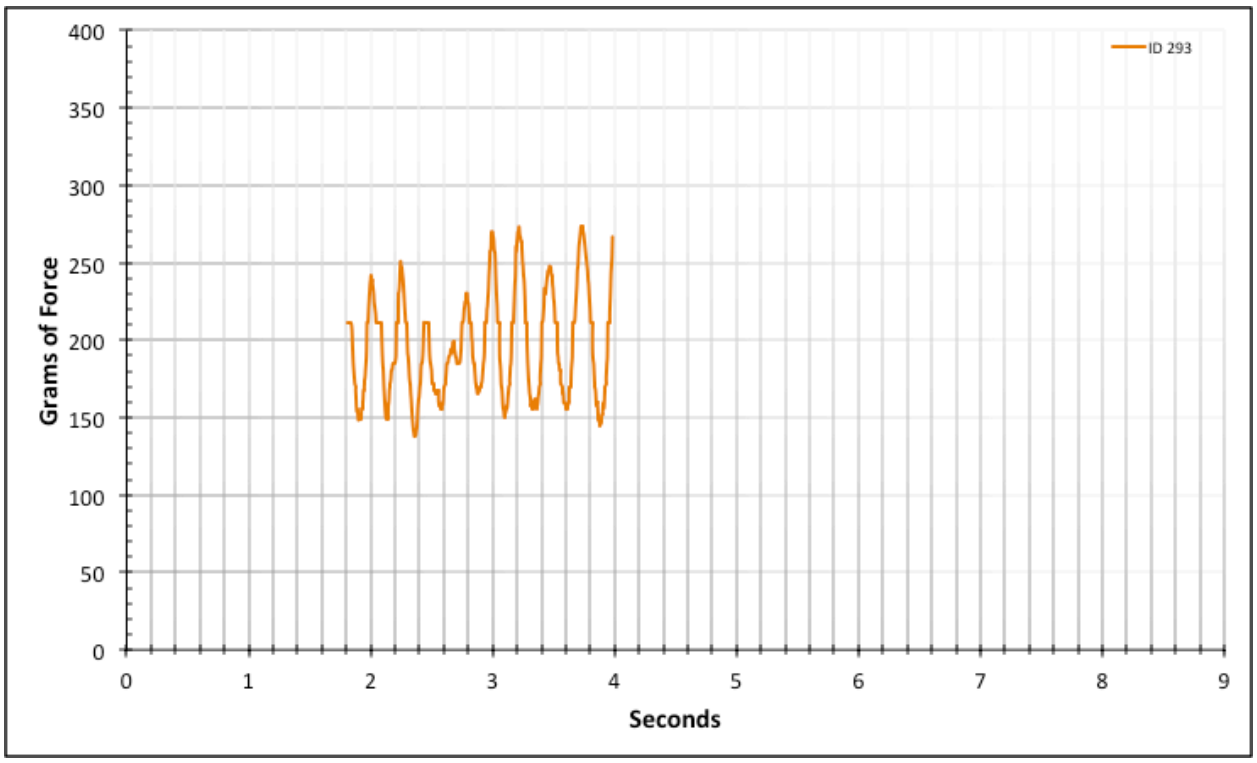

Figure A-6-426: Statistical Region Factory Baseline - Lubricated - ID 293 - #10, Bolt 3

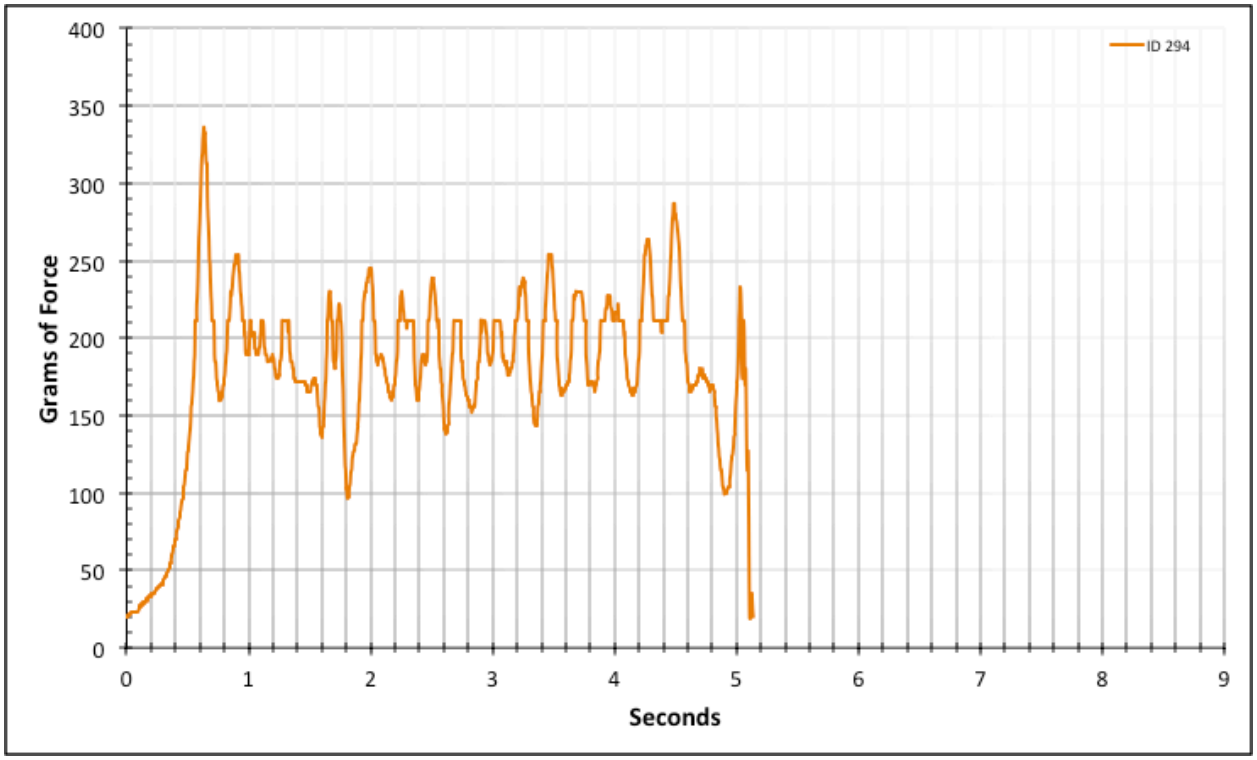

Figure A-6-427: Full Factory Baseline - Lubricated - ID 294 - #10, Bolt 3

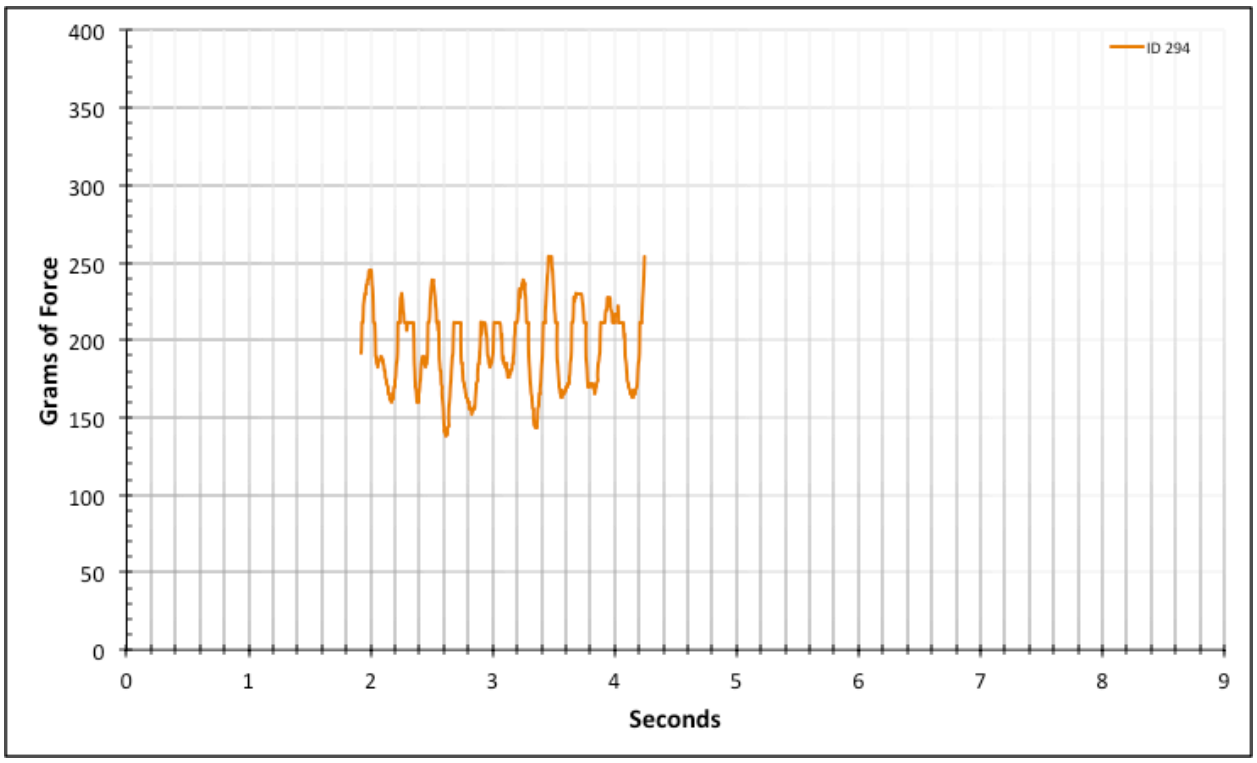

Figure A-6-428: Statistical Region Factory Baseline - Lubricated - ID 294 - #10, Bolt 3

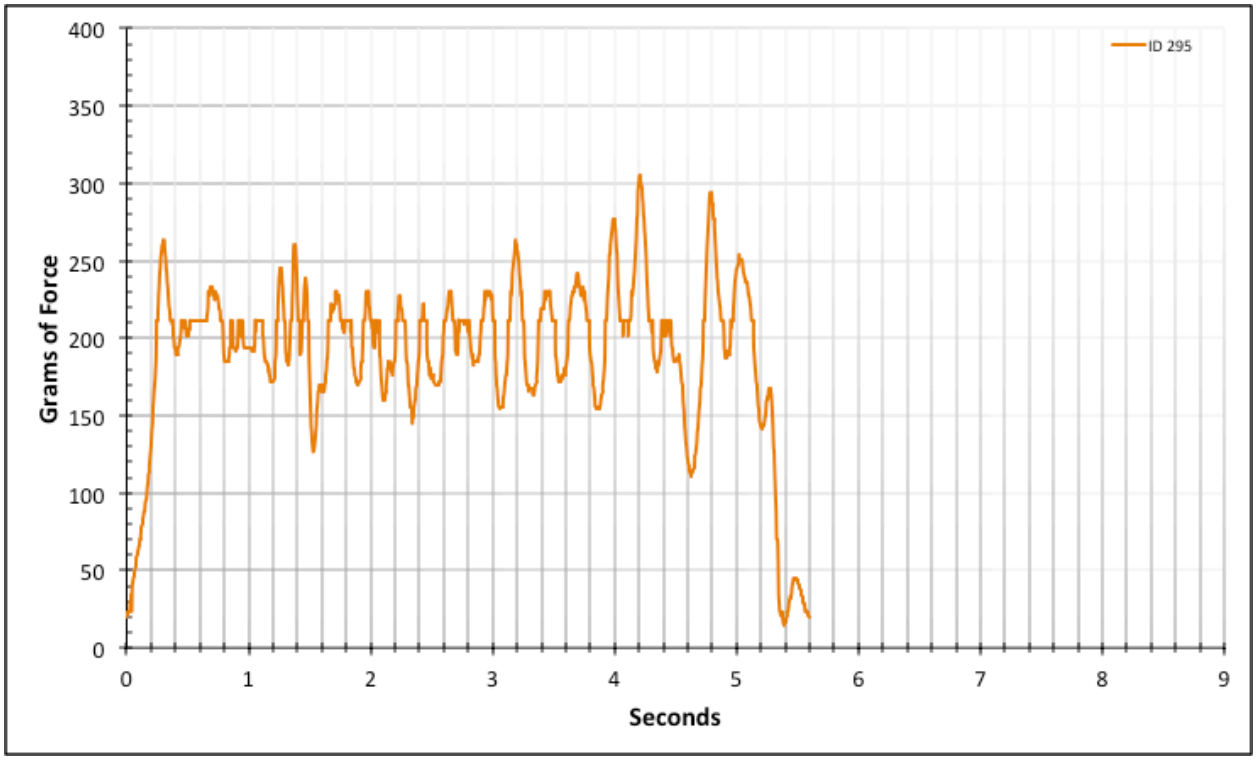

Figure A-6-429: Full Factory Baseline - Lubricated - ID 295 - #10, Bolt 3

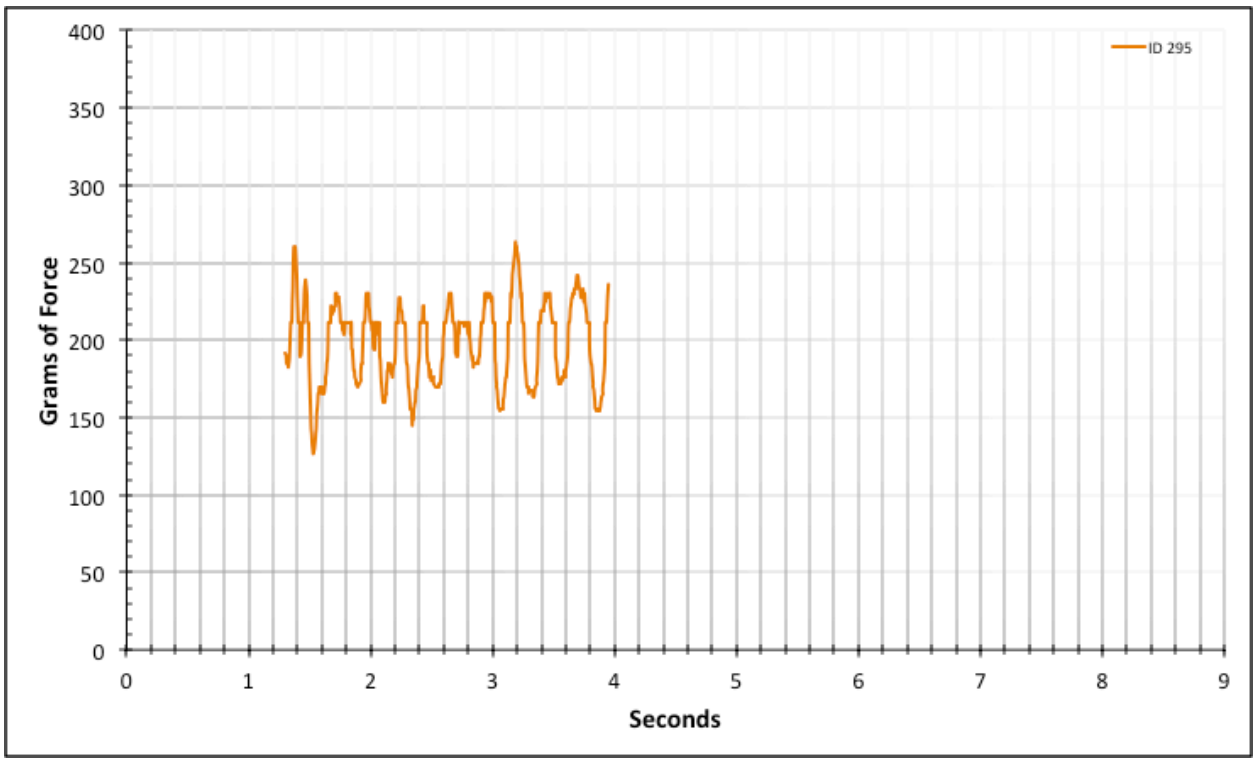

Figure A-6-430: Statistical Region Factory Baseline - Lubricated - ID 295 - #10, Bolt 3

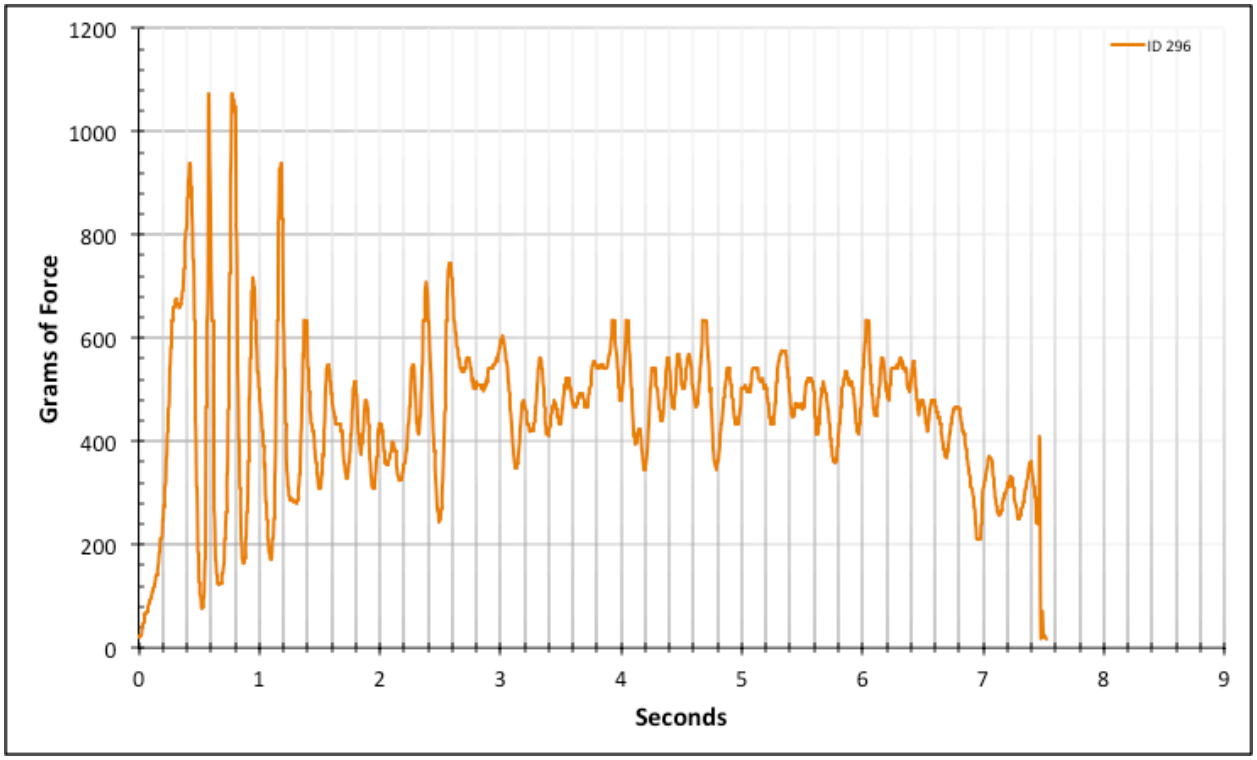

Figure A-6-431: Full Factory Baseline - Lubricated - ID 296 - #8, Bolt 1

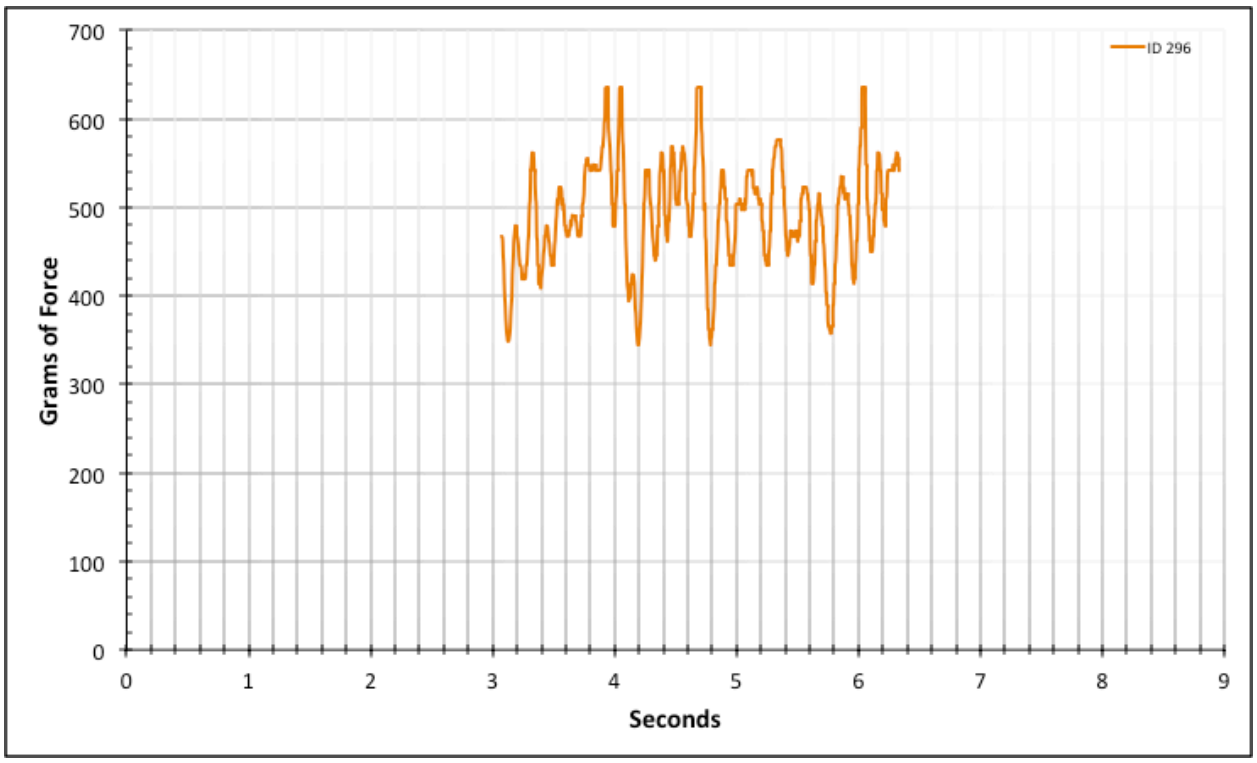

Figure A-6-432: Statistical Region Factory Baseline - Lubricated - ID 296 - #8, Bolt 1

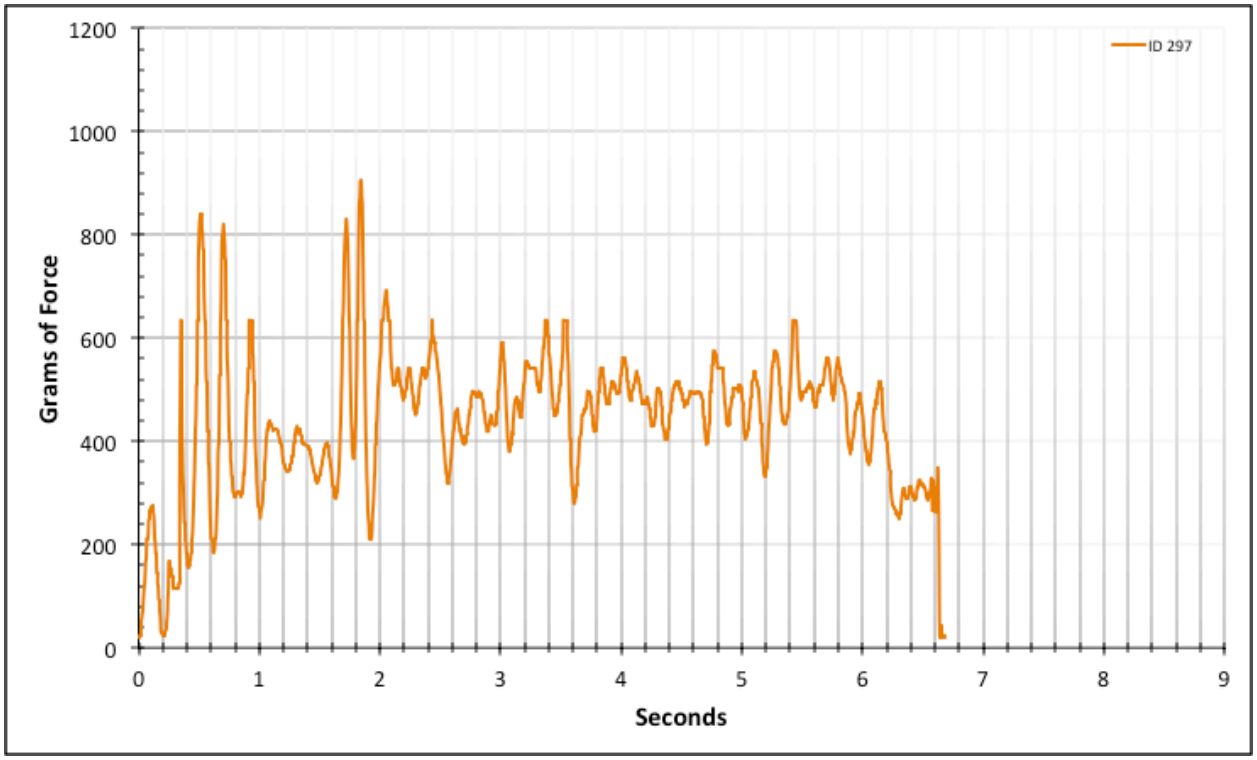

Figure A-6-433: Full Factory Baseline - Lubricated - ID 297 - #8, Bolt 1

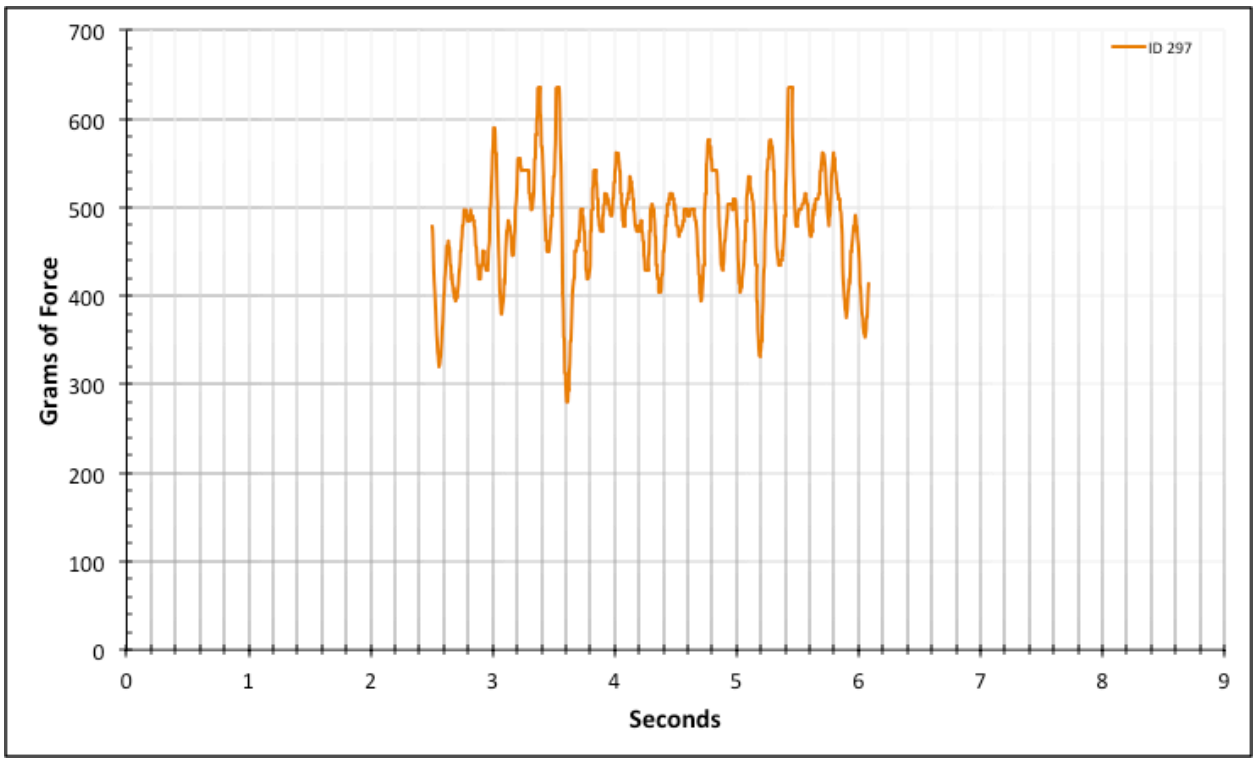

Figure A-6-434: Statistical Region Factory Baseline - Lubricated - ID 297 - #8, Bolt 1

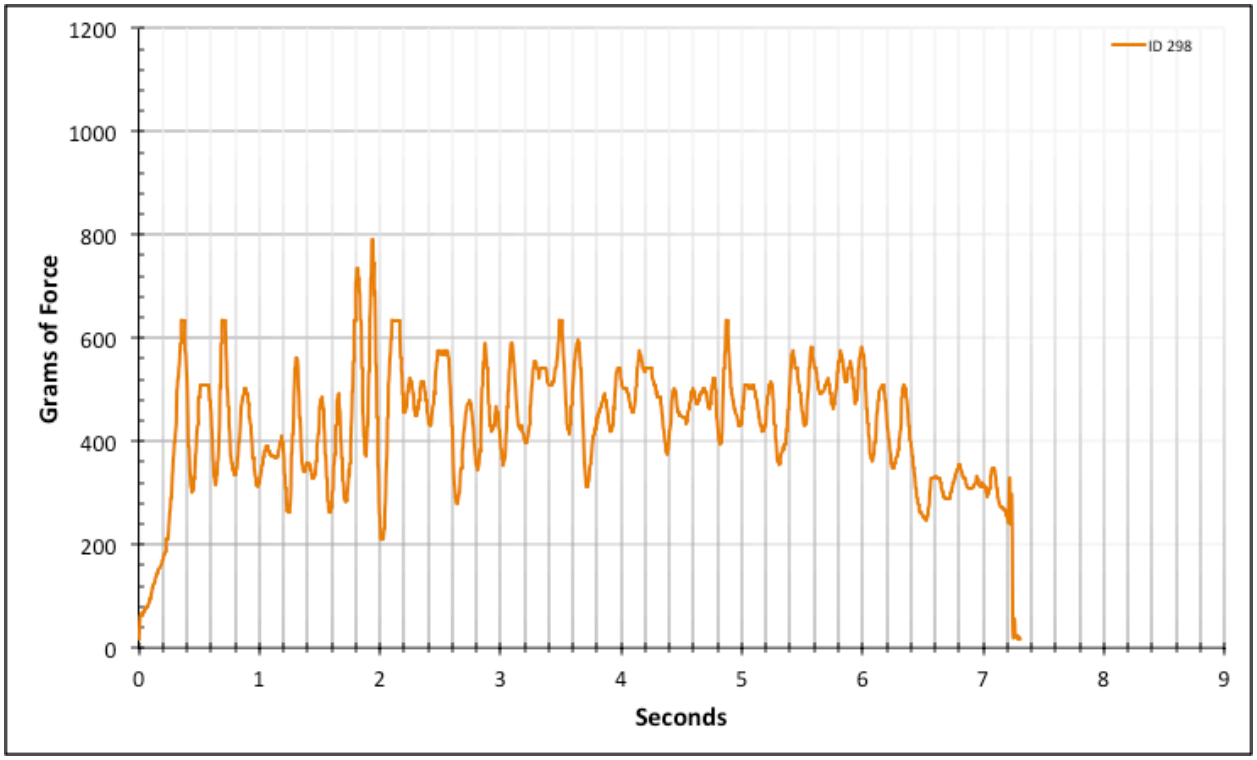

Figure A-6-435: Full Factory Baseline - Lubricated - ID 298 - #8, Bolt 1

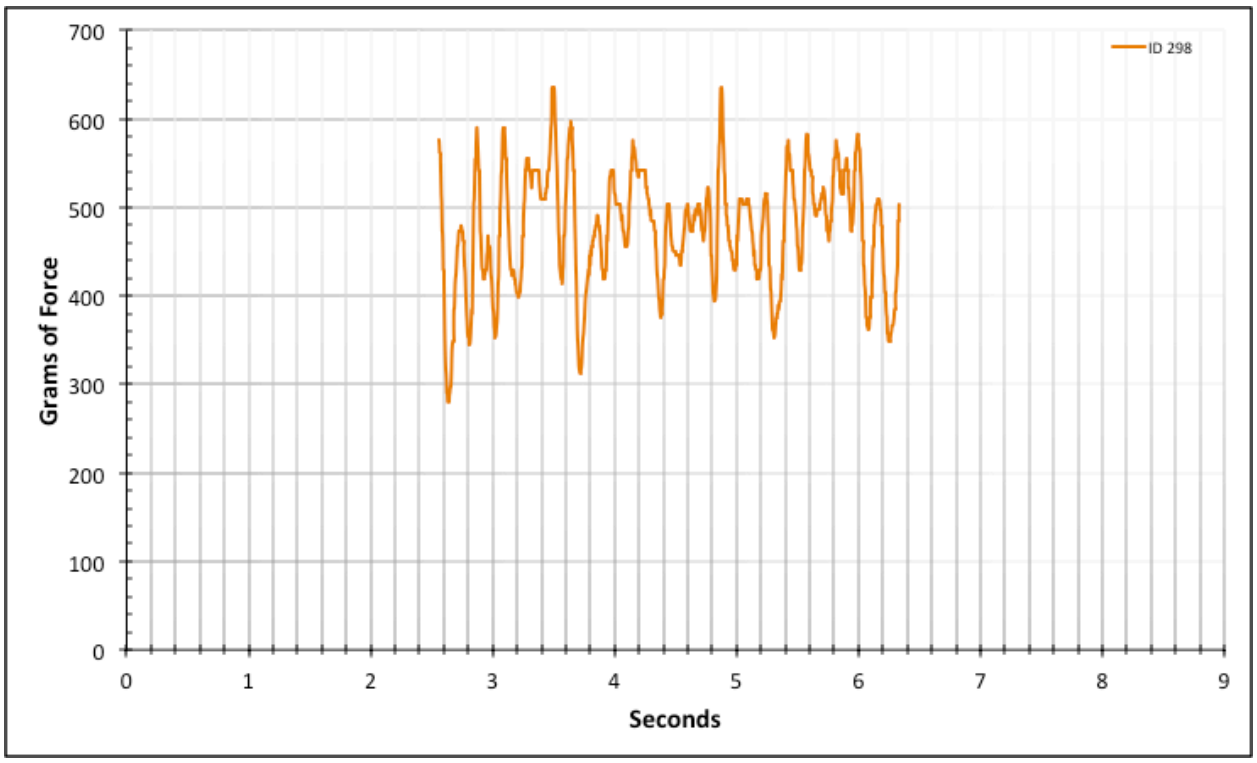

Figure A-6-436: Statistical Region Factory Baseline - Lubricated - ID 298 - #8, Bolt 1

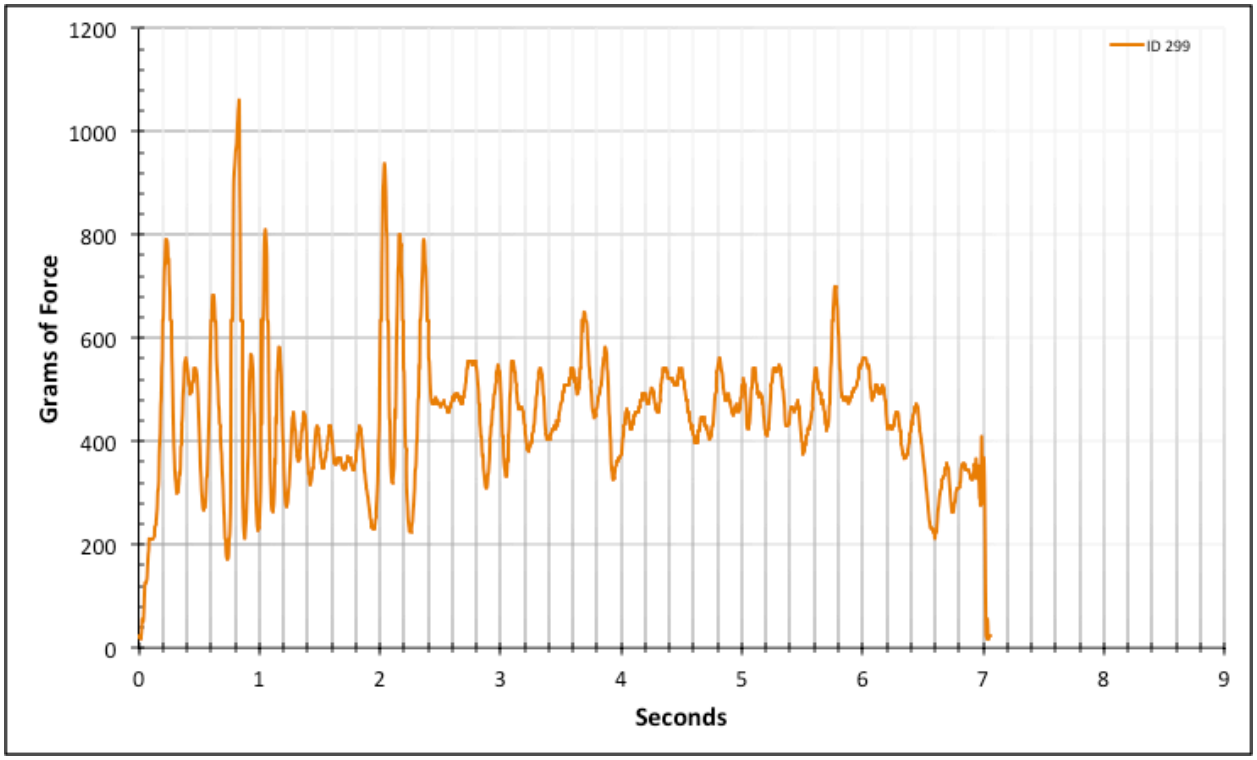

Figure A-6-437: Full Factory Baseline - Lubricated - ID 299 - #8, Bolt 1

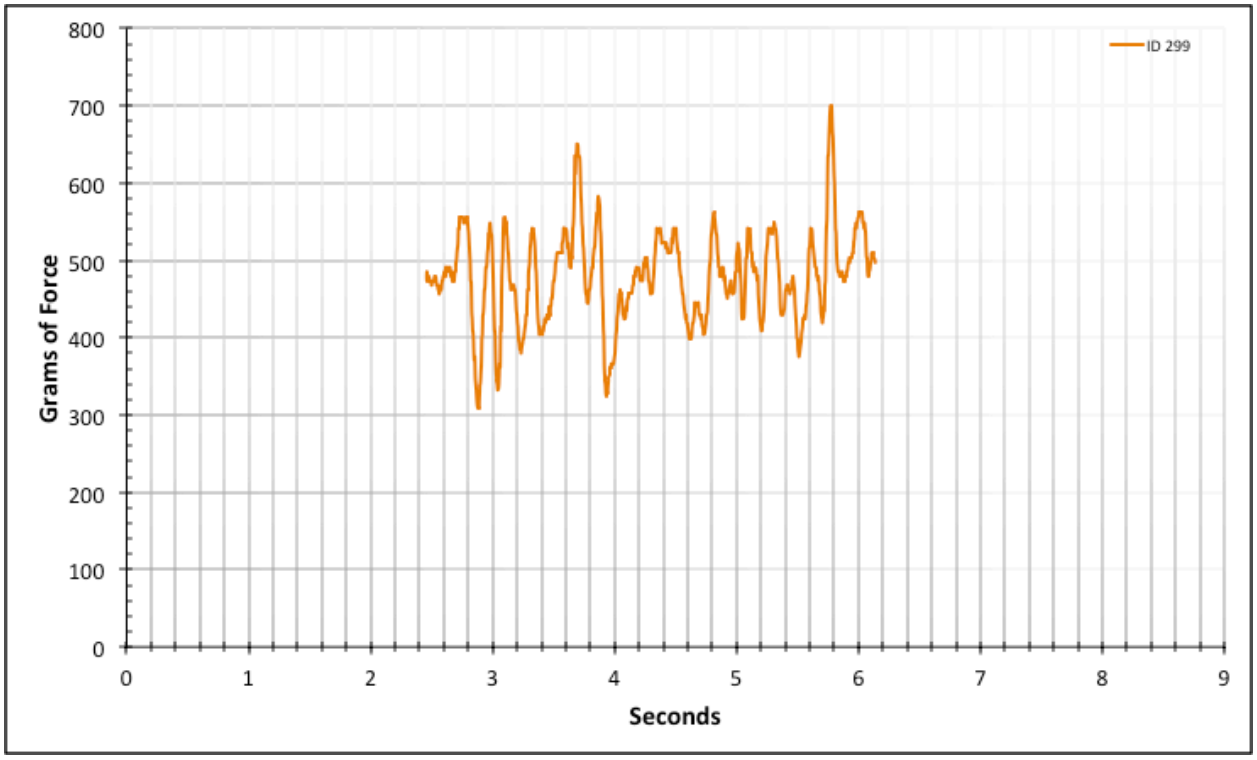

Figure A-6-438: Statistical Region Factory Baseline - Lubricated - ID 299 - #8, Bolt 1

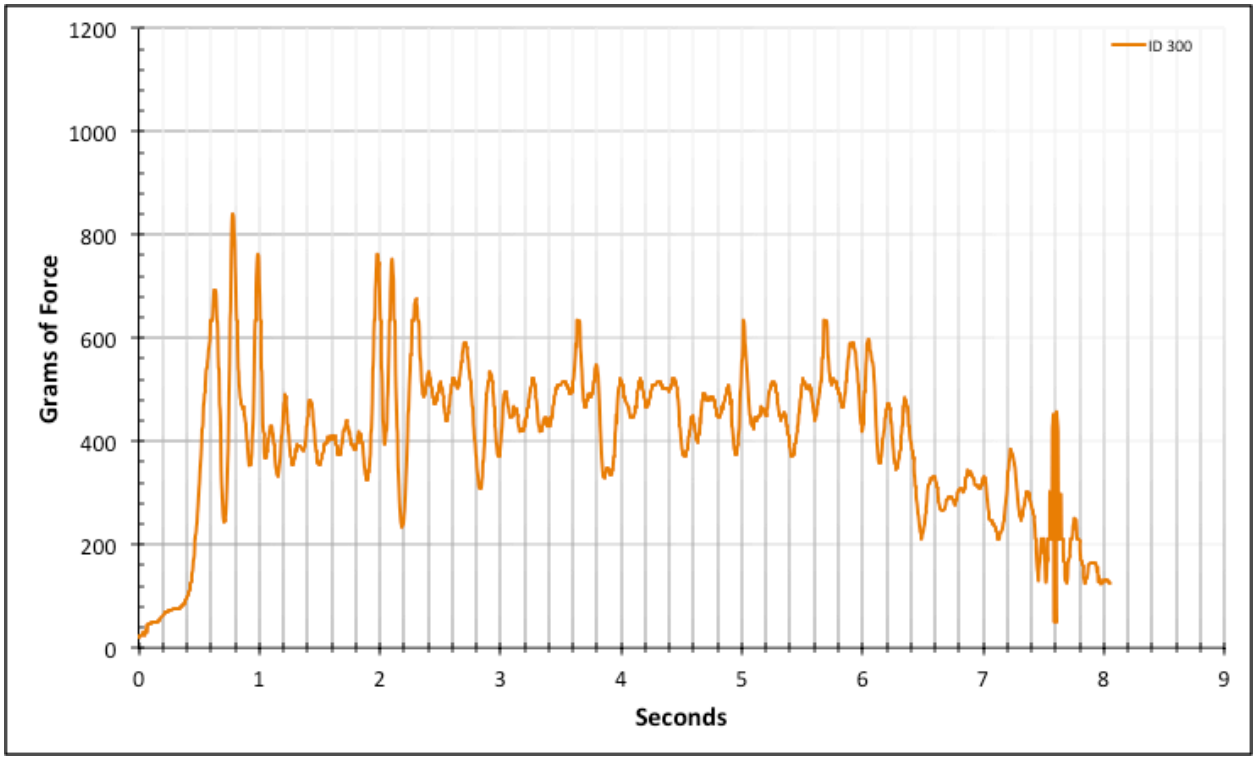

Figure A-6-439: Full Factory Baseline - Lubricated - ID 300 - #8, Bolt 1

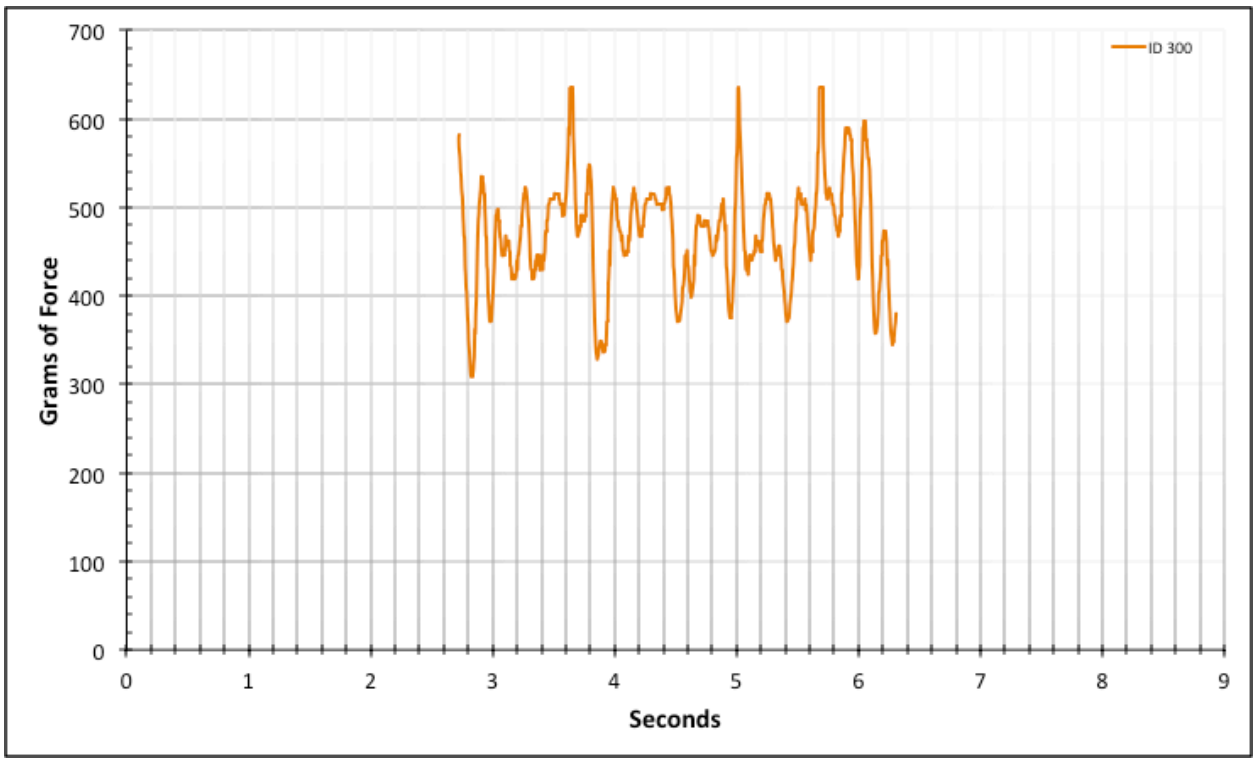

Figure A-6-440: Statistical Region Factory Baseline - Lubricated - ID 300 - #8, Bolt 1

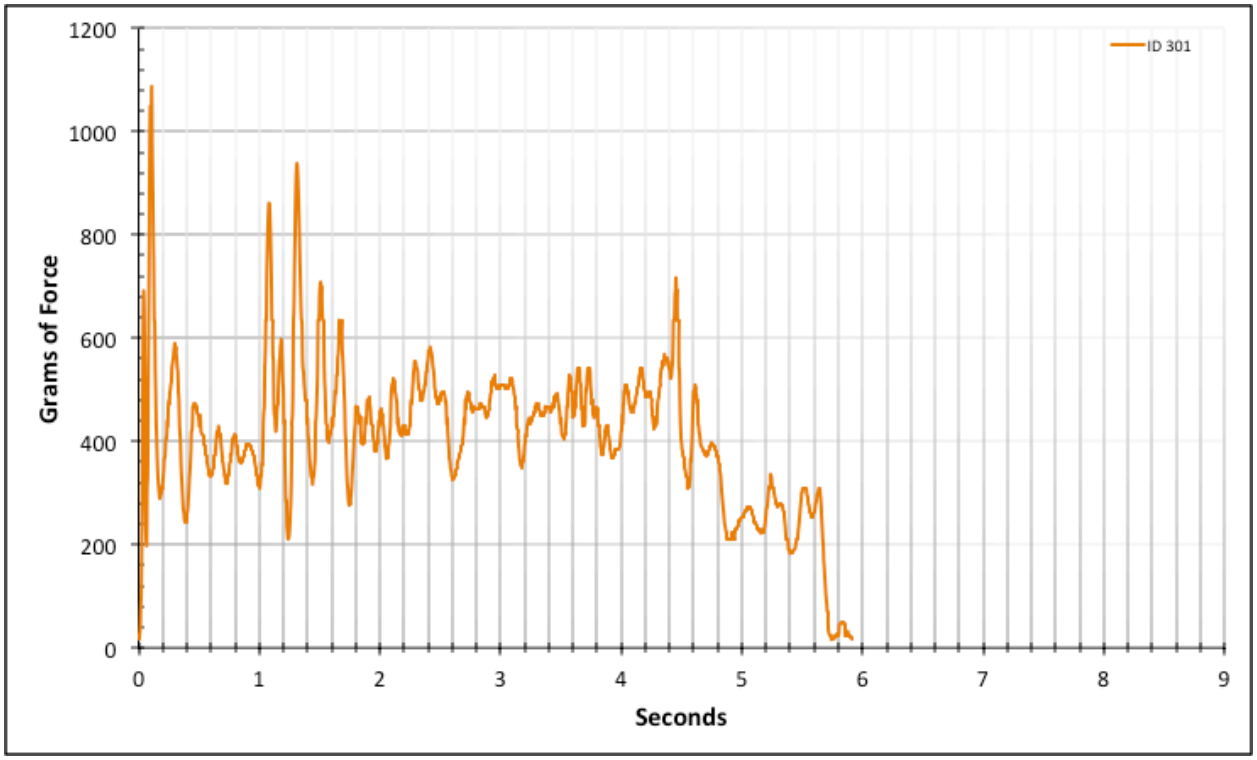

Figure A-6-441: Full Factory Baseline - Lubricated - ID 301 - #8, Bolt 2

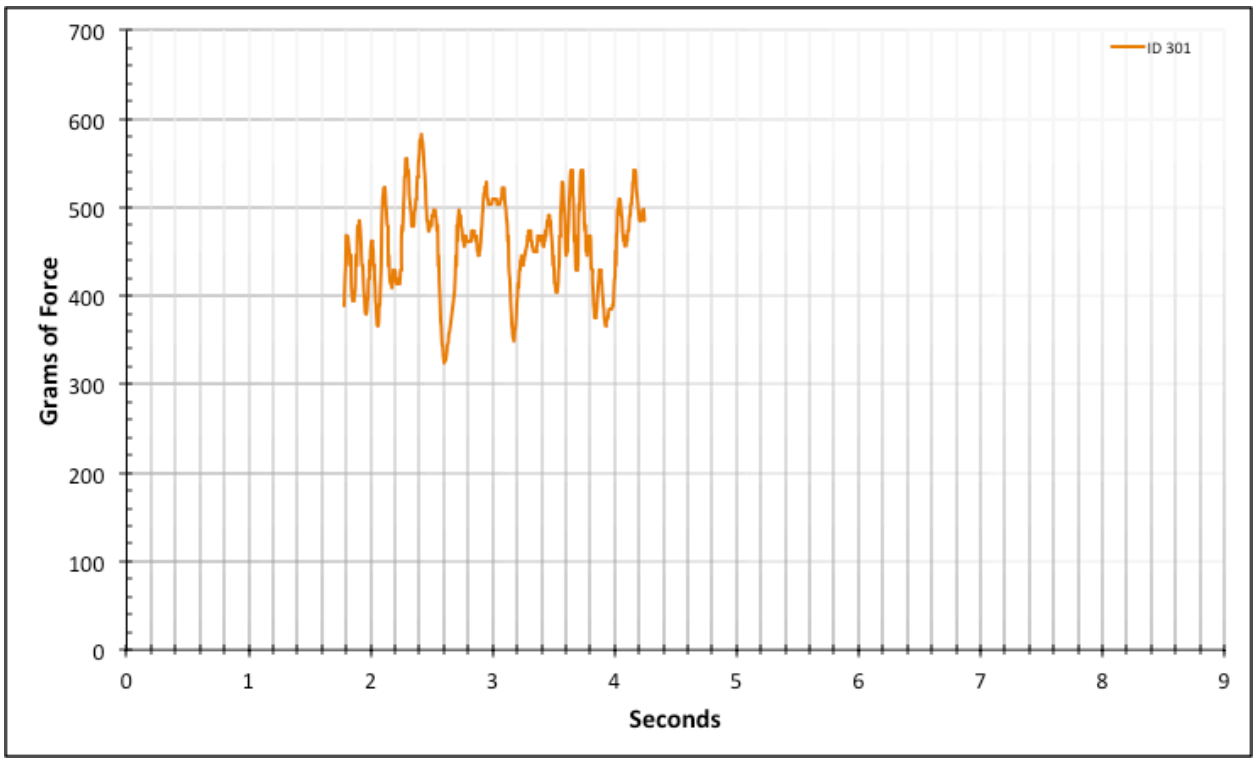

Figure A-6-442: Statistical Region Factory Baseline - Lubricated - ID 301 - #8, Bolt 2

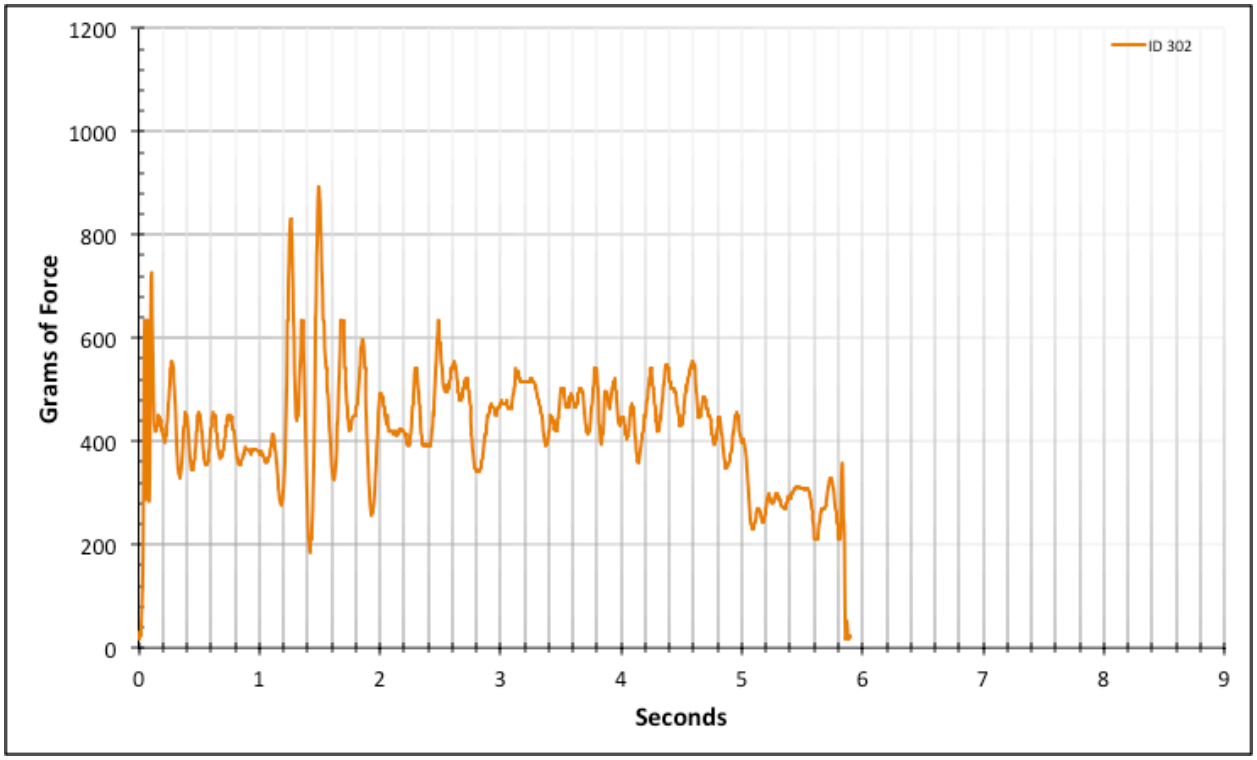

Figure A-6-443: Full Factory Baseline - Lubricated - ID 302 - #8, Bolt 2

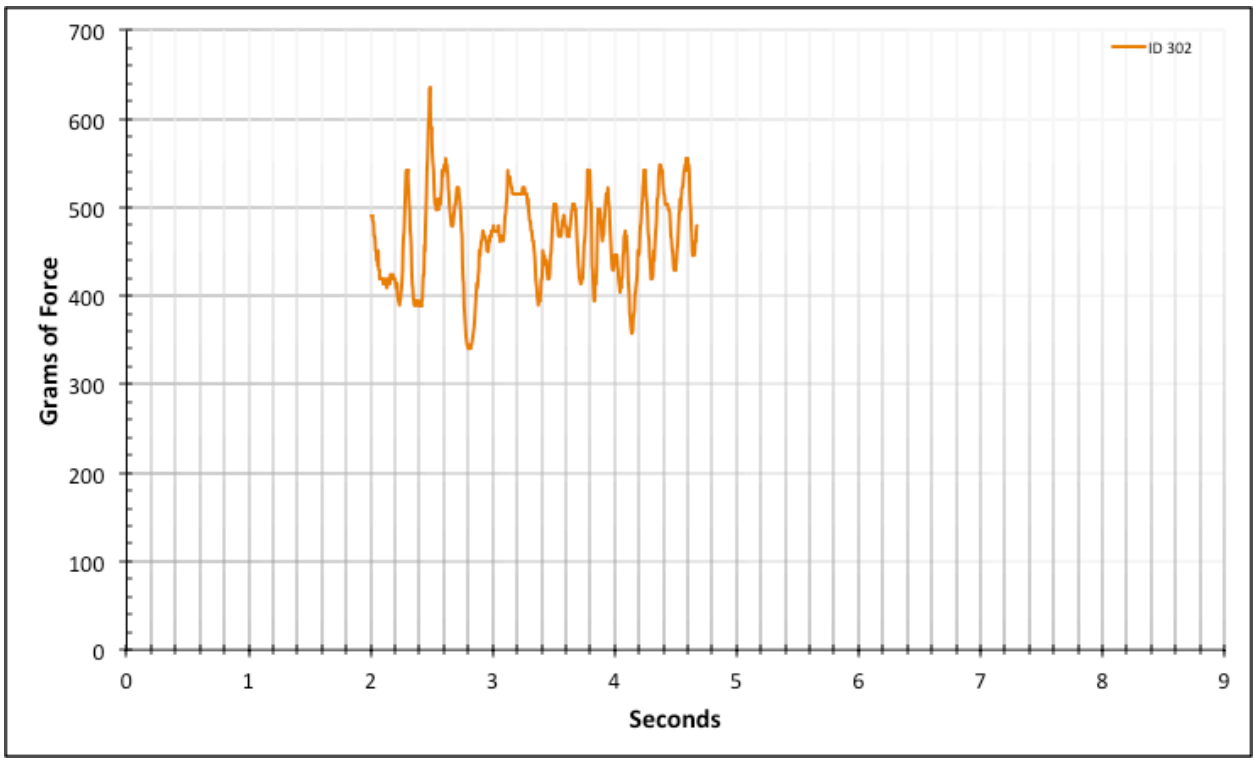

Figure A-6-444: Statistical Region Factory Baseline - Lubricated - ID 302 - #8, Bolt 2

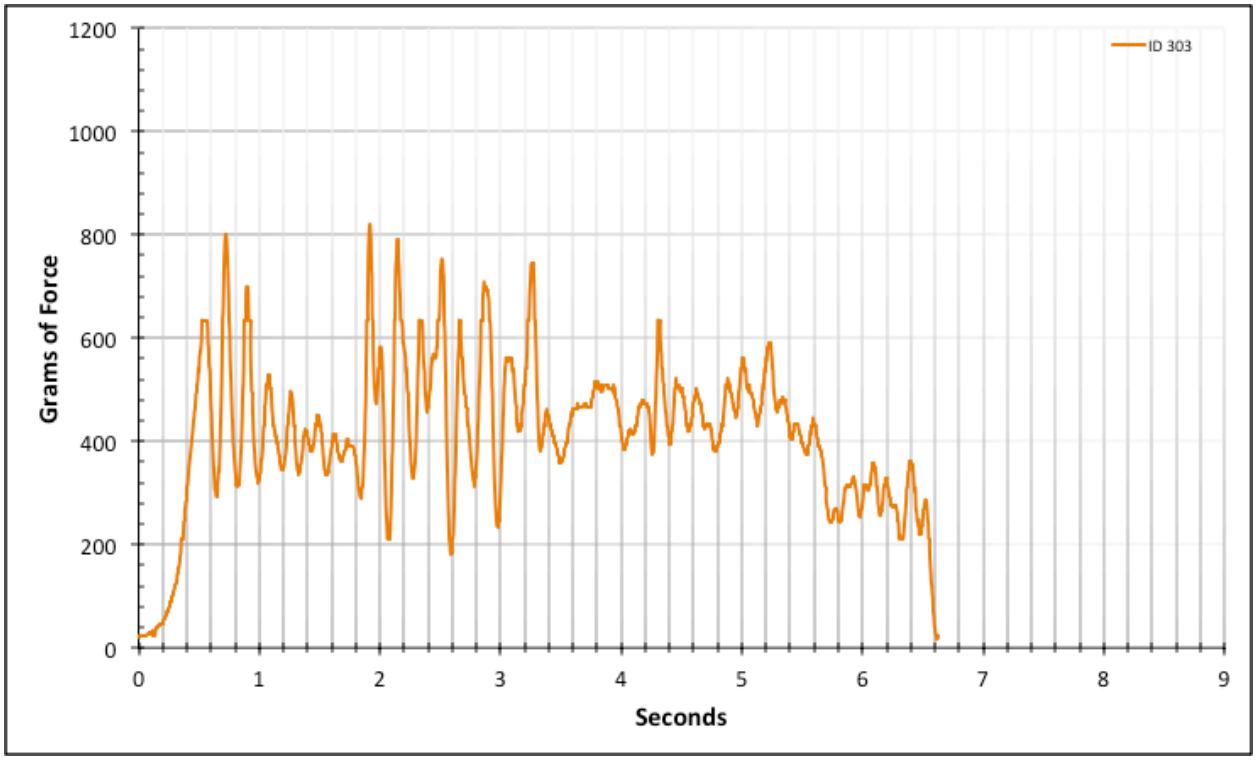

Figure A-6-445: Full Factory Baseline - Lubricated - ID 303 - #8, Bolt 2

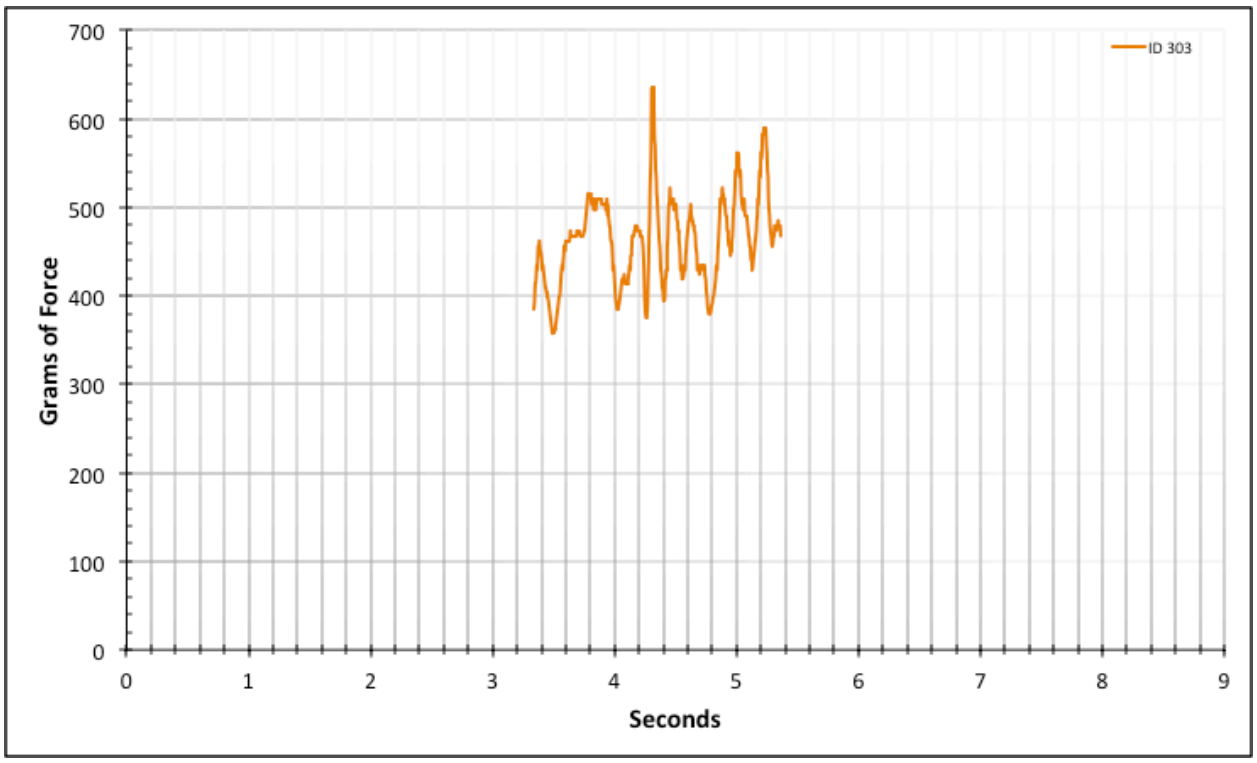

Figure A-6-446: Statistical Region Factory Baseline - Lubricated - ID 303 - #8, Bolt 2

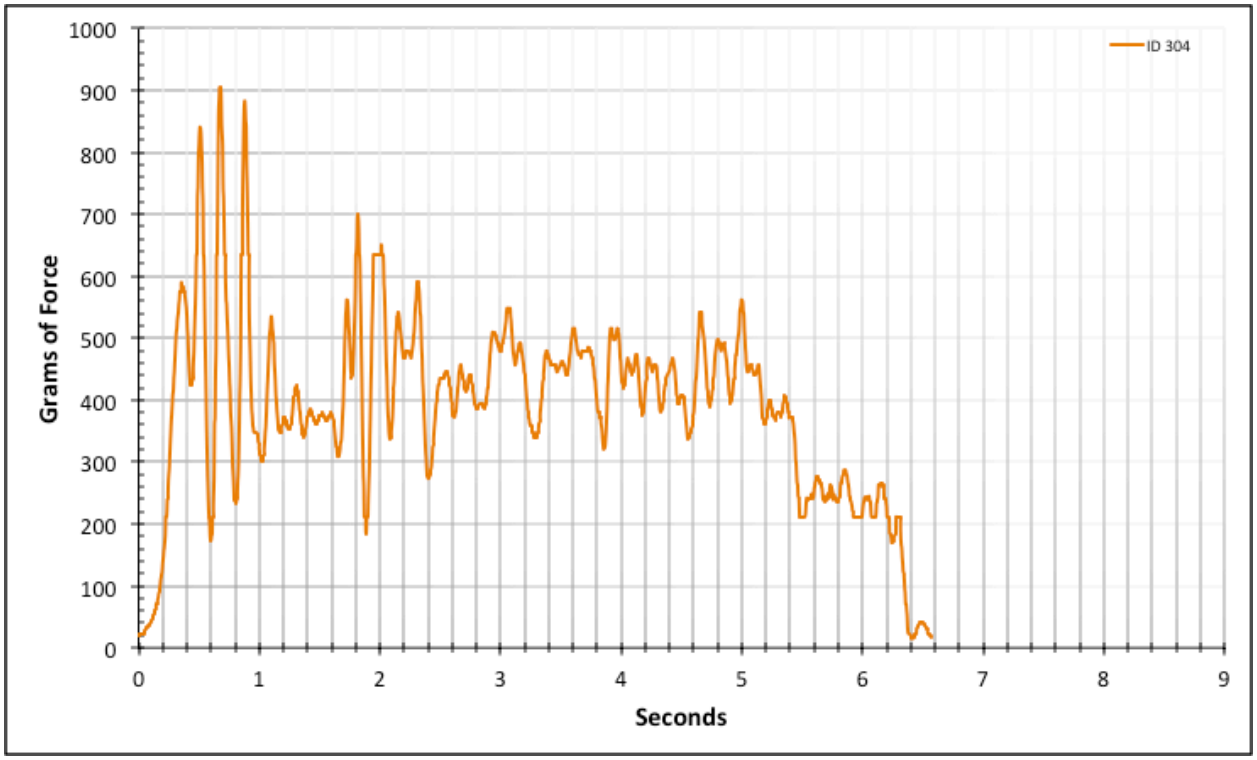

Figure A-6-447: Full Factory Baseline - Lubricated - ID 304 - #8, Bolt 2

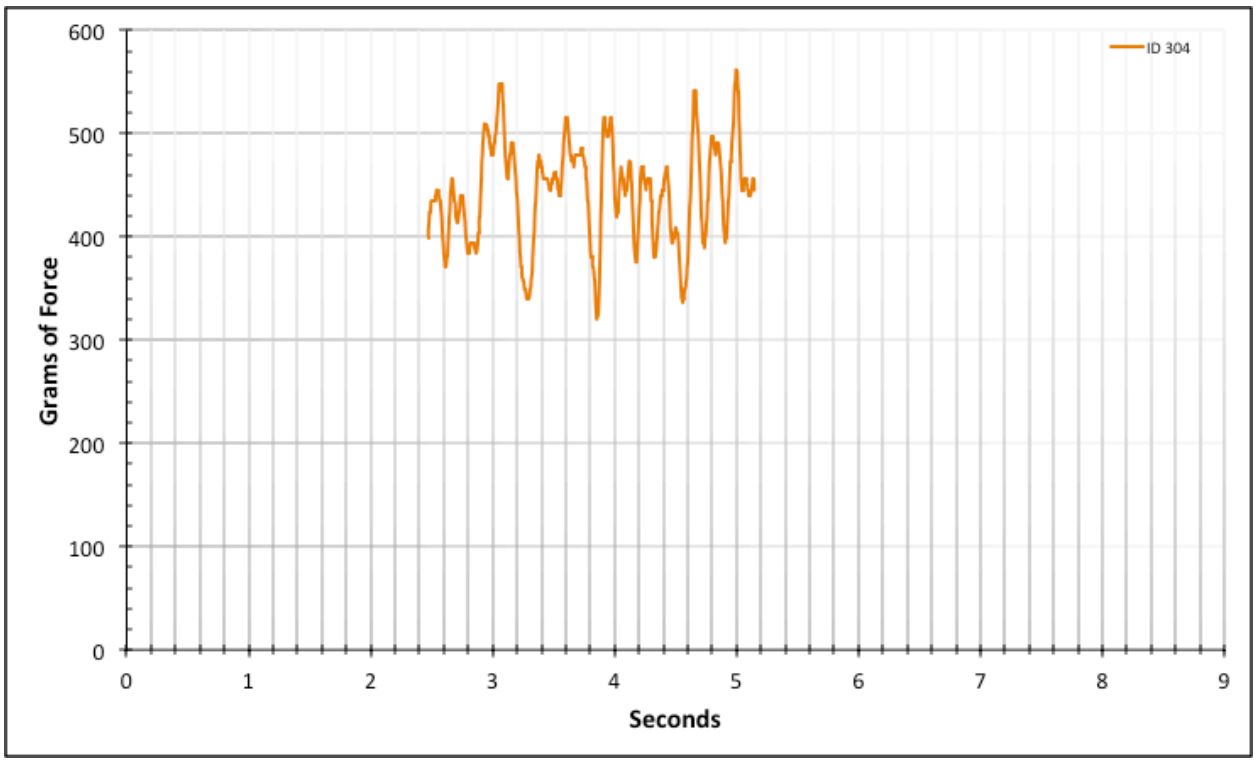

Figure A-6-448: Statistical Region Factory Baseline - Lubricated - ID 304 - #8, Bolt 2

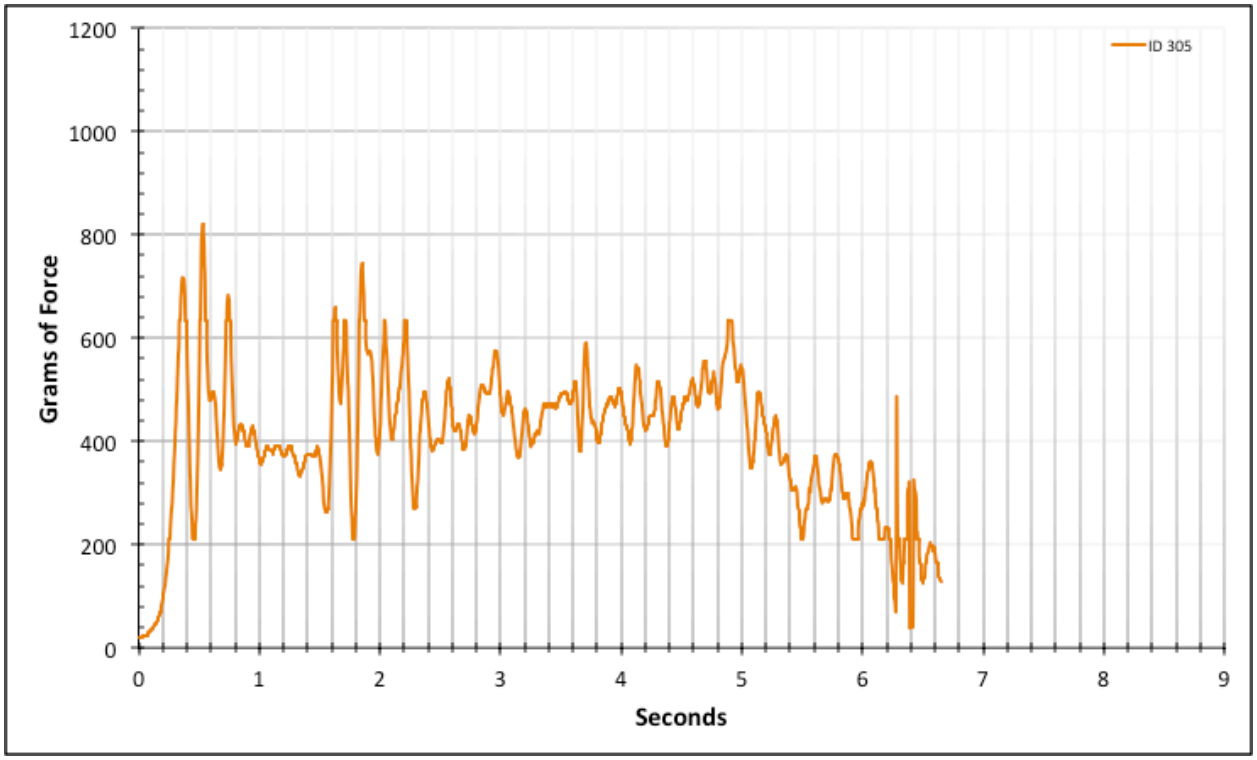

Figure A-6-449: Full Factory Baseline - Lubricated - ID 305 - #8, Bolt 2

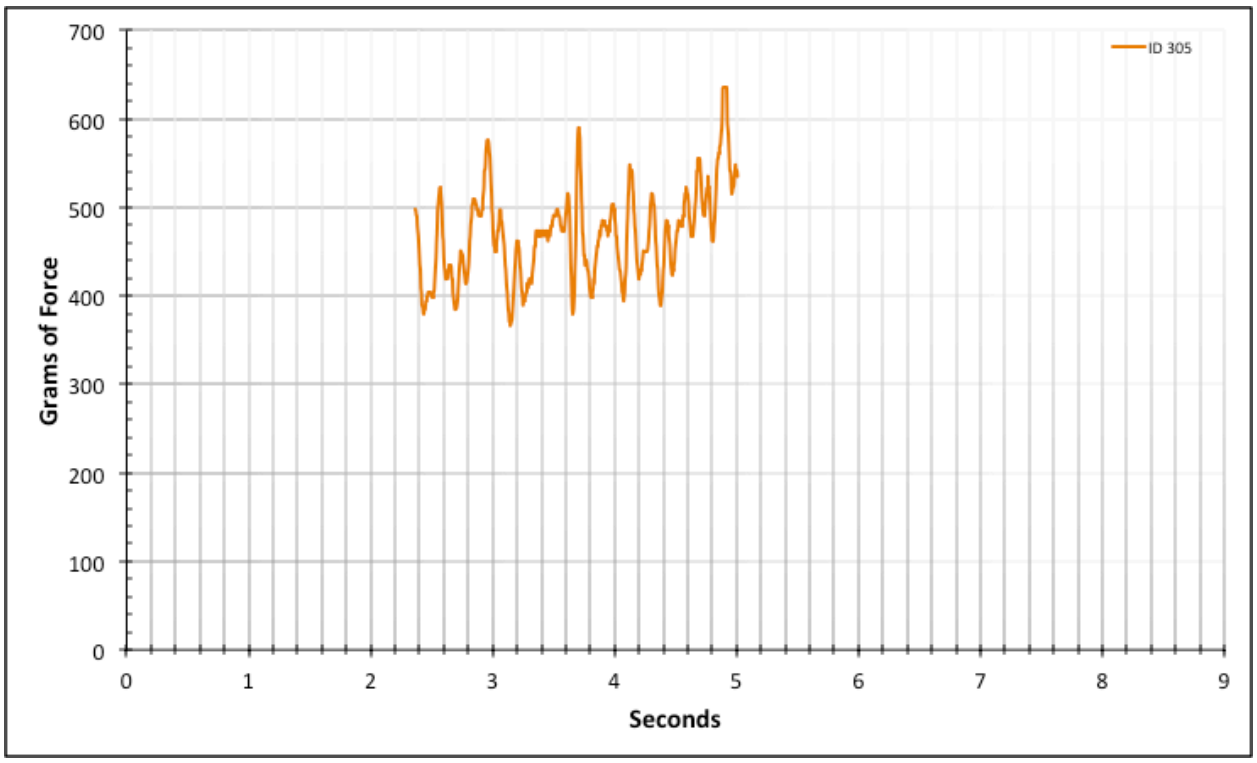

Figure A-6-450: Statistical Region Factory Baseline - Lubricated - ID 305 - #8, Bolt 2

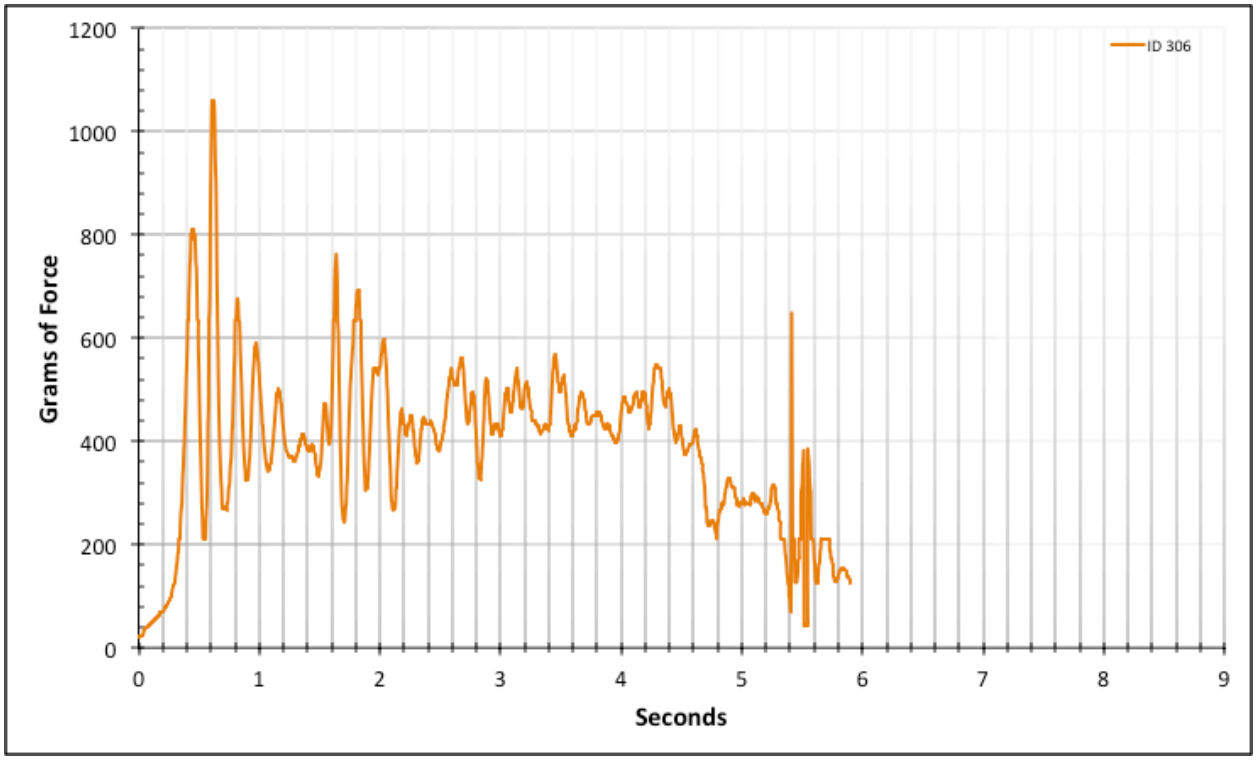

Figure A-6-451: Full Factory Baseline - Lubricated - ID 306 - #8, Bolt 3

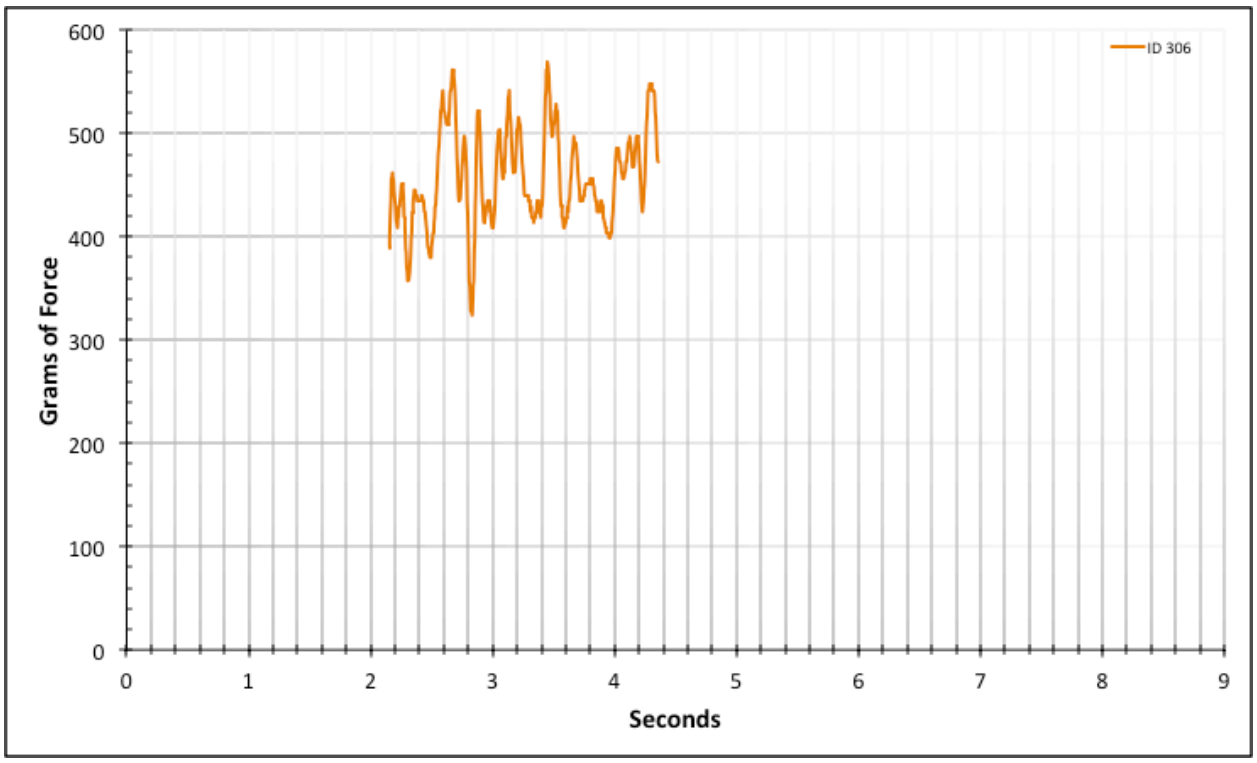

Figure A-6-452: Statistical Region Factory Baseline - Lubricated - ID 306 - #8, Bolt 3

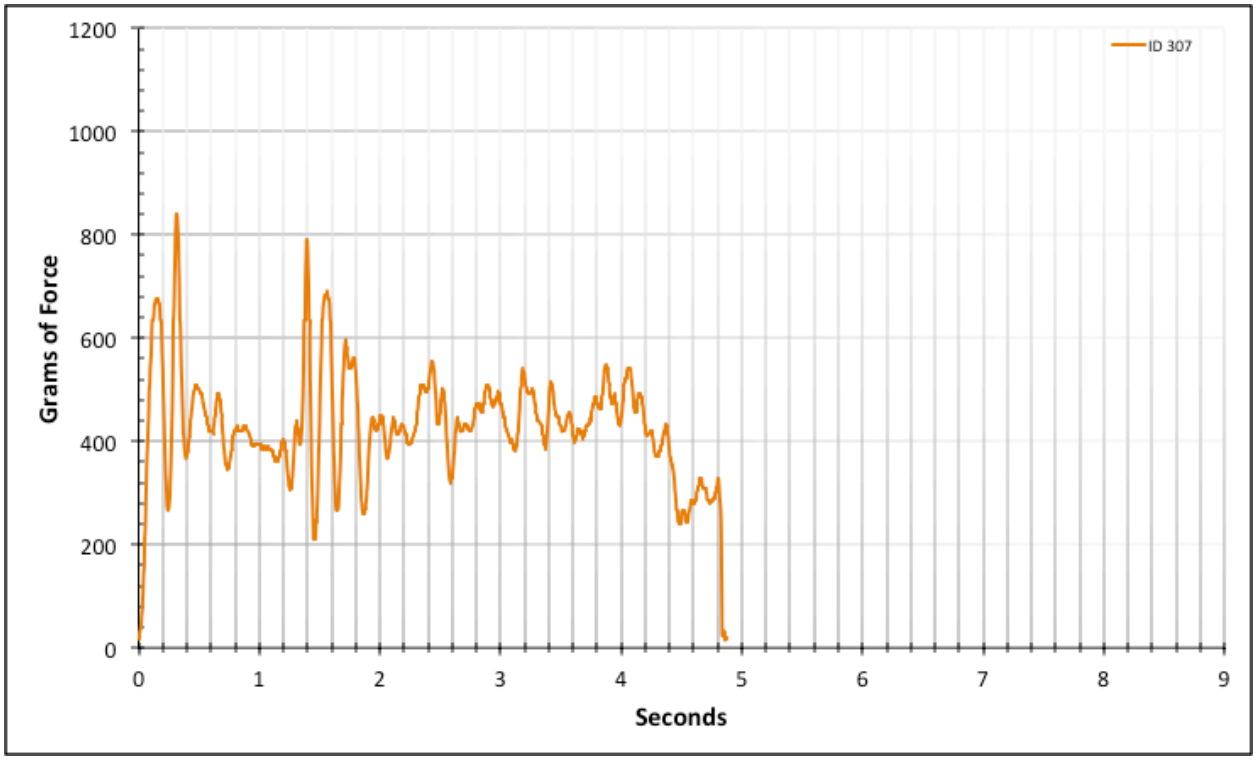

Figure A-6-453: Full Factory Baseline - Lubricated - ID 307 - #8, Bolt 3

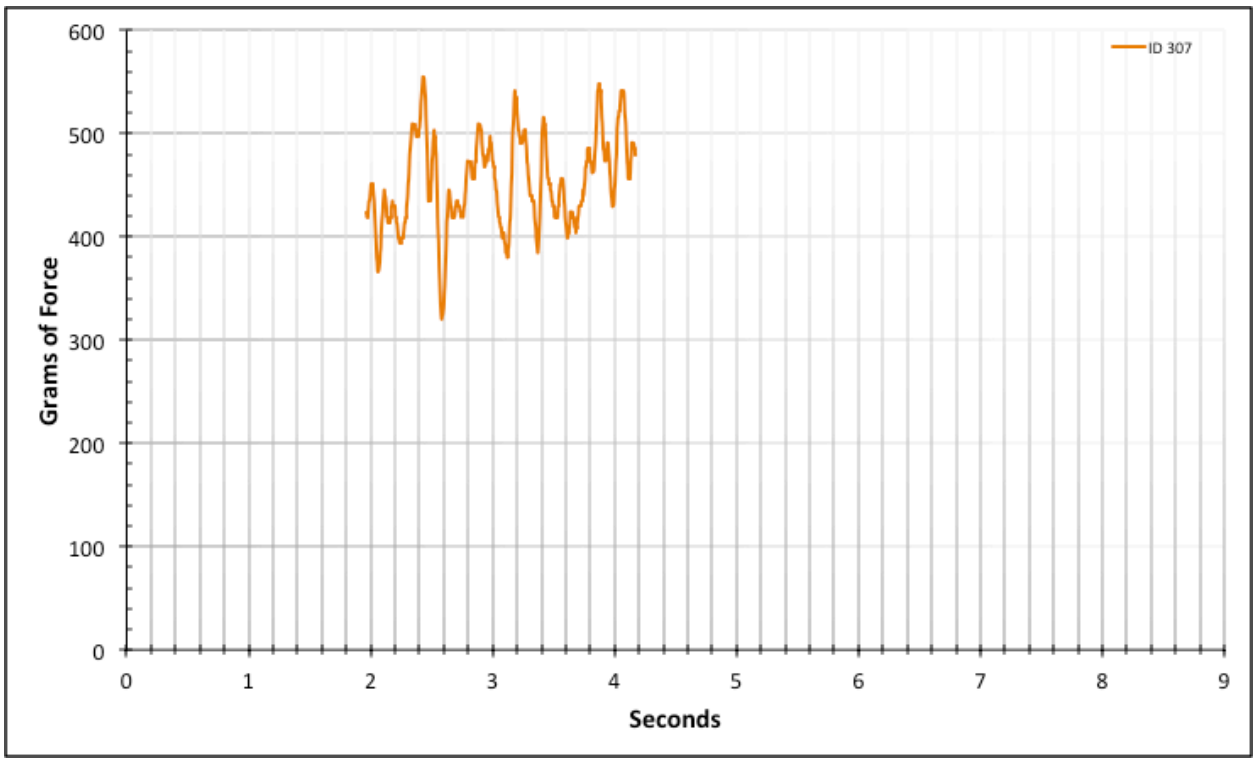

Figure A-6-454: Statistical Region Factory Baseline - Lubricated - ID 307 - #8, Bolt 3

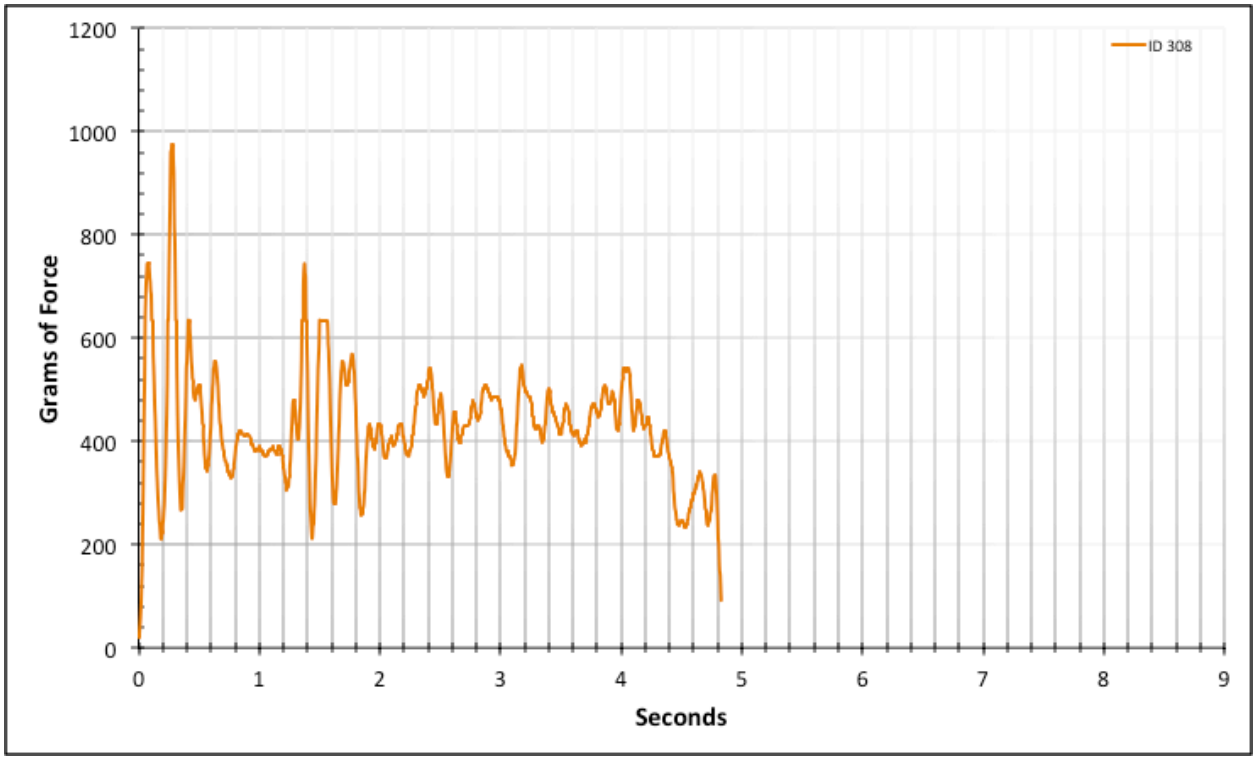

Figure A-6-455: Full Factory Baseline - Lubricated - ID 308 - #8, Bolt 3

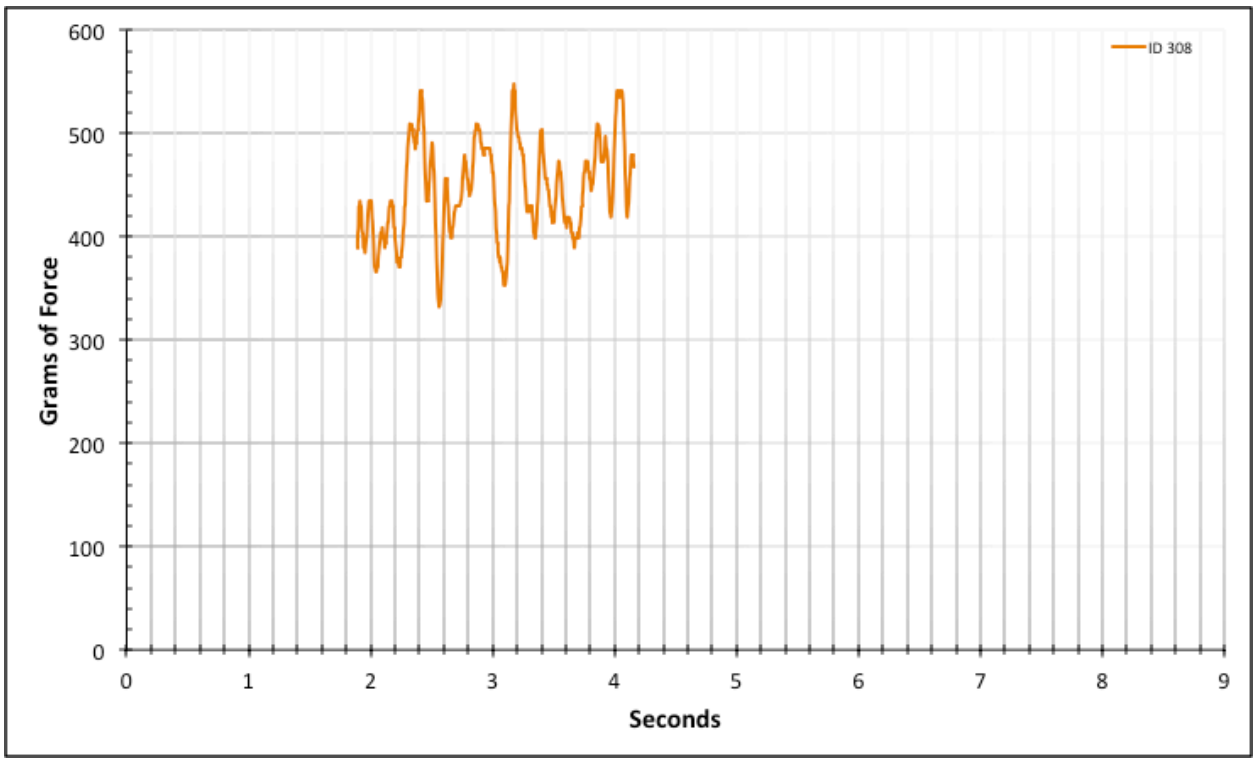

Figure A-6-456: Statistical Region Factory Baseline - Lubricated - ID 308 - #8, Bolt 3

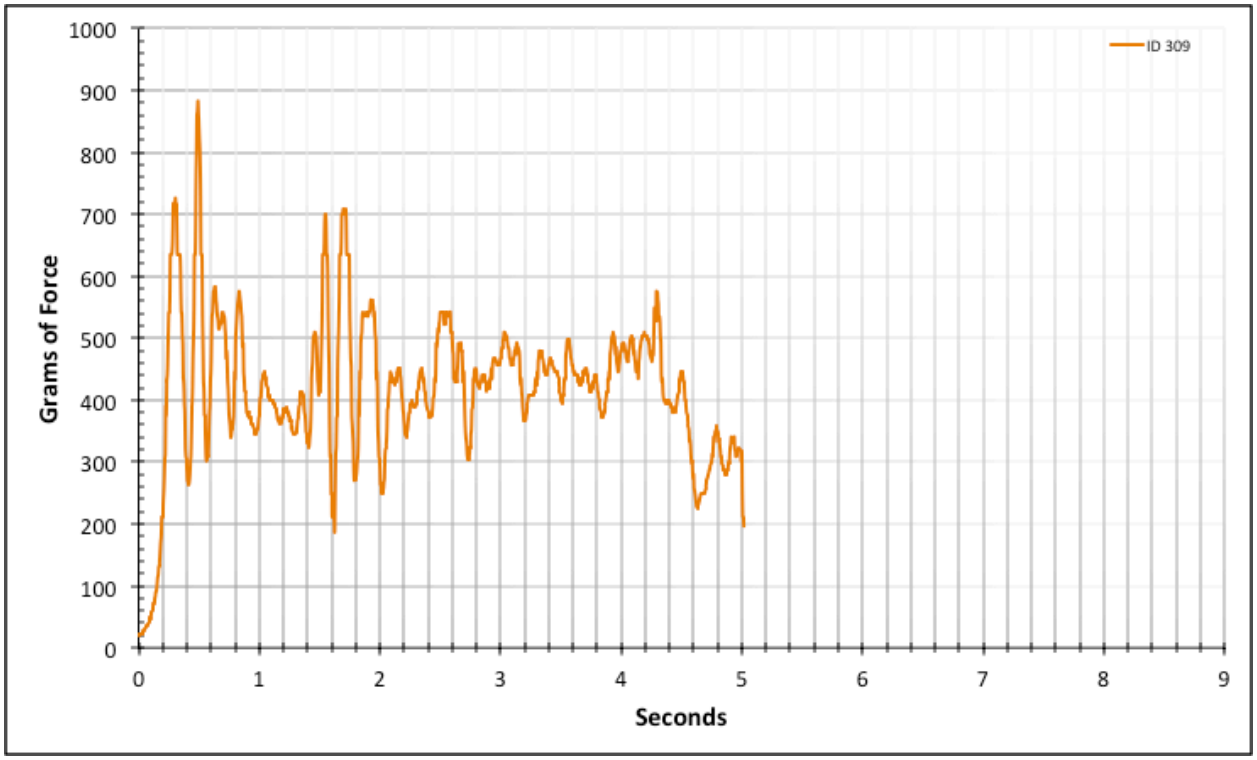

Figure A-6-457: Full Factory Baseline - Lubricated - ID 309 - #8, Bolt 3

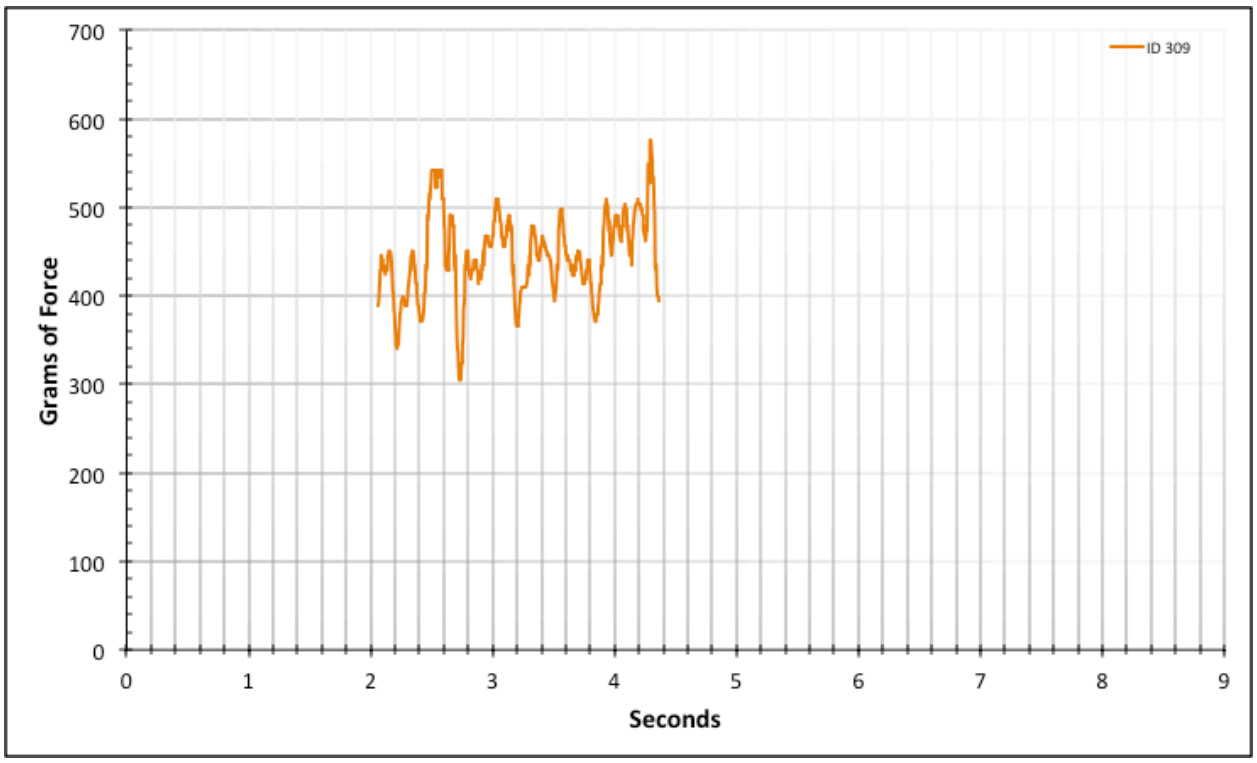

Figure A-6-458: Statistical Region Factory Baseline - Lubricated - ID 309 - #8, Bolt 3

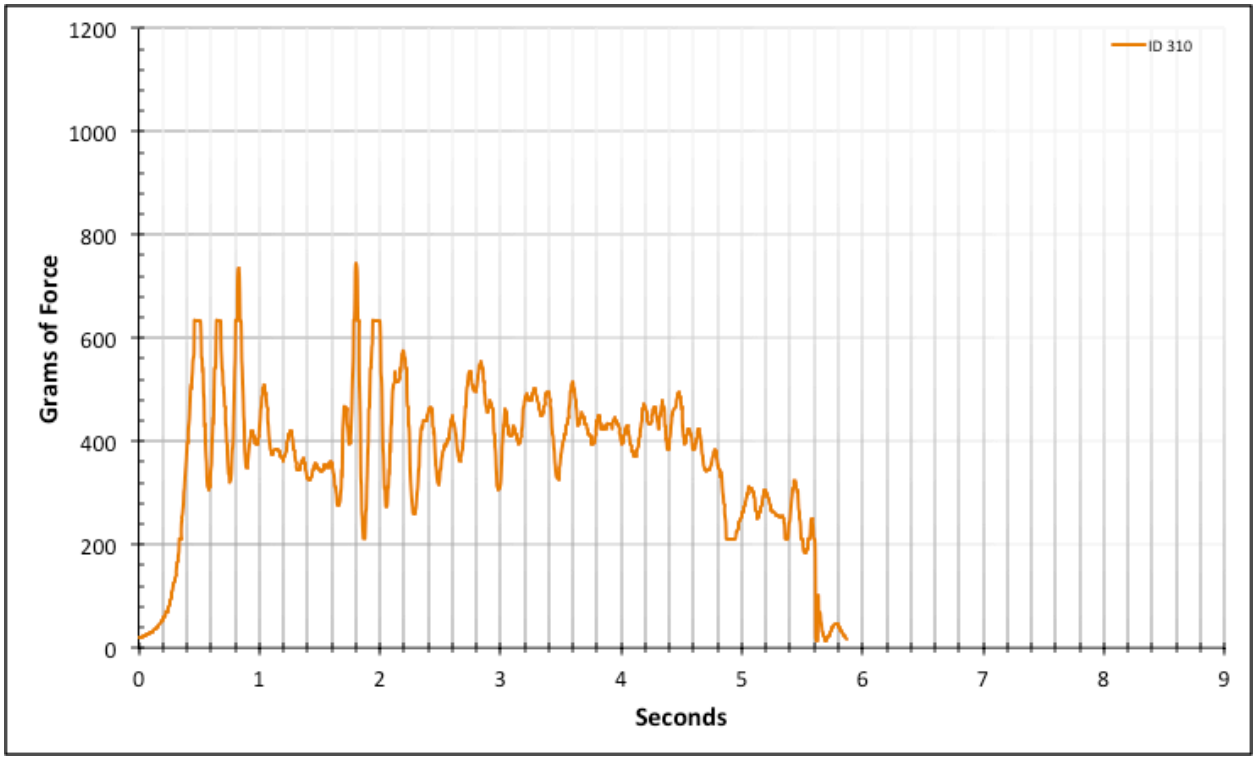

Figure A-6-459: Full Factory Baseline - Lubricated - ID 310 - #8, Bolt 3

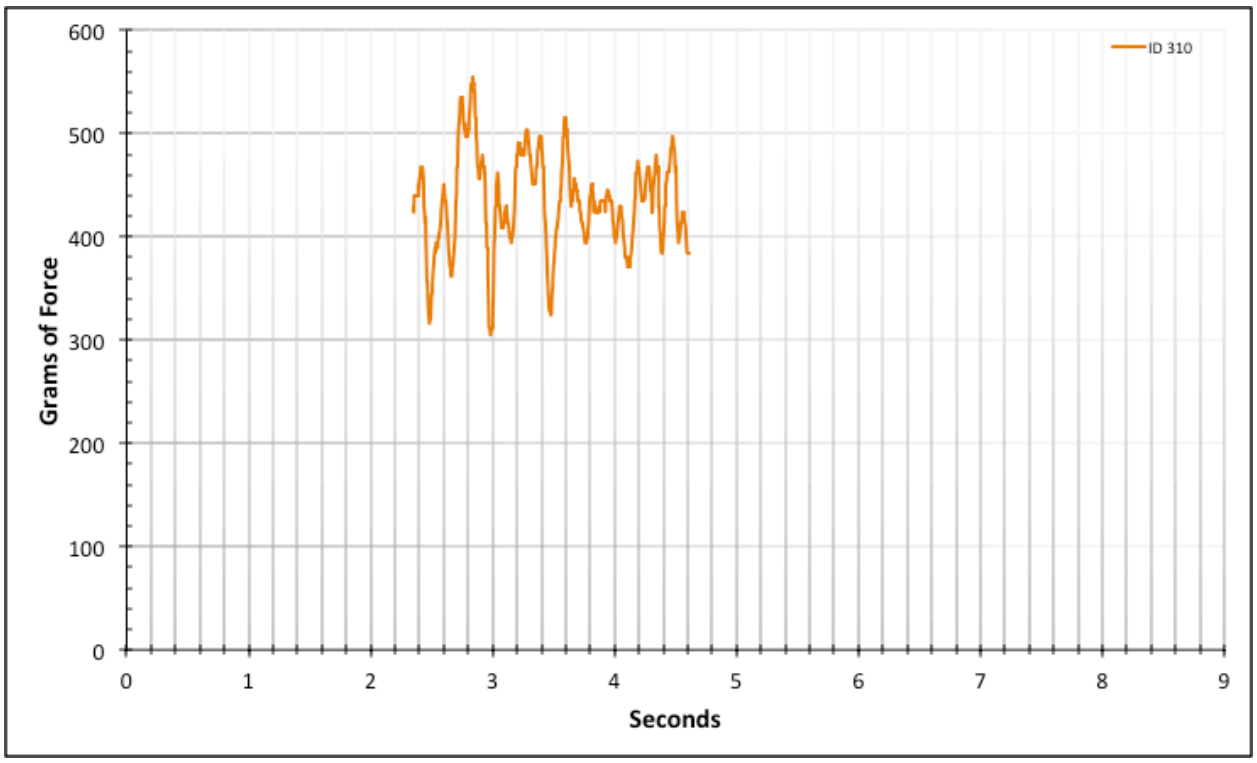

Figure A-6-460: Statistical Region Factory Baseline - Lubricated - ID 310 - #8, Bolt 3

Appendix B - Source Gauge Reader Code

B.1. default.nix

```
with import <nixpkgs> {};


haskell.lib.buildStackProject rec
{
   name = "gaugereader";


   ghc = haskell.compiler.ghc822;


   libs = [ git
            llvm_5
            libffi
            ffmpeg-full
            zlib
          ] ++ (if stdenv.isDarwin
              then [ darwin.cf-private
                     darwin.apple_sdk.frameworks.CoreFoundation
                     darwin.apple_sdk.frameworks.Kernel
                     darwin.apple_sdk.frameworks.Cocoa
                   ]
              else [ cudatoolkit8.lib
```

```
                cudatoolkit8.out
                linuxPackages.nvidia_x11
              ]
            );

  buildInputs = [ clang
                gcc
                haskell.compiler.ghc822
                stack
                pkgconfig
                which
              ] ++ libs;
}
```

B.2. gaugereader.cabal

```
name:              gaugereader
version:           0.1.0.0
synopsis:          Masked Occupancy Hough Transform for Gague Image Data Collection
description:       Masked Occupancy Hough Transform for Gague Image Data Collection
homepage:          https://github.com/TravisWhitaker/gaugereader
license:           MIT
license-file:      LICENSE
author:            Travis Whitaker
```

```
maintainer:          pi.boy.travis@gmail.com
copyright:           Travis Whitaker 2017
-- category:
build-type:          Simple
-- extra-source-files:  ChangeLog.md
cabal-version:       >=1.10


executable gaugereader
  main-is:             Main.hs
  other-modules:       GaugeReader.Color
                       GaugeReader.FrameIO
                       GaugeReader.Hough
  -- other-extensions:
  build-depends:       base >=4.10 && <4.11
                     , accelerate
                     , accelerate-llvm-native
                     , accelerate-io
                     , bytestring
                     , cassava
                     , ffmpeg-light
                     , JuicyPixels
                     , optparse-generic
                     , vector
```

```
  hs-source-dirs:      src
  default-language:    Haskell2010
  ghc-options:         -O2 -threaded -rtsopts
  if(!os(darwin))
    build-depends: accelerate-llvm-ptx
    cpp-options: -DCUDA
```

B.3. LICENSE

```
Copyright (c) 2018 Travis Whitaker
```

B.4. Setup.hs

```
import Distribution.Simple
main = defaultMain
```

B.5. Color.hs

```
{-# LANGUAGE FlexibleContexts
           , RebindableSyntax
           , ScopedTypeVariables
           , TypeOperators
           , ViewPatterns
           #-}

module GaugeReader.Color where
```

```
import Data.Array.Accelerate as A


rgbP :: Acc (Array DIM2 Word8)
    -> Acc (Array DIM2 Word8, Array DIM2 Word8, Array DIM2 Word8)
rgbP rgb =
   let (Z :. rgbh :. rgbw) = unlift (shape rgb) :: Z :. Exp Int :. Exp Int
       bwsh = lift (Z :. rgbh :. (div rgbw 3))
       rind :: Exp DIM2 -> Exp DIM2
       rind sh = let (Z :. bwh :. bww) = unlift sh :: Z :. Exp Int :. Exp Int
                 in lift (Z :. bwh :. (bww * 3))
       gind :: Exp DIM2 -> Exp DIM2
       gind sh = let (Z :. bwh :. bww) = unlift sh :: Z :. Exp Int :. Exp Int
                 in lift (Z :. bwh :. ((bww * 3) + 1))
       bind :: Exp DIM2 -> Exp DIM2
       bind sh = let (Z :. bwh :. bww) = unlift sh :: Z :. Exp Int :. Exp Int
                 in lift (Z :. bwh :. ((bww * 3) + 2))
       r = backpermute bwsh rind rgb
       g = backpermute bwsh gind rgb
       b = backpermute bwsh bind rgb
       in lift (r, g, b)


mixDown :: Exp Word8 -> Exp Word8 -> Exp Word8 -> Exp Word8
```

```
mixDown r g b = let r' = (fromIntegral r / 255) :: Exp Float
                    g' = (fromIntegral g / 255) :: Exp Float
                    b' = (fromIntegral b / 255) :: Exp Float
                in round (((r' + g' + b') / 3) * 255)

makeRed :: Acc (Array DIM2 Word8) -> Acc (Array DIM2 Word8)
makeRed rgb = let (r, g, b) = unlift (rgbP rgb) :: ( Acc (Array DIM2 Word8)
                                                   , Acc (Array DIM2 Word8)
                                                   , Acc (Array DIM2 Word8)
                                                   )
              in r

makeBW :: Acc (Array DIM2 Word8) -> Acc (Array DIM2 Word8)
makeBW rgb = let (r, g, b) = unlift (rgbP rgb) :: ( Acc (Array DIM2 Word8)
                                                  , Acc (Array DIM2 Word8)
                                                  , Acc (Array DIM2 Word8)
                                                  )
             in zipWith3 mixDown r g b

toTwoVal :: Acc (Array DIM2 Word8) -> Acc (Array DIM2 Bool)
toTwoVal bw =
   let bw32 = map fromIntegral bw :: Acc (Array DIM2 Word32)
       sm = the $ (sum (flatten bw32))
```

```
        (Z :. bwh :. bww) = unlift (shape bw) :: Z :. Exp Int :. Exp Int
        avg :: Exp Word32
        avg = div sm (fromIntegral (bwh * bww))
    in map (<= avg) bw32

rgbToTwoVal :: Acc (Array DIM2 Word8) -> Acc (Array DIM2 Bool)
rgbToTwoVal = toTwoVal . makeBW

twoValToBW :: Acc (Array DIM2 Bool) -> Acc (Array DIM2 Word8)
twoValToBW tv = map (\x -> if x then 255 else 0) tv

-- 8-bit grayscale image to RGB8 image for display purposes.
bwToRGB :: Acc (Array DIM2 Word8) -> Acc (Array DIM2 Word8)
bwToRGB bw =
    let (Z :. bwh :. bww) = unlift (shape bw) :: Z :. Exp Int :. Exp Int
        rgbsh = lift (Z :. bwh :. (3 * bww))
        bwind :: Exp DIM2 -> Exp DIM2
        bwind sh = let (Z :. rgbh :. rgbw) = unlift sh :: Z :. Exp Int :. Exp Int
                   in lift (Z :. rgbh :. (div rgbw 3))
    in backpermute rgbsh bwind bw
```

B.6. FramelO.hs

```
{-# LANGUAGE BangPatterns #-}
```

```
module GaugeReader.FrameIO where

import Codec.FFmpeg

import Codec.Picture

import qualified Data.Array.Accelerate    as A
import qualified Data.Array.Accelerate.IO as A

import Data.Bifunctor

import qualified Data.Vector.Storable as V

-- | Returns an RGB-ordered row-major array.
imgRGB8ToAccRGB8 :: Image PixelRGB8 -> A.Array A.DIM2 A.Word8
imgRGB8ToAccRGB8 (Image w h v) = A.fromVectors (A.Z A.:. h A.:. (3 * w)) v

-- | From an RGB-ordered row-major array.
accRGB8ToImgRGB8 :: A.Array A.DIM2 A.Word8 -> Image PixelRGB8
accRGB8ToImgRGB8 arr = let (A.Z A.:. h A.:. w) = A.arrayShape arr
                       in Image (div w 3) h (A.toVectors arr)
```

```
-- | Need to call Codec.FFmpeg.initFFmpeg before using this.
getFrameGetter :: FilePath -> IO (IO (Maybe (A.Array A.DIM2 A.Word8)), IO ())
getFrameGetter p = do
   (gf, cl) <- imageReader (File p)
   pure ((imgRGB8ToAccRGB8 <$>) <$> gf, cl)

-- | Need to call Codec.FFmpeg.initFFmpeg before using this.
getFrameTimeGetter :: FilePath
                   -> IO (IO (Maybe (A.Array A.DIM2 A.Word8, Double)), IO ())
getFrameTimeGetter p = do
   (gf, cl) <- imageReaderTime (File p)
   pure ((first imgRGB8ToAccRGB8 <$>) <$> gf, cl)

mkVidEncParams :: Int -- ^ Width
               -> Int -- ^ Height
               -> Int -- ^ Frames per second.
               -> EncodingParams
mkVidEncParams w h fps = EncodingParams {
   epWidth       = fromIntegral w
  , epHeight     = fromIntegral h
  , epFps        = fps
  , epCodec      = Nothing
  , epPixelFormat = Nothing
```

```
  , epPreset      = ""
  , epFormatName  = Nothing
  }
```

B.7. Hough.hs

```
{-# LANGUAGE FlexibleContexts
        , RebindableSyntax
        , ScopedTypeVariables
        , TypeOperators
        , ViewPatterns
        #-}

module GaugeReader.Hough where

import Data.Array.Accelerate as A

import qualified Prelude

-- 0 - 360
--indToRad :: Int -> Int -> Double
--indToRad m d = let fI = Prelude.fromIntegral
--              in ((fI d) / (fI m)) * 2 * pi
--
```

```
--indToRadExp :: Exp Int -> Exp Int -> Exp Double
--indToRadExp m d = ((fromIntegral d) / (fromIntegral m)) * 2 * pi


-- 0 - 180
indToRad :: Int -> Int -> Double
indToRad m d = let fI = Prelude.fromIntegral
               in ((fI d) / (fI m)) * pi


indToRadExp :: Exp Int -> Exp Int -> Exp Double
indToRadExp m d = ((fromIntegral d) / (fromIntegral m)) * pi


crop :: Exp Double  -- ^ Top crop frac
    -> Exp Double  -- ^ Bottom crop frac
    -> Exp Double  -- ^ Left crop frac
    -> Exp Double  -- ^ Right crop frac
    -> Acc (Array DIM2 Bool)
    -> Acc (Array DIM2 Bool)
crop t b l r occ =
   let (Z :. occh :. occw) = unlift (shape occ) :: Z :. Exp Int :. Exp Int
       tpix = round (t * (fromIntegral occh)) :: Exp Int
       bpix = round (b * (fromIntegral occh)) :: Exp Int
       lpix = round (l * (fromIntegral occw)) :: Exp Int
       rpix = round (r * (fromIntegral occw)) :: Exp Int
```

```
      res = lift (Z :. ((occh - tpix) - bpix) :. ((occw - lpix) - rpix)) :: Exp (Z :. Int :. Int)
      per oi =
        let (Z :. yi :. xi) = unlift oi :: Z :. Exp Int :. Exp Int
        in lift (Z :. (yi + tpix) :. (xi + lpix)) :: Exp (Z :. Int :. Int)
  in backpermute res per occ

circleMask :: Exp Int -> Acc (Array DIM2 Bool) -> Acc (Array DIM2 Bool)
circleMask rad occ =
  let (Z :. h :. w) = unlift (shape occ) :: Z :. Exp Int :. Exp Int
      circ :: Exp Double -> Exp (Z :. Int :. Int) -> Exp Bool
      circ r sh =
        let (Z :. y :. x) = unlift sh :: Z :. Exp Int :. Exp Int
            x' = (fromIntegral x) - (fromIntegral w / 2)
            y' = (fromIntegral y) - (fromIntegral h / 2)
        in (sqrt (x' * x' + y' * y')) <= r
      per :: Exp (Z :. Int :. Int) -> Exp (Z :. Int :. Int)
      per sh = if circ (fromIntegral rad) sh then sh else ignore
      def :: Acc (Array DIM2 Bool)
      def = fill (shape occ) (lift False)
  in permute (||) def per occ

hVals :: Exp Int -> Exp Int -> Acc (Array DIM2 Bool) -> Acc (Array DIM2 Word32)
hVals thetaCols rRows occ =
```

```
  let (Z :. occh :. occw) = unlift (shape occ) :: Z :. Exp Int :. Exp Int
      trep :: Acc (Array DIM3 Bool)
      trep = replicate (lift (Z :. thetaCols :. All :. All)) occ
      tw32 :: Acc (Array DIM3 Word32)
      tw32 = map (\b -> if b then 1 else 0) trep
      per :: Exp (Z :. Int :. Int :. Int) -> Exp (Z :. Int :. Int)
      per tri =
        let (Z :. trt :. try :. trx) = unlift tri :: Z :. Exp Int :. Exp Int :. Exp Int
            x     = ((fromIntegral trx) - ((fromIntegral occw) / 2)) :: Exp Double
            y     = -((fromIntegral try) - ((fromIntegral occh) / 2)) :: Exp Double
            theta = indToRadExp thetaCols trt
            r = (x * (cos theta) + y * (sin theta)) :: Exp Double
            rind = round r + (rRows `div` 2)
            resind = if (rind < rRows) && (rind >= 0)
                     then lift (Z :. rind :. trt)
                     else ignore
        in if (trep ! tri) then resind
                           else ignore
      def :: Acc (Array DIM2 Word32)
      def = fill (lift (Z :. rRows :. thetaCols)) 0
  in permute (+) def per tw32

hValDebugFrame :: Acc (Array DIM2 Word32) -> Acc (Array DIM2 Word8)
```

```
hValDebugFrame hvs =
  let flt = flatten hvs
      mx = fromIntegral (the (maximum flt))
      mn = fromIntegral (the (minimum flt))
      toFltRange :: Exp Word32 -> Exp Double
      toFltRange v32 = (fromIntegral v32 - mn) / (mx - mn)
      toByteRange :: Exp Double -> Exp Word8
      toByteRange vd = round (vd * 255)
  in map (toByteRange . toFltRange) hvs


maxPoint :: Acc (Array DIM2 Word32) -> Acc (Scalar DIM2)
maxPoint hvs =
  let hvsind :: Acc (Array DIM1 (DIM2, Word32))
      hvsind = flatten (indexed hvs)
      fight :: Exp (DIM2, Word32) -> Exp (DIM2, Word32) -> Exp (DIM2, Word32)
      fight x y  =
        let (xind, xval) = unlift x :: (Exp DIM2, Exp Word32)
            (yind, yval) = unlift y :: (Exp DIM2, Exp Word32)
        in if xval >= yval then x else y
      maxScalar :: Acc (Scalar (DIM2, Word32))
      maxScalar = fold1 fight hvsind
  in map fst maxScalar
```

```
-- | True if right, false if left.
lorR :: Acc (Array DIM2 Bool) -> Acc (Scalar Bool)
lorR occ =
  let (Z :. occh :. occw) = unlift (shape occ) :: Z :. Exp Int :. Exp Int
      lor :: Exp DIM2 -> Exp Bool -> Exp (Word32, Word32)
      lor i b = let (Z :. occy :. occx) = unlift i :: Z :. Exp Int :. Exp Int
                    v = if b then 1 else 0 :: Exp Word32
                in if (occx > (occw `div` 2))
                  then lift (0 :: Exp Word32, v) :: Exp (Word32, Word32)
                  else lift (v, 0 :: Exp Word32) :: Exp (Word32, Word32)
      lors = imap lor occ
      lrsum lrx lry = let (lx, rx) = unlift lrx :: (Exp Word32, Exp Word32)
                          (ly, ry) = unlift lry :: (Exp Word32, Exp Word32)
                      in lift (lx + ly, rx + ry)
      (l, r) = unlift (the (fold1All lrsum  lors))
  in unit (r > l)
```

B.8. Main.hs

```
{-# LANGUAGE BangPatterns
        , CPP
        , DeriveGeneric
        , DeriveAnyClass
        , FlexibleContexts
```

```
        , OverloadedStrings
        #-}

module Main where

import Codec.FFmpeg

import qualified Data.Array.Accelerate as A

#ifdef CUDA
import Data.Array.Accelerate.LLVM.PTX
#else
import Data.Array.Accelerate.LLVM.Native
#endif

import qualified Data.ByteString.Lazy as BL

import Data.Csv

import Data.Fixed

import Data.Monoid
```

```
import Options.Generic

import System.Environment
import System.IO

import GaugeReader.Color
import GaugeReader.FrameIO
import GaugeReader.Hough

data Needle = Needle {
    needleSeconds  :: !Double
  , needleAngle    :: !Double
  , needleRad      :: !Double
  , needleGrams    :: !Double
  } deriving ( Show
             , Generic
             , ToRecord
             )

tableHeader :: BL.ByteString
tableHeader = "time(seconds),angle(radians),radius(pixels),gauge(grams?)\n"

makeCrop :: Double -- ^ Top crop frac
```

```
        -> Double -- ^ Bottom crop frac
        -> Double -- ^ Left crop frac
        -> Double -- ^ Right crop frac
        -> Int    -- ^ Circle mask radius in pixels
        -> A.Array A.DIM2 A.Word8
        -> A.Array A.DIM2 A.Word8
makeCrop t b l r rad = run1 ( bwToRGB
                    . twoValToBW
                    . circleMask (A.constant rad)
                    . crop (A.constant t)
                        (A.constant b)
                        (A.constant l)
                        (A.constant r)
                    . toTwoVal
                    . makeBW
                    )

makeTrans :: Double -- ^ Top crop frac
         -> Double -- ^ Bottom crop frac
         -> Double -- ^ Left crop frac
         -> Double -- ^ Right crop frac
         -> Int    -- ^ Circle mask radius in pixels
         -> Int    -- ^ Theta columns
```

```
        -> Int    -- ^ Radius rows
        -> A.Array A.DIM2 A.Word8
        -> A.Array A.DIM2 A.Word8
makeTrans t b l r rad thCols rRows = run1 ( hValDebugFrame
                                  . hVals (A.constant thCols)
                                        (A.constant rRows)
                                  . circleMask (A.constant rad)
                                  . crop (A.constant t)
                                       (A.constant b)
                                       (A.constant l)
                                       (A.constant r)
                                  . toTwoVal
                                  . makeBW
                                  )

makeRec :: Double -- ^ Top crop frac
        -> Double -- ^ Bottom crop frac
        -> Double -- ^ Left crop frac
        -> Double -- ^ Right crop frac
        -> Int    -- ^ Circle mask radius in pixels
        -> Int    -- ^ Theta columns
        -> Int    -- ^ Radius rows
        -> A.Array A.DIM2 A.Word8
```

```
        -> (A.Scalar A.DIM2, A.Scalar Bool)
makeRec t b l r rad thCols rRows =
   let f arr = let circd = ( circleMask (A.constant rad)
                           . crop (A.constant t)
                                  (A.constant b)
                                  (A.constant l)
                                  (A.constant r)
                           . toTwoVal
                           . makeBW
                           ) arr
                   mp = ( maxPoint
                        . hVals (A.constant thCols)
                                (A.constant rRows)
                        ) circd
                   lr = lorR circd
               in A.lift (mp, lr)
   in run1 f


cropDebugPipeline :: FilePath -- ^ Input
                  -> FilePath -- ^ Output
                  -> Int      -- ^ Width in pixels
                  -> Int      -- ^ Height in pixels
                  -> Int      -- ^ Frames per second
```

```
                -> Double   -- ^ Top crop frac.
                -> Double   -- ^ Bottom crop frac.
                -> Double   -- ^ Left crop frac.
                -> Double   -- ^ Right crop frac.
                -> Int      -- ^ Circle mask radius in pixels
                -> IO ()
cropDebugPipeline i o w h fps t b l r rad = do
    (gf, incpl) <- getFrameGetter i
    wf          <- imageWriter (mkVidEncParams w h fps) o
    let f  = makeCrop t b l r rad
        f' = accRGB8ToImgRGB8 . f
        pipe :: Int -> IO ()
        pipe !i = do
            putStrLn ("Processing frame " ++ (show i))
            mfr <- gf
            case mfr of Nothing -> wf Nothing
                        Just fr -> wf (Just (f' fr)) *> pipe (i+1)
    pipe 1
    incpl


transDebugPipeline :: FilePath -- ^ Input
                   -> FilePath -- ^ Output
                   -> Int      -- ^ Width in pixels
```

```
                -> Int      -- ^ Height in pixels
                -> Int      -- ^ Frames per second
                -> Double   -- ^ Top crop frac.
                -> Double   -- ^ Bottom crop frac.
                -> Double   -- ^ Left crop frac.
                -> Double   -- ^ Right crop frac.
                -> Int      -- ^ Circle mask radius in pixels
                -> Int      -- ^ Theta columns.
                -> Int      -- ^ Radius rows.
                -> IO ()
transDebugPipeline i o w h fps t b l r rad tcols rrows = do
  (gf, incpl) <- getFrameGetter i
  wf          <- imageWriter (mkVidEncParams w h fps) o
  let f  = makeTrans t b l r rad tcols rrows
      f' = accRGB8ToImgRGB8 . f
      pipe :: Int -> IO ()
      pipe !i = do
        putStrLn ("Processing frame " ++ (show i))
        mfr <- gf
        case mfr of Nothing -> wf Nothing
                    Just fr -> wf (Just (f' fr)) *> pipe (i+1)
  pipe 1
  incpl
```

```
resToNeedle :: Int        -- ^ Theta columns
            -> Double     -- ^ Multiplicative calibration factor
            -> Double     -- ^ Exponential calibration factor
            -> ( (A.Scalar A.DIM2, A.Scalar Bool)
               , Double)  -- ^ Result.
            -> Needle
resToNeedle thCols af bf ((resp, reslr), t) =
    let (A.Z A.:. rad A.:. thInd) = A.indexArray resp A.Z
        ang = indToRad thCols thInd + (if (A.indexArray reslr A.Z)
                                       then pi
                                       else 0
                                      )
    in Needle t
               ang
               (fromIntegral rad)
               (af * (exp (ang * bf)))


tablePipeline :: FilePath -- ^ Input
              -> FilePath -- ^ Output
              -> Double   -- ^ Top crop frac
              -> Double   -- ^ Bottom crop frac
              -> Double   -- ^ Left crop frac
```

```
            -> Double   -- ^ Right crop frac
            -> Int      -- ^ Circle mask radius in pixels
            -> Int      -- ^ Theta columns.
            -> Int      -- ^ Radius rows.
            -> Double   -- ^ Multiplicative factor
            -> Double   -- ^ Exponential factor
            -> IO ()
tablePipeline i o t b l r rad tcols rrows af bf = do
    (gft, incpl) <- getFrameTimeGetter i
    h <- openFile o WriteMode
    BL.hPut h tableHeader
    let f = makeRec t b l r rad tcols rrows
        pipe :: Int -> IO [(A.Scalar A.DIM2, Double)]
        pipe !i = do
            putStrLn ("Processing frame " ++ (show i))
            mfrt <- gft
            case mfrt of Nothing      -> pure []
                         Just (fr, t) -> do
                             let !n = resToNeedle tcols af bf (f fr, t)
                             BL.hPut h (encode [n])
                             pipe (i+1)
    pipe 1
    hClose h
```

```
valFrac :: Double -> Bool
valFrac x = (x <= 0.5) && (x >= 0)

valTheta :: Int -> Bool
valTheta t = mod t 45 == 0

badFrac :: IO ()
badFrac = do
    putStrLn "Each crop fraction is expressed as a fraction of the"
    putStrLn "corresponding dimension, i.e. --top 0.25 --bottom 0.25 leaves one"
    putStrLn "with the middle 50% of the image's pixels."
    pure ()

badTheta :: IO ()
badTheta = do
    putStrLn "Theta resolution must be a multiple of 45. Although the angle is"
    putStrLn "reported in radians, the angular resolution is provided by the"
    putStrLn "user in degrees."

data Action = CropDebug { input  :: FilePath
                        , output :: FilePath
                        , width  :: Int
```

```
          , height :: Int
          , fps    :: Int
          , top    :: Double
          , bottom :: Double
          , left   :: Double
          , right  :: Double
          , radius :: Int
          }
| TransDebug { input     :: FilePath
          , output    :: FilePath
          , width     :: Int
          , height    :: Int
          , fps       :: Int
          , top       :: Double
          , bottom    :: Double
          , left      :: Double
          , right     :: Double
          , radius    :: Int
          , angleRes  :: Int
          , radiusRes :: Int
          }
| MakeTable { input      :: FilePath
          , output     :: FilePath
```

```
                , top        :: Double
                , bottom     :: Double
                , left       :: Double
                , right      :: Double
                , radius     :: Int
                , angleRes   :: Int
                , radiusRes  :: Int
                , multfactor :: Double
                , expfactor  :: Double
                }
        deriving ( Show
                 , Generic
                 , ParseRecord
                 )

doAction :: Action -> IO ()
doAction (CropDebug i o w h fps t b l r rad)
    | not (valFrac t && valFrac b && valFrac l && valFrac r) = badFrac
    | otherwise = cropDebugPipeline i o w h fps t b l r rad
doAction (TransDebug i o w h fps t b l r rad tcols rrows)
    | not (valFrac t && valFrac b && valFrac l && valFrac r) = badFrac
    | not (valTheta tcols) = badTheta
    | otherwise = transDebugPipeline i o w h fps t b l r rad tcols rrows
```

```
doAction (MakeTable i o t b l r rad tcols rrows af bf)
    | not (valFrac t && valFrac b && valFrac l && valFrac r) = badFrac
    | not (valTheta tcols) = badTheta
    | otherwise = tablePipeline i o t b l r rad tcols rrows af bf
main :: IO ()
main = do
    initFFmpeg
    getRecord "Hough Transform Gauge Video Reader" >>= doAction
```

B.9. stack.yaml

```
resolver: nightly-2018-01-14

packages:
- .

extra-deps:
- accelerate-1.1.1.0
- accelerate-io-1.0.0.1
- accelerate-llvm-1.1.0.0
- accelerate-llvm-native-1.1.0.1
- accelerate-llvm-ptx-1.1.0.0
- git: https://github.com/TravisWhitaker/ffmpeg-light
  commit: 6e737a4fa2d570f86d837ffa198df02372ffaf81
- git: https://github.com/TravisWhitaker/cuda.git
  commit: d37b12e422a8d54dfd6e6a773fe037d63512eff1
- git: https://github.com/TravisWhitaker/nvvm.git
  commit: eb2e04f6fb38660d56f2abe43ac96ac2016cdff2
system-ghc: true
```